GENETIC AND EPIGENETIC REGULATION OF INSECT DEVELOPMENT, REPRODUCTION, AND PHENOTYPIC PLASTICITY

EDITED BY: Wei Guo, S. Reddy Palli, Fei Li and Zhongxia Wu

PUBLISHED IN: Frontiers in Genetics and
Frontiers in Cell and Developmental Biology

frontiers Research Topics

ISSN 1664-8714
ISBN 978-2-88974-355-1
DOI 10.3389/978-2-88974-355-1

About Frontiers

Frontiers is more than just an open-access publisher of scholarly articles: it is a pioneering approach to the world of academia, radically improving the way scholarly research is managed. The grand vision of Frontiers is a world where all people have an equal opportunity to seek, share and generate knowledge. Frontiers provides immediate and permanent online open access to all its publications, but this alone is not enough to realize our grand goals.

Frontiers Journal Series

The Frontiers Journal Series is a multi-tier and interdisciplinary set of open-access, online journals, promising a paradigm shift from the current review, selection and dissemination processes in academic publishing. All Frontiers journals are driven by researchers for researchers; therefore, they constitute a service to the scholarly community. At the same time, the Frontiers Journal Series operates on a revolutionary invention, the tiered publishing system, initially addressing specific communities of scholars, and gradually climbing up to broader public understanding, thus serving the interests of the lay society, too.

Dedication to Quality

Each Frontiers article is a landmark of the highest quality, thanks to genuinely collaborative interactions between authors and review editors, who include some of the world's best academicians. Research must be certified by peers before entering a stream of knowledge that may eventually reach the public - and shape society; therefore, Frontiers only applies the most rigorous and unbiased reviews.
Frontiers revolutionizes research publishing by freely delivering the most outstanding research, evaluated with no bias from both the academic and social point of view. By applying the most advanced information technologies, Frontiers is catapulting scholarly publishing into a new generation.

What are Frontiers Research Topics?

Frontiers Research Topics are very popular trademarks of the Frontiers Journals Series: they are collections of at least ten articles, all centered on a particular subject. With their unique mix of varied contributions from Original Research to Review Articles, Frontiers Research Topics unify the most influential researchers, the latest key findings and historical advances in a hot research area! Find out more on how to host your own Frontiers Research Topic or contribute to one as an author by contacting the Frontiers Editorial Office: frontiersin.org/about/contact

GENETIC AND EPIGENETIC REGULATION OF INSECT DEVELOPMENT, REPRODUCTION, AND PHENOTYPIC PLASTICITY

Topic Editors:
Wei Guo, Institute of Zoology, Chinese Academy of Sciences (CAS), China
S. Reddy Palli, University of Kentucky, United States
Fei Li, Zhejiang University, China
Zhongxia Wu, Henan University, China

Citation: Guo, W., Palli, S. R., Li, F., Wu, Z. eds. (2022). Genetic and Epigenetic Regulation of Insect Development, Reproduction, and Phenotypic Plasticity. Lausanne: Frontiers Media SA. doi: 10.3389/978-2-88974-355-1

Table of Contents

frontiers in Genetics

ORIGINAL RESEARCH
published: 17 April 2020
doi: 10.3389/fgene.2020.00387

Genetic Variation May Have Promoted the Successful Colonization of the Invasive Gall Midge, *Obolodiplosis robiniae*, in China

*Yan-Xia Yao, Xing-Pu Shang, Jun Yang, Ruo-Zhu Lin, Wen-Xia Huai and Wen-Xia Zhao**

Key Laboratory of Forest Protection of National Forestry and Grassland Administration/Research Institute of Forest Ecology, Environment and Protection, Chinese Academy of Forestry, Beijing, China

Invasive species often cause serious economic and ecological damage. Despite decades of extensive impacts of invasives on bio-diversity and agroforestry, the mechanisms underlying the genetic adaptation and rapid evolution of invading populations remain poorly understood. The black locust gall midge, *Obolodiplosis robiniae*, a highly invasive species that originated in North America, spread widely throughout Asia and Europe in the past decade. Here, we used 11 microsatellite DNA markers to analyze the genetic variation of 22 *O. robiniae* populations in China (the introduced region) and two additional US populations (the native region). A relatively high level of genetic diversity was detected among the introduced populations, even though they exhibited lower diversity than the native US populations. Evidence for genetic differentiation among the introduced Chinese populations was also found based on the high *Fst* value compared to the relatively low among the native US populations. Phylogenetic trees, structure graphical output, and principal coordinate analysis plots suggested that the Chinese *O. robiniae* populations (separated by up to 2,540 km) cluster into two main groups independent of geographical distance. Genetic variation has been observed to increase rapidly during adaptation to a new environment, possibly contributing to population establishment and spread. Our results provide insights into the genetic mechanisms underlying successful invasion, and identify factors that have contributed to colonization by an economically important pest species in China. In addition, the findings improve our understanding of the role that genetic structure plays during invasion by *O. robiniae*.

Keywords: genetic diversity, genetic differentiation, genetic structure, population colonization, invasion success

OPEN ACCESS

Edited by:
Wei Guo,
Institute of Zoology (CAS), China

Reviewed by:
Chuan Ma,
Chinese Academy of Agricultural Sciences, China
Jagadish S. Bentur,
Agri Biotech Foundation, India

****Correspondence:***
Wen-Xia Zhao
zhaowx9501@126.com

Specialty section:
This article was submitted to Epigenomics and Epigenetics, a section of the journal Frontiers in Genetics

Received: *10 January 2020*
Accepted: *27 March 2020*
Published: *17 April 2020*

Citation:
Yao Y-X, Shang X-P, Yang J, Lin R-Z, Huai W-X and Zhao W-X (2020) Genetic Variation May Have Promoted the Successful Colonization of the Invasive Gall Midge, Obolodiplosis robiniae, in China. Front. Genet. 11:387. doi: 10.3389/fgene.2020.00387

INTRODUCTION

Obolodiplosis robiniae (Haldeman, 1847) (Diptera: Cecidomyiidae) is a North American species of gall midge that has recently been extensively introduced throughout Asia and Europe (CABI/EPPO, 2011) and is continuously expanding its range (Cierjacks et al., 2013; Stalazs, 2014; Badmin, 2016; Kostro-Ambroziak and Mieczkowska, 2017). It is specifically associated with host plants from

the genus *Robinia* (Fabaceae) (Stalazs, 2014). Its main host is *Robinia pseudoacacia* although it is occasionally found on *R. pseudoacacia* cv. 'Frisia' (Badmin, 2016). The gall midge causes leaf rolling and premature leaf shedding, resulting in the deterioration of the host and increased susceptibility to other pests, including wood borers such as longhorn beetles (Yang et al., 2006).

Obolodiplosis robiniae was first recorded in China (Qinhuangdao City, Hebei Province) in 2004 (Yang et al., 2006) and has since spread extensively. Its primary host (*R. pseudoacacia*) has been planted extensively across China, and *O. robiniae* is now found in most of these areas (Shang et al., 2015a). Chinese *O. robiniae* populations may produce between four and six generations per year (Wang, 2009; Mu et al., 2010; Shao et al., 2010; Liu, 2014), which is significantly higher than the rate in regions beyond China. For example, *O. robiniae* produces three to four generations per year in Italy (Duso et al., 2005) and Serbia (Mihajlovic et al., 2008), and a maximum of three generations per year in Korea (Lee et al., 2009).

Genetic diversity and population structure are important factors affecting the colonization of invasive species (Amouroux et al., 2013; Horst and Lau, 2015; Zhao et al., 2015). Invasive species often exhibit low genetic diversity during founding events, as new habitats are typically colonized by only a few individuals, representing a small proportion of the allelic diversity present in the source population (Nei et al., 1975; Tsutsui et al., 2003). However, when the founding individuals originate from multiple source populations, the genetic diversity of the founder population can be relatively high (Davis, 2009). This can contribute to invasion success by facilitating local adaptation to new environments and increasing new trait diversity (Facon et al., 2006). Besides, the invaders can rapidly evolve in isolation from other individuals of the same species when they were introduced into the new environments (Lee, 2002; Launey et al., 2010).

DNA-based molecular markers have been extensively used to examine the genetic diversity and population structure of a wide range of species. Microsatellite DNA markers (simple sequence repeats, SSRs) are suitable for routine genetic diversity analyses (Varshney et al., 2007; Kong et al., 2014; Kim et al., 2017), as they are ubiquitous among eukaryotes (Sharma et al., 2007), co-dominantly inherited, and highly polymorphic (Zong et al., 2015). Moreover, microsatellite analysis can yield valid results and improved phylogenetic trees compared to analyses involving other molecular markers (Schemerhorn et al., 2015). Due to their feasibility and practicality, microsatellite markers have been widely used in population genetics and ecological studies of various insects (Bonizzoni et al., 2000; Mezghani-Khemakhem et al., 2012; Anjos et al., 2016; Retamal et al., 2016; Duan et al., 2017; Kim et al., 2017; Simonato et al., 2019), including several invasive gall midge species (Bentur et al., 2011; Amouroux et al., 2013).

Previously, Shang et al. (2015b) investigated the genetic variation among Chinese *O. robiniae* populations using a partial mitochondrial DNA cytochrome c oxidase subunit I (COI) sequence marker. However, only 10 individuals exhibiting haplotypic variation and a mere four haplotypes were detected in 560 *O. robiniae* samples. Thus, the genetic mechanisms behind successful invasion, the genetic structure in the process of colonization, and the phylogenetic relationships among the Chinese *O. robiniae* populations remain poorly understood.

Accordingly, to gain further insight into the genetic structure of the Chinese *O. robiniae* populations and ascertain how the species has spread widely in new regions, we used 11 microsatellite markers to analyze the genetic structure of 22 Chinese *O. robiniae* populations. Two native populations from the United States (US) were also assessed based on the same loci for comparison with the Chinese populations, in order to explain how genetic diversity is altered during the invasion process.

MATERIALS AND METHODS

Sample Collection

We collected the gall midge larvae and pupae contained within rolled leaves of host trees growing in 22 cities across China (**Figure 1**). Generally, the rolled leaves were randomly picked from different trees; however, when infestation was low, individual trees were singled out for sample collection. Following collection, the rolled leaves were immediately transported to the laboratory in 60 cm × 40 cm plastic bags, in which they were maintained until adult emergence. From the samples collected at each location, 20 larger adults were selected, placed into a 1.5-mL centrifuge tube, and stored at −20°C for subsequent DNA extraction. Additionally, eight *O. robiniae* adults from two regions of the United States were obtained from the Quarantine Lab at the Institute of Forest Ecology, Environment, and Protection in the Chinese Academy of Forestry. Details of the sample collection and population codes are listed in **Table 1**.

DNA Extraction and Microsatellite Analyses

Genomic DNA was extracted from the entire *O. robiniae* body following the instructions described by Zhou et al. (2007) and stored at −20°C until needed. The 14 microsatellite loci (W3, W5, W8, W29, W31, W33, W35, W41, W46, W82, W83, W116, W126, and W132) developed by Yao et al. (2015) were initially selected to analyze the genotypes of 20 individuals per collection site (the exception being Zhengzhou, for which 16 individuals were analyzed) (**Table 1**). For each sample, we attempted to amplify all 14 loci; however, after two attempts, we were unable to amplify five loci (W29, W35, W41, W46, and W116) for many individuals; thus, these loci were not used in subsequent analyses. However, we assessed the applicability of two additional loci (W6 and W107; GenBank numbers: KP260520 and KP260530) that were not characterized by Yao et al. (2015), and we detected sufficient polymorphism among the analyzed samples. Hence, a total of 11 loci were used to genotype 444 *O. robiniae* individuals.

Microsatellite amplifications were performed in a 15 μL reaction volume containing 1 μL genomic DNA (10 ng), 1 μL of each primer (5 μmol/L), 7.5 μL 2X Taq PCR Master Mix (TIANGEN, Beijing, China), and 4.5 μL ddH_2O. The forward primer of each primer pair was labeled with a fluorescent dye (HEX, ROX, FAM, or TMARA; Sangon Biotech, Shanghai, China). The microsatellite cycling protocol was: 5 min at 95°C

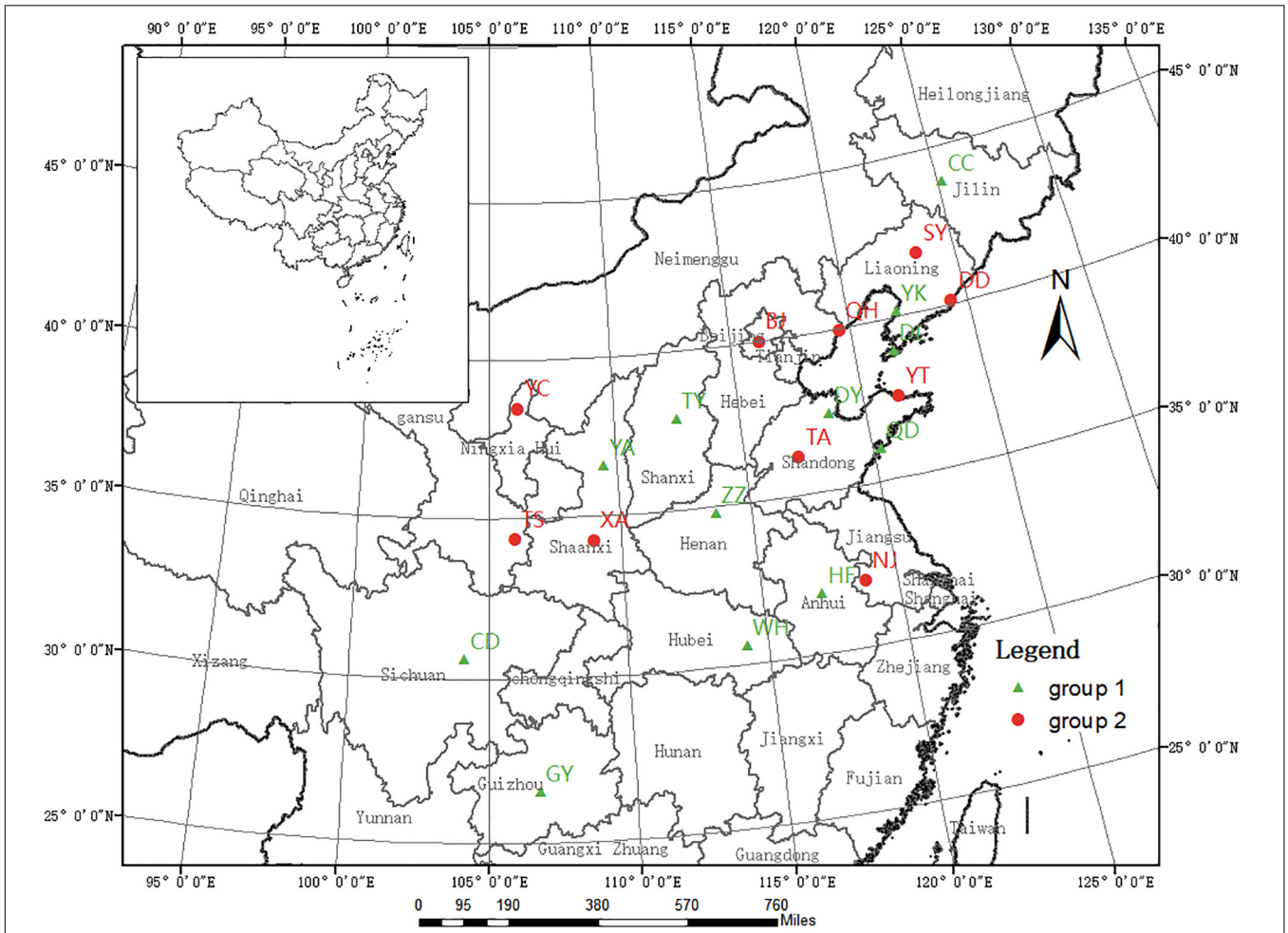

FIGURE 1 | Geographic locations of the 22 Chinese *Obolodiplosis robiniae* populations sampled. Population codes are listed in **Table 1**. (The source map was downloaded from the website http://www.webmap.cn/commres.do?method=dataDownload).

(initial denaturation step); followed by 30 cycles of 94°C for 30 s, 53°C (W3, W5, W6, and W8) or 56°C (the remaining loci) for 45 s, 72°C for 45 s, extension at 72°C for 10 min, and finally maintained at 16°C. PCR products were examined using a DNA analyzer (Applied Biosystems, Waltham, CA, United States) and the results were analyzed using Genotyping was carried out using a 3730xl automated DNA sequencer (Applied Biosystems, Waltham, CA, United States). Alleles were scored using GeneMarker software version 2.2. (Softgenetics LLC, State College, PA, United States).

Data Analyses

Genetic diversity was estimated by basic statistical analyses including number of alleles (*Na*), effective number of alleles (*Ne*), Shannon's information index (*I*), observed heterozygosity (*Ho*), expected heterozygosity (*He*), and Nei's (1973) expected heterozygosity (*Nei*), which were calculated using GenePop software version 4.3 (Rousset, 2008); genotype number (*GN*), gene diversity (*GD*), and polymorphism information content (*PIC*) were calculated using PowerMarker software version V3.25 (Liu and Muse, 2005). *F*-statistics and gene flow for each locus across populations were performed using PopGene software version 1.32 (Yeh et al., 2018). Deviations from the Hardy–Weinberg equilibrium (HWE) based on the Markov chain algorithm (10,000 steps) and linkage disequilibrium (LD) (10,000 permutations) were also examined by GenePop software. The genetic relationships between populations were assessed using a neighbor-joining dendrogram generated by PowerMarker and Molecular Evolutionary Genetics Analysis across Computing Platforms (MEGA X) (Kumar et al., 2018).

Populations differentiation was assessed by pairwise *Fst* values (based on 999 permutations) and gene flow (*Nm*) through AMOVA (analysis of molecular variance) approach which were performed using the Arlequin program version 3.5 (Excoffier and Lischer, 2010). The analyses can estimate variance and partitioning of the within- and among-population. Genetic structure analysis was performed with 100,000 Markov Chain Monte Carlo repetitions after a burn-in period of 200,000 interactions for each group number (*K*) using STRUCTURE software version 2.3.4 (Pritchard et al., 2000). The number of

TABLE 1 | Location of *Obolodiplosis robiniae* populations and the sample size used in this study.

Number	Code	Site	Latitude (N)	Longitude (E)	Altitude	Sample size
(1)	BJ	Beijing	40°00.184′	116°14.363′	76	20
(2)	CC	Changchun, Jilin	43°53.851′	125°16.329′	218	20
(3)	CD	Chengdu, Sichuan	30°38.245′	104°07.334′	510	20
(4)	DD	Dandong, Liaoning	40°06.906′	124°21.536′	33	20
(5)	DL	Dalian, Liaoning	38°58.531′	121°36.800′	67	20
(6)	DY	Dongying, Shandong	37°26.366′	118°34.448′	17	20
(7)	GY	Guiyang, Guizhou	26°33.531′	106°45.003′	1090	20
(8)	HF	Hefei, Anhui	31°52.824′	117°11.639′	39	20
(9)	NJ	Nanjing, Jiangsu	32°03.426′	118°50.820′	90	20
(10)	QD	Qingdao, Shandong	36°03.367′	120°20.934′	24	20
(11)	QH	Qinhuangdao, Hebei	39°56.161′	119°35.411′	17	20
(12)	SY	Shenyang, Liaoning	41°50.438′	123°25.690′	51	20
(13)	TA	Taian, Shandong	36°12.225′	117°07.104′	208	20
(14)	TS	Tianshui, Gansu	34°21.405′	106°00.034′	1460	20
(15)	TY	Taiyuan, Shanxi	37°54.592′	112°31.811′	798	20
(16)	WH	Wuhan, Hubei	30°36.733′	114°17.772′	40	20
(17)	XA	Xian, Shaanxi	34°15.474′	108°58.938′	428	20
(18)	YA	Yanan, Shaanxi	36°35.633′	109°29.535′	1121	20
(19)	YC	Yinchuan, Ningxia	38°28.933′	106°11.983′	1115	20
(20)	YK	Yingkou, Liaoning	40°12.432′	122°04.413′	15	20
(21)	YT	Yantai, Shandong	37°32.024′	121°25.657′	9	20
(22)	ZZ	Zhengzhou, Henan	34°48.509′	113°42.266′	95	16
(23)	US_f	Finger Lakes, NY, United States	42°45′	−76°41.4′W	–	5
(24)	US_g	Goat Island, NY, United States	43°48′	−79°42′W	–	3

subpopulations (K) was assumed to be from 1 to 22, without admixture and with correlated allele frequencies. To determine the most likely number of subpopulations, the optimum K-value was obtained by calculating the ΔK value (Evanno et al., 2005).

In addition, the Mantel test was conducted using the GenALEx 6.5 program (Peakall and Smouse, 2012) to determine correlations between Nei's genetic distance [was calculated using GenePop software based on Nei (1978)] and both geographical distance (km) and altitude (m). Significance was assessed by conducting 999 permutations. Moreover, a principal coordinate analysis (PCoA) was conducted using the same software.

RESULTS

Microsatellite Polymorphism and Diversity

In this study, locus polymorphism and diversity were determined based on 22 Chinese populations using 11 microsatellite markers, with each population consisting of 20 individual samples (except Zhengzhou, with 16 samples) (**Table 1**). Amplifying these microsatellite markers loci led to 436 polymorphic bands (**Supplementary Table S1**), representing 202 genotypes, ranging from 3 to 54 per primer pair. As shown in **Table 2**, there were 72 alleles among the 22 populations; the number of alleles (*Na*) observed per locus varied from 2 (W83 and W107) to 14 (W3 and W5), with a mean of 6.5 per locus. The effective numbers of alleles (*Ne*) varied from 1.4087 (W83) to 7.9971 (W3), with an average of 3.7255 per locus. The gene diversity index (*GD*) per locus ranged from 0.2901 (W83) to 0.8755 (W3), with an average of 0.6511, indicating that a high level of information was provided by the 11 microsatellite markers. Shannon's information index (*I*) ranged from 0.4767 (W83) to 2.2573 (W3), with a mean of 1.3188. The polymorphism information content (*PIC*) for the microsatellite loci ranged from 0.2494 (W83) to 0.8627 (W3), with an average of 0.6031. The observed

TABLE 2 | Polymorphism of microsatellite loci across Chinese *O. robiniae* populations.

Locus	*Na*	*GN*	*Ne*	*GD*	*I*	*Ho*	*He*	*PIC*
W3	14	54	7.9971	0.8755	2.2573	0.7477	0.8760	0.8627
W5	14	42	5.8768	0.8295	1.9743	0.7067	0.8308	0.8085
W6	4	6	2.2687	0.5601	0.9575	0.3471	0.5599	0.4973
W8	7	18	4.3609	0.7712	1.6184	0.3701	0.7716	0.7367
W31	5	14	4.2747	0.7661	1.5224	0.6697	0.7669	0.7281
W33	7	20	3.6391	0.7249	1.4660	0.6506	0.7260	0.6835
W82	5	12	3.3448	0.7010	1.3193	0.3532	0.7018	0.6487
W83	2	4	1.4087	0.2901	0.4767	0.3005	0.2905	0.2494
W107	2	3	1.6205	0.3829	0.5710	0.2271	0.3833	0.3096
W126	4	6	2.0018	0.5005	0.7223	0.4398	0.5010	0.3809
W132	8	23	4.1874	0.7603	1.6214	0.4207	0.7621	0.7284
Mean	6.5	18.3636	3.7255	0.6511	1.3188	0.4757	0.6518	0.6031

Number of alleles (Na), genotype number (GN), effective number of alleles (Ne), gene diversity (GD), Shannon's information index (I), observed heterozygosity (Ho), expected heterozygosity (He), polymorphism information content (PIC).

heterozygosity (*Ho*) ranged from 0.2271 (W107) to 0.7477 (W3) and expected heterozygosity (*He*) ranged from 0.2905 (W83) to 0.8760 (W3). For each locus, both *Na* and *Ho* values markedly changed among populations, whereas, *He* value minorly altered (**Supplementary Figure S1**). In addition, when we evaluated the within-sample HWE deviations for each locus across all 22 Chinese populations using the Markov chain algorithm (10,000 steps), we detected significant deviation from the expected value ($p < 0.05$) in 68 of 242 tests (28.10%) (**Supplementary Table S2**). Examination of genotypic LD between all pairs of alleles across all 22 populations, based on a permutation procedure (10,000 permutations), revealed a significant LD ($p < 0.05$) in 251 of 1210 tests (20.74%) from 11 loci in the 22 Chinese populations.

Population Genetic Diversity

The genetic diversity of 22 Chinese populations and two US populations was assessed. Six indices of genetic diversity (*Na*, *Ne*, *I*, *Ho*, *He*, and *Nei*) were evaluated. As shown in **Table 3**, for each Chinese population across all loci, the means of the above indices except *Na* were moderately or considerably lower than those of the native US populations, although the sample size of the Chinese populations (40) was markedly higher than that of the US populations (8). Regarding the three most important indices, *I*, *He*, and *Nei*, the lowest Chinese values (I = 0.7847, *He* = 0.4279, *Nei* = 0.4172) occurred in the DY population, and the highest (I = 1.1103, *He* = 0.6162, *Nei* = 0.6008) in the TS population. Increased values of these three indices occurred in the SY (I = 1.058, *He* = 0.6157, *Nei* = 0.6003), YT (I = 1.0761, *He* = 0.5825, *Nei* = 0.5677), and DD (I = 1.016, *He* = 0.5895, *Nei* = 0.5748) populations. The inbreeding coefficient (*Fis*) ranged from −0.0295 (TY) to 0.2011 (CD), with significant various observed for each locus among populations. Both US populations exhibited high *He* values of 0.6544 (US_f) and 0.6606 (US_g).

Genetic Differentiation in the Chinese Populations

The *Fst* per locus ranged from 0.1357 to 0.3770, with an average of 0.1994, and the *Fis* per locus ranged from −0.0037 (W3) to 0.3364 (W82) with an average of 0.0873 alleles per locus across populations (**Table 4**). Gene flow (*Nm*) ranged from 0.3093 at W31 to 1.5921 at W33 and averaged 1.0036. Meanwhile, the pairwise *Fst* ($p < 0.001$) values (**Supplementary Table S3**) between populations ranged from 0.022 (HF and WH) to 0.377 (BJ and GY), with an average value of 0.183. A total of 135 of the 213 *Fst* values (63.38%) were >0.15, while 48 (22.54%) were >0.25, which suggests that significant genetic differentiation

TABLE 3 | Genetic diversity of the *O. robiniae* populations across 11 microsatellite loci.

Code	Sample size	*Na*	*Ne*	*I*	*Ho*	*He*	*Nei*	*Fis*
BJ	40	3.3636	2.375	0.868	0.4591	0.4928	0.4805	0.0445
CC	40	3.7273	2.5568	0.9673	0.4364	0.5425	0.529	0.1751
CD	40	3.4545	2.1684	0.8976	0.4136	0.531	0.5177	0.2011
DD	40	3.5455	2.651	1.016	0.5591	0.5895	0.5748	0.0273
DL	40	3.1818	2.3375	0.8675	0.5636	0.5026	0.49	−0.1503
DY	40	3.2727	2.2412	0.7847	0.4409	0.4279	0.4172	−0.0569
GY	40	3.5455	2.0894	0.8164	0.3864	0.4705	0.4588	0.1578
HF	40	3.1818	2.5997	0.9554	0.4909	0.5742	0.5599	0.1232
NJ	40	3.8182	2.4202	0.9633	0.4364	0.5408	0.5273	0.1724
QD	40	3.3636	2.2096	0.8265	0.3682	0.4647	0.4531	0.1874
QH	40	3.6364	2.2661	0.9192	0.5318	0.5233	0.5102	−0.0423
SY	40	3.7273	2.797	1.058	0.5455	0.6157	0.6003	0.0914
TA	40	3.3636	2.0576	0.8347	0.439	0.4792	0.4672	0.0603
TS	40	4.0909	2.8428	1.1103	0.5045	0.6162	0.6008	0.1602
TY	40	3.6364	2.3278	0.9101	0.5273	0.5253	0.5122	−0.0295
WH	40	3.7273	2.5723	0.9797	0.5256	0.5599	0.5459	0.0371
XA	40	3.5455	2.535	0.9503	0.5182	0.5492	0.5355	0.0323
YA	40	3.8182	2.7608	0.9798	0.4199	0.5355	0.5221	0.1958
YC	40	3.8182	2.4284	0.9586	0.467	0.5369	0.5234	0.1078
YK	40	4.4545	2.6524	1.0623	0.4682	0.567	0.5528	0.1531
YT	40	4.2727	2.9205	1.0761	0.5081	0.5825	0.5677	0.1049
ZZ	30	3.4545	2.3364	0.912	0.4516	0.5346	0.5168	0.1261
CN mean	40	3.6363	2.4612	0.9415	0.4755	0.5346	0.5192	–
US_f	10	4.0909	3.2336	1.1472	0.5	0.6544	0.5875	0.1489
US_g	6	3.0909	2.6363	0.9632	0.5152	0.6606	0.5505	0.0642
US mean	8	3.5909	2.935	1.0552	0.5076	0.6575	0.569	–

Number of alleles (Na), effective number of alleles (Ne), Shannon's information index (I), observed heterozygosity (Ho), expected homozygosity (He), Nei's (1973) expected heterozygosity (Nei), inbreeding coefficient (Fis).

TABLE 4 | Summary of *F* statistics and gene flow for each locus.

Locus	*Fis*	*Fst*	*Nm*
W3	−0.0037	0.1487	1.4307
W5	0.0026	0.1460	1.4629
W6	0.0040	0.3770	0.4130
W8	0.2929	0.3198	0.5317
W31	−0.0441	0.1603	1.3093
W33	−0.0364	0.1357	1.5921
W82	0.3364	0.2379	0.8007
W83	−0.1980	0.1367	1.5792
W107	0.3182	0.1402	1.5337
W126	−0.0165	0.1379	1.5634
W132	0.2870	0.2230	0.8745
Mean	0.0873	0.1994	1.0036

Gene flow (Nm) estimated based on Nm = 0.25(1 – Fst)/Fst.

TABLE 5 | Population genetic variance revealed by 11 microsatellite loci through AMOVA analysis.

Source	Degree of freedom	Sum of squared deviations	Mean squared deviations	Variance component estimates	Percentage of variation
Chinese populations					
Among populations	21	622.846	29.659	0.665	18%
Among individuals	414	1371.394	3.313	0.353	10%
Within individuals	436	1136.500	2.607	2.607	72%
Total	871	3130.740		3.624	100%
Fst	0.183	0.001			
Nm	1.113				
P-value	<0.001				
US populations					
Among populations	1	7.496	7.496	0.354	9%
Among individuals	6	29.067	4.844	1.047	25%
Within individuals	8	22.000	2.750	2.750	66%
Total	15	58.563		4.151	100%
Fst	0.085				
Nm	2.685				
P-value	<0.03				

exists among the sampling sites and there is some restriction in gene flow between them (**Table 4**). The most noticeable genetic differentiation occurred between BJ and GY (*Fst* = 0.377), followed by GY and QH (*Fst* = 0.372), then DY and QH, DY and GY (*Fst* = 0.361 for both). According to the coefficient of genetic differentiation (*Fst* = 0.1830, $p < 0.001$), genetic variation within populations (81.66%) was substantially higher than that among populations (18.34%) ($p < 0.001$) (**Table 5**). Gene flow (*Nm*) ranged from 0.414 (BJ and GY) to 11.05 (HF and WH) (**Supplementary Table S4**), with an average of 1.113 (**Table 5**). All investigated loci contributed to the population differentiation ($p < 0.001$ for each individual locus). Regarding the native US populations, they had a relatively low *Fst* value (0.085, $p < 0.03$), a high *Nm* value (2.685), and variation within populations of 91%, while variation among populations was 9% ($p < 0.02$). This further indicates the existence of extensive genetic differentiation among the introduced populations.

Genetic Relationships and Population Structure Analysis

A dendrogram depicting the genetic relationships among the 22 Chinese populations was constructed based on the microsatellite data (**Figure 2**). The populations were divided into two main clusters, and each cluster was further separated into several sub-clusters. Group I contained populations from Northeast China (Jilin Province) to Southwest China (Guizhou Province), including Liaoning (YK, DL), Jilin (CC), Shanxi (TY), Shaanxi (YA), Shandong (DY, QD), Henan (ZZ), Sichuan (CD), Hubei (WH), Anhui (HF), and Guizhou (GY) provinces. Group II contained populations from North China (with the exception of the NJ population), including Beijing (BJ), Liaoning (SY, DD), Hebei (QH), Shandong (YT, TA), Shaanxi (XA), Gansu (TS), Ningxia (YC), and Jiangsu (NJ) provinces. Besides, some subdivided populations were clustered according to their spatial distribution, such as GY, HF, and WH located in the south of southern China, which clustered together in group I, whereas TA, DD, BJ, and QH located around Bohai Bay clustered together in group II.

The 436 Chinese *O. robiniae* samples were further assessed for population stratification using STRUCTURE software. Microsatellite data were analyzed with possible cluster numbers (K-values) ranging from 1 to 22. ΔK was clearly maximized when $K = 2$ ($\Delta K = 4298.3743$), indicating the occurrence of two distinct groups among the 22 populations (**Figure 3**), which validates the dendrogram-based grouping, and the second clade was grouped according to approximate geographical area. These results suggested different degrees of introgression in the populations, detected as differences in allelic frequencies among the populations. In addition, greater structuring ($K = 3$) revealed that QD, GY, and TY in group I had certain structural similarities to YT, SY, NJ, YC, and XA in group II.

In addition, PCoA based on the marker genotypes also revealed two distinct clusters of the Chinese populations (**Figure 4**), which were partly related to their geographical regions (group II contained populations from North China). The Mantel test revealed non-significant negative correlations between Nei's genetic distance (**Supplementary Table S5**) and geographical distance (km) ($r = -0.02$, $P = 0.456$; **Supplementary Figure S2**), and between Nei's genetic distance and altitude ($r = -0.026$, $P = 0.419$; **Supplementary Figure S3**), which indicates that genetic differentiation in the 22 Chinese populations may not be caused by geographical isolation.

DISCUSSION

In the present study, we detected a high degree of polymorphism among the assessed microsatellite loci. We also identified a relatively high level of genetic diversity among Chinese *O. robiniae* populations across all loci, with the average expected heterozygosity (He) and Nei's (1973) expected heterozygosity (*Nei*) being 0.5346 and 0.5192, respectively. The highest *He* was 0.6606, which occurred in the US_g population despite the fact that it consisted of only three *O. robiniae* individuals. Nonetheless, *He*, *Nei* (Shang et al., 2016), gene diversity index

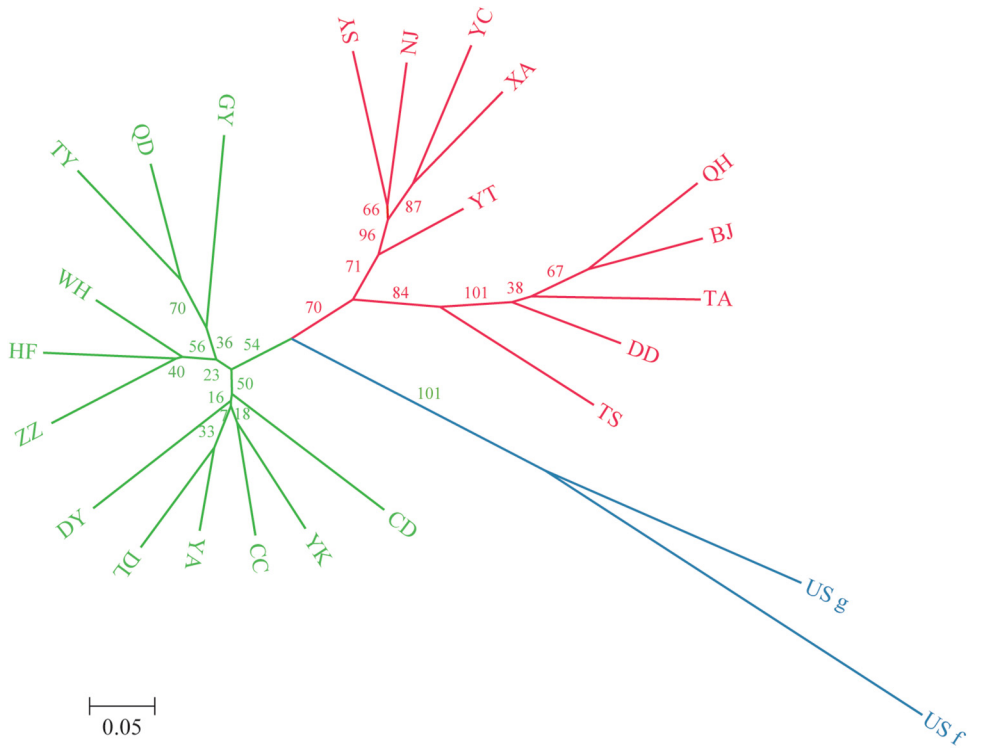

FIGURE 2 | Unrooted neighbor-joining dendrogram of the 24 *O. robiniae* populations based on Nei's distance using the allele frequencies of 11 microsatellite loci. Green represents the subpopulations of group 1, red represents the subpopulations of group 2, and blue represents the US populations.

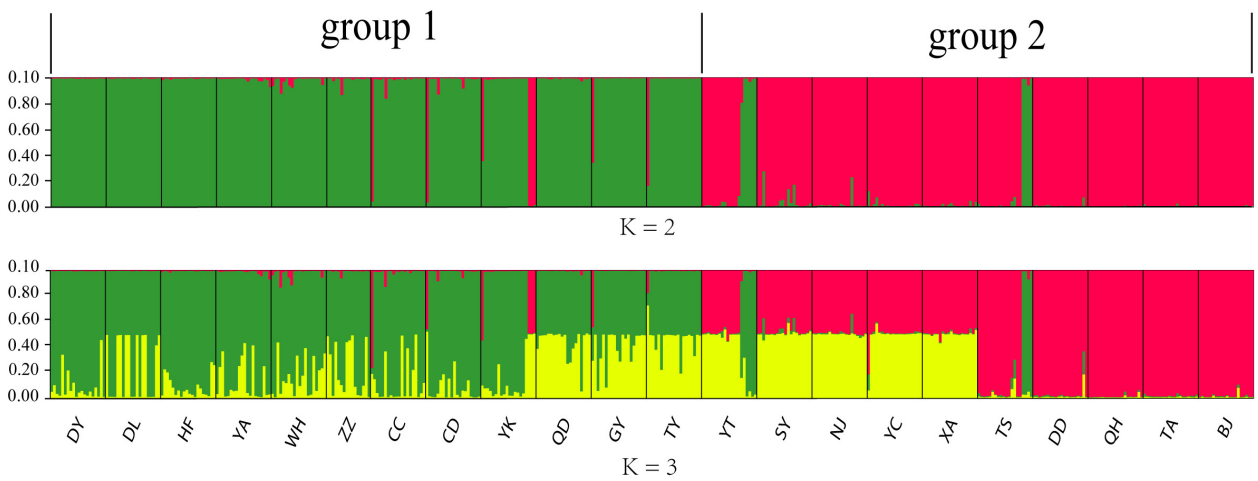

FIGURE 3 | Graphical output of the STRUCTURE analysis representing hierarchical data analyses to determine the number of genetic subpopulations (*K*) of *O. robiniae*. Each individual is represented by a single vertical bar.

(*GD*), and polymorphism information content (*PIC*) (Ren et al., 2014) are minimally influenced by sample size. Our results indicate significant differences in genetic diversity within the Chinese populations, as well as between the native and invasive populations. Shang et al. (2015b) detected a relatively low level of genetic diversity among Chinese *O. robiniae* populations using a COI marker. This discrepancy suggests that COI markers may be less suitable than microsatellite DNA markers for population analyses of a new invasive species, such as Chinese *O. robiniae*, as is the case with another invasive cecidomyiid, *Procontarinia mangiferae* (Amouroux et al., 2013).

The relatively high level of genetic diversity has likely contributed to the spread of *O. robiniae* across China in the past decade to the extent that this species is now established in most

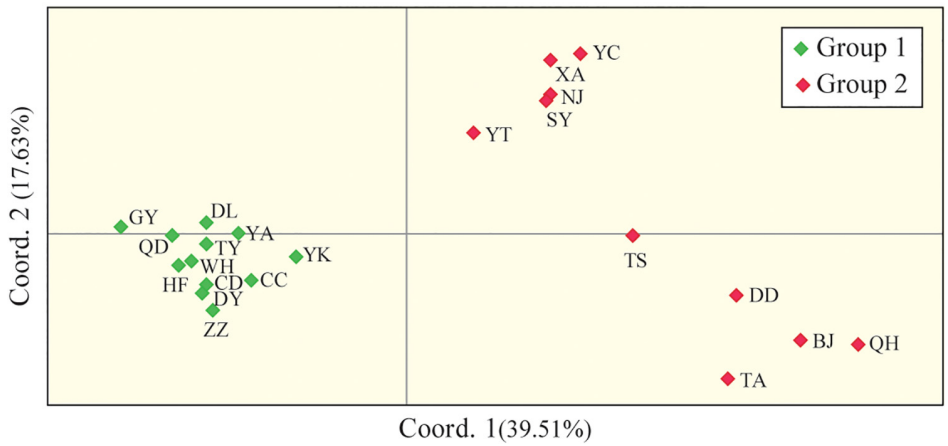

FIGURE 4 | Principal coordinate analysis (PCoA) of 436 Chinese *O. robiniae* individuals showing two distinct clusters of populations. Each population is represented by a diamond. Coord.1 (39.51%) and Coord.2 (17.63%) refer to the first and second principal component, respectively.

regions where its host exists (Shang et al., 2015a). *O. robiniae* has a short history in China, with initial detection occurring in 2004 (Yang et al., 2006), whereas its host was introduced over a century ago (Xu and Yang, 2006). Moreover, for the 22 Chinese populations analyzed, our results show a relatively high level of genetic differentiation (*Fst* = 0.1830) among populations from sites separated by distances of up to 2,540 km. Hence, the relatively high genetic diversity likely caused by significant differentiation among populations has been conducive to the rapid colonization and establishment of *O. robiniae* in China, and it is an important factor contributing to the successful invasion of *O. robiniae*.

The observed population differentiation likely resulted from rapid evolution during adaptation to the new environment. Invasive species may evolve rapidly in response to selection pressures driven by novel habitats (Sakai et al., 2001; Lee, 2002; Ochocki and Miller, 2017), and such rapid genetic adaptation might be important for invasive species (Shine et al., 2011) in order to increase fitness and invasion success (Suarez and Tsutsui, 2008; Roux and Wieczorek, 2009). Increasing the success of both their initial establishment and subsequent range expansion is a particularly effective strategy for introduced populations, as was shown for several invasive species during their colonization processes (Simberloff et al., 2013; Ochocki and Miller, 2017; Wu et al., 2019). Hence, differentiation among Chinese populations was likely accelerated by the rapid evolution of adaptations to the new environments, promoting successful invasion by *O. robiniae*.

Furthermore, high levels of genetic diversity in an invasive species might be caused by multiple introductions or large founding populations. It is thought that multiple introductions are associated with increased diversity because they supply increased variation and new genetic communities (Dlugosch and Parker, 2008). Multiple introductions are considered to produce invasive populations that are much more genetically diverse than a single source population (Sakai et al., 2001). As such, the successful establishment and invasion of many invasive species have been attributed to multiple introductions (Meixner et al., 2002; Kolbe et al., 2004; Cheng et al., 2008; Zalewski et al., 2010; Michaelides et al., 2018). For *O. robiniae*, in light of the short history in China, its high genetic diversity and colonization success might be also related to multiple independent invasive events.

Many studies have shown that the genetic structures of invasive species are well developed in their new ranges (Zeisset and Beebee, 2003; Herborg et al., 2007; Rollins et al., 2009; Zalewski et al., 2010). Indeed, the genetic diversity of invasive species is often higher than that of native populations (Marrs et al., 2008). In light of this, our neighbor-joining dendrogram and Bayesian STRUCTURE (K = 2) analyses indicated that the Chinese *O. robiniae* populations are divided into two independent clusters, although this division appears to be unrelated to geographical distribution. Meanwhile, gene flow was found among some Chinese populations, with QD, GY, and TY in group I having highly similar structures to YT, SY, NJ, YC, and XA in group II. In addition, some subgroups (GY, HF, and WH; TA, DD, BJ, and QH) were clustered according to their geographical distribution, which likely represents different routes of spread in the new environment. Furthermore, our results revealed that each group of the Chinese *O. robiniae* populations exhibited differences in geographical distribution and genetic distance, suggesting that the two groups do in fact represent two different sources. This implies the introduced populations likely experienced two independent invasive events, which initially shaped the genetic structure of the Chinese *O. robiniae* populations.

On the other hand, the fact that the division of the two groups was unrelated to geographical distribution (particularly for group I, which contained numerous genetically similar populations located in different geographical regions) suggests that human activity is likely another important contributing factor. Transport, business trips, and long-distance vacations have recently increased not only in frequency but also in distance. High levels of human-mediated dispersion can increase the

genetic diversity of an invasive population, thereby substantially modifying the genetic structure and potential management units (Perkins et al., 2013); these factors decrease the success of control measures for *O. robiniae* populations.

DATA AVAILABILITY STATEMENT

All datasets generated for this study are included in the article/**Supplementary Material**.

AUTHOR CONTRIBUTIONS

Y-XY and W-XZ: conceptualization, funding acquisition, project administration, and supervision. R-ZL, W-XH, and JY: data curation. Y-XY, X-PS, and JY: formal analysis, investigation, and resources. Y-XY and X-PS: methodology. Y-XY and R-ZL: software. Y-XY, R-ZL, and W-XH: validation. Y-XY, X-PS, R-ZL, and W-XH: visualization. Y-XY, X-PS, R-ZL, W-XH, JY, and W-XZ: writing – original draft and review and editing.

FUNDING

This work was funded by the Fundamental Research Funds of the Chinese Academy of Forestry (CAFYBB2017SZ003) and the National Key R&D Program of China (2016YFC1201200).

ACKNOWLEDGMENTS

We would like to thank Dr. Yan-Fei Zeng (Research Institute, Chinese Academy of Forestry) for discussions regarding the data. We also sincerely thank the other members of the Plant Quarantine Lab and Plant Pathology Lab of the Chinese Academy of Forestry for their helpful comments.

SUPPLEMENTARY MATERIAL

The Supplementary Material for this article can be found online at: https://www.frontiersin.org/articles/10.3389/fgene.2020.00387/full#supplementary-material

REFERENCES

Amouroux, P., Normand, F., Nibouche, S., and Delatte, H. (2013). Invasive mango blossom gall midge, *Procontarinia mangiferae* (Felt) (Diptera: Cecidomyiidae) in Reunion Island: ecological plasticity, permanent and structured populations. *Biol. Invasions* 15, 1677–1693. doi: 10.1017/S0007485314000480

Anjos, L. O., Peixoto, R. F. Jr., Chanquinie, D. M., Pinto, L. R., Creste, S. A., Dinardo-Miranda, L. L., et al. (2016). Microsatellite loci and genetic structure of artificial populations of *Cotesia flavipes* (Hymenoptera, Braconidae). *Genet. Mol. Res.* 15:gmr.15048851. doi: 10.4238/gmr15048851

Badmin, J. (2016). *Obolodiplosis robiniae* (Haldeman) (Diptera: Cecidomyiidae) on False–acacia cv Frisia. *Br. J. Entomol. Nat. Hist.* 29:245.

Bentur, J. S., Sinha, D. K., Padmavathy, R. C., Muthulakshmi, M., and Nagaraju, J. (2011). Isolation and characterization of microsatellite loci in the Asian rice gall midge (*Orseolia oryzae*) (Diptera: Cecidomyiidae). *Int. J. Mol. Sci.* 12, 755–772. doi: 10.3390/ijms12010755

Bonizzoni, M., Malacrida, A. R., Guglielmino, C. R., Gomulski, L. M., Gasperi, G., and Zheng, L. (2000). Microsatellite polymorphism in the Mediterranean fruit fly, *Ceratitis capitata*. *Insect Mol. Biol.* 9, 251–261. doi: 10.1046/j.1365-2583.2000.00184.x

CABI/EPPO (2011). *Obolodiplosis robiniae*. *Distribution Maps of Plant Pests*. Wallingford: *CABI*.

Cheng, X. Y., Cheng, F. X., Xu, R. M., and Xie, B. Y. (2008). Genetic variation in the invasive process of *Bursaphelenchus xylophilus* (Aphelenchida: Aphelenchoididae) and its possible spread routes in China. *Heredity* 100, 356–365. doi: 10.1038/sj.hdy.6801082

Cierjacks, A., Kowarik, I., Joshi, J., Hempel, S., Ristow, M., Lippe, M., et al. (2013). Biological flora of the British Isles: *Robinia pseudoacacia*. *J. Ecol.* 101, 1623–1640.

Davis, M. A. (2009). *Invasion Biology*. New York, NY: Oxford University Press.

Dlugosch, K. M., and Parker, I. M. (2008). Founding events in species invasions: genetic variation, adaptive evolution, and the role of multiple introductions. *Mol. Ecol.* 17, 431–449. doi: 10.1111/j.1365-294x.2007.03538.x

Duan, X., Wang, K., Su, S., Tian, R., Li, Y., and Chen, M. (2017). De novo transcriptome analysis and microsatellite marker development for population genetic study of a serious insect pest, *Rhopalosiphum padi* (L.) (Hemiptera: Aphididae). *PLoS One* 12:e0172513. doi: 10.1371/journal.pone.0172513

Duso, C., Fontana, P., and Tirello, P. (2005). Spread of the gall midge *Obolodiplosis robiniae* (Haldeman) injurious to black locust in Italy and Europe. *Inform. Fitopatol.* 55, 30–33.

Evanno, G., Regnaut, S., and Goudet, J. (2005). Detecting the number of clusters of individuals using the software STRUCTURE: a simulation study. *Mol. Ecol.* 14, 2611–2620. doi: 10.1111/j.1365-294x.2005.02553.x

Excoffier, L., and Lischer, H. E. L. (2010). Arlequin suite version 3.5: a new series of programs to perform population genetics analyses under Linux and Windows. *Mol. Ecol. Res.* 10, 564–567. doi: 10.1111/j.1755-0998.2010.02847.x

Facon, B., Genton, B. J., Shykoff, J., Jarne, P., Estoup, A., and David, P. A. (2006). General eco-evolutionary framework for understanding bioinvasions. *Trends Ecol. Evol.* 21, 130–135. doi: 10.1016/j.tree.2005.10.012

Haldeman, S. S. (1847). Description of several new and interesting animals. *Am. J. Agr. Sci.* 6, 191–194.

Herborg, L. M., Weetman, D., Van Oosterhout, C., and Hanfling, B. (2007). Genetic population structure and contemporary dispersal patterns of a recent European invader, the Chinese mitten crab, *Eriocheir sinensis*. *Mol. Ecol.* 16, 231–242. doi: 10.1111/j.1365-294x.2006.03133.x

Horst, C. P., and Lau, J. A. (2015). Genetic variation in invasive species response to direct and indirect species interactions. *Biol. Invasions* 17, 651–659. doi: 10.1111/j.1469-185X.2010.00123.x

Kim, S. R., Kim, K. Y., Jeong, J. S., Kim, M. J., Kim, K. H., Choi, K. H., et al. (2017). Population genetic characterization of the Japanese oak silkmoth, *Antheraea yamamai* (Lepidoptera: Saturniidae), using novel microsatellite markers and mitochondrial DNA gene sequences. *Genet. Mol. Res.* 16:gmr16029608. doi: 10.4238/gmr16029608

Kolbe, J. J., Glor, R. E., Schettino, L. R. G., Lara, A. C., Larson, A., and Losos, J. B. (2004). Genetic variation increases during biological invasion by a Cuban lizard. *Nature* 431, 177–181. doi: 10.1038/nature02807

Kong, L., Bai, J., and Li, Q. (2014). Comparative assessment of genomic SSR, EST–SSR and EST–SNP markers for evaluation of the genetic diversity of wild and cultured Pacific oyster, *Crassostrea gigas* Thunberg. *Aquaculture* 420-42, S85–S91.

Kostro-Ambroziak, A., and Mieczkowska, A. (2017). The first record of the black locust gall midge *Obolodiplosis robiniae* (Haldeman, 1847) (Diptera: Cecidomyiidae) from northeastern Poland. *Wiadomosci Entomol.* 36:755.

Kumar, S., Stecher, G., Li, M., Knyaz, C., and Tamura, K. (2018). MEGA X: molecular evolutionary genetics analysis across computing platforms. *Mol. Biol. Evol.* 35, 1547–1549. doi: 10.1093/molbev/msy096

Launey, S., Brunet, G., Guyomard, R., and Davaine, P. (2010). Role of introduction history and landscape in the range expansion of brown trout (*Salmo trutta* L.) in the Kerguelen Islands. *J. Hered.* 10, 270–283. doi: 10.1093/jhered/esp130

Lee, C. E. (2002). Evolutionary genetics of invasive species. *Trends Ecol. Evol.* 17, 386–391. doi: 10.1016/s0169-5347(02)02554-5

Lee, J. S., Jung, Y. M., Choi, K. S., Kim, I. K., Kwon, Y. D., Jeon, M. J., et al. (2009). Seasonal fluctuation and distribution of *Obolodiplosis robiniae* (Diptera: Cecidomyiidae) within crown of *Robinia pseudoacacia* (Fabaceae). *Korean J. App. Entomol.* 48, 447–451. doi: 10.5656/ksae.2009.48.4.447

Liu, K., and Muse, S. V. (2005). Powermarker: integrated analysis environment for genetic marker data. *BMC Bioinformatics* 21:2128–2129. doi: 10.1093/bioinformatics/bti282

Liu, Y. B. (2014). Management methods to control *Obolodiplosis robiniae*. *Gansu Agric.* 2, 87–88.

Marrs, R. A., Sforza, R., and Hufbauer, R. A. (2008). When invasion increases population genetic structure: a study with *Centaurea diffusa*. *Biol. Invasions* 10, 561–572. doi: 10.1007/s10530-007-9153-6

Meixner, M. D., Mcpheron, B. A., Silva, J. G., Gasparich, G. E., and Sheppard, W. S. (2002). The Mediterranean fruit fly in California: evidence for multiple introductions and persistent populations based on microsatellite and mitochondrial DNA variability. *Mol. Ecol. Notes* 11, 891–899. doi: 10.1046/j.1365-294x.2002.01488.x

Mezghani-Khemakhem, M., Bouktila, D., Casse, N., Maaroufi, H., Makni, M., and Makni, H. (2012). Development of new polymorphic microsatellite loci for the barley stem gall midge, *Mayetiola hordei* (Diptera: Cecidomyiidae) from an enriched library. *Int. J. Mol. Sci.* 13, 14446–14450. doi: 10.3390/ijms131114446

Michaelides, S. N., Goodman, R. M., Crombie, R. I., Kolbe, J. J., and Cowie, R. (2018). Independent introductions and sequential founder events shape genetic differentiation and diversity of the invasive green anole (*Aanolis carolinensis*) on pacific islands. *Divers. Distrib.* 24, 666–679. doi: 10.1111/ddi.12704

Mihajlovic, L., Glavendekic, M. M., Jakovljevic, I., and Marjanovic, S. (2008). *Obolodiplosis robiniae* (Haldeman) (Diptera: Cecidomyiidae) – a new invasive insect pest on black locust in Serbia. *Glas. Sumarskog Fakult. Univ. Beogr.* 97, 197–207. doi: 10.2298/gsf0897197m

Mu, X. F., Sun, J. S., Lu, W. F., Li, M., Qu, H. X., and Gao, Z. Y. (2010). Bionomics and control of *Obolodiplosis robiniae* in Beijing. *For. Pest Dis.* 29, 15–18.

Nei, M. (1973). Analysis of gene diversity in subdivided populations. *Proc. Natl. Acad. Sci.* 70, 3321–3323. doi: 10.1073/pnas.70.12.3321

Nei, M. (1978). Estimation of average heterozygosity and genetic distance from a Small Number of Individuals. *Genetics* 89, 583–590.

Nei, M., Maruyama, T., and Chakraborty, R. (1975). The bottleneck effect and genetic variability in populations. *Evolution* 29, 1–10. doi: 10.1111/j.1558-5646.1975.tb00807.x

Ochocki, B. M., and Miller, T. E. X. (2017). Rapid evolution of dispersal ability makes biological invasions faster and more variable. *Nat. Commun.* 8:14315. doi: 10.1038/ncomms14315

Peakall, R., and Smouse, P. E. (2012). GenAlEx 6.5: genetic analyses in Excel. Population genetic software for teaching and research—an update. *BMC Bioinformatics* 28, 2537–2539. doi: 10.1093/bioinformatics/bts460

Perkins, T. A., Phillips, B. L., Baskett, M. L., and Hastings, A. (2013). Evolution of dispersal and life history interact to drive accelerating spread of an invasive species. *Ecol. Lett.* 16, 1079–1087. doi: 10.1111/ele.12136

Pritchard, J. K., Stephens, M., and Donnelly, P. (2000). Inference of population structure using multilocus genotype data. *Genetics* 155, 945–959.

Ren, X. P., Jiang, H. F., Yan, Z. Y., Chen, Y., Zhou, X. J., Huang, L., et al. (2014). Genetic diversity and population structure of the major peanut (*Arachis hypogaea* L.) cultivars grown in China by SSR markers. *PLoS One* 9:e88091. doi: 10.1371/journal.pone.0088091

Retamal, R., Zaviezo, T., Malausa, T., Fauvergue, X., Le, G. I., and Toleubayev, K. (2016). Genetic analyses and occurrence of diploid males in field and laboratory populations of *Mastrus ridens* (Hymenoptera: Ichneumonidae), a parasitoid of the codling moth. *Biol. Control* 101, 69–77. doi: 10.1016/j.biocontrol.2016.06.009

Rollins, L. A., Woolnough, A. P., Wilton, A. N., Sinclair, R., and Sherwin, W. B. (2009). Invasive species can't cover their tracks: using microsatellites to assist management of starling (*Sturnus vulgaris*) populations in Western Australia. *Mol. Ecol.* 18, 1560–1573. doi: 10.1111/j.1365-294x.2009.04132.x

Rousset, F. (2008). Genepop'007: a complete reimplementation of the Genepop software for Windows and Linux. *Mol. Ecol. Resour.* 8, 103–106. doi: 10.1111/j.1471-8286.2007.01931.x

Roux, L. J., and Wieczorek, A. M. (2009). Molecular systematics and population genetics of biological invasions: towards a better understanding of invasive species management. *Ann. Appl. Biol.* 154, 1–17. doi: 10.1111/j.1744-7348.2008.00280.x

Sakai, A. K., Allendorf, F. W., Holt, J. S., Lodge, D. M., Molofsky, J., With, K. A., et al. (2001). The population biology of invasive species. *Ann. Rev. Ecol. Syst.* 32, 305–332.

Schemerhorn, B. J., Crane, Y. M., Cambron, S. E., Crane, C. F., and Shukle, R. H. (2015). Use of microsatellite and SNP markers for biotype characterization in Hessian fly. *J. Insect Sci.* 15:158. doi: 10.1093/jisesa/iev138

Shang, X. P., Yao, Y. X., Huai, W. X., and Zhao, W. X. (2016). Effects of sample size on genetic diversity index for population of *Obolodiplosis robiniae* in use of microsatellite DNA marker. *Plant Quar.* 1, 32–35.

Shang, X. P., Yao, Y. X., and Zhao, W. X. (2015a). Geographic distribution of an invasive insect pest,*Obolodiplosis robiniae* (Diptera: Cecidomyiidae) in China. *For. Pest Dis.* 34, 33–36.

Shang, X. P., Yao, Y. X., Huai, W. X., and Zhao, W. X. (2015b). Population genetic differentiation of the black locust gall midge *Obolodiplosis robiniae* (Haldeman) (Diptera: Cecidomyiidae): a North American pest invading Asia. *Bull. Entomol. Res.* 105, 736–742. doi: 10.1017/s000748531500070x

Shao, X. K., Ma, X. G., Shao, K. F., Lv, J., and Han, G. S. (2010). Occurrence, damage and control of *Obolodiplosis robiniae*. *J. Liaon. For. Sci. Technol.* 4, 31–32.

Sharma, P. C., Grover, A., and Kahl, G. (2007). Mining microsatellites in eukaryotic genomes. *Trends Biotechnol.* 25, 490–498. doi: 10.1016/j.tibtech.2007.07.013

Shine, R., Brown, G. P., and Phillips, B. L. (2011). An evolutionary process that assembles phenotypes through space rather than through time. *Proc. Natl. Acad. Sci. U.S.A.* 108, 5708–5711. doi: 10.1073/pnas.1018989108

Simberloff, D., Martin, J. L., Genovesi, P., Maris, V., Wardle, D. A., Aronson, J., et al. (2013). Impacts of biological invasions: what's what and the way forward. *Trends Ecol. Evol.* 28, 58–66. doi: 10.1016/j.tree.2012.07.013

Simonato, M., Pilati, M., Magnoux, E., Courtin, C., Sauné, L., Rousselet, J., et al. (2019). A population genetic study of the egg parasitoid *Baryscapus servadeii* reveals large scale automictic parthenogenesis and almost fixed homozygosity. *Biol. Control* 139:104097. doi: 10.1016/j.biocontrol.2019.104097

Stalazs, A. (2014). New records of some dipterans (Diptera: Cecidomyidae, Tephritidae) in north-eastern Lithuania. *Zool. Ecol.* 24, 55–57.

Suarez, A. V., and Tsutsui, N. D. (2008). The evolutionary consequences of biological invasions. *Mol. Ecol.* 17, 351–360. doi: 10.1111/j.1365-294X.2007.03456.x

Tsutsui, N. D., Suarez, A. V., and Grosberg, R. K. (2003). Genetic diversity, asymmetrical aggression, and recognition in a widespread invasive species. *Proc. Natl. Acad. Sci. U.S.A.* 100, 1078–1083. doi: 10.1073/pnas.0234412100

Varshney, R. K., Chabane, K., Hendre, P. S., Aggarwal, R. K., and Graner, A. (2007). Comparative assessment of EST-SSR, EST-SNP and AFLP markers for evaluation of genetic diversity and conservation of genetic resources using wild, cultivated and elite barleys. *Plant Sci.* 173, 638–649. doi: 10.1016/j.plantsci.2007.08.010

Wang, G. Y. (2009). *Primary Study on Biology, Ecology and Chemical Control of Obolodiplosis robiniae*. Master's dissertation, Shangdong Agriculture University, Taian.

Wu, N. N., Zhang, S. F., Li, X. W., Cao, Y. H., Liu, X. J., Wang, Q. H., et al. (2019). Fall webworm genomes yield insights into rapid adaptation of invasive species. *Nat. Ecol. Evol.* 3, 105–115. doi: 10.1038/s41559-018-0746-5

Xu, X. Q., and Yang, M. S. (2006). Review on utilization of *Robinia pseudoacacia*. *J. Hebei For. Sci. Technol.* S1:54.

Yang, Z. Q., Qiao, X. R., Bu, W. J., Yao, Y. X., Xiao, Y., and Han, Y. S. (2006). First discovery of an important invasive insect pest, *Obolodiplosis robiniae* (Diptera: Cecidomyiidae) in China. *Acta Entomol. Sin.* 49, 1050–1053.

Yao, Y. X., Zhao, W. X., and Shang, X. P. (2015). Development of polymorphic microsatellite markers of *Obolodiplosis robiniae* (Haldeman) (Diptera: Cecidomyiidae), a North American pest invading Asia. *J. Insect Sci.* 15:127. doi: 10.1093/jisesa/iev104

Yeh, F. C., Yang, R. C., Boyle, T. B. J., Ye, Z. H., and Mao, J. X. (2018). *POPGENE, the User-Friendly Shareware for Population Genetic Analysis*. Available at: http://wanfang.bjast.com.cn/D/ExternalResourceswdyx200204012%5E45.aspx, (accessed November 10, 2018).

Zalewski, A., Michalska-Parda, A., Bartoszewicz, M., Kozakiewicz, M., and Brzeziński, M. (2010). Multiple introductions determine the genetic structure of an invasive species population: American mink *Neovison vison* in Poland. *Biol. Conserv.* 143, 1355–1363. doi: 10.1016/j.biocon.2010.03.009

Zeisset, I., and Beebee, T. J. C. (2003). Population genetics of a successful invader: the marsh frog *Rana ridibunda* in Britain. *Mol. Ecol.* 12, 639–646. doi: 10.1046/j.1365-294x.2003.01775.x

Zhao, S. Y., Sun, S. G., Dai, C., Gituru, R. W., Chen, J. M., Wang, Q. F., et al. (2015). Genetic variation and structure in native and invasive *Solidago canadensis* populations. *Weed Res.* 55, 163–172.

Zhou, Z. X., Wan, F. H., Zhang, G. F., and Chen, B. (2007). A rapid method for extraction of genomic DNA of *Bemisia tabaci*. *Plant Protect.* 33, 131–133. doi: 10.3390/genes10090632

Zong, J. W., Zhao, T. T., Ma, Q. H., Liang, L. S., and Wang, G. X. (2015). Assessment of genetic diversity and population genetic structure of *Corylus mandshurica* in China using SSR markers. *PLoS One* 10:e0137528. doi: 10.1371/journal.pone.0137528

Conflict of Interest: The authors declare that the research was conducted in the absence of any commercial or financial relationships that could be construed as a potential conflict of interest.

frontiers in Cell and Developmental Biology

ORIGINAL RESEARCH
published: 05 May 2020
doi: 10.3389/fcell.2020.00311

The L-DOPA/Dopamine Pathway Transgenerationally Regulates Cuticular Melanization in the Pea Aphid *Acyrthosiphon pisum*

*Yi Zhang†, Xing-Xing Wang†, Hong-Gang Tian, Zhan-Feng Zhang, Zhu-Jun Feng, Zhan-Sheng Chen and Tong-Xian Liu**

Key Laboratory of Integrated Pest Management on Crops in Northwestern Loess Plateau, Ministry of Agriculture, Northwest A&F University, Xianyang, China

OPEN ACCESS

Edited by:
Wei Guo,
Institute of Zoology (CAS), China

Reviewed by:
Owain Rhys Edwards,
CSIRO Land and Water, Australia
Wei Zhang,
Peking University, China

***Correspondence:**
Tong-Xian Liu
txliu@nwsuaf.edu.cn

† These authors have contributed equally to this work

Specialty section:
This article was submitted to Epigenomics and Epigenetics, a section of the journal Frontiers in Cell and Developmental Biology

Received: *08 February 2020*
Accepted: *08 April 2020*
Published: *05 May 2020*

Citation:
Zhang Y, Wang X-X, Tian H-G, Zhang Z-F, Feng Z-J, Chen Z-S and Liu T-X (2020) The L-DOPA/Dopamine Pathway Transgenerationally Regulates Cuticular Melanization in the Pea Aphid Acyrthosiphon pisum. Front. Cell Dev. Biol. 8:311. doi: 10.3389/fcell.2020.00311

Maternal phenotypic regulations between different generations of aphid species help aphids to adapt to environmental challenges. The pea aphid *Acyrthosiphon pisum* has been used as a biological model for studies on phenotypic regulation for adaptation, and its alternative phenotypes are typically and physiologically based on maternal effects. We have observed an artificially induced and host-related maternal effect that may be a new aspect to consider in maternal regulation studies using *A. pisum*. Marked phenotypic changes in the cuticular melanization of daughter *A. pisum* were detected via *tyrosine hydroxylase* knockdown in the mothers during their period of host plants alternations. This phenotypic change was found to be both remarkable and repeatable. We performed several studies to understand its regulation and concluded that it may be controlled via the dopamine pathway. The downregulation and phenotypes observed were verified and described in detail. Additionally, based on histological and immunofluorescence analyses, the phenotypic changes caused by cuticular dysplasia were physiologically detected. Furthermore, we found that this abnormal development could not be reversed after birth. Transcriptome sequencing confirmed that this abnormal development represents a systemic developmental failure with numerous transcriptional changes, and chemical interventions suggested that transgenerational signals were not transferred through the nervous system. Our data show that transgenerational regulation (maternal effect) was responsible for the melanization failure. The developmental signals were received by the embryos from the mother aphids and were retained after birth. *APTH* RNAi disrupted the phenotypic determination process. We demonstrate that non-neuronal dopamine regulation plays a crucial role in the transgenerational phenotypic regulation of *A. pisum*. These results enhance our understanding of phenotyping via maternal regulation in aphids.

Keywords: *Acyrthosiphon pisum*, L-DOPA, RNA interference, maternal effect, tyrosine hydroxylase, phenotypic plasticity

INTRODUCTION

Environment-induced phenotypic changes are observed in many animal species and are an important physiological strategy that enables them to cope with environmental threats. Aphid species are normally serious agricultural pests that are highly adaptable (Van Emden and Harrington, 2017). The pea aphid *Acyrthosiphon pisum* (Harris) is utilized as a biological model of insect–plant interactions, phenotypic plasticity, and in symbiosis studies (Braendle et al., 2006). *A. pisum* has a transgenerational regulation system, and the biological features for their daughters can be modified between generations as different phenotypic development pathways, such as winged (alatae)–wingless (apterae) and sexual–asexual morphs, are determined by the mothers (Braendle et al., 2006; International Aphid Genomics Consortium, 2010). Winged and wingless *A. pisum* show diversity in their morphological, physiological, and behavioral features (Wratten, 1977; Sack and Stern, 2007). Furthermore, sexual and asexual individuals within this species differ mainly regarding their reproductive patterns and morphology (Miura et al., 2003). However, the mechanisms underlying the phenotypic regulations between different aphid generations are not yet fully understood.

The phenotypic controls and regulations of aphids are determined by the mother's generation (Van Emden and Harrington, 2017). Asexual aphids parthenogenetically produce embryos that develop directly within them. They can regulate organ and tissue formation patterns that are related to the different phenotypes of their daughters. For example, in *A. pisum*, wing and sex determination occur prenatally (MacKay and Wellington, 1977; Brisson, 2010); therefore, the phenotype of the aphids does not tend to change within a single generation in response to environmental changes (Brisson, 2010). The phenotypic regulation system of the mother aphids is primarily based on environmental conditions, such as temperature, photoperiod, physical contact (aphids density), and host nutrition status (Braendle et al., 2006). Maternal effects are observed in many aphid species and affect more than one generation (Zehnder and Hunter, 2007; Jeffs and Leather, 2014; Hu et al., 2016). Besides phenotypic regulations, biological and ecological features such as population dynamics, fecundity, and interspecies relationships (with ant and parasitoids) may be maternally regulated (Zehnder and Hunter, 2007; Tegelaar et al., 2013; Slater et al., 2019). Previous studies of transgenerational signal transmissions showed that there was little or no yolk in the viviparous oocytes and embryos, and no chorion. This was most likely because in addition to being dispensable, an eggshell could interfere with the maternal provisioning of the developing embryos (Bermingham and Wilkinson, 2009; Ogawa and Miura, 2014). In studies of the physiological basis, however, juvenile hormone (JH) and insulin pathways were found to possibly contribute to this regulation, but studies in which JH titers were manipulated have shown inconsistent results, and further research is required (Braendle et al., 2006; Huybrechts et al., 2010; Ishikawa et al., 2012). In brief, maternal effects play important roles for aphid environmental adaptations, but their mechanisms are still unclear.

The environment-induced morphs of aphids exhibit biological and physiological differences in many respects, including their cuticular sclerotization and melanization levels (Ishikawa and Miura, 2007). Insect cuticles are primarily composed of regular arrangements of catecholamines (for melanization), lipids, cuticle proteins, and chitin; they are present in various cuticular layers, and interact with each other (Filshie, 1982; Vukusic and Sambles, 2003; Moussian et al., 2006; Arakane et al., 2009; Gorman and Arakane, 2010; Noh et al., 2016). Physicochemical interactions among them constitute the foundation of cuticle formation, body shape, and surface appearance (Filshie, 1982; Wigglesworth, 1990; Anderson, 1966, 2011; Van de Kamp and Greven, 2010). The production of catecholamines eventually leads to pigment depositions in the exocuticle or epicuticle layers, and tyrosine hydroxylase (TH; the rate-limiting enzyme of dopamine biosynthesis) plays an important role in melanization regulation (Arakane et al., 2009; Noh et al., 2016).

Previous studies have described the melanization process for cuticular sclerotization and melanization of insects (catecholamine metabolize), which can be summarized as follows. In the cuticle, TH converts tyrosine into L-3,4-dihydroxyphenylalanine (L-DOPA) in the epidermal cells. Thereafter, L-DOPA decarboxylase (DDC) converts L-DOPA into dopamine. Acyldopamines, *N*-acetyldopamine (NADA) and *N*-β-alanyldopamine (NBAD), are synthesized from dopamine via the actions of the arylalkylamine-*N*-acetyltransferase (aaNAT) and NBAD synthase (ebony), respectively, and are transported to the extracellular tissues. Laccases (laccase 2, lac2) catalyze melanization (pigmentation) and sclerotization in the cuticles and other tissues (Suderman et al., 2006; Noh et al., 2016). Numerous insect species that were subjected to *TH* RNA interference (RNAi) treatments were shown to exhibit a pale body color (Gorman and Arakane, 2010; Ma et al., 2011; Lee et al., 2015). L-DOPA and dopamine are key chemicals upstream of catecholamine regulatory system.

The L-DOPA, which is functional upstream in animal melanization regulatory and nervous systems, is also found in plants, including the broad bean *Vicia faba,* the hosts of *A. pisum*. Pea aphids attack a variety of legume crops, including *V. faba*, white clover (*Trifolium repens*), and alfalfa (*Medicago sativa*) (Kanvil et al., 2014). *V. faba* are known to contain high levels of L-DOPA (Longo et al., 1974; Ingle, 2003; Zhang et al., 2016), which is a non-protein amino acid that participates in numerous plant and animal metabolic processes (Wise, 1978; Smeets and González, 2000) and also functions as an important secondary metabolite in plant chemical defenses against herbivores (Huang et al., 2011; Zhang et al., 2016). However, adapted pea aphids can sequester L-DOPA and use it for wound healing and UV-A resistance, which are processes related to melanization (Zhang et al., 2016). The L-DOPA environment could, thus, be important and aid the pea aphid in its adaptations for survival. This could occur either by balancing the L-DOPA self-synthesis and assimilation for stabilizing metabolic processes or by modifying the L-DOPA/dopamine biometabolic pathway. We have aimed to study in detail the transcriptomic profiles of the candidate genes in this pathway.

In the present study, we have detected remarkable and repeatable RNAi-related phenotypic changes in *A. pisum*, under hosts alternations. The phenomenon has been observed in response to *A. pisum TH* (*APTH*) knockdowns in the nymphs of RNAi-treated mothers during the period of transition between host plants (with high L-DOPA to low L-DOPA content). In response to this treatment, perturbations of the cuticle melanization and nymph development were observed. RNAi is widely used in gene function studies (Hannon, 2002), but its repression efficiency varies considerably among different insect species (Singh et al., 2017). Studies have shown that dsRNAs in the body fluid of *A. pisum* can be degraded, resulting in variable genetic downregulations (Huvenne and Smagghe, 2010; Christiaens et al., 2014; Singh et al., 2017).

To elucidate the mechanisms underlying the unexpected phenotypic changes in *A. pisum*, we investigated the transcriptional changes in the target genes, in response to the *APTH*-RNAi, and subsequently analyzed the L-DOPA and dopamine levels using liquid chromatography–mass spectrometry (LC/MS). We also performed detailed analyses of the phenotypic and biological changes in the nymphs, to compare the induced phenotypic changes and normal maternal phenotypic regulations. Histological examinations, immunofluorescence detection, transcriptomic analyses, and chemical interventions were also performed to understand the regulatory mechanisms underlying these transgenerational phenotypic changes.

MATERIALS AND METHODS

Insects and Plants

Red *A. pisum* were collected from *M. sativa* plants in Lanzhou, Gansu Province, China (N36°07′7″, E103°42′20″; Aug 2015) and reared on *V. faba* in Shaanxi, China, for approximately 5 years. Prior to the experiments, the aphids were cultured in low densities on *V. faba* and *T. repens* under long-day conditions (16:8 h L:D; 20 ± 1°C) for more than 30 generations at the Key Laboratory of Applied Entomology, Northwest A&F University, Yangling, Shaanxi, China.

Only wingless aphids were used in the experiments. They were replenished by rearing all the insects at densities in excess of 30 aphids/plant, for more than three generations. The aphids during the host transition period were used for the RNAi experiments. The newborn aphids (approximately 100 individuals for each experiment) on the *V. faba* (high L-DOPA content; **Supplementary Figure S10**) were immediately transferred and reared on *T. repens* (low L-DOPA content; **Supplementary Figure S10**) until they reached the adult stage. Phenotypic changes could also be observed in the *A. pisum* reared on *M. sativa* (also low L-DOPA content) during host plant alternations and RNAi from *V. faba*. However, given the impracticality of working with the much smaller *M. sativa* leaves, we selected *T. repens* (fit-size leaves for cells of 24-well plate) for the further experiments.

RNAi of *APTH* in *A. pisum*

The dsRNA of *APTH* was prepared for downregulation investigations, to modify the biosynthesis of L-DOPA. The dsRNA of the *lymphotoxin-alpha* gene (*lta*; Gene ID: 16992) of *Mus musculus* was used as a control (Chen et al., 2016). The synthesis and delivery methods (Barron et al., 2007; Zhang et al., 2016) of the dsRNAs are detailed in S1.1 (**Supplementary Material**), and the primers used to synthesize the *APTH* and *mus-lta* dsRNAs (designated as ds-TH1, ds-TH2, and ds-lta, respectively) are shown in **Supplementary Table S1** and **Supplementary Figure S1**.

L-DOPA and Dopamine Extractions and Assays

The injected aphids were reared on *T. repens* for 72 h after treatment and subsequently collected for LC/MS analysis. Newborn nymphs (within 30 min after birth) were collected from mothers between 72 and 96 h after the dsRNA treatments and prepared for LC/MS analysis. This methodology is detailed in S1.2 (**Supplementary Material**).

Observations of Phenotypic and Biological Changes

Phenotype Determination

Treated mothers and newborn nymphs were reared separately. Images of the mothers were captured 72 h after injection, whereas those of the nymphs were captured at each developmental stage. Individuals were prepared for imaging. Digital images were acquired using a Panasonic DMC-GH4 digital camera (Panasonic, Osaka, Japan) and a SDPTOP-SZN71 microscope system (Sunny, Hangzhou, Zhejiang, China).

Biological Parameters

The following biological parameters of the treated mothers (ds-TH and ds-lta) and their daughters were analyzed: proportion of abnormal producers (mothers); life span, survival rate, and duration of development for each stage (nymphs). This is further detailed in S1.3 (**Supplementary Material**).

Video Recording

Newborn (first instar) and new molted (second instar) nymphs were prepared for video recording (see S3 for more information, **Supplementary Material**).

Analysis of the Cuticle Morphology

Histological sectioning, staining (HE) and immunofluorescence were performed for abnormal (including low-tanning and over-tanning nymphs; **Supplementary Figure S11**) and control nymphs obtained from the ds-TH and ds-lta treatments, respectively. Five samples of the second thoracic (T2) segments of the third-instar of *A. pisum* from each treatment were selected for hematoxylin–eosin (HE) staining, and five samples of the cross-sections of the T2 segments of the third-instar nymphs from each treatment were selected for immunofluorescence assays. Transverse longitudinal sections, from the head to the tail, of the treated mother aphids were also collected 48 h after the dsRNA

injection for immunofluorescence experiments. The method is detailed in S1.3 (**Supplementary Material**). Digital images were acquired using a Nikon DS-Ri1 camera (Nikon, Tokyo, Japan), a Nikon 80i microscope system (Nikon, Tokyo, Japan), and Nis-Elements v. 3.22.14 (Build 736, Nikon, Tokyo, Japan). Cuticle thickness was determined from the digital images. All images showing Cy^{TM}3 fluorescence were captured and filtered using the default settings (brightness, contrast, and saturation) of software for comparison.

Transcriptome Sequencing

To analyze the systemic transcriptional changes between the two phenotypes, abnormal (including low-tanning and over-tanning nymphs; **Supplementary Figure S11**) and control nymphs obtained from the ds-TH and ds-lta treatments, respectively, were prepared for transcriptome sequencing. Since the embryos (inside the nymphs) could affect the transcriptomic data, the individuals were dissected and only the head with the antennae and legs were collected (**Supplementary Figure S12**). Approximately 400 samples from three developmental stages per treatment were frozen in liquid nitrogen for RNA extraction. As the RNA content in each sample tissue was relatively low, only one RNA sample per treatment (ds-TH and ds-lta) was successfully prepared. Extracted RNA was sent to the Wuhan Bioacme Corporation (Wuhan, China;[1]) for transcriptome sequencing and preliminary analysis (**Supplementary Table S3**). We also selected candidate genes (demonstrating relatively highly changed expression patterns) and analyzed the transcriptional changes in the newborn daughters of the abnormal nymph producers on the 3rd day after the dsRNA treatment. The sample collection protocol is detailed in S1.1 (**Supplementary Material**).

Testing the Dopamine Transition Signals of the Nervous System

The dopamine/L-DOPA biosynthesis inhibitor (metirosine) and dopamine receptor antagonists (SCH23390, Sulpiride and Pimozide) were injected into *A. pisum* to investigate the transition signals of the nervous system underlying this transgenerational phenomenon. The method is detailed in S1.4 (**Supplementary Material**), and the daughters of the treated aphids were reared for phenotypic detection (as described in section "Observations of phenotypic and biological changes").

Statistical Analyses

APTH transcriptomic data from the different treatments and aphids were subjected to Mann–Whitney *U*-tests (non-parametric). Values of the chemical amounts, body lengths, and developmental times were subjected to one-way analysis of variance. Differences among means were calculated using Duncan's test at a significance level of $P < 0.05$. Quantitative analyses of the L-DOPA and dopamine and the proportions of the abnormal nymph producers were subjected to a Student's *t*-test where $P < 0.05$ indicated significance. The survival data were analyzed using an χ^2 test where $P < 0.05$ also indicated significance. All data were processed using SPSS v. 22 (IBM Corp., Armonk, NY, United States). Immunofluorescence images were obtained and analyzed using CaseViewer (V 2.0, 3DHISTECH Ltd., H-1141 Budapest, Hungary). Charts and diagrams were constructed with Microsoft® Excel 2016 MSO (16.0.4266.1003; Redmond, WA, United States) and GraphPad Prism (V 8.0.2; San Diego, CA, United States).

[1]http://www.whbioacme.com

RESULTS

APTH Knockdown by RNAi in the Mother Aphids

Differences in *APTH* Repression in Different Parts of *A. pisum*

After the injection of dsRNAs (ds-TH1, ds-TH2, and ds-lta) into *A. pisum*, a significant reduction in the expression of *APTH*-RNAi was observed in the head on the second day (**Figure 1A**; *P* values are marked between the bars). In contrast, no significant transcriptional differences were detected in the abdomen (**Figure 1A**; *P* values are marked between the bars) or the whole body (**Figure 1A**; *P* values are marked between bars). Additional experiments with more replicates revealed that the abdominal *APTH* expression was unstable with the ds-TH1 and ds-TH2 treatments (**Figure 1A**; *P* values are marked between bars).

For more information and physiological background, the transcriptional differences in the expression of *APTH* between the different developmental stages are shown in **Supplementary Figures S2,S3** (head and abdomen, respectively) and the expression changes of *DDC* under *APTH*-RNAi are shown in **Supplementary Figures S5,S6**.

Duration of *APTH* Repression in the Heads of *A. pisum*

The downregulation of *APTH* in the head was relatively stable, and therefore, we analyzed the duration of *APTH* repression in the head. No significant reduction in *APTH* expression was detected in the heads of the dsRNA-treated aphids on the first day (**Figure 1B**; *P* values are marked between the bars). The dsRNA treatment reduced *APTH* expression on days 2 and 3 (**Figure 1B**; *P* values are marked between the bars). Thereafter, *APTH* expression was indistinguishable from that of the control individuals (**Figure 1B**; *P* values are marked between the bars). Additionally, the ds-TH1 treatment was slightly more effective than the ds-TH2 treatment.

L-DOPA and Dopamine Content of Mother Aphids With *APTH* Downregulation

LC/MS results showed that the L-DOPA content significantly decreased in aphids with *APTH* downregulation ($t = 3.908$, df = 34, $P < 0.001$; **Figure 1C**). A significant decrease in dopamine was also observed under the same conditions ($t = 3.438$, df = 34, $P = 0.002$; **Figure 1D**).

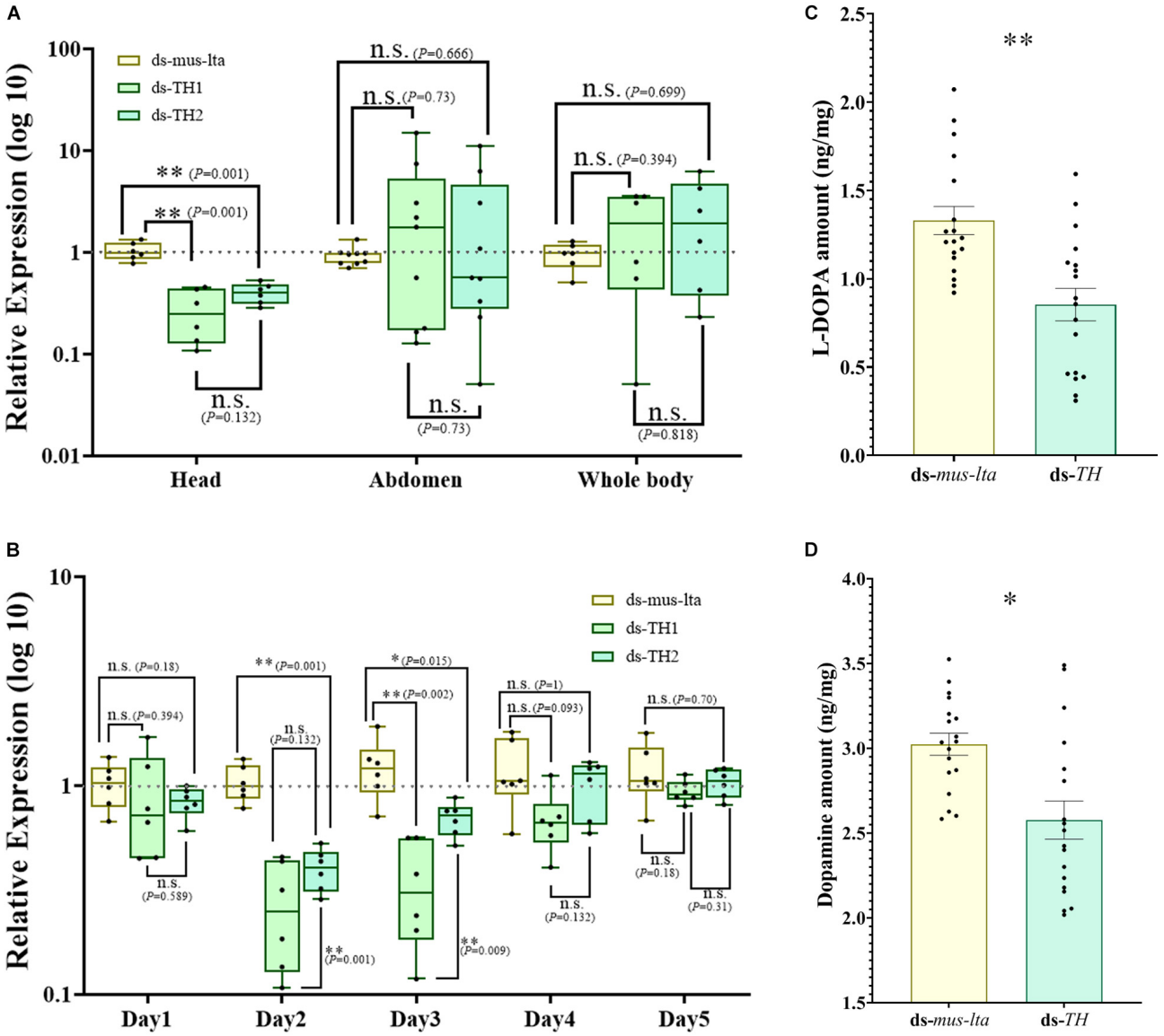

FIGURE 1 | *Tyrosine hydroxylase* RNAi in *Acyrthosiphon pisum*. **(A)** *APTH* transcriptional response to *APTH* RNAi in the head, abdomen, and whole body. n.s. indicates no significant difference according to Mann-Whitney *U*-test (non-parametric; $^{*}P < 0.05$, $^{**}P < 0.001$). Irregular *APTH* transcriptional response to *APTH* RNAi in the abdomen. n.s. indicates no significant difference. **(B)** Effect of RNAi suppression on *APTH* expression. n.s. indicates no significant difference according to Mann-Whitney *U*-test (non-parametric; $^{*}P < 0.05$, $^{**}P < 0.001$). Differences in L-DOPA **(C)** and dopamine **(D)** levels between aphids treated with *APTH* and those treated with *lta* RNAi. Each value represents the mean ± SEM; n.s. indicates no significant difference according to Student's *t*-test ($^{**}P < 0.001$).

TH Protein Analysis Using RNAi in Mother Aphids

The presence of the TH protein in the mother aphids and embryos treated with ds-TH and ds-lta was determined by immunofluorescence. Proteins were observed to be immune-positive in the mothers' cuticles and mostly in the embryos (**Figure 2**). Compared with the control treatments, in TH-RNAi–treated aphids, the TH fluorescence was detected only sparsely in the cuticles (**Figure 2A**). The fluorescence outline (red) of the head was difficult to identify in individuals with *APTH* downregulation.

Differences in immunofluorescence could also be observed in the embryos (**Figures 2C,D**). All embryos that could be identified in the longitudinal cuttings were collected and arranged by size for further comparison. Differences in the TH protein distributions could be detected in the embryo cuticles during the late developmental stages (from 15× to 30×; 400–1000 μm) between the two dsRNAs treatments, especially in the red fluorescence outlines (cuticle) of the embryo bodies. However, based on the detection of a strong fluorescence inside the embryos after the two treatments, we assume that the TH protein levels were not affected in the nervous system (**Figures 2C,D**).

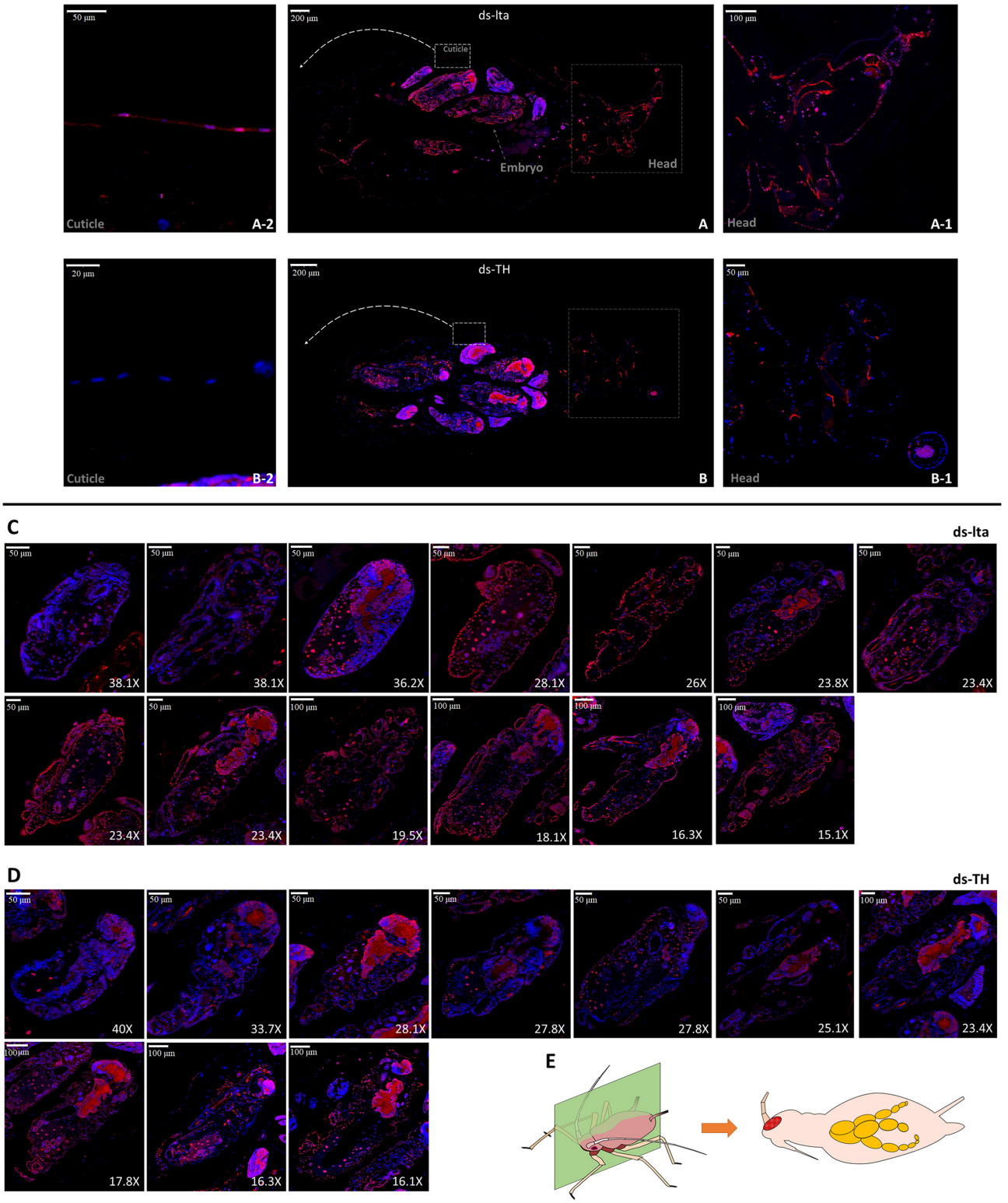

FIGURE 2 | TH immunofluorescence of treated mothers. The distribution of TH protein in *lta* dsRNA treated **(A)** and *APTH* dsRNA treated **(B)** adult aphids was determined by immunofluorescence. Anti-TH antibodies were detected using Cy3-conjugated rabbit IgG antibodies (red); Nuclei were stained with DAPI (blue). Head and cuticle were magnified and showed (ds-lta: head, A-1, cuticle, A-2; ds-TH: head, B-1, cuticle, B-2). All longitudinal slitting embryos inside [13 embryos/5 mothers from ds-lta treatments, **(C)**; and 10 embryos/5 mothers from ds-TH treatments, **(D)**] were selected and ordered by sizes. Transverse longitudinal sections from head to tail of *Acyrthosiphon pisum* samples **(E)**.

Original images and more replicates are provided in the supplemental information (*original images.rar*).

Phenotype Observations

Compared with the normal control mothers, the fourth-instar mothers with *APTH* knockdown did not differ in appearance. However, phenotypic alterations were observed in their daughters. The melanization levels in the heads, antennae, corniculi, and legs of the nymphs were substantially lower than those of their mothers (**Figure 3A**). Their legs were markedly curved and could not support their bodies (**Figures 3Ae**, Af). Low melanization levels were also evident in their exuviae (**Figures 3Ai**, Aj). After 8 d, most of the abnormal nymphs that reached the third instar failed to mature to the next developmental stage, whereas the control nymphs continued to develop into adults (**Figure 3Ak**). Excessive tanning could also be detected in the legs of the nymphs derived from the TH-RNAi mothers. Abnormal tanning (low- and over- tanning) may lead to a failure to molt (**Supplementary Figure S11**). The unabsorbed and unshed exuviae succumbed to fungal infections while still attached to the body (**Supplementary Figure S11**).

In the development monitoring experiments, the nymphs from the mothers subjected to the two treatments displayed differences in their body sizes and survival rates, during the 10-day monitoring period (**Figure 3B**; the original images are provided in supplemental information, *original images.rar*). A reduction in melanization was also detected by monitoring the early tanning after nymph molting. Nymphs subjected to different treatments and molting simultaneously exhibited very different tanning rates. Control aphids tanned faster than those treated with ds-TH (**Figure 3C**; original video 1: *1 instar 50X.mkv*; original video 2: *2 instar 20X.mkv*; Supplemental information). In addition, abnormal nymphs developed by day 7 after the TH dsRNA injections (ds-TH1 and ds-TH2) showed that most of the abnormal aphids were low-tanning individuals. However, two control nymphs with abnormal tanning were also observed on days 3 and 6 (**Figure 3D**).

Transcriptional and Biological Analyses of the Daughter Aphids

APTH Expression Analysis

APTH transcription levels in the daughter aphids were not affected by the RNAi treatments in the mothers. *APTH* expression levels in the newborn daughter nymphs (within 30 min after laying and no feeding) did not significantly change over 3 days after the dsRNAs treatments (**Figure 4A**; *P* values are marked between the bars).

L-DOPA and Dopamine Levels

There were no significant differences in the L-DOPA and dopamine levels between the nymphs laid by the mothers from the ds-TH and the ds-lta treatments (L-DOPA: $t = -0.479$, df = 28, $P = 0.636$; **Figure 4B**; dopamine: $t = 0.284$, df = 28, $P = 0.778$; **Figure 4C**).

Development Time and Body Size at Each Stage

The development times of the abnormal nymphs derived from the *APTH*-RNAi–treated mothers were significantly longer (without antenna) than those of the control nymphs in the first and second instars (1st instar: $F = 52.139$, df = 2, 56, $P < 0.001$; 2nd instar: $F = 158.137$, df = 2, 62, $P < 0.001$; **Figure 4D**). In contrast, the development times of the healthy nymphs (no obvious phenotypic changes) derived from the ds-TH–treated mothers did not significantly differ from those of the control. The survival rates of the abnormal third-instar nymphs were extremely low, and very few of these nymphs reached the fourth instar. The surviving nymphs from both the treatments had similar development times in the third instar ($t = -1.418$, df = 47, $P = 0.163$; **Figure 4D**).

The body sizes of the abnormal nymphs derived from the ds-TH–treated mothers were significantly smaller than those of the healthy individuals derived from these mothers (ds-TH) and of the control nymphs (ds-lta). This phenomenon was observed at all three developmental stages examined (1st instar: $F = 8.978$, df = 2, 66, $P < 0.001$; 2nd instar: $F = 37.569$, df = 2, 62, $P < 0.001$; and 3rd instar: $F = 63.932$, df = 2, 64, $P < 0.001$; **Figure 4E** and **Figure 3B**).

Lifespan and Survival Rates at Each Developmental Stage

The survival rates of the nymphs derived from the ds-TH–treated mothers were significantly lower than those of the control aphids in the first three developmental stages (1st instar: $\chi^2 = 21.664$, df = 1, $P < 0.001$; 2nd instar: $\chi^2 = 56.895$, df = 1, $P < 0.001$; and 3rd instar: $\chi^2 = 140.132$, df = 1, $P < 0.001$; **Figure 4F**). No abnormal nymphs (individuals showed low-tanning and over-tanning) reached the fourth instar. However, all healthy nymphs (ds-TH) survived through the last two stages. The lifespan of the abnormal nymphs was only half that of the control nymphs, and the difference was significant ($t = -15.135$, df = 60, $P < 0.001$; **Figure 4G**).

Cuticle Morphology in the Daughter Aphids of Treated Mothers

Histological analysis of the cuticle sections revealed that the cuticles of the daughter aphids (ds-TH) consisted of thinner layers (cuticle and epidermis, $t = 7.104$, df = 50, $P < 0.001$; **Figure 5B**) than those of the controls (ds-lta). Tissue abnormalities were also observed in the cuticle layers (**Figure 5**). The distinct cuticle layers were detected in the control nymphs (**Figure 5C**) but were indistinguishable from those derived from the ds-TH–treated mothers (**Figure 5D**). The microstructures of the epidermal cell layers in the latter (ds-TH) were also poorly defined (**Figure 5**).

The distribution of the TH proteins in the cuticles of the healthy and abnormal daughters was determined by immunofluorescence. Although the TH staining could be observed in the cuticle epidermal cells of the nymphs in both treatments (**Figures 5E,F**), the distribution of the TH protein was irregular in the cuticles of the abnormal nymphs (**Figure 5F**).

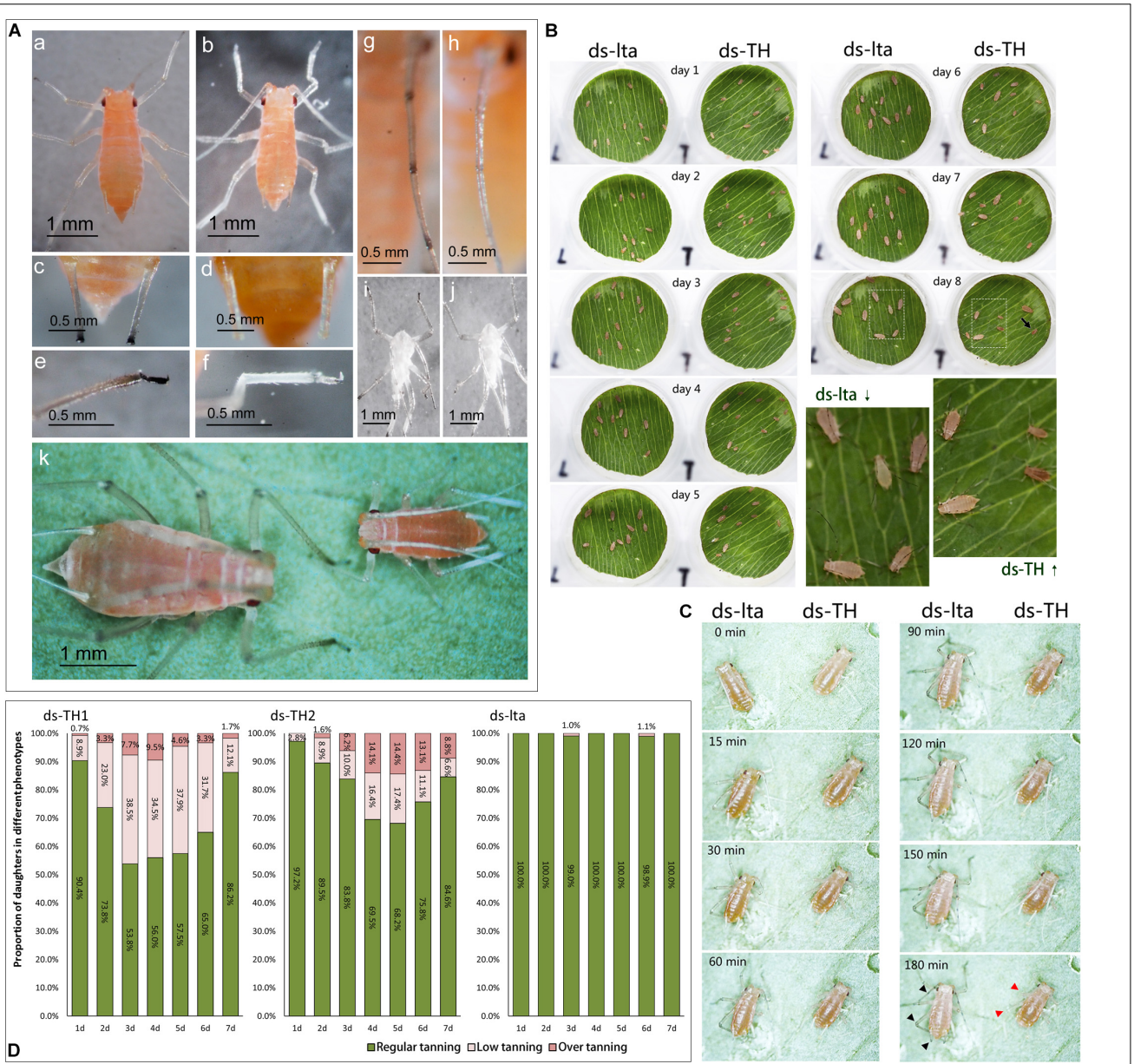

FIGURE 3 | Low or abnormal melanization in nymphs of *Acyrthosiphon pisum*. The second-instar nymphs selected for comparison were 12 h old **(A)**. Appearances of control (WT, wild type) and abnormally melanized aphids (a,b); relative differences in melanization of the cornicles of WT and abnormally melanized aphids (c.d); relative differences in melanization of the legs of WT and abnormally melanized aphids (e,f); relative differences in melanization in the antennae of WT and abnormally melanized aphids (g,h); relative differences in melanization of the exuviae of WT and abnormally melanized aphids (i,j); relative differences in the appearances of WT and abnormally melanized aphids of the same age (8 d post-hatching; k). Comparison of wild type (WT) and abnormally melanized aphids after 8 d of monitoring **(B)**; comparison of early melanization in WT and abnormally melanized aphids after 3 h of monitoring **(C)**; the arrow indicates an abnormal nymph at day 8; the red arrowhead indicates an abnormal melanin deposit and the black arrowhead indicates a melanin deposit in the control. Proportions of abnormal melanization in all nymphs after 7 d of monitoring mothers treated with different dsRNAs (ds-TH1, ds-TH2, and ds-lta, **D**); abnormal nymph producers selected from mothers treated with ds-TH1 and ds-TH2.

Relative Differences in Gene Expression Based on Transcriptome Sequencing

The transcriptomic results showed the transcriptional changes of the numerous genes between the two different daughter aphids. Heatmaps were constructed using candidate genes from cuticle proteins, melanization pathways, and chitin biosynthesis. The results showed differences in the transcription levels of these genes between the abnormally tanned (low- and over-tanned) and healthy individuals. The cuticle protein genes (CPs) were either upregulated or downregulated in response to the ds-TH treatment (**Figure 6A**). The transcription levels of the several candidate melanization genes were also altered.

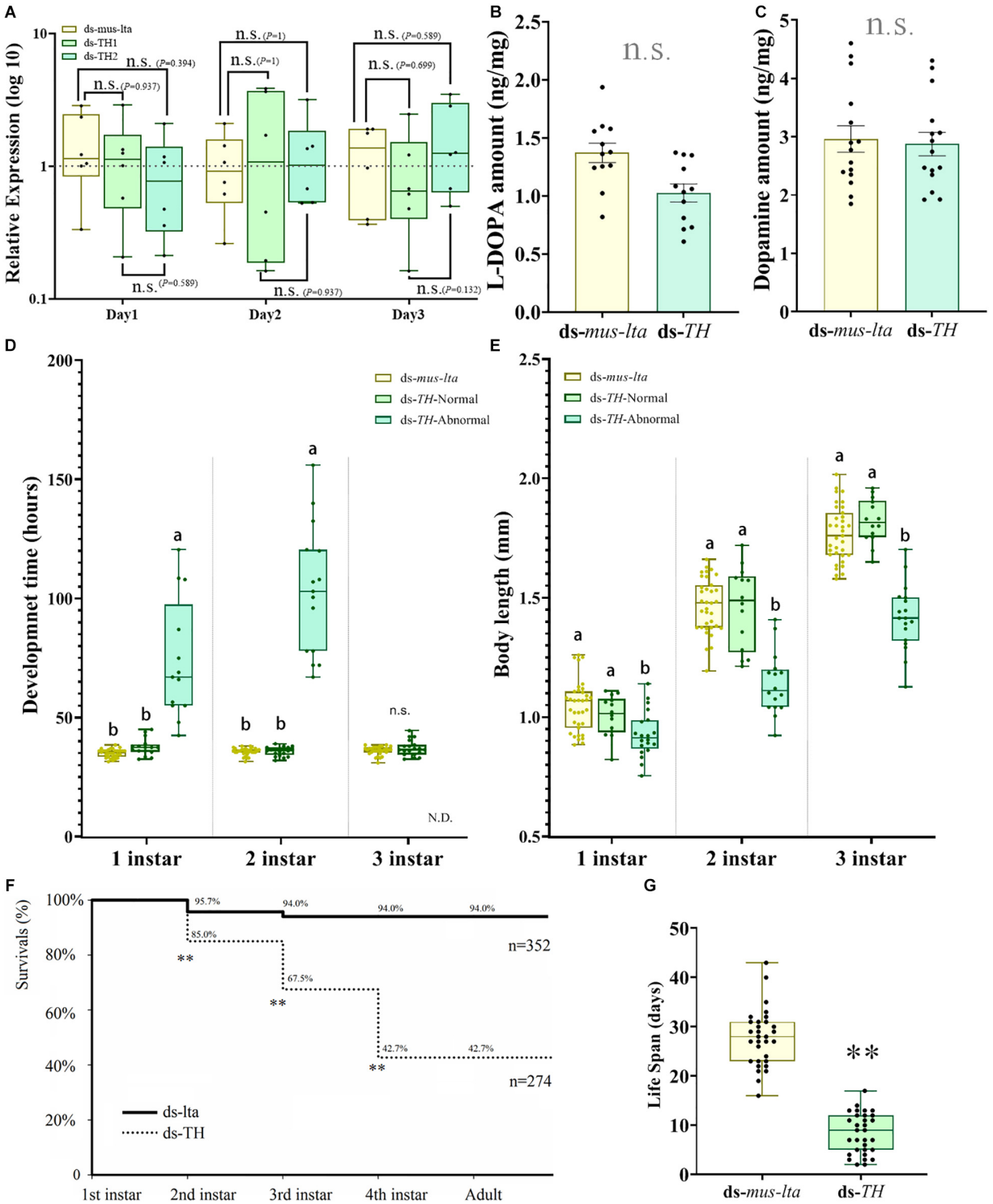

FIGURE 4 | Transcriptional, biochemical, and biological analyses of abnormal *Acyrthosiphon pisum* nymphs. **(A)** *APTH* transcription levels in 3-d-old nymphs derived from mothers treated with different dsRNAs. n.s. indicates no significant difference according to Mann-Whitney *U*-test (non-parametric; $^{*}P < 0.05$, $^{**}P < 0.001$). Relative differences in L-DOPA **(B)** and dopamine **(C)** levels between healthy and abnormal nymphs. n.s. indicates no significant difference according to Student's *t*-test. Comparative differences in development time **(D)** and body length **(E)** among healthy and abnormal nymphs derived from mothers treated with ds-TH and ds-lta. Different letters within the same fig indicate significant differences in the values (ANOVA; Duncan's test; $P < 0.05$), n.s. indicates no significant difference. N.D. (in D) denotes no data. Differences in survival rate **(F)** between healthy and abnormal nymphs derived from mothers administered ds-TH and ds-lta; differences in lifespan **(G)** between healthy and abnormal nymphs derived from mothers treated with ds-TH and ds-lta. ** in F indicates significant differences in the values (χ^2 test; $P < 0.001$). ** in G indicates significant differences in the values by Student's *t*-test ($P < 0.001$).

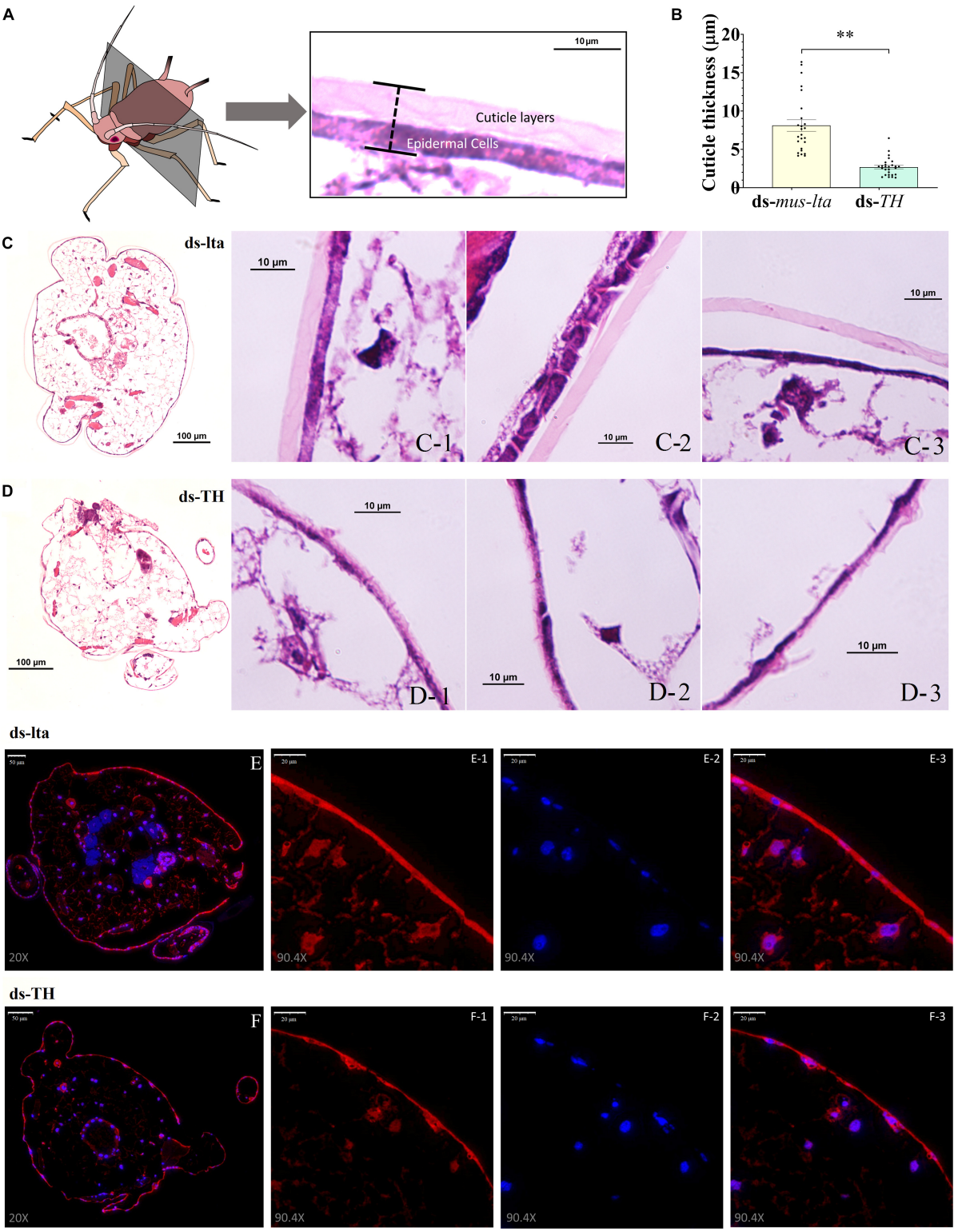

FIGURE 5 | Histology and TH immunofluorescence of daughters. Hematoxylin and eosin (H&E)-stained transverse sections of the cuticle at segment T2 **(A)** from third-instar pea aphid (*Acyrthosiphon pisum*) at × 10 and × 100 magnification. **(B)** Relative differences in cuticle thickness between healthy and abnormal aphids. Each value represents the mean ± SEM; Student's *t*-test (**$P < 0.001$). **(C)** H&E-stained histological sections of healthy nymphs (control). **(D)** H&E-stained histological sections of nymphs with abnormal cuticles. The distribution of TH protein in the cuticle of healthy **(E)** and abnormal **(F)** aphids was determined by immunofluorescence (× 20 and × 90.4 magnification). Anti-TH antibodies were detected using Cy3-conjugated rabbit IgG antibodies (red, E-1 and F-1, × 90.4 magnification); Nuclei were stained with DAPI (blue, E-2 and F-2, × 90.4); and merged images are shown in E-3 and F-3 (×90.4 magnification).

However, the expression levels of *TH*, the target gene of dsRNA, remained unchanged (**Figure 6B**). Only a slight alteration in the transcription levels was observed for chitin biosynthesis genes (**Figure 6C**).

Transcriptional verification by qRT-PCR of the selected candidate genes that exhibited relatively large exchange rate changes. The transcriptional results (qRT-PCR) showed different results from those of the transcriptomic data. Some results were similar, such as changes to XM_001949658.5 and XM_029488103.1 (XM_001949658.5, $t = -3.168$, df = 4, $P = 0.034$; XM_029488103.1, $t = -3.887$, df = 4, $P = 0.018$; **Figure 6D**). However, some other results of selected candidate genes that exhibited strong up- or downregulations in the transcriptomic analysis did not show a significant change in our transcriptional verifications (XM_001946681.5, $t = 0.002$, df = 4, $P = 0.999$; NM_001163201.1, $t = 1.354$, df = 4, $P = 0.247$; XM_003247688.4, $t = 11.416$, df = 4, $P = 0.201$; NM_001326676.1, $t = 5.681$, df = 4, $P = 0.809$; XM_001944914.5, $t = 0.807$, df = 4, $P = 0.465$; **Figure 6D**). Additional details are available in **Figures S12–S16** and the **Supplementary Material** (*Transcriptome sequencing.rar*).

Injection of a Dopamine Biosynthesis Inhibitor and Receptor Antagonists

To investigate whether dopamine-related pathways of the nervous system were involved in this transgenerational control system, we treated individual specimens with an inhibitor of dopamine biosynthesis or with receptor antagonists. Only individuals treated with the dopamine biosynthesis inhibitor (metirosine) gave birth to abnormal nymphs. We found that 7 of the 32 mothers were abnormal nymph producers, and phenotypic changes were detected in their daughters (**Table 1**). All individuals treated with dopamine receptor antagonists (SCH23390, Sulpiride and Pimozide) gave birth to normal and healthy offspring (**Table 1**). Typical low melanization of nymphs (no over-tanning individual found) were observed in metirosine-treated samples; this was similar to the phenotypic changes described previously in the daughter aphids of mothers with *APTH* knockdown (subsection "Phenotype observations").

DISCUSSION

Many of the phenotypic features of *A. pisum* are maternally determined and can lead to phenotypic changes in their daughters. In this study, artificially induced (RNAi) and host-related (under host transition period) transgenerational phenotypic regulations in *A. pisum* were observed. These findings are particularly useful for furthering our understanding of the mechanisms underlying the phenotypic determination in aphids. We detected strong, predictable, repeatable, and consistent phenotypic changes in the daughter aphids of the treated individuals. Low and high levels of cuticular melanization and sclerotization were detected in the nymphs. The periods of host transition, from feeding on *V. faba* (high L-DOPA content) to the *T. repens* (low L-DOPA content), and simultaneous treatments with *APTH* (converts L-tyrosine to L-DOPA) dsRNAs were both essential for this phenomenon. We suggested that the maternal effects played an important role, and a transgenerational system based on dopamine/L-DOPA signals between the mother and embryos could exist. This transgenerational regulation may be related to the phenotypic plasticity of the pea aphid but requires further investigation to improve our understanding.

TH, the target gene silenced by RNAi in this study, is a key regulatory enzyme upstream of melanization pathway (Hearing et al., 1980; Ma et al., 2011). Irregular and disordered transcriptional feedback in the abdomen showed strong but unclear dopamine-related regulation response patterns, and we hypothesize that this reaction was caused by the introduction of the *APTH* dsRNA. In this experiment, the dietary intake of the L-DOPA in the aphids was markedly reduced (host change). This severe reduction in L-DOPA assimilation could promote a reorganization of the internal biochemical environment. The reduction in L-DOPA content may have triggered endogenous L-DOPA biosynthesis and maintained its downstream reactions. The dopamine pathway is moderately susceptible to imbalances, and even weak interference from exogenous dsRNA could disrupt the transmission of molecular signals and cause irregular and disordered expression feedback of *APTH* in *A. pisum*.

Further analysis of the distribution of *TH* confirmed that *APTH* was downregulated in the insect cuticle and explained the irregular transcriptional feedback in the abdomen. Distribution differences of TH were detected in the developing cuticle tissues of the embryos. These results are consistent with the findings from a study using microarrays and *A. pisum* (Rabatel et al., 2013) and another study showing that external dsRNA could spread throughout the whole body in aphids (Wang et al., 2015). The nervous systems in embryos with strong positive fluorescence might be responsible for the irregular expression in the abdomen, and it is also possible that the dopamine-based neurological systems displayed strong feedback to the RNAi performance.

When *APTH* transcription was modified in the mothers, the disordered melanization phenotype was subsequently detected in the daughters. This indicated that the melanization failure is a systemic disorder of the daughter aphids' cuticle. Studies on the biological parameters from the abnormal aphids revealed that a maternal effect might determine this phenotype. Combining the results of *APTH* transcription detection and L-DOPA/dopamine content assays, which did not exhibit any significant differences, for the abnormal daughters, no transgenerational RNAi was observed. Furthermore, treated mothers continued to produce abnormal offspring even after the *APTH*-RNAi effect had weakened or disappeared altogether. Consequently, the phenotypic changes in the daughters may show long-term persistence and, generally, are irreversible. These conflicting results reflect the complexity of this phenomenon.

Furthermore, the daughter aphids with the abnormal phenotypes could not revert to the normal phenotypes at any subsequent stage in their lives, suggesting that these phenotypic changes were not directly induced by the RNAi (which could be recovered). Further experiments with the nymphs, including transcriptional analysis, L-DOPA/dopamine content analysis, and transcriptome sequencing, supported this conclusion. Melanization rate, body size, development time at

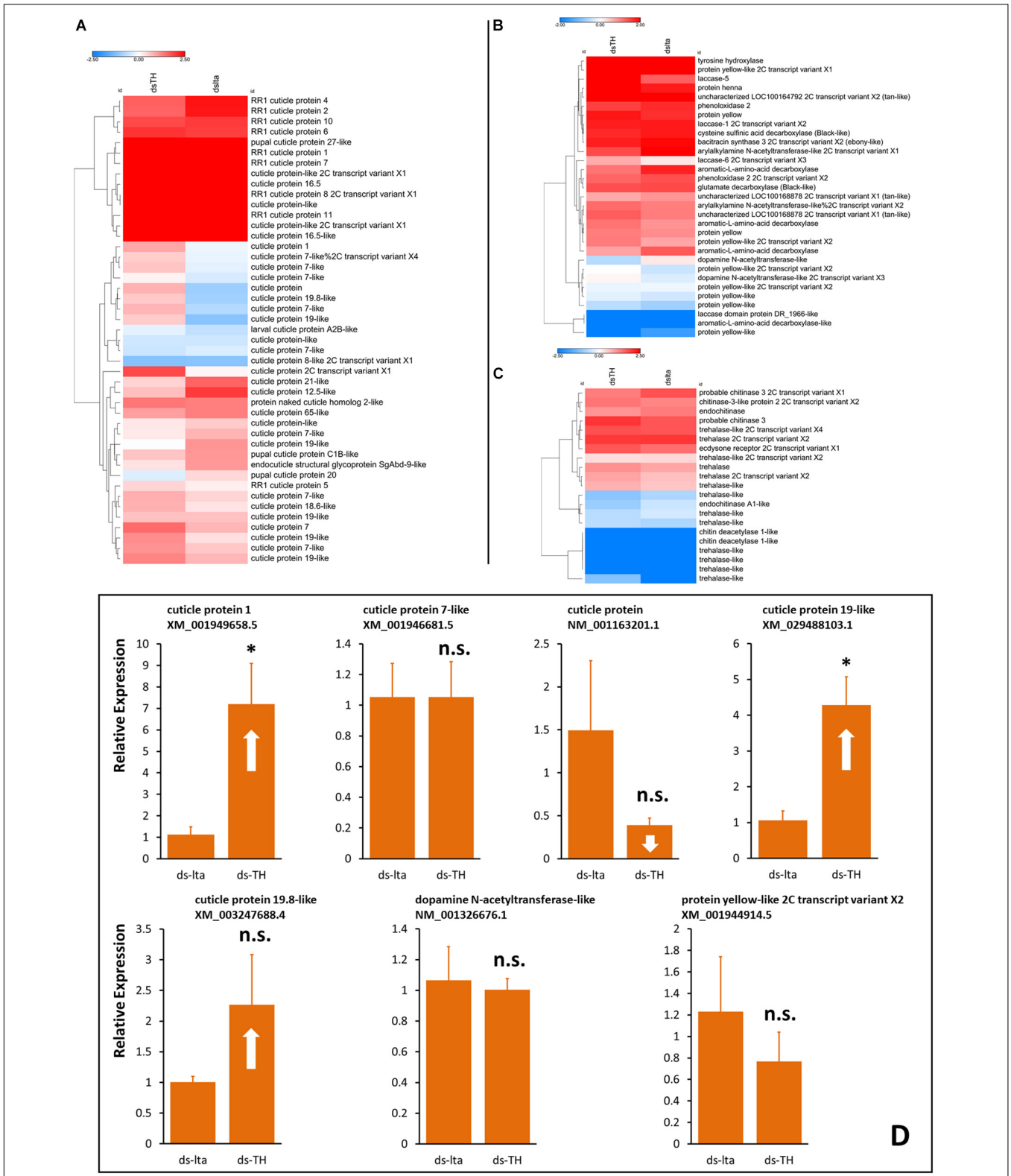

FIGURE 6 | Transcription analysis of daughters. Heatmaps of transcriptional differences in the candidate genes associated with cuticle proteins **(A)**, melanization **(B)**, and chitin biosynthesis **(C)**. Data were obtained from transcriptome sequencing of healthy and abnormal *Acyrthosiphon pisum* nymphs. Each sample prepared for RNA extraction consisted of more than 400 aphids without abdomens. Hierarchical clustering was performed using the Euclidean distance and the average linkage method. Transcription changes of selected genes from transcriptome results in new born aphids (whole body) were verified by qRT-PCR **(D)**, samples were collected from new daughters of abnormal-nymph-producers at the 3rd day after treatment. n.s. indicates no significant difference according to Student's *t*-test (*$P < 0.05$).

TABLE 1 | Abnormal offspring detection of *Acyrthosiphon pisum* under dsRNAs and chemicals (dopamine biosynthesis inhibitor and receptor antagonists) injections.

	Descriptions	Proportion of abnormal daughters (abnormal aphids/all daughters)		
		Day 3**	Day 4**	Day 5**
dsRNAs	ds-TH1* (dsRNA of *APTH*)	66/143 (46.15%)	51/116 (43.97%)	37/87 (42.53%)
	ds-TH2* (dsRNA of *APTH*)	21/130 (16.15%)	39/128 (30.47%)	42/132 (31.82%)
	ds-lta* (dsRNA control)	1/100 (1.00%)	0/95 (0)	0/113 (0)
Chemicals	Metirosine (dopamine biosynthesis inhibitor)	30/106 (28.30%)	11/119 (9.24%)	11/131 (8.40%)
	SCH23390 (D1 antagonist)	0/97 (0)	0/109 (0)	0/102 (0)
	Sulpiride (D2 and D3 antagonist)	0/73 (0)	0/90 (0)	0/90 (0)
	Pimozide (D2, D3, and D4 antagonist)	0/90 (0)	0/63 (0)	1/101 (0.99%)
	Saline (0.9%) (control)	0/146 (0)	0/123 (0)	0/101 (0)

See **Figure 3D for more details about dsRNAs injections. **After injections.*

each stage, and lifespan were markedly different between the abnormal and control nymphs. The abnormal aphids are born with signals that determine their future developmental patterns. This phenomenon is similar to the determination of wing and sexual dimorphism in aphids and is manifested as a maternal effect (Braendle et al., 2006; Dombrovsky et al., 2009; Brisson, 2010). Winged and sexual individuals differ from the typical parthenogenetic individuals in terms of their biological traits and appearance, including cuticular sclerotization and melanization (Kring, 1977; Ishikawa and Miura, 2007; Brisson, 2010). These differences are based on L-DOPA/dopamine reactions, and consequently, winged aphids are normally heavier than wingless aphids (Ishikawa and Miura, 2007).

We assumed that there was a connection between this induced phenotypic change and natural phenotypic regulations, as they may share a similar regulation pathway. Combining the results discussed above, several similarities were observed between our induced phenotypic changes and the natural maternal dimorphisms: (1) a certain proportion of the nymphs showed phenotypic changes (**Figure 3**; Müller et al., 2001; Wang et al., 2016); (2) the appearance of anomalous phenotypes in the offspring decreased over time, possibly because of signal attenuation in the mothers (**Figure 3**; Sutherland, 1969; Müller et al., 2001); and (3) the observed phenotypes in the transformed nymphs were generally permanent and irreversible (**Figure 3**). These similarities suggest that the phenotypic changes induced by the maternal *APTH*-RNAi was an atypical maternal effect in aphids. The fact that densely stimulated (physical contact) mothers can produce winged nymphs (irreversible phenotypic changes), whereas nutritional or photoperiod stimulations may induce mothers to generate sexual nymphs (irreversible phenotypic changes), reflect their adaptations to environmental changes (Nunes and Hardie, 1996; Miura et al., 2003; Sack and Stern, 2007; Dombrovsky et al., 2009).

The transcriptome sequencing results supported our hypothesis, as numerous transcriptional changes were observed, but candidate melanization gene expressions were relatively stable between the two samples. Heatmaps revealed no obvious differences between the abnormal and control nymphs with respect to the expression of the numerous candidate melanization genes (including *TH*) upstream of melanization regulation. In contrast, several genes downstream from *APTH*, including *laccase-like*, *yellow-like*, and *dopamine N-acetyltransferase-like* (Andersen, 2010), were either upregulated or downregulated in the abnormal nymphs in comparison to that in the control nymphs. Several *CPs* (Andersen et al., 1995) exhibited obvious changes between the abnormal and control nymphs, and these observations corroborated the identified microstructural collapses of the cuticle. The abnormally transcribed genes may be essential for cuticle formation, and their disruptions could cause the cuticle structures to collapse. The expression levels of several candidate chitin biosynthesis genes (Merzendorfer, 2006) in the abnormal nymphs were also slightly altered relative to those in the control nymphs. Our transcriptome sequencing results showed more changes than those that could be transcriptionally verified (**Supplementary Figure S16**). We also verified the transcriptional changes of the candidate genes (selected from transcriptome data) in the newborn aphids by qRT-PCR and found that while some candidate genes showed results similar to the transcriptome analysis (such as XM_001949658.5, XM_029488103.1, and XM_003247688.4), other genes (such as NM_001326676.1 and XM_001944914.5 of the melanization pathway) did not. We suggest that some genes might be directly regulated by the mothers, and daughter aphids that are born with transcriptional anomalies would not be able to revert to healthy individuals during further development processes. In contrast, other transcriptional changed genes may be downstream regulated after birth, and consequently, changes in their expression levels may not be detected in present study. However, the inefficiency of the RNAi of *A. pisum* made it difficult to further confirm the functions of the candidate *CPs* and reproduce the desired phenotypic change within a single generation by modifying these genes.

The malfunctioning cuticular layer observed with the transcriptional changes directly explained the physiological causes of these phenotypes. Cuticular dysplasia with microstructural collapse in *A. pisum* could result in abnormal melanization, which manifests as poor tanning. Analysis of the histological sections indicated that the cuticle and epidermal cells had thinned considerably, and there were anomalies in the cuticle layer, which is the site of melanin precipitation (Brey et al., 1985; Moussian, 2013). Malformed cuticular layers

cannot support melanization, even with enough substrates (L-DOPA and dopamine) and fully functional enzymes (including TH). Therefore, abnormal melanization may account for the observed phenotypic changes. The presence of the TH protein negated the RNA intergenerational interference and the irregular distribution of the TH protein provided evidence for the collapse of the cuticle structure. A malfunctioning cuticle layer would not support melanization, regardless of whether the substrates and key enzymes were sufficient and functional, respectively.

We hypothesized that L-DOPA, the reaction product of TH and one of the key chemicals that differ among *A. pisum* individuals, plays an important role in trans-generational regulation. In the present study, we observed the phenotypic changes in response to the changing levels of L-DOPA intake (host plant alternation) and L-DOPA self-synthesis modifications (*APTH*-RNAi). Our results suggest that L-DOPA and dopamine (the neurotransmitter derived from L-DOPA) might participate in the intergenerational signal transmission system. An L-DOPA/dopamine-based developmental signal is transmitted from the mothers to the embryos and determines the future developmental patterns of the nymphs. In this study, a disordered signal induced by *APTH* dsRNA was received by the embryos and caused pathological phenotypic changes thereafter.

The transgenerational signal might not be transmitted via the nervous system (dopamine and its receptors). Studies have shown that physical contact induces wing dimorphism in aphid offspring (Gallot et al., 2010; Vellichirammal et al., 2016), and this stimulation could affect the dopamine pathway (**Supplementary Figure S8**). However, the results of chemical intervention confirmed that transgenerational signals were not transferred through dopamine receptors and that only the dopamine biosynthesis inhibitor could induce similar phenotypic changes in the daughter aphids. Combined with the essential conditions of the host plant alternations (L-DOPA intake considerably reduced), L-DOPA/dopamine reductions must be the key factor, but dopamine receptor-based neurological regulation is not involved in this transgenerational phenotypic regulation. We suggest the presence of another downstream pathway, which is regulated by dopamine/L-DOPA content, that acts as a transgenerational signal between the mothers and embryos. Further research is required to fully understand this non-neuronal dopamine regulation.

We utilized RNAi and found that it could induce strong phenotypic changes in *A. pisum*. Variable RNAi efficiencies in aphids have previously been reported (Christiaens and Smagghe, 2014; Christiaens et al., 2014; Sapountzis et al., 2014; Singh et al., 2017; Cao et al., 2018). This investigation, however, has demonstrated a successful case for aphid RNAi based on the downregulation results of our target gene.

The aphid phenotypes observed were indicative of the complexity and flexibility of the transgenerational regulations. The present study shows that maternal phenotypic regulation systems of *A. pisum* can be affected in certain conditions, based on the transcriptional modifications. Mother aphids determine the developmental patterns of their daughters, and the dopamine pathway regulation is likely to be involved in cuticular development in daughter aphids via a pathway that does not depend on dopamine receptor-based neurological regulation. L-DOPA, the key chemical in this process, is present in both plants and aphids and functions in the physiological regulations of this process. However, how mother aphids transmit signals to their embryos and how the embryos receive them remains poorly understood. Future studies should focus on determining the genes that may be involved in this process.

DATA AVAILABILITY STATEMENT

All datasets generated for this study are included in the article/**Supplementary Material**.

AUTHOR CONTRIBUTIONS

YZ and T-XL designed the research. X-XW performed the research. Z-JF, Z-SC, and Z-FZ provided the assistance. YZ and X-XW analyzed the data. and YZ, H-GT, X-XW, and T-XL wrote the manuscript.

FUNDING

This research was supported by the Chinese Universities Scientific Fund (grant number, Z109021718).

ACKNOWLEDGMENTS

We are grateful for the assistance of all staff and students in the Key Laboratory of Applied Entomology, Northwest A&F University at Yangling, Shaanxi, China.

SUPPLEMENTARY MATERIAL

The Supplementary Material for this article can be found online at: https://www.frontiersin.org/articles/10.3389/fcell.2020.00311/full#supplementary-material

REFERENCES

Andersen, S. O. (2010). Insect cuticular sclerotization: a review. *Insect Biochem. Molec.* 40, 166–178. doi: 10.1016/j.ibmb.2009.10.007

Andersen, S. O., Hojrup, P., and Roepstorff, P. (1995). Insect cuticular proteins. *Insect Biochem. Molec.* 25, 153–176. doi: 10.1016/0965-1748(94)00052-J

Anderson, S. O. (1966). Covalent cross-links in a structural protein, resilin. *Acta Physiol. Scand. Suppl.* 263, 1–81.

Anderson, S. O. (2011). Are structural proteins in insect cuticles dominated by intrinsically disordered regions? *Insect Biochem. Mol. Biol.* 41, 620–627. doi: 10.1016/j.ibmb.2011.03.015

Arakane, Y., Lomakin, J., Beeman, R. W., Muthukrishnan, S., Gehrke, S. H., Kanost, M. R., et al. (2009). Molecular and functional analyses

of amino acid decarboxylases involved in cuticle tanning in *Tribolium castaneum*. *J. Biol. Chem.* 284, 16584–16594. doi: 10.1074/jbc.M901629200

Barron, A. B., Maleszka, J., Vander Meer, R. K., Robinson, G. E., and Maleszka, R. (2007). Comparing injection, feeding and topical application methods for treatment of honeybees with octopamine. *J. Insect Physiol.* 53, 187–194. doi: 10.1016/j.jinsphys.2006.11.009

Bermingham, J., and Wilkinson, T. L. (2009). Embryo nutrition in parthenogenetic viviparous aphids. *Physiol. Entomol.* 34, 103–109. doi: 10.1111/j.1365-3032.2008.00669.x

Braendle, C., Davis, G. K., Brisson, J. A., and Stern, D. L. (2006). Wing dimorphism in aphids. *Heredity* 97:192. doi: 10.1038/sj.hdy.6800863

Brey, P. T., Ohayon, H., Lesourd, M., Castex, H., Roucache, J., and Latge, J. P. (1985). Ultrastructure and chemical composition of the outer layers of the cuticle of the pea aphid *Acyrthosiphon pisum* (Harris). *Comp. Biochem. Phys. A* 82, 401–411. doi: 10.1016/0300-9629(85)90875-8

Brisson, J. A. (2010). Aphid wing dimorphisms: linking environmental and genetic control of trait variation. *Philos. Trans. R. Soc. B* 365, 605–616. doi: 10.1098/rstb.2009.0255

Cao, M., Gatehouse, J., and Fitches, E. (2018). A systematic study of RNAi effects and dsRNA stability in *Tribolium castaneum* and *Acyrthosiphon pisum*, following injection and ingestion of analogous dsRNAs. *Int. J. Mol. Sci.* 19:1079. doi: 10.3390/ijms19041079

Chen, N., Fan, Y. L., Bai, Y., Li, X. D., Zhang, Z. F., and Liu, T. X. (2016). Cytochrome P450 gene, *CYP4G51*, modulates hydrocarbon production in the pea aphid, *Acyrthosiphon pisum*. *Insect Biochem. Molec.* 76, 84–94. doi: 10.1016/j.ibmb.2016.07.006

Christiaens, O., and Smagghe, G. (2014). The challenge of RNAi-mediated control of hemipterans. *Curr. Opin. Insect Sci.* 6, 15–21. doi: 10.1016/j.cois.2014.09.012

Christiaens, O., Swevers, L., and Smagghe, G. (2014). DsRNA degradation in the pea aphid (*Acyrthosiphon pisum*) associated with lack of response in RNAi feeding and injection assay. *Peptides* 53, 307–314. doi: 10.1016/j.peptides.2013.12.014

Dombrovsky, A., Arthaud, L., Ledger, T. N., Tares, S., and Robichon, A. (2009). Profiling the repertoire of phenotypes influenced by environmental cues that occur during asexual reproduction. *Genome Res.* 19, 2052–2063. doi: 10.1101/gr.091611.109

Filshie, B. K. (1982). *Fine Structure of the Cuticle of Insects and Other Arthropods. Insect Ultrastructure*. Boston, MA: Springer, 281–312.

Gallot, A., Rispe, C., Leterme, N., Gauthier, J. P., Jaubert-Possamai, S., and Tagu, D. (2010). Cuticular proteins and seasonal photoperiodism in aphids. *Insect Biochem. Molec.* 40, 235–240. doi: 10.1016/j.ibmb.2009.12.001

Gorman, M. J., and Arakane, Y. (2010). Tyrosine hydroxylase is required for cuticle sclerotization and pigmentation in *Tribolium castaneum*. *Insect Biochem. Molec.* 40, 267–273. doi: 10.1016/j.ibmb.2010.01.004

Hannon, G. J. (2002). RNA interference. *Nature* 418, 244–251. doi: 10.1038/418244a

Hearing, V. J. Jr., Ekel, T. M., Montague, P. M., and Nicholson, J. M. (1980). Mammalin tyrosinase. Stoichiometry and measurement of reaction products. *BBA Biomembranes* 611, 251–268. doi: 10.1016/0005-2744(80)90061-3

Hu, X., Liu, X., Ridsdillsmith, T. J., Thieme, T., Zhao, H., and Liu, T. (2016). Effects of maternal diet on offspring fitness in the bird cherry-oat aphid. *Ecol. Entomol.* 41, 147–156. doi: 10.1111/een.12282

Huang, T., Jander, G., and de Vos, M. (2011). Non-protein amino acids in plant defense against insect herbivores: representative cases and opportunities for further functional analysis. *Phytochemistry* 72, 1531–1537. doi: 10.1016/j.phytochem.2011.03.019

Huvenne, H., and Smagghe, G. (2010). Mechanisms of dsRNA uptake in insects and potential of RNAi for pest control: a review. *J. Insect Physiol.* 56, 227–235. doi: 10.1016/j.jinsphys.2009.10.004

Huybrechts, J., Bonhomme, J., Minoli, S., Prunier-Leterme, N., Dombrovsky, A., Abdel-Latief, M., et al. (2010). Neuropeptide and neurohormone precursors in the pea aphid *Acyrthosiphon pisum*. *Insect Mol. Biol.* 19, 87–95. doi: 10.1111/j.1365-2583.2009.00951.x

Ingle, P. K. (2003). L-Dopa bearing plants. *Indian J. Nat. Prod. Resour.* 2, 126–133.

International Aphid Genomics Consortium (2010). Genome sequence of the pea aphid *Acyrthosiphon pisum*. *PLoS Biol.* 8:e1000313. doi: 10.1371/journal.pbio.1000313

Ishikawa, A., and Miura, T. (2007). Morphological differences between wing morphs of two Macrosiphini aphid species *Acyrthosiphon pisum* and *Megoura crassicauda* (Hemiptera, Aphididae). *Sociobiology* 50, 881–893.

Ishikawa, A., Ogawa, K., Gotoh, H., Walsh, T. K., Tagu, D., Brisson, J. A., et al. (2012). Juvenile hormone titer and gene expression during the change of reproductive modes in the pea aphid. *Insect Mol. Biol.* 12, 49–60. doi: 10.1111/j.1365-2583.2011.01111.x

Jeffs, C. T., and Leather, S. R. (2014). Effects of extreme, fluctuating temperature events on life history traits of the grain aphid, *Sitobion avenae*. *Entomol. Exp. Appl.* 150, 240–249. doi: 10.1016/j.jinsphys.2018.12.003

Kanvil, S., Powell, G., and Turnbull, C. (2014). Pea aphid biotype performance on diverse *Medicago* host genotypes indicates highly specific virulence and resistance functions. *B. Entomol. Res.* 104, 1–13. doi: 10.1017/S0007485314000443

Kring, J. B. (1977). Structure of the eyes of the pea aphid, *Acyrthosiphon pisum*. *Ann. Entomol. Soc. Am.* 70, 855–860. doi: 10.1093/aesa/70.6.855

Lee, K. S., Kim, B. Y., and Jin, B. R. (2015). Differential regulation of tyrosine hydroxylase in cuticular melanization and innate immunity in the silkworm *Bombyx mori*. *J. Asia Pac. Entomol.* 18, 765–770. doi: 10.1016/j.aspen.2015.09.008

Longo, R., Castellani, A., Sberze, P., and Tibolla, M. (1974). Distribution of l-dopa and related amino acids in *Vicia*. *Phytochemistry* 13, 167–171. doi: 10.1016/S0031-9422(00)91287-1

Ma, Z., Guo, W., Guo, X., Wang, X., and Kang, L. (2011). Modulation of behavioral phase changes of the migratory locust by the catecholamine metabolic pathway. *Proc. Natl. Acad. Sci. U.S.A.* 108, 3882–3887. doi: 10.1073/pnas.1015098108

MacKay, A., and Wellington, W. G. (1977). Maternal age as a source of variation in the ability of an aphid to produce dispersing forms. *Res. Popul. Ecol.* 18, 195–209. doi: 10.1007/BF02510847

Merzendorfer, H. (2006). Insect chitin synthases: a review. *J. Comp. Physiol. B* 176, 1–15. doi: 10.1007/s00360-005-0005-3

Miura, T., Braendle, C., Shingleton, A., Sisk, G., Kambhampati, S., and Stern, D. L. (2003). A comparison of parthenogenetic and sexual embryogenesis of the pea aphid *Acyrthosiphon pisum* (Hemiptera: Aphidoidea). *J. Exp. Zool. Part B* 295, 59–81. doi: 10.1002/jez.b.3

Moussian, B. (2013). "The arthropod cuticle," in *Arthropod Biology and Evolution*, eds A. Minelli, G. Boxshall, and G. Fusco (Berlin: Springer), 171–196. doi: 10.1007/978-3-662-45798-6_8

Moussian, B., Seifarth, C., Müller, U., Berger, J., and Schwarz, H. (2006). Cuticle differentiation during *Drosophila* embryogenesis. *Arthropod Struct. Dev.* 35, 137–152. doi: 10.1016/j.asd.2006.05.003

Müller, C. B., Williams, I. S., and Hardie, J. (2001). The role of nutrition, crowding and interspecific interactions in the development of winged aphids. *Ecol. Entomol.* 26, 330–340. doi: 10.1046/j.1365-2311.2001.00321.x

Noh, M. Y., Muthukrishnan, S., Kramer, K. J., and Arakane, Y. (2016). formation and pigmentation in beetles. *Curr. Opin. Insect Sci.* 17, 1–9. doi: 10.1016/j.cois.2016.05.004

Nunes, M. V., and Hardie, J. (1996). Differential photoperiodic responses in genetically identical winged and wingless pea aphids, *Acyrthosiphon pisum*, and the effects of day length on wing development. *Physiol. Entomol.* 21, 339–343. doi: 10.1111/j.1365-3032.1996.tb00875.x

Ogawa, K., and Miura, T. (2014). Aphid polyphenisms: trans-generational developmental regulation through viviparity. *Front. Physiol.* 5:1. doi: 10.3389/fphys.2014.00001

Rabatel, A., Febvay, G., Gaget, K., Duport, G., Baa-Puyoulet, P., Sapountzis, P., et al. (2013). Tyrosine pathway regulation is host-mediated in the pea aphid symbiosis during late embryonic and early larval development. *BMC Genomics* 14:235. doi: 10.1186/1471-2164-14-235

Sack, C., and Stern, D. L. (2007). Sex and death in the male pea aphid, *Acyrthosiphon pisum*: the life-history effects of a wing dimorphism. *J. Insect Sci.* 7, 1–9. doi: 10.1673/031.007.4501

Sapountzis, P., Duport, G., Balmand, S., Gaget, K., Jaubert-Possamai, S., Febvay, G., et al. (2014). New insight into the RNA interference response against cathepsin-L gene in the pea aphid, *Acyrthosiphon pisum*: molting or gut phenotypes

specifically induced by injection or feeding treatments. 2014. *Insect Biochem. Molec.* 51, 20–32. doi: 10.1016/j.ibmb.2014.05.005

Singh, I. K., Singh, S., Mogilicherla, K., Shukla, J. N., and Palli, S. R. (2017). Comparative analysis of double-stranded RNA degradation and processing in insects. *Sci. Rep.* 7:7059. doi: 10.1038/s41598-017-17134-2

Slater, J. M., Gilbert, L., Johnson, D. W., and Karley, A. J. (2019). Limited effects of the maternal rearing environment on the behaviour and fitness of an insect herbivore and its natural enemy. *PLoS One* 14:e0209965. doi: 10.1371/journal.pone.0209965

Smeets, W. J., and González, A. (2000). Catecholamine systems in the brain of vertebrates: new perspectives through a comparative approach. *Brain Res. Rev.* 33, 308–379. doi: 10.1016/S0165-0173(00)00034-5

Suderman, R. J., Dittmer, N. T., Kanost, M. R., and Kramer, K. J. (2006). Model reactions for insect cuticle sclerotization: cross-linking of recombinant cuticular proteins upon their laccase-catalyzed oxidative conjugation with catechols. *Insect Biochem. Mol. Biol.* 36, 353–365. doi: 10.1016/j.ibmb.2006.01.012

Sutherland, O. R. W. (1969). The role of crowding in the production of winged forms by two strains of the pea aphid, *Acyrthosiphon pisum*. *J. Insect Physiol.* 15, 1385–1410. doi: 10.1016/0022-1910(69)90199-1

Tegelaar, K., Glinwood, R., Pettersson, J., and Leimar, O. (2013). Transgenerational effects and the cost of ant tending in aphids. *Oecologia* 173, 779–790. doi: 10.1007/s00442-013-2659-y

Van de Kamp, T., and Greven, H. (2010). On the architecture of beetle elytra. *Entomol. Heute* 22, 191–204.

Van Emden, H. F., and Harrington, R. (eds). (2017). *Aphids as Crop Pests*. Wallingford: CABI.

Vellichirammal, N. N., Madayiputhiya, N., and Brisson, J. A. (2016). The genomewide transcriptional response underlying the pea aphid wing polyphenism. *Mol. Ecol.* 25, 4146–4160. doi: 10.1111/mec.13749

Vukusic, P., and Sambles, J. R. (2003). Photonic structures in biology. *Nature* 424:852. doi: 10.1038/nature01941

Wang, D., Liu, Q., Li, X., Sun, Y., Wang, H., and Xia, L. (2015). Double-stranded RNA in the biological control of grain aphid (*Sitobion avenae* F.). *Funct. Integr. Genomic* 15, 211–223. doi: 10.1007/s10142-014-0424-x

Wang, X. X., Zhang, Y., Zhang, Z. F., Tian, H. G., and Liu, T. X. (2016). Deciphering the function of octopaminergic signaling on wing polyphenism of the pea aphid *Acyrthosiphon pisum*. *Front. Physiol.* 7:603. doi: 10.3389/fphys.2016.00603

Wigglesworth, V. B. (1990). The distribution, function and nature of "cuticulin" in the insect cuticle. *J. Insect Physiol.* 36, 307–313. doi: 10.1016/0022-1910(90)90011-4

Wise, R. A. (1978). Catecholamine theories of reward: a critical review. *Brain Res.* 152, 215–247. doi: 10.1016/0006-8993(78)90253-6

Wratten, S. D. (1977). Reproductive strategy of winged and wingless morphs of the aphids *Sitobion avenae* and *Metopolophium dirhodum*. *Ann. Appl. Biol.* 85, 319–331. doi: 10.1111/j.1744-7348.1977.tb01918.x

Zehnder, C. Y., and Hunter, M. D. (2007). A comparison of maternal effects and current environment on vital rates of *Aphis nerii*, the milkweed–oleander aphid. *Ecol. Entomol.* 32, 172–180. doi: 10.1111/j.1365-2311.2007.00853.x

Zhang, Y., Wang, X. X., Zhang, Z. F., Chen, N., Zhu, J. Y., and Tian, H. G. (2016). Pea aphid *Acyrthosiphon pisum* sequesters plant-derived secondary metabolite L-DOPA for wound healing and UVA resistance. *Sci. Rep.* 6:23618. doi: 10.1038/srep23618

Conflict of Interest: The authors declare that the research was conducted in the absence of any commercial or financial relationships that could be construed as a potential conflict of interest.

frontiers in Genetics

ORIGINAL RESEARCH
published: 06 May 2020
doi: 10.3389/fgene.2020.00451

Imaginal Disc Growth Factor 6 (Idgf6) Is Involved in Larval and Adult Wing Development in *Bactrocera correcta* (Bezzi) (Diptera: Tephritidae)

*Yan Zhao, Zhihong Li, Xinyue Gu, Yun Su and Lijun Liu**

Department of Entomology, College of Plant Protection, China Agricultural University, Beijing, China

In insects, imaginal disk growth factors (IDGFs), an important component of the glycoside hydrolase 18 (GH18) family of chitinases, have been reported to be associated with the maintenance of the cuticle and molting. However, there is little knowledge of their function. In this study, imaginal disk growth factor 6 (*Idgf6*), which is an *Idgf*, was first identified and cloned from the guava fruit fly *Bactrocera correcta* (Bezzi) (Diptera: Tephritidae), one of the most serious pest insects in South China and surrounding Southeast Asian countries. This gene encodes IDGF6 protein with a conserved domain similar to ChiA chitinases, the glycoside hydrolase 18 (GH18) family of chitinases, according to NCBI BLAST. Phylogenetic analysis indicated that all *Idgf6s* were highly conserved among similar species. Subsequent temporal expression profiling revealed that *Idgf6* was highly expressed in both the late-pupal and mid-adult stages, suggesting that this gene plays a predominant role in pupal and adult development. Furthermore, RNA interference experiments against *Idgf6* in *B. correcta*, which led to the specific decrease in *Idgf6* expression, resulted in larval death as well as adult wing malformation. The direct effects of *Idgf6* silencing on *B. correcta* indicated its important role in development, and *Idgf6* might be further exploited as a novel insecticide target in the context of pest management.

Keywords: *Bactrocera correcta*, imaginal disk growth factor 6, RNA interference, death, wing malformation

OPEN ACCESS

Edited by:
Zhongxia Wu,
Henan University, China

Reviewed by:
Aishwarya Swaminathan,
University of Massachusetts Medical School, United States
Jyung-Hurng Liu,
National Chung Hsing University, Taiwan

****Correspondence:***
Lijun Liu
ljliu@cau.edu.cn

Specialty section:
This article was submitted to Epigenomics and Epigenetics, a section of the journal Frontiers in Genetics

Received: *02 February 2020*
Accepted: *14 April 2020*
Published: *06 May 2020*

Citation:
Zhao Y, Li Z, Gu X, Su Y and Liu L (2020) Imaginal Disc Growth Factor 6 (Idgf6) Is Involved in Larval and Adult Wing Development in Bactrocera correcta (Bezzi) (Diptera: Tephritidae). Front. Genet. 11:451. doi: 10.3389/fgene.2020.00451

INTRODUCTION

The epithelial apical extracellular matrix (ECM) is a specialized structure comprising secreted or transmembrane fibrous proteins and polysaccharides, whose composition varies widely, from chitinaceous cuticles of insects to cellulose in plants (Özturk-Çolak et al., 2016; Vuong-Brender et al., 2017; Cosgrove, 2005). Cuticle of insects is an exoskeleton covering the body and internal organs as an epithelial surface Exoskeleton is essential for controlling body shape, epithelial barrier formation, and epidermal wound healing and protects cells from direct contact with pathogens, toxins or pesticides (Galko and Krasnow, 2004; Yoshiyama et al., 2006; Moussian and Uv, 2010; Uv and Moussian, 2010; Turner, 2009; Toshio et al., 2010). It also further provides a challenge to maintain homeostasis of body fluids (Jaspers et al., 2014). Moreover, recent work has established an important role of the ECM in shaping various organs, such as *Drosophila* wings (Fernandes et al., 2010). Based on the conservation of amino acid sequences, several conserved motifs and protein

folding, chitinase has been divided into two families, named family 18 and family 19 glycosyl hydrolases (Coutinho and Henrissat, 1999; Henrissat, 1999). The glycoside hydrolase 18 (GH18) family, due to its characteristic glycol-18 domain, is a key family in insects that is widely distributed in all kingdoms, including bacteria, plants and animals (Tsai et al., 2001; Zhu Z. et al., 2004; Zhu et al., 2008a; Arakane and Muthukrishnan, 2010; Zhang et al., 2011a; Huang et al., 2012; Hussain and Wilson, 2013). Previous studies have shown that insects utilize multiple GH18 family chitinolytic enzymes for degrading, remodeling and binding to chitin and possibly for chitin synthesis (Zhu Q.S. et al., 2004).

Polypeptide factors with mitotic activity in invertebrates were first reported to be encoded by imaginal disk growth factors (IDGFs), belonging to group V chitinase, which are an important member of the GH18 family (Žurovcová and Ayala, 2002). *Idgfs* were originally identified and isolated from *Drosophila* S2 or imaginal disk cells on conditioned media (Kirkpatrick et al., 1995; Kawamura et al., 1999). In *Drosophila melanogaster*, there are six genes encoding IDGFs including *Idgf1*, *Idgf2*, *Idgf3*, *Idgf4*, *Idgf5*, and *Idgf6* (Kirkpatrick et al., 1995; Kawamura et al., 1999; Bryant, 2001; Varela et al., 2002). According to previous studies, in imaginal disk cell culture, *Idgfs* promote growth, proliferation, cell polarization, and motility (Kawamura et al., 1999). Some IDGFs are required for normal ECM formation, larval and adult molting or innate immune responses and wound healing (Zhang et al., 2011b; Kucerovaa et al., 2016; Pesch et al., 2016; Broz et al., 2017). Some studies have focused on the function of individual *Idgf* genes; for example, by individually knocking down genes in cuticle-secreting tissues, a large number of *Idgfs* have been shown to be involved in cuticle molting during the larval and pupal stages. This result was then supported by gene-specific spatial-temporal expression profiles and by developmental lethality profiles upon gene knockdown. Moreover, after the genes were knocked down, the mutants were highly susceptible to mechanical stresses and bacterial infections (Pesch et al., 2016). The non-enzymatic *Idgfs* play an important role in protecting newly synthesized cuticle matrix from degradation, which can stabilize and expand the size of ECM in larvae (Pesch et al., 2016). The target gene of our study, *Idgf6*, is one of the first identified *Idgf* genes; *Idgf6* was isolated by Kirkpatrick et al. and localized on the second chromosome at 53D (*Idgf6* is synonymous to Cht13 and DmDS47) (Kirkpatrick et al., 1995; Zhang et al., 2011b). Pesch et al. investigated the molecular network in *Idgf6* RNAi-induced mutants and showed that *Idgf6* RNAi-induced mutants exhibited the strongest lethality and most severe cuticle defects among other mutants (Pesch et al., 2016). *Idgf6* is critical for larval cuticle barrier formation and protection against invasive microorganisms and mechanical stresses (Pesch et al., 2016). Overall, few studies of this gene have focused on larval development, and knowledge of this gene in insect pupal and adult development is limited.

The guava fruit fly *Bactrocera correcta* (Bezzi) (Diptera: Tephritidae) is an economically important insect pest that is widely distributed in South China and other surrounding Southeast Asian countries (Liang et al., 1996; Drew and Raghu, 2002). This fruit fly infests a wide variety of types of commercial fruits, including guava, mango and peach, and vegetables in tropical and subtropical regions of the world (Liang et al., 1996; Bezzi, 1916; White and Elsomharris, 1992). Due to its polyphagous nature, along with its highly adaptive, reproductive and dispersal capabilities, it is considered to be a highly invasive fruit pest species that has been listed as a quarantine pest species by many countries and regions (White and Elsomharris, 1992). Therefore, the control of the guava fruit fly is thus increasingly important. Insect cuticle and molting have been the focuses of pest control research; consequently, clarification of insect *Idgf* gene expression should provide new knowledge that is useful for pest control (Togawa et al., 2007). Although *Idgfs* have been studied systematically in model insects such as *D. melanogaster*, relevant information is limited in*B. correcta*.

In the current study, we first cloned and identified the full-length cDNA of *Idgf6* from *B. correcta*, and previously, little was known about *Idgf6* in nonmodel organisms. We then analyzed the temporal expression pattern of *Idgf6* in eight different developmental stages of *B. correcta* using qRT-PCR. RNA interference technology was applied to explore the function of *Idgf6* in *B. correcta* at larval and adult stages. The *Idgf6* gene was found to play an important role in fruit fly development. Silencing of the *Idgf6* gene resulted in larval death and adult wing malformation. Our data reveal a critical role for *Idgf6* in

TABLE 1 | Primers used for cloning, real-time qRT-PCR amplification and dsRNA synthesis.

Gene	Primer	Sequence	Size (bp)
Bc 18s rRNA-rt	*18s*-rt-F	5'- GCGAGAGGTGAAATTCTTGG -3'	192
	18s-rt-R	5'- CGGGTAAGCGACTGAGAGAG -3'	
Bc Idgf6-rt	*Idgf6*-rt-F	5'-CGGACGAGAAGAGCAGC-3'	176
	Idgf6-rt-R	5'-GGCACGCAGTATGGGAT-3'	
Bc cloneIdgf6-1	*Idgf6*-whole seq-F	5'-GCGTGTATTTGCTTGTTG-3'	1398
	Idgf6-whole seq-R	5'-CGCAGTATGGGATATTTATC-3'	
Bc dsIdgf6	*Idgf6*-dsRNA-F	5'-AGCTGCCCTTGCGTGTAT-3'	542
	Idgf6-dsRNA-R	5'-GAACCATCAGCGCCTTCA-3'	

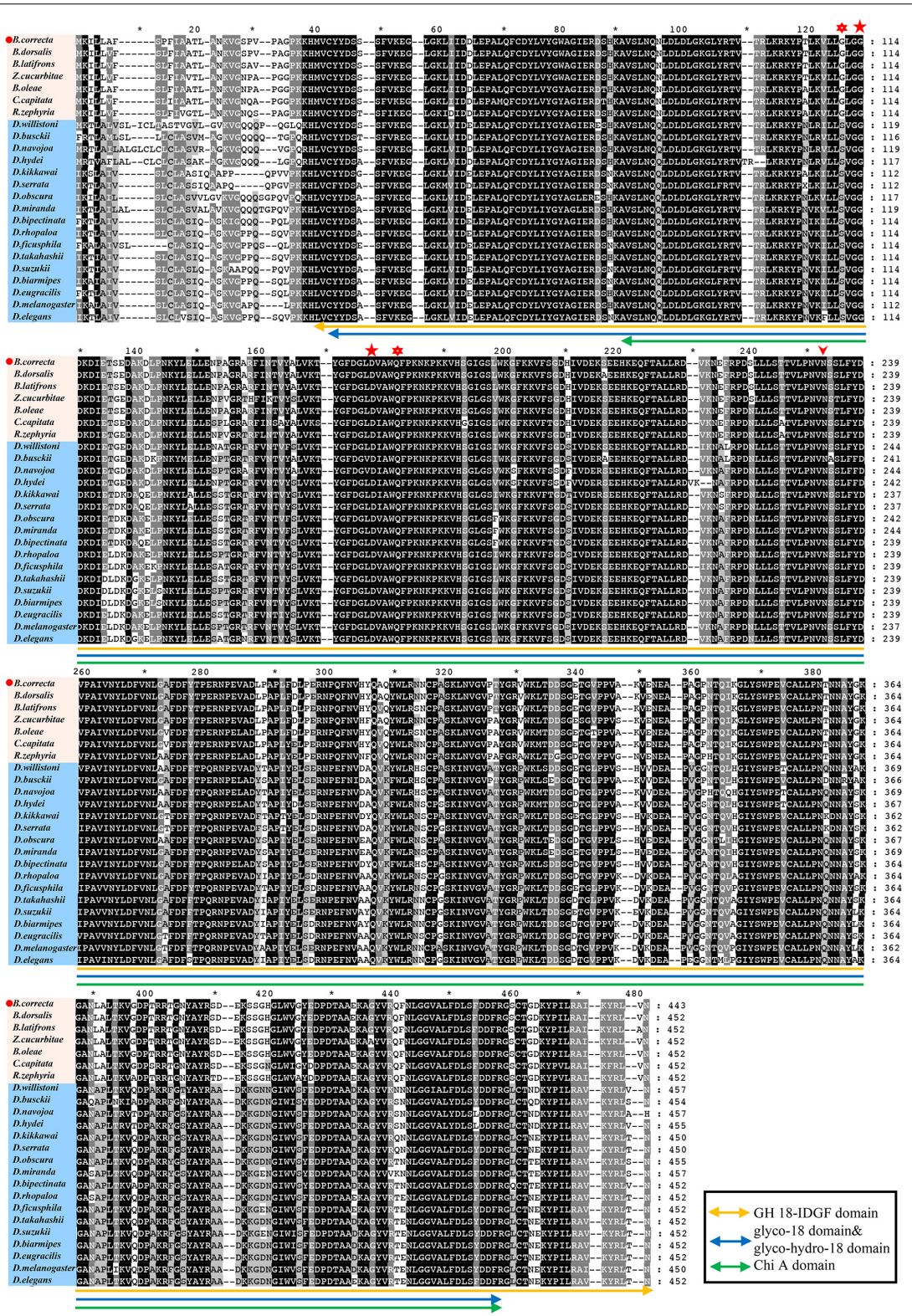

FIGURE 1 | Protein sequence alignments of IDGF6 proteins in Drosophilidae and Tephritidae fruit flies based on NCBI BLAST results. The alignments that present one predicted and conserved domain similar to ChiA chitinases, the glycoside hydrolase 18 (GH18) family of chitinases. Asterisks and star indicate the positions of residues that have been shown to be required for catalytic activity in bacterial chitinase (Watanabe et al., 1993). For the species both in Drosophilidae and Tephritidae, the second and third (star) match the required residues in chitinases, but the fourth (asterisks) is E in chitinases while Q in IDGFs. As for the first (asterisks), in Drosophilidae it is S, which matches the required residues in chitinases, but in Tephritidae it is G. All species IDGF sequences contain single consensus motif (arrowhead) for N-linked glycosylation (Kirkpatrick et al., 1995) that is missing in chitinase.

insect development and thus provide new insights into pest management.

MATERIALS AND METHODS

Experimental Insects

The *B. correcta* population used in this study was collected from Yunnan Province and was cultured in the laboratory at 25 ± 0.5 °C with 65 ± 5% relative humidity under a 14 h light/10 h dark photoperiod. All adults were maintained under the same conditions before starting the experiments to ensure the consistency of the experimental materials. The population had been cultured for approximately 10 generations to eliminate the influence of the local environment. The insects were fed artificial diets as previously described (Yuan et al., 2006). Two hundred individuals were maintained in three insect rearing cages (45 cm × 45 cm × 50 cm) in this experiment.

For temporal expression analysis, we collected samples from different stages: 1st instar larvae (2-day-old indicates 2 days post hatching), 3rd early instar larvae (5-day-old), 3rd instar larvae (7-day-old), early pupae (1-day-old indicates 1 day post pupating), medium pupae (5-day-old), late pupae (9-day-old), early adults (1 day post eclosion), and late adults (10 days post eclosion). Each stage had five replicates, and different numbers of individuals at each stage were collected to detect the expression because of different sizes of insects. Fifty individuals for 1st instar larvae, thirty individuals for 3rd instar larvae and all the pupa stages, ten for the adult stages. For the functional study, five replications were performed for each treatment, and each replicate contained 30 larvae. And for the functional study of the larval stage and adult stage, we obtained samples from 3rd instar larvae and 2-day-old adults, respectively. The samples were immersed in an RNA storage reagent (Tiangen, Beijing, China), immediately frozen with liquid nitrogen and stored at −80°C for further experiments.

Bioinformatics Analysis

RNA Extraction, Reverse Transcription, and cDNA Synthesis

RNA was extracted from the whole body using the RNAsimple Total RNA Kit (Tiangen, China) in accordance with the manufacturer's protocol. The extracted RNA was immediately dissolved in RNase-free water, and then was checked for quality, concentration, and purity using a NanoVue UV–Vis spectrophotometer (GE Healthcare Bio-Sciences, Uppsala, Sweden) at 260 and 280 nm. RNA integrity was checked by 1% agarose gel electrophoresis at 180 V for 16 min. Five biological replicates were conducted per treatment. Finally,

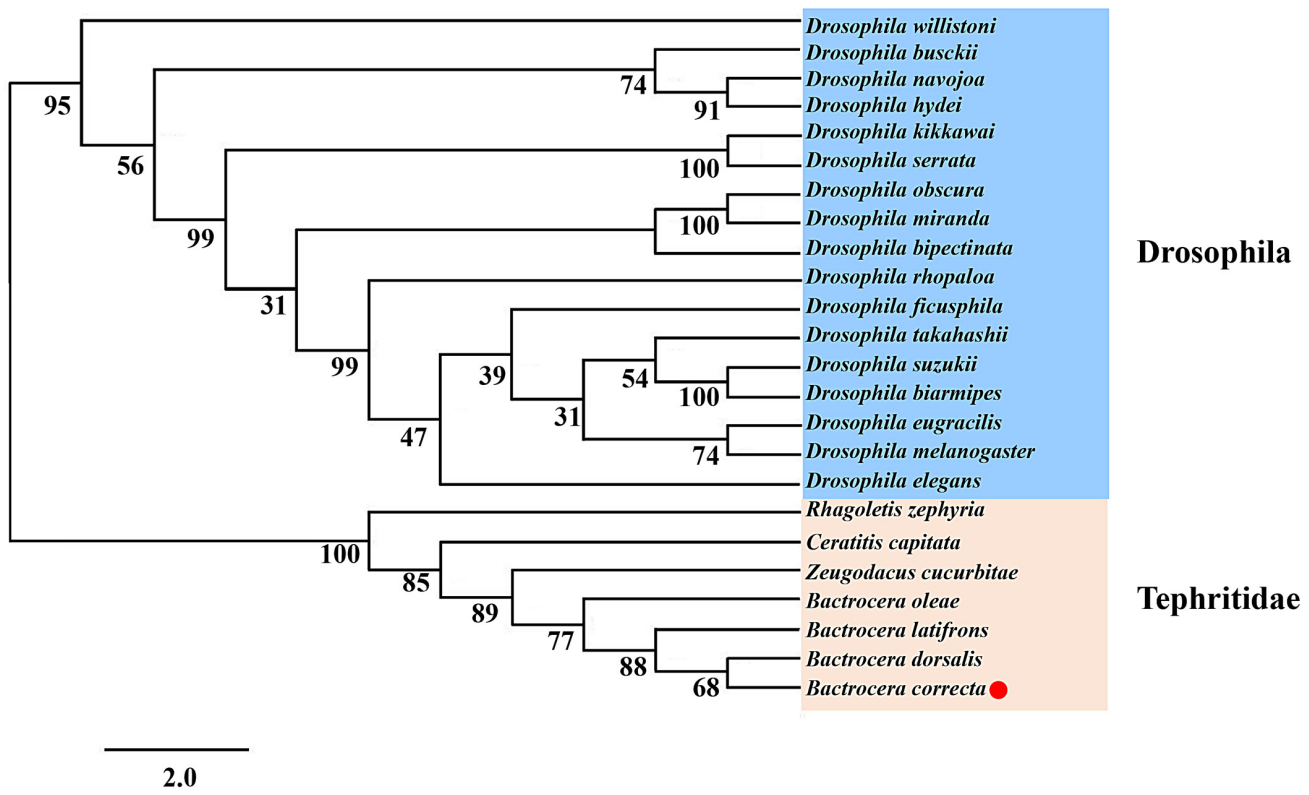

FIGURE 2 | Phylogenetic analysis of *Idgf6* using the maximum-likelihood method in RAxML. One hundred bootstrap iterations were conducted to obtain branch support values. The *B. correcta Idgf6* sequence we obtained is labeled with a red triangle. The amino acid and nucleotide sequences were downloaded from NCBI. The accession numbers of the genes are designated with the corresponding abbreviations and are listed in **Supplementary Table S1**.

first-strand cDNA was synthesized from 1000 ng of total RNA using the PrimeScript@ RT reagent Kit with gDNA Eraser (Perfect Real Time) (Takara, Japan) following the manufacturer's instructions.

ORF Cloning of *B. correcta Idgf6* and Sequence Analysis

To verify the ORF of *Idgf6* in *B. correcta*, primers were designed based on the conserved regions of *Idgf6* in *B. oleae*, *Ceratitis capitata*, and *D. melanogaster* (sequence from GenBank) and the sequence of *Idgf6* from the *B. correcta* transcriptome (No. MK450457). DNAMAN v.6.03 (Lynnon Biosoft, San Ramon, CA, United States) was used for sequence alignment. The primers for cloning are listed in **Table 1**. The open-reading frame (ORF) sequence of *Idgf6* was amplified using PrimeSTAR high-fidelity DNA polymerase (Takara, Dalian, China) following the manufacturer's protocol. The PCR products were isolated, purified and ligated into a pGEM-T Easy vector (Promega, Beijing, China) and sequenced by a company (BGI, Beijing, China).

The ORF and conserved domain were identified with ORF Finder software[1] and NCBI BLAST results[2]. To predict the conserved domains of *B. correcta Idgf6*, *Idgf6* protein sequences from 23 species in Drosophilidae and Tephritidae were collected by BlastP in GenBank (**Supplementary Table S1**) and aligned with the sequence of *B. correcta Idgf6* with ClustalX 2 software and GeneDoc 2.7.0 (Nicholas et al., 1997; Larkin et al., 2007).

Phylogenetic Analysis

The integrity of homologous amino acid sequences of other species was retrieved from the NCBI server. Sequences were first aligned by the conserved sequences using Geneious v10.22 (Kearse et al., 2012), and then phylogenetic analysis was performed using the maximum-likelihood method with RAxML software (Stamatakis, 2014). One thousand bootstrap iterations were conducted to obtain branch support values.

Temporal Expression Pattern of *Idgf6* by qRT-PCR

Following first-strand cDNA synthesis of *Idgf6*, qRT-PCR was performed using SYBR® Premix Ex Taq™ II (Tli RNaseH Plus) (Takara, Japan) on an ABI 7500 instrument (United States). The thermocycler conditions were 95°C for 30 s, followed by 40 cycles at 95°C for 5 s and 52°C for 34 s. Melting curve analysis was performed at the end of each expression analysis using the following conditions: 95°C for 15 s, followed by 52°C for 60 s. The sequences of the qRT-PCR primers used for the reference and target genes are described in **Table 1**. The relative expression level was calculated using the $2^{-\Delta\Delta CT}$ method (Chen and Wagner, 2012), with 18S rRNA as the reference gene (Gu et al., 2019). Fold changes were determined after the relative expression values were standardized using the lowest value.

Silencing of *Idgf6* by RNAi

Double-stranded RNA of *Idgf6* (ds*Idgf6*) was used to knock down *Idgf6* expression, and double-stranded RNA of green fluorescent protein (ds*GFP*) was used as the negative control. We synthesized dsRNAs with the T7 RiboMAX Express RNAi system (Promega, United States) using specific primers containing a T7 promotor sequence (**Table 1**). Then, dsRNA was purified using phenol, chloroform and ethanol, according to the manufacturer's instructions, and dissolved in RNase-free water.

The 3rd early instar larvae (5-day-old) of *B. correcta* were collected and placed into a 50 ml tube with 3 holes on the lid. Five replications were performed for each treatment, and each replicate contained 30 larvae. Three grams of artificial diet material with 30 μl of a dsRNA solution was used for feeding, and the concentration of the dsRNA solution for the primary exposure was 1000 ng/μl. The larvae were first fed with ds*GFP* and ds*Idgf6* for 48 h, and then transferred to a new artificial diet with the same treatment for another 48 h. After 96 h, the larvae developed to maturity. Larval mortality was counted, and larval body size was measured; 5 larvae were killed for RNAi efficiency detection. The remaining individuals were fed until the adult stage was reached and were used for phenotype observation on the 2nd day after emergence. The mortality of emerged individuals was recorded twenty days after the flies emerged.

Statistical Analysis

All experiments included five biological replicates. Statistical analysis was performed using SPSS 20 (IBM Corporation, United States). One-way ANOVA followed by Tukey's HSD tests was applied to gene expression data to test for significant differences among different developmental stages, and the

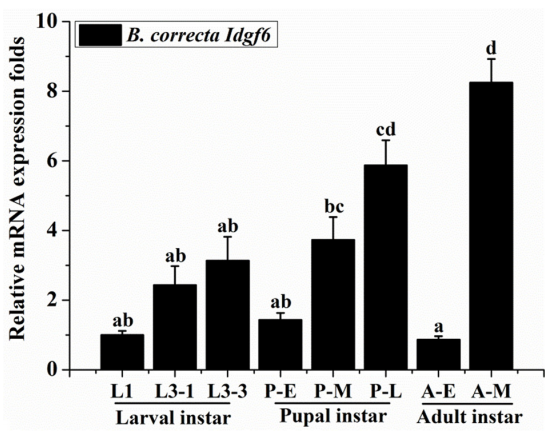

FIGURE 3 | The expression of *Idgf6* at eight developmental stages of *B. correcta*. The eight developmental stages examined include the 1st instar larvae (L1, 2-day-old indicates 2 days post hatching), 3rd early instar larvae (L3-1, 5-day-old), 3rd instar larvae (L3-3, 7-day-old), early pupae (P-E, 1-day-old indicates 1 day post pupating), medium pupae (P-M, 5-day-old), and late pupae (P-L, 9-day-old), early adults (A-E, 1 day post eclosion) and late adults (A-M, 10 days post eclosion). The results are presented as the relative expression after normalization against the endogenous *18S rRNA* gene. Expression is relative to the gene expression in 1st instar larvae (assigned a value of 1), and the same letter means there are no significant differences. Different letters above the bars represent significant differences at $P < 0.05$, as determined by ANOVA followed by Tukey's HSD tests.

[1]http://www.ncbi.nlm.nih.gov/gorf/gorf.html

[2]http://blast.ncbi.nlm.nih.gov/Blast.cgi

means were separated using a least significant difference test at a significance level of $P < 0.05$. An independent samples *t*-test ($P < 0.05$ and $P < 0.01$) was used to determine the significance of differences between the treatment and control in the dsRNA injection assay. All data are expressed as mean ± standard error (SE).

RESULTS

Cloning and Characterization of *Idgf6*

Idgf6 (GenBank accession no. MK450457) was cloned from *B. correcta*. Five ORFs, which were 1254 bp encoding 465 amino acids, were identified. Preliminary predictions of the conserved domains of the IDGF6 protein with NCBI BLAST showed that one conserved domain similar to ChiA chitinases, the glycoside hydrolase 18 (GH18) family of chitinases was predicted (**Figure 1**). Compared to the *Drosophila* species, which has one amino acid substituent, there are two amino acid substituents in the Tephritid fruit flies, which can eliminate the catalytic activity of chitinase (**Figure 1**). Besides, among all the Tephritid fruit flies, we found that there was one type of gene with the same domain as the phylogenetic tree (**Figures 1, 2**). Nucleotide sequence analysis revealed that the *Idgf6* of *B. correcta* had the highest identity with a homolog from *B. dorsalis* (96.73%), followed by the *Idgf6* of *B. oleae* (92.82%), *Zeugodacus cucurbitae* (90.67%), and *B. latifrons* (88.52%). Compared to the similar *Drosophila* species, the sequence had the highest identity with *Idgf6* of *D. navojoa* (73.44%).

Using the protein sequences, we analyzed the phylogenetic relationships between *Idgf6* in *B. correcta* and other *Idgf6s* with the maximum-likelihood method. The phylogenetic tree revealed the relationship between insect *Idgf6*s (**Figure 2**). All *Idgf6*s were highly conserved among similar species. The *Idgf6* in *B. correcta* was clustered close to that in *B. dorsalis*. We clearly observed that *Idgf6s* of the Tephritid fruit flies and the *Drosophila* fruit flies were clustered in two branches of the phylogenetic tree. The amino acid sequence alignment and evolutionary relationship suggested that *Idgf6s* were highly conserved among the Tephritid species.

Expression of *Idgf6* in Eight Different Developmental Stages of *B. correcta*

Using qRT-PCR, the expression levels of *Idgf6* differed significantly in certain developmental stages (Tukey HSD tests: $P < 0.05$). In the larval stage, *Idgf6* was expressed in the 1st instar and tended to stabilize until the 3rd instar. In the pupal stage, a lower level of mRNA expression was detected in early pupae, and its expression rose during medium pupae and reached the second highest level in late pupae ($P = 0.000$). In adults, the relative expression of *Idgf6* in late adults was significantly higher than that in early adults, and the highest expression level was measured in late adult individuals ($P = 0.001$). Overall,

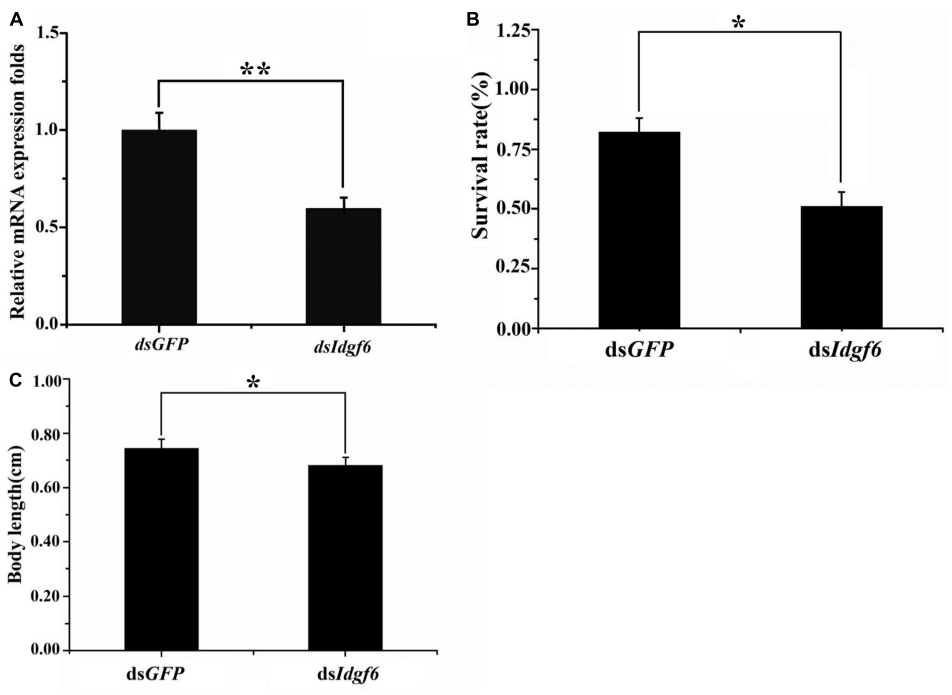

FIGURE 4 | Effect of silencing *Idgf6* in *B. correcta*. **(A)** The relative expression level of *Idgf6* after feeding ds*Idgf6*. **(B)** Larvae survival rate after exposure to dsRNA. **(C)** Larval body sizes after exposure to dsRNA. All the fruit flies in the functional study shown in **Figure 4** were 5-day-old 3rd early instar larvae exposed to dsRNA at a concentration of 1000 ng/μl for 96 h at 25 °C. Five replicates were conducted and the data were presented as mean ± SE. **indicates a statistically significant difference in *Idgf6* mRNA expression between the ds*Idgf6* group and the control ds*GFP* groups (*t*-tests: $P < 0.01$). *indicates a statistically significant difference in survival and body length between the ds*Idgf6* group and the control ds*GFP* group (*t*-test: $P < 0.05$).

within each stage, *Idgf6* expression is gradually up-regulated and specially enriched at the late (**Figure 3**). The different expression levels indicate that *Idgf6* has special physiological roles in different developmental stages.

Knocking Down *Idgf6* Caused Larval Death and Adult Malformation of *B. correcta*

The Functional Study of the Larval Stage

After 3rd early instar larvae of *B. correcta* were exposed to ds*Idgf6* at 1000 ng/μl for 96 h, the mRNA expression level of *Idgf6* was significantly reduced by 41.2% (P = 0.008) (**Figure 4A**). We also investigated the phenotypic changes of recipient insects after dsRNA treatment. Obvious increases in mortality were observed in treatment groups throughout the feeding period which increased by 37.8% as compared to the control ds*GFP* group (**Figure 4B**). Then, we measured the body size after feeding. The body sizes of surviving larvae in ds*GFP* and ds*Idgf6* groups were 0.7438 ± 0.1636 and 0.6861 ± 0.1452 after feeding, respectively. Thus, body size for the ds*Idgf6* group decreased by 8.4 % when compared to the control ds*GFP* group (**Figures 4C**, **5A**).

The Functional Study of the Pupal Stage

After all the fruit flies emerged, some individuals per treatment were found to exhibit two types of malformation compared with individuals fed ds*GFP* (**Figures 5B,C**). One type led to smaller body sizes, which accounted for 13.33%, and the other resulted in partly extensible wings, accounting for 6.67%, which led to a loss of flight capacity (**Figures 5D,E**). During subsequent development, 100% of deformed adults died before sexual maturity, approximately 5 days after emergence. In addition, there were no dead or malformed flies in the control groups, and all the flies lived for more than half a month.

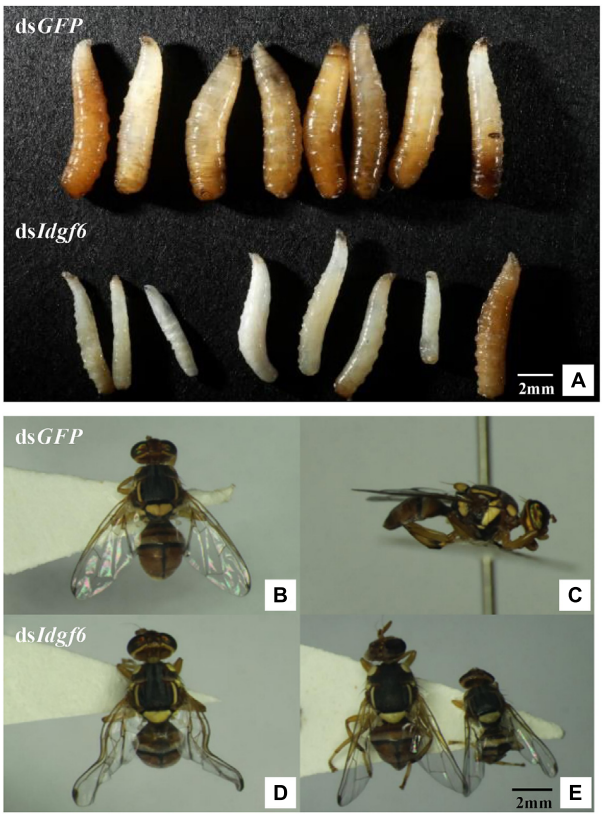

FIGURE 5 | *B. correcta* larval and adult malformed individuals after silencing. **(A)** Malformed phenotype of larvae after feeding ds*GFP* and ds*Idgf6*. **(B)** Front view of the phenotype of adults after feeding ds*GFP*. **(C)** Side view of the phenotype of adults after feeding ds*GFP*. **(D)** First type of malformed phenotype observed in adults after feeding ds*Idgf6*, which resulted in partly extended wings. **(E)** Second type of malformed phenotype of adults after feeding ds*Idgf6*, which led to smaller fruit flies.

DISCUSSION

In this study, the full-length cDNA sequence of *Idgf6* was cloned from *B. correcta*. There is one predicted and conserved domain in *B. correcta Idgf6* protein similar to ChiA chitinases, the glycoside hydrolase 18 (GH18) family of chitinases was predicted. In *D. melanogaster*, IDGFs have eight-chain alpha/beta barrel fold associated with GH 18 chitinase, but they have a known amino acid substituent that can eliminate the catalytic activity of chitinase (Kawamura et al., 1999). However, we found there are two amino acid substituents in the Tephritid fruit flies (**Figure 1**), which may play a similar role in eliminating the catalytic activity of chitinase. The presence of Chi A domain may indicate that *Idgf6* evolved from chitinases and gained new functions as a growth factor with the interaction of cell surface glycoproteins (Kawamura et al., 1999; Varela et al., 2002). Finally, using *Idgf6* nucleotide sequences of Drosophilidae and Tephritidae in GenBank, we applied the maximum-likelihood method to obtain a phylogenetic tree. *Idgf6* in *B. correcta* has high identity with homologues in other Tephritid fruit flies (**Figure 2**), and *Idgf6* in *B. correcta* has the closest relationship to *B. dorsalis Idgf6*.

Idgf genes play an important role in promoting growth, proliferation, cell polarization, and motility (Kawamura et al., 1999). In the present study, an examination of the temporal expression pattern of *Idgf6* revealed that the gene was detectable throughout the development of the insect and highly expressed in the late pupa and adult stages, with lower expression observed in other stages. These results indicate that this gene may play an important role in the whole stage of insect development, mainly in the pupa and adult stages. This result is consistent with previous findings in *D. melanogaster*, in which analysis of DS47 (IDGF6) protein production and mRNA expression during fly development indicated that both are present throughout the entire *D. melanogaster* life cycle, but are relatively lower in the embryos stage (Wang et al., 2009; Pesch et al., 2016). *Idgf6* is expressed in the cuticle producing organs, the mouth hooks, the epidermis, the tracheal system and the posterior spiracles, and especially in larvae, its message is made in the fat body and by hemocytes and secreted into the hemolymph

(Kirkpatrick et al., 1995; Pesch et al., 2016). Besides these, it's very interesting that within each stage, *Idgf6* expression is gradually up-regulated and specially enriched at the late, which may match its special requirement for molting into the next stage (Pesch et al., 2016).

Idgf6 was depleted at the larval stage, which caused partial larval death and adult wing malformation. However, the percentage of malformation was low, and the potential overlapping function between the six IDGF proteins could contribute to the incomplete penetrance in the RNAi experiments. These experimental results imply that *Idgf6* in *B. correcta* is related to larval mortality and adult wing development. Insect body contains hard, insoluble chitin, which is part of the exoskeleton, trachea, and the peritrophic membrane (PM) that surrounds the midgut food (Merzendorfer and Zimoch, 2003). Chitin is found in a number of different structures in addition to the cuticle and PM (Wilson and Cryan, 1997) whose synthesis occurs throughout insect development, including embryonic, larval, pupal and adult stages (Zhu Q.S. et al., 2004). Chitin in organs provides protection to insects against environmental and mechanical injuries, but it limits the growth and development of insects. Thus, the cuticles and PM are degraded periodically and reshuffled to allow growth and development (Merzendorfer and Zimoch, 2003). Insect chitinase plays a key role in degrading chitin in the old cuticles and PM during the larval molting and purulent process, and chitinase also plays a defensive role to prevent bacteria and fungi from penetrating PM. Therefore, in this study, knocking down the *Idgf6* gene in the larval stage may result in a decrease in the ability to degrade chitin in the old cuticles and a limitation in body size elongation. The decline in defensive ability makes the larvae susceptible to infection by bacteria, fungi, etc., resulting in an increase in larval mortality. According to a previous study, chitin is associated with wing joints in *B. dorsalis*, so it is speculated that the malformation of the adult wing after interference is related to this (Gu et al., 2019).

The GH18 genes of chitinases have potential use for pest management as biopesticides (Kramer and Muthukrishnan, 1997). Homologues of these genes exist in parasites and pests harmful to mankind and agriculture, such as mosquitos, lice and spotted wing *Drosophila* (Zhang et al., 2011b; Eichner et al., 2015; Fan et al., 2015). Insect chitinase genes have been suggested as targets for gene silencing via RNAi and have also been proposed as appropriate candidates in host-mediated silencing of pest genes (HMSPGs) for the control of diseases and insect pests of date palm (Zhu et al., 2008c; Niblett and Bailey, 2012; Al-Ayedh et al., 2016; Su et al., 2016; Cao et al., 2017). Therefore, it is of interest to focus on the functions of the genes involved in development and reproduction for future pest control. The target gene in our study, the *Idgf6* gene, provides a new target for a gene-specific search of pesticides, because the epithelial barrier was damaged and caused premature death of animals, and it is more sensitive to pathogenic infections. Blast searches showed that parts of the N-terminus of *Idgf6* were not conserved among insects, providing a specific target for insecticides. This opens the possibility to search for small molecules that may inhibit the function of insect species-specific *Idgf6* without affecting beneficial organisms. Chitin-ECM is the most important insect barrier against any environmental stresses. Hydrolase enzymes affecting function and the ECM protection system provide new strategies to eliminate already problematic animals in larval stages and prevent the growth of next generation pests (Pesch et al., 2016). Our research implies that silencing the *Idgf6* gene can cause larval death and adult wing malformation. Our findings indicate an essential role of *Idgf6* in larval mortality and adult wing development. Additionally, our results provide new insights into the function of *Idgfs* family members and may reveal a new potential gene for pest control.

DATA AVAILABILITY STATEMENT

All datasets generated for this study are included in the article/**Supplementary Material**. The datasets generated for this study can be found in the GenBank accession no. MK450457.

AUTHOR CONTRIBUTIONS

YZ, XG, and LL conducted statistical analysis of the whole data. YZ wrote the draft and revised manuscript. YZ, XG, ZL, YS, and LL provided statistical expertise and were involved in data analysis and interpretation of results. LL and ZL conceived and supervised the study. All authors reviewed and made contribution to the final manuscript.

FUNDING

This research was funded by Youth project of National Natural Science Foundation of China (No. 31801802 to LL) and Beijing Nature Science Foundation (No. 6172021 to ZL).

ACKNOWLEDGMENTS

We are grateful to Shaokun Guo from China Agricultural University for providing the sequence information and analysis results in transcriptome, Shiqian Feng from China Agricultural University for providing the methods of phylogenetic analysis, and Guoping Zhan and Chen Ma from Chinese Academy of Inspection and Quarantine for providing insects for this work. We are grateful to the reviewers for their review of the manuscript.

SUPPLEMENTARY MATERIAL

The Supplementary Material for this article can be found online at: https://www.frontiersin.org/articles/10.3389/fgene.2020.00451/full#supplementary-material

REFERENCES

Al-Ayedh, H., Rizwan-ul-Haq, M., Hussain, A., and Aljabr, A. M. (2016). Insecticidal potency of RNAi-based catalase knockdown in *Rhynchophorus ferrugineus* (Olivier) (Coleoptera: Curculionidae). *Pest Manag. Sci.* 72, 2118–2127. doi: 10.1002/ps.4242

Arakane, Y., and Muthukrishnan, S. (2010). Insect chitinase and chitinase-like proteins. *Cell. Mol. Life Sci.* 67, 201–216. doi: 10.1007/s00018-009-0161-9

Bezzi, M. (1916). On the fruit-flies of the genus Dacus (s. 1.) occurring in India, Burma, and Ceylon. *Bull. Entomol. Res.* 7:99. doi: 10.1017/S0007485300017430

Broz, V., Kucerova, L., Rouhova, L., Fleischmannova, J., Strnad, H., Bryant, P. J., et al. (2017). Drosophila imaginal disc growth factor 2 is a trophic factor involved in energy balance, detoxification, and innate immunity. *Sci. Rep.* 7:43273. doi: 10.1038/srep43273

Bryant, P. J. (2001). Growth factors controlling imaginal disc growth in Drosophila. *Novart. Fdn. Symp.* 237, 182–194. doi: 10.1002/0470846666.ch14

Cao, B. D., Bao, W. H., and Wuriyanghan, H. (2017). Silencing of target chitinase genes via oral delivery of dsRNA caused lethal phenotypic effects in mythimna separate (*Lepidoptera*: *Noctuidae*). *Appl. Biochem. Biotechnol.* 181, 860–866. doi: 10.1007/s12010-016-2254-x

Chen, B., and Wagner, A. (2012). Hsp90 is important for fecundity, longevity, and buffering of cryptic deleterious variation in wild fly populations. *BMC Evol. Biol.* 12:25. doi: 10.1186/1471-2148-12-25

Cosgrove, D. J. (2005). Growth of the plant cell wall. *Nat. Rev. Mol. Cell Biol.* 6, 850–861. doi: 10.1038/nrm1746

Coutinho, P. M., and Henrissat, B. (1999). "Carbohydrate-active enzymes: an integrated database approach," in *Recent Advances In Carbohydrate Bioengineering*, eds H. H. Gilbert, G. J. Davies, H. Henrissat, and B. Svensson (Cambridge: Royal Society), 3–12.

Drew, R. A. I., and Raghu, S. (2002). The fruit fly fauna (Diptera: Tephritidae: Dacinae) of the rainforest habitat of the Western Ghats, India. *Raffles B. Zool.* 50, 2.

Eichner, C., Harasimczuk, E., Nilsen, F., Grotmola, S., and Dalvin, S. (2015). Molecular characterisation and functional analysis of LsChi2, a chitinase found in the salmon louse (*Lepeophtheirus salmonis* salmonis, Krøyer 1838). *Exp. Parasitol.* 15, 39–48. doi: 10.1016/j.exppara.2015.01.011

Fan, X. J., Mi, Y. X., Ren, H., Zhang, C., Li, Y., and Xian, X. X. (2015). Cloning and functional expression of a chitinase cDNA from the apple leaf miner moth Lithocolletis ringoniella. *Biochem. Biokhimiia.* 80, 242–250. doi: 10.1134/S000629791502011X

Fernandes, I., Chanut-Delalande, H., Ferrer, P., Latapie, Y., Waltzer, L., Affolter, M., et al. (2010). Zona pellucida domain proteins remodel the apical compartment for localized cell shape changes. *Dev. Cell.* 18:76. doi: 10.1016/j.devcel.2009.11.009

Galko, M. J., and Krasnow, M. A. (2004). Cellular and genetic analysis of wound healing in drosophila Larvae. *PLoS. Biol.* 2:e239. doi: 10.1371/journal.pbio.0020239

Gu, X. Y., Li, Z. H., Su, Y., Zhao, Y., and Liu, L. (2019). Imaginal disc growth factor 4 regulates development and temperature adaptation in *Bactrocera dorsalis*. *Sci. Res.* 9:931. doi: 10.1038/s41598-018-37414-9

Henrissat, B. (1999). "Classification of chitinases modules," in *Chitin and Chitinases*, Vol. 87, eds P. Jolles and R. A. A. Muzzarelli (Basel: Birkhauser Verlag), 138–156.

Huang, Q. S., Xie, X. L., Liang, G., Gong, F., Wang, Y., Wei, X. Q., et al. (2012). The GH18 family of chitinases: their domain architectures, functions and evolutions. *Glycobiology* 22, 23–34. doi: 10.1093/glycob/cwr092

Hussain, M., and Wilson, J. B. (2013). New paralogues and revised time line in the expansion of the vertebrate GH18 family. *J. Mol. Evol.* 76, 240–260. doi: 10.1007/s00239-013-9553-4

Jaspers, M. H., Pflanz, R., Riedel, D., Kawelke, S., Feussner, I., and Schuh, R. (2014). The fatty acyl-CoA reductase Waterproof mediates airway clearance in Drosophila. *Dev. Biol.* 385, 23–31. doi: 10.1016/j.ydbio.2013.10.022

Kawamura, K., Shibata, T., Saget, O., Peel, D., and Bryant, P. J. (1999). A new family of growth factors produced by the fat body and active on Drosophila imaginal disc cells. *Development* 126, 211–219. doi: 10.1016/S0070-2153(08)60381-6

Kearse, M., Moir, R., Wilson, A., Stones-Havas, S., Cheung, M., Sturrock, S., et al. (2012). Geneious basic: an integrated and extendable desktop software platform for the organization and analysis of sequence data. *Bioinformatics* 28, 1647–1649. doi: 10.1093/bioinformatics/bts199

Kirkpatrick, R. B., Maticob, R. E., McNulty, D. E., Stricklerband, J. E., and Rosenberga, M. (1995). An abundantly secreted glycoprotein from Drosophila melanogaster is related to mammalian secretory proteins produced in rheumatoid tissues and by activated macrophages. *Gene* 153:154. doi: 10.1016/0378-1119(94)00756-i

Kramer, K. J., and Muthukrishnan, S. (1997). Insect chitinases: molecular biology and potential use as biopesticides. *Insect Biochem. Mol. Biol.* 27, 887–900. doi: 10.1016/j.ibmb.2011.03.001

Kucerovaa, L., Brozb, V., Arefina, B., Maaroufia, H. O., Hurychovaa, J., Strnadd, H., et al. (2016). The Drosophila chitinase-like protein IDGF3 is involved in protection against nematodes and in wound healing. *J. Innate Immun.* 8, 199–210. doi: 10.1159/000442351

Larkin, M. A., Blackshields, G., Brown, N. P., Chenna, R., McGettigan, P. A., McWilliam, H., et al. (2007). Clustal W and clustal X version 2.0. *Bioinformatics* 23, 2947–2948. doi: 10.1093/bioinformatics/btm404

Liang, G. Q., Yang, G. H., Liang, F., Situ, B. L., and Liang, X. D. (1996). Directory of bactrocera in Asia-Pacific(Chinese). *Inspect. Q. Depart. Entry* 1, 40–42.

Merzendorfer, H., and Zimoch, L. (2003). Chitin metabolism in insects: structure, function and regulation of chitin synthases and chitinases. *J. Exp. Biol.* 206, 4393–4412. doi: 10.1242/jeb.00709

Moussian, B., and Uv, A. E. (2010). An ancient control of epithelial barrier formation and wound healing. *Bioessays* 27, 987–990. doi: 10.1002/bies.20308

Niblett, C. L., and Bailey, A. M. (2012). Potential applications of gene silencing or RNA interference (RNAi) to control disease and insect pests of date palm. *Emir. J. Food Agric.* 24, 462–469.

Nicholas, K., Nicholas, H., Nicholas, K. B., Nicholas, H. B., Deerfield, D. W., Nicholas, H. B. J., et al. (1997). *GeneDoc: A Tool For Editing And Annotating Multiple Sequence Alignments. ver. 2.7.000.* Available online at: http://iubio.bio.indiana.edu/soft/molbio/ibmpc/genedoc-readme.html

Özturk-Çolak, A., Moussian, B., and Araújo, S. J. (2016). Drosophila, chitinous aECM and its cellular interactions during tracheal development. *Dev. Dyn.* 245, 259–267. doi: 10.1002/DVDY.24356

Pesch, Y. Y., Riedel, D., Patil, K. R., Loch, G., and Behr, M. (2016). Chitinases and Imaginal disc growth factors organize the extracellular matrix formation at barrier tissues in insects. *Sci. Rep.* 6:18340. doi: 10.1038/srep18340

Stamatakis, A. (2014). RAxML version 8: a tool for phylogenetic analysis and post-analysis of large phylogenies. *Bioinformatics* 30, 1312–1313. doi: 10.1093/bioinformatics/btu033

Su, C., Tu, G., Huang, S., Yang, Q., Shahzad, M. F., and Li, F. (2016). Genome-wide analysis of chitinase genes and their varied functions in larval moult, pupation and eclosion in the rice striped stem borer *Chilo suppressalis*. *Insect Mol. Biol.* 25, 401–412. doi: 10.1111/imb.12227

Togawa, T., Dunn, W. A., Emmons, A. C., and Willis, J. H. (2007). CPF and CPFL, two related gene families encoding cuticular proteins of *Anopheles gambiae* and other insects. *Insect Biochem. Mol. Biol.* 37, 688. doi: 10.1016/j.ibmb.2007.03.011

Toshio, S., Shigeru, A., Naoaki, S., Ryuta, M., Haruka, S., Miyuki, S., et al. (2010). Protein Crosslinking by transglutaminase controls cuticle morphogenesis in drosophila. *PLoS One* 5:e13477. doi: 10.1371/journal.pone.0013477

Tsai, Y. L., Hayward, R. E., Langer, R. C., Fidock, D. A., and Vinetz, J. M. (2001). Disruption of *Plasmodium falciparum* chitinase markedly impairs parasite invasion of mosquito midgut. *Infect. Immun.* 69, 4048–4054. doi: 10.1128/IAI.69.6.4048-4054.2001

Turner, J. R. (2009). Intestinal mucosal barrier function in health and disease. *Nat. Rev. Immunol.* 9, 799–809. doi: 10.1038/nri2653

Uv, A. E., and Moussian, B. (2010). The apical plasma membrane of Drosophila embryonic epithelia. *Eur. J. Cell Biol.* 89, 208–211. doi: 10.1016/j.ejcb.2009.11.009

Varela, P. F., Llera, A. S., Mariuzza, R. A., and Tormo, J. (2002). Crystal structure of imaginal disc growth factor-2: a member of a new family of growth-promoting glycoproteins from drosophila melanogaster. *J. Biol. Chem.* 277, 13229–13236. doi: 10.1074/jbc.M110502200

Vuong-Brender, T. T. K., Suman, S. K., and Labouesse, M. (2017). The apical ECM preserves embryonic integrity and distributes mechanical stress during morphogenesis. *Development* 144, 4336–4349. doi: 10.1242/dev.150383

Wang, H. B., Sakudoh, T., Kawasaki, H., Iwanaga, M., Araki, K., Fujimoto, H., et al. (2009). Purification and expression analysis of imaginal disc growth factor

in the silkworm, *Bombyx mori*. *J. Insect Physiol.* 55, 1065–1071. doi: 10.1016/j.jinsphys.2009.08.001

Watanabe, T., Kobori, K., Miyashita, K., Fujii, T., Sakai, H., Uchida, M., et al. (1993). Identification of glutamic acid 204 and aspartic acid 200 in chitinase A1 of *Bacillus circulans* WL-12 as essential residues for chitinase activity. *J. Biol. Chem.* 268, 18567–18572. doi: 10.1016/0005-2736(93)90077-D

White, I. M., and Elsomharris, M. M. (1992). Fruit flies of economic significance: their identification and bionomics. *Environ. Entomol.* 22, 1408–1408. doi: 10.1017/S0007485300041237

Wilson, T. G., and Cryan, J. R. (1997). Lufenuron, a chitin-synthesis inhibitor, interrupts development of Drosophila melanogaster. *J. Exp. Zool. Part B.* 278, 37–44. doi: 10.1002/(sici)1097-010x(19970501)278:1<37::aid-jez4>3.0.co;2-7

Yoshiyama, T., Namiki, T., Mita, K., Kataoka, H., and Niwa, R. (2006). Neverland is an evolutionally conserved Rieske-domain protein that is essential for ecdysone synthesis and insect growth. *Development* 133, 2565–2574. doi: 10.1242/dev.02428

Yuan, S. Y., Kong, Q., Xiao, C., Yang, S. S., Sun, W., Zhang, J. B., et al. (2006). Introduction to two kinds of artificial diets for mass rearing of adult *Bactrocera dorsalis* (Hendel) (Chinese). *J. Huazhong Agr. Univ.* 25, 371–374. doi: 10.13300/j.cnki.hnlkxb.2006.04.007

Zhang, J. Z., Zhang, X., Arakane, Y., Muthukrishnan, S., Kramer, K. J., Ma, E., et al. (2011a). Comparative genomic analysis of chitinase and chitinase-like genes in the African malaria mosquito (*Anopheles gambiae*). *PLoS One* 6:e19899. doi: 10.1371/journal.pone.0019899

Zhang, J. Z., Zhang, X., Arakane, Y., Muthukrishnan, S., Kramer, K. J., Ma, E., et al. (2011b). Identification and characterization of a novel chitinase-like gene cluster (AgCht5) possibly derived from tandem duplications in the African malaria mosquito, Anopheles gambiae. *Insect Biochem. Mol. Biol.* 41:528.

Zhu, Q. S., Arakane, Y., Banerjee, D., Beemanb, R. W., Kramera, K. J., and Muthukrishnan, S. (2008a). Domain organization and phylogenetic analysis of the chitinase-like family of proteins in three species of insects. *Insect Biochem. Mol. Biol.* 38:466. doi: 10.1016/j.ibmb.2007.06.010

Zhu, Q. S., Arakane, Y., Beeman, R. W., Kramer, K. J., and Muthukrishnan, S. (2008c). Functional specialization among insect chitinase family genes revealed by RNA interference. *Proc. Natl. Acad. Sci. U.S.A.* 105, 6650–6655. doi: 10.1073/pnas.0800739105

Zhu, Q. S., Arakane, Y., Beeman, R. W., Kramera, K. J., and Muthukrishnana, S. (2008b). Characterization of recombinant chitinase-like proteins of Drosophila melanogaster and *Tribolium castaneum*. *Insect Biochem. Mol. Biol.* 38:477. doi: 10.1016/j.ibmb.2007.06.011

Zhu, Q. S., Deng, Y. P., Vanka, P., Brown, S. J., Muthukrishnan, S., and Kramer, K. J. (2004). Computational identification of novel chitinase-like proteins in the Drosophila melanogaster genome. *Bioinformatics* 20, 161–169. doi: 10.1093/bioinformatics/bth020

Zhu, Z., Zheng, T., Homer, R. J., Kim, Y. K., Chen, N. Y., Cohn, L., et al. (2004). Acidic Mammalian Chitinase in Asthmatic Th2 Inflammation and IL-13 Pathway Activation. *Science* 304, 1678–1682. doi: 10.1126/science.1095336

Žurovcová, M., and Ayala, F. J. (2002). Polymorphism patterns in two tightly linked developmental genes, Idgf1 and Idgf3, of Drosophila melanogaster. *Genetics* 162, 177–188. doi: 10.1023/A:1020924028450

Conflict of Interest: The authors declare that the research was conducted in the absence of any commercial or financial relationships that could be construed as a potential conflict of interest.

frontiers in Cell and Developmental Biology

ORIGINAL RESEARCH
published: 08 May 2020
doi: 10.3389/fcell.2020.00300

Superficially Similar Adaptation Within One Species Exhibits Similar Morphological Specialization but Different Physiological Regulations and Origins

*Yi Zhang†, Xing-Xing Wang†, Zhu-Jun Feng, Hao-Su Cong, Zhan-Sheng Chen, Yu-Dan Li, Wen-Meng Yang, Song-Qi Zhang, Ling-Feng Shen, Hong-Gang Tian, Yi Feng and Tong-Xian Liu**

Key Laboratory of Integrated Pest Management on Crops in Northwestern Loess Plateau, Ministry of Agriculture, Northwest A&F University, Yangling, China

OPEN ACCESS

Edited by:
Wei Guo,
Institute of Zoology (CAS), China

Reviewed by:
Li Zhang,
Chinese Institute for Brain Research, Beijing (CIBR), China
Oldřich Nedvěd,
University of South Bohemia in České Budějovice, Czechia

***Correspondence:**
Tong-Xian Liu
txliu@nwafu.edu.cn;
txliu@nwsuaf.edu.cn

† These authors have contributed equally to this work

Specialty section:
This article was submitted to Epigenomics and Epigenetics, a section of the journal Frontiers in Cell and Developmental Biology

Received: *24 February 2020*
Accepted: *07 April 2020*
Published: *08 May 2020*

Citation:
Zhang Y, Wang X-X, Feng Z-J, Cong H-S, Chen Z-S, Li Y-D, Yang W-M, Zhang S-Q, Shen L-F, Tian H-G, Feng Y and Liu T-X (2020) Superficially Similar Adaptation Within One Species Exhibits Similar Morphological Specialization but Different Physiological Regulations and Origins. Front. Cell Dev. Biol. 8:300. doi: 10.3389/fcell.2020.00300

Animals have developed numerous strategies to contend with environmental pressures. We observed that the same adaptation strategy may be used repeatedly by one species in response to a certain environmental challenge. The ladybird *Harmonia axyridis* displays thermal phenotypic plasticity at different developmental stages. It is unknown whether these superficially similar temperature-induced specializations share similar physiological mechanisms. We performed various experiments to clarify the differences and similarities between these processes. We examined changes in the numbers and sizes of melanic spots in pupae and adults, and confirmed similar patterns for both. The dopamine pathway controls pigmentation levels at both developmental stages of *H. axyridis.* However, the aspartate-β-alanine pathway controls spot size and number only in the pupae. An upstream regulation analysis revealed the roles of *Hox* genes and elytral veins in pupal and adult spot formation. Both the pupae and the adults exhibited similar morphological responses to temperatures. However, they occurred in different body parts and were regulated by different pathways. These phenotypic adaptations are indicative of an effective thermoregulatory system in *H. axyridis* and explains how insects contend with certain environmental pressure based on various control mechanisms.

Keywords: environmental adaptation, *Harmonia axyridis*, melanization, multicolored Asian ladybird, phenotypic plasticity

INTRODUCTION

Many animal species including insects modify their morphology to adapt to rapidly changing environmental conditions. Similar physiological and biological characteristics may be observed more than once within the same species. The multicolored Asian ladybird *Harmonia axyridis* (Pallas) is a ubiquitous insect pest predator that displays number of color patterns (Tan, 1946; Koch, 2003; Michie et al., 2010). The pupae present with only one gradually changeable melanic spot pattern, with an orange background and numerous dark spots. In contrast, the adults have discrete elytral patterns with background and spot color either orange or black. This plasticity is

affected by both temperature and genetic background (Majerus et al., 2006; Michie et al., 2010, 2011; Knapp and Nedvěd, 2013). Recent studies established that the *pnr* gene determines elytra pattern background color in various color forms in *H. axyridis* (Ando et al., 2018; Gautier et al., 2018). However, the physiological and molecular mechanisms regulating thermally-induced spot size, shape, and number remain unclear.

The spot patterns of *H. axyridis* f. *succinea* are highly polymorphic across seasons and are temperature dependent. Seasonal phenotypic plasticity is advantageous for predictable environmental changes (Majerus et al., 2006; Michie et al., 2010, 2011; Knapp and Nedvěd, 2013). The adults and the pupae have low melanic body color (fewer and smaller spots) at high temperatures (Michie et al., 2010, 2011). This plasticity of body spot patterns to temperature is a thermal adaptation in *H. axyridis*. Dark-colored individuals rapidly increase their body temperature to warming by solar irradiation (Trullas et al., 2007). Similar thermal polyphenisms occur in butterflies and *Drosophila*. Cuticular melanization increases with decreasing temperature (Roland, 1982; Kingsolver, 1987; Gibert et al., 2000, 2016; Solensky and Larkin, 2003).

The numbers, sizes, and colors of the spots vary on the pupal dorsal cuticles and the adult elytra in *H. axyridis* f. *succinea* (Michie et al., 2011). Studies have shown that tyrosine-mediated cuticle pigmentation (melanization) plays a major role in cuticular melanin formation in numerous insect species (Michie et al., 2011; Sun et al., 2018a,b).

Insect cuticular melanization pathway is conserved among species. Tyrosine hydroxylase (TH) converts tyrosine to 3,4-dihydroxyphenylalanine (DOPA), and DOPA decarboxylase (DDC) converts DOPA to dopamine. The latter is a substrate for *N*-acetyldopamine (NADA) and *N*-β-alanyldopamine (NBAD) synthesized by arylalkylamine-*N*-acetyltransferase and NBAD synthase (ebony), respectively. *N*-acetyldopamine and NBAD are transported extracellularly and catalyzed by laccases (laccase 2, lac2) in cuticular melanization (pigmentation) and sclerotization (Suderman et al., 2006; Noh et al., 2016). Dopachrome is catalyzed by enzyme yellow to 5,6-dihydroxyindole-2-carboxylic acid, which polymerizes DOPA melanin. Aspartate decarboxylase (ADC) converts aspartic acid to β-alanine. The latter and dopamine are key substrates for ebony in NBAD formation. *ADC* and *ebony* downregulation limits β-alanine synthesis for NBAD production, leads to the accumulation of the melanin substrate dopamine, and enhances melanization (Borycz et al., 2002; Dai et al., 2015; Miyagi et al., 2015). Previous studies have shown that ebony and yellow determine spot patterns in numerous insect species (Wittkopp et al., 2002; Parchem et al., 2007; Futahashi et al., 2008, 2010; Wittkopp and Beldade, 2009; Arakane et al., 2010; Sharma et al., 2016).

Harmonia axyridis, that selected to investigate in this experiment, has been deployed as a biological control agent worldwide (Coderre et al., 1995; Dreistadt et al., 1995; Brown et al., 2007). The potential ecological impacts of introduction of *H. axyridis* must be considered (Koch, 2003; Koch and Galvan, 2007). Its environmental adaptation mediated by thermal phenotypic plasticity could be one reason that accounts for its global dispersal and possible negative ecological impact.

Thermal phenotypic plasticity is a major factor contributing to *H. axyridis* polymorphism. It is highly diverse and is directly induced by environmental stimuli. Melanic spot specialization is similar between pupae and adults. In this study, we examined the spot patterns in *H. axyridis* and their transcriptional regulation. The aims of this study were to compare thermally driven morphological changes at the phenotypical, physiological, and molecular levels in *H. axyridis* and to elucidate the mechanisms regulating its pigmentation patterns. Furthermore, we intended to compare the regulation differences of melanic spots formation between pupal dorsal cuticle and adult elytra to test our hypothesis that superficially similar phenotypic specification can be regulated through different molecular pathways.

MATERIALS AND METHODS

Insects

Multicolored Asian ladybird (*H. axyridis*; orange background with dark spots; f. *succinea*) were maintained in a laboratory (Yangling, Shannxi, China) at 27.5 ± 1°C, 50% relative humidity (RH), and a photoperiod of 14-h light and 10-h day cycle for >2 years. The beetles were reared on pea aphids (*Acyrthosiphon pisum*) fed with broad bean (*Vicia faba*).

Similar Morphological Change Patterns

Pupae

H. axyridis f. *succinea* larvae were reared at 15, 17.5, 20, 22.5, 25, 27.5, 30, 32.5, and 35°C (50% RH, 10,000 lx, 16L:8D) and prepared for sample collection and images analysis. Pupal samples were collected for both whole-body and segmental melanic spots analyses. Melanin spots of *H. axyridis* are color-uniform and have defined edges between them; therefore, the melanin levels can be calculated based on spots area proportion from images by pixels.

Top-, front-, and side-view images of the pupae ≥12 h post-pupation were captured with a Panasonic DMC-GH4 digital camera (Panasonic, Osaka, Japan; shutter speed: 1/250; aperture: F4.0; ISO: 320; picture style: faithful 0,0,0,0; white balance: color temperature, 3,000 K, AF mode: manual focus; metering mode: center-weighted average) coupled to the SDPTOP-SZN71 microscope system (Sunny, Hangzhou, Zhejiang, China; halogen lamp light temperature: 3,000 K). The percentages of spots on the whole body were calculated in ImageJ (v. 1.51j8; Wayne Rasband; National Institute of Health, Bethesda, MD, United States) and based on the spot area pixels proportions of whole-body pixels (projected areas, **Supplementary Figure S3C**). The melanin levels in all segments were also calculated (based on the spot area pixels proportions of all pixels for each segments).

First, the perimeter of the pupae (projected areas of dorsal position) was detected, and the pixel numbers inside the outline were calculated. Second, the edge of each melanic spot was then detected, and the pixels for each spot were calculated. Third, the total spot area for all spots and the percentage of this area to the whole-body area were calculated. At least 100 individuals were prepared for spots analysis of each temperature treatment.

Adults

Harmonia axyridis f. *succinea* larvae and pupae were reared at 15, 20, 25 and 30°C (50% RH, 1,000 lx, 16L:8D) and prepared for adult sample collection. Adult samples of both sexes were prepared for melanic spots area proportions analysis (as described in section"Pupae," **Supplementary Figure S3C**).

Adults of both sexes at ≥12 h post-eclosion were separated for imaging. The forewings (elytra) and hindwings were removed. Images of the elytra and top views of the wingless bodies were captured for analysis of the melanic spot area proportion. Melanic spot area proportion using the same equipment as for the pupae (section "Pupae").

The proportions of spots on the elytra and melanin on the abdomens were calculated in ImageJ and based on the proportions of spot area pixels as described in section "Pupae." At least 50 individuals were prepared for melanic spot analysis of each sex and temperature treatment.

To generate an average spots pattern, at least 15 separate images for each treatment were selected (adjust size and body orientation). After ensuring the following settings, the images were processed in Photoshop software (v. 13.0 × 64; Adobe, Mountain View, CA, United States): (1) set another 14 layers (including background image) of the basic images; (2) copied another 14 images in to each layer; (3) set: opacity: 100%,and fill opacity: 100% for all layers; (4) selected blend modes: screen, and obtained a preliminary overlaid image; (5) adjusted image: Brightness: -100, contrast: 30, and obtained a final image.

Physiological Regulatory Mechanisms

Modification of Target Gene Expression by RNAi

H. axyridis f. *succinea* transcriptomes (mixed samples with eggs, larvae, pupae, and adults) were sequenced before the experiments. Transcriptome sequencing and preliminary analysis were performed by Wuhan Bioacme Corp. (Wuhan, Hubei, China; http://www.whbioacme.com; Hiseq 4000 (PE150/125); NGS; 12 Gb clean data obtained). Target gene sequences (*HaTH,* MK584934.1; *Halac2,* MN650656; *Hayellow,* MN650659; *Hatan,* MN650658; *HaADC,* MN650660; and *Haebony,* MN650657) were obtained from *H. axyridis* transcriptome sequencing (open reading frames; ORF) and uploaded. Transcriptional analysis of the target genes under different temperature treatments was performed to detect correlations. This method is described in detail in **Supplementary Material S1.1**. The results are shown in **Supplementary Figure S1**.

The dsRNAs of the target genes were prepared in a T7 RiboMAX System (Promega, Madison, WI, United States). Two targets were selected for the RNAi. The primers used in the synthesis of the two dsRNAs are listed in **Supplementary Table S1**. Twelve-hour, fourth-instar larvae and pupae were injected with 250 nL dsRNA (∼100–5,000 ng μL^{-1}) for each of the target genes. A non-ladybird-related *GFP* gene was used as a control (Chen et al., 2016). The delivery of the dsRNAs is described in **Supplementary Material S1.1**. RNAi efficiency was measured by RT-Q-PCR (**Supplementary Material S1.1**). Effective dsRNAs were prepared for the subsequent experiments.

Phenotypic Observations

After dsRNA injection, the beetles were reared for pupation or eclosion. Treated individuals were prepared for the imaging of their melanin spots 12 h after ecdysis. Experiments conducted at 27.5°C. Digital images were acquired for phenotypic analysis (section "Pupae"). Adobe Photoshop CS6 (v. 13.0 × 64; Adobe, Mountain View, CA, United States) was used to remove the color channels.

Simulation of Dynamic Melanin Spot Changes in Pupae at Constant Temperature by Transcriptional Regulations of *HaADC* and *Haebony* Genes in the Aspartate-β-Alanine Pathway

To further confirm the critical role of genes in the aspartate-β-alanine pathway (*HaADC* and *Haebony*) in spots pattern regulation, we intended to reproduce melanin spot patterns induced by transcriptional modification (RNAi) at 32.5°C.

H. axyridis f. *succinea* larvae were reared at 32.5°C (50% RH, 1,000 lx, 16L:8D) to lower their melanin levels and prepared for injection with ds-*Haebony* and ds-*HaADC* (250 nL for each individual; ds-*Haebony*: 125, 250, 500, 1,000 ng μL^{-1}; ds-*HaADC*: 500, 1,000, 2,000, 4,000 ng μL^{-1}). A non-ladybird-related *GFP* gene was used as a control (250 nL, 5,000 ng μL^{-1}).

Cuticle Morphology

Histological sectioning and staining (hematoxylin–eosin; H&E) of pupae and adults were performed for cuticle morphology analysis. The protocol is described in **Supplementary Material S1.2**.

Immunofluorescence and *in situ* Hybridization

The distribution of key molecules (mRNA or protein) were analyzed to prove the connection between phenotypes and the regulation of key pathways. Tyrosine hydroxylase, the key cuticular melanization protein, was prepared for immunofluorescence. *HaADC* was selected for *in situ* hybridization. The protocols are described in **Supplementary Material S1.3**.

Upstream Spot Pattern Regulation

We screened and analyzed the upstream regulations of spots formation between the pupal and adult stages of *H. axyridis*, as supplementary evidence of the regulation differences between the two developmental stages.

Three *Hox* genes (*Ultrabithorax, Ubx,* MN927185*; Abdominal-A, Abd-A,* MN927187*;* and *Abdominal-B, Abd-B,* MN927186) associated with thoracic and abdominal segment formation were screened and prepared for a pupal spot pattern control study. For the adult experiments, elytral vein lengths were measured and the *Rhomboid* (*Rho*) gene associated with vein formation was prepared for an elytral spot pattern control study. The protocols are described in **Supplementary Material S1.4**.

Measurement of Veins of Elytra With Different Melanin Level

First, the R color channel was removed to enhance the vein contrast to the background (**Figure 5C-2**); then we measured the

length of the first vein (from the left, line a of **Figure 5C-2**) and the second vein (from the left, line b of **Figure 5C-2**) by pixels. Finally, the ratio of b to a (b/a) was calculated (**Figure 5C-3**).

Statistical Analyses

Melanin spot analyses under the various thermal treatments were subjected to one-way analysis of variance in SPSS (v. 22; IBM Corp., Armonk, NY, United States). Significantly different treatment means were identified by Duncan's test ($P < 0.05$). Immunofluorescence and *in situ* hybridization images were obtained and analyzed with CaseViewer v. 2.0 (3DHISTECH Ltd., Budapest, Hungary).

RESULTS

Similar Dynamic Changes in Pupal and Adult Melanin Spots With Temperature

In the pupae, the spot numbers and sizes decreased with increasing temperature (**Figure 1**). Under all temperature treatments, the largest spot was detected on the A3 segment (**Figures 1A,B**). In contrast, virtually no pigment spots were observed on the A1 segment; their frequency of occurrence was only 8% even at the lowest temperature (**Figure 1A**).

In the adults, the spot numbers and sizes also decreased with increasing temperature. The spot areas decreased with increasing temperature. Certain spots disappeared altogether (**Figures 1C,D**). Female adults had more and bigger melanin spots than male adults (**Figure 1C**). The data and statistical analyses are shown in **Supplementary Figures S1–S4**.

Phenotypic Similarities and Differences Under Certain Molecular Regulatory Pathways (RNAi)

All candidate genes were successfully downregulated (**Supplementary Figure S5**). Four of the six genes (*Halac2, HaTH, HaADC,* and *Haebony*) presented with melanization-related functions at both developmental stages. Similar phenotypic changes were detected in both the pupae and the adults under *Halac2* and *HaTH* RNAi (dopamine regulation pathway). Different phenotypic changes were detected between the pupae and the adults under *HaADC* and *Haebony* RNAi (aspartate-β-alanine regulation pathway).

Similar Phenotypic Changes

Melanization decreased with increasing dsRNA dose under *Halac2* RNAi and *HaTH* RNAi (**Figure 2**). These treatments induced similar phenotypic changes in both the pupae and the adults. Spot pigment (melanin) intensity diminished in response to these treatments (**Figure 2D**). Intermediate individuals confirmed that neither spot size nor number was affected by RNAi exposure (**Figures 2A,D**). Color fading was the main effect of *Halac2* and *HaTH* downregulation in the pupae.

The phenotypic changes observed in adults under *Halac2* and *HaTH* RNAi resembled those seen in pupae (**Figures 2B,C,E**). The melanin spots on the elytra, pronota, and abdomen were faded (**Figures 2B,C**). However, the numbers and sizes of the spots, even if without melanin, were not affected by any RNAi treatment. The edges of the spots were discerned with a blue channel filter (**Figure 2E**).

Phenotypic Differences Between Pupae and Adults

Pupae

Melanin spot numbers and sizes increased to more-or-less the same extent under both the *HaADC* and *Haebony* RNAi treatments (**Figure 2D**). The other parts of the cuticle remained orange. The A1 segment was the last to undergo pigmentation in response to *HaADC* and *Haebony* downregulation (**Figures 2A,D**).

Adults

The phenotypic changes in the adults under *HaADC* and *Haebony* RNAi did not involve melanin pattern alterations (**Figures 2B,C**). No obvious changes in spot size or number were observed under any of these treatments. Dark melanin line observed along the edge of the elytra was the only phenotypic changes. The borders of the melanin spots at the edges of the elytra were blurred. The entire elytra background turned orange-grey at the same post-emergence stage (**Figure 2E**).

Simulation of Dynamic Melanin Spot Changes in Pupae at Constant Temperature

Dynamic melanin spot changes were simulated by molecular regulation at a constant 32.5°C. Compared with the control, the insects administered with various dsRNA concentrations presented with variable melanin spot patterns. In the treated pupae, the melanin spot numbers and sizes increased with dsRNA dosage (*HaADC*-RNAi: $F = 70.911$; df = 4, 141; $P < 0.001$; *Haebony* RNAi: $F = 109.171$; df = 4, 135; $P < 0.001$; **Figure 3**). Enhanced pigmentation was observed for the T1 segments (pronotum) and the forewing (elytron) buds. The A1 segment was the last to undergo pigmentation under RNAi (**Figure 3A**).

Distribution Analyses of the Target Molecules in Two Regulatory Pathways

Tyrosine hydroxylase and ADC (the first step in aspartate-β-alanine and tyrosine-dopamine pathways) were selected to analyze the reactions in the cuticular tissues (**Figure 4A**). Tyrosine hydroxylase was localized to certain locations in the new cuticle where melanin spots develop after pupation (**Figures 4B–D**; white arrows). Relatively weak fluorescence was detected in the unpigmented area (**Figure 4D**; blue arrows). Tyrosine hydroxylase distribution matched that of the melanin spots on the elytra of newly-emerged adults (**Figures 4F–G**). *HaADC* mRNA distribution in the cuticle matched that of TH protein. Relatively stronger fluorescence was noted for the unpigmented position (**Figure 4E**). There was no clear *HaADC* distribution specificity in the elytra. However, comparatively weaker fluorescence was observed in the area with melanin spots (**Figure 4H**). *HaADC* mRNA was detected only in the in dorsal epidermis. In contrast, no fluorescence was measured in the ventral elytral cuticle (**Figure 4H**).

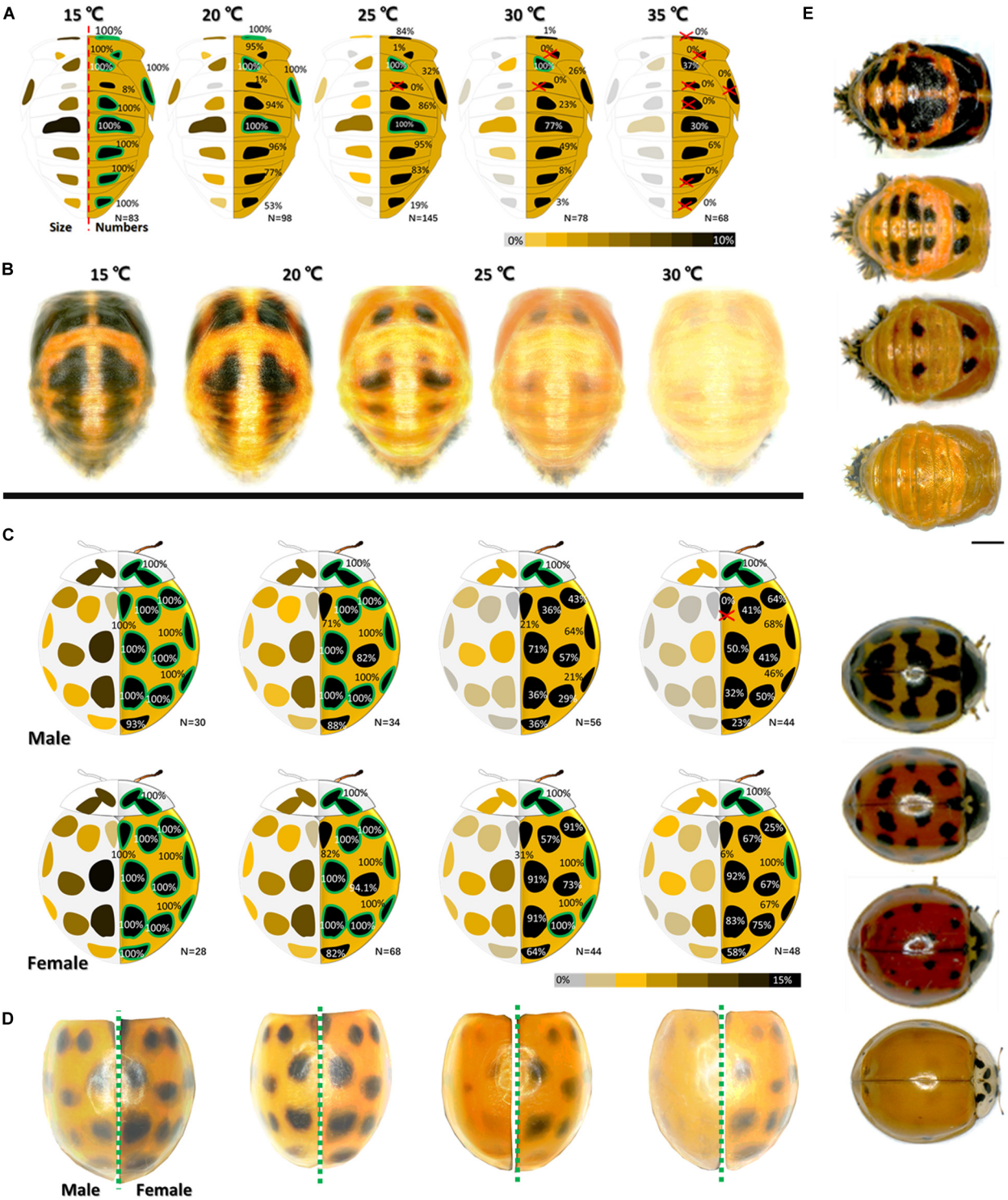

FIGURE 1 | Melanin spots dynamic changes (spots size and numbers) of pupae **(A)** and **(B)** and male and female adults **(C)** and **(D)** with temperature. In **(A)** and **(C)**, the average area ratio (size) of each spot is marked by colors on the left side of each sketch. Values (one spot area/dorsal area) are indicated by a heatmap with different colors (gray (0%)-yellow-brown-black). Occurrence frequency of each spot at particular temperature observed in our samples are marked on the right of each sketch. Spots with 100% occurrence frequency at particular temperature are marked with a green edge. Those with 0% occurrence frequency are marked by a red "×." In **(B)** and **(D)**, images (at least 15 images of similar size and positio) of pupa or elytra from the same temperature were overlaid to generated an average spots pattern. Randomly selected images of pupae and adults with different spot patterns are shown in **(E)**. See **Supplementary Figures S2, S3** for more details.

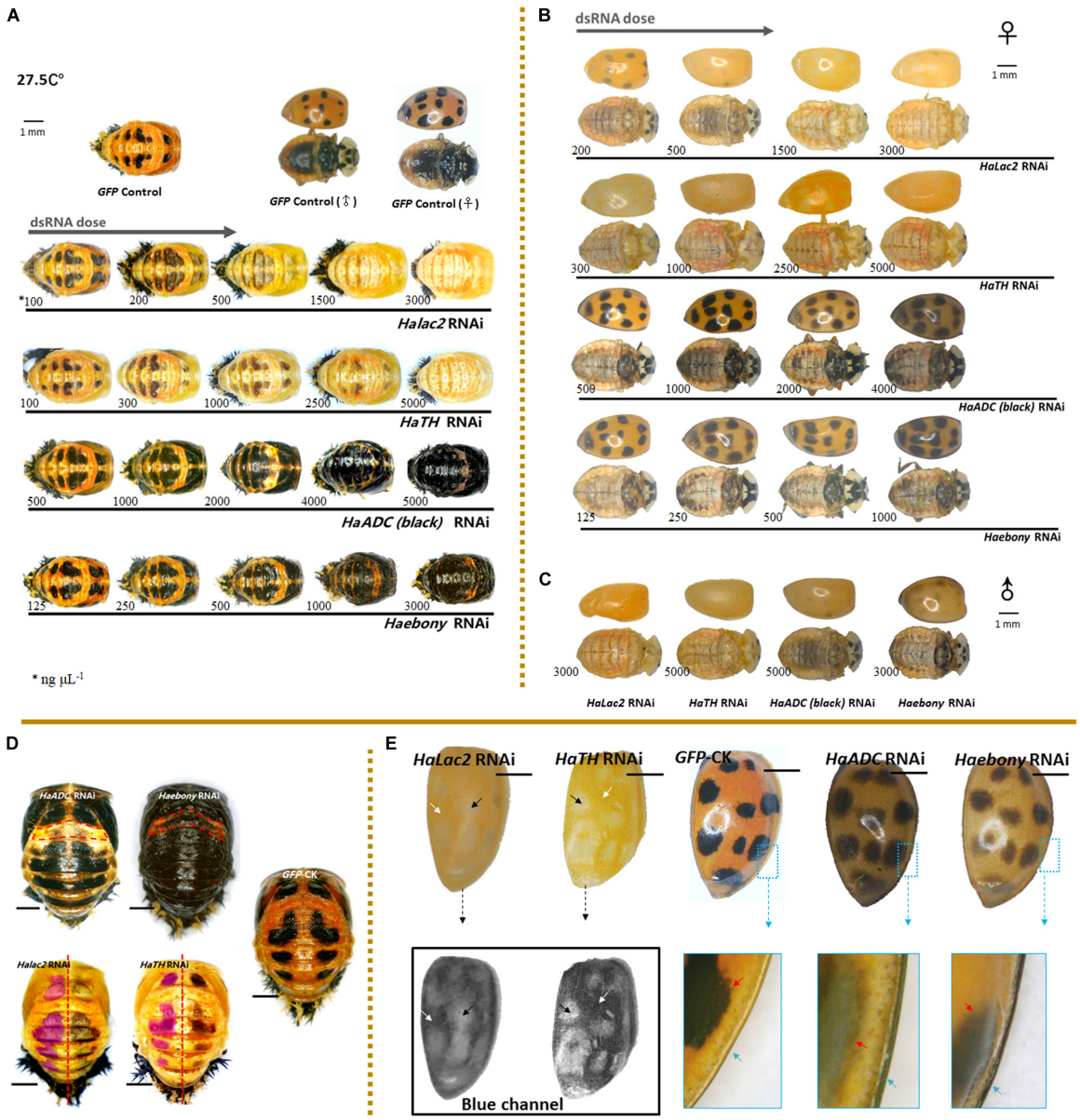

FIGURE 2 | Phenotypic changes in *Harmonia axyridis* under RNAi of candidate melanization genes. Pupae **(A)** and female adults **(B)** treated with different dsRNA concentrations. Male adults treated with highest dsRNA concentration **(C)**. Experiments conducted at 27.5°C. Mortality of samples and phenotypes of corpses shows in **Supplementary Figure S5**. Low melanic A1 segments have been indicated using dotted boxes in *HaADC* and *Haebony* RNAi; and spots areas are marked in translucent purplish red of *HaTH* and *Halac2* RNAi **(D)**. For adult elytra, red and green channels were removed to show phenotypic changes of *Halac2* and *HaTH* RNAi **(E)**; and white arrows indicate locations without any spots, black arrows indicate spot positions, red arrows indicate spot edges (inside the enlarged blue boxes). Concretions of dsRNAs are indicated under each sample, blue arrows indicate explanate elytron margins. Scale bars = 1 mm. See **Supplementary Figure S4** for more details on repression of candidate genes under RNAi.

Upstream Regulation of Spot Formation

Roles of Selected Hox Genes in Spot Patterns of Pupae

Pupal spot patterns were strongly influenced by the selected *Hox* (*Ha-Ubx, Ha-Abd-A,* and *Ha-Abd-B*) RNAi in the thoracic and abdominal segments (**Figure 5A**). Spots were detected in the A1 segment (which is normally devoid of spots) and decreased in T3 underwent *Ha-Ubx* RNAi. The spots on the A2 segment were enlarged. *Ha-Abd-A* downregulation caused the spots on the A2 segment to disappear. The spots on the A3 segment shrank while those on the A4 segment enlarged. *Ha-Abd-B* downregulation enlarged the spots on segments A3, A4, and A5.

Association Between Elytra Veins and Spot Patterns

The four main elytra veins had more branches in the melanized (spotted) areas than the unspotted areas (**Figure 5C**).

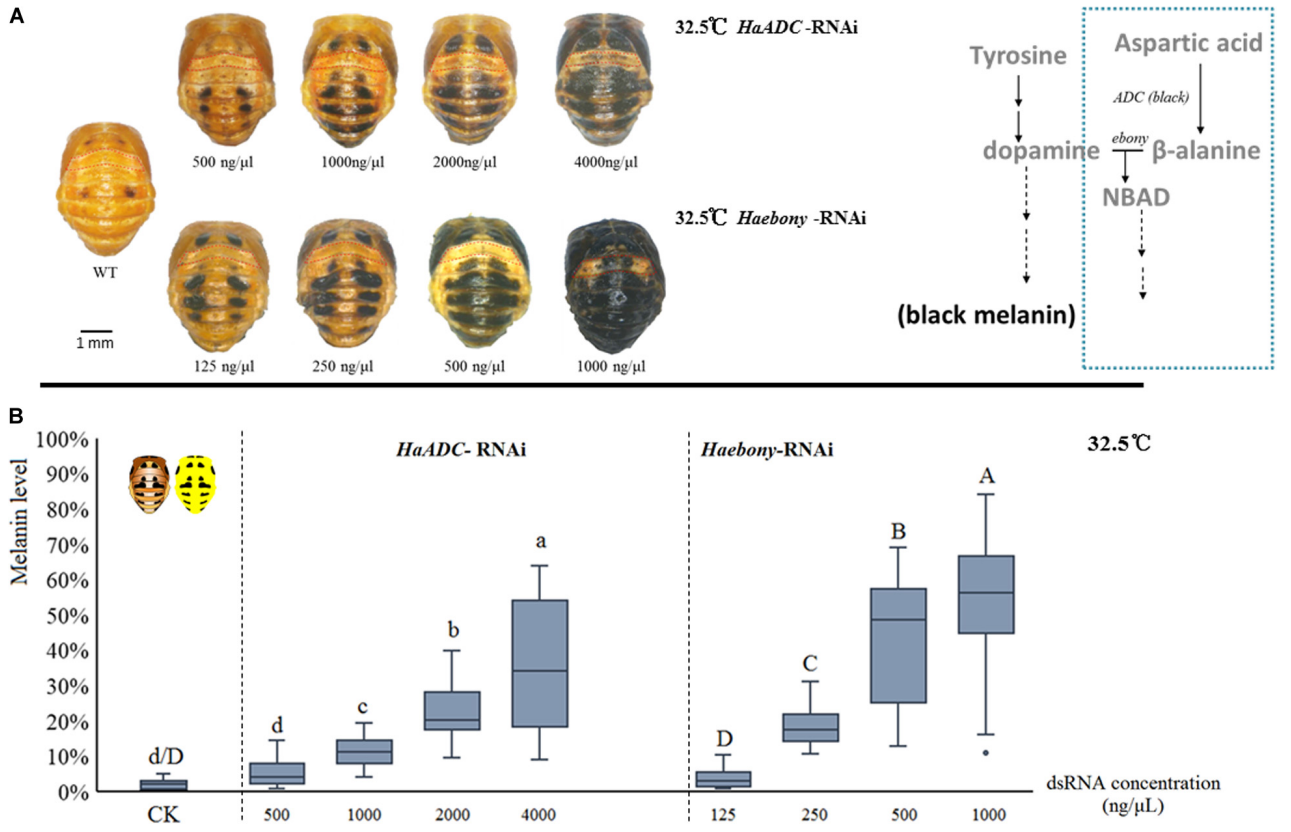

FIGURE 3 | Simulation of melanin spot patterns at high temperature (32.5°C) in pupae. Melanic spot pattern **(A)** and melanin level **(B)** changes under *HaADC* and *Haebony* RNAi were analyzed. Different letters indicate statistically significant differences (analysis of variance; Duncan's test; $P < 0.05$). A1 segments marked in red dotted box in **(A)**. Experiments were conducted at 32.5°C, at which pupal melanization is extremely low (WT of **A**). Scale bars = 1 mm.

The ratios of the second veins (b) to the sutural veins (a) are relatively higher in elytra with low melanization. The melanin level was significantly negatively correlated with b/a vein length ratio (Pearson correlations = -0.843; $P < 0.001$; **Figure 5C**). Downregulation of the vein formation-related gene *Ha-Rho* resulted in elytra shrinkage and folding and spot enlargement (**Figure 5D**).

DISCUSSION

Both the pupae and adults of *H. axyridis* display similar phenotypic plasticity when they developed at diverse temperatures. To determine if these phenotypic modifications in response to ambient temperature are sharing a same regulation system or not, we examined whether pupae and adults exhibit similar responses to temperature changes and whether their thermal phenotypic plasticities are regulated by similar molecular regulatory mechanisms. Here, both pupal and adult *H. axyridis* f. *succinea* displayed similar morphological structures dependent on temperature during development. However, the reaction mechanisms occurred in different body parts (dorsal cuticle and elytra) and developmental stages (pupa and adult) and were partly regulated by different molecular pathways (the aspartate-β-alanine pathway only functions in pupae). This superficially similar phenotypic adaptation among different body parts in *H. axyridis* enables the insect to cope with environmental pressure and abiotic stress.

The multicolored Asian ladybird *H. axyridis* presents thermally-induced cuticular color pattern plasticity in its pupal and adult stages (Michie et al., 2010, 2011). The color patterns of *H. axyridis* and other ladybird species may warn predators (Daloze et al., 1994; Dolenska et al., 2009; Prùchova et al., 2014), mate choice (Osawa and Nishida, 1992; Ueno et al., 1998) and enable it to contend with ambient temperature change (Trullas et al., 2007). Thermally controlled melanism has been reported for birds, snails, and other insects (Roland, 1982; Kingsolver, 1987; Lecompte et al., 1998; Gibert et al., 2000; Solensky and Larkin, 2003; Sharma et al., 2016; Galván et al., 2018). Dark cuticular pigmentation enables beetles to absorb heat rapidly at low temperatures, whereas low pigmentation levels reduce thermal absorption at high temperatures. Infrared thermal imaging confirmed these conclusions (**Supplementary Figure S2A**). The modification of cuticular melanization is an effective strategy for thermal adaptation.

Both the pupae and adults could regulate cuticular melanization level by controlling the numbers and sizes of their spots naturally for thermal adaptation. Various tissues

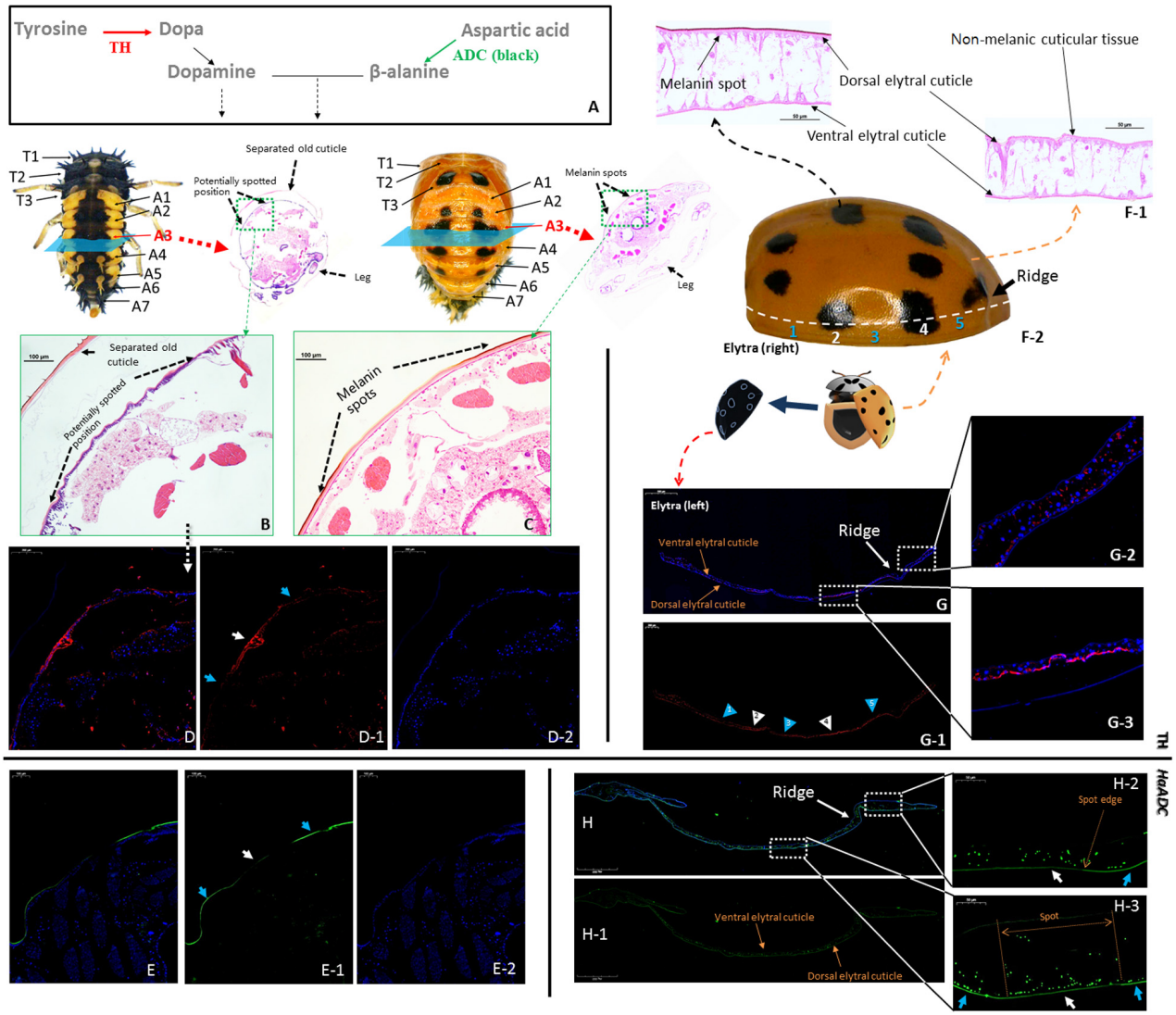

FIGURE 4 | Localization of tyrosine hydroxylase (TH) and aspartate decarboxylase (*HaADC* mRNA) in the pupal epidermis (**A–E**, molecular pathway is shown in **(A)** and elytra of adults **(F–H)**. H&E-stained histological sections of the A3 abdominal segment of pre-pupae **(B)** and pupae **(C)** of *Harmonia axyridis* with spot locations indicated. Two elytra were separated from one newly emerged adult. One of the elytra was collected for H&E-stained histological sections **(F-1)** and TH immunofluorescence assay **(G)**. The other elytra was used for spot detection based on symmetry **(F-2)**. Pre-pupa **(E)** and elytra **(H)** prepared for *in situ* hybridization of *HaADC* were collected from another individuals. White arrows indicate melanin spot location (and blue arrows indicate non-melanic position. Anti-TH (rabbit) antibodies detected with $Cy^{TM}3$-conjugated rabbit IgG antibodies (red) **(D,G)**. Localization of *HaADC* mRNA detected by *in situ* hybridization (probes used: **Supplementary Table S1**). Nuclei stained with DAPI (blue). Magnifications of the melanin spots **(E-2)** and a non-melanic position **(E-1)**. White arrows with numbers in **(G-1)** indicate melanin spot locations and blue arrows indicate non-melanic positions (blue). Position numbers of **(G-2)** and **(G-3)** correspond 1:1.

exhibiting thermosensitive melanic reaction were usually attached to the external integument and cover the body in different stages. The adult abdominal dorsal cuticle was covered by the elytra and lost its thermal sensitivity (**Supplementary Figure S4E**). This finding corroborates the hypothesis that melanic reaction, manifested by the regulation of spot size and number, is used for thermal adaptation in *H. axyridis*. Pupae and adults exhibited similar melanic responses to temperature changes in the form of changes to their spot patterns.

Melanization is the biochemical basis for this phenotypic plasticity (Suderman et al., 2006; Noh et al., 2016). Dopamine pathway was similar for both developmental stages. The candidate melanization genes undergo dynamic transcriptional changes at contrasting temperatures (Gibert et al., 2016, 2007). Knockdown of the dopamine pathway genes strongly influenced pigmentation (darkness) in both the pupae and the adults, but their spot shapes and numbers remained unaffected. These findings verified that candidate genes encoding melanin accumulation were functionally similar at both developmental stages and generated substrates for downstream dark pigmentation. However, they did not control either spot size or spot number.

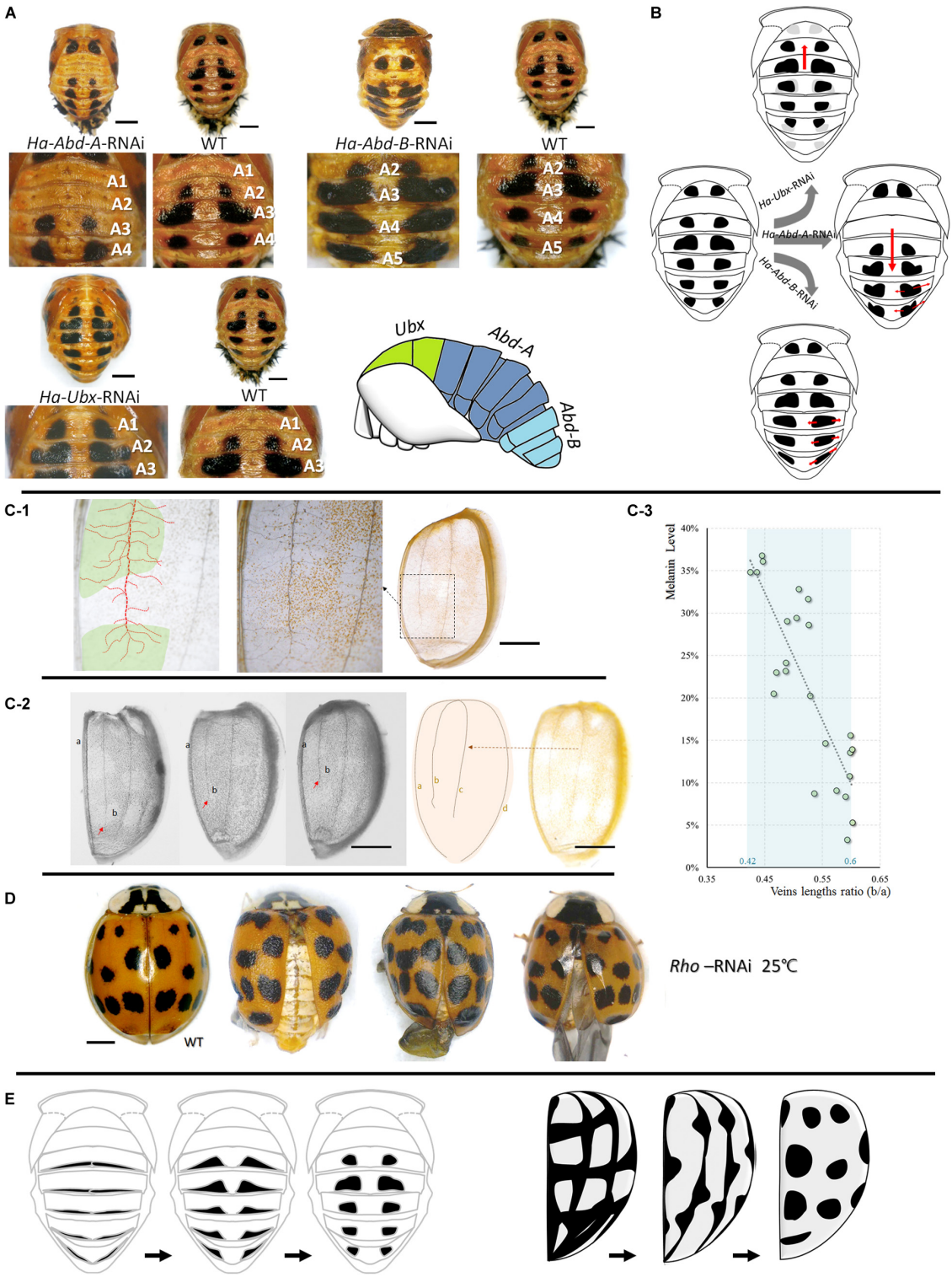

FIGURE 5 | Upstream regulations of spots formations in pupae and adults. Cuticular spot pattern changes under selected *Hox* genes (*Ha-Abd-A, Ha-Abd-B* and *Ha-Ubx*) RNAi of *Harmonia axyridis* pupae **(A,B)**. Connections between elytra spots and veins **(C,D)** and the hypothesis regarding the transformation of melanic tissues on abdominal cuticle (pupa, left) and elytra (adult, right) into spots-shape during adaptation process **(E)**. More branches observed in spot positions; dot lines in red indicated mean vein and branches, and spot positions are marked in green **(C-1)**. The ratio of the second vein (b) and the sutural vein (a) is relatively higher in elytra with low melanization **(C-2,C-3)**; red arrows indicate the lengths of second veins and are different among elytra. *Rhomboid* gene (*Ha-Rho*) downregulation caused shrinkage and folding of elytra, and enlarged spots **(D)**. The different original hypothesis of melanin spots of dorsal cuticle (pupa) and elytra (adult) are shown in **(E)**. Scale bars = 1 mm.

The genes of the aspartate-β-alanine pathway regulated cuticular melanic spot distribution patterns in the pupae but not in the adults of *H. axyridis*. Knockdown of these genes resulted in melanin spot enlargement and number increase in the pupae. We propose that the aspartate-β-alanine pathway is the key regulatory pathway for pupal cuticular melanin spot deposition in *H. axyridis*. Our spot simulation experiment strongly supports this conclusion. The two relevant genes in this pathway were upregulated prior to pupation in response to temperature increases (**Supplementary Figure S1**). However, knockdown of the genes degrading melanin did not affect the elytral spots in adult *H. axyridis*. Thus, we conclude that the superficial spot patterns of pupal and adult *H. axyridis* could be regulated by different molecular pathways.

Tyrosine hydroxylase and ADC are the key enzymes upstream of the dopamine regulation pathway and the aspartate-β-alanine regulation pathway, respectively. The distribution of TH and ADC differed between the adults and the pupae (pronota: **Supplementary Figures S7, S8**). In the pupal cuticle, fluorescence difference between TH distribution between the melanic and non-melanic tissues were observed, while *HaADC* fluorescence between the melanic and non-melanic tissues of the elytra was generally at the same level. This result supported our experiment that modifying *HaADC* and *Haebony* did not enlarge the elytral spots. *HaADC* had no positional specificity in the elytral cuticle cells. This finding was also supported by the observation that the aspartate-β-alanine pathway had negligible effect on the elytral spots.

Early pigmentation indirectly indicated the regulatory differences between the developmental stages of *H. axyridis* in terms of color pattern formation. In the early pigmentation phases, the newly-emerged adults exhibited asynchronous melanization among their various organs (pronotum and elytra; **Supplementary Figures S10B,C**). In contrast, pupal spot formation was almost synchronized among cuticle of thorax, abdomen and wings (**Supplementary Figure S10A**). Transcriptional analyses indicated that *HaADC* and *HaTH* were strongly upregulated in the pronota, elytra, and abdominal cuticle during pupal and adult development (**Supplementary Figure S9**). These results support our expectation that pupal and adult spot patterns were regulated differently.

Regulatory differences in color pattern formation were also observed among various *H. axyridis* color forms. Compared with the orange-colored (f. *succinea*) individuals, the genetically dark background forms, f. *conspicua* and f. *spectabilis,* also have pupal cuticles with an orange background; their melanization decreases with increasing temperatures similar to that observed in the orange background form (*succinea*; **Supplementary Figure S2E**). Thus, the pupal melanic modification system is conserved among the various *H. axyridis* forms determined by the pannier gene (Gautier et al., 2018), while their adult counterparts have entirely different elytra. Therefore, cuticular melanization in pupal and adult elytra might be controlled by different regulatory systems.

During adaptation, pupal abdominal and adult elytral spots may be synthesized from various melanic organs/tissues precursors. The results of our experiment involving the upstream regulation of spot patterns supported this speculation. In the pupae, the thoracic and abdominal spots could be changed in the forward or reverse direction under selected *Hox* RNAi (*Ha-Ubx, Ha-Abd-A,* and *Ha-Abd-B*; **Figure 5B**). These *hox* genes regulate segment formation (T2, T3 and A1-A7; **Supplementary Figure S11**; Hughes and Kaufman, 2002). Cuticular spots change under transcriptional *Ha-Ubx* and *Ha-Abd-A* regulation in insects (Gibert et al., 2007). We believe the pupal spots are transformed from the circular melanic regions at the edges of each segment (**Figure 5E**). In contrast, elytral spots were strongly associated with elytral second vein length and position along the apical–basal axis of wings. *Ha-Rho* downregulation enlarged elytral spots. This effect corroborates the connection between the elytral veins and spots. We proposed that the elytral spots formation might be connected to the elytral veins, but still need more evidences (**Figure 5E**). These melanic features are also found in various body parts of other insect species: wings (True et al., 1999; Shevtsova et al., 2011; Tomoyasu, 2017; Nijhout and McKenna, 2018); and abdomen (Hollocher et al., 2000; Brisson et al., 2005; Ahmed-Braimah and Sweigart, 2015; Miyagi et al., 2015). In *H. axyridis* f. *succinea*, however, they are thermosensitive and form spots. On an evolutionary timescale, environmental stress (thermostimulation and solar radiation) causes these distinct cuticular melanic areas to be similar and reacting to temperature when certain parts are exposed to these stimuli at various developmental stages.

Here, we assumed this superficially similar adaptation could occur in response to universal physical or chemical solutions, key environmental pressure, and time- or position-specific cuticle directly subjected to this pressure. Under these preconditions, similar strategies may potentially be selected to deal with environmental challenges based on a universal solution but via different molecular and physiological regulatory mechanisms.

CONCLUSION

In the present study, we confirmed that there are differences in regulation of melanin pattern between pupal and adult *H. axyridis*. Our data suggest that these similar adaptation strategies in melanin level regulation enable the insect to contend with temperature stress, albeit in different body parts in different developmental stages. Similar ecological adaptation strategies might be selected in the same animal species multiple times to cope with certain natural pressures. Further evidence for this biological strategy selection in other animal species is required to confirm its universality. This work may also help to clarify *H. axyridis* adaptation to its ambient environment and explain the observed variations in the distribution patterns of its melanin spots.

DATA AVAILABILITY STATEMENT

The datasets generated for this study can be found in the HaTH, MK584934.1; Halac2, MN650656; Hayellow, MN650659; Hatan, MN650658; HaADC, MN650660; Haebony, MN650657;HaUbx, MN927185; HaAbd-A, MN927187; HaAbd-B, MN927186.

AUTHOR CONTRIBUTIONS

YZ and T-XL designed research. X-XW and H-GT performed research. Z-JF, Z-SC, H-SC, Y-DL, L-FS, S-QZ, and W-MY provided assistance. YZ, X-XW, and YF analyzed data. YZ, H-GT, X-XW, and T-XL wrote the manuscript.

FUNDING

This research was supported by the Chinese Universities Scientific Fund (grant number, Z109021718).

ACKNOWLEDGMENTS

We are grateful for the assistance of all staff and students in the Key Laboratory of Applied Entomology, Northwest A&F University at Yangling, Shaanxi, China.

SUPPLEMENTARY MATERIAL

The Supplementary Material for this article can be found online at: https://www.frontiersin.org/articles/10.3389/fcell.2020.00300/full#supplementary-material

REFERENCES

Ahmed-Braimah, Y. H., and Sweigart, A. L. (2015). A single gene causes an interspecific difference in pigmentation in *Drosophila*. *Genetics* 200, 331–342. doi: 10.1534/genetics.115.174920

Ando, T., Matsuda, T., Goto, K., Hara, K., Ito, A., Hirata, J., et al. (2018). Repeated inversions within a pannier intron drive diversification of intraspecific colour patterns of ladybird beetles. *Nat. Commun.* 9:3843. doi: 10.1016/j.cub.2018.08.023

Arakane, Y., Dittmer, N. T., Tomoyasu, Y., Kramer, K. J., Muthukrishnan, S., Beeman, R. W., et al. (2010). Identification, mRNA expression and functional analysis of several yellow family genes in *Tribolium castaneum*. *Insect Biochem. Mol.* 40, 259–266. doi: 10.1016/j.ibmb.2010.01.012

Borycz, J., Borycz, J. A., Loubani, M., and Meinertzhagen, I. A. (2002). *Tan* and *ebony* genes regulate a novel pathway for transmitter metabolism at fly photoreceptor terminals. *J. Neurosci.* 22, 10549–10557. doi: 10.1523/JNEUROSCI.22-24-10549.2002

Brisson, J. A., Toni, D. C. D., Duncan, I., and Templeton, A. R. (2005). Abdominal pigmentation variation in *Drosophila polymorpha*: geographic variation in the trait, and underlying phylogeography. *Evolution* 59, 1046–1059. doi: 10.1111/j.0014-3820.2005.tb01043.x

Brown, P. M. J., Adriaens, T., Bathon, H., Cuppen, J., Goldarazena, A., Hägg, T., et al. (2007). "*Harmonia axyridis* in Europe: spread and distribution of a non-native coccinellid," in *From Biological Control to Invasion: the Ladybird Harmonia axyridis as a Model Species*, eds H. E. Roy and E. Wajnberg (Dordrecht: Springer), 5–21. doi: 10.1007/978-1-4020-6939-0_2

Chen, N., Fan, Y. L., Bai, Y., Li, X. D., Zhang, Z. F., and Liu, T. X. (2016). Cytochrome P450 gene, *CYP4G51*, modulates hydrocarbon production in the pea aphid, *Acyrthosiphon pisum*. *Insect Biochem. Mol.* 76, 84–94. doi: 10.1016/j.ibmb.2016.07.006

Coderre, D., Lucas, É, and Gagné, I. (1995). The occurrence of *Harmonia axyridis* (Pallas) (Coleoptera: Coccinellidae) in Canada. *Can. Entomol.* 127, 609–611. doi: 10.4039/Ent127609-4

Dai, F., Qiao, L., Cao, C., Liu, X., Tong, X., He, S., et al. (2015). Aspartate decarboxylase is required for a normal pupa pigmentation pattern in the silkworm, *Bombyx mori*. *Sci. Rep.* 5:10885. doi: 10.1038/srep10885

Daloze, D., Braekman, J. C., and Pasteels, J. M. (1994). Ladybird defence alkaloids: structural, chemotaxonomic and biosynthetic aspects (Col.: Coccinellidae). *Chemoecology* 5, 173–183. doi: 10.1007/BF01240602

Dolenska, M., Nedvěd, O., Veselý, P., Tesařová, M., and Fuchs, R. (2009). What constitutes optical warning signals of ladybirds (Coleoptera: Coccinellidae) towards bird predators: colour, pattern or general look? *Biol. J. Linn. Soc.* 98, 234–242. doi: 10.1111/j.1095-8312.2009.01277.x

Dreistadt, S. H., Hagen, K. S., and Bezark, L. G. (1995). *Harmonia axyridis* (Pallas) (Coleoptera: Coccinellidae), first western United States record for this Asiatic lady beetle. *Pan Pac. Entomol.* 71, 135–136.

Futahashi, R., Banno, Y., and Fujiwara, H. (2010). Caterpillar colour patterns are determined by a two-phase melanin gene prepatterning process: new evidence from *tan* and *laccase2*. *Evol. Dev.* 12, 157–167. doi: 10.1111/j.1525-142X.2010.00401.x

Futahashi, R., Sato, J., Meng, Y., Okamoto, S., Daimon, T., Yamamoto, K., et al. (2008). yellow and *ebony* are the responsible genes for the larval colour mutants of the silkworm *Bombyx mori*. *Genetics* 180, 1995–2005. doi: 10.1534/genetics.108.096388

Galván, I., Rodríguez-Martínez, S., and Carrascal, L. M. (2018). Dark pigmentation limits thermal niche position in birds. *Funct. Ecol.* 32, 1531–1540. doi: 10.1111/1365-2435.13094

Gautier, M., Yamaguchi, J., Foucaud, J., Loiseau, A., Ausset, A., Facon, B., et al. (2018). The genomic basis of colour pattern polymorphism in the harlequin ladybird. *Curr. Biol.* 28, 3296–3302. doi: 10.1016/j.cub.2018.08.023

Gibert, J. M., Mouchel-Vielh, E., De Castro, S., and Peronnet, F. (2016). Phenotypic plasticity through transcriptional regulation of the evolutionary hotspot gene tan in *Drosophila melanogaster*. *PLoS Genet.* 12:e1006218. doi: 10.1371/journal.pgen.1006218

Gibert, J. M., Peronnet, F., and Schlötterer, C. (2007). Phenotypic plasticity in *Drosophila* pigmentation caused by temperature sensitivity of a chromatin regulator network. *PLoS Genet.* 3:e30. doi: 10.1371/journal.pgen.0030030

Gibert, P., Moreteau, B., and David, J. R. (2000). Developmental constraints on an adaptive plasticity: reaction norms of pigmentation in adult segments of *Drosophila melanogaster*. *Evol. Dev.* 2, 249–260. doi: 10.1046/j.1525-142x.2000.00064.x

Hollocher, H., Hatcher, J. L., and Dyreson, E. G. (2000). Genetic and developmental analysis of abdominal pigmentation differences across species in the *Drosophila dunni* subgroup. *Evolution* 54, 2057–2071. doi: 10.1111/j.0014-3820.2000.tb01249.x

Hughes, C. L., and Kaufman, T. C. (2002). *Hox* genes and the evolution of the arthropod body plan1. *Evol. dev.* 4, 459–499. doi: 10.1046/j.1525-142X.2002.02034.x

Kingsolver, J. G. (1987). Evolution and coadaptation of thermoregulatory behavior and wing pigmentation pattern in pierid butterflies. *Evolution* 41, 472–490. doi: 10.1111/j.1558-5646.1987.tb05819.x

Knapp, M., and Nedvěd, O. (2013). Gender and timing during ontogeny matter: effects of a temporary high temperature on survival, body size and colouration in *Harmonia axyridis*. *PLoS One* 8:e74984. doi: 10.1371/journal.pone.0074984

Koch, R. L. (2003). The multicoloured Asian lady beetle, *Harmonia axyridis*: a review of its biology, uses in biological control, and non-target impacts. *J. Insect Sci.* 3:1. doi: 10.1093/jis/3.1.32

Koch, R. L., and Galvan, T. L. (2007). "Bad side of a good beetle: the North American experience with *Harmonia axyridis*," in *From Biological Control to Invasion: The Ladybird Harmonia Axyridis as a Model Species*, eds H. E. Roy and E. Wajnberg (Dordrecht: Springer), 23–35. doi: 10.1007/978-1-4020-6939-0_3

Lecompte, O., Madec, L., and Daguzan, J. (1998). Temperature and phenotypic plasticity in the shell colour and banding of the land snail *Helix aspersa*. *Compt. Rendus l'Acad. Sci. Ser. III Sci. Vie* 8, 649–654.

Majerus, M., Strawson, V., and Roy, H. (2006). The potential impacts of the arrival of the harlequin ladybird, *Harmonia axyridis* (Pallas) (Coleoptera: Coccinellidae), in Britain. *Ecol. Entomol.* 31, 207–215. doi: 10.1111/j.1365-2311.2006.00734.x

Michie, L. J., Mallard, F., Majerus, M. E. N., and Jiggins, F. M. (2010). Melanic through nature or nurture: genetic polymorphism and phenotypic plasticity in *Harmonia axyridis*. *J. Evol. Biol.* 23, 1699–1707. doi: 10.1111/j.1420-9101.2010.02043.x

Michie, L. J., Masson, A., Ware, R. L., and Jiggins, F. M. (2011). Seasonal phenotypic plasticity: wild ladybirds are darker at cold temperatures. *Evol. Ecol.* 25:1259. doi: 10.1007/s10682-011-9476-8

Miyagi, R., Akiyama, N., Osada, N., and Takahashi, A. (2015). Complex patterns of *cis*-regulatory polymorphisms in *ebony* underlie standing pigmentation variation in *Drosophila melanogaster*. *Mol. Ecol.* 24, 5829–5841. doi: 10.1111/mec.13432

Nijhout, H. F., and McKenna, K. Z. (2018). Wing morphogenesis in Lepidoptera. *Prog. Biophys. Mol. Biol.* 137, 88–94. doi: 10.1016/j.pbiomolbio.2018.04.008

Noh, M. Y., Muthukrishnan, S., Kramer, K. J., and Arakane, Y. (2016). Cuticle formation and pigmentation in beetles. *Curr. Opin. Insect Sci.* 17, 1–9. doi: 10.1016/j.cois.2016.05.004

Osawa, N., and Nishida, T. (1992). Seasonal variation in elytral colour polymorphism in *Harmonia axyridis* (the ladybird beetle): the role of non-random mating. *Heredity* 69, 297–307. doi: 10.1038/hdy.1992.129

Parchem, R. J., Perry, M. W., and Patel, N. H. (2007). Patterns on the insect wing. *Curr. Opin. Genet. Dev.* 17, 300–308. doi: 10.1016/j.gde.2007.05.006

Prùchova, A., Nedvěd, O., Veselı, P., Ernestova, B., and Fuchs, R. (2014). Visual warning signals of the ladybird *Harmonia axyridis*: the avian predators' point of view. *Entomol. Exp. Appl.* 151, 128–134. doi: 10.1111/eea.12176

Roland, J. (1982). Melanism and diel activity of alpine *Colias* (Lepidoptera: Pieridae). *Oecologia* 53, 214–221. doi: 10.1007/BF00545666

Sharma, A. I., Yanes, K. O., Jin, L., Garvey, S. L., Taha, S. M., and Suzuki, Y. (2016). The phenotypic plasticity of developmental modules. *EvoDevo* 7:15. doi: 10.1186/s13227-016-0053-7

Shevtsova, E., Hansson, C., Janzen, D. H., and Kjærandsen, J. (2011). Stable structural colour patterns displayed on transparent insect wings. *Proc. Natl. Acad. Sci. U.S.A.* 108, 668–673. doi: 10.1073/pnas.1017393108

Solensky, M. J., and Larkin, E. (2003). Temperature-induced variation in larval colouration in *Danaus plexippus* (Lepidoptera: Nymphalidae). *Ann. Entomol. Soc. Am.* 96, 211–216. doi: 10.1603/0013-8746(2003)096%5B0211:tvilci%5D2.0.co;2

Suderman, R. J., Dittmer, N. T., Kanost, M. R., and Kramer, K. J. (2006). Model reactions for insect cuticle sclerotization: cross-linking of recombinant cuticular proteins upon their laccase-catalyzed oxidative conjugation with catechols. *Insect Biochem. Molec.* 36, 353–365. doi: 10.1016/j.ibmb.2006.01.012

Sun, Y. X., Hao, Y. N., and Liu, T. X. (2018a). A β-carotene-amended artificial diet increases larval survival and be applicable in mass rearing of *Harmonia axyridis*. *Biol. Control* 123, 105–110. doi: 10.1016/j.biocontrol.2018.04.010

Sun, Y. X., Hao, Y. N., Yan, Y., Zhang, Y., Feng, Y., and Liu, T. X. (2018b). Morphological and biological characterization of a light-coloured mutant in the multicoloured Asian lady beetle, *Harmonia axyridis*. *Ecol. Evol.* 8, 9975–9985. doi: 10.1002/ece3.4379

Tan, C. C. (1946). Mosaic dominance in the inheritance of colour patterns in the lady-bird beetle, *Harmonia axyridis*. *Genetics* 31:195.

Tomoyasu, Y. (2017). Ultrabithorax and the evolution of insect forewing/hindwing differentiation. *Curr. Opin. Insect Sci.* 19, 8–15. doi: 10.1016/j.cois.2016.10.007

True, J. R., Edwards, K. A., Yamamoto, D., and Carroll, S. B. (1999). *Drosophila* wing melanin patterns form by vein-dependent elaboration of enzymatic prepatterns. *Curr. Biol.* 9, 1382–1391. doi: 10.1016/S0960-9822(00)80083-4

Trullas, S. C., van Wyk, J. H., and Spotila, J. R. (2007). Thermal melanism in ectotherms. *J. Therm. Biol.* 32, 235–245. doi: 10.1016/j.jtherbio.2007.01.013

Ueno, H., Sato, Y., and Tsuchida, K. (1998). Colour-associated mating success in a polymorphic Ladybird Beetle, *Harmonia axyridis*. *Funct. Ecol.* 12, 757–761. doi: 10.1046/j.1365-2435.1998.00245.x

Wittkopp, P. J., and Beldade, P. (2009). Development and evolution of insect pigmentation: genetic mechanisms and the potential consequences of pleiotropy. *Semin. Cell Dev. Biol.* 20, 65–71. doi: 10.1016/j.semcdb.2008.10.002

Wittkopp, P. J., True, J. R., and Carroll, S. B. (2002). Reciprocal functions of the *Drosophila* yellow and ebony proteins in the development and evolution of pigment patterns. *Development* 129, 1849–1858.

Conflict of Interest: The authors declare that the research was conducted in the absence of any commercial or financial relationships that could be construed as a potential conflict of interest.

frontiers in Cell and Developmental Biology

REVIEW
published: 29 May 2020
doi: 10.3389/fcell.2020.00361

Regulatory Mechanisms of Cell Polyploidy in Insects

Dani Ren[1†], Juan Song[1,2†], Ming Ni[1,3], Le Kang[1,2,3] and Wei Guo[1,2]**

[1] State Key Laboratory of Integrated Management of Pest Insects and Rodents, Institute of Zoology, Chinese Academy of Sciences, Beijing, China, [2] CAS Center for Excellence in Biotic Interactions, University of Chinese Academy of Sciences, Beijing, China, [3] College of Life Sciences, Hebei University, Baoding, China

Polyploidy cells undergo the endocycle to generate DNA amplification without cell division and have important biological functions in growth, development, reproduction, immune response, nutrient support, and conferring resistance to DNA damage in animals. In this paper, we have specially summarized current research progresses in the regulatory mechanisms of cell polyploidy in insects. First, insect hormones including juvenile hormone and 20-hydroxyecdysone regulate the endocycle of variant cells in diverse insect species. Second, cells skip mitotic division in response to developmental programming and conditional stimuli such as wound healing, regeneration, and aging. Third, the reported regulatory pathways of mitotic to endocycle switch (MES), including Notch, Hippo, and JNK signaling pathways, are summarized and constructed into genetic network. Thus, we think that the studies in crosstalk of hormones and their effects on canonical pathways will shed light on the mechanism of cell polyploidy and elucidate the evolutionary adaptions of MES through diverse insect species.

Keywords: endocycle, juvenile hormone, 20-hydroxyecdysone, mitotic/endocycle switch, cell cycle

OPEN ACCESS

Edited by:
Patrizio Dimitri,
Sapienza University of Rome, Italy

Reviewed by:
Igor V. Sharakhov,
Virginia Tech, United States
Igor Zhimulev,
Institute of Molecular and Cellular Biology (RAS), Russia

****Correspondence:***
Le Kang
lkang@ioz.ac.cn
Wei Guo
guowei@ioz.ac.cn

† These authors have contributed equally to this work

Specialty section:
This article was submitted to Epigenomics and Epigenetics, a section of the journal Frontiers in Cell and Developmental Biology

Received: *22 February 2020*
Accepted: *22 April 2020*
Published: *29 May 2020*

Citation:
Ren D, Song J, Ni M, Kang L and Guo W (2020) Regulatory Mechanisms of Cell Polyploidy in Insects. Front. Cell Dev. Biol. 8:361. doi: 10.3389/fcell.2020.00361

INTRODUCTION

Cell polyploidy generated by endocycle is a cell cycle variant that undergoes multiple rounds of nuclear genome duplication in the absence of cell division (Zielke et al., 2013). In canonical mitotic cell cycles, cells pass through Gap 1 phase (G1), synthesis phase (S), Gap 2 phase (G2) and end in mitosis (M), thus the genetic materials of the mother cell are duplicated and delivered to two daughter cells (**Figure 1A**). However, in endocycles, cells increase their genomic DNA content without cell division (Lee et al., 2009). Two variations of endocycle are endoreplication and endomitosis (Zielke et al., 2013). Endoreplication consists of successive Synthesis phase to Gap phase that completely skips mitosis (Lee et al., 2009; Maldonado et al., 2019; **Figure 1B**). Cells that undergoes endoreplication result in a single, enlarged, polyploid nucleus (Calvi, 2013). A special type of endoreplication is re-replication, in which DNA is initiated multiple times at individual origins of replication within a single S phase, provoking site-specific replication of an unique sequence (Lee et al., 2009; **Figure 1B**). Thus highly amplified and underreplicated DNA sequences at different loci form supersized multifiber-like chromosomes called polytene chromosomes (Stormo and Fox, 2017). While, endomitosis consists of G1, S, G2, and partial M phases, which produces cells with a single giant nucleus, which may subsequently fragment into a multinuclear appearance (Zielke et al., 2013; **Figure 1B**).

The biological purposes of endocycle include tissue growth, blood-brain barrier formation, immune response, nutrient support, and conferring resistance to DNA damage based on tiss

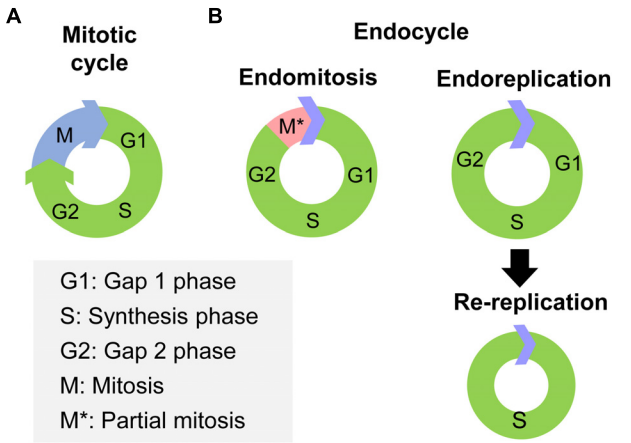

FIGURE 1 | The processes of mitotic cycle and endocycle. **(A)** The mitotic cycle comprises Gap 1 phase (G1), synthesis phase (S), Gap 2 phase (G2), and mitosis (M) phase. **(B)** The endocycle have two variations, endomitosis and endoreplication. Endomitosis consists of G1, S, and G2 phases and only a partial M phase. Endoreplication consists of repeated successions of S to G phase that completely skips mitosis phase. Re-replication is a special type of endoreplication, in which DNA replication is initiated multiple times at individual origin of replication within the same S phase.

types and developmental stages (Lilly and Spradling, 1996; Zhang et al., 2014; Lynch and Marinov, 2015; Bretscher and Fox, 2016; Wu et al., 2018; Zülbahar et al., 2018; Maldonado et al., 2019). Endocycle is considered a low-cost strategy to increase the cell and/or tissue size and efficiently produce massive molecules needed for specific functions, which avoids spending more time, materials, and energy to go through complete mitotic cycles (Edgar and Orr-Weaver, 2001; Lynch and Marinov, 2015; Maldonado et al., 2019). Thus, polyploidy cells have advantages in the adaptation of organisms to environment; however, they can also have detrimental effects on fertility and fitness owing to genomic instability, mitotic and meiotic abnormalities, and gene expression and epigenetic changes (Zhimulev, 1996; Van de Peer et al., 2017). On the other hand, unpredicted cell polyploidy is closely related to the development and progression of cancer in mammals (Storchova and Pellman, 2004; Davoli and de Lange, 2011; Fox and Duronio, 2013; Coward and Harding, 2014). Clinically, endocycle and polyploidy have been observed in cancerous tissues, with their occurrence ranging from 11% in stomach carcinoma to 54% in liver adenocarcinoma (Storchova and Pellman, 2004; Shu et al., 2018). Therefore, these findings provided important clues for revealing the essential roles of polyploidy in normal development and tissue, homeostasis, as well as the relationship between polyploidy and the progression of cancer in vertebrate animals.

Previously, some scientists have summarized the key genes that play a role in cell polyploidy and mainly focus on the cell division arrest. The interactive regulation of E2f1, cyclin E, and cyclin-dependent kinase (CDK) promote endocycle occurrence through bypassing many of the processes of mitosis in insects and mammals (Zielke et al., 2013). And the biological purposes of cell polyploidy in many different organisms are generally discussed (Edgar and Orr-Weaver, 2001; Lee et al., 2009; Fox and Duronio, 2013). Insects as the biggest groups in invertebrates have common phenomena of cell polyploidy; however, a thorough summary of previous studies involving in more extensive insect species is lacking except in *Drosophila*. Here we review the cells types with polyploidy and recent progresses in the regulatory mechanisms of cell polyploidy in insects with special emphasis on the aspects of hormones action and environmental stimuli. In addition, we constructed a regulatory network based on previous and recent reported signaling pathways involved in MES. Finally, we proposed a promising MES study system and potential directions in cell polyploidy study in insects.

POLYPLOID CELLS IN INSECTS

Polyploidy is commonly observed in highly metabolic tissues or cells in both complete and incomplete metamorphosis insects (**Table 1**). The fat body, midgut, muscle, Malpighian tubules, and nurse cells are the most reported tissues or cells with polyploidy (Zhimulev, 1996; Lee et al., 2009; Wu et al., 2018; Maldonado et al., 2019). The ploidy levels ranged from 4C in the fat body cells of *Locusta migratoria* to 2048C in the salivary glands of *Drosophila* and varied from 4C to 64C in different cells of single tissue (Hammond and Laird, 1985; Guo et al., 2014). Most of these polyploid tissues or cells can rapidly and massively synthesize proteins upon necessity during development, reproduction, immunity, flight, and other life activities (Ray et al., 2009; Fox and Duronio, 2013; Rangel et al., 2015; Wu et al., 2016).

In the fruit fly *Drosophila melanogaster*, larval growth is achieved primarily via endoreplication (Edgar and Nijhout, 2004). Most *Drosophila* larval tissues are composed mainly of polyploid cells including the salivary glands, fat body, germline cells, subperineurial glia, epidermis, gut, trachea, and Malpighian or renal tubules (Lee et al., 2009). The giant salivary gland cells undergo about 10 endocycles, resulting in polytene chromosomes (Hammond and Laird, 1985; Maldonado et al., 2019). In adult *Drosophila*, the maximum polyteny level is 64C in the midgut and 256C in Malpighian tubules, respectively (Lamb, 1982). *Drosophila* papillar cells become polyploid and naturally accumulate broken acentric chromosomes but do not apoptose/arrest the cell cycle, thus they can divide and survive despite high levels of DNA breakage (Zhang et al., 2014; Bretscher and Fox, 2016). The fat body generates polytenic cells through re-replication (Juhasz and Sass, 2005). In the female germline, nurse cells become polyploid during oogenesis, enabling them to provide vast amounts of maternal messages and products for the developing oocyte, whereas the somatic follicle cells that surround the egg undergo only three endocycles from stages 7–9 to reach a ploidy level of 16C, which facilitates the high levels of functional gene expression needed for reproduction (Calvi and Spradling, 1999; Royzman et al., 2002). Interestingly, the subperineurial glia expand enormously and become polyploid undergo both endoreplication and endomitosis, allowing it to accommodate

TABLE 1 | Tissues or cells with polyploidy in insects.

Order	Species	Tissue/cell type	Function	References
Diptera	*Drosophila melanogaster*	Brain/subperineurial glial cells	Blood-brain barrier	Unhavaithaya and Orr-Weaver, 2012; Zülbahar et al., 2018
		Ovary/nurse cells	Provide vast amounts of maternal messages and products for the developing oocyte	Royzman et al., 2002
		Ovary/follicle cells	Oocyte maturation and egg chamber development/eggshell gene amplification, DNA damage resistance	Calvi and Spradling, 1999
		Papillar cells	Repress the apoptotic response to DNA damage	Zhang et al., 2014; Bretscher and Fox, 2016
		Salivary glands	Synthesis and secretion glue proteins	Hammond and Laird, 1985; Buntrock et al., 2012
		Fat body	–	Juhasz and Sass, 2005
		Hindgut/rectal papillae	–	Fox and Duronio, 2013
		Trachea	–	Fox and Duronio, 2013
		Malpighian tubules	Absorb water, solutes, and wastes and excrete them as nitrogenous compounds	Lamb, 1982
		Renal tubules	–	Fox and Duronio, 2013
		Epidermis	–	Fox and Duronio, 2013
		Mechanosory bristle/shaft cells	–	Audibert et al., 2005
		Mechanosory bristle/socket cells	–	Audibert et al., 2005
	Calliphora erythrocephala	Ovary/nurse cells	–	Ribbert, 1979
	Aedes aegypti	Midgut	Immune response	Ray et al., 2009; Maldonado et al., 2019
	Culex pipiens	Midgut	Immune response	Ray et al., 2009; Maldonado et al., 2019
	Anopheles gambiae	Ovary/nurse cells	–	Zhimulev, 1996
	Anopheles albimanus	Ovary/nurse cells	–	Zhimulev, 1996
	Chironomus tentans	Salivary glands	–	Zhimulev et al., 2004
Orthoptera	*Locusta migratoria*	Fat body (female)	Massive synthesis of vitellogenin	Guo et al., 2014; Wu et al., 2016; Wu et al., 2018
		Fat body (male)	–	Ren et al., 2019
		Fat body-like tissue	–	Ren et al., 2019
		Ovary/follicle cells	Oocyte maturation and egg chamber development	Wu et al., 2016; Wu et al., 2018
Coleoptera	*Tribolium castaneum*	Midgut/intestinal stem cells	–	Parthasarathy and Palli, 2008
Lepidoptera	*Ephestia kuehniella*	Malpighian tubules	–	Buntrock et al., 2012
		Silk glands	High silk production	Buntrock et al., 2012
		Wing epithelium	Increase cell size	Edgar and Orr-Weaver, 2001
	Spodoptera frugiperda	Ovary	–	Meneses-Acosta et al., 2001
Hymenoptera	*Apis mellifera*	Malpighian tubules	–	Rangel et al., 2015
		Brain	–	Rangel et al., 2015
		Stinger	–	Rangel et al., 2015
		Leg	–	Rangel et al., 2015
		Thoracic muscle	–	Rangel et al., 2015
		Flight muscle	–	Rangel et al., 2015
	Bombus terrestris L.	Mandibular muscle (haploid male)	Keep pace with females in terms of muscular metabolic activity and efficiency	Aron et al., 2005
		Thoracic muscle (haploid male)	Keep pace with females in terms of muscular metabolic activity and efficiency	Aron et al., 2005
		Leg muscles (haploid male)	Keep pace with females in terms of muscular metabolic activity and efficiency	Aron et al., 2005
	Solenopsis invicta	Whole body	Body size and behavior	Scholes et al., 2013
	Pogonomyrmex badius	Whole body	Body size and behavior	Scholes et al., 2013
	Camponotus floridanus	Whole body	Body size and behavior	Scholes et al., 2013
	Atta texana	Whole body	Body size and behavior	Scholes et al., 2013

growing neurons, while simultaneously maintaining the blood-brain barrier, which otherwise would be disrupted through cell division (Unhavaithaya and Orr-Weaver, 2012; Zülbahar et al., 2018). During *Drosophila* pupal development, shaft and socket cells that form parts of the mechanosory bristle undergo two or three endocycles to produce cells with 8C or 16C DNA (Audibert et al., 2005). Therefore, the extensive cell polyploidy in *Drosophila* variant tissues and developmental stages displays the cellular potentials to remodel for various functions.

Polyploidy cells are also found in variant complete metamorphosis insect species. In mosquitoes, polyploidy cells arise in the anterior and posterior midgut of *Aedes aegypti*, yet only in anterior midgut *of Culex pipiens* during larval development (Ray et al., 2009). These polyploid midgut cells facilitate the fast production of immune proteins in a process known as priming (Maldonado et al., 2019). Polyploid chromosomes are formed in ovarian nurse cells of *Anopheles albimanus* and polytene chromosomes are formed in ovarian nurse cells of *Anopheles gambiae* and salivary glands of *Chironomus tentans* (Zhimulev, 1996; Zhimulev et al., 2004). In the *Calliphora erythrocephala*, nurse cells also developed polytene chromosomes post inbreeding and artificial selection (Ribbert, 1979). In the honey bee *Apis mellifera*, the Malpighian tubules is the most highly polyploid secretory cells, and the brain, stinger, leg, thoracic muscle, and flight muscle also generate polyploid cells (Rangel et al., 2015). In the bumble bee *Bombus terrestris L.*, cells in mandibular, thoracic, and leg muscles of the haploid male undergo one round of endoreduplication to become functionally diploid and get comparable size and function to those of the diploid female (Aron et al., 2005). Ploidy levels between and among worker castes of four highly polymorphic ant species, red imported fire ant *Solenopsis invicta*, Florida harvester ant *Pogonomyrmex badius*, Florida carpenter ant *Camponotus floridanus,* and Texas leaf-cutting ant *Atta texana*, are positively related to worker size, suggesting that worker task performance might benefit from endoreplication of certain tissues (Scholes et al., 2013). In the red flour beetle *Tribolium castaneum* larval stages, intestinal stem cells (ISC) conduct endoreplication for adult midgut polyploidic epithelium formation (Parthasarathy and Palli, 2008). In the flour moth *Ephestia kuehniella*, cells of Malpighian tubules and silk glands undergo endocycle through all larvae instars, and even, in the last instar, larvae nuclei are polyploid with a high DNA content, provoking a branched nucleus (Buntrock et al., 2012). In *Spodoptera frugiperda* sf9 ovarian cells, cell cycle arrests in G2/M phase to generate polynucleated cells (Meneses-Acosta et al., 2001).

In the migratory locust, *Locusta migratoria*, an incomplete metamorphosis insect species, fat body cells of female adults undergo extensive DNA replication to produce from 4C to 64C polyploidy cells during vitellogenesis. These polyploidy cells support the rapidly massive synthesis of vitellogenin, the main proteins in egg maturation, for dozens of oocytes in every gonadotrophic cycle. Besides, female locust follicle cells also undergo high levels of endoreplication during oocyte maturation to synthesize chorion protein for success chorionogenesis (Kimber, 1980; Guo et al., 2014; Wu et al., 2016, 2018). While in the male locust, the abdominal fat body (FB) undergoes endocycle and generates 4C to 8C polyploidy cells, while the fat body-like tissue (FLT) surrounding testis follicles is dominated by diploid cells instead of polyploidy cells (Ren et al., 2019). Thus, similar or same tissues in one species display different polyploidy levels between both genders or in different hemocal locations.

Both polyploid and polytene chromosomes originate by the endocycle. In the polytene chromosomes, the replicated sister chromatids remain attached and aligned and the chromosomes become visible. In polyploid cells, the replicated chromosome copies are dispersed and the chromosomes are not visible in the nucleus (Frawley and Orr-Weaver, 2015). Therefore, polytene chromosomes are specialized polyploid chromosomes. Transition between polytene and polyploid chromosome have been studied in *Drosophila* ovarian nurse cells (Bauer et al., 2012). Condensin II drives axial compaction and therefore force apart chromatids destroying a typical polytene chromosome structure, thus, polyploid chromosome are formed in the nurse cells (Bauer et al., 2012). It seems that polytene chromosomes formation are energy-saving to mainly skip duplicating heterochromatic regions, while polyploid chromosomes are advantageous to massively duplicate any gene upon necessity although its formation needs more energy (Frawley and Orr-Weaver, 2015; Stormo and Fox, 2017). Thus, we speculated that the use of different endoreplication strategies might indicate an adaptive trade-off between energy consuming in DNA amplification and the tissue demands for specific protein syntheses. Taken together, the extensive occurrence of cell polyploidy in variant insect species provide excellent study materials to decipher the regulatory mechanisms of endocycle in the light of evolution.

GENETIC NETWORK IN ENDOCYCLE

Although significantly different from the conventional cell cycle, endocycle uses regulatory pathways that also function in diploid cells (Lee et al., 2009; Calvi, 2013). Cyclin-dependent kinase (Cdk) 4/6 form an active complex with Cyclin D (CycD), phosphorylate and inactivate retinoblastoma protein (Rb), releasing transcription factor adenovirus E2 factor-1 (E2f1) from Rb-mediated repression (Swanson et al., 2015; Tigan et al., 2016). Cyclin E (CycE), which is activated by E2f1, together with cyclin-dependent kinase 2 (Cdk2), triggers S-phase by phosphorylating Sld2 and Sld3, which then recruit Dpb11 to replication origins, thereby activating the Mini-chromosome maintenance (Mcm) 2–7 DNA helicase (Zielke et al., 2011; Tanaka and Araki, 2012; Bell and Kaguni, 2013). Together with the origin recognition complex and Cdt1 (Cdc10 protein-dependent transcript 1), Cdc6 loads Mcm proteins onto DNA at the origins of replication to facilitate the formation of stable prereplication complex in G1 phase, thereby licensing these sites to initiate DNA replication in S phase (Sun et al., 2013; Wu et al., 2016; **Figure 2**).

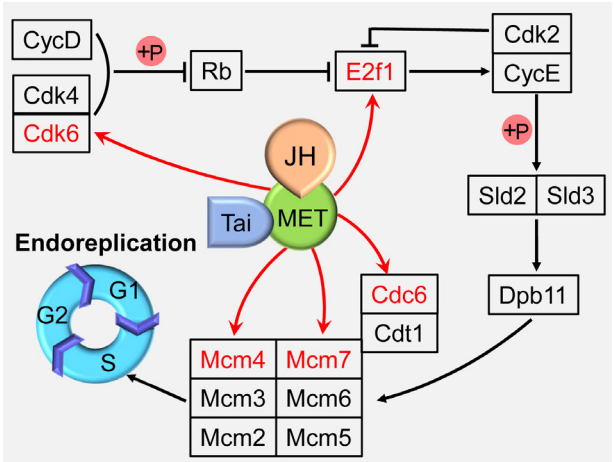

FIGURE 2 | Juvenile hormone (JH) regulation of the endoreplication. JH-Met/Tai ligand-receptor complex directly activates the expressions of cell cycle genes including minichromosome maintenance proteins 4 and 7 (Mcm4 and 7), cell division cycle 6 (Cdc6), cyclin-dependent kinase 6 (Cdk6), and adenovirus E2 factor-1 (E2f1) to regulate endoreplication and cell polyploidy. Met, Methoprene-tolerant; Tai, Taiman; CycD, cyclin D; Cdk2 and 4, Cyclin-dependent kinase 2 and 4; Rb, retinoblastoma; CycE, cyclin E; Cdt1, Cdc10 protein-dependent transcript 1; Mcm2, 3, 5, and 6, minichromosome maintenance protein 2, 3, 5, and 6.

ENDOCYCLE GOVERNED BY INSECT HORMONE

Juvenile hormone (JH) and 20-hydroxyecdysone (20E), as two dominant hormones that are involved in insect development, metamorphosis, and reproduction, play key roles in the regulation of cell polyploidy by binding to their respective nuclear receptors to initiate the expression of cell cycle genes (Fallon and Gerenday, 2010; Jindra et al., 2013; Yamanaka et al., 2013; Guo et al., 2014; Moriyama et al., 2016; Wu et al., 2016, 2018; Maldonado et al., 2019). Many studies have confirmed that the two hormones can regulate cell polyploidy in insects.

Juvenile hormone is a sesquiterpenoid produced by the corpora allata, and functions in cells by inducing the heterodimerization of its receptor, Methoprene-tolerant (Met) with Taiman (Tai). Met and Tai form a functional receptor to control insect development, metamorphosis, and reproduction (Jindra et al., 2013; Wang et al., 2017). The migratory locust, *Locusta migratoria* is the most well-studied insect species in the JH regulation on cell polyploidy. The adult fat body undergoes extensive DNA replication to highly polyploidy cells during vitellogenesis for successful reproduction under the regulation of JH (Nair et al., 1981; Oishi et al., 1985). In an effort to elucidate the mechanisms of JH action on female reproduction, digital gene expression profiling was employed to identify differentially expressed genes in JH-deprived fat bodies and those further treated with a JH analog (JHA). DNA replication pathway was identified as the top one "hit" after JHA treatment by Kyoto Encyclopedia of Genes and Genomes (KEGG) analyses (Guo et al., 2014). Further study revealed that Met binds directly on the E-box (CACGTG) or E-box-like (CACGCG) motifs in the promoter regions of Mcm4, Mcm7, and Cdc6 to activate the transcription of these genes, which promotes the endoreplication of fat body cells (Guo et al., 2014; Wu et al., 2016). In addition, JH-Met/Tai complex directly activates the transcription of Cdk6 and E2f1, and depletion of Cdk6 or E2f1 results in significantly decreased the cell polyploidy level, precocious mitotic entry for multinuclear appearance, and increased cell numbers in the fat body cells (Wu et al., 2018; **Figure 2**). These results indicate that JH is able to directly activate several cell cycle genes to enhance endoreplication process.

The ecdysteroid is also involved in cell cycle regulation in a different way from JH. The major ecdysteroid in insects such as 20E not only promotes molting at juvenile stages but also affects lifespan, learning, stress-induced responses, sleep regulation, social interactions, and sexual behavior in adults (Yamanaka et al., 2013). 20E mediate the switch between endocycle and site-specific endoreplication by binding to the ecdysone receptor (EcR) (Maldonado et al., 2019). Importantly, 20E also regulates DNA replication and polyploidy during insect metamorphosis (Sun et al., 2008). Correlations between epidermal DNA synthesis and hemolymph ecdysteroid levels have been revealed in the tobacco hornworm *Manduca sexta* and *Calpodes ethlius* (Wielgus et al., 1979; Dean et al., 1980). In *Plodia interpunctella*, imaginal wing cells arrest in G2 phase post 20E treatment by inducing a sharp decrease in the levels of cyclin A and B expression (Mottier et al., 2004). In cell line C7-10 from the mosquito *Aedes albopicus*, 20E application resulted in cell arrest in the G1 phase (Gerenday and Fallon, 2004). Further studies suggest that 20E treatment increases the expression of Cyclin E-Cdk2 inhibitory protein DACAPO, while decreases the expression of cyclin A (Fallon and Gerenday, 2010). In the wing discs of silkworm *Bombyx mori*, 20E directly activates c-Myc transcription, which subsequently stimulates the expression of cell cycle core regulators, including cyclinA, cyclinB, cyclinD, cyclinE, Cdc25, and E2F1 genes to promote endocycle progression and cell polyploidization during metamorphosis (Moriyama et al., 2016; **Figure 3**). These studies indicate that 20E promotes cell proliferation in low titer and initiates cell cycle arrest in high titer (Koyama et al., 2004; Moriyama et al., 2016). Thus, actions of 20E on cell polyploidy vary in different insect species in a dose-dependent way.

However, the interactions between JH and 20E in cell polyploidy regulation are still largely unknown. Classically, 20E counteracts on the function of JH during molting and metamorphosis (Liu P. C. et al., 2018; Liu S. et al., 2018). Studies of JH and 20E actions on cell polyploidy focus mainly on the aspects of DNA reduplication enhancement and cell division arrest, respectively. JH and 20E may jointly coordinate the timing of DNA reduplication and cell division during MES process.

ENVIRONMENT-EVOKED ENDOCYCLE

In response to pathogen, wound, and aging, some tissue cells are re-programmed, exiting their mitotic cell cycle to differentiate into polyploidy cells (Zielke et al., 2013). In *Drosophila*, ovarian pseudonurse cells raised the frequency of polytene chromosomes

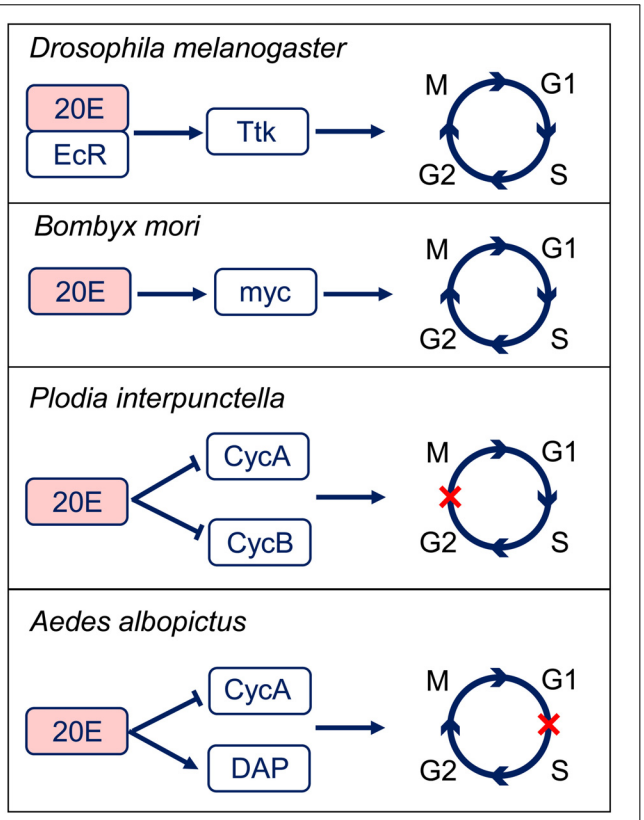

FIGURE 3 | 20-hydroxyecdysone (20E) regulation of the cell cycle progression. In *Drosophila melanogaster*, 20E-EcR positively regulates Tramtrack (Ttk) to transit the endocycle to mitotic cycle. In *Bombyx mori*, 20E promotes cell cycle progression through activation of c-Myc. In *Plodia interpunctella*, 20E induces an arrest of cells in G2 phase by decreasing the expressions of cyclin (Cyc) A and B. In *Aedes albopictus*, 20E application results in an accumulation of cells in G1 phase by decreasing CycA and increasing Dacapo (DAP) expresisons. EcR, ecdysone receptor.

in response to low temperature and protein-rich food (Mal'ceva et al., 1995). In *Anopheles albimanus*, the increase of cell DNA synthesis after challenged with different microorganism and *Plasmodium sp.* is considered as an adaptive immune response, which can be recalled quickly in next exposure to the same pathogens (Hernández-Martínez et al., 2013; Contreras-Garduño et al., 2015). In the adult *Drosophila* epidermis and hindgut, post-mitotic differentiated diploid cells respond to wounding by entering the endocycle, and this process is called wound-induced polyploidization (WIP) (Losick et al., 2016). In the honey bee *Apis mellifera*, endoreplication levels change with worker age in a tissue-specific manner, and there is a surprisingly significant decrease in cell ploidy in the leg and the thoracic muscles with aging (Rangel et al., 2015).

On the other hand, the mitotic cell cycle can be activated in some insects post stimuli. In *Aedes albopictus*, midgut generates an increase in regenerative cells after chemical and bacterial damages (Janeh et al., 2017). Besides, cell proliferation has been tested in *Aedes aegypti* midgut post viral infections and oxidative stress (Taracena et al., 2018). In *Drosophila*, starvation reduces E2f1 mRNA levels and blocks endocycling in salivary glands, whereas overexpression of E2f1 restores endocycles in starved fruit flies (Zielke et al., 2011). Inhibition of the target of rapamycin (TOR) in *Drosophila* prothoracic gland causes nutrient-dependent endocycle inhibition and developmental arrest (Ohhara et al., 2017). Thus, cell polyploidy displays adaptive plasticity to respond to unpredicted environment changes through remodeling the mitotic cycle to endocycle.

MOLECULAR MECHANISMS OF MITOSIS/ENDOCYCLE SWITCH

Cells switch from the mitotic cycle to the endocycle response to developmental signals or environmental stimuli, and become polyploidy rather than proliferation. This intermediate process is defined as the mitosis/endocycle switch (MES). The thrombopoetin and the Notch pathways have been identified as the major regulators of the mitotic-to-endocycle switch. The thrombopoetin pathway acts during differentiation of megakaryocytes, and the Notch pathway acts during the oogenesis and differentiation of trophoblasts (Zimmet and Ravid, 2000; Deng et al., 2001; López-Schier and St Johnston, 2001). Besides, the JNK pathway is also demonstrated to be required to promote mitosis prior to the transition, independent of the cell cycle components acted on by the Notch pathway (Jordan et al., 2006). In follicle cells, the Notch pathway stops proliferation and promotes a switch from the mitotic cycle to the endocycle (Sun and Deng, 2007). In contrast to Notch signal, Hedgehog (Hh) signal appears to promote follicle cell proliferation (Zhang and Kalderon, 2000).

The Notch signaling pathway in *Drosophila* follicle epithelium is a key upstream regulator of the MES. The ligand Delta expressed by oocytes activates the Notch receptor in follicle cells (Deng et al., 2001). Notch activity leads to downregulation of String (STG) and Dacapo (DAP), and upregulation of Cdh1/Fizzy-related (FZR) (Jordan et al., 2006). STG is a G2/M regulator Cdc25 phosphatase that removes inhibitory phosphates from Cdk1, allowing it to associate with CycA and CycB and initiate mitosis (Zielke et al., 2013). CycB-Cdk1 in return activates the STG by phosphorylation, which creates a positive feedback loop (Zielke et al., 2013). The activity of CycB-Cdk1 is further inactivated through phosphorylation (Welburn et al., 2007). Cdk1 can be phosphorylated on Tyr15 by Wee1 kinase, and on both Thr14 and Tyr15 by Myelin transcription factor 1 (Myt1) kinase (Parker and Piwnica-Worms, 1992; Mueller et al., 1995). Interestingly, Wee1 is phosphorylated and thereby inactivated by CycB-Cdk1, which creates a double negative feedback loop (Tang et al., 1993). CycA/CDK directly activates the Myb-MuvB (MMB) complex to induce transcription of a battery of cell cycle genes required for mitosis. AuroraB (AurB) is an MMB regulated gene, and knockdown of AurB and other subunits of the chromosomal passenger complex (CPC) induced endoreplication (Rotelli et al., 2019). Down-regulating of the CycE/CDK complex inhibitor DAP releases CycE/Cdk2, thus blocks S phase initiation (Zielke et al., 2013). FZR is a regulator of the APC ubiquitination complex that degrade CycA and CycB,

thereby reinforcing the block to mitosis (Zielke et al., 2013). FZR is negatively regulated by the homeodomain gene Cut, but Cut does not seem to regulate String (Stg) (Sun and Deng, 2005, 2007). String/Cdc25 and the transcription factor Cut are repressed by a zinc-finger transcription factor Hindsight (Hnt) (Sun and Deng, 2007). However, during oogenesis, Notch in *Drosophila* follicle cells is down-regulated and cooperate with Tramtrack (Ttk), a transcription factor that induces endocycle exit and entry in site-specific endoreplication (Sun et al., 2008). In the *Drosophila* bristle lineage, Ttk downregulates Cyclin E expression and is probably involved in the exit of the cells from the cell cycle (Audibert et al., 2005; **Figure 4**).

Hippo pathway in the *Drosophila* nervous system has been reported to be involved in the MES. Yki, an essential transcriptional activator of Hippo pathway, is required to establish the correct ploidy and is partly post-transcriptionally regulated miR-285. miR-285 is an upstream regulator of the Hippo pathway, which can directly target Yki cofactor Multiple Ankyrin repeats Single KH domain (Mask) to suppress Yki activity and down-regulates the expression of its downstream target cyclin E (CycE). Disturbance of CycE expression in subperineurial glial cell (SPG) causes abnormal endoreplication, which leads to aberrant DNA ploidy and defective septate junctions (Li et al., 2017). Moreover, the N-terminal asparagine amidohydrolase homolog Öbek counteracts the activity of Yki, as well as the activity of the fibroblast growth factor (FGF) receptor Heartless in glial cells to limit endoreplication and the consequent appearance of extra nuclei. However, other dividing cells are not affected by alteration of Öbek expression (Zülbahar et al., 2018). Cooperative activation of Yki and JNK upregulates *Drosophila* inhibitor-of-apoptosis protein 1 (Diap1) prevents mitotic entry by downregulating G2/M cyclin CycB, thereby inducing endoreplication (Cong et al., 2018). The protein level of *Drosophila* CycB is mediated by ubiquitination-mediated degradation, and Diap1 contains a RING domain and acts as an E3 ligase that could cause ubiquitination-mediated degradation of CycB in either direct or indirect manner (Xu et al., 2009; Shabbeer et al., 2013; Cong et al., 2018; **Figure 4**).

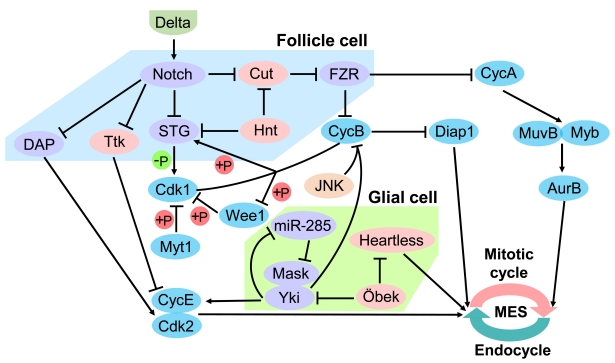

FIGURE 4 | Regulation of mitotic/endocycle switch. In the *Drosophila* follicle cell, Notch signaling pathway is a key upstream regulator of the mitotic/endocycle switch (MES). Activated Notch protein by the ligand Delta from oocytes terminates follicle cell proliferation and promotes MES by downregulating String (STG) and Dacapo (DAP) and upregulating FZR. In the *Drosophila* glial cell, Hippo signaling pathway is involved in MES. miR-285 suppresses Yki-Mask dimer activity by targeting Mask to downregulate cyclin E (CycE). Moreover, the N-terminal asparagine amidohydrolase homolog Öbek counteracts the activity of Yki and Heartless to limit endoreplication. FZR, Cdh1/Fizzy-related; Yki, Yorkie; Mask, Multiple Ankyrin repeats Single KH domain; Hnt, Hindsight; Ttk, Tramtrack; Cdk1 and 2, Cyclin-dependent kinase 1 and 2; Myt1, Myelin transcription factor 1; CycA and B, cyclin A and B; Diap1, *Drosophila* inhibitor-of-apoptosis protein 1; AurB, AuroraB.

A recent study in the migratory locust *Locusta migratoria* reported that FB cells undergo endocycle and become polyploidy, while FLT cells undergo rounds of mitotic cycle and dominated by diploid cells at the same developmental stages during male adult maturation. FB-FLT cells displayed different cell cycle strategy at the same developmental stages, avoiding the interference of developmental programming. Further analyses of comparative transcriptomes of FB-FLT provided valuable candidate cell cycle genes and transcription factors to investigate the molecular mechanism of MES (Ren et al., 2019). Probably, the FB-FLT of locust is one of novel promising systems to study MES.

The developmental signals and environmental stimuli can affect the performance of the MES. In endocycling cells, promoters of pro-apoptotic genes are silenced rendering them insensitive to DNA damage (Mehrotra et al., 2008). Starvation induces the pause of the M/E switch in *Drosophila* follicle cells, blocking the entry of egg chambers into vitellogenesis. Paused MES is induced by a reduction of insulin signal and involves a previously unknown crosstalk among FoxO, Cut, and Notch. FoxO is dispensable for the normal M/E switch. However, in paused MES, FoxO activates Cut expression cell-autonomously in follicle cells (Jouandin et al., 2014). Besides, MES regulation may vary in different tissues or cell types. The mitotic cyclins in endocycling follicle cells are regulated only by ubiquitin-dependent degradation, whereas in salivary glands, transcription of mitotic cyclins is terminated concomitantly with up-regulation of Fzr (Zielke et al., 2008; Maqbool et al., 2010). The suppression of mitotic regulators in endoreplicating salivary glands is mediated, at least in part, by the transcriptional repressor E2F2 (Zielke et al., 2011). Besides, Notch controls the switches of different cell cycle programs in follicle cells, yet the nurse cell endocycles are normal in Notch mutant clones (Lilly and Duronio, 2005).

In brief, *Drosophila* follicle cells and glial cells are two well-studied systems and locust FB-FLT would be a novel promising system to investigate the molecular mechanisms of MES (Sun and Deng, 2007; Li et al., 2017; Cong et al., 2018; Zülbahar et al., 2018; Ren et al., 2019). Developmentally controlled MES were regulated by Notch and Hippo signaling pathway; however, the environmental-stimulated MES have probable specific mechanisms which are condition-dependent.

PROSPECTS

Insects are the best models to study regulatory mechanisms of polyploidy, compared to vertebrates and plants. First, polyploidization can be observed at larvae and adult stages in both complete and incomplete metamorphosis insects.

Second, cells in different tissues of insects undergo endocycle during particular developmental stages or response to environmental stimuli.

Insect hormones play critical roles on cell polyploidy progression. JH promotes cell polyploidization by directly upregulating several DNA replication genes (Guo et al., 2014; Wu et al., 2016, 2018). However, whether JH also acts on cell division genes remains to be studied. Besides, the role of 20E played in cell cycle regulation is unclear, and the target genes of 20E in cell cycle process are also largely unknown. In some processes, JH plays a critical role in defining the action of 20E, and 20E also affects the function of JH (Jia et al., 2017; Liu P. C. et al., 2018; Liu S. et al., 2018). In addition, JH and 20E are reported to regulate MES-related genes and miRNA (Gerenday and Fallon, 2011; Dong et al., 2015; Wang et al., 2016; Song et al., 2019). Therefore, the crosstalk of JH and 20E in cell polyploidy regulation through MES need to be further investigated to clarify their biological functions and adaptive mechanisms to developmental programming and environmental changes.

Because MES is regulated by several canonical pathways, further studies should be conducted to decipher the relationships of these pathways and their interactions orchestrated by hormones. In addition, we attempt to answer whether these pathways are conserved in the regulation on MES in different tissue cells and diverse insect species. Therefore, studies of cell cycle genes and related pathways will shed light on the evolution of cell polyploidy and provide more target genes for pest control.

AUTHOR CONTRIBUTIONS

LK, WG, and DR designed the research. DR, JS, and MN collected the references. DR, JS, WG, and LK wrote the manuscript.

FUNDING

This work was supported by National Natural Science Foundation of China (31970481 and 31572333), Key Research Program of the Chinese Academy of Sciences (KJZD-SW-L07), Youth Innovation Promotion Association, CAS (No. 2016080), and Postdoctoral Foundation of China (2017M620907).

REFERENCES

Aron, S., de Menten, L., Van Bockstaele, D. R., Blank, S. M., and Roisin, Y. (2005). When hymenopteran males reinvented diploidy. *Curr. Biol.* 15, 824–827. doi: 10.1016/j.cub.2005.03.017

Audibert, A., Simon, F., and Gho, M. (2005). Cell cycle diversity involves differential regulation of Cyclin E activity in the *Drosophila* bristle cell lineage. *Development* 132, 2287–2297. doi: 10.1242/dev.01797

Bauer, C. R., Hartl, T. A., and Bosco, G. (2012). Condensin II promotes the formation of chromosome territories by inducing axial compaction of polyploid interphase chromosomes. *PLoS Genet.* 8:e1002873. doi: 10.1371/journal.pgen.1002873

Bell, S. P., and Kaguni, J. M. (2013). Helicase loading at chromosomal origins of replication. *Cold Spring Harb. Perspect. Biol.* 5:a010124. doi: 10.1101/cshperspect.a010124

Bretscher, H. S., and Fox, D. T. (2016). Proliferation of double-strand break-resistant polyploid cells requires *Drosophila* FANCD2. *Dev. Cell* 37, 444–457. doi: 10.1016/j.devcel.2016.05.004

Buntrock, L., Marec, F., Krueger, S., and Traut, W. (2012). Organ growth without cell division: somatic polyploidy in a moth, *Ephestia kuehniella*. *Genome* 55, 755–763. doi: 10.1139/g2012-060

Calvi, B. R. (2013). Making big cells: one size does not fit all. *Proc. Natl. Acad. Sci. U.S.A.* 110, 9621–9622. doi: 10.1073/pnas.1306908110

Calvi, B. R., and Spradling, A. C. (1999). Chorion gene amplification in *Drosophila*: A model for metazoan origins of DNA replication and S-phase control. *Methods* 18, 407–417. doi: 10.1006/meth.1999.0799

Cong, B., Ohsawa, S., and Igaki, T. (2018). JNK and Yorkie drive tumor progression by generating polyploid giant cells in *Drosophila*. *Oncogene* 37, 3088–3097. doi: 10.1038/s41388-018-0201-8

Contreras-Garduño, J., Rodríguez, M. C., Hernández-Martínez, S., Martínez-Barnetche, J., Alvarado-Delgado, A., Izquierdo, J., et al. (2015). *Plasmodium berghei* induced priming in *Anopheles albimanus* independently of bacterial co-infection. *Dev. Comp. Immunol.* 52, 172–181. doi: 10.1016/j.dci.2015.05.004

Coward, J., and Harding, A. (2014). Size does matter: why polyploid tumor cells are critical drug targets in the war on cancer. *Front. Oncol.* 4:123. doi: 10.3389/fonc.2014.00123

Davoli, T., and de Lange, T. (2011). The causes and consequences of polyploidy in normal development and cancer. *Annu. Rev. Cell Dev. Biol.* 27, 585–610. doi: 10.1146/annurev-cellbio-092910-154234

Dean, R. L., Bollenbacher, W. E., Locke, M., Smith, S. L., and Gilbert, L. I. (1980). Haemolymph ecdysteroid levels and cellular events in the intermoult/moult sequence of *Calpodes ethlius*. *J. Insect Physiol.* 26, 267–280. doi: 10.1016/0022-1910(80)90073-6

Deng, W. M., Althauser, C., and Ruohola-Baker, H. (2001). Notch-Delta signaling induces a transition from mitotic cell cycle to endocycle in *Drosophila* follicle cells. *Development* 128, 4737–4746.

Dong, D. J., Jing, Y. P., Liu, W., Wang, J. X., and Zhao, X. F. (2015). The steroid hormone 20-Hydroxyecdysone up-regulates Ste-20 family serine/threonine kinase Hippo to induce programmed cell death. *J. Biol. Chem.* 290, 24738–24746. doi: 10.1074/jbc.M115.643783

Edgar, B. A., and Orr-Weaver, T. L. (2001). Endoreplication cell cycles: more for less. *Cell* 105, 297–306. doi: 10.1016/s0092-8674(01)00334-8

Edgar, B. A., and Nijhout, H. F. (2004). "Growth and cell cycle control in *Drosophila*," in *Cell Growth – Control of Cell Size*. M. N. Hall, M. Raff, G. Thomas (Cold Spring Harbor, NY: Cold Spring Harb Perspect Biol) 23–83.

Fallon, A. M., and Gerenday, A. (2010). Ecdysone and the cell cycle: investigations in a mosquito cell line. *J. Insect Physiol.* 56, 1396–1401. doi: 10.1016/j.jinsphys.2010.03.016

Fox, D. T., and Duronio, R. J. (2013). Endoreplication and polyploidy: insights into development and disease. *Development* 140, 3–12. doi: 10.1242/dev.080531

Frawley, L. E., and Orr-Weaver, T. L. (2015). Polyploidy. *Curr. Biol.* 25, R353–R358. doi: 10.1016/j.cub.2015.03.037

Gerenday, A., and Fallon, A. M. (2004). Ecdysone-induced accumulation of mosquito cells in the G1 phase of the cell cycle. *J. Insect Physiol.* 50, 831–838. doi: 10.1016/j.jinsphys.2004.06.005

Gerenday, A., and Fallon, A. M. (2011). Increased levels of the cell cycle inhibitor protein, dacapo, accompany 20-hydroxyecdysone-induced G1 arrest in a mosquito cell line. *Arch. Insect Biochem. Physiol.* 78, 61–73. doi: 10.1002/arch.20440

Guo, W., Wu, Z., Song, J., Jiang, F., Wang, Z., Deng, S., et al. (2014). Juvenile hormone-receptor complex acts on mcm4 and mcm7 to promote polyploidy and vitellogenesis in the migratory locust. *PLoS Genet.* 10:e1004702. doi: 10.1371/journal.pgen.1004702

Hammond, M. P., and Laird, C. D. (1985). Chromosome structure and DNA replication in nurse and follicle cells of *Drosophila melanogaster*. *Chromosoma* 91, 267–278. doi: 10.1007/bf00328222

Hernández-Martínez, S., Barradas-Bautista, D., and Rodríguez, M. H. (2013). Differential DNA synthesis in *Anopheles albimanus* tissues induced by immune

challenge with different microorganisms. *Arch. Insect Biochem. Physiol*. 84, 1–14. doi: 10.1002/arch.21108

Janeh, M., Osman, D., and Kambris, Z. (2017). Damage-induced cell regeneration in the midgut of *Aedes albopictus* mosquitoes. *Sci. Rep*. 7:44594. doi: 10.1038/srep44594

Jia, Q., Liu, S., Wen, D., Cheng, Y., Bendena, W. G., Wang, J., et al. (2017). Juvenile hormone and 20-hydroxyecdysone coordinately control the developmental timing of matrix metalloproteinase-induced fat body cell dissociation. *J. Biol. Chem*. 292, 21504–21516. doi: 10.1074/jbc.M117.818880

Jindra, M., Palli, S. R., and Riddiford, L. M. (2013). The juvenile hormone signaling pathway in insect development. *Annu. Rev. Entomol*. 58, 181–204. doi: 10.1146/annurev-ento-120811-153700

Jordan, K. C., Schaeffer, V., Fischer, K. A., Gray, E. E., and Ruohola-Baker, H. (2006). Notch signaling through tramtrack bypasses the mitosis promoting activity of the JNK pathway in the mitotic-to-endocycle transition of *Drosophila* follicle cells. *BMC Dev. Biol*. 6:16. doi: 10.1186/1471-213X-6-16.

Jouandin, P., Ghiglione, C., and Noselli, S. (2014). Starvation induces FoxO-dependent mitotic-to-endocycle switch pausing during *Drosophila* oogenesis. *Development* 141, 3013–3021. doi: 10.1242/dev.108399

Juhasz, G., and Sass, M. (2005). Hid can induce, but is not required for autophagy in polyploid larval *Drosophila* tissues. *Eur. J. Cell Biol*. 84, 491–502. doi: 10.1016/j.ejcb.2004.11.010

Kimber, S. J. (1980). The secretion of the eggshell of *Schistocerca gregaria*: ultrastructure of the follicle cells during the termination of vitellogenesis and eggshell secretion. *J. Cell Sci*. 46, 455–477.

Koyama, T., Iwami, M., and Sakurai, S. (2004). Ecdysteroid control of cell cycle and cellular commitment in insect wing imaginal discs. *Mol. Cell Endocrinol*. 213, 155–166. doi: 10.1016/j.mce.2003.10.063

Lamb, M. J. (1982). The DNA content of polytene nuclei in midgut and Malpighian tubule cells of adult *Drosophila melanogaster*. *Wilehm. Roux Arch. Dev. Biol*. 191, 381–384. doi: 10.1007/BF00879628

Lee, H. O., Davidson, J. M., and Duronio, R. J. (2009). Endoreplication: polyploidy with purpose. *Genes Dev*. 23, 2461–2477. doi: 10.1101/gad.1829209

Li, D., Liu, Y., Pei, C., Zhang, P., Pan, L., Xiao, J., et al. (2017). miR-285-Yki/Mask double-negative feedback loop mediates blood-brain barrier integrity in *Drosophila*. *Proc. Natl. Acad. Sci. U.S.A*. 114, E2365–E2374. doi: 10.1073/pnas.1613233114

Lilly, M. A., and Duronio, R. J. (2005). New insights into cell cycle control from the *Drosophila* endocycle. *Oncogene* 24, 2765–2775. doi: 10.1038/sj.onc.1208610

Lilly, M. A., and Spradling, A. C. (1996). The *Drosophila* endocycle is controlled by cyclin E and lacks a checkpoint ensuring S-phase completion. *Genes Dev*. 10, 2514–2526. doi: 10.1101/gad.10.19.2514

Liu, P. C., Fu, X. N., and Zhu, J. S. (2018). Juvenile hormone-regulated alternative splicing of the taiman gene primes the ecdysteroid response in adult mosquitoes. *Proc. Natl. Acad. Sci. U.S.A*. 115, E7738–E7747. doi: 10.1073/pnas.1808146115

Liu, S., Li, K., Gao, Y., Liu, X., Chen, W., Ge, W., et al. (2018). Antagonistic actions of juvenile hormone and 20-hydroxyecdysone within the ring gland determine developmental transitions in *Drosophila*. *Proc. Natl. Acad. Sci. U.S.A*. 115, 139–144. doi: 10.1073/pnas.1716897115

López-Schier, H., and St Johnston, D. (2001). Delta signaling from the germ line controls the proliferation and differentiation of the somatic follicle cells during *Drosophila* oogenesis. *Genes Dev*. 15, 1393–1405. doi: 10.1101/gad.200901

Losick, V. P., Jun, A. S., and Spradling, A. C. (2016). Wound-induced polyploidization: regulation by Hippo and JNK signaling and conservation in mammals. *PLoS One* 11:e0151251. doi: 10.1371/journal.pone.0151251

Lynch, M., and Marinov, G. K. (2015). The bioenergetic costs of a gene. *Proc. Natl. Acad. Sci. U.S.A*. 112, 15690–15695. doi: 10.1073/pnas.1514974112

Mal'ceva, N. I., Gyurkovics, H., and Zhimulev, I. F. (1995). General characteristics of the polytene chromosomes from ovarian pseudonurse cells of the *Drosophila melanogaster* otu11 and fs(2)B mutants. *Chromosome Res*. 3, 191–200. doi: 10.1007/bf00710713

Maldonado, K. M., Mendoza, H. L., and Cruz Hernandez-Hernandez, F. (2019). Cell cycle dynamics and endoreplication in the mosquito midgut. *Am. J. Biomed. Sci. Res*. 5, 43–46. doi: 10.34297/ajbsr.2019.05.000871

Maqbool, S. B., Mehrotra, S., Kolpakas, A., Durden, C., Zhang, B., Zhong, H., et al. (2010). Dampened activity of E2F1-DP and Myb-MuvB transcription factors in *Drosophila* endocycling cells. *J. Cell Sci*. 123, 4095–4106. doi: 10.1242/jcs.064519

Mehrotra, S., Maqbool, S. B., Kolpakas, A., Murnen, K., and Calvi, B. R. (2008). Endocycling cells do not apoptose in response to DNA rereplication genotoxic stress. *Genes Dev*. 22, 3158–3171. doi: 10.1101/gad.1710208

Meneses-Acosta, A., Mendonça, R., Merchant, H., Covarrubias, L., and Ramírez, O. (2001). Comparative characterization of cell death between Sf9 insect cells and hybridoma cultures. *Biotechnol. Bioeng*. 72, 441–457. doi: 10.1002/1097-0290(20000220)72:4<441::aid-bit1006>3.0.co;2-3

Moriyama, M., Osanai, K., Ohyoshi, T., Wang, H. B., Iwanaga, M., and Kawasaki, H. (2016). Ecdysteroid promotes cell cycle progression in the *Bombyx* wing disc through activation of c-Myc. *Insect Biochem. Mol. Biol*. 70, 1–9. doi: 10.1016/j.ibmb.2015.11.008

Mottier, V., Siaussat, D., Bozzolan, F., Auzoux-Bordenave, S., Porcheron, P., and Debernard, S. (2004). The 20-hydroxyecdysone-induced cellular arrest in G2 phase is preceded by an inhibition of cyclin expression. *Insect Biochem. Mol. Biol*. 34, 51–60. doi: 10.1016/j.ibmb.2003.09.003

Mueller, P. R., Coleman, T. R., Kumagai, A., and Dunphy, W. G. (1995). Myt1: a membrane-associated inhibitory kinase that phosphorylates Cdc2 on both threonine-14 and tyrosine-15. *Science* 270, 86–90. doi: 10.1126/science.270.5233.86

Nair, K. K., Chen, T. T., and Wyatt, G. R. (1981). Juvenile hormone-stimulated polyploidy in adult locust fat body. *Dev. Biol*. 81, 356–360. doi: 10.1016/0012-1606(81)90300-6

Ohhara, Y., Kobayashi, S., and Yamanaka, N. (2017). Nutrient-dependent endocycling in steroidogenic tissue dictates timing of metamorphosis in *Drosophila melanogaster*. *PLoS Genet*. 13:e1006583. doi: 10.1371/journal.pgen.1006583

Oishi, M., Locke, J., and Wyatt, G. R. (1985). The ribosomal RNA genes of *Locusta migratoria*: copy number and evidence for underreplication in a polyploid tissue. *Can. J. Biochem. Cell Biol*. 63, 1064–1070. doi: 10.1139/o85-132

Parker, L., and Piwnica-Worms, H. (1992). Inactivation of the p34 cdc2-cyclin B complex by the human WEE1 tyrosine kinase. *Science* 257, 1955–1957. doi: 10.1126/science.1384126

Parthasarathy, R., and Palli, S. R. (2008). Proliferation and differentiation of intestinal stem cells during metamorphosis of the red flour beetle, *Tribolium castaneum*. *Dev. Dyn*. 237, 893–908. doi: 10.1002/dvdy.21475

Rangel, J., Strauss, K., Seedorf, K., Hjelmen, C. E., and Johnston, J. S. (2015). Endopolyploidy changes with age-related polyethism in the honey bee, *Apis mellifera*. *PLoS One* 10:e0122208. doi: 10.1371/journal.pone.0122208

Ray, K., Mercedes, M., Chan, D., Choi, C., and Nishiura, J. T. (2009). Growth and differentiation of the larval mosquito midgut. *J. Insect Sci*. 9, 1–13. doi: 10.1673/031.009.5501

Ren, D., Guo, W., Yang, P., Song, J., He, J., Zhao, L., et al. (2019). Structural and functional differentiation of a fat body-like tissue adhering to testis follicles facilitates spermatogenesis in locusts. *Insect Biochem. Mol. Biol*. 113:103207. doi: 10.1016/j.ibmb.2019.103207

Ribbert, D. (1979). Chromomeres and puffing in experimentally induced polytene chromosomes of *Calliphora erythrocephala*. *Chromosoma* 74, 269–298. doi: 10.1007/bf01190743

Rotelli, M. D., Policastro, R. A., Bolling, A. M., Killion, A. W., Weinberg, A. J., Dixon, M. J., et al. (2019). A Cyclin A-Myb-MuvB-Aurora B network regulates the choice between mitotic cycles and polyploid endoreplication cycles. *PLoS Genet*. 15:e1008253. doi: 10.1371/journal.pgen.1008253

Royzman, I., Hagihara, A. H., Dej, K. J., Bosco, G., Lee, J. Y., and Orr-Weaver, T. L. (2002). The E2F cell cycle regulator is required for *Drosophila* nurse cell DNA replication and apoptosis. *Mech. Dev*. 119, 225–237. doi: 10.1016/s0925-4773(02)00388-x

Scholes, D. R., Suarez, A. V., and Paige, K. N. (2013). Can endopolyploidy explain body size variation within and between castes in ants? *Ecol. Evol*. 3, 2128–2137. doi: 10.1002/ece3.623

Shabbeer, S., Omer, D., Berneman, D., Weitzman, O., Alpaugh, A., Pietraszkiewicz, A., et al. (2013). BRCA1 targets G2/M cell cycle proteins for ubiquitination and proteasomal degradation. *Oncogene* 32, 5005–5016. doi: 10.1038/onc.2012.522

Shu, Z., Row, S., and Deng, W. M. (2018). Endoreplication: the good, the bad, and the ugly. *Trends Cell Biol*. 28, 465–474. doi: 10.1016/j.tcb.2018.02.006

Song, J., Li, W., Zhao, H., and Zhou, S. (2019). Clustered miR-2, miR-13a, miR-13b and miR-71 coordinately target Notch gene to regulate oogenesis of the

migratory locust *Locusta migratoria*. *Insect Biochem. Mol. Biol.* 106, 39–46. doi: 10.1016/j.ibmb.2018.11.004

Storchova, Z., and Pellman, D. (2004). From polyploidy to aneuploidy, genome instability and cancer. *Nat. Rev. Mol. Cell Biol.* 5, 45–54. doi: 10.1038/nrm1276

Stormo, B. M., and Fox, D. T. (2017). Polyteny: still a giant player in chromosome research. *Chromosome Res.* 25, 201–214. doi: 10.1007/s10577-017-9562-z

Sun, J., Evrin, C., Samel, S. A., Fernandez-Cid, A., Riera, A., Kawakami, H., et al. (2013). Cryo-EM structure of a helicase loading intermediate containing ORC-Cdc6-Cdt1-MCM2-7 bound to DNA. *Nat. Struct. Mol. Biol.* 20, 944–951. doi: 10.1038/nsmb.2629

Sun, J. J., and Deng, W. M. (2005). Notch-dependent downregulation of the homeodomain gene cut is required for the mitotic cycle/endocycle switch and cell differentiation in *Drosophila* follicle cells. *Development* 132, 4299–4308. doi: 10.1242/dev.02015

Sun, J. J., and Deng, W. M. (2007). Hindsight mediates the role of Notch in suppressing hedgehog signaling and cell proliferation. *Dev. Cell* 12, 431–442. doi: 10.1016/j.devcel.2007.02.003

Sun, J. J., Smith, L., Armento, A., and Deng, W. M. (2008). Regulation of the endocycle/gene amplification switch by Notch and ecdysone signaling. *J. Cell Biol.* 182, 885–896. doi: 10.1083/jcb.200802084

Swanson, C. I., Meserve, J. H., McCarter, P. C., Thieme, A., Mathew, T., Elston, T. C., et al. (2015). Expression of an S phase-stabilized version of the CDK inhibitor Dacapo can alter endoreplication. *Development* 142, 4288–4298. doi: 10.1242/dev.115006

Tanaka, S., and Araki, H. (2012). Formation of pre-initiation complex: formation of the active helicase and establishment of replication forks. *Cold Spring Harb. Perspect. Biol.* 5:a010371. doi: 10.1101/cshperspect.a010371

Tang, Z., Coleman, T., and Dunphy, W. G. (1993). Two distinct mechanisms for negative regulation of the Wee1 protein kinase. *EMBO J.* 12, 3427–3436. doi: 10.1002/j.1460-2075.1993.tb06017.x

Taracena, M. L., Bottino-Rojas, V., Talyuli, O. A. C., Walter-Nuno, A. B., Oliveira, J. H. M., Angleró-Rodriguez, Y. I., et al. (2018). Regulation of midgut cell proliferation impacts *Aedes aegypti* susceptibility to dengue virus. *PLoS Negl. Trop. Dis.* 12:e0006498. doi: 10.1371/journal.pntd.0006498

Tigan, A. S., Bellutti, F., Kollmann, K., Tebb, G., and Sexl, V. (2016). CDK6-a review of the past and a glimpse into the future: from cell-cycle control to transcriptional regulation. *Oncogene* 35, 3083–3091. doi: 10.1038/onc.2015.407

Unhavaithaya, Y., and Orr-Weaver, T. L. (2012). Polyploidization of glia in neural development links tissue growth to blood-brain barrier integrity. *Genes Dev.* 26, 31–36. doi: 10.1101/gad.177436.111

Van de Peer, Y., Mizrachi, E., and Marchal, K. (2017). The evolutionary significance of polyploidy. *Nat. Rev. Genet.* 18, 411–424. doi: 10.1038/nrg.2017.26

Wang, D., Li, X. R., Dong, D. J., Huang, H., Wang, J. X., and Zhao, X. F. (2016). The steroid hormone 20-Hydroxyecdysone promotes the cytoplasmic localization of Yorkie to suppress cell proliferation and induce apoptosis. *J. Biol. Chem.* 291, 21761–21770. doi: 10.1074/jbc.m116.719856

Wang, Z., Yang, L., Song, J., Kang, L., and Zhou, S. (2017). An isoform of Taiman that contains a PRD-repeat motif is indispensable for transducing the vitellogenic juvenile hormone signal in *Locusta migratoria*. *Insect Biochem. Mol. Biol.* 82, 31–40. doi: 10.1016/j.ibmb.2017.01.009

Welburn, J. P., Tucker, J. A., Johnson, T., Lindert, L., Morgan, M., Willis, A., et al. (2007). How tyrosine 15 phosphorylation inhibits the activity of cyclin-dependent kinase 2-cyclin A. *J. Biol. Chem.* 282, 3173–3181. doi: 10.1074/jbc.m609151200

Wielgus, J. J., Bollenbacher, W. E., and Gilbert, L. I. (1979). Correlations between epidermal DNA synthesis and haemolymph ecdysteroid titre during the last larval instar of the tobacco hornworm, *Manduca sexta*. *J. Insect Physiol.* 25, 9–16. doi: 10.1016/0022-1910(79)90030-1

Wu, Z., Guo, W., Xie, Y., and Zhou, S. (2016). Juvenile hormone activates the transcription of cell-division-cycle 6 (Cdc6) for polyploidy-dependent insect vitellogenesis and oogenesis. *J. Biol. Chem.* 291, 5418–5427. doi: 10.1074/jbc.M115.698936

Wu, Z., Guo, W., Yang, L., He, Q., and Zhou, S. (2018). Juvenile hormone promotes locust fat body cell polyploidization and vitellogenesis by activating the transcription of Cdk6 and E2f1. *Insect Biochem. Mol. Biol.* 102, 1–10. doi: 10.1016/j.ibmb.2018.09.002

Xu, D., Woodfield, S. E., Lee, T. V., Fan, Y., Antonio, C., and Bergmann, A. (2009). Genetic control of programmed cell death (apoptosis) in *Drosophila*. *Fly* 3, 78–90. doi: 10.4161/fly.3.1.7800

Yamanaka, N., Rewitz, K. F., and O'Connor, M. B. (2013). Ecdysone control of developmental transitions: lessons from *Drosophila* research. *Annu. Rev. Entomol.* 58, 497–516. doi: 10.1146/annurev-ento-120811-153608

Zhang, B. Q., Mehrotra, S., Ng, W. L., and Calvi, B. R. (2014). Low levels of p53 protein and chromatin silencing of p53 target genes repress apoptosis in *Drosophila* endocycling cells. *PLoS Genet.* 10:e1004581. doi: 10.1371/journal.pgen.1004581

Zhang, Y., and Kalderon, D. (2000). Regulation of cell proliferation and patterning in *Drosophila* oogenesis by hedgehog signaling. *Development* 127, 2165–2176.

Zhimulev, I. F. (1996). Morphology and structure of polytene chromosomes. *Adv. Genet.* 34, 1–490. doi: 10.1016/s0065-2660(08)60533-7

Zhimulev, I. F., Belyaeva, E. S., Semeshin, V. F., Koryakov, D. E., Demakov, S. A., Demakova, O. V., et al. (2004). Polytene chromosomes: 70 years of genetic research. *Int. Rev. Cytol.* 241, 203–275. doi: 10.1016/s0074-7696(04)41004-3

Zielke, N., Edgar, B. A., and DePamphilis, M. L. (2013). Endoreplication. *Cold Spring Harb. Perspect. Biol.* 5:a012948. doi: 10.1101/cshperspect.a012948

Zielke, N., Kim, K. J., Tran, V., Shibutani, S. T., Bravo, M. J., Nagarajan, S., et al. (2011). Control of *Drosophila* endocycles by E2F and CRL4 (CDT2). *Nature* 480, 123–127. doi: 10.1038/nature10579

Zielke, N., Querings, S., Rottig, C., Lehner, C., and Sprenger, F. (2008). The anaphase-promoting complex/cyclosome (APC/C) is required for rereplication control in endoreplication cycles. *Genes Dev.* 22, 1690–1703. doi: 10.1101/gad.469108

Zimmet, J., and Ravid, K. (2000). Polyploidy: occurrence in nature, mechanisms, and significance for the megakaryocyte-platelet system. *Exp. Hematol.* 28, 3–16.

Zülbahar, S., Sieglitz, F., Kottmeier, R., Altenhein, B., Rumpf, S., and Klambt, C. (2018). Differential expression of Öbek controls ploidy in the *Drosophila* blood-brain barrier. *Development* 145:dev164111. doi: 10.1242/dev.164111

Conflict of Interest: The authors declare that the research was conducted in the absence of any commercial or financial relationships that could be construed as a potential conflict of interest.

frontiers in Genetics

ORIGINAL RESEARCH
published: 10 June 2020
doi: 10.3389/fgene.2020.00609

Involvement of Two Paralogous Methoprene-Tolerant Genes in the Regulation of Vitellogenin and Vitellogenin Receptor Expression in the Rice Stem Borer, *Chilo suppressalis*

*Lijun Miao[1], Nan Zhang[1], Heng Jiang[1], Fan Dong[1], Xuemei Yang[1], Xin Xu[1], Kun Qian[1], Xiangkun Meng[1] and Jianjun Wang[1,2]**

[1] College of Horticulture and Plant Protection, Yangzhou University, Yangzhou, China, [2] Joint International Research Laboratory of Agriculture and Agri-Product Safety of the Ministry of Education, Yangzhou University, Yangzhou, China

Besides the function of preventing metamorphosis in insects, the juvenile hormone (JH) plays a role in female reproduction; however, the underlying mechanism is largely unknown. The methoprene-tolerant (Met) protein belongs to a family of basic helix-loop-helix–Per-Arnt-Sim (bHLH-PAS) transcription factors and functions as the JH intracellular receptor. In this study, two full length cDNAs encoding *Met* (*CsMet1* and *CsMet2*) were isolated from the rice stem borer, *Chilo suppressalis.* Structural analysis revealed that both *CsMet1* and *CsMet2* exhibited typical bHLH, PAS-A, PAS-B, and PAC (PAS C terminal motif) domains. Comparative analysis of transcript level using reverse transcription-quantitative PCR (RT-qPCR) revealed that *CsMet1* was predominant in almost all examined developmental stages and tissues. Treatment with methoprene *in vivo* induces the transcription of both *CsMet1* and *CsMet2.* Notably, injection of dsCsMet1 and dsCsMet2 suppressed the expression levels of vitellogenin (*CsVg*) and Vg receptor (*CsVgR*). These findings revealed the potential JH signaling mechanism regulating *C. suppressalis* reproduction, and provided evidence that RNAi-mediated knockdown of *Met* holds great potential as a control strategy of *C. suppressalis.*

Keywords: *Chilo suppressalis*, juvenile hormone, methoprene-tolerant, vitellogenin, vitellogenin receptor, RNAi

OPEN ACCESS

Edited by:
Fei Li,
Zhejiang University, China

Reviewed by:
Weihua Ma,
Huazhong Agricultural University, China
Wei Dou,
Southwest University, China

****Correspondence:***
Jianjun Wang
wangjj@yzu.edu.cn

Specialty section:
This article was submitted to Epigenomics and Epigenetics, a section of the journal Frontiers in Genetics

Received: *20 February 2020*
Accepted: *19 May 2020*
Published: *10 June 2020*

Citation:
Miao L, Zhang N, Jiang H, Dong F, Yang X, Xu X, Qian K, Meng X and Wang J (2020) Involvement of Two Paralogous Methoprene-Tolerant Genes in the Regulation of Vitellogenin and Vitellogenin Receptor Expression in the Rice Stem Borer, Chilo suppressalis. Front. Genet. 11:609. doi: 10.3389/fgene.2020.00609

INTRODUCTION

The rice stem borer, *Chilo suppressalis* (Walker) (Lepidoptera: Crambidae), is one of the most serious rice pests in Asia, Middle East, and southern Europe, and causes large crop losses through feeding on the stems of rice. In China, the change of cultivation patterns has led to the frequent outbreaks of *C. suppressalis* in recent years (Mao et al., 2019). To date, spraying chemical insecticides remains the primary strategy for controlling *C. suppressalis*. However, intensive use of insecticides has driven *C. suppressalis* to develop resistance to a wide range of insecticides (Su et al., 2014; Lu et al., 2017; Yao et al., 2017). Hence, the development of RNA interference (RNAi)-mediated disruption of reproduction represents an alternative control strategy of *C. suppressalis* (Miao et al., 2020).

Insect reproduction is intricately regulated by three hormones, including the juvenile hormones (JHs), ecdysteroids, and insulin (Smykal and Raikhel, 2015; Roy et al., 2018; Al Baki et al., 2019). JH exerts its function through its intracellular receptor methoprene-tolerant (Met), a member of the family of the basic helix-loop-helix (bHLH)-Per-Arnt-Sim (PAS) transcription factors (Konopova and Jindra, 2007; Jindra et al., 2013, 2015). Since the first characterization of Met in *Drosophila melanogaster* (Wilson and Fabian, 1986), Met has been identified from a broad range of insect species, such as *Aedes aegypti* (Wang et al., 2007), *Tribolium castaneum* (Konopova and Jindra, 2007), *Nilaparvata lugens* (Lin et al., 2015), and *Helicoverpa armigera* (Ma et al., 2018). Interestingly, two Met paralogs, Met and Germ cell-expressed (Gce), are present across 12 *Drosophila* species (Baumann et al., 2010a,b). While mosquitoes and beetles possess only a single gene, two *Met* genes have also been identified in several Lepidopteran insects, including *Danaus plexippus* (Zhan et al., 2011), *Operophtera brumata* (Derks et al., 2015), and *Bombyx mori* (Guo et al., 2012; Suetsugu et al., 2013; Kayukawa and Shinoda, 2015). However, the role of two *Met* genes in the reproduction of Lepidopteran insects remains largely unknown.

The reproductive success of insects depends on vitellogenin (Vg) biosynthesis and uptake of Vg into developing oocytes mediated by vitellogenin receptor (VgR). Recently, we have characterized the *C. suppressalis CsVg* and *CsVgR* at the molecular levels (Huang et al., 2016; Miao et al., 2020). In this study, full-length cDNAs of two paralogous *Met* genes (named as *CsMet1* and *CsMet2*) were isolated from *C. suppressalis*. We report the structural features and temporal–spatial expression patterns of *CsMet1* and *CsMet2*. Furthermore, RNAi was employed to reveal the role of *CsMet1* and *CsMet2* in the regulation of *CsVg* and *CsVgR*.

MATERIALS AND METHODS

Insects Rearing and Sampling

Chilo suppressalis larvae was collected from rice stubbles of Yangzhou (32.39°N, 119.42°E) in 2013, and reared on an artificial diet in an incubator at 28 ± 1℃, 70 ± 5% RH, and a 16-h light/8-h dark photoperiod.

To examine the developmental expression profiles of *CsMet*, individuals were collected from larvae (third, fourth, fifth, and sixth instar), pupae at intervals of 2 days from pupation, and adults at intervals of 12 h from eclosion. For tissue expression analysis, tissues (including head, epidermis, midgut, hemolymph, and fat body) were dissected from the fifth-instar larva. All the samples were frozen immediately in liquid nitrogen and stored at -80°C until RNA isolation. Each experiment was performed with three biological replicates containing three to 10 individuals.

RNA Isolation, RT-PCR, and RACE

Total RNA was extracted using Trizol reagent (Invitrogen, Carlsbad, CA, United States). First-strand cDNA was synthesized from total RNA using the Primescript^{TM} First-Strand cDNA Synthesis Kit (TaKaRa, Dalian, China) according to the manufacturers' instruction.

The amino acid (aa) sequences of *B. mori BmMet1* (GenBank: NP001108458) and *BmMet2* (GenBank: BAJ05086) were searched against the transcriptome database of *C. suppressalis* in Insect Base[1], and specific primer pairs were designed based on the sequences of putative transcripts (**Table 1**). PCR reactions were performed with LA Taq^{TM} DNA polymerase (TaKaRa, Dalian, China). To obtain full length cDNA sequences of *CsMet1* and *CsMet2*, 5′-RACE and 3′-RACE were conducted using the SMART RACE cDNA Amplification Kit (Clontech, Mountain View, CA, United States), following the manufacturers' instructions. Gene specific primers (GSPs) used for RACE are listed in **Table 1**.

Molecular Cloning and Sequence Analysis

RT-PCR and RACE products were subcloned into the pMD18−T vector (TaKaRa) and sequenced. The molecular mass and isoelectric point (pI) of the deduced protein sequences were

[1]http://www.insect-genome.com/

TABLE 1 | Oligonucleotide primers used for RT-PCR, RACE, RT-qPCR, and RNAi.

Primer name	Sequence (5′ to 3′)	Description
W988Met1 F	ATGACATCATTGACTGGAGC	*CsMet1* RT-PCR
W989Met1 R	GGATTACAGGATTTCAGTTTCTGA	
W71Met1 R	CAACAGGCAGTCAGTCACCAAGT	*CsMet1* 5′-RACE
W72Met1 R	TGACATCATTGACTGGAGCCACTG	
W73Met1 F	TGTTGGTGTAGATTATGGGCGACG	*CsMet1* 3′-RACE
W74Met1 F	AAGTGGTGCAAGAAACTGGTGTCC	
W990Met2 F	AGAGAGATTCGAAACAAAGCG	*CsMet2* RT-PCR
W991Met2 R	TCGTTTGTACCAACACTGTC	
W75Met2 R	CCAGCATTTCGGCGACCTTGTTCTT	*CsMet2* 5′-RACE
W76Met2 R	CCAGTTCACCGATGGATTGGTTCAG	
W77Met2 F	GTGTTCGTGGGCATTGTCCGCTTGG	*CsMet2* 3′-RACE
W78Met2 F	TTTAGTCGGTGAGTCCTGCTATCGT	
EF1-α F	TGAACCCCCATACAGCGAATCC	RT-qPCR
EF1-α R	TCTCCGTGCCAACCAGAAATAGG	
W465Met1 qF	TGGCTTCCTCGAGATTGACA	RT-qPCR
W466Met1 qR	TCCTGATGCTACCCCAGATG	
W469Met2 qF	CAATCCATCGGTGAACTGGC	RT-qPCR
W470Met2 qR	GTTGAGTATGGACAGCAGCG	
W84VgR F	AGCCACTTCCCTACCTCCTA	RT-qPCR
W85VgR R	TAAGGCATTGGGGACTCGTT	
W976Vg F	AGCTCAGTCCGCTAAATGGA	RT-qPCR
W977Vg R	GCCCAGTTCGTGGTGTCTAT	
W463Met1 iF	TAATACGACTCACTATAGGGTCTGAC ATAGTGCACGCTCC	*CsMet1* RNAi
W464Met1 iR	TAATACGACTCACTATAGGGTGTGCG TACCCTTCTGACAC	
W467Met2 iF	TAATACGACTCACTATAGGGCAGGGG GCTCATTGTGGTAG	*CsMet2* RNAi
W468Met2 iR	TAATACGACTCACTATAGGGGTGCCG CGTTCTATACTCCA	

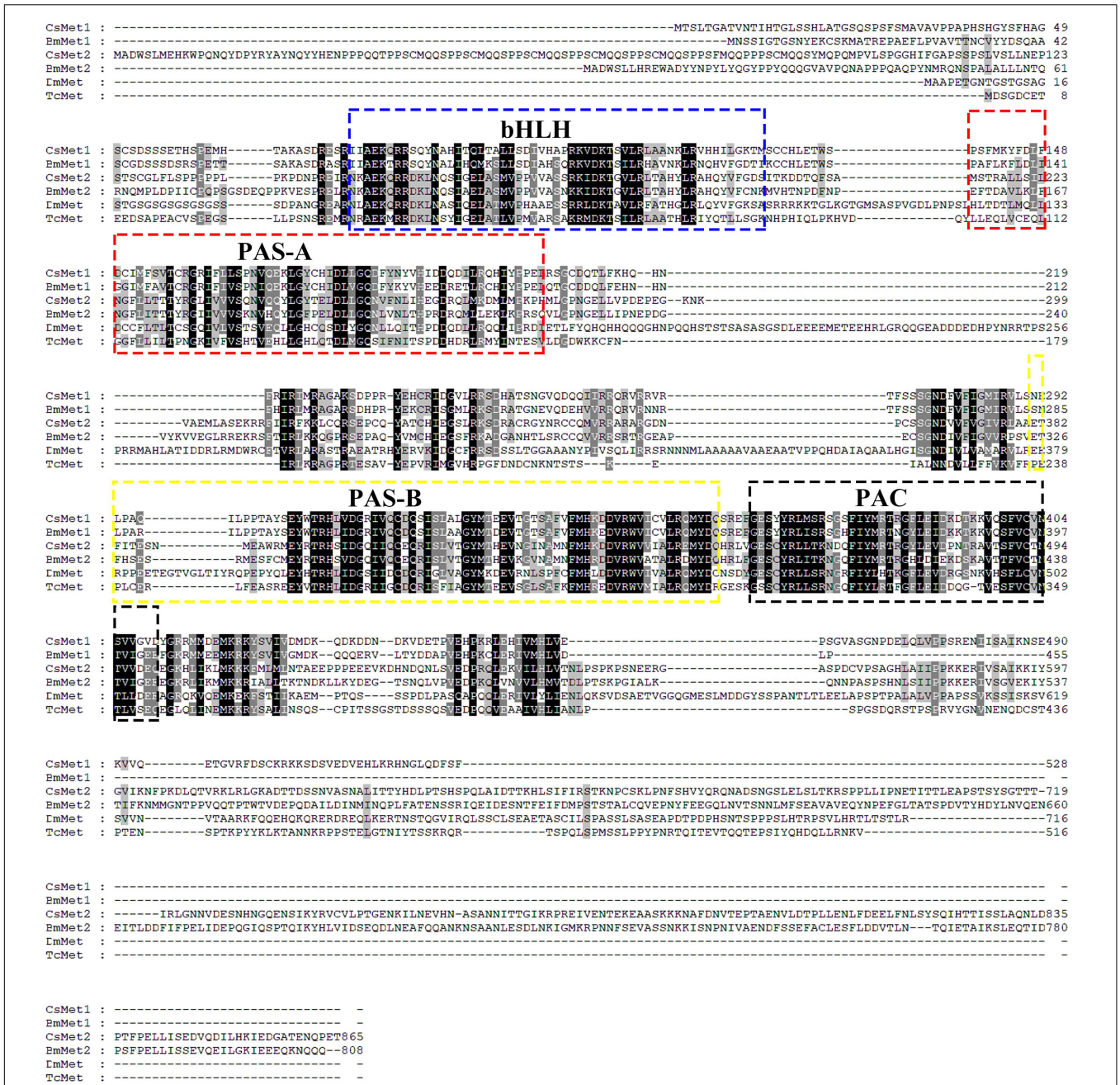

FIGURE 1 | Amino acid sequence alignments of *CsMet1*, *CsMet2* and other representative insect Mets. Met sequences were obtained from the following GenBank entries: NP001108458 for *B. mori BmMet1*, BAJ05086 for *B. mori BmMet2*, AAC14350 for *D. melanogaster DmMet* and NP 001092812 for *T. castaneum TcMet*.

predicted by using the online ExPASy proteomics server[2]. Conserved domains were predicted by NCBI conserved domain search tool[3] or by alignment to other published insect Mets. A phylogenetic tree was constructed with MEGA 7.0 using the neighbor-joining method with a *p*-distance model and a pairwise deletion of gaps (Kumar et al., 2016). The reliability of the NJ tree topology was statistically evaluated by bootstrap analysis with 1000 replicates.

Reverse Transcription-Quantitative PCR (RT-qPCR)

Reverse transcription-quantitative qPCR reactions were performed on the Bio-Rad CFX-96TM Real-time PCR system using TB Green™ Premix Ex Taq™ (Takara, Dalian, China) following the manufacturers' instructions.

[2]https://web.expasy.org/protparam/

[3]http://www.ncbi.nlm.nih.gov/Structure/cdd/wrpsb.cgi

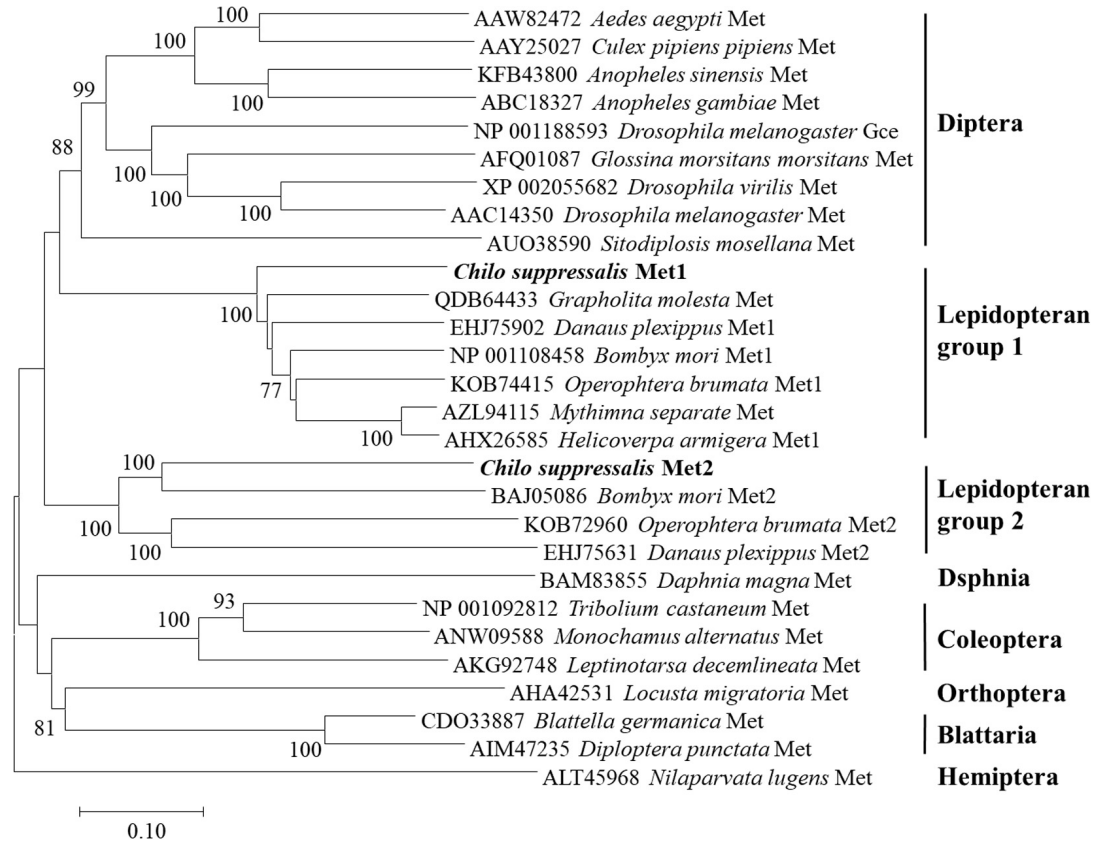

FIGURE 2 | Phylogenetic relationships of *CsMet1*, *CsMet2* and other insect Mets. The neighbor-joining tree was constructed by MEGA 7.0. Numbers indicated bootstrap support values (%) based on 1,000 replicates. Sequences were retrieved from GenBank protein database.

GSPs used are listed in **Table 1**. The stably expressed gene encoding EF1-α was used as a reference gene (Hui et al., 2011; Meng et al., 2019). The mRNA levels were normalized to reference gene with the $2^{-\Delta\Delta CT}$ method (Livak and Schmittgen, 2001). The means and standard errors for each time point were obtained from the average of three biologically independent samples.

Methoprene Treatment

To study effects of JH on expression of *CsMet*, newly emerged adult females were injected with 1 μL JH analog methoprene (3 μg/μL, Sigma–Aldrich, St. Louis, MO, United States) or same volume of acetone as control. Insects were collected for RT-qPCR analysis at 1, 6, 12, and 24 h after treatment, respectively, and experiments contained three biological replications.

RNA Interference

Double-strand RNAs (dsRNAs) against *CsMet1* or *CsMet2* were synthesized using TranscriptAid^{TM} T7 High Yield Transcription Kit (Thermo Fisher Scientific, Waltham, MA, United States). GSPs for dsRNA synthesis are listed in **Table 1**. Using a Nanoliter 2010 injector system (WPI, Sarasota, FL, United States), 1 μL solution of dsRNA (3 μg/μL) was injected into the abdomen of 6-day-old female pupae under a stereomicroscope. Equal dose of dsRNA for enhanced green fluorescent protein (EGFP) was injected as a control. A total of 40 pupae were injected per treatment, and each treatment was performed in triplicate. The treatment was repeated in newly emerged female adults (within 24 h), and insects were collected at 24 and 48 h after injection, respectively, for expression analysis of *CsMet1*, *CsMet2*, *CsVg*, and *CsVgR* by RT-qPCR.

Data Analysis

The statistical analysis was done using graphpad.prism.6 by one-way analysis of variance, followed by student's *t*-test. All data are presented as the mean ± SE.

RESULTS

Sequence and Structural Analysis of *CsMet1* and *CsMet2*

The full length *CsMet1* cDNA (GenBank accession number MN906993) was 2673 bp, with a 460 bp 5'-terminal untranslated region (UTR), a 1587 bp open reading frame (ORF), and a 626 bp 3′-UTR. The deduced *CsMet1* protein contained 528 aas with a

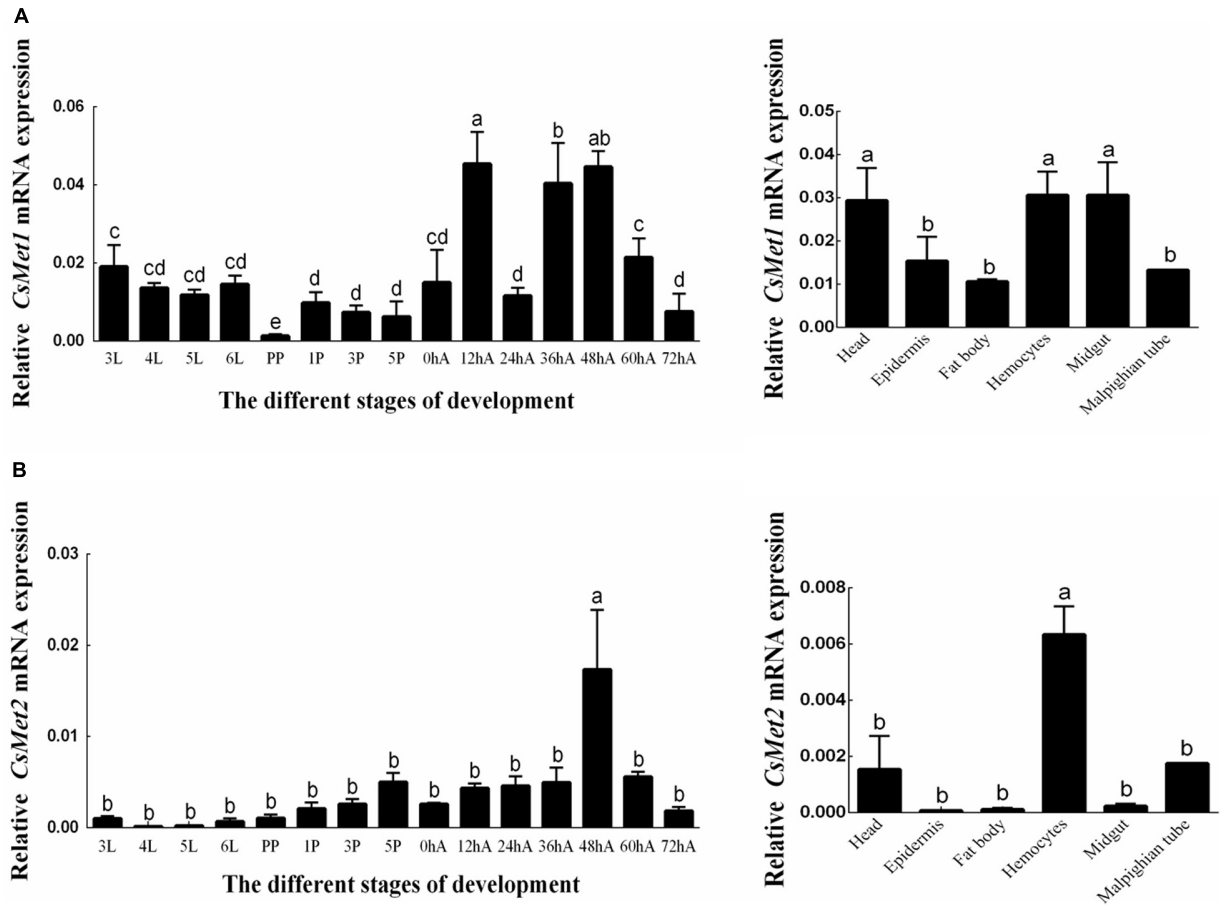

FIGURE 3 | Expression profiles of *CsMet1* **(A)** and *CsMet2* **(B)** in different developmental stages and various tissues from 5th instar larva. 3L: 3rd instar larvae; 4L: 4th instar larvae; 5L: 5th instar larvae; 6L: 6th instar larvae; PP: prepupae; 1P: 1-day-old pupae; 3P: 3-day-old pupae; 5P: 5-day-old pupae; 0hA: newly emerged female adults; 12hA: 12-h-old female adults; 24hA: 24-h-old female adults; 36hA: 36-h-old female adults; 48hA: 48-h-old female adults; 60hA: 60-h-old female adults; 72hA: 72-h-old female adults. Bars not sharing a common letter are significantly different.

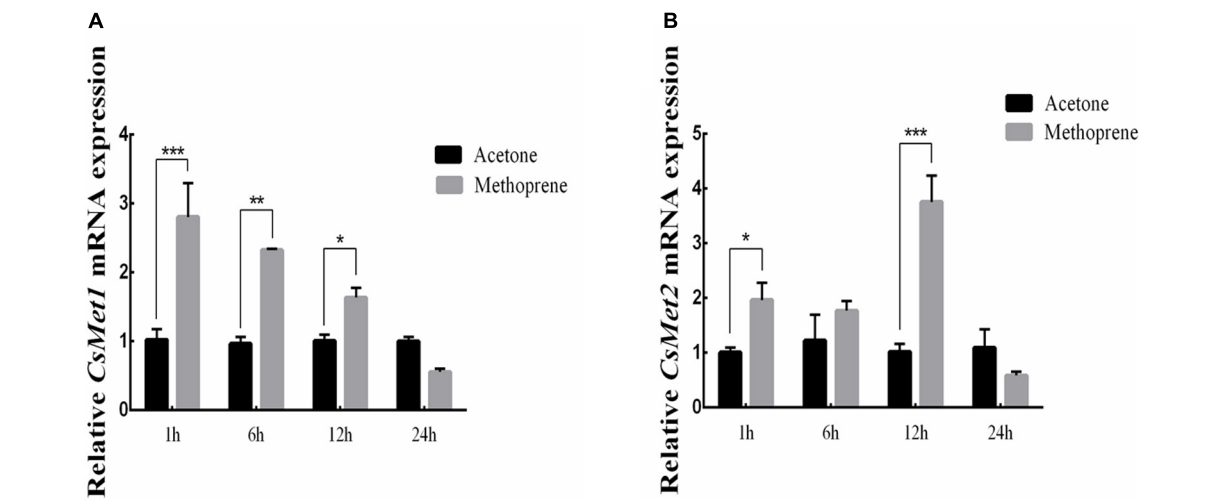

FIGURE 4 | Relative mRNA levels of *CsMet1* **(A)** and *CsMet2* **(B)** in the whole body insects after methoprene treatment in newly emerged female adults. The bars represent mean ± SE of three biological replicates. Asterisks indicate the significant differences between the groups (*$P < 0.05$, **$P < 0.01$, and ***$P < 0.001$).

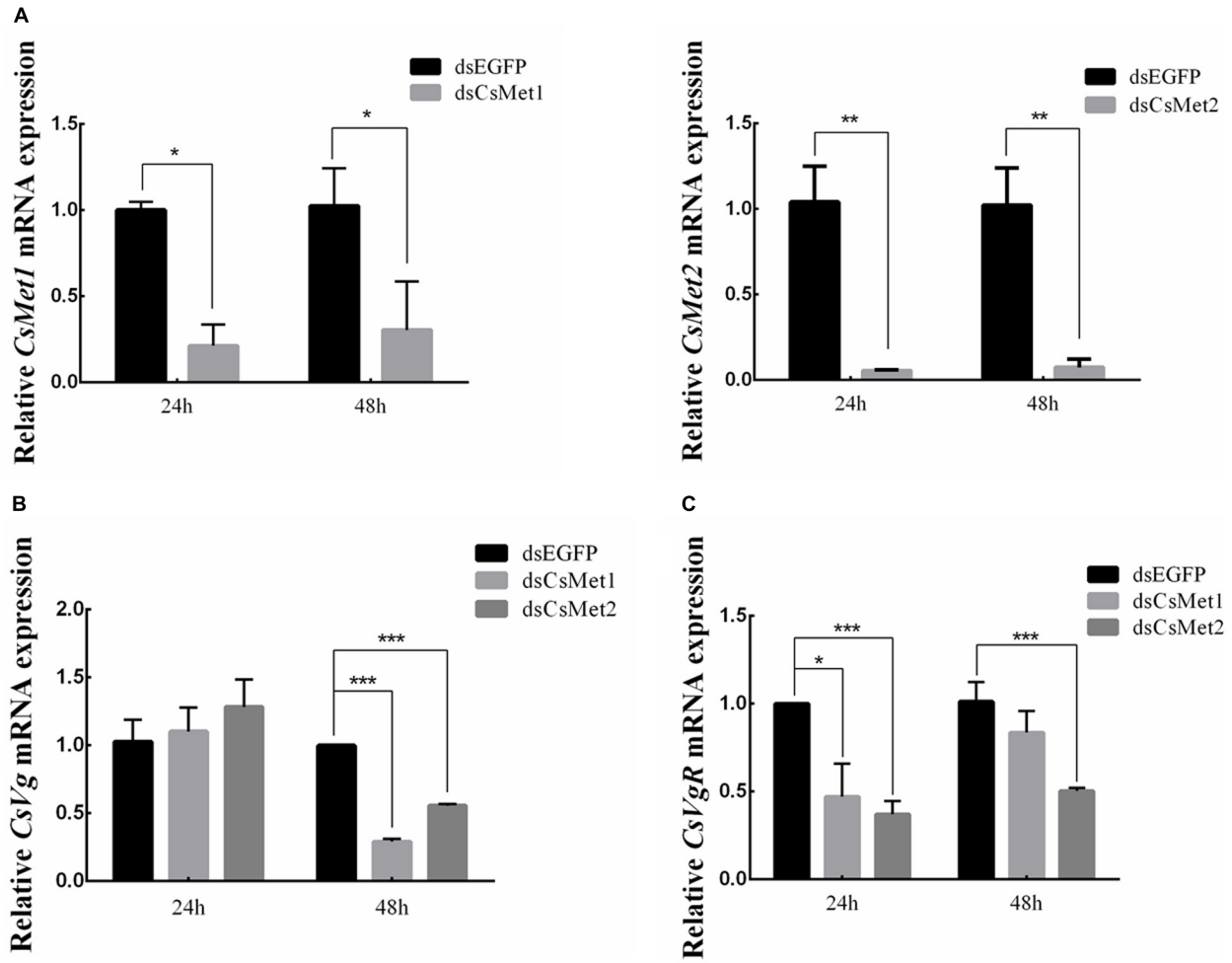

FIGURE 5 | Knockdown of *CsMet1* and *CsMet2*. dsRNAs were injected into 6-day-old female pupae followed by the second injection into the newly emerged female moths. The expression levels of *CsMet1*, *CsMet2* **(A)**, *CsVg* **(B)**, and *CsVgR* **(C)** in whole body insects were examined at 24 h and 48 h after treatment. The bars represent mean ± SE of three biological replicates. Asterisks indicate the significant differences between the groups (*$P < 0.05$, **$P < 0.01$, and ***$P < 0.001$).

predicted mass and pI of 60.34 kDa and 8.35, respectively. The 2824 bp *CsMet2* cDNA (GenBank accession number MN906994) contained an 85 bp 5′-UTR, a 2598 bp ORF encoding an 865 aa residue protein with a molecular mass of 97.37 kDa and a pI of 6.68, and a 141 bp 3′-UTR.

Structural analysis showed that the deduced protein of *CsMet1* and *CsMet2* had conserved domains of bHLH-PAS protein family including bHLH (DNA binding and dimerization regions), PAS-A (dimerization region), PAS-B (ligand binding and dimerization region), and PAC (PAS C terminal motif) domains (dimerization region) (**Figure 1**). Alignment of aa sequences demonstrated that *CsMet1* shared identity with other insect Met orthologs including *B. mori BmMet1* (60.98%) and *BmMet2* (21.88%), *D. melanogaster DmMet* (27.49%), and *T. castaneum TcMet* (28.30%). *CsMet2* shared 20.55, 44.19, 17.19, and 22.90% identity with *BmMet1*, *BmMet2*, *DmMet*, and *TcMet*, respectively. The aa identity between *CsMet1* and *CsMet2* was 21.71% (**Figure 1**). Phylogenetic analysis revealed that *CsMet1* and *CsMet2* were clustered into Lepidopteran group 1 and group 2 Met, respectively (**Figure 2**).

Temporal and Spatial Expression of *CsMet1* and *CsMet2*

The temporal expression patterns of *CsMet1* and *CsMet2* were detected from third instar to 3-day-old female adults and determined by RT-qPCR analysis. The results showed that the transcription level of *CsMet1* and *CsMet2* was detectable during all selected developmental stages. Specifically, the expression of *CsMet1* was relatively stable in the larval stage, sharply decreased in the prepupal stage, maintained at a low level during the pupal stage, and reached a peak in 12-h-old female adults (**Figure 3A**). The expression of *CsMet2* gradually increased from fourth instar to 5-day-old pupae. In the adult stage, the highest and lowest expression levels of *CsMet2* were observed in 48-h-old and 72-h-old female adults, respectively (**Figure 3B**).

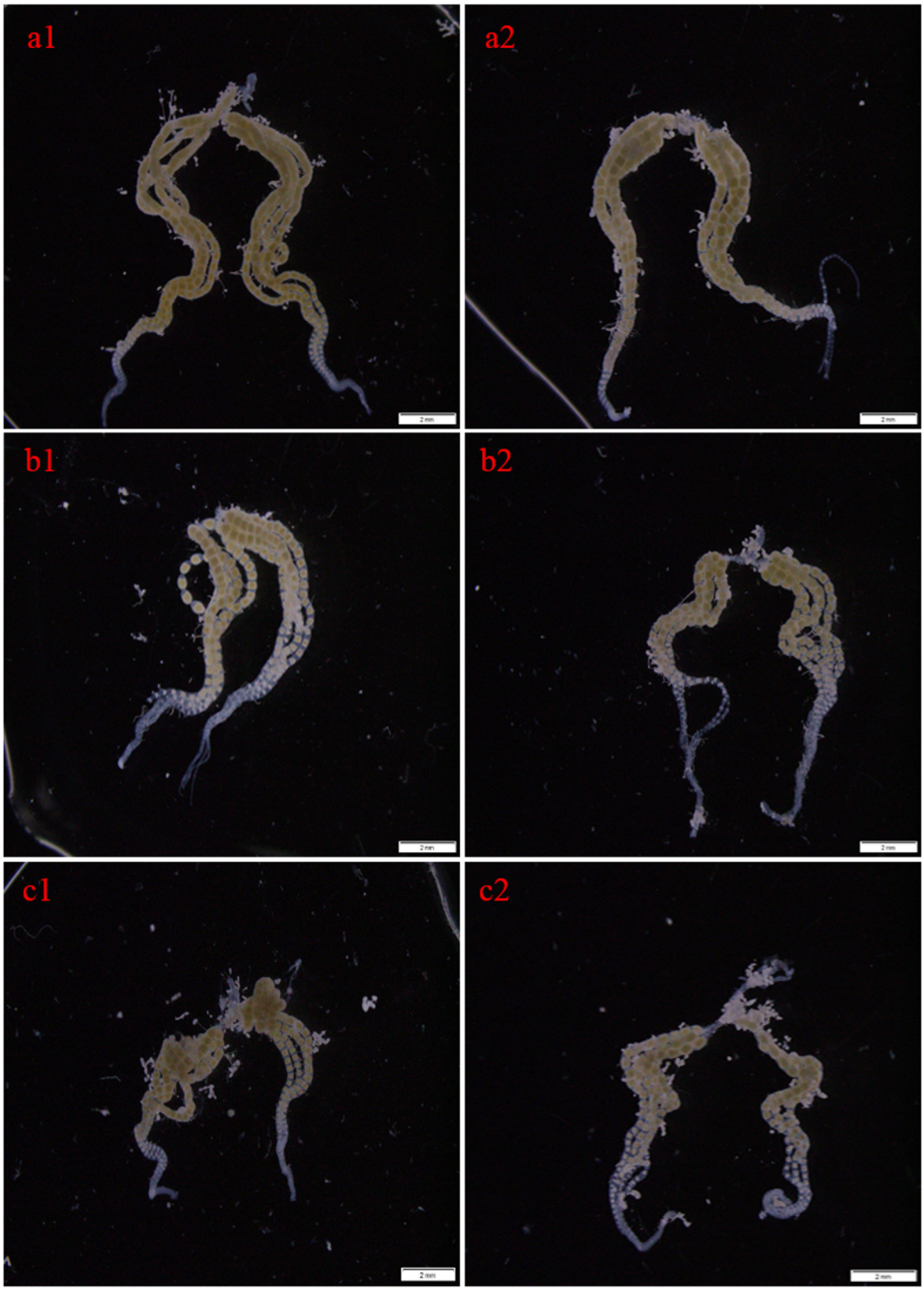

FIGURE 6 | Effects of RNAi-mediated knockdown of *CsMet1* and *CsMet2* on ovary development with dsEGFP as a control. The ovaries were dissected from female adults at 24 h after the second injection of dsEGFP (a1, a2), dsCsMet1 (b1, b2) and dsCsMet2 (c1, c2).

Analysis of the spatial expression profiles of *CsMet1* and *CsMet2* in fifth-instar larva showed that *CsMet1* was highly expressed in head, hemocytes, and midgut, while relatively low expression was observed in epidermis, fat body, and malpighian tube (**Figure 3A**). The highest expression level of *CsMet2* was observed in hemocytes, followed by head and Malpighian tube, whereas low expression was observed in epidermis, fat body, and midgut (**Figure 3B**).

Effect of JHA Treatment

To examine whether *CsMet1* and *CsMet2* were regulated by JH, JHA methoprene was injected into the newly emerged female adults. Compared with control, the results showed that *CsMet1* expression was upregulated by 2.74, 2.41, and 1.63 times at 1, 6, and 12 h after injection, respectively (**Figure 4A**). Similarly, transcription level of *CsMet2* was increased by 1.95, 1.45, and 3.68 times at 1, 6, and 1 2 h post-treatment, respectively (**Figure 4B**).

Effects of RNAi-Mediated Knockdown of *CsMet1* and *CsMet2*

To explore the role of *CsMet1* and *CsMet2* in the regulation of *CsVg* and *CsVgR*, female adults were collected at 24 and 48 h after the second dsRNA injection, respectively. The transcript level of *CsMet1* in dsCsMet1-injected female adults was suppressed by 78.74% (24 h) and 70.32% (48 h) compared with dsEGFP-injected insects, whereas the expression of *CsMet2* was significantly reduced by 94.69% (24 h) and 92.79% (48 h) (**Figure 5A**). Meanwhile, RNAi-mediated suppression of *CsMet1* and *CsMet2* decreased *CsVg* expression by 70.85 and 44.37% at 48 h post-treatment, respectively (**Figure 5B**). *CsVgR* expression in the dsCsMet1-treated and dsCsMet2-treated group decreased significantly by 52.91 and 62.98% at 24 h post-injection, respectively (**Figure 5C**). Furthermore, phenotypic observation revealed that silencing of both *CsMet1* and *CsMet2* resulted in suppressed ovarian development with decreased number of mature follicles (**Figure 6**).

DISCUSSION

The important roles played by JH in insect development and reproduction prompted the study on JH signaling, and the breakthrough had been the identification of transcription factor Met as an intracellular receptor for JH (Charles et al., 2011). Binding of JH to Met triggers dimerization of Met with another bHLH-PAS protein Taiman (Tai) to form a functional complex, which interacts with JH response elements (JHREs) of target genes (Smykal and Raikhel, 2015). While the *Met* null allele was expected to result in a lethal phenotype, the paralogous *Met* gene in *D. melanogaster*, *Gce*, ensured survival of the met null mutants (Baumann et al., 2010a,b). Similarly, two *Met* genes were also recently identified in several Lepidopteran insects (Zhan et al., 2011; Guo et al., 2012; Suetsugu et al., 2013; Derks et al., 2015; Kayukawa and Shinoda, 2015). However, only a single *Met* gene was found in those from other insect orders including *A. aegypti* (Dipteran, Wang et al., 2007), *T. castaneum* (Coleopteran, Konopova and Jindra, 2007), *Blattella germanica* (Blattarian, Lozano and Belles, 2014), *N. lugens* (Hemipteran, Lin et al., 2015), *Sitodiplosis mosellana* (Dipteran, Cheng et al., 2018), and so on. In this study, we isolated two paralogous *Met* genes, *CsMet1* and *CsMet2*, from *C. suppressalis*. Both proteins showed conserved domain organization of bHLH-PAS protein family (Ashok et al., 1998; Kayukawa and Shinoda, 2015; Ma et al., 2018). Phylogenetic analysis revealed that *CsMet1* and *CsMet2* were clustered into Lepidopteran group 1 and group 2 Met, respectively, providing further evidence of the occurrence of *Met* gene duplication in Lepidopteran insects.

The temporal and spatial expression patterns of a gene may provide hints as to its function. In this study, we found a marked reduction in expression levels of *CsMet1* in the prepupae stage, supporting its involvement in larval–pupal metamorphosis. Similar results were also observed in *HaMet1* of *H. armigera* (Ma et al., 2018) and *SmMet* of *S. mosellana* (Cheng et al., 2018), and was in agreement with the fact that JH exerts its anti-metamorphic effect through its receptor Met (Parthasarathy et al., 2008; Li et al., 2019). *CsMet2* transcript was hardly detected during the larval stage, and its expression reached the peak in 48-h-old female adults, suggesting that *CsMet2* was involved in JH signaling in adults, as had been reported for *BmMet2* in *B. mori* (Kayukawa and Shinoda, 2015). For tissue expression, *CsMet1* was highly expressed in larval head, midgut, and hemocytes, whereas *CsMet2* showed the highest expression in larval hemocytes. Interestingly, the temporal and spatial expression analysis revealed that *CsMet1* was dominant at almost all developmental stages and in all tissues examined. This result was somewhat different from the observation in *B. mori* that *BmMet2* transcript was more abundant than *BmMet1* transcript in the adult stage (Kayukawa and Shinoda, 2015). Whether *CsMet1* played a more important role in *C. suppressalis* needed further study in the future.

Juvenile hormone plays a crucial role in insect reproduction, but its molecular mode of action only became clear recently. It has been reported in *H. armigera*, *Diploptera punctata*, *N. lugens*, and S. *mosellana* that *Met* is significantly upregulated by JH III or JHA methoprene (Marchal et al., 2014; Zhao et al., 2014; Lin et al., 2015; Cheng et al., 2018). Our hormone treatment results also indicated that *CsMet1* and *CsMet2* expression was upregulated after JHA methoprene treatment. Further RNAi analysis revealed that knockdown of *CsMet1* and *CsMet2* resulted in significant decline of both *CsVg* and *CsVgR* expression in female adults, leading to decreased number of mature follicles in ovaries. Similarly, expression of *Vg* is regulated by JH via *Met* in *A. aegypti*, *H. armigera*, *D. punctata*, *N. lugens*, and *Bactrocera dorsalis* (Zou et al., 2013; Marchal et al., 2014; Lin et al., 2015; Ma et al., 2018; Yue et al., 2018). Downregulation of *VgR* transcription as well as suppressed ovarian development were also observed in dsMet-treated *H. armigera* and *Colaphellus bowringi* (Ma et al., 2018; Liu et al., 2019). Whether expression of *Vg* and *VgR* were directly regulated by Met was not well known.

It had been recently reported that knockdown of Krüppel-homolog 1 (Kr-h1), a direct target of JH-Met signaling, also decreased *VgR* expression in *C. bowringi* (Liu et al., 2019). On the other hand, Met is also a repressor of 20E pathway gene expression. It is likely that Met regulated the relative genes of 20E pathway (Zhao et al., 2014), which contributes to vitellogenis to some extent. Further study needs to be carried out to confirm these presumptions.

DATA AVAILABILITY STATEMENT

All datasets generated for this study are included in the article.

AUTHOR CONTRIBUTIONS

JW conceived and designed the study. LM, NZ, HJ, FD, XY, and XX performed the experiments. LM, JW, KQ, and XM wrote the manuscript. All authors reviewed and approved this submission.

FUNDING

This work was supported by the Special Fund for Agro-scientific Research in the Public Interest under Grant No. 201303017 and National Natural Science Foundation of China (31701807).

REFERENCES

Al Baki, M. A., Lee, D. W., Jung, J. K., and Kim, Y. (2019). Insulin signaling mediates previtellogenic development and enhances juvenile hormone-mediated vitellogenesis in a lepidopteran insect, *Maruca vitrata*. *BMC Dev. Biol.* 19:14. doi: 10.1186/s12861-019-0194-8

Ashok, M., Turner, C., and Wilson, T. G. (1998). Insect juvenile hormone resistance gene homology with the bHLH-PAS family of transcriptional regulators. *Proc. Natl. Acad. Sci. U.S.A.* 95, 2761–2766. doi: 10.1073/pnas.95.6.2761

Baumann, A., Barry, J., Wang, S., Fujiwara, Y., and Wilson, T. G. (2010a). Paralogous genes involved in juvenile hormone action in *Drosophila melanogaster*. *Genetics* 185, 1327–1336. doi: 10.1534/genetics.110.116962

Baumann, A., Fujiwara, Y., and Wilson, T. G. (2010b). Evolutionary divergence of the paralogs methoprene tolerant (Met) and germ cell expressed (gce) within the genus *Drosophila*. *J. Insect. Physiol.* 56, 1445–1455. doi: 10.1016/j.jinsphys

Charles, J. P., Iwema, T., Epa, V. C., Takaki, K., Rynes, J., and Jindra, M. (2011). Ligand-binding properties of a juvenile hormone receptor, methoprene-tolerant. *Proc. Natl. Acad. Sci. U.S.A.* 108, 21128–21133. doi: 10.1073/pnas.1116123109

Cheng, W. N., Li, X. J., Zhao, J. J., and Salzman, K. Z. (2018). Cloning and characterization of Methoprene-tolerant (Met) and Krüppel homolog 1 (Kr-h1) genes in the wheat blossom midge, *Sitodiplosis mosellana*. *Insect. Sci.* 27, 292–303. doi: 10.1111/1744-7917

Derks, M. F., Smit, S., Salis, L., Schijlen, E., Bossers, A., Mateman, C., et al. (2015). The genome of winter moth (*Operophtera brumata*) providesa genomic perspective on sexual dimorphism and phenology. *Genome. Biol. Evol.* 7, 2321–2332. doi: 10.1093/gbe/evv145

Guo, E., He, Q., Liu, S., Tian, L., Sheng, Z., Peng, Q., et al. (2012). MET is required for the maximal action of 20-hydroxyecdysone during *Bombyx* metamorphosis. *PLoS One* 7:e53256. doi: 10.1371/journal.pone.0053256

Huang, L., Lu, M. X., Han, G. J., Du, Y. Z., and Wang, J. J. (2016). Sublethal effects of chlorantraniliprole on development, reproduction and vitellogenin gene (*CsVg*) expression in the rice stem borer, *Chilo suppressalis*. *Pest. Manag. Sci.* 72, 2280–2286. doi: 10.1002/ps.4271

Hui, X. M., Yang, L. W., He, G. L., Yang, Q. P., Han, Z. J., and Li, F. (2011). RNA interference of ace1 and ace2 in *Chilo suppressalis* reveals their different contributions to motor ability and larval growth. *Insect Mol. Biol.* 20, 507–518. doi: 10.1111/j.1365-2583

Jindra, M., Bellés, X., and Shinoda, T. (2015). Molecular basis of juvenile hormone signaling. *Curr. Opin. Insect. Sci.* 11, 39–46. doi: 10.1016/j.cois.2015.08.004

Jindra, M., Palli, S. R., and Riddiford, L. M. (2013). The juvenile hormone signaling pathway in insect development. *Annu. Rev. Entomol.* 58, 181–204. doi: 10.1146/annurev-ento-120811-153700

Kayukawa, T., and Shinoda, T. (2015). Functional characterization of two paralogous JH receptors, methoprene tolerant 1 and 2, in the silkworm, *Bombyx mori* (Lepidoptera: Bombycidae). *Jpn. Soc. Appl. Entomol. Zool.* 50, 383–391. doi: 10.1007/s13355-015-0345-8

Konopova, B., and Jindra, M. (2007). Juvenile hormone resistance gene Methoprene-tolerant controls entry into metamorphosis in the beetle *Tribolium castaneum*. *Proc. Natl. Acad. Sci. U.S.A.* 104, 10488–10493. doi: 10.1073/pnas.0703719104

Kumar, S., Stecher, G., and Tamura, K. (2016). MEGA7: molecular evolutionary genetics analysis version 7.0 for bigger datasets. *Mol. Biol. Evol.* 33, 1870–1874. doi: 10.1093/molbev/msw054

Li, K., Jia, Q. Q., and Li, S. (2019). Juvenile hormone signaling- a mini review. *Insect. Sci.* 26, 600–606. doi: 10.1111/1744-7917.12614

Lin, X., Yao, Y., and Wang, B. (2015). Methoprene-tolerant (Met) and Krüpple-homologue 1 (Kr-h1) are required for ovariole development and egg maturation in the brown plant hopper. *Sci. Rep.* 5:18064. doi: 10.1038/srep18064

Liu, W., Guo, S., Sun, D., Zhu, L., Zhu, F., Lei, C. L., et al. (2019). Molecular characterization and juvenile hormone-regulated transcription of the vitellogenin receptor in the cabbage beetle *Colaphellus bowringi*. *Comp. Biochem. Physiol. A Mol. Integr. Physiol.* 229, 69–75. doi: 10.1016/j.cbpa.2018.12.004

Livak, K. J., and Schmittgen, T. D. (2001). Analysis of relative gene expression data using real-time quantitative PCR and the 2-ΔΔCT method. *Methods* 25, 402–408. doi: 10.1006/meth.2001.1262

Lozano, J., and Belles, X. (2014). Role of methoprene-tolerant (met) in adult morphogenesis and in adult ecdysis of *Blattella germanica*. *PLoS One* 9:e103614. doi: 10.1371/journal.pone.0103614

Lu, Y. H., Wang, G. R., Zhong, L. Q., Zhang, F. C., Bai, Q., Zheng, X. S., et al. (2017). Resistance monitoring of *Chilo suppressalis* (Walker) (Lepidoptera: Crambidae) to chlorantraniliprole in eight field populations from east and central china. *Crop. Prot.* 100, 196–202. doi: 10.1016/j.cropro.2017.07.006

Ma, L., Zhang, W., Liu, C., Chen, L., Xu, Y., Xiao, H., et al. (2018). Methoprene-tolerant (Met) is indispensable for larval metamorphosis and female reproduction in the cotton bollworm *Helicoverpa armigera*. *Front. Physiol.* 9:1601. doi: 10.3389/fphys.2018.01601

Mao, K., Li, W., Liao, X., Liu, C., Qin, Y., Ren, Z., et al. (2019). Dynamics of insecticide resistance in different geographical populations of *Chilo suppressalis* (Lepidoptera: Crambidae) in China 2016-2018. *J. Econ. Entomol.* 112, 1866–1874. doi: 10.1093/jee/toz109

Marchal, E., Hult, E. F., Huang, J., Pang, Z., Stay, B., and Tobe, S. S. (2014). Methoprene-tolerant (met) knockdown in the adult female cockroach, *Diploptera punctata* completely inhibits ovarian development. *PLoS One* 9:e106737. doi: 10.1371/journal.pone.0106737

Meng, X. K., Miao, L. J., Ge, H. C., Yang, X. M., Dong, F., Xu, X., et al. (2019). Molecular characterization of glutamate-gated chloride channel and its possible roles in development and abamectin susceptibility in the rice stem borer, *Chilo suppressalis*. *Pestic. Biochem. Physiol.* 155, 72–80. doi: 10.1016/j.pestbp

Miao, L. J., Zhang, N., Jiang, H., Dong, F., Yang, X. M., Xu, X., et al. (2020). Molecular characterization and functional analysis of the vitellogenin receptor in the rice stem borer, *Chilo suppressalis*. *Arch. Insect Biochem. Physiol.* 103:e21636. doi: 10.1002/arch.21636

Parthasarathy, R., Tan, A. J., and Palli, S. R. (2008). bHLH-PAS family transcription factor methoprene-tolerant plays a key role in JH action in preventing the premature development of adult structures during larval-pupal metamorphosis. *Mech. Dev.* 125, 601–616. doi: 10.1016/j.mod.2008.03.004

Roy, S., Saha, T. T., Zou, Z., and Raikhel, A. S. (2018). Regulatory pathways controlling female insect reproduction. *Annu. Rev. Entomol.* 63, 489–511. doi: 10.1146/annurev-ento-020117-043258

Smykal, V., and Raikhel, A. S. (2015). Nutritional control of insect reproduction. *Curr. Opin. Insect. Sci.* 11, 31–38. doi: 10.1016/j.cois.2015.08.003

Su, J., Zhang, Z., Wu, M., and Gao, C. (2014). Changes in insecticide resistance of the rice striped stem borer (Lepidoptera: Crambidae). *J. Econ. Entomol.* 107, 333–341. doi: 10.1603/ec13285

Suetsugu, Y., Futahashi, R., Kanamori, H., Keiko, K. O., Sasanuma, S., Narukawa, J., et al. (2013). Large scale full-length cDNA sequencing reveals a unique genomic landscape in a *Lepidopteran* model insect, *Bombyx mori*. *G3* 3, 1481–1492. doi: 10.1534/g3.113.006239

Wang, S. L., Baumann, A., and Wilson, T. G. (2007). *Drosophila melanogaster* Methoprene-tolerant (Met) gene homologs from three mosquito species: members of PAS transcriptional factor family. *J. Insect. Physiol.* 53, 246–253. doi: 10.1016/j.jinsphys.2006.07.011

Wilson, T. G., and Fabian, J. A. (1986). A *Drosophila melanogaster* mutant resistant to a chemical analog of juvenile hormone. *Dev. Biol.* 118, 190–201. doi: 10.1016/0012-1606(86)90087-4

Yao, R., Zhao, D. D., Zhang, S., Zhou, L. Q., Wang, X., Gao, C. F., et al. (2017). Monitoring and mechanisms of insecticide resistance in *Chilo suppressalis* (Lepidoptera: Crambidae), with special reference to diamides. *Pest. Manag. Sci.* 73, 1169–1178. doi: 10.1002/ps.4439

Yue, Y., Yang, R. L., Wang, W. P., Zhou, Q. H., Chen, E. H., Yuan, G. R., et al. (2018). Involvement of Met and Kr-h1 in JH-mediated reproduction of female *Bactrocera dorsalis* (Hendel). *Front Physiol.* 9:482. doi: 10.3389/fphys.2018.00482

Zhan, S., Merlin, C., Boore, J. L., and Reppert, S. M. (2011). The monarch butterfly genome yields insights into long-distance migration. *Cell* 147, 1171–1185. doi: 10.1016/j.cell.2011.09.052

Zhao, W. L., Liu, C. Y., Liu, W., Wang, D., Wang, J. X., and Zhao, X. F. (2014). Methoprene-tolerant 1 regulates gene transcription to maintain insect larval status. *J. Mol. Endocrinol.* 53, 93–104. doi: 10.1530/JME-14-0019

Zou, Z., Saha, T. T., Roy, S., Shin, S. W., Backman, T. W., Grike, T., et al. (2013). Juvenile hormone and its receptor, methoprene-tolerant, control the dynamics of mosquito gene expression. *Proc. Natl. Acad. Sci. U.S.A.* 110, 2173–2181. doi: 10.1073/pnas.1305293110

Conflict of Interest: The authors declare that the research was conducted in the absence of any commercial or financial relationships that could be construed as a potential conflict of interest.

frontiers in Cell and Developmental Biology

ORIGINAL RESEARCH
published: 11 June 2020
doi: 10.3389/fcell.2020.00369

Coding and Non-coding RNAs: Molecular Basis of Forest-Insect Outbreaks

*Sufang Zhang[1], Sifan Shen[1], Zhongwu Yang[2], Xiangbo Kong[1], Fu Liu[1] and Zhang Zhen[1]**

[1] Key Laboratory of Forest Protection of State Forestry and Grassland Administration, Research Institute of Forest Ecology, Environment and Protection, Chinese Academy of Forestry, Beijing, China, [2] Forestry Comprehensive Development Center of Guilin, Guilin, China

Insect population dynamics are closely related to 'human' ecological and economic environments, and a central focus of research is outbreaks. However, the lack of molecular-based investigations restricts our understanding of the intrinsic mechanisms responsible for insect outbreaks. In this context, the moth *Dendrolimus punctatus* Walker can serve as an ideal model species for insect population dynamics research because it undergoes periodic outbreaks. Here, high-throughput whole-transcriptome sequencing was performed using *D. punctatus,* sampled during latent and outbreak periods, to systemically explore the molecular basis of insect outbreaks and to identify the involved non-coding RNA (ncRNA) regulators, namely microRNAs, long non-coding RNAs, and circular RNAs. Differentially expressed mRNAs of *D. punctatus* from different outbreak periods were involved in developmental, reproductive, immune, and chemosensory processes; results that were consistent with the physiological differences in *D. punctatus* during differing outbreak periods. Targets analysis of the non-coding RNAs indicated that long non-coding RNAs could be the primary ncRNA regulators of *D. punctatus* outbreaks, while circular RNAs mainly regulated synapses and cell junctions. The target genes of differentially expressed microRNAs mainly regulated the metabolic and reproductive pathways during the *D. punctatus* outbreaks. Developmental, multi-organismal, and reproductive processes, as well as biological adhesion, characterized the competing endogenous RNA network. Chemosensory and immune genes closely related to the outbreak of *D. punctatus* were further analyzed in detail: from their ncRNA regulators' analysis, we deduce that both lncRNA and miRNA may play significant roles. This is the first report to examine the molecular basis of coding and non-coding RNAs' roles in insect outbreaks. The results provide potential biomarkers for control targets in forest insect management, as well as fresh insights into underlying outbreak-related mechanisms, which could be used for improving insect control strategies in the future.

Keywords: forest insect, outbreak, whole-transcriptome sequencing, lncRNA, ceRNA

OPEN ACCESS

Edited by:
Wei Guo,
Institute of Zoology (CAS), China

Reviewed by:
Shanchun Yan,
Northeast Forestry University, China
Lilin Zhao,
Institute of Zoology (CAS), China

***Correspondence:**
Zhang Zhen
zhangzhen@caf.ac.cn

Specialty section:
This article was submitted to Epigenomics and Epigenetics, a section of the journal Frontiers in Cell and Developmental Biology

Received: *11 February 2020*
Accepted: *24 April 2020*
Published: *11 June 2020*

Citation:
Zhang S, Shen S, Yang Z, Kong X, Liu F and Zhen Z (2020) Coding and Non-coding RNAs: Molecular Basis of Forest-Insect Outbreaks. Front. Cell Dev. Biol. 8:369. doi: 10.3389/fcell.2020.00369

KEY MESSAGE

Understanding how an outbreak of insects happens is a key topic of forest pest research, but the underpinning molecular mechanisms remain unclear. We systemically analyzed the gene expression differences and their non-coding regulators, and deduced the corresponding developmental, reproductive, chemosensory, and immune processes as key terms related to pest outbreaks of a moth. This work deepens our understanding of outbreak-related mechanisms and supplies potential biomarkers or control targets for forest insect management.

INTRODUCTION

As the most abundant and diverse animals on earth, insects play important roles in ecosystems, and their population dynamics are closely related to humans' ecological and economic environments. Outbreaks are the central focus of insect population research, long attracting the attention of both entomologists and ecologists (Hunter, 1995). Investigations on why insect outbreaks occur have been performed, considering such reasons as nutrition (Quezada García et al., 2015), natural enemies (Berryman et al., 1987), environmental factors (Veran et al., 2015; Fuentealba et al., 2017), host resistance (Elderd et al., 2013), and population interactions (Lu et al., 2010). Yet, in the same habitat, only small numbers of species may undergo an outbreak, while most of the other co-occurring species maintain low and stable population sizes within the community (Alison, 1991). This indicates that outbreaking species may respond to changes in biological and/or abiotic factors differently from that of non-outbreaking species, and the former may have an intrinsic motivation differing from the latter (Myers, 1993). To date, the physiological responses of outbreak species to some factors have been heavily researched (Berryman, 1988; Veran et al., 2015); however, the molecular basis of these responses is still unclear, which limits our understanding of the intrinsic mechanisms responsible for insect outbreaks.

Dendrolimus spp. (Lepidoptera; Lasiocampidae) are major destructive pests of conifer forests (Xiao, 1992) and *Dendrolimus punctatus* Walker is the most widely distributed species in China (Chen, 1990; Billings, 1991; Luo et al., 2018), making it the most important pine tree defoliator. Notably, *D. punctatus* is a periodic outbreaking species; once it outbreaks, the caterpillars feeding on pine needles can quickly cause the large-scale destruction of pine forests, in a phenomenon called "Fire without smoke." *D. punctatus* present different physiological characteristics during different outbreak stages. During the low-density latent period, the egg production and female ratio of *D. punctatus* are maintained at a certain level; during the ascending period, the egg production, female ratios, and population density increase considerably, with the degree of population aggregation also increasing; in the declining period, the body size, emergence rate, and female ratio of pine caterpillars all decrease to very low levels, while their rates of parasitism rise to a high level, additionally, their density drops rapidly to a very low level (Billings, 1991; Zhang et al., 2002). Collectively, these characteristics indicate that population density and several physiological characteristics, such as reproduction, immunity, or chemosensory system, are closely linked to the outbreak stages of *D. punctatus*. Outbreak of other insects also infer the importance of these physiological characteristics (Guo et al., 2011; Wang et al., 2013). Thus, *D. punctatus* offers a good model insect for investigating forest outbreak mechanisms, though the genetic mechanisms underlying this phenomenon remain generally unexplored.

With the advent of modern sequencing technology and acquisition of genomic information on outbreaking species, studies of insect outbreak mechanisms can now move from their ecological and physiological levels to understanding their basis at the molecular level (Kang et al., 2004; Wang et al., 2014). Accordingly, it is essential to investigate the molecular mechanisms that drive the occurrence of outbreak insects at multiple stages of an outbreak. Furthermore, biological processes are regulated not only by protein coding genes but also by non-coding RNA (ncRNA), such as microRNA (miRNA), long non-coding RNA (lncRNA), and circular RNA (circRNA) (Costa, 2005; Hansen et al., 2013; Beermann et al., 2016; Hombach and Kretz, 2016). The miRNAs—small ncRNAs of 20–30 nt—are well-known regulators of insect development and reproduction (Wei et al., 2009; He et al., 2016; Belles, 2017; Roy et al., 2018). LncRNAs are ncRNA longer than 200 bp (Amaral et al., 2008; Chen et al., 2016; Wu et al., 2016), which play important epigenetic regulating functions because they can form complexes with chromatin regulators at appropriate genomic regions in the cis and trans forms (Kretz et al., 2012; Mercer and Mattick, 2013). The circRNAs are newly discovered ncRNAs that form rings without the 5′-cap and 3′-polyadenylated tail (Wilusz and Sharp, 2013; Ling-Ling and Li, 2015), and they can originate from exons, introns, or intergenic regions (Zhang et al., 2013; Jeck and Sharpless, 2014; Li et al., 2015). Both lncRNAs and circRNAs can regulate gene expression through lncRNA/circRNA–miRNA–gene networks and they are also called "miRNA sponges" (Hansen et al., 2013). In particular, circRNA can regulate the splicing, transcription, and expression of genes, and subsequently regulate physiological characteristics (Li et al., 2015; Wang et al., 2017). With the development of next-generation sequencing technologies and bioinformatics, it is now possible to explore the molecular basis of dynamic population changes of outbreaking insects and to analyze the various regulators and modifiers of gene expression levels, such as miRNA, lncRNA, and circRNA, as well as the networks formed among different regulators and protein-coding genes (Yvonne et al., 2014; Li et al., 2017a; Wang et al., 2019).

In this comprehensive study, high-throughput whole-transcriptome sequencing was performed using populations of *D. punctatus* at low-density (latent period) and high-density (outbreak period) to systemically explore the molecular basis of different physiological characteristics during these two periods and to identify the involved regulating lncRNAs, circRNAs, and miRNAs. Furthermore, the chemosensory and immune genes and their regulating ncRNAs, which maybe closely

linked to outbreak stages of *D. punctatus*, were analyzed in detail. This study is the first to not only identify the ncRNAs in *D. punctatus* but also explore the coding and non-coding RNA-based molecular mechanisms of forest insect outbreaks. These results will enhance our understanding of the unique ecological and evolutionary characteristics of the population dynamics-related mechanisms of outbreak insects.

MATERIALS AND METHODS

Sampling, RNA Extraction, and RNA Quantification

Dendrolimus punctatus pupae of different densities during different outbreak stages (low-density latent period and high-density outbreak period) were collected from Quanzhou, Guilin City, in Guangxi Province, China. The low-density insects was collected from an area where less than 10% of the trees were damaged by *D. punctatus*, and the insects were rare on the damaged trees; the high-density insects was collected from an area where more than 80% of the trees were damaged by *D. punctatus*; many insects were visible on these pine tree and so they were easy to collect. These two sampling areas were located in two neighboring villages of the same town (low-density *D. punctatus*: ca. N25°58′4.72″, E111°14′47.19″; high-density *D. punctatus*: ca. N25°49′36.90″, E111°21′21.95″). All the sample specimens were collected from host Masson pine (*Pinus massoniana*) trees (ca. 10-years old) Approximately 50 pupae were collected from each low- or high-density population, and maintained in our laboratory under a 16-h light:8-h dark photoperiod at 26 ± 2°C and 50% ± 10% relative humidity. Newly emerged male and female *D. punctatus* were collected and immediately frozen in liquid nitrogen. Four groups were used: males of low-density, females of low-density, males of high-density, and females of high-density. Three biological replications were prepared for each sample.

Total RNA per sample was extracted using TRIzol (Invitrogen, Carlsbad, CA, United States). RNA degradation and contamination, especially with DNA, were checked using 1.5% agarose gels. The concentration and purity of RNA were both measured by a NanoDrop 2000 spectrophotometer (Thermo Fisher Scientific, Wilmington, DE, United States), and its integrity was assessed using the RNA Nano 6000 Assay Kit of the Agilent Bioanalyzer 2100 System (Agilent Technologies, CA, United States).

Library Preparation for lncRNA-Seq, Clustering, and Sequencing

From each sample, a total of 1.5 μg RNA was used as input material after first removing the ribosomal RNA (rRNA) with the Ribo-Zero rRNA Removal Kit (Epicentre, Madison, WI, United States). Sequencing libraries were generated using the NEBNext® Ultra™ Directional RNA Library Prep Kit for Illumina® (NEB, United States), by following the manufacturer's recommendations. Unique index codes were added to attribute the sequences to each sample. Briefly, fragmentation was carried out using divalent cations under an elevated temperature in the NEBNext First Strand Synthesis Reaction Buffer (5×). First-strand cDNA was synthesized using a random hexamer primer and reverse transcriptase; next, second-strand cDNA synthesis was performed using DNA polymerase I and RNase H. The remaining overhangs were converted into blunt ends through exonuclease/polymerase activities. After the adenylation of the DNA fragments' 3′ ends, NEB Next adaptors with hairpin-loop structures were ligated to them to prepare for the hybridization. To select insert fragments that were preferentially 150–200 bp in length, library fragments were first purified with AMPure XP beads (Beckman Coulter, Beverly, MA, United States). Then, 3 μL of USER enzyme (NEB) was used with the size-selected, adaptor-ligated cDNA, at 37°C for 15 min, before running the PCR. Then, the PCR was performed using Phusion High-Fidelity DNA polymerase, universal PCR primers, and an index (X) primer. Ensuing PCR products were then purified (AMPure XP system) and library quality assessed on an Agilent Bioanalyzer 2100.

The clustering of index-coded samples was done in an acBot Cluster Generation System, with a TruSeq PE Cluster Kitv3-cBot-HS (Illumina), according to the manufacturer's instructions. After this cluster generation, the library preparations were sequenced on an Illumina HiSeq platform, and paired-end reads were generated.

Library Preparation for Small RNA-Seq, Clustering, and Sequencing

For the small RNA library preparation, 1.5 μg of total RNA per sample was used with an NEBNext® Multiplex Small RNA Library Prep Set for Illumina® (NEB), by following the manufacturer's recommendations, to which index codes were added to attribute the sequences to each sample.

Briefly, the 3′ SR and 5′ SR adaptors were ligated, and M-MuLV reverse transcriptase was used to synthesize the first stand chain. Then, PCR amplifications were performed using Long AmpTaq 2 × Master Mix, an SR primer, and an index (X) primer. PCR products were purified on 8% polyacrylamide gels (run at 100 V, for 80 min). DNA fragments of 140–160 bp (i.e., length of small ncRNA plus the 3′ and 5′ adaptors) were recovered and dissolved in an 8-μL elution buffer. Finally, all the PCR products were purified by the AMPure XP system, and library quality assessed.

The clustering of these index-coded samples was performed in a cBot Cluster Generation System, with a TruSeq PE Cluster Kit v4-cBot-HS (Illumina), according to the manufacturer's instructions. After this cluster generation, each library preparation was sequenced on an Illumina HiSeq 2500 platform and 50-bp single-end reads generated.

Quality Control

Raw data (i.e., raw reads) in the 'fastq' format were first processed using in-house perl scripts. In this step, clean data were obtained by removing from the raw data those reads containing adapters and poly-Ns, as well as any low quality

reads. Additionally, the Q20, Q30, GC-content, and sequence duplication level of the clean data were calculated. For small RNA-Seq data, reads were trimmed and cleaned by removing sequences shorter than 15 nt or longer than 35 nt. Finally, at least 16.28 Gb of clean data for each lncRNA sequencing sample, with a Q30 > 92.99%, and more than 14.30 Mb of clean data for each small RNA-Seq sample, with a Q30 > 99.43%, were obtained. All downstream analyses were thus performed using only high-quality clean data.

lncRNA Identification

The transcriptome was assembled using StringTie (v1.3.1) software[1], based on the reads mapped to the reference genome of *D. punctatus* (Daehwan et al., 2015; Pertea et al., 2016). The assembled transcripts were then annotated using the gff compare program[2]. The unknown transcripts were used to screen for putative lncRNAs. To sort the ncRNA candidates among the unknown transcripts, four computational approaches, namely CPC/CNCI/Pfam/CPAT, were combined and used (Lei et al., 2007; Kai et al., 2013; Liang et al., 2013; Finn et al., 2014). Those transcripts exceeding 200 nt in length, and having more than two exons, were selected as lncRNA candidates (Kelley and Rinn, 2012; Lv et al., 2013); these were further screened using CPC/CNCI/Pfam/CPAT, which has the ability to distinguish not only protein-coding from non-coding genes but also different types of lncRNAs—including lincRNA, intronic lncRNA, anti-sense lncRNA, sense lncRNA.

miRNA Identification

Use the Bowtie tools software (Langmead and Salzberg, 2012), clean reads were used as queries against the Silva, GtRNAdb, Rfam, and Repbase databases for sequence alignments, and to filter out rRNA, transfer RNA, small nuclear RNA, small nucleolar RNA, other ncRNAs as well as any repeats. The remaining reads were used to detect miRNAs through comparisons with *D. punctatus* genome (Zhang et al., 2020) and known miRNAs from the miRBase (v21)[3], and novel miRNA were predicted by miRDeep3 (Friedländer et al., 2012).

CircRNA Identification and Target Prediction

CircRNA Identifier (CIRI) was used to predict the circRNAs (Yang Y. et al., 2017). CIRI scans the SAM files, twice. In the first scan, CIRI detects junction reads of circRNA candidates, by using paired-end mapping and GT–AG splicing signals. Then, it re-scans the SAM alignment to eliminate false-positive candidates derived from incorrectly mapped reads of homologous genes or repetitive sequences. We used the miRanda (Doron et al., 2008) and RNA hybrid (Rehmsmeier et al., 2004) tools for predicting circRNA target miRNAs and the corresponding target genes of miRNAs.

[1]https://ccb.jhu.edu/software/stringtie/index.shtml

[2]http://ccb.jhu.edu/software/stringtie/gffcompare.shtml

[3]http://www.mirbase.org/

Expression Analysis

StringTie (v1.3.1) was used to calculate the fragments per kilobase of exon per million fragments mapped (FPKM) values, for both lncRNAs and coding genes, in each sample (Pertea et al., 2016). Gene FPKMs were computed by summing the FPKMs of transcripts in each gene group; FPKMs were calculated based on the length of the fragments and the read counts mapped to this fragment. The expression levels of miRNA and circRNA were each quantified using TPM (transcript per million) (Fahlgren et al., 2007).

Differential Expression Analysis

The differential expression analysis was performed using the 'DESeq' (v1.10.1) (Anders and Huber, 2012). DESeq provides statistical routines for determining differential expression in digital gene expression data, by using a model based on the negative binomial distribution. The resulting *P*-values are adjusted using the Benjamini and Hochberg's approach (Haynes, 2013) for controlling the false discovery rate (FDR). Genes with an adjusted *P*-value < 0.01 and absolute value of $\log_2$ (fold-change) > 1 were designated as differentially expressed.

Gene Functional Annotation

The mRNAs and targets of ncRNAs were queried in a BLAST algorithm-based search against the NR, SWISSPROT, KEGG, and KOG databases (using cut-off threshold of 1e-5), from which the most similar sequence targets were selected for functional annotations. Then, the molecular functions, biological processes, and cellular components of the genes were assigned a gene ontology (GO) annotation by Blast2GO (Stefan et al., 2008). The GO enrichment analysis of differentially expressed genes (DEGs) was carried out using the 'topGO' (Alexa and Rahnenfuhrer, 2010), and KOBAS software (Xie et al., 2011) was used to test for the statistical enrichment of these DEGs in KEGG pathways.

Competing Endogenous RNA (ceRNA) Network Analysis

Differentially expressed ncRNAs and mRNAs between low- and high-density *D. punctatus* groups were also analyzed. The miRNA response elements were first identified, by screening the circRNA, lncRNA, and mRNA sequences. Then, the STRING database (Cytoscape 3.4.0) was used to identify protein–protein interactions among the products of these DEGs.

Validation by Real Time Quantitative PCR (qRT-PCR)

To verify our RNA-Seq results, a total of thirteen DEGs, three lncRNAs, three miRNAs, and three circRNAs, were randomly selected to detect their respective expression levels by qRT-PCR. The RNAs used for this validation were the same as those of Illumina-sequenced RNAs. PimeScipt RT reagent Kit (TaKaRa, Dalian, China) was used to synthase cDNA (for mRNA, lncRNA and circRNA) with random hexamers. Mir-X^{TM} miRNA First Strand Synthesis and the SYBR® qRT-PCR Kit (Takara, Dalian, China) were used to synthesize the DNA template for miRNA, for which miRNA primers were designed according to the Kit's

manual. The qRT-PCR was carried out with the SYBR Green PCR kit (TaKaRa, Dalian, China). Beta-actin (for mRNA, lncRNA, and circRNA) and U6 (for miRNA) served as controls. All primers used for qRT-PCR can be found in **Supplementary Table S1**. All qRT-PCR reactions were performed in a Roche LightCycler 480 (Stratagene, La Jolla, CA, USA), using this program: 2 min at 95°C, 40 cycles of 20 s at 95°C, 20 s at 58°C, and 20 s at 72°C; finally, a melting curve analysis (58°C to 95°C) was conducted to evaluate the specificity of obtained PCR products. Ct values were calculated in Roche qPCR software (v1.5.1) by applying the second derivative method. Each PCR reaction was done in triplicate. Data are presented as the $\log_2$ (fold-change) in expression and were compared with RNA-Seq results.

RESULTS

Overview of Sequencing and ncRNA Predictions

In all, 209.24 Gb of clean data with a Q30 > 92.99% were obtained (**Supplementary Table S2**), and this data mapped onto the *D. punctatus* reference genome assembly, by using HISAT2 (Daehwan et al., 2015; **Supplementary Table S3**). A total of 55,684 lncRNAs were predicted, most of them being lincRNAs (41,324; 74.2%), followed by intronic-lncRNAs (7,384; 13.3%), antisense-lncRNAs (4,120; 7.4%), and sense lncRNAs (2,856; 5.1%) (**Figure 1A**). For the lengths of lncRNA and mRNA, they had similar distribution patterns (**Supplementary Figures S1A,B**) but more of the mRNAs contained four or more exons (**Supplementary Figures S1C,D**). Most of the ORFs were shorter than 100 bp from the lncRNA, yet longer than 200 bp from the mRNA (**Supplementary Figures S1E,F**). Additionally, the mRNAs were characterized by more isoforms than were lncRNAs (**Supplementary Figure S1G**), indicating the former are more complex than the latter. Finally, the expression levels of lncRNAs and mRNAs were generally similar (**Supplementary Figure S1H**).

Overall, 15,698 circRNAs were predicted in *D. punctatus* according to CIRI, with most of these derived from exons < 3,000 bp whereas most of those derived from intergenic regions were longer than 3,000 bp (**Figure 1B**). Compared with mRNAs, the expression levels of circRNAs were higher (**Supplementary Figure S2**).

For the miRNAs, 193.67 Mb of clean reads were acquired, with at least 14.30 Mb per sample, and their Q30 was > 99.43%. From them, any reads less than 15 nt and longer than 35 nt were first removed, the remaining reads were mapped onto the *D. punctatus* reference data (**Supplementary Table S4**). This yielded 3,738 miRNAs, of which most were between 20 nt and 22 nt (**Figure 1C**); however, the length distributions of known and novel miRNAs differed (**Supplementary Figures S3A,B**). The first nucleotide bias analysis indicated that as the total length of a miRNA increased, so did the bias for U serving as the first nucleotide (**Supplementary Figure S3C**). Additionally, there was evidence of miRNA nucleotide bias at the last position for U and C (**Supplementary Figure S3D**).

Expression Differences and Functional Analyses of Coding RNAs Between Low and High Density *D. punctatus*

To analyze the molecular responses of *D. punctatus* during different stages of outbreaks, we compared and selected the DEGs using DESeq (Anders and Huber, 2012). The DEG numbers indicated that the differences between sexes in *D. punctatus* (occurring at both low and high densities) were much greater than those found between densities (both male and female) (**Table 1**).

Then we focused on analyzing gene expression differences in *D. punctatus* from different outbreak stages. An MA plot of the differences between low- and high-density insects showed the more DEGs in males than females (**Supplementary Figures S4A,B**). The GO annotation of DEGs in females at low- versus high-density mainly focused on multicellular organism process, developmental process, multi-organism process, reproduction, and immune system process (**Figure 2A**). The top-10 enriched GO terms for DEGs between low- and high-density female insects revealed that, apart from basic metabolic processes, also included were olfactory-related sensory perception of smell, regulation of postsynaptic membrane potential, chromatin silencing at rDNA (**Table 2**). These differences indicated that *D. punctatus* females from high-density and low-density populations mainly differ on their development, reproduction, immunity, and olfaction. To detect, in greater detail, further possible differences between low- and high-density insects, we analyzed the up- and down-regulated genes separately. According to their GO enrichment results, this

TABLE 1 | Numbers of differentially expressed coding and non-coding RNAs between sexes and population densities of *Dendrolimus punctatus*.

	mRNA			lncRNA			miRNA			circRNA		
DEG Set	all	up	down	all	up	down	all	up	down	all	up	down
Low-♀: Low-♂	6470	3388	3082	473	122	351	581	152	429	77	62	15
High-♀: High-♂	8309	4144	4165	954	417	537	288	40	248	80	55	25
Low-♀: High-♀	561	333	228	138	59	79	347	161	186	39	28	11
Low-♂: High-♂	1371	895	476	169	89	80	239	107	132	81	36	45

Low, samples from low density; High, samples from high density; all, the number of total DEGs; up, the number of up-regulated DEGs; Down, the number of donw-regulated DEGs.

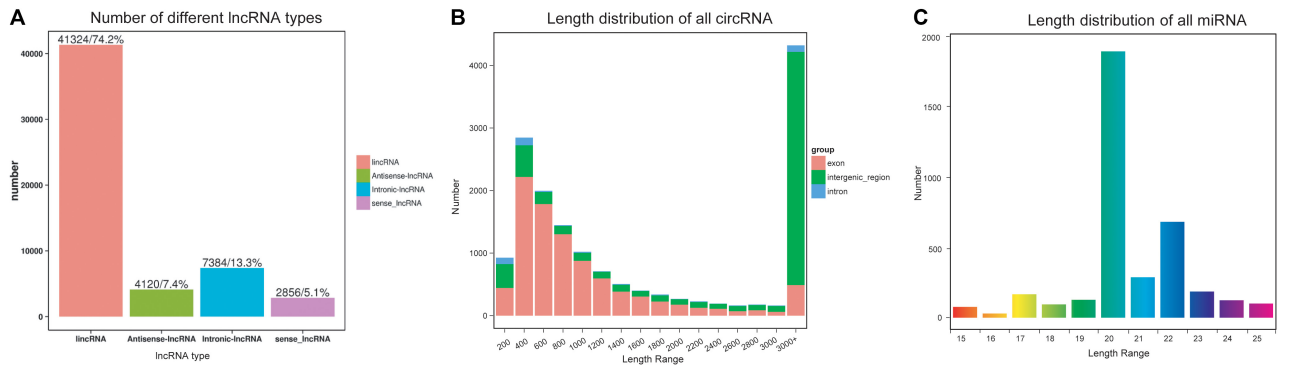

FIGURE 1 | Characteristics of non-coding RNAs in *Dendrolimus punctatus*. **(A)** Classification of the predicted novel lncRNAs; **(B)** length distribution of the circRNAs; **(C)** length distribution of the miRNAs.

activity was very different between low- and high-density females of *D. punctatus*: the latter's up-regulated genes were involved in biological regulation, localization, response to stimulus, signaling, developmental process, multi-organism process, and reproduction (**Figure 2B**); however, the down-regulated genes of these high-density females were involved in multicellular organism process, development process, multi-organism process, reproduction, reproduction process, and immune system process (**Figure 2C**). Thus, the low-density *D. punctatus* females have better developmental, reproductive, and immune capabilities.

For males of *D. punctatus*, a GO term analysis of DEGs between those at low- and high-density revealed they differed significantly in developmental process, multi-organism process, reproduction, and immune system process, as well as the presynaptic process involved in chemical synaptic transmission (**Figure 2D**). Up- and down-regulated DEGs between low- and high-density males of *D. punctatus* showed different characteristics from the females. The up-regulated genes were involved in biological regulation, localization, response to stimulus, and signaling (much like females), but no developmental and reproductive processes were evidently enriched. Additionally, the presynaptic process involved in chemical synaptic transmission was represented to a higher degree in up-regulated DEGs than among the total genes (**Figure 2E**). The down-regulated genes were similar to those of females, in that they were mainly involved in multicellular organismal process, developmental process, multi-organism process, reproduction, and immune system process (**Figure 2F**). These results indicated the low-density males of *D. punctatus* put more energy into development, production, and immune functions than high-density conspecific individuals, while the males at high-density allocate more energy into basic metabolism and olfactory functions.

Functions of Non-coding RNAs in the Differential Characteristics of Low- and High-Density *D. punctatus*

To analyze the functions of ncRNAs (lncRNA, miRNA, and circRNA) in regulating the outbreak of *D. punctatus*, the differentially expressed ncRNAs were first identified. Using a cutoff of fold change ≥ 2 coupled to an FDR < 0.05, we distinguished 473 and 954 differentially expressed lncRNAs between sexes of *D. punctatus* from low- and high-density populations, respectively; and likewise, 138 and 169 differentially expressed lncRNAs between low- vs.

TABLE 2 | Enriched GO term of DEGs (differentially expressed genes) between low- and high-density female *Dendrolimus punctatus*.

GO.ID	Term	Annotated	Significant	Expected	KS
GO:0006278	RNA-dependent DNA biosynthetic process	331	7	4.9	<1e-30
GO:0090305	nucleic acid phosphodiester bond hydrolysis	342	7	5.06	<1e-30
GO:0015074	DNA integration	90	1	1.33	<1e-30
GO:0090304	nucleic acid metabolic process	1933	25	28.62	4.0e-28
GO:0043551	regulation of phosphatidylinositol 3-kinase activity	27	1	0.4	5.5e-13
GO:0006334	nucleosome assembly	47	1	0.7	1.7e-08
GO:0006259	DNA metabolic process	709	10	10.5	4.8e-05
GO:0050911	detection of chemical stimulus involved in sensory perception of smell	96	0	1.42	0.00098
GO:0060078	regulation of postsynaptic membrane potential	11	3	0.16	0.00106
GO:0000183	chromatin silencing at rDNA	14	1	0.21	0.00312

Annotated, Annotated gene numbers of the term; Significant, Annotated DEGs numbers of the term; Expected, expected numbers of annotated DEGs numbers of the term; KS, significant statistics of the term.

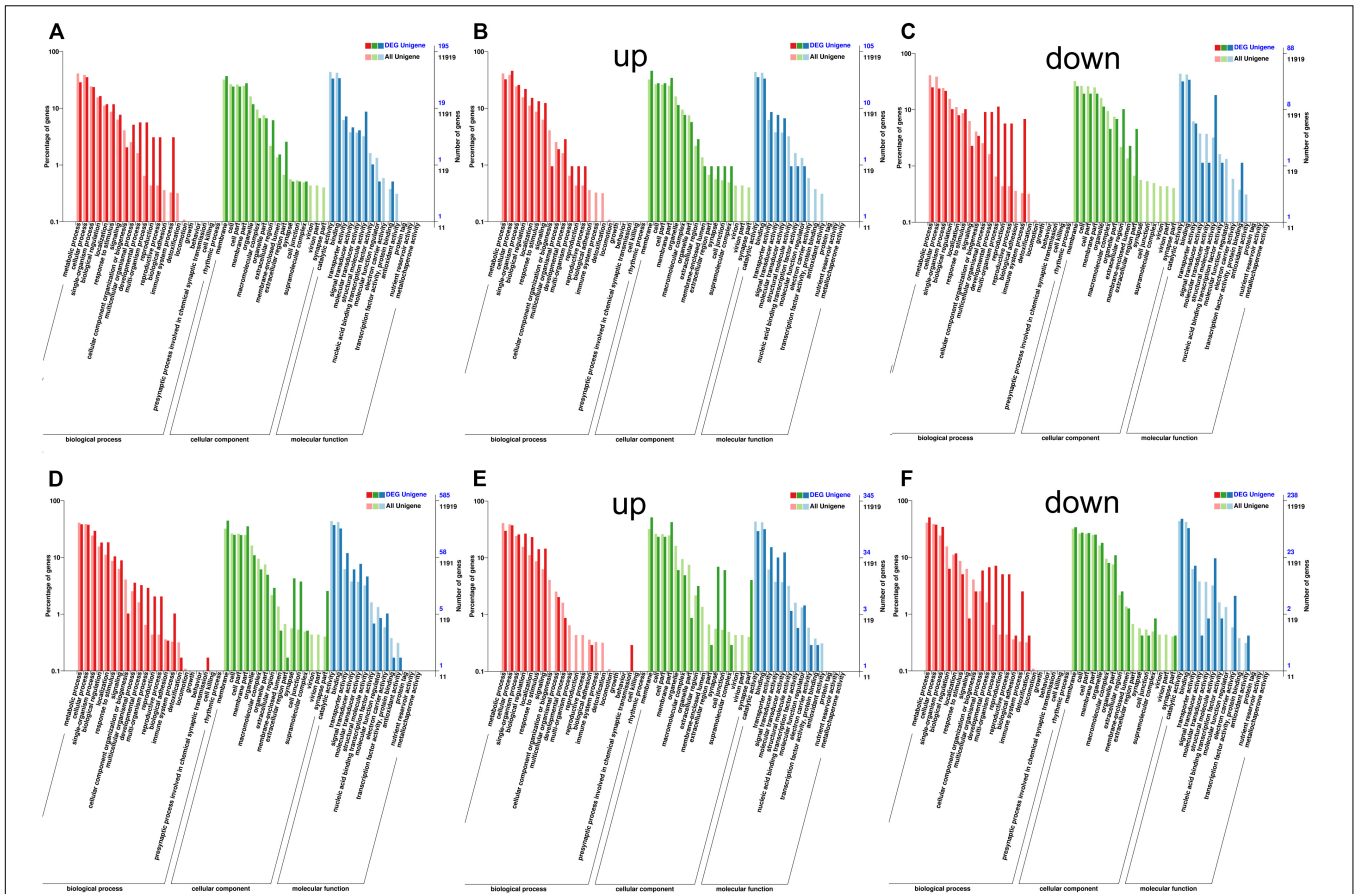

FIGURE 2 | GO annotation of the DEGs (differentially expressed genes) identified between low- vs. high-density *Dendrolimus punctatus*. **(A–C)** For females: total DEGs **(A)**, up-regulated genes **(B)**, and down-regulated genes **(C)**. **(D–F)** For males: total DEGs **(D)**, up-regulated genes **(E)**, and down-regulated genes **(F)**.

high-density *D. punctatus* in females and males, respectively (**Table 1**). According to a Volcano plot of DEGs targeted by mRNAs and lncRNAs, the ratio values of differently expressed lncRNAs to mRNAs between low- and high-density areas (**Supplementary Figures S5A,B**) was higher than those between females and males (**Supplementary Figures S5C,D**); this indicated a stronger regulatory role of lncRNAs in generating differences found between low- and high-density insects than those between sexes. Applying the same cutoff criteria as above, 77 and 80 differentially expressed circRNAs between sexes of *D. punctatus* from low- and high-density areas, and 39 and 81 differentially expressed circRNAs between low- vs. high-density *D. punctatus* in females and males were identified, respectively (**Table 1**). Likewise, for differentially expressed miRNAs, 581 and 288 of them were found between female and male *D. punctatus* from low- and high-density populations, respectively, with 347 and 239 identified between low- vs. high-density *D. punctatus* in the females and males, respectively (**Table 1**).

Next, the targets of differently expressed ncRNAs between low- and high-density *D. punctatus* insects were further analyzed to explore the regulating roles of ncRNAs during this insect's outbreaks. The lncRNAs may regulate the associated mRNA genes of neighboring (cis target) and overlapping (trans targets) (Li et al., 2017a). Hence, both the cis and trans targets of lncRNAs were predicted and analyzed. For females, the cis targets of differentially expressed lncRNA between low- and high-density insects were mainly involved in developmental and multi-organism processes, reproduction, and behavior, while the trans targets were involved in biological regulation, response to stimulus, signaling, and cellular component organization or biogenesis (**Figures 3A,B**). The differently expressed mRNAs (**Figure 2A**) and the targets of differently expressed lncRNAs between low- and high-density females of *D. punctatus* were both involved in metabolism, development, and reproduction; however, their enriched GO terms revealed some divergence, in that mRNAs were more specific to the immunity term, whereas lncRNAs' targets were more specific to the behavior term. For males, the cis targets of differentially expressed lncRNAs between low- and high-density insects were mainly involved in reproduction and the presynaptic process involved in chemical synaptic transmission, while the trans targets participated in multicellular organismal, developmental, and immune system processes, as well as reproduction and cell killing (**Figures 3C,D**). In sum, the GO terms of differently expressed mRNAs and targets of differently expressed lncRNAs from male insects at low- and high-density

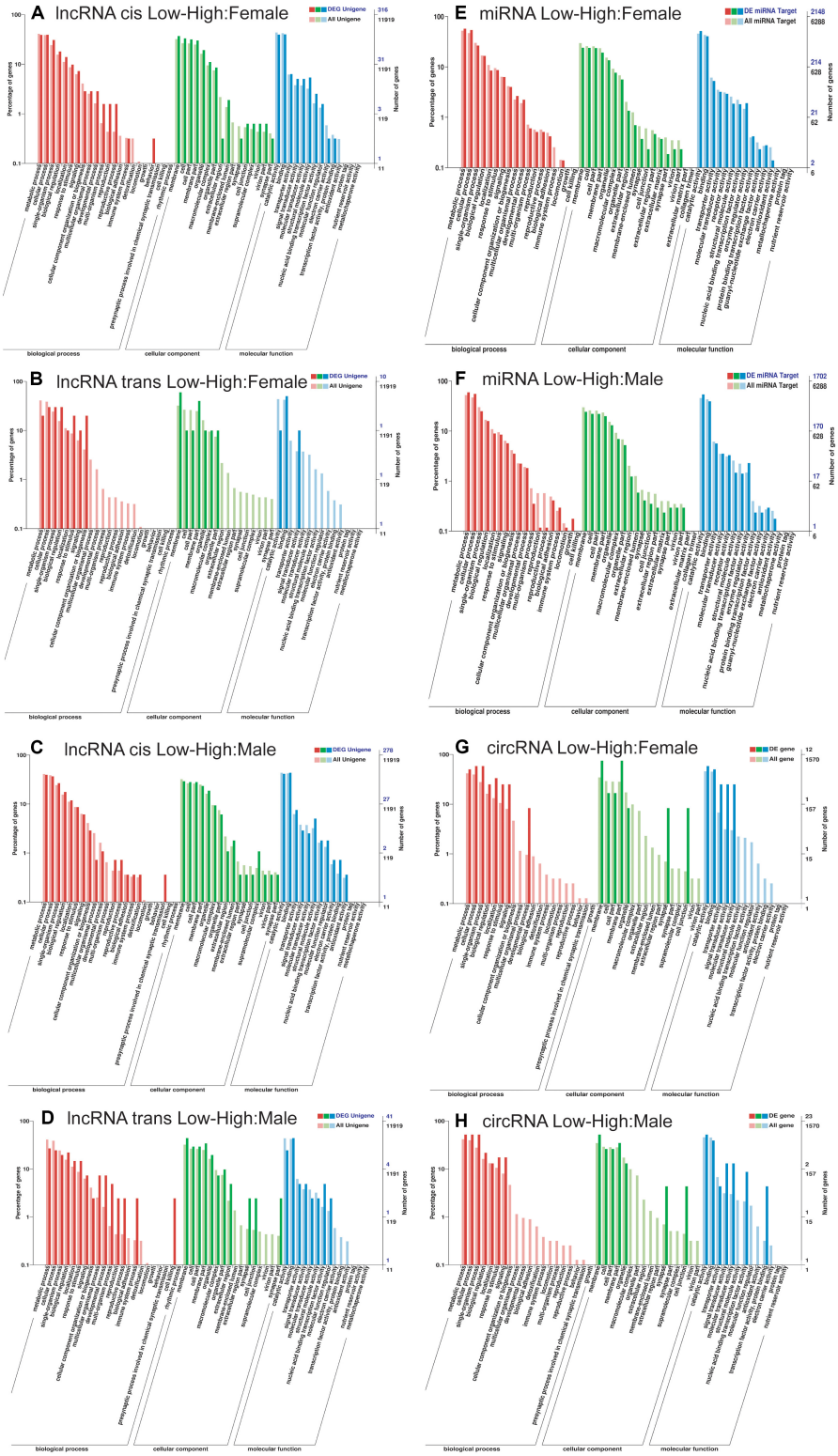

FIGURE 3 | GO annotation of the targets of differently expressed non-coding RNAs identified between low- vs. high-density *Dendrolimus punctatus*. **(A–D)** lncRNAs: cis **(A)** and trans **(B)** GO annotations of differentially expressed lncRNAs between *D. punctatus* females from the low- and high-density populations. Likewise, cis **(C)** and trans **(D)** GO annotations of the differentially expressed lncRNAs between *D. punctatus* males from the low- and high-density populations. **(E,F)** miRNAs: GO annotation of the targets of differentially expressed miRNAs between low- vs. high-densities in females **(E)** and males **(F)**. **(G,H)** circRNAs: GO annotation of genes targeted by the differentially expressed circRNAs between low- vs. high-densities in females **(G)** and males **(H)**.

were coincident, indicating a primary regulator role for lncRNA in *D. punctatus* outbreaks.

The respective functions of miRNAs related the differing characteristics of low- and high-density populations of *D. punctatus* were then analyzed. In females, there were fewer target genes of differentially expressed miRNAs between low- and high-density *D. punctatus* than targets of all the miRNAs in the immune system process (**Figure 3E**). Because miRNAs play negative regulatory roles on their target genes (Ghildiyal and Zamore, 2009), these results indicated that miRNA play more regulatory roles in the low-density insect. In males, fewer target genes of differentially expressed miRNAs between low- and high- density *D. punctatus* populations were found than targets of all the miRNAs in both the multi-organism process and reproduction terms (**Figure 3F**). This indicated that these miRNAs function in metabolic and reproductive adjustments that occur between low- and high-density males of *D. punctatus*.

The targeted genes of differentially expressed circRNAs between low- and high-density populations of *D. punctatus* were also analyzed. In females, these mainly participated in the biological process category of development, the cellular component category of synapse and cell junction, and the molecular function categories of transporter, signal transducer, and molecular transducer activities (**Figure 3G**). In males, they were primarily involved in the cellular component category of synapse and cell junction, as well as molecular function categories of protein binding and signal transducer, molecular transducer, nucleic acid-binding transcription factor, and transcription factor activities (**Figure 3H**). These results revealed the different targeted genes of the differentially expressed circRNAs; interestingly, the category synapse and cell junction was enriched in both comparisons.

To verify the RNA-Seq data, we selected thirteen mRNA, three lncRNA, three miRNA, and three circRNA randomly. Their respective fold-change values in expression between low- and high-density *D. punctatus* were tested by qRT-PCR. These results verified the reliability of the initial set of RNA-Seq results (**Supplementary Figure S6**).

Construction of ceRNA Networks in *D. punctatus*

The circRNAs, lncRNAs, and mRNAs may bind to the same miRNA response elements competitively in a regulatory network, which is referred to as a ceRNA network (Salmena et al., 2011). **Figure 4A** shows the total numbers of differentially expressed coding and ncRNAs in different situations. The ratios of ncRNAs targeting DEGs between low- and high-density populations are higher than those between males and females, indicating the regulatory functions of ncRNAs were stronger in the outbreak process than between sexes. Then, to derive a ceRNA network, we screened the relationships between miRNA vs. mRNA, miRNAs vs. circRNA and miRNAs vs. lncRNA (**Supplementary Table S5**), using the following parameters: number of miRNAs interacting with the candidate ceRNAs > 5 and $P < 0.05$ (Li et al., 2014). From this, a total of 55,707,481 ceRNA relationships with 41,508 nodes were obtained. With such a complex network, it was necessary to extract the critical RNAs and perform a follow-up analysis: score for all the nodes in the network were obtained and the top 10% of nodes were kept for further examination. A GO annotation of these critical RNAs indicated their involvement in developmental, multi-organism, and reproduction processes, as well as biological adhesion (**Figure 4B**), and these GO terms also figured prominently among the DEGs distinguished between low- and high-density *D. punctatus* populations. Taken together, these results indicated that an operating ceRNA regulatory network is crucial during insect outbreaks.

Differently Expressed Chemosensory and Immune Genes Between Low- and High-Density *D. punctatus* and Their ncRNA Regulators

The chemosensory and immune system closely related to the physiological characteristics during different outbreak stages of *D. punctatus*, as indicated in the previous research (Billings, 1991; Zhang et al., 2002). Our transcriptomic results also illustrated their critical roles in the outbreak process of this defoliating insect. Accordingly, we further analyzed these two gene families in low- and high-density *D. punctatus*. Heatmaps (**Figure 5**) showed that relative expression levels of chemosensory and immune genes not only differed greatly between sexes, but also between individuals at low-and high-density, especially in male insects.

Then, we investigated in depth the differently expressed chemosensory and immune genes between low- and high-density *D. punctatus* and their ncRNA regulators. In females, the expression of five chemosensory genes was statistically different between low- and high-density *D. punctatus* (**Figure 6A**): it was greater for *DpunCSP8* and *DpunOBP20* in low-density females, but greater for *DpunOBP22*, *DpunOBP46*, and *DpunOR56* in high-density females. 14 lncRNAs contained *DpuncCSP8* as their target (**Supplementary Figure S7A**), yet only MSTRG.120627.1 was expressed significantly higher in high-density females (**Figure 6B**). Eight, six, and six lncRNAs respectively contained *DpuncOBP20*, *DpuncOBP22*, and *DpuncOBP46* as targets (**Supplementary Figures S7B–D**), but none of these lncRNAs were expressed in a significantly different way between low- and high-density females. Six miRNAs contained *DpuncOR56* as their target, of which three were significantly down-regulated in females at high-density (**Figure 6C**, **Supplementary Figure S7E**), the reverse of *DpunOR56*'s expression. Three immune genes, *Serpin-4L*, *DpunGap11*, and *DpunTalin1*, were found expressed significantly higher in high-density than in low-density females of *D. punctatus* (**Figure 6D**). No ncRNA regulator could be found for Serpin-4L. Eight lncRNAs contained *DpunGap11* as a target (**Supplementary Figure S7F**), with only MSTRG.146927.1 expressed at a significantly higher level in the high-density than low-density females (**Figure 6E**). *DpunTalin1* was target of one lncRNA (**Supplementary Figure S7G**), one miRNA (**Supplementary Figure S7H**), and seven circRNAs (**Supplementary Figure S7I**); however, none of these ncRNAs were expressed in a significantly different way between low- and high-density females.

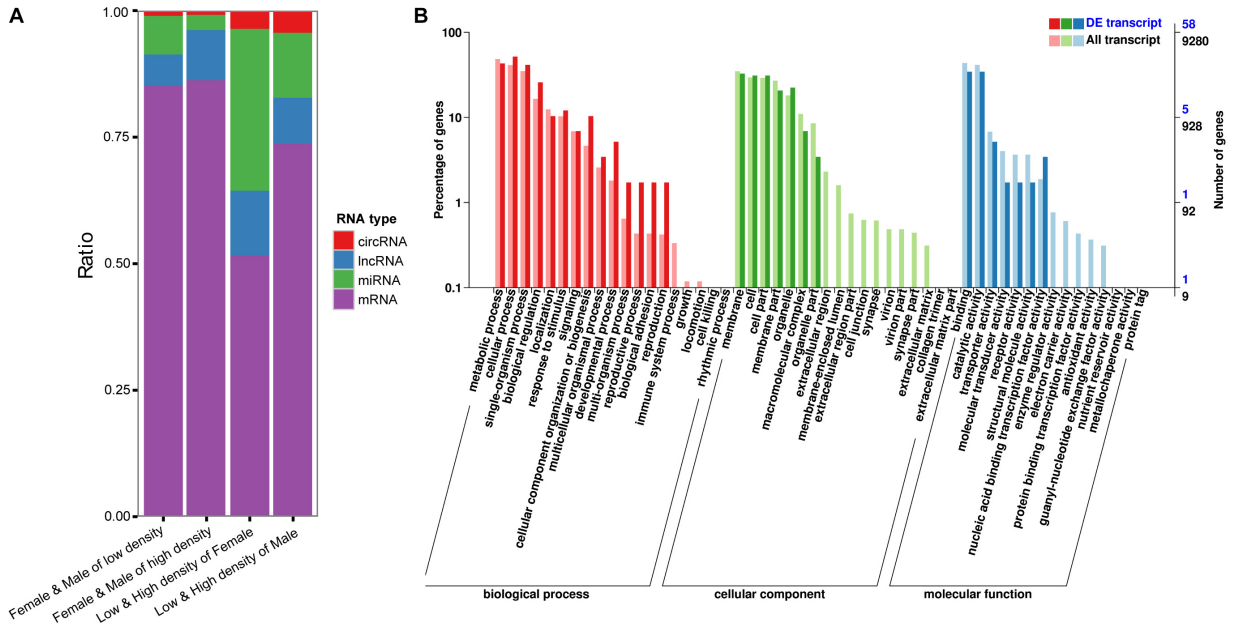

FIGURE 4 | (A) Total numbers of differentially expressed coding and ncRNAs in four situations tested; **(B)**. GO annotation of critical genes in the ceRNA network.

Next, we considered the situations of low- vs. high-density males of *D. punctatus*, finding more differently expressed chemosensory or immune genes in males than females between low- and high-density populations of *D. punctatus* (**Figure 7**). Ten chemosensory genes were expressed at significantly differently levels between low- and high-density males of *D. punctatus* (**Figure 7A**): *DpunCSP7*, *Dpund17*, *DpunIR21*, and *DpunIR25a* were expressed more in low-density males, whereas *DpunCSP19*, *DpunOBP1*, *DpunPBP1*, *next-OR60*, and *DpunSNMP1* were all expressed more in high-density males. Among these chemosensory genes, an lncRNA regulator, MSTRG.120685.1, of both *DpunCSP17* (**Figure 7B**) and *DpunCSP19* (**Figure 7C**), had significantly more expression in high-density males, as did another lncRNA regulator, MSTRG.120685.1, of *next-IR1* (**Figure 7D**); *DpunPBP1* was regulated by 30 lncRNAs (**Figure S8E**), of which eight were expressed significantly more in high-density males (**Figure 7E**). The ncRNA regulators of other chemosensory genes did not undergo a significantly different level of expression between low- and high-density males of *D. punctatus* (**Supplementary Figure S8**). Eleven immune genes were expressed significantly and differently between low- and high-density male *D. punctatus* (**Figure 7F**), of which six were down-regulated and five were up-regulated in high-density males. Among these immune genes, the lncRNA regulator, MSTRG.156626.2, of *DpunCASP3* (**Figure 7G**), was expressed significantly more in low-density males, as was the miRNA regulator, asu-miR-34-5p, of *DpunKn* (**Figure 7H**). Similarly, another miRNA regulator, unconservative_000344F_pilon_5149037, of *DpunCLIP-serpin 3* (**Figure 7I**), had significantly greater expression in high-density males, as did the lncRNA regulator MSTRG.226902.1 of *DpunSerpin easter-L* (**Figure 7J**) and both lncRNA regulators, MSTRG.165722.1 and MSTRG.165710.3, of *DpunPGRP2* (**Figure 7K**). Finally, *DpunHemocytin* and *DpunHemocytin-2* were both regulated by a miRNA that was expressed significantly higher in low-density males (**Figures 7L,M**). The ncRNA regulators of other immune genes did show any significantly expressed differences between low- and high-density males of *D. punctatus* (**Supplementary Figure S9**).

DISCUSSION

Insect species that experience outbreaks undergo extreme fluctuations in population density and consequently are capable of exerting substantial ecological and economic effects over large areas (Baltensweiler and Fischlin, 1988; Pener and Simpson, 2009). Understanding the large-scale and long-term dynamic mechanisms of outbreaking insects is therefore necessary to develop effective management strategies to mitigate these occurrences. Hence, in this study we employed whole-transcriptome sequencing and bioinformatics technology to comprehensively analyze the outbreak-related functions of coding and ncRNAs profiles and ceRNA networks in a typical forest insect pest, the defoliating moth *D. punctatus*.

Currently, molecular mechanism-related studies of *D. punctatus* outbreak characteristics remain limited to mRNAs (Yang et al., 2016; Yang C.H. et al., 2017; Zhang et al., 2016, 2018), while the study of ncRNAs in forest insects is generally limited. Our study is the first to identify and quantify expression levels of lncRNA, circRNA, and miRNA in *D. punctatus*. We identified 55,684 novel lncRNAs, in addition to 5,698 novel

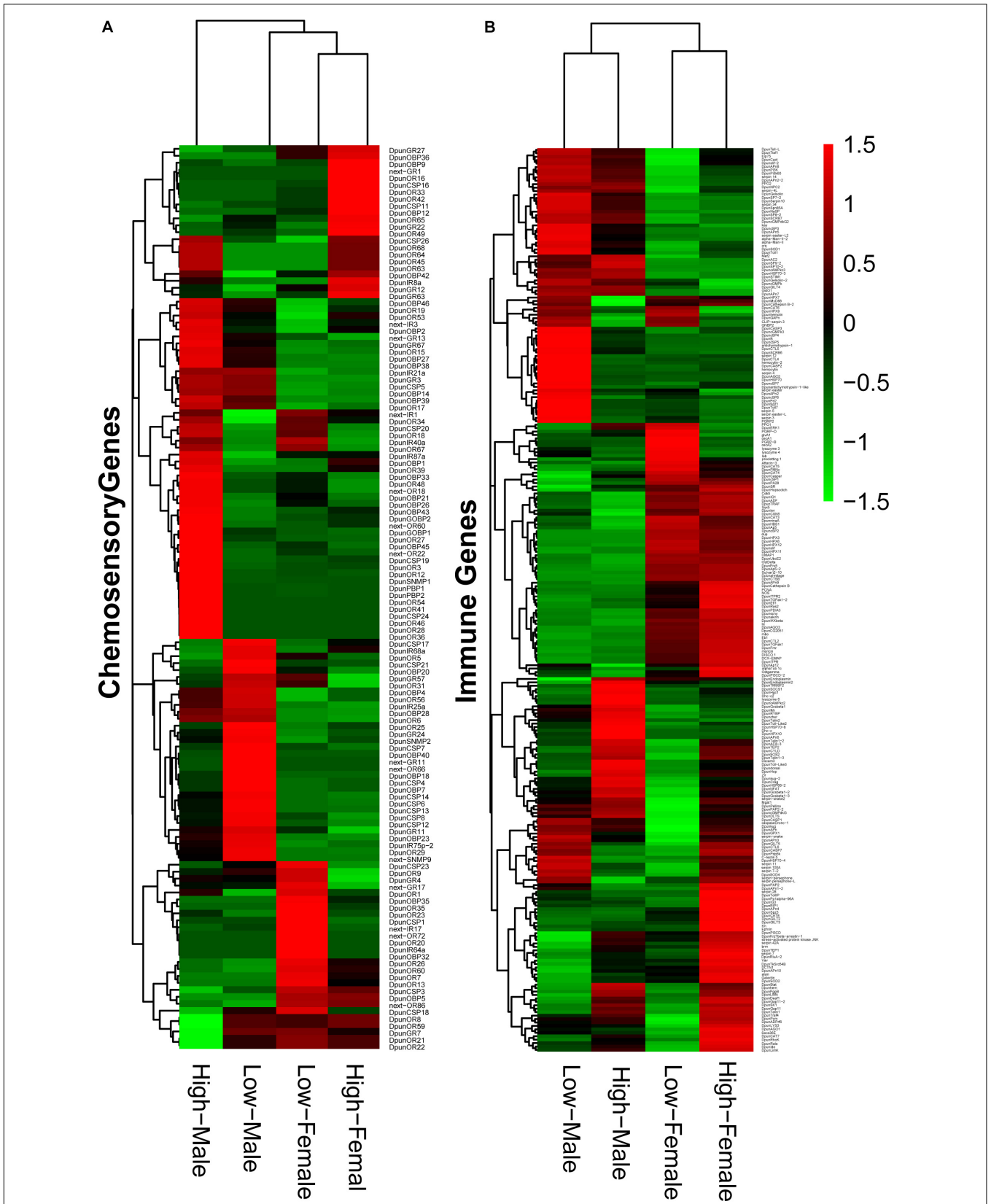

FIGURE 5 | Expression of chemosensory genes **(A)** and immune genes **(B)** in male and female *Dendrolimus punctatus* from low- and high-density populations.

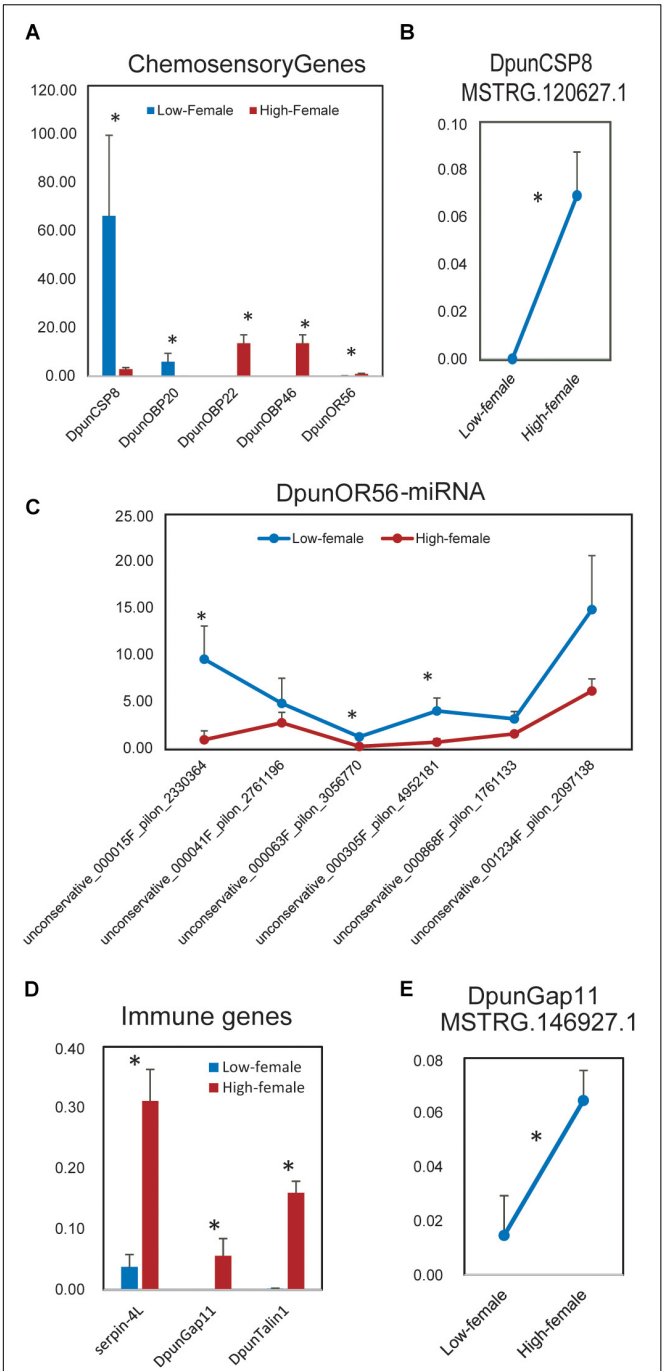

FIGURE 6 | Differently expressed chemosensory and immune genes and their significant differently expressed non-coding RNA regulators between low- vs. high-density females of *Dendrolimus punctatus*. **(A)** Differently expressed chemosensory genes; **(B)** significant differently expressed lncRNA regulator of *DpunCSP8*; **(C)** miRNA regulators of DpunOR56; **(D)** differently expressed immune genes; **(E)** significant differently expressed lncRNA regulator of DpunGap11.

circRNAs and 3,521 novel miRNAs. Furthermore, differentially expressed coding and non-coding RNAs were identified between the low- and high-density *D. punctatus* populations, for which functional annotations revealed their specific regulatory roles in this pest's outbreaks.

Firstly, the differentially expressed mRNAs related to *D. punctatus* population density were investigated. The differences arising between low- and high-population densities in males and females were various. In females, the DEGs were mainly involved in metabolism, development, reproduction and immunity, while in males, in addition to metabolism, development, reproduction, and immunity, the DEGs contributed to synapse junctions. Reproduction and immunity differences between low and high density of both sexes are consistent with other research in which fertility and parasitism rates differed during the non-outbreak and outbreak stages of *D. punctatus* (Zhang et al., 2002). The synapse is involved in neuron-related activities, such as learning and memory (Priyamvada et al., 2009; Fiumara et al., 2015). We posit that the differences in synaptic capabilities found between low- and high-density male insects reflect their varied neural activities. In this way, the molecular basis of differences in physiological traits of low- and high-density *D. punctatus* could be outlined.

The ncRNAs appear to play important roles in cellular functions, particularly in organismal responses to biotic and abiotic stresses (Gomes et al., 2013), and our results suggest the regulatory functions of ncRNAs in insect outbreaks are also significant. The lncRNAs participate in the regulation of different biological processes, albeit in disparate ways (Long et al., 2017; Marchese et al., 2017). Our results indicate that lncRNAs have regulatory functions during the outbreaking process of *D. punctatus*. In females of *D. punctatus*, the targets of differentially expressed lncRNAs between low- and high-density populations were mostly involved in metabolism, development, reproduction, and behavior. These functions are similar to those of their differently expressed mRNAs. Additionally, in males, the functions of the targets of differentially expressed lncRNAs were consistent with those of differently expressed mRNAs. Consequently, we conclude that lncRNAs are the primary ncRNA regulators of molecular differences that arise in this insect when its population is at low versus high density. The regulatory functions of lncRNAs during insect reproduction have been demonstrated (Wen et al., 2016; Maeda et al., 2018), and our work here indicates that reproductive regulation of lncRNAs can also affect different stages of insect outbreaks. Immune-related regulatory functions of lncRNAs are extensively researched in animals and humans (Atianand et al., 2017; Chen et al., 2017; Mowel et al., 2018), but a focus on insects has been limited. Our results demonstrated that immune-related regulatory functions of lncRNAs also operate in insects, and this may, in part, explain the resulting different immune capabilities of low- and high-density individuals of *D. punctatus*.

The circRNA revealed the existence of different regulatory functions between sexes in low- and high-density *D. punctatus* populations, but they both participated in synapse and cell junction. This result is consistent with previous findings in which synapse regulation was determined to be a vital function of circRNAs (Westholm et al., 2014; You et al., 2015). As newly found ncRNAs, research on the functioning of circRNAs remains limited to humans and a few vertebrate species (Li et al., 2017b;

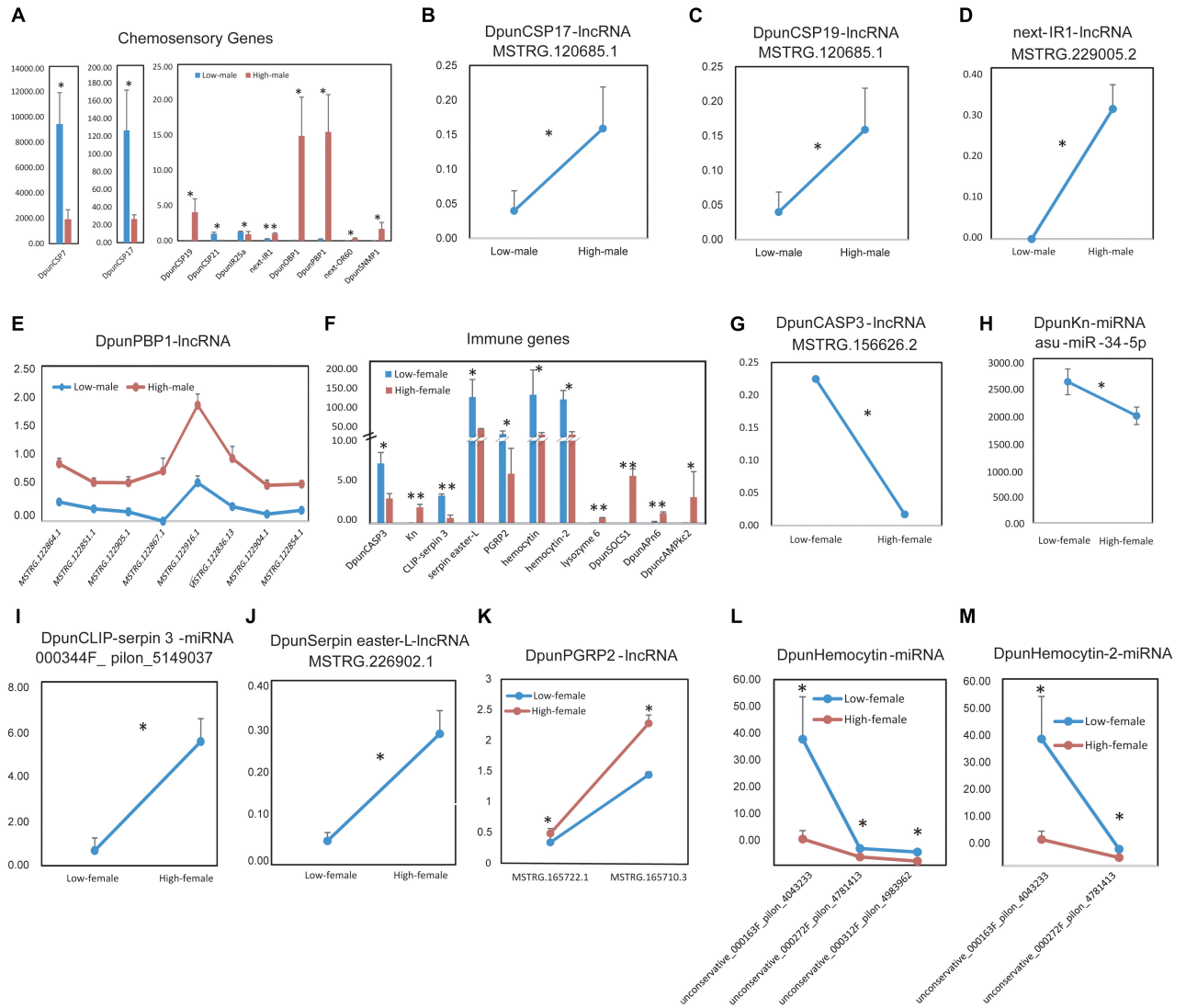

FIGURE 7 | Differently expressed chemosensory and immune genes and their significant differently expressed non-coding RNA regulators between low- vs. high-density males of *Dendrolimus punctatus*. **(A)** Differently expressed chemosensory genes; **(B–E)** significant differently expressed non-coding RNA regulators of chemosensory genes in **(A)**. **(F)** Differently expressed immune genes; **(G–M)** significant differently expressed non-coding RNA regulators of immune genes in **(F)**.

Xiu et al., 2019; Zhang et al., 2019). The regulatory functions of circRNAs in insects during changes in their population density deserve further research.

Being important epigenetic regulators of mRNA translation, miRNAs' involvement is implicated in many critical biological processes, such as learning, reproduction, development, metabolism, immunity, and aging (Priyamvada et al., 2009; Nan et al., 2012; Fiumara et al., 2015; Mehta and Baltimore, 2016; Ling et al., 2017; Meuti et al., 2018; Roy et al., 2018). However, miRNAs often operate in networks (Guo et al., 2016), and genome-wide analyses of miRNAs can help to reveal the complexity inherent to these networks (Li Y. et al., 2017). Our whole-transcriptome sequencing of both coding and non-coding RNAs could facilitate the identification of miRNA and miRNA–mRNA interacting pairs in *D. punctatus*. Functional annotations of the target genes of differentially expressed miRNAs indicated they are chiefly involved in regulating the immune and reproductive pathways during outbreaks of *D. punctatus*. Further functional analyses are essential to confirm the roles of miRNAs in insect outbreaks.

The "ceRNA hypothesis," proposed by Salmena et al. (2011), describes how lncRNAs or circRNAs could inhibit miRNAs to positively regulate targeted mRNAs, by unifying the functions of several coding and ncRNAs. No ceRNAs were previously reported in *D. punctatus*, and so here we analyzed the ceRNA network related to *D. punctatus* outbreaks for the first time. Key genes analysis of the *D. punctatus* population density-related ceRNA network indicated that the developmental process, multi-organism process, reproduction process, and biological adhesion were components of its ceRNA network. These findings provide a

theoretical basis for further investigations of the outbreak-related mechanisms of *D. punctatus* and other similar insects.

Besides the basic metabolic processes, our results indicated that chemosensory and immune genes play important roles in outbreak of *D. punctatus*. We found that chemosensory and immune genes that were differently expressed between low- and high-density *D. punctatus* characterized the males more than females. The lncRNAs were the main regulators for these DEGs, yet miRNA regulators were also found in several of these genes. Most of these lncRNA regulators had the same expression pattern as their mRNA targets, but some of them also showed reverse expression patterns vis-à-vis their mRNA targets, such as lncRNA MSTRG.120685.1 and *DpunCSP17*. These results suggest a complex regulation effect imparted by lncRNAs (Rinn and Chang, 2012). miRNA can regulate the olfactory activities of insects (Guo et al., 2018), and we also found that olfactory receptor was regulated by miRNAs in *D. punctatus*; but the regulatory roles of miRNA for immune gene were more comment in *D. punctatus*. Most of these miRNAs' expression patterns were the opposite of their mRNA targets, a finding consistent with other research (Ghildiyal and Zamore, 2009). Nevertheless, some unexpected cases were also found in our study. For example, the expression levels of miRNA regulators of *DpunHemocytin* and *DpunHemocytin-2* as well as those these two genes were all down-regulated in the high-density population of *D. punctatus* insects. The reasons for these unexpected results may be inaccurate target predictions (Riffo-Campos et al., 2016) or that the miRNA acts as a subsidiary regulators of these genes, highlighting the need for further mechanistic research. Our work indicates that ncRNAs are crucial regulators during outbreaks of *D. punctatus*, but the mechanisms underpinning interactions between differently expressed genes and their ncRNA regulators merits further investigation.

CONCLUSION

In this study, we elucidated the coding and non-coding profiles of control and outbreak insects from a whole-transcriptome analysis. The results indicated that the physiological differences between low- and high-density *D. punctatus* matched well to the functions of identified DEGs. Accordingly, we may deduce that reproduction, immunity, and multi-organism processes, and the chemosensory system, are the key signal pathways involved in this insect's outbreaks. Analysis of three kinds of ncRNAs suggested that lncRNAs are the primary regulators, while miRNAs function mainly in the immune and reproduction adjustments made at different outbreak stages in *D. punctatus*. Further analysis of those chemosensory and immune genes closely related to outbreaking *D. punctatus* showed that its males contain more DEGs than do females between low- and high-density insects, and by analyzing their non-coding RNA regulators we deduced that lncRNA and miRNA play important roles during the outbreak process. To the best of our knowledge, this is the first report to have examined lncRNAs, circRNAs, miRNAs, and mRNAs expression levels and their functions in an outbreaking insect species. These findings increase our understanding of ceRNA networks and can generally aid and guide further exploration of their regulatory functions in key physiological processes required for insect outbreaks to emerge. However, the outbreak of an insect population is a complicated process: the regulatory relationships among the factors we identified above, along with initiating factors of this process, remain unclear, and so further functional-related research on these key DEGs and their non-coding regulators is necessary. Our work provides new and timely insights into the mechanisms underlying insect outbreaks that could inform control strategies to mitigate them.

DATA AVAILABILITY STATEMENT

Raw reads from sequencing are deposited in the Sequence Read Archive (SRA) database with NCBI accessiona SRR10481893–SRR10481916.

AUTHOR CONTRIBUTIONS

ZZ and SZ designed the research. SZ, SS, ZY, XK, and FL, collated the sample, performed the research and/or analyzed the data. SZ wrote the manuscript. ZZ revised the manuscript. All authors reviewed the manuscript.

FUNDING

This research was funded by the National Key Research and Development Program of China (2017YFD0600102), The Fundamental Research Funds for the Central Non-profit Research Institution of CAF (CAFYBB2017QB003), The National Key Research and Development Program of China (2018YFC1200400), and The National Nature Science Foundation of China (31670657).

ACKNOWLEDGMENTS

We thank Charlesworth Author Services for English editing of this work.

SUPPLEMENTARY MATERIAL

The Supplementary Material for this article can be found online at: https://www.frontiersin.org/articles/10.3389/fcell.2020.00369/full#supplementary-material

FIGURE S1 | Structural features and expression comparisons of lncRNAs and mRNAs in *Dendrolimus punctatus*. **(A)** Lengths of lncRNAs; **(B)** lengths of mRNAs; **(C)** exon numbers of lncRNAs; **(D)** exon numbers of mRNAs; **(E)** ORF lengths of lncRNAs; **(F)** ORF lengths of mRNAs; **(G)** the alternatively spliced isoforms of lncRNAs and mRNAs; **(H)** the expression levels of lncRNAs and mRNAs.

FIGURE S2 | FPKM comparisons for the mRNAs and circRNAs.

FIGURE S3 | Characterization of miRNAs in *Dendrolimus punctatus*. **(A,B)** Length distributions of known **(A)** and novel **(B)** miRNAs identified in this study; **(C)** first nucleotide bias of miRNAs; **(D)** nucleotide bias analysis at each miRNA position.

FIGURE S4 | MA plot of the differences between low- and high-density *Dendrolimus punctatus* in females **(A)** and males **(B)**.

FIGURE S5 | Volcano plot of mRNA and lncRNA-targeted DEGs in *Dendrolimus punctatus* between low- vs. high-density population in females **(A)**, males **(B)**, and between sexes in low- **(C)** and high- **(D)** density populations.

FIGURE S6 | Real-time PCR validation of the RNA-Seq data. The *x*-axis shows the RNA names, and the *y*-axis is their $\log_2$ (fold change) based on the ratio of high-density and low-density insects.

FIGURE S7 | All non-coding RNA regulators of differently expressed chemosensory and immune genes between low- vs. high-density females of *Dendrolimus punctatus*. **(A–D)** lncRNA regulators of *DpunCSP8*, *DpunOBP20*, *DpunOBP22*, *DpunOBP46*; **(E)** miRNA regulators of *DpunOR56*; **(F)** lncRNA regulators of *DpunGap11*; **(G–I)** lncRNA, miRNA, and circRNA regulators of *DpunTalin1*.

FIGURE S8 | All non-coding RNA regulators of differently expressed chemosensory genes between low- vs. high-density males of *Dendrolimus punctatus*. **(A,B)** lncRNA and circRNA regulators of *DpunCSP7*; **(C–F)** lncRNA regulators of *DpunCSP17*, *DpunCSP19*, *DpunCSP21*, and *DpunIR25a*; **(G,H)** lncRNA and miRNA regulators of *DpunNext-IR1*; **(I–K)** lncRNA regulators of *DpunPBP1*, *DpunNext-OR60*, and *DpunSNPM1*.

FIGURE S9 | All non-coding RNA regulators of differently expressed immune genes between low- vs. high-density males of *Dendrolimus punctatus*. **(A,B)** lncRNA and circRNA regulators of *DpunCASP3*; **(C,D)** lncRNA and miRNA regulators of *DpunKn*; **(E,F)** lncRNA and miRNA regulators of *DpunCLIP-serpin 3*; **(G,H)** lncRNA regulators of *DpunSerpin easter-L* and *DpunPGRP2*; **(I)** miRNA regulators of *DpunHemocytin*; **(J,K)** lncRNA and miRNA regulators of *DpunHemocytin-2*; **(L,M)** lncRNA and circRNA regulators of *DpunAPn6*; **(N,O)** lncRNA and miRNA regulators of *DpuncAMPkc2*.

TABLE S1 | Primers used for the gene expression validation with Real-time PCR.

TABLE S2 | Summary of the sequenced data for *D. punctatus*.

TABLE S3 | Sequence alignment results for the comparison of sequencing data to selected reference genomes.

TABLE S4 | Sequence alignment results for the comparison of sequenced miRNAs to selected reference genomes.

TABLE S5 | circRNA, lncRNA, and mRNA gene numbers that correlated to miRNA.

REFERENCES

Alexa, A., and Rahnenfuhrer, J. (2010). *topGO: Enrichment Analysis for Gene Ontology. R Package (Version 2.18 ed.)*.

Alison, F. H. (1991). Traits that distinguish outbreaking and nonoutbreaking macrolepidoptera feeding on northern hardwood trees. *Oikos* 60, 275–282. doi: 10.2307/3545068

Amaral, P. P., Dinger, M. E., Mercer, T. R., and Mattick, J. S. (2008). The eukaryotic genome as an RNA machine. *Science* 319:1787. doi: 10.1126/science.1155472

Anders, S., and Huber, W. (2012). *Differential Expression of RNA-Seq Data At The Gene Level - the DESeq Package". R Package*.

Atianand, M. K., Caffrey, D. R., and Fitzgerald, K. A. (2017). Immunobiology of long noncoding RNAs. *Ann. Rev. Immunol.* 35, 177–198. doi: 10.1146/annurev-immunol-041015-055459

Baltensweiler, W., and Fischlin, A. (1988). "The larch budmoth in the alps," in *Dynamics of Forest Insect Populations. Population Ecology (Theory and Application)*, ed. A. A. Berryman (Boston, MA: Springer).

Beermann, J., Piccoli, M.-T., Viereck, J., and Thum, T. (2016). Non-coding RNAs in development and disease: background, mechanisms, and therapeutic approaches. *Physiol. Rev.* 96, 1297–1325. doi: 10.1152/physrev.00041.2015

Belles, X. (2017). MicroRNAs and the evolution of insect metamorphosis. *Annu. Rev. Entomol.* 62, 111–125. doi: 10.1146/annurev-ento-031616-034925

Berryman, A. A. (1988). *Dynamics of Forest Insect Populations: Patterns, Causes, Implications*. New York, NY: Plenum Press.

Berryman, A. A., Stenseth, N. C., and Isaev, A. S. (1987). Natural regulation of herbivorous forest insect populations. *Oecologia* 71, 174–184. doi: 10.1007/BF00377282

Billings, R. F. (1991). The pine caterpillar *Dendrolimus punctatus* in viet nam; recommendations for integrated pest management. *Forest Ecol. Manag.* 39, 97–106. doi: 10.1016/0378-1127(91)90167-T

Chen, B., Zhang, Y., Zhang, X., Jia, S., Chen, S., and Kang, L. (2016). Genome-wide identification and developmental expression profiling of long noncoding RNAs during *Drosophila metamorphosis*. *Sci. Rep.* 6:23330. doi: 10.1038/srep23330

Chen, C. (ed.). (1990). "Species, geographic distributions, and biological characteristics of pine caterpillars in China," in *Integrated Management of Pine Caterpillars in China*, (Beijing: China Forestry Publishing House), 5–18.

Chen, Y. G., Satpathy, A. T., and Chang, H. Y. (2017). Gene regulation in the immune system by long noncoding RNAs. *Nat. Immunol.* 18, 962–972. doi: 10.1038/ni.3771

Costa, F. F. (2005). Non-coding RNAs: new players in eukaryotic biology. *Gene* 357, 83–94. doi: 10.1016/j.gene.2005.06.019

Daehwan, K., Ben, L., and Salzberg, S. L. (2015). HISAT: a fast spliced aligner with low memory requirements. *Nat. Methods* 12, 357–360. doi: 10.1038/nmeth.3317

Doron, B., Manda, W., Aaron, G., Marks, D. S., and Chris, S. (2008). The microRNA.org resource: targets and expression. *Nucleic Acids Res.* 36, 149–153.

Elderd, B. D., Rehill, B. J., Haynes, K. J., and Dwyer, G. (2013). Induced plant defenses, host-pathogen interactions, and forest insect outbreaks. *Proc. Natl. Acad. Sci. U.S.A.* 110, 14978–14983. doi: 10.1073/pnas.1300759110

Fahlgren, N., Howell, M. D., Kasschau, K. D., Chapman, E. J., Sullivan, C. M., Cumbie, J. S., et al. (2007). High-throughput sequencing of *Arabidopsis* microRNAs: evidence for frequent birth and death of MIRNA genes. *PLoS One* 2:e219. doi: 10.1371/journal.pone.0000219

Finn, R. D., Alex, B., Jody, C., Penelope, C., Eberhardt, R. Y., Eddy, S. R., et al. (2014). Pfam: the protein families database. *Nucleic Acids Res.* 42, 222–230.

Fiumara, F., Rajasethupathy, P., Antonov, I., Kosmidis, S., Sossin, W. S., and Kandel, E. R. (2015). MicroRNA-22 gates long-term heterosynaptic plasticity in *Aplysia* through presynaptic regulation of CPEB and downstream targets. *Cell Rep.* 11, 1866–1875. doi: 10.1016/j.celrep.2015.05.034

Friedländer, M. R., Mackowiak, S. D., Li, N., Chen, W., and Rajewsky, N. (2012). miRDeep2 accurately identifies known and hundreds of novel microRNA genes in seven animal clades. *Nucleic Acids Res.* 40, 37–52. doi: 10.1093/nar/gkr688

Fuentealba, A., Pureswaran, D., Bauce, E., and Despland, E. (2017). How does synchrony with host plant affect the performance of an outbreaking insect defoliator? *Oecologia* 184, 847–857. doi: 10.1007/s00442-017-3914-3914

Ghildiyal, M., and Zamore, P. D. (2009). Small silencing RNAs: an expanding universe. *Nat. Rev. Genet.* 10, 94–108. doi: 10.1038/nrg2504

Gomes, A. Q., Nolasco, S., and Soares, H. (2013). Non-coding RNAs: multi-tasking molecules in the cell. *Intern. J. Mol. Sci.* 14, 16010–16039. doi: 10.3390/ijms140816010

Guo, W., Wang, X., Ma, Z., Xue, L., Han, J., Yu, D., et al. (2011). CSP and takeout genes modulate the switch between attraction and repulsion during behavioral phase change in the *Migratory locust*. *PLoS Genet.* 7:e1001291. doi: 10.1371/journal.pgen.1001291

Guo, X., Ma, Z., Du, B., Li, T., Li, W., Xu, L., et al. (2018). Dop1 enhances conspecific olfactory attraction by inhibiting miR-9a maturation in locusts. *Nat. Commun.* 9:1193. doi: 10.1038/s41467-018-03437-z

Guo, Y., Alexander, K., Clark, A. G., Grimson, A., and Yu, H. (2016). Integrated network analysis reveals distinct regulatory roles of transcription factors and microRNAs. *RNA* 22, 1663–1672. doi: 10.1261/rna.048025.114

Hansen, T. B., Jensen, T. I., Clausen, B. H., Bramsen, J. B., Finsen, B., Damgaard, C. K., et al. (2013). Natural RNA circles function as efficient microRNA sponges. *Nature* 495, 384–388. doi: 10.1038/nature11993

Haynes, W. (2013). "Benjamini-hochberg method," in *Encyclopedia of Systems Biology*, eds W. Dubitzky, O. Wolkenhauer, K.-H. Cho, and H. Yokota (New York, NY: Springer), 78–78. doi: 10.1007/978-1-4419-9863-7_1215

He, J., Chen, Q., Wei, Y., Jiang, F., Yang, M., Hao, S., et al. (2016). MicroRNA-276 promotes egg-hatching synchrony by up-regulating *brm* in locusts. *Proc. Natl. Acad. Sci. U.S.A.* 113, 584–589. doi: 10.1073/pnas.1521098113

Hombach, S., and Kretz, M. (2016). "Non-coding RNAs: classification, biology and functioning," in *Non-Coding RNAs in Colorectal Cancer*, eds O. Slaby and G. A. Calin (Cham: Springer International Publishing), 3–17. doi: 10.1007/978-3-319-42059-2_1

Hunter, A. F. (1995). "Chapter 3 - ecology, life history, and phylogeny of outbreak and nonoutbreak species," in *Population Dynamics*, eds N. Cappuccino and P. W. Price (San Diego: Academic Press), 41–64. doi: 10.1016/b978-012159270-7/50004-x

Jeck, W. R., and Sharpless, N. E. (2014). Detecting and characterizing circular RNAs. *Nat. Biotechnol.* 32, 453–461. doi: 10.1038/nbt.2890

Kai, C., Lei, W., Xu, C., Zhang, X., Xing, L., Zuo, H., et al. (2013). Influence on surgical treatment of intertrochanteric fracture with or without preoperative skeletal traction. *Nucleic Acids Res.* 41:e74.

Kang, L., Chen, X., Zhou, Y., Liu, B., Zheng, W., Li, R., et al. (2004). The analysis of large-scale gene expression correlated to the phase changes of the migratory locust. *Proc. Natl. Acad. Sci. U.S.A.* 101, 17611–17615. doi: 10.1073/pnas.0407753101

Kelley, D., and Rinn, J. (2012). Transposable elements reveal a stem cell-specific class of long noncoding RNAs. *Genome Biol.* 13:R107.

Kretz, M., Webster, D. E., Flockhart, R. J., Lee, C. S., Zehnder, A., Lopez-Pajares, V., et al. (2012). Suppression of progenitor differentiation requires the long noncoding RNA ANCR. *Genes Dev.* 26:338. doi: 10.1101/gad.182121.111

Langmead, B., and Salzberg, S. L. (2012). Fast gapped-read alignment with Bowtie 2. *Nat. Methods* 9, 357–359. doi: 10.1038/nmeth.1923

Lei, K., Yong, Z., Zhi-Qiang, Y., Xiao-Qiao, L., Shu-Qi, Z., Liping, W., et al. (2007). CPC: assess the protein-coding potential of transcripts using sequence features and support vector machine. *Nucleic Acids Res.* 35:W345.

Li, J.-H., Liu, S., Zhou, H., Qu, L.-H., and Yang, J.-H. (2014). starBase v2.0: decoding miRNA-ceRNA, miRNA-ncRNA and protein-RNA interaction networks from large-scale CLIP-Seq data. *Nucleic Acids Res.* 42, D92–D97. doi: 10.1093/nar/gkt1248

Li, X., Ao, J., and Wu, J. (2017a). Systematic identification and comparison of expressed profiles of lncRNAs and circRNAs with associated co-expression and ceRNA networks in mouse germline stem cells. *Oncotarget* 8, 26573–26590. doi: 10.18632/oncotarget.15719

Li, X., Liu, C.-X., Xue, W., Zhang, Y., Jiang, S., Yin, Q.-F., et al. (2017b). Coordinated circRNA biogenesis and function with NF90/NF110 in viral infection. *Mol. Cell* 67, 214–227. doi: 10.1016/j.molcel.2017.05.023

Li, Y., Li, S., Li, R., Xu, J., Jin, P., Chen, L., et al. (2017). Genome-wide miRNA screening reveals miR-310 family members negatively regulate the immune response in *Drosophila melanogaster* via co-targeting, *Drosomycin*. *Dev. Compar. Immunol.* 68, 34–45. doi: 10.1016/j.dci.2016.11.014

Li, Z., Huang, C., Bao, C., Chen, L., Lin, M., Wang, X., et al. (2015). Exon-intron circular RNAs regulate transcription in the nucleus. *Nat. Struct. Mol. Biol.* 22, 256–264. doi: 10.1038/nsmb.2959

Liang, S., Haitao, L., Dechao, B., Guoguang, Z., Kuntao, Y., Changhai, Z., et al. (2013). Utilizing sequence intrinsic composition to classify protein-coding and long non-coding transcripts. *Nucleic Acids Res.* 41:e166. doi: 10.1093/nar/gkt646

Ling, L., Kokoza, V. A., Zhang, C., Aksoy, E., and Raikhel, A. S. (2017). MicroRNA-277 targets insulin-like peptides 7 and 8 to control lipid metabolism and reproduction in *Aedes aegypti* mosquitoes. *Proc. Natl. Acad. Sci. U.S.A.* 114:E8017.

Ling-Ling, C., and Li, Y. (2015). Regulation of circRNA biogenesis. *RNA Biol.* 12, 381–388. doi: 10.1080/15476286.2015.1020271

Long, Y., Wang, X., Youmans, D. T., and Cech, T. R. (2017). How do lncRNAs regulate transcription? *Sci. Adv.* 3:eaao2110. doi: 10.1126/sciadv.aao2110

Lu, Y., Wu, K., Jiang, Y., Xia, B., Li, P., Feng, H., et al. (2010). Mirid bug outbreaks in multiple crops correlated with wide-scale adoption of Bt cotton in China. *Science* 328, 1151–1154. doi: 10.1126/science.1187881

Luo, D., Lai, M., Xu, C., Shi, H., and Liu, X. (2018). Life history traits in a capital breeding pine caterpillar: effect of host species and needle age. *BMC Ecol.* 18:24. doi: 10.1186/s12898-018-0181-180

Lv, J., Cui, W., Liu, H., He, H., Xiu, Y., Guo, J., et al. (2013). Identification and characterization of long non-coding RNAs related to mouse embryonic brain development from available transcriptomic data. *PLoS One* 8:e71152. doi: 10.1371/journal.pone.00071152

Maeda, R. K., Sitnik, J. L., Frei, Y., Prince, E., Gligorov, D., Wolfner, M. F., et al. (2018). The lncRNA male-specific abdominal plays a critical role in *Drosophila* accessory gland development and male fertility. *PLoS Genet.* 14:e1007519. doi: 10.1371/journal.pgen.1007519

Marchese, F. P., Raimondi, I., and Huarte, M. (2017). The multidimensional mechanisms of long noncoding RNA function. *Genome Biol.* 18, 206–206. doi: 10.1186/s13059-017-1348-1342

Mehta, A., and Baltimore, D. (2016). MicroRNAs as regulatory elements in immune system logic. *Nat. Rev. Immunol.* 16:279. doi: 10.1038/nri.2016.40

Mercer, T. R., and Mattick, J. S. (2013). Structure and function of long noncoding RNAs in epigenetic regulation. *Nat. Struct. Mol. Biol.* 20, 300–307. doi: 10.1038/nsmb.2480

Meuti, M., Bautista-Jimenez, R., and Reynolds, J. (2018). MicroRNAs are likely part of the molecular toolkit regulating adult reproductive diapause in the mosquito, *Culex pipiens*. *PLoS One* 13:e0203015. doi: 10.1371/journal.pone.00203015

Mowel, W. K., Kotzin, J. J., McCright, S. J., Neal, V. D., and Henao-Mejia, J. (2018). Control of immune cell homeostasis and function by lncRNAs. *Trends Immunol.* 39, 55–69. doi: 10.1016/j.it.2017.08.009

Myers, J. H. (1993). Population outbreaks in forest Lepidoptera. *Am. Sci.* 81, 240–251.

Nan, L., Michael, L., Kajia, C., Masashi, A., Gert-Jan, H., Kennerdell, J. R., et al. (2012). The microRNA miR-34 modulates ageing and neurodegeneration in *Drosophila*. *Nature* 482, 519–523. doi: 10.1038/nature10810

Pener, M. P., and Simpson, S. J. (2009). Locust phase polyphenism: an update. *Adv. Insect Physiol.* 36, 1–72.

Pertea, M., Kim, D., Pertea, G. M., Leek, J. T., and Salzberg, S. L. (2016). Transcript-level expression analysis of RNA-seq experiments with HISAT, StringTie and Ballgown. *Nat. Protoc.* 11:1650. doi: 10.1038/nprot.2016.095

Priyamvada, R., Ferdinando, F., Robert, S., Doron, B., Puthanveettil, S. V., Russo, J. J., et al. (2009). Characterization of small RNAs in *Aplysia* reveals a role for miR-124 in constraining synaptic plasticity through CREB. *Neuron* 63, 803–817. doi: 10.1016/j.neuron.2009.05.029

Quezada García, R., Seehausen, M. L., and Bauce, É (2015). Adaptation of an outbreaking insect defoliator to chronic nutritional stress. *J. Evol. Biol.* 28, 347–355. doi: 10.1111/jeb.12571

Rehmsmeier, M., Steffen, P., Hochsmann, M., and Giegerich, R. (2004). Fast and effective prediction of microRNA/target duplexes. *RNA* 10, 1507–1517. doi: 10.1261/rna.5248604

Riffo-Campos, ÁL., Riquelme, I., and Brebi-Mieville, P. (2016). Tools for sequence-based miRNA target prediction: what to choose? *Intern. J. Mol. Sci.* 17:1987. doi: 10.3390/ijms17121987

Rinn, J. L., and Chang, H. Y. (2012). Genome regulation by long noncoding RNAs. *Annu. Rev. Biochem.* 81, 145–166. doi: 10.1146/annurev-biochem-051410-092902

Roy, S., Saha, T. T., Zou, Z., and Raikhel, A. S. (2018). Regulatory pathways controlling female insect reproduction. *Annu. Rev. Entomol.* 63, 489–511. doi: 10.1146/annurev-ento-020117-043258

Salmena, L., Poliseno, L., Tay, Y., Kats, L., and Pandolfi, P. P. (2011). A ceRNA hypothesis: the rosetta stone of a hidden RNA language? *Cell* 146, 353–358. doi: 10.1016/j.cell.2011.07.014

Stefan, G., Juan Miguel, G. G., Javier, T., Williams, T. D., Nagaraj, S. H., María José, N., et al. (2008). High-throughput functional annotation and data mining with the Blast2GO suite. *Nucleic Acids Res.* 36, 3420–3435. doi: 10.1093/nar/gkn176

Veran, S., Simpson, S. J., Sword, G. A., Deveson, E., Piry, S., Hines, J. E., et al. (2015). Modeling spatiotemporal dynamics of outbreaking species: influence of environment and migration in a locust. *Ecology* 96, 737–748. doi: 10.1890/14-0183.1

Wang, J., Ren, Q., Hua, L., Chen, J., Zhang, J., Bai, H., et al. (2019). Comprehensive analysis of differentially expressed mRNA, lncRNA and circRNA and their ceRNA networks in the longissimus dorsi muscle of two different pig breeds. *Intern. J. Mol. Sci.* 20:1107. doi: 10.3390/ijms20051107

Wang, X., Fang, X., Yang, P., Jiang, X., Jiang, F., Zhao, D., et al. (2014). The locust genome provides insight into swarm formation and long-distance flight. *Nat. Commun.* 5:2957. doi: 10.1038/ncomms3957

Wang, Y., Wang, Q., Gao, L., Zhu, B., Luo, Y., Deng, Z., et al. (2017). Integrative analysis of circRNAs acting as ceRNAs involved in ethylene pathway in tomato. *Physiol. Plant.* 161, 311–321. doi: 10.1111/ppl.12600

Wang, Y., Yang, P., Cui, F., and Kang, L. (2013). Altered Immunity in Crowded Locust Reduced Fungal (*Metarhizium anisopliae*) Pathogenesis. *PLoS Pathog.* 9:e1003102. doi: 10.1371/journal.pone.01003102

Wei, Y., Chen, S., Yang, P., Ma, Z., and Kang, L. (2009). Characterization and comparative profiling of the small RNA transcriptomes in two phases of locust. *Genome Biol.* 10:R6. doi: 10.1186/gb-2009-10-1-r6

Wen, K., Yang, L., Xiong, T., Di, C., Ma, D., Wu, M., et al. (2016). Critical roles of long noncoding RNAs in *Drosophila* spermatogenesis. *Genome Res.* 26, 1233–1244. doi: 10.1101/gr.199547.115

Westholm, J. O., Miura, P., Olson, S., Shenker, S., Joseph, B., Sanfilippo, P., et al. (2014). Genome-wide analysis of *Drosophila* circular RNAs reveals their structural and sequence properties and age-dependent neural accumulation. *Cell Rep.* 9, 1966–1980. doi: 10.1016/j.celrep.2014.10.062

Wilusz, J. E., and Sharp, P. A. (2013). A circuitous route to noncoding RNA. *Science* 340, 440–441. doi: 10.1126/science.1238522

Wu, Y., Cheng, T., Liu, C., Liu, D., Zhang, Q., Long, R., et al. (2016). Systematic identification and characterization of long non-coding RNAs in the silkworm, *Bombyx mori*. *PLoS One* 11:e0147147. doi: 10.1371/journal.pone.0147147

Xiao, G. (1992). *Forest Insects of China*. Beijing: China Forestry Publishing House.

Xie, C., Mao, X., Huang, J., Ding, Y., Wu, J., Dong, S., et al. (2011). KOBAS 2.0: a web server for annotation and identification of enriched pathways and diseases. *Nucleic Acids Res.* 39, 316–322.

Xiu, Y., Jiang, G., Zhou, S., Diao, J., Liu, H., Su, B., et al. (2019). Identification of potential immune-related circRNA-miRNA-mRNA regulatory network in intestine of *Paralichthys olivaceus* during *Edwardsiella tarda* Infection. *Front. Genet.* 10:731. doi: 10.3389/fgene.2019.00731

Yang, C.-H., Yang, P.-C., Li, J., Yang, F., and Zhang, A.-B. (2016). Transcriptome characterization of *Dendrolimus punctatus* and expression profiles at different developmental stages. *PLoS One* 11:e0161667. doi: 10.1371/journal.pone.0161667

Yang, C.-H., Yang, P.-C., Zhang, S.-F., Shi, Z.-Y., Kang, L., and Zhang, A.-B. (2017). Identification, expression pattern, and feature analysis of cuticular protein genes in the pine moth *Dendrolimus punctatus* (Lepidoptera: Lasiocampidae). *Insect Biochem. Mol. Biol.* 83(Suppl. C), 94–106. doi: 10.1016/j.ibmb.2017.03.003

Yang, Y., Fan, X., Mao, M., Song, X., Wu, P., Zhang, Y., et al. (2017). Extensive translation of circular RNAs driven by N6-methyladenosine. *Cell Res.* 27:626. doi: 10.1038/cr.2017.31

You, X., Vlatkovic, I., Babic, A., Will, T., Epstein, I., Tushev, G., et al. (2015). Neural circular RNAs are derived from synaptic genes and regulated by development and plasticity. *Nat. Neurosci.* 18, 603–610. doi: 10.1038/nn.3975

Yvonne, T., John, R., and Pier Paolo, P. (2014). The multilayered complexity of ceRNA crosstalk and competition. *Nature* 505, 344–352. doi: 10.1038/nature12986

Zhang, S., Kong, X., Ze, S., Wang, H., Lin, A., Liu, F., et al. (2016). Discrimination of cis-trans sex pheromone components in two sympatric Lepidopteran species. *Insect Biochem. Mol. Biol.* 73, 47–54. doi: 10.1016/j.ibmb.2016.04.004

Zhang, S., Shen, S., Peng, J., Zhou, X., Kong, X., Ren, P., et al. (2020). Chromosome-level genome assembly of an important pine defoliator, *Dendrolimus punctatus* (Lepidoptera; Lasiocampidae). *Mol. Ecol. Resour.* Accepted. doi: 10.1111/1755-0998.13169

Zhang, S.-F., Zhang, Z., Kong, X.-B., Wang, H.-B., and Liu, F. (2018). Dynamic changes in chemosensory gene expression during the *Dendrolimus punctatus* mating process. *Front. Physiol.* 8:1127. doi: 10.3389/fphys.2017.01127

Zhang, Y., Zhang, X. O., Chen, T., Xiang, J. F., Yin, Q. F., Xing, Y. H., et al. (2013). Circular intronic long noncoding RNAs. *Mol. Cell* 51, 792–806. doi: 10.1016/j.molcel.2013.08.017

Zhang, Z., Li, D., and Cha, G. (2002). Time series analysis and complex dynamics of mason pine caterpillar, *Dendrolimus punctatus* walker (Lepidoptera: Lasiocampidae). *Acta Ecol. Sin.* 22, 1061–1067.

Zhang, Z., Tang, J., He, X., Zhu, M., Gan, S., Guo, X., et al. (2019). Comparative transcriptomics identify key hypothalamic circular RNAs that participate in sheep (*Ovis aries*) reproduction. *Animals* 9:557. doi: 10.3390/ani9080557

Conflict of Interest: The authors declare that the research was conducted in the absence of any commercial or financial relationships that could be construed as a potential conflict of interest.

frontiers in Genetics

ORIGINAL RESEARCH
published: 23 June 2020
doi: 10.3389/fgene.2020.00452

DNA Methylation and Demethylation Are Regulated by Functional DNA Methyltransferases and DnTET Enzymes in *Diuraphis noxia*

*Pieter H. du Preez, Kelly Breeds, N. Francois V. Burger, Hendrik W. Swiegers, J. Christoff Truter and Anna-Maria Botha**

Department of Genetics, Stellenbosch University, Stellenbosch, South Africa

Aphids are economically important insect pests of crops worldwide. Despite resistant varieties being available, resistance is continuously challenged and eventually broken down, posing a threat to food security. In the current study, the epigenome of two related Russian wheat aphid (*Diuraphis noxia*, Kurdjumov) biotypes (i.e., SA1 and SAM) that differ in virulence was investigated to elucidate its role in virulence in this species. Whole genome bisulfite sequencing covered a total of 6,846,597,083 cytosine bases for SA1 and 7,397,965,699 cytosine bases for SAM, respectively, of which a total of 70,861,462 bases (SA1) and 74, 073,939 bases (SAM) were methylated, representing 1.126 ± 0.321% (SA1) and 1.105 ± 0.295% (SAM) methylation in their genomes. The sequence reads were analyzed for contexts of DNA methylation and the results revealed that RWA has methylation in all contexts (CpG, CHG and CHH), with the majority of methylation within the CpG context (± 5.19%), while the other contexts show much lower levels of methylation (CHG – ± 0.27%; CHH – ± 0.34%). The top strand was slightly (0.02%) more methylated than the bottom strand. Of the 35,493 genes that mapped, we also analyzed the contexts of methylation of each of these and found that the CpG methylation was much higher in genic regions than in intergenic regions. The CHG and CHH levels did not differ between genic and intergenic regions. The exonic regions of genes were more methylated (±0.56%) than the intronic regions. We also measured the 5mC and 5hmC levels between the aphid biotypes, and found little difference in 5mC levels between the biotypes, but much higher levels of 5hmC in the virulent SAM. RWA had two homologs of each of the *DNA methyltransferases 1* (*DNMT1a* and *DNMT1b*) and *DNMT3s* (*DNMT3a* and *DNMT3b*), but only a single *DNMT2*, with only the expression of *DNMT3* that differed significantly between the two RWA biotypes. RWA has a single ortholog of Ten eleven translocase (*DnTET*) in the genome. Feeding studies show that the more virulent RWA biotype SAM upregulate *DnDNMT3* and *DnTET* in response to wheat expressing antibiosis and antixenosis.

Keywords: whole genome bisulfite sequencing, DNMT and TET, global methylation (5mC), global hydroxymethylation (5hmC), Russian wheat aphid

OPEN ACCESS

Edited by:
Wei Guo,
Institute of Zoology (CAS), China

Reviewed by:
Bing Chen,
Hebei University, China
Owain Rhys Edwards,
CSIRO Land and Water, Australia

****Correspondence:***
Anna-Maria Botha
ambo@sun.ac.za

Specialty section:
This article was submitted to Epigenomics and Epigenetics, a section of the journal Frontiers in Genetics

Received: *14 January 2020*
Accepted: *14 April 2020*
Published: *23 June 2020*

Citation:
du Preez PH, Breeds K, Burger NFV, Swiegers HW, Truter JC and Botha A-M (2020) DNA Methylation and Demethylation Are Regulated by Functional DNA Methyltransferases and DnTET Enzymes in Diuraphis noxia. Front. Genet. 11:452. doi: 10.3389/fgene.2020.00452

INTRODUCTION

Diuraphis noxia (Kurdjumov, Hemiptera: Aphididae—or Russian wheat aphid, RWA) biotypes are morphologically similar, yet display vast differences in their capacity to damage wheat cultivars upon feeding (i.e., their virulence) (Botha, 2013). In South Africa, the virulence of the four wild type and the mutant RWA biotypes is as follows in order from least to most virulent: SA1 < SA2 < SA3 < SA4 < SAM (Swanevelder et al., 2010; Jankielsohn, 2016). Despite the emergence of new RWA biotypes in South Africa (Tolmay et al., 2007; Jankielsohn, 2011, 2016), and other parts of the world, including the United States of America (USA) (Haley et al., 2004; Burd et al., 2006; Randolph et al., 2009) and Argentina (Clua et al., 2004), the molecular mechanism(s) underlying the development of new biotypes is currently unknown (Shufran and Payton, 2009; Botha et al., 2014a). The known genealogy of SA1 and SAM (Swanevelder et al., 2010), their genetic similarity (Burger and Botha, 2017) and their position on either end of the virulence spectrum, renders them particularly useful in the present study, to improve the understanding of the process of biotypification. The possibility of a link between RWA methylation and biotype virulence has previously been suggested (Gong et al., 2012; Breeds et al., 2018). In 2012, Gong et al. investigated the methylation of four genes encoding salivary gland proteins (putative effector genes) in RWA biotypes US1 and US2, and found these genes to be differentially methylated in the different biotypes. In the initial investigation of South African RWA methylation (Breeds et al., 2018), the different biotypes exhibited different banding patterns (after restriction of their DNA with methylation-sensitive enzymes), methylation levels and methylation trends, all of which support a role for methylation in biotypification.

The epigenetic modification of DNA methylation involves the covalent addition of a methyl group to the 5′ position of cytosine (Glastad et al., 2011; Lyko and Maleszka, 2011). In insects, methylation occurs predominantly within genes (Walsh et al., 2010; Zemach et al., 2010; Glastad et al., 2011; Lyko and Maleszka, 2011), where to date it is reported to perform two major functions. Firstly, intragenic methylation affects alternative splicing by recruiting or interfering with different DNA binding factors (Hunt et al., 2013b; Glastad et al., 2014; Yan et al., 2015), and secondly, it prevents the initiation of spurious transcription at cryptic binding sites within genes (Hunt et al., 2010, 2013a,b). Three classes of DNA methyltransferase (DNMT) proteins are involved in methylation of DNA and these perform different functions, with DNMT3 and DNMT1 establishing and maintaining methylation patterns, respectively, but with a less clear function for DNMT2. This class is known to show strong conservation in sequence and is suggested to be an ancient DNA methyltransferase that changed its substrate specificity from DNA to tRNA (Sunita et al., 2008; Iyer et al., 2011; Jurkowski and Jeltsch, 2011; Raddatz et al., 2013). Insects have a variety of combinations of the *DNMT* genes, with some lineages having lost one (e.g., *Bombyx mori* and *Triboleum castaneum*) or two (e.g., *Drosophila melanogaster* and *Anopheles gambiae*) classes of *DNMTs*, and others having multiple homologs (e.g., *Apis mellifera*, *Nasonia vitripennis,* and *Acyrthosiphon pisum*) within a certain *DNMT* class (Kunert et al., 2003; Marhold et al., 2004; Walsh et al., 2010; Xiang et al., 2010; Glastad et al., 2011; Feliciello et al., 2013). Despite their important function in DNA methylation, knowledge of RWA *DNMTs* is still lacking.

DNA methylation is removed through the process of demethylation, which can occur both passively and actively, with 5-hydroxymethylcytosine (5hmC) being a measurable intermediate of one of the active demethylation pathways (Branco et al., 2012; Kohli and Zhang, 2013). Hydroxymethylcytosine is formed through the oxidation of 5mC by ten-eleven translocation enzymes (TETs) (Tahiliani et al., 2009; Shen et al., 2014). The presence of 5hmC has only been reported in a few insects including *A. mellifera*, *T. castaneum*, *N. vitripennis* and *D. melanogaster* (Cingolani et al., 2013; Feliciello et al., 2013; Wojciechowski et al., 2014; Delatte et al., 2016; Pegoraro et al., 2016; Rasmussen et al., 2016). To determine the presence and extent of 5hmC in the RWA, an antibody specific to 5hmC was used, providing the first insight into RWA demethylation.

The objective in this study was firstly to sequence and compare the epigenome of RWA biotypes SA1 and SAM, and determine the level, location (e.g., intergenic or genic, exonic or intronic), and contexts of DNA methylation (i.e., CpG, CHH, CHG) within the genomes of these RWA biotypes with differential virulence. Secondly, to quantify global methylation (5mC) and demethylation (5hmC) in the South African biotypes with shared genealogy; and thirdly, to characterize the DNA methyltransferases (*DNMTs*) and ten-eleven translocase enzyme-like (*TET*) genes and expression in these aphids, to relate these observations to the reported difference in virulence levels of the South African RWA biotypes SA1 and SAM.

MATERIALS AND METHODS

Aphid Rearing

For whole genome bisulfite sequencing and measurement of global methylation (5mC) and hydroxymethylation (5hmC) levels, colonies of apterous parthenogenetic female aphids of South African RWA biotypes SA1 and SAM were separately established in BugDorm cages (MegaView Science Education Services Co. Ltd., Taiwan) in an insectary with the following conditions: 22.5 ± 2.5°C, 40% relative humidity, and continuous artificial lighting from high pressure sodium lamps as previously described (Breeds et al., 2018). In all instances triplicate colonies of each biotype were established. Stock colonies of RWA biotype SA1 were maintained on the wheat line Tugela (susceptible) and biotype SAM on the near isogenic wheat line Tugela-*Dn1* (resistant). To avoid any environmental effects due to feeding on different wheat plants, aphid biotypes were transferred to the susceptible cultivar "SST356" 1 month prior to DNA extraction for the whole genome bisulfite sequencing. In all instances, treatments were conducted using separate BugDorm cages in triplicate ($n = 3 \times 2$).

For *DnDNMT* expression analysis (0h), RWA biotype SA1 was maintained on the "SST 356" wheat cultivar (susceptible), while the highly virulent SAM biotype was maintained on "SST 398" (RWA resistant), and then transferred to the susceptible

"SST 356" wheat cultivar 1 month prior to RNA extraction and cDNA synthesis.

For the RNAseq analysis, colonies of apterous parthenogenetic female aphids of South African RWA biotypes SA1 and SAM were separately established in BugDorm cages (MegaView Science Education Services Co. Ltd., Taiwan) in an insectary with the following conditions: 22.5 ± 2.5°C, 40% relative humidity, and continuous artificial lighting from high pressure sodium lamps as previously described (Breeds et al., 2018). RWA biotype SA1 was maintained on the wheat line Tugela (susceptible) and biotype SAM on the near isogenic wheat line Tugela-*Dn5* (resistant). Multiple individual replicates, consisting of 50 aphids of various life stages, were collected for each biotype. Collected aphids were flash frozen in liquid nitrogen and RNA was extracted following the protocol of Qiagen's RNeasy RNA extraction kit performing the optional on column Qiagen DNase treatment. Extracted RNA was assessed for quality through both bleach-gel electrophoresis (Aranda et al., 2012) and with an Agilent 2100 Bioanalyser using the RNA Nano 6000 kit (Babu and Gassmann, 2016). Three RNA samples, from each biotype, representing three biological repeats, with the highest RIN values (at least above 7) were used in subsequent analysis.

For the *DnDNMT* and *DnTET* host-shifts, RWA biotypes SA1 and SAM were maintained on the susceptible "SST 356" wheat cultivar, and then transferred to either near isogenic wheat lines Tugela (susceptible), or Tugela-*Dn1* (resistant), or Tugela-*Dn5* (resistant) prior to RNA extraction and cDNA synthesis. Aphids were sampled at 0, 6, and 48 h post host-shifting. In all instances, treatments were conducted using separate BugDorm cages using separate plants in triplicate ($n = 3 \times 2$).

For the quantitation of DNMT proteins, both biotypes were maintained on the "SST 356" wheat cultivar before protein extraction. In all instances, treatments were conducted using separate BugDorm cages in triplicate ($n = 3 \times 2$). All SST cultivars were obtained from SENSAKO (Pty) Ltd., (South Africa).

Identification, Cloning and Sequencing of RWA *DNMTs* and *Ten Eleven Translocation-Like (TET-Like) Genes*

DNMT and TET sequences of the pea aphid (*Acyrthosiphon pisum*) were obtained through GenBank and used as BLAST (Altschul et al., 1997) queries against the NCBI's non-redundant (nr) database to obtain homologs from the Class Insecta. The obtained sequences were then aligned using MAFFT v.7.4 (Katoh and Standley, 2013) and through use of maximum parsimony the obtained sequences were phylogenetically rendered through use of PAUP v4.0a136.

Primers were designed (**Table S1**) to amplify the transcripts of identified RWA *DNMTs* and *TET-like genes* using Primer3 (Rozen and Skaletsky, 2000). The primers were then used in a primer BLAST analysis against the RWA SAM biotype reference genome (GCA_001465515.1) to ensure they only matched genes of interest. RNA extractions and cDNA synthesis were performed for both RWA biotypes SA1 and SAM as previously described (Burger et al., 2017).

PCR reactions for sequencing were performed using Phusion High-Fidelity DNA Polymerase (NEB) and following the manufacturer's protocol. PCR products were then ligated into the pTZ57R/T vector (InsTAclone PCR cloning kit, Thermo Scientific) overnight at 4°C. For PCR reactions showing non-specific amplification, gel fragments containing bands of the expected product size were excised and subjected to five freeze-thaw cycles (liquid nitrogen/60°C oven) in 20 μl of distilled water and the obtained DNA was quantified through spectrophotometry (NanoDrop 2000, Thermo). Based on these results, differing amounts of freeze-thawed DNA were used, in accordance with the kit's recommendations on the optimal quantity of PCR product for ligation.

Transformation of DH5α competent cells (Thermo Scientific) was performed through heat shock following the manufacturers' protocol and recombinant colonies were cultured and screened as previously performed (Burger et al., 2017). Plasmid minipreps (derived from at least one colony per PCR product) were submitted to the Central Analytical Facility (CAF) of Stellenbosch University for bi-directional Sanger sequencing using universal M13 forward and reverse primers (**Table S1**).

After Sanger sequencing, raw sequences were imported into Geneious v.9.1.8 and trimmed on either end to remove poor quality or ambiguous base calls. A VecScreen BLAST (http://www.ncbi.nlm.nih.gov/tools/vecscreen/) was then performed using the trimmed sequences to remove any vector DNA. The sequences for both SA1 and SAM biotypes (at least one forward and one reverse per PCR product) were aligned with the respective gene from which primers were designed using Primer 3 (Sievers et al., 2011).

Sequencing, Transcriptome Assembly, and Quality Control

RNA samples were sent for sequencing at Macrogen Inc., South Korea where six libraries were prepared using the TruSeq Stranded mRNA Sample Preparation Guide, Part #15031047 Rev. E. Paired-end library construction was performed using the Illumina TruSeq stranded mRNA kit and the subsequent libraries were sequenced on the Illumina NovaSeq 6000 system to obtain 100 bp paired-end reads for three replicates of both the *Diuraphis noxia* SAM and SA1 biotypes.

Raw reads obtained from the NovaSeq 6000 system were analyzed through use of FASTQC (Andrews, 2010) and trimmed of all poor quality reads and sequencing adaptors through use of Trimmomatic (Bolger et al., 2014). The trimmed reads were then used to perform a strand specific *de novo* assembly through use of the Trinity software suite (Haas et al., 2013). The assembled transcriptome's quality was assessed through mapping the reads back to the assembled transcripts using Bowtie2 (Langmead and Salzberg, 2012), and to assess the percentage of reads utilized to construct the transcriptome. A BUSCO v4.2 (Simão et al., 2015) analysis was also performed using the Insecta homolog set (accessed on 2020/02, https://buscos.ezlab.org/datasets/prerelease/viridiplantae_odb10.tar.gz) to establish the number of represented essential orthologs. To assess if sequencing depth was adequate to generate a high quality *de*

novo assembly, successively increasing sub-samplings of total sequencing data for individual samples were performed and assembled separately. These were then compared through the use of BLASTx to the NCBI's nr (protein) database, and the SwissProt uniprotKB and TrEMBL databases to assess the number of full-length BLAST matches obtained for the assembled transcripts from the differently sized assemblies.

Basic statistics such as the number of transcripts, transcript average length, transcript average %GC content, transcript N50 and transcript Ex90N50 were also calculated. All transcripts were analyzed through use of OmicsBox v1.2 (OmicsBox—Bioinformatics Made Easy, BioBam Bioinformatics, March 3, 2019, https://www.biobam.com/omicsbox) by performing BLASTx and BLASTn searches, respectively to the NCBI's nr and nt databases (accessed on 2019/08/21). Blast2GO (Götz et al., 2008) was then used to assign gene ontologies (GO) and KOG terms to all transcripts.

To compare the differential gene expression between the least and most virulent biotypes, transcript abundance quantification was performed using RSEM (Li and Dewey, 2011) for each sample using the obtained *de novo* transcripts. Average expression and the coefficient of variation was calculated per gene for the two biotypes SA1 and SAM separately. For this purpose FPKM (fragments per kilobase of transcript per million) values were used but also estimated by RSEM. We also identified differentially expressed (DE) genes between biotypes SA1 and SAM using edgeR (Robinson et al., 2010) based on gene-level expected counts estimated by RSEM. Only genes with greater than two counts-per-million in at least three samples were retained for DE analysis and we considered genes DE if they had a fold-change (FC) $\geq$1.5 and $p < 0.05$ after adjusting for multiple testing using the Benjamini–Hochberg (BH) procedure (Benjamini and Hochberg, 1995).

Augustus v3.3.3 (Stanke et al., 2006) was utilized to predict protein coding genes from the assembled transcripts using the *Acyrthosiphon pisum* (pea pahid) training set. Through use of a Trinity provided script, the GATK v.3.8 pipeline for variant calling (Van der Auwera et al., 2013) was applied between the transcripts from the biotypes. Variants were accepted as true if they possessed an FS score above 30 (Phred-scaled *p*-value using Fisher's exact test to detect strand bias) and a QD score <2 (Variant Confidence/Quality by Depth). Variants were also required to be present in all 3 biological replicates of one biotype and absent in all 3 biological replicates of the other biotype.

Analysis of *DNMT* and *TET* Expression

For *DNMT* gene expression analyses, 20 apterous aphids were collected in triplicate for each biotype ($3 \times n = 60$) and their heads were removed with a liquid nitrogen-cooled scalpel by cutting carefully posterior to the prothorax (**Figure S1**) and RNA was extracted as previously described (Burger et al., 2017). cDNA synthesis was performed using the iScript™ cDNA Synthesis kit (BioRad) in accordance with the provided protocol, applying 350 to 400 ng of total RNA as template per 20 µl reaction.

For the host-shift experiment, RNA was isolated from apterous aphid whole-body homogenates prepared using a micro-pestle in liquid nitrogen cooled Eppendorf tubes. Each treatment was represented by three biological replicates consisting of 30 aphids each ($n = 90$). The frozen aphids were ground with micro-pestles and RNA was extracted using RNeasy Mini Kit (Qiagen), following the manufacturers recommended protocol for insect material. cDNA synthesis was performed using SensiFAST cDNA Synthesis Kit (Bioline), with 200 ng of input RNA.

Primer pairs for RT-qPCR (**Table S2**) were designed using Primer3 from the CDS regions of the RWA sequenced *DNMTs* and *TET* to yield products of between 100 bp and 200 bp in size. Primers were used in a primerBLAST analysis against the assembled RWA SAM biotype reference genome (GCA_001465515.1) to ensure they only matched the *DNMT* and *TET* genes from which they were designed. The relative expression of *DNMT1*, *DNMT2,* and *DNMT3* (in sampled aphid heads of the RWA biotypes SA1 and SAM), as well as the relative expression of *DnTET* (whole aphids of RWA biotypes SA1 and SAM that underwent host-shifts) was quantified as previously described (Burger et al., 2017). All samples and standards were quantified in triplicate along with a no template control as a measure of contamination. A five point, two times serial dilution of a zero-hour SA1 sample was used to generate quantification standards. The relative expression of *DnDNMT3* and *TET* were calculated using Pfaffl's mathematical model (Pfaffl, 2001) for each time point (0, 6, and 48 h). A CFX96 Real-Time System (Bio-Rad) was used to perform the real-time PCR analysis. Each reaction started with a denaturation step at 95°C for 3 min, followed 40 cycles of amplification, consisting of a denaturation step at 95°C for 10 s, an annealing step at the relevant temperature for each primer set (**Table S2**) for 30 s, and an extension step at 72°C for 30 s. A melt curve analysis was also performed for each reaction, to verify the absence of non-specific amplification: The incubation temperature was increased in 5 s intervals, 0.5°C at a time, from 65 to 95°C. The ribosomal genes *L27* and *L32* were used as reference genes as they have previously been shown to be constitutively expressed, respectively, in RWA and the pea aphid (Shakesby et al., 2009; Sinha and Smith, 2014).

Measuring DNMT Protein Activity

For the extraction of aphid protein, three replicates of 150 apterous aphids ($n = 450$) of biotypes SA1 and SAM were collected, flash-frozen and stored at −80°C until use. A micropestle was used to grind aphids into a fine powder, to which 100 µl phosphate buffered saline (50 mM NaH_2PO_4, 50 mM Na_2HPO_4 and 150 mM NaCl, pH 7.5), 10 µl phenylmethylsulphonyl fluoride (1 mM) and 10 µl dithiothreitol (1 mM) were added. Homogenized mixtures were centrifuged at 15 000 rpm (4°C) for 10 min to pellet the cell debris and the resulting supernatant was transferred to a clean Eppendorf tube. Protein concentrations were quantified using the Bradford protein assay (Bradford, 1976) with Bovine Serum Albumin as standard (BioRad, USA), and the Glomax®-Multi Detection plate reader (Promega, USA) as described by Rylatt and Parish (1982).

DNA methyltransferase protein activity was quantified following the guidelines provided with Abcam's colourimetric DNMT Activity Quantification kit (Abcam, UK), and using

the maximum recommended amount of nuclear extract, 5 µl (ranging from 7.69 to 10.96 µg, standardized using the formula below) of each of the three biological replicates per biotype ($n = 3$). DNA methyltransferase activity in OD/h/µg (optical density/hour/microgram) was calculated using the formula below.

$$\text{Protein activity} = \frac{(\text{Sample OD} - \text{Blank OD})}{[\text{Protein amount (ug) x hour}]} \text{ x } 1000$$

An ANOVA was performed to test for significant differences between the sample means, with the level of significance set at $p \leq 0.05$.

Quantifying Levels of Global Methylation (5mC) and Hydroxymethylation (5hmC)

Global levels of methylation were determined utilizing a colourimetric Methylated DNA Quantification kit (Abcam) using 150 ng DNA of the three biological repeats per biotype ($n = 3$). A slight modification of the protocol was followed in the "methylation capture" section, whereby incubation of DNA and diluted capture antibody was performed for 15 h at room temperature in the dark to allow for optimal antibody binding, as opposed to 1 h at room temperature. The final plate incubation, after addition of the developer solution, was carried out for the maximum recommended time of 10 min. Absorbance at 450 nm was read in triplicate ($n = 9$) within five min of adding the stop solution, using the Glomax®-Multi Detection System. Relative methylation levels were calculated for each sample using the following formula:

$$\textit{Relative 5mC \%} = \frac{(\textit{Sample OD} - \textit{Negative control OD})/S}{(\textit{Positive control OD} - \textit{Negative control OD}) \; x\, 2/P} \; x\, 100$$

where 5mC is 5-methylcytosine, OD is optical density, S is the amount of sample DNA in ng and P is the amount of positive control in ng. An ANOVA was performed to test for significant differences between the sample means, with the level of significance set at $p \leq 0.05$.

Global hydroxymethylation levels were quantified using a colourimetric Hydroxymethylated DNA Quantification kit (Abcam), in accordance with the provided protocol. Freshly extracted DNA sample from each biotype were loaded in triplicate ($n = 3$), and standardized using the formula below (refer to S, the amount of sample DNA). The final plate incubation was carried out for 10 min, where after absorbance at 450 nm was read using the Glomax®-Multi Detection System. Relative hydroxymethylation levels were calculated for each sample using the following formula:

$$\textit{Relative 5hmC \%} = \frac{(\textit{Sample OD} - \textit{Negative control II OD})/S}{(\textit{Positive control OD} - \textit{Negative control II OD}) \; x\, 5/P} \; x\, 100$$

where 5hmC is 5-hydroxymethylcytosine, OD is optical density, S is the amount of sample DNA in ng and P is the amount of positive control in ng. An ANOVA was performed to test for significant differences between the sample means, with the level of significance set at $p \leq 0.05$.

Statistical Analysis

Microsoft Excel (2010)/XLSTAT Premium (Addinsoft Inc. USA) were used for the statistical analysis, and SigmaPlot (2001) was used to plot graphs showing the average readings and standard deviation. An ANOVA was performed to test for significant differences between the sample means, with the level of significance set at $p \leq 0.05$. The model assumptions of ANOVA (i.e., homoscedasticity and normality of the residuals), were tested for using Levene's test and the Shapiro-Wilk test, respectively (significance set at $p \leq 0.05$ for both tests). If the ANOVA null hypothesis—that the means of the treatment groups are equal—was rejected, a Fisher's LSD test was then performed.

Whole Genome Bisulfite Sequencing (WGBS) and Analysis

A total of 100 apterous female aphids of South African RWA biotypes SA1 and SAM were used for DNA extraction performed as described previously (Burger and Botha, 2017) (GenBank ID GCA_001465515.1; BioProject PRJNA297165). Three independent biological repeats of each biotype were conducted of each biotype ($n = 3$). Samples consisting of 2 µg DNA, of both RWA biotypes SA1 and SAM were submitted to Macrogen Inc., South Korea for bisulfite treatment, library preparation and sequencing.

DNA samples were treated with the EZ DNA Methylation Lightning kit (Zymo Research) and used to construct the sequencing library utilizing the TruSeq DNA Methylation Library Kit™ (Illumina) ($n = 1$) or Accel-NGS® Methyl-Seq (Swift Biosciences) for Illumina ($n = 2$), 5′ tags were generated through random priming, followed by selective 3′ tagging. Illumina P7 and P5 adapters were ligated through amplification to the 5′ and 3′ ends, respectively. The Illumina HiSeq X platform was used to sequence the bisulfite treated samples.

The obtained sequencing data was analyzed for quality using FastQC (Andrews, 2010). After inspecting the adapter content, per base sequence content, and per base sequence quality, Trimmomatic (Bolger et al., 2014) was used to remove adapter sequences and trim the paired-end reads for quality. A sliding window over 15 bp was used to trim for a quality score of 20, along with a headcrop of 10. The Illuminaclip parameter was used to search for and remove adapter sequences from the reads. After trimming, all reads were filtered for a minimum read length of 40 bp.

The Bismark software program (Krueger and Andrews, 2011) was used to analyze the methylation status of the trimmed and filtered sequence reads. Using the RWA SAM biotype reference genome (GenBank ID GCA_001465515.1; BioProject PRJNA297165), the observed over expected number of cytosine bases for each methylation context was calculated as follows:

$$C_pG_{\frac{O}{E}} = \frac{F_{C_pG}}{F_C.F_G}$$

$$CHG_{\frac{O}{E}} = \frac{F_{CAG} + F_{CTG} + F_{CCG}}{3(F_C.F_{1-G}.F_G)}$$

$$CHH_{\frac{O}{E}} = \frac{F_{CAA} + F_{CAT} + F_{CAC} + F_{CTA} + F_{CTT} + F_{CTG} + F_{CGA} + F_{CGT} + F_{CGG}}{9(F_C.2F_{1-G})}$$

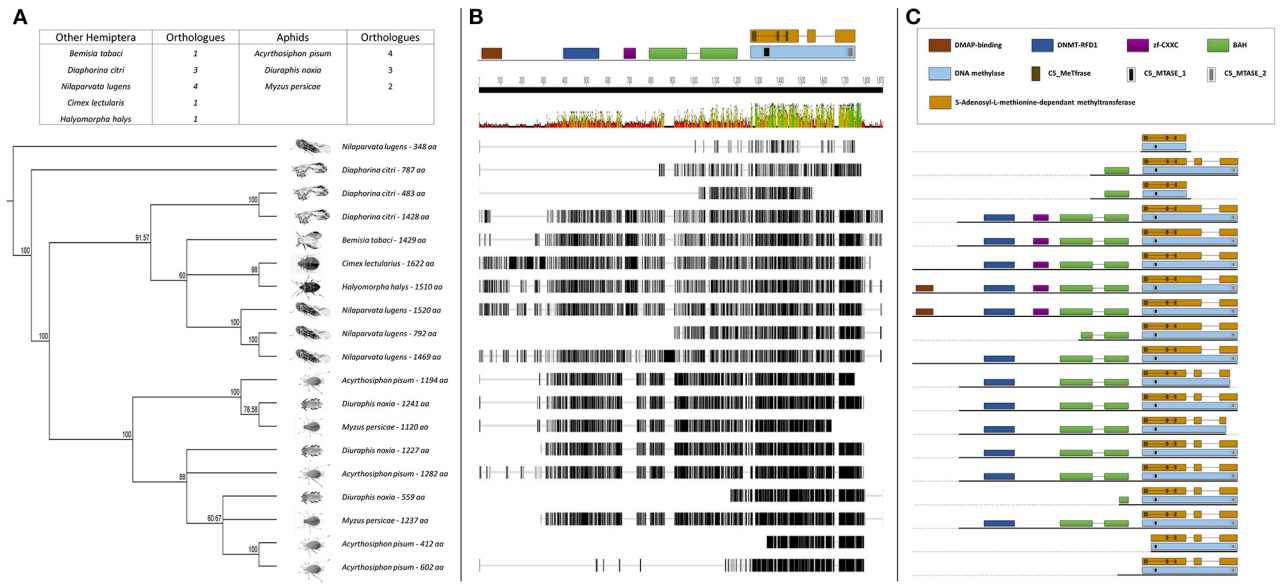

FIGURE 1 | (A) Phylogenetic analysis of the DNMT1 amino acid sequences from eight Hemipterans species using MAFFT v7.4 and Paup v4.0a136. Included in the analysis are *Acyrthosiphon pisum, Bemisia tabaci, Cimex lectularius*, *Diaphorina citri, Diuraphis noxia, Halyomorpha halys, Myzus persicae,* and *Nilaparvata lugens*; **(B)** Comparison of the *DNMT1* gene sequence from the different hemipteran species in **(A)**, showing the level of conservation on gene sequence level; and **(C)** Comparison of the conservancy on functional motifs within the *DNMT1* gene sequence from the different hemipteran species in **(A)**. Indicated are functional and/or structural motifs.

Where F represents the frequency of the subscripted nucleotide/dinucleotide/trinucleotide, in the reference genome. As a reference genome is not available for biotype SA1, the calculations were only performed for biotype SAM.

The R-package DSS-single (Wu et al., 2015) was used to calculate which genes are significantly differentially methylated (p-value < 0.05) between SA1 and SAM from the WGBS data. For the analysis, only genic CpG loci, with at least a ten times coverage in both biotypes, across all three repeats were considered. This amounted to 613,730 CpG sites. A Wald test (Wald, 1943) was conducted for differentially methylated loci with the DMLTest function. The optional "smoothing" algorithm of this function, which uses methylation data of nearby loci to generate "pseudo replicates" is only recommended for datasets where methylation loci are dense (Feng et al., 2014). Due to the high AT content and low methylation levels in RWA, methylation loci are sparse and the "smoothing" algorithm was not employed. The CallDMR function was then used to identify differentially methylated regions using information from the differentially methylated loci, such as the number of CpG sites in a region and the percentage of sites in a region scored as significant. This information is used to calculate a combined score for each region, referred to as an area statistic, which can be used to sort regions based on the degree of differentiation in CpG methylation (Wu et al., 2015). The Blast2GO suite (Conesa et al., 2005; Conesa and Götz, 2008) was used to search for the gene ontologies (GO) and KOG terms (Burger and Botha, 2017) of genes containing a differentially methylated region.

RESULTS

Classes of DNA Methyltransferases in RWA

The BLASTp analysis performed using the insect DNMTs against the RWA proteins, revealed three DNMT subfamilies. Comparison of the DNMTs of RWA with other aphids (i.e., *A. pisum* and *Myzus persicae*), as well as with other distant hemipteran species (i.e., *Bemisia tabaci, Cimex lectularius*, *Diaphorina citri, Halyomorpha halys,* and *Nilaparvata lugen*) confirmed that as with other hemipterans, RWA have three DNMT subfamilies of genes, i.e., *DNMT1, DNMT2*, *DNMT3* (**Figures 1–3**). With the DNMT1 and DNMT3 sequences, those from RWA were mostly similar to that of *M. persicae* and then *A. pisum,* than to the other hemipterans included in the study. Whereas, those from *N. lugens* (the brown planthopper) and *D. citri* (Asian citrus psyllid) the most distant from the plant aphids. In the case of DNMT2, the separation was less distinct. These observations were strongly supported by bootstrap values.

Further sequence analysis revealed that the RWA had two homologs of each of the DNMT1s (DNMT1a and DNMT1b) and DNMT3s (DNMT3a and DNMT3b) (**Figures 1A**, **3A**), but only a single DNMT2 (**Figure 2B**) protein. The RWA DNMTs contained several functional motifs that were recognizable and contributing to the ascribed function, all shared between the plant aphids (**Figures 1C**, **2C**, **3C**).

To assess whether the DNMTs differ between RWA biotypes, an alignment of the DNMT sequences obtained between the SA1 and SAM biotypes was conducted which revealed 36 SNPs between the biotypes (**Figures S2–S7**).

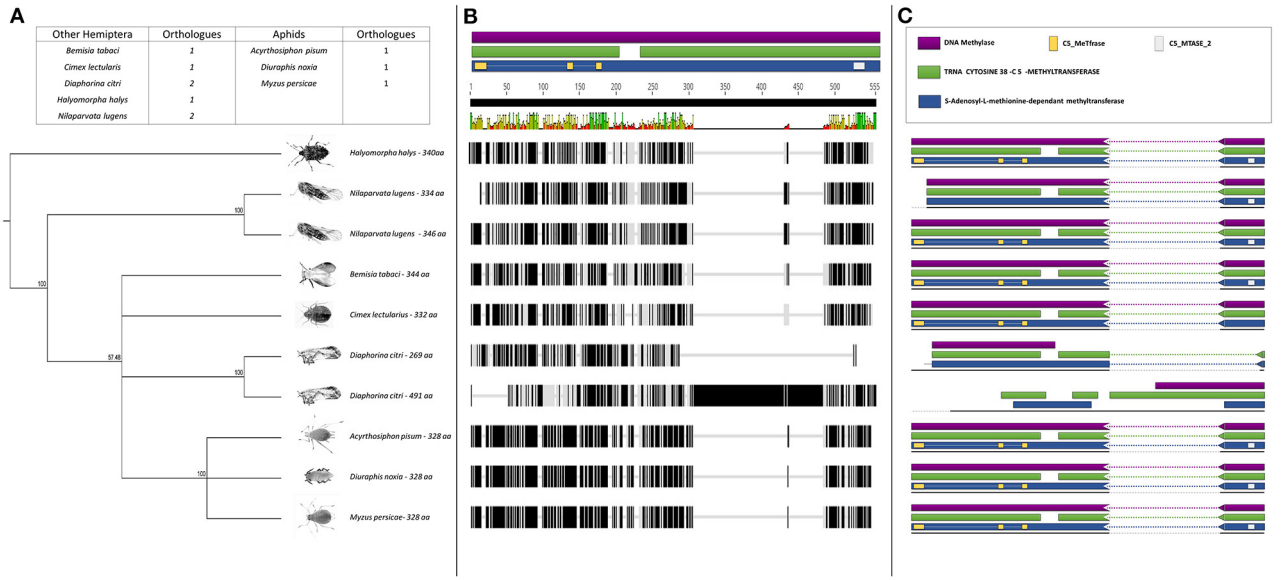

FIGURE 2 | (A) Phylogenetic analysis of the DNMT2 amino acid sequences from eight Hemipterans species using MAFFT v7.4 and Paup v4.0a136. Included in the analysis are *Acyrthosiphon pisum, Bemisia tabaci, Cimex lectularius*, *Diaphorina citri, Diuraphis noxia, Halyomorpha halys, Myzus persicae,* and *Nilaparvata lugens*; **(B)** Comparison of the *DNMT2* gene sequence from the different hemipteran species in **(A)**, showing the level of conservation on gene sequence level; and **(C)** Comparison of the conservancy on functional motifs within the *DNMT2* gene sequence from the different hemipteran species in **(A)**. Indicated are functional and/or structural motifs.

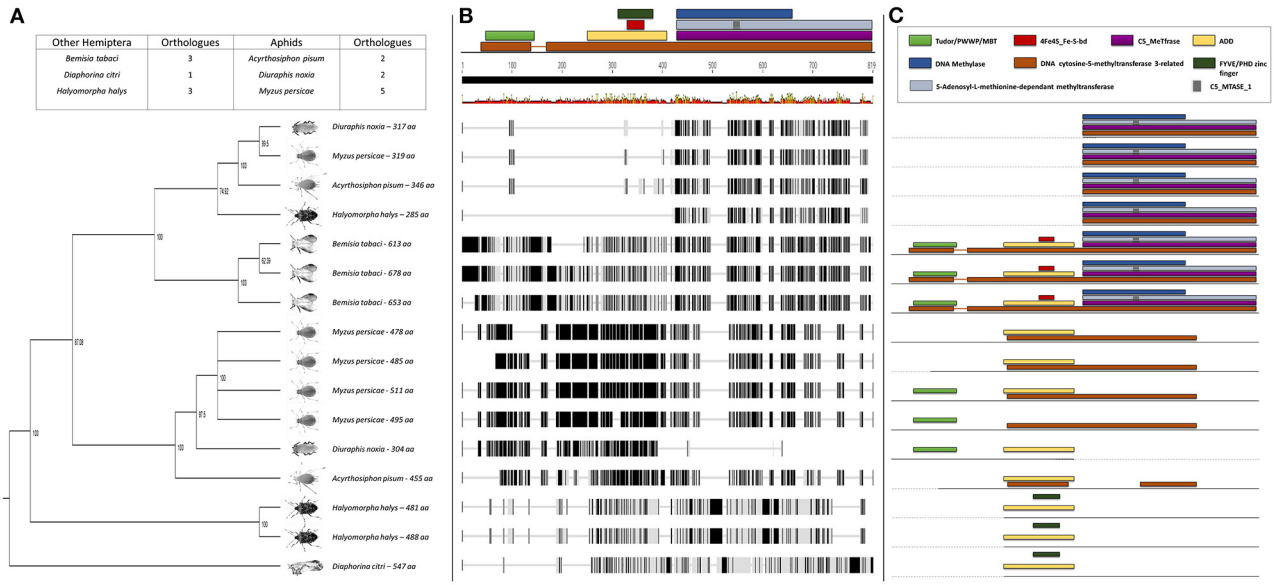

FIGURE 3 | (A) Phylogenetic analysis of the DNMT3 amino acid sequences from eight Hemipterans species using MAFFT v7.4 and Paup v4.0a136. Included in the analysis are *Acyrthosiphon pisum, Bemisia tabaci, Cimex lectularius*, *Diaphorina citri, Diuraphis noxia, Halyomorpha halys, Myzus persicae,* and *Nilaparvata lugens*; **(B)** Comparison of the *DNMT3* gene sequence from the different hemipteran species in **(A)**, showing the level of conservation on gene sequence level; and **(C)** Comparison of the conservancy on functional motifs within the *DNMT3* gene sequence from the different hemipteran species in **(A)**. Indicated are functional and/or structural motifs.

We used the transcriptome data to investigate the expression pattern of known methylation genes in RWA biotypes SA1 and SAM (**Figures 5**, **6**). We again found the full complement of DNA methyltransferases which was expressed in different transcript levels, with minimal differences in *DnDNMT1* and *DnDNMT2* between the RWA biotypes, with fewer *DnDNMT3* transcripts in the more virulent SAM (9.51 ± 6.9) than in the less virulent SA1 (31.45 ± 2.4) ($p = 0.006$).

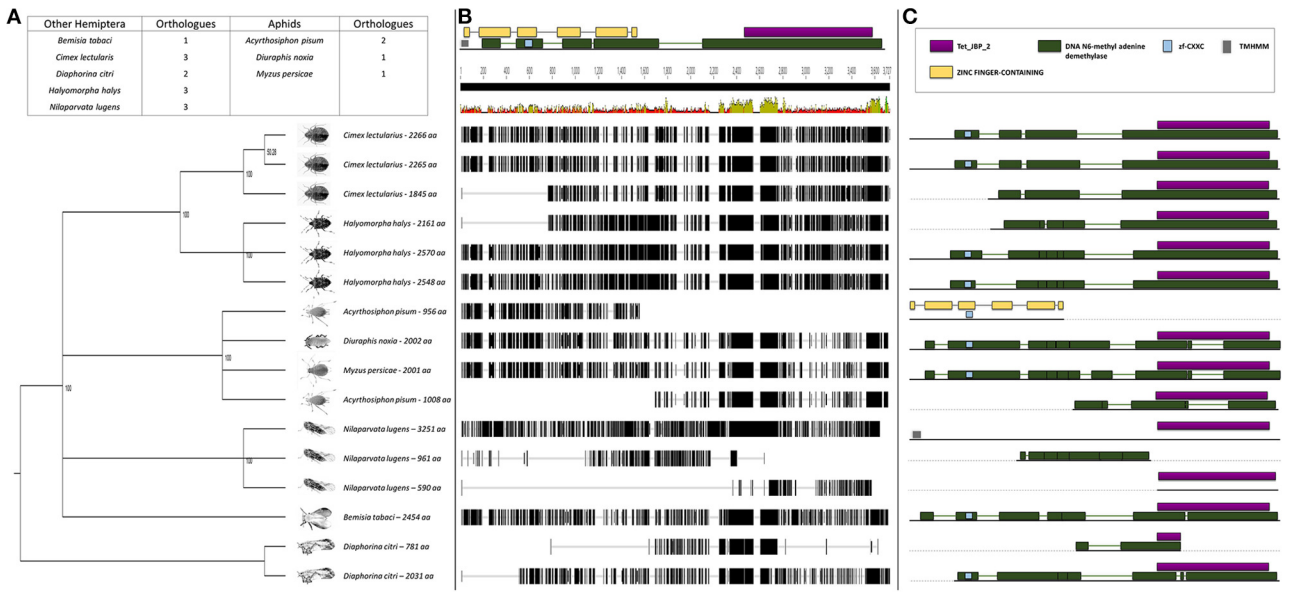

FIGURE 4 | (A) Phylogenetic analysis of the N6-methyl adenine demethylase (TET-like) amino acid sequences from eight Hemipterans species using MAFFT v7.4 and Paup v4.0a136. Included in the analysis are *Acyrthosiphon pisum, Bemisia tabaci, Cimex lectularius*, *Diaphorina citri, Diuraphis noxia, Halyomorpha halys, Myzus persicae,* and *Nilaparvata lugens*; **(B)** Comparison of the *N6-methyl adenine demethylase* (*TET-like*) gene sequence from the different hemipteran species in **(A)** showing the level of conservation on gene sequence level; and **(C)** Comparison of the conservancy on functional motifs within the *N6-methyl adenine demethylase* (*TET-like*) gene sequence from the different hemipteran species in **(A)**. Indicated are Tet_JBP_2, DNA N6-methyl adenine demethylase, zf-CXXC, TMHMM, and Zinc finger-containing motifs.

To measure whether the observed SNPs had any bearing on gene expression between less and more virulent RWA biotypes, the expression of aphid head *DNMTs* among the RWA biotypes was also investigated. Biotype SAM's *DNMT1* expression was higher than that measured in biotype SA1, but the difference in expression was not significant (p-value = 0.416 for *L27* and 0.362 for *L32*), as was the expression of *DNMT2* (**Figure 5A**). The expression of *DNMT3* however showed the most inter-biotype variation of the three *DNMT* subfamilies, and revealed that the *DNMT3* expression levels of SAM (most virulent aphid biotype) were significantly lower than that measured in SA1 (Fisher's LSD test; p-value of ≤ 0.1).

To establish whether the difference in the DNMT gene expression equates into measurable differences in total DNMT protein activity, the DNMT protein activity was determined (**Figure 5B**). The concentration of DNMT protein activity within the biotypes ranged from 44.80 to 53.54 OD/h/μg, with biotype SAM exhibiting the lower DNMT protein activity of the biotypes. However, the DNMT protein activity levels did not differ significantly between the biotypes ($p \leq 0.05$).

Sequence Analysis and Expression of *DnTET* in RWA Biotypes

To shed light on the observed difference in global demethylation but not methylation levels, the *TET (N6-methyl adenine demethylase)* genes responsible for oxidation within the methylation pathway were studied (Wojciechowski et al., 2014). We were able to isolate and sequence the *DnTET* ortholog from RWA. Comparison of the DnTET (N6-methyl adenine demethylase) protein sequences in RWA with other aphids (i.e., *A. pisum, M. persicae)* and with other distant hemipteran species (i.e., *B. tabaci, C. lectularius*, *D. citri, H. halys,* and *N. lugen*) confirmed that all these species have recognizable TET-like sequences in their genomes (**Figure 4**). Clustering of the sequences group the aphids closer to each other than to the other hemipterans, with strong bootstrap support (**Figure 4A**). Further analysis revealed that unlike *A. pisum* and some of the other hemipteran species, RWA has only a single form of TET (**Figure 4B**), which contain several functional motifs including DNA N6-methyl adenine demethylase (**Figure 4C**).

We also used the transcriptome data to investigate the expression pattern of the *TET (N6-methyl adenine demethylase)* genes responsible for oxidation within the methylation pathway in RWA biotypes SA1 and SAM (**Figure 6C**). We found more *DnTET* transcripts in the more virulent SAM (5.81 ± 0.38) than in the less virulent SA1 (2.59 ± 2.3) ($p = 0.014$).

Expression of DNA Methylation Genes During Feeding Studies

To assess further whether the sequenced *DnDNMT* and *DnTET* genes expressed in RWA biotypes SA1 and SAM, differ when challenged with different host plants, the RWA biotypes were reared on susceptible host plants ($n = 3$) (**Table 1**) and then moved to two resistant wheat cultivars (Tugela-*Dn1* and Tugela-*Dn5*). The lines were selected based on the fact that they are near isogenic and differ only with regard to the resistance gene present (i.e., *Dn1* expressing antibiosis—harmful

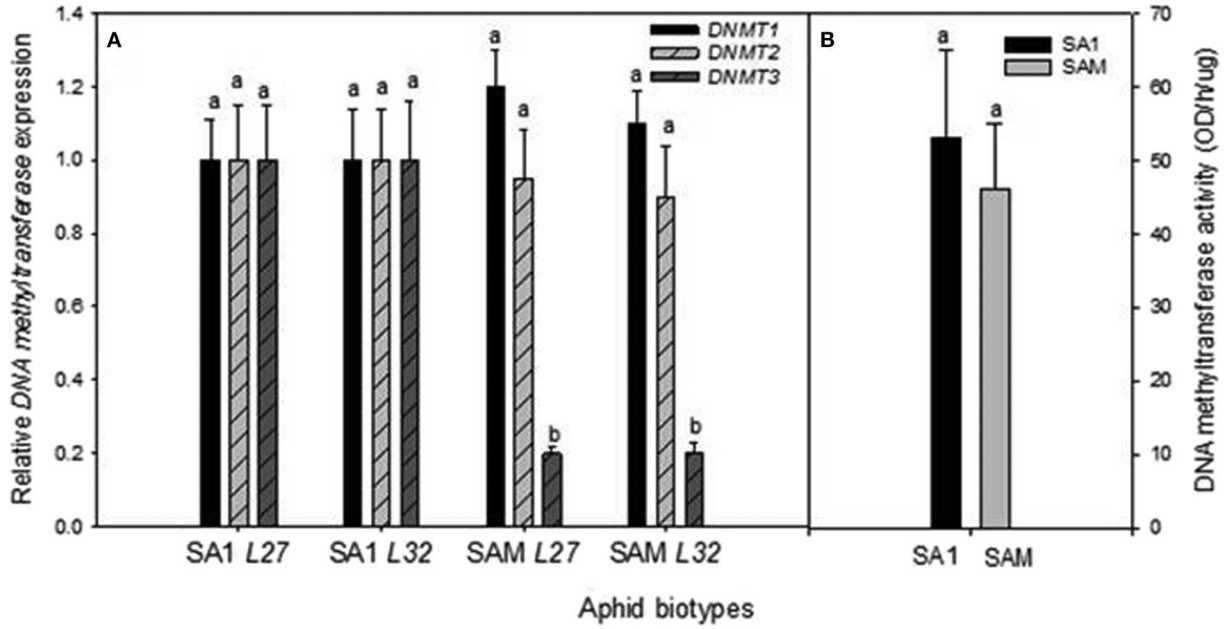

FIGURE 5 | (A) Comparison of the average relative expression (R mean) of *DNMTs* in South African RWA biotype heads. Fold changes in expression are shown relative to the SA1 samples, the expression of which was set at 1. *DNMTs* expression is presented when normalized against the reference genes *L27* and *L32*, respectively, and the error bars indicate standard deviation. Different alphabetical letters indicate statistical significance ($p \leq 0.05$). **(B)** DNA Methyltransferase protein activity (OD/h/μg) measured in South African RWA biotypes SA1 and SAM, with error bars indicating the standard deviation.

TABLE 1 | Relative expression of *DNMT3* and *TET* in RWA biotypes SA1 and SAM when feeding on a susceptible cultivar SST.

Relative gene expression	**Aphid biotype**			
	SA1		**SAM**	
Reference genes	***Lr27***	***Lr32***	***Lr27***	***Lr32***
DNMT	0.852 ± 0.126	0.734 ± 0.084	1.308 ± 0.531	0.749 ± 0.221
TET	0.758 ± 0.114	0.652 ± 0.072	1.222 ± 0.304	0.721 ± 0.223

Lr27 and Lr32 was used as reference genes.

to the aphid and *Dn5* expressing antibiosis and antixenosis—non-palatable) (**Figure 7**). The measured *DnDNMT* expression increased significantly in both aphid biotypes when challenged with a new feeding environment (i.e., *Dn5* expressing both antibiotic and antixenotic) ($p \leq 0.05$). The relative expression almost doubled in the less virulent biotype SA1, but even more in the more virulent biotype SAM (± six-fold *Lr27*; ±11-fold *Lr32*) within 6 h after host-shifting.

To assess whether the sequenced *DnTET* gene was also differentially expressed in RWA, biotypes SA1 and SAM during feeding after host-shifting, the expression of *DnTET* was also measured (**Figure 8**). The measured *DnTET* expression increased slightly but not significantly after 6 h in the less virulent SA1 biotypes when challenged with the *Dn5* wheat line (antibiotic and antixenotic) ($p > 0.05$), but significantly in SA1 after 48 h when challenged with the antibiotic wheat line Tugela-*Dn1* (*Lr27*) ($p \leq 0.05$). In contrast, the *DnTET* expression of virulent biotype SAM remained the same when challenged with the antibiotic wheat line Tugela-*Dn1*, but increased significantly within the first 6 h after host-shifting from the susceptible Tugela to the wheat line containing the *Dn5* resistance gene ($p \leq 0.05$).

Global Methylation and Hydroxymethylation Quantification

To quantify the global levels of methylation (5mC) and dehydroxymenthylation (5hmC), antibodies specific to these (i.e., 5mC and 5hmC) were used. The use of the 5mC antibody revealed similar levels of global methylation between the less virulent SA1 and more virulent SAM biotype, with the measured levels, ranging between 0.14 and 0.16% (**Figure 9**). The hydroxymethylation levels, however differed significantly ranging from 0.12 to 0.46% (**Figure 9**), with biotype SA1 displaying the lowest, and biotype SAM displaying the highest 5hmC levels, respectively ($p \leq 0.05$).

Whole Genome Bisulfite Sequencing

The whole genome bisulfite sequencing produced a total of 6,846,597,083 raw reads for SA1 and 7,397,965,699 raw reads for SAM, respectively, of which a total of 70,861,462 bases (SA1) and 74,073,939 bases (SAM) were methylated, which represents 1.126 ± 0.321% (SA1) and 1.105 ± 0.295% (SAM) methylation in the genome (**Tables S3, S4**). The sequence reads were analyzed for contexts of DNA methylation within the genome (**Table S5**) and the results revealed that RWA has methylation in all contexts

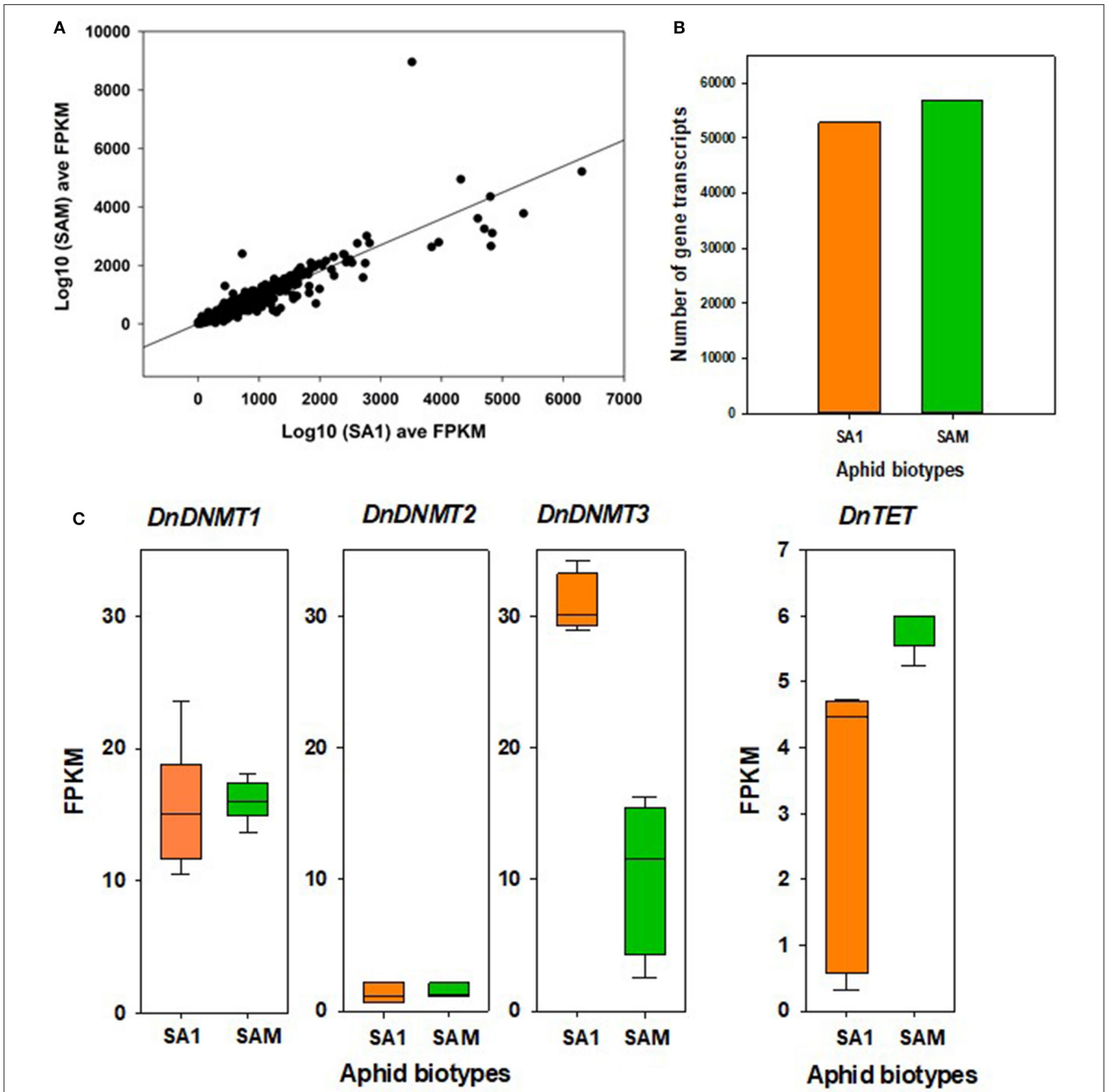

FIGURE 6 | Differential gene expression between RWA biotypes SA1 and SAM. **(A)** SA1 and SAM gene expression as log10 fragments per kilobase of transcript per million mapped reads (FPKM) average over three biological replicates for transcripts retained for differential expression (DE) analysis with edgeR ($n = 64,214$). Benjamini-Hochberg (BH) corrected $p > 0.05$ and absolute fold change [FC] > 1.5). **(B)** Comparison of number of transcripts expressed in SA1 and SAM. **(C)** Significant differences were observed in the expression of *DnDNMT3* and *DnTET* in SA1 and SAM; edgeR; BH corrected $p > 0.05$ and absolute fold change [FC] > 1.5.

(CpG, CHG, and CHH), with the majority of methylation within the CpG context (±5.19%), while the other contexts show much lower levels of methylation (CHG—±0.27%; CHH—±0.34%). The reads were then subjected to quality analysis, aligned and mapped to the RWA biotype SAM reference genome (GenBank ID GCA_001465515.1; BioProject PRJNA297165). Of the methylated reads, most of the methylation was located in genic regions (±1.58%), but intergenic methylation was also present (±0.808%) (**Table S6**). Methylation was evenly distributed between both strands, with the top strand only

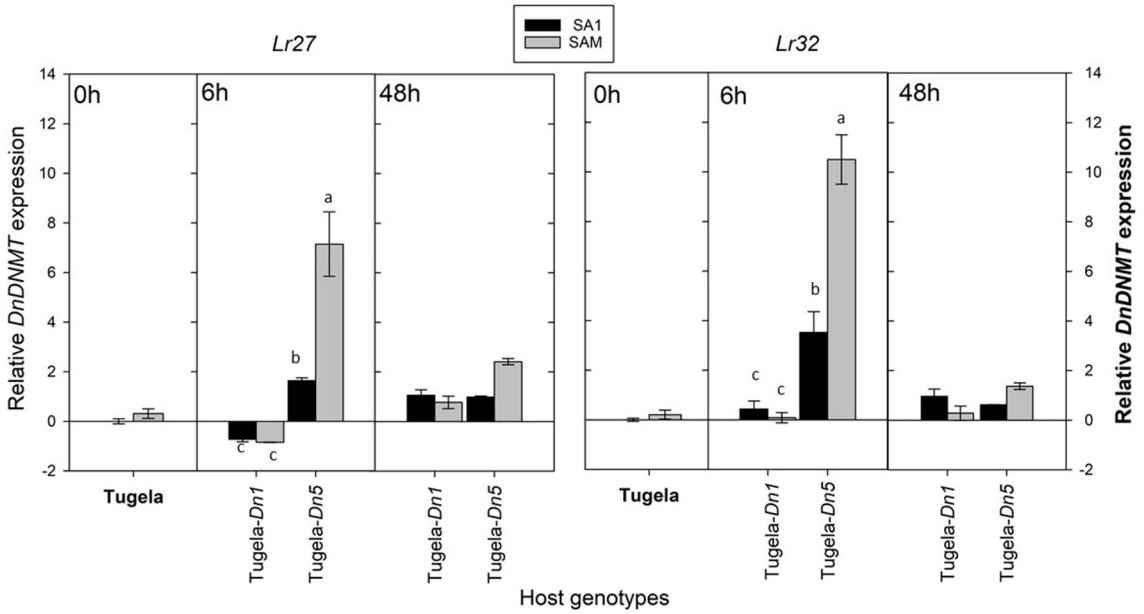

FIGURE 7 | A comparison of the average relative expression (R mean) of *DnDNMT* of South African RWA biotypes after transfer to different host plants after 6 and 48 h of feeding. Fold changes in expression are shown relative to the SA1 samples, the expression of which was set at 1. *DnDNMT* expression is presented when normalized against the reference genes *L27* and *L32* respectively, and the error bars indicate standard deviation. Different alphabetic letters indicate significant differences ($p \leq 0.05$).

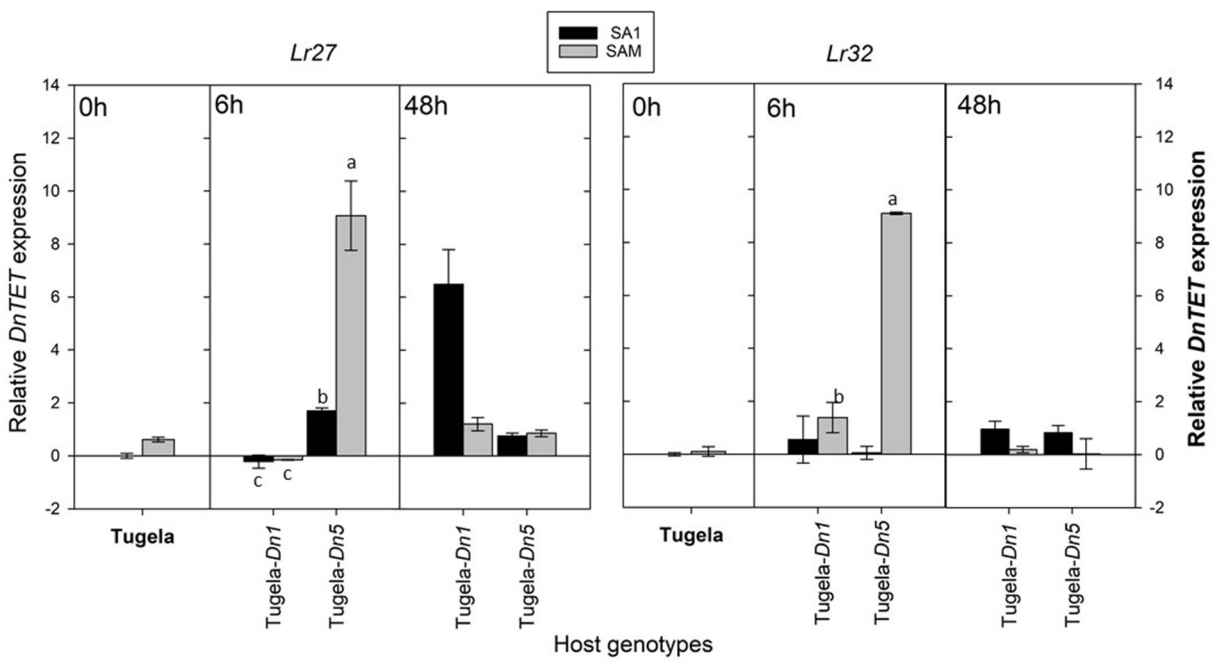

FIGURE 8 | A comparison of the average relative expression (R mean) of *DnTET* of South African RWA biotypes after transfer to different host plants after 6 and 48 h of feeding. Fold changes in expression are shown relative to the SA1 samples, the expression of which was set at 1. *DnTET* expression is presented when normalized against the reference genes *L27* and *L32,* respectively, and the error bars indicate standard deviation. Different alphabetic letters indicate significant differences ($p \leq 0.05$).

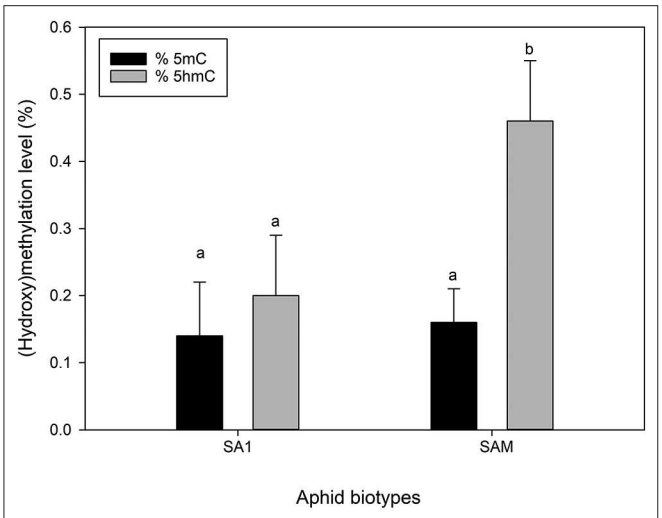

FIGURE 9 | Comparison of global 5 mC (black) and 5 hmC (gray) levels of the South African RWA biotypes. The error bars indicate standard deviation and different alphabetic letters indicate significant differences ($p \leq 0.05$).

containing 0.02% more methylated calls than the bottom strand (**Table S7**). Within genes exonic regions were found to be overall more methylated (±0.56%) than the intronic regions (**Table S8**), and the most represented context of methylation (i.e., CpG, CHG, or CHH) was in the CpG context, followed by the CHG context, with the least in the CHH context (**Table S9**).

Using the SAM biotype reference genome, the observed over expected number of cytosine bases were also calculated (**Figure 10**). This is commonly seen for the CpG context, denoted as $CpG_{O/E}$ (Hunt et al., 2010), with the data on all three contexts of cytosine methylation available from the Bismark pipeline, the other, often overlooked $CHG_{O/E}$ and $CHH_{O/E}$ ratios were also included in this study. After calculating these ratios, it was revealed that the observed CpG context, unlike with the other contexts was lower than expected (**Figure 10**). This is particularly so for the observed CpG context in exonic regions (**Figure 10A**).

After analysis, we identified 40 differentially methylated genes (DMEs) when we compared the genes that were differentially methylated between the less and more virulent biotypes (**Figure 11**; **Figures S8A1-3, B1-9, C1-13**). Even though based on broad functional categories, the differences between the least virulent SA1 and most virulent SAM seems minimal (**Figure 11**), further analyses of their involvement into biochemical pathways revealed that these DMEs had distinctly different predicted functions (even when involved within the same pathway, **Figures S8A1-3**). Interesting examples include the selective methylation of genes in more virulent SAMs, but not SA1, which include include DMEs involved in the irinotecan metabolism (**Figure S8A3**); metabolism of cytotoxicity by cytochrome P450 (**Figures S8C10, C11**); steroid hormone biosynthesis (**Figure S8C2**) and wax biosynthesis (**Figure S8C**).

DISCUSSION

Integrated pest management programs against RWA depend heavily on the breeding of wheat cultivars that provide resistance (Tolmay et al., 1997; Smith and Clement, 2012; Botha, 2013; Sinha and Smith, 2014). The effectiveness of these cultivars, however, is often short-lived as aphids overcome the resistance they impart (Botha et al., 2005, 2010; Tagu et al., 2008; Sinha and Smith, 2014). Understanding how new aphid biotypes develop, as well as the mechanisms they employ to exert their virulence enabling them to breakdown plant resistance, are of utmost importance if resistant cultivars are to be used to their full potential (Botha et al., 2014a). The availability of the highly virulent mutant RWA biotype (SAM) (Swanevelder et al., 2010), alongside South Africa's naturally occurring biotypes (SA1, SA2, SA3, and SA4) (Walters et al., 1980; Tolmay et al., 2007; Jankielsohn, 2011, 2016) presents a unique opportunity for the study of biotypification. Despite having developed from SA1, which only renders *dn3*-containing cultivars susceptible (Jankielsohn, 2011), SAM has the remarkable ability to overcome the resistance of all the *Dn* genes that have been introduced and/or documented (Botha, 2013; Botha et al., 2014a). SAM thus serves as a model to resolve aphid biotypification.

In the present study, we investigated the DNMT protein family, as they catalyze the covalent addition of a methyl group to the 5′ position of cytosine in the methylation pathway. *DNMT2* seemed the most conserved with only a single form of the protein responsible for stabilizing tRNA and the regulation of protein synthesis in response to environmental cues (Becker and Weigel, 2015). In contrast, *DNMT1* and *DNMT3* with two forms each, are responsible for maintaining and establishing methylation patterns, respectively (Goll and Bestor, 2005; Goll et al., 2006; Jeltsch et al., 2006). Owing to the important role of these proteins in changing methylation patterns, it is not surprising that variations in these genes occur. RWA is also not the only insect showing multiple homologs within a specific DNMT class. Some insect lineages were shown to lack one (e.g., *B. mori* and *T. castaneum*) or two (e.g., *D. melanogaster* and *A.gambiae*) classes of *DNMTs*, while others have multiple homologs (e.g., *A. mellifera*, *N. vitripennis* and *A. pisum*) within a certain *DNMT* class (Kunert et al., 2003; Marhold et al., 2004; Walsh et al., 2010; Xiang et al., 2010; Glastad et al., 2011; Feliciello et al., 2013).

The limited available literature on aphid *DNMTs* prompted an investigation into the baseline *DNMT* expression (i.e., expression of aphids not challenged with resistance) of South African RWA. It is widely assumed that the insect DNMTs have the same functions as their mammalian orthologs (Wang et al., 2006; Glastad et al., 2014). *DNA methyltransferase 3* (*DNMT3)* was the only gene of which the expression was significantly different between the two RWA biotypes. *DNMT3* has long been known as a *de novo* methyltransferase (Okano et al., 1999; Goll and Bestor, 2005), which establishes new methylation patterns by methylating previously unmethylated sites (Kunert et al., 2003; Schaefer and Lyko, 2007). The *DNMT3* expression of the virulent biotype used in this study, SAM, is down-regulated

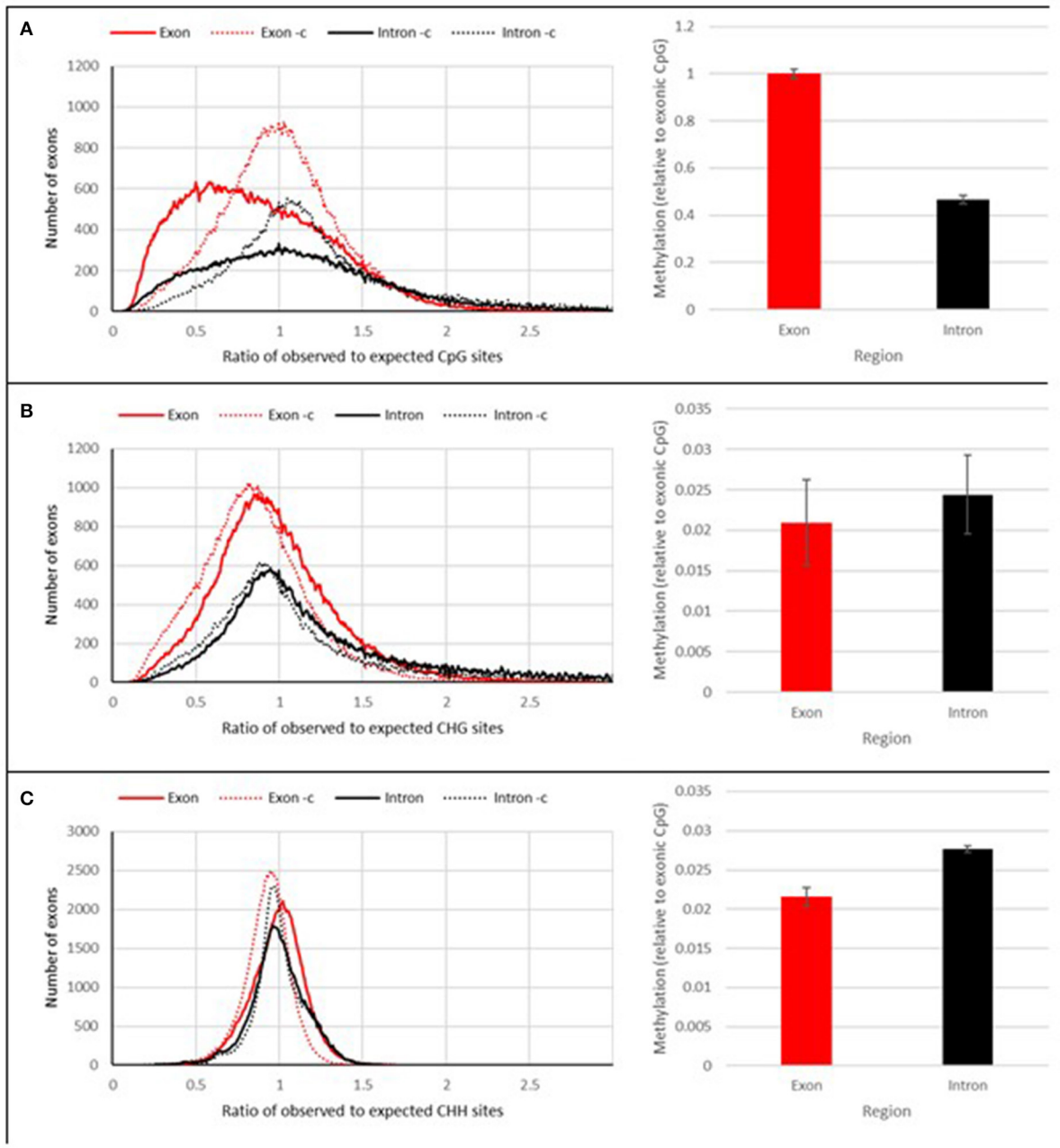

FIGURE 10 | DNA methylation context. The calculated observed over expected number of cytosine bases in the genome of RWA. **(A)**, $CpG_{(O/E)}$ **(B),** $CHG_{(O/E)}$, **(C)** $CHH_{(O/E)}$.

in comparison to the less virulent biotype, SA1, and this decrease in expression could therefore be advantageous from a virulence perspective.

A role for *DNMT3A* in the facilitation of transcription has also been identified, with *DNMT3A*-dependent methylation of gene bodies promoting transcription by antagonizing polycomb repression (Wu et al., 2010). Although the aphid effector genes are yet to be identified (Botha et al., 2005, 2014b), it is possible that they contain *DNMT3A* binding sites within their gene bodies, and that their transcription could be facilitated by *DNMT3A* binding and subsequent methylation. In the current study, SA1's *DNMT3A* expression, and therefore DNMT3A protein production, is up-regulated in comparison to the more virulent biotype. The fact that SA1 has higher *DNMT3A* expression (and perhaps greater effector protein production) under unchallenged conditions, may provide some insight into why SA1 is the least virulent biotype. Therefore, quantifying the *DNMT3A* expression of aphids challenged by resistance may

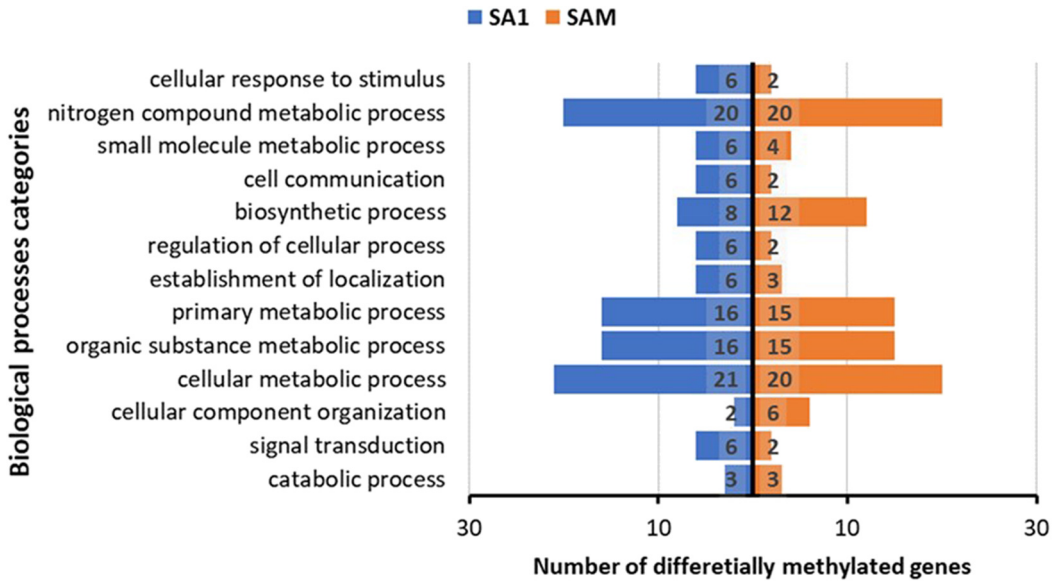

FIGURE 11 | Differentially methylated genes (DMEs) differ in numbers between the less virulent biotype SA1 and more virulent SAM when group in broad biological process categories.

yield valuable information on *DNMT3A*'s possible involvement in effector transcription.

Other functions of *DNMT3* include its role in the removal of 5mC and 5hmC (Chen et al., 2012, 2013) and a proposed involvement in the maintenance of methylation, by being able to "methylate sites missed by DNMT1 activity" (Jones and Liang, 2009). However, as the *DNMT3*-mediated removal of 5mC and 5hmC is dependent on certain redox conditions (Chen et al., 2012, 2013), and has only been shown to occur *in vitro* (Chen et al., 2012, 2013), it is difficult to draw conclusions regarding the *DNMT3* expression and its potential demethylating and dehydroxymethylating activities in RWA. The DNA methyltransferase 3 protein is assumed to help maintain methylation in densely methylated areas of mammalian genomes (Jones and Liang, 2009).

The hydroxylation of methylated cytosines by TET enzymes, resulting in the formation of 5hmC, is one of various active demethylation mechanisms (Tahiliani et al., 2009; Branco et al., 2012). The initial functional characterization of TETs was performed in mammals, which have three TET enzymes, namely TET1, TET2, and TET3 (Iyer et al., 2009; Tahiliani et al., 2009). In contrast to this, invertebrates possess only a single TET ortholog (Pastor et al., 2013; Wojciechowski et al., 2014), which has been identified in insects containing hydroxymethylation, including *A. mellifera* (Cingolani et al., 2013; Wojciechowski et al., 2014), *T. castaneum* (Feliciello et al., 2013), *N. vitripennis* (Pegoraro et al., 2016) and *D. melanogaster* (Dunwell et al., 2013). In 2014, Wojciechowski et al. functionally characterized the *A. mellifera* TET ortholog, AmTET, and concluded that, like the mammalian TETs, AmTET is capable of hydroxylating 5mC to form 5hmC. This provided the first evidence that TETs play a similar role in insects, as they do in mammals. The presence of measurable amounts of 5hmC in the RWA biotypes tested, suggests that at least one active demethylation pathway (i.e., hydroxylation of 5mC by TET) is present in RWA, as confirmed in the current study when we sequenced the *DnTET* ortholog. We then studied the expression of this gene in the RWA biotypes after challenging the aphids through differential feeding, as this was previously shown to be perceived as stressful (Burger et al., 2017). Interestingly, when SA1 feeds on wheat with an antibiotic mode of resistance (e.g., Tugela-*Dn1*), an oxidative burst (elevated H_2O_2) occurs at the feeding sites (Botha et al., 2014b; Burger et al., 2017), and the expression of *DnTET* more than doubles. Whereas, when SA1 feed on wheat expressing both antibiosis and antixenosis (e.g., Tugela-*Dn5*), not only is the aphid challenged by the elevated H_2O_2 but also by volatile substances that make the wheat unpalatable (Botha et al., 2014b), resulting in the tripling of *DnTET* expression. A similar trend is not observed with the expression of *DnTET* in SAM. Biotype SAM feeding, however, is not associated with an oxidative burst or increased peroxidase activity levels, because SAM "avoids" detection by wheat hosts (Botha et al., 2014a).

In the present study, we also studied the epigenome of RWA biotypes SA1 (least virulent SA biotype) and SAM (most virulent SA biotype). The whole-genome bisulfite sequencing indicated that the genomes of these biotypes were globally more methylated (i.e., 1.126 ± 0.321% for SA1; 1.105 ± 0.295% for SAM) than previously reported for insect genomes. For example, the global methylation levels of *A. mellifera* (Lyko et al., 2010), *B. mori* (Xiang et al., 2010), the ants *Camponotus floridanus* and *Harpegnathos saltator* (Bonasio et al., 2012) and *N. vitripennis* (Beeler et al., 2014) are all between 0.1 and 0.2%.

However, when quantified using the antibody-based methods, the global methylation levels (0.14–0.16%) are in line with other reports of insect methylation. Panikar et al. (2015) investigated adult *D. melanogaster* methylation, also through an

antibody-based method, found the adult *D. melanogaster* genome to be ∼0.5% methylated. Russian wheat aphids thus have low, but detectable levels of methylation which are ∼0.2 to 0.4-fold of that of the model organism *D. melanogaster*, as measured using the same technique, which allows a more direct comparison. Although other authors have reported lower levels of adult *D. melanogaster* methylation using bisulfite sequencing (0% – Lyko et al., 2000), liquid chromatography tandem mass spectrometry (0.034% – Capuano et al., 2014) and thin layer chromatography (0.05–0.1% – Gowher et al., 2000).

The sequence reads were analyzed for contexts of DNA methylation within the genome and the results revealed that RWA has methylation in all contexts (CpG, CHG and CHH), with the majority of methylation within the CpG context (±5.19%), but still notable methylation in the other contexts (CHG—± 0.27%; CHH—± 0.34%), with most of the methylation located in the genic regions. A similar finding was recently reported by Mathers et al. (2019) in the green peach aphid, *Myzus persicae*. The authors found that exons are highly enriched for methylated CpGs, particularly at the 3′ end of genes. Their findings also alludes to sex-biased differential methylation of genes involved in aphid sexual differentiation.

The model organisms, mice (*Mus musculus*) and zebra fish (*Danio rerio*), showed very low levels of CHH and CHG methylation (1% and lower) when compared to the 74.2% and 80.3% CpG methylation observed, respectively. Low levels of CHG (0.26%) and CHH (0.17%) were also reported for the honeybee (*Apis mellifera*) (Feng et al., 2010). In another insect example, the over expression of DNMT2-like protein in fruit flies (*Drosophila melanogaster*) resulted in observable CpT and CpA methylation (Kunert et al., 2003).

We also wanted to assess whether the DNA strands (top vs. bottom) were methylated equally and found that the top strands were slightly more methylated (0.06%) than the bottom ones. However, interestingly the difference between the methylation of the top and bottom strands were significantly more in the more virulent SAM (0.09%), than SA1 (0.02%). This was not an unexpected finding, as biotype SAM was previously found to exhibit the highest level of hemimethylation (at the external cytosine) when its methylation was investigated using the Methylation-Sensitive Amplification Polymorphism (MSAP) technique (Breeds et al., 2018). Hemimethylated DNA arises during DNA replication, as the newly synthesized daughter strand contains unmodified cytosines (Jeltsch, 2002; Goll and Bestor, 2005). When the levels of 5-hmC were measured using the antibody based method, earlier observations (Breeds et al., 2018) were confirmed, as the levels of 5hmC differed significantly between the aphid biotypes, with SAM much higher than that measured in the less virulent SA1 ($p < 0.05$; **Figure 9**).

Analysis of the 40 differentially methylated genes (DMEs) revealed that the less and more virulent biotypes had distinctly different DMEs. As previously indicated, DMEs in the more virulent biotype SAM include DMEs involved in the irinotecan metabolism where is it seemingly regulates the conversion between SN-38 and SN38G which regulates secretion. SN-38 produced in the body by carboxylesterase is the active metabolite of irinotecan (Fujita et al., 2015), with its mechanism of action thought to be its interaction with the cleavable complex of DNA and a nuclear protein topoisomerase I. This then results in a blockade of DNA replication (Hsiang and Liu, 1988; Hertzberg et al., 1989) which causes double-strand DNA breakage and cell death. This process may be linked to the metabolism of xenobiotics by cytochrome P450 and ascorbate and aldarate metabolism that may enable SAM to counter its feeding environment better than its parent, the less virulent SA1. In locusts, it was demonstrated that an ascorbate-recycling system in the midgut lumen can act as an effective antioxidant defense in caterpillars that feed on prooxidant-rich foods, emphasizing the importance of a defensive strategy in herbivorous insects based on the maintenance of conditions in the gut lumen that reduce or eliminate the potential prooxidant behavior of ingested phenols (Barbehenn et al., 2001). Interestingly, more virulent SAM also selectively methylates genes associated with steroid hormone biosynthesis and wax biosynthesis, both pathways producing chemicals that affect the physiological processes associated with insect development and insect survival (Niwa and Niwa, 2016). The less virulent SA1 have DMEs associated with the glutathione biosynthesis which may signal stress responses.

Collectively, the results suggest that RWA biotype SAM has a greater capacity to actively methylate/demethylate its DNA than its parent SA1. Thus, it can be concluded with fair confidence that SAM undergoes more methylation/demethylation than its parent biotype SA1. However, the question that remains is whether this ability to actively methylate/demethylate occurs at specific sets of genes depending on the environmental cue/stress RWA is faced with, as opposed to occurring globally (although global, genome-wide demethylation was measured). As gene bodies are the predominant sites of methylation in insects (Zemach et al., 2010; Glastad et al., 2011; Lyko and Maleszka, 2011), it is likely that it is in these regions that methylation will be removed. Also, removal of intragenic methylation of certain genes may alter the transcripts that are produced, by exposing cryptic binding sites or intragenic promoters (Maunakea et al., 2010; Hunt et al., 2013a) and/or affect the splice variants that are produced, through methylation's involvement in alternative splicing (Lyko and Maleszka, 2011; Shukla et al., 2011; Bonasio et al., 2012; Maunakea et al., 2013; Glastad et al., 2014; Yan et al., 2015). As demethylation can occur in a matter of hours (Glastad et al., 2011), the greater capability of SAM to demethylate its genome, may provide SAM with more flexibility to adapt to changing environments, and therefore may underlie SAM's ability to overcome plant resistance. However, this is an aspect that requires further investigation in future.

DATA AVAILABILITY STATEMENT

The whole epigenome sequencing data from SA1 (accession SRX4643785) and SAM (accession SRX4643786) were deposited to the National Center for Biotechnology Information (NCBI) (GEO SUBMISSION GSE119504) (https://www.ncbi.nlm.nih.gov/gds/?term=diuraphis%20noxia) with Bioproject number PRJNA489432.

AUTHOR CONTRIBUTIONS

A-MB conceived and designed the experiments as well as drafted the manuscript. Aphid rearing and sampling was performed by KB and NB. DNMT expression and TET expression was performed by KB and JT respectively, while DNMT and TET sequencing was performed by KB and HS, respectively. Alignments and phylogentic analyses of DNMT and TET sequences were performed by NB while 5mC and 5hmC analyses were performed by KB, NB, and A-MB. Whole genome bisulfite sequencing and its analysis was performed by PP and NB. All authors edited and reviewed the final manuscript.

SUPPLEMENTARY MATERIAL

The Supplementary Material for this article can be found online at: https://www.frontiersin.org/articles/10.3389/fgene.2020.00452/full#supplementary-material

REFERENCES

Altschul, S. F., Madden, T. L., Schäffer, A. A., Zhang, J., Zhang, Z., Miller, W., et al. (1997). Gapped BLAST and PSI-BLAST: a new generation of protein database search programs. *Nucleic Acids Res.* 25, 3389–3402. doi: 10.1093/nar/25.17.3389

Andrews, S. (2010). *FastQC: A Quality Control Tool for High Throughput Sequence Data*. Available online at: http://www.bioinformatics.babraham.ac.uk?/projects/fastqc/ (accessed October 6, 2011).

Aranda, P. S., LaJoie, D. M., and Jorcyk, C. L. (2012). Bleach gel: a simple agarose gel for analyzing RNA quality. *Electroph* 33, 366–369. doi: 10.1002/elps.201100335

Babu, C. V. S., and Gassmann, M. (2016). *Assessing Integrity of Plant RNA With the Agilent 2100 Bioanalyzer System*. Waldbronn: Agilent Technologies.

Barbehenn, R. V., Bumgarner, S. L. F.,Roosen, E., and Martin, M. M. (2001). Antioxidant defenses in caterpillars: role of the ascorbate-recycling system in the midgut lumen. *J. Insect Physiol.* 47, 349–357 doi: 10.1016/S0022-1910(00)00125-6

Becker, C., Weigel, D. (2015). Epigenetic variation: origin and transgenerational inheritance. *Curr. Opinion Plant Biol.* 15, 562–7. doi: 10.1016/j.pbi.2012.08.004

Beeler, S. M., Wong, G. T., Zheng, J. M., Bush, E. C., Remnant, E. J., Benjamin, P., et al. (2014). Whole-genome DNA methylation profile of the jewel wasp (*Nasonia vitripennis*). *G3* 4, 383–388. doi: 10.1534/g3.113.008953

Benjamini, V., and Hochberg, V. (1995). Controlling the false discovery rate: a practical and powerful approach to multiple testing. *J. R. Stat. Soc. B.* 57, 289–300. doi: 10.1111/j.2517-6161.1995.tb02031.x

Bolger, A. M., Lohse, M., and Usadel, B. (2014). Trimmomatic: a flexible trimmer for Illumina sequence data. *Bioinformatics* 30, 2114–2120. doi: 10.1093/bioinformatics/btu170

Bonasio, R., Li, Q., Lian, J., Mutti, N. S., Jin, L., Zhao, H., et al. (2012). Genome-wide and caste-specific DNA methylomes of the ants *Camponotus floridanus* and *Harpegnathos saltator*. *Curr. Biol.* 22, 1755–1764. doi: 10.1016/j.cub.2012.07.042

Botha, A.-M. (2013). A coevolutionary conundrum: the arms race between *Diuraphis noxia* (Kurdjumov) a specialist pest and its host *Triticum aestivum* (L.). *Arthropod Plant Interact.* 7, 359–372. doi: 10.1007/s11829-013-9262-3

Botha, A.-M., Burger, N. F. V., and van Eck, L. (2014a). Hypervirulent *Diuraphis noxia* (Hemiptera: Aphididae) biotype SAM avoids triggering defenses in its host (*Triticum aestivum*) (Poales: Poaceae) during feeding. *Environ. Entomol.* 43, 672–681. doi: 10.1603/EN13331

Botha, A.-M., Li, Y., and Lapitan, N. L. V. (2005). Cereal host interactions with Russian wheat aphid: a review. *J. Plant Interact.* 1, 211–222. doi: 10.1080/17429140601073035

Botha, A.-M., Swanevelder, Z. H., and Lapitan, N. L. V. (2010). Transcript profiling of wheat genes expressed during feeding by two different biotypes of *Diuraphis noxia*. *Environ. Entomol.* 39, 1206–1231. doi: 10.1603/EN09248

Botha, A.-M., van Eck, L., Burger, N. F. V., and Swanevelder, Z. H. (2014b). Near-isogenic lines of *Triticum aestivum* with distinct modes of resistance exhibit dissimilar transcriptional regulation during *Diuraphis noxia* feeding. *Biol. Open* 3, 1116–1126. doi: 10.1242/bio.201410280

Bradford, M. M. (1976). A rapid and sensitive method for the quantitation of microgram quantities of protein utilizing the principle of protein-dye binding. *Anal. Biochem.* 72, 248–254. doi: 10.1016/0003-2697(76)90527-3

Branco, M. R., Ficz, G., and Reik, W. (2012). Uncovering the role of 5-hydroxymethylcytosine in the epigenome. *Nat. Rev. Genet.* 13, 7–13. doi: 10.1038/nrg3080

Breeds, K., Burger, N. F. V., and Botha, A.-M (2018). New insights into the methylation status of virulent *Diuraphis noxia* (Hemiptera: Aphididae) biotypes. *J. Econ. Entomol.* 111, 1395–1403. doi: 10.1093/jee/toy039

Burd, J. D., Porter, D. R., Puterka, G. J., Haley, S. D., and Peairs, F. B. (2006). Biotypic variation among North American Russian wheat aphid (Homoptera: Aphididae) populations. *J. Econ. Entomol.* 99, 1862–1866. doi: 10.1093/jee/99.5.1862

Burger, N. F. V., and Botha, A. M. (2017). Genome of Russian wheat aphid an economically important cereal aphid. *Stand. Genomic Sci.* 12:90. doi: 10.1186/s40793-017-0307-6

Burger, N. F. V., Venter, E., and Botha, A.-M (2017). Profiling *Diuraphis noxia* (Hemiptera: Aphididae) transcript expression of the biotypes SA1 and SAM feeding on various *Triticum aestivum* varieties. *J. Econ. Entomol.* 110, 692–701. doi: 10.1093/jee/tow313

Capuano, F., Mülleder, M., Kok, R., Blom, H. J., and Ralser, M. (2014). Cytosine DNA methylation is found in *Drosophila melanogaster* but absent in *Saccharomyces cerevisiae*, *Schizosaccharomyces pombe*, and other yeast species. *Anal. Chem.* 86, 3697–3702. doi: 10.1021/ac500447w

Chen, C.-C., Wang, Y., and Shen, K. J. (2012). The mammalian *de novo* DNA methyltransferases DNMT3A and DNMT3B are also DNA 5-hydroxymethylcytosine dehydroxymethylases. *J. Biol. Chem.* 287, 33116–33121. doi: 10.1074/jbc.C112.406975

Chen, C.-C., Wang, Y., and Shen, K. J. (2013). DNA 5-methylcytosine demethylation activities of the mammalian DNA methyltransferases. *J. Biol. Chem.* 288, 9084–9091. doi: 10.1074/jbc.M112.445585

Cingolani, P., Cao, X., Khetani, R. S., Chen, C.-C., Coon, M., Sammak, A., et al. (2013). Intronic non-CG DNA hydroxymethylation and alternative mRNA splicing in honey bees. *BMC Genomics* 14:666. doi: 10.1186/1471-2164-14-666

Clua, A., Castro, A. M., Ramos, S., Gimenez, D. O., and Vasicek, A. (2004). The biological characteristics and distribution of the greenbug, *Schizaphis graminum*, and Russian wheat aphid, *Diuraphis noxia* (Hemiptera: Aphididae), in Argentina and Chile. *Eur. J. Entomol.* 101, 193–198. doi: 10.14411/eje.2004.024

Conesa, A., and Götz, S. (2008). Blast2GO: a comprehensive suite for functional analysis in plant genomics. *Int. J. Plant Genomics*. 2008:619832. doi: 10.1155/2008/619832

Conesa, A., Götz, S., García-Gómez, J. M., Terol, J., Talón, M., and Robles, M. (2005). Blast2GO: A universal tool for annotation, visualization and analysis in functional genomics research. *Bioinformatics* 21, 3674–3676. doi: 10.1093/bioinformatics/bti610

Delatte, B., Wang, F., Ngoc, L. V., Collignon, E., Bonvin, E., Deplus, R., et al. (2016). Transcriptome-wide distribution and function of RNA hydroxymethylcytosine. *Science* 351, 282–285. doi: 10.1126/science.aac5253

Dunwell, T. L., McGuffin, L. J., Dunwell, J. M., and Pfeifer, G. P. (2013). The mysterious presence of a 5-methylcytosine oxidase in the *Drosophila* genome. Possible explanations. *Cell Cycle* 12, 3357–3365. doi: 10.4161/cc.26540

Feliciello, I., Parazajder, J., Akrap, I., and Ugarković, D. (2013). First evidence of DNA methylation in insect *Tribolium castaneum*. Environmental regulation of DNA methylation within heterochromatin. *Epigenetics* 8, 534–541. doi: 10.4161/epi.24507

Feng, H., Conneely, K. N., and Wu, H. (2014). A Bayesian hierarchical model to detect differentially methylated loci from single nucleotide resolution sequencing data. *Nucl. Acids Res.* 42:e69. doi: 10.1093/nar/gku154

Feng, S., Cokus, S. J., Zhang, X., Chen, P.-Y., Bostick, M., Goll, M. G., et al. (2010). Conservation and divergence of methylation patterning in plants and animals. *Proc. Natl. Acad. Sci. U S A.* 107, 8689–8694. doi: 10.1073/pnas.1002720107

Fujita, K. I., Kubota, Y., Ishida, H., and Sasaki, Y. (2015). Irinotecan, a key chemotherapeutic drug for metastatic colorectal cancer. *World J. Gastroenterol.* 21, 12234–12248. doi: 10.3748/wjg.v21.i43.12234

Glastad, K. M., Hunt, B. G., and Goodisman, M. A. D. (2014). Evolutionary insights into DNA methylation in insects. *Curr. Opin. Insect Sci.* 1, 25–30. doi: 10.1016/j.cois.2014.04.001

Glastad, K. M., Hunt, B. G., Yi, S. V., and Goodisman, M. A. D. (2011). DNA methylation in insects: on the brink of the epigenomic era. *Insect Mol. Biol.* 20, 553–565. doi: 10.1111/j.1365-2583.2011.01092.x

Goll, M. G., and Bestor, T. H. (2005). Eukaryotic cytosine methyltransferases. *Annu. Rev. Biochem.* 74, 481–514. doi: 10.1146/annurev.biochem.74.010904.153721

Goll, M. G., Kirpekar, F., Maggert, K. A., Yoder, J. A., Hsieh, L., Zhang, X., et al. (2006). Methylation of $tRNA^{Asp}$ by the DNA methyltransferase homolog Dnmt2. *Science* 311, 395–398. doi: 10.1126/science.1120976

Gong, L., Cui, F., Sheng, C., Lin, Z., Reeck, G., Xu, J., et al. (2012). Polymorphism and methylation of four genes expressed in salivary glands of Russian wheat aphid (Homoptera: Aphididae). *J. Econ. Entomol.* 105, 232–241. doi: 10.1603/EC11289

Götz, S., Garcia-Gomez, J. M., Terol, J., Williams, T. D., Nagaraj, S. H., Nueda, M. J., et al. (2008). High-throughput functional annotation and data mining with the Blast2GO suite. *Nucleic Acids Res.* 36, 3420–3435 doi: 10.1093/nar/gkn176

Gowher, H., Leismann, O., and Jeltsch, A. (2000). DNA of *Drosophila melanogaster* contains 5-methylcytosine. *EMBO J.* 19, 6918–6923. doi: 10.1093/emboj/19.24.6918

Haas, B. J., Papanicolaou, A., Yassour, M., Grabherr, M., Blood, P. D., Bowden, J., et al. (2013). *De novo* transcript sequence reconstruction from RNA-seq using the Trinity platform for reference generation and analysis. *Nat. Prot.* 8:1494. doi: 10.1038/nprot.2013.084

Haley, S. D., Peairs, F. B., Walker, C. B., Rudolph, J. B., and Randolph, T. L. (2004). Occurrence of a new Russian wheat aphid biotype in Colorado. *Crop Sci.* 44, 1589–1592. doi: 10.2135/cropsci2004.1589

Hertzberg, R. P., Caranfa, M. J., Holden, K. G., Jakas, D. R., Gallagher, G., Mattern, M. R., et al. (1989). Modification of the hydroxyl lactone ring of camptothecin: inhibition of mammalian topoisomerase I and biological activity. *J. Med. Chem.* 32, 715–720. doi: 10.1021/jm00123a038

Hsiang, Y. H., and Liu, L. F. (1988). Identification of mammalian DMA topoisomerase I as an intercellular target of the anticancer drug camptothecin. *Cancer Res.* 48, 1722–1726.

Hunt, B. G., Brisson, J. A., Yi, S. V., and Goodisman, M. A. D. (2010). Functional conservation of DNA methylation in the pea aphid and the honeybee. *Genome Biol. Evol.* 2, 719–728. doi: 10.1093/gbe/evq057

Hunt, B. G., Glastad, K. M., Yi, S. V., and Goodisman, M. A. D. (2013a). Patterning and regulatory associations of DNA methylation are mirrored by histone modifications in insects. *Genome Biol. Evol.* 5, 591–598. doi: 10.1093/gbe/evt030

Hunt, B. G., Glastad, K. M., Yi, S. V., and Goodisman, M. A. D. (2013b). The function of intragenic DNA methylation: insights from insect epigenomes. *Integr. Comp. Biol.* 53, 319–328. doi: 10.1093/icb/ict003

Iyer, L. M., Abhiman, S., and Aravind, L. (2011). Natural history of eukaryotic DNA methylation systems. *Prog. Mol. Biol. Transl. Sci.* 101, 25–104. doi: 10.1016/B978-0-12-387685-0.00002-0

Iyer, L. M., Tahiliani, M., Rao, A., and Aravind, L. (2009). Prediction of novel families of enzymes involved in oxidative and other complex modifications of bases in nucleic acids. *Cell Cycle* 8, 1698–1710. doi: 10.4161/cc.8.11.8580

Jankielsohn, A. (2011). Distribution and diversity of Russian wheat aphid (Hemiptera: Aphididae) biotypes in South Africa and Lesotho. *J. Econ. Entomol.* 104, 1736–1741. doi: 10.1603/EC11061

Jankielsohn, A. (2016). Changes in the Russian wheat aphid (Hemiptera: Aphididae) biotype complex in South Africa. *J. Econ. Entomol.* 109, 907–912. doi: 10.1093/jee/tov408

Jeltsch, A. (2002). Beyond Watson and crick: DNA methylation and molecular enzymology of DNA methyltransferases. *Chembiochem* 3, 274–293. doi: 10.1002/1439-7633(20020402)3:4<274::AID-CBIC274>3.0.CO;2-S

Jeltsch, A., Nellen, W., and Lyko, F. (2006). Two substrates are better than one: dual specificities for Dnmt2 methyltransferases. *Trends Biochem. Sci.* 31, 306–308. doi: 10.1016/j.tibs.2006.04.005

Jones, P. A., and Liang, G. (2009). Rethinking how DNA methylation patterns are maintained. *Nat. Rev. Genet.* 10, 805–811. doi: 10.1038/nrg2651

Jurkowski, T. P., and Jeltsch, A. (2011). On the evolutionary origin of eukaryotic DNA methyltransferases and Dnmt2. *PLoS ONE* 6:e28104. doi: 10.1371/journal.pone.0028104

Katoh, K., and Standley, D. M. (2013). MAFFT multiple sequence alignment software version 7: improvements in performance and usability. *Mol. Biol. Evol.* 30, 772–780. doi: 10.1093/molbev/mst010

Kohli, R. M., and Zhang, Y. (2013). TET enzymes, TDG and the dynamics of DNA demethylation. *Nature* 502, 472–479. doi: 10.1038/nature12750

Krueger, F., and Andrews, S. R. (2011). Bismark: a flexible aligner and methylation caller for bisulfite-seq applications. *Bioinformatics* 27, 1571–1572. doi: 10.1093/bioinformatics/btr167

Kunert, N., Marhold, J., Stanke, J., Stach, D., and Lyko, F. (2003). A Dnmt2-like protein mediates DNA methylation in *Drosophila*. *Development* 130, 5083–5090. doi: 10.1242/dev.00716

Langmead, B., and Salzberg, S. L. (2012). Fast gapped-read alignment with Bowtie 2. *Nat. Method* 9:357. doi: 10.1038/nmeth.1923

Li, B., and Dewey, C. N. (2011). RSEM: accurate transcript quantification from RNA-Seq data with or without a reference genome. *BMC Bioinform.* 12:323. doi: 10.1186/1471-2105-12-323

Lyko, F., Foret, S., Kucharski, R., Wolf, S., Falckenhayn, C., and Maleszka, R. (2010). The honey bee epigenomes: differential methylation of brain DNA in queens and workers. *PLoS Biol.* 8:e1000506. doi: 10.1371/journal.pbio.1000506

Lyko, F., and Maleszka, R. (2011). Insects as innovative models for functional studies of DNA methylation. *Trends Genet.* 27, 127–131. doi: 10.1016/j.tig.2011.01.003

Lyko, F., Ramsahoye, B. H., Jaenisch, R. (2000). DNA methylation in Drosophila melanogaster. *Nature* 408, 538–540. Available online at: https://www.nature.com/articles/35046205

Marhold, J., Rothe, N., Pauli, A., Mund, C., Kuehle, K., Brueckner, B., et al. (2004). Conservation of DNA methylation in dipteran insects. *Insect Mol. Biol.* 13, 117–123. doi: 10.1111/j.0962-1075.2004.00466.x

Mathers, T. C., Mugford, T. S., Percival-Alwyn, L. Y., Chen, K., and Swarbreck, D. (2019). Sex-specific changes in the aphid DNA methylation landscape. *Mol. Ecol.* 28, 4228–4241. doi: 10.1111/mec.15216

Maunakea, A. K., Chepelev, I., Cui, K., and Zhao, K. (2013). Intragenic DNA methylation modulates alternative splicing by recruiting MeCP2 to promote exon recognition. *Cell Res.* 23, 1256–1269. doi: 10.1038/cr.2013.110

Maunakea, A. K., Nagarajan, R. P., Bilenky, M., Ballinger, T. J., D'Souza, C., Fouse, S. D., et al. (2010). Conserved role of intragenic DNA methylation in regulating alternative promoters. *Nature* 466, 253–257. doi: 10.1038/nature09165

Niwa, Y. S., and Niwa, R. (2016). Transcriptional regulation of insect steroid hormone biosynthesis and its role in controlling timing of molting and metamorphosis. *Dev. Growth Differ.* 58, 94–105. doi: 10.1111/dgd.12248

Okano, M., Bell, D. W., Haber, D. A., and Li, E. (1999). DNA methyltransferases Dnmt3a and Dnmt3b are essential for *de novo* methylation and mammalian development. *Cell* 99, 247–257. doi: 10.1016/S0092-8674(00)81656-6

Panikar, C. S., Rajpathak, S. N., Abhyankar, V., Deshmukh, S., and Deobagkar, D. D. (2015). Presence of DNA methyltransferase activity and CpC methylation in *Drosophila melanogaster*. *Mol. Biol. Rep.* 42, 1615–1621. doi: 10.1007/s11033-015-3931-5

Pastor, W. A., Aravind, L., and Rao, A. (2013). TETonic shift: biological roles of TET proteins in DNA demethylation and transcription. *Nat. Rev. Mol. Cell Biol.* 14, 341–356. doi: 10.1038/nrm3589

Pegoraro, M., Bafna, A., Davies, N. J., Shuker, D. M., and Tauber, E. (2016). DNA methylation changes induced by long and short photoperiods in *Nasonia*. *Genome Res.* 26, 203–210. doi: 10.1101/gr.196204.115

Pfaffl, M. W. (2001). A new mathematical model for relative quantification in real-time RT–PCR. *Nucleic Acids Res.* 29:e45. doi: 10.1093/nar/29.9.e45

Raddatz, G., Guzzardob, P. M., Olovac, N., Fantappied, M. R., Ramppe, M., Schaefera, M., et al. (2013). Dnmt2-dependent methylomes lack defined

DNA methylation patterns. *Proc. Natl. Acad. Sci. U.S.A.* 110, 8627–8631. doi: 10.1073/pnas.1306723110

Randolph, T. L., Peairs, F., Weiland, A., Rudolph, J. B., and Puterka, G. J. (2009). Plant responses to seven Russian wheat aphid (Hemiptera: Aphididae) biotypes found in the United States. *J. Econ. Entomol.* 102, 1954–1959. doi: 10.1603/029.102.0528

Rasmussen, E. M. K., Vågbø, C. B., Münch, D., Krokan, H. E., Klungland, A., Amdam, G. V., et al. (2016). DNA base modifications in honey bee and fruit fly genomes suggest an active demethylation machinery with species- and tissue-specific turnover rates. *Biochem. Biophys. Rep*. 6, 9–15. doi: 10.1016/j.bbrep.2016.02.011

Robinson, M. D., McCarthy, D. J., and Smyth, G. K. (2010). edgeR: a Bioconductor package for differential expression analysis of digital gene expression data. *Bioinform* 26, 139–140. doi: 10.1093/bioinformatics/btp616

Rozen, S., and Skaletsky, H. (2000). "Primer3 on the WWW for general users and for biologist programmers," in *Bioinformatics Methods and Protocols*, edited by S. Misener and S. A. Krawetz (Totowa, NJ: Humana Press), 365–386. doi: 10.1385/1-59259-192-2:365

Rylatt, D. B. and Parish, C. R. (1982). Protein determination on an automatic spectrophotometer. *Anal. Biochem.* 121, 213–214. doi: 10.1016/0003-2697(82)90578-4

Schaefer, M., and Lyko, F. (2007). DNA methylation with a sting: an active DNA methylation system in the honeybee. *BioEssays* 29, 208–211. doi: 10.1002/bies.20548

Shakesby, A. J., Wallace, I. S., Isaacs, H. V., Pritchard, J., Roberts, D. M., and Douglas, A. E. (2009). A water-specific aquaporin involved in aphid osmoregulation. *Insect Biochem. Mol. Biol.* 39, 1–10. doi: 10.1016/j.ibmb.2008.08.008

Shen, L., Song, C. X., He, C., and Zhang, Y. (2014). Mechanism and function of oxidative reversal of DNA and RNA methylation. *Annu. Rev. Biochem*. 83, 585–614. doi: 10.1146/annurev-biochem-060713-035513

Shufran, K. A., and Payton, T. L. (2009). Limited genetic variation within and between Russian wheat aphid (Hemiptera: Aphididae) biotypes in the United States. *J. Econ. Entomol.* 102, 440–445. doi: 10.1603/029.102.0157

Shukla, S., Kavak, E., Gregory, M., Imashimizu, M., Shutinoski, B., Kashlev, M., et al. (2011). CTCF-promoted RNA polymerase II pausing links DNA methylation to splicing. *Nature* 479, 74–79. doi: 10.1038/nature10442

Sievers, F., Wilm, A., Dineen, D., Gibson, T. J., Karplus, K., Li, W., et al. (2011). Fast, scalable generation of high-quality protein multiple sequence alignments using Clustal Omega. *Mol. Syst. Biol.* 7:539. doi: 10.1038/msb.2011.75

Simão, F. A., Waterhouse, R. M., Ioannidis, P., Kriventseva, E. V., and Zdobnov, E. M. (2015). BUSCO: assessing genome assembly and annotation completeness with single-copy orthologs. *Bioinformatics* 31, 3210–3212. doi: 10.1093/bioinformatics/btv351

Sinha, D. K., and Smith, C. M. (2014). Selection of reference genes for expression analysis in *Diuraphis noxia* (Hemiptera: Aphididae) fed on resistant and susceptible wheat plants. *Sci. Rep*. 4:5059. doi: 10.1038/srep05059

Smith, C. M., and Clement, S. L. (2012). Molecular bases of plant resistance to arthropods. *Annu. Rev. Entomol.* 57, 309–328. doi: 10.1146/annurev-ento-120710-100642

Stanke, M., Schöffmann, O., Morgenstern, B., and Waack, S. (2006). Gene prediction in eukaryotes with a generalized hidden Markov model that uses hints from external sources. *BMC Bioinform*. 7:62. doi: 10.1186/1471-2105-7-62

Sunita, S., Tkaczuk, K. L., Purta, E., Kasprzak, J. M., Douthwaite, S., Bujnicki, J. M., et al. (2008). Crystal structure of the *Escherichia coli* 23S rRNA:m5C methyltransferase RlmI (YccW) reveals evolutionary links between RNA modification enzymes. *J. Mol. Biol.* 383, 652–666. doi: 10.1016/j.jmb.2008.08.062

Swanevelder, Z. H., Surridge, A. K. J., Venter, E., and A.-Botha, M. (2010). Limited endosymbiont variation in *Diuraphis noxia* (Hemiptera: Aphididae) biotypes from the United States and South Africa. *J. Econ. Entomol.* 103, 887–897. doi: 10.1603/ec09257

Tagu, D., Klingler, J. P., Moya, A., and Simon, J.-C. (2008). Early progress in aphid genomics and consequences for plant-aphid interactions studies. *Mol. Plant Microbe Interact*. 21, 701–708. doi: 10.1094/MPMI-21-6-0701

Tahiliani, M., Koh, K. P., Shen, Y., Pastor, W. A., Bandukwala, H., Brudno, Y., et al. (2009). Conversion of 5-methylcytosine to 5-hydroxymethylcytosine in mammalian DNA by MLL partner TET1. *Science* 324, 930–935. doi: 10.1126/science.1170116

Tolmay, V. L., Lindeque, R. C., and Prinsloo, G. J. (2007). Preliminary evidence of a resistance-breaking biotype of the Russian wheat aphid, *Diuraphis noxia* (Kurdjumov) (Homoptera: Aphididae), in South Africa. *Afr. Entomol.* 15, 228–230. doi: 10.4001/1021-3589-15.1.228

Tolmay, V. L., van Lill, D., and Smith, M. F. (1997). The influence of Demeton-S-Methyl/Parathion and Imidacloprid on the yield and quality of Russian wheat aphid resistant and susceptible wheat cultivars. *S. Afr. J. Plant Soil* 14, 107–111. doi: 10.1080/02571862.1997.10635091

Van der Auwera, G. A., Carneiro, M. O., Hartl, C., Poplin, R., del Angel, G., Levy-Moonshine, A., et al. (2013). From FastQ data to high-confidence variant calls: the genome analysis toolkit best practices pipeline. *Curr. Prot. Bioinform*. 43, 11–10. doi: 10.1002/0471250953.bi1110s43

Wald, A. (1943). Tests of statistical hypotheses concerning several parameters when the number of observations is large. *Trans. Am. Math. Soc*. 54, 426–482. doi: 10.1090/S0002-9947-1943-0012401-3

Walsh, T. K., Brisson, J. A., Robertson, K., Gordon, K., Jaubert-Possamai, S., Tagu, D., et al. (2010). A Functional DNA methylation system in the pea aphid, *Acyrthosiphum pisum*. *Insect Mol. Biol.* 19, 215–228. doi: 10.1111/j.1365-2583.2009.00974.x

Walters, M. C., Penn, F., du Toit, F., Botha, T. C., and Aalbersberg, K. (1980). The Russian wheat aphid. Farming in South Africa, Leaflet series, wheat. *G3*, 1–6.

Wang, Y., Jorda, M., Jones, P. L., Maleszka, R., Ling, X., Robertson, H. M., et al. (2006). Functional CpG methylation system in a social insect. *Science* 314, 645–647. doi: 10.1126/science.1135213

Wojciechowski, M., Rafalski, D., Kucharski, R., Misztal, K., Maleszka, J., Bochtler, M., et al. (2014). Insights into DNA hydroxymethylation in the honeybee from in-depth analyses of TET dioxygenase. *Open Biol.* 4:140110. doi: 10.1098/rsob.140110

Wu, H., Coskun, V., Tao, J., Xie, W., Ge, W., Yoshikawa, K., et al. (2010). Dnmt3a-dependent nonpromoter DNA methylation facilitates transcription of neurogenic genes. *Science* 329, 444–448. doi: 10.1126/science.1190485

Wu, H., Xu, T., Feng, H., Chen, L., Li, B., Yao, B., et al. (2015). Detection of differentially methylated regions from whole-genome bisulfite sequencing data without replicates. *Nucleic Acids Res.* 43:e141. doi: 10.1093/nar/gkv715

Xiang, H., Zhu, J., Chen, Q., Dai, F., Li, X., Li, M., et al. (2010). Single base-resolution methylome of the silkworm reveals a sparse epigenomic map. *Nat. Biotechnol.* 28, 516–520. doi: 10.1038/nbt.1626

Yan, H., Bonasio, R., Simola, D. F., Liebig, J., Berger, S. L., and Reinberg, D. (2015). DNA methylation in social insects: how epigenetics can control behavior and longevity. *Annu. Rev. Entomol.* 60, 435–452. doi: 10.1146/annurev-ento-010814-020803

Zemach, A., McDaniel, I. E., Silva, P., and Zilberman, D. (2010). Genome-wide evolutionary analysis of eukaryotic DNA methylation. *Science* 328, 916–919. doi: 10.1126/science.1186366

Conflict of Interest: The authors declare that the research was conducted in the absence of any commercial or financial relationships that could be construed as a potential conflict of interest.

frontiers in Genetics

ORIGINAL RESEARCH
published: 26 June 2020
doi: 10.3389/fgene.2020.00636

Poly(A) Binding Protein Is Required for Nuclear Localization of the Ecdysteroidogenic Transcription Factor Molting Defective in the Prothoracic Gland of *Drosophila melanogaster*

*Takumi Kamiyama[1], Wei Sun[2,3], Naoki Tani[4], Akira Nakamura[4] and Ryusuke Niwa[3]**

[1]Graduate School of Life and Environmental Sciences, University of Tsukuba, Tsukuba, Japan, [2]Laboratory of Evolutionary and Functional Genomics, School of Life Sciences, Chongqing University, Chongqing, China, [3]Life Science Center for Survival Dynamics, Tsukuba Advanced Research Alliance (TARA), University of Tsukuba, Tsukuba, Japan, [4]Department of Germline Development, Institute of Molecular Embryology and Genetics, Kumamoto University, Kumamoto, Japan

OPEN ACCESS

Edited by:
Wei Guo,
Institute of Zoology (CAS), China

Reviewed by:
Xavier Belles,
Instituto de Biología Evolutiva (IBE), Spain
Shun-Fan Wu,
Nanjing Agricultural University, China

***Correspondence:**
Ryusuke Niwa
ryusuke-niwa@tara.tsukuba.ac.jp

Specialty section:
This article was submitted to Epigenomics and Epigenetics, a section of the journal Frontiers in Genetics

Received: *19 February 2020*
Accepted: *26 May 2020*
Published: *26 June 2020*

Citation:
Kamiyama T, Sun W, Tani N, Nakamura A and Niwa R (2020) Poly(A) Binding Protein Is Required for Nuclear Localization of the Ecdysteroidogenic Transcription Factor Molting Defective in the Prothoracic Gland of Drosophila melanogaster. Front. Genet. 11:636. doi: 10.3389/fgene.2020.00636

Steroid hormone signaling contributes to the development of multicellular organisms. In insects, ecdysteroids, like ecdysone and the more biologically-active derivative 20-hydroxyecdysone (20E), promote molting and metamorphosis. Ecdysone is biosynthesized in the prothoracic gland (PG), *via* several steps catalyzed by ecdysteroidogenic enzymes that are encoded by Halloween genes. The spatio-temporal expression pattern of ecdysteroidogenic genes is strictly controlled, resulting in a proper fluctuation of the 20E titer during insect development. However, their transcriptional regulatory mechanism is still elusive. A previous study has found that the polyadenylated tail [poly(A)] deadenylation complex, called Carbon catabolite repressor 4-Negative on TATA (CCR4-NOT) regulates the expression of *spookier* (*spok*), which encodes one of the ecdysteroidogenic enzymes in the fruit fly *Drosophila melanogaster*. Based on this finding, we speculated whether any other poly(A)-related protein also regulates *spok* expression. In this study, we reported that poly(A) binding protein (Pabp) is involved in *spok* expression by regulating nuclear localization of the transcription factor molting defective (Mld). When *pabp* was knocked down specifically in the PG by transgenic RNAi, both *spok* mRNA and Spok protein levels were significantly reduced. In addition, the *spok* promoter-driven green fluorescence protein (GFP) signal was also reduced in the *pabp*-RNAi PG, suggesting that Pabp is involved in the transcriptional regulation of *spok*. We next examined which transcription factors are responsible for Pabp-dependent transcriptional regulation. Among the transcription factors acting in the PG, we primarily focused on the zinc-finger transcription factor Mld, as Mld is essential for *spok* transcription. Mld was localized in the nucleus of the control PG cells, while Mld abnormally accumulated in the cytoplasm

of *pabp*-RNAi PG cells. In contrast, *pabp*-RNAi did not affect the nuclear localization of other transcription factors, including ventral vein lacking (Vvl) and POU domain motif 3 (Pdm3), in PG cells. From these results, we propose that Pabp regulates subcellular localization in the PG, specifically of the transcription factor Mld, in the context of ecdysone biosynthesis.

Keywords: poly(A) binding protein, nuclear localization, insect development, ecdysone biosynthesis, Halloween gene

INTRODUCTION

Ecdysteroids, like ecdysone and the more biologically-active derivative 20-hydroxyecdysone (20E), regulate several biological events in insects (Niwa and Niwa, 2014; Uryu et al., 2015). The 20-hydroxyecdysone titers are temporally changed during insect development, where proper fluctuations of 20E titers are essential for insect development (Riddiford, 1993; Nijhout, 1994; Bellés, 2020). Ecdyone is biosynthesized in an endocrine organ named the prothoracic gland (PG) *via* several steps catalyzed by step-specific enzymes (Niwa and Niwa, 2014). The enzymes are encoded by a group of genes often called the Halloween gene (Rewitz et al., 2007). Therefore, the regulation of ecdysteroidogenic genes expression is essential to achieve proper fluctuations of 20E titers (Niwa and Niwa, 2016). However, the molecular mechanism by which the expression of ecdysteroidogenic genes is regulated is yet to be fully elucidated.

Previously, we have reported that polyadenylated tail [poly(A)] degradation complex, called Carbon catabolite repressor 4-Negative on TATA (CCR4-NOT) is involved in the regulation of ecdysteroidogenic gene expression in the fruit fly *Drosophila melanogaster* (Zeng et al., 2018). By knocking down the gene *phosphoglycerate kinase promoter directed over production* (*Pop2*), which encodes a vital component of the CCR4-NOT complex, specifically in the PG, *D. melanogaster* animals show a larval-arrested phenotype. Furthermore, the expression levels of some ecdysteroidogenic genes are strongly decreased in these animals. Based on this finding, we hypothesized that other poly(A) related protein(s) may also contribute to the expression of ecdysteroidogenic genes.

In this study, we revealed that poly(A) binding protein (Pabp) contributes to the expression of ecdysteroidogenic genes. The knockdown of the *pabp* gene in the PG caused first instar-arrest and a decrease in ecdysteroidogenic gene expression, especially *spookier* (*spok*). Interestingly, the nuclear localization of the transcription factor molting defective (Mld), a transcriptional activator of *spok*, was disrupted in PG cells of *pabp*-RNAi larvae. Our results suggest that Pabp positively regulates ecdysteroidogenic gene expression by regulating ecdysteroidogenic transcription factors.

MATERIALS AND METHODS

D. melanogaster Strains

D. melanogaster flies were reared on a standard agar-cornmeal medium at 25 or 17°C under a 12:12 h light/dark cycle. w^{1118} served as a control strain. *phm-GAL4#22* (a gift from Michael B. O'Connor, University of Minnesota, MN; McBrayer et al., 2007; Yamanaka et al., 2013) was used as the strain to drive forced gene expression in the PG. *UAS-dicer2* (#24650) was obtained from the Bloomington *Drosophila* Stock Center. *UAS-pabp-IR* (#22007) and *UAS-mld-IR* (#17329) were obtained from the Vienna *Drosophila* Resource Center. Transgenic RNAi experiments were conducted by crossing these *UAS RNAi* lines with *w*, *UAS-dicer2*, and *phm-GAL4#22/TM6 Ubi-GFP*. A strain carrying the 1.45 kb *spok* promoter-fused GFP cassette (*spok>GFP*) was previously described (Komura-Kawa et al., 2015).

Generating Anti-Mld Antibody

Rabbit polyclonal anti-Mld antibody was raised against the peptide: NH_2-MSANRRRRSASAASSIAAET-COOH, which corresponds to 1–20 amino acid residues of the mature Mld protein (Neubueser et al., 2005).

Immunostaining

Immunostaining of prothoracic glands was performed as described previously (Imura et al., 2017). Briefly, dissected larval tissues were fixed in 3.7% formaldehyde in phosphate-buffered saline (PBS) for 30 min at room temperature. Samples were then washed with PBS + 0.3% Triton X-100 (Nacalai tesque, Kyoto Japan) and incubated overnight at 4°C with primary antibodies: rabbit anti-Mld antibody (1:200), guinea pig anti-*Spok* antibody (1:200; Gibbens et al., 2011), rabbit anti-Phantom (Phm) antibody (1:200; Parvy et al., 2005), rat anti-Ventral vein lacking (Vvl) antibody (1:3,000; Anderson et al., 1995), and guinea pig anti-POU domain motif 3 (Pdm3; 1:100; Chen et al., 2012). As fluorescent secondary antibodies, we used goat anti-guinea pig Alexa Fluor 488 (Life Technologies, Carlsbad, CA, USA) and goat anti-rabbit Alexa Fluor 555 (Life Technologies, Carlsbad, CA, USA). The secondary antibodies were diluted 1:200 and incubated for 2.5 h at room temperature. Nuclear stains used in this study were 4',6-diamidino-2-phenylindole (DAPI; Sigma-Aldrich, St. Louis, MO, USA) and TOPRO3 (Thermo Fisher Scientific, Waltham, MA, USA). For DAPI staining, after the incubation with the secondary antibodies, the samples were washed and then incubated with 1 μg/ml (final concentration) of DAPI for 1 h. For TOPRO3 staining, the samples were incubated with the secondary antibodies along with 10 μg/ml (final concentration) of RNase A (Takara Bio, Kusatsu, Japan). The samples were then washed, followed by the 1-h incubation with 10 μm TOPRO3 (Thermo Fisher Scientific, Waltham, MA, USA). Confocal images were captured using the LSM 700 laser scanning confocal microscope (Carl Zeiss, Oberkochen, Germany). Images were processed using the ImageJ software (Schneider et al., 2012).

Quantitative Reverse Transcription-Polymerase Chain Reaction

RNA was isolated from the whole bodies of the second instar larvae using the RNAiso Plus reagent (TaKaRa, Shiga, Japan). Genomic DNA digestion and cDNA synthesis were performed using the ReverTra Ace qPCR RT Kit (TOYOBO, Tokyo, Japan). Quantitative reverse transcription-polymerase chain reaction (qRT-PCR) was performed using the THUNDERBIRD SYBR qPCR Mix (TOYOBO, Tokyo, Japan) with a Thermal Cycler Dic TP800 System (TaKaRa, Shiga, Japan). Serial dilutions of a plasmid containing the open reading frame (ORF) of each gene were used as a standard. The expression levels of the target genes were normalized to an endogenous control *ribosomal protein 49* (*rp49*) in the same sample. Primers amplifying *noppera-bo* (*nobo*), *neverland* (*nvd*), *shroud* (*sro*), *spok*, *phm*, *disembodied* (*dib*), *shadow* (*sad*), and *rp49* have been described previously (McBrayer et al., 2007; Niwa et al., 2010; Enya et al., 2014).

GFP Reporter Assay

A *spok* promoter-driven GFP reporter assay was performed as described previously (Komura-Kawa et al., 2015). Briefly, *spok>GFP/CyO Act-GFP*; *UAS-deicer2*, *phm22-GAL4/TM6 Ubi-GFP* was established and crossed with *UAS-pabp-IR*. Eggs were laid on grape plates with yeast pastes at 25°C for 2 h. The GFP-negative first instar larvae were picked up and transferred into vials with standard cornmeal food. They were dissected 60 h after egg laying (AEL) and then immunostained.

RESULTS

Pabp Plays an Essential Role in the PG During Larval Development

To examine the importance of Pabp in the PG, we observed the developmental progress of *pabp*-RNAi larvae, for which we used a PG-specific driver (*phm22-GAL4*, hereafter *phm>*) to knock down *pabp* expression by transgenic RNAi. We found that PG-specific *pabp*-RNAi caused a larval-arrest phenotype. Eighty eight percent of *phm>pabp*-RNAi animals were arrested at the second larval instar and even 132 h AEL or later, while only few animals molted into the third larval instar or pupariated at the same time point (**Figures 1A–C**). The arrested second instar larvae failed to pupariate and died. This result suggests that the Pabp function in the PG is essential for larval development.

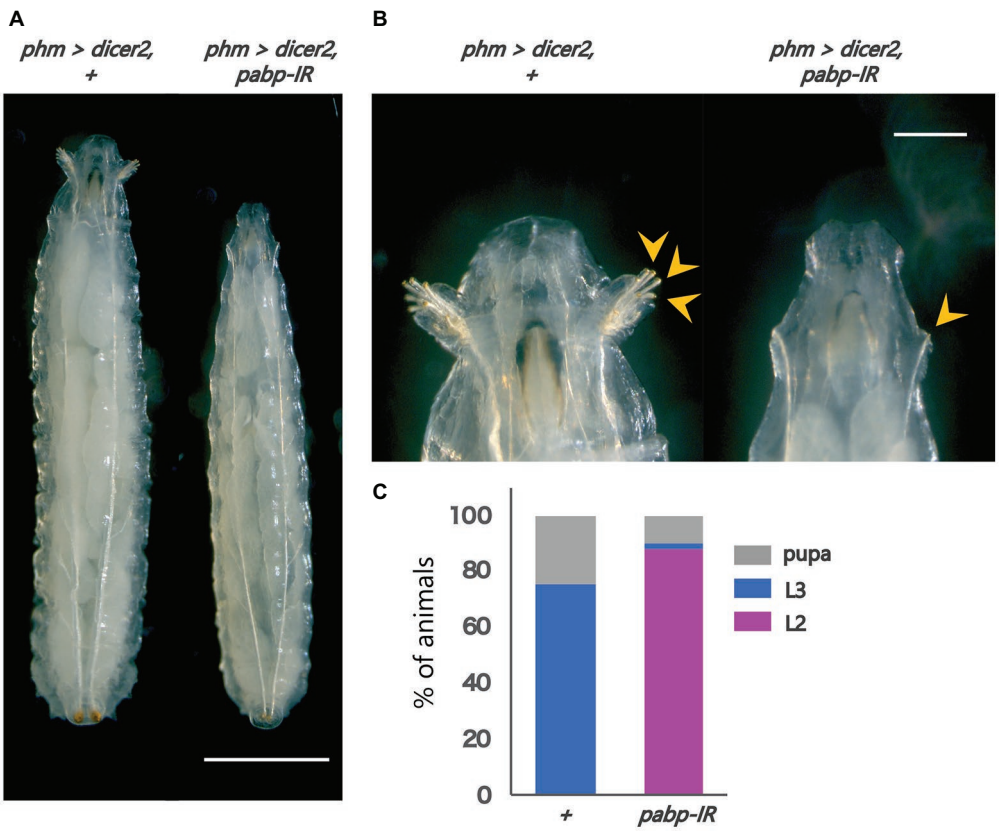

FIGURE 1 | Pabp function is required in the PG for larval development. Phenotypes caused by PG-specific *pabp*-RNAi at 132 h AEL. **(A)** Whole bodies of the control and RNAi larvae. Scale bar: 5 mm **(B)** Magnified intensity of **Figure 1A**. Scale bar: 2 mm. (Left) *phm>dicer2*, + larvae molted in the third larval instar as judged by the branched morphology of the anterior tracheal pits (yellow arrowheads), typical features of third instar larvae. (Right) *phm>dicer2*, *pabp-IR* larvae raised at the second larval instar and exhibit singular insertions of anterior tracheal pits. **(C)** The developmental progression of *phm>dicer2*, + (N = 41) and *phm>dicer2*, and *pabp-IR* (N = 49) animals at 132 h AEL. L2: second instar larva, L3: third instar larva.

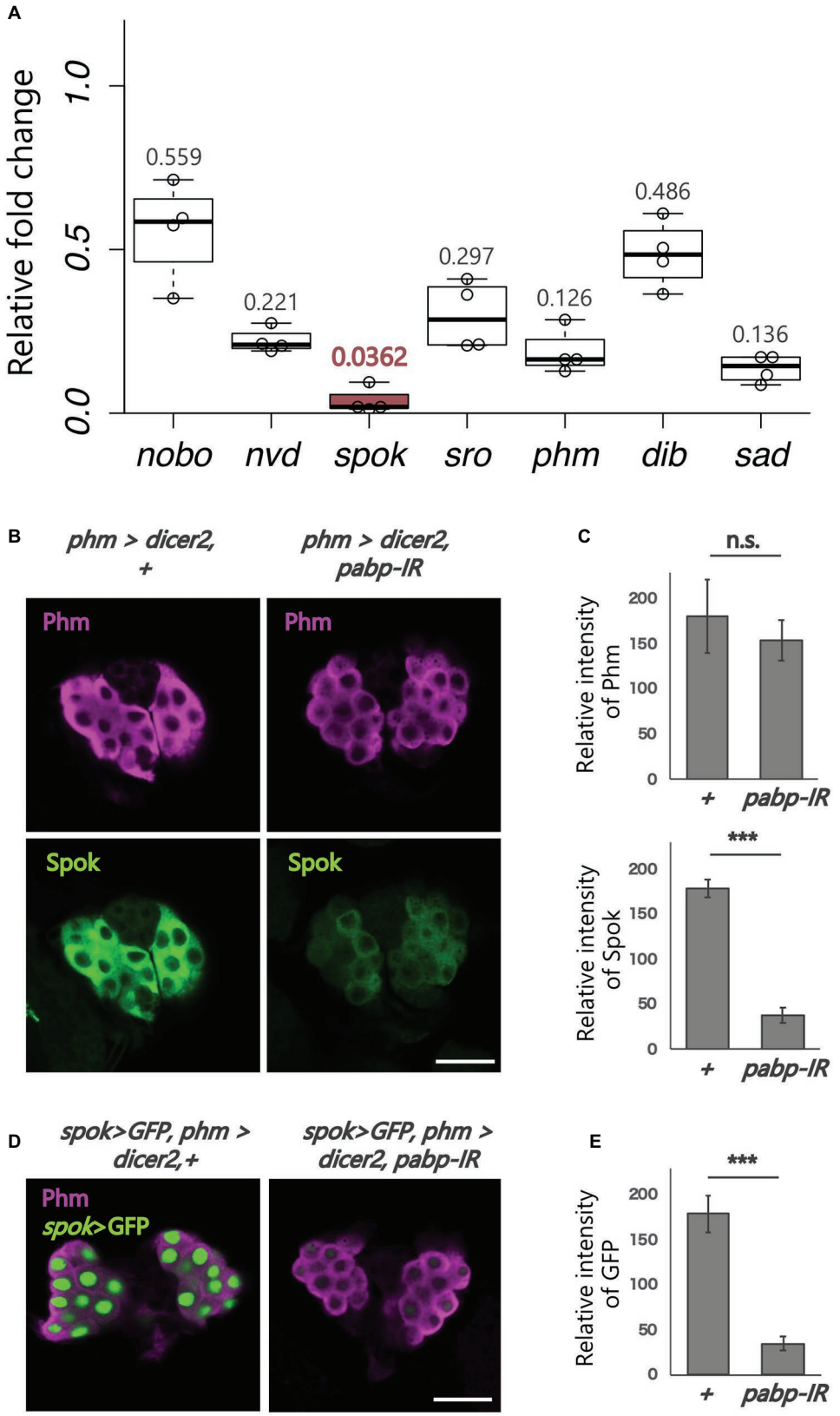

FIGURE 2 | Continued

FIGURE 2 | Expression analysis of ecdysteroidogenic genes. All photos are single-plane confocal images. **(A)** Relative expression levels of seven ecdysteroidogenic genes in *phm>dicer2*, *pabp-IR* at 60 h AEL compared to controls (*phm>dicer2*, +) based on the quantitative reverse transcription-polymerase chain reaction (qRT-PCR; $N = 4$). RNA was isolated from the whole bodies of the second instar larvae. **(B)** Immunostaining of the PG cells from *phm>dicer2*, + and *phm>dicer2*, and *pabp-IR* second instar larvae at 60 h AEL with antibodies against Phm (magenta) and Spok (green). **(C)** Quantifications of fluorescence intensities of Phm and Spok in the PG (each $N = 3$). Error bars represent standard deviations. *** and n.s. indicate $p < 0.001$ and non-significance ($p > 0.05$), respectively, by Student's *t*-test. **(D)** Fluorescence images of the PG cells from *phm>dicer2*, + and *phm>dicer2*, *pabp-IR* larvae with *spok* enhancer/promoter-driven nuclear localized-GFP construct (*spok>GFP*) at 60 h AEL. **(E)** Quantification of GFP fluorescence intensity in the PG nuclei ($N = 4$). The bar plots are drawn in the same manner as **(C)**. PG cells are immunostained with anti-Phm antibody (magenta). Scale bar: 20 μm.

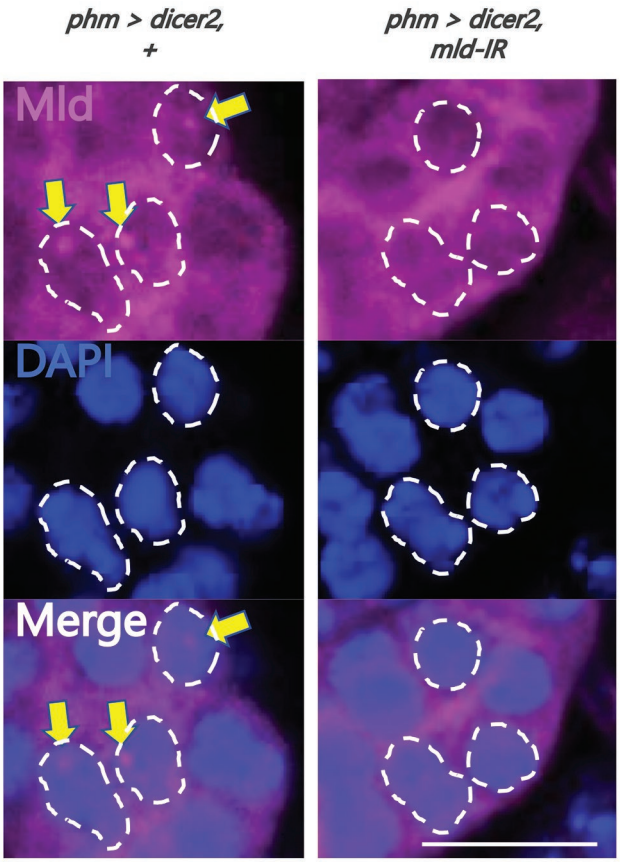

FIGURE 3 | Evaluation of newly-generated anti-molting defective (Mld) antibody. Magnified image of prothoracic gland (PG) cells. All photos are single-plane confocal images. Tissues were stained with anti-Mld antibody (magenta) and 4',6-diamidino-2-phenylindole (DAPI; blue). Representative nuclei are outlined by dashed lines. Mld signals were detected in the nuclei of the PG cells of *phm>dicer2*, + (yellow arrow) at 36 h after egg laying (AEL). In contrast, the signal disappeared in *phm>dicer2* and *pabp-IR*. Scale bar: 10 μm.

PG-Specific Knockdown of *pabp* Strongly Reduces the Expression of Ecdysteroidogenic Enzyme Genes, Especially *spookier*

Next, we examined whether *pabp* knockdown in the PG changes the expression of ecdysteroidogenic genes. We conducted qRT-PCR to examine the expression levels of seven ecdysteroidogenic genes (Chávez et al., 2000; Warren et al., 2002, 2004; Niwa et al., 2004, 2010; Namiki et al., 2005; Ono et al., 2006; Yoshiyama et al., 2006; Chanut-delalande et al., 2014; Enya et al., 2014) in the second instar larvae of control and *pabp*-RNAi animals. The expression levels of all ecdysteroidogenic genes examined were suppressed in *pabp*-RNAi animals. However, specifically, the suppression levels were different among these seven genes. In particular, the suppression level of *spok*, encoding an ecdysteroidogenic cytochrome P450 enzyme, substantially decreased (**Figure 2A**). Consistent with this result, the Spok protein level also substantially decreased in the PG of *pabp*-RNAi animals as compared to control animals, while the protein level of another ecdysteroidogenic P450 enzyme Phm was only slightly affected (**Figures 2B,C**).

To determine whether *spok* expression is transcriptionally and/or translationally disrupted in the *pabp*-RNAi animals, we conducted a GFP reporter assay *in vivo*. The *spok* enhancer region, which is sufficient for *spok* transcription in the PG, has been identified in our previous study (Komura-Kawa et al., 2015). We found that the *spok* enhancer-driven GFP level was

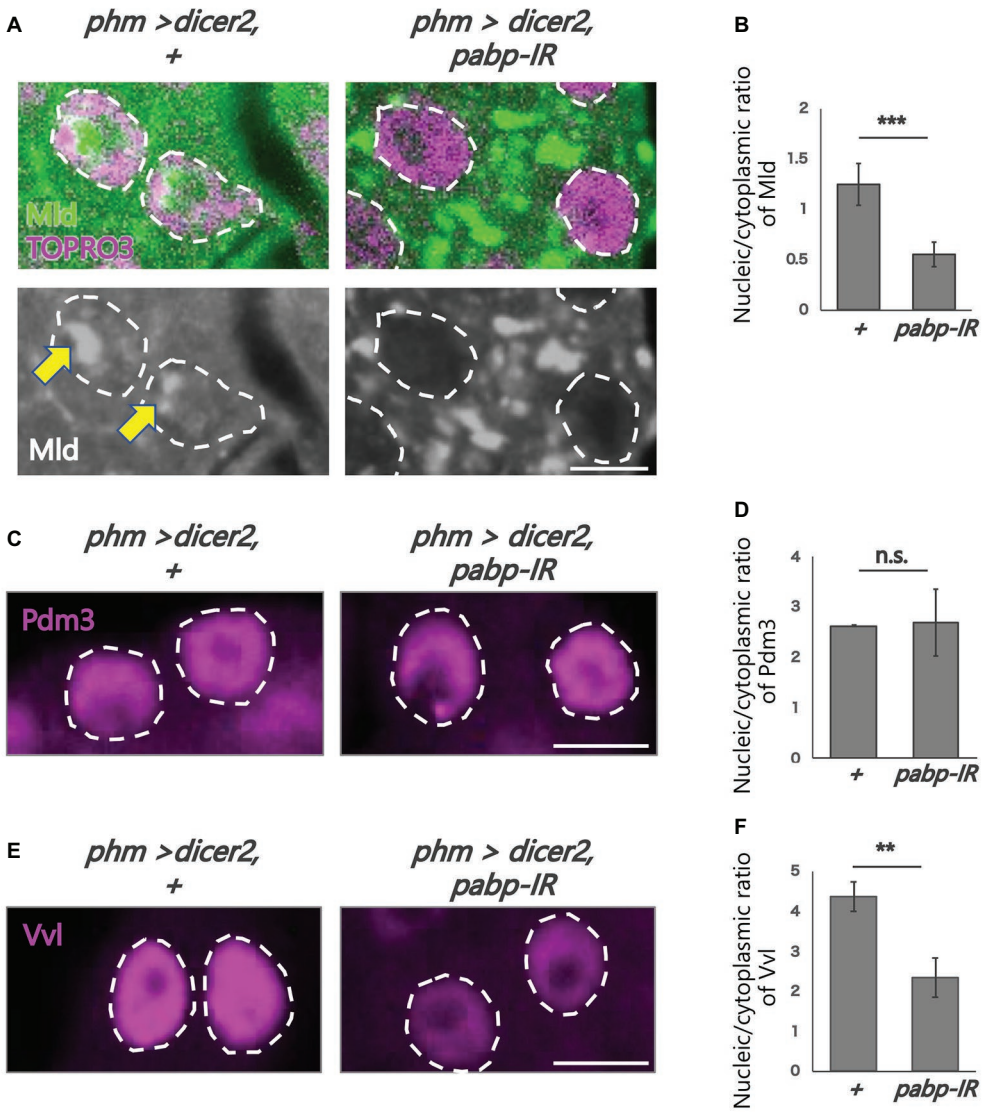

FIGURE 4 | Subcellular localization of transcription factors in the PG cells. All photos are single-plane confocal images. **(A,C,E)** Immunostaining of the PG cells from *phm>dicer2*, + and *phm>dicer2*, *pabp-IR* second instar larvae at 60 h AEL with the antibodies against Mld (green), POU domain motif 3 (Pdm3; magenta), Ventral vein lacking (Vvl; magenta), respectively. Dashed lines indicate the shape of nuclei. **(A)** Nuclei are stained by TOPRO3 (magenta). Bottom panels are single channels of Mld (grayscale). Scale bar: 5 μm. **(B,D,F)** Quantifications of fluorescence intensities of Mld ($N = 5$), Pdm3 ($N = 3$), and Vvl ($N = 3$) in the PG nuclei. Error bars represent standard deviations. ***, ** and n.s. indicate $p < 0.001$, $p < 0.005$ and non-significance ($p > 0.005$), respectively, by Student's *t*-test.

almost diminished in PG cells of *pabp*-RNAi animals, suggesting that *pabp* knockdown disrupts *spok* transcription (**Figures 2D,E**).

Reduction of the Expression of *spok* Correlates With Mislocalization of Its Transcriptional Activator Mld

To analyze the molecular mechanism of suppression of *spok* transcription, we focused on the transcription factor Mld. Mld is a zinc-finger type DNA binding protein involved in ecdysone biosynthesis in the PG (Neubueser et al., 2005). Moreover, we have previously reported that Mld is crucial for transcription of *spok*, acting on the upstream region of the *spok* gene locus (Danielsen et al., 2014; Komura-Kawa et al., 2015). In this study, we newly-generated an anti-Mld antibody to visualize Mld protein *in vivo* by immunostaining. Before the immunostaining experiment, we examined the specificity of the newly-generated anti-Mld antibody. We observed that the Mld signal was observed in the nucleus of PG cells in control animals. In contrast, the Mld signal in the PG nucleus disappeared in *mld*-RNAi animals (**Figure 3**), confirming that the immunostaining signal in the PG nucleus corresponds to Mld protein localization. We then conducted immunostaining with an anti-Mld antibody against *pabp*-RNAi PG cells. Surprisingly, we found that nuclear localization of Mld was disrupted in the *pabp*-RNAi PG cells, although Mld is localized in the nucleus of control PG cells (**Figures 4A,B**).

These results suggest that Pabp regulates the transcription of *spok* by mediating the nuclear localization of Mld.

Next, we examined whether such mislocalization is selective for Mld, but not for other transcription factors in PG cells. To address this issue, we examined the nuclear localization of two other transcription factors such as Vvl and Pdm3, in the *pabp*-RNAi PG cells. Vvl is a POU-domain transcription factor involved in the regulation of the transcription of all known ecdysteroidogenic genes in PG cells (Danielsen et al., 2016). Pdm3 is also a POU-domain transcription factor that is enriched in PG cells (Ou et al., 2016), whereas, its role in PG cells has not yet been elucidated. An immunohistological analysis using anti-Vvl and anti-Pdm3 antibodies revealed that nuclear localization of Vvl and Pdm3 was maintained in the nucleus, even in *pabp*-RNAi PG cells. Nevertheless, the Vvl signal did slightly decrease (**Figures 4C–F**). Taken together, these results suggest that Pabp regulates the nuclear localization specifically of Mld.

DISCUSSION

In this study, we revealed that Pabp is required for the nuclear localization of the ecdysteroidogenic transcription factor Mld. First, the PG-specific knockdown of *pabp* reduced ecdysteroidogenic gene expression, especially that of *spok*. Second, that reduction of *spok* expression correlated well with the mislocalization of its transcription factor Mld. Third, mislocalization did not occur for all transcription factors but did occur specifically for Mld. In conjunction with our previous data showing that Mld is crucial for inducing *spok* expression through the Mld-response element in *spok* promoter region (Uryu et al., 2018), we propose that Pabp positively regulates *spok* expression *via* mediating nuclear localization of Mld in PG cells (**Figure 5**).

The predicted ORF of *mld* encodes a protein that belongs to the family of the zinc-finger associated domain (ZAD) containing C_2H_2 zinc-finger proteins (ZFPs; Neubueser et al., 2005). A previous study has shown that modification or depletion of ZAD disrupts nuclear localization of ZAD-ZFPs (Zolotarev et al., 2016). In conjunction with our observation, this fact raises the possibility that ZAD may be involved in the Pabp-dependent nuclear localization of ZAD-ZFPs, whereas, this hypothesis has yet been experimentally examined. It would also be intriguing to examine whether the subcellular localization of Ouija board (Ouib) and Séance (Séan), other ZAD-ZFP transcription factors of *spok* and *nvd*, respectively (Komura-Kawa et al., 2015; Uryu et al., 2018), are also affected by *pabp*-RNAi. Currently, we failed to generate anti-Ouib and anti-Séan specific antibodies.

This is the first report showing a novel function of Pabp in controlling the nuclear localization of a transcription factor for ecdysone biosynthesis. In the last decade, several transcription factors for ecdysone biosynthesis have been identified (Niwa and Niwa, 2016), while the regulation of subcellular localization of these transcription factors has not been rigorously studied; except DHR4 (Ou et al., 2011). Pabp and other poly(A)-related proteins might be critical research targets for understanding the nuclear and cytoplasmic translocation of ecdysteroidogenic transcription factors in the future.

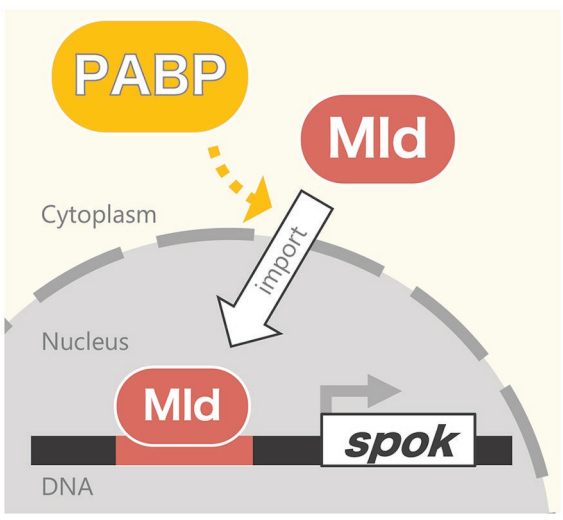

FIGURE 5 | Model of the Pabp function contributing nuclear localization of Mld for *spok* transcription.

DATA AVAILABILITY STATEMENT

The raw data supporting the conclusions of this article will be made available by the authors, without undue reservation, to any qualified researcher.

AUTHOR CONTRIBUTIONS

Study conception: TK, WS, and RN. Investigation (performing of the experiments): TK, NT, and RN. Investigation (data analysis): TK, WS, NT, AN, and RN. Writing/manuscript preparation (writing the initial draft): TK and RN. Writing/manuscript preparation (critical review, commentary, or revision): TK, WS, NT, AN, and RN. Funding acquisition: AN and RN. All authors contributed to the article and approved the submitted version.

FUNDING

This work was supported by a grant from AMED-CREST, AMED to RN (19gm1110001h0003) and the program of the Joint Usage/Research Center for Developmental Medicine, Institute of Molecular Embryology and Genetics, Kumamoto University to RN. We received for an open access publication fee from our institution.

ACKNOWLEDGMENTS

We thank Cheng-Ting Chien, Michael B. O'Connor, Makoto Sato, Bloomington Stock Center, KYOTO Stock Center (DGRC), the National Institute of Genetics, the Vienna *Drosophila* RNAi Center, and the *Drosophila* Genomics Resource Center for stocks and reagents. We also thank Outa Uryu and Reiko Kise for their technical assistance.

REFERENCES

Anderson, M. G., Perkins, G. L., Chittick, P., Shrigley, R. J., and Johnson, W. A. (1995). Drifter, a *Drosophila* POU-domain transcription factor, is required for correct differentiation and migration of tracheal cells and midline glia. *Genes Dev.* 9, 123–137. doi: 10.1101/GAD.9.1.123

Bellés, X. (2020). *Insect metamorphosis: From natural history to regulation of development and evolution. 1st Edn*. Cambridge, MA, USA: Academic Press.

Chanut-delalande, H., Hashimoto, Y., Pelissier-monier, A., Spokony, R., Dib, A., Kondo, T., et al. (2014). Pri peptides are mediators of ecdysone for the temporal control of development. *Nat. Cell Biol.* 16, 1035–1044. doi: 10.1038/ncb3052

Chávez, V. M., Marqués, G., Delbecque, J. P., Kobayashi, K., Hollingsworth, M., Burr, J., et al. (2000). The *Drosophila disembodied* gene controls late embryonic morphogenesis and codes for a cytochrome P450 enzyme that regulates embryonic ecdysone levels. *Development* 127, 4115–4126.

Chen, C. K., Chen, W. Y., and Chien, C. T. (2012). The POU-domain protein Pdm3 regulates axonal targeting of R neurons in the *Drosophila* ellipsoid body. *Dev. Neurobiol.* 72, 1422–1432. doi: 10.1002/dneu.22003

Danielsen, E. T., Moeller, M. E., Dorry, E., Komura-Kawa, T., Fujimoto, Y., Troelsen, J. T., et al. (2014). Transcriptional control of steroid biosynthesis genes in the *Drosophila* prothoracic gland by Ventral veins lacking and Knirps. *PLoS Genet.* 10:e1004343. doi: 10.1371/journal.pgen.1004343

Enya, S., Ameku, T., Igarashi, F., Iga, M., Kataoka, H., Shinoda, T., et al. (2014). A Halloween gene *noppera-bo* encodes a glutathione S-transferase essential for ecdysteroid biosynthesis via regulating the behaviour of cholesterol in *Drosophila*. *Sci. Rep.* 4:6586. doi: 10.1038/srep06586

Gibbens, Y. Y., Warren, J. T., Gilbert, L. I., and O'Connor, M. B. (2011). Neuroendocrine regulation of *Drosophila* metamorphosis requires TGFβ/activin signaling. *Development* 138, 2693–2703. doi: 10.1242/dev.063412

Imura, E., Yoshinari, Y., Shimada-Niwa, Y., and Niwa, R. (2017). Protocols for visualizing steroidogenic organs and their interactive organs with immunostaining in the fruit fly *Drosophila melanogaster*. *J. Vis. Exp.* 122:55519. doi: 10.3791/55519

Komura-Kawa, T., Hirota, K., Shimada-Niwa, Y., Yamauchi, R., Shimell, M. J., Shinoda, T., et al. (2015). The *Drosophila* zinc finger transcription factor Ouija board controls ecdysteroid biosynthesis through specific regulation of spookier. *PLoS Genet.* 11:e1005712. doi: 10.1371/journal.pgen.1005712

McBrayer, Z., Ono, H., Shimell, M., Parvy, J. P., Beckstead, R. B., Warren, J. T., et al. (2007). Prothoracicotropic hormone regulates developmental timing and body size in *Drosophila*. *Dev. Cell* 13, 857–871. doi: 10.1016/j.devcel.2007.11.003

Namiki, T., Niwa, R., Sakudoh, T., Shirai, K. I., Takeuchi, H., and Kataoka, H. (2005). Cytochrome P450 CYP307A1/Spook: a regulator for ecdysone synthesis in insects. *Biochem. Biophys. Res. Commun.* 337, 367–374. doi: 10.1016/j.bbrc.2005.09.043

Neubueser, D., Warren, J. T., Gilbert, L. I., and Cohen, S. M. (2005). *molting defective* is required for ecdysone biosynthesis. *Dev. Biol.* 280, 362–372. doi: 10.1016/j.ydbio.2005.01.023

Nijhout, H. F. (1994). *Insect hormones*. Princetion, NJ, USA: Princeton University Press.

Niwa, R., Matsuda, T., Yoshiyama, T., Namiki, T., Mita, K., Fujimoto, Y., et al. (2004). CYP306A1, a cytochrome P450 enzyme, is essential for ecdysteroid biosynthesis in the prothoracic glands of *Bombyx* and *Drosophila*. *J. Biol. Chem.* 279, 35942–35949. doi: 10.1074/jbc.M404514200

Niwa, R., Namiki, T., Ito, K., Shimada-Niwa, Y., Kiuchi, M., Kawaoka, S., et al. (2010). *Non-molting glossy/shroud* encodes a short-chain dehydrogenase/reductase that functions in the "Black Box" of the ecdysteroid biosynthesis pathway. *Development* 137, 1991–1999. doi: 10.1242/dev.045641

Niwa, R., and Niwa, Y. S. (2014). Enzymes for ecdysteroid biosynthesis: their biological functions in insects and beyond. *Biosci. Biotechnol. Biochem.* 78, 1283–1292. doi: 10.1080/09168451.2014.942250

Niwa, Y. S., and Niwa, R. (2016). Transcriptional regulation of insect steroid hormone biosynthesis and its role in controlling timing of molting and metamorphosis. *Develop. Growth Differ.* 58, 94–105. doi: 10.1111/dgd.12248

Ono, H., Rewitz, K. F., Shinoda, T., Itoyama, K., Petryk, A., Rybczynski, R., et al. (2006). *Spook* and *spookier* code for stage-specific components of the ecdysone biosynthetic pathway in *Diptera*. *Dev. Biol.* 298, 555–570. doi: 10.1016/j.ydbio.2006.07.023

Ou, Q., Magico, A., and King-Jones, K. (2011). Nuclear receptor DHR4 controls the timing of steroid hormone pulses during *Drosophila* development. *PLoS Biol.* 9:e1001160. doi: 10.1371/journal.pbio.1001160

Ou, Q., Zeng, J., Yamanaka, N., Brakken-Thal, C., O'Connor, M. B., and King-Jones, K. (2016). The insect prothoracic gland as a model for steroid hormone biosynthesis and regulation. *Cell Rep.* 16, 1-16. doi: 10.1016/j.celrep.2016.05.053

Parvy, J. P., Blais, C., Bernard, F., Warren, J. T., Petryk, A., Gilbert, L. I., et al. (2005). A role for βFTZ-F1 in regulating ecdysteroid titers during post-embryonic development in *Drosophila melanogaster*. *Dev. Biol.* 282, 84–94. doi: 10.1016/j.ydbio.2005.02.028

Rewitz, K. F., O'Connor, M. B., and Gilbert, L. I. (2007). Molecular evolution of the insect Halloween family of cytochrome P450s: phylogeny, gene organization and functional conservation. *Insect Biochem. Mol. Biol.* 37, 741–753. doi: 10.1016/j.ibmb.2007.02.012

Riddiford, L. M. (1993). "Hormones and *Drosophila* development" in *The development of Drosophila melanogaster*. eds. M. Bate and A. Martinez-Arias (Cold Spring Harbor, NY, USA: Cold Spring Harbor Laboratory Press), 899–939.

Schneider, C. A., Rasband, W. S., and Eliceiri, K. W. (2012). NIH image to imageJ: 25 years of image analysis. *Nat. Methods* 9, 671–675. doi: 10.1038/nmeth.2089

Uryu, O., Ameku, T., and Niwa, R. (2015). Recent progress in understanding the role of ecdysteroids in adult insects: germline development and circadian clock in the fruit fly *Drosophila melanogaster*. *Zoological Lett.* 1:32. doi: 10.1186/s40851-015-0031-2

Uryu, O., Ou, Q., Komura-Kawa, T., Kamiyama, T., Iga, M., Syrzycka, M., et al. (2018). Cooperative control of ecdysone biosynthesis in *Drosophila* by transcription factors Séance, Ouija board, and Molting defective. *Genetics* 208, 605–622. doi: 10.1534/genetics.117.300268

Warren, J. T., Petryk, A., Marque, G., Jarcho, M., Parvy, J. P., Dauphin-villemant, C., et al. (2002). Molecular and biochemical characterization of two P450 enzymes in the ecdysteroidogenic pathway of *Drosophila melanogaster*. *Proc. Natl. Acad. Sci. U. S. A.* 99, 11043–11048. doi: 10.1073/pnas.162375799

Warren, J. T., Petryk, A., Marqués, G., Parvy, J. P., Shinoda, T., Itoyama, K., et al. (2004). Phantom encodes the 25-hydroxylase of *Drosophila melanogaster* and *Bombyx mori*: a P450 enzyme critical in ecdysone biosynthesis. *Insect Biochem. Mol. Biol.* 34, 991–1010. doi: 10.1016/j.ibmb.2004.06.009

Yamanaka, N., Romero, N. M., Martin, F. A., Rewitz, K. F., Sun, M., O'Connor, M. B., et al. (2013). Neuroendocrine control of *Drosophila* larval light preference. *Science* 341, 1113–1116. doi: 10.1126/science.1241210

Yoshiyama, T., Namiki, T., Mita, K., Kataoka, H., and Niwa, R. (2006). Neverland is an evolutionally conserved Rieske-domain protein that is essential for ecdysone synthesis and insect growth. *Development* 133, 2565–2574. doi: 10.1242/dev.02428

Zeng, J., Kamiyama, T., Niwa, R., and King-Jones, K. (2018). The *Drosophila* CCR4-NOT complex is required for cholesterol homeostasis and steroid hormone synthesis. *Dev. Biol.* 443, 10–18. doi: 10.1016/j.ydbio.2018.08.012

Zolotarev, N. A., Maksimenko, O. G., Georgiev, P. G., and Bonchuk, A. N. (2016). ZAD-domain is essential for nuclear localization of insulator proteins in *Drosophila melanogaster*. *Acta Nat.* 8, 97–102. doi: 10.32607/20758251-2016-8-3-97-102

Conflict of Interest: The authors declare that the research was conducted in the absence of any commercial or financial relationships that could be construed as a potential conflict of interest.

frontiers in Genetics

ORIGINAL RESEARCH
published: 03 July 2020
doi: 10.3389/fgene.2020.00683

Histone Deacetylase 11 Knockdown Blocks Larval Development and Metamorphosis in the Red Flour Beetle, *Tribolium castaneum*

*Smitha George and Subba Reddy Palli**

Department of Entomology, University of Kentucky, Lexington, KY, United States

Post-translational modifications (PTM) such as methylation, acetylation, phosphorylation, and ubiquitination of histones and other proteins regulate expression of genes. The acetylation levels of these proteins are determined by the balance of expression of histone acetyltransferase (HATs) and histone deacetylases (HDACs). We recently reported that class I HDACs (HDAC1 and HDAC3) play important roles in juvenile hormone (JH) suppression of metamorphosis in the red flour beetle, *Tribolium castaneum*. Here, we report on the function of a single class IV HDAC member, HDAC11. Injection of dsRNA targeting *T. castaneum HDAC11* gene into newly molted last instar larvae induced knockdown of the target gene and arrested larval development and prevented metamorphosis into the pupal stage. Dark melanized areas were detected in larvae that showed developmental arrest and mortality. Developmental expression studies showed an increase in HDAC11 mRNA levels beginning at the end of the penultimate larval stage. These higher levels were maintained during the final instar larval and pupal stages. A JH analog, hydroprene, suppressed *HDAC11* expression in the larvae. Sequencing of RNA isolated from control and dsHDAC11 injected larvae identified several differentially expressed genes, including those involved in JH action, ecdysone response, and melanization. The acetylation levels of core histones showed an increase in TcA cells exposed to dsHDAC11. Also, an increase in histone H3 acetylation, specifically H3K9, H3K18 and H3K27, were detected in HDAC11 knockdown larvae. These studies report the function of HDAC11 in insects other than *Drosophila* for the first time and show that HDAC11 influences the acetylation levels of histones and expression of multiple genes involved in *T. castaneum* larval development.

Keywords: juvenile hormone, epigenetics, histone deacetylase 11, histone H3, dsRNA

OPEN ACCESS

Edited by:
Enrique Medina-Acosta, State University of the North Fluminense Darcy Ribeiro, Brazil

Reviewed by:
Rodrigo Nunes Da Fonseca, Federal University of Rio de Janeiro, Brazil
Yoonseong Park, Kansas State University, United States

***Correspondence:**
Subba Reddy Palli
rpalli@email.uky.edu; rpalli@uky.edu

Specialty section:
This article was submitted to Epigenomics and Epigenetics, a section of the journal Frontiers in Genetics

Received: *27 March 2020*
Accepted: *04 June 2020*
Published: *03 July 2020*

Citation:
George S and Palli SR (2020) Histone Deacetylase 11 Knockdown Blocks Larval Development and Metamorphosis in the Red Flour Beetle, Tribolium castaneum. Front. Genet. 11:683. doi: 10.3389/fgene.2020.00683

INTRODUCTION

Two major insect hormones, ecdysteroids (20-hydroxyecdysone, 20E, is the most active form) and juvenile hormones (JH) regulate many aspects of insect life, including postembryonic development (Riddiford, 1996; Wyatt et al., 1996; Hartfelder, 2000; Singtripop et al., 2000; Min et al., 2004; Giray et al., 2005; Hrdy et al., 2006; Futahashi and Fujiwara, 2008). These hormones have been extensively studied because of their involvement in the regulation of multiple biological processes,

including diapause, reproduction, and polyphenism (Wigglesworth, 1934; Riddiford, 1994, 2012). Juvenile hormones are sesquiterpenoids secreted by the corpora allata that mediate a variety of functions in insects (Jindra et al., 2013). The JH signaling cascade is a complex molecular process that includes multiple players such as JH receptor, *Methoprene-tolerant* (*Met*) (Wilson and Fabian, 1986; Konopova and Jindra, 2007) and, its heterodimeric partner, SRC, steroid receptor co-activator homolog (Li et al., 2011; Zhang et al., 2011). The JH-receptor complex binds to the juvenile hormone response elements (JHRE) present in the promoters of JH-response genes and regulate their expression (Kayukawa et al., 2012; Cui et al., 2014). 20-hydroxyecdysone binds to a heterodimer of two nuclear receptors, ecdysone receptor (EcR) and ultraspiracle (USP) and ecdysone response elements present in the promoters of ecdysone-induced transcription factors including E75, E74, Broad complex (BR-C) and E93 and regulate their expression (Palli et al., 2005). These ecdysone induced transcription factors, in turn, regulate expression of multiple genes important for growth, development, molting and metamorphosis (Riddiford et al., 2000).

Hormones represent attractive targets for the development of environmentally friendly insect control methods. Hindering this effort is the lack of knowledge on the molecular basis of hormone action. Research in epigenetics-based gene regulation has facilitated the discovery of various post-translational modification mechanisms (PTM) such as methylation, acetylation, phosphorylation, and ubiquitination. The role of acetylation in the regulation of 20E induced gene expression in *Drosophila melanogaster* has been reported (Bodai et al., 2012). The CREB-binding protein (CBP) mediates acetylation of histone H3K27 and antagonizes "Polycomb" silencing in *D. melanogaster* (Tie et al., 2009). The CBP also functions in regulating the expression of hormone response genes in *Tribolium castaneum* (Roy et al., 2017; Xu et al., 2018) and *Blattella germanica* (Fernandez-Nicolas and Belles, 2016). Since acetylation is a key component in the regulation of gene expression, we decided to explore the function of histone deacetylases (HDACs) in the red flour beetle, *T. castaneum.* Recent findings from our lab have demonstrated that class I HDACs (HDAC1 and HDAC3) play important roles in JH suppression of metamorphosis in *T. castaneum* (George et al., 2019; George and Palli, 2020). Here, we focused on the function of sole class IV HDAC member, HDAC11 (TC007473), to study its role in *T. castaneum* development.

Human HDACs identified to date can be grouped into four classes; Class I-IV based on their structure, phylogeny, and function. Class I HDACs are ubiquitously expressed and play essential roles in proliferation, whereas classes II and IV have a tissue-specific function (Lehrmann et al., 2002). HDAC11 first described in 2002 is a unique member class IV HDAC family since it is not homologous with RPD3 or HDA1 yeast enzymes (Gao et al., 2002). Selective/class-specific inhibitors targeting HDAC11 have been developed for treating patients with myeloproliferative neoplasms (MPN) (Yue et al., 2020). HDAC11 shows some sequence similarity to class I and II HDACs and is highly conserved in invertebrates and plants (Yang and Seto, 2008). HDAC11 depletion in neuroblastoma cell lines induces cell death mediated by apoptotic programs (Thole et al., 2017). HDAC11 knockout study in mice identified an age-dependent brain region-specific function in regulating *FEZ1* (fasciculation and elongation protein zeta 1), a gene associated with schizophrenia (Bryant et al., 2017). HDAC11 knockout mice showed resistance to high-fat-diet-induced obesity and metabolic syndrome, suggesting that HDAC11 functions as a critical metabolic regulator (Sun et al., 2018). However, not much information is available on HDAC11 function in insects. Functions of *D. melanogaster* histone deacetylases were studied by RNA interference and microarrays and showed that HDAC1 and HDAC3 control expression of genes involved in multiple processes including lipid metabolism, cell cycle regulation and signal transduction (Foglietti et al., 2006). However, three other HDACs tested did not show any detectable functions (Foglietti et al., 2006). Also, overexpression of HDAC 3, 6 or 11 suppressed CGG repeat-induced neurodegeneration in *D. melanogaster* Fragile X Tremor Ataxia Syndrome model suggesting that HDAC activators might be used to repress transcription of fragile X syndrome gene (Todd et al., 2010). In the current studies, we employed RNAi, RNA sequencing, and RT-qPCR to elucidate the role of HDAC11 in *T. castaneum*. Knockdown of HDAC11 during the larval stage induced arrest in larval development, melanization, and mortality. RNA isolated from *T. castaneum* larvae injected with double-stranded RNA (dsRNA) targeting the gene coding for HDAC11 (dsHDAC11) or dsmalE (a control dsRNA targeting *E. coli* malE gene) was sequenced, and differential gene expression analysis was conducted. Genes involved in hormone action and multiple biological processes such as melanization were identified as differentially expressed genes in HDAC11 knockdown larvae.

MATERIALS AND METHODS

Insects and Cells

Insects (*T. castaneum*, GA-1 strain) (Haliscak and Beeman, 1983) were maintained in a Percival incubator set at 30°C and 65 ± 5% relative humidity with complete dark conditions on organic wheat flour (Heartland Mill, Marienthal, KS) mixed with 10% baker's yeast (MP biomedicals, Solon, OH, United States). The *T. castaneum* cells, BCIRL-TcA-CLG1 (TcA), were cultured in EX-CELL 420 (Sigma-Aldrich, St-Louis, MO, United States) medium supplemented with 10% Fetal Bovine Serum (FBS, VWR-Seradigm, Radnor, PA, United States) at 28°C as described previously (Goodman et al., 2012).

Hormone Treatments

Both *S*-Hydroprene (Ethyl 3, 7, 11-trimethyl-2, 4-dodecadienoate) and JH III were purchased from Sigma-Aldrich. The hydroprene was dissolved in cyclohexane at 2 μg/μl concentration and one microliter of this solution was applied on the integument of each last instar larva. One microliter of cyclohexane solvent alone was applied to each control larva. For cell culture experiments, JH III was prepared in DMSO at 10 mM concentration and one microliter per ml of culture medium was

added to achieve a final concentration of 10 μM. Control cells were treated with the same volume of DMSO.

Double-Stranded RNA Synthesis (dsRNA), RNA Isolation, cDNA Synthesis and Quantitative Reverse Transcription PCR (RT-qPCR)

T. castaneum HDAC11 ortholog was identified using the *D. melanogaster* HDAC11 sequence available at the FlyBase (Thurmond et al., 2019). Specific primers targeting two regions of *HDAC11* and containing T7 polymerase promoter at the 5′ end (**Supplementary Table S1**) and genomic DNA isolated from *T. castaneum* were used to PCR amplify the fragment of HDAC11. The PCR fragment used as a template for dsRNA synthesis. Primers used to amplify a fragment of JH receptor, Met, from *T. castaneum* (TcMet) have been reported previously (Parthasarathy et al., 2008). The MEGAscript T7 kit (Invitrogen, United States) was used for dsRNA synthesis. Purification, quality check, and quantification of dsRNA were performed as described previously (George et al., 2019). dsRNA prepared using a fragment of *Escherichia coli* maltose-binding proteins (malE) was used as a control.

Total RNA was isolated from treated and control insects using TRI reagent-RT (Molecular Research Center, Inc. Cincinnati, OH, United States). The RNA was converted to cDNA using M-MLV reverse transcriptase (Invitrogen-ThermoFisher Scientific). RT-qPCR was performed using iTaq Universal SYBR Green Supermix (Bio-Rad, Hercules, CA, United States) in Applied Biosystems StepOnePlus Real-time PCR instrument. The qPCR mixture contained 2 μl of diluted cDNA (1:5), 0.4 μl gene-specific primer mix, 2.6 μl nuclease-free water, and 5 μl SYBR green in a 10 μl final volume. The qPCR cycling conditions were: initial holding stage 95°C (20 s), followed by 40 cycles of denaturation at 95°C (5 s), annealing, and extension at 60°C (30 s) along with melting curve. The relative mRNA levels were calculated using *RP49* as a reference gene.

Differential Gene Expression Analysis

Total RNA extracted from three biological replicates of larvae at 12 h after treatment with dsHDAC11 or dsmalE using the TRI reagent-RT and used for RNA-seq library preparation following the protocol described previously (Ma et al., 2014; Hunt, 2015; Kalsi and Palli, 2017). Raw reads were analyzed following CLC genomic workbench pipeline (Version 11.0.1, Qiagen, United States). Blast2GO Pro Plugin in the CLC workbench was used to determine the GO terms. The GO terms were used for predicting functions of differentially expressed genes. The GO terms were represented using Web Gene Ontology Annotation Plot (WEGO) as described previously (Ye et al., 2006).

Western Blot Analysis

We used Acetylated-Lysine (Ac-K^2-100) MultiMab™ Rabbit mAb mix (Cell signaling #9814) to detect proteins post-translationally modified by acetylation. Histone H3 antibody sampler kit #9927 (Cell Signaling, Danvers, MA, United States) that includes Lys9, Lys14, Lys18, Lys27, and Lys56 specific antibodies were used to detect various lysine acetylation sites of histone H3. Band density was determined by Image-J software and normalized with loading control protein, ß-Actin. The Anti-rabbit IgG, HRP-linked antibody (Cell signaling #7074), was used for chemiluminescence detection. The blots were developed with Supersignal™ West Femto Maximum sensitivity Substrate (Thermo Fisher, Scientific, Rockford, IL, United States).

Statistical Analysis

The statistical analyses were performed using JMP Pro 14.0 (SAS Institute Inc., Cary, NC, United States) to test for statistical differences among treatments. *Post-hoc* tests were conducted using the Tukey-Kramer HSD method ($\alpha = 0.05$). One-way ANOVA was performed for comparison between treatments.

RESULTS

Tribolium castaneum HDAC11

T. castaneum HDAC11 contains a single Zn+ dependent catalytic domain surrounded by a short N- and C- terminus (**Figure 1A**). Phylogenetic analysis of HDACs in *T. castaneum* revealed that TcHDAC11 is closer to Class I deacetylases (HDAC1, HDAC3, and HDAC8) than to class II (**Figure 1B**). *T. castaneum* HDAC11 open reading frame consists of 314–331 residues with a molecular mass of 35.2–37.2 kDa and one catalytic

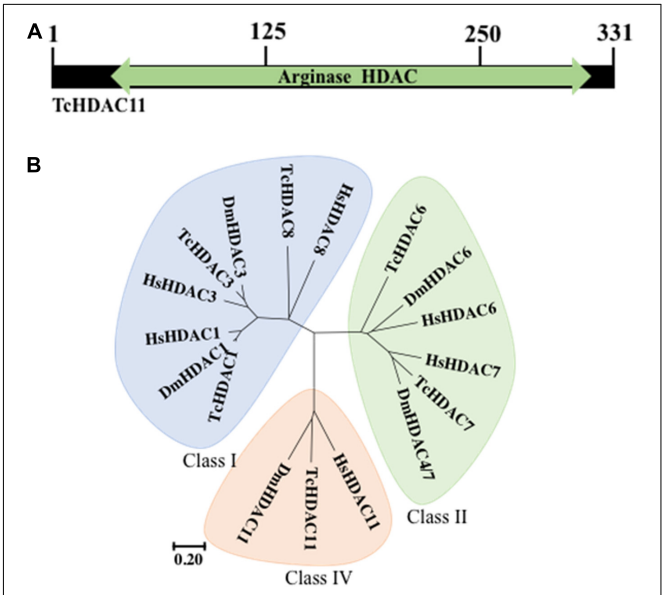

FIGURE 1 | TcHDAC11 catalytic domain and phylogeny. **(A)** Schematic representation of the TcHDAC11 with the catalytic domain marked. The numbers on the top show the position of amino acids. The data for this Figure is obtained from NCBI (Geer et al., 2002). **(B)** Phylogenetic tree demonstrating the relationship between HDAC classes. The tree was inferred using the Neighbor-joining method. Evolutionary analyses were conducted in MEGA7 (Kumar et al., 2016). The tree was drawn to scale, with branch lengths and the evolutionary distances used to infer the phylogenetic tree as the same units. The identification of HDACs in *T. castaneum* was reported previously (George et al., 2019).

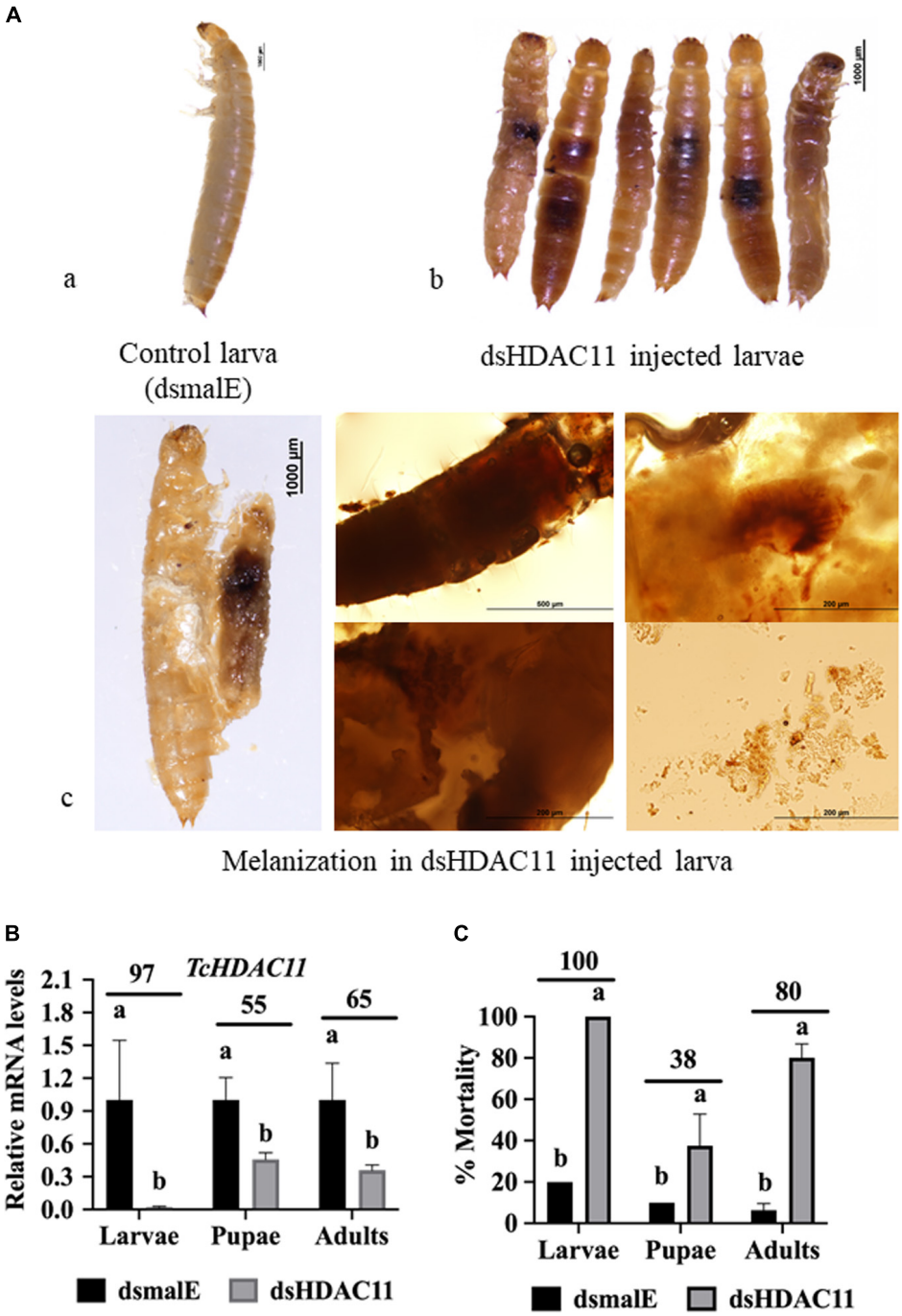

FIGURE 2 | Phenotypes and mortality induced by dsRNA mediated knockdown of *HDAC11* in *T. castaneum*. **(A) a:** Control larvae injected with dsmalE pupated and later emerged as healthy adults. **b:** dsHDAC11 was injected into the newly molted last instar larvae. Phenotypes were photographed on the fifth day after injection. Knockdown of the *HDAC11* gene affected larval development resulting in pigmentation, growth retardation, and mortality. **c:** Light microscopic images of melanization in HDAC11 knockdown larvae. A high degree of hard melanization was detected inside the body. **(B)** Newly molted last instar larvae, pupae or adults were injected with dsHDAC11 or dsmalE. Total RNA was isolated from treated insects at 72 h after injection and used to determine relative mRNA levels of TcHDAC11. Knockdown efficiency was calculated by comparing TcHDAC11 mRNA levels in dsTcHDAC11 and dsmalE treated insects. Mean ± SE (n = 3–5) are shown. Means marked with different letters are significantly different from each other, $P \leq 0.05$ by ANOVA. **(C)** Newly molted last instar larvae, pupae or adults were injected with dsHDAC11 or dsmalE. The mortality was recorded until death or adult eclosion. Mean ± SE (n = 30) are shown. Means marked with different letters are significantly different from each other, $P \leq 0.05$ by ANOVA.

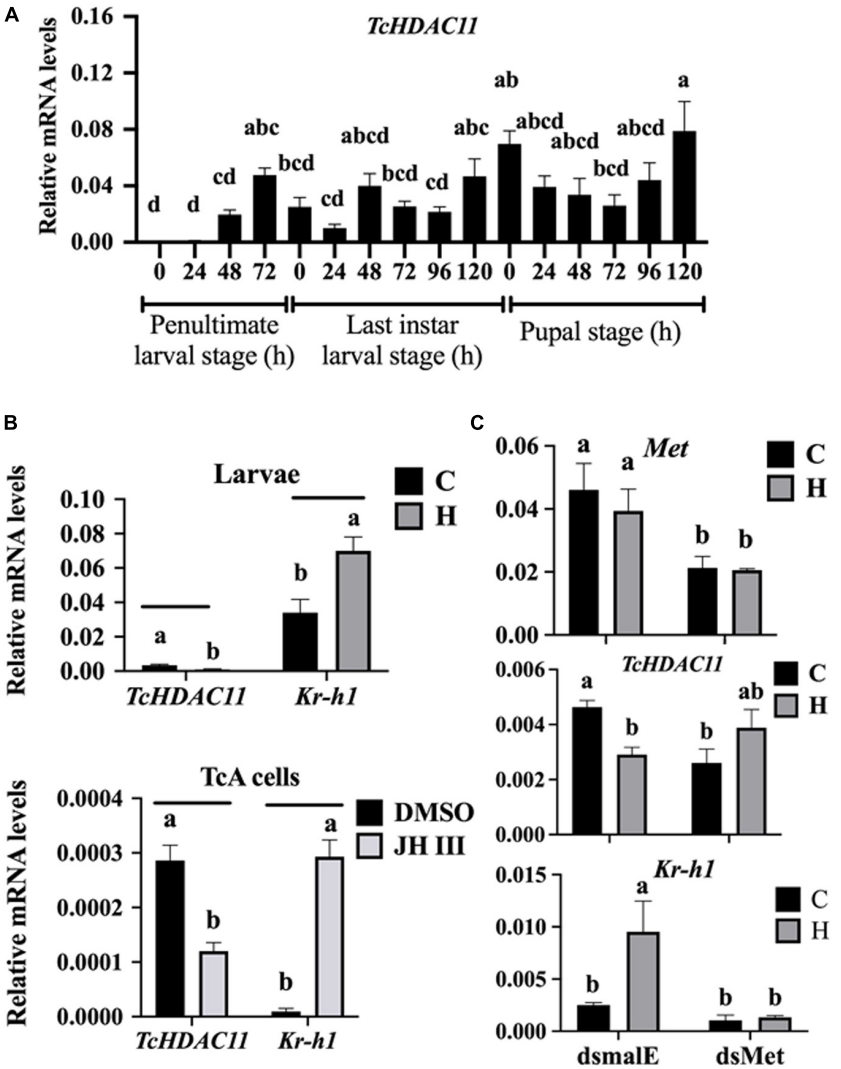

FIGURE 3 | Developmental expression profile and JH induction of *HDAC11* in *T. castaneum* determined by RT-qPCR. **(A)** HDAC11 mRNA levels were determined during the penultimate, last larval, and pupal stages at 24 h intervals. Total RNA was isolated from a pool of two larvae for each replication and subjected to RT-qPCR analysis to determine the relative mRNA levels. The HDAC11 mRNA levels were normalized using RP49. Results expressed as Mean ± SE (n = 4). Means marked with different letters are significantly different from each other, $P \leq 0.05$ by ANOVA. **(B)** JH suppresses the expression of *HDAC11* in *T. castaneum* larvae and TcA cells. S-Hydroprene (JH analog) dissolved in cyclohexane was topically applied to 48 h old last instar larvae (0.5 μL of 2 μg/μL). Total RNA was isolated from larvae collected at 6 h after treatment and subjected to RT-qPCR. Similarly, TcA cells were treated with 10 μm of JH III in DMSO or DMSO alone for 6 h. Total RNA isolated from larvae was used to quantify Kr-h1 and HDAC11 mRNA levels. Mean ± SE (n = 4) are shown. **(C)** Met is required for suppression of *HDAC11* by hydroprene. dsMet or dsmalE was injected into day 0 last instar larvae. At 48 h after injection, the larvae were treated with hydroprene. Total RNA isolated from larvae was used to quantify *Kr-h1*, *HDAC11* and, *Met* mRNA levels. The data shown are mean ± SE (n = 4). C, cyclohexane; H, hydroprene.

domain (**Figure 1A**). Comparison between the *T. castaneum* full-length HDAC11 amino acid sequence with those from *D. melanogaster* and human HDAC11s amino acid sequences showed 54 and 58 percent amino acid identity, respectively (**Supplementary Figure S1**).

HDAC11 Knockdown Arrests Larval Development

To determine HDAC11 function in larval, pupal development, and metamorphosis, the dsHDAC11 was injected into newly molted last instar larvae (day 0), freshly formed white-colored pupae and adults. The control insects injected with dsmalE (**Figure 2Aa**) pupated after 5–6 days after dsRNA injection and later emerged as healthy adults. However, developmental arrest and mortality were observed in 100% of dsHDAC11 injected larvae (**Figure 2Ab**). The arrested larvae showed dark pigmentation inside their body (**Figure 2Ac**). Dark melanized patches of tissues attached to the integument were detected in dissected larvae. Injection of dsHDAC11 reduced mRNA levels of the target gene by 97, 55, and 65% in larvae, pupae and adults, respectively, when compared to their levels in control insects

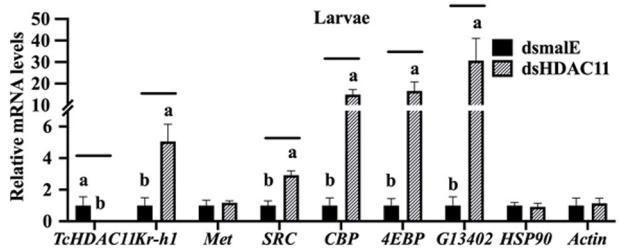

FIGURE 4 | *HDAC11* knockdown in the last instar larvae of *T. castaneum* affects the expression of genes involved in JH action and response. The knockdown of *HDAC11* in newly molted last instar larvae caused an upregulation of genes involved in JH action (*SRC*, *CBP*) and JH response (*Kr-h1*, *4EBP*, *G13402)*. dsHDAC11 or dsmalE was injected into newly molted last instar larvae. Total RNA was extracted at 12 h after treatment, and the mRNA levels of JH-response genes (*Kr-h1*, *4EBP*, *G13402*), genes involved in JH action (*Met*, *SRC*, *CBP*), *HSP90* and *Actin* were quantified. Mean ± SE (n = 4) are shown. Means marked with different letters are significantly different from each other, $P \leq 0.05$ by ANOVA.

injected with dsmalE (**Figure 2B**). Injection of dsHDAC11 also induced 100, 38, and 80% mortality in larvae, pupae and adults, respectively (**Figure 2C**). In contrast, the control insects injected with dsmalE showed less than 20% mortality (**Figure 2C**).

Developmental Expression and JH Suppression of TcHDAC11

No HDAC11 mRNA was detected in *T. castaneum* larvae soon after molting into the penultimate larval stage (**Figure 3A**). Then the HDAC11 mRNA levels increased gradually, reaching the maximum levels by the end of the penultimate larval stage (**Figure 3A**). The HDAC11 mRNA was detected throughout the last instar larval and pupal stages, albeit with some fluctuations in their levels (**Figure 3A**). In general, higher levels of HDAC11 mRNA were detected at the end of the penultimate and last instar larval stages when compared to those at the beginning of these stages. Also, higher levels of HDAC11 mRNA were detected in the pupae when compared to those in the larval stages.

To test if JH suppresses HDAC11 gene expression, the last instar larvae were treated with JH analog hydroprene in cyclohexane or cyclohexane alone. As shown in **Figure 3B**, significantly lower levels of HDAC11 mRNA were detected in larvae treated with hydroprene when compared to those in the control larvae treated with cyclohexane. Similarly, lower levels of HDAC11 mRNA were detected in TcA cells exposed to JH III, when compared to those in the control cells exposed to DMSO (**Figure 3B**). Also, the JH-response gene, *Kr-h1*, was induced by hydroprene in larvae and JH III in cells (**Figure 3B**). These data suggest that JH suppresses HDAC11 gene expression. To determine whether or not JH suppression of the HDAC11 gene requires the JH receptor, Met, *T. castaneum* last instar larvae were injected with dsMet or dsmalE and then treated with hydroprene or cyclohexane. As shown in **Figure 3C**, dsMet injected larvae showed significantly lower levels of Met mRNA when compared to those in larvae injected with dsmalE. As expected, the HDAC11 mRNA levels decreased in dsmalE

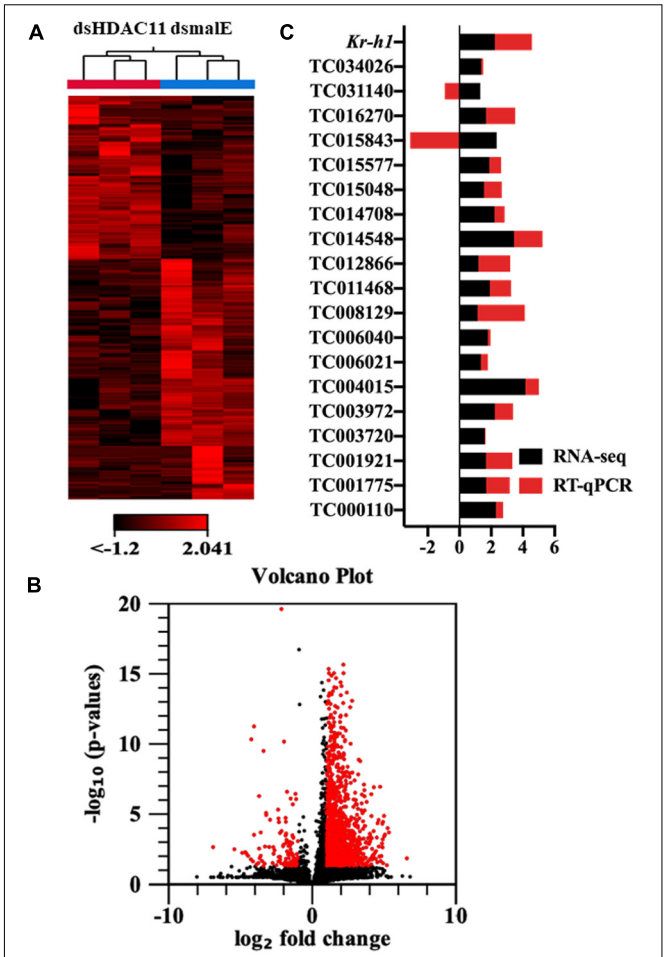

FIGURE 5 | *HDAC11* knockdown in the last instar larvae of *T. castaneum* affects the transcription of genes involved in multiple pathways. **(A)** The heatmap of differentially expressed genes in dsHDAC11 and dsmalE treated insects. **(B)** Differentially expressed genes identified after *HDAC11* knockdown represented as the volcano plot. The X and Y-axis represent the $-\log_{10}$ *P*-values and $\log_2$ fold change of mean normalized values, respectively. The red dots indicate the genes that showed a ≥2-fold difference in expression with a $P \leq 0.05$. **(C)** RNA-seq data is verified and compared with RT-qPCR represented as a stacked bar graph. RT-qPCR confirmed the expression of 20 selected genes from the up-regulated group (**Supplementary Data Sheet**_RNA-seq data).

injected larvae treated with hydroprene but not in dsMet injected larvae treated with hydroprene. Also, the *Kr-h1* gene was induced in dsmalE injected larvae but not in dsMet injected larvae. These data suggest that Met is required for JH suppression of HDAC11 gene expression.

Identification of Genes Affected by HDAC11 Knockdown

The effect of Knockdown of HDAC11 on the expression of JH response genes in larvae were tested using RT-qPCR. *T. castaneum* last instar larvae were injected with dsHDAC11 or dsmalE A, the total RNA isolated from these larvae was used to determine mRNA levels of HDAC11 and genes known

TABLE 1 | Expression changes of hormone-response genes identified in larvae treated with dsHDAC11.

Gene symbol	Gene description	Fold Change[a]	*P*-value[b]
Kr-h1	Krüppel homolog 1	4.68	0.00
LOC655028	ecdysone-induced protein 74EF	2.03	0.00
EcR	ecdysone receptor	2.18	0.03
Tcjheh-r1	juvenile hormone epoxide hydrolase-like protein 1	28.14	0.01
Tcjheh-r2	juvenile hormone epoxide hydrolase-like protein 2	2.03	0.01
Tcjheh-r5	juvenile hormone epoxide hydrolase-like protein 5	2.40	0.00
LOC661705	Phosphoenol pyruvate carboxykinase [GTP]	3.14	0.00
LOC659239	Krueppel homolog 2	3.87	0.00
TcSRC	nuclear receptor coactivator 1	2.24	0.02
LOC660434	broad-complex core protein isoform 6-like	2.59	0.02
LOC658929	nuclear hormone receptor FTZ-F1	2.03	0.04
USP	ultraspiracle nuclear receptor	2.08	0.00
LOC664565	CREB-binding protein	7.73	0.00
LOC660626	Hairy	9.33	0.00
LOC658656	Apterous A	4.67	0.00

[a]*Experiment – Fold Change (normalized values).* [b]*Baggerley's test: normalized values.*

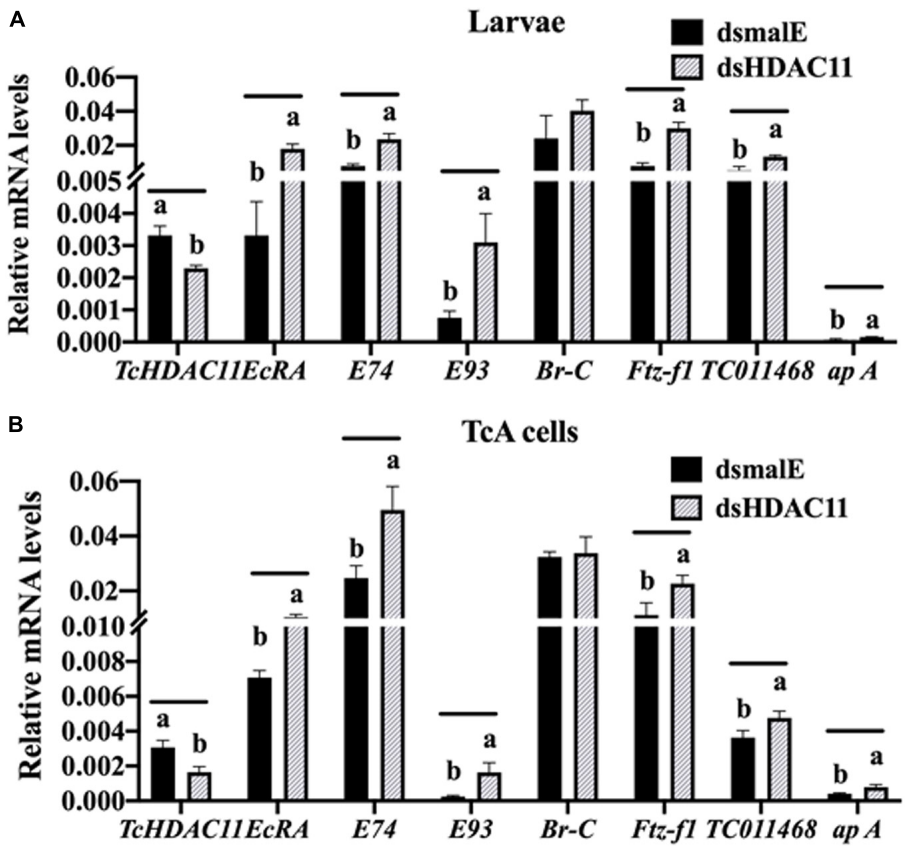

FIGURE 6 | RT-qPCR validation of RNA-seq data in *Tribolium* larvae and TcA cells. **(A)** Differentially expressed genes predicted by RNA-seq analysis are verified by RT-qPCR. Total RNA was extracted at 12 h after injection was used to quantify mRNA levels. Mean ± SE of four replications is shown. Means marked with different letters are significantly different from each other, $P \leq 0.05$ by *t*-test. **(B)** TcA cells were treated with dsHDAC11 or dsmalE. Total RNA was extracted 72 h after dsRNA treatment was used to quantify mRNA levels. Mean ± SE of four replications is shown. Means marked with different letters are significantly different from each other, $P \leq 0.05$ by ANOVA.

TABLE 2 | JH-response genes that showed an increase in expression in dsHDAC11 treated larvae.

Gene symbol	Gene description	JH		dsHDAC11	
		Fold change	*P*-value	Fold change	*P*-value
LOC660562	rho GTPase-activating protein 100F	115.45	0.020	29.80	0.002
Kr-h1	Krüppel homolog 1	29.91	0.000	4.68	0.000
LOC662658	4-hydroxyphenylpyruvate dioxygenase	3.46	0.000	4.00	0.000
LOC100141923	sodium-coupled monocarboxylate transporter 2-like	202.63	0.004	3.82	0.014
LOC660154	projectin	13.63	0.030	3.68	0.000
LOC659434	fibroblast growth factor receptor homolog 1	95.55	0.030	3.63	0.000
LOC661127	uncharacterized LOC661127	4.02	0.030	3.38	0.000
LOC107398485	sodium-independent sulfate anion transporter-like	4.28	0.030	3.21	0.004
LOC658154	alpha-2C adrenergic receptor	8.08	0.001	2.90	0.012
LOC100142605	ankyrin-3	2.90	0.008	2.38	0.007
LOC103314138	voltage-dependent T-type calcium channel subunit alpha-1G	6.85	0.020	2.14	0.000

TABLE 3 | COG5048 domains identified in genes up-regulated in dsHDAC11 treated larvae.

Gene symbol	Gene description	Locus tag	Fold change	*P*-value
LOC658487	Zinc finger protein GLIS2 homolog	TC000326	2.49	0.000
LOC659757	Zinc finger protein Gfi-1	TC031695	6.19	0.000
Kr-h1	Krüppel homolog 1	TC012990	4.68	0.000
LOC660309	Krueppel-like factor 8	TC006125	2.23	0.000
Pho	Pleiohomeotic	TC015577	3.69	0.000
LOC662411	Zinc finger protein 184	TC015048	2.92	0.040
LOC103313120	Zinc finger protein OZF	N/A	3.99	0.050
LOC103314758	Zinc finger protein ZFP69	TC033495	3.11	0.010
LOC107397979	Gastrula zinc finger protein XlCGF26.1-like	N/A	8.52	0.030

N/A, not available.

TABLE 4 | Genes involved in melanin biosynthesis that showed an increase in their expression in *HDAC11* knockdown larvae.

Gene symbol	Gene description	Locus Tag	Fold Change	*P*-value
Ddc	dopa decarboxylase	TC013480	4.46	0.000
Dat	dopamine N acetyltransferase	TC008204, Nat	2.50	0.000
Lac1	laccase 1	TC000821, TcLac1	2.36	0.000
Th	tyrosine hydroxylase	TC002496	3.39	0.000
Y-2	yellow-2	TC003539	4.97	0.000

to be involved in JH-response. The mRNA levels of HDAC11 decreased and those of three JH-response genes (*Kr-h1*, *4EBP*, *G13402*), SRC, and CBP increased significantly in dsHDAC11 injected larvae when compared to those in larvae injected with dsmalE (**Figure 4**). However, the expression of Met and two housekeeping genes, Actin and HSP90, were not affected by *HDAC11* knockdown (**Figure 4**). These data suggest that HDAC11 may influence the expression of JH-response as well as genes coding for proteins involved in JH action.

The RNA isolated from dsHDAC11 and dsmalE injected larvae at 12 h after treatment were sequenced and assembled into transcriptomes and used to identify other targets of HDAC11. Run summary and total read counts of sequencing output are shown in **Supplementary Table S2**. A heatmap representing the overall pattern of normalized mean expression values of differentially expressed genes (DEGs) is shown in **Figure 5A**. The DEGs are shown as a volcano plot with red dots indicating statistically significant genes after the EDGE test between treatment and control (**Figure 5B**). We identified 1913 DEGs (**Supplementary Data Sheet**), 95% (1815) of these genes are up-regulated, and 5% (98) are down-regulated. Hormone response genes *Kr-h1*, ecdysone induced protein 74EF, and ecdysone receptor are among the up-regulated genes (**Supplementary Data Sheet**, dsHDAC11-DEG, **Table 1**). Web-based GO analysis of differently expressed genes showed enrichment of GO terms for binding, especially nucleic acid and protein binding, biological regulation, pigmentation, and developmental process (**Supplementary Figure S2**). To confirm the results from RNA-seq analysis, we selected 20 genes based on their predicted function and expression levels and verified by RT-qPCR using the RNA isolated from *T. castaneum* larvae. Eighteen out of 20 genes tested showed a positive correlation

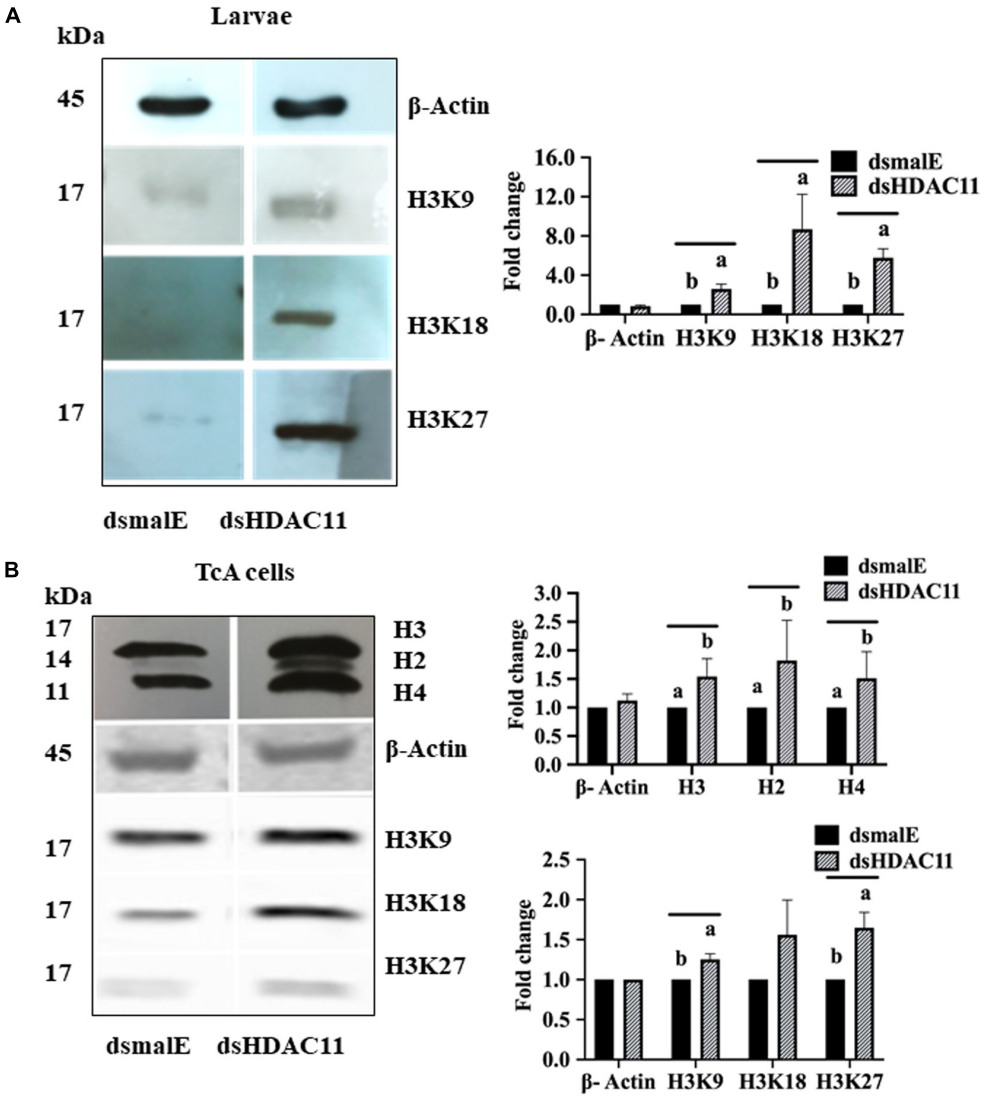

FIGURE 7 | *HDAC11* knockdown affects acetylation levels of histone H3 in *T. castaneum*. **(A)** The total protein extracted from dsHDAC11 or dsmalE injected larvae were resolved on SDS-PAGE gels, transferred to western blots, and probed with antibodies recognizing Acetyl-Histone H3 (Antibody Sampler Kit # 9927-Cell Signaling (H3K9, H3K14, H3K18, H3K27, and H3K56). ß-actin served as a loading control. The HRP-linked IgG (#7074-Cell Signaling) was used as a secondary antibody. Band densities were determined by Image-J software and normalized with loading control protein-ß-Actin. The Mean + SE (n = 3) band densities are shown. Means marked with different letters are significantly different from each other, $P \leq 0.05$ by ANOVA. **(B)** Acetylated-Lysine (Ac-K^2-100) MultiMab^{TM} Rabbit mAb mix #9814 was used to detect acetylation levels of proteins extracted from TcA cells exposed to dsHDAC11 or dsmalE. The acetylation levels of histone H3K9, H3K18 and H3K27 increased in HDAC11 knockdown cells were detected as described in **Figure 7A**. The band densities were quantified and plotted as described in **Figure 7A**. The Mean + SE (n = 3) band densities are shown. Means marked with different letters are significantly different from each other, $P \leq 0.05$ by ANOVA.

in their expression levels determined by the two methods (**Figure 5C**). RT-qPCR analysis of RNA isolated from larvae (**Figure 6A**) and TcA cells (**Figure 6B**) also verified an increase in expression levels of EcRA, E74, E93 Ftz-f1, TC011468 and ap A increase predicted by differential gene expression analysis of transcriptomes of larvae treated with dsHDAC11 or dsmalE. A comparison of up-regulated genes between JH III treated TcA cells (Roy and Palli, 2018), and dsHDAC11 treated larvae identified eleven common genes, including the *Kr-h1* (**Table 2**). Nine genes that code for proteins containing zinc finger, COG5048 domains found in *Kr-h1* are also up-regulated in *HDAC11* knockdown larvae (**Table 3**). Since dsHDAC1 (George et al., 2019) and dsHDAC11 induced 100% mortality, we compared DEGs between these two datasets and identified several common genes (**Supplementary Data Sheet**_dsHDAC1 vs. dsHDAC11). Notably, the expression of CBP was up-regulated by seven-fold in both treatments. Since dsHDAC11 larval phenotypes showed enhanced pigmentation, we searched for genes coding for enzymes involved in melanization in our RNA-seq data. Interestingly, several genes coding for enzymes known to function in melanin biosynthesis were up-regulated in dsHDAC11 injected larvae (**Table 4**).

HDAC11 Knockdown Increases Acetylation Levels of Histone H3

Increase in acetylation levels of H3K9, H3K18, and H3K27 was detected in dsHDAC11 treated larvae compared to the levels in dsmalE treated larvae (**Figure 7A**). Also, TcA cells exposed to dsHDAC11 showed an increase in acetylation levels of core histones H3, H2, and H4 (**Figure 7B**) compared with control cells treated with dsmalE. An increase in acetylation levels of H3K9, H3K18 and H3K27 was detected in dsHDAC11 treated cells compared to control cells treated with dsmalE (**Figure 7B**). These data suggest that H3 is one of the targets for HDAC11 deacetylation.

DISCUSSION

We recently reported on the function of class I HDACs in JH suppression of metamorphosis in *T. castaneum* (George et al., 2019). Here, we investigated the role of the sole member of class IV HDACs, HDAC11. HDAC11 knockdown induced complete lethality during the larval stage. Human HDAC11 is biochemically distinct from other HDACs but phylogenetically closely related to class I HDACs (De Ruijter et al., 2003). Similarly, phylogenetic analysis of HDACs in *T. castaneum* revealed that TcHDAC11 is close to class I than to class II deacetylases (**Figure 1B**).

Interestingly, we observed that knockdown of the *HDAC11* gene during the final instar larval stage of the red flour beetle, *T. castaneum* resulted in a dark-colored larval phenotype that eventually died. Human HDAC11 is reported to be involved in the regulation of different inflammatory responses and diverse immune functions (Yanginlar and Logie, 2018). Dopa decarboxylase (Ddc) and phenoloxidase (PO) are necessary for insect cuticular melanization, and the molecular action of 20-hydroxyecdysone on various transcription factors leads to Ddc expression in *Manduca sexta* (Hiruma and Riddiford, 2009). Strict regulation of immune response and melanization is crucial for the proper development and survival of insects. RNA-seq data showed that the genes coding for enzymes (Tyrosine hydrolase, *Ddc*, Yellow-2, Laccase 1, Dopamine N acetyltransferase) known to be involved in insect melanin biosynthesis are up-regulated in HDAC11 knockdown larvae (**Table 4**). In *D. melanogaster*, microbial infection triggers activation of phenoloxidases; serine proteases and serine protease inhibitors (serpins) control the sites of infection (Tang, 2009). Differential expression of genes coding for several serine proteases, toll-like receptors, and serpins were observed in HDAC11 knockdown samples (Datasheet_melanization terms). Melanization and toll pathway share similar serine proteases in *D. melanogaster* (Dudzic et al., 2019).

Inhibition of HDAC11 induced the expression of p53 in human liver cancer cells and promoted apoptosis (Gong et al., 2019). HDAC11 is reported to be overexpressed in several carcinomas, and HDAC11 depletion causes cell death and inhibits metabolic activity in controlling proliferation in several human carcinoma cell lines (colon, prostate, ovarian cell lines) (Deubzer et al., 2013). Similarly, HDAC11 depletion in human neuroblastoma cells triggers caspase activation and caspase-dependent apoptosis (Thole et al., 2017). HDAC11 depletion in MYCN-driven neuroblastoma cell lines strongly induces cell death, mostly mediated by apoptotic programs (Thole et al., 2017). Inhibitor studies in mouse models showed that HDAC11 plays an important role in oncogene-induced hematopoiesis in myeloproliferative neoplasms (MPNs) (Yue et al., 2020). Based on these previous findings, it is tempting to hypothesize that HDAC11 knockdown may induce the death of some internal tissues resulting in the dark color detected in larvae. However, further work is required to identify specific tissues/cells involved and to uncover mechanisms behind the phenotype detected after HDAC11 knockdown in *T. castaneum* larvae.

Another finding of this research is the discovery that HDAC11 is required for larval development and metamorphosis in *T. castaneum*. This is the first report on the role of HDAC11 on the growth and development of insect larvae. RNA sequencing and RT-qPCR analysis showed that knockdown in HDAC11 affects the expression of JH and 20E response genes as well as those coding for proteins involved in the action of these two hormones. Since both JH and 20E play critical roles in larval development and metamorphosis (Jindra et al., 2013); HDAC11

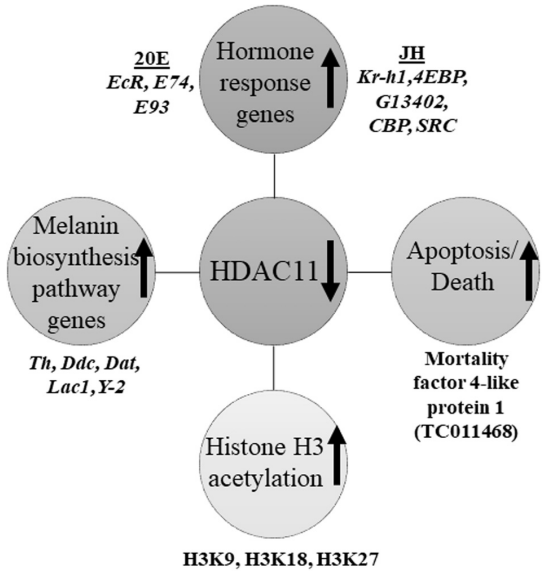

FIGURE 8 | Schematic representation of HDAC11 action in the red flour beetle. Here we summarized the results RNA sequencing and RT-qPCR analysis showed that knockdown in HDAC11 affects the expression of JH and 20E response genes as well as those coding for proteins involved in the action of these two hormones. Since both JH and 20E play critical roles in larval development and metamorphosis, HDAC11 may have blocked larval development and metamorphosis by affecting the action of these two hormones. The GO terms for pigmentation is significantly enriched in HDAC11 knockdown samples compared to the control. RNA-seq data showed that the genes coding for enzymes (Tyrosine hydrolase, *Ddc*, Yellow-2, Laccase 1, Dopamine N acetyltransferase) involved in insect melanin biosynthesis are up-regulated. RNAi mediated knockdown of HDAC11 induces mortality in larvae, pupae, and adults. Mortality factor 4-like protein 1 (TC011468) and apterous A (TC003972) were identified as differentially expressed genes in HDAC11 knockdown larvae. HDAC11 knockdown resulted in an increase in acetylation levels of histones H3, especially H3K18 and H3K27.

may block larval development and metamorphosis by affecting the action of these two hormones. RNA-seq analysis revealed several genes, including transcription factor sox-10, Hairy, CBP, SRC, chromatin remodeler SWI/SNF complex subunit SMARCC2, polycomb complex protein BMI-1-A, polycomb protein Scm, BTB/POZ, ultrabithorax, EcR, tramtrack, ecdysone-induced protein 74EF, and nuclear hormone receptor FTZ-F1 that showed an increase in expression in HDAC11 knockdown larvae. These data suggest that the deacetylation of histones and other proteins by HDAC11 may lead to a decrease in expression of these genes involved in JH and 20E action and response. However, the precise mechanisms involved in the arrest in larval development induced by HDAC11 knockdown remains to be elucidated. Further studies are required to uncover molecular mechanisms governing these phenotypes.

Apterous A (ap A, TC003972) and mortality factor 4-like protein 1 (TC011468) are significantly up-regulated in dsHDAC11 treated larvae. RT-qPCR reconfirmed RNA-seq predictions (**Figures 6A,B**). In *D. melanogaster*, apterous encodes a member of LIM (*Lin11*, *Isl-1& Mec-3*) homeobox transcription factor which contributes to the identity of wing cells, JH production, and neuronal pathfinding (Cohen et al., 1992). Mortality factor 4-like protein 1 (TC011468), also known as NuA4 complex subunit EAF3 homolog-like protein is a MORF-related gene and part of the Tip60 chromatin remodeling complex in *D. melanogaster*. Tip60 is involved in DNA repair by acetylating phosphorylated H2AV in *D. melanogaster* (Kusch et al., 2004). Mortality factor 4 like 1 protein regulates chromatin remodeling and mediates epithelial cell death in a mouse model of pneumonia (Zou et al., 2015). Interestingly, HDAC inhibitors activity leads to the modulation of expression of various genes and in turn, induces growth arrest, differentiation, and apoptotic cell death (Marks et al., 2000). Moreover, HDAC11 overexpression inhibits the cell cycle progression in fibroblast of Balb/c-3T3 cells. Also, the HDAC11 transcript was identified as a platelet-derived growth factor (PDGF) target, and HDAC11 mRNA abundance correlates inversely with proliferative status (Bagui et al., 2013). We identified fibroblast growth factor receptor homolog 1, ankyrin-3 as common genes up-regulated in HDAC11 knockdown larvae, or JH III treated cells (**Table 2**). Nuclear hormone receptors and their transcriptional coregulators were expressed in neural stem cells, and their expression was altered during differentiation induced by fibroblast growth factor 2 (FGF2) withdrawal. FGF2 withdrawal strongly induced the mRNA expression of HDAC11 in mouse cells (Androutsellis-Theotokis et al., 2013). Chromatin modifier, HDAC11, regulates lymph node metastasis development and dissemination in the breast cancer experimental model (Leslie et al., 2019). Human HDAC11 expression is limited to kidney, heart, brain, skeletal muscle, and testis, suggesting a tissue-specific function (Gao et al., 2002). Small interfering RNAs (siRNAs) that selectively inhibited HDAC11 expression, significantly up-regulated OX40L, and induced apoptosis in Hodgkin lymphoma (HL) cell lines. Silencing HDAC11 increased the production of tumor necrosis-α (TNF-α) and IL-17 in the supernatants of HL cells. An HDAC inhibitor study in human cell lines revealed that HDAC11 plays an essential role in regulating OX40 ligand expression in Hodgkin lymphoma (Buglio et al., 2011). The protein "Eiger" is the close homolog for OX40L in *T. castaneum* and *D. melanogaster* eiger (egr) encodes the TNF superfamily ligand that activates the intracellular JNK pathway, which mediates cell death, tumor suppression, and growth regulation (Igaki et al., 2002; Shklover et al., 2015). Our studies revealed that HDAC11 is essential for survival, and RNAi mediated knockdown induce developmental arrest and mortality.

HDAC11 regulates oligodendrocyte-specific gene expression and cell development in the cell line of rats by deacetylation of histone H3K9/K14 (Liu et al., 2009). Our western blots analysis showed that HDAC11 regulates acetylation levels of H3, specifically H3K9, H3K18 and H3K27. As demonstrated for HDAC1 in *T. castaneum* (George et al., 2019), HDAC11 may also influence acetylation levels of histones, especially H3, and regulate promoter access and, consequently, the expression of genes involved in JH and 20E action and response. In conclusion, we showed that HDAC11 knockdown affects hormone action and melanin biosynthesis and thereby arrest in development and metamorphosis of the red flour beetle, *T. castaneum* (**Figure 8**).

DATA AVAILABILITY STATEMENT

We have deposited the short-read (Illumina HiSeq 4000) sequence data in the NCBI SRA (accession numbers PRJNA495026 and PRJNA612004). BioSample metadata are available in the NCBI BioSample database (http://www.ncbi.nlm.nih.gov/biosample/) under accession numbers SAMN10203356, SAMN10203357, SAMN14356366, and SAMN14356367).

AUTHOR CONTRIBUTIONS

SG and SP designed the experiments, and wrote the manuscript. SG carried out the experiments. Both authors contributed to the article and approved the submitted version.

FUNDING

This work was supported by grants from the National Institute of Health (GM070559-14) and the National Institute of Food and Agriculture, US Department of Agriculture (HATCH project 2351177000).

ACKNOWLEDGMENTS

We thank Najla Albishi for help with microscopic techniques and Hunt lab for RNA-seq analysis.

SUPPLEMENTARY MATERIAL

The Supplementary Material for this article can be found online at: https://www.frontiersin.org/articles/10.3389/fgene.2020.00683/full#supplementary-material

REFERENCES

Androutsellis-Theotokis, A., Chrousos, G. P., Mckay, R. D., Decherney, A. H., and Kino, T. (2013). Expression profiles of the nuclear receptors and their transcriptional coregulators during differentiation of neural stem cells. *Horm. Metab. Res.* 45, 159–168. doi: 10.1055/s-0032-1321789

Bagui, T. K., Sharma, S. S., Ma, L., and Pledger, W. J. (2013). Proliferative status regulates HDAC11 mRNA abundance in nontransformed fibroblasts. *Cell Cycle* 12, 3433–3441. doi: 10.4161/cc.26433

Bodai, L., Zsindely, N., Gaspar, R., Kristo, I., Komonyi, O., and Boros, I. M. (2012). Ecdysone induced gene expression is associated with acetylation of histone H3 lysine 23 in *Drosophila melanogaster*. *PLoS One* 7:e40565. doi: 10.1371/journal.pone.0040565

Bryant, D. T., Landles, C., Papadopoulou, A. S., Benjamin, A. C., Duckworth, J. K., Rosahl, T., et al. (2017). Disruption to schizophrenia-associated gene Fez1 in the hippocampus of HDAC11 knockout mice. *Sci. Rep.* 7: 11900.

Buglio, D., Khaskhely, N. M., Voo, K. S., Martinez-Valdez, H., Liu, Y. J., and Younes, A. (2011). HDAC11 plays an essential role in regulating OX40 ligand expression in Hodgkin lymphoma. *Blood* 117, 2910–2917. doi: 10.1182/blood-2010-08-303701

Cohen, B., Mcguffin, M. E., Pfeifle, C., Segal, D., and Cohen, S. M. (1992). apterous, a gene required for imaginal disc development in *Drosophila* encodes a member of the LIM family of developmental regulatory proteins. *Genes Dev.* 6, 715–729. doi: 10.1101/gad.6.5.715

Cui, Y., Sui, Y., Xu, J., Zhu, F., and Palli, S. R. (2014). Juvenile hormone regulates *Aedes aegypti* Kruppel homolog 1 through a conserved E box motif. *Insect. Biochem. Mol. Biol.* 52, 23–32. doi: 10.1016/j.ibmb.2014.05.009

De Ruijter, A. J., Van Gennip, A. H., Caron, H. N., Kemp, S., and Van Kuilenburg, A. B. (2003). Histone deacetylases (HDACs): characterization of the classical HDAC family. *Biochem. J.* 370, 737–749. doi: 10.1042/bj20021321

Deubzer, H. E., Schier, M. C., Oehme, I., Lodrini, M., Haendler, B., Sommer, A., et al. (2013). HDAC11 is a novel drug target in carcinomas. *Int. J. Cancer* 132, 2200–2208. doi: 10.1002/ijc.27876

Dudzic, J. P., Hanson, M. A., Iatsenko, I., Kondo, S., and Lemaitre, B. (2019). More than black or white: melanization and toll share regulatory serine proteases in *Drosophila*. *Cell Rep.* 27, 1050–1061.

Fernandez-Nicolas, A., and Belles, X. (2016). CREB-binding protein contributes to the regulation of endocrine and developmental pathways in insect hemimetabolan pre-metamorphosis. *Biochim. Biophys. Acta* 1860, 508–515. doi: 10.1016/j.bbagen.2015.12.008

Foglietti, C., Filocamo, G., Cundari, E., De Rinaldis, E., Lahm, A., Cortese, R., et al. (2006). Dissecting the biological functions of *Drosophila* histone deacetylases by RNA interference and transcriptional profiling. *J. Biol. Chem.* 281, 17968–17976. doi: 10.1074/jbc.m511945200

Futahashi, R., and Fujiwara, H. (2008). Juvenile hormone regulates butterfly larval pattern switches. *Science* 319:1061. doi: 10.1126/science.1149786

Gao, L., Cueto, M. A., Asselbergs, F., and Atadja, P. (2002). Cloning and functional characterization of HDAC11, a novel member of the human histone deacetylase family. *J. Biol. Chem.* 277, 25748–25755. doi: 10.1074/jbc.m111871200

Geer, L. Y., Domrachev, M., Lipman, D. J., and Bryant, S. H. (2002). CDART: protein homology by domain architecture. *Genome Res.* 12, 1619–1623. doi: 10.1101/gr.278202

George, S., Gaddelapati, S. C., and Palli, S. R. (2019). Histone deacetylase 1 suppresses Krüppel homolog 1 gene expression and influences juvenile hormone action in *Tribolium castaneum*. *Proc. Natl. Acad. Sci. U.S.A.* 116, 17759–17764. doi: 10.1073/pnas.1909554116

George, S. and Palli, S. R. (2020). Histone deacetylase 3 is required for development and metamorphosis in the red flour beetle, *Tribolium castaneum*. *BMC Genomics*. 21:420. doi: 10.1186/s12864-020-06840-3

Giray, T., Giovanetti, M., and West-Eberhard, M. J. (2005). Juvenile hormone, reproduction, and worker behavior in the neotropical social wasp *Polistes canadensis*. *Proc. Natl. Acad. Sci. U.S.A.* 102, 3330–3335. doi: 10.1073/pnas.0409560102

Gong, D., Zeng, Z., Yi, F., and Wu, J. (2019). Inhibition of histone deacetylase 11 promotes human liver cancer cell apoptosis. *Am. J. Transl. Res.* 11, 983–990.

Goodman, C. L., Stanley, D., Ringbauer, J. A. Jr., Beeman, R. W., and Silver, K. (2012). A cell line derived from the red flour beetle *Tribolium castaneum* (Coleoptera: Tenebrionidae). *Vitro Cell Dev. Biol. Anim.* 48, 426–433. doi: 10.1007/s11626-012-9524-x

Haliscak, J. P., and Beeman, R. W. (1983). Status of malathion resistance in five genera of beetles infesting farm-stored corn, wheat, and oats in the United States. *J. Econ. Entomol.* 76, 717–722. doi: 10.1093/jee/76.4.717

Hartfelder, K. (2000). Insect juvenile hormone: from "status quo" to high society. *Braz. J. Med. Biol. Res.* 33, 157–177. doi: 10.1590/s0100-879x2000000200003

Hiruma, K., and Riddiford, L. M. (2009). The molecular mechanisms of cuticular melanization: the ecdysone cascade leading to dopa decarboxylase expression in *Manduca sexta*. *Insect. Biochem. Mol. Biol.* 39, 245–253. doi: 10.1016/j.ibmb.2009.01.008

Hrdy, I., Kuldova, J., Hanus, R., and Wimmer, Z. (2006). Juvenile hormone III, hydroprene and a juvenogen as soldier caste differentiation regulators in three *Reticulitermes* species: potential of juvenile hormone analogues in termite control. *Pest. Manag. Sci.* 62, 848–854. doi: 10.1002/ps.1244

Hunt, A. G. (2015). A rapid, simple, and inexpensive method for the preparation of strand-specific RNA-Seq libraries. *Methods Mol. Biol.* 1255, 195–207. doi: 10.1007/978-1-4939-2175-1_17

Igaki, T., Kanda, H., Yamamoto-Goto, Y., Kanuka, H., Kuranaga, E., Aigaki, T., et al. (2002). Eiger, a TNF superfamily ligand that triggers the *Drosophila* JNK pathway. *EMBO J.* 21, 3009–3018. doi: 10.1093/emboj/cdf306

Jindra, M., Palli, S. R., and Riddiford, L. M. (2013). The juvenile hormone signaling pathway in insect development. *Annu. Rev. Entomol.* 58, 181–204. doi: 10.1146/annurev-ento-120811-153700

Kalsi, M., and Palli, S. R. (2017). Cap n collar transcription factor regulates multiple genes coding for proteins involved in insecticide detoxification in the red flour beetle, *Tribolium castaneum*. *Insect. Biochem. Mol. Biol.* 90, 43–52. doi: 10.1016/j.ibmb.2017.09.009

Kayukawa, T., Minakuchi, C., Namiki, T., Togawa, T., Yoshiyama, M., Kamimura, M., et al. (2012). Transcriptional regulation of juvenile hormone-mediated induction of Krüppel homolog 1, a repressor of insect metamorphosis. *Proc. Natl. Acad. Sci. U.S.A.* 109, 11729–11734. doi: 10.1073/pnas.1204951109

Konopova, B., and Jindra, M. (2007). Juvenile hormone resistance gene Methoprene-tolerant controls entry into metamorphosis in the beetle *Tribolium castaneum*. *Proc. Natl. Acad. Sci. U.S.A.* 104, 10488–10493. doi: 10.1073/pnas.0703719104

Kumar, S., Stecher, G., and Tamura, K. (2016). MEGA7: molecular evolutionary genetics analysis version 7.0 for bigger datasets. *Mol. Biol. Evol.* 33, 1870–1874. doi: 10.1093/molbev/msw054

Kusch, T., Florens, L., Macdonald, W. H., Swanson, S. K., Glaser, R. L., Yates, J. R., et al. (2004). Acetylation by Tip60 is required for selective histone variant exchange at DNA lesions. *Science* 306, 2084–2087. doi: 10.1126/science.1103455

Lehrmann, H., Pritchard, L. L., and Harel-Bellan, A. (2002). Histone acetyltransferases and deacetylases in the control of cell proliferation and differentiation. *Adv. Cancer Res.* 86, 41–65. doi: 10.1016/s0065-230x(02)86002-x

Leslie, P. L., Chao, Y. L., Tsai, Y. H., Ghosh, S. K., Porrello, A., Van Swearingen, A. E. D., et al. (2019). Histone deacetylase 11 inhibition promotes breast cancer metastasis from lymph nodes. *Nat. Commun.* 10:4192.

Li, M., Mead, E. A., and Zhu, J. (2011). Heterodimer of two bHLH-PAS proteins mediates juvenile hormone-induced gene expression. *Proc. Natl. Acad. Sci. U.S.A.* 108, 638–643. doi: 10.1073/pnas.1013914108

Liu, H., Hu, Q., D'ercole, A. J., and Ye, P. (2009). Histone deacetylase 11 regulates oligodendrocyte-specific gene expression and cell development in OL-1 oligodendroglia cells. *Glia* 57, 1–12. doi: 10.1002/glia.20729

Ma, L., Pati, P. K., Liu, M., Li, Q. Q., and Hunt, A. G. (2014). High throughput characterizations of poly(A) site choice in plants. *Methods* 67, 74–83. doi: 10.1016/j.ymeth.2013.06.037

Marks, P. A., Richon, V. M., and Rifkind, R. A. (2000). Histone deacetylase inhibitors: inducers of differentiation or apoptosis of transformed cells. *J. Natl. Cancer Inst.* 92, 1210–1216. doi: 10.1093/jnci/92.15.1210

Min, K. J., Jones, N., Borst, D. W., and Rankin, M. A. (2004). Increased juvenile hormone levels after long-duration flight in the grasshopper, *Melanoplus sanguinipes*. *J. Insect Physiol.* 50, 531–537. doi: 10.1016/j.jinsphys.2004.03.009

Palli, S. R., Hormann, R. E., Schlattner, U., and Lezzi, M. (2005). Ecdysteroid receptors and their applications in agriculture and medicine. *Vitam. Horm.* 73, 59–100. doi: 10.1016/s0083-6729(05)73003-x

Parthasarathy, R., Tan, A., and Palli, S. R. (2008). bHLH-PAS family transcription factor methoprene-tolerant plays a key role in JH action in preventing the premature development of adult structures during larval-pupal metamorphosis. *Mech. Dev.* 125, 601–616. doi: 10.1016/j.mod.2008.03.004

Riddiford, L. M. (1994). Cellular and molecular actions of juvenile-hormone.1. General-considerations and premetamorphic actions. *Adv. Insect. Physiol.* 24, 213–274. doi: 10.1016/s0065-2806(08)60084-3

Riddiford, L. M. (1996). Juvenile hormone: the status of its "status quo" action. *Arch. Insect. Biochem. Physiol.* 32, 271–286. doi: 10.1002/(sici)1520-6327(1996)32:3/4<271::aid-arch2>3.0.co;2-w

Riddiford, L. M. (2012). How does juvenile hormone control insect metamorphosis and reproduction? *Gen. Comp. Endocrinol.* 179, 477–484. doi: 10.1016/j.ygcen.2012.06.001

Riddiford, L. M., Cherbas, P., and Truman, J. W. (2000). Ecdysone receptors and their biological actions. *Vitam. Horm.* 60, 1–73. doi: 10.1016/s0083-6729(00)60016-x

Roy, A., George, S., and Palli, S. R. (2017). Multiple functions of CREB-binding protein during postembryonic development: identification of target genes. *BMC Genomics* 18:996. doi: 10.1186/s12864-017-4373-3

Roy, A., and Palli, S. R. (2018). Epigenetic modifications acetylation and deacetylation play important roles in juvenile hormone action. *BMC Genomics* 19:934. doi: 10.1186/s12864-017-4373-934

Shklover, J., Levy-Adam, F., and Kurant, E. (2015). The role of *Drosophila* TNF Eiger in developmental and damage-induced neuronal apoptosis. *FEBS Lett.* 589, 871–879. doi: 10.1016/j.febslet.2015.02.032

Singtripop, T., Wanichacheewa, S., and Sakurai, S. (2000). Juvenile hormone-mediated termination of larval diapause in the bamboo borer, Omphisa fuscidentalis. *Insect. Biochem. Mol. Biol.* 30, 847–854. doi: 10.1016/s0965-1748(00)00057-6

Sun, L., Marin De Evsikova, C., Bian, K., Achille, A., Telles, E., Pei, H., et al. (2018). Programming and regulation of metabolic homeostasis by HDAC11. *eBio Med.* 33, 157–168. doi: 10.1016/j.ebiom.2018.06.025

Tang, H. (2009). Regulation and function of the melanization reaction in *Drosophila*. *Fly* 3, 105–111. doi: 10.4161/fly.3.1.7747

Thole, T. M., Lodrini, M., Fabian, J., Wuenschel, J., Pfeil, S., Hielscher, T., et al. (2017). Neuroblastoma cells depend on HDAC11 for mitotic cell cycle progression and survival. *Cell Death Dis.* 8:e2635. doi: 10.1038/cddis.2017.49

Thurmond, J., Goodman, J. L., Strelets, V. B., Attrill, H., Gramates, L. S., Marygold, S. J., et al. (2019). FlyBase 2.0: the next generation. *Nucleic Acids Res.* 47, D759–D765.

Tie, F., Banerjee, R., Stratton, C. A., Prasad-Sinha, J., Stepanik, V., Zlobin, A., et al. (2009). CBP-mediated acetylation of histone H3 lysine 27 antagonizes *Drosophila* Polycomb silencing. *Development* 136, 3131–3141. doi: 10.1242/dev.037127

Todd, P. K., Oh, S. Y., Krans, A., Pandey, U. B., Di Prospero, N. A., Min, K.-T., et al. (2010). Histone Deacetylases suppress CGG repeat-induced neurodegeneration via transcriptional silencing in models of fragile X tremor ataxia syndrome. *PLoS Genet.* 6:e1001240. doi: 10.1371/journal.pone.001001240

Wigglesworth, V. B. (1934). Factors controlling moulting and 'metamorphosis' in an insect. *Nature* 133, 725–726. doi: 10.1038/133725b0

Wilson, T. G., and Fabian, J. (1986). A *Drosophila melanogaster* mutant resistant to a chemical analog of juvenile hormone. *Dev. Biol.* 118, 190–201. doi: 10.1016/0012-1606(86)90087-4

Wyatt, G. R., Davey, K. G., and Evans, P. D. (1996). Cellular and molecular actions of juvenile hormone. II. roles of juvenile hormone in adult insects. *Adv. Insect. Physiol.* 26, 1–15.

Xu, J., Roy, A., and Palli, S. R. (2018). CREB-binding protein plays key roles in juvenile hormone action in the red flour beetle, *Tribolium castaneum*. *Sci. Rep.* 8:1426.

Yang, X. J., and Seto, E. (2008). The Rpd3/Hda1 family of lysine deacetylases: from bacteria and yeast to mice and men. *Nat. Rev. Mol. Cell Biol.* 9, 206–218. doi: 10.1038/nrm2346

Yanginlar, C., and Logie, C. (2018). HDAC11 is a regulator of diverse immune functions. *Biochim. Biophys. Acta Gen. Regul. Mech.* 1861, 54–59. doi: 10.1016/j.bbagrm.2017.12.002

Ye, J., Fang, L., Zheng, H., Zhang, Y., Chen, J., Zhang, Z., et al. (2006). WEGO: a web tool for plotting GO annotations. *Nucleic Acids Res.* 34, W293–W297.

Yue, L., Sharma, V., Horvat, N. P., Akuffo, A. A., Beatty, M. S., Murdun, C., et al. (2020). HDAC11 deficiency disrupts oncogene-induced hematopoiesis in myeloproliferative neoplasms. *Blood* 135, 191–207. doi: 10.1182/blood.2019895326

Zhang, Z. L., Xu, J. J., Sheng, Z. T., Sui, Y. P., and Palli, S. R. (2011). Steroid receptor co-activator is required for juvenile hormone signal transduction through a bHLH-PAS transcription factor, methoprene tolerant. *J. Biol. Chem.* 286, 8437–8447. doi: 10.1074/jbc.m110.191684

Zou, C., Li, J., Xiong, S., Chen, Y., Wu, Q., Li, X., et al. (2015). Mortality factor 4 like 1 protein mediates epithelial cell death in a mouse model of pneumonia. *Sci. Transl. Med.* 7:311ra171. doi: 10.1126/scitranslmed.aac7793

Conflict of Interest: The authors declare that the research was conducted in the absence of any commercial or financial relationships that could be construed as a potential conflict of interest.

frontiers in Genetics

ORIGINAL RESEARCH
published: 10 July 2020
doi: 10.3389/fgene.2020.00723

Investigation of Isoform Specific Functions of the V-ATPase a Subunit During *Drosophila* Wing Development

*Dongqing Mo, Yao Chen, Na Jiang, Jie Shen and Junzheng Zhang**

Department of Entomology and MOA Key Lab of Pest Monitoring and Green Management, College of Plant Protection, China Agricultural University, Beijing, China

The vacuolar ATPases (V-ATPases) are ATP-dependent proton pumps that play vital roles in eukaryotic cells. Insect V-ATPases are required in nearly all epithelial tissues to regulate a multiplicity of processes including receptor-mediated endocytosis, protein degradation, fluid secretion, and neurotransmission. Composed of fourteen different subunits, several V-ATPase subunits exist in distinct isoforms to perform cell type specific functions. The 100 kD a subunit (Vha100) of V-ATPases are encoded by a family of five genes in *Drosophila*, but their assignments are not fully understood. Here we report an experimental survey of the *Vha100* gene family during *Drosophila* wing development. A combination of CRISPR-Cas9 mutagenesis, somatic clonal analysis and *in vivo* RNAi assays is used to characterize the requirement of Vha100 isoforms, and mutants of *Vha100-2*, *Vha100-3, Vha100-4,* and *Vha100-5* genes were generated. We show that *Vha100-3* and *Vha100-5* are dispensable for fly development, while *Vha100-1* is not critically required in the wing. As for the other two isoforms, we find that *Vha100-2* regulates wing cuticle maturation, while *Vha100-4* is the single isoform involved in developmental patterning. More specifically, *Vha100-4* is required for proper activation of the Wingless signaling pathway during fly wing development. Interestingly, we also find a specific genetic interaction between *Vha100-1* and *Vha100-4* during wing development. Our results revealed the distinct roles of *Vha100* isoforms during insect wing development, providing a rationale for understanding the diverse roles of V-ATPases.

Keywords: V-ATPase a subunit, wing development, *Drosophila melanogaster*, V-ATPase isoform, V100-2

OPEN ACCESS

Edited by:
Wei Guo,
Institute of Zoology (CAS), China

Reviewed by:
Lihua Huang,
South China Normal University, China
Aishwarya Swaminathan,
University of Massachusetts Medical School, United States
Xubo Zhang,
Shanxi University, China

***Correspondence:**
Junzheng Zhang
zhangjz@cau.edu.cn

Specialty section:
This article was submitted to Epigenomics and Epigenetics, a section of the journal Frontiers in Genetics

Received: *20 March 2020*
Accepted: *15 June 2020*
Published: *10 July 2020*

Citation:
Mo D, Chen Y, Jiang N, Shen J and Zhang J (2020) Investigation of Isoform Specific Functions of the V-ATPase a Subunit During Drosophila Wing Development. Front. Genet. 11:723. doi: 10.3389/fgene.2020.00723

INTRODUCTION

The vacuolar ATPases (V-ATPases) are ubiquitous proton pumps which play important roles in eukaryotic cells (Forgac, 2007). V-ATPases transport proton into intracellular compartments, and are therefore crucial for pH homeostasis in organelles such as endosomes, secretory vesicles, synaptic vesicles, and lysosomes (Hinton et al., 2009). The V-ATPases are generally required for a broad spectrum of cellular processes, including endosomal trafficking, lysosomal degradation, and exocytosis (Forgac, 2007). Insect V-ATPases are expressed in nearly all epithelial tissues and are well-known for their roles in physiological activities such as secretion of K + and

Na + and formation of fluid (Wieczorek et al., 2009). Moreover, recent studies have illuminated the importance of V-ATPases for insect development. In *Drosophila melanogaster*, mutations that dampen the V-ATPases activity are reported to disrupt the formation of eye, wing and egg chambers (Yan et al., 2009; Buechling et al., 2010; Hermle et al., 2010; Vaccari et al., 2010). Further studies demonstrated that V-ATPases are involved in regulation of cell proliferation, cell fate determination and tissue patterning through modification of key developmental signaling pathways (Kobia et al., 2013; Gleixner et al., 2014; Portela et al., 2018; Ren et al., 2018).

The V-ATPase is a large protein complex composed of 14 different subunits that are organized into the cytosolic V1 region and the membrane-bound V0 region (Nelson, 2003). Region V1 hydrolyzes ATP and provides energy to pump protons through the protein lipid pores formed in region V0 (Jianhua et al., 2015). The V1 region contains eight subunits while the V0 domain is assembled by six different subunits (Forgac, 2007). The regulatory C subunit is located in the V1 domain and interacts with subunit a in the V0 domain (Wilkens et al., 2004; Inoue and Forgac, 2005; Cipriano et al., 2008). Therefore, the C subunit is well positioned to control the reversible dissociation of the V-ATPase complex (Inoue et al., 2005; Forgac, 2007). The C subunit is encoded by *Vha44* in *Drosophila*, which is required for endolysosomal acidification and regulates elimination of nurse cells in the ovary (Mondragon et al., 2019), cell competition in the eye imaginal disk (Nagata et al., 2019), and apical endocytosis in the wing disk epithelial cells (Gleixner et al., 2014). Ectopic *Vha44* expression is shown to impair endolysosomal degradation and induce invasive cell behavior in the developing wing disk (Petzoldt et al., 2013) as well as differentiation defects in the eye disk (Portela et al., 2018).

Many of the V-ATPase subunits exist in multiple isoforms which are often expressed in a cell type specific manner (Toei et al., 2010). In *Drosophila*, the V-ATPase multigene family consists of 33 different genes (Julian, 1999; Allan et al., 2005). Apart from five subunits in the V1 region and the accessory subunits VhaAC45 and VhaM8.9, other V-ATPase subunits are encoded by two to five genes (Allan et al., 2005). In vertebrates, isoforms of subunit a in the V0 domain contain information necessary for targeting the V-ATPase complexes to the appropriate plasma membrane (Toyomura et al., 2003; Qi et al., 2007; Saw et al., 2011). In *Drosophila*, the V-ATPase a subunit is encoded by *Vha100-1*, *Vha100-2*, *Vha100-3*, *Vha100-4,* and *Vha100-5* with specific tissue distribution patterns (Toei et al., 2010). Previous studies have suggested that Vha100-1 is an isoform required for synaptic vesicle exocytosis in the nervous system (Hiesinger et al., 2005). Loss of *Vha100-1* leads to vesicle accumulation in synaptic terminals (Wang et al., 2014), neuronal degeneration (Williamson et al., 2010a), and defects in brain wiring (Williamson et al., 2010b). RNAi knock-down experiments indicate that *Vha100-2* is involved in regulation of neural stem cells proliferation (Wissel et al., 2018), acid generation of the midgut (Overend et al., 2016), elimination of nurse cells in the ovary (Mondragon et al., 2019), and cell competition in the eye disk (Nagata et al., 2019). Similar as *Vha100-2*, knock-down of *Vha100-4* also leads to acidification defect in the larval midgut (Overend et al., 2016). The roles of *Vha100-3* and *Vha100-5* are still unclear, and our understanding of whether and how Vha100 isoforms collaboratively regulate the development of specific tissue is incomplete.

In order to further investigate the functional diversity of the V-ATPase a subunit isoforms, we generated and characterized mutants of *Vha100-2, -3, -4,* and *-5*. We found that among the five isoforms, *Vha100*-3 and *Vha100*-5 are dispensable for fly development. We further demonstrated that *Vha100-2* is specifically required for wing cuticle formation, while *Vha100-4* is involved in Wingless signaling activation. Comparative studies revealed that *Vha100-1* and *Vha100-4* execute both independent and redundant function during fly wing development. Our studies uncovered the isoform specific functions of the V-ATPase a subunit during *Drosophila* wing development.

MATERIALS AND METHODS

Fly Genetics

Fly stocks and all fly crosses were maintained at 25°C on standard fly food. The following fly stocks were used: *hh*-Gal4, UAS-*mCD8-gfp/TM6B* (Ren et al., 2018); *Vha100-2* RNAi (TH04790.N; TsingHua Fly Center); *FRT42D*, $Vha44^{KG00915}$*/Cyo* (#111534; Kyoto Stock Center); *FRT42D*, $Vha44^{K05440}$*/Cyo* (#111081; Kyoto Stock Center); *FRT82B,* $Vha100\text{-}1^{1}$*/TM3, Sb* (#39669; Bloomington Drosophila Stock Center); *w;Sco/Cyo* (#2555; Bloomington Drosophila Stock Center); and *w;TM3/TM6B* (#2537; Bloomington Drosophila Stock Center). The *Ubx-FLP; FRT82B, Ubi-RFP/TM6B, Ubx-FLP; FRT42D, Ubi-RFP/Cyo,* and *Ubx-FLP; FRT42D, Ubi-GFP*/*Cyo* stocks were used to generate mosaic mutant clones in the wing disks (Ren et al., 2018). The *sens−GFP* reporter was described before (Sarov et al., 2016) and obtained from Bloomington Drosophila Stock Center (#38666). The *fz3*-LacZ reporter was described before (Sato et al., 1999).

CRISPR-Cas9 Mediated Mutagenesis

The sgRNA targets were designed against the genomic sequences of *Vha100-2, Vha100-3, Vha100-4,* and *Vha100-5* with CRISPR Optimal Target Finder[1] (Gratz et al., 2014). Templates for sgRNA transcription were generated by annealing of two DNA oligonucleotides and subsequent PCR amplification (Bassett et al., 2013). *In vitro* transcription was performed with the T7 RiboMAX^{TM} Kit (Promega, P1320) and the sgRNAs were purified by phenol-choloroform extraction and isopropanol precipitation. Cas9 mRNA was transcribed with the mMESSAGE mMACHINE® T7 Transcription Kit (Ambion), using a linearized plasmid containing the Cas9 cDNA (Addgene plasmid 42251) as template. The Cas9 mRNA were polyadenylated with the Escherichia *coli* Poly(A) polymerase Kit (NEB), and purified with the RNeasy Mini Kit (QIAGEN). 15 μg of Cas9 mRNA and 7.5 μg sgRNA were mixed with DEPC water in a 30 μl volume for embryo injection. Fly embryos of the w^{1118} strain (#5905; Bloomington Drosophila Stock Center) were injected using standard protocols by Fungene Biotech (Beijing, China).

[1] http://tools.flycrispr.molbio.wisc.edu/targetFinder/

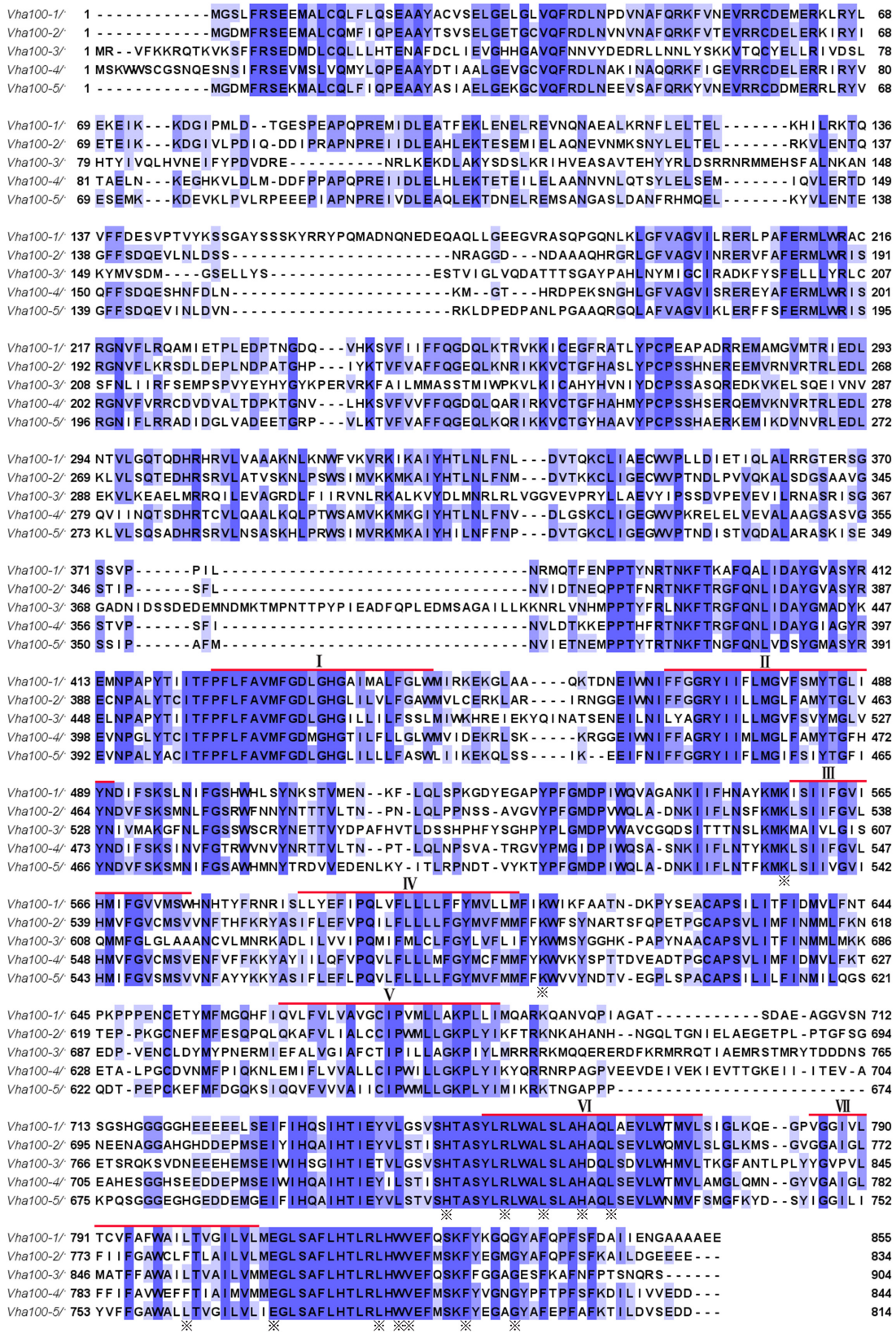

FIGURE 1 | Continued

FIGURE 1 | Amino acid sequences and structures of V-ATPase subunit a isoforms in *Drosophila*. Alignment of the five *Drosophila* V-ATPase a subunit isoform sequences (Vha100-1, Vha100-2, Vha100-3, Vha100-4, and Vha100-5) is shown. Identical residues are indicated by blue shades and similar residues are labeled by light purple shades. The seven putative transmembrane helices predicted from topographical analysis are shown with a red bar. The residues whose mutation has a significant effect on activity or assembly of the V-ATPase are indicated by asterisks. GenBank accession numbers assigned to Vha100-1, Vha100-2, Vha100-3, Vha100-4, and Vha100-5 are AAF56861, AAF55551, AAM68427, AAF55550, and AAF53116, respectively.

TABLE 1 | The sequence identity (and similarity) between pairs of *Drosophila* a subunit isoforms.

Pairs of isoforms	Identity and (similarity)	Pairs of isoforms	Identity and (similarity)
Vha100-1 and Vha100-2	58% (71%)	Vha100-2 and Vha100-4	65% (79%)
Vha100-1 and Vha100-3	36% (51%)	Vha100-2 and Vha100-5	65% (79%)
Vha100-1 and Vha100-4	53% (67%)	Vha100-3 and Vha100-4	33% (51%)
Vha100-1 and Vha100-5	57% (71%)	Vha100-3 and Vha100-5	35% (53%)
Vha100-2 and Vha100-3	35% (54%)	Vha100-4 and Vha100-5	56% (72%)

Males developed from the injected embryos (G0) were outcrossed to virgin females of *TM3/TM6B* (for *Vha100-2* and *Vha100-4*) or *Sco/Cyo* (for *Vha100-3* and *Vha100-5*). Single G1 males were each crossed to 4–5 females of the corresponding balancer stocks and the progenies (G2) bearing the same balancer chromosome were maintained as an independent stock. About 50 G2 stocks were established from each injection, and mutations were screened by PCR test of genomic DNAs. Primer pairs were designed to generate PCR products covering the target sites, which were compared with the control sequences amplified from w^{1118} genomic DNA. The primers used are: V100-2F: AACGTTGTCGTTGGCTGAAGCA; V100-2R: ATGT CATCCTGGATGTCGGGCA; V100-3F: CTGCGCATCGTGG ACAGTCTG; V100-3R: GAATGATCAGGTTGAAGGAGC; V100-4F: GCTGTGCTCCGAAAGTGAG; V100-4R: ACCT TGTGACCCTCCTTGTT; V100-5F: CAGTTATAACACTCG ATTTGA; and V100-5R: TTGAGTTCTTGCATGTGCCGGA. Mutant alleles were identified and named as $Vha100\text{-}2^{D2}$, $Vha100\text{-}3^{D3}$, $Vha100\text{-}4^{D4}$, and $Vha100\text{-}5^{D5}$. FRT82B (#2035; Bloomington Drosophila Stock Center) was recombined into the $Vha100\text{-}2^{D2}$ and $Vha100\text{-}4^{D4}$ mutant genomes by standard genetic crosses for further mosaic analysis.

mRNA *in situ* Hybridization in *Drosophila* Wing Imaginal Disks

The coding regions of *Vha100-2* (1208 bp–1430 bp of GeneBank #AAF55551) and *Vha100-4* (982 bp–1240 bp of GeneBank #AAF55550) were used to generate antisense RNA probes for *in situ* hybridization. An autofluorescent alkaline phosphatase substrate (Vector) was used to visualize mRNA in the rhodamine channel, and mutant clones were marked by immunofluorescence staining of GFP protein as described before (Su et al., 2011).

Immunofluorescence Staining

Wing disks dissected from third-instar larvae were fixed in 4% paraformaldehyde for 15 min, blocked in PBS containing 0.1% Triton X–100 and 0.2% BSA for 1 h, and incubated overnight at 4°C with the following primary antibodies: mouse anti-Cut (1:100; 2B10; and DSHB), mouse anti-Wingless (1:200; 4D4; and DSHB), mouse anti-Notch intracellular domain NICD (1:200; C17.9C6; and DSHB), mouse anti- Notch extracellular domain NECD (1:200; C458.2H; and DSHB), mouse anti-Dl (1:200; C594.9B; and DSHB), rabbit anti-GFP (1:2000; A11122; and Thermo Fisher), and rabbit anti-Caspase3 (1:200; Cell signaling). Alexa fluor-conjugated secondary antibodies (1:400; Invitrogen) were used. Alexa fluor-568 conjugated phalloidin was used to label cell morphology (1:200; Thermo Fisher). The fluorescence images were acquired with Leica SP8 confocal microscope and processed in Photoshop and ImageJ.

TABLE 2 | Summary of CRISPR-Cas9 sgRNA sequences.

Gene symbol	sgRNA-1 sequence	sgRNA-2 sequence
Vha100-2	GATGTTCCGTAGTGAGGAGA	GTATACCTCCGTATCTGAGC
Vha100-3	GATTTCGACGACTGTCCAGT	GCACAGCTTCGCTTTGAACA
Vha100-4	GCAAATGTATCTGCAGCCGG	GTTGCCGCCTTGGGCGAGGT
Vha100-5	GGGCGTAGGCTGCCTCCGGC	GTTTCGCGATCTGAACGAGG

Eosin Y and FB28 Staining and Microscopy of the Adult Wing

Adult flies with correct genotypes were collected and fixed overnight in isopropanol. Dissected adult wings were mounted in Euparal mounting media (BioQuip). For Eosin Y and FB28 staining experiments, 2 days old files were fixed in formaldehyde phosphate buffer, washed several times with PBS, and stained with FB28 solution (1 mg/ml; Sigma-Aldrich) at room temperature for 1 h or 0.5% Eosin Y at 55°C for 35 min. Adult wings were then dissected and mounted in 80% glycerol. The images were captured with a Leica DMIL inverted microscope equipped with a QICAM Fast 1394 digital camera.

RESULTS

Vha100 Isoforms Are Differentially Required for Fly Development

The a subunit of the V-ATPase is encoded by five genes in *Drosophila*, which are spread at different locations throughout

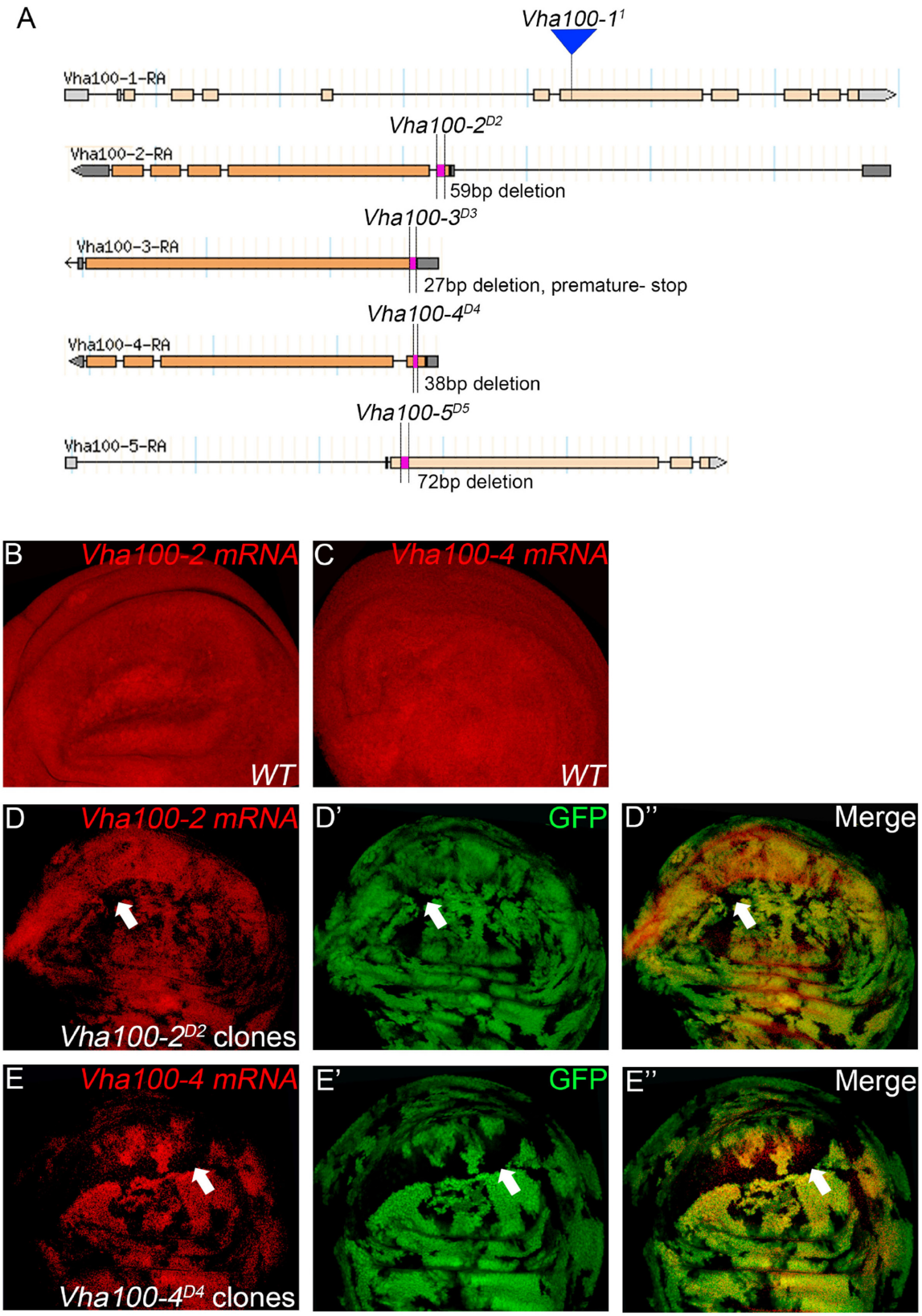

FIGURE 2 | Continued

FIGURE 2 | Generation and verification of *Vha100* mutants. **(A)** Schematic illustration of *Vha100* mutant alleles. The *Vha100-1*^{1} is a loss of function allele caused by mutation in the splice acceptor site. CRISPR-Cas9 mediated deleterious alleles are generated for other members of the *Vha100* family. The position and molecular nature of each allele is labeled. **(B–E)** *In situ* hybridization in *Drosophila* wing imaginal disks. In wild type wing disks, *Vha100-2* **(B)** and *Vha100-4* **(C)** are ubiquitously expressed. In *Vha100-2*^{D2} mutant clones, the mRNA levels (red) are significantly down-regulated **(D)**. The mRNA levels of *Vha100-4* (red) are significantly down-regulated in *Vha100-4*^{D4} clones **(E)**. The down-regulation of *Vha100-2* (n = 11) and *Vha100-4* (n = 14) in mutant clones is fully penetrant. The mutant clones are marked by absence of GFP. Representative mutant clones are indicated by arrows. Scale bars: 10 μm.

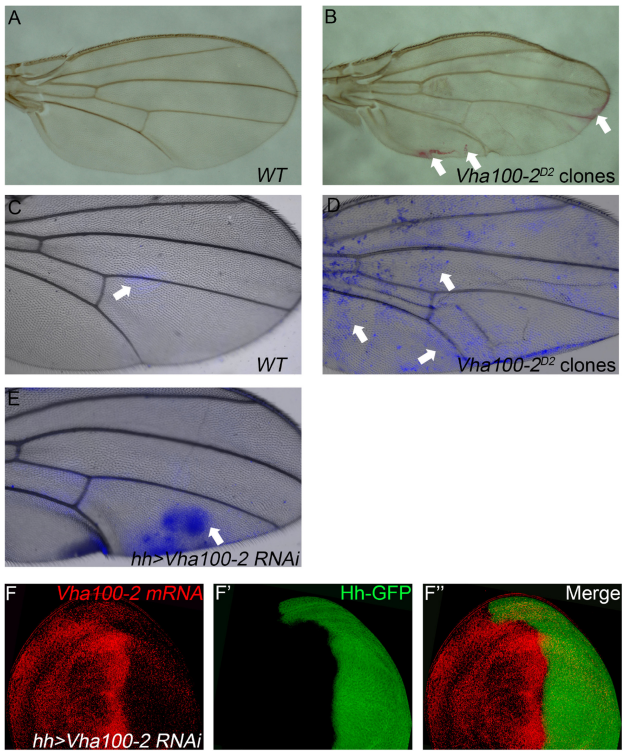

FIGURE 3 | *Vha100-2* is specifically required for wing cuticle formation. **(A,B)** Penetration of Eosin Y through the wing cuticle. The adult wing of *Ubx-FLP; FRT82B, Ubi-RFP* stock is used as wild type control, which is resistant to Eosin Y penetration **(A)**. By contrast, patches with Eosin Y staining (red) are observed in fly wings harboring homozygous *Vha100-2*^{D2} mutant clones **(B)**. **(C–E)** Penetration of FB28 through the wing cuticle. In wild-type control wings, the FB28 dye (blue) shows limited penetration competency **(C)**. The FB28 dye (blue) scatters into the wing bearing homozygous *Vha100-2*^{D2} clones **(D)**. In *Vha100-2* RNAi expression area, the penetration of the FB28 dye (blue) is evident **(E)**. **(F)** The mRNA level of *Vha100-2* (red) are down-regulated in RNAi expressing cells (marked by GFP). Representative Eosin Y and FB28 staining patches are indicated by arrows. The down-regulation of *Vha100-2* in RNAi expressing region is fully penetrant (n = 7). Scale bars: 0.5 mm in **(A–E)** and 10 μm in **(F)**.

the genome (**Supplementary Figures S1A–D**). The -1, -2, -3, -4, and -5 isoform comprises 855, 834, 904, 844, and 814 amino acid residues, respectively. A hidden Markov model (Krogh et al., 2001; http://www.cbs.dtu.dk/services/TMHMM-2.0/) predicated that these isoforms have closely similar structures with seven putative transmembrane regions, which are conserved among the five isoforms (**Figure 1**). High conservation is also evident for the hydrophilic amino and hydrophobic carboxy terminals of fly Vha100 isoforms (**Figure 1**). Detailed analysis of sequence homology reveals that Vha100-3 is the most diverse member of the family, while the other isoforms share a similarity about 70% between each other (**Table 1**). A number of residues of the a subunit have been experimentally demonstrated to be important for the activity or assembly of V-ATPase complex in yeast (Leng et al., 1996, 1998), which were later found to be conserved in mouse orthologs (Nishi and Forgac, 2000; Toyomura et al., 2000). All of these residues are conserved in the fly isoforms, with the exception of L800 (the Vha100-1 numbering), which is conserved in -3 and -5 but is a phenylalanine in -2 and -4 (**Figure 1**). It is likely that the less conserved regions may render different functions of Vha100 isoforms. Construction of a phylogenetic tree (Minh et al., 2013; Trifinopoulos et al., 2016) using the mouse, fly and yeast sequences reveals that the development of multiple isoforms of the a subunit appears to have occurred independently in these species (**Supplementary Figure S1E**).

Previous studies have isolated several *Vha100-1* mutant alleles and revealed a neuronal specific role of *Vha100-1* during fly development (Hiesinger et al., 2005). For the other four isoforms, mutagenesis analyses have not been reported yet. To better understand how Vha100 isoforms function in different developmental contexts, we generated *Vha100-2*, *Vha100-3*, *Vha100-4,* and *Vha100-5* mutants by CRISPR-Cas9 mediated genome editing (**Table 2**). Mutations with small deletions were identified by genomic DNA PCR (**Supplementary Figure S2**) and used for further analysis (**Figure 2A**). Homozygous *Vha100-3*^{D3} and *Vha100-5*^{D5} mutant flies are viable and fertile with normal appearance of body structure and tissue morphology. Previous studies have shown that the expression of *Vha100-3* is restricted to the testes in adult males, while the mRNA of *Vha100-5* is undetectable by *in situ* hybridization in fly larvae (Wang et al., 2004; Allan et al., 2005). We reason that these two isoforms might perform specific physiological roles, but are dispensable for fly development. Therefore, we moved on to examine the roles of *Vha100-1*, *Vha100-2*, and *Vha100-4* in fly wing development.

As *Vha100-1*^{1} (Hiesinger et al., 2005), *Vha100-2*^{D2}, and *Vha100-4*^{D4} are homozygous lethal mutants, somatic mosaic clones were generated using the FLP-FRT system to examine their roles in wing development. The FLP recombinase catalyzes exchange of the homologous chromosome arms and induces the generation of homozygous mutant cell clones with randomized size and location (Xu and Rubin, 1993). Importantly, the wild type cells surrounding the mutant clones serve as rigorous internal control for developmental studies (Theodosiou and Xu, 1998). Taking advantage of the FLP-FRT system, we evaluated whether *Vha100-2*^{D2} and *Vha100-4*^{D4} (**Figure 2A**) behave as loss-of-function alleles by examining their mRNA levels in mutant mosaic clones. Both *Vha100-2* (**Figure 2B**) and *Vha100-4* (**Figure 2C**) were ubiquitously expressed in wing

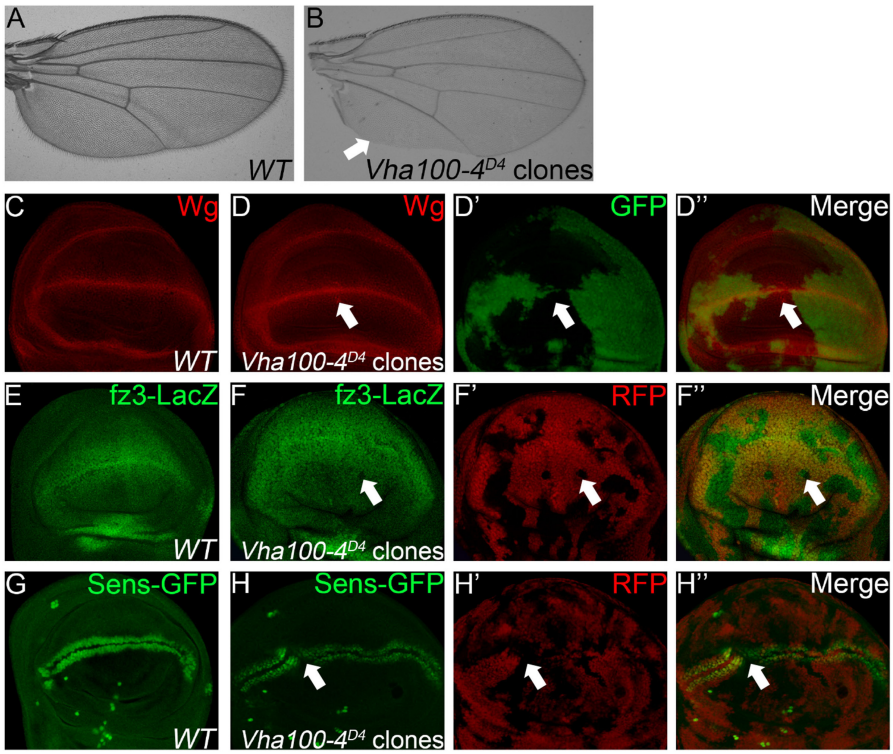

FIGURE 4 | *Vha100-4* is required for proper activation of the Wg signaling pathway. **(A,B)** The adult wing of W^{1118} stock is used as wild type control **(A)**. Wing margin notches and marginal bristle loss are observed in homozygous $Vha100\text{-}4^{D4}$ mutant clones **(B)**. **(C,D)** Immunostaining shows that Wg (red) is expressed by cells at the D/V boundary in the pouch of wild type wing disk **(C)**. Wg proteins (red) are accumulated in a subset of mutant $Vha100\text{-}4^{D4}$ clones (n = 7/13; **D**). **(E,F)** The Wg signaling reporter *fz3-LacZ* (green) is expressed by all cells in the pouch area of wing disk **(E)**. Expression of *fz3-LacZ* (green) is dampened in $Vha100\text{-}4^{D4}$ mutant clones (n = 6/11; **F**). **(G,H)** Sens-GFP (green) is expressed in two rows of cells which are above and below the D/V boundary **(G)**. Expression of the *Sens-GFP* reporter (green) was inhibited in a subset of $Vha100\text{-}4^{D4}$ mutant clones (n = 7/12; **H**). The mutant clones are marked by absence of GFP **(D)** or RFP **(F,H)**. Representative mutant clones are indicated by arrows. Scale bars: 0.5 mm in **(A,B)** and 10 μm in **(C–H)**.

disk cells. Compared with the neighboring wild type cells, the expression level of *Vha100-2* were significantly down-regulated in $Vha100\text{-}2^{D2}$ homozygous cells (**Figure 2D**). The expression of *Vha100-4* were also obviously decreased in $Vha100\text{-}4^{D4}$ clones (**Figure 2E**).

Vha100-2 Is Specifically Required for Wing Cuticle Formation

We first examined the overall requirement of V-ATPase activity during wing development, and the contributions of distinct Vha100 isoforms were further dissected. Two mutants of the regulatory C subunit *Vha44* were tested (**Supplementary Figure S3A**) and both of them resulted in various developmental defects including loss of wing marginal bristles and nicking of wing margin (**Supplementary Figures S3B–D**). We then investigated whether *Vha44* regulates Notch (N) and Wingless (Wg) signaling activity, two major signaling pathways that were affected by mutations of other V-ATPase subunits (Vaccari et al., 2010; Kobia et al., 2013; Gleixner et al., 2014; Portela et al., 2018; Ren et al., 2018). In the wild type imaginal wing disk, the N target gene *cut* is produced in a narrow stripe of cells along the dorsal/ventral (D/V) boundary (**Supplementary Figure S3E**). In $Vha44^{K05440}$ mutant clones, the expression of Cut is abolished when the clones are located at the D/V boundary (**Supplementary Figure S3F**). Clones of *Vha44* mutant cells also displayed various degrees of accumulation of the ligand molecule Delta (Dl) and N protein itself, which were detected as intracellular puncta (**Supplementary Figures S3G–J**). During fly wing development, the Wg protein is generated at the D/V boundary (**Supplementary Figure S3K**) and transported throughout the wing disk to activate down-stream targets (Swarup and Verheyen, 2012). In *Vha44* mutant cells, the expression level of Wg was not significantly affected, while the distribution of Wg protein in signal receiving cells was altered (**Supplementary Figure S3L**). As a consequence, the activity of Wg signaling was dampened in *Vha44* mutant cells (**Supplementary Figures S3M,N**), which was monitored by a *fz3*-LacZ reporter (Sato et al., 1999). In addition, we found that $Vha44^{K05440}$ mutant cells displayed aberrant cellular cortex morphology (**Supplementary Figures S3O,P**) and likely underwent apoptosis (**Supplementary Figures S3Q,R**).

In contrast to the *Vha44* mutants, fly wings harboring homozygous $Vha100\text{-}2^{D2}$ mutant clones displayed wrinkles in the wing surface, without disruption of the vein patterns

and wing margin integrity (**Figures 3A,B**). In agreement with the lack of patterning defects in the adult wing, the expression of Cut remained unaltered in *Vha100-2*^{D2} mutant clones (**Supplementary Figure S4A**). The expression level and distribution of Wg, N, and Dl proteins were also normal in *Vha100-2*^{D2} mutant cells (**Supplementary Figures S4B–D**), suggesting that Vha100-2 is not required for these two pathways. Furthermore, phalloidin staining showed that *Vha100-2*^{D2} mutant had little influence for cell morphology (**Supplementary Figure S4E**). Wrinkling of the wing surface is often associated with defective cuticle deposition (Moussian, 2010). To further characterize the role of *Vha100-2* on wing cuticle formation, we analyzed the cuticle impermeability by FB28 and Eosin Y staining (Wang et al., 2016, 2017). Wild-type wings with an intact cuticle layer is almost resistant to Eosin Y penetration (**Figure 3A**). By contrast, wings harboring homozygous *Vha100-2*^{D2} mutant clones showed patches of Eosin Y staining (**Figure 3B**). Similarly, a polysaccharide-specific dye FB28 was able to penetrate through the cuticle of wings bearing *Vha100-2*^{D2} mutant clones (**Figures 3C,D**). We further confirmed the role of *Vha100-2* in cuticle integrity by knock-down of *Vha100-2* expression in the posterior compartment of the wing. Regional specific inhibition of *Vha100-2* led to wrinkles in the RNAi expressing area as well as diffusion of the FB28 dye (**Figure 3E**). Consistent with the adult wing phenotype, RNAi knock-down led to attenuation of *Vha100-2* mRNA level when examined in the wing disk (**Figure 3F**). Taken together, our results suggest that *Vha100-2* might be involved in cuticle formation of the wing.

Vha100-4 Is Required for Proper Activation of the Wg Signaling Pathway

When *Vha100-4*^{D4} mutant clones were induced in the wing, marginal notches and bristle loss were observed (**Figures 4A,B**). These marginal defects are typically resulted from disruption of N or Wg signaling activity (Logan and Nusse, 2004). Interestingly, we found that neither the target Cut nor the signaling molecules (N and Dl) were changed in *Vha100-4*^{D4} mutant cells (**Supplementary Figure S5**). On the other hand, aggregation of Wg proteins were observed in some mutant cells (**Figures 4C,D**), and the expression of the Wg activity reporter *fz3*-LacZ (**Figures 4E,F**), and *sens*-GFP (**Figures 4G,H**) were dampened in a subset of *Vha100-4*^{D4} mutant clones. Collectively, these findings provide evidence that Vha100-4 is likely involved in Wg signaling activation during fly wing development.

Vha100-1 Performs Redundant Function With Vha100-4

Although previous studies suggest that Vha100-1 functions in the neuronal system to regulate fly development (Hiesinger et al., 2005; Wang et al., 2014), we noticed that ectopic veins were formed in wings bearing *Vha100-1*^{1} mutant clones (**Figures 5A,B**). However, N and Wg signaling were not affected in *Vha100-1*^{1} mutant cells (**Supplementary Figures S6A,B**). In addition, we noticed that *Vha100-1*^{1} mutant cells did not undergo apoptosis (**Supplementary Figure S6C**) and displayed

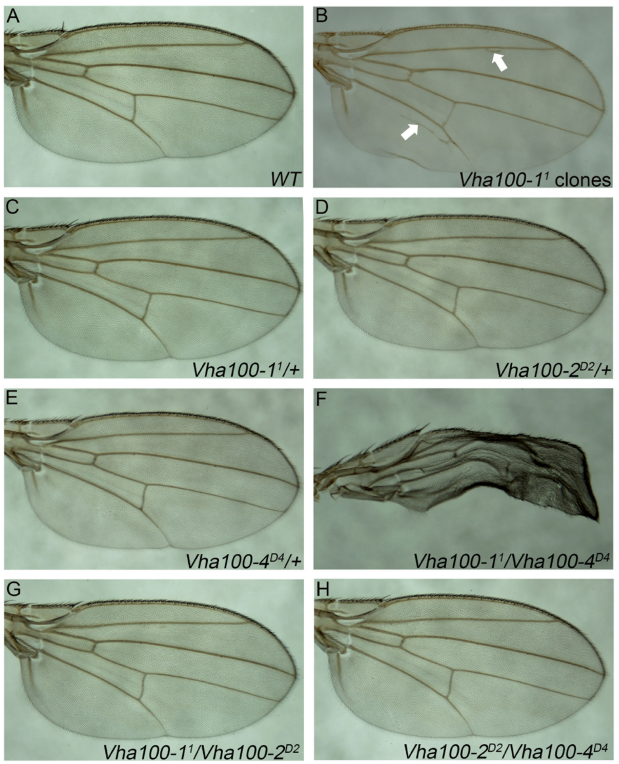

FIGURE 5 | *Vha100-1* and *Vha100-4* perform redundant functions during fly wing development. **(A,B)** The adult wing of *W*^{1118} stock is used as wild type control **(A)**. Ectopic veins (marked by arrows) are formed in wings bearing *Vha100-1*^{1} mutant clones **(B)**. **(C–H)** Compensation tests among *Vha100-1*, *Vha100-2,* and *Vha100-4*. The adult wings of heterozygous *Vha100-1*^{1} **(C)**, *Vha100-2*^{D2} **(D)**, and *Vha100-4*^{D4} **(E)** flies are indistinguishable from wild type controls. *Trans*-heterozygous *Vha100-1*^{1}/*Vha100-4*^{D4} flies show severe wing developmental defects **(F)**. Wings of *Vha100-2*^{D2}/*Vha100-1*^{1} **(G)** and *Vha100-2*^{D2}/*Vha100-4*^{D4} **(H)** flies display normal developmental patterns. Scale bars: 0.5 mm.

normal cell morphology (**Supplementary Figure S6D**). The overall patterning and wing margin integrity was not affected by *Vha100-1*^{1} mutant clones, suggesting that Vha100-1 might function in specific processes during vein cell differentiation.

Mutations of *Vha100-1*, *Vha100-2,* and *Vha100-4* were unable to fully recapture the wing defects caused by *Vha44* mutant, despite that they are all essential genes required for normal development. These results indicate that these isoforms may function redundantly and the loss of single isoform can be compensated by the remaining family members in certain developmental contexts. To test this hypothesis, we crossed *Vha100-1*^{1}, *Vha100-2*^{D2}, and *Vha100-4*^{D4} flies with each other and examined the wing phenotypes in the *trans*-heterozygous progenies. For each mutant allele, the heterozygotes were indistinguishable with wild type controls (**Figures 5C–E**). The wings of *Vha100-1*^{1}/*Vha100-4*^{D4} flies were severely malformed (**Figure 5F**), indicating a strong genetic interaction and functional redundancy between *Vha100-1* and *Vha100-4*. Combination of *Vha100-2*^{D2} with either *Vha100-1*^{1} (**Figure 5G**) or *Vha100-4*^{D4} (**Figure 5H**)

shows no effect on fly development and wing morphology, suggesting that Vha100-2 likely functions independently of the other two isoforms.

DISCUSSION

The V-ATPases are highly conserved multi-subunit pumps that transport hydrogen ions in exchange for ATP. Present in the endo-membranes of all eukaryotic cells, they are well known regulators for acidification of various intracellular compartments (Forgac, 2007). Studies in the larval midgut of the tobacco hornworm *Manduca sexta* are among the first reports to reveal that V-ATPases also pump protons across the plasma membranes of many specialized animal cells (Wieczorek et al., 2009). The great diversity of functions that the V-ATPases serve in eukaryotic organisms is recognized as a remarkable feature (Forgac, 2007; Wieczorek et al., 2009). Several subunits of the V-ATPases are encoded by multiple isoforms, and tissue specific expression of different isoforms have been demonstrated as a common strategy to fulfill the diverse requirement for V-ATPases (Toei et al., 2010). However, whether different isoforms are used in the same tissue to execute distinct functions is still an open question.

Here we report that isoforms of the V-ATPase a subunit are differentially required for *Drosophila* wing development. We provide genetic evidence that three of the five Vha100 isoforms (*Vha100-1*, *Vha100-2,* and *Vha100-4*) are involved in fly wing development. Somatic clonal analysis show that *Vha100-1* regulates vein formation, while *Vha100-2* functions in cuticle deposition and *Vha100-4* participates in Wg signaling transduction. It is likely that *Vha100-1* regulates vein formation through pathways transduced by other signaling molecules, such as bone morphogenetic protein (BMP), and epidermal growth factor (EGF) during fly wing development (Blair, 2007). Our results strongly support a model that V-ATPases might exist as multiple subtypes composed by diverse subunit isoforms in the same cells to meet the diversified demands. The accumulation of signaling molecules and alteration of signaling activities are not always fully penetrant in *Vha100* mutant cells, which is also noticed in previous studies on other V-ATPase subunits (Yan et al., 2009; Vaccari et al., 2010; Ren et al., 2018). During tissue development, the V-ATPase regulates acidification of cellular organelles which are necessary for protein sorting, trafficking, and turnover (Forgac, 2007). It is conceivable that disrupting V-ATPase activity results in aberrant trafficking and degradation of signaling molecules, a highly dynamic process that might be only partially captured by conventional genetic analysis. In addition, our compensation tests suggest that beyond their specialized roles, *Vha100-1,* and *Vha100-4* likely function redundantly for wing patterning and growth. This redundancy may also help to explain the minor defects observed when *Vha100-1* and *Vha100-4* single mutant clones were induced in the wing. Our observations suggest that the V-ATPases subtypes are able to constitute a coordinated network in cells. Further studies are required to dissect the exact mechanisms underlying the mode of action for V-ATPases.

Previous studies using RNAi knock-down experiments indicate that *Vha100-2* is involved in the development of multiple fly tissues (Wang et al., 2014; Overend et al., 2016; Mondragon et al., 2019; Nagata et al., 2019). We find that *Vha100-2* is the sole isoform required for wing cuticle integrity. This is the first report regarding a role of V-ATPases in insect cuticle formation. The cuticle is a multifunctional tissue that covers the whole body of insects, which provides significant protections from life threatening dangers such as dehydration, predators and pathogen infection (Moussian, 2010). It is possible that V-ATPases might regulate membrane trafficking and secretion of the cuticle components in wing epithelia cells in a similar fashion as reported in *Caenorhabditis elegans* (Liégeois et al., 2007). However, V-ATPases may as well function in other steps during cuticle formation, which needs to be further explored.

DATA AVAILABILITY STATEMENT

The raw data supporting the conclusions of this article will be made available by the authors, without undue reservation, to any qualified researcher.

AUTHOR CONTRIBUTIONS

DM performed the mosaic screen and identified the *Vha44* mutants. DM, YC, and NJ performed the immunostaining analyses. JZ performed the mRNA *in situ* hybridization. DM, YC, NJ, and JZ performed the statistical analyses for wing phenotypes. DM prepared the original draft. JS and JZ reviewed and edited the manuscript. JS and JZ supervised the project. All authors approved the final manuscript submitted for publication.

FUNDING

This work was supported by the National Natural Science Foundation of China (31772526 and 31970478 to JZ and 31872295 to JS).

ACKNOWLEDGMENTS

We thank Drs. Alan Jian Zhu, Yun Zhao, Renjie Jiao, Tao Wang, Wei Wu, the Bloomington Stock Center, the Kyoto Fly Stock Center, the TsingHua Fly Stock Center, and the Developmental Studies Hybridoma Bank (DSHB) for fly stocks and antibodies. We thank Drs. Yinqiao Zhang and Zhenyong Du for help with construction of the phylogenetic tree.

SUPPLEMENTARY MATERIAL

The Supplementary Material for this article can be found online at: https://www.frontiersin.org/articles/10.3389/fgene.2020.00723/full#supplementary-material

REFERENCES

Allan, A. K., Juan, D., Davies, S. A., and Julian, A. T. D. (2005). Genome-wide survey of V-ATPase genes in *Drosophila* reveals a conserved renal phenotype for lethal alleles. *Physiol. Genom.* 22, 128–138. doi: 10.1152/physiolgenomics.00233.2004

Bassett, A. R., Tibbit, C., Ponting, C. P., and Liu, J. L. (2013). Highly efficient targeted mutagenesis of *Drosophila* with the CRISPR/Cas9 system. *Cell Rep.* 4, 220–228. doi: 10.1016/j.celrep.2013.06.020

Blair, S. S. (2007). Wing vein patterning in *Drosophila* and the analysis of intercellular signaling. *Annu. Rev. Cell Dev. Biol.* 23, 293–319. doi: 10.1146/annurev.cellbio.23.090506.123606

Buechling, T., Bartscherer, K., Ohkawara, B., Chaudhary, V., Spirohn, K., Niehrs, C., et al. (2010). Wnt/Frizzled signaling requires dPRR, the *Drosophila* homolog of the prorenin receptor. *Curr. Biol.* 20, 1263–1268. doi: 10.1016/j.cub.2010.05.028

Cipriano, D. J., Wang, Y., Bond, S., Hinton, A., Jefferies, K. C., Qi, J., et al. (2008). Structure and regulation of the vacuolar ATPases. *Biochim. Biophys. Acta* 1777, 599–604.

Forgac, M. (2007). Vacuolar ATPases: rotary proton pumps in physiology and pathophysiology. *Nat. Rev. Mol. Cell Biol.* 8, 917–929. doi: 10.1038/nrm2272

Gleixner, E. M., Canaud, G., Hermle, T., Guida, M. C., Kretz, O., Huber, T. B., et al. (2014). V-ATPase/ mTOR signaling regulates megalin-mediated apical endocytosis. *Cell Rep.* 8, 10–19. doi: 10.1016/j.celrep.2014.05.035

Gratz, S. J., Ukken, F. P., Rubinstein, C. D., Thiede, G., Donohue, L. K., Cummings, A. M., et al. (2014). Highly specific and efficient CRISPR/Cas9-catalyzed homology-directed repair in *Drosophila*. *Genetics* 196, 961–971. doi: 10.1534/genetics.113.160713

Hermle, T., Saltukoglu, D., Grucnewald, J., Walz, G., Simons, M., Gru, J., et al. (2010). Regulation of Frizzled-dependent planar polarity signaling by a V-ATPase subunit. *Curr. Biol.* 20, 1269–1276. doi: 10.1016/j.cub.2010.05.057

Hiesinger, P. R., Fayyazuddin, A., Mehta, S. Q., Rosenmund, T., Schulze, K. L., Zhai, R. G., et al. (2005). The v-ATPase V0 subunit a1 is required for a late step in synaptic vesicle exocytosis in *Drosophila*. *Cell* 121, 607–620. doi: 10.1016/j.cell.2005.03.012

Hinton, A., Bond, S., and Forgac, M. (2009). V-ATPase functions in normal and disease processes. *Pflugers Arch.* 457, 589–598. doi: 10.1007/s00424-007-0382-4

Inoue, T., and Forgac, M. (2005). Cysteine-mediated cross-linking indicates that subunit C of the V-ATPase is in close proximity to subunits E and G of the V1 domain and subunit a of the V0 domain. *J. Biol. Chem.* 280, 27896–27903. doi: 10.1074/jbc.m504890200

Inoue, T., Wang, Y., Jefferies, K., Qi, J., Hinton, A., and Forgac, M. (2005). Structure and regulation of the V-ATPases. *J. Bioenerg. Biomembr.* 37, 393–398.

Jianhua, Z., Samir, B., and John, L. R. (2015). Electron cryomicroscopy observation of rotational states in a eukaryotic V-ATPase. *Nature* 521, 241–245. doi: 10.1038/nature14365

Julian, A. T. D. (1999). The multifunctional *Drosophila melanogaster* V-ATPase is encoded by a multigene family. *J. Bioenerg. Biomembr.* 31, 75–83.

Kobia, F., Duchi, S., Deflorian, G., and Vaccari, T. (2013). Pharmacologic inhibition of vacuolar HC ATPase reduces physiologic and oncogenic Notch signaling. *Mol. Oncol.* 8, 207–220. doi: 10.1016/j.molonc.2013.11.002

Krogh, A., Larsson, B., von Heijne, G., and Sonnhammer, E. L. (2001). Predicting transmembrane protein topology with a hidden Markov model: application to complete genomes. *J. Mol. Biol.* 305, 567–580. doi: 10.1006/jmbi.2000.4315

Leng, X. H., Manolson, M., and Forgac, M. (1998). Function of the COOH-terminal domain of Vph1p in activity and assembly of the yeast V-ATPase. *J. Biol. Chem.* 273, 6717–6723. doi: 10.1074/jbc.273.12.6717

Leng, X. H., Manolson, M., Liu, Q., and Forgac, M. (1996). Site-directed mutagenesis of the 100-kDa subunit (Vph1p) of the yeast vacuolar (H+□)-ATPase. *J. Biol. Chem.* 271, 22487–22493. doi: 10.1074/jbc.271.37.22487

Liégeois, S., Benedetto, A., Michaux, G., Belliard, G., and Labouesse, M. (2007). Genes required for osmoregulation and apical secretion in *Caenorhabditis elegans*. *Genetics* 175, 709–724. doi: 10.1534/genetics.106.066035

Logan, C. Y., and Nusse, R. (2004). The Wnt signaling pathway in development and disease. *Annu. Rev. Cell Dev. Biol.* 20, 781–810.

Minh, B. Q., Nguyen, M. A. T., and von Haeseler, A. (2013). Ultrafast approximation for phylogenetic bootstrap. *Mol. Biol. Evol.* 30, 1188–1195. doi: 10.1093/molbev/mst024

Mondragon, A. A., Yalonetskaya, A., Ortega, A. J., Elguero, J., Chung, W. S., and McCall, K. (2019). Lysosomal machinery drives extracellular acidification to direct non- apoptotic cell death. *Cell Rep.* 27, 11–19.

Moussian, B. (2010). Recent advances in understanding mechanisms of insect cuticle differentiation. *Insect. Biochem. Mol. Biol.* 40, 363–375. doi: 10.1016/j.ibmb.2010.03.003

Nagata, R., Nakamura, M., Sanaki, Y., and Igaki, T. (2019). Cell competition is driven by autophagy. *Dev. Cell.* 51, 99–112.

Nelson, N. (2003). A journey from mammals to yeast with vacuolar H+-ATPase (V-ATPase). *J. Bioenerg. Biomembr.* 35, 281–289.

Nishi, T., and Forgac, M. (2000). Molecular cloning and expression of three isoforms of the 100-kDa a subunit of the mouse vacuolar proton-translocating ATPase. *J. Biol. Chem.* 275, 6824–6830. doi: 10.1074/jbc.275.10.6824

Overend, G., Luo, Y., Henderson, L., Douglas, A. E., Davies, S. A., and Dow, J. A. (2016). Molecular mechanism and functional significance of acid generation in the *Drosophila* midgut. *Sci. Rep.* 6:27242.

Petzoldt, A. G., Gleixner, E. M., Fumagalli, A., Vaccari, T., and Simons, M. (2013). Elevated expression of the V-ATPase C subunit triggers JNK-dependent cell invasion and overgrowth in a *Drosophila* epithelium. *Dis. Model. Mech.* 6, 689–700. doi: 10.1242/dmm.010660

Portela, M., Yang, L., Paul, S., Li, X., Veraksa, A., Parsons, L. M., et al. (2018). Lgl reduces endosomal vesicle acidification and Notch signaling by promoting the interaction between Vap33 and the V-ATPase complex. *Sci. Signal.* 11:eaar1976. doi: 10.1126/scisignal.aar1976

Qi, J., Wang, Y., and Forgac, M. (2007). The vacuolar (H+)-ATPase: subunit arrangement and in vivo regulation. *J. Bioenerg. Biomembr.* 39, 423–426. doi: 10.1007/s10863-007-9116-8

Ren, L., Mo, D., Li, Y., Liu, T., Yin, H., Jiang, N., et al. (2018). A genetic mosaic screen identifies genes modulating Notch signaling in *Drosophila*. *PLoS One* 13:e0203781. doi: 10.1371/journal.pone.0203781

Sarov, M., Barz, C., Jambor, H., Hein, M. Y., Schmied, C., Suchold, D., et al. (2016). A genome-wide resource for the analysis of protein localisation in *Drosophila*. *eLife* 5:e12068.

Sato, A., Kojima, T., Ui-Tei, K., Miyata, Y., and Saigo, K. (1999). Dfrizzled-3, a new *Drosophila* Wnt receptor, acting as an attenuator of Wingless signaling in wingless hypomorphic mutants. *Development* 126, 4421–4430.

Saw, N. M., Kang, S. Y., Parsaud, L., Han, G. A., Jiang, T., Grzegorczyk, K., et al. (2011). Vacuolar H(+)-ATPase subunits Voa1 and Voa2 cooperatively regulate secretory vesicle acidification, transmitter uptake, and storage. *Mol. Biol. Cell.* 22, 3394–3409. doi: 10.1091/mbc.e11-02-0155

Su, Y., Ospina, J. K., Zhang, J., Michelson, A. P., Schoen, A. M., and Zhu, A. J. (2011). Sequential phosphorylation of smoothened transduces graded hedgehog signaling. *Sci. Signal.* 4:ra43. doi: 10.1126/scisignal.2001747

Swarup, S., and Verheyen, E. M. (2012). Wnt/Wingless signaling in *Drosophila*. *Cold Spring Harb. Perspect. Biol.* 4:a007930.

Theodosiou, N. A., and Xu, T. (1998). Use of FLP/FRT system to study *Drosophila* development. *Methods* 14, 355–365. doi: 10.1006/meth.1998.0591

Toei, M., Saum, R., and Forgac, M. (2010). Regulation and isoform function of the V-ATPases. *Biochemistry* 49, 4715–4723. doi: 10.1021/bi100397s

Toyomura, T., Murata, Y., Yamamoto, A., Oka, T., Sun-Wada, G. H., Wada, Y., et al. (2003). From lysosomes to the plasma membrane: localization of vacuolar-type H+ -ATPase with the a3 isoform during osteoclast differentiation. *J. Biol. Chem.* 278, 22023–22030. doi: 10.1074/jbc.m302436200

Toyomura, T., Oka, T., Yamaguchi, C., Wada, Y., and Futai, M. (2000). Three subunit a isoforms of mouse vacuolar H(+)-ATPase. *Preferential expression of the a3* isoform during osteoclast differentiation. *J. Biol. Chem.* 275, 8760–8765. doi: 10.1074/jbc.275.12.8760

Trifinopoulos, J., Nguyen, L.-T., von Haeseler, A., and Minh, B. Q. (2016). W-IQ-TREE: a fast online phylogenetic tool for maximum likelihood analysis. *Nucleic Acids Res.* 44, W232–W235.

Vaccari, T., Duchi, S., Cortese, K., Tacchetti, C., and Bilder, D. (2010). The vacuolar ATPase is required for physiological as well as pathological activation of the Notch receptor. *Development* 137, 1825–1832. doi: 10.1242/dev.045484

Wang, D., Epstein, D., Khalaf, O., Srinivasan, S., Williamson, W. R., Fayyazuddin, A., et al. (2014). Ca2+-Calmodulin regulates SNARE assembly and spontaneous neurotransmitter release via v-ATPase subunit V0 a1. *J. Cell Biol.* 205, 21–31. doi: 10.1083/jcb.201312109

Wang, J., Kean, L., Yang, J., Allan, A. K., Davies, S. A., Herzyk, P., et al. (2004). Function-informed transcriptome analysis of *Drosophila* renal tubule. *Genome Biol.* 5:R69.

Wang, Y., Carballo, R. G., and Moussian, B. (2017). Double cuticle barrier in two global pests, the whitefly *Trialeurodes vaporariorum* and the bedbug *Cimex lectularius*. *J. Exp. Biol.* 220, 1396–1399. doi: 10.1242/jeb.156679

Wang, Y., Yu, Z., Zhang, J., and Moussian, B. (2016). Regionalization of surface lipids in insects. *Proc. Biol. Sci.* 283:20152994. doi: 10.1098/rspb.2015.2994

Wieczorek, H., Beyenbach, K. W., Huss, M., and Vitavska, O. (2009). Vacuolar-type proton pumps in insect epithelia. *J. Exp. Biol.* 212, 1611–1619. doi: 10.1242/jeb.030007

Wilkens, S., Inoue, T., and Forgac, M. (2004). Three-dimensional structure of the vacuolar ATPase: localization of subunit H by difference imaging and chemical cross-linking. *J. Biol. Chem.* 279, 41942–41949. doi: 10.1074/jbc.m407821200

Williamson, W. R., Wang, D., Haberman, A. S., and Hiesinger, P. R. (2010a). A dual function of V0-ATPase a1 provides an endolysosomal degradation mechanism in *Drosophila melanogaster* photoreceptors. *J. Cell Biol.* 189, 885–899. doi: 10.1083/jcb.201003062

Williamson, W. R., Yang, T., Terman, J. R., and Hiesinger, P. R. (2010b). Guidance receptor degradation is required for neuronal connectivity in the *Drosophila* nervous system. *PLoS Biol.* 8:e1000553. doi: 10.1371/journal.pone.01000553

Wissel, S., Harzer, H., Bonnay, F., Burkard, T. R., Neumüller, R. A., and Knoblich, J. A. (2018). Time-resolved transcriptomics in neural stem cells identifies a v-ATPase/Notch regulatory loop. *J. Cell Biol.* 217, 3285–3300. doi: 10.1083/jcb.201711167

Xu, T., and Rubin, G. M. (1993). Analysis of genetic mosaics in developing and adult *Drosophila* tissues. *Development* 117, 1223–1237.

Yan, Y., Denef, N., and Schucpbach, T. (2009). The vacuolar proton pump, V-ATPase, is required for notch signaling and endosomal trafficking in *Drosophila*. *Dev. Cell.* 17, 387–402. doi: 10.1016/j.devcel.2009.07.001

Conflict of Interest: The authors declare that the research was conducted in the absence of any commercial or financial relationships that could be construed as a potential conflict of interest.

frontiers in Genetics

ORIGINAL RESEARCH
published: 06 August 2020
doi: 10.3389/fgene.2020.00887

Transcriptional Control of Quality Differences in the Lipid-Based Cuticle Barrier in *Drosophila suzukii* and *Drosophila melanogaster*

*Yiwen Wang[1,2], Jean-Pierre Farine[3], Yang Yang[1], Jing Yang[1], Weina Tang[2], Nicole Gehring[1], Jean-François Ferveur[3] and Bernard Moussian[1,4]**

[1] Section Animal Genetics, Interfaculty Institute of Cell Biology, University of Tübingen, Tübingen, Germany, [2] School of Pharmaceutical Science and Technology, Tianjin University, Tianjin, China, [3] Centre des Sciences du Goût et de l'Alimentation, UMR-CNRS 6265, Université de Bourgogne, Dijon, France, [4] CNRS, Inserm, Institut de Biologie Valrose, Université Côte d'Azur, Nice, France

OPEN ACCESS

Edited by:
Zhongxia Wu,
Henan University, China

Reviewed by:
Amy Tsurumi,
Massachusetts General Hospital and Harvard Medical School, United States
Pengcheng Yang,
Beijing Institutes of Life Science (CAS), China

***Correspondence:**
Bernard Moussian
bernard.moussian@uni-tuebingen.de

Specialty section:
This article was submitted to Epigenomics and Epigenetics, a section of the journal Frontiers in Genetics

Received: *27 March 2020*
Accepted: *20 July 2020*
Published: *06 August 2020*

Citation:
Wang Y, Farine J-P, Yang Y, Yang J, Tang W, Gehring N, Ferveur J-F and Moussian B (2020) Transcriptional Control of Quality Differences in the Lipid-Based Cuticle Barrier in Drosophila suzukii and Drosophila melanogaster. Front. Genet. 11:887. doi: 10.3389/fgene.2020.00887

Cuticle barrier efficiency in insects depends largely on cuticular lipids. To learn about the evolution of cuticle barrier function, we compared the basic properties of the cuticle inward and outward barrier function in adults of the fruit flies *Drosophila suzukii* and *Drosophila melanogaster* that live on fruits sharing a similar habitat. At low air humidity, *D. suzukii* flies desiccate faster than *D. melanogaster* flies. We observed a general trend indicating that in this respect males are less robust than females in both species. Xenobiotics penetration occurs at lower temperatures in *D. suzukii* than in *D. melanogaster*. Likewise, *D. suzukii* flies are more susceptible to contact insecticides than *D. melanogaster* flies. Thus, both the inward and outward barriers of *D. suzukii* are less efficient. Consistently, *D. suzukii* flies have less cuticular hydrocarbons (CHC) that participate as key components of the cuticle barrier. Especially, the relative amounts of branched and desaturated CHCs, known to enhance desiccation resistance, show reduced levels in *D. suzukii*. Moreover, the expression of *snustorr* (*snu*) that encodes an ABC transporter involved in barrier construction and CHC externalization, is strongly suppressed in *D. suzukii*. Hence, species-specific genetic programs regulate the quality of the lipid-based cuticle barrier in these two Drosophilae. Together, we conclude that the weaker inward and outward barriers of *D. suzukii* may be partly explained by differences in CHC composition and by a reduced Snu-dependent transport rate of CHCs to the surface. In turn, this suggests that *snu* is an ecologically adjustable and therefore relevant gene in cuticle barrier efficiency.

Keywords: insect, cuticle, *Drosophila*, barrier, lipid

INTRODUCTION

Fruit flies of the genus *Drosophila* including *Drosophila*, *Sophophora*, and Hawaiian *Drosophila* (O'Grady and DeSalle, 2018b) commonly live on fruits that serve as a site for feeding, mating, oviposition, and development. Usually, despite of the common macrohabitat, i.e., orchards, *Drosophila* flies of different species may occupy their specific microhabitats and largely avoid each

other in time and space (Mitsui et al., 2006; Beltrami et al., 2012; O'Grady and DeSalle, 2018a; Plantamp et al., 2019). Some species such as *Drosophila suzukii* prefer, for instance, immature fruits (Lee et al., 2011; Walsh et al., 2011; Silva-Soares et al., 2017; Olazcuaga et al., 2019), while others like *Drosophila melanogaster* prefer rotten fruits (Versace et al., 2016).

Microhabitat choice is complex and involves along with behavior and diet preference chemo-physical environmental constraints. A major challenge in microhabitat choice is availability of water including air humidity. One strategy to cope with the water problem is to adapt the efficiency of the cuticular barrier to the specific needs. Molecular mechanisms modulating a cuticle barrier against water loss (desiccation) and accounting for adaptation to different humidity conditions have been analyzed only in a few cases. The differences in desiccation resistance between the closely related East-Australian *Drosophila birchii* and *Drosophila serrata*, for instance, rely on the composition of cuticular hydrocarbons (CHCs) that serve as a barrier at the cuticle surface (Chung et al., 2014). In *D. birchii*, the expression level of *mFas* that codes for a fatty acid synthase producing methyl-branched CHCs is suppressed compared to its expression level in *D. serrata*. Thus, reduced methyl-branched CHCs may explain why *D. birchii* is more sensitive to desiccation than *D. serrata*.

Several genes involved in cuticular desiccation resistance have been identified and characterized in *D. melanogaster*. The ABC transporters Oskyddad (Osy) and Snustorr (Snu) and the extracellular protein Snustorr-snarlik (Snsl) are needed for the constitution of the cuticle surface comprising the envelope, the outermost cuticle layer and the CHC overlay (Moussian, 2010; Zuber et al., 2018; Wang et al., 2020). Mutations in *osy*, *snu*, and *snsl* cause rapid water loss and subsequent death. Likewise, RNA interference against *cyp4g1* coding for a P450 oxidative decarbonylase required for CHC production enhances desiccation sensitivity (Qiu et al., 2012). It is yet unexplored whether the expression and function of these genes is under environmental control. In a genome-wide study, they were not found to be associated with CHC profile changes in wild-type *D. melanogaster* flies (Dembeck et al., 2015).

In this work, we sought to compare the cuticle barrier efficiency in *D. melanogaster* and *D. suzukii* in order to gain more insight in the ecology and evolution of this trait in fruit flies.

MATERIALS AND METHODS

Fly Stocks

In the summer of 2018, five *D. suzukii* wild-type flies (2 females and 3 males) were collected from cherries from a cherry tree in a private garden in Tübingen, Germany. With these five flies, we established a *D. suzukii* stock, that we named "Tübingen 2018." In 2019, we harvested several dozens of blackberries in a private garden in Tübingen; around 40 flies eclosed from these fruits and were used to set up a new line that was called "Brombeere 2019." A third *D. suzukii* wild-type stock was established in 2018 starting from around 20 flies eclosed from several dozens of cherries from the city Bad Wimpfen, Germany, that is about 90 km to the north of Tübingen. The wild-type *D. melanogaster* stock was established from five female and five male flies collected in a wine orchard in Dijon in 2000 ("Dijon 2000"). All flies were raised in polysterol bottles containing standard corn meal food supplied with fresh baker's yeast. A filter paper was stuck into *D. suzukii* culture bottles. The identical laboratory environment for both species ensures comparability of the data.

Determination of Body Water Content

Ten male or female 5-days old flies were weighed on a micro-balance before drying for 2 h at 90°C. They were weighed for a second time after drying. The difference between the fresh and the dry weighs was used to evaluate the amount of water.

Desiccation Assay

In each assay, groups of ten six to 10 days old flies were collected on ice and incubated in a petri dish containing silica (Sigma Aldrich) at 22°C. The petri dish was sealed with parafilm during the experiment. The experiment was repeated at least three times. Control flies survive for several hours in the petri dish without silica.

Eosin Y Penetration Assay

According to our recently published protocol (Wang et al., 2016), ten to twenty flies of each sex and species were incubated for 20 min with Eosin Y (0.5%, Sigma-Aldrich) at different temperatures. After staining, flies were washed with tap water at room temperature. Wings were cut off using micro-scissors, observed under a Leica EZ4 stereomicroscope and imaged using the in-built Leica camera and software.

Insecticide Treatment

Ten flies of each species were incubated in vials that contained either 0, 0.05 or 0.1 μg chlorpyriphos (stock solution 1 mg/ml acetone). Lethality was recorded during 4 h of incubation at the end of which all flies died when exposed at the highest insecticide amounts. This experiment was repeated at least three times.

Identification of Genes and Quantitative Real-Time PCR

To design qPCR primers, *D. melanogaster*, and *D. suzukii* transcript sequences were retrieved from flybase (flybase.org). Primers (**Table 1**) amplifying 100–120 bp were designed using the online primer3 software[1]. Total RNA was extracted (RNEasy kit, Qiagen) from five freshly eclosed male or female flies (0 to 3 h old) to prepare the cDNA template (Omniscript RT kit, Qiagen) for the qPCR reaction (FastStart Essential DNA Green Master, Roche) on a Roche Nano LightCycler. This experiment was repeated four times. Data were analyzed with the inbuilt software of Roche and Microsoft Excel. The $2^{-\Delta\Delta CT}$ method was applied to calculate the gene expression levels. The transcript levels of the reference gene *RpS20* coding for ribosomal protein S20 were used to normalize gene expression.

[1] http://primer3.ut.ee

TABLE 1 | Sequences of primers for qPCR used in this study.

Gene	Forward primer	Reverse primer
D. suz app	GGTGTCGTTTCGCAGTTCAG	TGGCTTTCTTTGTTTCTTCGGT
D. mel app	GAAAAGAAAGTCCCTGGGCG	ATCATCGTGTTGTCGTGCAG
D. suz osy	GGTGTTTGGTGGCTGGTATC	TGGTCTGACTCAGCATCACC
D. mel osy	GCAATATGTGACCGACGATG	GCGGTACAGCAACTGTGAGA
D. suz cyp4g1	CATCGATGAGAACGATGTGG	TGTCGTGACCCTCGAACATA
D. mel cyp4g1	ATGGCCAACAGGCATTACT	TGTCGGTGGAGTGGACAATA
D. suz desat1	CCACTCGTGGCTTCTTCTTC	ATGGGCATCAACAGCATGTA
D. mel desat1	ACGTAACCTGGCTGGTGAAC	TCTTGTAGTCCCAGGGGAAG
D. suz fas1	AGAGGCGAGAACCACTTTCA	AGGTGGTGGACAAGAACCTG
D. mel fas1	CGTACGACCCCTCTGTTGAT	ACCACCTTGAGACGTCCATC
D. suz fas2	CTTGATCTCCGTGCTCATCA	CAAGACGGAGCAGGCTAATC
D. mel fas2	CAGCAACATCGAGGAGTTCA	GCTTCTGGTGGACGCTAAAG
D. suz fas3	AAGCTTGTTTCGCTTTGGAA	AGCTCCACCAAAACCAAATG
D. mel fas3	AACGGTGTGCATCATTTTGA	CAGGAGGTCTTCGTCTTTGC
D. suz farO	AGAAGCCGATGCTGATGAGT	ATGGATATCCGGATGGTTGA
D. mel farO	AGTATCCGAACGCACTTGCT	GAAGAGATGCGCCAGATAGC
D. suz acc	CGGGAACAGTGACATTTGTG	CTGTTCAGCTTCTCCGGAAC
D. mel acc	AACAACGGAGTCACCCACA	CAGGTCACAACCGATGTACG
D. suz snu	GCAAGAAGAAGAACGCCAAC	TGCAAGACAGCAAAGTGGTC
D. suz snu #2	TTCCTCATCTCCTCGGTGTG	CCAGATCACTCCAGACAGCA
D. mel snu	TACACCCACTTCGGGTCTTC	AGTGCCGAGTGGAAAGCTAA
D. suz snsl	GTGGAACTGGGTCCTCAGAA	TTTTCTCCGTGGAGGTCATC
D. mel snsl	TCTGGCCCGTCAACTTTATC	CACTGGTTTCTTGGCCTGAT
D. suz rps20	CTGCTGCACCCAAGGATATT	AGTCTTACGGGTGGTGATGC
D. mel rps20	TTCGCATCACCACCCGT AAGAC	TTGTGGATTCTCATCTGGAA GCG

Determination of CHCs

To extract CHs, 6-h or 5-day old flies were frozen for 5 min at −20°C, prior to the extraction procedure. For wing analysis, wings were cut off using micro-scissors. Each pair of wings was immersed for 10 min at room temperature in vials containing 20 µl of hexane. For whole fly extraction, each individual was immersed under similar conditions in 30 µl of hexane. In all cases, the solution also contained 3.33 ng/µl of C26 (*n*-hexacosane) and 3.33 ng/µl of C30 (*n*-triacontane) as internal standards. After removing the wings or the fly bodies, the extracts were stored at −20°C until analysis. All extracts were analyzed using a Varian CP3380 gas chromatograph fitted with a flame ionization detector, a CP Sil 5CB column (25 m × 0.25 mm internal diameter; 0.1 m film thickness; Agilent), and a split–splitless injector (60 ml/min split-flow; valve opening 30 s after injection) with helium as carrier gas (velocity = 50 cm/s at 120°C). The temperature program began at 120°C, ramping at 10°C/min to 140°C, then ramping at 2 C/min to 290°C, and holding for 10 min. The chemical identity of the CHCs was checked using gas chromatography-mass spectrometry system equipped with a CP Sil 5CB column (Everaerts et al., 2010). The amount (ng/insect) of each component was calculated based on the readings obtained from the internal standards. For the sake of clarity we only show the sum (in ng) of desaturated CHs (ΣDesat), the sum of linear saturated CHs (ΣLin), and the sum of methyl-branched CHs (ΣBr) and their respective percentages calculated based on the overall CHs sum (ΣCHCs).

RESULTS

Drosophila suzukii Is More Sensitive to Dryness Than *Drosophila melanogaster*

To learn about ecological similarities and differences between *D. suzukii* and *D. melanogaster*, we first compared their desiccation resistance (**Figure 1**). *D. suzukii* males were dead within 4 h after exposing them to dry conditions, while most *D. melanogaster* males survived until 5 h of exposition to dryness. They died between 6 and 8 h under this condition. *D. suzukii* females started to die after 5 h of exposure to dryness and after 10 h, their lethality reached 90%. The *D. melanogaster* females reached the 90% lethality rate after 15 h under the same condition. In conclusion, *D. suzukii* and *D. melanogaster* females live longer under dry conditions (<10% air humidity) than males. However, both *D. suzukii* males and females are more sensitive to dryness than *D. melanogaster* males and females.

D. suzukii Flies Are Heavier Than *D. melanogaster* Flies but Contain a Lesser Proportion of Water

Body mass and body water content are reported to be positively correlated to desiccation resistance (Ferveur et al., 2018). We determined these two parameters in *D. suzukii* and *D. melanogaster* males and females (**Table 2**). *D. suzukii* males are 58% heavier than *D. melanogaster* males, while *D. suzukii* females are 75% heavier than *D. melanogaster* females. These differences are statistically significant (see **Table 2**). Water represents 76% and 82% of the *D. suzukii* female and male body mass, respectively, while in *D. melanogaster* females and males it represents 80% and 87%, respectively. These differences have a low statistical significance (see **Table 2**). Thus, *D. suzukii* flies weight more than *D. melanogaster* flies, but, by trend, contain proportionally less water.

The Inward Barrier Is More Permeable in *D. suzukii* Than in *D. melanogaster*

Our results suggest that the outward barrier is less efficient in *D. suzukii* flies than in *D. melanogaster* flies. Using an Eosin Y incubation assay (Wang et al., 2016, 2017), we tested whether the inward barrier function also differs between *D. suzukii* and *D. melanogaster* (**Figure 2**). In particular, we measured the permeability of the wing cuticle, given that this flat organ allows to produce an unambiguous scoring under light microscopy. The Eosin Y penetration temperature in wings lies between 37 and 40°C in both *D. suzukii* sexes, whereas its range is 55 to 60°C in both *D. melanogaster* male and female flies. Thus, the inward barrier of the *D. suzukii* wing cuticle is more permeable than the *D. melanogaster* wing cuticle.

To further evaluate the inward barrier efficiency, we also compared the sensitivity of *D. suzukii* and *D. melanogaster* to the contact insecticide Chlorpyrifos (**Figure 3**). In general, *D. suzukii*

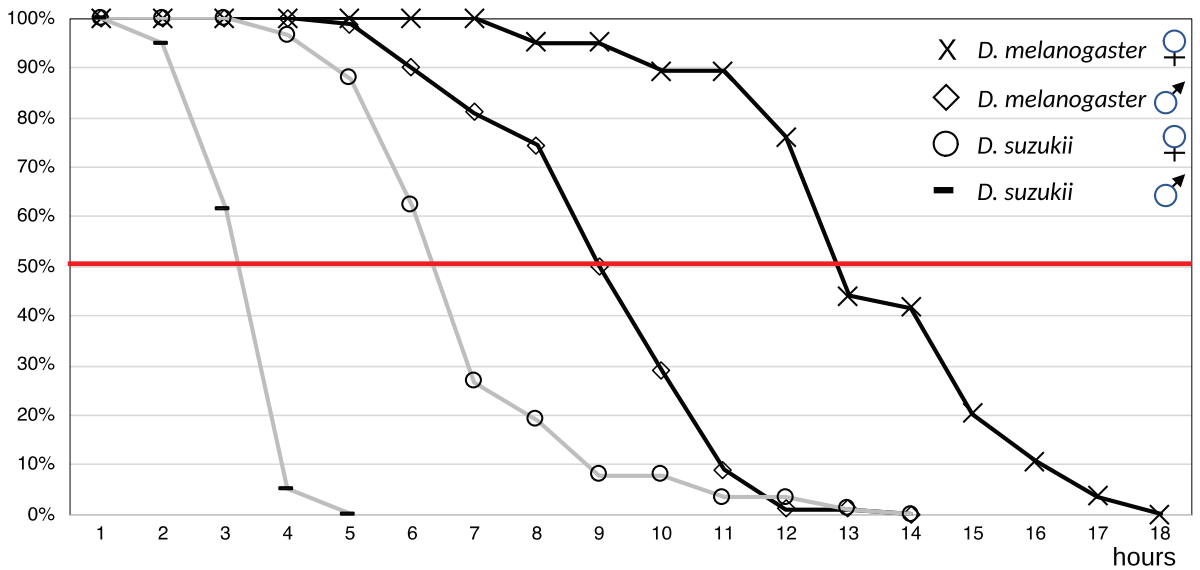

FIGURE 1 | *D. suzukii* and *D. melanogaster* flies were incubated at low air humidity (<10%). Survival of flies was recorded until all flies had died. Females and males were tested separately as it is known that females are generally more robust than males. The TL50 values are 3–4 h for *D. suzukii* males, 6–7 h for *D. suzukii* females, 9–10 h for *D. melanogaster* males, and 13–14 h for *D. melanogaster* females. Following a log-rank test, the *p*-values for the differences between males and between females of both species were calculated; they are <0.0001 for both comparisons.

flies are more susceptible to Chlorpyrifos than *D. melanogaster* flies. We also observed that females of both species were more resistant against Chlorpyrifos than males. This finding is consistent with the assumption that the inward barrier is weaker in *D. suzukii* than in *D. melanogaster*.

CHC Composition Differs Between *D. suzukii* and *D. melanogaster*

The function of both the outward and inward barriers relies on the presence of surface CHCs. To test whether barrier differences between *D. suzukii* and *D. melanogaster* are reflected by the CHC composition, we performed GC/MS analysis of surface lipids of the whole body and of dissected wings (**Figure 4**). Our results are consistent with studies reporting CHC profiles in *D. suzukii* (Snellings et al., 2018) and *D. melanogaster* (Everaerts et al., 2010). On average, 1115 ng CHCs per male and 1404 ng CHCs per female were extracted from the body surface of *D. suzukii*. The body surface extracts of each *D. melanogaster* male contains 1506 ng CHCs on average, while each female *D. melanogaster* has 2095 ng CHCs on its body surface. The desaturation rates of *D. suzukii* male and female body CHCs are 63.1% and 59.1%, respectively. The desaturation rates of *D. melanogaster* male and female body CHCs are 59.3% and 71.1%, respectively. Around 6.5% of body CHCs on *D. suzukii* males and 10.4% on *D. suzukii* females are methylated. The methylation rates on *D. melanogaster* male and female body CHCs are 21.3% and 19.4%, respectively. We conclude that both the total amounts and the composition of body CHCs considerably differ between *D. suzukii* and *D. melanogaster*. In a nutshell, *D. melanogater* males and females have more branched, desaturated and total, but less linear CHCs than their *D. suzukii* counterparts. The CHC relative compositions of dissected *D. suzukii* and *D. melanogaster* wings are similar to the respective whole body CHC relative compositions.

TABLE 2 | Body mass and water content of *D. suzukii* and *D. melanogaster* flies.

	Body mass (mg)	Water content (%)
D. suzukii female	1.9 ± 0.04	76 ± 0.6
D. suzukii male	1.2 ± 0.015	82 ± 1
D. melanogaster female	1.1 ± 0.09	80 ± 3.8
D. melanogaster male	0.76 ± 0.03	87 ± 3.1

The p-values following a Student's t-test for body mass mean differences between the sexes of the two species are 0.001 (females) and 0.0002 (males). The p-values following a Student's t-test for water content mean differences between the sexes of the two species are 0.02 (females) and 0.1 (males). The standard deviation for the values of both traits are given in ±.

Expression of Key Genes Involved Barrier Formation Varies in *D. suzukii* and *D. melanogaster*

To learn about the molecular mechanisms underlying CHC composition in *D. suzukii* and *D. melanogaster*, we monitored the expression levels of genes that code for enzymes involved in CHC formation (**Figure 5**). We used quantitative real-time PCR (qPCR), to record the expression levels of *fas1*, *fas2*, *fas3*, *cyp4g1*, *farO*, *acc*, *desat1,* and *app* transcripts in newly hatched flies. Compared to *D. melanogaster* females, the expression of genes encoding the first key enzymes of fatty acid synthesis FAS1 and ACC were low in *D. suzukii* females. However, these genes showed similar expression levels in *D. melanogaster* and *D. suzukii* males. Likewise, the expression of *farO* was similar

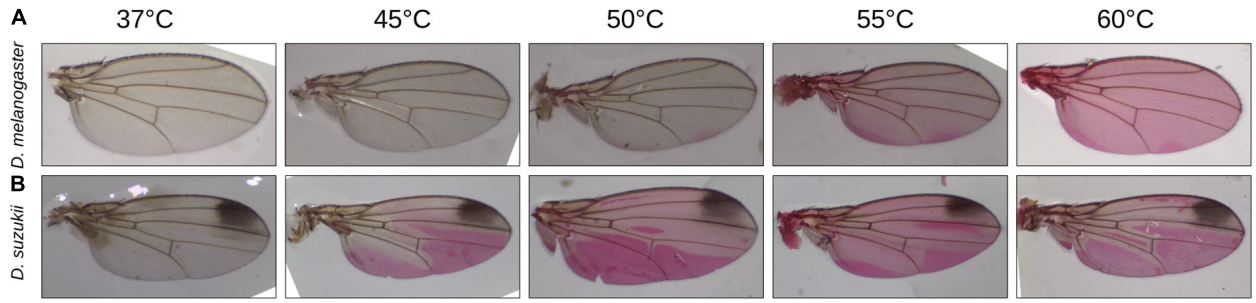

FIGURE 2 | The inward barrier efficiency was tested in an Eosin Y penetration assay. As a read out, we choose to score dye penetration into the wing tissue in dependence of the incubation temperature. Here, we show the results for the male wings. Dye penetration into the wing of *D. suzukii* flies started at 40°C **(A)**, while Eosin Y penetrated the *D. melanogaster* wing at 55°C **(B)**. Penetration temperature was similar in males and females in both species. Female wings are shown in **Supplementary Figure S1**. It is worth mentioning that both strains were captured in the wild and are not isogenized; hence, variation of staining intensity and wing size is expected.

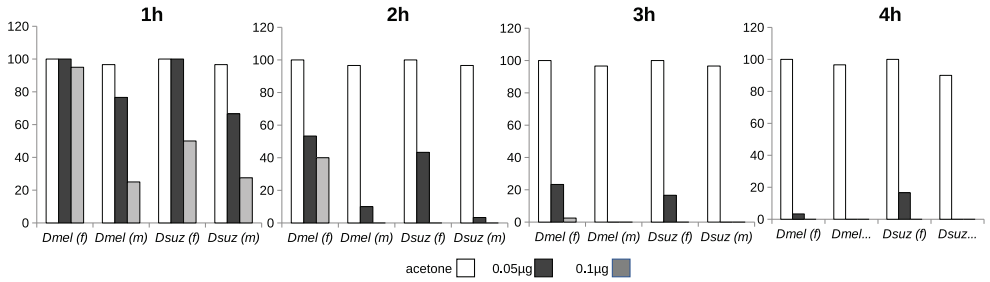

FIGURE 3 | Groups of flies were exposed to three different amounts of chlorpyrifos for 4 h. Survival was recorded every hour. At least 30 flies were tested in each experiment.

in *D. melanogaster* and *D. suzukii* males and females. While *fas3* expression was higher in *D. suzukii* males than in *D. melanogaster* males, it did not differ between *D. melanogaster* and *D. suzukii* females. The expression of the gene coding for the terminal CHC producing enzyme Cyp4g1 was lower in *D. suzukii* males as compared to *D. melanogaster* males whereas it did not differ between females of the two species. In both sexes, *app* transcript levels were higher in *D. suzukii*, while the expression levels of both *fas2* and *desat1* were around 100 times higher in *D. suzukii* than in *D. melanogaster*.

We also examined the expression levels of *oskyddad* (*osy*), *snustorr* (*snu*), and *snustorr snarlik* (*snsl*), all three coding for proteins required for the construction of the cuticle barrier (**Figure 5**). The expression of *snsl* did not differ significantly in both sexes of the two species. Levels of *osy* transcripts were higher in *D. suzukii* females and males than in *D. melanogaster*. However, *snu* expression was dramatically reduced in both *D. suzukii* females and males compared to same-sex *D. melanogaster* flies. We obtained identical results when we compared the expression levels of *snu* in both *D. suzukii* and *D. melanogaster* female and male dissected wing buds (**Supplementary Figure S3**).

Initially, *snu* was characterized in *D. melanogaster* as a key gene involved in barrier efficiency in a genetic approach in the laboratory (Zuber et al., 2018; Wang et al., 2020). Indeed, mutations in *snu* are lethal underlining its role in barrier function. Here, the quantitative variation of its expression correlating with cuticle barrier efficiency in *D. suzukii* and *D. melanogaster* suggests that it is also important in nature. To underpin this notion, we repeated the analysis of its expression changing two parameters. First, in order to rule out line-specific gene expression, we quantified *snu* transcript levels in two additional *D. suzukii* wild-type lines (see section "Materials and Methods"). Second, to exclude primer-specific effects, we designed a new set of *D. suzukii snu*-specific primers for these experiments (**Table 1**). The expression of *snu* was significantly reduced by more than 80% in *D. suzukii* compared to *D. melanogaster* in these experiments (**Supplementary Figure S3**).

Overall, the expression of some key genes coding for proteins and enzymes involved in lipid-based barrier construction and function show a substantial variation between *D. suzukii* and *D. melanogaster*. Especially, the expression divergence of *snu* is intriguing as its transcript levels have been shown to correlate with barrier efficiency in *D. melanogaster* (Wang et al., 2020).

DISCUSSION

Desiccation

Desiccation resistance is conveyed by a combination of the behavioral repertoire and physiological and physical properties of the organism. In case of incipient drought, an animal,

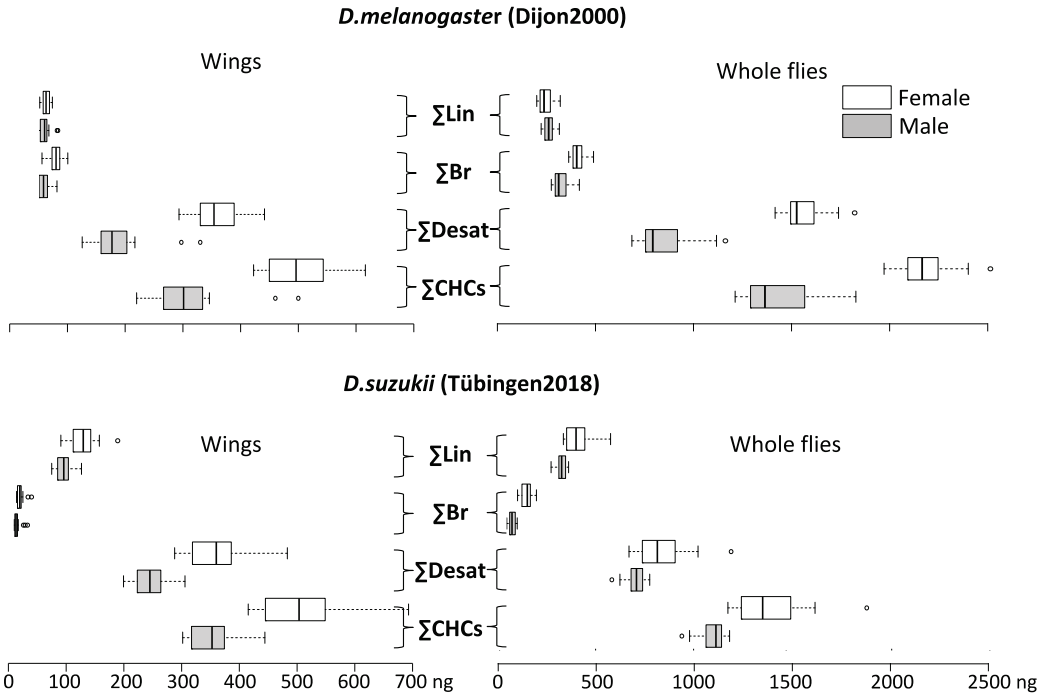

FIGURE 4 | Amounts (in ng) and composition of wings (left panels) and whole body (right) CHCs in individual *D. melanogaster* **(top)** and *D. suzukii* **(bottom)** were determined by gas chromatography and mass spectrometry. The amounts of sum linear (ΣLin), sum branched (ΣBr) and sum desaturated (ΣDesat) CHCs were calculated based on the overall sum of CHCs (ΣCHCs). See **Supplementary Figure S2** for all detected CHCs and **Table 3** for the statistical analysis of these data.

for instance, may respond by taking up and storing more water and initiate fortification of its barrier against evaporation. These responses and their amplitude depend, of course, on the genetic constitution of the organism. Hypothetically, the micro-environment of an insect has a decisive impact on the quality of a responsive trait and the expression dynamics of the underlying genes. Under identical conditions, the response may vary at several levels. In dimorphic species, a difference in this regard may prevail between sexes. Response variation is probably more accentuated between species than within species.

In our inter-species comparative approach, we found that *D. suzukii* is more sensitive to low air humidity than *D. melanogaster*. This is in agreement with a work published by Terhzaz et al. (2018). Since all flies were reared under similar laboratory conditions, we can rule out possible experimental bias for this observation. Indeed, both species were shown to be responsive to environmental cues. *D. suzukii* appears in two morphs, i.e., the summer and the winter morph with distinct ecological traits. The winter morph, for instance, is more robust at low humidity conditions than the summer morph (Toxopeus et al., 2016; Fanning et al., 2019). *D. melanogaster* as a cosmopolitan species also shows geographical variation (Rajpurohit et al., 2017; Dong et al., 2019). We believe that there are two physiological explanations for the inter-species differences. The first one implies that the difference in water shortage tolerance between these two species relies on total body water content. Indeed, we found that the overall body water content in *D. suzukii* is lower than in *D. melanogaster*. However, the water-content hypothesis is not very plausible given that *D. suzukii* males which contain relatively more water than females are less robust than females at lower air humidity. The second physiological explanation underscores that the water loss rate through the three major routes respiration, excretion or cuticular transpiration may be higher or faster in *D. suzukii* than in *D. melanogaster*. For a number of different *Drosophila* species including *D. melanogaster* (*D. suzukii* was not included in that study), it was proposed that especially cuticular transpiration accounts for the highest water loss rate, whereas excretion (<6%), and respiration (<10%) are rather negligible in this regard (Gibbs et al., 2003).

TABLE 3 | *p*-values of the Wilcoxon test on differences of the wing and whole body total (CHCs), desaturated (Desat), branched (Br), and linear (Lin) CHC amounts between *D. suzukii* and *D. melanogaster* males and females presented in **Figure 4**.

	Wings (*D. s* vs *D. m*)		**Whole Body (*D. s* vs *D. m*)**	
	Males	**Females**	**Males**	**Females**
Σ CHCs	0.021	0.837	1.907×10^{-6}	1.907×10^{-6}
Σ Desat	0.0007	0.588	0.0005	9.556×10^{-5}
Σ Br	9.529×10^{-5}	9.502×10^{-5}	9.542×10^{-5}	9.555×10^{-5}
Σ Lin	9.529×10^{-5}	9.542×10^{-5}	0.0001	9.542×10^{-5}

Except for the differences of total and desaturated CHC amounts in female wings, all differences are statistically significant.

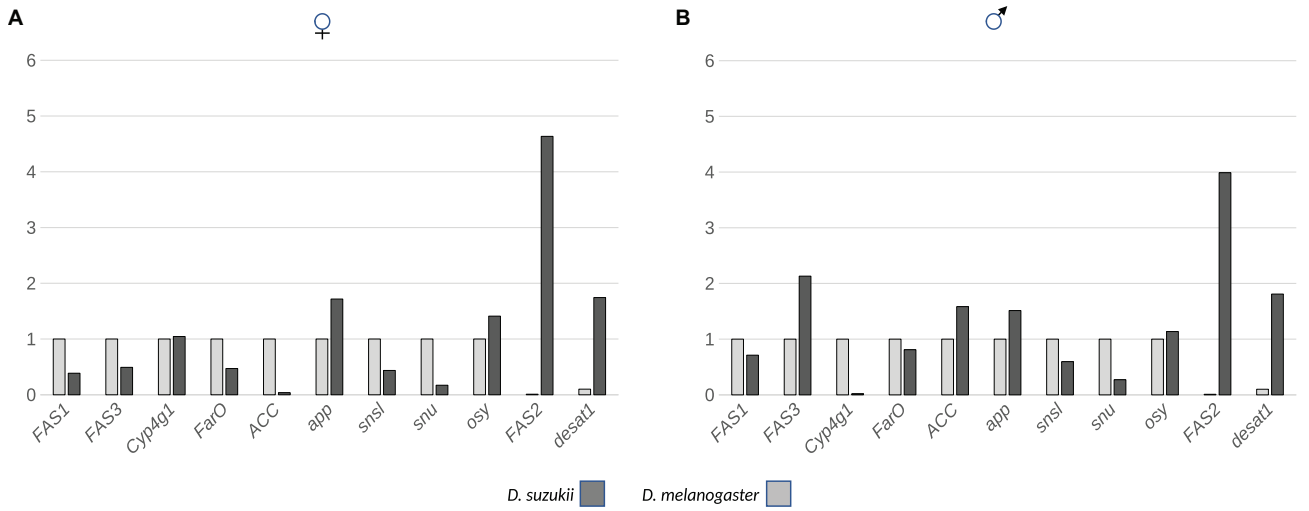

FIGURE 5 | The expression of genes coding for enzymes and proteins involved in lipid (CHC) biosynthesis and transport was monitored by qPCR in females **(A)** and males **(B)** of *D. suzukii* and *D. melanogaster*. For all transcripts except for *FAS2* and *desat1*, the *D. melanogaster* expression levels were set to 1. For FAS2, the expression level of the *D. melanogaster* transcript was set to 0.01, and the expression level of the *D. melanogaster desat1* transcript was set to 0.1. The *p*-values following a Student's *t*-test are 0.04 (female; f) and 0.33 (male; m) for *FAS1*, 0.29 (f) and 0.004 (m) for *FAS3*, 0.88 (f) and 0.004 (m) for *Cyp4G1*, 0.05 (f) and 0.048 (m) for *FarO*, 0.007 (f) and 0.04 (m) for *ACC*, 0.002 (f) and 0.046 (m) for *app*, 0.098 (f) and 0.49 (m) for *snsl*, 0.03 (f) and 0.003 (m) for *snu*, 0.047 (f) and 0.006 (m) for *osy*, 0.02 (f) and 0.0007 (m) for *FAS2* and 0.009 (f) and 0.009 (m) for *desat1* expression differences.

The CHC Barrier and Gene Expression

According to the assumption of Gibbs et al. (2003), we think that a weaker outward barrier in *D. suzukii* may explain the observed difference in desiccation resistance between these species. Indeed, we found that *D. suzukii* flies have less CHCs on their surface than *D. melanogaster* flies suggesting that the CHC-based barrier is weaker in *D. suzukii*. However, Gibbs et al. (2003) reported that the quality of the cuticle barrier does not seem to depend on the CHC amounts in the *Drosophila* species studied. On the other hand, several recent works suggested that reduced CHC levels do cause enhanced desiccation (Qiu et al., 2012). Gibbs et al. (2003) also argued that the CHC melting temperature Tm that depends on CHC composition did not correlate with the water loss rate in their work. This is, however, in conflict with more recent findings. Higher proportions of desaturated CHCs confer increased desiccation resistance to *D. melanogaster* flies in experimentally selected lines (Ferveur et al., 2018). In another study, Chung et al. (2014) demonstrated that higher amounts of branched CHCs in *D. serrata* (29%) entail a higher desiccation resistance compared to *D. birchii* (3%). In analogy, our study reveals that *D. suzukii* has proportionally less branched CHCs (6% in males and 13% in females of the total amounts of CHCs) than *D. melanogaster* (23% in males and 19% in females of the total amounts of CHCs). We conclude that these traits may contribute to the difference in desiccation resistance observed between *D. suzukii* and *D. melanogaster*.

Remarkably, the CHC profiles in *D. suzukii* and *D. melanogaster* did not correlate with expression profiles of genes coding for lipid synthesis or modification enzymes. For instance, *FASN2* that codes for a microsomal fatty acid synthase catalyzing the formation of methyl-branched fatty acids, is expressed at higher levels in *D. suzukii* than in *D. melanogaster*, while the relative amounts of branched CHCs is reduced in *D. suzukii*. Moreover, the expression of *Desat1* that codes for a fatty acid desaturase responsible for fatty acid desaturation is enhanced in *D. suzukii* although the relative amounts of desaturated CHCs are lower in this species. Either the gene expression levels do not reflect the enzyme levels, or the catalytic activity of enzymes in *D. suzukii* is lower than in *D. melanogaster*. Alternatively, the limiting process of CHC amounts may not be their production but their externalization and deposition on the cuticle. Consistent with this interpretation, we found that the expression of *snu* coding for an ABC transporter involved in barrier construction and function (Zuber et al., 2018; Wang et al., 2020) is reduced in *D. suzukii* compared to *D. melanogaster*. Thus, it is possible that less CHCs accumulate on the cuticle of *D. suzukii* because of reduced Snu activity that should be tested in biochemical experiments. This interpretation is in line with our recent findings that in *D. melanogaster* flies with low *snu* expression in the wing have decreased CHC levels and compromised wing cuticle barrier function (Wang et al., 2020). Possibly, the expression divergence between *D. melanogaster* and *D. suzukii* relies on a species-specific regulatory network and involves more target genes than *snu* alone (Wittkopp, 2007). One such target gene may be *osy*, also coding for an ABC transporter needed for cuticle barrier efficiency and acting independently from Snu (Wang et al., 2020). The expression of *osy* is, in contrast to *snu*, slightly but significantly upregulated in *D. suzukii* compared to *D. melanogaster*. Obviously, this upregulation is not sufficient to equate the cuticle barrier efficiency in *D. suzukii* with the one in *D. melanogaster*. Admittedly, this is a compelling but simplified scenario as we do neglect an important point.

The experiments presented in this work were done in a constant laboratory environment. Thus, we did not analyze the gene x environment (GxE) interaction in our desiccation assay. In other words, in nature, a complex, changing environment, gene expression variation may be different (Gibson, 2008; Hodgins-Davis and Townsend, 2009). For instance, the barrier of *D. suzukii* flies might be more robust under natural conditions than in the laboratory. Whether these differences may account for lifestyle differences between *D. suzukii* and *D. melanogaster* remains to be investigated.

To what extent can we apply our view on the situation of the outward barrier in *D. suzukii* and *D. melanogaster* to the situation of the inward barrier? Our experiments showed that the weaker outward barrier function of *D. suzukii* flies is paralleled by their weaker inward barrier function. Xenobiotics including both the inert dye Eosin Y and the insecticide Chlorpyrifos did penetrate the cuticle of *D. suzukii* more efficiently than in *D. melanogaster*. Thus, in a simple scenario, the CHC composition that defines the outward barrier function, would also be responsible for the inward barrier function in both species.

CONCLUSION

We would like to share two concluding remarks with the reader. First, we are aware that some differences in barrier efficiency between *D. suzukii* and *D. melanogaster* may be due to some geographical differences between the cities of Tübingen (Germany) and Dijon (France), where the respective strains studied here were captured. Indeed, barrier efficiency varies among geographically separated *D. melanogaster* populations (Dong et al., 2019). *D. suzukii* populations also display genomic variations (Tait et al., 2017) that may have an impact on their desiccation tolerance. However, the difference of desiccation sensitivity between these two species is similar to that reported in a previous study indicating that *D. melanogaster* is more resistant under low air humidity than *D. suzukii* (Terhzaz et al., 2018). This confirms that inter-specific differences are higher than possible geographical intraspecific differences.

Second, here we focussed on the cuticle as a potential site of water loss during desiccation. Recently, Terhzaz et al. (2018) showed that differences in a neuroendocrine control of water loss through the Malpighian tubules, i.e., excretory water loss in *D. suzukii* and *D. melanogaster* could also explain differences in desiccation resistance. Hence, as mentioned above, besides cuticular transpiration control, other mechanisms of water homeostasis may account for performance differences between *Drosophila* species adapted to environments with variable hygrometry. Continuing work in this direction to gather the complexity of desiccation resistance or sensitivity may ultimately serve to design strategies for successful *Drosophila* pest management.

DATA AVAILABILITY STATEMENT

The raw data supporting the conclusions of this article will be made available by the authors, without undue reservation, to any qualified researcher.

AUTHOR CONTRIBUTIONS

YW, J-PF, YY, JY, WT, NG, J-FF, and BM performed experiments and analyzed data. J-FF and BM designed and supervised experiments. J-FF revised the manuscript. BM wrote and revised the manuscript.

FUNDING

This work was supported by a grant to BM by the German Research Foundation (DFG, MO1714/9-1) and a grant to YY by the National Science Foundation of China (NSFC, 31761133021).

SUPPLEMENTARY MATERIAL

The Supplementary Material for this article can be found online at: https://www.frontiersin.org/articles/10.3389/fgene.2020.00887/full#supplementary-material

FIGURE S1 | As in males shown in **Figure 2**, Eosin Y penetrates the wings of *D. suzukii* females at lower temperatures as the wings of *D. melanogaster* females.

FIGURE S2 | Here we show the array of CHCs in weight (ng) and percentage (%) as determined in wings and whole bodies of *D. suzukii* and *D. melanogaster flies*.

FIGURE S3 | **(A)** As in the whole body shown in **Figure 5**, *snu* expression is reduced also in *D. suzukii* wings of males and females compared to *D. melanogaster*. **(B)** The expression of *snu* is reduced in three different stocks of *D. suzukii* flies (males and females mixed) compared to *D. melanogaster* flies. The *p*-values after a Student's *t*-test are 0.0004 for the expression differences of *snu* between female wings and 0.02 for the expression differences between male wings shown in **(A)**. The *p*-values for the expression differences of *snu* between *D. melanogaster* and the different *D. suzukii* lines are 0.013 (Tübingen 2018), 0.009 (Brombeere), and 0.008 (Bad Wimpfen) shown in **(B)**.

REFERENCES

Beltrami, M., Medina-Munoz, M. C., Del Pino, F., Ferveur, J. F., and Godoy-Herrera, R. (2012). Chemical cues influence pupation behavior of *Drosophila* simulans and *Drosophila buzzatii* in nature and in the laboratory. *PLoS One* 7:e39393. doi: 10.1371/journal.pone.0039393

Chung, H., Loehlin, D. W., Dufour, H. D., Vaccarro, K., Millar, J. G., and Carroll, S. B. (2014). A single gene affects both ecological divergence and mate choice in *Drosophila*. *Science* 343, 1148–1151. doi: 10.1126/science.1249998

Dembeck, L. M., Boroczky, K., Huang, W., Schal, C., Anholt, R. R., and Mackay, T. F. (2015). Genetic architecture of natural variation in cuticular hydrocarbon composition in *Drosophila melanogaster*. *eLife* 4:e09861.

Dong, W., Dobler, R., Dowling, D. K., and Moussian, B. (2019). The cuticle inward barrier in *Drosophila melanogaster* is shaped by mitochondrial and nuclear genotypes and a sex-specific effect of diet. *PeerJ* 7:e7802. doi: 10.7717/peerj.7802

Everaerts, C., Farine, J. P., Cobb, M., and Ferveur, J. F. (2010). *Drosophila* cuticular hydrocarbons revisited: mating status alters cuticular profiles. *PLoS One* 5:e9607. doi: 10.1371/journal.pone.0009607

Fanning, P. D., Johnson, A. E., Luttinen, B. E., Espeland, E. M., Jahn, N. T., and Isaacs, R. (2019). Behavioral and physiological resistance to desiccation in spotted wing *Drosophila* (Diptera: Drosophilidae). *Environ. Entomol.* 48, 792–798. doi: 10.1093/ee/nvz070

Ferveur, J. F., Cortot, J., Rihani, K., Cobb, M., and Everaerts, C. (2018). Desiccation resistance: effect of cuticular hydrocarbons and water content in *Drosophila melanogaster* adults. *PeerJ* 6:e4318. doi: 10.7717/peerj.4318

Gibbs, A. G., Fukuzato, F., and Matzkin, L. M. (2003). Evolution of water conservation mechanisms in *Drosophila*. *J. Exp. Biol.* 206, 1183–1192. doi: 10.1242/jeb.00233

Gibson, G. (2008). The environmental contribution to gene expression profiles. *Nat. Rev. Genet.* 9, 575–581. doi: 10.1038/nrg2383

Hodgins-Davis, A., and Townsend, J. P. (2009). Evolving gene expression: from G to E to GxE. *Trends Ecol. Evol.* 24, 649–658. doi: 10.1016/j.tree.2009.06.011

Lee, J. C., Bruck, D. J., Curry, H., Edwards, D., Haviland, D. R., Van Steenwyk, R. A., et al. (2011). The susceptibility of small fruits and cherries to the spotted-wing *Drosophila*, *Drosophila suzukii*. *Pest Manag. Sci.* 67, 1358–1367. doi: 10.1002/ps.2225

Mitsui, H., Takahashi, K. H., and Kimura, M. T. (2006). Spatial distributions and clutch sizes of *Drosophila* species ovipositing on cherry fruits of different stages. *Population Ecol.* 48, 233–237. doi: 10.1007/s10144-006-0260-5

Moussian, B. (2010). Recent advances in understanding mechanisms of insect cuticle differentiation. *Insect. Biochem. Mol. Biol.* 40, 363–375. doi: 10.1016/j.ibmb.2010.03.003

O'Grady, P., and DeSalle, R. (2018a). Hawaiian *Drosophila* as an evolutionary model clade: days of future past. *Bioessays* 40:e1700246.

O'Grady, P. M., and DeSalle, R. (2018b). Phylogeny of the genus *Drosophila*. *Genetics* 209, 1–25.

Olazcuaga, L., Rode, N. O., Foucaud, J., Facon, B., Ravigne, V., Ausset, A., et al. (2019). Oviposition preference and larval performance of *Drosophila suzukii* (Diptera: Drosophilidae), spotted-wing *Drosophila*: effects of fruit identity and composition. *Environ. Entomol.* 48, 867–881. doi: 10.1093/ee/nvz062

Plantamp, C., Henri, H., Andrieux, T., Regis, C., Mialdea, G., Dray, S., et al. (2019). Phenotypic plasticity in the invasive pest *Drosophila suzukii*: activity rhythms and gene expression in response to temperature. *J. Exp. Biol.* 222:jeb199398. doi: 10.1242/jeb.199398

Qiu, Y., Tittiger, C., Wicker-Thomas, C., Le Goff, G., Young, S., Wajnberg, E., et al. (2012). An insect-specific P450 oxidative decarbonylase for cuticular hydrocarbon biosynthesis. *Proc. Natl. Acad. Sci. U.S.A.* 109, 14858–14863. doi: 10.1073/pnas.1208650109

Rajpurohit, S., Hanus, R., Vrkoslav, V., Behrman, E. L., Bergland, A. O., Petrov, D., et al. (2017). Adaptive dynamics of cuticular hydrocarbons in *Drosophila*. *J. Evol. Biol.* 30, 66–80.

Silva-Soares, N. F., Nogueira-Alves, A., Beldade, P., and Mirth, C. K. (2017). Adaptation to new nutritional environments: larval performance, foraging decisions, and adult oviposition choices in *Drosophila suzukii*. *BMC Ecol.* 17:21. doi: 10.1186/s12898-017-0131-2

Snellings, Y., Herrera, B., Wildemann, B., Beelen, M., Zwarts, L., Wenseleers, T., et al. (2018). The role of cuticular hydrocarbons in mate recognition in *Drosophila suzukii*. *Sci. Rep.* 8:4996.

Tait, G., Vezzulli, S., Sassu, F., Antonini, G., Biondi, A., Baser, N., et al. (2017). Genetic variability in Italian populations of *Drosophila suzukii*. *BMC Genet.* 18:87. doi: 10.1186/s12863-017-0558-7

Terhzaz, S., Alford, L., Yeoh, J. G., Marley, R., Dornan, A. J., Dow, J. A., et al. (2018). Renal neuroendocrine control of desiccation and cold tolerance by *Drosophila suzukii*. *Pest Manag. Sci.* 74, 800–810.

Toxopeus, J., Jakobs, R., Ferguson, L. V., Gariepy, T. D., and Sinclair, B. J. (2016). Reproductive arrest and stress resistance in winter-acclimated *Drosophila suzukii*. *J. Insect. Physiol.* 89, 37–51.

Versace, E., Eriksson, A., Rocchi, F., Castellan, I., Sgado, P., and Haase, A. (2016). Physiological and behavioral responses in *Drosophila melanogaster* to odorants present at different plant maturation stages. *Physiol. Behav.* 163, 322–331.

Walsh, D. B., Bolda, M. P., Goodhue, R. E., Dreves, A. J., Lee, J. C., Bruck, D. J., et al. (2011). *Drosophila suzukii* (Diptera: Drosophilidae): invasive pest of ripening soft fruit expanding its geographic range and damage potential. *J. Intergr. Pest Manag.* 2, G1–G7.

Wang, Y., Carballo, R. G., and Moussian, B. (2017). Double cuticle barrier in two global pests, the whitefly *Trialeurodes vaporariorum* and the bedbug Cimex lectularius. *J. Exp. Biol.* 220, 1396–1399.

Wang, Y., Norum, M., Oehl, K., Yang, Y., Zuber, R., Yang, J., et al. (2020). Dysfunction of Oskyddad causes Harlequin-type ichthyosis-like defects in *Drosophila melanogaster*. *PLoS Genet.* 16:e1008363. doi: 10.1371/journal.pgen.1008363

Wang, Y., Yu, Z., Zhang, J., and Moussian, B. (2016). Regionalization of surface lipids in insects. *Proc. Biol. Sci.* 283:20152994.

Wittkopp, P. J. (2007). Variable gene expression in eukaryotes: a network perspective. *J. Exp. Biol.* 210, 1567–1575.

Zuber, R., Norum, M., Wang, Y., Oehl, K., Gehring, N., Accardi, D., et al. (2018). The ABC transporter Snu and the extracellular protein Snsl cooperate in the formation of the lipid-based inward and outward barrier in the skin of *Drosophila*. *Eur. J. Cell. Biol.* 97, 90–101.

Conflict of Interest: The authors declare that the research was conducted in the absence of any commercial or financial relationships that could be construed as a potential conflict of interest.

frontiers in Cell and Developmental Biology

REVIEW
published: 07 August 2020
doi: 10.3389/fcell.2020.00679

Rhodnius, Golden Oil, and *Met*: A History of Juvenile Hormone Research

*Lynn M. Riddiford**

Department of Biology, Friday Harbor Laboratories, University of Washington, Friday Harbor, WA, United States

Juvenile hormone (JH) is a unique sesquiterpenoid hormone which regulates both insect metamorphosis and insect reproduction. It also may be utilized by some insects to mediate polyphenisms and other life history events that are environmentally regulated. This article details the history of the research on this versatile hormone that began with studies by V. B. Wigglesworth on the "kissing bug" *Rhodnius prolixus* in 1934, through the discovery of a natural source of JH in the abdomen of male *Hyalophora cecropia* moths by C. M. Williams that allowed its isolation ("golden oil") and identification, to the recent research on its receptor, termed *Methoprene-tolerant* (*Met*). Our present knowledge of cellular actions of JH in metamorphosis springs primarily from studies on *Rhodnius* and the tobacco hornworm *Manduca sexta*, with recent studies on the flour beetle *Tribolium castaneum,* the silkworm *Bombyx mori*, and the fruit fly *Drosophila melanogaster* contributing to the molecular understanding of these actions. Many questions still need to be resolved including the molecular basis of competence to metamorphose, differential tissue responses to JH, and the interaction of nutrition and other environmental signals regulating JH synthesis and degradation.

Keywords: juvenile hormone, *Rhodnius prolixus*, *Hyalophora cecropia*, *Manduca sexta*, *Methoprene-tolerant*

OPEN ACCESS

Edited by:
Subba Reddy Palli,
University of Kentucky, United States

Reviewed by:
Xavier Belles,
Institut de Biología Evolutiva (IBE), Spain
Thomas Roeder,
University of Kiel, Germany

***Correspondence:**
Lynn M. Riddiford
lmr@uw.edu

Specialty section:
This article was submitted to Epigenomics and Epigenetics, a section of the journal Frontiers in Cell and Developmental Biology

Received: *25 May 2020*
Accepted: *06 July 2020*
Published: *07 August 2020*

Citation:
Riddiford LM (2020) Rhodnius, Golden Oil, and Met: A History of Juvenile Hormone Research. Front. Cell Dev. Biol. 8:679. doi: 10.3389/fcell.2020.00679

INTRODUCTION

Serendipity is often the key to novel and fundamental discoveries. Physiologists early on are taught the August Krogh Principle: "For a large number of problems there will be some animal of choice or a few such animals on which it can be most conveniently studied" (Krogh, 1929). The history of juvenile hormone (JH) research is filled with examples of this as will be clear in the following account.

Experimental endocrinology began with Berthold who in 1849 transplanted testes into castrated roosters and showed that they caused the return of the normal secondary sex characteristics (enlarged combs and wattles) (Soma, 2006). In 1856, Brown-Séquard showed that the adrenal gland was essential to life (Aminoff, 2017), then later showed that mammalian testicular extracts influence secondary sex characteristics in other animals and purportedly aging in men as well (Brown-Séquard, 1889). The first work on hormonal control of metamorphosis was that of Gudernatsch (1912) who found that extracts of mammalian thyroid were sufficient to cause precocious metamorphosis of frog tadpoles, indicating a universality of function of these extracts. All these findings showed that endocrine organ extracts contained substances that when injected into the blood could act on particular target organ(s); these substances were named "hormones" (Starling, 1905).

Stefan Kopeć working in Cracow, Poland between 1908 and 1912 was the first to show that in insects, unlike in birds and mammals, the secondary sex characteristics were not dependent on gonadal hormones (Cymborowski, 1981). He went on to demonstrate in the gypsy moth, *Lymantria dispar,* that the brain secreted a hormone that was necessary for metamorphosis (Kopeć, 1917, 1922). This "brain hormone" was the first known neurosecretory hormone in insects and was later called "prothoracicotropic hormone" (PTTH) when the particular pair of cells was isolated and shown to stimulate ecdysone secretion by the prothoracic glands of the tobacco hornworm, *Manduca sexta*, *in vitro* (Agui et al., 1979).

WIGGLESWORTH AND *Rhodnius*

In 1934, working with the bloodsucking, kissing bug, *Rhodnius prolixus* (the vector of Chagas disease), Vincent B. Wigglesworth was the first to show that there was a hormone that circulated in the nymphal hemolymph that prevented metamorphosis. *Rhodnius* was ideal for these experiments since they only molted after a blood meal and they could be parabiosed (i.e., two could be attached together by the anterior ends so that they shared circulating hemolymph). Normally a nymph would molt 6 days after feeding, but when decapitated immediately after feeding, it never molted (Wigglesworth, 1934; **Figure 1**). If, however, decapitation was delayed until 3 days after feeding, the molt proceeded normally. Through a series of parabiosis experiments, Wigglesworth (1934) then showed that there was a hormone released from the head after feeding that initiated the molting process. Moreover, parabiosis experiments with penultimate fourth and final fifth instar nymphs showed that there was also a hormone released from the head region that inhibited metamorphosis (**Figure 2**). Parabiosis of a fed headless fourth instar to a headless metamorphosing nymph caused precocious metamorphosis of the fourth instar nymph. In contrast, a fed headless fifth instar nymph parabiosed to a molting fourth instar nymph formed a supernumerary nymph. Histological studies showed that the head contained a brain and the posterior sympathetic ganglion that innervated a single median gland, the corpus allatum, located at the back of the head above the subesophageal ganglion in a hemolymph-filled sinus (**Figure 2**). Moreover, the corpus allatum showed cyclical changes during larval molting and metamorphosis. Based on these studies, Wigglesworth (1934) concluded that both the "molting" and "inhibitory" hormones come from the corpus allatum.

From further parabiosis and corpus allatum implantation experiments, Wigglesworth (1936) concluded that the corpus allatum was the source of the inhibitory hormone for metamorphosis. In 1940, he further showed by implantations of various organs into fed decapitated fourth instar nymphs that only the corpus allatum secreted the "inhibitory hormone" and the brain (the dorsal half) the "molting hormone" (Wigglesworth, 1940). At this point, he named the metamorphosis-inhibitory hormone "juvenile hormone." He also compared the abdominal epidermal changes during a nymphal molt and at metamorphosis. Based on this comparison, Wigglesworth hypothesized that metamorphosis at the cellular level occurs only when the molting hormone is present and activates the "imaginal system" (Wigglesworth, 1940). If, however, JH is also present, it activates the nymphal system and prevents the production of

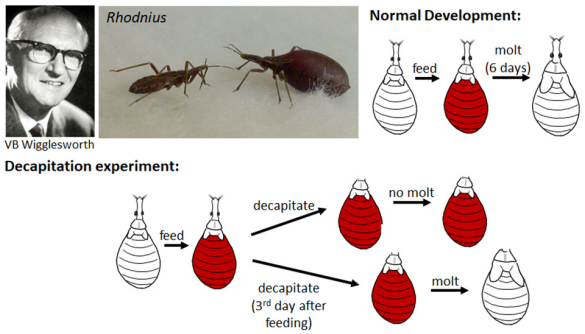

FIGURE 1 | Top: Vincent B. Wigglesworth (left); non-fed (left) and blood-fed (right) nymphs of *Rhodnius prolixus* (center); cartoon of the normal development of a nymph which after feeding on a blood meal (orange) molts to the next nymphal instar 6 days later. **Bottom**: Cartoon of decapitation experiments shows that decapitation immediately after feeding prevents the molting but decapitation 3 days after feeding does not. Photos of Wigglesworth from Phillips (2004) and of *Rhodnius* taken by Timothy Bradley and Catherine Loudon from Knight (2014) (reproduced with permission).

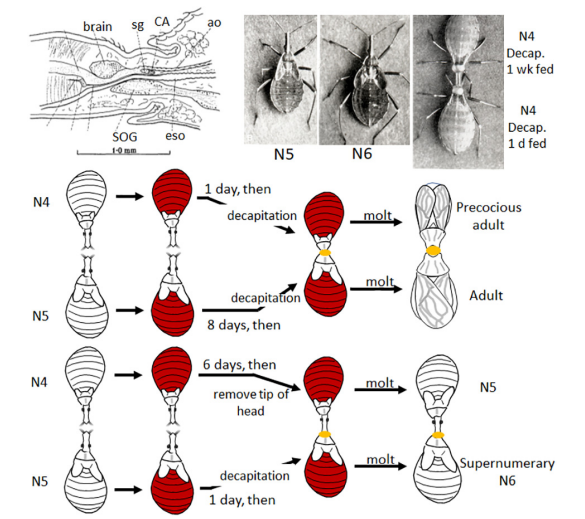

FIGURE 2 | Top: Diagram of brain and corpus allatum (CA) of *Rhodnius* (modified from Figure 2 in Wigglesworth, 1934); *Rhodnius* 5th instar (N5), supernumerary 6th instar (N6), and parabiosed, fed and decapitated (decap) 4th instar (N4) (top one decapitated one week after feeding, the bottom 1 day after feeding) nymphs [photos from Plates I and II in Wigglesworth (1954), reproduced with permission]. **Bottom**: Cartoon of two parabiosis experiments: (1) (top) a 4th instar nymph decapitated 1 day after feeding and parabiosed to a 5th instar nymph decapitated 8 days after feeding (thus ready to molt) molted to a precocious adult; (2) a parabiosed 4th instar nymph with only the tip of the head removed (leaving the CA intact) 6 days after feeding parabiosed to a 5th instar nymph decapitated only 1 day after feeding caused the latter to molt to a supernumerary 6th instar nymph (Wigglesworth, 1934). See text for details. ao, aorta; eso, esophagus; sg, sympathetic ganglion; SOG, subesophageal ganglion.

adult structures. Later guided by the findings of Williams (1947, 1948) on the wild silkmoth, *Hyalophora* (formerly *Platysamia*) *cecropia* (commonly called Cecropia) (see below), Wigglesworth (1952) showed that the thoracic glands of *Rhodnius* secreted the molting hormone after activation by a hormone from the brain.

Wigglesworth also showed that the corpus allatum reactivated in the adult and regulated ovarian maturation in the female and accessory gland development in the male (Wigglesworth, 1936). The corpora allata were first described in the goat moth caterpillar, *Cossus cossus,* as "petits ganglions de la tete" (Lyonet, 1762). Later Nabert (1912) described their structure for many different insects, but their function(s) was unknown. Holmgren in 1909 and Ito in 1918 had noted changes in size of the corpora allata associated with reproductive maturation in termites and Lepidoptera, respectively (as cited in Wigglesworth, 1985), but no one had experimentally tackled the problem. Thus, Wigglesworth was the first to demonstrate that a hormone regulated reproduction in insects; and, moreover, that hormone was JH, the same hormone that regulated metamorphosis.

His findings spawned a whole series of experiments in many different insects on the role of the corpora allata in reproduction. In most insects, the corpora allata were found necessary for ovarian maturation —the grasshopper, *Melanoplus differentialis* (Pfeiffer, 1939), various flies (Thomsen, 1940; Vogt, 1942), and the cockroach, *Leucophaea maderae* (Scharrer, 1946). However, in a few insects such as the walking stick, *Carausius* (formerly *Dixippus*) *morosus* (Pflugfelder, 1937) and the silkmoth, *Bombyx mori* (Bounhiol, 1939), egg development occurred normally after allatectomy. These early studies were also notable for the number of women working in this area–Isabella Pfeiffer, Ellen Thomsen, Marguerite Vogt, and Berta Scharrer. Studies since then show that JH plays nearly a universal role in the regulation of insect reproduction although the details of the precise role it plays depends on the insect's life history (see reviews by Wigglesworth, 1985; Wyatt and Davey, 1996; Raikhel et al., 2005; Santos et al., 2019).

CONFIRMATION OF THE CORPORA ALLATA AS THE SOURCE OF JH

Bounhiol (1938) working with the silkworm, *B. mori*, showed that removal of the corpora allata (allatectomy) from early instar larvae caused precocious metamorphosis but removal in the final (fifth) instar had no effect on the onset of metamorphosis (**Figure 3**, top). The allatectomized larva formed a normal cocoon and subsequently a normal pupa and adult. At about the same time, Pflugfelder (1937) and Radtke (1942) showed that loss of the corpora allata caused precocious metamorphosis in *Carausius*, and the mealworm, *Tenebrio molitor*, respectively.

At the end of the 1930s, Piepho (1938a) and Kühn and Piepho (1940) used larval integumental (epidermis plus overlying cuticle) implants in *Galleria* larvae to study hormonal control of molting and metamorphosis. The implants molted with the host and produced the type of cuticle dictated by the hormonal environment. Thus, implants from both last instar larvae (**Figure 3**, bottom center) and first instar larvae (**Figure 3**, bottom right) that were placed in a final instar larval host metamorphosed with the host.

Also, in the late 1930s, Helen Tsui-ying Lee at Sun Yat-sen University in Canton, China studied the prothoracic glands of lepidopteran larvae and their innervation and was the first to suggest that these glands were endocrine in nature and worthy of study by insect physiologists (Lee, 1948). However, her study was not published until 1948 due to the Japanese invasion of China in 1938. By the time of the publication of her article, the Japanese scientist Soichi Fukuda had published his classic articles on the commercial silkworm, *B. mori*, showing the role of the prothoracic glands in pupation (Fukuda, 1940a,b) and of both the corpora allata and prothoracic glands in larval molting (Fukuda, 1944).

WILLIAMS AND *Hyalophora cecropia* (CECROPIA), A NATURAL SOURCE OF JH

Carroll M. Williams grew up in Richmond, VA and loved to play around the James River that ran through the city. There he encountered among the insects he collected, the large saturniid moth, *H. cecropia*, whose pupal quiescence (diapause) inside its cocoon over the winter intrigued him. When he began his postdoctoral studies as a Junior Fellow in the Department of Biology at Harvard University in 1941, he started to work on this problem. His first studies concerned the role of the brain and prothoracic glands [recently implicated by Wigglesworth (1940) and Bounhiol (1945) to be involved in the metamorphosis of *Rhodnius* and *Bombyx*, respectively] in promoting development of the Cecropia pupa into the moth in the spring. In a series of extirpation and implantation experiments, he showed that the brain was responsible for activating the prothoracic glands to cause adult development (Williams, 1946, 1947, 1948, 1952). Moreover, chilling the pupae at 6°C for at least 10 weeks was sufficient to allow activation of the brain when the pupae were brought back to room temperature (Williams, 1956a).

Serendipitous Discovery of a Natural Source of JH

In the experiments described above on the role of the brain in terminating diapause, Williams became intrigued with the technique of parabiosis that Wigglesworth had used. Saturniid moths do not feed as adults so mate, lay their eggs and die within about 10 days. Therefore, Williams hypothesized that parabiosis of an adult to a pupa might allow the moth to live longer. When he parabiosed a headless Cecropia moth to a chilled diapausing pupa and kept the pair at 25°C, the moth did live longer. To his surprise, however, the pupa developed into a "second pupa" rather than to a normal adult! Although this experiment were done in the early 1950s, it was not published until 1963 (Williams, 1963). In a series of experiments to explore this phenomenon, he discovered that the "second pupa" was only formed when the parabiotic partner was either a Cecropia or a *Samia cynthia* (Cynthia) male moth (Williams, 1959,

1963; **Figure 4**). Cecropia pupae parabiosed to female moths of either species or to *Antheraea polyphemus* (Polyphemus) moths developed into normal adults. Moreover, the abdomens of the male Cecropia or Cynthia moths were sufficient to cause the formation of the second pupae and therefore were the repository for the "juvenile hormone" from the corpora allata that was responsible for the phenomenon (Williams, 1956b, 1959, 1963).

He found that chilled Polyphemus pupae were the best assay animals for JH activity (Williams, 1959) and proceeded to make ether extracts of Cecropia abdomens to isolate the hormone (Williams, 1956b; **Figure 4**). This extract was yellow due to the carotenoids in Cecropia fat body so he called it the "golden oil." During his sabbatical year in Wigglesworth's laboratory in Cambridge, he further purified and characterized the "golden oil" (Williams, 1956b). Using this extract, Wigglesworth painted his initials VBW on abraded cuticle of final instar nymphs of *Rhodnius* and showed that these initials were present as newly synthesized nymphal cuticle surrounded by adult cuticle after metamorphosis (Wigglesworth, 1958), confirming that this hormone could act on various insect orders. The JH in this "golden oil" was not chemically determined until 1967 when Röller et al. (1967) at the University of Wisconsin identified the active compound as the sesquiterpenoid methyl *dl-trans,trans,cis*-10-epoxy-7-ethyl-3,11-dimethyl-2,6-tridecadienoate (JH I) (for a review of the chemistry, see Röller and Dahm, 1968; **Figure 5**) and subsequently showed that the same compound was released from male Cecropia corpora allata *in vitro* (Röller and Dahm, 1970). Meyer et al. (1968) found a second hormone, JH II (methyl *dl-trans,trans,cis*-10,11-epoxy-3, 7, 11-trimethyl-2,6-tridecadienoate) (**Figure 5**) as a minor component of the "golden oil." Nearly 10 years later Shirk et al. (1976) showed that the JH was stored in the male accessory gland, not in the abdominal fat body (**Figure 4**). Moreover, the male corpora allata secreted JH acid that was then converted into JH by JH esterase in the accessory gland (Peter et al., 1981).

Juvenile hormones I and II were subsequently shown to be found only in Lepidoptera (Schooley et al., 1984). JH III (**Figure 5**) was first isolated by culturing adult female corpora allata of another lepidopteran, the tobacco hawk moth, *M. sexta* (Judy et al., 1973) and subsequently shown to be the JH of most other insects (Schooley et al., 1984). JH 0 and 4-methyl-JH I (**Figure 5**) were found in *Manduca* embryos (Bergot et al., 1980). JHs with modifications of the epoxide moiety are found

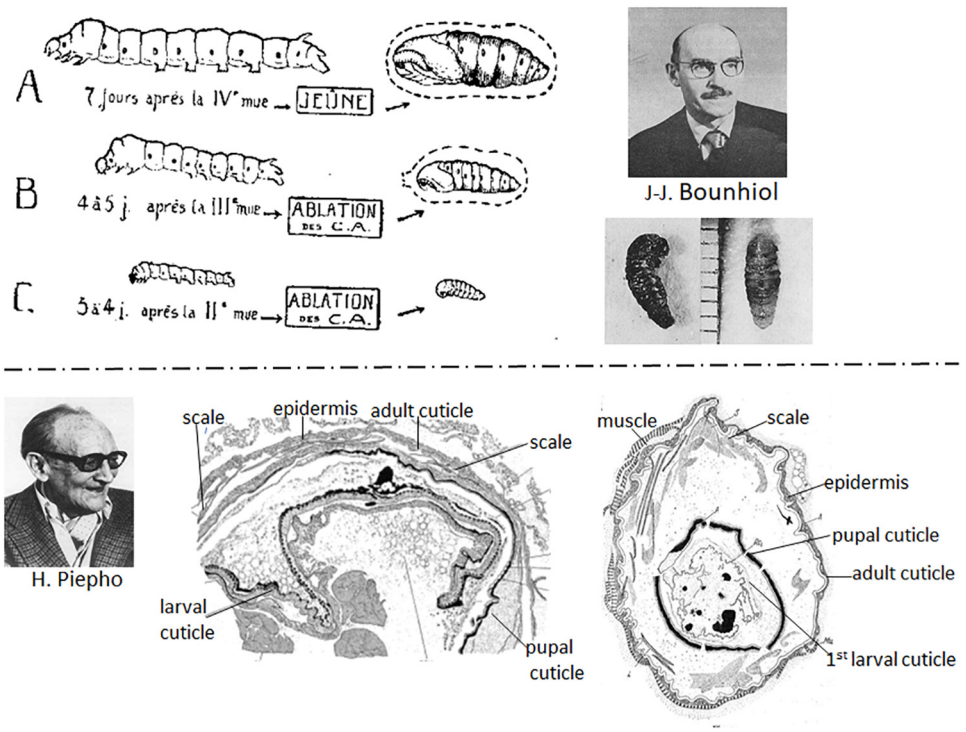

FIGURE 3 | Top: (Left) Diagram of effects of removal of the corpora allata (CA) (allatectomy) from the silkworm *Bombyx mori*. (A) Normal 5th instar larva and pupa; (B) allatectomized 4th instar larva formed a precocious pupa; (C) allatectomized 3rd instar larva formed a precocious pupa (figure from Bounhiol, 1938). (Right) Jean-Jacques Bounhiol (above); photo of pupae formed from allatectomized 4th (left) and 3rd (right) instar larvae (from Bounhiol, 1938) (bottom). **Bottom**: (Left) Hans Piepho. (Center) Result of an implant of 5th instar *Galleria* integument (epidermis plus cuticle) into another 5th instar *Galleria* larva that subsequently metamorphosed to a pupa and an adult. The implanted epidermis formed a pupal cuticle, then an adult cuticle with scales (from Piepho, 1938a). (Right) Result of an implant of 1st instar integument into a 5th instar larva after metamorphosis of the host. The implant formed a pupal, then an adult cuticle (from Piepho, 1938b). Photo of Bounhiol from Lamy and Delsol (1980) (reproduced with permission from Elsevier Masson) and that of Piepho from Hintze-Podufal (1996) (reproduced with permission from www.schweizerbart.de/journals/entomologia).

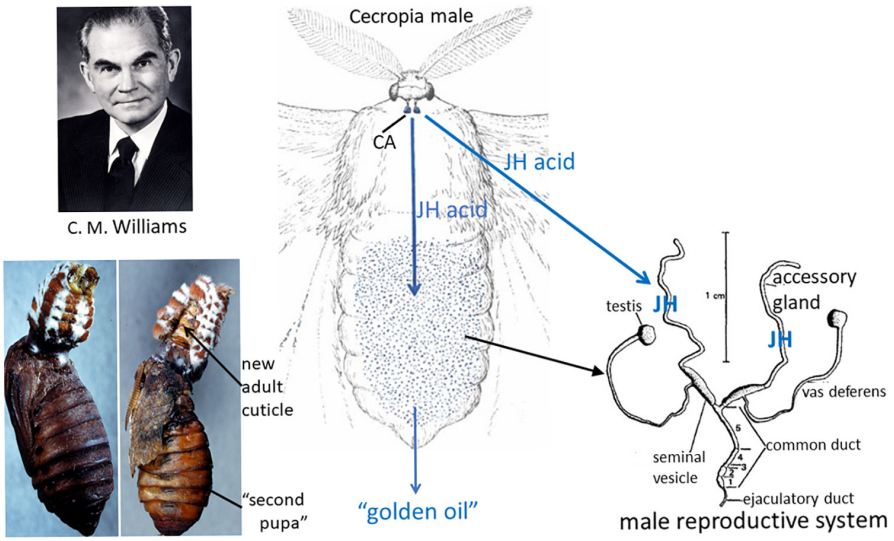

FIGURE 4 | Left: (Top) Carroll M. Williams. Photo from his memoir in the National Academy of Sciences Memoir collection. (Bottom) Cecropia male abdomen parabiosed to a chilled diapausing Cecropia pupa (left); after 21 days, the "second pupa" had formed and the abdomen had molted to a scaleless adult abdomen (right, arrow) (from the original slides taken by Muriel V. Williams that were used for the black-and-white Figures 3, 4 in Williams, 1963). **Center**: Diagram of the Cecropia male moth whose corpora allata (CA) synthesize and secrete juvenile hormone (JH) acid and from whose abdomen the "golden oil" that contained JH was extracted (drawing of the moth modified from a figure in Williams, 1958). **Right**: Reproductive system of a male saturniid moth (modified Figure 1 in Shepherd, 1974). The accessory glands of Cecropia males synthesize JH from the JH acid that is secreted from the CA, then store the hormone (Shirk et al., 1976; Peter et al., 1981).

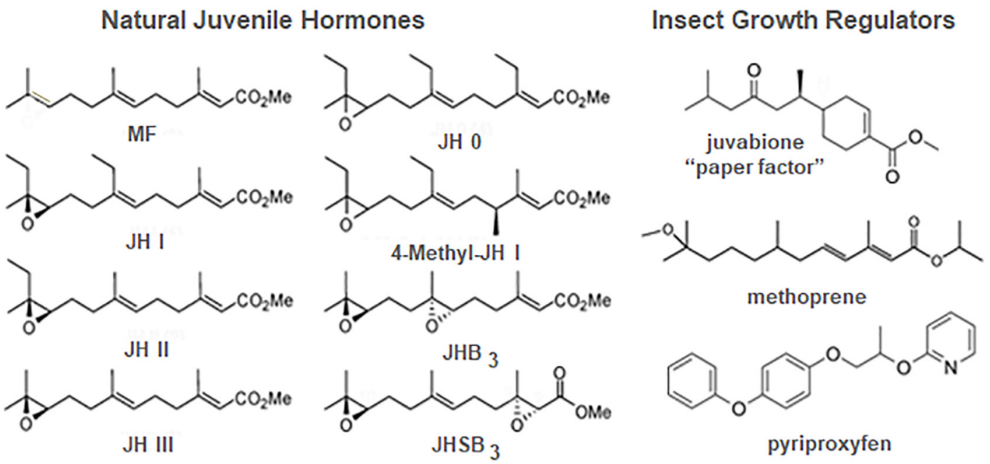

FIGURE 5 | Structures of the natural juvenile hormones (JH) **(left)** and some JH analogs known as insect growth regulators (IGRs) **(right)**. JHB_3, JH bisepoxide; $JHSB_3$, JH skipped bisepoxide; MF, methyl farnesoate. Prepared by Xavier Belles.

in the Diptera and Hemiptera. JH III bisepoxide (JHB3) was first identified in *Drosophila melanogaster* (Richard et al., 1989), and JH III skipped bisepoxide (JHSB3) was first found in the stink bug, *Plautia stali* (Kotaki et al., 2009; **Figure 5**).

Insect Growth Regulators

In his first article on the extraction of JH from the Cecropia male abdomen, Williams also commented on the efficacy of topical application of this extract in disrupting metamorphosis. He then suggested that "...in addition to the theoretical interest of the JH, it seems likely that the hormone, when identified and synthesized, will prove to be an effective insecticide. This prospect is worthy of attention because insects can scarcely evolve a resistance to their own hormone" (Williams, 1956b). In 1964, Karel Sláma from Czechoslovakia came to the Williams laboratory at Harvard University to work bringing his favorite study insect, the linden bug, *Pyrrhocoris apterus*. Although he brought linden seeds to feed the bugs, he used glass jars containing an upright paper towel to mimic a tree to rear the insects. Surprisingly, none of the nymphs

metamorphosed under these conditions. Initially suspecting that JH might be airborne within the Williams laboratory, Sláma reared at home some *Pyrrhocoris* shipped directly from Czechoslovakia but again no metamorphosis occurred; only supernumerary nymphs appeared. They then started a systematic search for a source of the hormone in the rearing conditions that resulted in the discovery that the source was the paper towels in the rearing jars (Sláma and Williams, 1965, 1966; Williams and Sláma, 1966). It proved only to be in American, not European, paper towels because the American paper towels and other paper products were made from balsam fir and European paper products were made from pine. Bowers et al. (1966) isolated and identified this "paper factor" from balsam fir as the methyl ester of todomatuic acid (juvabione) (**Figure 5**). Juvabione proved effective as a JH mimic only for the family Pyrrhocoridae, with other insects, even those in a closely related family Lygaeidae such as the milkweed bug *Oncopeltus fasciatus*, being unaffected. Such specificity gave rise to the hope that selective JH analogs might be found for prevention of metamorphosis of various pestiferous insects that would not harm beneficial insects such as honeybees.

Zoëcon founded in 1968 by Carl Djerassi, an organic chemist at Stanford University, was the first company formed to search for chemicals that had JH action on particular insects which they named insect growth regulators (IGRs). Methoprene (**Figure 5**) was first registered in 1975 by the Environmental Protection Agency as Altosid and used primarily in mosquito breeding areas as a larvicide. In treated water, larvae did not metamorphose to the adult, thus reducing the population (Staal, 1975). Today methoprene or another more potent IGR, pyriproxyfen (**Figure 5**), is still used in integrated pest management schemes to control mosquitoes, particularly those that are resistant to chemical insecticides (Walton and Eldridge, 2020). Methoprene is also used in combination with pyriproxyfen (Rust et al., 2016) or adulticides (Rust and Hemsarth, 2019) in flea collars and other flea products to prevent metamorphosis of flea larvae and kill the adults. Unfortunately, resistance to the IGRs has arisen (Parthasarathy et al., 2012), but combinations of IGRs or with other insecticides such as discussed above in flea control have reduced its impact.

THE TOBACCO HORNWORM (*Manduca sexta*) AND LARVAL ENDOCRINE PHYSIOLOGY

In the 1970s, the tobacco hornworm (*M. sexta*) became popular for the study of insect growth, molting and metamorphosis. *Manduca* thrived on a completely defined diet (Bell and Joachim, 1976) under laboratory conditions and was utilized initially by the laboratories of Carroll Williams, Fotis Kafatos, and Lynn Riddiford at Harvard University and Larry Gilbert's laboratory first at Northwestern University, then at the University of North Carolina. Jim Truman as a Junior Fellow at Harvard in the Riddiford and Williams groups showed using simple ligation experiments that the release of PTTH from the larval brain occurred during a certain time of day when the larvae were reared under a light:dark cycle (Truman, 1972; Truman and Riddiford, 1974). PTTH then activated the prothoracic glands to release ecdysone that with its biologically active metabolite, 20-hydroxyecdysone (20E) (see Riddiford et al., 2001), initiated and orchestrated the subsequent molt. The ligature experiments also appeared to indicate that JH necessary for larval molting was released slightly later than PTTH (Truman, 1972) and that JH was again necessary at the time of head capsule slippage during the molt for normal epidermal and cuticular pigmentation (Truman et al., 1973). Later Fain and Riddiford (1976) showed that the apparent delay of JH for the larval molt was due to the slow activation of the prothoracic glands by PTTH. The chance appearance of a *black* mutant larva in the Harvard tobacco hornworm colony (Safranek and Riddiford, 1975) allowed the development of a sensitive bioassay for JH (Fain and Riddiford, 1975). This assay showed that JH was present in the fourth (penultimate) instar larval hemolymph in declining amounts through the feeding and the molting periods and rose again at ecdysis to the fifth and final larval instar.

Fred Nijhout, a graduate student of Williams, subsequently showed that the final larval instar was dependent on a threshold size attained at the time of ecdysis (Nijhout and Williams, 1974a; Nijhout, 1975a). When the larva surpassed the threshold size for metamorphosis, it fed and grew in the final instar to a critical weight that started the endocrine events leading to metamorphosis (Nijhout and Williams, 1974b; Nijhout, 1975b). Subsequent studies by many on both *Manduca* and *Bombyx* have shown that these events are the decline of JH release by the corpora allata, the rise of a specific esterase to degrade JH in the hemolymph and tissues followed by the release of PTTH once the JH titer was sufficiently low (reviewed in Goodman and Granger, 2005; Hiruma and Kaneko, 2013; Nijhout et al., 2014). The subsequent release of ecdysone from the prothoracic glands was relatively small, but in the absence of JH caused the cessation of feeding and the onset of wandering behavior to search for a pupation site (Dominick and Truman, 1985).

During this period, Gibbs and Riddiford (1977) devised a sensitive *Manduca* larval assay for PTTH and showed that the region of the brain containing the lateral neurosecretory cells had the highest PTTH activity. Subsequently, Larry Gilbert's laboratory identified the pair of PTTH cells in that region (Agui et al., 1979) and studied the control of the prothoracic glands by PTTH (see reviews by Gilbert et al., 2002; Smith and Rybczynski, 2012). Much later *Manduca* PTTH was cloned and recombinant PTTH shown to be active (Gilbert et al., 2000; Shionoya et al., 2003), and *in situ* hybridization of its mRNA showed that only this pair of cells contained PTTH mRNA (Shionoya et al., 2003).

In addition, Gilbert's laboratory and Bhaskaran's laboratory at Texas A&M University studied the control of the corpora allata by the brain (Bhaskaran et al., 1980, 1990; see also review by Goodman and Granger, 2005). Both allatotropic and allatoinhibin activities were uncovered, but the allatotropin isolated and sequenced from adult *Manduca* brains was inactive in larvae (Kataoka et al., 1989).

CELLULAR ACTIONS OF JUVENILE HORMONE

Early Studies

The cellular actions of JH were first addressed by Wigglesworth (1940; 1963; 1973) in his studies of its action on the abdominal epidermis of *Rhodnius*. He found that cells responded to the molting hormone at metamorphosis in a particular pattern within the segment and that could be blocked by JH given at different times. He concluded that whereas the molting hormone activates the epidermal cells to begin growth, JH "merely ensures [perhaps by some action at the level of genes (Wigglesworth, 1954), perhaps indirectly by some action upon the cytoplasm (Wigglesworth, 1953)], that the larval pattern is maintained among the activated epidermal cells" (Wigglesworth, 1963). Later Lawrence (1969) found that treatment of *Oncopeltus* with JH at a specific time in the final nymphal instar caused the formation of adult cuticle with larval pigmentation. Willis et al. (1982) extended this study to *Pyrrhocoris*, the Colorado potato beetle, *Leptinotarsa decemlineata*, and various Lepidoptera, showing that there were two effects of JH—one causing a mosaic cuticle which has discrete patches of different stage-specific cuticle due to differing epidermal sensitivity to JH and the other a composite cuticle produced by a single cell which combines features of two metamorphic stages due to differing temporal JH sensitivity of different morphological characteristics.

Control of Cellular Commitment

The *Manduca* larva provided an epidermis that could be readily cultured and produce cuticle *in vitro* in response to the proper hormonal regimen. A new larval cuticle was synthesized by fourth instar larval epidermis when exposed to 20E immediately after explantation from an intermolt feeding larva (Riddiford et al., 1979, 1980). If, however, cultured in hormone-free media for 24 h, then exposed to 20E, it formed a pupal cuticle (Mitsui and Riddiford, 1978; Riddiford et al., 1980). When final larval instar epidermis was exposed to a low concentration of 20E followed by a high concentration, thereby mimicking the prewandering and pupal molt concentrations of ecdysteroid (Bollenbacher et al., 1981), it formed a pupal cuticle (Mitsui and Riddiford, 1976, 1978). Therefore, one could ask about the direct action of JH on the epidermis under defined conditions.

The abdominal epidermis of *Manduca* is polymorphic in that it first makes a larval cuticle under the influence of JH when exposed to ecdysteroid for the penultimate and final larval molts. Then when exposed to low ecdysteroid in the absence of detectable JH during the pre-wandering peak of ecdysteroid, the epidermis becomes unable to produce a larval cuticle either *in vivo* (when implanted into a penultimate stage larva and allowed to go through final larval molt) (Riddiford, 1976, 1978) or *in vitro* in response to 20E and JH (Mitsui and Riddiford, 1978). Instead it produces pupal cuticle. Hence, in response to the hormonal conditions alone, a single epidermal cell can switch from producing a larval cuticle to a pupal cuticle and therefore is now pupally committed. Although the epidermal cells of beetle (*T. molitor*) (and lepidopteran) larvae are electrically coupled through gap junctions through which small molecules move readily (Caveney and Podgorski, 1975), the cells of the abdominal segment of *Manduca* respond to this ecdysteroid-induced change of commitment in a particular pattern (Truman et al., 1974; Riddiford, 1978) that turns out to be same as the cell-by-cell induction of the Bric-à-brac-Tramtrack-Broad (BTB) transcription factor Broad by 20E (Zhou and Riddiford, 2001).

In *Drosophila* during the molt, 20E initiates a transcription factor cascade called the "Ashburner cascade." This cascade was first defined by Ashburner et al. (1974) as a series of salivary gland chromosomal puffs (expansions of the polytene DNA strands) induced by 20E *in vitro* that corresponded to the puffs seen *in vivo* at the time of wandering just before and during pupariation. Many of the puffs were later found to encode transcription factors (Thummel, 1990). The same cascade of transcription factors is seen in *Manduca* abdominal epidermis at both the fourth-fifth larval molt and metamorphosis (summarized in Hiruma and Riddiford, 2010) with the exception that Broad is not induced at the fifth larval molt, but only at the time of the ecdysteroid peak that initiates wandering. Thus, *Manduca* larval abdominal epidermis proved to be an ideal system in which to study the action of JH at the cellular and molecular levels. As seen above, when exposed to 20E in the absence of JH, this epidermis first expresses *broad* as it becomes pupally committed. Once committed, it henceforth only makes pupal cuticle when next confronted with a molting concentration of ecdysteroid, whether *in vivo* or *in vitro* (Hiruma and Riddiford, 2010). Once *broad* is activated by the ecdysteroid, its mRNA levels fluctuate during the wandering and prepupal periods directed by the levels of 20E present. Then after pupal ecdysis, *broad* mRNAs disappear from the epidermis over the first 3 days of pupal life and never reappear during the pupal-adult molt or in the adult epidermis (Zhou and Riddiford, 2002). However, when JH is given to the freshly ecdysed pupa, the *broad* transcripts reappear when the ecdysteroid titer arises for the subsequent molt and a "second pupa" rather than an adult is formed. Thus, JH prevents the ecdysteroid-induced switching on of *broad* in the larval epidermis and the ecdysteroid-induced switching off of *broad* in the pupal epidermis.

Drosophila Development, JH and Stage-Specifying Transcription Factors

To elucidate how JH acted to direct the action of ecdysteroid in the polymorphic epidermis, one had to turn to *Drosophila* with its wealth of genetic and molecular biological approaches. *Drosophila* along with the other higher Diptera has however the disadvantage for studying JH action on metamorphosis in that nearly all of the larval tissues except for the Malpighian tubules and the nervous system are discarded at metamorphosis. The adult head and thorax are made from imaginal discs that make larval cuticle and proliferate throughout larval life, then differentiate at metamorphosis, whereas the abdomen comes from abdominal histoblasts (Perez, 1910; Svácha, 1992; Fristrom and Fristrom, 1993). These histoblasts do not divide but make larval cuticle that lies above them during larval life. Then during the prepupal period after pupariation, they begin to

divide. The pupal cuticle of the abdomen then is made by reprogrammed larval epidermal cells and histoblasts. After head eversion to form the intact pupa inside the puparium, the proliferated histoblasts spread out from their nests in each abdominal segment, displacing the larval epidermal cells to form the adult epidermis (Ninov et al., 2007, 2009). The displaced larval cells are then engulfed by phagocytic hemocytes (Williams and Truman, 2005). When the ecdysteroid titer rises for the adult molt beginning about 18 h after pupariation (Handler, 1982), the imaginal epidermal cells first respond by undergoing adult commitment and patterning, then as the ecdysteroid titer declines form the adult cuticle beginning about 48–52 h after pupariation (Fristrom and Fristrom, 1993; Zhou and Riddiford, 2002; Ninov et al., 2009).

Normally Broad is present in the histoblasts and their derivatives until about 30 h after pupariation, then disappears (Zhou and Riddiford, 2002). By contrast, when JH is applied at the time of pupariation, the pupa appears normal but the resultant adult is a mosaic of a normal head and thorax and a pupal abdomen (Ashburner, 1970; Postlethwait, 1974). Under these conditions, Broad persists in the adult abdominal epidermis throughout adult development (Zhou and Riddiford, 2002). Furthermore, when *broad-Z1* was overexpressed in the whole animal using a heat shock GAL4 promoter between 30 and 36 h and again at about 48 h after pupariation, a second pupa was formed, indicating that the structures developing from the imaginal discs as well as from the histoblasts were capable of forming pupal cuticle. Thus, the presence of Broad in the cell allows it to make pupal cuticle in response to ecdysteroid and prevents the production of adult cuticle.

During adult development, ecdysone and 20E rise in the absence of JH, and the adult-specifying transcription factor E93 appears (Ureña et al., 2014, 2016). Uyehara et al. (2017) have recently shown that E93 directly acts on the chromatin structure in the enhancers of specific genes, opening up some adult-specific genes such as *nubbin* (important in wing vein formation) for activation and closing the chromatin on others such as *broad*, thus suppressing its expression. Broad and E93 are pupal- and adult-specifying transcription factors respectively throughout the Holometabola (Truman and Riddiford, 2019; Bellés, 2020) and thus fulfill the prediction of Williams and Kafatos (1971) that there are three master regulatory genes that successively activate the larval, pupal, and adult gene sets as metamorphosis proceeds. The idea that the unique features of the larva, pupa, and adult were the results of stage-specific gene sets was nullified by the finding that the same cuticle gene was expressed in the epidermis of two different metamorphic stages to produce a particular type of cuticle (Willis, 1986). This finding however does not negate the hypothesis that there are master regulatory genes that dictate the stage. The stage-specifying transcription factors Broad (pupal) and E93 (adult) along with Krüppel homolog 1 (Kr-h1) in the larva (see below) that regulate each stage and each other (Truman and Riddiford, 2019; Bellés, 2020) seem to be the long-sought regulators.

Williams and Kafatos (1971) also postulated that there is a larval master regulatory gene. *Kr*-h1 may be such a gene. Although initially discovered in *Drosophila* as important for metamorphosis (Pecasse et al., 2000), Kr-h1 is present throughout the insects including the primitive firebrat, *Thermobia domestica* (Konopova et al., 2011), and is necessary to prevent precocious metamorphosis (Minakuchi et al., 2009; Lozano and Belles, 2011). Kr-h1 appears in the embryo at the time that JH appears and is present throughout larval life, then disappears during metamorphosis to the pupa (see review by Truman and Riddiford, 2019). The presence of JH ensures that Kr-h1 will appear when 20E rises for the larval molt and may stabilize Kr-h1 during the larval intermolt period. Kr-h1 disappears at the onset of metamorphosis only to reappear during the molt to the pupa when ecdysteroids again are acting in the presence of JH to prevent adult development of imaginal disc derivatives, the extent of which depends on the species studied. See, for example, the pupal-adult intermediate formed after allatectomy of the Cecropia prepupa (Williams, 1961) versus the normal pupa formed by allatectomized *Bombyx* or *Galleria* larvae (Bounhiol, 1938; Piepho, 1942). However, Kr-h1 does not appear to be a nymph- or larval-specifying factor since its suppression by RNAi in the embryo does not prevent the production of a nymph or larva (Smykal et al., 2014). Instead, the role of Kr-h1 is likely its repression of the expression of the adult-specifying E93 as is seen in both the hemimetabolous cockroach, *Blattella germanica* (Belles and Santos, 2014; Ureña et al., 2016) and the holometabolous *Drosophila* and flour beetle, *Tribolium castaneum* (Ureña et al., 2016). This role of Kr-h1 has been emphasized in naming the molecular pathway underlying the "*status quo*" action of JH in metamorphosis the Met-Kr-h1-E93 (MEKRE93) pathway (Belles and Santos, 2014).

JUVENILE HORMONE RECEPTOR

In 1967 when JH was identified as a sesquiterpenoid (Röller et al., 1967), hormones were thought to be only steroids, peptides or proteins with intracellular receptors for the steroids and membrane receptors for the peptides and proteins. The sesquiterpenoid nature of JH allows it to enter the cell (Mitsui et al., 1979) but also allows it to interact with the membrane (Davey, 1996, 2000; Wyatt and Davey, 1996; Goodman and Cusson, 2012). The search for these JH receptors turned out to be long and tortuous and is not over yet.

Intracellular Receptors

JP29

The "*status quo*" action of JH during larval life is assumed to be intracellular since it directs nuclear ecdysteroid action during the larval molts and must be absent for ecdysteroids to initiate metamorphosis. A JH binding protein (JHBP) was isolated from *Manduca* larval hemolymph that bound JH and protected it from the hemolymph esterases but not the JH-specific esterase that appeared once the larva attained the critical weight for metamorphosis (reviewed by Goodman and Cusson, 2012). JHBP is also thought to have other functions including presentation of JH to the cell (see review by Goodman and Cusson, 2012). However, studies *in vitro* showed that JH I alone was just as effective as the combination of JH I and JHBP in the culture

medium in preventing the 20E-induced pupal commitment of the *Manduca* abdominal epidermis (Riddiford, 1978).

The search for the intracellular JH receptor in *Manduca* utilized photoaffinity-labeled JHs and JH analogs (synthetic compounds that could be photo-cross-linked to cellular protein(s) to which they bound to allow the subsequent isolation of the protein) (Prestwich et al., 1994). This search yielded a 29 kDa nuclear protein (JP29) which at first was thought to be the JH receptor (Palli et al., 1994). Later studies by Charles et al. (1996) showed that the apparent tight, specific binding of JH I to JP29 was an artifact of a co-purifying esterase that removed the tritiated ester group of JH I used to monitor that binding. Moreover, JP29 was found to bind to the insecticyanin granules in the epidermis and to be regulated by 20E during a larval molt but not after pupal commitment (Shinoda et al., 1997). The role of JP29 in the epidermis is unknown.

USP

Ultraspiracle (USP) was shown to be the heterodimeric partner of the ecdysone receptor (EcR) necessary for the action of 20E in tissues, but 20E only bound specifically and tightly to EcR (see review by Riddiford et al., 2001). The *usp* null mutant in *Drosophila* initiates the molt normally at the end of the first instar and makes the second instar cuticle, but is unable to ecdyse (Oro et al., 1992). Rescue to the mid-third instar was afforded by one heat shock pulse of *usp* in the first instar (apparently due to the persistence of USP protein in the larva through the onset of the second instar molt) (Hall and Thummel, 1998). Thereafter, however, the larva entered a "stationary phase" instead of wandering at the expected time of the onset of metamorphosis. Twenty-four hours later, a new cuticle composed of both larval and pupal cuticle proteins covered the posterior region of the body, but the anterior region had only partially everted imaginal discs, and death ensued. Interestingly, the onset of glue protein synthesis in the salivary glands necessary for gluing the puparium to the substrate at the time of pupariation occurred normally at the mid-third instar transition but the glue was not secreted nor did the glands later die as normally occurs. Thus, it appears that USP is needed as a partner for EcR during the larval molts when the ecdysteroid titer is high but is not essential for low ecdysteroid action that causes glue protein synthesis. This latter action may be due to the ecdysteroid sitting on the EcR and causing derepression (Schubiger et al., 2005).

In 1997, Jones and Sharp (1997) found that recombinant *Drosophila* USP specifically bound JH III and JH III acid [the natural JH and its acid metabolite found in *Drosophila* third (final) larval instar hemolymph (Jones et al., 2013)] and suggested that it might be the JH receptor in the larva (Jones and Sharp, 1997; Jones et al., 2006). Unfortunately, the binding of JH III to USP showed about 100-fold lower affinity than one would expect for a hormone receptor. Later studies showed that the potential binding pocket of USP was filled by an unknown phospholipid under *in vivo* conditions (Billas et al., 2001; Sasorith et al., 2002). Also, a *Drosophila* USP-GFP reporter construct that was properly activated by 20E in explanted larval brains and salivary glands was not responsive to JH III alone nor to a combination of 20E and JH III (Beck et al., 2009). Only when the explants were pretreated with JH III before adding the 20E did JH III have an effect—that of reducing the activation produced by 20E. These and other studies (reviewed in Riddiford, 2008) strongly suggested that USP was not the JH receptor during larval life.

Instead USP may be the receptor for methyl farnesoate during the mid-third instar transition in *Drosophila* when methyl farnesoate is the predominant juvenoid in the hemolymph (Jones et al., 2013) and can be converted to JH bis-epoxide (Wen et al., 2015; see **Figure 5** for structures of methyl farnesoate and JH bis-epoxide). The Jones group found that USP bound methyl farnesoate with an affinity similar to that of the binding of the retinoid X receptor (RXR) to its ligand 9-*cis*-retinoic acid and that point mutations of USP in residues in the apparent ligand binding pocket decreased this binding 4–10-fold. The usp^2 null mutant could be rescued by USP through metamorphosis but not by the mutant USPs, which instead showed abnormal development at the time of wandering. Thus, the mutated USP apparently could not bind the circulating methyl farnesoate to allow normal metamorphic development although it did not interfere with the normal first and second instar molts. What exact role the methyl farnesoate-USP complex is playing at the onset of metamorphosis remains a mystery that needs exploring.

Methoprene-Tolerant (Met) Encodes the JH Receptor

In 1986, Tom Wilson took a different approach to look for the JH receptor. He mutagenized *Drosophila* with ethyl methanesulfonate, then reared the larvae on diet containing a high concentration of the JH analog methoprene (Wilson and Fabian, 1986; **Figure 6A**, top). Screening with methoprene or JH III that prevents metamorphosis of the abdomen (see above section for JH effects on *Drosophila*) yielded a mutant that was about 100-fold more resistant to JH than the parental wild-type, which they named *Methoprene-tolerant* (*Met*). Because increased levels of JH were needed in the *Met* mutant for both its metamorphic and reproductive effects, they suggested that the Met protein might be involved in JH reception.

This hypothesis was not confirmed until Konopova and Jindra (2007) showed that Met expression was necessary in the flour beetle, *T. castaneum*, to prevent premature metamorphosis. Suppression of Met expression by RNAi in third or fourth instar larvae yielded premature pupation after the fifth or sixth instar (of a total of 7 larval instars) (**Figure 6A**, bottom). A few of these survived to form miniature adults. Moreover, neither methoprene nor JH III application was effective to cause the formation of "second pupae" by *Tribolium* pupae that had been given Met RNAi. Thus, the loss of Met in *Tribolium* prevented the usual metamorphic responses to JH and therefore fit the criteria for a JH receptor.

As discussed above, the higher Diptera have an extreme form of metamorphosis whereby the larval body is discarded except for the nervous system and the Malpighian tubules; and the adult arises from imaginal cells and discs that have proliferated during larval life or in the case of the abdominal histoblasts during the prepupal period (Perez, 1910; Fristrom and Fristrom, 1993). In *Drosophila* larvae, JH is present and declines before metamorphosis (Bownes and Rembold, 1987; Sliter et al., 1987) but seems to have no role in larval life. Dietary JH caused only

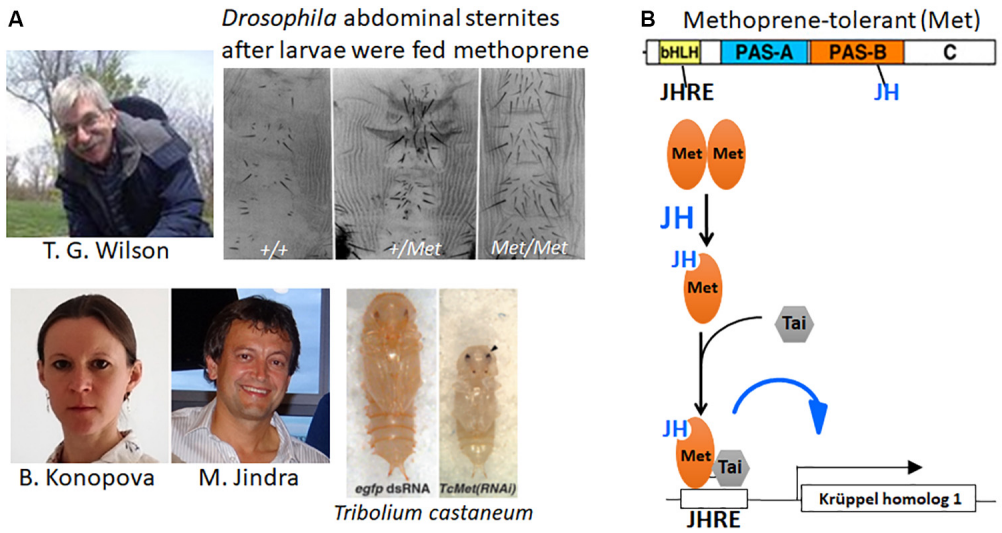

FIGURE 6 | (A) *Top:* (Left) Tom Wilson (photo was taken by Emily Wilson and used with her permission). The adult abdominal sternites of the *Methoprene-tolerant* (*Met*$^{+}$) mutant of *Drosophila melanogaster* after the larvae fed on diet containing methoprene (modified from Figure 2 of Wilson and Fabian, 1986). +/+, homozygous wild type; +/*Met*, heterozygous *Met* mutant; *Met*/*Met*, homozygous Met mutant. *Bottom*: Barbora Konopova and Marek Jindra and the precocious pupa they obtained after giving *Met* RNAi to a 4th instar larva of *Tribolium castaneum* (right) compared with a normal pupa that formed after *egfp* RNAi had been given to a 4th instar larva (left) (modified from Figure 3 in Konopova and Jindra, 2007). Photos of Barbora Konopova from her Research Gate file (used with her permission) and of Marek Jindra taken by Masako Asahina (used with Dr. Jindra's permission). **(B)** *Top*: Cartoon of the Met protein showing its various domains: bHLH, basic helix-loop-helix domain; the Period-Arylhydrocarbon receptor nucleotide translocator-Single-minded (PAS) A and B domains; the C terminal domain. The bHLH domain binds to the juvenile hormone (JH) response element (JHRE) on the target gene promoter; JH binds to the Pas B domains of Met (Charles et al., 2011) and Germ cell-expressed (Gce) [the paralog of Met (Baumann et al., 2010)] (Bittova et al., 2019). *Bottom*: Cartoon of events occurring when JH enters a target cell. The unliganded Met is thought to exist as a homodimer (Godlewski et al., 2006). When JH is present, it binds to Met causing the dissociation of the dimer and the binding of Taiman (Tai) to Met, then both Tai and Met bind to the JHRE on the promoters of Krüppel homolog 1 (Kr-h1) and other JH target genes (Jindra et al., 2015a).

a prolongation of the final larval instar followed by a normal appearing puparium that developed to the pharate adult but did not eclose (Bryant and Sang, 1968; Riddiford and Ashburner, 1991). These pharate adults had abdominal defects similar to those found when JH was applied at pupariation (Ashburner, 1970; Postlethwait, 1974) as well as nervous system defects (Restifo and Wilson, 1998; Riddiford et al., 2010, 2018). In contrast to other holometabolous insects, when *Drosophila* larvae were genetically allatectomized by overexpressing cell death genes in the corpora allata, the larvae formed normal puparia but died at or shortly after head eversion to the pupa (Liu et al., 2009; Riddiford et al., 2010). The discrepancy between the *Met* null mutant surviving to the adult and the death of the allatectomized pupa was found to be due to the existence of a second, closely related gene named *germ cell-expressed* (*gce*) (Baumann et al., 2010). *Met–gce* double mutants die at head eversion (Abdou et al., 2011) just as allatectomized prepupae do. *Met* and *gce* are paralogous genes with *gce* representing the ancestral gene (Baumann et al., 2010).

Methoprene-tolerant is a member of the basic-helix-loop-helix (bHLH)-Period (per)-Aryl hydrocarbon receptor nuclear translocator (Arnt)-Single-minded (sim) (PAS) domain family of transcription factors (**Figure 6B**). Charles et al. (2011) found that recombinant Met bound both methoprene and JH III with high affinity in the PAS-B domain. Subsequent studies have shown that the Met-JH complex heterodimerizes with a cofactor Taiman [also known as steroid response coactivator (SRC) and ßFtz-F1 Interacting Steroid Receptor Coactivator (FISC)] and forms a complex that binds to a JH-response element on the mosquito *early trypsin* gene (Li et al., 2011; Jindra et al., 2015a; Liu et al., 2018) and on the *Kr-h1* gene in *Tribolium* and *Blattella* (Zhang et al., 2011; Lozano et al., 2014). Both Met and Gce bind JH III and methyl farnesoate as well as the JH analogs methoprene and pyriproxyfen, and this binding is necessary for the induction of Kr-h1 in *Drosophila* larvae (Jindra et al., 2015b; Wen et al., 2015; Bittova et al., 2019).

Membrane Receptor

Based on studies with *Rhodnius* follicular cell epithelium (Davey and Huebner, 1974; Davey, 1996), Davey postulated that JH has a membrane receptor for its role in oocyte maturation–increasing the intercellular spaces so that vitellogenin can enter the oocyte. This receptor appeared to activate the sodium-potassium ATPase ("sodium pump") in the cells causing them to lose water and consequently shrink to create the intercellular spaces (termed "patency"). Abortive attempts were made to isolate this receptor (Davey, 1996). Recently, Jing et al. (2018) showed in the locust that JH causes the phosphorylation of the follicular cell Na-K-ATPase, thus activating it and causing increased patency.

Juvenile hormone activation of the *early trypsin* gene in the mosquito, *Aedes aegypti*, involves the activation of the phospholipase C pathway and the phosphorylation of both Met

and Tai which enhances the binding of Met–Tai intracellular dimer on the promoter of the *early trypsin* gene (Liu et al., 2015; Ojani et al., 2016). How this activation of the membrane phospholipids occurs is still unknown.

QUESTIONS FOR THE FUTURE

Why Is Not JH Required for the First Two Instars in Insects?

In his early experiments, Wigglesworth (1934) parabiosed a decapitated fed first instar nymph to a fed final instar nymph that had been decapitated after the critical period for the adult molt. The first instar nymph molted to a miniature adult with adult abdominal pigmentation and patterning, precocious genitalia and rudimentary wings. Similarly, Piepho (1938b) showed that an integumental (epidermis and overlying cuticle) implant from a first instar *Galleria* larva in a final instar larva formed both a pupal cuticle and an adult cuticle with scales when the host metamorphosed (**Figure 2**, bottom right). Thus, the cells of early instar animals are capable of forming adult structures when exposed to the proper hormonal environments. Yet under normal conditions in the presence of JH in the immature stages, they form nymphal (*Rhodnius*) or larval (*Galleria*) structures at the molt.

Recent studies have shown, however, that JH is not necessary for progress through the first and second instars after hatching (Daimon et al., 2012; see also reviews by Jindra, 2019; Truman and Riddiford, 2019; Bellés, 2020). Although the corpora allata begin secreting JH about two-thirds of the way through embryogenesis and continue at least to hatching, neither Met nor Kr-h1 is necessary for development of the first or second instar larvae or nymphs respectively of the silkworm *Bombyx* and the linden bug, *Pyrrhocoris* (Smykal et al., 2014; Daimon et al., 2015). Only in the third instar does one begin to see the effects of the absence of JH in terms of the precocious appearance of adult characters in *Pyrrhocoris* or of *broad* mRNA in *Bombyx*. In the latter without the JH receptor Met, most larvae die in the molt to the third instar with mosaic patches of larval and pupal cuticle (Daimon et al., 2015). To resolve this conundrum of the lack of a requirement for JH for the first two instars, Daimon et al. (2015) have proposed that for metamorphosis to occur requires the appearance of a "competence factor" which is necessary to induce *broad* expression. Once this factor appears, the presence of JH at the time of ecdysteroid rise for the molt is necessary to keep *broad* suppressed.

Besides its "*status quo*" action during ecdysteroid-induced molts, JH also is essential for maintaining proliferative growth and suppressing morphogenesis in imaginal cells and discs during the intermolt growth periods of Lepidoptera (Truman et al., 2006). Morphogenetic growth in preparation for metamorphosis normally begins in the final instar when the JH titer declines after the larva has attained the critical weight for metamorphosis (Zhou and Riddiford, 2001; MacWhinnie et al., 2005; Allee et al., 2006). At this time, *broad* mRNA appears in the imaginal cells followed sometime later by the onset of the morphogenetic proliferation. The onset of *broad* expression only requires sucrose feeding, but proliferation requires protein as well (MacWhinnie et al., 2005; Truman et al., 2006; Suzuki et al., 2013). The switch from proliferative growth in the early instars to morphogenetic growth in the final instar requires only the decline of JH and can occur in the absence of ecdysteroid (Truman et al., 2006). However, it requires the presence of a "metamorphosis initiation factor" which is dependent on nutrient input and may be similar to the "competence factor" seen in third instar *Bombyx* larvae (Daimon et al., 2015; Inui and Daimon, 2017). The nutrient input appears to trigger insulin signaling that is necessary for the wing discs to become competent to metamorphose (Koyama et al., 2008; Suzuki et al., 2013).

The requirement for either a nymph or a larva to undergo two feeding instars before metamorphosis holds throughout the insects (Truman, 2019; Truman and Riddiford, 2019). Once they enter the third feeding instar, JH is then necessary to prevent metamorphosis until a threshold size to form a viable adult is achieved. The identities of the "competence factor" for metamorphosis and the "metamorphosis initiation factor" and the necessary interactions between nutrition and hormones to achieve this threshold size are critical problems yet to be solved.

Why Do *Drosophila* Imaginal Discs and Histoblasts Differ in Their Response to JH?

In higher Diptera, metamorphosis entails the loss of all larval tissues except for the nervous system and the Malpighian tubules (Perez, 1910; Fristrom and Fristrom, 1993). As discussed above in the section on *Drosophila* development, the adult develops externally from the imaginal discs and the abdominal histoblasts and internally from imaginal cells associated with larval tissues. For the epidermis, only the abdominal histoblasts are sensitive to JH, and that sensitivity occurs during their proliferation during the prepupal period. The histoblasts contain both JH receptors, Met and Gce (Baumann et al., 2017). Normally they begin to express *broad* mRNA during the late third instar and continue to do so during their proliferation and spreading until about 24 h after pupariation (Zhou and Riddiford, 2002). Broad protein then disappears from these cells by 30 h after pupariation. When JH was applied at pupariation, Broad protein remained in the abdominal epidermis at least until 72 h after pupariation and these cells make pupal cuticle rather than adult cuticle (Zhou and Riddiford, 2002). Thus, JH seems to be most effective on adult abdominal differentiation when given during the time of histoblast proliferation, but why this is so remains mysterious.

Juvenile hormone has no effect on the metamorphosis of *Drosophila* imaginal discs, even when fed to larvae throughout larval life (Riddiford and Ashburner, 1991) or when given at the time of pupariation or early during the prepupal period (Ashburner, 1970; Postlethwait, 1974). The discs contain only one of the two JH receptors, Met, albeit at low levels; Gce has not been detected in any (Baumann et al., 2017). They however contain the necessary cofactor Taiman. Yet even

when *gce* or *gce* and *Met* were overexpressed in the larval wing disc, JH in the diet did not prevent the subsequent metamorphosis of the disc to a normal adult structure (Baumann et al., 2017). This result suggests that the lack of JH effects on imaginal discs is not due to the lack of JH receptors.

For imaginal disc structures, there are two critical periods of adult development: (1) about 30–36 h after pupariation, when morphogenesis of adult hairs and bristles occurs; and (2) about 48–52 h after pupariation just before adult cuticle is deposited (Fristrom and Fristrom, 1993). Timed overexpression of *broad* during these two periods was sufficient to cause the head and thoracic structures to form a "second pupa" (Zhou and Riddiford, 2002), indicating that these imaginal cells can make pupal cuticle. These experiments also suggested that Broad had to be present for pupal differentiation to occur. But why exogenous JH causes high re-expression of Broad in the developing adult abdominal epidermis and only traces of it in the developing adult head and thorax (Zhou and Riddiford, 2002) remains an enigma.

Importantly, when JH was applied at pupariation, Kr-h1 was expressed in the developing adult legs and eyes unlike its lack of expression at this time in control flies (Minakuchi et al., 2008). Thus, these discs can respond to the JH by maintaining Kr-h1 expression but they still undergo metamorphosis. Since they differentiated into normal adult structures, these discs presumably express E93. This presumed E93 expression is counter to the suppression of E93 by Kr-h1 as is normally seen in other species (Belles and Santos, 2014; Ureña et al., 2016). Further elucidation of the interaction of JH, Kr-h1, Broad, and E93 in different *Drosophila* tissues during development and metamorphosis is clearly needed.

How Is the Secretion of JH Regulated?

Over the years, we have learned much about how the synthesis and secretion of JH is regulated in both immature insects and adults by hormones (neuropeptides, ecdysteroids, and JH itself) and nutritional signals (see reviews by Stay and Tobe, 2007; Goodman and Cusson, 2012; Hiruma and Kaneko, 2013; Marchal et al., 2013; Noriega, 2014; Santos et al., 2019; Bendena et al., 2020). The mechanisms involved in this regulation such as the role of microRNAs are only beginning to be studied (Bendena et al., 2020). Particularly important is a deeper understanding of this regulation by environmental (both internal and external) signals in the role of JH in the control of polyphenisms ranging from pigmentary changes to organization of insect societies (Nijhout, 1995; Miura, 2019).

OTHER ROLES OF JH

Juvenile hormone has a myriad of actions in insects beyond its well-known effects on insect metamorphosis and reproduction. This diversity of action may stem at least partially from its uniqueness among animal hormones in terms of its chemical structure as a sesquiterpenoid and its receptor as a member of the bHLH family of transcription factors. The immediate precursor of JH, methyl farnesoate, is found in the Crustacea which are ancestral to the insects and is involved in reproductive maturation and possibly in early development (Nagaraju, 2011; Qu et al., 2018; Miyakawa et al., 2018). In the crustacean *Daphnia magna* where methyl farnesoate is necessary for environmental male sex determination (Olmstead and Leblanc, 2002; LeBlanc and Medlock, 2015; Toyota et al., 2015), the Met receptor for methyl farnesoate was found to differ in only one amino acid in its binding pocket from the insect *Tribolium* Met

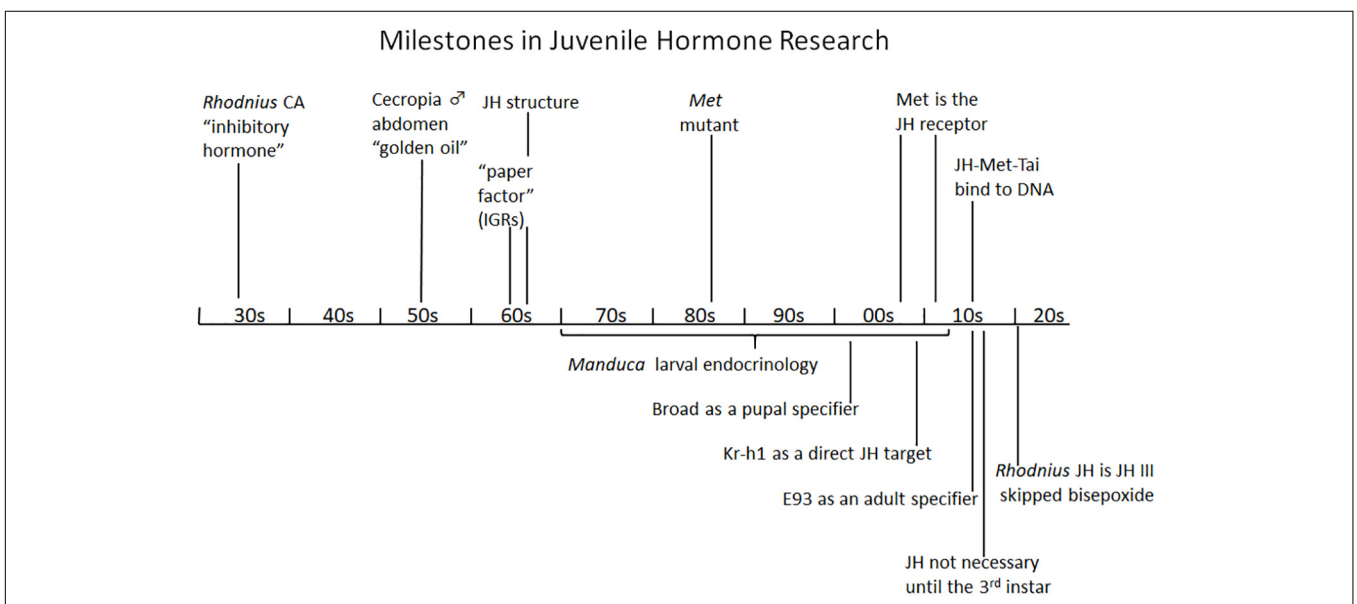

FIGURE 7 | Summary diagram of milestones in juvenile hormone research. See text for details. CA, corpus allatum; IGR, insect growth regulator; JH, juvenile hormone; Kr-h1, Krüppel homolog 1; Met, *Methoprene-tolerant*; Tai, Taiman.

(Miyakawa et al., 2013, 2018). This difference was found to favor the binding affinity for methyl farnesoate over JH III.

SUMMARY

Figure 7 shows the major milestones in the progress of research on JH from the time of its discovery by Wigglesworth in the 1930s to the present which have been detailed in this short review. This progress has been from the phenomenological to the underlying molecular basis of its action. The JH I and II of Cecropia were identified in 1967 and 1968, then the JH III of most other insects as well as JH 0 in Lepidoptera and JH III bis-epoxide in the higher Diptera were identified in the 1970s and 1980s, but it was not until 2020 that the JH of *Rhodnius* was shown to be JHSB3 (Villalobos-Sambucaro et al., 2020). Now that we have the receptors and know something about its downstream effectors, we should be able to delve further into the molecular modes of action of this unique hormone that controls so many aspects of the insect's life history.

AUTHOR CONTRIBUTIONS

LR was the sole author of this manuscript.

ACKNOWLEDGMENTS

I thank Dr. James Truman for the drawings in **Figures 1**, **2**, for helpful discussion during the writing of this manuscript, and critical comments on the article as a whole; Dr. Bronislaw Cymborowski for comments on Stefan Kopec; Drs. Xavier Belles and Judy Willis for critical comments on the final manuscript; and Dr. Belles for providing **Figure 5**.

REFERENCES

Abdou, M. A., Heb, Q., Wen, D., Zyaan, O., Wang, J., Xu, J., et al. (2011). *Drosophila* Met and Gce are partially redundant in transducing juvenile hormone action. *Insect Biochem. Mol. Biol.* 41, 938–945. doi: 10.1016/j.ibmb.2011.09.003

Agui, N., Granger, N. A., Gilbert, L. I., and Bollenbacher, W. E. (1979). Cellular localization of the insect prothoracicotropic hormone: *in vitro* assay of a single neurosecretory cell. *Proc. Natl. Acad. Sci. U.S.A.* 76, 5694–5698. doi: 10.1073/pnas.76.11.5694

Allee, J. P., Pelletier, C. L., Fergusson, E. K., and Champlin, D. T. (2006). Early events in adult eye development of the moth, *Manduca sexta*. *J. Insect Physiol* 52, 450–460. doi: 10.1016/j.jinsphys.2005.12.006

Aminoff, M. J. (2017). The life and legacy of Brown-Séquard. *Brain* 140, 1525–1532.

Ashburner, M. (1970). Effects of juvenile hormone on adult differentiation of *Drosophila melanogaster*. *Nature* 227, 187–189. doi: 10.1038/227187a0

Ashburner, M., Chihara, C., Meltzer, P., and Richards, G. (1974). Temporal control of puffing activity in polytene chromosomes. *Cold Spring Harb. Symp. Quant. Biol.* 38, 655–662. doi: 10.1101/sqb.1974.038.01.070

Baumann, A., Fujiwara, Y., and Wilson, T. G. (2010). Evolutionary divergence of the paralogs *Methoprene tolerant* (*Met*) and *germ cell expressed* (*gce)* within the genus *Drosophila*. *J. Insect Physiol.* 56, 1445–1455. doi: 10.1016/j.jinsphys.2010.05.001

Baumann, A. A., Texada, M. J., Chen, H. M., Etheredge, J. N., Miller, D. L., Picard, S., et al. (2017). Genetic tools to study juvenile hormone action in *Drosophila*. *Sci. Rep.* 7:2132. doi: 10.1038/s41598-017-02264-4

Beck, Y., Delaporte, C., Moras, D., Richards, G., and Billas, I. M. (2009). The ligand-binding domains of the three RXR-USP nuclear receptor types support distinct tissue and ligand specific hormonal responses in transgenic *Drosophila*. *Dev. Biol.* 330, 1–11. doi: 10.1016/j.ydbio.2008.12.042

Bell, R. A., and Joachim, F. G. (1976). Techniques for rearing laboratory colonies of tobacco hornworms and pink bollworms. *Ann. Entomol. Soc. Am.* 69, 365–373. doi: 10.1093/aesa/69.2.365

Bellés, X. (2020). *Insect Metamorphosis: From Natural History to Regulation of Development and Evolution*. New York, NY: Academic Press.

Belles, X., and Santos, C. G. (2014). The MEKRE93 (Methoprene tolerant-Krüppel homolog 1-E93) pathway in the regulation of insect metamorphosis, and the homology of the pupal stage. *Insect Biochem. Mol. Biol.* 52, 60–68. doi: 10.1016/j.ibmb.2014.06.009

Bendena, W. G., Hui, J. H. L., Sang, I. C.-S., and Tobe, S. S. (2020). Neuropeptide and microRNA regulators of juvenile hormone production. *Gen. Comp. Endocrinol.* 295:113507. doi: 10.1016/j.ygcen.2020.113507

Bergot, B. J., Jamieson, G. C., Ratcliff, M. A., and Schooley, D. A. (1980). JH Zero: new naturally occurring insect juvenile hormone from developing embryos of the tobacco hornworm. *Science* 210, 336–338. doi: 10.1126/science.210.4467.336

Bhaskaran, G., Dahm, K. H., Barrera, P., Pacheco, J. L., Peck, K. E., and Muszynska-Pytel, M. (1990). Allatinhibin, a neurohormonal inhibitor of juvenile hormone biosynthesis in *Manduca sexta*. *Gen. Comp. Endocrinol.* 78, 123–136. doi: 10.1016/0016-6480(90)90053-o

Bhaskaran, G., Jones, G., and Jones, D. (1980). Neuroendocrine regulation of corpus allatum activity in *Manduca sexta*: sequential neurohormonal and nervous inhibition in the last-instar larva. *Proc. Natl. Acad. Sci. U.S.A.* 77, 4407–4411. doi: 10.1073/pnas.77.8.4407

Billas, I. M., Moulinier, L., Rochel, N., and Moras, D. (2001). Crystal structure of the ligand-binding domain of the ultraspiracle protein USP, the ortholog of retinoid X receptors in insects. *J. Biol. Chem.* 276, 7465–7474. doi: 10.1074/jbc.m008926200

Bittova, L., Jedlicka, P., Dracinsky, M., Kirubakaran, P., Vondrasek, J., Hanus, R., et al. (2019). Exquisite ligand stereoselectivity of a *Drosophila* juvenile hormone receptor contrasts with its broad agonist repertoire. *J. Biol. Chem.* 294, 410–423. doi: 10.1074/jbc.ra118.005992

Bollenbacher, W. E., Smith, S. L., Goodman, W., and Gilbert, L. I. (1981). Ecdysteroid titer during larval-pupal-adult development of the tobacco hornworm, *Manduca sexta*. *Gen. Compar. Endocrinol.* 44, 302–306. doi: 10.1016/0016-6480(81)90005-8

Bounhiol, J.-J. (1938). Recherches expérimentales sur le déterminisme de la métamorphose chez les Lépidopterès. *Bull. Biol. Fr. Belg. Suppl.* 24, 1–199.

Bounhiol, J. J. (1939). Recentes recherches experimentales sur les insects. Les fonctions des corps allates *(corpora allata)*. *Arch. Zool. Exper. Gen.* 81, 54–63.

Bounhiol, J.-J. (1945). Destin independent lors de la nymphose des trois parties formées dans un ver a soie par deux ligatures plus ou moins espacées. *C. R. Acad. Ser. Soc. Biol. Bordeaux* 139, 842–844.

Bowers, W. S., Fales, H. M., Thompson, M. J., and Uebel, E. C. (1966). Juvenile hormone: identification of an active compound from balsam fir. *Science* 154, 1020–1021. doi: 10.1126/science.154.3752.1020

Bownes, M., and Rembold, H. (1987). The titre of juvenile hormone during the pupal and adult stages of the life cycle of *Drosophila melanogaster*. *Eur. J. Biochem.* 164, 709–712. doi: 10.1111/j.1432-1033.1987.tb11184.x

Brown-Séquard, D. R. (1889). Note on the effects produced on man by subcutaneous injections of a liquid obtained from the testicles of animals. *Lancet* 134, 105–107. doi: 10.1016/s0140-6736(00)64118-1

Bryant, P. J., and Sang, J. H. (1968). *Drosophila*: lethal derangements of metamorphosis and modifications of gene expression caused by juvenile hormone mimics. *Nature* 220, 393–394. doi: 10.1038/220393a0

Caveney, S., and Podgorski, C. (1975). Intercellular communication in a positional field. Ultrastructural correlates and tracer analysis of communication between

insect epidermal cells. *Tissue Cell* 7, 559–574. doi: 10.1016/0040-8166(75)90026-9

Charles, J. P., Iwema, T., Epa, V. C., Takaki, K., Rynes, J., and Jindra, M. (2011). Ligand-binding properties of a juvenile hormone receptor, Methoprene-tolerant. *Proc. Natl. Acad. Sci. U.S.A.* 108, 21128–21133. doi: 10.1073/pnas.1116123109

Charles, J.-P., Wojtasek, H., Lentz, A. J., Thomas, B. A., Bonning, B. C., Palli, S. R., et al. (1996). Purification and reassessment of ligand binding by the recombinant, putative juvenile hormone receptor of the tobacco hornworm, *Manduca sexta*. *Arch. Insect Biochem. Physiol.* 31, 371–393. doi: 10.1002/(sici)1520-6327(1996)31:4<371::aid-arch2>3.0.co;2-z

Cymborowski, B. (1981). "Stefan Kopeć," in *Proceedings of the Part 1 International Conference Regulation of Insect Development and Behaviour*, eds F. Sehnal, A. Zabza, J. J. Menn, and B. Cymborowski (Wrocław: Wrocław Technical University Press), I–II.

Daimon, T., Kozaki, T., Niwa, R., Kobayashi, I., Furuta, K., Namiki, T., et al. (2012). Precocious metamorphosis in the juvenile hormone-deficient mutant of the silkworm, *Bombyx mori*. *PLoS Genet.* 8:e1002486. doi: 10.1371/journal.pgen.1002486

Daimon, T., Uchibori, M., Nakao, H., Sezutsu, H., and Shinoda, T. (2015). Knockout silkworms reveal a dispensable role for juvenile hormones in holometabolous life cycle. *Proc. Natl. Acad. Sci. U.S.A.* 112, E4226–E4235. doi: 10.1073/pnas.1506645112

Davey, K. G. (1996). Hormonal control of the follicular epithelium during vitellogenin uptake. *Invert. Reprod. Dev.* 30, 249–254. doi: 10.1080/07924259.1996.9672551

Davey, K. G. (2000). The modes of action of juvenile hormones: some questions we ought to ask. *Insect Biochem. Mol. Biol.* 30, 663–669. doi: 10.1016/s0965-1748(00)00037-0

Davey, K. G., and Huebner, E. (1974). The response of the follicle cells of *Rhodnius prolixus* to juvenile hormone and antigonadotropin *in vitro*. *Can. J. Zool.* 52, 1407–1412. doi: 10.1139/z74-178

Dominick, O. S., and Truman, J. W. (1985). The physiology of wandering behavior in *Manduca sexta*. II. The endocrine control of wandering behavior. *J. Exp. Biol.* 117, 45–68.

Fain, M. J., and Riddiford, L. M. (1975). Juvenile hormone titers in the hemolymph during late larval development of the tobacco hornworm, *Manduca sexta* (L.). *Biol. Bull.* 149, 506–521. doi: 10.2307/1540383

Fain, M. J., and Riddiford, L. M. (1976). Reassessment of the critical periods for prothoracicotropic hormone and juvenile hormone secretion in the tobacco hornworm, *Manduca sexta*. *Gen. Comp. Endocrinol.* 30, 131–141. doi: 10.1016/0016-6480(76)90092-7

Fristrom, D., and Fristrom, J. W. (1993). "The metamorphic development of the adult epidermis," in *The Development of Drosophila melanogaster*, Vol. II, eds M. Bate and A. Martinez-Arias (Plainview, NY: Cold Spring Harbor Laboratory Press), 843–897.

Fukuda, S. (1940a). Induction of pupation in silkworm by transplanting the prothoracic gland. *Proc. Imp. Acad. Japan* 16, 414–416. doi: 10.2183/pjab1912.16.414

Fukuda, S. (1940b). Hormonal control of molting and pupation in the silkworm. *Proc. Imp. Acad. Japan* 16, 417–420. doi: 10.2183/pjab1912.16.417

Fukuda, S. (1944). The hormonal mechanism of larval molting and metamorphosis in the silkworm. *J. Fac. Sci. Tokyo Univ. Sec. IV* 6, 477–532.

Gibbs, D., and Riddiford, L. M. (1977). Prothoracicotropic hormone in *Manduca sexta*: localization by a larval assay. *J. Exp. Biol.* 66, 255–266.

Gilbert, L. I., Rybczynski, R., Song, Q., Mizoguchi, A., Morreale, R., Smith, W. A., et al. (2000). Dynamic regulation of prothoracic gland ecdysteroidogenesis: *Manduca sexta* recombinant prothoracicotropic hormone and brain extracts have identical effects. *Insect Biochem. Mol. Biol.* 30, 1079–1089. doi: 10.1016/s0965-1748(00)00083-7

Gilbert, L. I., Rybczynski, R., and Warren, J. T. (2002). Control and biochemical nature of the ecdysteroidogenic pathway. *Annu. Rev. Entomol.* 47, 883–916. doi: 10.1146/annurev.ento.47.091201.145302

Godlewski, J., Wang, S., and Wilson, T. G. (2006). Interaction of bHLH-PAS proteins involved in juvenile hormone reception in *Drosophila*. *Biochem. Biophys. Res. Commun.* 342, 1305–1311. doi: 10.1016/j.bbrc.2006.02.097

Goodman, W. G., and Cusson, M. (2012). "The juvenile hormones," in *Insect Endocrinology*, ed. L. I. Gilbert (Amsterdam: Elsevier), 310–365.

Goodman, W. G., and Granger, N. A. (2005). "The juvenile hormones," in *Comprehensive Molecular Insect Science*, eds L. I. Gilbert, K. Iatrou, and S. S. Gill (Amsterdam: Elsevier), 319–408.

Gudernatsch, J. F. (1912). Feeding experiments on tadpoles. I. The influence of specific organs given as food on growth and differentiation. A contribution to the knowledge of organs with internal secretion. *Wilhelm Roux Arch. Entwickl. Mech. Org.* 35, 457–483. doi: 10.1007/bf02277051

Hall, B. L., and Thummel, C. S. (1998). The RXR homolog ultraspiracle is an essential component of the *Drosophila* ecdysone receptor. *Development* 125, 4709–4717.

Handler, A. M. (1982). Ecdysteroid titers during pupal and adult development in *Drosophila melanogaster*. *Dev. Biol.* 93, 73–82. doi: 10.1016/0012-1606(82)90240-8

Hintze-Podufal, C. (1996). In Memoriam. Hans Piepho, 1909–1993. *Entomol. Gener.* 20, 221–223.

Hiruma, K., and Kaneko, Y. (2013). Hormonal regulation of insect metamorphosis with special reference to juvenile hormone biosynthesis. *Curr. Top. Dev. Biol.* 103, 73–100. doi: 10.1016/b978-0-12-385979-2.00003-4

Hiruma, K., and Riddiford, L. M. (2010). Developmental expression of mRNAs for epidermal and fat body proteins and hormonally regulated transcription factors in the tobacco hornworm. *Manduca sexta*. *J. Insect Physiol.* 56, 1390–1395. doi: 10.1016/j.jinsphys.2010.03.029

Inui, T., and Daimon, T. (2017). Implantation assays using the integument of early stage *Bombyx* larvae: insights into the mechanisms underlying the acquisition of competence for metamorphosis. *J. Insect Physiol.* 100, 35–42. doi: 10.1016/j.jinsphys.2017.05.002

Jindra, M. (2019). Where did the pupa come from? The timing of juvenile hormone signalling supports homology between stages of hemimetabolous and holometabolous insects. *Philos. Trans. R. Soc. Lond. B Biol. Sci.* 374, 20190064. doi: 10.1098/rstb.2019.0064

Jindra, M., Bellés, X., and Shinoda, T. (2015a). Molecular basis of juvenile hormone signaling. *Curr. Opin. Insect Sci.* 11, 39–46. doi: 10.1016/j.cois.2015.08.004

Jindra, M., Uhlirova, M., Charles, J.-P., Smykal, V., and Hill, R. J. (2015b). Genetic evidence for function of the bHLH-PAS protein Gce/Met as a juvenile hormone receptor. *PLoS Genet.* 11:e1005394. doi: 10.1371/journal.pgen.1005394

Jing, Y. P., An, H., Zhang, S., Wang, N., and Zhou, S. (2018). Protein kinase C mediates juvenile hormone-dependent phosphorylation of Na^+/K^+-ATPase to induce ovarian follicular patency for yolk protein uptake. *J. Biol. Chem.* 293, 20112–20122. doi: 10.1074/jbc.ra118.005692

Jones, D., Jones, G., and Teal, P. E. (2013). Sesquiterpene action, and morphogenetic signaling through the ortholog of retinoid X receptor, in higher Diptera. *Gen. Comp. Endocrinol.* 194, 326–335.

Jones, G., Jones, D., Teal, P., Sapa, A., and Wozniak, M. (2006). The retinoid-X receptor ortholog, ultraspiracle, binds with nanomolar affinity to an endogenous morphogenetic ligand. *FEBS J.* 273, 4983–4996. doi: 10.1111/j.1742-4658.2006.05498.x

Jones, G., and Sharp, P. A. (1997). Ultraspiracle: an invertebrate nuclear receptor for juvenile hormones. *Proc. Natl. Acad. Sci. U.S.A.* 94, 13499–13503. doi: 10.1073/pnas.94.25.13499

Judy, K. J., Schooley, D. A., Dunham, L. L., Hall, M. S., Bergot, J., and Siddall, J. B. (1973). Isolation, structure, and absolute configuration of a new natural juvenile hormone from *Manduca sexta*. *Proc. Natl. Acad. Sci. U.S.A.* 70, 1509–1513. doi: 10.1073/pnas.70.5.1509

Kataoka, H., Toschi, A., Li, J. P., Carney, R. L., Schooley, D. A., and Kramer, S. J. (1989). Identification of an allatotropin from adult *Manduca sexta*. *Science* 243, 1481–1483. doi: 10.1126/science.243.4897.1481

Knight, K. (2014). *Rhodnius* respiration depends on multiple factors. *J. Exp. Biol.* 217:2622. doi: 10.1242/jeb.111104

Konopova, B., and Jindra, M. (2007). Juvenile hormone resistance gene *Methoprene-tolerant* controls entry into metamorphosis in the beetle *Tribolium castaneum*. *Proc. Natl. Acad. Sci. U.S.A.* 104, 10488–10493. doi: 10.1073/pnas.0703719104

Konopova, B., Smykal, V., and Jindra, M. (2011). Common and distinct roles of juvenile hormone signaling genes in metamorphosis of holometabolous and hemimetabolous insects. *PLoS One* 6:e28728. doi: 10.1371/journal.pone.0028728

Kopeć, S. (1917). Experiments on metamorphosis of insects. *Bull. Int. Acad. Sci. Cracovie (B)* 57–60.

Kopeć, S. (1922). Studies on the necessity of the brain for the inception of insect metamorphosis. *Biol. Bull.* 42, 323–342. doi: 10.2307/1536759

Kotaki, T., Shinada, T., Kaihara, K., Ohfune, Y., and Numata, H. (2009). Structure determination of a new juvenile hormone from a heteropteran insect. *Org. Lett.* 11, 5234–5237. doi: 10.1021/ol902161x

Koyama, T., Syropyatova, M. O., and Riddiford, L. M. (2008). Insulin/IGF signaling regulates the change in commitment in imaginal discs and primordia by overriding the effect of juvenile hormone. *Dev. Biol.* 324, 258–265. doi: 10.1016/j.ydbio.2008.09.017

Krogh, A. (1929). The progress of physiology. *Science* 70, 200–204.

Kühn, A., and Piepho, H. (1940). Über die ausbildung der schuppen in hauttransplantaten von schmetterlingen. *Biol. Zbl.* 60, 1–22.

Lamy, M., and Delsol, M. (1980). Jean-Jacques bounhiol, 1905-1979. *Ann. Endocrinol.* 41, 153–156.

Lawrence, P. A. (1969). Cellular differentiation and pattern formation during metamorphosis of the milkweed bug *Oncopeltus*. *Dev. Biol.* 19, 12–40. doi: 10.1016/0012-1606(69)90068-2

LeBlanc, G. A., and Medlock, E. K. (2015). Males on demand: the environmental-neuro-endocrine control of male sex determination in daphnids. *FEBS J.* 282, 4080–4093. doi: 10.1111/febs.13393

Lee, H. T.-Y. (1948). A comparative morphological study of the prothoracic glandular bands of some lepidopterous larvae with special reference to their innervation. *Ann. Ent. Soc. Amer.* 41, 200–205. doi: 10.1093/aesa/41.2.200

Li, M., Mead, E. A., and Zhu, J. (2011). Heterodimer of two bHLH-PAS proteins mediates juvenile hormone-induced gene expression. *Proc. Natl. Acad. Sci. U.S.A.* 108, 638–643. doi: 10.1073/pnas.1013914108

Liu, P., Fu, X., and Zhu, J. (2018). Juvenile hormone-regulated alternative splicing of the *taiman* gene primes the ecdysteroid response in adult mosquitoes. *Proc. Natl. Acad. Sci. U.S.A.* 115, E7738–E7747. doi: 10.1073/pnas.1808146115

Liu, P., Peng, H. J., and Zhu, J. (2015). Juvenile hormone-activated phospholipase C pathway enhances transcriptional activation by the Methoprene-tolerant protein. *Proc. Natl. Acad. Sci. U.S.A.* 112, E1871–E1879. doi: 10.1073/pnas.1423204112

Liu, Y., Sheng, Z., Liu, H., Wen, D., He, Q., Wang, S., et al. (2009). Juvenile hormone counteracts the bHLH-PAS transcription factors MET and GCE to prevent caspase-dependent programmed cell death in *Drosophila*. *Development* 136, 2015–2025. doi: 10.1242/dev.033712

Lozano, J., and Belles, X. (2011). Conserved repressive function of Krüppel homolog 1 on insect metamorphosis in hemimetabolous and holometabolous species. *Sci. Rep.* 1:163. doi: 10.1038/srep00163

Lozano, J., Kayukawa, T., Shinoda, T., and Belles, X. (2014). A role for Taiman in insect metamorphosis. *PLoS Genet.* 10:e1004769. doi: 10.1371/journal.pgen.1004769

Lyonet, P. (1762). *Traite Anatomique de la Chenille, qui Ronge le Bois de Saule*. Cambridge: viaLibri Limited.

MacWhinnie, S. G. B., Allee, J. P., Nelson, C. A., Riddiford, L. M., Truman, J. W., and Champlin, D. T. (2005). The role of nutrition in creation of the eye imaginal disc and initiation of metamorphosis in *Manduca sexta*. *Dev. Biol.* 285, 285–297. doi: 10.1016/j.ydbio.2005.06.021

Marchal, E., Hult, E. F., Huang, J., Stay, B., and Tobe, S. S. (2013). *Diploptera punctata* as a model for studying the endocrinology of arthropod reproduction and development. *Gen. Comp. Endocrinol.* 188, 85–93. doi: 10.1016/j.ygcen.2013.04.018

Meyer, A. S., Schneiderman, H. A., Hanzmann, E., and Ko, J. H. (1968). The two juvenile hormones from the cecropia silk moth. *Proc. Natl. Acad. Sci. U.S.A.* 60, 853–860. doi: 10.1073/pnas.60.3.853

Minakuchi, C., Namiki, T., and Shinoda, T. (2009). Krüppel homolog 1, an early juvenile hormone-response gene downstream of *Methoprene-tolerant*, mediates its anti-metamorphic action in the red flour beetle *Tribolium castaneum*. *Dev. Biol.* 325, 341–350. doi: 10.1016/j.ydbio.2008.10.016

Minakuchi, C., Zhou, X., and Riddiford, L. M. (2008). Krüppel homolog 1 (Kr-h1) mediates juvenile hormone action during metamorphosis of *Drosophila melanogaster*. *Mech. Dev.* 125, 91–105. doi: 10.1016/j.mod.2007.10.002

Mitsui, T., and Riddiford, L. M. (1976). Pupal cuticle formation by *Manduca sexta* epidermis *in vitro*: patterns of ecdysone sensitivity. *Dev. Biol.* 54, 172–186. doi: 10.1016/0012-1606(76)90297-9

Mitsui, T., and Riddiford, L. M. (1978). Hormonal requirements for the larval-pupal transformation of the epidermis of *Manduca sexta in vitro*. *Dev. Biol.* 62, 193–205. doi: 10.1016/0012-1606(78)90101-x

Mitsui, T., Riddiford, L. M., and Bellamy, G. (1979). Metabolism of juvenile hormone by the epidermis of the tobacco hornworm, *Manduca sexta*. *Insect Biochem.* 9, 637–643. doi: 10.1016/0020-1790(79)90103-3

Miura, T. (2019). Juvenile hormone as a physiological regulator mediating phenotypic plasticity in pancrustaceans. *Dev. Growth Diff.* 61, 85–96. doi: 10.1111/dgd.12572

Miyakawa, H., Sato, T., Song, Y., Tollefsen, K. E., and Iguchi, T. (2018). Ecdysteroid and juvenile hormone biosynthesis, receptors and their signaling in the freshwater microcrustacean Daphnia. *J. Steroid Biochem. Mol. Biol.* 184, 62–68. doi: 10.1016/j.jsbmb.2017.12.006

Miyakawa, H., Toyota, K., Hirakawa, I., Ogino, Y., Miyagawa, S., Oda, S., et al. (2013). A mutation in the receptor Methoprene-tolerant alters juvenile hormone response in insects and crustaceans. *Nat. Comm.* 4:1856. doi: 10.1038/ncomms2868

Nabert, A. (1912). Die Corpora allata der Insekten. *Zeitschr. Wiss. Zool.* 104, 181–358.

Nagaraju, G. P. (2011). Reproductive regulators in decapod crustaceans: an overview. *J. Exp. Biol.* 214, 3–16. doi: 10.1242/jeb.047183

Nijhout, H. F. (1975a). A threshold size for metamorphosis in the tobacco hornworm, *Manduca sexta* (L.). *Biol. Bull.* 149, 214–225. doi: 10.2307/1540491

Nijhout, H. F. (1975b). Dynamics of juvenile hormone action in larvae of the tobacco hornworm, *Manduca sexta* (L.). *Biol. Bull.* 149, 568–579. doi: 10.2307/1540387

Nijhout, H. F. (1995). *Insect Hormones*. Princeton, NJ: Princeton University Press.

Nijhout, H. F., Riddiford, L. M., Mirth, C., Shingleton, A. W., Suzuki, Y., and Callier, V. (2014). The developmental control of size in insects. *Wiley Interdiscip. Rev. Dev. Biol.* 3, 113–134. doi: 10.1002/wdev.124

Nijhout, H. F., and Williams, C. M. (1974a). Control of moulting and metamorphosis in the tobacco hornworm, *Manduca sexta* (L.): growth of the last-instar larva and the decision to pupate. *J. Exp. Biol.* 61, 481–491.

Nijhout, H. F., and Williams, C. M. (1974b). Control of moulting and metamorphosis in the tobacco hornworm, *Manduca sexta* (L.): cessation of juvenile hormone secretion as a trigger for pupation. *J. Exp. Biol.* 61, 493–501.

Ninov, N., Chiarelli, D. A., and Martín-Blanco, E. (2007). Extrinsic and intrinsic mechanisms directing epithelial cell sheet replacement during *Drosophila* metamorphosis. *Development* 134, 367–379. doi: 10.1242/dev.02728

Ninov, N., Manjón, C., and Martín-Blanco, E. (2009). Dynamic control of cell cycle and growth coupling by ecdysone, EGFR, and PI3K signaling in *Drosophila* histoblasts. *PLoS Biol.* 7:e1000079. doi: 10.1371/journal.pbio.1000079

Noriega, F. G. (2014). Juvenile hormone biosynthesis in insects: what is new, what do we know, and what questions remain? *Int. Sch. Res. Notices* 2014:967361. doi: 10.1155/2014/967361

Ojani, R., Liu, P., Fu, X., and Zhu, J. (2016). Protein kinase C modulates transcriptional activation by the juvenile hormone receptor Methoprene-tolerant. *Insect Biochem. Mol. Biol.* 70, 44–52. doi: 10.1016/j.ibmb.2015.12.001

Olmstead, A. W., and Leblanc, G. A. (2002). Juvenoid hormone methyl farnesoate is a sex determinant in the crustacean *Daphnia magna*. *J. Exp. Zool.* 293, 736–739. doi: 10.1002/jez.10162

Oro, A. E., McKeown, M., and Evans, R. M. (1992). The *Drosophila* retinoid X receptor homolog ultraspiracle functions in both female reproduction and eye morphogenesis. *Development* 115, 449–462.

Palli, S. R., Touhara, K., Charles, J.-P., Bonning, B. C., Atkinson, J. K., Trowell, S. C., et al. (1994). A nuclear juvenile hormone-binding protein from larvae of *Manduca sexta*: a putative receptor for the metamorphic action of juvenile hormone. *Proc. Natl. Acad. Sci. U.S.A.* 91, 6191–6195. doi: 10.1073/pnas.91.13.6191

Parthasarathy, R., Farkas, R., and Palli, S. R. (2012). Recent progress in juvenile hormone analogs (JHA) research. *Adv. Insect Physiol.* 43, 353–436. doi: 10.1016/b978-0-12-391500-9.00005-x

Pecasse, F., Beck, Y., Ruiz, C., and Richards, G. (2000). Kruüppel-homolog, a stage-specific modulator of the prepupal ecdysone response, is essential for *Drosophila* metamorphosis. *Dev. Biol.* 221, 53–67. doi: 10.1006/dbio.2000.9687

Perez, C. (1910). Recherches histologiques sur la metamorphose des Muscides *Calliphora erythrocephalea* Mg. *Arch. Zool. Exp. Gen.* 4, 1–274, 1–XVI.

Peter, M. G., Shirk, P. D., Dahm, K. H., and Röller, H. (1981). On the specificity of juvenile hormone biosynthesis in the male *Cecropia* moth. *Z. Naturforsch.* 36c, 579–585. doi: 10.1515/znc-1981-7-812

Pfeiffer, I. W. (1939). Experimental study of the function of the corpora allata in the grasshopper, *Melanoplus differentialis*. *J. Exp. Zool.* 82, 439–461. doi: 10.1002/jez.1400820307

Pflugfelder, O. (1937). Bau, entwicklung und funktion der Corpora allata und cardiaca von *Dixippus morosus*. *Br. Z. Wiss. Zool.* 149, 477–512.

Phillips, K. (2004). Happy anniversary JEB! *J. Exp. Biol.* 207, 1–3. doi: 10.1242/jeb.00776

Piepho, H. (1938a). Wachstum und totale metamorphose an hautimplantaten bei der wachsmotte *Galleria mellonella*. L. *Biol Zbl.* 58, 356–366.

Piepho, H. (1938b). Über die experimentelle ausl?sbarkeit überzähliger häutungen und vorzeitiger verpuppung an hautstücken bei kleinschmetterlingen. *Naturwissenschaften* 52, 141–142. doi: 10.1007/bf00631948

Piepho, H. (1942). Untersuchungen zur entwicklungsphysiologie der insektenmetamorphose : über die puppenhäutung der wachsmotte *Galleria mellonella* L. *Wilhelm Roux Arch. EntwMech. Org.* 141, 500–583. doi: 10.1007/bf00596490

Postlethwait, J. H. (1974). Juvenile hormone and the adult development of *Drosophila*. *Biol. Bull.* 147, 119–135. doi: 10.2307/1540573

Prestwich, G. D., Touhara, K., Riddiford, L. M., and Hammock, B. D. (1994). Larva lights: a decade of photoaffinity labeling with juvenile hormone analogues. *Insect Biochem. Mol. Biol.* 24, 747–761. doi: 10.1016/0965-1748(94)90104-x

Qu, Z., Bendena, W. G., Tobe, S. S., and Hui, J. (2018). Juvenile hormone and sesquiterpenoids in arthropods: biosynthesis, signaling, and role of MicroRNA. *J. Steroid Biochem. Mol. Biol.* 184, 69–76. doi: 10.1016/j.jsbmb.2018.01.013

Radtke, A. (1942). Hemmung der verpuppung beim mehlkäfer *Tenebroadio molitor L. Naturwissenschafen* 29, 451–453, 469.

Raikhel, A. S., Brown, M. R., and Belles, X. (2005). "Hormonal control of reproductive processes," in *Comprehensive Molecular Insect Science*, Vol. 3, eds L. I. Gilbert, K. Iatrou, and S. S. Gill (Amsterdam: Elsevier), 433–491. doi: 10.1016/b0-44-451924-6/00040-5

Restifo, L. L., and Wilson, T. G. (1998). A juvenile hormone agonist reveals distinct developmental pathways mediated by ecdysone-inducible Broad-complex transcription factors. *Dev. Genet.* 22, 141–159. doi: 10.1002/(sici)1520-6408(1998)22:2<141::aid-dvg4>3.0.co;2-6

Richard, D. S., Applebaum, S. W., and Gilbert, L. I. (1989). Developmental regulation of juvenile hormone biosynthesis by the ring gland of *Drosophila melanogaster*. *J. Comp. Physiol. B. Biochem. System. Environ. Physiol.* 159, 383–387. doi: 10.1007/bf00692410

Riddiford, L. M. (1976). Hormonal control of insect epidermal cell commitment *in vitro*. *Nature* 259, 115–117. doi: 10.1038/259115a0

Riddiford, L. M. (1978). Ecdysone-induced change in cellular commitment of the epidermis of the tobacco hornworm, *Manduca sexta*, at the initiation of metamorphosis. *Gen. Comp. Endocrinol.* 34, 438–446. doi: 10.1016/0016-6480(78)90284-8

Riddiford, L. M. (2008). Juvenile hormone action: a 2007 perspective. *J. Insect Physiol.* 54, 895–901. doi: 10.1016/j.jinsphys.2008.01.014

Riddiford, L. M., and Ashburner, M. (1991). Effects of juvenile hormone mimics on larval development and metamorphosis of *Drosophila melanogaster*. *Gen. Comp. Endocrinol.* 82, 172–183. doi: 10.1016/0016-6480(91)90181-5

Riddiford, L. M., Cherbas, P., and Truman, J. W. (2001). Ecdysone receptors and their biological actions. *Vitam. Horm.* 60, 1–73. doi: 10.1016/s0083-6729(00)60016-x

Riddiford, L. M., Curtis, A. T., and Kiguchi, K. (1979). Culture of the epidermis of the tobacco hornworm, *Manduca sexta*. *Tissue Cult. Assn. Man.* 5, 975–985.

Riddiford, L. M., Kiguchi, K., Roseland, C. R., Chen, A. C., and Wolfgang, W. J. (1980). "Cuticle formation and sclerotization *in vitro* by the epidermis of the tobacco hornworm, *Manduca sexta*," in *Invertebrate Systems In Vitro*, eds E. Kurstak, K. Maramorosch, and A. Dubendorfer (Amsterdam: Elsevier), 103–115.

Riddiford, L. M., Truman, J. W., Mirth, C. K., and Shen, Y. (2010). A role for juvenile hormone in the prepupal development of *Drosophila melanogaster*. *Development* 137, 1117–1126. doi: 10.1242/dev.037218

Riddiford, L. M., Truman, J. W., and Nern, A. (2018). Juvenile hormone reveals mosaic developmental programs in the metamorphosing optic lobe of *Drosophila melanogaster*. *Biol. Open* 7:bio034025. doi: 10.1242/bio.034025

Rust, M. K., and Hemsarth, W. (2019). Synergism of adulticides and insect growth regulators against larval cat fleas (Siphonaptera: Pulicidae). *J. Med. Entomol.* 56, 790–795. doi: 10.1093/jme/tjy239

Rust, M. K., Lance, W., and Hemsarth, H. (2016). Synergism of the IGRs methoprene and pyriproxyfen against larval cat fleas (Siphonaptera: Pulicidae). *J. Med. Entomol.* 53, 629–633. doi: 10.1093/jme/tjw010

Röller, H., and Dahm, K. H. (1968). The chemistry and biology of juvenile hormone. *Rec. Prog. Horm. Res.* 24, 651–680. doi: 10.1016/b978-1-4831-9827-9.50018-6

Röller, H., and Dahm, K. H. (1970). The identity of juvenile hormone produced by corpora allata *in vitro*. *Naturwissenschaften* 9, 454–455. doi: 10.1007/bf00607739

Röller, H., Dahm, K. H., Sweeley, C. C., and Trost, B. M. (1967). The structure of juvenile hormone. *Angew. Chem.* 6, 179–180.

Safranek, L., and Riddiford, L. M. (1975). The biology of the black larval mutant of the tobacco hornworm. *Manduca sexta*. *J. Insect Physiol.* 21, 1931–1938. doi: 10.1016/0022-1910(75)90225-5

Santos, C. G., Humann, F. C., and Hartfelder, K. (2019). Juvenile hormone signaling in insect oogenesis. *Curr. Opin. Insect Sci.* 31, 43–48. doi: 10.1016/j.cois.2018.07.010

Sasorith, S., Billas, I. M., Iwema, T., Moras, D., and Wurtz, J. M. (2002). Structure-based analysis of the ultraspiracle protein and docking studies of putative ligands. *J. Insect Sci.* 2:25. doi: 10.1093/jis/2.1.25

Scharrer, B. (1946). The role of the corpora allata in the development of *Leucophaea* (Orthoptera). *Endocrinology* 38, 35–45. doi: 10.1210/endo-38-1-35

Schooley, D. A., Baker, F. C., Tsai, L. W., Miller, C. A., and Jamieson, G. C. (1984). "Juvenile hormones 0, I, and II exist only in Lepidoptera," in *Biosynthesis, Metabolism and Mode of Action of Insect Hormones*, eds J. A. Hoffmann and M. Porchet (Berlin: Springer Verlag), 373–383. doi: 10.1007/978-3-642-69922-1_36

Schubiger, M., Carré, C., Antoniewski, C., and Truman, J. W. (2005). Ligand-dependent de-repression via EcR/USP acts as a gate to coordinate the differentiation of sensory neurons in the *Drosophila* wing. *Development* 132, 5239–5248. doi: 10.1242/dev.02093

Shepherd, J. G. (1974). Activation of saturniid moth sperm by a secretion of the male reproductive tract. *J. Insect Physiol.* 20, 2107–2122. doi: 10.1016/0022-1910(74)90037-7

Shinoda, T., Hiruma, K., Charles, J.-P., and Riddiford, L. M. (1997). Hormonal regulation of JP29 during larval development and metamorphosis in the tobacco hornworm, *Manduca sexta*. *Arch. Insect Biochem. Physiol.* 34, 409–428. doi: 10.1002/(sici)1520-6327(1997)34:4<409::aid-arch2>3.0.co;2-n

Shionoya, M., Matsubayashi, H., Asahina, M., Kuniyoshi, H., Nagata, S., Riddiford, L. M., et al. (2003). Molecular cloning of the prothoracicotropic hormone from the tobacco hornworm, *Manduca sexta*. *Insect Biochem. Mol. Biol.* 33, 795–801. doi: 10.1016/s0965-1748(03)00078-x

Shirk, P. D., Dahm, K. H., and Röller, H. (1976). The accessory sex glands as the repository for juvenile hormone in male cecropia moths. *Zeitschr. Naturforsch. Sec. C Biosci.* 31, 199–200. doi: 10.1515/znc-1976-3-421

Sláma, K., and Williams, C. M. (1965). Juvenile hormone activity for the bug *Pyrrhocoris apterus*. *Proc. Natl. Acad. Sci. U.S.A.* 54, 411–414. doi: 10.1073/pnas.54.2.411

Sláma, K., and Williams, C. M. (1966). The juvenile hormone. V. The sensitivity of the bug, *Pyrrhocoris apterus*, to a hormonally active factor in American paper-pulp. *Biol. Bull.* 130, 235–246.

Sliter, T. J., Sedlak, B. J., Baker, F. C., and Schooley, D. A. (1987). Juvenile hormone in *Drosophila melanogaster*. Idenitfication and titer determination during development. *Insect Biochem.* 17, 161–165. doi: 10.1016/0020-1790(87)90156-9

Smith, W., and Rybczynski, R. (2012). "Prothoracicotropic hormone," in *Insect Endocrinology*, ed. L. I. Gilbert (Amsterdam: Elsevier), 1–62. doi: 10.1016/b978-0-12-384749-2.10001-9

Smykal, V., Daimon, T., Kayukawa, T., Takaki, K., Shinoda, T., and Jindra, M. (2014). Importance of juvenile hormone signaling arises with competence of insect larvae to metamorphose. *Dev. Biol.* 390, 221–230. doi: 10.1016/j.ydbio.2014.03.006

Soma, K. K. (2006). Testosterone and aggression: berthold, birds and beyond. *J. Neuroendocrin.* 18, 543–551. doi: 10.1111/j.1365-2826.2006.01440.x

Staal, G. B. (1975). Insect growth regulators with juvenile hormone activity. *Ann. Rev. Entomol.* 20, 417–460. doi: 10.1146/annurev.en.20.010175.002221

Starling, E. H. (1905). Croonian lecture: on the chemical correlation of the function of the body. *Lancet* 2, 339–341. doi: 10.1016/s0140-6736(01)11877-5

Stay, B., and Tobe, S. S. (2007). The role of allatostatins in juvenile hormone synthesis in insects and crustaceans. *Ann. Rev. Entomol.* 52, 277–299. doi: 10.1146/annurev.ento.51.110104.151050

Suzuki, Y., Koyama, T., Hiruma, K., Riddiford, L. M., and Truman, J. W. (2013). A molt timer is involved in the metamorphic molt in *Manduca sexta* larvae. *Proc. Natl. Acad. Sci. U.S.A.* 110, 12518–12525. doi: 10.1073/pnas.1311405110

Svácha, P. (1992). What are and what are not imaginal discs: reevaluation of some basic concepts (Insecta. Holometabola). *Dev. Biol.* 154, 101–117. doi: 10.1016/0012-1606(92)90052-i

Thomsen, E. (1940). Relation between corpus allatum and ovaries in adult flies (Muscidre). *Nature* 145, 28–29. doi: 10.1038/145028a0

Thummel, C. S. (1990). Puffs and gene regulation–molecular insights into the *Drosophila* ecdysone regulatory hierarchy. *BioEssays* 12, 561–568. doi: 10.1002/bies.950121202

Toyota, K., Miyakawa, H., Hiruta, C., Furuta, K., Ogino, Y., Shinoda, T., et al. (2015). Methyl farnesoate synthesis is necessary for the environmental sex determination in the water flea *Daphnia pulex*. *J. Insect Physiol.* 80, 22–30. doi: 10.1016/j.jinsphys.2015.02.002

Truman, J. W. (1972). Physiology of insect rhythms I. Circadian organization of the endocrine events underlying the moulting cycle of larval tobacco hornworms. *J. Exp. Biol.* 57, 805–820.

Truman, J. W. (2019). The evolution of insect metamorphosis. *Curr. Biol.* 29, R1252–R1268.

Truman, J. W., Hiruma, K., Allee, J. P., MacWhinnie, S. G. B., Champlin, D. T., and Riddiford, L. M. (2006). Juvenile hormone is required to couple imaginal disc formation with nutrition in insects. *Science* 312, 1385–1388. doi: 10.1126/science.1123652

Truman, J. W., and Riddiford, L. M. (1974). Physiology of insect rhythms. III. The temporal organization of the endocrine events underlying pupation of the tobacco hornworm. *J. Exp*. Biol. 60, 371–382.

Truman, J. W., and Riddiford, L. M. (2019). The evolution of insect metamorphosis: a developmental and endocrine view. *Philos. Trans. R. Soc. B* 374:20190070. doi: 10.1098/rstb.2019.0070

Truman, J. W., Riddiford, L. M., and Safranek, L. (1973). Hormonal control of cuticle coloration in the tobacco hornworm: basis of an ultrasensitive bioassay for juvenile hormone. *J. Insect Physiol.* 19, 195–203. doi: 10.1016/0022-1910(73)90232-1

Truman, J. W., Riddiford, L. M., and Safranek, L. (1974). Temporal patterns of response to ecdysone and juvenile hormone in the epidermis of the tobacco hornworm, *Manduca sexta*. *Dev. Biol.* 39, 247–262. doi: 10.1016/0012-1606(74)90238-3

Ureña, E., Chafino, S., Manjón, C., Franch-Marro, X., and Martin, D. (2016). The occurrence of the holometabolous pupal stage requires the interaction between E93, Krüppel-homolog 1 and Broad-Complex. *PLoS Genet.* 12:e1006020. doi: 10.1371/journal.pgen.1006020

Ureña, E., Manjón, C., Franch-Marro, X., and Martin, D. (2014). Transcription factor E93 specifies adult metamorphosis in hemimetabolous and holometabolous insects. *Proc. Natl. Acad. Sci. U.S.A.* 111, 7024–7029. doi: 10.1073/pnas.1401478111

Uyehara, C. M., Nystrom, S. L., Niederhuber, M. J., Leatham-Jensen, M., Ma, Y., Buttitta, L. A., et al. (2017). Hormone-dependent control of developmental timing through regulation of chromatin accessibility. *Genes Dev.* 31, 862–875. doi: 10.1101/gad.298182.117

Villalobos-Sambucaro, M. J., Nouzova, M., Ramirez, C. E., Eugenia Alzugaray, M., Fernandez-Lima, F., Ronderos, J. R., and Noriega, F. G. (2020). The juvenile hormone described in *Rhodnius prolixus* by Wigglesworth is juvenile hormone III skipped bisepoxide. *Sci. Rep.* 10:3091. doi: 10.1038/s41598-020-59495-1

Vogt, M. (1942). Weiteres zur frage der artspezifität gonadotroper hormone. Untersuchungen an *Drosophila*-arten. *Wilhelm Roux Arch.* 141, 424–454. doi: 10.1007/bf00596488

Walton, W. E., and Eldridge, B. E. (2020). *UC IPM Pest Notes:Mosquitoes*. Oakland, CA: UC ANR Publication, 7451.

Wen, D., Rivera-Perez, C., Abdou, M., Jia, Q., He, Q., Liu, X., et al. (2015). Methyl farnesoate plays a dual role in regulating *Drosophila* metamorphosis. *PLoS Genet.* 11:e1005038. doi: 10.1371/journal.pgen.1005038

Wigglesworth, V. B. (1934). The physiology of ecdysis in *Rhodnius prolixus* (Hemiptera) II. Factors controlling moulting and metamorphosis. *Quart. J. Microsc. Sci.* 77, 191–222.

Wigglesworth, V. B. (1936). The function of the corpus allatum in the growth and reproduction of *Rhodnius prolixus* (Hemiptera). *Quart. J. Microsc. Sci.* 79, 91–121.

Wigglesworth, V. B. (1940). The determination of characters at metamorphosis in *Rhodnius prolixus* (Hemiptera). *J. Exp. Biol.* 17, 201–223.

Wigglesworth, V. B. (1952). The thoracic gland in *Rhodnius prolixus* (Hemiptera) and its role in moulting. *J. Exp. Biol.* 29, 561–570.

Wigglesworth, V. B. (1953). Determination of cell function in an insect. *J. Embryol. Exp. Morph.* 1, 269–277.

Wigglesworth, V. B. (1954). *The Physiology of Insect Metamorphosis*. Cambridge: Cambridge University Press.

Wigglesworth, V. B. (1958). Some methods for assaying extracts of the juvenile hormone in insects. *J. Insect Physiol.* 2, 73–84. doi: 10.1016/0022-1910(58)90031-3

Wigglesworth, V. B. (1963). The action of moulting hormone and juvenile hormone at the cellular level in *Rhodnius prolixus*. *J. Exp. Biol.* 40, 231–245.

Wigglesworth, V. B. (1973). The role of the epidermal cells in moulding the surface pattern of the cuticle in *Rhodnius* (Hemiptera). *J. Cell Sci.* 12, 683–705.

Wigglesworth, V. B. (1985). "Historical perspectives," in *Comprehensive Insect Physiology, Biochemistry and Pharmacology*, Vol. 7, eds G. A. Kerkut and L. I. Gilbert (Oxford: Pergamon Press), 1–24.

Williams, C. M. (1946). Physiology of insect diapause: the role of the brain in the production and termination of pupal dormancy in the giant silkworm, *Platysamia cecropia*. *Biol. Bull.* 90, 234–243. doi: 10.2307/1538121

Williams, C. M. (1947). Physiology of insect diapause. II. Interaction between the pupal brain and prothoracic glands in the metamorphosis of the giant silkworm, *Platysamia cecropia*. *Biol. Bull.* 93, 89–98. doi: 10.2307/1538279

Williams, C. M. (1948). Physiology of insect diapause. III. The prothoracic glands in the Cecropia silkworm, with special reference to their significance in embryonic and postembryonic development. *Biol. Bull.* 94, 60–65. doi: 10.2307/1538210

Williams, C. M. (1952). Physiology of insect diapause. IV. The brain and prothoracic glands as an endocrine system in the Cecropia silkworm. *Biol. Bull.* 103, 120–138. doi: 10.2307/1538411

Williams, C. M. (1956a). Physiology of insect diapause. X. An endocrine mechanism for the influence of temperature on the diapausing pupa of the Cecropia silkworm. *Biol. Bull.* 110, 201–218. doi: 10.2307/1538982

Williams, C. M. (1956b). The juvenile hormone of insects. *Nature* 178, 212–213. doi: 10.1038/178212b0

Williams, C. M. (1958). The juvenile hormone of insects. *Sci. Am.* 198, 67–75.

Williams, C. M. (1959). The juvenile hormone. I. Endocrine activity of the corpora allata of the adult Cecropia silkworm. *Biol. Bull.* 116, 323–338. doi: 10.2307/1539218

Williams, C. M. (1961). The juvenile hormone. II. Its role in the endocrine control of molting, pupation, and adult development in the Cecropia silkworm. *Biol. Bull.* 121, 572–585. doi: 10.2307/1539456

Williams, C. M. (1963). The juvenile hormone. III. Its accumulation and storage in the abdomens of certain male moths. *Biol. Bull.* 124, 355–367. doi: 10.2307/1539485

Williams, C. M., and Kafatos, F. C. (1971). Theoretical aspects of the action of Juvenile Hormone. *Bull. Soc. Entom. Suisse* 44, 151–162.

Williams, C. M., and Sláma, K. (1966). The juvenile hormone. VI. Effects of the "Paper Factor" on the growth and metamorphosis of the bug, *Pyrrhocoris apterus*. *Biol. Bull.* 130, 247–253. doi: 10.2307/1539701

Williams, D. W., and Truman, J. W. (2005). Cellular mechanisms of dendrite pruning in *Drosophila*: insights from *in vivo* time-lapse of remodeling dendritic

arborizing sensory neurons. *Development* 132, 3631–3642. doi: 10.1242/dev.01928

Willis, J. H. (1986). The paradigm of stage-specific gene sets in insect metamorphosis: time for revision! *Arch. Insect Biochem. Physiol.* 3, 47–57. doi: 10.1002/arch.940030707

Willis, J. H., Rezaur, R., and Sehnal, F. (1982). Juvenoids cause some insects to form composite cuticles. *J. Embryol. Exp. Morphol.* 71, 25–40.

Wilson, T. G., and Fabian, J. (1986). A *Drosophila melanogaster* mutant resistant to a chemical analog of juvenile hormone. *Dev. Biol.* 118, 190–201. doi: 10.1016/0012-1606(86)90087-4

Wyatt, G. R., and Davey, K. G. (1996). Cellular and molecular actions of juvenile hormone. II. Roles of juvenile hormone in adult insects. *Adv. Insect Physiol.* 26, 1–155. doi: 10.1016/s0065-2806(08)60030-2

Zhang, Z., Xu, J., Sheng, Z., Sui, Y., and Palli, S. R. (2011). Steroid receptor co-activator is required for juvenile hormone signal transduction through a bHLH-PAS transcription factor, Methoprene tolerant. *J. Biol. Chem.* 286, 8437–8447. doi: 10.1074/jbc.m110.191684

Zhou, B., and Riddiford, L. M. (2001). Hormonal regulation and patterning of the Broad-Complex in the epidermis and wing discs of the tobacco hornworm, *Manduca sexta*. *Dev. Biol.* 231, 125–137. doi: 10.1006/dbio.2000.0143

Zhou, X., and Riddiford, L. M. (2002). Broad specifies pupal development and mediates the 'status quo' action of juvenile hormone on the pupal-adult transformation in *Drosophila* and *Manduca*. *Development* 129, 2259–2269.

Conflict of Interest: The author declares that the research was conducted in the absence of any commercial or financial relationships that could be construed as a potential conflict of interest.

frontiers in Cell and Developmental Biology

REVIEW
published: 20 August 2020
doi: 10.3389/fcell.2020.00837

Pheromonal Regulation of the Reproductive Division of Labor in Social Insects

Jin Ge[1,2†], Zhuxi Ge[1,2†], Dan Zhu[1,2] and Xianhui Wang[1,2]*

[1] State Key Laboratory of Integrated Management of Pest Insects and Rodents, Institute of Zoology, Chinese Academy of Sciences, Beijing, China, [2] CAS Center for Excellence in Biotic Interactions, University of Chinese Academy of Sciences, Beijing, China

The reproductive altruism in social insects is an evolutionary enigma that has been puzzling scientists starting from Darwin. Unraveling how reproductive skew emerges and maintains is crucial to understand the reproductive altruism involved in the consequent division of labor. The regulation of adult worker reproduction involves conspecific inhibitory signals, which are thought to be chemical signals by numerous studies. Despite the primary identification of few chemical ligands, the action modes of primer pheromones that regulate reproduction and their molecular causes and effects remain challenging. Here, these questions were elucidated by comprehensively reviewing recent advances. The coordination with other modalities of queen pheromones (QPs) and its context-dependent manner to suppress worker reproduction were discussed under the vast variation and plasticity of reproduction during colony development and across taxa. In addition to the effect of QPs, special attention was paid to recent studies revealing the regulatory effect of brood pheromones. Considering the correlation between pheromone and hormone, this study focused on the production and perception of pheromones under the endocrine control and highlighted the pivotal roles of nutrition-related pathways. The novel chemicals and gene pathways discovered by recent works provide new insights into the understanding of social regulation of reproductive division of labor in insects.

Keywords: division of labor, queen pheromone, juvenile hormone, olfactory receptor, caste

OPEN ACCESS

Edited by:
Zhongxia Wu,
Henan University, China

Reviewed by:
Yongliang Fan,
Northwest A&F University, China
Lei Zhao,
University of Wisconsin-Madison, United States

****Correspondence:***
Xianhui Wang
wangxh@ioz.ac.cn

† These authors have contributed equally to this work

Specialty section:
This article was submitted to Epigenomics and Epigenetics, a section of the journal Frontiers in Cell and Developmental Biology

Received: *30 June 2020*
Accepted: *05 August 2020*
Published: *20 August 2020*

Citation:
Ge J, Ge Z, Zhu D and Wang X (2020) Pheromonal Regulation of the Reproductive Division of Labor in Social Insects. Front. Cell Dev. Biol. 8:837. doi: 10.3389/fcell.2020.00837

INTRODUCTION

Insect societies provide excellent model systems for research on organization principles. A signature and defining trait of eusocial insects is the reproductive division of labor, expressed as strong reproductive skew, in which a single or a few females (queen) monopolize colony reproduction, while all other females (workers) care for eggs laid by the queen (Wilson, 1971). Unraveling the mechanism underlying reproductive skew provides an avenue to understand the influence of social interaction on individual phenotypic plasticity and its consequent task allocation.

Social insects are well known to utilize chemical signals to regulate their behavior (Leonhardt et al., 2016). Empirical evidence and theoretical consideration indicated the importance of pheromones in regulating adult worker reproduction. These pheromones, predicted by classical paradigms, are specific components to dominant females [queen pheromones (QPs)] and

are closely correlated with fertility. On the basis of this criterion, early studies have identified queen mandibular pheromones (QMPs) in honeybees and cuticular hydrocarbons (CHCs) in ants as queen primer pheromones to inhibit worker reproduction (Le Conte and Hefetz, 2008). However, two questions remain unsettled, including (1) the modes of action of chemical components and (2) the pheromonal production and the modulation of pheromones on worker physiology.

This study aimed to review research progresses focusing on the above two questions mainly in the last 10 years, from ultimate and proximate perspective. The influence of context and the coordination with other modalities in reproductive regulation were discussed under the complexity of reproductive skew at colony levels. In addition to QPs, the effect of brood was considered. Given the strong association between pheromone and hormone, we focused on the production and perception of pheromones in response to endocrine factors. Taking advantage of exquisite bioassays, chemical analysis, genomics, and genetic manipulation, recent discoveries have found molecular innovation of chemicals and gene pathways, largely expanding the understanding of social regulation of reproduction in insects.

REPRODUCTIVE SIGNALING: A COMBINATION OF SENSORY MODALITIES

The modalities that queens or foundresses utilize to regulate workers could be generally categorized into either "behavioral" or "chemical." In primitive eusocial species lacking morphologically defined castes, aggressive dominance behavior is a universal approach to generate reproductive skew and could be aided by visual cues serving as "badges of status" (Tibbetts and Lindsay, 2008). By contrast, in highly social species with a large colony, queens were unable to afford physical contact with every worker. Therefore, chemical communication is hypothesized to be a reliable way to regulate worker reproduction (Le Conte and Hefetz, 2008; Kocher and Grozinger, 2011). Despite a correlation between CHCs and fertility of dominant breeders in many primitively eusocial wasps (Sledge et al., 2001; Dapporto et al., 2007; Bhadra et al., 2010), the queen CHC blends alone failed to inhibit the subordinates' ovarian development in *Polistes satan*. Therefore, these studies supported the hypothesis that fertility-linked compounds only play addictive roles in the reproductive regulation of primitively eusocial species (Oi et al., 2019). However, a recent study in *Lasioglossum malachurum* sweat bees has revealed that the over production of macrocyclic lactones acts as QPs by influencing worker behavior and decreasing ovarian activations. This study for the first time described a QP with a primer function in a eusocial hymenopteran species other than species with morphologically distinct castes (Steitz and Ayasse, 2020). Similar to the complexity of modalities regulating reproduction in primitively eusocial species, mounting evidence of QPs in highly eusocial species did not exclude the participation of behavioral interaction in affecting worker reproduction. In *Bombus impatiens* bumblebees, directly contacting with a caged queen could fully activate worker ovaries, suggesting that queen-initiated behavior may be responsible for the inhibition of worker reproduction (Padilla et al., 2016). Taken together, the orchestration of pheromone and behavior in regulating worker reproduction seem more complex than previously conceived. Given that the transmission of each sensory modality is under the selection of environmental factors, reproductive signaling is possibly affected by species-specific life-history traits. In the case of sweat bees, living in below-ground nests renders visual cues useless and is likely to make chemical compounds as an honest signal of dominance. How various modalities (i.e., behavior, chemical compounds and visual cues) interact to regulate reproduction remains an open question. Finally, the establishment of reproductive hierarchy requires the cognition of nestmates' fertility which integrates various sensory modalities, such as behavior, chemicals and visual cues. The outcome of behavioral interaction could be inferred by the color pattern or chemical fingerprints of opponents (Reichert and Quinn, 2017), thus eliciting associative learning after dominance contest.

In addition to numerous works focusing on reproductive signaling from queens and nestmate workers, recent studies have examined the roles of brood in reproductive regulation. When kept with young larvae, *B. impatiens* workers showed reduced ovarian activation and oviposition. Moreover, this effect was in a quantity-dependent manner; the presence of 10 larvae completely suppresses egg laying, regardless of worker age, relatedness to brood, or brood parentage/sex (Starkey et al., 2019a). Exposure to the odors from larvae, however, was insufficient to suppress ovarian activation and workers fail to differentiate between larvae and pupae on the basis of olfactory cues (Starkey et al., 2019b). Therefore, in bumblebees, odors alone could not explain regulatory effect of brood and workers might use multiple information sources or rely on behavioral interaction to regulate their reproduction. A subsequent study further showed a synergistic effect of queens and larvae on worker reproduction-related genes, where the combined effect of queen and larvae outweighed their separate effect, indicating that the two coordinate to maintain reproductive monopoly (Orlova et al., 2020). The regulatory effect of young offspring, including eggs, is likely to evolve across social species, given the widespread trade-off between reproduction and brood care (Schultner et al., 2017). In highly eusocial *Apis mellifera* and primitively eusocial *Ooceraea biroi*, the worker's ovary activation is suppressed by larvae signals which are identified as chemical compound in honeybees (Mohammedi et al., 1998; Maisonnasse et al., 2010; Ulrich et al., 2016). Eggs could also convey inhibitory signals to workers in a highly eusocial insect; the surface hydrocarbons of *Camponotus floridanus* queen-laid eggs induce workers to refrain from oviposition, thus regulating worker reproduction in subcolonies (Endler et al., 2004).

EVOLUTIONARY ORIGIN OF QPS

Two scenarios regarding the evolutionary origin of QPs prevail. Widely discussed and supported in CHC QPs is the sender-precursor scenario. This hypothesis posits that QPs were

derived from a preadaptation on the sender, who already produces a precursor as functionless physiological byproducts or to serve unrelated purpose (Wyatt, 2014; Stokl and Steiger, 2017). Under this scenario, two predictions could be proposed. The first one is that QPs evolve from chemical cues of solitary ancestors, as byproducts of ovary development. This hypothesis is robustly supported by the universal physiological link between odor and fertility (Van Oystaeyen et al., 2014; Holman, 2018). In solitary and primitive eusocial species without morphologically distinct castes, ovarian activation usually triggers substantial changes in cuticular compounds (Liebig, 2010; Oi et al., 2019). Thus, the chemical by-products of fertility gradually evolved into honest fertility indices and subsequently into dedicated QPs in highly eusocial species (Peeters and Liebig, 2009). Even though widely accepted as one of the most convincing explanations regarding QP evolution, the mechanisms underlying functional transition from fertility recognition cues to ovarian developmental deterrents remain elusive. The second prediction is that QPs may be derived from sex pheromones. From an ultimate perspective, sex pheromones advertise female fecundity to potential mates and thus are able to serve as honest indicators of fertility and evolve secondarily as QPs (Ayasse et al., 2001). A support for this prediction came from the shared structure between fertility signals in social species and contact pheromones in solitary species (Smith et al., 2009, 2012). However, limited studies have demonstrated a joint function in a certain species. The only evidence comes from honeybees in which chemicals from QMPs not only attract males from long distance but also induce worker sterility (Le Conte and Hefetz, 2008). The evolution of QP's dual functions is possibly constrained by the life-cycle separation between mating and ovarian activation. For instance, in the sweat bee, gynes mate before overwintering but initiate reproduction in the ensuing summer. Sex pheromones are not used as QPs, because of their quantitative decrease after mating (Steitz and Ayasse, 2020).

In contrast to the sender–precursor scenario, the sensory exploitation hypothesis predicted that QPs could evolve *de novo* acting on pre-existing gene-regulatory networks that are linked with the regulation of reproduction in receiver workers. A notable case under this scenario is the honeybee QMPs. On the one hand, the 4-hydroxy-3-methoxyphenylethanol (HVA) in QMPs could directly suppress the worker reproduction by acting on dopamine receptors instead of stimulating the sensory system (Beggs et al., 2007; Beggs and Mercer, 2009). On the other hand, the QMPs unexpectedly showed reduced ovary size, number of eggs and the number of viable offspring in phylogenetically distantly related fruit fly *Drosophila melanogaster*, suggesting the exploitation of conserved physiological pathways (Camiletti et al., 2013; Galang et al., 2019). This finding was further verified by a recent study demonstrating a remarkable cross activity of honeybee QMP in bumblebees, in which the egg laying of workers and queens are inhibited by non-native QMP blend (Princen et al., 2019). Another hypothesis under the sensory exploitation scenario is that QPs evolve from oviposition deterring pheromones. In solitary insects, especially herbivores, females reduce egg laying to avoid intra-specific competition in response to conspecific chemical signals deposited on oviposition substrates (Peter, 2002). However, this hypothesis lacks any empirical evidence.

The two above-mentioned scenarios are in line with the two hypotheses regarding the ultimate cause of the reproductive skew in social insects. In particular, the sender-precursor scenario corresponds to the queen signal hypothesis which postulates that workers regulate their own reproduction on the basis of their own fitness interest thus adjusting their behavior in accordance to queen signals that honestly indicate queen fertility (Keller and Nonacs, 1993; Grueter and Keller, 2016). By contrast, under the "sensory exploitation" scenario, which corresponds to "queen control" hypothesis, the queen could potentially deceive or manipulate the workers against their own interests even though the signals are still honest (Keller, 2009; Smith and Liebig, 2017). This sensory exploitation could be evolutionarily stable in the long run, by leading to either a queen–worker arm race, to workers evolving counter–adaptations, or to limited personal cost of workers' sterility (Kocher and Grozinger, 2011; Peso et al., 2015). From a proximate perspective, the evolution of manipulative QPs requires the queens to be immune to the pheromones themselves, considering the inhibitory effect of honeybee QMP on bumblebee queens (Princen et al., 2019).

CHEMICAL NATURE OF PHEROMONES

Studies in recent years have focused on the role of CHCs as QPs. Synthesized in oenocytes, the arrays of long-chained linear and branched, saturated, and unsaturated hydrocarbons are highly abundant in insect epicuticle, conveying recognition cues related to sex, age, and nestmates (Oi et al., 2015). Mounting evidence showed that CHCs are conserved honest fertility cues, from primitively eusocial wasps to advanced eusocial ants (Liebig, 2010). A recent study identified CHC as a royal pheromone in termites, which appears to predate its use as QP in social Hymenoptera (Funaro et al., 2018). However, the unequivocal identification of CHCs with priming function is limited in a handful of species, thus preventing the generalization of the chemical nature of QP. The inhibitory effect of isolated CHC signal on ovarian activation were observed in ants, wasps, and bumblebees, implying that CHCs are a conserved class of signals in regulating reproduction (Van Oystaeyen et al., 2014). However, the uniformity of CHCs as QPs is challenged by subsequent studies regarding its methodological bias and logical pitfall. First, because of CHCs abundance and ease in detection and spectral/structural analysis, the research preference for CHCs inevitably caused negligence of other compounds (Amsalem and Hefetz, 2018). Therefore, recent reviews and studies called for attention to be paid to the exocrine glands, which are the sources of many described trial and alarm pheromones (Dani and Turillazzi, 2018; Villalta et al., 2018; Hefetz, 2019). Up to date, the only QP found in exocrine glands is the chemical blends in the honeybee mandibular glands, which are immensely hypertrophied in queens (Slessor et al., 1988). Indeed, the queen-specific specialization has been reported in various glands and species, such as honeybees (Katzav-Gozansky et al., 1997), halictid bees (Steitz and Ayasse, 2020),

and ants (Smith et al., 2012), but dedicated examination of their compounds functioning as QPs has been seldom performed. Second, although non-volatile CHCs are able to avoid sensory habituation caused by saturation, their higher expression in queens compared with workers cannot guarantee the uniqueness of QPs predicted by theory (Hefetz, 2019). Most of the identified CHC QPs are common in queens and workers but present in greatest quantities in queens (Van Oystaeyen et al., 2014). Regulation via the QP higher in queens than in workers could be problematic because of a dilution of pheromones in populous colonies (Orlova and Hefetz, 2014). Workers possibly activate their ovaries as under queenless conditions. Overall, despite the certain roles of CHCs in adverting the queen's presence, these fertility cues are not sufficient to serve as conserved signals for the regulatory function in reproduction. Glandular sources and other queen-qualitatively specific compounds should be considered in the search for queen primer pheromones (**Figure 1**).

Recent studies and reviews have proposed several guidelines in seeking unknown QPs (Amsalem and Hefetz, 2018; Villalta et al., 2018; Hefetz, 2019). Firstly, QPs may be multicomponent and pleiotropic. The specificity of communication is theoretically enhanced when compound blends are used as pheromones. Multiple components may contribute to the reliability of queen signaling because of the complexity of social signals within a colony. In honeybees, the QPs consists of six components, all of which are necessary for the inhibition of gyne rearing (Wanner et al., 2007; Matsuura et al., 2010). Besides, QPs could also elicit releaser effects, such as retinue behavior in ants and honeybee workers (Villalta et al., 2018), grooming in wasps (Holman et al., 2010), and shaking in termites (Funaro et al., 2018). Secondly, the QPs usually work in a context dependent manner to prevent misinterpretation (Orlova and Amsalem, 2019). A growing body of evidence has identified various forms of social context responsible for the expression of QP regulatory effects, including

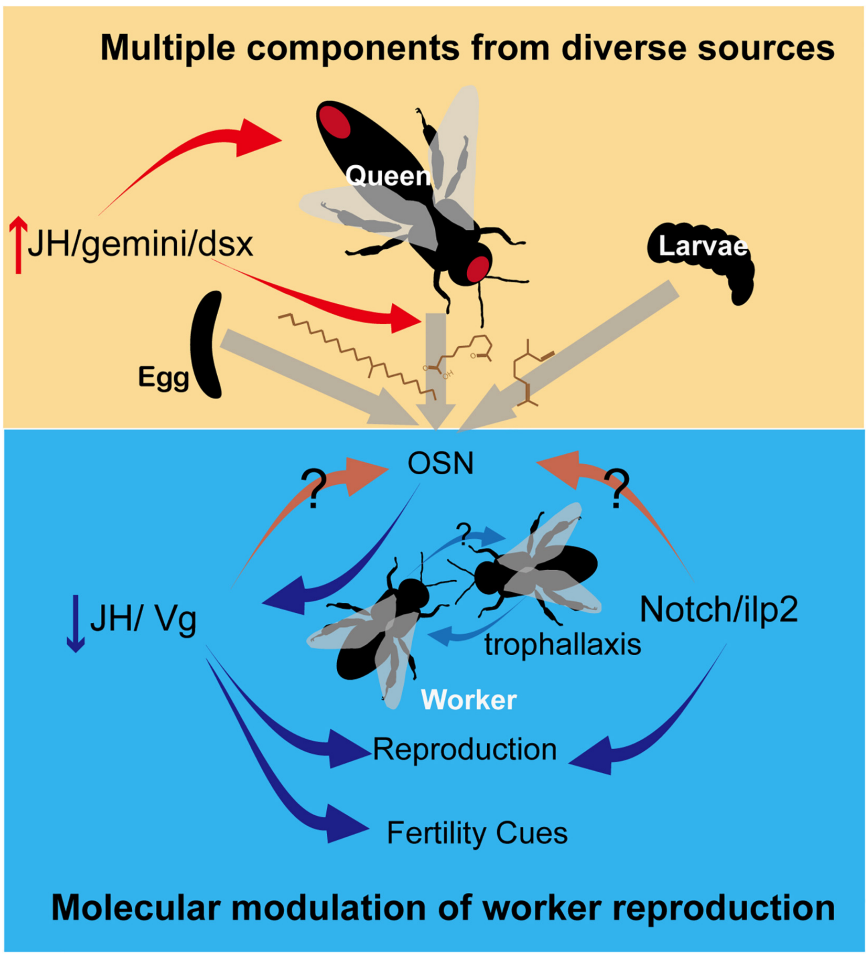

FIGURE 1 | Pheromonal regulation of worker reproduction in social insects. Primer pheromones, including CHCs and other glandular compounds, are released by queens, eggs and larvae to suppress worker ovarian development. The production of pheromones is influenced by gonadotropin JH or by transcriptional factor gemini or dsx. In recipient workers, the primer pheromones down-regulate nutrition-related pathways including JH/Vg or Notch/ilp to inhibit worker reproduction, via activating OSN in antennae. These nutrition-related pathways may increase the sensitivity of OSN to pheromones in turn. An amplification of effect is possible due to trophallaxis among workers. Moreover, a down-regulated JH level results in a reduction of fertility cues emitted by workers, therefore maintaining reproductive skew in a colony. Red ellipses in the upper panel show glands in queens. Red and blue arrows depict stimulatory and inhibitory effects, respectively.

chemical background (Funaro et al., 2018), behavioral repertoire (Padilla et al., 2016), or the presence of brood (Hoover et al., 2003) or nestmates (Kikuchi et al., 2007). Social context may influence QP dispersion within the colony. For example, in honeybees and ants, the frequent occurrence of licking or trophallaxis possibly helps to transfer QP and accelerate the dispersion of QP from queen to workers and among workers (Naumann et al., 1991; Soroker et al., 1995). In addition, thermal regulation by workers is an alternative way to facilitate QP dispersion. The capacity of honeybee and bumble workers to produce heat may promote the active space of QPs (Stabentheiner et al., 2010), which generally increase QP volatility as temperature increases (Gibbs, 1995).

PHEROMONAL PRODUCTION

The production of QPs in queens is still mysterious in most social insect species, but it could be inferred by their link with reproduction. A large body of studies have revealed the role of juvenile hormone in the production of CHCs. The linkage between CHCs and fertility in social insects could be explained by the universal hormone pleiotropy reported in primitively and advanced eusocial species, in which Juvenile Hormone (JH) serves as CHC regulator and gonadotropin hormone (Slessor et al., 1988; Cuvillier-Hot et al., 2002; Holman et al., 2010; Kelstrup et al., 2014; Oliveira et al., 2017). The up-regulation of JH via the application of methoprene (a JH analog) leads to a shift of worker CHC profile to that of the queen (Brent et al., 2016; Oliveira et al., 2017). Thus, the hormones involved in ovarian development could affect the synthesis or transport of CHCs. However, the genes responsible for the synthesis of CHC fertility signal in social insects have only been reported in termites. *Neofem4*, a cytochrome P450 gene, is more expressed in *Cryptotermes secundus* queens than in workers. Silencing this gene by using RNAi alters the queen odors to those of a worker and induces a worker butting behavior, indicating the onset of reproductive replacement differentiation (Korb et al., 2009; Hoffmann et al., 2014). However, less information is available regarding the production of QP in exocrine glands. In Cape honeybees, the synthesis of QMPs is controlled by alternative splicing of the CP-2 transcription factor *gemini*. Altering the splice pattern of *gemini* by siRNA feeding results in ovary activation and increased amount of queen-specific pheromones 9-oxo-2-decenoic acid (9-ODA) and 9-hydroxy-2-decenoic acid (9-HDA). As methyl p-hydroxybenzoate (HOB) and HVA are not affected by the knockdown of specific *gemini*, this gene possibly acts on the biosynthesis of fatty acid-derived components (Jarosch et al., 2011; Jarosch-Perlow et al., 2018). The synthesis of QMP is also influenced by the sex determination pathway. The knockdown of *Doublesex (dsx)* in queenless honeybee workers results in reduced ovary development and a reduced level of pheromonal fertility signals, indicating that the regulatory network is co-opted during eusocial evolution to regulate pheromone production (Velasque et al., 2018). Considering the honesty of QPs in indicating fertility predicted by the sender–precursor scenario (see section "EVOLUTIONARY ORIGIN OF QPS"), gonadotropin may be pivotal in the production of QPs besides CHCs. In addition to gonadotropin, nutrition is likely to be an alternative proximate factor governing QP production, because it activates reproduction directly on vitellogenin (vg) or indirectly through JH (Kapheim, 2017). Nutrition is also the key to influence reproductive physiology and drives caste determination in honeybees (Metcalf and Whitt, 1977; Mutti et al., 2011).

PHEROMONAL PERCEPTION

A key issue regarding pheromone-regulated reproduction is how QPs are perceived and what sort of genetic and physiological specializations facilitate signal perception in social insects. Semio-chemicals are basically detected by olfactory sensory neurons in porous sensory hairs located on chemosensory organs, especially the antennae. The knock-down of Orco, an olfactory co-receptor, impairs a series of social behavior including worker dueling to become gametes in *Harpegnathos saltator* ants (Yan et al., 2017). Electroantennography demonstrated that workers respond specifically to the putative QPs in several species, such as *Pachycondyla inversa*, *Apis cerana*, and *A. mellifera* (D'Ettorre et al., 2004; Dong et al., 2017). Moreover, single sensilla recording in ants verified that QP candidate CHCs are responded by basiconic sensilla (Ozaki et al., 2005; Sharma et al., 2015). Investigations of the glomeruli in the antennal lobe where ORNs are projected to in the brain have revealed female-specific or caste-specific structural specialization relevant to QP perception. In *C. floridanus*, females have about approximately 140 T6 glomeruli, whereas males completely lack these glomeruli (Nakanishi et al., 2010). In *O. biroi*, basiconic sensilla and CHC responsive ORs are found only on the ventral surface of the female antennal club (McKenzie et al., 2016). A correlation between glomeruli numbers and worker polymorphism exists in *Atta vollenweideri* (Kelber et al., 2010). Given their central role in chemosensory perception, peripheral circuits substantially contribute to the specificity and plasticity of QP perception. For instance, *C. floridanus* workers are able to detect and distinguish enantiomers of a proposed QP (3-methylheptacosane) by using sensilla basiconica structures (Sharma et al., 2015). Electrophysiological responses to several CHCs decrease with the transition from non-reproductive *H. saltator* workers to gamergates, implying a potential mechanism to tolerate the mutually inhibitory or self-inhibitory effects of QPs on gamergates (Gospocic et al., 2017).

Recent works have implied possible correlation between pheromonal perception and endocrine factors. In honeybees, JH treatment influences the retinue behavior of young workers to QMP. The latter influence is likely due to the reduced levels of an octopamine (OA) receptor in the antennae (Vergoz et al., 2009). Indeed, JH application induces a dramatic change in gene expression in the neural system, including the brain and antennae (Pandey and Bloch, 2015). A similar modulation of responsiveness to social cues has also been reported in Vg. A knockdown of a Vg ortholog called *Vg-like A* in the fat body of young ant workers reduced brood care and increased nestmate care, a task usually performed by old workers. This work

revealed that *Vg-like A* drives behavioral maturation by mediating responses to social cues (Kohlmeier et al., 2018). Thus, divergent Vg or JH titer may lead to differential responses to QPs among castes. Further study should investigate the mechanisms of sensory threshold modulation by endocrine factors in primitively and advanced eusocial species.

Analysis based on genome has revealed that 9-exon ORs particularly expanded in ants are specifically expressed in females, indicating a possible interaction with social signals, such as CHCs (Smith et al., 2011, 2012; Zhou et al., 2012; Oxley et al., 2014; McKenzie et al., 2016). The knowledge of OR with ligands in QPs is limited in two species. In honeybees, AmOr11, specifically bounds to the QMP component 9-ODA (Wanner et al., 2007). In *H. saltator*, HsOr263 is highly expressed in workers and responsible in binding a candidate reproductive signal, due to its strong responses to gamergate extract and a predicted QP (13, 23-DiMeC37) (Pask et al., 2017). Whether and how the olfactory plasticity of QP perception is influenced by modulation of OR expression levels remain to be determined, because alterations in a single odorant receptor may lead to a significant effect on animal odor perception.

PHEROMONAL EFFECTS AT MOLECULAR LEVELS

Few studies have revealed the global effect of QPs on the genetic and epigenetic networks of workers. In *Solenopsis invicta*, under queenright conditions, numerous genes are differentially expressed between foragers and non-foragers. However, in absence of the queen, these differences disappear at transcriptional level, implying a possibility that QP participates in task allocation among workers (Manfredini et al., 2014). A comparative study further showed that exposure to QPs leads to similar trancriptic responses in two ant and two bee species (genera: *Lasius*, *Apis*, and *Bombus*). With functions involving lipid biosynthesis and transport, olfaction, production of cuticle, oogenesis, and histone (de) acetylation, QP-sensitive genes seem to be peripheral in the gene co-expression network and caste-specific expression (Holman et al., 2019). In addition to the effect of QP on gene expression, the application of QP results in a change in the level of DNA methylation in honeybee and *Lasius* ants. However, the DNA methylation level is not affected by QP in *Bombus terrestris* (Holman et al., 2016). The QMP in honeybees also exerts epigenetic modifications to RNA and histones in the brain, potentially affecting aging-related genes (Junior et al., 2020). Although promising, these findings mainly examined the global level of epigenetic effect, while the mechanism of QP perception on epigenetics and epigenetically targeted genes remain unknown.

Studies concerning the specific molecular effects of reproductive pheromonal regulation in adult individuals are scarce. Duncan et al. (2016) provided the first molecular mechanism directly linking ovary activity in adult worker bees with the presence of the queen. QMP inhibits worker reproduction by stimulating Notch signaling in ovary tissues in the region where germ cells are specified. In the absence of the queen, the Notch receptor in the cells of germarium renders these cells refractory to Notch signaling. This finding provided support for the reproductive ground plan hypothesis (West-Eberhard, 1987; Page and Amdam, 2007), by revealing the targeted control of worker fertility through co-option of a conserved cell-signaling pathway (Duncan et al., 2016). In addition to the Notch, alternative pathways have been proposed in primitively eusocial species. For example, in *B. terrestris*, Vg expression is lower in the presence of newly mated queens than same-age virgin queens regardless of queen ovarian inactivation under both conditions (Amsalem et al., 2014). In *Polistes dominula* paper wasps, 3-h group formation is sufficient to down-regulate the JH level in low-ranked subordinates, suggesting the hyper-sensitivity of JH in response to nestmate cues, including pheromones (Tibbetts et al., 2018). This result was reminiscent of the finding that JH could mediate the threshold to social signals in turn. Given the gonadotropic and physiological functions of JH in the primitively social species (Amsalem et al., 2014; Kelstrup et al., 2017), a negative feedback loop exists between pheromones and JH to enhance the efficiency of regulation (**Figure 1**). Recent studies on parthenogenetic clonal raider ants (*O. biroi*) revealed the molecular mechanism underlying the brood control of reproductive skew. A single gene, called insulin-like peptide 2 (*ilp2*) was identified on the basis of brain transcriptome. This gene was more up-regulated in reproductives than in non-reproductives (Chandra et al., 2018). Larval signals suppress *ilp2* to inhibit adult reproduction, thus potentially amplifying reproductive asymmetries (Chandra et al., 2018). These studies have partially revealed the signal transduction from social cues, including pheromones to reproductive outcome, and highlighted the importance of nutrition-related pathways. Whether pheromones directly affect the ovary or act via signaling between neural circuits are yet to be determined. Although ovarian development was extensively used as a proxy to reproduction, ovarian activation may be decoupled from reproduction because the ovary is possibly involved in the task allocation of workers, as demonstrated by the meta-analysis in some ant species (Pamminger and Hughes, 2017). Further studies should pay attention to the functional discrimination between ovarian activation and egg laying in reproduction.

CONCLUSION

Considerable advances on the pheromonal regulation of reproduction have been achieved in the last decades. Several discoveries of variation and plasticity of reproductive partitioning within and across species provided not only valuable data for constructing evolutionary routes of chemical communication but also hints for the identification of key components via a comparative approach.

Despite the strong association between CHCs and fertility, the unequivocal identification of CHC as queen pheromone. QP is rather limited. The contexts, such as colony, nestmates, and brood, in the regulation of worker reproduction demonstrated that pheromones are released from more than one source with multiple components and should work in combination with other

modalities (**Figure 1**). This argument helps settle the existing controversies among the chemical nature, evolutionary origin, and conservation of reproductive signaling.

Current works in both primitively eusocial and advanced eusocial species indicated the co-option of conserved pathways in pheromonal regulation of reproduction and highlighted the coordination among social cues, endocrine factors and reproduction (**Figure 1**). Studies on model species, such as honeybees and radial colonial ants, have demonstrated evolutionary innovations of nutrition-related pathways responsible for pheromonal effects. However, the mechanism of production and reception of pheromones remains largely unknown. With the aid of advances in genetic manipulation, future works could elucidate the genetic network underlying QP production, thereby contributing to loss-of-function experiments to identify the causal relationships between semiochemicals and reproduction. The reverse chemical ecology, based on the genome and identification of the olfactory receptors will be an effective approach for the screening of new components.

AUTHOR CONTRIBUTIONS

XW and JG designed the research. JG and ZG collected the references. All authors wrote the manuscript.

FUNDING

This work was supported by the National Natural Science Foundation of China (31772531 and 31930012), Science and Technology Service Network Initiative of the Chinese Academy of Sciences (KFJ-STS-ZDTP-073).

REFERENCES

Amsalem, E., and Hefetz, A. (2018). Preface: pheromone-mediation of female reproduction and reproductive dominance in social species. *J. Chem. Ecol.* 44, 747–749. doi: 10.1007/s10886-018-0992-7

Amsalem, E., Malka, O., Grozinger, C., and Hefetz, A. (2014). Exploring the role of juvenile hormone and vitellogenin in reproduction and social behavior in bumble bees. *BMC Evol. Biol.* 14:45. doi: 10.1186/1471-2148-14-45

Ayasse, M., Paxton, R., and Tengö, J. (2001). Mating behavior and chemical communication in the order hymenoptera. *Annu. Rev. Entomol.* 46, 31–78. doi: 10.1146/annurev.ento.46.1.31

Beggs, K. T., Glendining, K. A., Marechal, N. M., Vergoz, V., Nakamura, I., Slessor, K. N., et al. (2007). Queen pheromone modulates brain dopamine function in worker honey bees. *Proc. Natl. Acad. Sci. U.S.A.* 104, 2460–2464. doi: 10.1073/pnas.0608224104

Beggs, K. T., and Mercer, A. R. (2009). Dopamine receptor activation by honey bee queen pheromone. *Curr. Biol.* 19, 1206–1209. doi: 10.1016/j.cub.2009.05.051

Bhadra, A., Mitra, A., Deshpande, S. A., Chandrasekhar, K., Naik, D. G., Hefetz, A., et al. (2010). Regulation of reproduction in the primitively eusocial wasp *Ropalidia marginata*: on the trail of the queen pheromone. *J. Chem. Ecol.* 36, 424–431. doi: 10.1007/s10886-010-9770-x

Brent, C. S., Penick, C. A., Trobaugh, B., Moore, D., and Liebig, J. (2016). Induction of a reproductive-specific cuticular hydrocarbon profile by a juvenile hormone analog in the termite *Zootermopsis nevadensis*. *Chemoecology* 26, 195–203. doi: 10.1007/s00049-016-0219-8

Camiletti, A. L., Percival-Smith, A., and Thompson, G. J. (2013). Honey bee queen mandibular pheromone inhibits ovary development and fecundity in a fruit fly. *Entomo. Exp. Appl.* 147, 262–268. doi: 10.1111/eea.12071

Chandra, V., Fetter-Pruneda, I., Oxley, P. R., Ritger, A. L., McKenzie, S. K., Libbrecht, R., et al. (2018). Social regulation of insulin signaling and the evolution of eusociality in ants. *Science* 361, 398–402. doi: 10.1126/science.aar5723

Cuvillier-Hot, V., Gadagkar, R., Peeters, C., and Cobb, M. (2002). Regulation of reproduction in a queenless ant: aggression, pheromones and reduction in conflict. *Proc. Biol. Sci.* 269, 1295–1300. doi: 10.1098/rspb.2002.1991

Dani, F. R., and Turillazzi, S. (2018). Chemical communication and reproduction partitioning in social wasps. *J. Chem. Ecol.* 44, 796–804. doi: 10.1007/s10886-018-0968-7

Dapporto, L., Santini, A., Dani, F. R., and Turillazzi, S. (2007). Workers of a Polistes paper wasp detect the presence of their queen by chemical cues. *Chem. Senses* 32, 795–802. doi: 10.1093/chemse/bjm047

D'Ettorre, P., Heinze, J., Schulz, C., Francke, W., and Ayasse, M. (2004). Does she smell like a queen? Chemoreception of a cuticular hydrocarbon signal in the ant *Pachycondyla inversa*. *J. Exp. Biol.* 207, 1085–1091. doi: 10.1242/jeb.00865

Dong, S., Wen, P., Zhang, Q., Li, X., Tan, K., and Nieh, J. (2017). Resisting majesty: *Apis cerana*, has lower antennal sensitivity and decreased attraction to queen mandibular pheromone than *Apis mellifera*. *Sci. Rep.* 7:44640. doi: 10.1038/srep44640

Duncan, E. J., Hyink, O., and Dearden, P. K. (2016). Notch signalling mediates reproductive constraint in the adult worker honeybee. *Nat. Commun.* 7:12427. doi: 10.1038/ncomms12427

Endler, A., Liebig, J., Schmitt, T., Parker, J. E., Jones, G. R., Schreier, P., et al. (2004). Surface hydrocarbons of queen eggs regulate worker reproduction in a social insect. *Proc. Natl. Acad. Sci. U.S.A.* 101, 2945–2950. doi: 10.1073/pnas.0308447101

Funaro, C. F., Boroczky, K., Vargo, E. L., and Schal, C. (2018). Identification of a queen and king recognition pheromone in the subterranean termite *Reticulitermes flavipes*. *Proc. Natl. Acad. Sci. U.S.A.* 115, 3888–3893. doi: 10.1073/pnas.1721419115

Galang, K., Croft, J., Thompson, G., and Percival-Smith, A. (2019). Analysis of the Drosophila melanogaster anti-ovarian response to honey bee queen mandibular pheromone. *Insect Mol. Biol.* 28, 99–111. doi: 10.1111/imb.12531

Gibbs, A. (1995). Physical properties of insect cuticular hydrocarbons: model mixtures and lipid interactions. *Comp. Biochem. Phys. B* 112, 667–672. doi: 10.1016/0305-0491(95)00119-0

Gospocic, J., Shields, E. J., Glastad, K. M., Lin, Y., Penick, C. A., Yan, H., et al. (2017). The *Neuropeptide corazonin* controls social behavior and caste identity in ants. *Cell* 170, 748–759. doi: 10.1016/j.cell.2017.07.014

Grueter, C., and Keller, L. (2016). Acoustical communication in social insects. *Curr. Opin. Neurobiol.* 38, 6–11. doi: 10.1007/978-3-0348-8878-3_10

Hefetz, A. (2019). The critical role of primer pheromones in maintaining insect sociality. *Z. Naturforsch. C. J. Biosci.* 74, 221–231. doi: 10.1515/znc-2018-0224

Hoffmann, K., Gowin, J., Hartfelder, K., and Korb, J. (2014). The scent of royalty: a p450 gene signals reproductive status in a social insect. *Mol. Biol. Evol.* 31, 2689–2696. doi: 10.1093/molbev/msu214

Holman, L. (2018). Queen pheromones and reproductive division of labor: a meta-analysis. *Behav. Ecol.* 29, 1199–1209. doi: 10.1093/beheco/ary023

Holman, L., Helantera, H., Trontti, K., and Mikheyev, A. S. (2019). Comparative transcriptomics of social insect queen pheromones. *Nat. Commun.* 10:1593. doi: 10.1038/s41467-019-09567-2

Holman, L., Jørgensen, C. G., Nielsen, J., and d'Ettorre, P. (2010). Identification of an ant queen pheromone regulating worker sterility. *Proc. Biol. Sci.* 277, 3793–3800. doi: 10.1098/rspb.2010.0984

Holman, L., Trontti, K., and Helantera, H. (2016). Queen pheromones modulate DNA methyltransferase activity in bee and ant workers. *Biol. Lett.* 12:20151038. doi: 10.1098/rsbl.2015.1038

Hoover, S. E., Keeling, C. I., Winston, M. L., and Slessor, K. N. (2003). The effect of queen pheromones on worker honey bee ovary development. *Naturwissenschaften* 90, 477–480. doi: 10.1007/s00114-003-0462-z

Jarosch, A., Stolle, E., Crewe, R. M., and Moritz, R. F. (2011). Alternative splicing of a single transcription factor drives selfish reproductive behavior in honeybee workers (*Apis mellifera*). *Proc. Natl. Acad. Sci. U.S.A.* 108, 15282–15287. doi: 10.1073/pnas.1109343108

Jarosch-Perlow, A., Yusuf, A. A., Pirk, C. W. W., Crewe, R. M., and Moritz, R. F. A. (2018). Control of mandibular gland pheromone synthesis by alternative splicing of the CP-2 transcription factor gemini in honeybees (*Apis mellifera* carnica). *Apidologie* 49, 450–458. doi: 10.1007/s13592-018-0571-5

Junior, C. A. C., Ronai, I., Hartfelder, K., and Oldroyd, B. P. (2020). Queen pheromone modulates the expression of epigenetic modifier genes in the brain of honey bee workers. *bioRxiv* [Preprint], doi: 10.1101/2020.03.04.977058

Kapheim, K. M. (2017). Nutritional, endocrine, and social influences on reproductive physiology at the origins of social behavior. *Curr. Opin. Insect Sci.* 22, 62–70. doi: 10.1016/j.cois.2017.05.018

Katzav-Gozansky, T., Soroker, V., Hefetz, A., Cojocaru, M., Erdmann, D., and Francke, W. (1997). Plasticity of caste-specific Dufour's gland secretion in the honey bee (*Apis mellifera* L.). *Naturwissenschaften* 84, 238–241. doi: 10.1007/s001140050386

Kelber, C., Rossler, W., and Kleineidam, C. J. (2010). Phenotypic plasticity in number of glomeruli and sensory innervation of the antennal lobe in leaf-cutting ant workers (*A. vollenweideri*). *Dev. Neurobiol.* 70, 222–234. doi: 10.1002/dneu.20782

Keller, L. (2009). Adaptation and the genetics of social behaviour. *Philos. T. R. Soc. B* 364, 3209–3216. doi: 10.1098/rstb.2009.0108

Keller, L., and Nonacs, P. (1993). The role of queen pheromones in social insects: queen control or queen signal? *Anim. Behav.* 45, 787–794. doi: 10.1006/anbe.1993.1092

Kelstrup, H. C., Hartfelder, K., Esterhuizen, N., and Wossler, T. C. (2017). Juvenile hormone titers, ovarian status and epicuticular hydrocarbons in gynes and workers of the paper wasp Belonogaster longitarsus. *J. Insect Physiol.* 98, 83–92. doi: 10.1016/j.jinsphys.2016.11.014

Kelstrup, H. C., Hartfelder, K., Nascimento, F. S., and Riddiford, L. M. (2014). The role of juvenile hormone in dominance behavior, reproduction and cuticular pheromone signaling in the caste-flexible epiponine wasp, *Synoeca surinama*. *Front. Zool.* 11:78. doi: 10.1186/s12983-014-0078-5

Kikuchi, T., Tsuji, K., Ohnishi, H., and Le Breton, J. (2007). Caste-biased acceptance of non-nestmates in a polygynous ponerine ant. *Anim. Behav.* 73, 559–565. doi: 10.1016/j.anbehav.2006.04.015

Kocher, S. D., and Grozinger, C. M. (2011). Cooperation, conflict, and the evolution of queen pheromones. *J. Chem. Ecol.* 37, 1263–1275. doi: 10.1007/s10886-011-0036-z

Kohlmeier, P., Feldmeyer, B., and Foitzik, S. (2018). Vitellogenin-like A-associated shifts in social cue responsiveness regulate behavioral task specialization in an ant. *PLoS Biol.* 16:e2005747. doi: 10.1371/journal.pbio.2005747

Korb, J., Weil, T., Hoffmann, K., Foster, K. R., and Rehli, M. (2009). A gene necessary for reproductive suppression in termites. *Science* 324, 758–758. doi: 10.1126/science.1170660

Le Conte, Y., and Hefetz, A. (2008). Primer pheromones in social hymenoptera. *Annu. Rev. Entomol.* 53, 523–542. doi: 10.1146/annurev.ento.52.110405.091434

Leonhardt, S. D., Menzel, F., Nehring, V., and Schmitt, T. (2016). Ecology and evolution of communication in social insects. *Cell* 164, 1277–1287. doi: 10.1016/j.cell.2016.01.035

Liebig, J. (2010). Hydrocarbon profiles indicate fertility and dominance status in ant, bee, and wasp colonies. *Insect Hydrocarb.* 2010, 254–281. doi: 10.1017/CBO9780511711909.014

Maisonnasse, A., Alaux, C., Beslay, D., Crauser, D., Gines, C., Plettner, E., et al. (2010). New insights into honey bee (*Apis mellifera*) pheromone communication. Is the queen mandibular pheromone alone in colony regulation? *Front. Zool.* 7:18. doi: 10.1186/1742-9994-7-18

Manfredini, F., Lucas, C., Nicolas, M., Keller, L., Shoemaker, D., and Grozinger, C. M. (2014). Molecular and social regulation of worker division of labour in fire ants. *Mol. Ecol.* 23, 660–672. doi: 10.1111/mec.12626

Matsuura, K., Himuro, C., Yokoi, T., Yamamoto, Y., Vargo, E. L., and Keller, L. (2010). Identification of a pheromone regulating caste differentiation in termites. *Proc. Natl. Acad. Sci. U.S.A.* 107, 12963–12968. doi: 10.1073/pnas.1004675107

McKenzie, S. K., Fetter-Pruneda, I., Ruta, V., and Kronauer, D. J. (2016). Transcriptomics and neuroanatomy of the clonal raider ant implicate an expanded clade of odorant receptors in chemical communication. *Proc. Natl. Acad. Sci. U.S.A.* 113, 14091–14096. doi: 10.1073/pnas.1610800113

Metcalf, R. A., and Whitt, G. S. (1977). Intra-nest relatedness in the social wasp *Polistes metricus*. *Behav. Ecol. Sociobiol.* 2, 339–351. doi: 10.1007/BF00299504

Mohammedi, A., Paris, A., Crauser, D., and Le Conte, Y. (1998). Effect of aliphatic esters on ovary development of queenless bees (*Apis mellifera* L.). *Naturwissenschaften* 85, 455–458. doi: 10.1007/s001140050531

Mutti, N. S., Dolezal, A. G., Wolschin, F., Mutti, J. S., Gill, K. S., and Amdam, G. V. (2011). IRS and TOR nutrient-signaling pathways act via juvenile hormone to influence honey bee caste fate. *J. Exp. Biol.* 214, 3977–3984. doi: 10.1242/jeb.061499

Nakanishi, A., Nishino, H., Watanabe, H., Yokohari, F., and Nishikawa, M. (2010). Sex-specific antennal sensory system in the ant *Camponotus japonicus*: glomerular organizations of antennal lobes. *J. Comp. Neurol.* 518, 2186–2201. doi: 10.1002/cne.22326

Naumann, K., Winston, M. L., Slessor, K. N., Prestwich, G. D., and Webster, F. X. (1991). Production and transmission of honey bee queen (*Apis mellifera* L.) mandibular gland pheromone. *Behav. Ecol. Sociobiol.* 29, 321–332. doi: 10.1007/bf00165956

Oi, C. A., Oliveira, R. C., van Zweden, J. S., Mateus, S., Millar, J. G., Nascimento, F. S., et al. (2019). Do primitively eusocial wasps use queen pheromones to regulate reproduction? a case study of the paper wasp *Polistes satan*. *Front. Ecol. Evol.* 7:199. doi: 10.3389/fevo.2019.00199

Oi, C. A., van Zweden, J. S., Oliveira, R. C., Van Oystaeyen, A., Nascimento, F. S., and Wenseleers, T. (2015). The origin and evolution of social insect queen pheromones: novel hypotheses and outstanding problems. *Bioessays* 37, 808–821. doi: 10.1002/bies.201400180

Oliveira, R. C., Vollet-Neto, A., Akemi Oi, C., van Zweden, J. S., Nascimento, F., Sullivan Brent, C., et al. (2017). Hormonal pleiotropy helps maintain queen signal honesty in a highly eusocial wasp. *Sci. Rep.* 7, 1–12. doi: 10.1038/s41598-017-01794-1

Orlova, M., and Amsalem, E. (2019). Context matters: plasticity in response to pheromones regulating reproduction and collective behavior in social Hymenoptera. *Curr. Opin. Insect Sci.* 35, 69–76. doi: 10.1016/j.cois.2019.07.004

Orlova, M., and Hefetz, A. (2014). Distance from the queen affects workers' selfish behaviour in the honeybee (*A. mellifera*) colony. *Behav. Ecol. Sociobiol.* 68, 1693–1700. doi: 10.1007/s00265-014-1777-9

Orlova, M., Starkey, J., and Amsalem, E. (2020). A small family business: synergistic and additive effects of the queen and the brood on worker reproduction in a primitively eusocial bee. *J. Exp. Biol.* 223:547. doi: 10.1242/jeb.217547

Oxley, P. R., Ji, L., Fetter-Pruneda, I., McKenzie, S. K., Li, C., Hu, H., et al. (2014). The genome of the clonal raider ant *Cerapachys biroi*. *Curr. Biol.* 24, 451–458. doi: 10.1016/j.cub.2014.01.018

Ozaki, M., Wada-Katsumata, A., Fujikawa, K., Iwasaki, M., Yokohari, F., Satoji, Y., et al. (2005). Ant nestmate and non-nestmate discrimination by a chemosensory sensillum. *Science* 309, 311–314. doi: 10.1126/science.1105244

Padilla, M., Amsalem, E., Altman, N., Hefetz, A., and Grozinger, C. M. (2016). Chemical communication is not sufficient to explain reproductive inhibition in the bumblebee *Bombus impatiens*. *R. Soc. Open Sci.* 3:160576. doi: 10.1098/rsos.160576

Page, R. E. Jr., and Amdam, G. V. (2007). The making of a social insect: developmental architectures of social design. *Bioessays* 29, 334–343. doi: 10.1002/bies.20549

Pamminger, T., and Hughes, W. O. (2017). Testing the reproductive groundplan hypothesis in ants (Hymenoptera: Formicidae). *Evolution* 71, 153–159. doi: 10.1111/evo.13105

Pandey, A., and Bloch, G. (2015). Juvenile hormone and ecdysteroids as major regulators of brain and behavior in bees. *Curr. Opin. Insect. Sci.* 12, 26–37. doi: 10.1016/j.cois.2015.09.006

Pask, G. M., Slone, J. D., Millar, J. G., Das, P., Moreira, J. A., Zhou, X., et al. (2017). Specialized odorant receptors in social insects that detect cuticular hydrocarbon cues and candidate pheromones. *Nat. Commun.* 8:297. doi: 10.1038/s41467-017-00099-1

Peeters, C., and Liebig, J. (2009). "Fertility signaling as a general mechanism of regulating reproductive division of labor in ants," in *Organization of Insect Societies: From Genome to Socio-Complexity*, eds J. Gadau and J. Fewell (Cambridge: Harvard University Press), 220–242.

Peso, M., Elgar, M. A., and Barron, A. B. (2015). Pheromonal control: reconciling physiological mechanism with signalling theory. *Biol. Rev.* 90, 542–559. doi: 10.1111/brv.12123

Peter, A. (2002). "Oviposition pheromones in herbivorous and carnivorous insects," in *Chemoecology of Insect Eggs and Egg Depositions*, eds M. Hilker and T. Meiners (Oxford: Blackwell Publishing), 235–263. doi: 10.1002/9780470760253.ch9

Princen, S. A., Van Oystaeyen, A., Petit, C., van Zweden, J. S., Wenseleers, T., and Smiseth, P. (2019). Cross-activity of honeybee queen mandibular pheromone in bumblebees provides evidence for sensory exploitation. *Behav. Ecol.* 31, 303–310. doi: 10.1093/beheco/arz191

Reichert, M. S., and Quinn, J. L. (2017). Cognition in contests: mechanisms, ecology, and evolution. *Trends Ecol. Evol.* 32, 773–785. doi: 10.1016/j.tree.2017.07.003

Schultner, E., Oettler, J., and Helantera, H. (2017). The role of brood in eusocial Hymenoptera. *Q. Rev. Biol.* 92, 39–78. doi: 10.1086/690840

Sharma, K. R., Enzmann, B. L., Schmidt, Y., Moore, D., Jones, G. R., Parker, J., et al. (2015). Cuticular hydrocarbon pheromones for social behavior and their coding in the ant antenna. *Cell Rep.* 12, 1261–1271. doi: 10.1016/j.celrep.2015.07.031

Sledge, M. F., Boscaro, F., and Turillazzi, S. (2001). Cuticular hydrocarbons and reproductive status in the social wasp *Polistes dominulus*. *Behav. Ecol. Sociobiol.* 49, 401–409. doi: 10.1007/s002650000311

Slessor, K. N., Kaminski, L. A., King, G. G. S., Borden, J. H., and Winston, M. L. (1988). Semiochemical basis of the retinue response to queen honey bees. *Nature* 332, 354–356. doi: 10.1038/332354a0

Smith, A. A., Holldobler, B., and Liebig, J. (2009). Cuticular hydrocarbons reliably identify cheaters and allow enforcement of altruism in a social insect. *Curr. Biol.* 19, 78–81. doi: 10.1016/j.cub.2008.11.059

Smith, A. A., Holldobler, B., and Liebig, J. (2012). Queen-specific signals and worker punishment in the ant *Aphaenogaster cockerelli*: the role of the Dufour's gland. *Anim. Behav.* 83, 587–593. doi: 10.1016/j.anbehav.2011.12.024

Smith, A. A., and Liebig, J. (2017). The evolution of cuticular fertility signals in eusocial insects. *Curr. Opin. Insect Sci.* 22, 79–84. doi: 10.1016/j.cois.2017.05.017

Smith, C. D., Zimin, A., Holt, C., Abouheif, E., Benton, R., Cash, E., et al. (2011). Draft genome of the globally widespread and invasive Argentine ant (*Linepithema humile*). *Proc. Natl. Acad. Sci. U.S.A.* 108, 5673–5678. doi: 10.1073/pnas.1008617108

Soroker, V., Vienne, C., and Hefetz, A. (1995). Hydrocarbon dynamics within and between nestmates in *Cataglyphis niger* (Hymenoptera: Formicidae). *J. Chem. Ecol.* 21, 365–378. doi: 10.1007/bf02036724

Stabentheiner, A., Kovac, H., and Brodschneider, R. (2010). Honeybee colony thermoregulation - regulatory mechanisms and contribution of individuals in dependence on age, location and thermal stress. *PLoS One* 5:e8967. doi: 10.1371/journal.pone.0008967

Starkey, J., Brown, A., and Amsalem, E. (2019a). The road to sociality: brood regulation of worker reproduction in the simple eusocial bee *Bombus impatiens*. *Anim. Behav.* 154, 57–65. doi: 10.1016/j.anbehav.2019.06.004

Starkey, J., Derstine, N., and Amsalem, E. (2019b). Do bumble bees produce brood pheromones? *J. Chem. Ecol.* 45, 725–734. doi: 10.1007/s10886-019-01101-4

Steitz, I., and Ayasse, M. (2020). Macrocyclic lactones act as a queen pheromone in a primitively eusocial sweat bee. *Curr. Biol.* 30, 1136–1141. doi: 10.1016/j.cub.2020.01.026

Stokl, J., and Steiger, S. (2017). Evolutionary origin of insect pheromones. *Curr. Opin. Insect Sci.* 24, 36–42. doi: 10.1016/j.cois.2017.09.004

Tibbetts, E. A., Fearon, M. L., Wong, E., Huang, Z. Y., and Tinghitella, R. M. (2018). Rapid juvenile hormone downregulation in subordinate wasp queens facilitates stable cooperation. *Proc. R. Soc. B* 285:2645. doi: 10.1098/rspb.2017.2645

Tibbetts, E. A., and Lindsay, R. (2008). Visual signals of status and rival assessment in *Polistes dominulus* paper wasps. *Biol. Lett.* 4, 237–239. doi: 10.1098/rsbl.2008.0048

Ulrich, Y., Burns, D., Libbrecht, R., and Kronauer, D. J. (2016). Ant larvae regulate worker foraging behavior and ovarian activity in a dose-dependent manner. *Behav. Ecol. Sociobiol.* 70, 1011–1018. doi: 10.1007/s00265-015-2046-2

Van Oystaeyen, A., Oliveira, R. C., Holman, L., van Zweden, J. S., Romero, C., Oi, C. A., et al. (2014). Conserved class of queen pheromones stops social insect workers from reproducing. *Science* 343, 287–290. doi: 10.1126/science.1244899

Velasque, M., Qiu, L., and Mikheyev, A. S. (2018). The doublesex sex determination pathway regulates reproductive division of labor in honey bees. *bioRxiv* [Preprint], doi: 10.1101/314492

Vergoz, V., McQuillan, H. J., Geddes, L. H., Pullar, K., Nicholson, B. J., Paulin, M. G., et al. (2009). Peripheral modulation of worker bee responses to queen mandibular pheromone. *Proc. Natl. Acad. Sci. U.S.A.* 106, 20930–20935. doi: 10.1073/pnas.0907563106

Villalta, I., Abril, S., Cerda, X., and Boulay, R. (2018). Queen control or queen signal in ants: what remains of the controversy 25 years after Keller and Nonacs' seminal paper? *J. Chem. Ecol.* 44, 805–817. doi: 10.1007/s10886-018-0974-9

Wanner, K. W., Nichols, A. S., Walden, K. K., Brockmann, A., Luetje, C. W., and Robertson, H. M. (2007). A honey bee odorant receptor for the queen substance 9-oxo-2-decenoic acid. *Proc. Natl. Acad. Sci. U.S.A.* 104, 14383–14388. doi: 10.1073/pnas.0705459104

West-Eberhard, M. J. (1987). "Flexible strategy and social evolution," in *Animal Societies. Theories and Facts*, eds Y. Ito, J. L. Brown, and J. Kikkawa (Tokyo: Japan Scientific Societies Press), 35–51.

Wilson, E. O. (1971). *The Insect Societies*. Cambridge: Harvard University Press.

Wyatt, T. D. (2014). *Pheromones and Animal Behavior: Chemical Signals and Signatures*. Cambridge: Cambridge University Press.

Yan, H., Opachaloemphan, C., Mancini, G., Yang, H., Gallitto, M., Mlejnek, J., et al. (2017). An engineered orco mutation produces aberrant social behavior and defective neural development in ants. *Cell* 170, 736–747. doi: 10.1016/j.cell.2017.06.051

Zhou, X., Slone, J. D., Rokas, A., Berger, S. L., Liebig, J., Ray, A., et al. (2012). Phylogenetic and transcriptomic analysis of chemosensory receptors in a pair of divergent ant species reveals sex-specific signatures of odor coding. *PLoS Genet.* 8:e1002930. doi: 10.1371/journal.pgen.1002930

Conflict of Interest: The authors declare that the research was conducted in the absence of any commercial or financial relationships that could be construed as a potential conflict of interest.

frontiers in Genetics

REVIEW
published: 10 September 2020
doi: 10.3389/fgene.2020.01027

Diversity of Insect Sesquiterpenoid Regulation

Stacey S. K. Tsang[1†], Sean T. S. Law[1†], Chade Li[1†], Zhe Qu[1], William G. Bendena[2], Stephen S. Tobe[3] and Jerome H. L. Hui[1]*

[1] Simon F.S. Li Marine Science Laboratory, State Key Laboratory of Agrobiotechnology, School of Life Sciences, The Chinese University of Hong Kong, Hong Kong, China, [2] Department of Biology, Queen's University, Kingston, ON, Canada, [3] Department of Cell and Systems Biology, University of Toronto, Toronto, ON, Canada

Insects are arguably the most successful group of animals in the world in terms of both species numbers and diverse habitats. The sesquiterpenoids juvenile hormone, methyl farnesoate, and farnesoic acid are well known to regulate metamorphosis, reproduction, sexual dimorphism, eusociality, and defense in insects. Nevertheless, different insects have evolved with different sesquiterpenoid biosynthetic pathway as well as products. On the other hand, non-coding RNAs such as microRNAs have been implicated in regulation of many important biological processes, and have recently been explored in the regulation of sesquiterpenoid production. In this review, we summarize the latest findings on the diversity of sesquiterpenoids reported in different groups of insects, as well as the recent advancements in the understanding of regulation of sesquiterpenoid production by microRNAs.

Keywords: insect, sesquiterpenoid, juvenile hormone, microRNA, evolution

OPEN ACCESS

Edited by:
Zhongxia Wu,
Henan University, China

Reviewed by:
Wen Liu,
Huazhong Agricultural University, China
Deng Huimin,
South China Normal University, China

***Correspondence:**
Jerome H. L. Hui
jeromehui@cuhk.edu.hk

[†] These authors have contributed equally to this work

Specialty section:
This article was submitted to Epigenomics and Epigenetics, a section of the journal Frontiers in Genetics

Received: *29 May 2020*
Accepted: *11 August 2020*
Published: *10 September 2020*

Citation:
Tsang SSK, Law STS, Li C, Qu Z, Bendena WG, Tobe SS and Hui JHL (2020) Diversity of Insect Sesquiterpenoid Regulation. Front. Genet. 11:1027. doi: 10.3389/fgene.2020.01027

DIVERSE BIOSYNTHETIC PATHWAYS AND TYPES OF INSECT SESQUITERPENOIDS

In insects and crustaceans, sesquiterpenoid hormones including farnesoic acid (FA), methyl farnesoate (MF) and juvenile hormone (JH) regulate the development, metamorphosis and reproduction (Cheong et al., 2015). The beginning step in the biosynthesis of the sesquiterpenoids starts from acetyl-CoA which goes through the universal eukaryotic mevalonate (MVA) pathway to synthesize farnesyl pyrophosphate (FPP) (Tobe and Bendena, 1999; Belles et al., 2005; Hui et al., 2010, 2013). In the presence of FPP pyrophosphatase, FPP is then converted to farnesol and can further generate farnesal with the catalyzation by farnesol dehydrogenase. Farnesoic acid (FA) will then be generated via further dehydrogenation with farnesal dehydrogenase in different insects. A summary of the sesquiterpenoid biosynthetic pathway is shown in **Figure 1**.

Despite all insects utilizing a common biosynthetic pathway in the production of FA, diverse pathways have evolved in the downstream process of sesquiterpenoids production. For insects in the order blattodea, coleoptera, diptera, and orthoptera, esterification of FA occurs in the corpora allata (CA), which will form MF catalyzed by a *SAM*-dependent juvenile hormone acid *O*-methyltransferase (JHAMT) (Shinoda and Itoyama, 2003). In insects such as cockroaches (Huang et al., 2015), honeybees (Bomtorin et al., 2014), locusts (Marchal et al., 2011), and pea aphids (Daimon and Shinoda, 2013), MF is oxidized by epoxidase CYP15A1 in formation of JH-III (**Figure 1**). Direct applications of FA on fruit flies increased the biosynthesis of MF and JH-III in both larval and adult stages, while JHB3 biosynthesis is inhibited in larvae (Bendena et al., 2011).

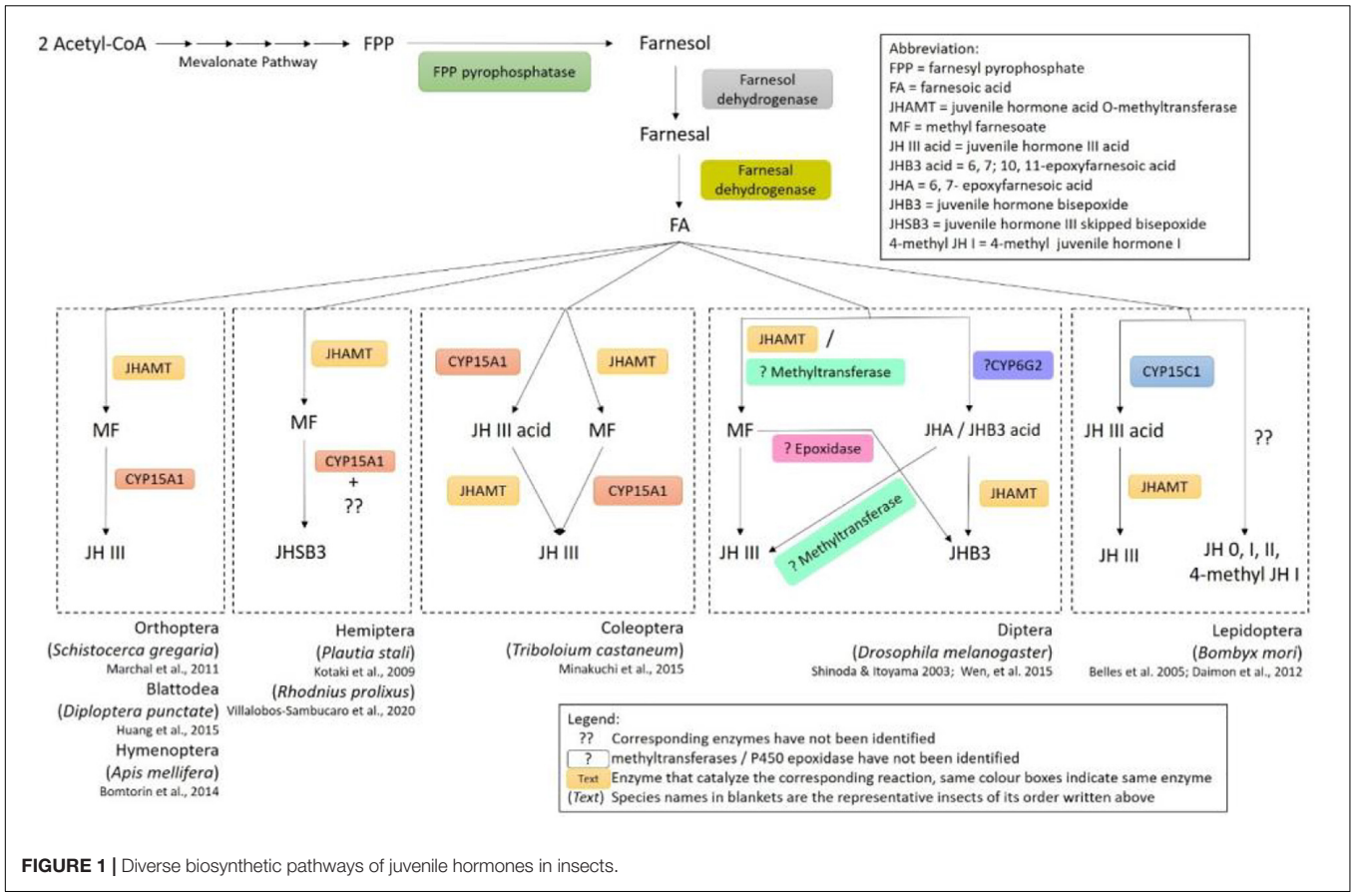

FIGURE 1 | Diverse biosynthetic pathways of juvenile hormones in insects.

TABLE 1 | Different types of juvenile hormones isolated from hexapods.

Type of JH	Chemical structure	Insects	Tissue extracted	References
JH-0	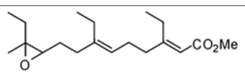	Lepidopterans	EG	Bergot et al., 1980
JH-I	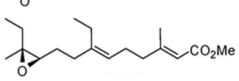		LE, EG	Röller et al., 1967
JH-II	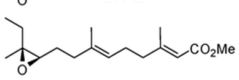		LE, EG	Meyer et al., 1968
4-Methyl JH-I	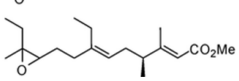		EG	Bergot et al., 1981
JH-III	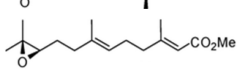	All insects	CA	Judy et al., 1973
JHB3	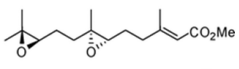	Dipterans	CA	Richard et al., 1989
JHSB3	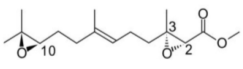	Hemipterans	CA	Kotaki et al., 2009

CA, corpora allata; EG, egg; LE, lipid extract.

Moreover, diverse biosynthetic pathways for production of JH-III have also been identified in other insects (**Figure 1**). For instance, in the coleopterans such as beetles, CYP15A1 can first oxidize FA to form JH-III acid, followed by methylation with JHAMT resulting in the formation of JH-III (Minakuchi et al., 2015; Jiang et al., 2017); while in lepidopterans, the conversion of FA to JH-III acid is performed with another epoxidase CYP15C1 followed by subsequent methylation by JHAMT (Daimon et al., 2012; **Figure 1**). Furthermore, different sesquiterpenoid products have also been identified in various types of insects (**Figure 1** and **Table 1**). In the dipterans including flies, JH-III bisepoxide (JHB3) has been identified

(Richard et al., 1989). In the hemipterans like the stinkbugs, JH-III skipped bisepoxide (JHSB3) is formed (Kotaki et al., 2009); and in the lepidopterans such as moths, specific JH homologs including JH-I, JH-II, JH-0, and 4-methyl JH-I are produced (Belles et al., 2005; **Figure 1** and **Table 1**). It is worth mentioning that JH-I is found in the male accessory glands of the cecropia moth, and whether it performs the suspected hormonal function remains unknown (Paroulek and Sláma, 2014; De Loof and Schoofs, 2019).

DIVERSE ROLES OF SESQUITERPENOIDS IN INSECTS

Regulation of Metamorphosis

A special feature of insects is that they have evolved with distinct modes of metamorphosis, including hemimetaboly (incomplete) and holometaboly (complete) (Sehnal et al., 1996). These biological events are collectively controlled by sesquiterpenoids that inhibit metamorphosis, and ecdysteroids such as 20-hydroxyecysone (20E) that trigger metamorphosis (Konopova et al., 2011; Liu et al., 2018; Niwa and Niwa, 2014a,b). In general, sesquiterpenoid inhibits ecdysteroids action, and when their biosynthesis in the CA is suppressed via the inhibition of JHAMT and 3-hydroxy-3-methylglutaryl Coenzyme-A reductase (HMGR), metamorphosis can then occur (Cheong et al., 2015; Liu et al., 2018; Qu et al., 2018). An overview is shown in **Figure 2**.

In the best studied holometabolous insect, the fly *Drosophila melanogaster*, sesquiterpenoids exert *status quo* function to prevent metamorphosis in the early larval stage (Cheong et al., 2015; Qu et al., 2018). Sesquiterpenoids JH-III, JHB3, and their immediate precursor MF can all bind to the *C*-terminal of the intracellular receptor Methoprene-tolerant (Met) or its paralog named Germ-cell expressed (Gce) in *Drosophila*, which encodes a transcription factor of the bHLH-PAS family (Ashok et al., 1988; Jindra et al., 2015; Wen et al., 2015). The binding affinities of sesquiterpenoids to Gce are differ with a rank order of JH-III > JHB3 > MF which is in line with their developmental potency (Bittova et al., 2019). After the binding of JH with Met or Gce in formation of a functional complex, another bHLH-PAS protein that acts as the steroid receptor co-activator [Taiman (Tai)] in *D. melanogaster* or SRC in other insect species is recruited, which together binds to the specific JH response element (JHRE) on the promoter region of *Krüppel homolog 1* (*Kr-h1*) to activate transcription (Kayukawa et al., 2012; Qu et al., 2018). Previous studies have demonstrated that *Kr-h1* can transduce the JH signal to repress 20E primary responsive genes, including *ecdysone receptor* (*EcR*), *Broad-complex* (*Br-C*), ecdysone-inducible proteins *E75* and *E93*, which subsequently inhibit 20E biosynthesis in the prothoracic gland (Kayukawa et al., 2016; Liu et al., 2018); and can also inhibit the expression of steroidogenic enzyme gene *Spok* by binding to the Kr-h1 binding site (KBS) and turn on the methylation which in turns also leads to the suppression of ecdysone biosynthesis (Song and Zhou, 2019; Zhang T. et al., 2018; **Figures 2**, **3**).

In other holometabolous insects including beetle *Tribolium castaneum*, moths *Bombyx mori* and *Helicoverpa armigera*, as well as hemimetabolous insects including cockroach *Blattella germanica*, planthopper *Nilaparvata lugens*, and stinkbug *Pyrrhocoris apterus* and *Rhodnius prolixus*, *Kr-h1* has also exhibited anti-metamorphic effects (Minakuchi et al., 2009; Konopova et al., 2011; Lozano and Belles, 2011; Kayukawa et al., 2017; Li et al., 2018; Zhang W. N. et al., 2018).

During the larval-pupal transition in *Drosophila*, 20E binds to EcR proteins and Ultraspiracle (Usp) to form a heterodimer (Riddiford et al., 2000), and this complex will further trigger the transcription of 20E primary-response genes including *Br-C*, *E74*, *E75*, and *E93*. These downstream genes have been identified with essential functions in molting. For instances, E93 enables the larval tissues to execute apoptosis and promotes the formation of adult tissues (Ureña et al., 2016); and the Gce/Tai (but not Met/Tai) complex activates E75A functions in preimaginal molts (Dubrovsky et al., 2011). In beetle *T. castaneum*, Met has also proven to bind JH with high affinity via the highly conserved hydrophobic pocket within its PAS-B domain (Charles et al., 2011). In lepidopteran, USP can also bind JH (Dubrovsky, 2005). In moth *Manduca*, JP29 isolated from epidermis has also been suggested as another potential JH receptor, which has found to be highly specific to JH binding but with low affinity (Truman and Riddiford, 2002).

Regulation of Reproduction

Apart from repressing metamorphosis in insects, sesquiterpenoids also play an important role in stimulating reproduction in adult insects, including processes such as vitellogenesis, oogenesis and polyploidization (Wyatt and Davey, 1996). In female *Drosophila,* sesquiterpenoids have long been known to regulate the oogenesis and vitellogenesis (Postlethwait and Weiser, 1973; Swevers et al., 2005; Riddiford, 2012). The titer of JH is promoted with expression of ecdysis triggering hormone (ETH) binding to its receptor (ETHR) whose synthesis is governed by 20E (Meiselman et al., 2017; Roy et al., 2018).

Similar but diverse mechanisms have also been discovered in other insects. In the beetle *T. castaneum,* JH-mediated *Met* and *Kr-h1* promote vitellogenin (Vg) synthesis in the fat body (Parthasarathy et al., 2010; **Figure 4Ai**), and *Met* can also trigger insulin-like peptides (ILPs) *ILP2* and *ILP3* by AKT pathway to phosphorylate the fork head transcription factor (FOXO) and induce *Vg* expression (Sheng et al., 2011; **Figure 4Aii**). In mosquito *Aedes aegypti*, expression of *Kr-h1* triggered by Met together with Cycle and steroid receptor coactivator SRC/FISC after adult emergence supported that sesquiterpenoid is essential for previtellogenic development (Zhu et al., 2010; Shin et al., 2012). In migratory locust *Locusta migratoria*, JH together with Met/SRC complex are found to be pivotal in maintaining *Vg* expression and oocyte development (Song et al., 2014), and can promote cell polyploidization by regulating the expression of *cyclin-dependent kinase 6* (*Cdk6*) and *adenovirus E2 factor-1* (*E2f1*) (Wu et al., 2016; Wu Z. et al., 2018; **Figure 4Aiii**). JH activates Na^+/K^+-ATPase for the induction of patency in vitellogenic follicular epithelium, where Vg can then reach the surface of maturing oocyte (Jing et al., 2018). In the stinkbug *P. apterus*, nevertheless, Vg synthesis is mainly regulated by JH signaling genes *Met* and *Tai* independent of Kr-h1 (Smykal et al., 2014).

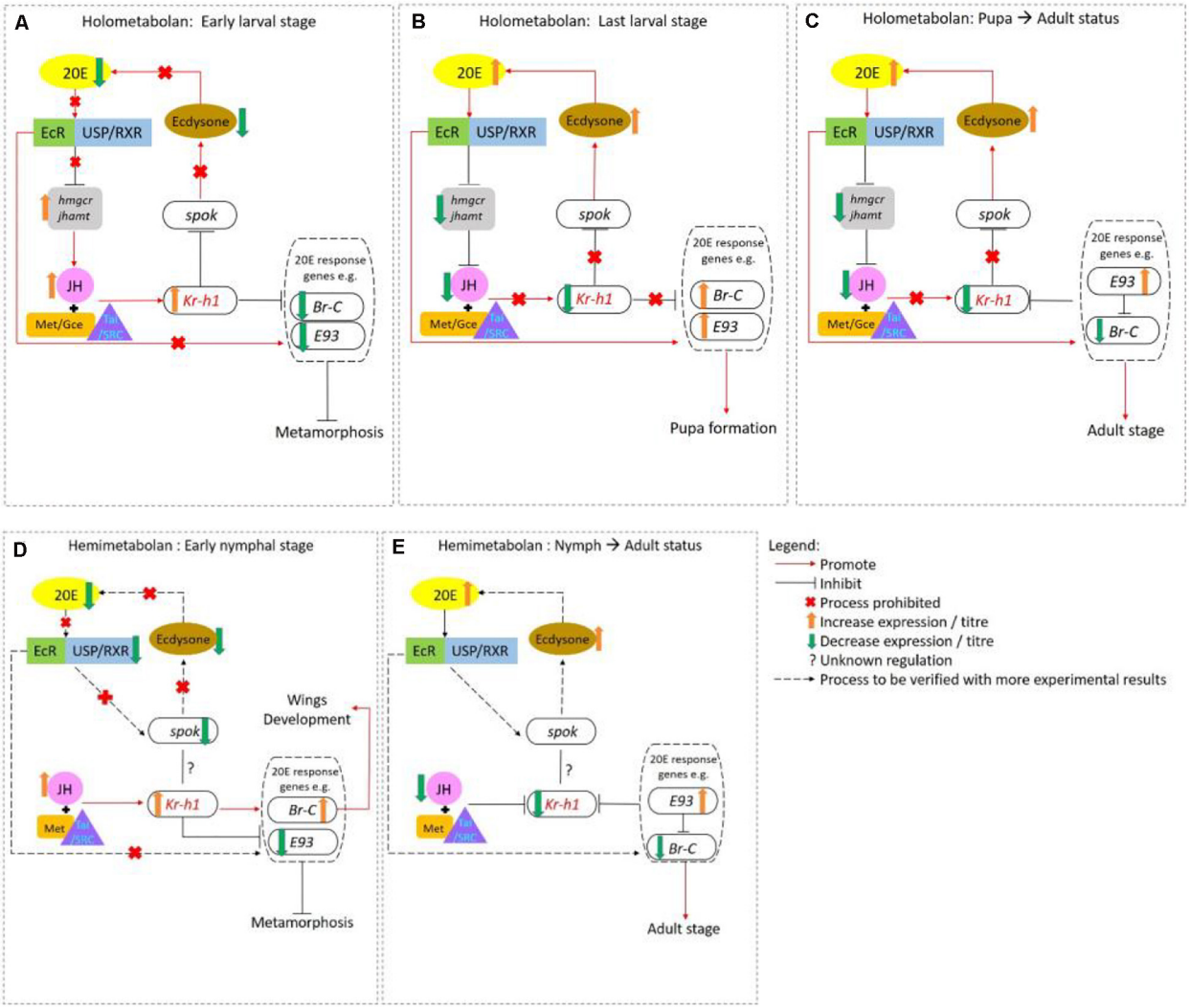

FIGURE 2 | Interaction of sesquiterpenoid juvenile hormone (JH) and ecdysteroid during metamorphosis in holometabolans **(A–C)** and hemimetabolans **(D,E)**. **(A)** In early larval stages of holometabolous insects, JH-Met/Tai receptor complex activates the transcription of primary JH-early responsive gene *Kr-h1* which prevents immature larvae from precocious larval development by inhibiting *Br-C*, *E93,* and *Spok* expression. **(B)** When JH levels drastically drop in the last larval stage, 20E acts through EcR/USP to activate the transcription of 20E-early responsive genes such as *Br-C*, *E93, E74*, *E75*, *Ftz-f1* and initiate larval-pupal transition. **(C)** At the end of the pupal stage, the *Br-C* levels decline again which upregulates the expression of *E93* that drives the pupa-adult transition. In hemimetabolous insect, JH titer remains high from hatching until the last nymphal stage. **(D)** During the early nymphal, high *Kr-h1* expression level is maintained by JH which inhibits metamorphosis by repressing *E93* expression. **(E)** In the last nymphal stage, the JH titers fall followed by the *Kr-h1* expression level. For details, please refer to main text and Truman, 2019.

In addition, sesquiterpenoids can mediate insect reproduction under different light conditions. In aphids, reproductive polyphenism alternates their reproductive modes from parthenogenesis to sexual reproduction given different photoperiodic duration. In *Acyrthosiphon pisum*, enhanced sesquiterpenoid degradation by juvenile hormone esterase (JHE) accounts for the lower JH titer during short-day conditions that produces sexual morphs, in contrast to the higher JH titer in parthenogenetic morphs during long-day conditions (Ishikawa et al., 2012; **Figure 4B**). In beetle *Colaphellus bowringi*, high sesquiterpenoid titer upregulates expression of vitellogenin receptor (VgR) via JH-Met-Kr-h1 signaling and promotes Vg synthesis and ovary development during short-day period, while low JH titer initiates reproductive diapause and promotes lipid storage in the fat body instead of Vg synthesis during the long-day period (Liu et al., 2016, 2019; **Figure 4C**).

Sexual Dimorphism and Dimorphic Behavior

Sexual dimorphism is commonly observed in insects. Nevertheless, the extreme sexually dimorphic traits of juvenile-like females without pupation and ephemeral winged males after a pupal stage in scale insects have raised questions as to how these features could arise. By transcriptomic and qRT-PCR analyses

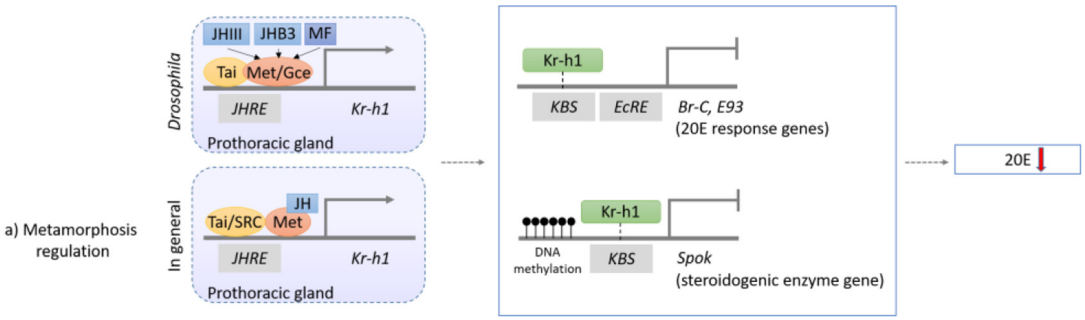

FIGURE 3 | Schematic diagram showing the mechanism of sesquiterpenoids in metamorphosis regulation in *Drosophila* and other insects. In fly *Drosophila*, JH-III, JHB3, and MF will bind to the JH receptor Met or Gce, while in other insects, JH-III will bind to Met in other insects (for details, please refer to text). The complex will then further dimerize with Tai and bind to specific JHRE to initiate the expression of *Kr-h1*. Kr-h1 protein will then bind to the KBS to inhibit expressions of 20E response genes (*Br-C* and *E93*), and will also bind to KBS and initiates DNA methylation of a steroidogenic enzyme gene *Spok*, which will all result in the lower titer of 20E and inhibition of metamorphosis.

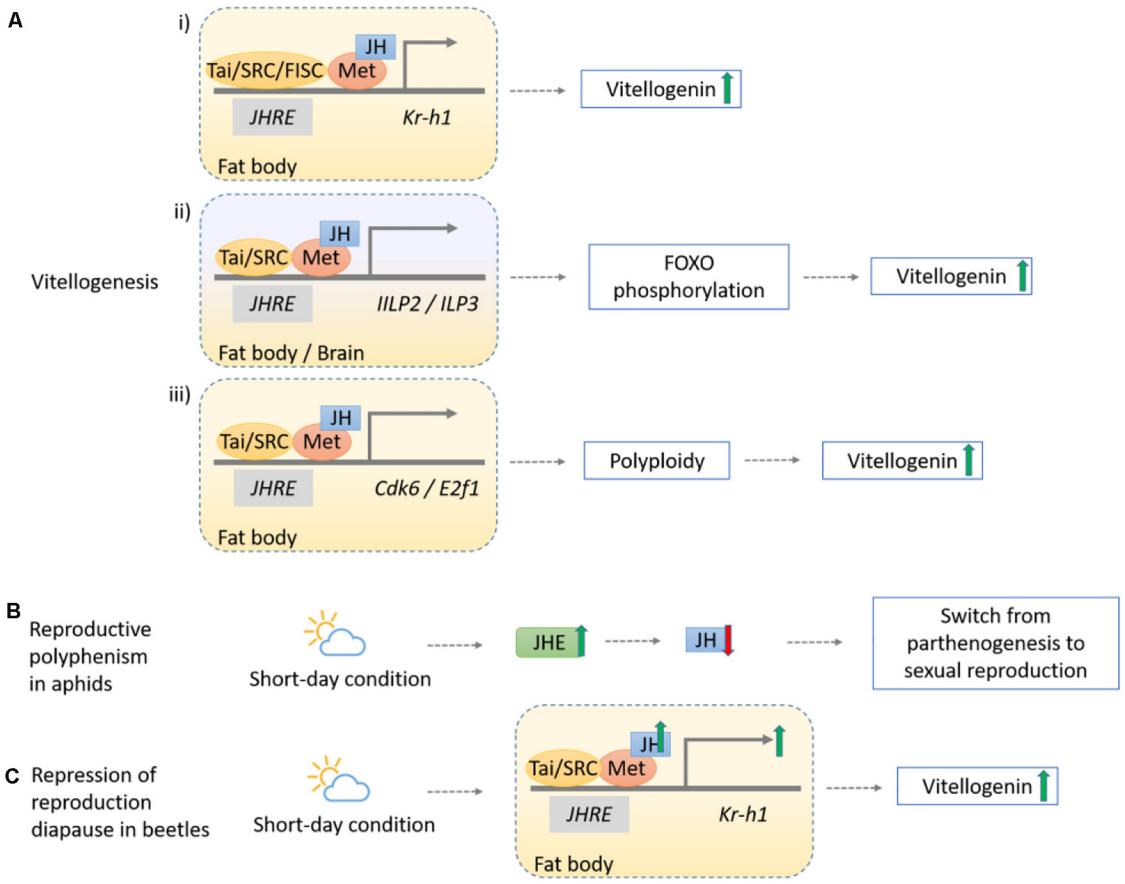

FIGURE 4 | Schematic diagram showing the mechanisms of sesquiterpenoids in regulation of insect reproduction**. (Ai)** The JH-Met-Tai/SRC complex upregulates Kr-h1 to increase Vg synthesis level, as observed in *T. castaneum*, *A. aegypti* (with an additional complex FISC), *L. migratoria* but not in *P. apterus*. **(Aii)** The JH-Met-Tai complex initiates transcriptions of *ILP2* and *ILP3*, which phosphorylates the fork head transcription factor (FOXO) through ILP signaling pathway and induces *Vg* expression in *T. castaneum*. **(Aiii)** The JH-Met-Tai/SRC complex promotes expression of core mediators in cell cycle progression, *Cdk6* and *E2f1*, to facilitate vitellogenesis in *L. migratoria*. **(B)** Reproductive polyphenism in aphid *A. pisum* occurs during the short-day condition given the increased JHE activity, and the lowering of JH result in the switch from parthenogenesis to sexual reproduction. **(C)** Repression of reproduction diapause in beetles *C. bowringi* initiates in short-day condition where the upregulation of the JH-Met-Kr-h1 pathway genes expression increases Vg synthesis.

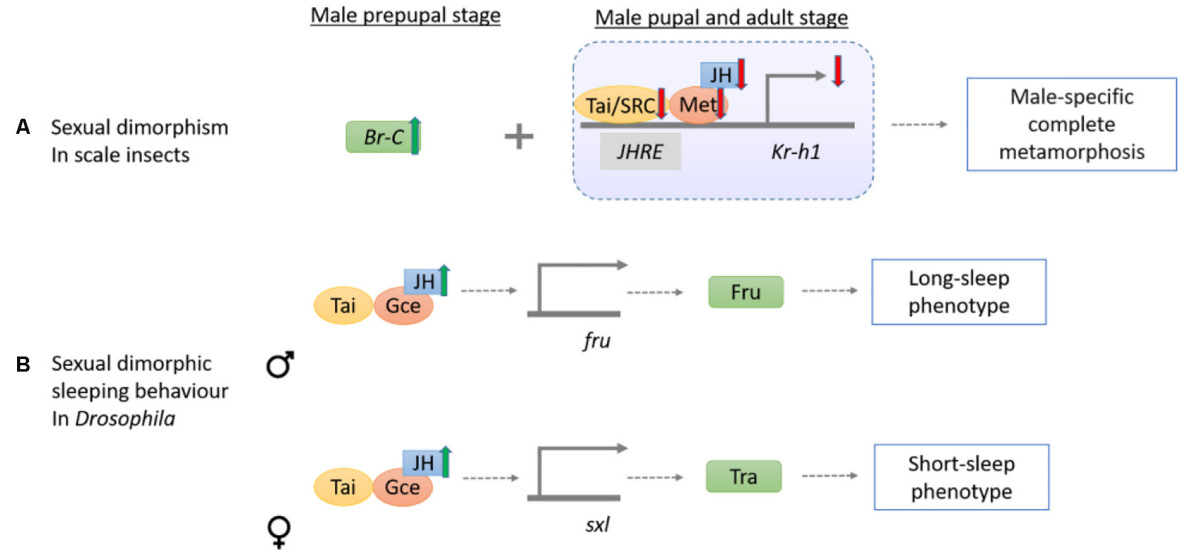

FIGURE 5 | Schematic diagram showing the mechanisms of sesquiterpenoids in regulation of insect sexual dimorphism and dimorphic behavior. **(A)** In scale insects, sexual dimorphism of winged male adults is linked to the signaling of JH, Met, Tai/SRC, and *Kr-h1*, whereas they are increased in early developmental stages but decreased during the pupal and adult stages. **(B)** The sexual dimorphic sleeping behavior in *Drosophila* is maintained by the JH-Gce signal on the *fru* and *sxl* genes in male and female, respectively. *fru* then encodes Fru for inducing long-sleep pattern in male while *sxl* induces Tra for short-sleep phenotype in female.

of post-embryonic stages of *Ericerus pela*, lower *Met*, *Tai,* and *Kr-h1* expression levels are found in pupal and adult males as compared to females. Together with a surge in *Br-C* expression in male prepupal stage, the sex-specific regulation lead to the complete metamorphosis in males but not in females (Yang et al., 2015; **Figure 5A**). In another scale insect *Planococcus kraunhiae*, qRT-PCR analysis on a daily sampling of different development stages reveal that expression levels of *Kr-h1* are higher in male-biased embryos and early nymphs, and lower during prepupal and after pupal stages (Vea et al., 2016). However, elevation of JH or *Met*, *Tai,* and *Kr-h1* gene expressions as observed in *E. pela* is not found in the adult *P. kraunhiae* females.

In *Drosophila*, JH can also control sexual dimorphic behaviors including locomotory and sleeping activities (Belgacem and Martin, 2007; Wu B. et al., 2018; **Figure 5B**). In the presence of JH by overexpression of *JHAMT*, longer sleep in males and shorter sleep in females are observed (Wu B. et al., 2018). Interestingly, *gce* mutant male flies sleep less while female sleep more but mutation in the *Met* dose not exhibit a similar result (Wu B. et al., 2018). The binary switch gene *sex-lethal* (Sxl) can impose female development via promoting expression of *fruitless* (*fru*), *doublesex* (*dsx*), and *transformer* (*tra*). Male development occurs when sxl is turned off (Kappes et al., 2011). In the *jhamt* and *gce* mutant, Fru, sxl, and tra transcript level were almost halved. Decreasing sleep time occurred when *fru* in male flies and when female *tra* was expressed in Fru neurons of males, suggesting JH-Gce signaling can potentially act as a regulatory pathway in sexually dimorphic sleep pattern (Wu B. et al., 2018).

Eusociality

Some insects such as ants, bees, termites and wasps are well known for their eusociality in which they live cooperatively in a colony and only some individuals are reproductive. Such processes have also been linked to JH.

Across ant species, the effects of JH act with different eusocial complexity (**Figure 6A**). For ants with simple, queenless societies, e.g., *Streblognathus* and *Diacamma*, low JH titer is recorded in the gamergates with high individual ranks within the hierarchy, and elevated JH level result in a loss of the reproductive status of the alpha workers (Sommer et al., 1993; Cuvillier-Hot et al., 2004; Brent et al., 2006). For species that have secondarily revert to queenless, simple societies, e.g., *Dinoponera quadriceps*, JH application can increase the regressed ovaries in queenless ants (Norman et al., 2019). For ants with complex society such as *Pogonomyrmex rugosus*, JH analogs (methoprene) stimulate the production of queens and upregulate *Vg* gene expression. The effect of JH in ants is interpreted as mimicking the effect of hibernation (Libbrecht et al., 2013), where low temperature or the associated photoperiod changes up-regulate the insulin/insulin-like growth factor signaling pathway (IIS) genes in queens. No direct result has proven the relationship of IIS and JH in ants to date, and yet, the production of JH in the CA is affected by the release of neuropeptides regulated by IIS in *Drosophila* (Tu et al., 2005). JH may also directly or indirectly regulate of caste polyethism via changing the division of labor and maternal effects. Elevated JH titer can alter the behavior of workers of *Acromyrmex octospinosus* leaf-cutting ants by making them more active, threat responsive, and less interested in intranida works such as taking care of larva and fungal cultivation (Norman and Hughes, 2016). During the maternal stage of *Pogonomyrmex* harvest ants, additional JH also resulted in a 50% increase in worker body size and significantly reduced in total number of progeny reared (Cahan et al., 2011).

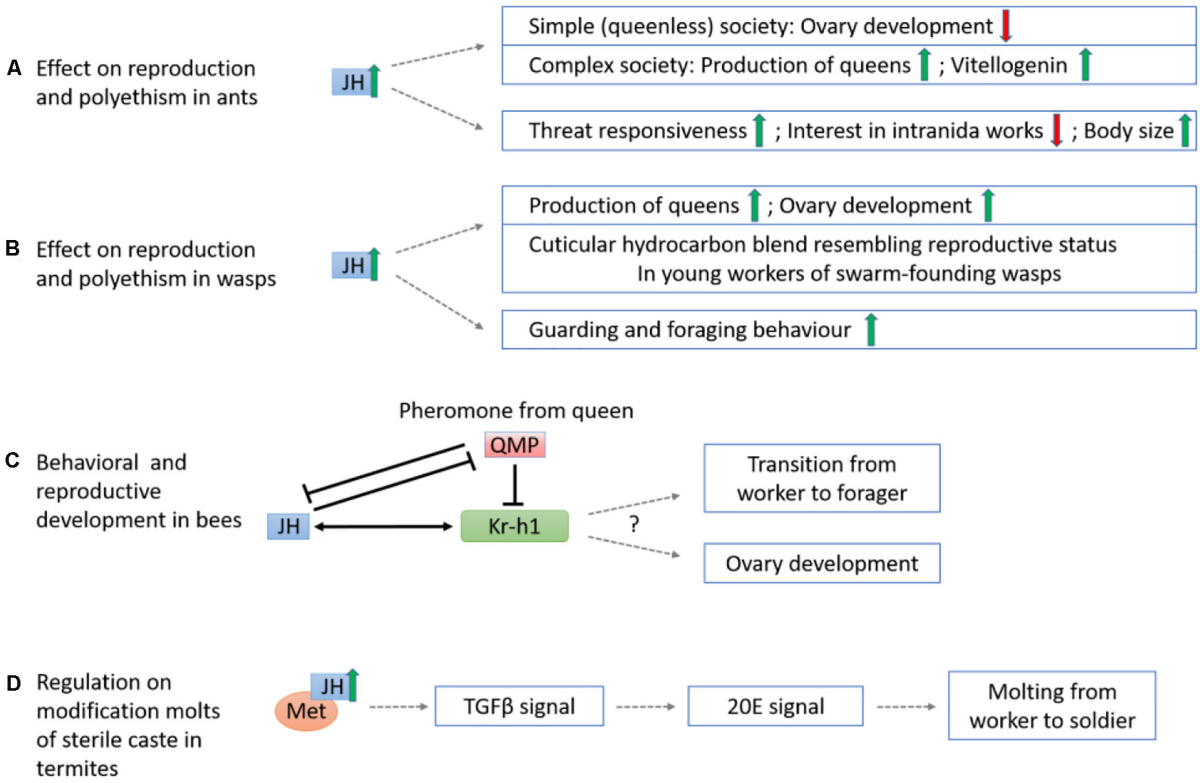

FIGURE 6 | Schematic diagram showing the mechanisms of sesquiterpenoids in regulation of insect eusociality. **(A)** The effect of JH on reproduction and polyethism in ants. The elevation of JH represses ovary development in simple, queenless societies but promotes queen production and vitellogenin expression in complex societies. JH also induces threat responsiveness and reduces interest in intraida works in ants, and may also increase their body size. **(B)** The effect of JH on reproduction and polyethism in wasps. JH generally stimulates the production of queens and ovary development, and mediates cuticular hydrocarbon blend resembling reproductive status in young workers of swarm-founding wasps. Besides, JH triggers the guarding and foraging behavior. **(C)** The queen releases QMP which downregulates JH and *Kr-h1* and thus inhibits ovary development of workers and the transition from in-hive worker to forager in bees. **(D)** The increase of JH in JH-Met signaling pathway induces TGFβ and 20E signals that promote the modification molts from worker to soldier in the sterile caste of termite *Z. nevadensis*.

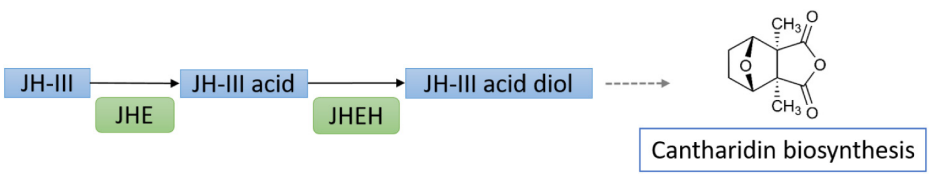

FIGURE 7 | Schematic diagram showing the potential involvement of juvenile hormone in regulation of insect defensive toxin production. The metabolism of JH-III through its degradation pathway by JHE and JHEH is essential for the biosynthesis of the defensive toxin cantharidin in blister beetles.

Similarly, JH also appears to have different effects on wasp species with various eusociality (**Figure 6B**). Previous studies indicated JH could modulate age polyethism and promote the production of foragers in highly eusocial species such as *Polybiine* wasps (O'Donnell and Jeanne, 1993; O'Donnell, 1998), and could mediate both age polyethism (Shorter and Tibbetts, 2009) and reproductive division of labor in primitively eusocial species such as *Polistes*. Application of JH analog methoprene promotes the onset of guarding behavior, the number of foraging females, and stimulates the production of queens (Barth et al., 1975; Röseler et al., 1980, 1984, 1985; Lozano et al., 2015; Giray et al., 2005). Nevertheless, in other primitive eusocial species such as *Ropalidia marginata* that has both post-imaginal regulation of reproductive division of labor and age polyethism, JH could only accelerate ovarian development but not age polyethism (Agrahari and Gadagkar, 2003). For caste-flexible swarm-founding wasp *Synoeca surinama*, JH functions as gonadotropin and directly modifies the cuticular hydrocarbon blend of young workers to resemble that of a reproductive one but does not necessarily link to dominance behavior (Kelstrup et al., 2014).

It is worth also noting that the response to JH could be different among members of the same colony. In *Polistes canadensis,* the effect of JH on ovaries are different between queens and workers as a potential trophic advantage of the queens

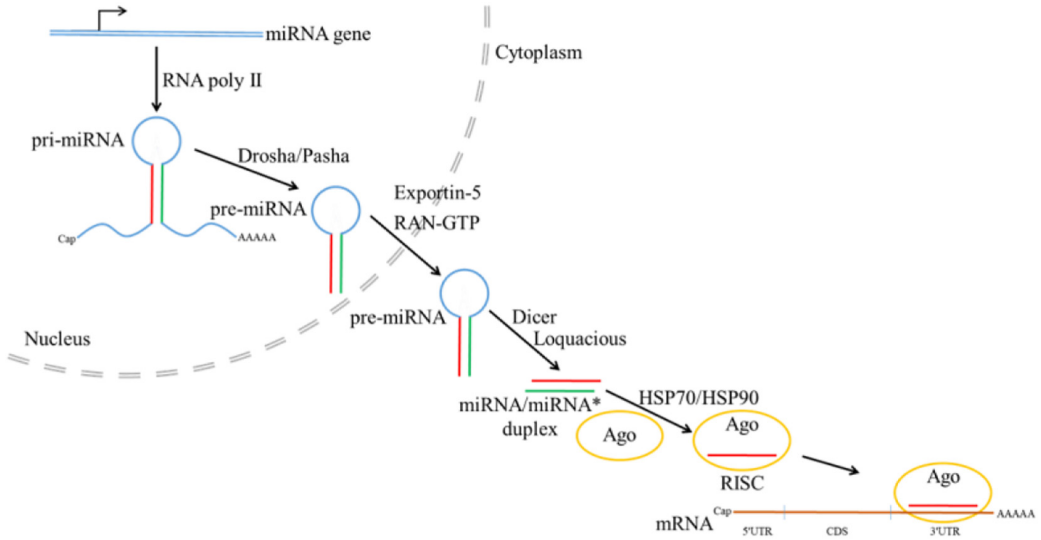

FIGURE 8 | Canonical microRNA biogenesis pathway in *Drosophila* (the figure is summarized from Bartel, 2004; Denli et al., 2004; Kim et al., 2009; Iwasaki et al., 2010; Cao et al., 2017; Qu et al., 2018).

over the workers (Giray et al., 2005), while in *Polistes dominulus* where queens nest cooperatively with other queens, JH has a stronger effect on the dominance, fertility, and aggressiveness of large queens (Tibbetts and Izzo, 2009; Tibbetts et al., 2011, 2018). In species *Polistes metricus* with non-cooperative nest-founding queen pattern, JH leads to an increase of fertility for all individuals, but among the cooperative workers, large workers increase their fertility in response to JH more while small workers do not (Tibbetts and Sheehan, 2012).

In honeybees *Apis mellifera*, repression of ovary development, of in-hive workers, were induced by the downregulation of *Kr-h1* expression controlled by the queen's release of mandibular pheromone (QMP) (Grozinger and Robinson, 2007; **Figure 6C**). In methoprene (JH analog)-treated workers, *Kr-h1* expression is no longer repressed by QMP suggesting an antagonistic relationship between sesquiterpenoids and QMP. In addition, the transition of working to foraging behavior were also found to link to a higher JH titer and *Kr-h1* level (Grozinger and Robinson, 2007). On the other hand, in the bumblebee *Bombus terrestris*, similar to the honeybee mentioned above, QMP reduces *Kr-h1* level but the difference in *Kr-h1* expression between the working and foraging bees are not significant (Shpigler et al., 2010). However, among a group of queenless workers, the dominant individuals have a higher *Kr-h1* expression with active ovaries whereas subordinate individuals have a downregulated *Kr-h1* expression level with undeveloped ovaries (Shpigler et al., 2010). These studies highlighted the possible roles of sesquiterpenoids in the eusociality in bees.

In termites, eusociality is maintained through differentiation into reproductive caste and sterile soldier caste, in which a higher JH titer induces differentiation of workers via an intermediate presoldier stage to become sterile soldiers (Roisin, 1996). Transcriptomic and RNA interference (RNAi) analyses in three molting stages (worker, presoldier and soldier) of termite *Zootermopsis nevadensis* show that the JH-Met and transforming growth factor beta (TGFβ) pathways are involved in the ecdysteroid synthesis for molting in soldier formation (Masuoka et al., 2018; **Figure 6D**). However, suppression on *Kr-h1* via RNAi has no effect on JH analog induced molting, demonstrating that the molting effect mainly depends on JH-Met induced pathways (Masuoka et al., 2018). This in turn also suggested that JH may alternatively promotes molting instead of solely inhibiting metamorphosis.

Defense

Terpenes in plants have been the major focus on the understanding the plant defense against the insects, and the role of sesquiterpenoids in insect defense has also been documented in a much lesser extent when comparing to the aforementioned roles. In blister beetles, sesquiterpenoid cantharidin is produced and released as a defensive toxin during disturbance (Carrel et al., 1993). Transcriptomic analyses on *Mylabris cichorii* identified that the mevalonate pathway in synthesis of JH is correlated with the cantharidin biosynthesis (Huang et al., 2016). In another blister beetle *Epicauta chinensis*, RNAi knockdown of *CYP15A1* and JH epoxide hydrolase (JHEH) result in inhibition of cantharidin biosynthesis, suggesting degradation of JH-III is essential in producing potential precursors of cantharidin (Jiang et al., 2017; **Figure 7**).

MicroRNA REGULATIONS ON SESQUITERPENOIDS

Non-coding RNAs such as microRNAs (miRNAs) have been implicated in regulation of many important biological processes (Lucas and Raikhel, 2013; Wang et al., 2014; Yang et al., 2014; Cao et al., 2017; Qu et al., 2018). In canonical

TABLE 2 | Published studies of potential microRNA regulators on insect sesquiterpenoid pathway genes.

Species	Target	miRNA	Validation methods	References
Ae. aegypti	*HMGR*	miR-31–5p	*In silico* prediction	Nouzova et al., 2018
	PP-MevD	Bantam-3p, miR-34-5p	*In silico* prediction	
	ALDH	miR-34–5p	*In silico* prediction	
	FPPS	miR-9a-5p, miR-317-3p	*In silico* prediction	
An. gambiae	*JHAMT*	miR-278	*In vitro*	Qu et al., 2017
	Met	miR-8, miR-14, miR-34, miR-278	*In vitro*	
Dr. melanogaster	*JHAMT*	Bantam	*In vivo*	
	JHAMT	miR-252, miR-304	*In vitro*	
	Gce	Let-7, miR-8, miR-14, miR-34, miR-278, miR-304	*In vitro*	
Tr. castaneum	*JHAMT*	bantam, miR-252a, miR-304, let-7, miR-92b	*In vitro*	
	Met	miR-92b	*In vitro*	
	Met	miR-6-3p, miR-9a-3p, miR-9d-3p, miR-11-3p, miR-13-3p, miR-13a-3p, miR-2944a-3p, miR-2944b-3p, miR-2944c-3p, miR-3804a-5p, miR-3893-3p	*In silico* prediction	Wu et al., 2017
	Kr-h1	miR-6-3p, miR-9a-3p, miR-11-3p, miR-13-3p, miR-13a-3p, miR-2548-3p, miR-2944a-3p, miR-2944b-3p, miR-2944c-3p, miR-31a, miR-31b-5p, miR-31c-5p, miR-3893-3p, miR-6531-5p	*In silico* prediction	
Lo. migratoria	*Kr-h1*	Let-7, miR-278	*In vivo*	Song et al., 2018
Bl. germanica	*Kr-h1*	miR-2 family (miR-2, miR-13a, and miR-13b)	*In vivo*	Lozano et al., 2015
Da. pulex	*JHAMT*	Bantam, miR-92, miR-252b	*In vitro*	Qu et al., 2017
	Met	Bantam, miR-278	*In vitro*	
N. denticulata	*JHAMT*	Bantam, miR-92, miR-252	*In vitro*	
	Met	miR-8, miR-34, miR-278	*In vitro*	
S. maritima	*JHAMT*	Let-7, miR-34, miR-252, miR-278	*In vitro*	
Ta. tridentatus	*JHAMT*	Bantam, let-7, miR-34, miR-92, miR-278	*In vitro*	
	Met	Bantam, let-7, miR-8, miR-34, miR-252	*In vitro*	

For details, please refer to the text.

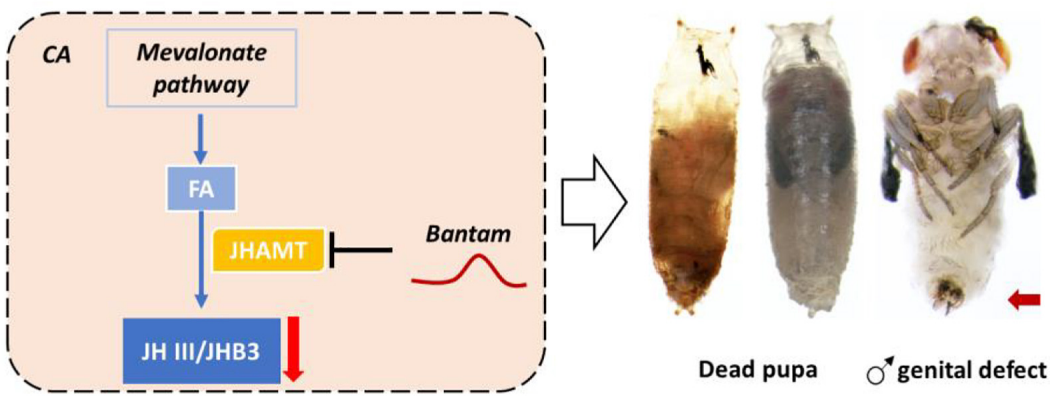

FIGURE 9 | MicroRNA bantam regulates JH titer via targeting *JHAMT* in *D. melanogaster*. Up-regulation of bantam repressed expression of *JHAMT* and reduced the titer of JH III and JHB3, which resulted in dead pupa and male genital defects.

miRNA biogenesis pathway in insects (**Figure 8**), primary miRNA transcript (pri-miRNA) is first transcribed from miRNA gene by RNA polymerase II, followed by processing by Drosha with the help of partner Pasha to generate the precursor miRNA (pre-miRNA) (Denli et al., 2004; Kim et al., 2009). Transported from nucleus to cytoplasm with the help of Exportin-5 and RAN-GTP, pre-miRNA is further processed by Dicer and Loquacious to produce miRNA/miRNA* duplex, which will be loaded into the Argonaute (Ago) by HSP70/HSP90 chaperone machinery to form mature RNA-induced silencing complex (RISC) after strand selection (Bartel, 2004; Kim et al., 2009; Iwasaki et al., 2010). Recently, miRNAs have been explored in the regulation of sesquiterpenoids. In *Blattella germanica*,

silencing the expression of *Dicer-1* shows that miRNAs regulation is related to metamorphosis (Gomez-Orte and Belles, 2009), and treatment of methoprene on *Drosophila* S2 cells also reveal the differential expression of miR-34, miR-100, miR-125, and let-7 (Sempere et al., 2003).

In many insects, miRNAs have also been found to potentially regulate different sesquiterpenoid pathway genes (**Table 2**). For instances, in mosquito *A. aegypti*, four JH biosynthetic enzyme genes including *3-hydroxy-3-methylglutaryl-coenzyme A reductase* (*HMGR*), *diphosphomevalonate decarboxylase* (*PP-MevD*), *aldehyde dehydrogenase* (*ALDH*), and *farnesyl-pyrophosphate synthase* (*FPPS*) were *in silico* predicted to be potentially regulated by miRNAs (Nouzova et al., 2018). In addition, in the adult female mosquito, mosquito specific miR-1890 targets JH-controlled chymotrypsin-like SP, *JHA15* that involve in the regulation of blood digestion, ovary development and egg deposition (Lucas et al., 2015).

In *T. castaneum*, developmental defects and lethality are observed after knocking down *Dcr-1* and *Ago-1*, and *in silico* prediction showed that putative JH receptor *Met* and JH-inducible transcription factor *Kr-h1* were targeted by 11 miRNAs and 14 miRNAs respectively (Wu et al., 2017).

In *L. migratoria*, Ago-1-dependent miRNAs are involved in oogenesis (Song et al., 2013), with let-7 and miR-278 caused decrease of yolk protein precursors results in defects of ovarian development and oocyte maturation through *Kr-h1* (Song et al., 2018), and application of miR-2/13/71 agomiR leads to inhibition of oocyte maturation and ovarian growth whilst the expression level of this miRNA cluster could be decreased to achieve vitellogenesis and oogenesis (Song et al., 2019).

In *B. germanica*, expression of Dicer-1 whose depletion causes sterile females, is negatively related to JH levels, indicating the important roles of miRNAs and interaction between miRNAs and JH in oogenesis (Tanaka and Piulachs, 2012). Specifically, treatment with miR-2-inhibitor on last instar resulted metamorphic defects, and treatment with miR-2 mimic on the Dicer-1-depleted juvenile can complete metamorphosis from nymph to adults (Lozano et al., 2015).

In order to strengthen ability of adaptation, brown planthoppers, *Nilaparvata lugens*, shows polyphenism with two phenotypes, long-winged and short-winged morphs. miR-34, whose expression level can be upregulated or downregulated by JH and 20E, respectively, can target insulin receptor-1 to be involved in the modulation of wing polyphenism (Ye et al., 2019).

In *H. armigera*, 20E and JH are involved in the control of climbing behaviors of single nucleopolyhedrovirus (*HaSNPV*) infected larvae. Methoprene treatment decreases expression of *Br-C Z2* and increases expression of these miRNAs miR-8 and miR-429 which could target *Br-C Z2* (Zhang S. et al., 2018), implying the miRNA-mediated crosstalk between 20E and JH.

In *Drosophila*, miRNA *bantam* has been found to interact with *JHAMT* both *in silico*, *in vitro*, and *in vivo* (Qu et al., 2017). The overexpression of microRNA *bantam* in the brain decreases expression levels of JHAMT.; The knockdown of *bantam* increases the expression level of *JHAMT* (Qu et al., 2017; **Figure 9**). Hormonal measurement in *bantam* mutants demonstrates decreased sesquiterpenoid levels and male genital defects. *bantam* mutant phenotypes can be rescued by exogenous sesquiterpenoid application (Qu et al., 2017). In other arthropods including other insects, crustaceans, myriapod and chelicerate, the roles of *bantam* and other miRNAs on *JHAMT* and *Met* have also been tested both *in silico* and *in vitro*, revealing a conserved system of miRNAs in regulation of sesquiterpenoids established in the arthropod ancestor (Qu et al., 2017; **Table 2**). A list summarizing the latest knowledge on miRNA regulation of sesquiterpenoid pathway genes are shown in **Table 2**.

AUTHOR CONTRIBUTIONS

SSKT, SL, CL, and JH wrote the first draft of the manuscript. All authors proofread the final version of the manuscript.

FUNDING

This work was supported by the Hong Kong Research Grant Council (RGC) General Research Fund (GRF) (14100919, 14100420). SSKT, SL, and CL were supported by studentships by the Chinese University of Hong Kong.

REFERENCES

Agrahari, M., and Gadagkar, R. (2003). Juvenile hormone accelerates ovarian development and does not affect age polyethism in the primitively eusocial wasp, *Ropalidia marginata*. *J. Insect Physiol.* 49, 217–222. doi: 10.1016/s0022-1910(02)00268-8

Ashok, M., Turner, C., and Wilson, T. G. (1988). Insect juvenile hormone resistance gene homology with the bHLH-PAS family of transcriptional regulators. *Proc. Natl. Acad. Sci. U.S.A.* 95, 2761–2766. doi: 10.1073/pnas.95.6.2761

Bartel, D. P. (2004). MicroRNAs: genomics, biogenesis, mechanism, and function. *Cell* 116, 281–297. doi: 10.1016/s0092-8674(04)00045-5

Barth, R. H., Lester, L. J., Sroka, P., Kessler, T., and Hearn, R. (1975). Juvenile HORMONE PROMOTES DOMINANCE BEHAVIOR AND OVARIAN DEVELOPMENT IN SOCIAL WASPs (*Polistes annularis*). *Experientia* 31, 691–692.

Belgacem, Y. H., and Martin, J. R. (2007). Hmgcr in the corpus allatum controls sexual dimorphism of locomotor activity and body size via the insulin pathway in Drosophila. *PLoS One* 2:e187. doi: 10.1371/journal.pone.0000187

Belles, X., Martin, D., and Piulachs, M. D. (2005). The mevalonate pathway and the synthesis of juvenile hormone in insects. *Annu. Rev. Entomol.* 50, 181–199. doi: 10.1146/annurev.ento.50.071803.130356

Bendena, W. G., Zhang, J., Burtenshaw, S. M., and Tobe, S. S. (2011). Evidence for differential biosynthesis of juvenile hormone (and related) sesquiterpenoids in *Drosophila melanogaster*. *Gen. Comp. Endocrinol.* 172, 56–61. doi: 10.1016/j.ygcen.2011.02.014

Bergot, B. J., Baker, F. C., Cerf, D. C., Jamieson, G., and Schooley, D. A. (1981). *Juvenile Hormone Biochemistry*, eds G. E. Pratt and G. T. Brooks (Amsterdam: Elsevier), 33–45.

Bergot, B. J., Jamieson, G. C., Ratcliff, M. A., and Schooley, D. A. (1980). JH zero: new naturally occurring insect juvenile hormone from developing embryos of the tobacco hornworm. *Science* 210, 336–338. doi: 10.1126/science.210.4467.336

Bittova, L., Jedlicka, P., Dracinsky, M., Kirubakaran, P., Vondrasek, J., Hanus, R., et al. (2019). Exquisite ligand stereoselectivity of a Drosophila juvenile hormone receptor contrasts with its broad agonist repertoire. *J. Biol. Chem.* 294, 410–423. doi: 10.1074/jbc.RA118.005992

Bomtorin, A. D., Mackert, A., Rosa, G. C., Moda, L. M., Martins, J. R., Bitondi, M. M. G., et al. (2014). Juvenile hormone biosynthesis gene expression in the corpora allata of honey bee (*Apis mellifera L.*) female castes. *PLoS One* 9:e86923. doi: 10.1371/journal.pone.0086923

Brent, C., Peeters, C., Dietemann, V., Crewe, R., and Vargo, E. (2006). Hormonal correlates of reproductive status in the queenless ponerine ant, Streblognathus peetersi. *J. Comp. Physiol. A Neuroethol. Sens. Neural Behav. Physiol.* 192, 315–320.

Cahan, S. H., Graves, C. J., and Brent, C. S. (2011). Intergenerational effect of juvenile hormone on offspring in *Pogonomyrmex* harvester ants. *J. Comp. Physiol. B* 181, 991–999. doi: 10.1007/s00360-011-0587-x

Cao, J. Q., Tong, W. S., Yu, H. Y., Tobe, S. S., Bendena, W. G., and Hui, J. H. L. (2017). The role of microRNAs in *Drosophila* regulation of insulin-like peptides and ecdysteroid signaling: Where are we now? *Adv. Insect Physiol.* 53, 55–85. doi: 10.1016/bs.aiip.2017.02.002

Carrel, J. E., McCairel, M. H., Slagle, A. J., Doom, J. P., Brill, J., and McCormick, J. P. (1993). Cantharidin production in a blister beetle. *Experientia* 49, 171–174. doi: 10.1007/BF01989424

Charles, J. P., Iwema, T., Epa, V. C., Takaki, K., Rynes, J., and Jindra, M. (2011). Ligand-binding properties of a juvenile hormone receptor, Methoprene-tolerant. *Proc. Natl. Acad. Sci. U.S.A.* 108, 21128–21133. doi: 10.1073/pnas.1116123109

Cheong, S. P., Huang, J., Bendena, W. G., Tobe, S. S., and Hui, J. H. (2015). Evolution of Ecdysis and metamorphosis in arthropods: the rise of regulation of juvenile hormone. *Integr. Comp. Biol.* 55, 878–890. doi: 10.1093/icb/icv066

Cuvillier-Hot, V., Lenoir, A., and Peeters, C. (2004). Reproductive monopoly enforced by sterile police workers in a queenless ant. *Behav. Ecol.* 15, 970–975.

Daimon, T., and Shinoda, T. (2013). Function, diversity, and application of insect juvenile hormone epoxidases (CYP15). *Biotechnol. Appl. Biochem.* 60, 82–91. doi: 10.1002/bab.1058

Daimon, T., Kozaki, T., Niwa, R., Kobayashi, I., Furuta, K., Namiki, T., et al. (2012). Precocious metamorphosis in the juvenile hormone-deficient mutant of the silkworm, Bombyx mori. *PLoS Genet.* 8:e1002486. doi: 10.1371/journal.pgen.1002486

De Loof, A., and Schoofs, L. (2019). Mode of action of Farnesol, the "Noble Unknown" in particular in Ca2+ homeostasis, and its juvenile hormone-esters in evolutionary retrospect. *Front. Neurosci.* 13:141. doi: 10.3389/fnins.2019.00141

Denli, A. M., Tops, B. B., Plasterk, R. H., Ketting, R. F., and Hannon, G. J. (2004). Processing of primary microRNAs by the Microprocessor complex. *Nature* 432, 231–235. doi: 10.1038/nature03049

Dubrovsky, E. B. (2005). Hormonal cross talk in insect development. *Trends Endocrinol. Metab.* 16, 6–11. doi: 10.1016/j.tem.2004.11.003

Dubrovsky, E. B., Dubrovskaya, V. A., Bernardo, T., Otte, V., DiFilippo, R., and Bryan, H. (2011). The Drosophila FTZ-F1 nuclear receptor mediates juvenile hormone activation of E75A gene expression through an intracellular pathway. *J. Biol. Chem.* 286, 33689–33700. doi: 10.1074/jbc.M111.273458

Giray, T., Giovanetti, M., and West-Eberhard, M. J. (2005). Juvenile hormone, reproduction, and worker behavior in the neotropical social wasp Polistes Canadensis. *Proc. Natl. Acad. Sci. U.S.A.* 102, 3330–3335. doi: 10.1073/pnas.0409560102

Gomez-Orte, E., and Belles, X. (2009). MicroRNA-dependent metamorphosis in hemimetabolan insects. *Proc. Natl. Acad. Sci. U.S.A.* 106, 21678–21682. doi: 10.1073/pnas.0907391106

Grozinger, C. M., and Robinson, G. E. (2007). Endocrine modulation of a pheromone-responsive gene in the honey bee brain. *J. Comp. Physiol. A Neuroethol. Sens. Neural. Behav. Physiol.* 193, 461–470. doi: 10.1007/s00359-006-0202-x

Huang, J., Marchal, E., Hult, E. R., and Tobe, S. S. (2015). Characterization of the juvenile hormone pathway in the viviparous cockroach, *Diploptera punctate*. *PLoS One* 10:e0117291. doi: 10.1371/journal.pone.0117291

Huang, Y., Wang, Z., Zha, S., Wang, Y., Jiang, W., Liao, Y., et al. (2016). De novo transcriptome and expression profile analysis to reveal genes and pathways potentially involved in cantharidin biosynthesis in the blister beetle *Mylabris cichorii*. *PLoS One* 11:e0146953. doi: 10.1371/journal.pone.0146953

Hui, J. H., Benena, W. G., and Tobe, S. S. (2013). "Future perspectives for research on the biosynthesis of juvenile hormones and related sesquiterpenoids in Arthropod endocrinology and ecotoxicology," in *Juvenile Hormone and Juvenoids: Moldeling Biological Effects and Environmental*, ed. J. Devillers (New York, NY: CRC Press), 15–30.

Hui, J. H. L., Hayward, A., Bendena, W. G., Takahashi, T., and Tobe, S. S. (2010). Evolution and functional divergence of enzymes involved in sesquiterpenoid hormone biosynthesis in crustaceans and insects. *Peptides* 31, 451–455. doi: 10.1016/j.peptides.2009.10.003

Ishikawa, A., Ogawa, K., Gotoh, H., Walsh, T. K., Tagu, D., Brisson, J. A., et al. (2012). Juvenile hormone titre and related gene expression during the change of reproductive modes in the pea aphid. *Insect Mol. Biol.* 21, 49–60. doi: 10.1111/j.1365-2583.2011.01111.x

Iwasaki, S., Kobayashi, M., Yoda, M., Sakaguchi, Y., Katsuma, S., Suzuki, T., et al. (2010). Hsc70/Hsp90 chaperone machinery mediates ATP-dependent RISC loading of small RNA duplexes. *Mol. Cell* 39, 292–299. doi: 10.1016/j.molcel.2010.05.015

Jiang, M., Lu, S., and Zhang, Y. (2017). Characterization of juvenile hormone related genes regulating cantharidin biosynthesis in *Epicauta chinensis*. *Sci. Rep.* 7:2308. doi: 10.1038/s41598-017-02393-w

Jindra, M., Uhlirova, M., Charles, J. P., Smykal, V., and Hill, R. J. (2015). Genetic evidence for function of the bHLH-PAS Protein Gce/Met as a juvenile hormone receptor. *PLoS Genet.* 11:e1005394. doi: 10.1371/journal.pgen.1005394

Jing, Y.-P., An, H., Zhang, S., Wang, N., and Zhou, S. (2018). Protein kinase C mediates juvenile hormone-dependent phosphorylation of Na+/K+-ATPase to induce ovarian follicular patency for yolk protein uptake. *J. Biol. Chem.* 293, 20112–20122. doi: 10.1074/jbc.RA118.005692

Judy, K. J., Schooley, D. A., Dunham, L. L., Hall, M. S., Bergot, B. J., and Siddall, J. B. (1973). Isolation, structure, and absolute configuration of a new natural insect juvenile hormone from Manduca sexta. *Proc. Natl. Acad. Sci. U.S.A.* 70, 1509–1513. doi: 10.1073/pnas.70.5.1509

Kappes, G., Deshpande, G., Mulvey, B. B., Horabin, J. I., and Schedl, P. (2011). The Drosophila Myc gene, diminutive, is a positive regulator of the Sex-lethal establishment promoter, Sxl-Pe. *Proc. Natl. Acad. Sci. U.S.A.* 108, 1543–1548. doi: 10.1073/pnas.1017006108

Kayukawa, T., Jouraku, A., Ito, Y., and Shinoda, T. (2017). Molecular mechanism underlying juvenile hormone-mediated repression of precocious larval–adult metamorphosis. *Proc. Natl. Acad. Sci. U.S.A.* 114, 1057–1062. doi: 10.1073/pnas.1615423114

Kayukawa, T., Minakuchi, C., Namiki, T., Togawa, T., Yoshiyama, M., Kamimura, M., et al. (2012). Transcriptional regulation of juvenile hormone-mediated induction of Krüppel homolog 1, a repressor of insect metamorphosis. *Proc. Natl. Acad. Sci. U.S.A.* 109, 11729–11734. doi: 10.1073/pnas.1204951109

Kayukawa, T., Nagamine, K., Ito, Y., Nishita, Y., Ishikawa, Y., and Shinoda, T. (2016). Krüppel homolog 1 inhibits insect metamorphosis via direct transcriptional repression of broad-complex, a Pupal Specifier Gene. *J. Biol. Chem.* 291, 1751–1762. doi: 10.1074/jbc.M115.686121

Kelstrup, H. C., Hartfelder, K., Nascimento, F. S., and Riddiford, L. M. (2014). The role of juvenile hormone in dominance behavior, reproduction and cuticular pheromone signaling in the caste-flexible epiponine wasp, *Synoeca surinama*. *Front. Zool.* 11:78. doi: 10.1186/s12983-014-0078-5

Kim, V. N., Han, J., and Siomi, M. C. (2009). Biogenesis of small RNAs in animals. *Nat. Rev. Mol. Cell Biol.* 10, 126–139. doi: 10.1038/nrm2632

Konopova, B., Smykal, V., and Jindra, M. (2011). Common and distinct roles of juvenile hormone signaling genes in metamorphosis of holometabolous and hemimetabolous insects. *PLoS One* 6:e28728. doi: 10.1371/journal.pone.0028728

Kotaki, T., Shinada, T., Kaihara, K., Ohfune, Y., and Numata, H. (2009). Structure determination of a new juvenile hormone from a Heteropteran insect. *Org. Lett.* 11, 5234–5237. doi: 10.1021/ol902161x

Li, K. L., Yuan, S. Y., Nanda, S., Wang, W. X., Lai, F. X., Fu, Q., et al. (2018). The Roles of E93 and Kr-h1 in Metamorphosis of *Nilaparvata lugens*. *Front. Physiol.* 9:1677. doi: 10.3389/fphys.2018.01677

Libbrecht, R., Corona, M., Wende, F., Azevedo, D. O., Serrao, J. E., and Keller, L. (2013). Interplay between insulin signaling, juvenile hormone, and vitellogenin regulates maternal effects on polyphenism in ants. *Proc. Natl. Acad. Sci. U.S.A.* 110, 11050–11055. doi: 10.1073/pnas.1221781110

Liu, S., Li, K., Gao, Y., Chen, W., Ge, W., Feng, Q., et al. (2018). Antagonistic actions of juvenile hormone and 20-hydroxyecdysone within the ring gland

determine developmental transitions in Drosophila. *Proc. Natl. Acad. Sci. U.S.A.* 115, 139–144. doi: 10.1073/pnas.1716897115

Liu, W., Guo, S., Sun, D., Zhu, L., Zhu, F., Lei, C. L., et al. (2019). Molecular characterization and juvenile hormone-regulated transcription of the vitellogenin receptor in the cabbage beetle *Colaphellus bowringi*. *Comp. Biochem. Physiol. A. Mol. Integr. Physiol.* 229, 69–75. doi: 10.1016/j.cbpa.2018.12.004

Liu, W., Li, Y., Zhu, L., Zhu, F., Lei, C. L., and Wang, X. P. (2016). Juvenile hormone facilitates the antagonism between adult reproduction and diapause through the methoprene-tolerant gene in the female *Colaphellus bowringi*. *Insect Biochem. Mol. Biol.* 74, 50–60. doi: 10.1016/j.ibmb.2016.05.004

Lozano, J., and Belles, X. (2011). Conserved repressive function of Krüppel homolog 1 on insect metamorphosis in hemimetabolous and holometabolous species. *Sci. Rep.* 1:163. doi: 10.1038/srep00163

Lozano, J., Montañez, R., and Belles, X. (2015). MiR-2 family regulates insect metamorphosis by controlling the juvenile hormone signaling pathway. *Proc. Natl. Acad. Sci. U.S.A.* 112, 3740–3745. doi: 10.1073/pnas.1418522112

Lucas, K., and Raikhel, A. S. (2013). Insect microRNAs: biogenesis, expression profiling and biological functions. *Insect Biochem. Mol. Biol.* 43, 24–38. doi: 10.1016/j.ibmb.2012.10.009

Lucas, K. J., Zhao, B., Roy, S., Gervaise, A. L., and Raikhel, A. S. (2015). Mosquito-specific microRNA-1890 targets the juvenile hormone-regulated serine protease JHA15 in the female mosquito gut. *RNA Biol.* 12, 1383–1390. doi: 10.1080/15476286.2015.1101525

Marchal, E., Zhang, J., Badisco, L., Verlinden, H., Hult, E. F., Van Wielendaele, P., et al. (2011). Final steps in juvenile hormone biosynthesis in the desert locust, *Schistocerca gregaria*. *Insect Biochem. Mol. Biol.* 41, 219–227. doi: 10.1016/j.ibmb.2010.12.007

Masuoka, Y., Yaguchi, H., Toga, K., Shigenobu, S., and Maekawa, K. (2018). TGFβ signaling related genes are involved in hormonal mediation during termite soldier differentiation. *PLoS Genet.* 14:e1007338. doi: 10.1371/journal.pgen.1007338

Meiselman, M., Lee, S. S., Tran, R., Dai, H., Ding, Y., Rivera-Perez, C., et al. (2017). Endocrine network essential for reproductive success in *Drosophila melanogaster*. *Proc. Natl. Acad. Sci. U.S.A.* 114, E3849–E3858. doi: 10.1073/pnas.1620760114

Meyer, A. S., Schneiderman, H. A., Hanzmann, E., and Ko, J. H. (1968). The two juvenile hormones from the cecropia silk moth. *Proc. Natl. Acad. Sci. U.S.A.* 60, 853–860. doi: 10.1073/pnas.60.3.853

Minakuchi, C., Ishii, F., Washidu, Y., Ichikawa, A., Tanaka, T., Miura, K., et al. (2015). Expressional and functional analysis of CYP15A1, a juvenile hormone epoxidase, in the red flour beetle *Tribolium castaneum*. *J. Insect Physiol.* 80, 61–70. doi: 10.1016/j.jinsphys.2015.04.008

Minakuchi, C., Namiki, T., and Shinoda, T. (2009). Krüppel homolog 1, an early juvenile hormone-response gene downstream of Methoprene-tolerant, mediates its anti-metamorphic action in the red flour beetle *Tribolium castaneum*. *Dev. Biol.* 325, 341–350. doi: 10.1016/j.ydbio.2008.10.016

Niwa, R., and Niwa, Y. S. (2014a). Enzymes for ecdysteroid biosynthesis: their biological functions in insects and beyond. *Biosci. Biotechnol. Biochem.* 78, 1283–1292. doi: 10.1080/09168451.2014.942250

Niwa, Y. S., and Niwa, R. (2014b). Neural control of steroid hormone biosynthesis during development in the fruit fly *Drosophila melanogaster*. *Genes Genet. Syst.* 89, 27–34. doi: 10.1266/ggs.89.27

Norman, V. C., and Hughes, W. (2016). Behavioural effects of juvenile hormone and their influence on division of labour in leaf-cutting ant societies. *J. Exp. Biol.* 219, 8–11. doi: 10.1242/jeb.132803

Norman, V. C., Pamminger, T., Nascimento, F., and Hughes, W. (2019). The role of juvenile hormone in regulating reproductive physiology and dominance in Dinoponera quadriceps ants. *PeerJ* 7:e6512. doi: 10.7717/peerj.6512

Nouzova, M., Etebari, K., Noriega, F. G., and Asgari, S. (2018). A comparative analysis of corpora allata-corpora cardiaca microRNA repertoires revealed significant changes during mosquito metamorphosis. *Insect Biochem. Mol. Biol.* 96, 10–18. doi: 10.1016/j.ibmb.2018.03.007

O'Donnell, S. (1998). Reproductive caste determination in eusocial wasps (Hymenoptera : Vespidae). *Annu. Rev. Entomol.* 43, 323–346. doi: 10.1146/annurev.ento.43.1.323

O'Donnell, S., and Jeanne, R. L. (1993). Methoprene accelerates age polyethism in workers of a social wasp *Polybia occidentalis*. *Physiol. Entomol.* 18, 189–194.

Paroulek, M., and Sláma, K. (2014). Production of the sesquiterpenoid, juvenile hormone-1 (JH-I), and of vitamin E in the accessory sexual (colleterial) glands of adult male moths, *Hyalophora cecropia* (Linnaeus, 1758), (Lepidoptera: Saturniidae). *Life Exc. Biol.* 2, 102–124. doi: 10.9784/LEB2(2)Paroulek.01

Parthasarathy, R., Sun, Z., Bai, H., and Palli, S. R. (2010). Juvenile hormone regulation of vitellogenin synthesis in the red flour beetle, *Tribolium castaneum*. *Insect Biochem. Mol. Biol.* 40, 405–414. doi: 10.1016/j.ibmb.2010.03.006

Postlethwait, J. H., and Weiser, K. (1973). Vitellogenesis induced by Juvenile Hormone in the Female Sterile Mutant apterous-four in *Drosophila melanogaster*. *Nat. New Biol.* 244, 284–285. doi: 10.1038/newbio244284a0

Qu, Z., Bendena, W. G., Nong, W., Siggens, K. W., Noriega, F. G., Kai, Z. P., et al. (2017). MicroRNAs regulate the sesquiterpenoid hormonal pathway in Drosophila and other arthropods. *Proc. Biol. Sci.* 284:20171827. doi: 10.1098/rspb.2017.1827

Qu, Z., Bendena, W. G., Tobe, S. S., and Hui, J. H. L. (2018). Juvenile hormone and sesquiterpenoids in arthropods: biosynthesis, signaling, and role of MicroRNA. *J. Steroid Biochem.* 184, 69–76. doi: 10.1016/j.jsbmb.2018.01.013

Richard, D. S., Applebaum, S. W., Sliter, T. J., Baker, F. C., Schooley, D. A., Reuter, C. C., et al. (1989). Juvenile hormone bisepoxide biosynthesis in vitro by the ring gland of *Drosophila melanogaster*: a putative juvenile hormone in the higher Diptera. *Proc. Natl. Acad. Sci. U.S.A.* 86, 1421–1425.

Riddiford, L. M. (2012). How does juvenile hormone control insect metamorphosis and reproduction? *Gen. Comp. Endocrinol.* 179, 477–484. doi: 10.1016/j.ygcen.2012.06.001

Riddiford, L. M., Cherbas, P., and Truman, J. W. (2000). Ecdysone receptors and their biological actions. *Vitam. Horm.* 60, 1–73.

Roisin, Y. (1996). Castes in humivorous and litter-dwelling neotropical nasute termites (Isoptera, Termitidae). *Ins. Soc.* 43, 375–389. doi: 10.1007/BF01258410

Röller, H., Dahm, K. H., Sweely, C. C., and Trost, B. M. (1967). The structure of the juvenile hormone. *Angew. Chem. Int. Ed.* 6, 179–180.

Röseler, P. F., Röseler, I., and Strambi, A. (1980). The activity of corpora allata in dominant and subordinated females of the wasp *Polistes gallicus*. *Insectes Soc.* 27, 97–107.

Röseler, P. F., Röseler, I., and Strambi, A. (1985). Role of ovaries and ecdysteroids in dominance hierarchy establishment among foundresses of the primitively social wasp, *Polistes gallicus*. *Behav. Ecol. Sociobiol.* 18, 9–13.

Röseler, P. F., Röseler, I., Strambi, A., and Augier, R. (1984). Influence of insect hormones on the establishment of dominance hierarchies among foundresses of the paper wasp, *Polistes gallicus*. *Behav. Ecol. Sociobiol.* 15, 133–142. doi: 10.1007/BF00299381

Roy, S., Saha, T. T., Zou, Z., and Raikhel, A. S. (2018). Regulatory pathways controlling female insect reproduction. *Annu. Rev. Entomol.* 63, 489–511. doi: 10.1146/annurev-ento-020117-043258

Sehnal, F., Svacha, P., and Zrzavy, J. (1996). "Evolution of insect metamorphosis," in *Metamorphosis. Postembryonic reprogramming of gene expression in amphibian and insect cells*, eds L. I. Gilbert, J. R. Tata, and B. G. Atkinson (San Diego, CA: Academic Press.), 3–58.

Sempere, L. F., Sokol, N. S., Dubrovsky, E. B., Berger, E. M., and Ambros, V. (2003). Temporal regulation of microRNA expression in *Drosophila melanogaster* mediated by hormonal signals and broad-Complex gene activity. *Dev. Biol.* 259, 9–18.

Sheng, Z., Xu, J., Bai, H., Zhu, F., and Palli, S. R. (2011). Juvenile hormone regulates vitellogenin gene expression through insulin-like peptide signaling pathway in the red flour beetle, *Tribolium castaneum*. *J. Biol. Chem.* 286, 41924–41936. doi: 10.1074/jbc.M111.269845

Shin, S. W., Zou, Z., Shah, T. T., and Raikhel, A. S. (2012). bHLH-PAS heterodimer of methoprene-tolerant and cycle mediates circadian expression of juvenile hormone-induced mosquito genes. *Proc. Natl. Acad. Sci. U.S.A.* 109, 16576–16581. doi: 10.1073/pnas.1214209109

Shinoda, T., and Itoyama, K. (2003). Juvenile hormone acid methyltransferase: a key regulatory enzyme for insect metamorphosis. *Proc. Natl. Acad. Sci. U.S.A.* 100, 11986–11991. doi: 10.1073/pnas.2134232100

Shorter, J. R., and Tibbetts, E. A. (2009). The effect of juvenile hormone on temporal polyethism in the paper wasp *Polistes dominulus*. *Insect. Soc.* 56, 7–13. doi: 10.1007/s00040-008-1026-1

Shpigler, H., Patch, H. M., Cohen, M., Fan, Y., Grozinger, C. M., and Bloch, G. (2010). The transcription factor Krüppel homolog 1 is linked to hormone mediated social organization in bees. *BMC Evol. Biol.* 10:120. doi: 10.1186/1471-2148-10-120

Smykal, V., Bajgar, A., Provaznik, J., Fexova, S., Buricova, M., Takaki, K., et al. (2014). Juvenile hormone signaling during reproduction and development of the linden bug, *Pyrrhocoris apterus*. *Insect Biochem. Mol. Biol.* 45, 69–76. doi: 10.1016/j.ibmb.2013.12.003

Sommer, K., Hölldobler, B., and Rembold, H. (1993). Behavioral and physiological aspects of reproductive control in a Diacamma species from Malaysia (Formicidae, Ponerinae). *Ethology* 94, 162–170. doi: 10.1111/j.1439-0310.1993.tb00556.x

Song, J., Guo, W., Jiang, F., Kang, L., and Zhou, S. (2013). Argonaute 1 is indispensable for juvenile hormone mediated oogenesis in the migratory locust, *Locusta migratoria*. *Insect Biochem. Mol. Biol.* 43, 879–887. doi: 10.1016/j.ibmb.2013.06.004

Song, J., Li, W., Zhao, H., Gao, L., Fan, Y., and Zhou, S. (2018). The microRNAs let-7 and miR-278 regulate insect metamorphosis and oogenesis by targeting the juvenile hormone early-response gene Krüppel-homolog 1. *Development* 145:dev170670. doi: 10.1242/dev.170670

Song, J., Li, W., Zhao, H., and Zhou, S. (2019). Clustered miR-2, miR-13a, miR-13b and miR-71 coordinately target Notch gene to regulate oogenesis of the migratory locust *Locusta migratoria*. *Insect Biochem. Mol. Biol.* 106, 39–46. doi: 10.1016/j.ibmb.2018.11.004

Song, J., Wu, Z., Wang, Z., Deng, S., and Zhou, S. (2014). Krüppel-homolog 1 mediates juvenile hormone action to promote vitellogenesis and oocyte maturation in the migratory locust. *Insect Biochem. Mol. Biol.* 52, 94–101. doi: 10.1016/j.ibmb.2014.07.001

Song, J., and Zhou, S. (2019). Post-transcriptional regulation of insect metamorphosis and oogenesis. *Cell. Mol. Life Sci.* 77, 1893–1909. doi: 10.1007/s00018-019-03361-5

Swevers, L., Raikhel, A., Sappington, T., Shirk, P., and Iatrou, K. (2005). "Vitellogenesis and post-vitellogenic maturation of the insect ovarian follicle," in *Comprehensive Insect Physiology, Biochemistry, Pharmacology and Molecular Biology*, Vol. 3, eds L. Gilbert, S. Gill, and K. Iatrou (Amsterdam: Elsevier), 87–155. doi: 10.1016/B0-44-451924-6/00093-4

Tanaka, E. D., and Piulachs, M. D. (2012). Dicer-1 is a key enzyme in the regulation of oogenesis in panoistic ovaries. *Biol. Cell* 104, 452–461. doi: 10.1111/boc.201100044

Tibbetts, E. A., and Izzo, A. S. (2009). Endocrine mediated phenotypic plasticity- Condition-dependent effects of JH on dominance and fertility of wasp queens. *Horm. Behav.* 56, 527–531. doi: 10.1016/j.yhbeh.2009.09.003

Tibbetts, E. A., and Sheehan, M. J. (2012). The effect of juvenile hormone on Polistes wasp fertility varies with cooperative behavior. *Horm. Behav.* 61, 559–564. doi: 10.1016/j.yhbeh.2012.02.002

Tibbetts, E. A., Levy, S., and Donajkowski, K. (2011). Reproductive plasticity in *Polistes* paper wasp workers and the evolutionary origins of sociality. *J. Insect Physiol.* 57, 995–999. doi: 10.1016/j.jinsphys.2011.04.016

Tibbetts, E. A., Fearon, M. L., Wong, E., Huang, Z. Y., and Tinghitella, R. M. (2018). Rapid juvenile hormone downregulation in subordinate wasp queens facilitates stable cooperation. *Proc. Biol. Sci.* 285:20172645. doi: 10.1098/rspb.2017.2645

Tobe, S. S., and Bendena, W. G. (1999). The regulation of juvenile hormone production in arthropods: functional and evolutionary perspectives. *Ann. N.Y. Acad. Sci.* 300–310. doi: 10.1111/j.1749-6632.1999.tb07901.x

Truman, J. W. (2019). The evolution of insect metamorphosis. *Curr. Biol.* 29, R1252–R1268. doi: 10.1016/j.cub.2019.10.009

Truman, J. W., and Riddiford, L. M. (2002). Endocrine insights into the evolution of metamorphosis in insects. *Annu. Rev. Entomol.* 47, 467–500. doi: 10.1146/annurev.ento.47.091201.145230

Tu, M. P., Yin, C. M., and Tatar, M. (2005). Mutations in insulin signaling pathway alter juvenile hormone synthesis in *Drosophila melanogaster*. *Gen. Comp. Endocrinol.* 142, 347–356. doi: 10.1016/j.ygcen.2005.02.009

Ureña, E., Chafino, S., Manjón, C., Franch-Marro, X., and Martín, D. (2016). The Occurrence of the Holometabolous Pupal Stage Requires the Interaction between E93, Krüppel-Homolog 1 and Broad-Complex. *PLoS Genet.* 12:e1006020. doi: 10.1371/journal.pgen.1006020

Vea, I. M., Tanaka, S., Shiotsuki, T., Jouraku, A., Tanaka, T., and Minakuchi, C. (2016). Differential juvenile hormone variations in scale insect extreme sexual dimorphism. *PLoS One* 11:e0149459. doi: 10.1371/journal.pone.0149459

Wang, C., Feng, T., Wan, Q., Kong, Y., and Yuan, L. (2014). miR-124 controls Drosophila behavior and is required for neural development. *Int. J. Dev. Neurosci.* 38, 105–112. doi: 10.1016/j.ijdevneu.2014.08.006

Wen, D., Rivera-Perez, C., Abdou, M., Jia, Q., He, Q., Liu, X., et al. (2015). Methyl farnesoate plays a dual role in regulating drosophila metamorphosis. *PLoS Genet.* 13:e1005038. doi: 10.1371/journal.pgen.1005038

Wu, B., Ma, L., Zhang, E., Du, J., Liu, S., Price, J., et al. (2018). Sexual dimorphism of sleep regulated by juvenile hormone signaling in Drosophila. *PLoS Genet.* 14:e1007318. doi: 10.1371/journal.pgen.1007318

Wu, W., Xiong, W., Li, C., Zhai, M., Li, Y., Ma, F., et al. (2017). MicroRNA-dependent regulation of metamorphosis and identification of microRNAs in the red flour beetle, *Tribolium castaneum*. *Genomics* 109, 362–373. doi: 10.1016/j.ygeno.2017.06.001

Wu, Z., Guo, W., Xie, Y., and Zhou, S. (2016). Juvenile hormone activates the transcription of cell-division-cycle 6 (Cdc6) for Polyploidy-dependent Insect Vitellogenesis and Oogenesis. *J. Biol. Chem.* 291, 5418–5427. doi: 10.1074/jbc.M115.698936

Wu, Z., Guo, W., Yang, L., He, Q., and Zhou, S. (2018). Juvenile hormone promotes locust fat body cell polyploidization and vitellogenesis by activating the transcription of Cdk6 and E2f1. *Insect Biochem. Mol. Biol.* 102, 1–10.

Wyatt, G. R., and Davey, K. G. (1996). Cellular and molecular actions of juvenile hormone. II. Roles of juvenile hormone in adult insects. *Adv. Insect Physiol.* 26, 1–155.

Yang, M., Wei, Y., Jiang, F., Wang, Y., Guo, X., He, J., et al. (2014). MicroRNA-133 inhibits behavioral aggregation by controlling dopamine synthesis in locusts. *PLoS Genet.* 10:e1004206. doi: 10.1371/journal.pgen.1004206

Yang, P., Chen, X. M., Liu, W. W., Feng, Y., and Sun, T. (2015). Transcriptome analysis of sexually dimorphic Chinese white wax scale insects reveals key differences in developmental programs and transcription factor expression. *Sci. Rep.* 5:8141. doi: 10.1038/srep08141

Ye, X., Xu, L., Li, X., He, K., Hua, H., Cao, Z., et al. (2019). miR-34 modulates wing polyphenism in planthopper. *PLoS Genet.* 15:e1008235. doi: 10.1371/journal.pgen.1008235

Zhang, S., An, S., Hoover, K., Li, Z., Li, X., Liu, X., et al. (2018). Host miRNAs are involved in hormonal regulation of HaSNPV-triggered climbing behaviour in Helicoverpa armigera. *Mol. Ecol.* 27, 459–475. doi: 10.1111/mec.14457

Zhang, T., Song, W., Zheng, L., Qian, W., Wei, L., Yang, Y., et al. (2018). Krüppel homolog 1 represses insect ecdysone biosynthesis by directly inhibiting the transcription of steroidogenic enzymes. *Proc. Natl. Acad. Sci. U.S.A.* 115, 3960–3965. doi: 10.1073/pnas.1800435115

Zhang, W. N., Ma, L., Liu, C., Chen, L., Xiao, H. J., and Liang, G. M. (2018). Dissecting the role of Krüppel homolog 1 in the metamorphosis and female reproduction of the cotton bollworm, *Helicoverpa armigera*. *Insect Mol. Biol.* 27, 492–504. doi: 10.1111/imb.12389

Zhu, J., Busche, J. M., and Zhang, X. (2010). Identification of juvenile hormone target genes in the adult female mosquitoes. *Insect Biochem. Mol. Biol.* 40, 23–29. doi: 10.1016/j.ibmb.2009.12.004

Conflict of Interest: The authors declare that the research was conducted in the absence of any commercial or financial relationships that could be construed as a potential conflict of interest.

frontiers in Cell and Developmental Biology

REVIEW
published: 22 September 2020
doi: 10.3389/fcell.2020.576571

Special Significance of Non-*Drosophila* Insects in Aging

Siyuan Guo[1,2], *Xianhui Wang*[1,2] *and Le Kang*[1,2]*

[1] State Key Laboratory of Integrated Management of Pest Insects and Rodents, Institute of Zoology, Chinese Academy of Sciences, Beijing, China, [2] CAS Center for Excellence in Biotic Interactions, University of Chinese Academy of Sciences, Beijing, China

Aging is the leading risk factor of human chronic diseases. Understanding of aging process and mechanisms facilitates drug development and the prevention of aging-related diseases. Although many aging studies focus on fruit fly as a canonical insect system, minimal attention is paid to the potentially significant roles of other insects in aging research. As the most diverse group of animals, insects provide many aging types and important complementary systems for aging studies. Insect polyphenism represents a striking example of the natural variation in longevity and aging rate. The extreme intraspecific variations in the lifespan of social insects offer an opportunity to study how aging is differentially regulated by social factors. Insect flight, as an extremely high-intensity physical activity, is suitable for the investigation of the complex relationship between metabolic rate, oxidative stress, and aging. Moreover, as a "non-aging" state, insect diapause not only slows aging process during diapause phase but also affects adult longevity during/after diapause. In the past two decades, considerable progress has been made in understanding the molecular basis of aging regulation in insects. Herein, the recent research progress in non-*Drosophila* insect aging was reviewed, and its potential utilization in aging in the future was discussed.

Keywords: non-*Drosophila* insects, aging, phenotypic plasticity, flight, diapause

OPEN ACCESS

Edited by:
Zhongxia Wu,
Henan University, China

Reviewed by:
Thomas Roeder,
University of Kiel, Germany
Zhangwu Zhao,
China Agricultural University, China

***Correspondence:**
Le Kang
lkang@ioz.ac.cn

Specialty section:
This article was submitted to Epigenomics and Epigenetics, a section of the journal Frontiers in Cell and Developmental Biology

Received: *26 June 2020*
Accepted: *04 September 2020*
Published: *22 September 2020*

Citation:
Guo S, Wang X and Kang L (2020) Special Significance of Non-Drosophila Insects in Aging. Front. Cell Dev. Biol. 8:576571. doi: 10.3389/fcell.2020.576571

INTRODUCTION

Aging is regarded as the greatest risk factor of most chronic pathological conditions (Kennedy et al., 2014), and becoming a socioeconomic problem worldwide (He et al., 2016). Between 2000 and 2050, the percentage of population aged above 60 years is projected to increase from approximately 11% to 22% worldwide (United Nations, 2017). As the aging population rapidly grows, aging-related chronic conditions contribute to the biggest proportion of global healthcare burden, and they are estimated to become the next global public health challenge (World Health Organization, 2017). Thus, understanding of aging mechanisms and identifying aging regulators are becoming increasingly important.

Aging is an extraordinary complex process with a time-dependent loss of structure, function, and physiological integrity (Lopez-Otin et al., 2013). Nine molecular aging hallmarks and seven pillars of aging mechanisms have been characterized, including dysfunction or alterations in metabolism, inflammation, stress adaptation, proteostasis, intercellular communication, mitochondrial functions, telomere state, genomic stability, and epigenetics (Lopez-Otin et al., 2013; Kennedy et al., 2014). Most of the current knowledges about aging mechanisms were contributed by canonical model organisms, including yeast (*Saccharomyces cerevisiae*), worm

(*Caenorhabditis elegans*), fruit fly (*Drosophila melanogaster*), and house mouse (*Mus musculus*). Fruit fly is a canonical insect model with advantages of rapid life cycle, high fecundity, convenient and precise genetic manipulation, and easy maintenance (Helfand and Rogina, 2003). Studies on fruit fly aging made remarkable contributions to the understanding of conserved aging-regulatory mechanisms, such as endocrine regulation (Toivonen and Partridge, 2009), oxidative stress (Le Bourg, 2001), epigenetic alterations (Solovev et al., 2018), mitochondrial dysfunctions (Guo, 2012), and genomic instability (Li et al., 2013). Moreover, *Drosophila* contains approximately 70% of known disease-related genes in humans (Reiter et al., 2001). Thus, *Drosophila* has been widely used in modeling aging-related diseases of humans and screening for anti-aging drugs (Piper and Partridge, 2018). However, only focusing on a few number of model species ignores the diversity of longevity and aging traits that have evolved in nature, and the diversity provides an opportunity to study various regulators and mechanisms involved in aging plasticity and senescence evolution (Valenzano et al., 2017). Therefore, more non-canonical systems are required for deep understanding of aging biology.

As the most diverse group of living animals (Mayhew, 2007), insects have the characteristics of phenotypic plasticity, flight, and diapause (**Figure 1**), which are considerably essential for aging studies. With single genotype, the lifespan of polyphenic insects, especially social insects, can substantially vary depending on the environment (Keller and Jemielity, 2006), thereby providing an opportunity to study the effects of environmental and social factors on aging. Insect flight achieves the highest metabolic rate known (Kammer and Heinrich, 1978), and excessive oxidative stress associated with hyperactive respiratory metabolism may be the potential aging accelerator (Finkel and Holbrook, 2000). In addition, a special stage of developmental arrest called diapause has evolved in many insect species, enabling them to survive extreme conditions, such as winter (Denlinger, 2002). Diapause results in low metabolic activity and a profound extension of insect lifespan, thereby providing an opportunity to understand the mechanism underlying lifespan extension (Denlinger, 2008; Hahn and Denlinger, 2010).

In the past two decades, advances in genomics, genetic manipulation, and gene editing technology enable the aging studies to approach the multiple phenotypes and molecular levels in the non-*Drosophila* insects. Considerable progress has been achieved in explaining these fantastic aging traits in insects. Here, the recent advances in aging studies of non-*Drosophila* insects were discussed, and the special values of insects as model systems for aging biology were highlighted.

PHENOTYPIC PLASTICITY AND AGING IN INSECTS

Studies conducted in twins demonstrated that approximately 25% of the variation in human longevity is due to genetic factors, while the rest is due to individual behavior and environmental factors (Herskind et al., 1996; Sebastiani and Perls, 2012). The studies on diet, exercise, chemical exposure, and social connection all demonstrate to affect aging and lifespan in humans through complex and largely unknown mechanisms (Lopez-Otin et al., 2016; Yang et al., 2016; Krutmann et al., 2017; Duggal et al., 2018). Understanding the mechanisms underlying the effects of modifiable environments on aging could help develop treatments to promote human health span.

Many insects have evolved the ability of one genotype to produce more than one alternative phenotype when exposed to different environments (Whitman and Ananthakrishnan, 2009; Simpson et al., 2011). Polyphenic insects offer striking examples of natural variation in longevity, such as reproductives and workers in social insects, gregarious and solitary locusts, spring and summer butterflies, and winged and wingless aphids (Keller and Jemielity, 2006; Pener and Simpson, 2009; Ogawa and Miura, 2014; Freitak et al., 2019). Unlike canonical model species, polyphenic insects exhibit up to 100-fold changes in longevity in response to environmental changes (Remolina and Hughes, 2008), revealing their specific value in studying the effects of environmental factors on aging. Moreover, a number of environmental factors are involved in regulating the phenotypic plasticity of insects (Whitman and Ananthakrishnan, 2009; Simpson et al., 2011). Diet, reproduction, behavior, social interaction, population density, photoperiodic cues, and temperature contribute to lifespan variations in polyphenic insects (Keller and Jemielity, 2006; Pener and Simpson, 2009; Ogawa and Miura, 2014; Freitak et al., 2019). Therefore, the extreme lifespan differences and enormous influencing factors provide an opportunity to deeply understand the mechanisms behind aging plasticity induced by complex environmental changes.

The differences in the lifespan of divergent morphs of butterflies, aphids, and locusts are suitable samples for studying the effects of photoperiodic cues and temperature, environmental stress, and population density on aging, respectively (Pener and Simpson, 2009; Ogawa and Miura, 2014; Freitak et al., 2019). Although previous studies have discovered some interesting aging characteristics, such as key roles of population density at the early life on locust aging (Boerjan et al., 2011) and the positive relationship between immune activity and longevity in seasonally polyphenic butterfly (Freitak et al., 2019), the mechanisms remain unknown.

SOCIAL INSECTS IN AGING

Social insects such as honey bees, bumble bees, ants, and termites, represent the ideal model systems to investigate the mechanisms behind the effects of social factors on aging because of the enormous intraspecific variation in their lifespan and aging rate (Keller and Jemielity, 2006; Kramer et al., 2016). Highly reproductive honeybee queens can survive for two years, whereas sterile workers can only survive between few weeks and one year (Seeley, 1978; Winston, 1987). The reproductives of social ants and termites can live up to 30 years (Hölldobler and Wilson, 1990), while workers frequently have 10-fold shorter lifespans (Kramer and Schaible, 2013). Moreover, the aging rate and lifespan of workers considerably vary depending

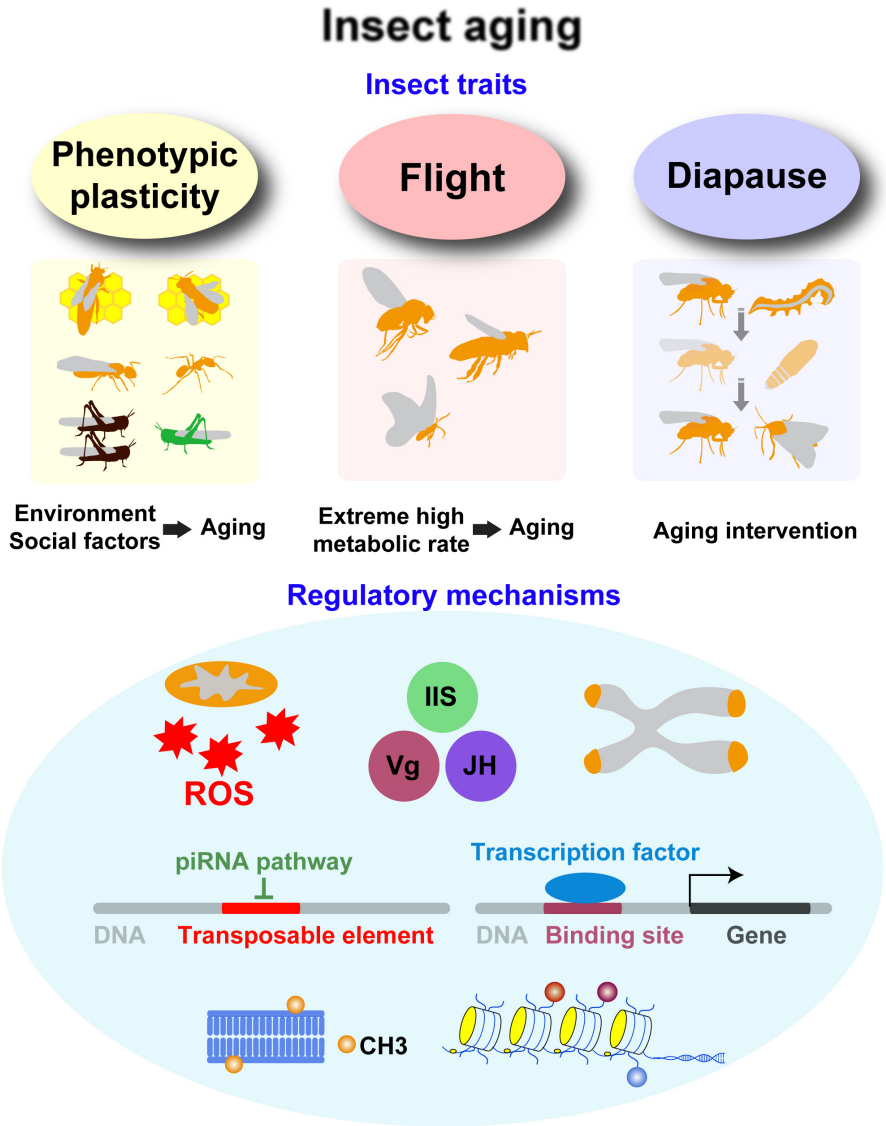

FIGURE 1 | Overview of insect traits with aging-regulatory functions and major molecular mechanisms underlying the effects of these insect traits. Phenotypic plasticity, flight, and diapause have effects on aging. The representative insects and the research implications are shown. Several factors, such as oxidative stress, endocrine factors, telomere, transposable elements, transcription factors, and epigenetics, play important roles in the effects of these insect traits.

on environmental and task changes. For example, the tasks of honeybee workers change in an orderly and usually age-dependent manner, with young workers performing nursing duties and old ones foraging (Winston, 1987). The timing of transition from in-hive tasks to foraging is the most significant predictor of worker lifespan, because foragers senesce faster than their same-aged nurse counterparts (Seehuus et al., 2006a; Behrends et al., 2007; Münch et al., 2008; Quigley et al., 2018). Honeybee workers can revert from foraging duties to hive activities, and this reversion is associated with the reversal of aging biomarkers (Amdam et al., 2005; Baker et al., 2012; Herb et al., 2012). Some eusocial ants possess a type of social organization that enables adult workers to become reproductive individuals or gamergates following removal of queen (Brunner et al., 2011). With the reallocation of tasks, the fertile workers could achieve an extended lifespan (Hartmann and Heinze, 2003; Schneider et al., 2011; Kohlmeier et al., 2017).

Several mechanisms are involved in regulating caste-specific aging rate in social insects. First, the difference in antioxidant capacity is one of the putative reasons. The level of vitellogenin (Vg), which protects organisms from oxidative stress (Seehuus et al., 2006b), is higher in honeybee individuals with longer lifespan; for instance, it is higher in queens than in workers and higher in nurses than in foragers (Amdam et al., 2005; Corona et al., 2007; Münch and Amdam, 2010). Polyunsaturated fatty acids that are high in pollen but negligible in royal jelly may result in the cellular membrane of honeybee workers becoming more susceptible to lipid peroxidation than that of queens

(Haddad et al., 2007; Martin et al., 2019). However, the role of antioxidant genes in queen-biased longevity is controversial. Some studies on honeybees and ants revealed a lower level of antioxidant genes in reproductives than in workers (Parker et al., 2004; Corona et al., 2005; Schneider et al., 2011). Second, endocrine factors also play key roles in caste-specific aging phenotypes. The interaction between insulin/IGF (insulin-like growth factor)-like signaling (IIS), juvenile hormone (JH), and Vg jointly regulates longevity and reproduction (Rodrigues and Flatt, 2016). However, the aging-regulatory functions of endocrine network are not conserved across social insects. For example, unlike the fire ant and several primitively eusocial insects (Robinson and Vargo, 1997; Bloch et al., 2002), in honeybee workers, JH appears to be life-shortening hormone because JH and Vg are configured in a mutually repressive regulatory circuitry during adult stage (Guidugli et al., 2005; Page and Amdam, 2007). Less conserved interaction pathways between endocrine factors (e.g., microRNAs) may contribute to species variation in the longevity regulation of endocrine network (Marco et al., 2010; Nunes et al., 2013). Third, the difference in the maintenance of genomic stability and telomere may be one of potential mechanisms. The heads of termite reproductives, not the major workers, prevent aging-related genomic damages caused by transposable element activity through continued upregulation of the piRNA pathway (Elsner et al., 2018). Telomerase activity displays a 70-fold increase in brains of adult honeybee queens compared to those of adult workers (Korandová and Frydrychová, 2016). The piRNA pathway and telomerase being primarily in germline suggests that the reproductives of highly social insects could be regarded as equivalent to germline of a colony, whereas the workers are equivalent to disposable soma (Elsner et al., 2018). The reproductives have evolved germline-corresponding anti-aging mechanisms to sustain themselves through generations. The fourth potential mechanism is epigenetic regulation. Caste-specific methylation profiles are associated with conserved aging-regulatory pathways, including IIS components, IIS-related metabolic systems, JH-responsive genes, and telomere maintenance (Bonasio et al., 2012; Foret et al., 2012), suggesting that DNA methylation may contribute to the aging differences between queens and workers. Genomic demethylation by pharmacological inhibition increases Vg expression and extends the lifespan of worker bees (Cardoso-Júnior et al., 2018), indicating the potential roles of DNA methylation in regulating aging in workers.

Although considerable progress has been achieved in understanding the mechanism behind aging divergences in social insects, research evidence remains lacking in some important related issues. Many aging-regulatory genes display differences at the transcriptional level between castes in social insects, suggesting that transcriptional regulation plays crucial roles in caste-specific aging trajectories. Epigenetics connects environmental inputs with transcription and thus may be the key to the aging differences between castes (Benayoun et al., 2015). However, the interplay between many types of epigenetic mechanisms and caste-specific aging is rarely studied, although the crucial roles of histone modifications and microRNAs in establishing caste-specific transcriptional programs and caste differentiation have been proposed (Weaver et al., 2007; Bonasio et al., 2010; Spannhoff et al., 2011; Guo et al., 2013; Simola et al., 2013, 2016; Shi et al., 2015; Ashby et al., 2016; Wojciechowski et al., 2018).

FLIGHT AND AGING IN INSECTS

Metabolic rates may be related to aging and longevity. The rate of living theory proposed at the beginning of the 20th century suggests that a slowed rate of metabolism is associated with lengthened longevity (Rubner, 1916). In line with this view, recent studies revealed that increased resting metabolic rate is a risk factor for mortality in humans (Ruggiero et al., 2008; Jumpertz et al., 2011). High metabolic rates have been hypothesized to come with a cost in terms of increased level of reactive oxygen species (ROS), the byproducts of mitochondrial metabolism, which leads to accelerated aging through damaging macromolecules, including DNA, lipid, and proteins (Harman, 1956; Finkel and Holbrook, 2000). Data from humans revealed that changes in metabolic rates are accompanied by changes in oxidative stress and may underlie variation in aging rate (Redman et al., 2018). However, the relationship between metabolic rate, ROS, and lifespan is highly complex. The positive relationship between metabolic rate and ROS production provokes great debate (Speakman, 2005), and the beneficial roles of ROS in regulating lifespan, metabolism, and development have been demonstrated (Santos et al., 2018). The true mechanisms of the association between metabolic rates and aging are not well understood.

Insect flight has the highest metabolic rate (Kammer and Heinrich, 1978) and profound effects on aging process. In line with the early metabolic and locomotor senescence in *Drosophila* after forcing flight (Lane et al., 2014), aging is accelerated in honeybee workers after transitioning from infrequently flying nurses to frequently flying foragers (Seehuus et al., 2006a; Behrends et al., 2007). Moreover, foraging bees with flight restriction do not display aging-related learning deficits as the free-flying ones (Tolfsen et al., 2011). Flight restriction similarly decreases the mitochondrial damage and extends lifespan to approximately threefold of the normal in houseflies (Agarwal and Sohal, 1994; Yan and Sohal, 2000). These results collectively implicated the negative effects of flight on insect aging. However, flight experience is not always detrimental. For instance, flight restriction leads to increased oxidative damage in brains of honey bees and early senescence of flight performance in fruit flies (Tolfsen et al., 2011; Lane et al., 2014). A high flight activity rate within the activity days has no negative effects on longevity in two bee species in the fields (Straka et al., 2014). In Glanville fritillary butterfly (*Melitaea cinxia*), peak flight metabolic rates are positively associated with lifespan (Niitepõld and Hanski, 2013). Flight treatment alone has no effect on the longevity of some butterflies, including Glanville fritillary butterfly (Woestmann et al., 2017), Mormon fritillary (*Speyeria mormonia*) (Niitepõld and Boggs, 2015), speckled wood butterfly (*Pararge aegeria*) (Gibbs and Van Dyck, 2010), and squinting bush brown butterfly (*Bicyclus anynana*) (Saastamoinen et al., 2010). Therefore, the

effects of flight behavior on insect longevity and aging seem to vary depending on species, flight traits, physiological states, and some other factors.

Elevated oxidative stress is considered as the primarily mechanism underlying the negative effects of flight on lifespan. In insects, flight could induce oxidative stress by increasing ROS generation from respiratory metabolism and altering membrane lipid composition that is more susceptible to ROS (Sohal et al., 1984; Yan and Sohal, 2000; Magwere et al., 2006; Williams et al., 2008; Margotta et al., 2018). Elevated oxidative stress in insects is deleterious in most cases. An increase in oxidative stress by pharmacological and genetic manipulations shortens lifespan in some insects (Phillips et al., 1989; Parkes et al., 1998; Kirby et al., 2002; Duttaroy et al., 2003; Cui et al., 2004; Margotta et al., 2018). However, the mechanism underlying the non-negative effects of insect flight on lifespan has not yet been studied. One potential explanation for these effects is that the oxidative stress generated by moderate flight may induce long-term stress response, thus protecting organisms from damage accumulation (Gems and Partridge, 2008). Another possible explanation is that some insects may evolve specific antioxidant mechanisms. For example, to resist oxidative stress during hovering flight, the tobacco hornworm (*Manduca sexta*) fed with nectar sugar generated antioxidant compounds by shunting glucose via low-energy pentose phosphate pathways (Levin et al., 2017). In addition, ROS does not always play negative roles in insect longevity; it could extend longevity by inducing diapause in cotton bollworm (*Helicoverpa armigera*) (Zhang et al., 2017).

Studies on the mechanisms behind the effects of insect flight on aging mainly focused on oxidative stress, and few studies on other aging-regulatory mechanisms are available. Insect flight induces substantial changes in endocrine status and gene expression (Rademakers and Beenakkers, 1977; Goldsworthy, 1983; Margotta et al., 2013; Kvist et al., 2015; Woestmann et al., 2017). Whether and how these endocrine and transcriptional changes influence aging process remain elusive. Moreover, insect flight experience influences oxidative damage in a tissue-dependent manner (Williams et al., 2008; Margotta et al., 2013, 2018). Flight-susceptible tissues may further affect systemic aging through inter-tissue crosstalk (Demontis et al., 2013). However, the key tissues and signals involved are still unknown. Lastly, insect species vary widely in flight traits, such as wingbeat frequency, flight duration, and wing morphology (Molloy et al., 1987; Dudley, 2002). Such variations in flight traits have effects on the differences in flight metabolic properties (Casey et al., 1985; Feller and Nachtigall, 1989; Darveau et al., 2014), and they may be involved in species variation in the effects of flight on aging through unknown mechanisms.

DIAPAUSE AND AGING IN INSECTS

How to extend lifespan has always fascinated people throughout human history. Science fictions depict that humans extend lifespan and reach the future through achieving hypometabolic states and cryonics. Interestingly, this specific ability is common in insects. Diapause, a state of programmed arrest of development coupled with suppressed metabolic activity, helps insects to survive unfavorable environmental conditions (Denlinger, 2002). During diapause, insects do not experience the same fast "aging clock" as in direct development, resulting in drastically extended lifespan (Tatar and Yin, 2001). Moreover, insects have evolved diapause at different life cycle stages, including eggs, larvae, pupae, and adults, thereby providing opportunities to study the effects of various diapause types on aging (Denlinger, 2002). Studying insect diapause could provide new insights into aging interventions and lifespan extension (Denlinger, 2008).

Insect systems demonstrate organismal and genetic links between diapause and aging. Similar with *Drosophila*, which undergoes a negligible senescence during reproductive diapause (Tatar et al., 2001a,b), adult monarch butterflies and grasshoppers with reproductive diapause induced by surgical removal of the *corpora allata* have doubled lifespan (Herman and Tatar, 2001; Tatar and Yin, 2001). In addition, a handful of evidence revealed the roles of pupal and larval diapauses on the extension of pre-adult longevity (Lu et al., 2013; Lin and Xu, 2016; Lin et al., 2016; Zhang et al., 2017; Wang et al., 2018). Noteworthy, diapause not only slows aging during diapause phase, but also has species-dependent effects on adult longevity after diapause. For example, maize stalk borer (*Busseola fusca*) and spotted stem borer (*Chilo partellus*) have shortened adult lifespans after diapause (Gebre-Amlak, 1989; Dhillon and Hasan, 2018), but cotton bollworm (*H. armigera*) and multivoltine bruchid (*Kytorhinus sharpianus*) display extended lifespans after diapause (Ishihara and Shimada, 1995; Chen et al., 2014).

Transcriptional regulation may play a crucial role in diapause-related aging regulation (Denlinger, 2002). Several key transcription factors involved have been characterized. In the mosquito *Culex pipiens*, transcription factor FoxO, which is regulated by insulin and JH signaling, alters the expression of aging-regulatory genes during diapause (Sim and Denlinger, 2008, 2013a,b; Sim et al., 2015). In the moth *H. armigera*, accumulation of FoxO induced by high ROS activity during diapause also promote lifespan extension (Zhang et al., 2017). The diapause-related ROS increase is attributed to the downregulation of hexokinase expression, which is regulated by transcription factors CREB, c-Myc, and POU (Lin and Xu, 2016). In addition, repression of mitochondrial activity, which may be related to lifespan extension of diapause, is regulated by a network of transcription factors HIF-1α, CREB, Smad1, POU, and TFAM (Lin et al., 2016; Li et al., 2018; Wang et al., 2020). Except for transcription factors, epigenetic mechanism may also influence the transcriptional alterations of aging-regulatory genes during diapause (Reynolds, 2017). Studies have proposed that DNA methylation (Pegoraro et al., 2016), histone modifications (Lu et al., 2013; Hickner et al., 2015; Sim et al., 2015; Reynolds et al., 2016), non-coding RNAs (Reynolds et al., 2013, 2017; Poupardin et al., 2015; Yocum et al., 2015; Reynolds, 2019), and RNA methylation (Jiang et al., 2019) may all contribute to diapause-related transcriptional changes and phenotypes. The phenomenon of extended adult lifespan after diapause in some insects suggests that the expression levels of aging-regulatory genes persist after diapause termination. The possible cause of species variation in this phenomenon is

species-specific transcriptional maintenance. The transcriptional regulatory mechanisms underlying diapause seem to vary across insects. Interspecific comparisons revealed little transcriptional similarity among diapauses across invertebrates (Ragland et al., 2010). DNA methylation play roles in diapause regulation in the wasp *Nasonia vitripennis* but not in the silkmoth *Bombyx mori* (Pegoraro et al., 2016; Yuichi et al., 2016).

Some gaps exist in understanding the effects of diapause on aging. Although a great variation in the expression of aging-related genes during diapause has been documented, experimental evidence of cause-and-effect relationships between gene expression and aging is still lacking. Moreover, whether the expression levels of these diapause-induced aging-regulatory genes persist after diapause termination and the underlying mechanisms involved are unclear.

CONCLUSION AND PERSPECTIVE

Substantial progress has been achieved in enhancing the understanding of the molecular basis of aging regulation in insect aging. Obviously, these underlying molecular mechanisms were highly intertwined processes. Transcriptional differences are the most observed differences in aging-regulatory genes involved in endocrine regulation, oxidative stress responses, maintenance of telomere, and genomic stability (Amdam et al., 2005; Corona et al., 2007; Bonasio et al., 2010; Elsner et al., 2018). These transcriptional differences may be attributed to variations in transcription factors and epigenetic states, which in turn are influenced by endocrine factors (Sim and Denlinger, 2008, 2013a; Vaiserman et al., 2018). The mechanisms mentioned above also play critical roles in mammalian and human aging (Lopez-Otin et al., 2013). For instance, reduced insulin signaling is related to extended longevity in social insects and mammals (Tatar et al., 2003; Corona et al., 2007; Ament et al., 2008), although the insulin pathways considerably vary across species (Corona et al., 2007; Smýkal et al., 2020). DNA methylation is closely related to aging from insects to mammals (Herb et al., 2012; Yan et al., 2015; Horvath and Raj, 2018), although the differences in genomic DNA methylation between insects and vertebrates are highly significant (de Mendoza et al., 2020). This finding suggests that aging-regulatory pathways are evolutionarily conserved, although the detailed mechanisms may vary across species. Thus, aging studies on non-*Drosophila* insects could expand the understanding of aging regulators and help develop anti-aging interventions. Here, several perspectives for further studies on insect aging are provided as follows.

First, studying the aging mechanisms underlying aging plasticity in non-social insects is highly valuable. Transcription regulation represents one of the key mechanisms underlying aging regulation, and it is the downstream of environment-induced epigenetic changes. Thus, transcriptome analysis could be used to screen key aging genes and pathways underlying aging plasticity in these species.

Second, determining epigenetic mechanisms underlying aging plasticity is essential. A large number of studies suggest that epigenetic factors have potential roles in aging regulation in polyphenic insects. Epigenetic marks are plastic, and many drugs targeting epigenetic enzymes are available (Heerboth et al., 2014). Investigating the link between epigenetic information and environment cues and the epigenetic mechanisms behind insect aging could provide new insights into treatments for aging retardation and reversal.

Third, the effects of insect flight and diapause on aging vary largely depending on insect species. The diversity of insects offers rich resources for cross-species comparisons. Thus, interspecific analysis could help elucidate the mechanisms underlying the beneficial effects of insect flight and diapause on adult longevity, which may reveal new strategies to prevent collapse during aging.

Thousands of insect genomes have been sequenced (Li et al., 2019), and gene editing tools have been developed in various insects (Gantz and Akbari, 2018; Hillary et al., 2020). A strong and growing arsenal of powerful technologies provides a huge support for elucidating the molecular mechanisms underlying insect aging. These novel insect models are expected to result in groundbreaking discoveries and ultimately promote human healthy aging in the future.

AUTHOR CONTRIBUTIONS

LK and XW designed the research. SG collected the references. SG, LK, and XW wrote the manuscript. All authors contributed to the article and approved the submitted version.

FUNDING

This study was supported by the National Natural Science Foundation of China (Grant Nos. 31920103004, 31930012, and 31772531).

REFERENCES

Agarwal, S., and Sohal, R. S. (1994). DNA oxidative damage and life expectancy in houseflies. *Proc. Natl. Acad. Sci. U S A.* 91, 12332–12335. doi: 10.1073/pnas.91.25.12332

Amdam, G. V., Aase, A. L. T. O., Seehuus, S.-C., Kim Fondrk, M., Norberg, K., and Hartfelder, K. (2005). Social reversal of immunosenescence in honey bee workers. *Exp. Gerontol.* 40, 939–947. doi: 10.1016/j.exger.2005.08.004

Ament, S. A., Corona, M., Pollock, H. S., and Robinson, G. E. (2008). Insulin signaling is involved in the regulation of worker division of labor in honey bee colonies. *Proc. Natl. Acad. Sci. U S A.* 105, 4226–4231. doi: 10.1073/pnas.0800630105

Ashby, R., Forêt, S., Searle, I., and Maleszka, R. (2016). MicroRNAs in honey bee caste determination. *Sci. Rep.* 6:18794. doi: 10.1038/srep18794

Baker, N., Wolschin, F., and Amdam, G. V. (2012). Age-related learning deficits can be reversible in honeybees Apis mellifera. *Exp. Gerontol.* 47, 764–772. doi: 10.1016/j.exger.2012.05.011

Behrends, A., Scheiner, R., Baker, N., and Amdam, G. V. (2007). Cognitive aging is linked to social role in honey bees (Apis mellifera). *Exp. Gerontol.* 42, 1146–1153. doi: 10.1016/j.exger.2007.09.003

Benayoun, B. A., Pollina, E. A., and Brunet, A. (2015). Epigenetic regulation of ageing: linking environmental inputs to genomic stability. *Nat. Rev. Mol. Cell Bio.* 16, 593–610. doi: 10.1038/nrm4048

Bloch, G., Wheeler, D. E., and Robinson, G. E. (2002). "Endocrine influences on the organization of insect societies," in *Hormones Brain and Behavior*, D.W. Pfaff, A.P. Arnold, A.M. Etgen, S.E. Fahrbach & R.T. Rubin, (San Diego: Academic Press), 1027–1068. doi: 10.1016/b978-008088783-8.00030-9

Boerjan, B., Sas, F., Ernst, U. R., Tobback, J., Lemiere, F., Vandegehuchte, M. B., et al. (2011). Locust phase polyphenism: Does epigenetic precede endocrine regulation? *Gen. Comp. Endocr.* 173, 120–128. doi: 10.1016/j.ygcen.2011.05.003

Bonasio, R., Li, Q., Lian, J., Mutti, N. S., Jin, L., Zhao, H., et al. (2012). Genome-wide and caste-specific DNA methylomes of the ants Camponotus floridanus and Harpegnathos saltator. *Curr. Biol.* 22, 1755–1764. doi: 10.1016/j.cub.2012.07.042

Bonasio, R., Zhang, G., Ye, C., Mutti, N. S., Fang, X., Qin, N., et al. (2010). Genomic Comparison of the Ants Camponotus floridanus and Harpegnathos saltator. *Science* 329, 1068–1071. doi: 10.1126/science.1192428

Brunner, E., Kroiss, J., Trindl, A., and Heinze, J. (2011). Queen pheromones in Temnothorax ants: control or honest signal? *BMC Evol. Biol.* 11:55. doi: 10.1186/1471-2148-11-55

Cardoso-Júnior, C. A. M., Guidugli-Lazzarini, K. R., and Hartfelder, K. (2018). DNA methylation affects the lifespan of honey bee (Apis mellifera L.) *workers - Evidence for a regulatory module that involves vitellogenin expression but is independent of juvenile hormone function*. *Insect. Biochem. Mol. Biol.* 92, 21–29. doi: 10.1016/j.ibmb.2017.11.005

Casey, T. M., May, M. L., and Morgan, K. R. (1985). Flight energetics of euglossine bees in relation to morphology and wing stroke frequency. *J. Exp. Biol.* 116, 271–289.

Chen, C., Xia, Q., Xiao, H., Xiao, L., and Xue, F. (2014). A comparison of the life-history traits between diapause and direct development individuals in the cotton bollworm, Helicoverpa armigera. *J. Insect. Sci.* 14:19. doi: 10.1093/jis/14.1.19

Corona, M., Hughes, K. A., Weaver, D. B., and Robinson, G. E. (2005). Gene expression patterns associated with queen honey bee longevity. *Mech. Age. Dev.* 126, 1230–1238. doi: 10.1016/j.mad.2005.07.004

Corona, M., Velarde, R. A., Remolina, S., Moran-Lauter, A., Wang, Y., Hughes, K. A., et al. (2007). Vitellogenin, juvenile hormone, insulin signaling, and queen honey bee longevity. *Proc. Natl. Acad. Sci. U S A.* 104, 7128–7133. doi: 10.1073/pnas.0701909104

Cui, X., Wang, L., Zuo, P., Han, Z., Fang, Z., Li, W., et al. (2004). D-Galactose-caused life shortening in Drosophila melanogaster and Musca domestica is associated with oxidative stress. *Biogerontology* 5, 317–325. doi: 10.1007/s10522-004-2570-3

Darveau, C.-A., Billardon, F., and Bélanger, K. (2014). Intraspecific variation in flight metabolic rate in the bumblebee Bombus impatiens repeatability and functional determinants in workers and drones. *J. Exp. Biol.* 217, 536–544. doi: 10.1242/jeb.091892

de Mendoza, A., Lister, R., and Bogdanovic, O. (2020). Evolution of DNA methylome diversity in eukaryotes. *J. Mol. Biol.* 432, 1687–1705. doi: 10.1016/j.jmb.2019.11.003

Demontis, F., Piccirillo, R., Goldberg, A. L., and Perrimon, N. (2013). The influence of skeletal muscle on systemic aging and lifespan. *Aging Cell* 12, 943–949. doi: 10.1111/acel.12126

Denlinger, D. L. (2002). Regulation of diapause. *Annu. Rev. Entomol.* 47, 93–122. doi: 10.1146/annurev.ento.47.091201.145137

Denlinger, D. L. (2008). Why study diapause? *Entomol. Res.* 38, 1–9. doi: 10.1111/j.1748-5967.2008.00139.x

Dhillon, M. K., and Hasan, F. (2018). Consequences of diapause on post-diapause development, reproductive physiology and population growth of Chilo partellus (Swinhoe). *Physiol. Entomol.* 43, 196–206. doi: 10.1111/phen.12243

Dudley, R. (2002). *The biomechanics of insect flight: form, function, evolution*. Princeton, NJ: Princeton University Press, doi: 10.1515/9780691186344

Duggal, N. A., Pollock, R. D., Lazarus, N. R., Harridge, S., and Lord, J. M. (2018). Major features of immunesenescence, including reduced thymic output, are ameliorated by high levels of physical activity in adulthood. *Aging Cell* 17:e12750. doi: 10.1111/acel.12750

Duttaroy, A., Paul, A., Kundu, M., and Belton, A. (2003). A Sod2 null mutation confers severely reduced adult life span in Drosophila. *Genetics* 165, 2295–2299.

Elsner, D., Meusemann, K., and Korb, J. (2018). Longevity and transposon defense, the case of termite reproductives. *Proc. Natl. Acad. Sci. U S A.* 115, 5504–5509. doi: 10.1073/pnas.1804046115

Feller, P., and Nachtigall, W. (1989). Flight of the honey bee. *J. Comp. Physio. B* 158, 719–727.

Finkel, T., and Holbrook, N. J. (2000). Oxidants, oxidative stress and the biology of ageing. *Nature* 408, 239–247. doi: 10.1038/35041687

Foret, S., Kucharski, R., Pellegrini, M., Feng, S., Jacobsen, S. E., Robinson, G. E., et al. (2012). DNA methylation dynamics, metabolic fluxes, gene splicing, and alternative phenotypes in honey bees. *Proc. Natl. Acad. Sci. U S A* 109, 4968–4973. doi: 10.1073/pnas.1202392109

Freitak, D., Tammaru, T., Sandre, S.-L., Meister, H., and Esperk, T. (2019). Longer life span is associated with elevated immune activity in a seasonally polyphenic butterfly. *J. Evol. Biol.* 32, 653–665. doi: 10.1111/jeb.13445

Gantz, V. M., and Akbari, O. S. (2018). Gene editing technologies and applications for insects. *Curr. Opin. Insect. Sci.* 28, 66–72. doi: 10.1016/j.cois.2018.05.006

Gebre-Amlak, A. (1989). Phenology and fecundity of maize stalk borer Busseola fusca (Fuller) in Awassa. *South. Ethiopia. Insect. Sci. Appl.* 10, 131–137. doi: 10.1017/s1742758400010274

Gems, D., and Partridge, L. (2008). Stress-response hormesis and aging: "that which does not kill us makes us stronger". *Cell Metab.* 7, 200–203. doi: 10.1016/j.cmet.2008.01.001

Gibbs, M., and Van Dyck, H. (2010). Butterfly flight activity affects reproductive performance and longevity relative to landscape structure. *Oecologia* 163, 341–350. doi: 10.1007/s00442-010-1613-5

Goldsworthy, G. J. (1983). The endocrine control of flight metabolism in locusts. *Adv. Insect. Physiol.* 17, 149–204. doi: 10.1016/S0065-2806(08)60218-0

Guidugli, K. R., Nascimento, A. M., Amdam, G. V., Barchuk, A. R., Omholt, S., Simões, Z. L. P., et al. (2005). Vitellogenin regulates hormonal dynamics in the worker caste of a eusocial insect. *FEBS Lett.* 579, 4961–4965. doi: 10.1016/j.febslet.2005.07.085

Guo, M. (2012). Drosophila as a model to study mitochondrial dysfunction in Parkinson's disease. *Cold Spring Harb. Perspect Med.* 2:a009944. doi: 10.1101/cshperspect.a009944

Guo, X., Su, S., Skogerboe, G., Dai, S., Li, W., Li, Z., et al. (2013). Recipe for a busy bee: microRNAs in honey bee caste determination. *PLoS One* 8:e81661. doi: 10.1371/journal.pone.0081661

Haddad, L. S., Kelbert, L., and Hulbert, A. J. (2007). Extended longevity of queen honey bees compared to workers is associated with peroxidation-resistant membranes. *Exp. Gerontol.* 42, 601–609. doi: 10.1016/j.exger.2007.02.008

Hahn, D. A., and Denlinger, D. L. (2010). Energetics of insect diapause. *Annu. Rev. Entomol.* 56, 103–121. doi: 10.1146/annurev-ento-112408-085436

Harman, D. (1956). Aging: a theory based on free radical and radiation chemistry. *J. Gerontol.* 11, 298–300. doi: 10.1093/geronj/11.3.298

Hartmann, A., and Heinze, J. (2003). Lay eggs, live longer: division of labor and life span in a clonal ant species. *Evolution* 57, 2424–2429. doi: 10.1111/j.0014-3820.2003.tb00254.x

He, W., Goodkind, D., and Kowal, P. (2016). *An Aging World: 2015. International Population Reports*. Suitland, MA: United States Census Bureau, doi: 10.1007/978-3-642-19335-4_63

Heerboth, S., Lapinska, K., Snyder, N., Leary, M., Rollinson, S., and Sarkar, S. (2014). Use of epigenetic drugs in disease: An overview. *Genet. Epigenet* 1, 9–19. doi: 10.4137/GEG.S12270

Helfand, S. L., and Rogina, B. (2003). Genetics of aging in the fruit fly. *Drosophila melanogaster*. *Annu. Rev. Genet* 37, 329–348. doi: 10.1146/annurev.genet.37.040103.095211

Herb, B. R., Wolschin, F., Hansen, K. D., Aryee, M. J., Langmead, B., Irizarry, R., et al. (2012). Reversible switching between epigenetic states in honeybee behavioral subcastes. *Nat. Neurosci.* 15, 1371–1373. doi: 10.1038/nn.3218

Herman, W. S., and Tatar, M. (2001). Juvenile hormone regulation of longevity in the migratory monarch butterfly. *Proc. Biol. Sci.* 268, 2509–2514. doi: 10.1098/rspb.2001.1765

Herskind, A. M., Mcgue, M., Holm, N. V., Sorensen, T. I. A., Harvald, B., and Vaupel, J. W. (1996). The heritability of human longevity: A population-based study of 2872 Danish twin pairs born 1870-1900. *Hum. Genet* 97, 319–323. doi: 10.1007/BF02185763

Hickner, P. V., Mori, A., Zeng, E., Tan, J. C., and Severson, D. W. (2015). Whole transcriptome responses among females of the filariasis and arbovirus vector mosquito Culex pipiens implicate TGF-β signaling and chromatin modification as key drivers of diapause induction. *Funct. Integr. Genom.* 15, 439–447. doi: 10.1007/s10142-015-0432-5

Hillary, V. E., Ceasar, S. A., and Ignacimuthu, S. (2020). "Genome engineering in insects: focus on the CRISPR/Cas9 system," in *Genome Engineering via CRISPR-Cas9 System*, eds V. Singh and P. K. Dhar (Academic Press), 219–249. doi: 10.1016/B978-0-12-818140-9.00018-0

Hölldobler, B., and Wilson, E. O. (1990). *The ants*. Cambridge, MA: Belknap Press of Harvard University Press.

Horvath, S., and Raj, K. (2018). DNA methylation-based biomarkers and the epigenetic clock theory of ageing. *Nat. Rev. Genet.* 19, 371–384. doi: 10.1038/s41576-018-0004-3

Ishihara, M., and Shimada, M. (1995). Trade-off in allocation of metabolic reserves: effects of diapause on egg production and adult longevity in a multivotine bruchid. *Kytorhinus sharpianus*. *Funct. Ecol.* 9, 618–624. doi: 10.2307/2390152

Jiang, T., Li, J., Qian, P., Xue, P., Xu, J., Chen, Y., et al. (2019). The role of N6-methyladenosine modification on diapause in silkworm (Bombyx mori) strains that exhibit different voltinism. *Mol. Reprod. Dev.* 86, 1981–1992. doi: 10.1002/mrd.23283

Jumpertz, R., Hanson, R. L., Sievers, M. L., Bennett, P. H., Nelson, R. G., and Krakoff, J. (2011). Higher energy expenditure in humans predicts natural mortality. *J. Clin. Endocrinol. Metab.* 96, E972–E976. doi: 10.1210/jc.2010-2944

Kammer, A. E., and Heinrich, B. (1978). Insect flight metabolism. *Adv. Insect. Phys.* 13, 133–228. doi: 10.1016/S0065-2806(08)60266-0

Keller, L., and Jemielity, S. (2006). Social insects as a model to study the molecular basis of ageing. *Exp. Gerontol.* 41, 553–556. doi: 10.1016/j.exger.2006.04.002

Kennedy, B. K., Berger, S. L., Brunet, A., Campisi, J., Cuervo, A. M., Epel, E. S., et al. (2014). Geroscience: linking aging to chronic disease. *Cell* 159, 708–712. doi: 10.1016/j.cell.2014.10.039

Kirby, K., Hu, J., Hilliker, A. J., and Phillips, J. P. (2002). RNA interference-mediated silencing of Sod2 in Drosophila leads to early adult-onset mortality and elevated endogenous oxidative stress. *Proc. Natl. Acad. Sci. U S A.* 99, 16162–16167. doi: 10.1073/pnas.252342899

Kohlmeier, P., Negroni, M. A., Kever, M., Emmling, S., Stypa, H., Feldmeyer, B., et al. (2017). Intrinsic worker mortality depends on behavioral caste and the queens' presence in a social insect. *Sci. Nat.* 104:34. doi: 10.1007/s00114-017-1452-x

Korandová, M., and Frydrychová, R. Č. (2016). Activity of telomerase and telomeric length in Apis mellifera. *Chromosoma* 125, 405–411. doi: 10.1007/s00412-015-0547-4

Kramer, B. H., and Schaible, R. (2013). Colony size explains the lifespan differences between queens and workers in eusocial Hymenoptera. *Biol. J. Linn. Soc.* 109, 710–724. doi: 10.1111/bij.12072

Kramer, B. H., Van Doorn, G. S., Weissing, F. J., and Pen, I. (2016). Lifespan divergence between social insect castes: challenges and opportunities for evolutionary theories of aging. *Curr. Opin. Insect. Sci.* 16, 76–80. doi: 10.1016/j.cois.2016.05.012

Krutmann, J., Bouloc, A., Sore, G., Bernard, B. A., and Passeron, T. (2017). The skin aging exposome. *J. Dermatol. Sci.* 85, 152–161. doi: 10.1016/j.jdermsci.2016.09.015

Kvist, J., Mattila, A. L. K., Somervuo, P., Ahola, V., Koskinen, P., Paulin, L., et al. (2015). Flight-induced changes in gene expression in the Glanville fritillary butterfly. *Mol. Ecol.* 24, 4886–4900. doi: 10.1111/mec.13359

Lane, S. J., Frankino, W. A., Elekonich, M. M., and Roberts, S. P. (2014). The effects of age and lifetime flight behavior on flight capacity in Drosophila melanogaster. *J. Exp. Biol.* 217, 1437–1443. doi: 10.1242/jeb.095646

Le Bourg, E. (2001). Oxidative stress, aging and longevity in Drosophila melanogaster. *FEBS Lett.* 498, 183–186. doi: 10.1016/s0014-5793(01)02457-7

Levin, E., Lopez-Martinez, G., Fane, B., and Davidowitz, G. (2017). Hawkmoths use nectar sugar to reduce oxidative damage from flight. *Science* 355, 733–734. doi: 10.1126/science.aah4634

Li, F., Zhao, X., Li, M., He, K., Huang, C., Zhou, Y., et al. (2019). Insect genomes: progress and challenges. *Insect. Mol. Biol.* 28, 739–758. doi: 10.1111/imb.12599

Li, H., Lin, X., Geng, S., and Xu, W. (2018). TGF-β and BMP signals regulate insect diapause through Smad1-POU-TFAM pathway. *Biochim. Biophys. Acta Mol. Cell Res.* 1865, 1239–1249. doi: 10.1016/j.bbamcr.2018.06.002

Li, W., Prazak, L., Chatterjee, N., Grüninger, S., Krug, L., Theodorou, D., et al. (2013). Activation of transposable elements during aging and neuronal decline in Drosophila. *Nat. Neurosci.* 16, 529–531. doi: 10.1038/nn.3368

Lin, X., Tang, L., Yang, J., and Xu, W. (2016). HIF-1 regulates insect lifespan extension by inhibiting c-Myc-TFAM signaling and mitochondrial biogenesis. *Biochim. Biophys. Acta Mol. Cell Res.* 1863, 2594–2603. doi: 10.1016/j.bbamcr.2016.07.007

Lin, X., and Xu, W. (2016). Hexokinase is a key regulator of energy metabolism and ROS activity in insect lifespan extension. *Aging* 8, 245–259. doi: 10.18632/aging.100885

Lopez-Otin, C., Blasco, M. A., Partridge, L., Serrano, M., and Kroemer, G. (2013). The hallmarks of aging. *Cell* 153, 1194–1217. doi: 10.1016/j.cell.2013.05.039

Lopez-Otin, C., Galluzzi, L., Freije, J. M. P., Madeo, F., and Kroemer, G. (2016). Metabolic Control of Longevity. *Cell* 166, 802–821. doi: 10.1016/j.cell.2016.07.031

Lu, Y., Denlinger, D. L., and Xu, W. (2013). Polycomb repressive complex 2 (PRC2) protein ESC regulates insect developmental timing by mediating H3K27me3 and activating prothoracicotropic hormone gene expression. *J. Biol. Chem.* 288, 23554–23564. doi: 10.1074/jbc.M113.482497

Magwere, T., Pamplona, R., Miwa, S., Martinez-Diaz, P., Portero-Otin, M., Brand, M. D., et al. (2006). Flight activity, mortality rates, and lipoxidative damage in Drosophila. *J. Gerontol. A Biol. Sci. Med. Sci.* 61, 136–145. doi: 10.1093/gerona/61.2.136

Marco, A., Hui, J. H. L., Ronshaugen, M., and Griffiths-Jones, S. (2010). Functional shifts in insect microRNA evolution. *Genome Biol. Evol.* 2, 686–696. doi: 10.1093/gbe/evq053

Margotta, J. W., Mancinelli, G. E., Benito, A. A., Ammons, A., Roberts, S. P., and Elekonich, M. M. (2013). Effects of flight on gene expression and aging in the honey bee brain and flight muscle. *Insects* 4, 9–30. doi: 10.3390/insects4010009

Margotta, J. W., Roberts, S. P., and Elekonich, M. M. (2018). Effects of flight activity and age on oxidative damage in the honey bee, Apis mellifera. *J. Exp. Biol.* 221:jeb183228. doi: 10.1242/jeb.183228

Martin, N., Hulbert, A. J., Brenner, G. C., Brown, S. H. J., Mitchell, T. W., and Else, P. L. (2019). Honey bee caste lipidomics in relation to life-history stage and the long life of the queen. *J. Exp. Biol.* 222:jeb207043. doi: 10.1242/jeb.207043

Mayhew, P. J. (2007). Why are there so many insect species? Perspectives from fossils and phylogenies. *Biol. Rev.* 82, 425–454. doi: 10.1111/j.1469-185X.2007.00018.x

Molloy, J., Kyrtatas, V., Sparrow, J., and White, D. (1987). Kinetics of flight muscles from insects with different wingbeat frequencies. *Nature* 328, 449–451. doi: 10.1038/328449a0

Münch, D., and Amdam, G. V. (2010). The curious case of aging plasticity in honey bees. *FEBS Lett.* 584, 2496–2503. doi: 10.1016/j.febslet.2010.04.007

Münch, D., Amdam, G. V., and Wolschin, F. (2008). Ageing in a eusocial insect: molecular and physiological characteristics of life span plasticity in the honey bee. *Funct. Ecol.* 22, 407–421. doi: 10.1111/j.1365-2435.2008.01419.x

Niitepõld, K., and Boggs, C. L. (2015). Effects of increased flight on the energetics and life history of the butterfly Speyeria mormonia. *PLoS One* 10:e0140104. doi: 10.1371/journal.pone.0140104

Niitepõld, K., and Hanski, I. (2013). A long life in the fast lane: positive association between peak metabolic rate and lifespan in a butterfly. *J. Exp. Biol.* 216, 1388–1397. doi: 10.1242/jeb.080739

Nunes, F. M. F., Ihle, K. E., Mutti, N. S., Simões, Z. L. P., and Amdam, G. V. (2013). The gene vitellogenin affects microRNA regulation in honey bee Apis mellifera fat body and brain. *J. Exp. Biol.* 216, 3724–3732. doi: 10.1242/jeb.089243

Ogawa, K., and Miura, T. (2014). Aphid polyphenisms: trans-generational developmental regulation through viviparity. *Front. Physiol.* 5:1. doi: 10.3389/fphys.2014.00001

Page, R. E. Jr., and Amdam, G. V. (2007). The making of a social insect: developmental architectures of social design. *BioEssays* 29, 334–343. doi: 10.1002/bies.20549

Parker, J. D., Parker, K. M., Sohal, B. H., Sohal, R. S., and Keller, L. (2004). Decreased expression of Cu-Zn superoxide dismutase 1 in ants with extreme lifespan. *Proc. Natl. Acad. Sci. U S A.* 101, 3486–3489. doi: 10.1073/pnas.0400222101

Parkes, T., Kirby, K., Phillips, J., and Hilliker, A. (1998). Transgenic analysis of the cSOD-null phenotypic syndrome in Drosophila. *Genome* 41, 642–651. doi: 10.1139/g98-068

Pegoraro, M., Bafna, A., Davies, N. J., Shuker, D. M., and Tauber, E. (2016). DNA methylation changes induced by long and short photoperiods in Nasonia. *Gen. Res.* 26, 203–210. doi: 10.1101/gr.196204.115

Pener, M. P., and Simpson, S. J. (2009). Locust phase polyphenism: an update. *Adv. Insect. Phys.* 36, 1–272. doi: 10.1016/S0065-2806(08)36001-9

Phillips, J. P., Campbell, S. D., Michaud, D., Charbonneau, M., and Hilliker, A. J. (1989). Null mutation of copper-zinc superoxide-dismutase in Drosophila confers hypersensitivity to paraquat and reduced Longevity. *Proc. Natl. Acad. Sci. U S A.* 86, 2761–2765. doi: 10.1073/pnas.86.8.2761

Piper, M. D. W., and Partridge, L. (2018). Drosophila as a model for ageing. *Biochim. Biophys. Acta Mol. Basis Dis.* 1864, 2707–2717. doi: 10.1016/j.bbadis.2017.09.016

Poupardin, R., Schöttner, K., Korbelová, J., Provazník, J., Doležel, D., Pavlinic, D., et al. (2015). Early transcriptional events linked to induction of diapause revealed by RNAseq in larvae of drosophilid fly, Chymomyza costata. *BMC Genomics* 16:720. doi: 10.1186/s12864-015-1907-4

Quigley, T. P., Amdam, G. V., and Rueppell, O. (2018). "Honeybee Workers as Models of Aging," in *Conn's Handbook of Models for Human Aging (Second Edition)*, eds J. L. Ram and P. M. Conn (Cambridge: Academic Press), 533–547. doi: 10.1016/b978-0-12-811353-0.00040-3

Rademakers, L. H. P. M., and Beenakkers, A. M. T. (1977). Changes in the secretory activity of the glandular lobe of the corpus cardiacum of Locusta migratoria induced by flight. *Cell Tissue Res.* 180, 155–171. doi: 10.1007/BF00231949

Ragland, G. J., Denlinger, D. L., and Hahn, D. A. (2010). Mechanisms of suspended animation are revealed by transcript profiling of diapause in the flesh fly. *Proc. Natl. Acad. Sci. U S A.* 107, 14909–14914. doi: 10.1073/pnas.1007075107

Redman, L. M., Smith, S. R., Burton, J. H., Martin, C. K., Il'yasova, D., and Ravussin, E. (2018). Metabolic slowing and reduced oxidative damage with sustained caloric restriction support the rate of living and oxidative damage theories of aging. *Cell Metab.* 27, 805–815. doi: 10.1016/j.cmet.2018.02.019

Reiter, L. T., Potocki, L., Chien, S., Gribskov, M., and Bier, E. (2001). A systematic analysis of human disease-associated gene sequences in Drosophila melanogaster. *Genome Res.* 11, 1114–1125. doi: 10.1101/gr.169101

Remolina, S. C., and Hughes, K. A. (2008). Evolution and mechanisms of long life and high fertility in queen honey bees. *Age* 30:177. doi: 10.1007/s11357-008-9061-4

Reynolds, J. A. (2017). Epigenetic influences on diapause. *Adv Insect Phys.* 53, 115–144. doi: 10.1016/bs.aiip.2017.03.003

Reynolds, J. A. (2019). Noncoding RNA regulation of dormant states in evolutionarily diverse animals. *Biol. Bull.* 237, 192–209. doi: 10.1086/705484

Reynolds, J. A., Bautista-Jimenez, R., and Denlinger, D. L. (2016). Changes in histone acetylation as potential mediators of pupal diapause in the flesh fly, Sarcophaga bullata. *Insect. Biochem. Mol. Biol.* 76, 29–37. doi: 10.1016/j.ibmb.2016.06.012

Reynolds, J. A., Clark, J., Diakoff, S. J., and Denlinger, D. L. (2013). Transcriptional evidence for small RNA regulation of pupal diapause in the flesh fly, Sarcophaga bullata. *Insect. Biochem. Mol. Biol.* 43, 982–989. doi: 10.1016/j.ibmb.2013.07.005

Reynolds, J. A., Peyton, J. T., and Denlinger, D. L. (2017). Changes in microRNA abundance may regulate diapause in the flesh fly, Sarcophaga bullata. *Insect. Biochem. Mol. Biol.* 84, 1–14. doi: 10.1016/j.ibmb.2017.03.002

Robinson, G. E., and Vargo, E. L. (1997). Juvenile hormone in adult eusocial Hymenoptera: gonadotropin and behavioral pacemaker. *Arch. Insect. Biochem. Physiol.* 35, 559–583. doi: 10.1002/(sici)1520-6327(1997)35:4<559::aid-arch13>3.0.co;2-9

Rodrigues, M. A., and Flatt, T. (2016). Endocrine uncoupling of the trade-off between reproduction and somatic maintenance in eusocial insects. *Curr. Opin. Insect. Sci.* 16, 1–8. doi: 10.1016/j.cois.2016.04.013

Rubner, M. (1916). Machinery of metabolism. *JAMA* 66:1879. doi: 10.1111/jgs.12740

Ruggiero, C., Metter, E. J., Melenovsky, V., Cherubini, A., Najjar, S. S., Ble, A., et al. (2008). High basal metabolic rate is a risk factor for mortality: the Baltimore Longitudinal Study of Aging. *J. Gerontol. A Biol. Sci. Med. Sci.* 63, 698–706. doi: 10.1093/gerona/63.7.698

Saastamoinen, M., Van Der Sterren, D., Vastenhout, N., Zwaan, B. J., and Brakefield, P. M. (2010). Predictive adaptive responses: condition-dependent impact of adult nutrition and flight in the tropical butterfly Bicyclus anynana. *Am. Nat.* 176, 686–698. doi: 10.1086/657038

Santos, A. L., Sinha, S., and Lindner, A. B. (2018). The good, the bad, and the ugly of ROS: new insights on aging and aging-related diseases from eukaryotic and prokaryotic model organisms. *Oxid. Med. Cell Longev.* 2018:1941285. doi: 10.1155/2018/1941285

Schneider, S. A., Schrader, C., Wagner, A. E., Boesch-Saadatmandi, C., Liebig, J., Rimbach, G., et al. (2011). Stress resistance and longevity are not directly linked to levels of enzymatic antioxidants in the ponerine ant Harpegnathos saltator. *PLoS One* 6:e14601. doi: 10.1371/journal.pone.0014601

Sebastiani, P., and Perls, T. T. (2012). The genetics of extreme longevity: lessons from the new England centenarian study. *Front. Genet.* 3:277. doi: 10.3389/fgene.2012.00277

Seehuus, S.-C., Krekling, T., and Amdam, G. V. (2006a). Cellular senescence in honey bee brain is largely independent of chronological age. *Exp. Gerontol.* 41, 1117–1125. doi: 10.1016/j.exger.2006.08.004

Seehuus, S.-C., Norberg, K., Gimsa, U., Krekling, T., and Amdam, G. V. (2006b). Reproductive protein protects functionally sterile honey bee workers from oxidative stress. *Proc. Natl. Acad. Sci. U S A.* 103, 962–967. doi: 10.1073/pnas.0502681103

Seeley, T. D. (1978). Life history strategy of the honey bee, Apis mellifera. *Oecologia* 32, 109–118. doi: 10.1007/BF00344695

Shi, Y., Zheng, H., Pan, Q., Wang, Z., and Zeng, Z. (2015). Differentially expressed microRNAs between queen and worker larvae of the honey bee (Apis mellifera). *Apidologie* 46, 35–45. doi: 10.1007/s13592-014-0299-9

Sim, C., and Denlinger, D. L. (2008). Insulin signaling and FOXO regulate the overwintering diapause of the mosquito Culex pipiens. *Proc. Natl. Acad. Sci. U S A.* 105, 6777–6781. doi: 10.1073/pnas.0802067105

Sim, C., and Denlinger, D. L. (2013a). Juvenile hormone III suppresses forkhead of transcription factor in the fat body and reduces fat accumulation in the diapausing mosquito, Culex pipiens. *Insect. Mol. Biol.* 22, 1–11. doi: 10.1111/j.1365-2583.2012.01166.x

Sim, C., and Denlinger, D. L. (2013b). Insulin signaling and the regulation of insect diapause. *Front. Physiol.* 4:189. doi: 10.3389/fphys.2013.00189

Sim, C., Kang, D. S., Kim, S., Bai, X., and Denlinger, D. L. (2015). Identification of FOXO targets that generate diverse features of the diapause phenotype in the mosquito Culex pipiens. *Proc. Natl. Acad. Sci. U S A* 112, 3811–3816. doi: 10.1073/pnas.1502751112

Simola, D. F., Graham, R. J., Brady, C. M., Enzmann, B. L., Desplan, C., Ray, A., et al. (2016). Epigenetic (re)programming of caste-specific behavior in the ant Camponotus floridanus. *Science* 351:aac6633. doi: 10.1126/science.aac6633

Simola, D. F., Ye, C., Mutti, N. S., Dolezal, K., Bonasio, R., Liebig, J., et al. (2013). A chromatin link to caste identity in the carpenter ant Camponotus floridanus. *Gen. Res.* 23, 486–496. doi: 10.1101/gr.148361.112

Simpson, S. J., Sword, G. A., and Lo, N. (2011). Polyphenism in insects. *Curr. Biol.* 21, R738–R749. doi: 10.1016/j.cub.2011.06.006

Smýkal, V., Pivarči, M., Provazník, J., Bazalová, O., Jedlička, P., Lukšan, O., et al. (2020). Complex evolution of insect insulin receptors and homologous decoy receptors, and functional significance of their multiplicity. *Mol. Biol. Evol.* 37, 1775–1789. doi: 10.1093/molbev/msaa048

Sohal, R., Allen, R., Farmer, K., and Procter, J. (1984). Effect of physical activity on superoxide dismutase, catalase, inorganic peroxides and glutathione in the adult male housefly, Musca domestica. *Mech. Age. Dev.* 26, 75–81. doi: 10.1016/0047-6374(84)90069-1

Solovev, I., Shaposhnikov, M., Kudryavtseva, A., and Moskalev, A. (2018). "Drosophila melanogaster as a model for studying the epigenetic basis of aging," in *Epigenetics of Aging and Longevity*, eds A. Moskalev and A. M. Vaiserman (Boston: Academic Press), 293–307. doi: 10.1016/b978-0-12-811060-7.00014-0

Spannhoff, A., Kim, Y. K., Raynal, N. J. M., Gharibyan, V., Su, M., Zhou, Y., et al. (2011). Histone deacetylase inhibitor activity in royal jelly might facilitate caste switching in bees. *EMBO Rep.* 12, 238–243. doi: 10.1038/embor.2011.9

Speakman, J. R. (2005). Body size, energy metabolism and lifespan. *J. Exp. Biol.* 208, 1717–1730. doi: 10.1242/jeb.01556

Straka, J., černá, K., Macháčková, L., Zemenová, M., and Keil, P. (2014). Life span in the wild: the role of activity and climate in natural populations of bees. *Funct. Ecol.* 28, 1235–1244. doi: 10.1111/1365-2435.12261

Tatar, M., Bartke, A., and Antebi, A. (2003). The endocrine regulation of aging by insulin-like signals. *Science* 299, 1346–1351. doi: 10.1126/science.1081447

Tatar, M., Chien, S. A., and Priest, N. K. (2001a). Negligible senescence during reproductive dormancy in Drosophila melanogaster. *Am. Nat.* 158, 248–258. doi: 10.1086/321320

Tatar, M., Kopelman, A., Epstein, D., Tu, M. P., Yin, C. M., and Garofalo, R. S. (2001b). A mutant Drosophila insulin receptor homolog that extends life-span and impairs neuroendocrine function. *Science* 292:107. doi: 10.1126/science.1057987

Tatar, M., and Yin, C. M. (2001). Slow aging during insect reproductive diapause: why butterflies, grasshoppers and flies are like worms. *Exp. Gerontol.* 36, 723–738. doi: 10.1016/s0531-5565(00)00238-2

Toivonen, J. M., and Partridge, L. (2009). Endocrine regulation of aging and reproduction in Drosophila. *Mol. Cell Endocrinol.* 299, 39–50. doi: 10.1016/j.mce.2008.07.005

Tolfsen, C. C., Baker, N., Kreibich, C., and Amdam, G. V. (2011). Flight restriction prevents associative learning deficits but not changes in brain protein-adduct formation during honeybee ageing. *J. Exp. Biol.* 214, 1322–1332. doi: 10.1242/jeb.049155

United Nations (2017). *World Population Ageing 2017-Highlights*. New York: Department of Economic and Social Affairs.

Vaiserman, A. M., Lushchak, V., and Koliada, A. K. (2018). "Epigenetics of Longevity in Social Insects," in *Epigenetics of Aging and Longevity*, (Netherland: Elsevier), 271–289. doi: 10.1016/b978-0-12-811060-7.00013-9

Valenzano, D. R., Aboobaker, A., Seluanov, A., and Gorbunova, V. (2017). Non-canonical aging model systems and why we need them. *EMBO J.* 36, 959–963. doi: 10.15252/embj.201796837

Wang, T., Geng, S., Guan, Y., and Xu, W. (2018). Deacetylation of metabolic enzymes by Sirt2 modulates pyruvate homeostasis to extend insect lifespan. *Aging* 10, 1053–1072. doi: 10.18632/aging.101447

Wang, X., Geng, S., Zhang, X., and Xu, W. (2020). P-S6K is associated with insect diapause via the ROS/AKT/ S6K/CREB/HIF-1 pathway in the cotton bollworm. *Helicoverpa armigera*. *Insect Biochem. Mol. Biol.* 120:103262. doi: 10.1016/j.ibmb.2019.103262

Weaver, D. B., Anzola, J. M., Evans, J. D., Reid, J. G., Reese, J. T., Childs, K. L., et al. (2007). Computational and transcriptional evidence for microRNAs in the honey bee genome. *Genome Biol.* 8:R97. doi: 10.1186/gb-2007-8-6-r97

Whitman, D. W., and Ananthakrishnan, T. N. (2009). *Phenotypic plasticity of insects: Mechanisms and consequences*. Enfield, NH: Science Publishers.

Williams, J. B., Roberts, S. P., and Elekonich, M. M. (2008). Age and natural metabolically-intensive behavior affect oxidative stress and antioxidant mechanisms. *Exp. Gerontol.* 43, 538–549. doi: 10.1016/j.exger.2008.02.001

Winston, M. L. (1987). *The biology of the honey bee*. Cambridge, MA: Harvard University Press.

Woestmann, L., Kvist, J., and Saastamoinen, M. (2017). Fight or flight? - Flight increases immune gene expression but does not help to fight an infection. *J. Evol. Biol.* 30, 501–511. doi: 10.5061/dryad.38c5g

Wojciechowski, M., Lowe, R., Maleszka, J., Conn, D., Maleszka, R., and Hurd, P. J. (2018). Phenotypically distinct female castes in honey bees are defined by alternative chromatin states during larval development. *Genome Res.* 28, 1532–1542. doi: 10.1101/gr.236497.118

World Health Organization (2017). *Global strategy and action plan on ageing and health*. Switzerland: WHO.

Yan, H., Bonasio, R., Simola, D. F., Liebig, J., Berger, S. L., and Reinberg, D. (2015). DNA methylation in social insects: how epigenetics can control behavior and longevity. *Annu. Rev. Entomol.* 60, 435–452. doi: 10.1146/annurev-ento-010814-020803

Yan, L., and Sohal, R. S. (2000). Prevention of flight activity prolongs the life span of the housefly, Musca domestica, and attenuates the age-associated oxidative damamge to specific mitochondrial proteins. *Free Radic. Biol. Med.* 29, 1143–1150. doi: 10.1016/s0891-5849(00)00423-8

Yang, Y. C., Boen, C., Gerken, K., Li, T., Schorpp, K., and Harris, K. M. (2016). Social relationships and physiological determinants of longevity across the human life span. *Proc. Natl. Acad. Sci. U S A* 113, 578–583. doi: 10.1073/pnas.1511085112

Yocum, G. D., Rinehart, J. P., Horvath, D. P., Kemp, W. P., Bosch, J., Alroobi, R., et al. (2015). Key molecular processes of the diapause to post-diapause quiescence transition in the alfalfa leafcutting bee Megachile rotundata identified by comparative transcriptome analysis. *Physiol. Entomol.* 40, 103–112. doi: 10.1111/phen.12093

Yuichi, E., Tsubouchi, H., and Sakamoto, K. (2016). Does DNA methylation play a role in photoperiodic diapause of moths? *J. Entomol. Zool. Stud.* 4, 458–460.

Zhang, X., Wang, T., Lin, X., Denlinger, D. L., and Xu, W. (2017). Reactive oxygen species extend insect life span using components of the insulin-signaling pathway. *Proc. Natl. Acad. Sci. U S A* 114, E7832–E7840. doi: 10.1073/pnas.1711042114

Conflict of Interest: The authors declare that the research was conducted in the absence of any commercial or financial relationships that could be construed as a potential conflict of interest.

frontiers in Genetics

ORIGINAL RESEARCH
published: 24 September 2020
doi: 10.3389/fgene.2020.566320

Transcriptomic and Epigenomic Dynamics of Honey Bees in Response to Lethal Viral Infection

Hongmei Li-Byarlay[1†], Humberto Boncristiani[2†], Gary Howell[3], Jake Herman[2], Lindsay Clark[4], Micheline K. Strand[5], David Tarpy[1,6] and Olav Rueppell[2†]*

[1] Department of Entomology and Plant Pathology, North Carolina State University, Raleigh, NC, United States, [2] Department of Biology, University of North Carolina at Greensboro, Greensboro, NC, United States, [3] High Performance Cluster, Office of Information Technology, North Carolina State University, Raleigh, NC, United States, [4] High Performance Computing in Biology, University of Illinois at Urbana-Champaign, Urbana, IL, United States, [5] Army Research Office, Army Research Laboratory, Research Triangle Park, NC, United States, [6] W.M. Keck Center for Behavioral Biology, North Carolina State University, Raleigh, NC, United States

OPEN ACCESS

Edited by:
Wei Guo,
Chinese Academy of Sciences (CAS), China

Reviewed by:
Sufang Zhang,
Chinese Academy of Forestry, China
Richard Alan Katz,
Fox Chase Cancer Center, United States

***Correspondence:**
Hongmei Li-Byarlay
hli-byarlay@centralstate.edu

†Present address:
Hongmei Li-Byarlay, Agricultural Research and Development Program, Central State University, Wilberforce, OH, United States
Humberto Boncristiani, Department of Entomology, University of Florida, Gainesville, FL, United States
Olav Rueppell, Department of Biological Sciences, University of Alberta, Edmonton, AB, Canada

Specialty section:
This article was submitted to Epigenomics and Epigenetics, a section of the journal Frontiers in Genetics

Received: 27 May 2020
Accepted: 17 August 2020
Published: 24 September 2020

Citation:
Li-Byarlay H, Boncristiani H, Howell G, Herman J, Clark L, Strand MK, Tarpy D and Rueppell O (2020) Transcriptomic and Epigenomic Dynamics of Honey Bees in Response to Lethal Viral Infection. Front. Genet. 11:566320. doi: 10.3389/fgene.2020.566320

Honey bees (*Apis mellifera* L.) suffer from many brood pathogens, including viruses. Despite considerable research, the molecular responses and dynamics of honey bee pupae to viral pathogens remain poorly understood. Israeli Acute Paralysis Virus (IAPV) is emerging as a model virus since its association with severe colony losses. Using worker pupae, we studied the transcriptomic and methylomic consequences of IAPV infection over three distinct time points after inoculation. Contrasts of gene expression and 5 mC DNA methylation profiles between IAPV-infected and control individuals at these time points – corresponding to the pre-replicative (5 h), replicative (20 h), and terminal (48 h) phase of infection – indicate that profound immune responses and distinct manipulation of host molecular processes accompany the lethal progression of this virus. We identify the temporal dynamics of the transcriptomic response to with more genes differentially expressed in the replicative and terminal phases than in the pre-replicative phase. However, the number of differentially methylated regions decreased dramatically from the pre-replicative to the replicative and terminal phase. Several cellular pathways experienced hyper- and hypo-methylation in the pre-replicative phase and later dramatically increased in gene expression at the terminal phase, including the MAPK, Jak-STAT, Hippo, mTOR, TGF-beta signaling pathways, ubiquitin mediated proteolysis, and spliceosome. These affected biological functions suggest that adaptive host responses to combat the virus are mixed with viral manipulations of the host to increase its own reproduction, all of which are involved in anti-viral immune response, cell growth, and proliferation. Comparative genomic analyses with other studies of viral infections of honey bees and fruit flies indicated that similar immune pathways are shared. Our results further suggest that dynamic DNA methylation responds to viral infections quickly, regulating subsequent gene activities. Our study provides new insights of molecular mechanisms involved in epigenetic that can serve as foundation for the long-term goal to develop anti-viral strategies for honey bees, the most important commercial pollinator.

Keywords: alternative splicing, transcriptome, DNA methylation, immune genes, pupa, IAPV, gene expression, comparative genomics

AUTHOR SUMMARY

Honey bees, the most important managed pollinators, are experiencing unsustainable mortality. Israeli Acute Paralysis Virus (IAPV) causes economically important disease in honey bees, and it is emerging as a model system to study viral pathogen-host interactions in pollinators. The pupation stage is important for bee development but individuals are particularly vulnerable for parasitic mite infestations and viral infections. Currently, it is unclear how honey bee pupae respond to this virus. However, these responses, including gene expression and DNA methylomic changes, are critical to understand so that anti-viral genes can be identified and new anti-viral strategies be developed. Here, we use next-generation sequencing tools to reveal the dynamic changes of gene expression and DNA methylation as pupae succumb to IAPV infections after 5, 20, and 48 h. We found that IAPV causes changes in regions of DNA methylation more at the beginning of infection than later. The activity of several common insect immune pathways are affected by the IAPV infections, as are some other fundamental biological processes. Expression of critical enzymes in DNA methylation are also induced by IAPV in a temporal manner. By comparing our results to other virus studies of honey bees and fruit flies, we identified common anti-viral immune responses. Thus, our study provides new insight on the genome responses of honey bees over the course of a fatal virus infection with theoretical and practical implications.

INTRODUCTION

Infectious disease results from the breakdown of an organism's normal physiological state because of the presence or proliferation of a pathogen. This disruption can be molecularly characterized by transcriptome profiling to permit a systemic understanding of host-pathogen interactions, particularly in combination with other system-level approaches (Arvey et al., 2012; Tanca et al., 2013; Gardy and Loman, 2018). Transcriptomic and epigenomic changes in response to pathogen infections are important to understand because they are interdependent but relate to different temporal dynamics.

DNA methylation of Cytosine (5 mC) is a central epigenetic regulator of gene expression and alternative splicing (Zemach et al., 2010; Li-Byarlay et al., 2013), affecting diverse aspects of organismal function and disease (Edwards and Myers, 2007). Epigenetic programming may also be the target of host manipulations by pathogens (De Monerri and Kim, 2014) and affect host defenses and susceptibility to infection (Merkling et al., 2015; Kuss-Duerkop et al., 2018). The virus induced changes in host immune response and gene expression via DNA methylation is still a new study field. It is understudied whether changing host DNA methylation such as gene expression of certain antiviral immune genes is a main mechanism utilized by DNA or RNA viruses to manipulate immune responses. Genome-wide analyses of methylome and transcriptome indicated that the infection of DNA tumor virus induced hypermethylation of host genes during viral persistence (Kuss-Duerkop et al., 2018). In plants, DNA hypomethylation was reported after 24 h of viral infection (Pavet et al., 2006).

Honey bees (*Apis mellifera* L.) were the first insects in which a fully functional 5 mC DNA methylation system was discovered (Wang et al., 2006; Kucharski et al., 2008). Social hymenopterans, such as bees, wasps, and ants, have low levels of DNA methylation (Hunt et al., 2010; Glastad et al., 2015; Bewick et al., 2017). The methylated 5 mC sites can be one of three different kinds (CpG dinucleotides, CHG, and CHH, H represents A, T or C) (Lyko et al., 2010). The CpG is the most common kind in honey bees. CpG DNA methylation in insects occurs predominantly in gene bodies, associated with histone modifications and alternative splicing (Lyko et al., 2010; Zemach et al., 2010; Hunt et al., 2013; Li-Byarlay et al., 2013; Glastad et al., 2014; Yan et al., 2014; Glastad et al., 2016). Its phenotypic consequences range from behavioral plasticity (Herb et al., 2012; Opachaloemphan et al., 2018) to alternative development trajectories (Kucharski et al., 2008; Glastad et al., 2019) and disease responses (Galbraith et al., 2015). Especially the study from Herb et al. (2012) showed gene expression differences related to differentially methylated regions (DMRs) and also suggests wider effect because many DMRs are related to transcription factors, in which the alternative splicing may affect their function. Despite this breath of effects, few studies have investigated the role of CpG DNA methylation in insect development, immune system, and disease (Mukherjee et al., 2015; Burggren, 2017; Vilcinskas, 2017; Grozinger and Flenniken, 2019).

Honey bees are the most important managed pollinator in agriculture and crop production (Calderone, 2012). However, recent declines in honey bee health have led to unsustainably high annual colony losses in the apicultural industry (Calderone, 2012; Kulhanek et al., 2017) for which multiple, potentially interacting factors are likely the cause (Cornman et al., 2012; Goulson et al., 2015). One major contributor to widespread colony mortality is pathogenic viral infection. Many of the most important viruses are either associated with or can be directly vectored by parasitic *Varroa* mites (Bailey et al., 1963; Chen and Siede, 2007; Di Prisco et al., 2011; Gisder and Genersch, 2017). Pathogenic viral stressors affect the morphology, physiology, behavior, and growth of honey bees at different developmental stages (Chen and Siede, 2007; Runckel et al., 2011; Cornman et al., 2012; McMenamin and Genersch, 2015), ultimately leading to reduced colony productivity and mortality. The developmental pupal stage is critical for many viral diseases because the *Varroa* mite feeds on the pupae for a prolonged time (Di Prisco et al., 2011).

Honey bees employ a combination of individual- and group-level defenses against pathogens (Wilson-Rich et al., 2009). The main innate immune pathways of insects are present in honey bees and respond to virus infections (Evans et al., 2006; Brutscher et al., 2015), including the Toll, Janus kinase and Signal Transducer and Activator of Transcription (JAK-STAT), Immune Deficiency (Imd), c-Jun NH2-Terminal Kinase (JNK) pathways, antimicrobial peptides (AMPs), endocytosis, and phagocytosis mechanisms (Brutscher et al., 2015). Activation of some immune pathways, such as the RNAi mechanism, can lead to increased virus resistance (Brutscher et al., 2017). Thus, we understand that some honey bee genes respond to virus infection but a systematic

characterization of the temporal dynamics of the immune responses and the general transcriptome and methylome have not been investigated, although such studies can yield important information (Lemaitre and Hoffmann, 2007).

Israeli Acute Paralysis Virus (IAPV) has been associated with colony losses (Cox-Foster et al., 2007; Maori et al., 2009; Tantillo et al., 2015), particularly during the winter (Chen et al., 2014). IAPV belongs to the picornavirus-like family Dicistroviridae, that includes single-strand, positive sense RNA viruses that are pathogenic to a range of insects (Bonning and Miller, 2010). IAPV is relatively common in honey bees and affects all life history stages and castes (Chen et al., 2014). When cells are infected, the positive strand of RNA is released into the cytosol and translated by the host ribosomes. Then the assembled complexes for viral replication synthesize negative-sense RNA from which more descendant positive strands of the RNA are produced. These are assembled with viral proteins into virions that are then released to infect other cells (Nagy and Pogany, 2012; Chen et al., 2014). Covert infections persist through vertical and horizontal transmission, but IAPV can also readily cause paralysis and death of infected individuals (Maori et al., 2007). Acute infections of IAPV profoundly affect cellular transcription at the pupal stage (Boncristiani et al., 2013), and microarray analyses of larvae and adults indicate significant and stage-specific responses to IAPV infection (Chen et al., 2014). Parallel transcriptomic and epigenomic profiling of adult IAPV infection identified some additional molecular responses, including expression changes in immune genes and epigenetic pathways (Galbraith et al., 2015). However, little overlap of identified responses within and among studies leave the molecular characterization of IAPV infection in honey bees unresolved, and more detailed studies of dynamic responses in the time-course of IAPV infection are needed.

Here, we experimentally test the hypothesis that viral infections can affect not only transcriptomic profiles but also induce DNA methylomic changes in honey bee pupae. Specifically, we compared the complete transcriptome and methylome profiles across three distinct phases of a lethal IAPV infection. Furthermore, we tested if our results indicate significant overlap of immune genes with fruit flies as well as other stages of honey bees under IAPV viral infections.

RESULTS

Temporal Viral Infections Cause Transcriptomic Changes in Gene Expressions

The transcriptomes of whole honey bee pupae injected with PBS or infected with IAPV were compared at three time points: 5, 20, and 48 h post-injection (**Figure 1**). On average, IAPV-infected pupae yielded slightly more RNA-seq reads than the corresponding PBS controls (5 h: IAPV = 46,001,777 vs. PBS = 41,666,177; 20 h: IAPV = 47,915,086 vs. PBS = 42,429,737; and 48 h: IAPV = 42,649,987 vs. PBS = 39,248,297). Coverage thus varied among individual samples from 41x to 65x (**Supplementary Table 1**). Differentially expressed genes (DEGs) increased with disease progression over time from 432 after 5 h to 5,913 after 20 h and 5,984 after 48 h (**Supplementary Table 2**).

Relative to the PBS control, IAPV-infected pupae had 198 genes significantly up-regulated and 234 genes significantly down-regulated after 5h; 2,738 genes were significantly up-regulated and 3,175 genes significantly down-regulated after 20 h; and 3,021 genes significantly up-regulated and 2,963 genes significantly down-regulated after 48 h (**Supplementary Figures 1–3**). DEG overlap between all significantly up- or down-regulated genes was significant in all pairwise directional comparisons (up- and down-regulated genes separately) among the three time points (**Figure 2**; up-regulated 5 h vs. 20 h: $p < 0.05$; all other tests: $p < 0.001$). For the > 8-fold DEGs, significant overlap was found for all pairwise comparisons among the IAPV up-regulated gene sets ($p < 0.001$) and also for the down-regulated gene sets at 20 and 48 h ($p < 0.001$) (**Supplementary Table 2**).

Gene Enrichment and Functional Analyses

To identify IAPV-induced expression patterns across all genes regardless of significance threshold, GO Mann-Whitney *U*-tests and a Weighted Gene Co-expression Network Analysis were performed on the expression differences between IAPV infected and control samples at three time points. Post 5h of IAPV infection, multiple biological process GO terms were observed with upregulation of RNA processing (ncRNA, tRNA, and rRNA) as the most significant GO terms ($p < 0.001$). Only one term was significantly downregulated at this time point: "small GTPase mediated signal transduction." 20 h post IAPV infection, no GO terms passed the strictest significance threshold ($p < 0.001$) for upregulation, and GO term "translation" was the most significantly downregulated ($p < 0.001$). Finally, in post 48h IAPV infected samples, there was still no term passing the strictest significance in upregulation, and GO terms of "translation," "homophilic cell adhesion," and "aminoglycan metabolic process" were the most significantly downregulated (**Figure 3**). As to molecular function, significant GO terms associated with downregulation in post 20 and 48 h IAPV infected samples were "structural molecules," "structural constituent of ribosome," "structural constituent of cuticle," and "chitin binding" (**Supplementary Figure 4**). As to cellular component, significant GO terms associated with downregulation in post 20 and 48 h IAPV infected samples were "ribosomal subunit," "ribonucleoprotein complex," and "intracellular non-membrane organelle" (**Supplementary Figure 4**). Although numerous other terms were less significantly enriched in up- or down-regulated genes, no other GO terms surpassed the most stringent significance criterion.

Viral and Ribosomal RNA Content

Four transcripts (IAPV, Deformed Wing Virus (DWV), Large Sub-Unit rRNA (LSU rRNA), and Small Sub-Unit rRNA (SSU-rRNA) accounted for 63.5% of all sequenced reads (**Supplementary Figure 5**). As expected, a large number of

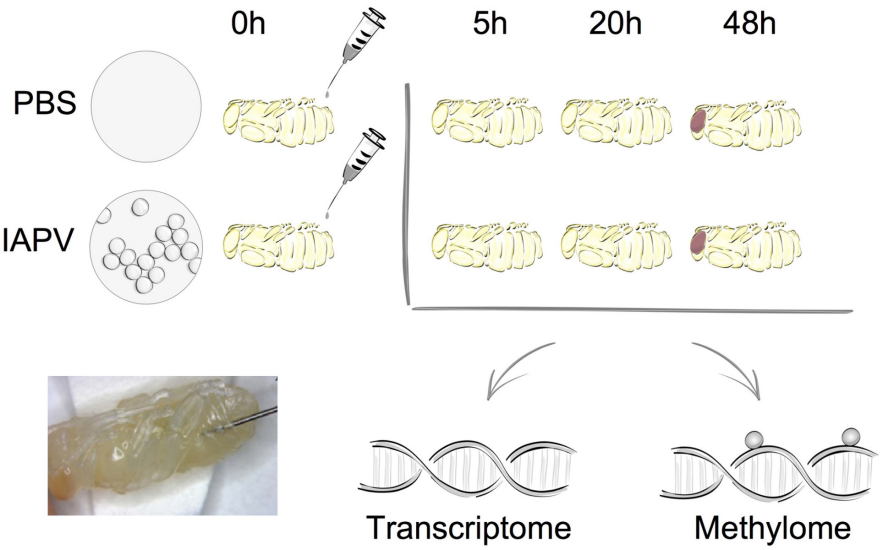

FIGURE 1 | Overall experimental design. The two experimental groups included either sham treatment (PBS injection) or Israeli Acute Paralysis Virus (IAPV) inoculations via injection. At each investigated time point (5, 20, or 48 h post-injection) three biological replicates were collected, each consisting of one whole pupa that was individually processed for further transcriptomic and methylomic analyses.

IAPV reads was observed in the IAPV-infected pupae, with the proportion being similarly high at 20 h (86% ave) and 48 h (90% ave). Additionally, five of nine control samples (all time points included) had a large proportion of reads mapping to DWV.

Comparative Transcriptomic Analyses of Immune Genes With Other Pathogen Infection in Honey Bees and *Drosophila*

A comparison with a previously published list of 186 immune genes from Evans et al. (2006) showed that 1 and 89 of them were represented in our 5 h, 20 h/48 h DEG lists respectively (**Figure 4A** and **Supplementary Tables 3**, **4**). The overlap between immune genes and our DEGs was significant for up-regulated DEGs at 5 h and down-regulated DEGs at 20 h (**Supplementary Tables 3, 4**). Comparison of our data with IAPV-induced gene expression changes in adult honey bees in Galbraith et al. (2015) revealed 6 and 358 genes overlapped, indicating a significant directional overlap of our up- and down-regulated DEGs at 5 h and 20 h/48 h with DEGs in adults (**Figure 4C**, for specific gene names, see **Supplementary Tables 3, 4**). When compared to immune genes associated with anti-viral responses in *Drosophila* (Xu et al., 2012), 11, 212, and 219 genes overlapped in our 5h, 20h, and 48h DEG lists (**Supplementary Table 5**), representing significant directional overlap of our up- and down-regulated DEGs at 20 h and 48 h (for specific gene names see **Supplementary Table 5**).

Temporal Dynamics of Genes and Molecular Pathways Based on Transcriptomic Data

Analyses of the three infection time points revealed dramatic changes of gene expression levels from several key metabolic and immune pathways, including lipid metabolism, the Jak-STAT pathway, and AMPs. With regards to lipid metabolism, the expression of the gene *Cyp6as5* was significantly increased in the infected samples from 5 to 20 h, and from 20 to 48 h, similarly to 9 more genes that displayed similar expression profiles (**Supplementary Figure 7**).

In the Jak-STAT immune pathway, the expression of gene *SoS* was significantly increased in the infected samples from 20 to 48 h (**Supplementary Figure 6**). Nine more genes displaying similar expression profiles as *SoS* after viral infection were identified (**Supplementary Figure 7**). Among the AMP genes, the expression of gene *defensin-1* was significantly increased in the infected samples from 5 to 20 h, and from 20 to 48 h (**Supplementary Figure 6**). The gene expression of EGFR and a group of other genes were transiently downregulated from 5 to 20 h post-infection and from 20 to 48 h post-infection by IAPV (**Supplementary Figure 7**). Gene *GB55029* (uncharacterized) showed an increase from 5 to 20 h infection, but then a significant decrease of expression from 20 to 48 h infection (**Supplementary Figure 7**).

Differentially Spliced Genes

Number of genes with significant isoform switches in samples 5, 20, and 48 h post IAPV infection were 193, 620, and 990 (**Supplementary Figure 8** and **Supplementary Table 6**). Number of significant differential transcripts usage (DTU) or alternative splicing is much higher post 20 and 48 h of IAPV infection (**Supplementary Figure 9**). All the splicing events are categorized in **Table 1**. Among all the categories, there are significant trends of DTU to be in shorter 3′ UTRs, longer 5′ UTRs, Exon gain, Transcription Start Site (TSS) more downstream in 20 and 48 h IAPV post infection treatments (**Figure 5**).

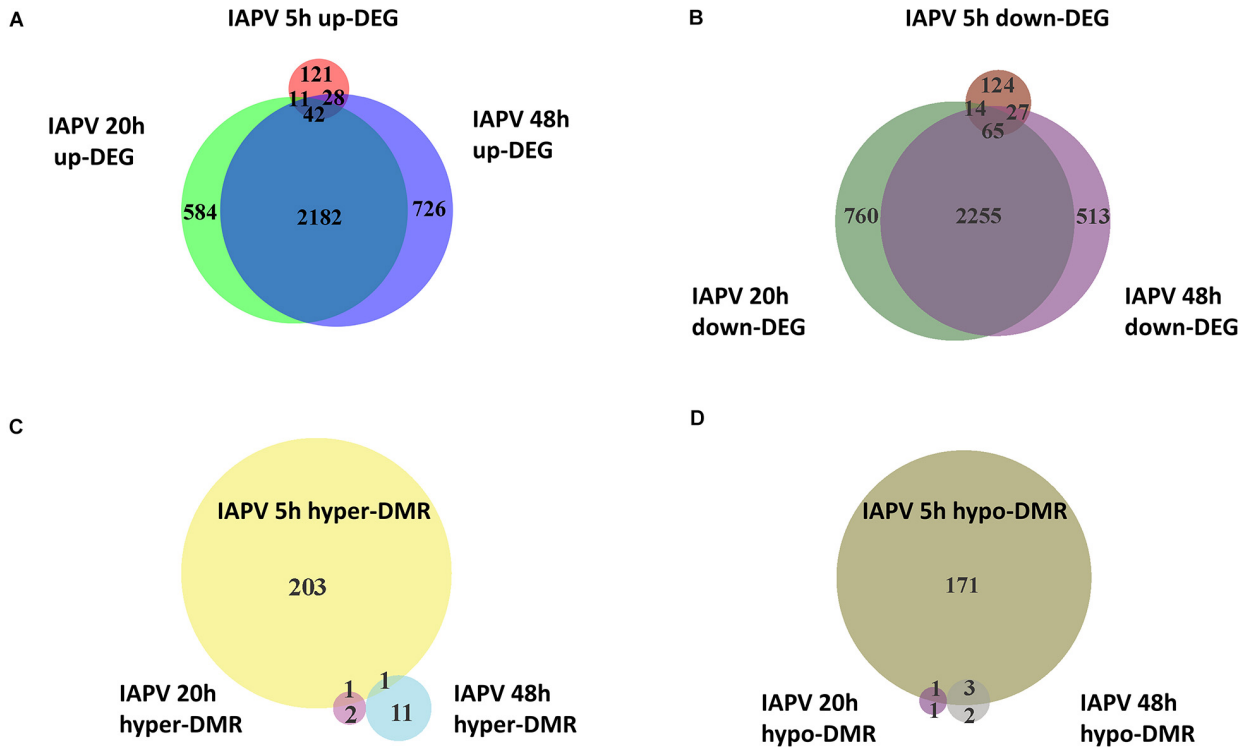

FIGURE 2 | Directional overlap of differentially regulated genes among time points. **(A)** Venn diagram showing genes that were differentially expressed as up-regulated (FDR < 0.05). Number of DEGs only in post IAPV 5, 20, and 48 h are 121, 584, and 726. Number of genes between IAPV 5 and 20 h only overlap is 11. Number of DEGs between IAPV 5 and 48 h only overlap is 28. Number of DEGs between IAPV 20 and 48 h only overlap is 2182. Number of DEGs from IAPV 5–20–48 h overlap is 42. **(B)** Venn diagram showing genes that are differentially expressed as down-regulated (FDR < 0.05). Number of DEGs only in post IAPV 5, 20, and 48 h are 124, 760, and 513. Number of DEGs between IAPV 5 and 20 h only overlap is 14. Number of DEGs between IAPV 5 and 48 h only overlap is 27. Number of DEGs between IAPV 20 and 48 h only overlap is 2255. Number of DEGs from IAPV 5–20–48 h overlap is 65. **(C)** Venn diagram showing genes that are differentially methylated (percent methylation difference larger than 10%, $q < 0.01$) as hyper-methylation among three time points (5, 20, and 48 h after IAPV infection). Number of DMRs only in post IAPV 5, 20, and 48 h are 203, 2, and 11. Number of DMRs between IAPV 5 and 20 h only overlap is 1. Number of DMRs between IAPV 5 and 48 h only overlap is 1. **(D)** Venn diagram showing genes that are differentially methylated (percent methylation difference larger than 10%, $q < 0.01$) as hypo-methylation among three time points (5, 20, and 48 h after IAPV infection). Number of DMRs only in post IAPV 5, 20, and 48 h are 171, 1, and 2. Number of DMRs between IAPV 5 and 20 h only overlap is 1. Number of DMRs between IAPV 5 and 48 h only overlap is 3.

Enzymes Involved in DNA Methylation

Gene expression differences were also identified in the DNA methylation system, specifically the two important enzymes, *DNA methyl-transferase 1* (*DNMT1*) and *3* (*DNMT3*). When compared between IAPV and control samples, *DNMT1* (*GB47348*) was significantly down-regulated 1.5-fold ($p < 0.001$) at 20 h post-infection, and 1.7-fold ($p < 0.001$) at 48 h post-infection (**Figure 6**). Similarly, *DNMT3* (*GB55485*) was significantly down-regulated 1.7-fold ($p < 0.001$) in 20 h post-infection samples, and 2.7-fold ($p < 0.001$) in 48 h post-infection samples (**Figure 6**). There was no significant difference of gene expression between IAPV and controls post 5 h post-viral infection (**Figure 6**).

Changes of DNA Methylation After Viral Infections and Comparative Methylomic Analysis

Total methylated 5 mC sites in CpG, CHG, and CHH settings were 1,955,471; 878,838; and 1,433,905 respectively (**Figure 7**). The ratio of methylated CpG sites versus total CpG sites was highest in 5 h PBS control (10%), followed by 5 h IAPV post-infection samples, 20 h PBS control, 20 h IAPV post-infection samples, 48 h control, and lowest in 48 h IAPV post-infection samples (about 4%) (**Figure 7**). The whole genome-wide Pearson correlation matrix for CpG base profiles across all samples at each time point (5, 20, and 48 h post-infection) are listed in **Supplementary Figure 10**.

We identified 523, 5, and 18 differentially methylated regions (DMRs) between IAPV and control groups in the 5, 20, and 48 h post-infection samples, respectively (**Supplementary Table 7** for a detailed gene list). Significant overlap of DMRs existed between 5 and 20 h ($p < 0.05$) and 5 and 48 h ($p < 0.0001$) comparisons (**Supplementary Table 4**).

Our comparison of our DMR lists with the previously published immune genes of Evans et al. (2006) revealed 5 and 1 gene were overlapping with the DMRs at 5 h and 20 h/48 h post-infection, respectively (**Figure 4B** and **Supplementary Tables 3, 4**). Comparison of our data with IAPV-induced methylation changes in adult honey bees of Galbraith et al. (2015)

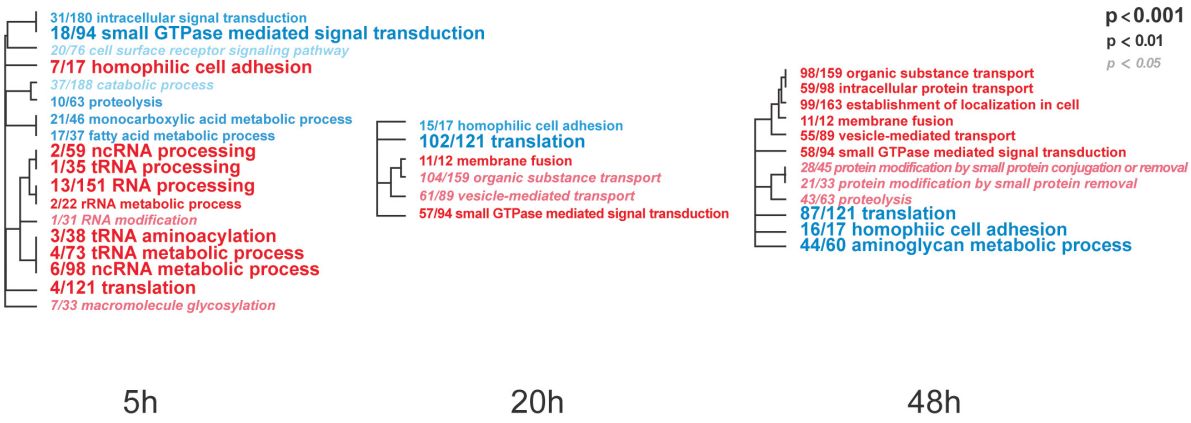

FIGURE 3 | Overall trends in biological processes affected by progressing IAPV infection. Gene Ontology Mann-Whitney U tests of the expression differences between IAPV and control samples at the three time points included all data points regardless of their individual level of statistical significance. Red and blue fonts indicate GO terms that are enriched in up- and down-regulated DEGs in IAPV relative to control samples, respectively. Font size indicates the level of significance for the particular GO term and clustering is based on empirical GO-term similarity in our dataset.

revealed 14 and 1 genes were overlapped with DMRs at 5 h and 20 h/48 h (**Figure 4D**, for specific gene names see **Supplementary Tables 3, 4**).

We examined the genome-wide Pearson correlation matrix for CpG base profiles across all samples at each time point. Overall samples after 5 h infection have the highest correlation (0.72–0.87), and samples after 48 h infection have the lowest correlation (0.69–0.73); specific coefficients are listed in **Supplementary Figure 10**).

Differential DNA Methylation Leads to Differential Gene Expression Later in Several Immune Pathways

To look into the potential association between gene expression and CpG methylation, we studied whether genes that showed early changes of CpG methylation also exhibited significant changes of gene expression later. A list of 38 immune genes that were hypo- or hyper-methylated at the first time point (5 h post-IAPV infection), were found differentially expressed later (48 h post IAPV infection) (**Supplementary Table 8**). These cellular pathways included the MAPK (mitogen-activated protein kinase) pathway, JAK/STAT (Janus kinase/signal transducer and activator of transcription) pathway, Hippo signaling pathway, mTOR (mammalian target of rapamycin) signaling pathway, TGF-beta (transforming growth factor-beta) signaling pathway, ubiquitin mediated proteolysis, and spliceosome. Interestingly, we detected 12 genes from this group with differentially spliced patterns with a significant statistical q value (**Table 2**).

Comparative Methylomic Analyses of Immune Genes With Other Pathogen Infection

The comparison with a previously published list of 186 immune genes from Evans et al. (2006), showed that 5 (*GB45248*, *GB46478*, *GB55483*, *GB51399*, and *GB41850*) and 1 (*GB46478*) genes overlapped in our 5h and 48h DMR lists, respectively (**Supplementary Table 3**). There was no significant directional overlap of the list of immune genes and our hyper- or hypo-regulated DMRs at 5, 20, and 48 h (**Supplementary Tables 3, 4**). Comparison of our data with IAPV-induced gene expression changes in adult honey bees in Galbraith et al. (2015) revealed 19, 1 (*GB51998*), and 1 genes (*GB42022*) overlapped, indicating no significant directional overlap of our hyper- or hypo-regulated DMRs at 5, 20, and 48 h (**Supplementary Tables 3, 4**). When compared to immune genes associated with anti-viral responses in *Drosophila* (Xu et al., 2012), 20, 1 (*GB17743*), and 1 genes (*GB15242*) overlapped in our 5, 20, and 48 h DMR lists (**Supplementary Table 5**).

Motif

To reveal the potential regulation of CpG methylation, we examined the 6-mer motif of each CpG site, including the 2 nucleotides upstream and downstream of each CpG site. Analysis of 6-mer motifs from 5 h DMRs showed no common pattern of the motif (**Supplementary Figure 11**). Similarly, analysis of motifs from 20 h DMRs containing CpG sites revealed little signal beyond the selected central CpG sites in the middle of 6-mer motifs. However, DMRs from 48 h post- IAPV infection tend to have a T or C following the central CpG (**Supplementary Figure 11**).

DISCUSSION

To test our hypothesis that viral infections not only affects gene expression profiles but also DNA methylomic marks in honey bee pupae, we compared the complete transcriptome and methylome responses across three distinct phases (5, 20, and 48 h) of a lethal IAPV infection. While methylation is most affected early during the infection, differential gene expression increases over time and severity of the infection. Many up- and down-regulated genes

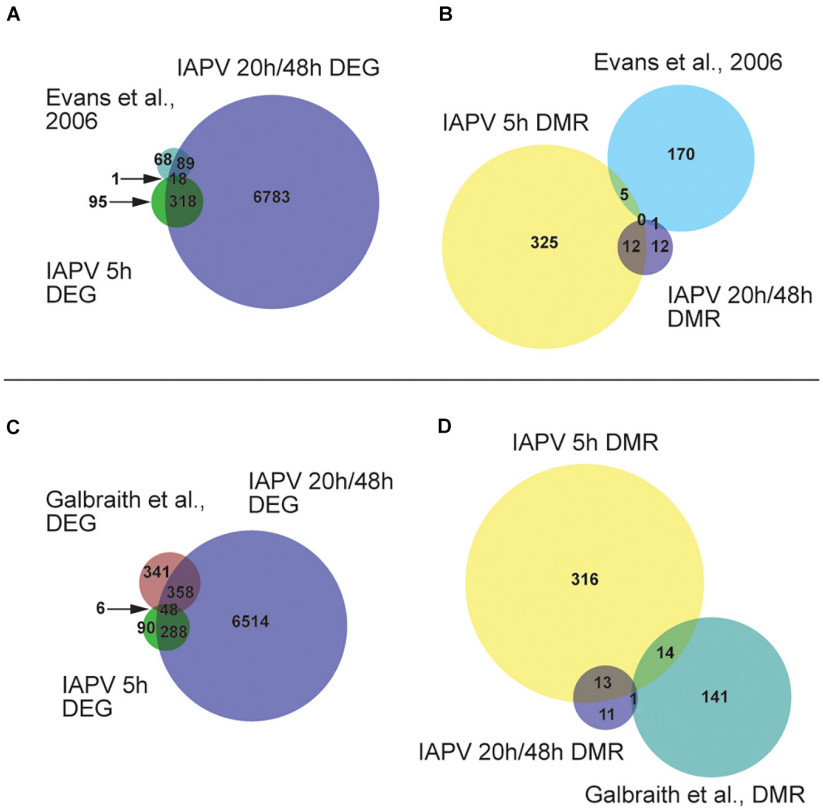

FIGURE 4 | Comparisons or our results to other studies revealed significant overlap. **(A)** Venn diagram showing overlap of genes that are differentially expressed (FDR < 0.05; $p < 0.05$). Number of DEGs (differentially expressed genes) only in IAPV 5, 20/48 h, or Evans et al. (2006) immune gene list is 95, 6783, or 68. Number of DEGs overlap between IAPV 20 h/48 h and Evans et al. is 89. Number of DEGs overlap between IAPV 5 and 20 h/48 h is 318. Number of DEGs overlap between IAPV 5 h and Evans et al. is 1. **(B)** differentially methylated (>10%, $p < 0.05$) among three time points (5, 20, and 48 h after viral infection) and immune gene list from Gisder and Genersch (2017). Number of DMRs (differentially methylated regions) only in IAPV 5, 20/48 h, or Evans et al. (2006) immune gene list is 325, 12, or 170. Number of DMRs overlap between IAPV 20 h/48 h and Evans et al. is 1. Number of DMRs overlap between IAPV 5 and 20/48 h is 12. Number of DMRs overlap between IAPV 5 h and Evans et al. is 5. **(C)** Venn diagram showing overlap of DEGs (FDR < 0.05; $p < 0.05$) compared to Galbraith et al. Number of DEGs only in IAPV 5, 20/48 h, or Galbraith et al. is 90, 6514, or 341. Number of DEGs overlap between IAPV 20 h/48 h and Galbraith et al. is 358. Number of DEGs overlap between IAPV 5 and 20 h/48 h is 288. Number of DEGs overlap between IAPV 5 h and Galbraith et al. is 6. **(D)** differentially methylated (>10%, $p < 0.05$) among three time points (5, 20, and 48 h after IAPV infection) and immune gene list from Galbraith et al. DMR list. Number of DMRs (differentially methylated regions) only in IAPV 5, 20 h/48 h, or Galbraith et al. DMR list is 316, 11, or 141. Number of DMRs overlap between IAPV 20 h/48 h and Galbraith et al. is 1. Number of DMRs overlap between IAPV 5 and 20 h/48 h is 14. Number of DMRs overlap between IAPV 5 h and Galbraith et al. is 13.

are involved in RNA processing and translations, proteolysis, and metabolic processes (**Figure 3**). A collection of genes have differential transcript usage or alternative splicing post IAPV infections (**Figure 5**). When compared to differentially expressed genes from adult honey bee and fruit fly post viral infection, we have discovered significant overlap of our IAPV-responsive genes with immune genes from these other studies (Evans et al., 2006).

The pupal stage is a critical phase for metamorphosis and an important temporal window for *Varroa* mite parasitism. Our study, which incorporates and confirms the separate observations of adult or larval honey bees (Cox-Foster et al., 2007; Cornman et al., 2013; Chen et al., 2014; Galbraith et al., 2015), includes new observations that provide a more complete understanding of how the pupae respond to lethal viral attack. Previous studies showed that honey bee pupae can respond to disease with increased immune gene expression to decrease the success of parasites and pathogens (Kuster et al., 2014; Brutscher et al., 2017). Our results reveal that rapid epigenetic changes in response to viral infection precede and presumably trigger profound and widespread transcriptome responses in honey bees. A combination of both transcriptomics and methylomics at multiple time points can reveal the role of and the relation between 5 mC methylation and gene expression profiles under viral infection of insects (Huang et al., 2019).

Alternative splicing in response to viral infection can affect subsequent gene expression through several mechanisms (De Maio et al., 2016). Our results of differential transcript usage or alternative splicing indicated the viral infection can cause large changes in alternative splicing of the bee hosts, which brings a new perspective on molecular mechanisms of IAPV virus pathogenesis. It is known that RNA virus can alter host mRNA splicing (Dubois et al., 2014; Chan et al., 2019). Previous research revealed that DNA methylation is linked to regulate

TABLE 1 | Isoform switch consequences investigated.

Category	Consequence	Description	Post 5 h	Post 20 h	Post 48 h
1	Tss	Change in transcription start site	120	407	602
2	Tts	Change in transcription termination site	21	169	246
3	Last exon	Last exon changed	9	97	130
4	Intron retention	Difference in intron retention	26	100	186
5	Intron structure	Different exon-exon junctions used	160	552	875
6	Exon number	Different number of exons	86	373	627
7	ORF seq similarity	Jaccard similarity of AA sequences below 0.9	47	211	281
8	ORF genomic	Change in genomic position of ORF	97	382	540
9	5 utr length	Difference in length of 5′ UTR	131	433	653
10	3 utr length	Difference in length of 3′ UTR	27	190	284
11	NMD status	Change in sensitivity to nonsense-mediated decay	5	45	76
12	Coding potential	Change in coding potential probability, above or below 0.7	5	30	36
13	Domains identified	Change in which protein domains were identified	19	96	119
14	Domain length	Change in length of overlapping domains	3	20	26
15	IDR identified	Difference in presence of intrinsically disordered regions	19	112	159
16	IDR length	Difference in length of intrinsically disordered regions	5	38	45
17	IDR type	Difference in presence of binding site in IDR	7	42	63
18	Signal peptide identified	Change in presence of signal peptide	1	8	14

Numbers of significant genes are shown.

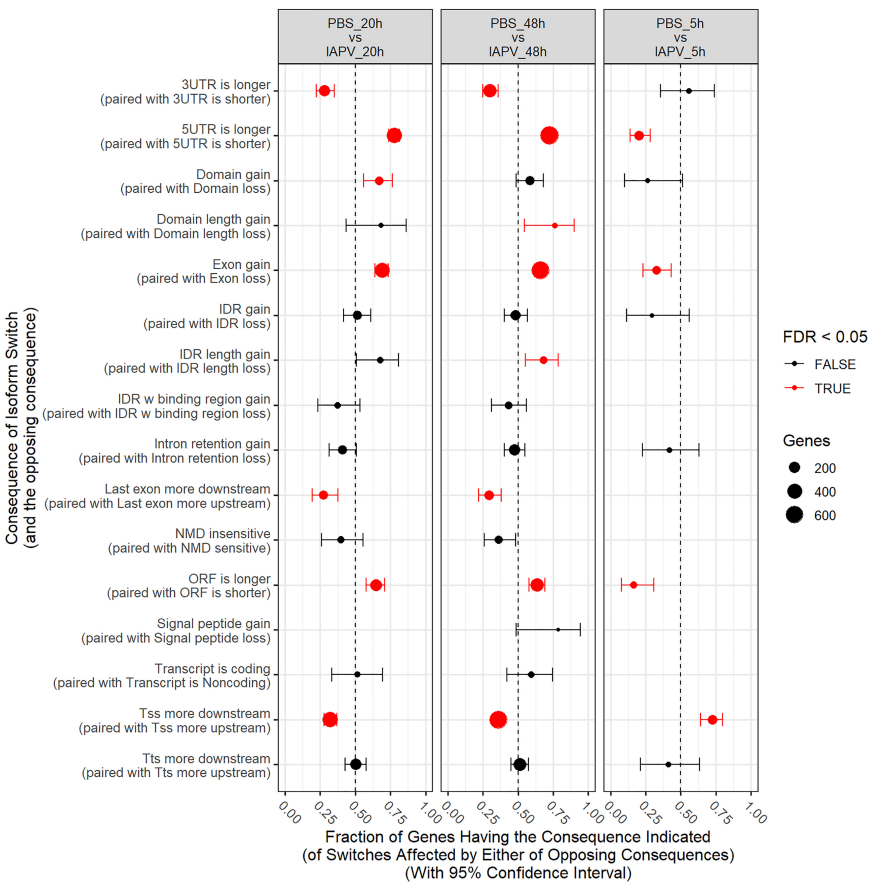

FIGURE 5 | Significant trends in consequences of isoform switches or alternative splicing were observed, and were generally similar at 20 and 48 h, often with opposite consequences at 5 h. Fraction of genes having the consequence indicated with 95% Confidence Interval. UTR-untranslated region, ITR-Inverted Terminal Repeat, ORF-open reading frame, NMD- nonsense-mediated decay, TSS-transcription start site, TTS-transcription terminal site.

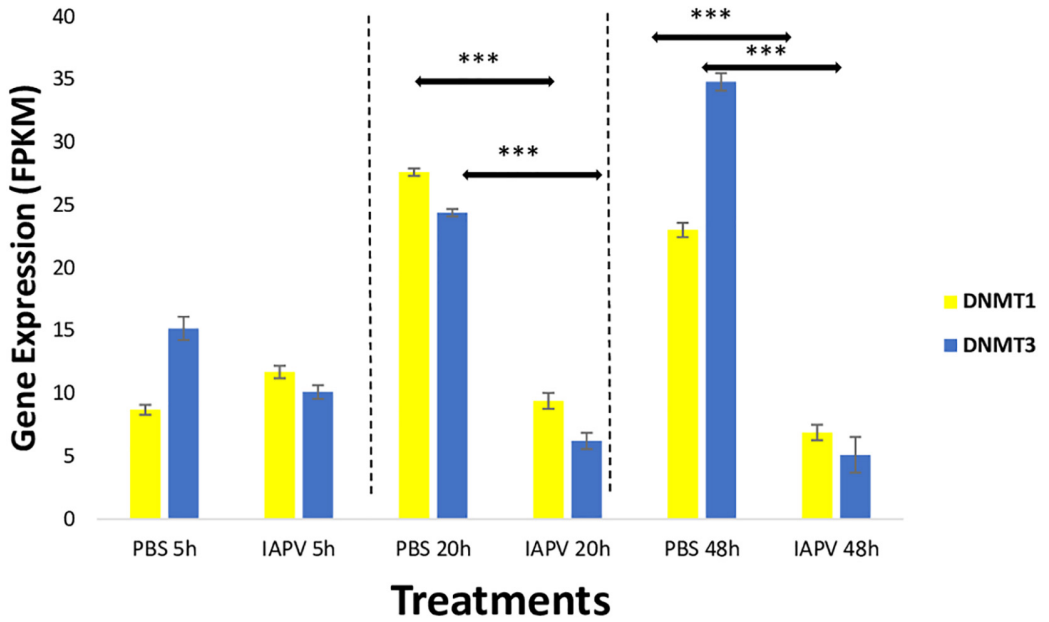

FIGURE 6 | Gene expression patterns (mean ± SE) of the major DNA Methyl-Transferases (DNMTs). Both DNMT1 (GB47348) and DNMT3 (GB55485) showed significant down-regulation when comparing sham control (N = 3) and IAPV samples (N = 3) after 20 and 48 h after IAPV infection respectively. ***$p < 0.001$. False Discovery Rate (FDR) < 0.05.

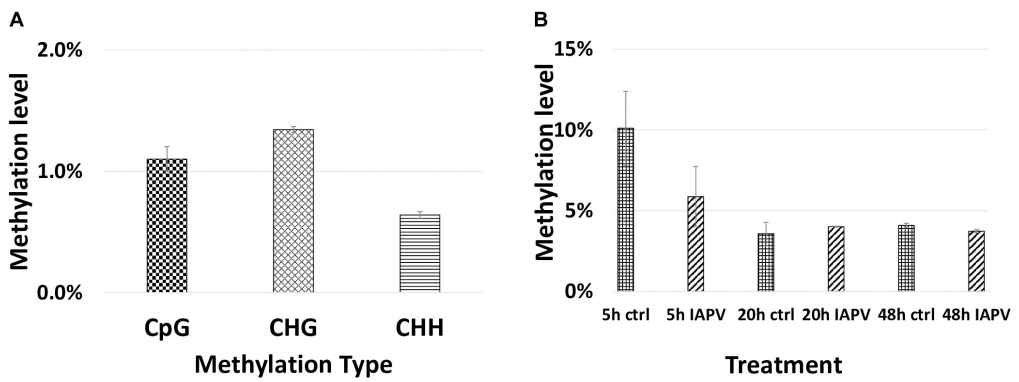

FIGURE 7 | Genome wide methylation patterns. **(A)** Total methylated 5 mC sites in each group (CpG, CHG, and CHH) are shown. **(B)** Methylated CpG sites/Total CpG sites are shown for each treatment and time point.

alternative splicing in honeybees via RNA interference knocking down DNMT3 (Li-Byarlay et al., 2013).

The epigenetic changes we report here are interesting because the 5 mC methylome profile indicated a large amount of DMRs after 5 h IAPV infection. However, DMR number dramatically dropped after 20 h and 48 h of infection. This phenomenon may be explained by the cell death and apoptosis after severe infections after 20 and 48 h. We propose a possible explanation is that 5 mC changes as a primary host-defense mechanism responding to viral infection at the onset. During the early stage of viral infection, 5 mC methylation may be the first to react leading to molecular changes genome-wide, potentially interacting with the transcription process such as transcription factor binding. The mechanism on how to induce abnormal methylation at the molecular and cellular levels by viral infection is yet to be determined. A few potential explanations are that pathogenic infection may lead to cellular proliferation and inaccuracy in epigenetic processes, or molecular signaling pathways involved in the infection response affect these epigenetic processes. Previous studies showed that viral infection can change 5 mC methylation in human cancer (Kusano et al., 2006; Toyota and Yamamoto, 2011). Other studies also showed that changes in epigenetics marks can affect immune responses, cell-cycle checkpoints, cell death, and cell fate (Toyota and Yamamoto, 2011; Turner and Diaz-Munoz, 2018).

In honey bees, some evidence links 5 mC methylation marks to gene regulation (Kucharski et al., 2008; Li-Byarlay et al., 2013; Wang and Li-Byarlay, 2015; Li-Byarlay, 2016; Glastad et al., 2019)

TABLE 2 | A list of twelve immune genes that were hypo- or hyper-methylated first post 5 h of viral infection, then gene expression and splicing patterns changed significantly post 48 h of viral infection ($q < 0.05$).

Gene.function	BEEBASE	X5h.meth.diff	X48h.DEG. log2_fold_ change	Gene name	Consequences_ 5h	Consequences_ 20h	Consequences_ 48h
Hippo signaling pathway	GB53036	−40.02	1.63	Serine/threonine-protein kinase Warts, transcript variant X2	NA	NA	5
Lysine degradation	GB47635	−38.66	−0.5	Suppressor of variegation 3–9, transcript variant X1	NA	NA	1,4,6,8,9,17
FoxO signaling pathway	GB54054	−26.65	2.08	Ubiquitin carboxyl-terminal hydrolase 7, transcript variant X1	1,4,5,8,9,15	NA	NA
Spliceosome	GB46655	−16.15	1.78	Splicing factor U2AF 50 kDa subunit, transcript variant X1	NA	5,6,8,9	NA
Lysine degradation	GB43459	24.34	−2.42	Histone-lysine N-methyltransferase trithorax, transcript variant X2	NA	NA	4,6,10
Ubiquitin mediated proteolysis	GB42193	26.51	1.53	Ubiquitin-conjugating enzyme E2-22 kDa, transcript variant X1	NA	1,5,7,8,14	NA
Ubiquitin mediated proteolysis	GB45517	29.47	0.65	E3 ubiquitin-protein ligase Nedd-4, transcript variant X6	NA	NA	2,3,5,6,8,10,17,
TGF-beta signaling pathway	GB43676	30.93	1.37	Activin receptor type-1, transcript variant X1	NA	NA	5,6,8
uncharacterized	GB41710	31.91	−2.07	Uncharacterized LOC408494, transcript variant X3	NA	5,6,7	1,6
mTOR signaling pathway	GB52079	33.8	−0.56	Rapamycin-insensitive companion of mTOR, transcript variant X2	NA	NA	1,5,9
Lysosome	GB54097	40.23	2.52	Malvolio, transcript variant X1	NA	1,5,8,9	1,5,8,9
RNA transport	GB51710	45.25	1	Eukaryotic initiation factor 4A-I, transcript variant X3	NA	NA	2,3,6,10,11

Gene.function (column 1) showed immune pathways involved. BEEBASE (column 2) showed the gene ID in BEEBASE. X5h.meth.diff (column 3) showed changes of DNA methylation level of the gene/region when comparing post 5h IAPV infection samples and control samples. X48h.DEG.log2_fold_change (column 4) showed fold change of gene expression in log2 scale when comparing post 48h IAPV infection samples and control samples. GENENAME (column 5) showed gene names. Consequences_5h, consequences_20h and consequences_48h (column 6–8) are the detected categories of alternative splicing listed in the first column of ***Table 1****. Details of gene IDs and q-values are in* ***Supplementary Table 8****.*

but limited reports showed 5 mC methylation are associated with change of gene expressions (Herb et al., 2012). The data here indicates that 38 of the initially differentially methylated genes subsequently exhibit significant changes of gene expression (**Table 1**), and 12 of these genes displayed significant changes in their splicing events. In general, the epigenetic control of 5 mC methylation and gene expression has been reported for plants and mammals (Allis and Jenuwein, 2016; Saripalli et al., 2020), but the function of 5 mC methylation in the regulation of genes in insects is still not clear (Li-Byarlay et al., 2013; Wang and Li-Byarlay, 2015). One hypothesis is that DNA methylation is involved in cell signaling or involved in the regulation of co-transcription via transcription factors (Toyota et al., 2009; Shukla et al., 2011; Marina et al., 2016).

DNA methyl-transferases 1 and 3 are critical enzymes for a functional methylation system. Our data show the IAPV infection reduced the gene expression of these two key enzymes over time. This finding is consistent with previous reports showing that viral infection can change the expression of DNMTs in animal and cell studies (Fang et al., 2012; Tian et al., 2013). The significant fold change of these enzymes is moderate but sufficient to cause dramatic changes in the global DNA methylome, as indicated in previous studies (Wang et al., 2006; Kucharski et al., 2008; Li-Byarlay et al., 2013). The DNA methylation changes in turn can have further consequences for widespread gene expression patterns. We found more DMR post 5 h IAPV infection, when the DNMTs are not yet differently expressed. Possible explanation is that the initial viral infection induced the methylation changes at the initial stage by other potential molecular mechanism such as histone modifications (Paschos and Allday, 2010; Dantas Machado et al., 2015). DNMTs may be regulated to restore homeostasis which may explain why fewer DMRs at the later stages (Matilainen et al., 2017).

At every time-point, we identified numerous differentially expressed genes that confirmed the profound consequences of IAPV infection (Boncristiani et al., 2013). Such effects can certainly be caused by cell expansion or loss, rather than direct effects on gene activity. However, the systemic consequences for the health and function of the organism may be similar: the level of immunity might drop due to declining cell numbers or lowered gene activity per cell. Molecular pathways from differentially expressed and methylated genes indicated that the MAPK signaling pathway, Jak/STAT signaling pathway, Hippo signaling pathway, mTOR signaling pathway, TGF-beta signaling pathway, ubiquitin mediated proteolysis, and spliceosome are critical to respond to viral infections. Both MAPK and Jak/STAT signaling pathway are immune pathways with antiviral immune response in honey bees and dipterans (Dostert et al., 2005; Lemaitre and Hoffmann, 2007; Cirimotich et al., 2010; Chen et al., 2014; Galbraith et al., 2015; Brutscher et al., 2015; Grozinger and Flenniken, 2019). The Hippo signaling pathway is highly conserved from insects to mammals, which regulates

cell death and differentiation (Munoz-Wolf and Lavelle, 2017). Previous study also showed differentially expressed genes regulated by IAPV in honey bee brood are involved in the mTOR, TGF-beta pathways, and ubiquitin mediated proteolysis (Chen et al., 2014).

In addition, our data showed that IAPV infection can induce *Defensin-1*, a key antimicrobial peptide responding to viral infections (Kuster et al., 2014; Brutscher et al., 2015). P450 genes are known as responding to oxidative stress in *Drosophila* during larval development (Li et al., 2008). In honey bees, P450s are involved in xenobiotic detoxification (Johnson et al., 2009; Berenbaum and Johnson, 2015). From a wider perspective, Chikungunya virus infection specifically activates the MAPK signaling pathways in humans (Varghese et al., 2016) and is a stress-responsive part of the intestinal innate immunity of *C. elegans* (Sakaguchi et al., 2004). Recent report showed that MAPK may play a role in regulating certain P450 genes (Yang et al., 2020). On the other hand, IAPV infection presumably causes major deregulation of the cellular homeostasis through the cooption of the cellular machinery to replicate itself (Boncristiani et al., 2013). Thus, deregulation of ribosome biosynthesis (**Figure 3**) and major energetic pathways is not surprising. Interestingly, transcriptomic analyses of Colony Collapse Disorder, which had been associated with IAPV (Cox-Foster et al., 2007), have shown similar immune responses (Johnson et al., 2009; Aufauvre et al., 2014). The methylomic profile of pupae 48 h after IAPV infection indicated genes involved in anti-parasitoid immune response (Howell et al., 2012; Haddad et al., 2016) to be affected. One of these genes that overlaps with a previous genomic study of honey bee immune genes (Evans et al., 2006) is Peroxin 23, a protein involved in peroxisomal protein import and associated with autophagosome formation in *Drosophila* muscles and central nervous system (Hazelett et al., 2012; Zirin et al., 2015). Compared to a previous report of the 5 mC methylomic profiles of honey bee adults infected with IAPV (Galbraith et al., 2015), our analysis revealed only one overlapping gene (GB51998), which is related to ATP binding, circadian regulation of gene expression systems (Claridge-Chang et al., 2001), and muscle morphogenesis and function in *Drosophila* (Schnorrer et al., 2010).

The list of identified DMRs linked to genes associated with ATP binding, phagosome, fatty acid degradation, RNA transport, and RNA degradation. Lipid metabolism, signaling, and biosynthesis are related to virus-host interactions (Chukkapalli et al., 2012). Fatty acid degradation and metabolism also responded to cold stress in other insects and might indicate increased energetic demands of stressed organisms (Vermeulen et al., 2013). Alternatively, IAPV may remodel the host cells by hijacking the lipid signaling pathways and synthesis process for its own replication, similar to virus manipulation of host RNA replication and transport mechanisms (Nagy and Pogany, 2012; Boncristiani et al., 2013).

Our study only represents a first step in the understanding of the intricate interplay of viruses and their honey bee host's physiology. Future research needs to characterize the temporal transcriptome trends in more detail and tissue-specificity. Pupae are particularly relevant but also challenging because the ongoing metamorphosis entails drastic hormonal and presumably transcriptional changes even in the absence of disease. The discovered functional pathways need to be functionally investigated, particularly the putative 5 mC methylation control of immune genes.

MATERIALS AND METHODS

Bee Samples and Virus Preparation

All honey bee samples were acquired from unselected experimental hives in the research apiary of the University of North Carolina Greensboro. A previously prepared and characterized IAPV solution in PBS was used for inoculations (Boncristiani et al., 2013). White-eyed pupae were either injected with PBS solution as control treatment or with 10^4 genome copies of IAPV in 1.0 μl of the viral suspension per pupa. Pupae were maintained on folder filter papers in a sterile lab incubator at 32°C and 60% R.H. After 5, 20, and 48 h of injections, each individual pupal sample was flash-frozen in liquid nitrogen and then stored in a −80°C freezer. **Figure 1** illustrates the experimental design.

RNA-Seq Library Preparation and Sequencing

Treatment control (PBS-injection) and IAPV-infected pupae were compared across three time points (5, 20, and 48 h). Three pupae were collected for each treatment and each time point for a total of 18 samples. Dual extraction of nucleic acid (RNA and DNA) from each pupa was carried out using the MasterPure dual extraction kit (Epicenter, MC85200). Briefly, whole pupae were individually homogenized and lysed first by using a micropestle. The lysed cells were mixed with extraction buffer and centrifuged to remove proteins and undesired debris of the cell. Subsequent RNA and DNA fractions were treated with DNase and RNase accordingly. RNA-seq library preparation and sequencing were performed by the Genomic Sciences Laboratory of the North Carolina State University. Total RNA from each pupa was used to generate tagged Illumina libraries, using the NEBNext® RNA Library Prep Kit (New England Biolab). All RNA-seq libraries were sequenced in two flow cells on the Illumina Next-Seq 500 (paired-end 150 bp length reads).

BS-Seq Library Preparation and Sequencing

Bisulfite (BS) conversion of the genomic DNA from the above-mentioned dual extraction of each sample was carried out by using the EZ DNA Methylation-Lightning Kit (Zymo Research, D5030, Irvine, CA, United States). BS-converted DNA (100 ng) of each sample was used for preparing the BS-seq library via the TruSeq DNA Methylation Kit (Illumina, EGMK91324, San Diego, CA, United States). The quality of the libraries was checked using Qubit assays (Q32850, Life Technologies) and with the 2100 Bioanalyzer (Agilent Technologies, Inc.). The pooled 18 libraries were run on two replicate lanes of the Illumina

NextSeq 500 (150 bp paired-end reads) by the Genomic Sciences Laboratory at NCSU.

Bioinformatic Analyses

Overall quality control analysis of all resulting data was carried out by using FastQC.[1] Raw data were trimmed by Trimmomatic (java -jar PE -phred33 ILLUMINACLIP:TruSeq3-PE.fa:2:30:10 MINLEN:36). TopHat2 v.2.0.12 (Kim et al., 2013) was used to align trimmed RNA-seq reads to the *Apis mellifera* 4.5 reference genome. General alignment parameters were chosen to allow three mismatches per segment, 12 mismatches per read, and gaps of up to 3 bp (tophat –read-mismatches 12 –segment-mismatches 3 –read-gap-length 3 –read-edit-dist 15 –b2-sensitive) to minimize the possibility that small sequence differences of our samples with the reference genome would bias expression estimates. These settings resulted in the successful alignment of 35% of raw reads (117–143 million per sample). Reconstructed transcripts were aligned with Cufflinks (v2.2.1) to the *Apis mellifera* OGS 3.2 allowing gaps of up to 1 bp (cufflinks –overlap-radius 1 –library-type fr-firststrand). To annotate promoters and transcription starts, we employed the "cuffcompare" command using OGS3.2 gff file (cuffcompare -s -CG -r).

Cuffdiff2 (v.2.1.1) (Kim et al., 2013) was used to test for differential expression between IAPV and control groups (n = 3 pupae treated as biological replicates at each of the 3 different time points) with the multiple mapping correction and a false discovery rate threshold set at 0.05. All three IAPV groups (IAPV_5h, IAPV_20h, and IAPV_48h) were compared to their corresponding sham-control groups (PBS_5h, PBS_20h, PBS_48h) to identify differentially expressed genes (DEGs). The data were explored and visualized with CummeRbundv.2.0.0[2] and custom R scripts (Rsoftwarev.2.15.0).[3] Differentially expressed genes with similar expression temporal dynamics were analyzed by cufflinks in R. Total of output of gene numbers is set to be 10 (for example, consider gene GB49890 (cyp6as5), we can find nine other genes in the database with similar expression patterns, then plot the expression patterns in **Supplementary Figure 7**).

Whole genome BS-Seq analysis was carried out by trimming the sequences using trim_galore (version 0.4.1)[4] (trim_galore./file1_R1_001.fastq.gz./file1_R2_001.fastq.gz -q 20 –paired –phred33 -o). The Bismark tool (Krueger and Andrews, 2011) (bismark –bowtie2 –path_to_bowtie -p 8 path_to_genome_files/–1/file1 –2/file2) was employed for whole genome alignment. Brief procedures included Genome Conversion, Genome Alignment, Deduplication, and Methylation calls. Differentially methylated regions and genes (DMRs) were produced by methylKit in R (version 1.3.8) with percent methylation difference larger than 10% and $q < 0.01$ for the difference (Akalin et al., 2012).

The reference genome and official gene set were the same as described before. The sequencing raw data are published at the NCBI database (Sequence Read Archive (SRA) submission: SUB3404557, BioProject: PRJNA429508). All codes for the bioinformatic analyses are online.[5]

To determine overlap between DEG lists, either up- or down-regulated genes were compared between different time points. This directional overlap analysis avoids artifacts that can confound undirected DEG comparisons (Lawhorn et al., 2018). The analysis was compared focusing on DEGs with a more than 8-fold difference, and with DMRs (either hyper- or hypo-methylated). All overlap analyses were performed with hypergeometric tests to calculate the p-value for overlap based on the cumulative distribution function (CDF) of the hypergeometric distribution as published previously (Li-Byarlay et al., 2013). GO Mann-Whitney U tests were carried out on the gene expression data using codes published in Github.[6] These analyses search for patterns of up- or down-regulation in genes associated with particular GO-terms based on their signed, uncorrected p-values regardless of significance thresholds (Wright et al., 2015).

For differentially transcript usage or spliced genes, transcript-level counts were quantified using Salmon1 v1.2.1 (Patro et al., 2017) against the A. mellifera HAv3.1 annotation. Viral RNAs were included in the transcriptome used for alignment but were omitted from isoform analysis. Salmon results were imported directly into the IsoformSwitchAnalyzeR R package (Vitting-Seerup and Sandelin, 2017; Vitting-Seerup and Sandelin, 2019), which normalizes transcript counts based on abundances and uses the TMM method to adjust effective library size. The version of IsoformSwitchAnalyzeR used was 1.11.3, obtained from GitHub commit 5a7ab4a due to a bug in version 1.11.2 on Bioconductor. Although CDS were annotated in the GFF file for A. mellifera, these caused problems in IsoformSwitchAnalyzeR due to inclusion of stop codons, as well as some transcripts having no annotated CDS or CDS that were obviously incorrect. Therefore, the analyzeORF function was used to predict open reading frames *de novo* from the transcript sequences, which in the vast majority of cases resulted in agreement with the published annotation. Nucleotide and amino acid sequences for all transcripts for significant genes were then exported for analysis with external tools: CPAT9 was used to determine whether a transcript was likely to be coding (Wang et al., 2013). It was run from the webserver using the *Drosophila* (dm3, BDGP release 5) assembly. A coding probability of 0.7 was used as the cutoff for classifying a transcript as coding or non-coding. Pfam10 (Punta et al., 2012) version 32.0 was used to predict protein domains, using pfam_scan v1.6 run on the Biocluster.

Statistical Analysis of Differential Transcript Usage

A design matrix was constructed in which the condition was the combination of treatment and time point (six conditions total),

[1]http://www.bioinformatics.babraham.ac.uk/projects/fastqc/

[2]http://compbio.mit.edu/cummeRbund/

[3]http://www.r-project.org/

[4]http://www.bioinformatics.babraham.ac.uk/projects/trim_galore/

[5]https://www.researchgate.net/publication/343237015_RNAseq_and_BSseq_codes_for_public

[6]https://github.com/z0on/GO_MWU

and DWV infection (determined by alignment of reads to the DWV mRNA) was included as a covariate. Sample degradation was excluded as a covariate as it introduced singularity into the model at 48 h. The contrasts tested were IAPV_5h – PBS_5h, IAPV_20h – PBS_20h, and IAPV_48h – PBS_48h. The preFilter function in IsoformSwitchAnalyzeR was used with default settings to filter transcripts and genes. Genes were removed if they only had one isoform or if they did not have at least 1 RPKM in at least one condition. Transcripts were removed if they had no expression in any condition. After filtering, 15,808 isoforms belonging to 4,667 genes remained.

Differential transcript usage (DTU) was assessed using DEXSeq from within IsoformSwitchAnalyzeR (Anders et al., 2012; Ritchie et al., 2015; Vitting-Seerup and Sandelin, 2019). Genes were only retained for further analysis if they had an FDR < 0.05 for DTU, and if isoform usage (proportion of counts from a gene belonging to a given isoform) changed by at least 0.1 for at least two isoforms in opposite directions (i.e., the isoforms "switched").

Enrichment of Overlapping Genes Among Different Studies

To test whether our DEGs and DMRs had significant overlap with known immune genes, these lists were compared to published immune genes (Evans et al., 2006) using hypergeometric tests. Additionally, a directional overlap analysis was performed on our DEGs (separated by up- or down-regulation) with a previous RNA-seq study of IAPV infection in adult honey bee workers (Galbraith et al., 2015).

To identify potential motifs that are targeted for epigenetic modification after IAPV infection, differentially methylated regions (DMR) were analyzed post 5, 20, and 48 h IAPV infection generating 6-mer sequence logos with the online tool weblogo.[7]

DATA AVAILABILITY STATEMENT

The sequencing raw data are published at the NCBI database (Sequence Read Archive (SRA) submission: SUB3404557, BioProject: PRJNA429508).

[7] https://weblogo.berkeley.edu

AUTHOR CONTRIBUTIONS

HL-B, MS, DT, and OR conceptualized the scientific idea and aims. HB performed the viral infection experiments. HL-B prepared the samples and performed sequencing experiments and bioinformatics analyses. GH provided assistance on the computational techniques on High Performance Cluster. JH and LC provided additional analysis of GO and splicing. HL-B wrote the manuscript with all co-authors input. All authors contributed to the article and approved the submitted version.

FUNDING

The National Research Council Postdoctoral Fellowship, USDA NIFA Evans Allen fund (NI191445XXXXG002), NSF HBCU-UP grant (1900793), and Illumina Go Mini Challenge Grant supported HL-B. Major research funding was from the U.S. Army Research Laboratory grants #W911NF04D0003 and #W911NF1520045 to OR, DT, and MS.

ACKNOWLEDGMENTS

We thank Karl M. Glastad (University of Pennsylvania), Marce Lorenzen (NCSU), Andrew Petersen (NCSU), and HPCBio at University of Illinois on bioinformatics consulting, Karmi Oxman and Susan Balfe for the graphic designs, and Conrad Zagory, Jr. at CSU for critical reviews on the English writing.

SUPPLEMENTARY MATERIAL

The Supplementary Material for this article can be found online at: https://www.frontiersin.org/articles/10.3389/fgene.2020.566320/full#supplementary-material

REFERENCES

Akalin, A., Kormaksson, M., Li, S., Garrett-Bakelman, F. E., Figueroa, M. E., Melnick, A., et al. (2012). methylKit: a comprehensive R package for the analysis of genome-wide DNA methylation profiles. *Genome Biol.* 13:R87.

Allis, C. D., and Jenuwein, T. (2016). The molecular hallmarks of epigenetic control. *Nat. Rev. Genet.* 17, 487–500. doi: 10.1038/nrg.2016.59

Anders, S., Reyes, A., and Huber, W. (2012). Detecting differential usage of exons from RNA-seq data. *Genome Res.* 22, 2008–2017. doi: 10.1101/gr.133744.111

Arvey, A., Tempera, I., Tsai, K., Chen, H.-S., Tikhmyanova, N., Klichinsky, M., et al. (2012). An atlas of the epstein-barr virus transcriptome and epigenome reveals host-virus regulatory interactions. *Cell Host Microbe* 12, 233–245. doi: 10.1016/j.chom.2012.06.008

Aufauvre, J., Misme-Aucouturier, B., Viguès, B., Texier, C., Delbac, F., and Blot, N. (2014). Transcriptome analyses of the honeybee response to *Nosema ceranae* and insecticides. *PLoS One* 9:e91686. doi: 10.1371/journal.pone.0091686

Bailey, L., Gibbs, A., and Woods, R. (1963). Two viruses from adult honey bees (*Apis mellifera* Linnaeus). *Virology* 21, 390–395. doi: 10.1016/0042-6822(63)90200-9

Berenbaum, M. R., and Johnson, R. M. (2015). Xenobiotic detoxification pathways in honey bees. *Curr. Opin. Insect Sci.* 10, 51–58. doi: 10.1016/j.cois.2015.03.005

Bewick, A. J., Vogel, K. J., Moore, A. J., and Schmitz, R. J. (2017). Evolution of DNA methylation across insects. *Mol. Biol. Evol.* 34, 654–665.

Boncristiani, H. F., Evans, J. D., Chen, Y., Pettis, J., Murphy, C., Lopez, D. L., et al. (2013). In-vitro infection of pupae with Israeli Acute Paralysis Virus suggests variation for susceptibility and disturbance of transcriptional homeostasis in honey bees (*Apis mellifera*). *PLoS One* 8:e73429. doi: 10.1371/journal.pone.0073429

Bonning, B. C., and Miller, W. A. (2010). Dicistroviruses. *Annu. Rev. Entomol.* 55, 129–150. doi: 10.1146/annurev-ento-112408-085457

Brutscher, L. M., Daughenbaugh, K. F., and Flenniken, M. L. (2015). Antiviral defense mechanisms in honey bees. *Curr. Opin. Insect Sci.* 10, 71–82. doi: 10.1016/j.cois.2015.04.016

Brutscher, L. M., Daughenbaugh, K. F., and Flenniken, M. L. (2017). Virus and dsRNA-triggered transcriptional responses reveal key components of honey bee antiviral defense. *Sci. Rep.* 7:6448.

Burggren, W. W. (2017). Epigenetics in insects: mechanisms, phenotypes and ecological and evolutionary implications. *Adv. Insect Physiol.* 53, 1–30. doi: 10.1016/bs.aiip.2017.04.001

Calderone, N. W. (2012). Insect pollinated crops, insect pollinators and US agriculture: trend analysis of aggregate data for the period 1992–2009. *PLoS One* 7:e37235. doi: 10.1371/journal.pone.0037235

Chan, C. Y., Low, J. Z. H., Gan, E. S., Ong, E. Z., Zhang, S. L.-X., Tan, H. C., et al. (2019). Antibody-dependent dengue virus entry modulates cell intrinsic responses for enhanced infection. *mSphere* 4:e00528-19.

Chen, Y. P., Pettis, J. S., Corona, M., Chen, W. P., Li, C. J., Spivak, M., et al. (2014). Israeli acute paralysis virus: epidemiology, pathogenesis and implications for honey bee health. *PLoS Pathog.* 10:e1004261. doi: 10.1371/journal.ppat.1004261

Chen, Y. P., and Siede, R. (2007). "Honey bee viruses," in *Advances in Virus Research*, Vol. 70, eds K. Maramorosch, A. J. Shatkin, and F. A. Murphy (Salt Lake City, UT: Academic Press), 33–80.

Chukkapalli, V., Heaton, N. S., and Randall, G. (2012). Lipids at the interface of virus–host interactions. *Curr. Opin. Microbiol.* 15, 512–518. doi: 10.1016/j.mib.2012.05.013

Cirimotich, C. M., Dong, Y., Garver, L. S., Sim, S., and Dimopoulos, G. (2010). Mosquito immune defenses against *Plasmodium* infection. *Dev. Comp. Immunol.* 34, 387–395. doi: 10.1016/j.dci.2009.12.005

Claridge-Chang, A., Wijnen, H., Naef, F., Boothroyd, C., Rajewsky, N., and Young, M. W. (2001). Circadian regulation of gene expression systems in the *Drosophila* head. *Neuron* 32, 657–671. doi: 10.1016/s0896-6273(01)00515-3

Cornman, R. S., Boncristiani, H., Dainat, B., Chen, Y., Weaver, D., and Evans, J. D. (2013). Population-genomic variation within RNA viruses of the Western honey bee, *Apis mellifera*, inferred from deep sequencing. *BMC genomics.* 14:154. doi: 10.1186/1471-2164-14-154

Cornman, R. S., Tarpy, D. R., Chen, Y., Jeffreys, L., Lopez, D., Pettis, J. S., et al. (2012). Pathogen webs in collapsing honey bee colonies. *PLoS One* 7:e43562. doi: 10.1371/journal.pone.0043562

Cox-Foster, D. L., Conlan, S., Holmes, E. C., Palacios, G., Evans, J. D., Moran, N. A., et al. (2007). A metagenomic survey of microbes in honey bee colony collapse disorder. *Science* 318, 283–287. doi: 10.1126/science.1146498

Dantas Machado, A. C., Zhou, T., Rao, S., Goel, P., Rastogi, C., Lazarovici, A., et al. (2015). Evolving insights on how cytosine methylation affects protein–DNA binding. *Brief. Funct. Genomics* 14, 61–73. doi: 10.1093/bfgp/elu040

De Maio, F. A., Risso, G., Iglesias, N. G., Shah, P., Pozzi, B., Gebhard, L. G., et al. (2016). The dengue virus NS5 protein intrudes in the cellular spliceosome and modulates splicing. *PLoS Pathog.* 12:e1005841. doi: 10.1371/journal.ppat.1005841

De Monerri, N. C. S., and Kim, K. (2014). Pathogens hijack the epigenome: a new twist on host-pathogen interactions. *Am. J. Pathol.* 184, 897–911.

Di Prisco, G., Pennacchio, F., Caprio, E., Boncristiani, H. F. Jr., Evans, J. D., and Chen, Y. (2011). *Varroa destructor* is an effective vector of Israeli acute paralysis virus in the honeybee, *Apis mellifera*. *J. Gen. Virol.* 92, 151–155. doi: 10.1099/vir.0.023853-0

Dostert, C., Jouanguy, E., Irving, P., Troxler, L., Galiana-Arnoux, D., Hetru, C., et al. (2005). The Jak-STAT signaling pathway is required but not sufficient for the antiviral response of drosophila. *Nat. Immunol.* 6, 946–953. doi: 10.1038/ni1237

Dubois, J., Terrier, O., and Rosa-Calatrava, M. (2014). Influenza viruses and mRNA splicing: doing more with less. *mBio* 5:e00070-14.

Edwards, T. M., and Myers, J. P. (2007). Environmental exposures and gene regulation in disease etiology. *Environ. Health Perspect.* 115, 1264–1270. doi: 10.1289/ehp.9951

Evans, J. D., Aronstein, K., Chen, Y. P., Hetru, C., Imler, J. L., Jiang, H., et al. (2006). Immune pathways and defence mechanisms in honey bees *Apis mellifera*. *Insect Mol. Biol.* 15, 645–656. doi: 10.1111/j.1365-2583.2006.00682.x

Fang, J., Hao, Q., Liu, L., Li, Y., Wu, J., Huo, X., et al. (2012). Epigenetic changes mediated by microRNA miR29 activate cyclooxygenase 2 and lambda-1 interferon production during viral infection. *J. Virol.* 86, 1010–1020. doi: 10.1128/jvi.06169-11

Galbraith, D. A., Yang, X., Niño, E. L., Yi, S., Grozinger, C., and Schneider, D. S. (2015). Parallel epigenomic and transcriptomic responses to viral infection in honey bees (*Apis mellifera*). *PLoS Pathog.* 11:e1004713. doi: 10.1371/journal.ppat.1004713

Gardy, J. L., and Loman, N. J. (2018). APPLICATIONS OF NEXT-GENERATION SEQUENCING Towards a genomics-informed, real-time, global pathogen surveillance system. *Nat. Rev. Genet.* 19, 9–20. doi: 10.1038/nrg.2017.88

Gisder, S., and Genersch, E. (2017). Viruses of commercialized insect pollinators. *J. Invertebr. Pathol.* 147, 51–59. doi: 10.1016/j.jip.2016.07.010

Glastad, K. M., Gokhale, K., Liebig, J., and Goodisman, M. A. (2016). The caste-and sex-specific DNA methylome of the termite *Zootermopsis nevadensis*. *Sci. Rep.* 6:37110.

Glastad, K. M., Goodisman, M. A., Yi, S. V., and Hunt, B. G. (2015). Effects of DNA methylation and chromatin state on rates of molecular evolution in insects. *G3* 6, 357–363. doi: 10.1534/g3.115.023499

Glastad, K. M., Hunt, B. G., and Goodisman, M. A. (2019). Epigenetics in insects: genome regulation and the generation of phenotypic diversity. *Annu. Rev. Entomol.* 64, 185–203. doi: 10.1146/annurev-ento-011118-111914

Glastad, K. M., Hunt, B. G., and Goodisman, M. A. D. (2014). Evolutionary insights into DNA methylation in insects. *Curr. Opin. Insect Sci.* 1, 25–30. doi: 10.1016/j.cois.2014.04.001

Goulson, D., Nicholls, E., Botias, C., and Rotheray, E. L. (2015). Bee declines driven by combined stress from parasites, pesticides, and lack of flowers. *Science* 347:1255957. doi: 10.1126/science.1255957

Grozinger, C. M., and Flenniken, M. L. (2019). Bee viruses: ecology, pathogenicity, and impacts. *Annu. Rev. Entomol.* 64, 205–226. doi: 10.1146/annurev-ento-011118-111942

Haddad, N., Mahmud Batainh, A., Suleiman Migdadi, O., Saini, D., Krishnamurthy, V., Parameswaran, S., et al. (2016). Next generation sequencing of *Apis mellifera syriaca* identifies genes for *Varroa* resistance and beneficial bee keeping traits. *Insect Sci.* 23, 579–590. doi: 10.1111/1744-7917.12205

Hazelett, D. J., Chang, J. C., Lakeland, D. L., and Morton, D. B. (2012). Comparison of parallel high-throughput RNA sequencing between knockout of TDP-43 and its overexpression reveals primarily nonreciprocal and nonoverlapping gene expression changes in the central nervous system of Drosophila. *G3* 2, 789–802. doi: 10.1534/g3.112.002998

Herb, B. R., Wolschin, F., Hansen, K. D., Aryee, M. J., Langmead, B., Irizarry, R., et al. (2012). Reversible switching between epigenetic states in honeybee behavioral subcastes. *Nat. Neurosci.* 15, 1371–1373. doi: 10.1038/nn.3218

Howell, L., Sampson, C. J., Xavier, M. J., Bolukbasi, E., Heck, M. M., and Williams, M. J. (2012). A directed miniscreen for genes involved in the *Drosophila* anti-parasitoid immune response. *Immunogenetics* 64, 155–161. doi: 10.1007/s00251-011-0571-3

Huang, H., Wu, P., Zhang, S., Shang, Q., Yin, H., Hou, Q., et al. (2019). DNA methylomes and transcriptomes analysis reveal implication of host DNA methylation machinery in BmNPV proliferation in *Bombyx mori*. *BMC genomics.* 20:736. doi: 10.1186/s12864-019-6146-7

Hunt, B. G., Brisson, J. A., Yi, S. V., and Goodisman, M. A. D. (2010). Functional conservation of DNA methylation in the pea aphid and the honeybee. *Genome Biol. Evol.* 2, 719–728. doi: 10.1093/gbe/evq057

Hunt, B. G., Glastad, K. M., Yi, S. V., and Goodisman, M. A. D. (2013). The function of intragenic DNA methylation: insights from insect epigenomes. *Integr. Comp. Biol.* 53, 319–328. doi: 10.1093/icb/ict003

Johnson, R. M., Evans, J. D., Robinson, G. E., and Berenbaum, M. R. (2009). Changes in transcript abundance relating to colony collapse disorder in honey bees (*Apis mellifera*). *Proc. Natl. Acad. Sci. U. S. A.* 106, 14790–14795. doi: 10.1073/pnas.0906970106

Kim, D., Pertea, G., Trapnell, C., Pimentel, H., Kelley, R., and Salzberg, S. L. (2013). TopHat2: accurate alignment of transcriptomes in the presence of insertions, deletions and gene fusions. *Genome Biol.* 14:R36.

Krueger, F., and Andrews, S. R. (2011). Bismark: a flexible aligner and methylation caller for Bisulfite-Seq applications. *Bioinformatics* 27, 1571–1572. doi: 10.1093/bioinformatics/btr167

Kucharski, R., Maleszka, J., Foret, S., and Maleszka, R. (2008). Nutritional control of reproductive status in honeybees via DNA methylation. *Science* 319, 1827–1830. doi: 10.1126/science.1153069

Kulhanek, K., Steinhauer, N., Rennich, K., Caron, D. M., Sagili, R. R., Pettis, J. S., et al. (2017). A national survey of managed honey bee 2015–2016 annual colony losses in the USA. *J. Apic. Res.* 56, 328–340. doi: 10.1080/00218839.2017.1344496

Kusano, M., Toyota, M., Suzuki, H., Akino, K., Aoki, F., Fujita, M., et al. (2006). Genetic, epigenetic, and clinicopathologic features of gastric carcinomas with the CpG island methylator phenotype and an association with Epstein–Barr virus. *Cancer* 106, 1467–1479. doi: 10.1002/cncr.21789

Kuss-Duerkop, S. K., Westrich, J. A., and Pyeon, D. (2018). DNA tumor virus regulation of host DNA methylation and its implications for immune evasion and oncogenesis. *Viruses* 10:82. doi: 10.3390/v10020082

Kuster, R. D., Boncristiani, H. F., and Rueppell, O. (2014). Immunogene and viral transcript dynamics during parasitic *Varroa destructor* mite infection of developing honey bee (*Apis mellifera*) pupae. *J. Exp. Biol.* 217, 1710–1718. doi: 10.1242/jeb.097766

Lawhorn, C. M., Schomaker, R., Rowell, J. T., and Rueppell, O. (2018). Simple comparative analyses of differentially expressed gene lists may overestimate gene overlap. *J. Comput. Biol.* 25, 606–612. doi: 10.1089/cmb.2017.0262

Lemaitre, B., and Hoffmann, J. (2007). The host defense of *Drosophila melanogaster*. *Annu. Rev. Immunol.* 25, 697–743.

Li, H. M., Buczkowski, G., Mittapalli, O., Xie, J., Wu, J., Westerman, R., et al. (2008). Transcriptomic profiles of *Drosophila melanogaster* third instar larval midgut and responses to oxidative stress. *Insect Mol. Biol.* 17, 325–339. doi: 10.1111/j.1365-2583.2008.00808.x

Li-Byarlay, H. (2016). The function of DNA methylation marks in social insects. *Front. Ecol. Evol.* 4:57. doi: 10.3389/fevo.2016.00057

Li-Byarlay, H., Li, Y., Stroud, H., Feng, S., Newman, T. C., Hou, K. K., et al. (2013). RNA interference knockdown of DNA methyl-transferase 3 affects gene alternative splicing in the honey bee. *Proc. Natl. Acad. Sci. U.S.A.* 110, 12750–12755. doi: 10.1073/pnas.1310735110

Lyko, F., Foret, S., Kucharski, R., Wolf, S., Falckenhayn, C., and Maleszka, R. (2010). The honey bee epigenomes: differential methylation of brain DNA in queens and workers. *PLoS Biol.* 8:e1000506. doi: 10.1371/journal.pbio.1000506

Maori, E., Lavi, S., Mozes-Koch, R., Gantman, Y., Peretz, Y., Edelbaum, O., et al. (2007). Isolation and characterization of Israeli acute paralysis virus, a dicistrovirus affecting honeybees in Israel: evidence for diversity due to intra- and inter-species recombination. *J. Gen. Virol.* 88(Pt 12), 3428–3438. doi: 10.1099/vir.0.83284-0

Maori, E., Paldi, N., Shafir, S., Kalev, H., Tsur, E., Glick, E., et al. (2009). IAPV, a bee-affecting virus associated with Colony Collapse Disorder can be silenced by dsRNA ingestion. *Insect Mol. Biol.* 18, 55–60. doi: 10.1111/j.1365-2583.2009.00847.x

Marina, R. J., Sturgill, D., Bailly, M. A., Thenoz, M., Varma, G., Prigge, M. F., et al. (2016). TET-catalyzed oxidation of intragenic 5-methylcytosine regulates CTCF-dependent alternative splicing. *EMBO J.* 35, 335–355. doi: 10.15252/embj.201593235

Matilainen, O., Quirós, P. M., and Auwerx, J. (2017). Mitochondria and epigenetics–crosstalk in homeostasis and stress. *Trends Cell Biol.* 27, 453–463. doi: 10.1016/j.tcb.2017.02.004

McMenamin, A. J., and Genersch, E. (2015). Honey bee colony losses and associated viruses. *Curr. Opin. Insect Sci.* 8, 121–129. doi: 10.1016/j.cois.2015.01.015

Merkling, S. H., Bronkhorst, A. W., Kramer, J. M., Overheul, G. J., Schenck, A., and Van Rij, R. P. (2015). The epigenetic regulator G9a mediates tolerance to RNA virus infection in Drosophila. *PLoS Pathog.* 11:e1004692. doi: 10.1371/journal.ppat.1004692

Mukherjee, K., Twyman, R. M., and Vilcinskas, A. (2015). Insects as models to study the epigenetic basis of disease. *Prog. Biophys. Mol. Biol.* 118, 69–78. doi: 10.1016/j.pbiomolbio.2015.02.009

Munoz-Wolf, N., and Lavelle, E. C. (2017). Hippo interferes with antiviral defences. *Nat. Cell Biol.* 19, 267–269. doi: 10.1038/ncb3502

Nagy, P. D., and Pogany, J. (2012). The dependence of viral RNA replication on co-opted host factors. *Nat. Rev. Microbiol.* 10, 137–149. doi: 10.1038/nrmicro2692

Opachaloemphan, C., Yan, H., Leibholz, A., Desplan, C., and Reinberg, D. (2018). Recent advances in behavioral (epi) genetics in eusocial insects. *Annu. Rev. Genet.* 52, 489–510. doi: 10.1146/annurev-genet-120116-024456

Paschos, K., and Allday, M. J. (2010). Epigenetic reprogramming of host genes in viral and microbial pathogenesis. *Trends Microbiol.* 18, 439–447. doi: 10.1016/j.tim.2010.07.003

Patro, R., Duggal, G., Love, M. I., Irizarry, R. A., and Kingsford, C. (2017). Salmon provides fast and bias-aware quantification of transcript expression. *Nat. Methods* 14, 417–419. doi: 10.1038/nmeth.4197

Pavet, V., Quintero, C., Cecchini, N. M., Rosa, A. L., and Alvarez, M. E. (2006). Arabidopsis displays centromeric DNA hypomethylation and cytological alterations of heterochromatin upon attack by *Pseudomonas syringae*. *Mol. Plant Microbe Interact.* 19, 577–587. doi: 10.1094/mpmi-19-0577

Punta, M., Coggill, P. C., Eberhardt, R. Y., Mistry, J., Tate, J., Boursnell, C., et al. (2012). The Pfam protein families database. *Nucleic Acids Res.* 40, D290–D301.

Ritchie, M. E., Phipson, B., Wu, D., Hu, Y., Law, C. W., Shi, W., et al. (2015). limma powers differential expression analyses for RNA-sequencing and microarray studies. *Nucleic Acids Res.* 43:e47. doi: 10.1093/nar/gkv007

Runckel, C., Flenniken, M. L., Engel, J. C., Ruby, J. G., Ganem, D., Andino, R., et al. (2011). Temporal analysis of the honey bee microbiome reveals four novel viruses and seasonal prevalence of known viruses, *Nosema*, and *Crithidia*. *PLoS One* 6:e20656. doi: 10.1371/journal.pone.0020656

Sakaguchi, A., Matsumoto, K., and Hisamoto, N. (2004). Roles of MAP kinase cascades in *Caenorhabditis elegans*. *J. Biochem.* 136, 7–11. doi: 10.1093/jb/mvh097

Saripalli, G., Sharma, C., Gautam, T., Singh, K., Jain, N., Prasad, P., et al. (2020). Complex relationship between DNA methylation and gene expression due to Lr28 in wheat-leaf rust pathosystem. *Mol. Biol. Rep.* 47, 1339–1360. doi: 10.1007/s11033-019-05236-1

Schnorrer, F., Schonbauer, C., Langer, C. C. H., Dietzl, G., Novatchkova, M., Schernhuber, K., et al. (2010). Systematic genetic analysis of muscle morphogenesis and function in *Drosophila*. *Nature* 464, 287–291. doi: 10.1038/nature08799

Shukla, S., Kavak, E., Gregory, M., Imashimizu, M., Shutinoski, B., Kashlev, M., et al. (2011). CTCF-promoted RNA polymerase II pausing links DNA methylation to splicing. *Nature* 479, 74–79. doi: 10.1038/nature10442

Tanca, A., Deligios, M., Addis, M. F., and Uzzau, S. (2013). High throughput genomic and proteomic technologies in the fight against infectious diseases. *J. Infect. Dev. Ctries.* 7, 182–190. doi: 10.3855/jidc.3027

Tantillo, G., Bottaro, M., Di Pinto, A., Martella, V., Di Pinto, P., and Terio, V. (2015). Virus infections of honeybees *Apis mellifera*. *Ital. J. Food Saf.* 4, 157–168.

Tian, F., Zhan, F., VanderKraats, N. D., Hiken, J. F., Edwards, J. R., Zhang, H., et al. (2013). DNMT gene expression and methylome in Marek's disease resistant and susceptible chickens prior to and following infection by MDV. *Epigenetics* 8, 431–444. doi: 10.4161/epi.24361

Toyota, M., Suzuki, H., Yamashita, T., Hirata, K., Imai, K., Tokino, T., et al. (2009). Cancer epigenomics: implications of DNA methylation in personalized cancer therapy. *Cancer Sci.* 100, 787–791. doi: 10.1111/j.1349-7006.2009.01095.x

Toyota, M., and Yamamoto, E. (2011). DNA methylation changes in cancer. *Prog. Mol. Biol. Transl. Sci.* 101, 447–457.

Turner, M., and Diaz-Munoz, M. D. (2018). RNA-binding proteins control gene expression and cell fate in the immune system. *Nat. Immunol.* 19, 120–129. doi: 10.1038/s41590-017-0028-4

Varghese, F. S., Thaa, B., Amrun, S. N., Simarmata, D., Rausalu, K., Nyman, T. A., et al. (2016). The antiviral alkaloid berberine reduces chikungunya virus-induced mitogen-activated protein kinase signaling. *J. Virol.* 90, 9743–9757. doi: 10.1128/jvi.01382-16

Vermeulen, C. J., Sorensen, P., Gagalova, K. K., and Loeschcke, V. (2013). Transcriptomic analysis of inbreeding depression in cold-sensitive *Drosophila melanogaster* shows upregulation of the immune response. *J. Evol. Biol.* 26, 1890–1902. doi: 10.1111/jeb.12183

Vilcinskas, A. (2017). The impact of parasites on host insect epigenetics. *Adv. Insect Physiol.* 53, 145–165. doi: 10.1016/bs.aiip.2017.05.001

Vitting-Seerup, K., and Sandelin, A. (2017). The landscape of isoform switches in human cancers. *Mol. Cancer Res.* 15, 1206–1220. doi: 10.1158/1541-7786.mcr-16-0459

Vitting-Seerup, K., and Sandelin, A. (2019). IsoformSwitchAnalyzeR: analysis of changes in genome-wide patterns of alternative splicing and its functional consequences. *Bioinformatics* 35, 4469–4471. doi: 10.1093/bioinformatics/btz247

Wang, L., Park, H. J., Dasari, S., Wang, S., Kocher, J.-P., and Li, W. (2013). CPAT: coding-potential assessment tool using an alignment-free logistic regression model. *Nucleic Acids Res.* 41:e74. doi: 10.1093/nar/gkt006

Wang, Y., Jorda, M., Jones, P. L., Maleszka, R., Ling, X., Robertson, H. M., et al. (2006). Functional CpG methylation system in a social insect. *Science* 314, 645–647. doi: 10.1126/science.1135213

Wang, Y., and Li-Byarlay, H. (2015). Physiological and molecular mechanisms of nutrition in honey bees. *Adv. Insect Physiol.* 49, 25–58. doi: 10.1016/bs.aiip.2015.06.002

Wilson-Rich, N., Spivak, M., Fefferman, N. H., and Starks, P. T. (2009). Genetic, individual, and group facilitation of disease resistance in insect societies. *Annu. Rev. Entomol.* 54, 405–423. doi: 10.1146/annurev.ento.53.103106.093301

Wright, R. M., Aglyamova, G. V., Meyer, E., and Matz, M. V. (2015). Gene expression associated with white syndromes in a reef building coral, *Acropora hyacinthus*. *BMC Genomics* 16:371. doi: 10.1186/s12864-015-1540-2

Xu, J., Grant, G., Sabin, L. R., Gordesky-Gold, B., Yasunaga, A., Tudor, M., et al. (2012). Transcriptional pausing controls a rapid antiviral innate immune response in *Drosophila*. *Cell Host Microbe* 12, 531–543. doi: 10.1016/j.chom.2012.08.011

Yan, H., Simola, D. F., Bonasio, R., Liebig, J., Berger, S. L., and Reinberg, D. (2014). Eusocial insects as emerging models for behavioural epigenetics. *Nat. Rev. Genet.* 15, 677–688. doi: 10.1038/nrg3787

Yang, X., Deng, S., Wei, X., Yang, J., Zhao, Q., Yin, C., et al. (2020). MAPK-directed activation of the whitefly transcription factor CREB leads to P450-mediated imidacloprid resistance. *Proc. Natl. Acad. Sci. U.S.A.* 117, 10246–10253. doi: 10.1073/pnas.1913603117

Zemach, A., McDaniel, I. E., Silva, P., and Zilberman, D. (2010). Genome-wide evolutionary analysis of eukaryotic DNA methylation. *Science* 328, 916–919. doi: 10.1126/science.1186366

Zirin, J., Nieuwenhuis, J., Samsonova, A., Tao, R., and Perrimon, N. (2015). Regulators of autophagosome formation in *Drosophila* muscles. *PLoS Genet.* 11:e1005006. doi: 10.1371/journal.pgen.1005006

Conflict of Interest: The authors declare that the research was conducted in the absence of any commercial or financial relationships that could be construed as a potential conflict of interest.

frontiers in Genetics

ORIGINAL RESEARCH
published: 26 October 2020
doi: 10.3389/fgene.2020.573603

A Mechanosensory Receptor TMC Regulates Ovary Development in the Brown Planthopper *Nilaparvata lugens*

*Ya-Long Jia†, Yi-Jie Zhang†, Di Guo, Chen-Yu Li, Jun-Yu Ma, Cong-Fen Gao and Shun-Fan Wu**

College of Plant Protection, Nanjing Agricultural University, State and Local Joint Engineering Research Center of Green Pesticide Invention and Application, Nanjing, China

Transmembrane channel-like (TMC) genes encode a family of evolutionarily conserved membrane proteins. Mutations in the TMC1 and TMC2 cause deafness in humans and mice. However, their functions in insects are is still not well known. Here we cloned three *tmc* genes, *Nltmc3*, *Nltmc5*, and *Nltmc7* from brown planthoppers. The predicted amino acid sequences showed high identity with other species homologs and have the characteristic eight or nine transmembrane domains and TMC domain architecture. We detected these three genes in all developmental stages and examined tissues. Interestingly, we found *Nltmc3* was highly expressed in the female reproductive organ especially in the oviduct. RNAi-mediated silencing of *Nltmc3* substantially decreased the egg-laying number and impaired ovary development. Our results indicate that *Nltmc3* has an essential role in the ovary development of brown planthoppers.

Keywords: TMC, reproduction, mechanoreceptors, *Nilaparvata lugens*, expression pattern

OPEN ACCESS

Edited by:
Wei Guo,
Institute of Zoology, Chinese Academy of Sciences (CAS), China

Reviewed by:
LinQuan Ge,
Yangzhou University, China
Haijun Xu,
Zhejiang University, China

***Correspondence:**
Shun-Fan Wu
wusf@njau.edu.cn

† These authors have contributed equally to this work

Specialty section:
This article was submitted to Epigenomics and Epigenetics, a section of the journal Frontiers in Genetics

Received: *17 June 2020*
Accepted: *02 September 2020*
Published: *26 October 2020*

Citation:
Jia Y-L, Zhang Y-J, Guo D, Li C-Y, Ma J-Y, Gao C-F and Wu S-F (2020) A Mechanosensory Receptor TMC Regulates Ovary Development in the Brown Planthopper Nilaparvata lugens. Front. Genet. 11:573603. doi: 10.3389/fgene.2020.573603

INTRODUCTION

Transmembrane channel-like (TMC) proteins have been identified from insects to mammals (Keresztes et al., 2003; Kurima et al., 2003; Guo et al., 2016). Eight TMC proteins were presented in vertebrates including humans and mice (Keresztes et al., 2003; Kurima et al., 2003). They can be grouped into three subfamilies A, B, and C, in terms of their sequence homology and similarities of the genomic structures of their respective genes (Keresztes et al., 2003). The TMC protein subfamily A consists of three proteins, TMC1, TMC2, and TMC3; subfamily B contains two proteins, TMC5 and TMC6; And subfamily C include three members, TMC4, TMC7, and TMC8 (Keresztes et al., 2003; Kurima et al., 2003). In *Caenorhabditis elegans*, two *tmc* genes have been cloned (Chatzigeorgiou et al., 2013). However, the *Drosophila* genome only encodes one *tmc* homolog (Guo et al., 2016). All *tmc* genes are strongly predicted to encode proteins with at least six transmembrane domains and a novel conserved CWETXVGQEly(K/R)LtvXD amino-acid sequence motif that termed as TMC domain (Keresztes et al., 2003; Kurima et al., 2003).

TMC1 and TMC2, first identified in deaf human patients, are essential for hearing in mice (Kawashima et al., 2015). TMC1 and TMC2 are necessary for the mechano-transduction currents of hair cells (Pan et al., 2013, 2018). Recent studies have showed that TMC1 and TMC2 are pore-forming subunits of mechanosensory transduction channels (Pan et al., 2018; Jia et al., 2019). The

tmc1 gene in *C. elegans* was reported to encode a sodium-sensitive cation channel and participates in nociceptive neuron-mediated alkaline and salt chemo-sensation (Chatzigeorgiou et al., 2013; Zhang et al., 2015; Wang et al., 2016). Recent studies showed that TMC proteins in nematodes modulate egg laying and membrane excitability through a background leak conductance (Yue et al., 2018). In *Drosophila*, the *tmc* gene was involved in proprioception, food texture detection and egg-laying texture discrimination (Guo et al., 2016; Zhang et al., 2016; Wu et al., 2019).

The brown planthopper (BPH), *Nilaparvata lugens* (Stål), (Hemiptera: Delphacidae), is a serious pest on rice in China. It has cause loss of rice production more than $300 million annually in Asia (Min et al., 2014). Chemical insecticides are mainly used for BPH control. However, due to the large scale and intensive use of insecticides, BPH has evolved high levels of resistance to many of the major classes of insecticide (Wu et al., 2018). Hence, it is urgent to find new insecticide targets to develop novel insecticides. Although *tmc* genes have been characterized in mice, nematodes, and fruit flies, few studies have been performed to investigate functions of *tmc* genes in other insects. In this study, we characterized the *tmc* gene family of the BPH. We found that three *tmc* genes were present in the genome of BPH. The expression of these three *tmc* genes were investigated and we found that silencing of *Nltmc3* gene, which is homology of *tmc* gene in *Drosophila* and *C. elegans*, impairs the egg-laying and ovary development in BPH.

MATERIALS AND METHODS

Insects

Nilaparvata lugens was collected from a rice field at the Plant Protection Station of Jiangpu County (Jiangsu, China). They were reared on Taichung Native 1 (TN1) rice seedlings in the laboratory. The rearing conditions were 27 ± 1°C, with 70 ± 10% relative humidity and a 16 h:8 h (Light:Dark) photoperiod.

Identification and Cloning of *Nltmc* Genes

The amino acid sequence of *D. melanogaster* TMC protein was used to screen against *N. lugens* genomic and transcriptomic databases for identification of its homologs in *N. lugens*. Open reading frames (ORFs) were predicted with EditSeq (version 5.02, DNAstar, Madison, WI, United States).

Total RNA was isolated from whole insects using the TRIzol Reagent (Invitrogen, Carlsbad, CA, United States) following the manufacturer's protocol. Residual genomic DNA was removed by RQ1 RNase-Free DNase (Promega). Single-stranded cDNA was synthesized from the total RNA with M-MLV reverse transcriptase and oligo $(dT)_{18}$ (BioTeke, Beijing, China). The forward primer Nltmc-comp-F and the reverse primer Nltmc-comp-R were used to amplify the full-length or fragment gene by means of PCR on cDNA from adult *N. lugens* using TransTaq HiFi DNA Polymerase (TransGen Biotech, Beijing, China). The purified PCR products were sub-cloned into pGEM® -T easy vector (Promega, Madison, WI) and then sequenced using the 3730 XL DNA analyzer (Applied Biosystems, Carlsbad, CA, United States. The primers corresponding to each gene are listed in **Table 1**.

Sequence Analysis and Phylogenetic Tree Construction

The exon and intron architectures of *Nltmc* genes were predicted based on the alignments of putative cDNA against their corresponding genomic sequences in Spidey[1], and then structured on the website of GSDS v2.0[2] (Hu et al., 2015). The transmembrane segments and topology of NlTMC proteins were predicted by TMHMM v2.0[3]. Multiple alignments of

[1]http://www.ncbi.nlm.nih.gov/spidey/

[2]http://gsds.cbi.pku.edu.cn/index.php

[3]http://www.cbs.dtu.dk/services/TMHMM-2.0/

TABLE 1 | The primers used in this study.

Primers	Primers sequence
For fragment cloning	
Nltmc3-F1	AGCTTCGAGCAGACGACAAACCAA
Nltmc3-R1	CTTGCGTTCTCCTGCATCCT
Nltmc3-F2	GGCAGTTTGTGAAACGTGAA
Nltmc3-R2	AGCGAACAAGTCCCAGAACGC
Nltmc3-F3	GGCTTCAAAGAAGCTCTGCTTGAG
Nltmc3-R3	TTGCGTCCGATTTGAGGTCA
Nltmc5-F1	ATGACCAATGACCCATTGGCTG
Nltmc5-R1	ATTGGCGTCTTGCGTTGTTG
Nltmc5-F2	TTTGTTGGTGAATGTAAAACA
Nltmc5-R2	TGCCCTGAGGTATAATGACGA
Nltmc5-F3	TCTATGTGCGGTGGCGTTTA
Nltmc5-R3	TACCGTACGCCAGCTATCAGAGA
Nltmc7-F1	AGCACTACGCACATCAACGA
Nltmc7-R1	TTAACTGTTGGGCAAGTCGACA
Nltmc7-F2	GCTGTCACCTTCTTGTGAGCTA
Nltmc7-R2	TGTTCCCACATTTTTCGCCG
For qPCR	
Q*Nltmc3*-F	GACAGAGTAAACTGTCTGAG
Q*Nltmc3*-R	AGCGAACAAGTCCCAGAACGC
Q*Nltmc5*-F	GCTATGGTACGGCAGTCTGA
Q*Nltmc5*-R	TGTCAACGTGTGCTACTCCA
Q*Nltmc7*-F	AGCACTACGCACATCAACGA
Q*Nltmc7*-R	CTTGCAGGCGAAATGTGTCT
QNl18s-F	CGCTACTACCGATTGAA
QNl18s-R	GGAAACCTTGTTACGACTT
dsRNA synthesis	
T7-*Nltmc3*-F1	**TAATACGACTCACTATAGGG**AGAGCGTTATTCGTGCGTGT
T7-*Nltmc3*-R1	**TAATACGACTCACTATAGGG**AAGCTCCTTAGGCAACGCTT
T7-*Nltmc5*-F1	**TAATACGACTCACTATAGGG**ACTCAACAGTCACACCTCGG
T7-*Nltmc5*-R1	**TAATACGACTCACTATAGGG**TTCAGCCGCTAGAAGCAGTT
T7-*Nltmc7*-F1	**TAATACGACTCACTATAGGG**AGCGCTGTGCTACTTCTTGT
T7-*Nltmc7*-R1	**TAATACGACTCACTATAGGG**CGAGTAGTAGCGAGGCACTG
T7-*gfp*-F	**TAATACGACTCACTATAGGG**AAGGGCGAGGAGCTGTTCACCG
T7-*gfp*-R	**TAATACGACTCACTATAGGG**CAGCAGGACCATGTGATCGCGC

the complete amino acid sequences were performed with Clustal Omega[4]. Phylogenetic tree was constructed using MEGA 5.2.2 software with the Maximum Likelihood method and bootstrapped with 1,000 replications. The branch support values are expressed as percentages. The accession numbers of the sequences used in the phylogenetic analysis are listed in **Table 2**.

Gene Expression Profile Analysis

Developmental stage samples were collected from eggs (n = 100∼120), first-instar (n = 80), second-instar (n = 60), third-instar (n = 230), fourth-instar (n = 15∼20), fifth-instar nymphs (n = 15), and adults of both sexes and wing forms: brachypterous female (BF), macropterous female (MF), brachypterous male (BM), and macropterous male adults (MM) (n = 10). Eggs were collected at 4 days (central development stage) after the oviposition since the egg stage is 6–7 days. Nymphs were collected every 24 h from the beginning of each instar until molting and all adults were collected 4 days after eclosion.

Different tissue samples including head, wing, gut, Malpighian tubule (MT), female reproductive organ (FRO), ovary (OA), oviduct (OU), copulatory pouch (CP), and spermatheca (SE) were dissected from brachypterous female adults collected 4 days after eclosion. The first-strand cDNA was synthesized with HiScript® II Q RT SuperMix for qPCR (+ gDNA wiper) kit (Vazyme, Nanjing, China) using an oligo$(dT)_{18}$ primer and 500 ng total RNA template in a 10 μl reaction, following the instructions.

Real-time qPCRs were employed to investigate relative expression of *Nltmc* genes in the various samples using the UltraSYBR Mixture (with ROX) Kit (CWBIO, Beijing, China). The PCR was performed in 20 μl reaction including 4 μl of 10-fold diluted cDNA, 1 μl of each primer (10 μM), 10 μl 2× UltraSYBR Mixture, and 6 μl RNase-free water. The standard two-step PCR cycle conditions were as follows: 95°C for 10 min, and then 40 cycles of amplification consisting of 95°C for 15 s, 60°C for 40 s, followed by melting curve analysis. Pairs of gene-specific primers used for real-time qPCR were designed using the Primer Premier 5 Software (**Table 1**). The relative quantification of *Nltmc* was calculated according to the comparative $2^{-\Delta\Delta CT}$ method (Livak and Schmittgen, 2001).

[4]http://www.ebi.ac.uk/Tools/msa/clustalo

TABLE 2 | Accession numbers of amino acid sequences used in the phylogenetic and sequence alignment analysis.

Protein name	Accession number	Protein name	Accession number
AaTMC5	XP_021695152.1	HsTMC1	NP_619636.2
AaTMC7	XP_021708478.1	HsTMC2	NP_542789.2
AgTMCah	XP_308243.4	HsTMC3	NP_001074001.1
AgTMCbh	XP_310494.4	HsTMC4	NP_001138775.2
AgTMCch	XP_320512.3	HsTMC5	NP_001248770.1
AmTMC2	XP_006568703.2	HsTMC7	NP_079123.3
AmTMC7	XP_395471.3	HsTMC8	XP_024306385.1
BmTMC1	XP_012552239.2	MmTMC1	NP_083229.1
BmTMC6	XP_021203376.1	MmTMC2	NP_619596.1
BmTMC7	XP_021209073.1	MmTMC3	NP_808363.3
CeTMC1	NP_508221.3	MmTMC4	NP_861541.2
CeTMC2	NP_001335510.1	MmTMC5	XP_011240226.1
DmTMC	NP_001303362.1	MmTMC6	NP_663414.3
DrTMC1	NP_001299610.1	MmTMC7	NP_766064.2
DrTMC2	NP_001289166.1	MmTMC8	NP_001182017.1
DrTMC3	NP_001289166.1	MpTMC3	XP_022160746.1
DrTMC4	XP_002664983.1	MpTMC7	XP_022166873.1
DrTMC5	XP_005163977.1	MsTMC3	XP_025190709.1
DrTMC6	NP_001002705.1	MsTMC7	XP_025195716.1
HaTMC3	XP_021194056.1	PrTMC2	XP_022125523.1
HaTMC7	XP_021199860.1	PrTMC5	XP_022121573.1
HhTMC2	XP_014287845.1	PrTMC7	XP_022124079.1
HhTMC7	XP_014275019.1	PtTMC3	XP_015917737.1
PtTMC5	XP_021003906.1	PtTMC7	XP_015908754.1
PhTMCc	XP_002427541.1	VdTMC3	XP_022643750.1

Double-Stranded RNA (dsRNA) Preparation and Injection

The fragment coding sequence of *Nltmc* genes and green fluorescent protein (*gfp*) were amplified by PCR using specific primers conjugated with the T7 RNA polymerase (**Table 1**). PCR-generated DNA templates were then used to synthesize dsRNA, which contains T7 promoter sequences at each end. We used a MEGAscript T7 transcription kit (Ambion, Austin, TX, United States) to produce the specific dsRNA of each gene as the manufacturer's instruction. The quality and size of the dsRNA products were verified by 1% agarose gel electrophoresis. Thirty fully mated female adults (collected 4 days after eclosion) were injected with approximately 50 nl of purified dsRNA (5,000 ng/μl) via mesothorax and were reared with rice seedlings. A set of 6–10 insects at 3 days after injection was selected to verify dsRNA knockdown efficiency by qRT-PCR. The remaining individuals were used for observations of eggs laid and female survival. Four to six biological replications were performed.

Egg-Laying, Survival Assay and Quantification of Egg Number

For egg-laying assay, RNAi injected females (fully mated) were transferred vials with fresh rice seedlings. Number of laid eggs were counted under a stereomicroscope (Zeiss) after 3 days. The female survival was recorded 8 days after injection of dsRNA. At least four to six vials per treatment were observed. Ovaries of mated females were prepared under the stereomicroscope (Zeiss). Pictures of ovaries were taken using a light microscope with a digital video camera (Zeiss, ProgRes 3008 mF, Jenoptik, Jena, Germany). The number of eggs per ovary were measured and counted.

Statistics

Experimental data was analyzed using GraphPad Prism 6 software (GraphPad Software Inc., San Diego, CA, United States). The two-tailed unpaired Student's t-test or one-way analysis of variance (ANOVA) of Duncan's multi-range test were used to test the differences between two or more than two normal distribution data.

RESULTS

Sequence Analysis of *tmc* Gene Family in *N. lugens*

We identified three *tmc* genes in the genome and transcriptome database of *N. lugens*. These three *tmc* genes were cloned by PCR and then confirmed by DNA sequencing (**Table 1**). One fragment and two full-lengths of different cDNA clones were obtained. These sequences were designated *Nltmc3* (GenBank accession number: MT576068), *Nltmc5* (MT576067), and *Nltmc7* (MT576069) according to their similarity to other invertebrate and vertebrate *tmc* genes (Keresztes et al., 2003; Kurima et al., 2003).

We cloned the fragment of *Nltmc3* gene that consists of 4,476-bp cDNA encoding 1,492 amino acids. We tried to clone the full-length of this gene using 5′-RACE and 3′-RACE technology. Unfortunately, we did not get the positive results. We then cloned the full-length of *Nltmc5* and *Nltmc7* gene. The complete ORF of *Nltmc5* and *Nltmc7* encodes 692 and 780 amino acids, respectively. Exon-intron organization was analyzed by comparing cloned cDNAs and the corresponding genomic sequence, revealing that *Nltmc3* is located on scaffold 754 and scaffold 3202, *Nltmc5* is located on scaffold 943, and *Nltmc7* is located on scaffold 2298 (**Figure 1**). TMHMM2.0 strongly predicts the presence of eight or nine transmembrane-spanning domains in each of the TMC proteins. They all encode a conserved TMC domain that share the completely conserved amino acid triplet C (cysteine) – W (tryptophan) – E (glutamic acid), predicted to be located on the extracellular loop upstream of TM6 (**Figures 2–4**) (Keresztes et al., 2003). Amino-acid sequence comparisons between the NlTMC proteins and other species TMC proteins show high overall amino acid similarity at the transmembrane region and TMC domain (**Figures 2–4**). The encoded protein of NlTMC3, similar with CeTMC1, CeTMC2, and DmTMC, has large ORFs. BLASTP analyses of protein sequence alignment showed that NlTMC3 had 60, 66, and 66%, sequence similarity with the TMC proteins of *Drosophila melanogaster* and *C. elegans*. Interestingly, we found two internal repeats between TM5 and TM6 in the *Nltmc3* gene (**Figure 2**). In mammals, eight TMC proteins can be grouped into three subfamilies A, B, and C, based on sequence homology (Keresztes et al., 2003). Phylogenetic tree comparison showed that NlTMC3 clustered with MmTMC1, MmTMC2, MmMTC3, CeTMC1, CeTMC2, and DmTMC, which belongs to A subfamily. NlTMC5 is assembled in a group that contains MmTMC5 and MmTMC6, which belongs to B subfamily. And NlTMC7 clustered with MmTMC7 and HsTMC7 that belongs to C subfamily (**Figure 5**).

Developmental and Tissue-Specific Expression Patterns of *Nltmc* Genes

The relative expression level of three *Nltmc* genes in different developmental stages and tissues were measured by qPCR (**Figure 6**). The results showed that the expression levels of the *Nltmc* genes varied between the developmental stages including egg, 1st–5th instar nymph, and 4-day old adults (MM, MF, BM, and BF). Among them, *Nltmc3* and *Nltmc7* were highly

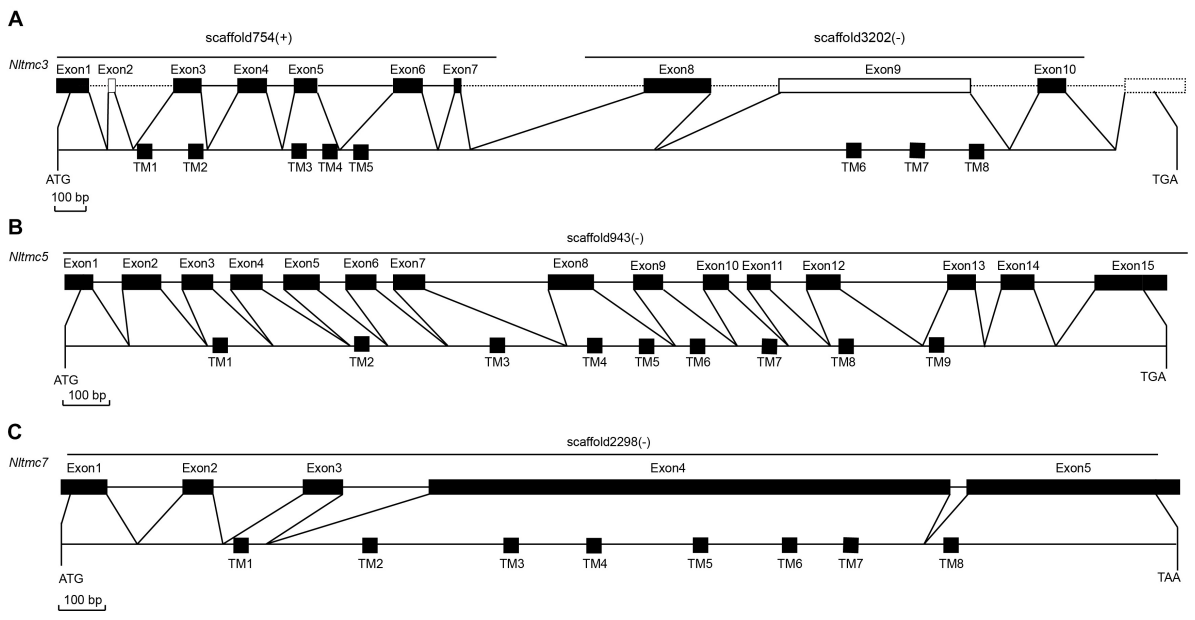

FIGURE 1 | Genomic structures of *Nltmc3* **(A)**, *Nltmc5* **(B)**, and *Nltmc7* **(C)** genes and the domain structures of encoded proteins. The exon–intron organization of *Nltmc* genes was determined by sequence comparison between genomic sequence and putative cDNA sequence. The top line of every gene represents the original genomic scaffold sequences. The predicted start codon (ATG), stop codon (TAG or TAA) and the scaffold of gene locus (" + " represent the same orientation with scaffold; " – " represent the reverse orientation with scaffold) are also shown in the corresponding positions. The bottom line represents the full-length sequence of the transcript. The transmembrane regions are indicated by the black squares. In the predicted topologies of the receptors, the transmembrane regions are indicated as TM1-8 or TM1-9.

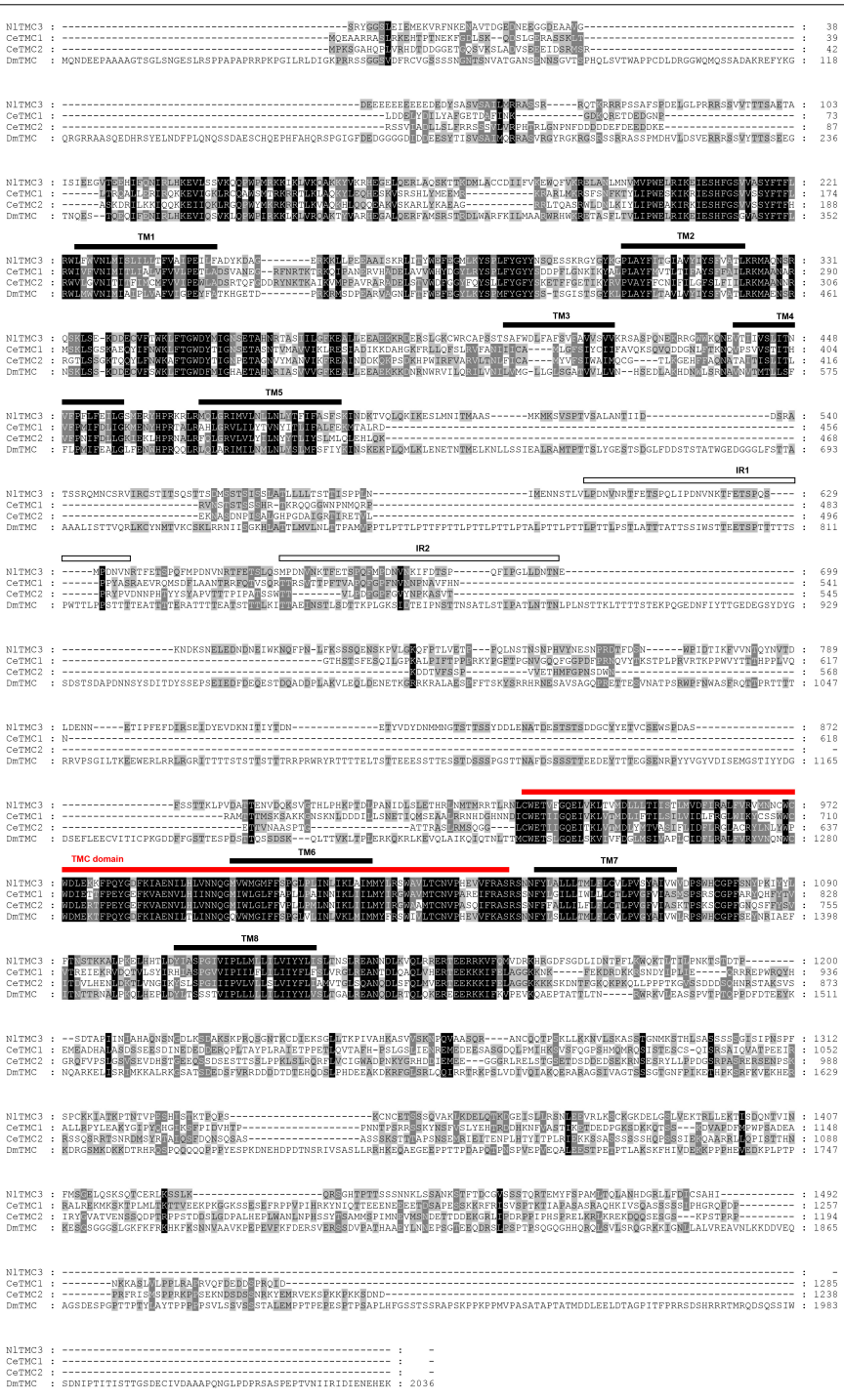

FIGURE 2 | Amino acid sequence alignment of NlTMC3 and orthologs genes from *Caenorhabditis elegans* (CeTMC1: NP_508221.3; CeTMC2: NP_001335510.1), and *Drosophila melanogaster* (DmTMC: NP_001303362.1). The amino acid position is shown on the right. Identical residues between orthologs sequences are shown as white characters against the black background, and conservative substitutions shown as shading. Black lines represent the transmembrane domain (TM), white squares represent the internal repeats (IRs), and red line represents TMC domain.

expressed in the nymphs compared with other developmental stages. *Nltmc5* was more highly expressed in MM and MF than BM and BF adults indicated that *Nltmc5* might involve in the wing polymorphism in BPH (**Figures 6A,D,G**).

We further investigated the relative expression level of three *Nltmc* genes in various female adult tissues, including the head, wing, gut, Malpighian tubules (MT) and FRO using qPCR method. In the examined tissues, all *Nltmc* genes were

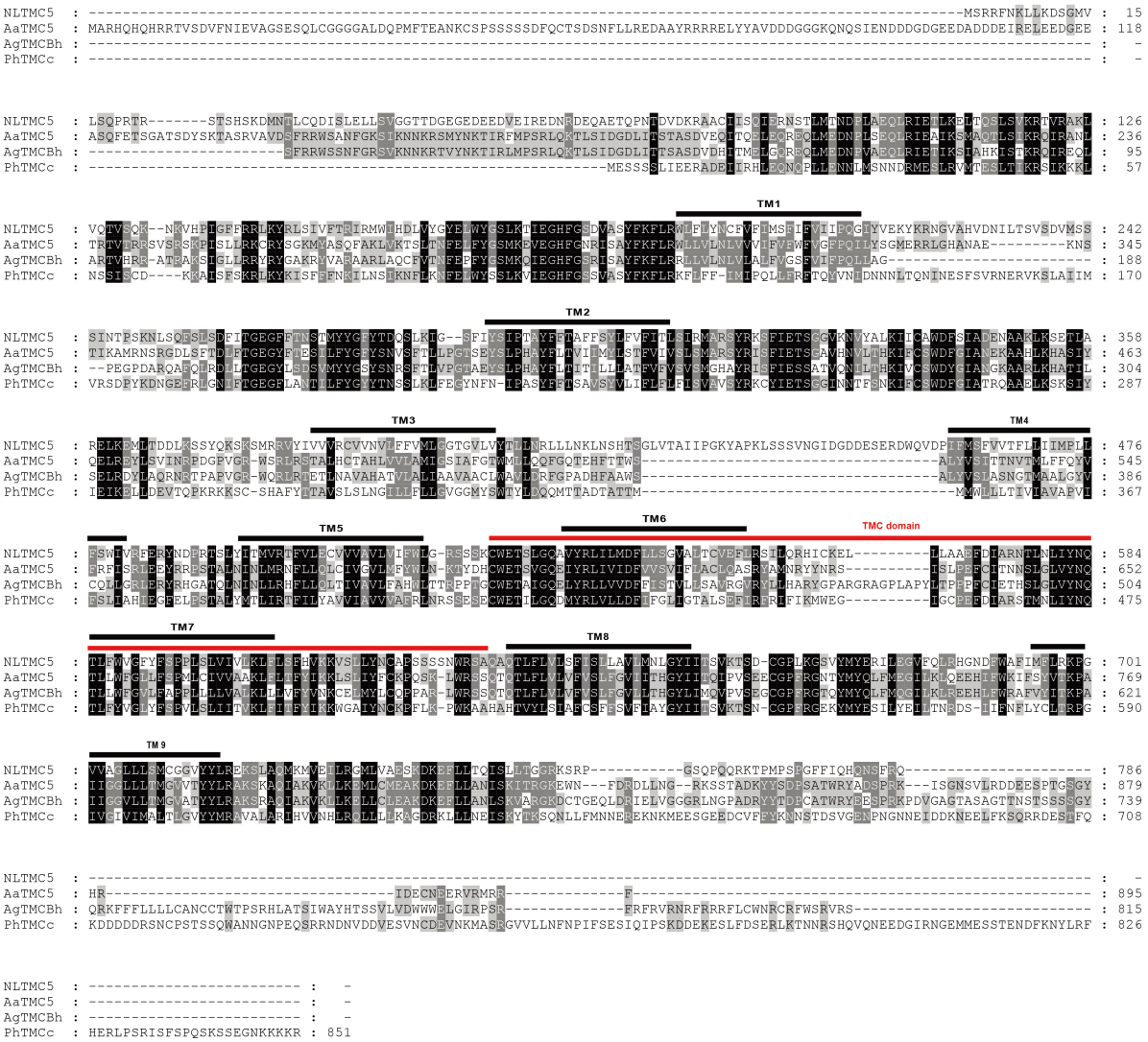

FIGURE 3 | Amino acid sequence alignment of NlTMC5 and orthologs genes from *Aedes aegypti* (XP_021695152.1), *Anopheles gambiae* (XP_310494.4), and *Pediculus humanus corporis* (XP_002427541.1). The amino acid position is shown on the right. Identical residues between orthologs sequences are shown as white characters against the black background, and conservative substitutions shown as shading. Black lines represent the transmembrane domain (TM), and red line represents TMC domain.

mostly expressed in reproductive organs compared with other tissues (**Figures 6B,E,H**). This indicated that these genes could be involved in reproduction in the BPH. We next examined the expression pattern of three *Nltmc* genes within the FRO (**Figures 6C,F,I**). Interestingly, *Nltmc3* was highly expressed in the oviduct (OU). While, *Nltmc5* was the most expressed in the ovary (OA). And *Nltmc7* was almost expressed equally in the four examined tissues (**Figures 6C,F,I**).

Silencing of *Nltmc3* Affects Egg-Laying of *N. lugens*

Next, we tested whether *Nltmc* genes are involved in the egg laying of *N. lugens*. Using RNAi technology, we silenced all of the *Nltmc* genes in the *N. lugens* (**Figures 7A–C**). The dsRNA-injection did not negatively affect the survival of *N. lugens* (**Figure 7D**). However, the *dsNltmc3*-injected planthoppers showed the decreased eggs (**Figure 7E**). While silencing *Nltmc5* and *Nltmc7* had little impact on the egg-laying rate of BPH (**Figure 7E**).

Silencing of *Nltmc3* Leads to Undeveloped Ovaries of *N. lugens*

Next, we investigated the underlying mechanism of *Nltmc3* involved in the egg laying of *N. lugens*. We did not observe any developmental defects of BPH after *Nltmc3* gene silencing (data not shown). We then examined ovary development in females at 7-day-adulthood (3-day after injection of dsRNA). For *dsgfp*-injected females, ovaries were fully developed (**Figure 7F**). By

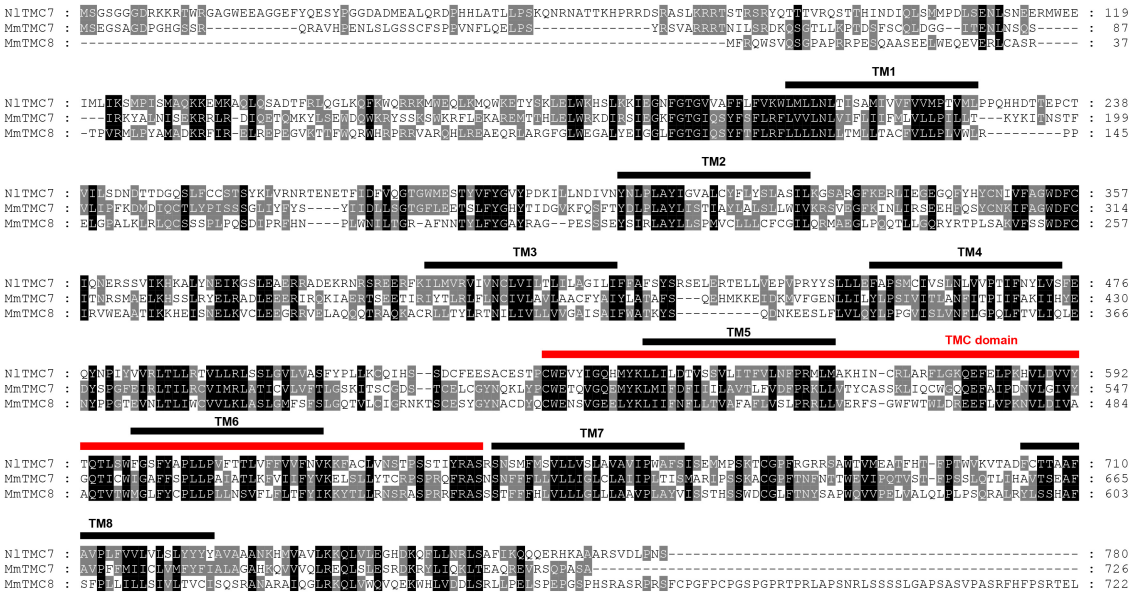

FIGURE 4 | Amino acid sequence alignment of NlTMC7 and orthologs genes from *Mus musculus* (MmTMC7: NP_766064.2; MmTMC8: NP_001182017.1). The amino acid position is shown on the right. Identical residues between orthologs sequences are shown as white characters against the black background, and conservative substitutions shown as shading. Black lines represent the transmembrane domain (TM), and red line represents TMC domain.

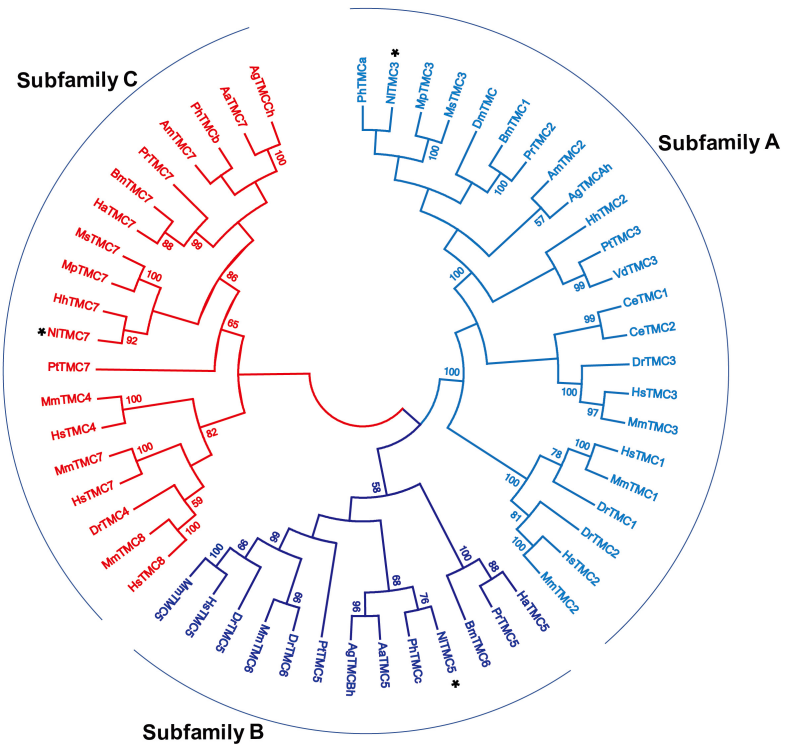

FIGURE 5 | Phylogenetic analysis of three NlTMCs and various TMC proteins. Maximum likelihood tree was constructed by MEGA software. The numbers at the nodes of the branches represent the percentage of bootstrap support (1,000 replications) for each branch. The gene names followed by their GenBank accession numbers are listed in **Table 2**. Aa, *Aedes aegypti*; Ag, *Anopheles gambiae*; Am, *Apis mellifera*; Bm, *Bombyx mori*; Ce, *Caenorhabditis elegans*; Dm, *Drosophila melanogaster*; Dr, *Danio rerio*; Ha, *Helicoverpa armigera*; Hh, *Halyomorpha halys*; Hs, *Homo sapiens*; Mm, *Mus musculus*; Mp, *Myzus persicae*; Ms, *Melanaphis sacchari*; Pr, *Pieris rapae*; Pt, Parasteatoda tepidariorum; Vd, *Varroa destructor*; Ph, *Pediculus humanus corporis*.

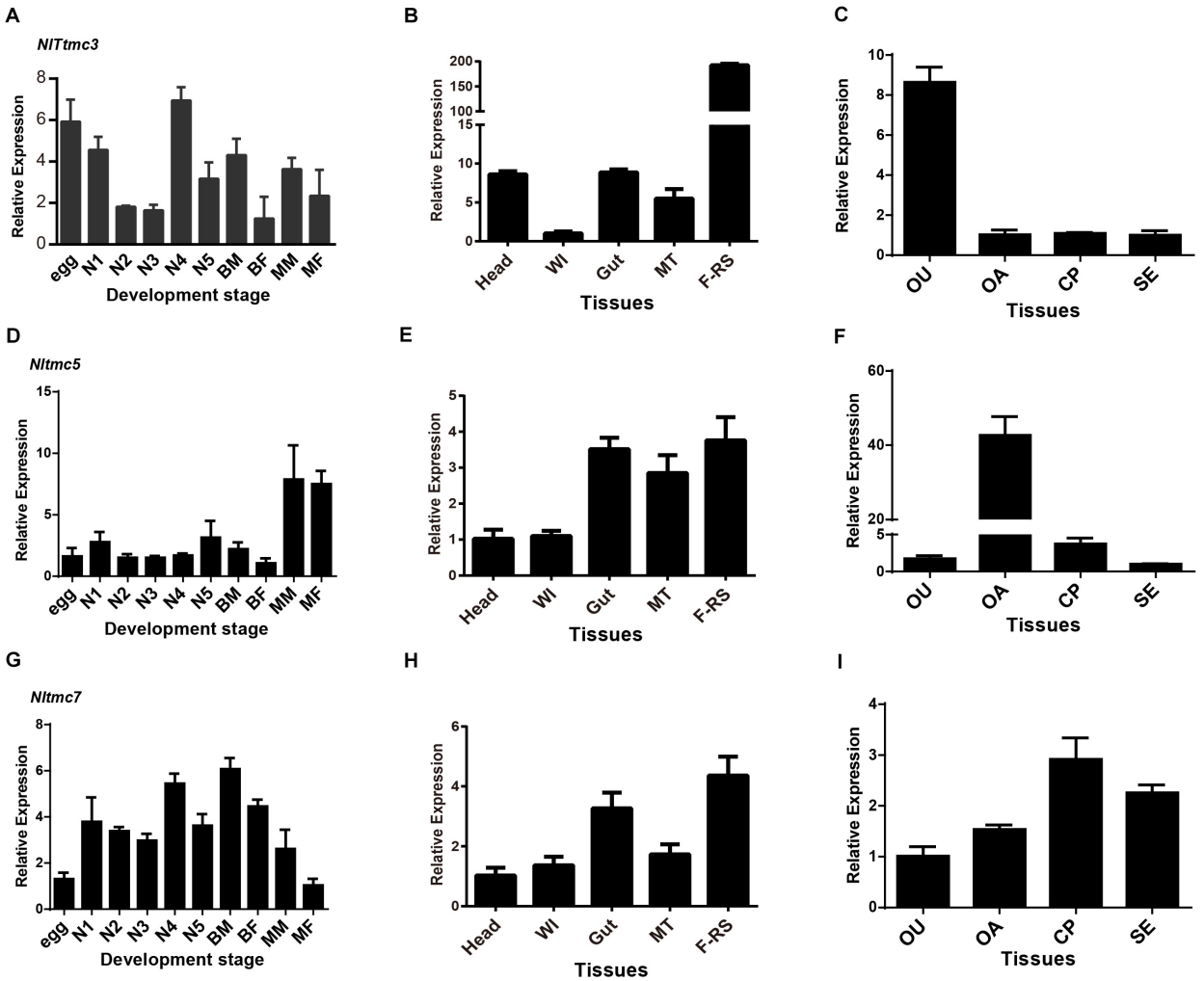

FIGURE 6 | The expression patterns of three *Nltmc* genes. **(A,D,G)** Expression patterns of three *Nltmc* genes at different developmental stages including egg, 1st to 5th instar nymphs, and adults of MF (macropterous female), BF (brachypterous female), MM (macropterous male), and BM (brachypterous male). **(B,E,H)** Expression patterns of three *Nltmc* genes in various tissues including head, wing (WI), gut, Malpighian tubule (MT), and female reproductive organ (FRO). **(C,F,I)** Expression patterns of three *Nltmc* gene in the four female reproductive organ regions including the oviduct (OU), ovary (OA), copulatory pouch (CP), and the spermatheca (SE). Data are expressed as the mean ± s.e.m. ($n > 3$).

contrast, ovaries of dsNltmc3-injected females were small and poorly developed (**Figure 7F**). In the *Nltmc3*-RNAi planthoppers, we observed less detained eggs per ovary (**Figure 7G**). However, silencing *Nltmc5* and *Nltmc7* has no impact on the ovarian development in the BPH (**Figures 7F,G**).

DISCUSSION

Eight *tmc* genes were cloned in vertebrate (Keresztes et al., 2003; Kurima et al., 2003). All TMC proteins are strongly predicted to encode at least six conserved transmembrane domains and a conserved TMC domain (Kurima et al., 2003). In insects, the *tmc* gene was only cloned and investigated in *Drosophila* (Guo et al., 2016; Zhang et al., 2016). There is only one *tmc* gene in the *Drosophila* genome (Guo et al., 2016). And two *tmc* genes were found in the *C. elegans* genome (Jia et al., 2019). They all belongs to subfamily A *tmc* gene family. In this study, we identified three *tmc* genes in the BPH genome, suggestive of diverse separation of the *tmc* genes in different species. They can be sub-divided into three subfamilies A, B and C. There are three *tmc* genes in BPH. Three TMC proteins in BPH were well clustered with other species' TMC proteins. They are homologs with *Myzus persicae tmc3*, *Aedes aegypti tmc5*, and *Myzus persicae tmc7*, respectively, thus, we used homologs genes' names for the three *tmc* genes of the BPH. Interestingly, we found that the *Nltmc3* gene was highly expressed in the FRO. The RNAi-based functional analysis indicated that *Nltmc3* was involved in female fecundity and ovary development.

NlTMC3 protein exhibits sequence conservation with TMC subfamily A members in other species including *Drosophila* and

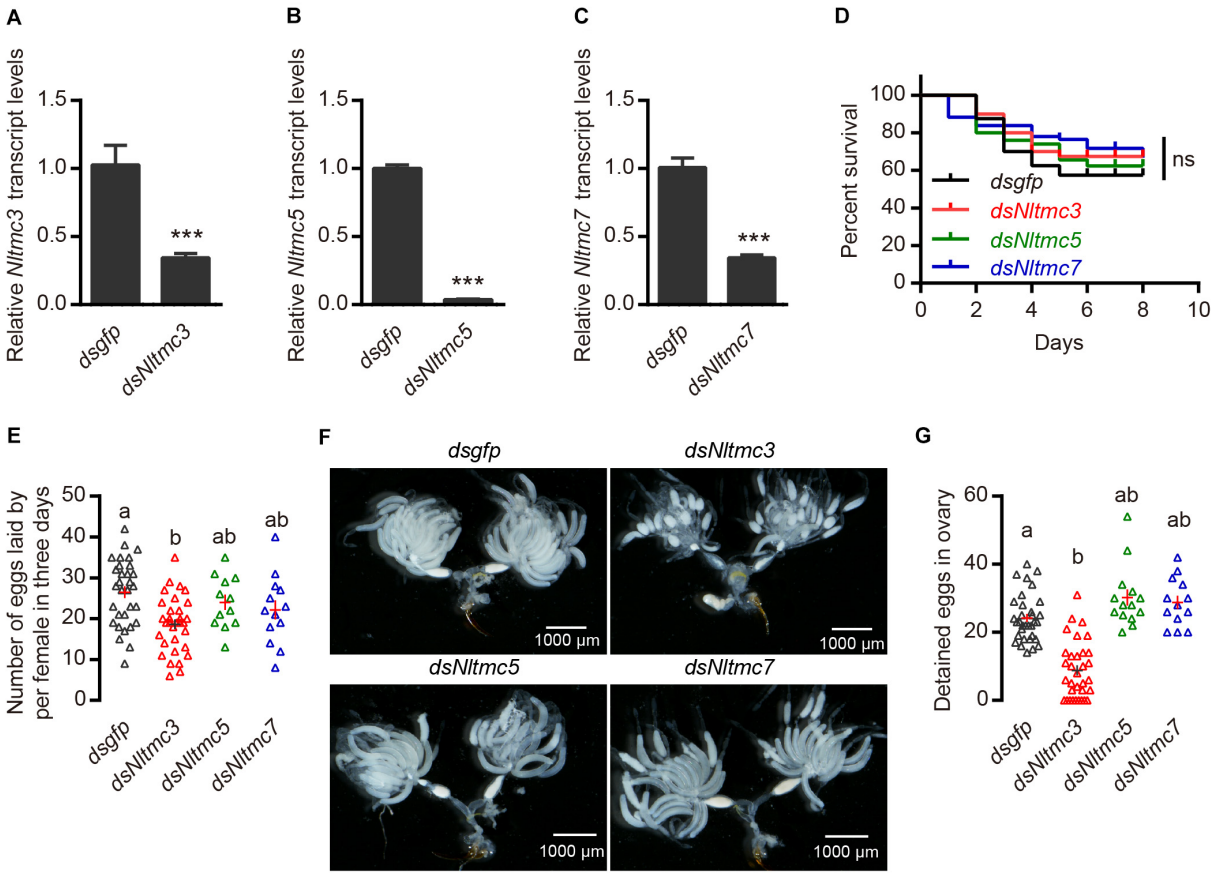

FIGURE 7 | RNAi-mediated silencing of *Nltmc3* gene reduce eggs laid of female brown planthopper. **(A–C)** Downregulation of three *Nltmc* genes using *Nltmc*-RNAi leads to a reduction in mRNA expression level. **(D)** No significant difference was observed in survival between *dsNltmc* and *dsgfp*. **(E)** Silencing of *Nltmc3* gene by *dsNltmc3* resulted in a significant reduction of eggs laid. While silence of *Nltmc5* and *Nltmc7* gene have no impacts on egg-laying of brown planthopper. **(F)** The effect of RNAi on the ovary development in the *dsgfp* (control), *dsNltmc3*, *dsNltmc5*, and *dsNltmc7* groups. Scale bar = 1,000 μm. **(G)** The detained eggs in ovary measured at 4 days old females injected with dsRNA for *Nltmc3*, *Nltmc5*, *Nltmc7*, or *gfp*. Groups that share at least one letter (e.g., a vs ab) are statistically indistinguishable, and groups that have different letters (e.g., a vs b) are statistically different. One-way ANOVA followed by Tukey's multiple comparisons test, $p < 0.05$. All data are presented as means ± s.e.m.

C. elegans, in the putative transmembrane domains (**Figure 2**). NlTMC3 is much larger than its nematode or mouse homologs. A similar result was also found in the fruit fly (Guo et al., 2016). Besides this, we discovered one internal repeat between TM5 and TM6 (**Figure 2**). It is of interest to determine whether this repeat has any physiological meanings in the future. We found two other *tmc* genes, *Nltmc5* and *Nltmc7*, which belong to subfamily B and C, respectively. From our phylogenetic analysis, we also found their homology gene in silkworm, mosquito and honeybee (**Figure 5**). However, these two subfamily genes were lost in the genome of *Drosophila* and *C. elegans*.

We also examined the distribution pattern of three *Nltmc* genes. The results revealed a ubiquitous expression of *Nltmc* genes in all developmental stages and examined tissues, indicating the possibility of a vast array of physiological functions for *Nltmc* genes. *tmc1* and *tmc2* are components of the mechano-transduction channel for sound transduction in the hair cells of the mammalian inner ear (Kurima et al., 2002; Vreugde et al., 2002; Pan et al., 2013). However, they are very broadly expressed which indicated that they might also functions in other tissues. In mammals, three other *tmc* genes (*tmc3*, *tmc4*, and *tmc7*) are also expressed in hair cells but their functions in hearing are largely unknown (Kurima et al., 2003; Kawashima et al., 2015; Scheffer et al., 2015). In *C. elegans*, TMC proteins are expressed in both neurons and muscle cells (Chatzigeorgiou et al., 2013; Zhang et al., 2015; Yue et al., 2018). *Cetmc1* is required for the ASH nociceptive neuron-mediated alkaline and salt chemo-sensation (Chatzigeorgiou et al., 2013; Wang et al., 2016). Recent studies showed that TMC proteins in *C. elegans* mediate a background Na^+-leak conductance in the egg-laying circuit (HSN neurons and vulval muscles) (Yue et al., 2018). In *Drosophila*, TMC protein was expressed on the larval class I and class II dendritic arborization neurons and bipolar dendrite neurons that acts in proprioception (Guo et al., 2016). The *tmc* gene and TMC-expressing multi-dendritic neurons in the fruit fly labellum are required for food texture detection (Zhang et al., 2016). Our studies showed that sweet neurons inhibit texture discrimination by signaling TMC-expressing mechanosensitive

neurons when deciding where to deposit their eggs in *Drosophila* (Wu et al., 2019). These results indicated that TMC-expressing neurons play opposing roles in hardness discrimination in two different behavioral decisions.

We found that *Nltmc3* was highly expressed in the FRO especially on the oviduct which indicated that this gene might influence reproductive physiology in the BPH. Indeed, knockdown of *Nltmc3* led to reduction of female fertility and undeveloped ovaries (**Figure 7**). In *C. elegans*, adult worms lacking either *Cetmc1* or *Cetmc2* retained more eggs in the uterus and had significantly less progenies. A more severely defective egg-laying phenotype was observed in double mutant worms (Yue et al., 2018). Our previous studies showed that interference of β-adrenergic-like octopamine receptor (NlOA2B2) signaling pathway had a strong impact on the egg laying of the female BPH (Wu et al., 2017). OA2B2 has already been established in *D. melanogaster* to be important for ovulation of eggs (Lim et al., 2014; Li et al., 2015). However, we did not observe more retained eggs in the *Nltmc3*-silenced BPHs. These results indicate that silencing *Nltmc3* gene has little impairment on the ovulation of BPHs. We observed a dramatic reduction in the number of mature eggs in the ovaries of females injected with dsRNA of *Nltmc3*, as compared with the *dsgfp*-injected females. Hence, our results indicated that NlTMC3 is required for ovary development and fecundity in *N. lugens*. In many insects, the amino acid/target of rapamycin (TOR) and insulin nutritional signaling pathways have vital roles in insect reproduction (Roy et al., 2018). Former studies have showed that silencing of the TOR gene in BPHs leads to unmatured eggs (Lu et al., 2016). The TOR nutritional signaling pathway and juvenile hormone (JH) regulation of vitellogenesis has been known for a long time (Zhai et al., 2015; Zhuo et al., 2017; Roy et al., 2018; Zhang et al., 2019). The possible involvement of NlTMC3 in TOR or JH signaling in *N. lugens* females needs further investigation.

In summary, we found that the *Nltmc3* plays a critical role in female *N. lugens* ovary development, and *Nltmc3* knockdown leads to reduction of female fertility. Further studies should be conducted to clarify how NlTMC3 influences female *N. lugens* reproduction.

DATA AVAILABILITY STATEMENT

The datasets presented in this study can be found in online repositories. The names of the repository/repositories and accession number(s) can be found below: https://www.ncbi.nlm.nih.gov/nuccore/MT576067.

AUTHOR CONTRIBUTIONS

S-FW conceived and designed the experiments. Y-LJ, Y-JZ, DG, C-YL, and J-YM performed the experiments. S-FW, Y-LJ, DG, C-YL, and C-FG analyzed the data. S-FW, Y-LJ, and Y-JZ wrote and revised the manuscript. All authors commented on the manuscript. All authors contributed to the article and approved the submitted version.

FUNDING

This research was supported by the National Natural Science Foundation of China (Nos. 31772205 and 31830075), and the Top-notch Academic Programs Project of Jiangsu Higher Education Institutions (PPZY2015B157).

REFERENCES

Chatzigeorgiou, M., Bang, S., Hwang, S. W., and Schafer, W. R. (2013). tmc-1 encodes a sodium-sensitive channel required for salt chemosensation in *C. elegans*. *Nature* 494, 95–99. doi: 10.1038/nature11845

Guo, Y., Wang, Y., Zhang, W., Meltzer, S., Zanini, D., Yu, Y., et al. (2016). Transmembrane channel-like (tmc) gene regulates *Drosophila* larval locomotion. *Proc. Natl. Acad. Sci. U.S.A.* 113, 7243–7248. doi: 10.1073/pnas.1606537113

Hu, B., Jin, J., Guo, A.-Y., Zhang, H., Luo, J., and Gao, G. (2015). GSDS 2.0: an upgraded gene feature visualization server. *Bioinformatics* 31, 1296–1297. doi: 10.1093/bioinformatics/btu817

Jia, Y., Zhao, Y., Kusakizako, T., Wang, Y., Pan, C., Zhang, Y., et al. (2019). TMC1 and TMC2 proteins are pore-forming subunits of mechanosensitive ion channels. *Neuron* 105, 310–321. doi: 10.1016/j.neuron.2019.10.017

Kawashima, Y., Kurima, K., Pan, B., Griffith, A. J., and Holt, J. R. (2015). Transmembrane channel-like (TMC) genes are required for auditory and vestibular mechanosensation. *Pflugers Arch.* 467, 85–94. doi: 10.1007/s00424-014-1582-3

Keresztes, G., Mutai, H., and Heller, S. (2003). TMC and EVER genes belong to a larger novel family, the TMC gene family encoding transmembrane proteins. *BMC Genomics* 4:24. doi: 10.1186/1471-2164-4-24

Kurima, K., Peters, L. M., Yang, Y., Riazuddin, S., Ahmed, Z. M., Naz, S., et al. (2002). Dominant and recessive deafness caused by mutations of a novel gene, TMC1, required for cochlear hair-cell function. *Nat. Genet.* 30, 277–284. doi: 10.1038/ng842

Kurima, K., Yang, Y., Sorber, K., and Griffith, A. J. (2003). Characterization of the transmembrane channel-like (TMC) gene family: functional clues from hearing loss and *Epidermodysplasia verruciformis*. *Genomics* 82, 300–308. doi: 10.1016/s0888-7543(03)00154-x

Li, Y., Fink, C., El-Kholy, S., and Roeder, T. (2015). The octopamine receptor octß2R is essential for ovulation and fertilization in the fruitfly *Drosophila melanogaster*. *Arch. Insect Biochem. Physiol.* 88, 168–178. doi: 10.1002/arch.21211

Lim, J., Sabandal, P. R., Fernandez, A., Sabandal, J. M., Lee, H.-G., Evans, P., et al. (2014). The octopamine receptor Octβ2R regulates ovulation in *Drosophila melanogaster*. *PLoS One* 9:e104441. doi: 10.1371/journal.pone.0104441

Livak, K. J., and Schmittgen, T. D. (2001). Analysis of relative gene expression data using real-time quantitative PCR and the 2-ΔΔCT method. *Methods* 25, 402–408. doi: 10.1006/meth.2001.1262

Lu, K., Chen, X., Liu, W.-T., and Zhou, Q. (2016). TOR pathway-mediated juvenile hormone synthesis regulates nutrient-dependent female reproduction in *Nilaparvata lugens* (Stål). *Int. J. Mol. Sci.* 17:438. doi: 10.3390/ijms17040438

Min, S., Lee, S. W., Choi, B.-R., Lee, S. H., and Kwon, D. H. (2014). Insecticide resistance monitoring and correlation analysis to select appropriate insecticides against *Nilaparvata lugens* (Stål), a migratory pest in Korea. *J. Asia Pac. Entomol.* 17, 711–716. doi: 10.1016/j.aspen.2014.07.005

Pan, B., Akyuz, N., Liu, X.-P., Asai, Y., Nist-Lund, C., Kurima, K., et al. (2018). TMC1 forms the pore of mechanosensory transduction channels in vertebrate inner ear hair cells. *Neuron* 99, 736–753.e736.

Pan, B., Géléoc, G. S., Asai, Y., Horwitz, G. C., Kurima, K., Ishikawa, K., et al. (2013). TMC1 and TMC2 are components of the mechanotransduction channel

in hair cells of the mammalian inner ear. *Neuron* 79, 504–515. doi: 10.1016/j.neuron.2013.06.019

Roy, S., Saha, T. T., Zou, Z., and Raikhel, A. S. (2018). Regulatory pathways controlling female insect reproduction. *Annu. Rev. Entomol.* 63, 489–511. doi: 10.1146/annurev-ento-020117-043258

Scheffer, D. I., Shen, J., Corey, D. P., and Chen, Z.-Y. (2015). Gene expression by mouse inner ear hair cells during development. *J. Neurosci.* 35, 6366–6380. doi: 10.1523/jneurosci.5126-14.2015

Vreugde, S., Erven, A., Kros, C. J., Marcotti, W., Fuchs, H., Kurima, K., et al. (2002). Beethoven, a mouse model for dominant, progressive hearing loss DFNA36. *Nat. Genet.* 30:257. doi: 10.1038/ng848

Wang, X., Li, G., Liu, J., Liu, J., and Xu, X. Z. S. (2016). TMC-1 mediates alkaline sensation in *C. elegans* through nociceptive neurons. *Neuron* 91, 146–154. doi: 10.1016/j.neuron.2016.05.023

Wu, S. F., Ja, Y. L., Zhang, Y. J., and Yang, C. H. (2019). Sweet neurons inhibit texture discrimination by signaling TMC-expressing mechanosensitive neurons in *Drosophila*. *eLife* 8:e46165.

Wu, S. F., Jv, X. M., Li, J., Xu, G. J., Cai, X. Y., and Gao, C. F. (2017). Pharmacological characterisation and functional roles for egg-laying of a β-adrenergic-like octopamine receptor in the brown planthopper *Nilaparvata lugens*. *Insect. Biochem. Mol. Biol.* 87, 55–64. doi: 10.1016/j.ibmb.2017.06.008

Wu, S. F., Zeng, B., Zheng, C., Mu, X. C., Zhang, Y., Hu, J., et al. (2018). The evolution of insecticide resistance in the brown planthopper (*Nilaparvata lugens* Stål) of China in the period 2012-2016. *Sci. Rep.* 8:4586.

Yue, X., Zhao, J., Li, X., Fan, Y., Duan, D., Zhang, X., et al. (2018). TMC proteins modulate egg laying and membrane excitability through a background leak conductance in *C. elegans*. *Neuron* 97, 571–585.e575.

Zhai, Y., Sun, Z., Zhang, J., Kang, K., Chen, J., and Zhang, W. (2015). Activation of the TOR signalling pathway by glutamine regulates insect fecundity. *Sci. Rep.* 5:10694.

Zhang, J.-L., Yuan, X.-B., Chen, S.-J., Chen, H.-H., Xu, N., Xue, W.-H., et al. (2019). The histone deacetylase NlHDAC1 regulates both female and male fertility in the brown planthopper, *Nilaparvata lugens*. *Open Biol.* 8:180158. doi: 10.1098/rsob.180158

Zhang, L., Gualberto, D. G., Guo, X., Correa, P., Jee, C., and Garcia, L. R. (2015). TMC-1 attenuates *C. elegans* development and sexual behaviour in a chemically defined food environment. *Nat. Commun.* 6:6345.

Zhang, Y. V., Aikin, T. J., Li, Z., and Montell, C. (2016). The basis of food texture sensation in *Drosophila*. *Neuron* 91, 863–877. doi: 10.1016/j.neuron.2016.07.013

Zhuo, J.-C., Xue, J., Lu, J.-B., Huang, H.-J., Xu, H.-J., and Zhang, C.-X. (2017). Effect of RNAi-mediated knockdown of NlTOR gene on fertility of male *Nilaparvata lugens*. *J. Insect. Physiol.* 98, 149–159. doi: 10.1016/j.jinsphys.2017.01.002

Conflict of Interest: The authors declare that the research was conducted in the absence of any commercial or financial relationships that could be construed as a potential conflict of interest.

frontiers in Genetics

ORIGINAL RESEARCH
published: 29 October 2020
doi: 10.3389/fgene.2020.602863

Mosquito Diversity and Population Genetic Structure of Six Mosquito Species From Hainan Island

Siping Li[1], Feng Jiang[3], Hong Lu[2], Xun Kang[1], Yanhong Wang[2], Zhen Zou[2], Dan Wen[2], Aihua Zheng[2], Chunxiang Liu[2], Qiyong Liu[4], Le Kang[2,3], Qianfeng Xia[1] and Feng Cui[2]**

[1] Key Laboratory of Tropical Translational Medicine of Ministry of Education and School of Tropical Medicine and Laboratory Medicine, Hainan Medical University, Haikou, China, [2] State Key Laboratory of Integrated Management of Pest Insects and Rodents, Institute of Zoology, Chinese Academy of Sciences, Beijing, China, [3] Beijing Institutes of Life Science, Chinese Academy of Sciences, Beijing, China, [4] State Key Laboratory of Infectious Diseases Prevention and Control, WHO Collaborating Centre for Vector Surveillance and Management, National Institute for Communicable Disease Control and Prevention, Chinese Center for Disease Control and Prevention, Beijing, China

OPEN ACCESS

Edited by:
Zhongxia Wu,
Henan University, China

Reviewed by:
Jinbao Gu,
Southern Medical University, China
Chun-xiao Li,
Beijing Institute of Microbiology and Epidemiology, China

***Correspondence:**
Feng Cui
cuif@ioz.ac.cn
Qianfeng Xia
xiaqianfeng@sina.com

Specialty section:
This article was submitted to Epigenomics and Epigenetics, a section of the journal Frontiers in Genetics

Received: *04 September 2020*
Accepted: *12 October 2020*
Published: *29 October 2020*

Citation:
Li S, Jiang F, Lu H, Kang X, Wang Y, Zou Z, Wen D, Zheng A, Liu C, Liu Q, Kang L, Xia Q and Cui F (2020) Mosquito Diversity and Population Genetic Structure of Six Mosquito Species From Hainan Island. Front. Genet. 11:602863. doi: 10.3389/fgene.2020.602863

Hainan is a tropical island in southern China with abundant mosquito species, putting Hainan at risk of mosquito-borne virus disease outbreaks. The population genetic diversity of most mosquito species on Hainan Island remains elusive. In this study, we report the diversity of mosquito species and the genetic diversity of the predominant species on Hainan. Field populations of adults or larvae were collected from 12 regions of Hainan Island in 2018 and 2019. A fragment of the mitochondrial cytochrome c oxidase subunit I (*coxI*) gene was sequenced from 1,228 mosquito samples and used for species identification and genetic diversity analysis. Twenty-three known mosquito species from the genera *Aedes*, *Armigeres*, *Culex*, *Mansonia*, and *Anopheles* and nine unconfirmed mosquito species were identified. *Aedes albopictus*, *Armigeres subalbatus*, and *Culex pipiens quinquefasciatus* were the most prevalent mosquito species on Hainan. The regions north of Danzhou, Tunchang, and Qionghai exhibited high mosquito diversity (26 species). The order of the total haplotype diversity and nucleotide diversity of the populations from high to low was as follows: *Culex tritaeniorhynchus*, *Ar. subalbatus*, *Culex pallidothorax*, *Culex gelidus*, *Ae. albopictus*, and *C. p. quinquefasciatus*. Tajima's *D* and Fu's F_S tests showed that *Ae. albopictus*, *C. p. quinquefasciatus*, *C. tritaeniorhynchus*, and *C. gelidus* had experienced population expansion, while the *Ar. subalbatus* and *C. pallidothorax* populations were in genetic equilibrium. Significant genetic differentiation existed in the overall populations of *Ae. albopictus*, *Ar. subalbatus*, *C. p. quinquefasciatus*, and *C. pallidothorax*. The *Ae. albopictus* populations on Hainan were characterized by frequent gene exchange with populations from Guangdong and four other tropical countries, raising the risk of viral disease outbreaks in these regions. Two subgroups were reported in the *Ar. subalbatus* populations for the first time. Our findings may have important implications for vector control on Hainan Island.

Keywords: *Aedes*, *Armigeres*, *Culex*, *Mansonia*, *Anopheles*, cytochrome c oxidase subunit I

INTRODUCTION

Hainan Island is located in southern China and has an area of 33,920 km^2. The climate of Hainan is a tropical maritime monsoon climate with an annual average temperature of 24.2°C and an annual average rainfall of 1,684 mm. Hainan has become a China Pilot Free Trade Zone, with increasing international tourism and commercial trade, under the Belt and Road policy. The natural and cultural conditions of Hainan result in abundant mosquito species. A total of 44 mosquito species in 9 genera have been reported in Hainan based on classical morphological classification, among which 28 species have available molecular markers, such as mitochondrial cytochrome c oxidase subunit I (*coxI*) gene sequences (Zhan et al., 2000; Wang et al., 2012; Sun et al., 2014; Lian et al., 2015). The common species include *Anopheles sinensis*, *Anopheles dirus*, *Anopheles tessellatus*, *Anopheles minimus*, *Aedes albopictus*, *Aedes aegypti*, *Culex tritaeniorhynchus*, *Culex pipiens quinquefasciatus*, *Armigeres subalbatus*, etc. (Zhao et al., 2017). However, the distribution and population genetic diversity of most mosquito species in Hainan have not been reported.

The abundant mosquito diversity put Hainan at risk of mosquito-borne virus disease outbreaks. There have been several outbreaks of Japanese encephalitis virus, which is mainly transmitted by *C. tritaeniorhynchus* (Zheng et al., 2011; Zhao et al., 2017). Dengue fever, caused by *Aedes*-transmitted Dengue viruses, is endemic in Hainan (Zheng et al., 2011). Hainan has also been confirmed as a potential natural focus of other mosquito-borne viruses such as Ross River virus and chikungunya virus (Zhao et al., 2017). Therefore, knowledge of the mosquito species, distribution, and population genetic diversity on the island is key for the control of mosquitoes and mosquito-borne virus diseases on Hainan.

The *coxI* gene is a valuable and reliable diagnostic tool for studying the genetic diversity and establishing the intraspecific relationships of mosquitoes (Walton et al., 2000; Cook et al., 2005; Zhong et al., 2013). In this study, we used the *coxI* gene to investigate the diversity and population genetic diversity of field collected mosquitoes from 12 regions of Hainan in 2018 and 2019. In total, 23 known mosquito species from the genera *Aedes*, *Armigeres*, *Culex*, *Mansonia*, and *Anopheles* and nine unconfirmed mosquito species were identified. The genetic diversity of six dominant species was analyzed.

MATERIALS AND METHODS

Mosquito Collection

Mosquitoes were collected from twelve regions: Haikou (HK), Wenchang (WC), and Lingao (LG) in the north; Sanya (SY), Lingshui (LS), and Ledong (LD) in the south; Dongfang (DF) and Danzhou (DZ) in the west; Qionghai (QH) and Wanning (WN) in the east; and Tunchang (TC) and Wuzhishan (WZS) in the central part of Hainan Island, from June to October 2019 (**Supplementary Figure 1**). In seven of the regions (HK, WC, SY, LS, DF, TC, and WZS) mosquitoes were collected from June to September 2018 (**Supplementary Figure 1**). HK, LG, WN, DZ, and LS were reported to have outbreaks of Dengue fever (Wu et al., 2007). Malaria was epidemic in WN, DF, and LD (Xiao et al., 2010). SY, LD, and HK ever outbroke with Japanese encephalitis (Fu et al., 2002; Wang J. X. et al., 2015). Each region included one sampling site, except for HK, which included three sites, and DZ, which included two sites. Several special sampling habitats included a maple deer field at TC, a virgin forest at LS, and a wetland inhabited by water birds at HK. Adult mosquitoes were captured using a human lure or light trap and stored in liquid nitrogen or RNAlater (Thermo Fisher Scientific, Waltham, MA, United States). Larvae were collected from discarded buckets and bottles, puddles, and ditches, brought to the laboratory, then raised to the adult stage before being stored in liquid nitrogen.

DNA Extraction and Polymerase Chain Reaction Amplification

Genomic DNA was extracted from one leg of each specimen using the hot sodium hydroxide and Tris (Hot SHOT) method (Montero-Pau et al., 2008). Briefly, one leg was placed in 50 μL of alkaline lysis buffer (50 mM NaOH), followed by incubation in a thermocycler at 95°C for 30 min. Then, 6 μL of Tris-HCl (pH 7.5) was added. Appropriate forward (GGTCAACAAATCATAAAGATATTGG) and reverse (TAAACTTCAGGGTGACCAAAAAATCA) primers (Folmer et al., 1994) were used to amplify a 710 bp *coxI* gene fragment. Polymerase chain reaction (PCR) was performed in a reaction mixture containing 12.5 μL of Premix Taq (Takara Bio, Beijing, China), 1 μL of 10 mM primers, 1.5 μL of DNA, and 10 μL of distilled water. The thermal cycling conditions included a 5 min initial denaturation step at 94°C, followed by 34 cycles of 30 s of denaturation at 94°C, 30 s annealing at 55°C and 41 s elongation at 72°C, and a final elongation at 72°C for 12 min. The product was checked by 1% agarose gel electrophoresis and sent to a company (Beijing Tianyi Huiyuan Bioscience & Technology Inc., Beijing, China) for sequencing.

Data Analysis

After removing the bases corresponding to irregular peak patterns, clean *coxI* sequences from 611 to 626 bp were obtained from 1,227 mosquito samples and deposited into the GenBank database. These sequences were aligned with the *coxI* gene sequences of different species of mosquitoes downloaded from GenBank using ClustalW of MEGA7.0 (**Supplementary Table 1**). When the nucleotide identity of a specimen with the homologous *coxI* sequence of a mosquito species in GenBank was over 99%, the specimen was regarded as belonging to the same species as the reference species. Sliding window analysis was performed using DnaSP V.5.10.01 to reveal the number of haplotypes, haplotype diversity, nucleotide diversity, and variable sites (Librado and Rozas, 2009). The partitioning of genetic variation within and among populations was calculated via the analysis of molecular variance (AMOVA) with 1,000 permutations implemented in Arlequin v. 3.5 (Excoffier and Lischer, 2010). The pairwise fixation index (*F*st) between the Hainan populations was calculated with the distance method. The *F*st between Hainan

TABLE 1 | Species and numbers of mosquitoes collected in Hainan based on the nucleotide sequences of *coxI*.

Species	Location											
	HK	WC	LD	SY	LG	DZ	DF	QH	WN	LS	TC	WZS
Aedes albopictus	28	23	35	41	12	21	33	15	21	48	50	25
Ae. vexans								4			2	
Ae. aegypti			3									
Ae. malayensis	3											
Armigeres subalbatus	26	24		15		33	3	1		15	5	29
Culex pipiens quinquefasciatus	78	2	109	65	1	135	38	16			2	93
C. gelidus	15					7		7			51	
C. vishnui	4				2			4			17	
C. pseudovishnui								4				
C. tritaeniorhynchus	3					6		45			37	
C. pallidothorax		12			1	22						65
C. fuscanus						16					1	9
C. sitiens					98	13						
C. cinctellus								1				
C. bitaeniorhynchus								1				
C. fuscocephala								19			5	
Mansonia uniformis								1			35	
Anopheles barbirostris											4	
An. tessellatus											4	
An. aconitus								1			1	
An. vagus						2		2			2	
An. sinensis						1						
An. kochi											1	

and other regions of China or overseas sites was calculated with haplotype frequencies. The significance level was tested with 10,000 random permutations (Slatkin and Hudson, 1991). Gene flow (Nm) was calculated as (1 – *F*st)/2*F*st (Halbert et al., 2012). Tajima's *D* and Fu's *Fs* values of the neutrality test were applied to examine recent population expansion when the null hypothesis of neutrality was rejected due to significant negative values (Tajima, 1989; Fu, 1997). Phylogenetic trees for the *Aedes*, *Anopheles*, and *Culex* genera and *Ar. subalbatus* were constructed based on the nucleotide sequences of *coxI* using the neighbor-joining method (p-distance model and pairwise deletion) in MEGA 7.0. The statistical significance of tree branching was tested by performing 1,000 bootstrap replications.

FIGURE 1 | Distribution of mosquito species on Hainan. Triangles indicate collection sites. A, *Ae. albopictus*. B, *Ae. vexans*. C, *Ae. aegypti*. D, *Ae. malayensis*. E, *Ar. subalbatus*. F, *C. p. quinquefasciatus*. G, *C. gelidus*. H, *C. tritaeniorhynchus*. I, *C. sitiens*. J, *C. vishnui*. K, *C. pallidothorax*. L, *C. fuscanus*. M, *C. fuscocephala*. N, *C. pseudovishnui*. O, *C. cinctellus*. P, *C. bitaeniorhynchus*. Q, *An. barbirostris*. R, *An. tessellatus*. S, *An. vagus*. T, *An. sinensis*. U, *An. aconitus*. V, *An. kochi*. W, *M. uniformis*. Unconfirmed mosquito species are numbered from 1 to 9.

RESULTS

Mosquito Species Identification

The *coxI* sequences of single mosquitoes from Hainan were obtained and aligned with the *coxI* sequences of different species of mosquitoes downloaded from GenBank. Twenty-three known mosquito species in five genera were identified in the two years of the investigation in Hainan (**Table 1**), including *Ae. albopictus*, *Ae. aegypti*, *Aedes vexans*, *Aedes malayensis*, *Ar. subalbatus*, *C. p. quinquefasciatus*, *Culex gelidus*, *Culex vishnui*, *C. tritaeniorhynchus*, *Culex pallidothorax*, *Culex fuscanus*, *Culex fuscocephala*, *Culex pseudovishnui*, *Culex sitiens*,

Culex cinctellus, *Culex bitaeniorhynchus*, *Mansonia uniformis*, *Anopheles barbirostris*, *An. tessellatus*, *Anopheles vagus*, *An. sinensis*, *Anopheles kochi*, and *Anopheles aconitus*. In addition to the known species, nine samples showed a nucleotide identity between 87 and 96% with known mosquito species. Therefore, they were treated as unconfirmed mosquito species and excluded from any further analyses (**Supplementary Table 2**). *Ae. albopictus* was the most prevalent mosquito species on Hainan Island and was found at all 12 sampling locations. *C. p. quinquefasciatus* and *Ar. subalbatus* were second to *Ae. albopictus* in terms of their distribution across the island. From the overall distribution of the mosquitoes, it was clear that the regions north of the line from Danzhou to Tunchang and Qionghai were characterized by plentiful mosquito species; 22 known and 4 unconfirmed mosquito species were found in these areas. In contrast, only 6 known and 5 unconfirmed mosquito species were found in regions south of this line (**Figure 1**).

Neighbor-joining phylogenetic trees were constructed for the Hainan mosquitoes of the *Aedes*, *Culex*, and *Anopheles* genera with reference sequences of mosquitoes from other regions. In the *Aedes* genus, the four species formed distinct clades with 99% bootstrap values (**Figure 2A**). In the *Culex* genus, each species formed a distinct clade supported by a 100% bootstrap value except for *C. tritaeniorhynchus*, which was split into two subclades with a 71% bootstrap value. Furthermore, *C. vishnui*, *C. pseudovishnui*, and *C. tritaeniorhynchus* clustered together with a 95% bootstrap value, forming the acknowledged *C. vishnui* complex (**Figure 2B**; Kumar et al., 2017). In the *Anopheles* genus, the six species formed distinct clades with 100% bootstrap values (**Figure 3A**).

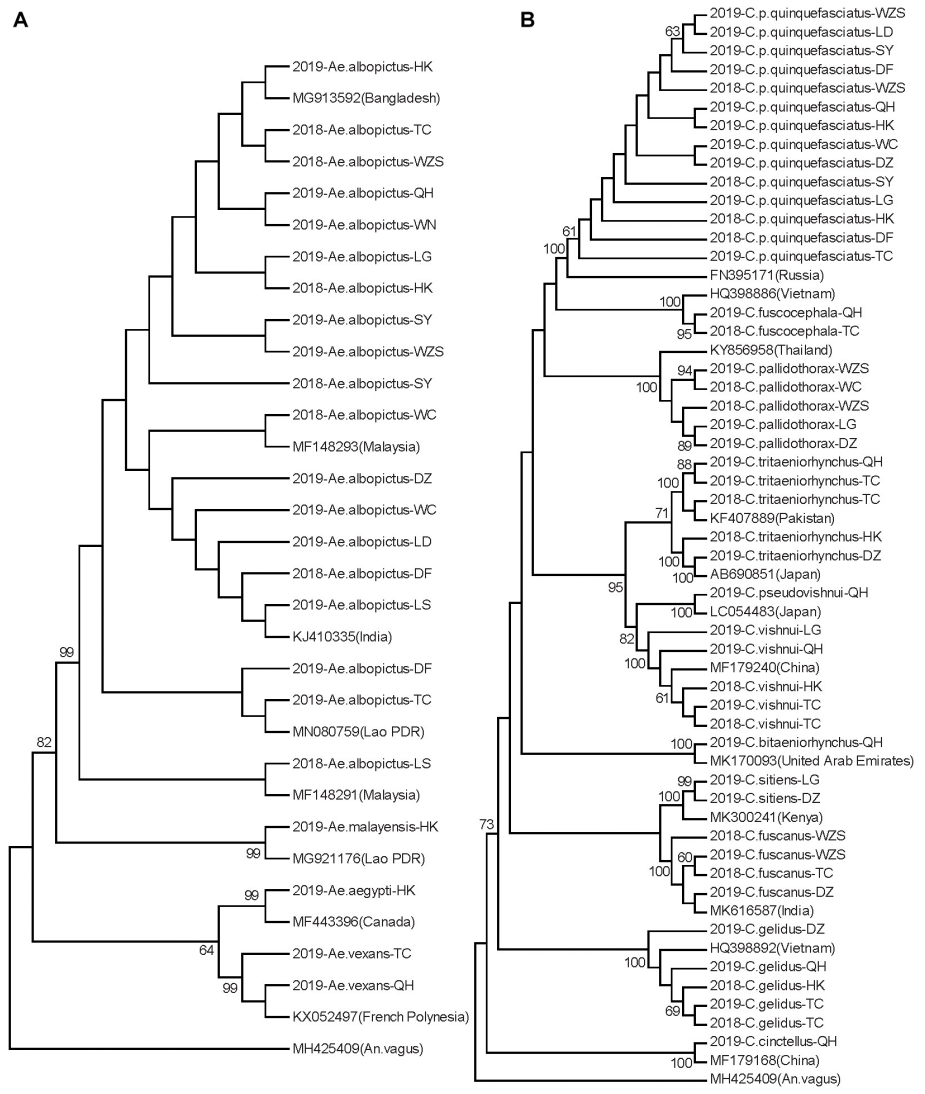

FIGURE 2 | Neighbor-joining phylogenetic trees of *Aedes* and *Culex* genus mosquitoes from Hainan based on the nucleotide sequences of *coxI*. **(A)** *Aedes* genus. **(B)** *Culex* genus. The Hainan samples are named according to the year-species-collection site. Sequences of mosquitoes with accession numbers in GenBank from other regions (in brackets) are referenced. The sequence of *Anopheles vagus* is used as the outgroup. Bootstrap values over 60 are indicated.

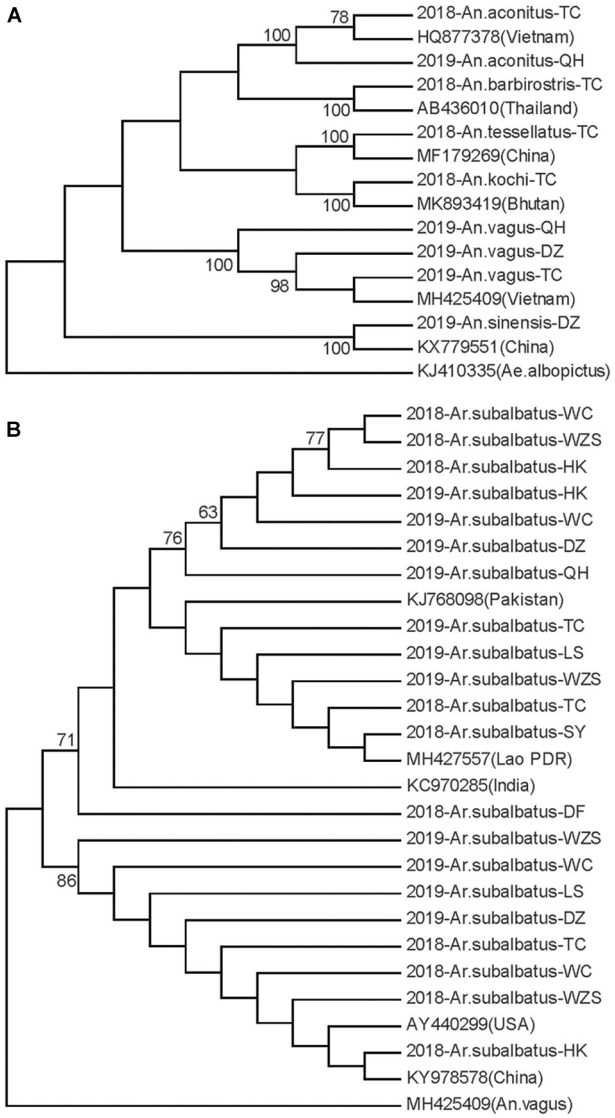

FIGURE 3 | Neighbor-joining phylogenetic trees of the *Anopheles* genus and *Armigeres subalbatus* from Hainan based on the nucleotide sequences of *coxI*. **(A)** *Anopheles* genus. **(B)** *Ar. subalbatus*. The Hainan samples are named according to the year-species-collection site. Sequences of mosquitoes with accession numbers in GenBank from other regions (in brackets) are referenced. The sequence of *Aedes albopictus* or *Anopheles vagus* is used as an outgroup. Bootstrap values over 60 are indicated.

Genetic Diversity of *Ae. albopictus* Populations

Ae. albopictus was collected in 12 regions of Hainan. In total, 33 variable sites and 46 haplotypes were detected (**Table 2**). Haplotypes 1 and 5 were the most widely distributed haplotypes (**Supplementary Table 3**). The total haplotype diversity (H_d) was 0.62, and the nucleotide diversity (π) was 0.17. The highest diversity was found in the DF population, and the lowest diversity was found in the WN population (**Table 2**). Pairwise population differentiation was evaluated with the fixation index (*F*st) using the distance method (**Table 3**). High significant pairwise population differentiation was observed between DF and the other populations (*F*st between 0.17 and 0.24). However, the Nm values between DF and the other populations were larger than 1 (from 1.55 to 2.44), indicating frequent gene exchange between them (**Table 3**). The DZ and HK populations showed significant but low differentiation (*F*st < 0.1) from some populations due to more frequent gene exchange. The molecular variance analysis (AMOVA) showed that the majority of the genetic variance occurred within populations (92.68%) (**Supplementary Table 4**). The total *F*st was 0.07 ($P < 0.001$), and Nm was 6.64, reflecting low population differentiation. Tajima's *D* value (−2.10) and Fu's F_s value (−29.15) for the overall populations both reached a significant level, reflecting significant population expansion (**Table 2**). Regarding the specific populations, SY and TC presented significant negative *D* and F_s values. WC and DZ exhibited significant negative F_s values.

The *F*st values between Hainan populations and those of other regions from China or overseas were also calculated according to the haplotype frequencies (**Table 4**). The haplotype sequences of the *Ae. albopictus* populations from Henan, Fujian, Yunnan, Guangdong in China, the Congo, the United States of America (United States), Italy, the Lao People's Democratic Republic, Singapore, Japan, Thailand, and Pakistan were downloaded from GenBank. The Hainan populations exhibited the largest divergence from the United States population (*F*st = 0.42, $P < 0.01$) and the least divergence from the Congo population (*F*st = 0.09, $P < 0.01$). There was frequent gene flow between the Hainan populations and the Henan, Yunnan, Guangdong, Congo, Lao People's Democratic Republic, Singapore, or Thailand populations (Nm from 1 to 5.3).

Genetic Diversity of *Ar. subalbatus* Populations

Ar. subalbatus was collected from nine regions of Hainan. The phylogenetic analysis showed that two subgroups were clustered with over 70% bootstrap values. The TC, WZS, LS, HK, DZ, and WC populations contained individuals from both subgroups (**Figure 3B**). Genetic diversity was analyzed among the HK, WC, SY, DZ, LS, and WZS populations because they presented a sample size of more than 10 individuals.

There were 16 haplotypes with 22 variable sites, and only one haplotype appeared in all populations (**Table 2** and **Supplementary Table 5**). The two subgroups did not share any haplotypes. The total haplotype diversity and nucleotide diversity were 0.74 (H_d) and 0.42 (π), respectively. HK exhibited the lowest haplotype diversity, and SY exhibited the lowest nucleotide diversity. WC showed the highest haplotype and nucleotide diversity (**Table 2**). Tajima's *D* tests and Fu's F_s test for the overall populations did not present statistically significant negative values, suggesting that the *Ar. subalbatus* populations of Hainan were in genetic equilibrium. Only LS exhibited a significant negative *D* value, implying population expansion (**Table 2**). Significant genetic differentiation existed in half of the pairs of the six populations, especially those including

TABLE 2 | Haplotype and nucleotide diversity of the *coxI* gene of six mosquito species and the neutrality test.

	Location	N	H	Variable sites	Haplotype diversity ($H_d \pm$ SD)	Nucleotide diversity ($\pi \times 10^2$)	Tajima's *D*	Fu's F_S
Aedes albopictus	HK	28	6	6	0.50 ± 0.11	0.20	−0.62	−1.17
	WC	23	8	7	0.75 ± 0.08	0.21	−1.07	−3.62*
	LD	35	5	4	0.63 ± 0.06	0.14	−0.37	−0.97
	SY	41	9	8	0.62 ± 0.07	0.14	−1.54*	−5.37*
	LG	12	2	1	0.41 ± 0.13	0.07	0.54	0.74
	DZ	21	9	8	0.73 ± 0.10	0.26	−0.95	−4.16*
	DF	33	8	9	0.77 ± 0.04	0.26	−0.82	−1.86
	QH	15	4	4	0.47 ± 0.15	0.13	−1.07	−0.77
	WN	21	2	1	0.38 ± 0.10	0.06	0.66	0.94
	LS	48	6	6	0.54 ± 0.06	0.11	−1.30	−2.33
	TC	50	14	12	0.68 ± 0.07	0.18	−1.75*	−10.95**
	WZS	25	4	4	0.41 ± 0.11	0.10	−1.12	−0.88
	Total	352	46	33	0.62 ± 0.03	0.17	−2.10*	−29.15*
Armigeres subalbatus	HK	26	4	9	0.40 ± 0.11	0.33	−0.45	2.26
	WC	24	6	10	0.82 ± 0.05	0.53	0.70	1.55
	SY	15	4	7	0.62 ± 0.12	0.22	−1.31	0.38
	DZ	33	6	11	0.58 ± 0.09	0.33	−0.82	0.55
	LS	15	5	9	0.63 ± 0.13	0.26	−1.56*	−0.33
	WZS	29	7	12	0.78 ± 0.06	0.53	0.26	1.08
	Total	142	16	22	0.74 ± 0.03	0.42	−0.96	−2.71
Culex pipiens quinquefasciatus	HK	78	2	1	0.36 ± 0.05	0.06	0.93	1.48
	LD	54	9	20	0.57 ± 0.07	0.22	−2.15*	−6.03*
	SY	65	2	1	0.12 ± 0.05	0.02	−0.56	−0.32
	DZ	113	10	44	0.51 ± 0.04	0.21	−2.63**	−3.13
	DF	38	3	2	0.10 ± 0.07	0.02	−1.49*	−1.41*
	QH	16	2	1	0.13 ± 0.11	0.02	−1.16	−0.70
	WZS	93	5	9	0.08 ± 0.04	0.03	−2.25**	−3.72*
	Total	457	23	62	0.35 ± 0.03	0.11	−2.63**	−29.07**
Culex tritaeniorhynchus	DZ	6	5	32	0.93 ± 0.12	1.94	−0.91	1.12
	QH	45	37	56	0.99 ± 0.01	0.96	−1.89*	−25.29*
	TC	37	25	36	0.97 ± 0.02	0.67	−1.83*	−17.90*
	Total	88	63	70	0.98 ± 0.01	0.91	−1.96*	−25.32*
Culex gelidus	HK	15	5	4	0.71 ± 0.09	0.14	−0.92	−1.86*
	DZ	7	3	2	0.67 ± 0.09	0.14	0.21	−0.24
	QH	7	4	3	0.81 ± 0.13	0.18	−0.30	−1.22
	TC	51	14	16	0.79 ± 0.05	0.27	−1.69*	−7.45*
	Total	80	15	17	0.75 ± 0.04	0.22	−1.76*	−8.55**
Culex pallidothorax	WC	12	4	5	0.76 ± 0.08	0.30	0.50	0.78
	DZ	22	7	7	0.86 ± 0.03	0.30	1.07	−0.26
	WZS	65	9	9	0.63 ± 0.06	0.29	−0.12	−1.12
	Total	99	13	13	0.79 ± 0.03	0.38	−0.13	−1.97

*$P < 0.05$, **$P < 0.01$. N, sample number; H, haplotype number.

the SY population, which showed significant differentiation from all other populations except for LS (*F*st between 0.10 and 0.26, **Table 5**), largely because all individuals from SY belonged to a single subgroup (**Figure 3B**). Genetic exchange frequently occurred between most populations (Nm values from 1.41 to 88.97) (**Table 5**). The total *F*st was 0.10 ($P < 0.01$), and Nm was 4.50. Most of the total variation existed within populations (89.52%) (**Supplementary Table 6**). However, when AMOVA was applied to the two subgroups, 77.06% of the total variation was found to exist between the subgroups (**Supplementary Table 6**). The *F*st between subgroups was 0.77 ($P < 0.01$), and Nm was less than 1, indicating that gene flow failed to prevent the subgroup differentiation caused by genetic drift.

The genetic differentiation of the Hainan *Ar. subalbatus* populations from those of Pakistan or India was analyzed using haplotype frequencies. The Hainan populations exhibited greater differentiation from the Pakistan population

TABLE 3 | Pairwise genetic differentiation (*F*st; lower triangle) and gene flow (Nm; upper triangle) between *Aedes albopictus* populations on Hainan.

Location	HK	WC	LD	SY	LG	DZ	DF	QH	WN	LS	TC	WZS
HK		11.09	4.30	8.34	58.75	6.01	1.87	32.22	14.55	8.63	14.85	20.74
WC	0.04		12.94	31.45	–	11.30	2.31	–	78.28	–	–	53.39
LD	0.10**	0.04		21.23	56.63	6.05	2.44	28.86	12.72	17.82	54.03	12.72
SY	0.06*	0.02	0.02		–	9.10	1.71	–	–	–	–	–
LG	0.01	−0.02	0.01	−0.04		148.00	2.00	–	–	–	–	–
DZ	0.08**	0.04	0.08*	0.05*	0.01		1.80	20.47	14.54	8.31	10.28	11.88
DF	0.21**	0.18**	0.17**	0.23**	0.20**	0.22**		2.08	1.55	1.57	1.96	1.71
QH	0.05	−0.01	0.02	−0.02	−0.06	0.02	0.19**		–	–	–	–
WN	0.03	0.01	0.04	−0.02	−0.07	0.03	0.24**	−0.03		–	–	–
LS	0.05*	−0.01	0.03	−0.01	−0.05	0.06*	0.24**	−0.02	−0.03		–	–
TC	0.03*	−0.01	0.01	−0.01	−0.04	0.05*	0.20**	−0.03	−0.02	−0.01		–
WZS	0.02	0.01	0.04	−0.01	−0.06	0.04	0.22**	−0.03	−0.04	−0.02	−0.01	

*$P < 0.05$, **$P < 0.01$. When Fst is negative, Nm is not available.

TABLE 4 | Pairwise genetic differentiation (*F*st; lower triangle) and gene flow (Nm; upper triangle) between different geographical populations of *Aedes albopictus*.

Location	HN	HEN	FJ	YN	GD	CG	United States	IT	LA	SG	JP	TL	PT
HN		1.02	0.89	2.97	1.74	5.30	0.68	0.89	3.00	1.00	0.86	1.67	0.88
HEN	0.33**		2.21	2.36	4.42	0.25	3.17	1.68	1.67	1.23	3.77	1.88	0.89
FJ	0.36**	0.18*		1.47	2.92	0.26	1.30	1.12	0.99	0.99	1.61	1.36	1.75
YN	0.14*	0.17**	0.25**		17.94	0.43	0.76	1.63	10.76	1.94	1.49	9.31	1.61
GD	0.22**	0.10**	0.15**	0.03*		0.36	1.57	2.30	2.15	2.39	2.36	5.49	1.82
CG	0.09**	0.67**	0.65**	0.58*			0.21	0.24	0.81	0.32	0.23	0.40	0.22
United States	0.42**	0.14	0.28**	0.30**	0.71*			0.85	0.73	0.66	2.26	0.82	0.45
IT	0.36**	0.23*	0.31**	0.18**	0.68**	0.37**			1.00	1.00	1.23	1.46	0.74
LA	0.14**	0.30**	0.34**	0.19	0.38**	0.41**	0.33**			1.14	0.97	3.92	1.08
SG	0.33**	0.29**	0.34**	0.17**	0.61**	0.43**	0.33**	0.31**			2.37	1.66	0.92
JP	0.37**	0.12	0.24**	0.18**	0.68**	0.18**	0.29**	0.34**	0.17**			1.38	0.7
TL	0.23**	0.21**	0.27**	0.05	0.55	0.38**	0.25**	0.11**	0.23**	0.27**			1.49
PT	0.36**	0.36**	0.40**	0.24**	0.69**	0.53**	0.40**	0.32**	0.35**	0.42**	0.25**		

*HN, Hainan, 352 samples. HEN, Henan, 10. FJ, Fujian, 28. YN, Yunnan, 9. GD, Guangdong, 11. CG, Congo, 127. United States, 35. IT, Italy, 14. LA, Lao DPR, 154. SG, Singapore, 36. JP, Japan, 15. TL, Thailand, 29. PT, Pakistan, 11. *$P < 0.05$, **$P < 0.01$. When Fst is negative, Nm is not available.*

(*F*st = 0.30, $P < 0.01$) than the Indian population (*F*st = 0.13, $P < 0.05$) but showed frequent gene flow with both populations (**Supplementary Table 7**).

Genetic Diversity of *C. p. quinquefasciatus* Populations

The collection of *C. p. quinquefasciatus* populations was performed in seven regions. In total, 23 haplotypes with 62 variable sites were identified, and only one haplotype appeared in all populations (**Table 2** and **Supplementary Table 8**). The total haplotype diversity and nucleotide diversity were comparatively low (H_d = 0.35, π = 0.11), but LD and DZ showed the highest diversity (H_d of approximately 0.5, π of approximately 0.2). Tajima's *D* tests and Fu's F_s test for the overall populations presented statistically significant negative values (**Table 2**), indicating significant population expansion. LD, DF and WZS exhibited significant negative *D* and F_s values, and DZ showed a significant negative *D*. The largest pairwise population differentiation existed between HK and SY (*F*st = 0.18, $P < 0.01$). HK exhibited significant differentiation from all six other populations, followed by LD and DZ, which showed significant differentiation from five populations (**Table 6**). Frequent gene flow occurred between most populations (Nm from 2.31 to 143.25) (**Table 6**). The total *F*st was 0.10 ($P < 0.01$), and Nm was 4.50. The majority of the variation (90.43%) existed within populations (**Supplementary Table 9**). Compared with the populations from Turkey, the United Kingdom, Serbia, and Canada, the Hainan populations exhibited no significant genetic differentiation. The pairwise divergence between all populations was not significant (**Supplementary Table 10**).

Genetic Diversity of Populations of Other Mosquito Species

C. tritaeniorhynchus was collected at TC, QH, and DZ. There were 63 haplotypes and 70 variable sites detected in these populations in total (**Table 2** and **Supplementary Table 11**). The total haplotype diversity and nucleotide diversity were quite high (H_d = 0.98, π = 0.91), and these populations experienced expansion during their history with significant negative Tajima's *D* and Fu's F_s values (**Table 2**). No significant genetic differentiation was observed for these populations (**Supplementary Table 12**).

TABLE 5 | Pairwise genetic differentiation (*F*st; lower triangle) and gene flow (Nm; upper triangle) between *Armigeres subalbatus* populations on Hainan.

Location	HK	WC	SY	DZ	LS	WZS
HK		14.68	1.41	–	2.27	1.86
WC	0.03		4.38	17.68	30.54	10.68
SY	0.26**	0.10*		2.25	88.97	4.30
DZ	−0.05	0.03	0.18**		4.12	2.22
LS	0.18**	0.02	0.01	0.11**		19.71
WZS	0.21**	0.04	0.10*	0.18**	0.02	

*$P < 0.05$, **$P < 0.01$. When Fst is negative, Nm is not available.

TABLE 6 | Pairwise genetic differentiation (*F*st; lower triangle) and gene flow (Nm; upper triangle) between *Culex pipiens quinquefasciatus* populations on Hainan.

Location	HK	LD	SY	DZ	DF	QH	WZS
HK		3.36	2.31	3.58	2.80	3.55	2.63
LD	0.13**		10.15	4.61	7.87	17.68	5.33
SY	0.18**	0.05**		5.62	19.54	19.03	57.87
DZ	0.12**	0.10**	0.08**		7.49	12.62	5.22
DF	0.15**	0.06**	0.02	0.06**		143.25	–
QH	0.12*	0.03	0.03	0.04	0.01		–
WZS	0.16**	0.09**	0.01	0.09**	−0.01	−0.01	

*$P < 0.05$, **$P < 0.01$. When Fst is negative, Nm is not available.

TABLE 7 | Pairwise genetic differentiation (*F*st; lower triangle) and gene flow (Nm; upper triangle) between *Culex pallidothorax* populations on Hainan.

Location	WC	DZ	WZS
WC		2.12	2.70
DZ	0.19**		0.90
WZS	0.16*	0.36**	

*$P < 0.05$, **$P < 0.01$. When Fst is negative, Nm is not available.

C. gelidus was collected at TC, HK, DZ, and QH. Fifteen haplotypes and 17 variable sites were detected (**Table 2** and **Supplementary Table 13**). The total haplotype diversity was 0.75, and the total nucleotide diversity was 0.22. The Tajima's *D* and Fu's F_s values for the overall populations presented significant negative values, indicating population expansion (**Table 2**). No significant genetic differentiation was observed for these populations (**Supplementary Table 14**).

C. pallidothorax was collected at WC, DZ and WZS. Thirteen haplotypes and 13 variable sites were found in these populations (**Table 2** and **Supplementary Table 15**). The total haplotype diversity was 0.79, and the total nucleotide diversity was 0.38. The overall populations were in genetic equilibrium due to non-significant negative Tajima's *D* and Fu's F_s values (**Table 2**). Significant genetic differentiation existed between the pairs of the three populations, and the largest differentiation appeared between DZ and WZS (*F*st = 0.36, $P < 0.01$) due to limited genetic exchange between them (Nm less than 1) (**Table 7**). The total *F*st was 0.33 ($P < 0.001$), and Nm was 1.01. A considerable proportion (33.06%) of genetic variance existed among populations (**Supplementary Table 16**).

DISCUSSION

In the investigation of mosquito populations at Hainan from 2018 to 2019, we found 23 known species in five genera, including four *Aedes*, 11 *Culex*, six *Anopheles*, one *Mansonia*, and one *Armigeres* species based on the *coxI* sequences. In addition, nine specimens were not confirmed due to their low identities with the *coxI* sequences of known mosquitoes in GenBank. Although *coxI* has emerged as the most commonly used marker for barcoding, this marker sometimes does not contain enough information to distinguish certain mosquito species of *Anopheles and Culex* (Bourke et al., 2013; Laurito et al., 2013). Another limitation of the barcoding approach is the recombination within mitochondrial genes may lead to complex sequence patterns when species with divergent mitochondrial DNA genomes interbreed (Chan et al., 2014). To avoid potential errors from the unique *coxI* barcoding, we used an over 99% cutoff in the nucleotide identity with the published homologous reference sequences of mosquito species.

The predominant species at Hainan probably changed with time. In previous studies, *Ae. albopictus*, *Ae. aegypti*, *C. tritaeniorhynchus*, *C. p. quinquefasciatus*, *An. dirus*, *An. sinensis*, *An. tessellates*, *An. minimus*, and *An. barbirostris* have been found to be broadly distributed on Hainan (Zhao et al., 2017). However, in this study, *Ae. albopictus*, *C. p. quinquefasciatus*, and *Ar. subalbatus* were the most prevalent species. *Ar. subalbatus* was detected in nine regions, whereas it was only found in Haikou, Sanya and Baoting before 2014 (Su et al., 1994; Zhan et al., 2000; Wang X. et al., 2015). *Ae. aegypti*, *An. sinensis*, *An. tessellates*, and *An. barbirostris* were found only in one region. *C. tritaeniorhynchus* was collected in four regions. We did not collect any *An. dirus* or *An. minimus* specimens.

The richness and dominant mosquito species of Hainan Island are different from those of other tropical islands. In an investigation conducted from 2005 to 2012 on Taiwan Island, 26 mosquito species from 8 genera were identified (Su et al., 2014). The most prevalent species on Taiwan Island were *C. tritaeniorhynchus*, *C. sitiens* and *An. sinensis*, differing considerably from the situation on Hainan. Thirteen species were commonly observed on Hainan and Taiwan Islands. Eight species of *Aedes* and *Culex* were found in 2013 on Tongatapu Island, which is located in the South Pacific Ocean (Swan and Harding, 2017). *Ae. aegypti* was the most prevalent species on Tongatapu Island, followed by *Ae. albopictus*. *C. sitiens*, *C. p. quinquefasciatus*, *Ae. albopictus*, *Ae. aegypti*, and *Ae. vexans*, which existed on all three islands.

The Hainan *Ae. albopictus* populations showed frequent gene flow with the Yunnan and Guangdong populations but not with the Fujian populations. Fang et al. (2018) reported that Hainan *Ae. albopictus* only exhibited frequent gene flow with the Yunnan population and that gene exchange between Hainan and Guangdong or Fujian populations was blocked. We also found that the Hainan *Ae. albopictus* populations showed frequent gene flow with the Congo, Lao People's Democratic Republic, Singapore, and Thailand populations. Our results remind us that the risk of outbreaks of *Ae. albopictus*-borne human viruses, such

as Dengue virus and Zika virus, is elevated in these tropical areas considering the frequent gene flow between them, especially between Guangdong and Hainan.

Ar. subalbatus is known to be the vector for parasites of many human diseases, such as Japanese encephalitis virus and the filarial worm *Wuchereria bancrofti* (Das et al., 1983). Two subgroups are reported in the *Ar. subalbatus* populations on Hainan for the first time. The *Ar. subalbatus* specimens registered in GenBank from Pakistan, India and the Lao People's Democratic Republic all belong to one subgroup, while the *Ar. subalbatus* specimens from a lab in United States (AY440299) (Bartholomay et al., 2004) and Yunnan in China (KY978578) (Li and Chen, 2018) are closely related to the other subgroup. *Ar. subalbatus* has become one of the most prevalent species at Hainan according to this investigation. The overall populations remained in genetic equilibrium. Six populations contained individuals from the two subgroups. A high ratio of variation (77.06%) existed between the two subgroups. This is a dominant cause of the high haplotype and nucleotide diversity of the *Ar. subalbatus* populations on Hainan. The genetic divergence between the two subgroups was quite high (Fst = 0.77), and gene flow between them was blocked. It is possible that in the future, the accumulation of genetic differences will lead to reproductive isolation between the two subgroups and, thus, the formation of new species.

In conclusion, our results showed a high diversity of mosquito species and their population genetic characteristics on Hainan Island. These results may have important implications for vector control and shed light on understanding the evolutionary processes of these mosquito species.

DATA AVAILABILITY STATEMENT

The datasets presented in this study can be found in online repositories. The names of the repository/repositories and accession number(s) can be found below: https://www.ncbi.nlm.nih.gov/genbank/, MT541015–MT541156, MT541161–MT541779, MT566458–MT566913, MT575769–MT575771, MT576036, MT586701, MT590372, MT596915, MT606009, and MT613992.

AUTHOR CONTRIBUTIONS

FC, QX, and LK designed the experiments. FC and SL wrote the manuscript. SL performed the experiments and conducted the data analysis. SL, FJ, HL, XK, YW, ZZ, DW, AZ, CL, QL, and FC collected mosquitoes from the fields. All authors contributed to the article and approved the submitted version.

FUNDING

This work was supported by grants of the Major Special Projects for Infectious Diseases during the 13th 5-year plan of China (No. 2017ZX10303404), the State Key Research Development Program of China (No. 2019YFC1200201), and the Open Foundation of Key Laboratory of Tropical Translational Medicine of Ministry of Education, Hainan Medical University.

ACKNOWLEDGMENTS

We thank Dr. Zushi Huang from the Institute of Zoology, Chinese Academy of Sciences for giving suggestions on genetic analysis.

SUPPLEMENTARY MATERIAL

The Supplementary Material for this article can be found online at: https://www.frontiersin.org/articles/10.3389/fgene.2020.602863/full#supplementary-material

REFERENCES

Bartholomay, L. C., Cho, W. L., Rocheleau, T. A., Boyle, J. P., Beck, E. T., Fuchs, J. F., et al. (2004). Description of the transcriptomes of immune response-activated hemocytes from the mosquito vectors *Aedes aegypti* and *Armigeres subalbatus*. *Infect. Immun.* 72, 4114–4126. doi: 10.1128/iai.72.7.4114-4126.2004

Bourke, B. P., Oliveira, T. P., Suesdek, L., Bergo, E. S., and Sallum, M. A. (2013). A multi-locus approach to barcoding in the *Anopheles strodei* subgroup (Diptera: Culicidae). *Parasit Vect.* 6:111. doi: 10.1186/1756-3305-6-111

Chan, A., Chiang, L. P., Hapuarachchi, H. C., Tan, C. H., Pang, S. C., Lee, R., et al. (2014). DNA barcoding: complementing morphological identification of mosquito species in Singapore. *Parasit Vect.* 7:569. doi: 10.1186/s13071-014-0569-4

Cook, S., Diallo, M., Sall, A. A., Cooper, A., and Holmes, E. C. (2005). Mitochondrial markers for molecular identification of *Aedes* mosquitoes (Diptera: Culicidae) involved in transmission of arboviral disease in West Africa. *J. Med. Entomol.* 42, 19–28. doi: 10.1603/0022-2585(2005)042[0019:mmfmio]2.0.co;2

Das, P., Bhattacharya, S., Chakraborty, S., Palit, A., Das, S., Ghosh, K. K., et al. (1983). Diurnal manbiting activity of *Armigeres subalbatus* (Coquillett, l898) in a village in WestBengal. *Indian J. Med. Res.* 78, 794–798.

Excoffier, L., and Lischer, H. (2010). Arlequin suite ver 3.5: a new series of programs to perform population genetics analyses under Linux and Windows. *Mol. Ecol. Resour.* 10, 564–567. doi: 10.1111/j.1755-0998.2010.02847.x

Fang, Y., Zhang, J., Wu, R., Xue, B., Qian, Q., and Gao, B. (2018). Genetic polymorphism study on *Aedes albopictus* of different geographical regions based on DNA barcoding. *Biomed Res. Int.* 2018:1501430. doi: 10.1155/2018/1501430

Folmer, O., Black, M., Hoeh, W., Lutz, R., and Vrijenhoek, R. (1994). DNA primers for amplification of mitochondrial cytochrome c oxidase subunit I from diverse metazoan invertebrates. *Mol. Mar. Biol. Biotech.* 3, 294–302.

Fu, Y. (1997). Statistical tests of neutrality of mutations against population growth, hitchhiking and background selection. *Genetics* 147, 915–925.

Fu, Y., Li, Z. L., Wang, C. X., Zhu, J., Pan, L. W., Chen, Y. B., et al. (2002). Investigation of an outbreak of Japanese B encephalitis in hainan province. *China Trop. Med.* 2, 105–107.

Halbert, N. D., Gogan, P. J., Hedrick, P. W., Wahl, J. M., and Derr, J. N. (2012). Genetic population substructure in bison at Yellowstone National Park. *J. Hered.* 103, 360–370. doi: 10.1093/jhered/esr140

Kumar, N. P., Rajavel, A. R., and Jambulingam, P. (2017). Development of a PCR methodology to distinguish species members of *Culex vishnui* subgroup (Diptera: Culicidae) based on DNA barcodes. *Insect Sci.* 24, 336–340. doi: 10.1111/1744-7917.12344

Laurito, M., de Oliveira, T. M., Almiron, W. R., and Sallum, M. A. M. (2013). COI barcode versus morphological identification of *Culex* (*Culex*) (Diptera: Culicidae) species: a case study using samples from Argentina and Brazil. *Mem. Inst. Oswaldo Cruz.* 108, 110–122. doi: 10.1590/0074-0276130457

Li, X., and Chen, B. (2018). Sequencing and analysis of the complete mitochondrial genome of *Armigeres subalbatus* (Diptera: Culicidae). *Acta Entomol. Sin.* 61, 114–121.

Lian, G., Ke, M., Wu, B., Wang, H., Feng, Z., Yang, Z., et al. (2015). DNA-barcode based molecular identification for eleven common mosquito species at frontier ports. *Chinese Front. Health Quarant.* 3, 1004–9770.

Librado, P., and Rozas, J. (2009). DnaSP v5: a software for comprehensive analysis of DNA polymorphism data. *Bioinformatics* 25, 1451–1452. doi: 10.1093/bioinformatics/btp187

Montero-Pau, J., Gomez, A., and Munoz, J. (2008). Application of an inexpensive and high-throughput genomic DNA extraction method for the molecular ecology of zooplanktonic diapausing eggs. *Limnol. Oceanogr.* 6, 218–222. doi: 10.4319/lom.2008.6.218

Slatkin, M., and Hudson, R. R. (1991). Pairwise comparisons of mitochondrial DNA sequences in stable and exponentially growing populations. *Genetics* 129, 555–562.

Su, C., Yang, C., Teng, H., Lu, L., Lin, C., Tsai, K., et al. (2014). Molecular epidemiology of Japanese encephalitis virus in mosquitoes in Taiwan during 2005–2012. *PLoS Negl. Trop. Dis.* 8:e3122. doi: 10.1371/journal.pntd.0003122

Su, S., Gu, B., Cai, W., and Chen, D. (1994). An investigation about mosquito species in Baoting region of Hainan island. *J. Med. Pest Control* 10, 123–127.

Sun, D., Wang, S., Zen, L., Li, S., and Zhuo, K. (2014). Survey of the diversity of *Anopheles* species in Hainan province. *J. Pathog. Biol.* 9, 271–274.

Swan, T., and Harding, J. (2017). The distribution and occurrence of mosquito larvae (Diptera: Culicidae) in the Tongatapu Island Group, Kingdom of Tonga. *Austral. Entomol.* 56, 160–168. doi: 10.1111/aen.12219

Tajima, F. (1989). Statistical method for testing the neutral mutation hypothesis by DNA polymorphism. *Genetics* 123, 597–601.

Walton, C., Handley, J. M., Tun-Lin, W., Collins, F. H., Harbach, R. E., Baimai, V., et al. (2000). Population structure and population history of *Anopheles dirus* mosquitoes in Southeast Asia. *Mol. Biol. Evol.* 17, 962–974. doi: 10.1093/oxfordjournals.molbev.a026377

Wang, G., Li, C., Guo, X., Xing, D., Dong, Y., Wang, Z., et al. (2012). Identifying the main mosquito species in china based on DNA barcoding. *PLoS One* 7:e47051. doi: 10.1371/journal.pone.0047051

Wang, J. X., Liang, Y. Q., Yang, C. X., Wu, Y. Y., and Zhang, X. B. (2015). Epidemic characteristics of epidemic encephalitis B in Xiuying District of Haikou City from 2005 to 2013. *Hainan Med. J.* 26, 1691–1692.

Wang, X., Yang, X., Zhao, W., and Lin, C. (2015). Analysis of surveillance data of mosquito density from 2012 to 2014 in Haikou city, Hainan, China. *Chinese J. Vect. Biol. Control* 26, 424–426.

Wu, W. X., Jin, Y. M., Sun, Y. L., Zeng, X. J., Su, X. Y., Jia, P. B., et al. (2007). Analysis of results of sentinel monitoring of transmission vector of dengue fever in Hainan Province in 2006. *China Trop. Med.* 7, 1863–1864.

Xiao, D., Long, Y., Wang, S. Q., Li, L., Yan, S. P., Xu, D. Z., et al. (2010). Survey of number, density and composition of Anopheles in Hainan Province from 2O06 to 2008. *China Trop. Med.* 10, 265–277.

Zhan, D., Long, Z., Liu, G., Tang, T., and An, J. (2000). Surveillance of vector mosquitoes in Sanya region of Hainan island. *J. Med. Pest Control* 16, 354–356.

Zhao, X., Hou, N., Chen, C., Zhang, Q., Zhao, J., and Lu, Y. (2017). Analysis of mosquito vector species and epidemic situation of mosquito-borne viruses in Hainan Province. *Hainan Med. J.* 28, 1174–1178.

Zheng, Y., Wang, Z., and Lian, G. (2011). Review on arbovirus studies in Hainan province, China. *Chinese J. Vect. Biol. Control* 22, 607–610.

Zhong, D. B., Lo, E., Hu, R., Metzger, M. E., Cummings, R., Bonizzoni, M., et al. (2013). Genetic analysis of invasive *Aedes albopictus* populations in Los Angeles county, California and its potential public health impact. *PLoS One* 8:e68586. doi: 10.1371/journal.pone.0068586

Conflict of Interest: The authors declare that the research was conducted in the absence of any commercial or financial relationships that could be construed as a potential conflict of interest.

frontiers in Genetics

ORIGINAL RESEARCH
published: 03 November 2020
doi: 10.3389/fgene.2020.585320

Functional Analysis of Nuclear Factor Y in the Wing-Dimorphic Brown Planthopper, *Nilaparvata lugens* (Hemiptera: Delphacidae)

*Hao-Hao Chen[1], Yi-Lai Liu[1], Xin-Yang Liu[1], Jin-Li Zhang[1] and Hai-Jun Xu[1,2,3]**

[1] Institute of Insect Sciences, Zhejiang University, Hangzhou, China, [2] Ministry of Agriculture Key Laboratory of Molecular Biology of Crop Pathogens and Insect Pests, Zhejiang University, Hangzhou, China, [3] State Key Laboratory of Rice Biology, Zhejiang University, Hangzhou, China

Nuclear factor Y (NF-Y) is a heterotrimeric transcription factor with the ability to bind to a CCAAT box in nearly all eukaryotes. However, the function of NF-Y in the life-history traits of insects is unclear. Here, we identified three NF-Y subunits, *Nl*NF-YA, *Nl*NF-YB, and *Nl*NF-YC, in the wing-dimorphic brown planthopper (BPH), *Nilaparvata lugens*. Spatio-temporal analysis indicated that *NlNF-YA*, *NlNF-YB*, and *NlNF-YC* distributed extensively in various body parts of fourth-instar nymphs, and were highly expressed at the egg stage. RNA interference (RNAi)-mediated silencing showed that knockdown of *NlNF-YA*, *NlNF-YB*, or *NlNF-YC* in third-instar nymphs significantly extended the fifth-instar duration, and decreased nymph-adult molting rate. The addition of 20-hydroxyecdysone could specifically rescue the defect in adult molting caused by *NlNF-YA*^{RNAi}, indicating that *Nl*NF-Y might modulate the ecdysone signaling pathway in the BPH. In addition, *NlNF-YA*^{RNAi}, *NlNF-YB*^{RNAi}, or *NlNF-YC*^{RNAi} led to small and moderately malformed forewings and hindwings, and impaired the normal assembly of indirect flight muscles. Adult BPHs treated with *NlNF-YA*^{RNAi}, *NlNF-YB*^{RNAi}, or *NlNF-YC*^{RNAi} produced fewer eggs, and eggs laid by these BPHs had arrested embryogenesis. These findings deepen our understanding of NF-Y function in hemipteran insects.

Keywords: ***Nilaparvata lugens*, nuclear factor Y, wing development, ecdysone, reproduction**

OPEN ACCESS

Edited by:
Wei Guo,
Chinese Academy of Sciences (CAS), China

Reviewed by:
LinQuan Ge,
Yangzhou University, China
Junzheng Zhang,
China Agricultural University, China

***Correspondence:**
Hai-Jun Xu
haijunxu@zju.edu.cn

Specialty section:
This article was submitted to Epigenomics and Epigenetics, a section of the journal Frontiers in Genetics

Received: *20 July 2020*
Accepted: *12 October 2020*
Published: *03 November 2020*

Citation:
Chen H-H, Liu Y-L, Liu X-Y, Zhang J-L and Xu H-J (2020) Functional Analysis of Nuclear Factor Y in the Wing-Dimorphic Brown Planthopper, Nilaparvata lugens (Hemiptera: Delphacidae). Front. Genet. 11:585320. doi: 10.3389/fgene.2020.585320

INTRODUCTION

Nuclear transcription factor Y (NF-Y) is an evolutionarily conserved transcription factor that exists in almost all organisms, from prokaryotes to eukaryotes (Dorn et al., 1987; Laloum et al., 2013). NF-Y exerts differential regulation on a wide variety of genes through binding to a CCAAT box, one of the most ubiquitous elements in eukaryotic promoters (Li et al., 1992; Mantovani, 1998; Suzuki et al., 2001). NF-Y consists of three subunits, NF-YA, NF-YB, and NF-YC, all required for DNA-binding (McNabb et al., 1995; Sinha et al., 1995; Bi et al., 1997; Mantovani, 1999). Accumulated evidence indicates that animal NF-Y is essential for numerous biological processes involved in proliferation and apoptosis, cancer and tumorigenesis, stress responses, growth, and development (Li et al., 2018). For instance, the deletion of the mouse *NF-YA* homolog causes early embryo lethality (Bhattacharya et al., 2003). Down-regulation of mouse *NF-YA* was found to reduce the expression of several cell cycle control genes in differentiated muscle cells, suggesting NF-YA

is involved in specifying myogenic fate (Gurtner et al., 2003). Knockdown or overexpression of the *Drosophila melanogaster NF-YA* homolog in all tissues results in lethality at the larval stage, indicating that a certain level of NF-YA is necessary for viability in flies (Yoshioka et al., 2007). However, he contribution of NF-Y homologs to the life-history traits of other insect species has yet to be reported.

The wing-dimorphic brown planthopper (BPH), *Nilaparvata lugens* (Hemiptera: Delphacidae), is the most destructive pest of rice in Asia (Xue et al., 2014), causing a loss in rice production of more than $300 million annually in Asia. It feeds exclusively on the phloem sap of the rice plant and transmits plant viruses such as rice ragged stunt virus and rice grassy stunt virus, resulting in loss of plant vigor and reduced yield (Backus et al., 2005; Otuka, 2013). The BPH is a hemimetabolous insect, the newly hatched first-instar nymphs look like miniature adults except for the absence of wings and sexual immaturity, and grow gradually within increasing stages. The BPH has five nymphal stages, and wing buds grow with each of these stages, but short- and long-winged morphs are externally indistinguishable until the adults emerge (Xu and Zhang, 2017). Long-winged BPH adults have well-developed forewings, hindwings, and indirect flight muscles (IFM), whereas, short-winged adults have undeveloped forewings and rudimentary hindwings (Xu and Zhang, 2017; Zhang et al., 2019). Wing dimorph and high fecundity are the two most important biological features contributing to the ecological success of the BPH (Zhang et al., 2019). Recently, facilitated by the development of genetic tools (Xu et al., 2013; Xue et al., 2018) and genomic information (Xue et al., 2014), the molecular basis underlying wing dimorphism (Xu et al., 2015) and population resurgence (Wu et al., 2020) are emerging, which offers a basis for the design of new control agents to combat BPH infestation.

In the present study, we identified the BPH *NF-YA* (*NlNF-YA*), *NF-YB* (*NlNF-YB*), and *NF-YC* (*NlNF-YC*) homologs by searching the BPH genomic and transcriptomic databases. RNA interference (RNAi)-mediated gene silencing showed that *Nl*NF-YA, *Nl*NF-YB, and *Nl*NF-YC all played pivotal roles in nymph growth, wing formation, IFM development, and reproduction. In addition, we found that NF-Y regulated adult eclosion most likely through linking to the ecdysone signaling pathway. Our findings deepen our understanding of the function of NF-Y in hemipteran insects.

MATERIALS AND METHODS

Insects

The BPH strain was originally collected from a rice field in Hangzhou, China. Insects were reared on rice seedlings (rice variety: Xiushui 134) in a walk-in chamber at 26 ± 0.5°C, with a light: dark photoperiod of 16: 8 h and relative humidity of 50 ± 5%.

Gene Identification and Sequence Analysis

The amino acid sequences of *Drosophila* NF-Y homologs were used to screen BPH genomic and transcriptomic databases for homologs. Total RNA was isolated from BPH nymphs using RNAiso plus (Takara #9109) according to the manufacturer's protocol. For cDNA syntheses, 450 ng of total RNA was reversely transcribed in a 10 μL reaction with HiScript QRT SuperMix (Vazyme #R223-01). The *NlNF-YA*, *NlNF-YB*, and *NlNF-YC* sequences were amplified from cDNA using fidelity DNA polymerase (Toyobo #930700) with NlNF-YA-F/R, NlNF-YB-F/R, and NlNF-YC-F/R primer pairs, respectively (**Supplementary Table 1**). The PCR product was cloned and the sequence was determined by Sanger sequencing.

To identify the exon-intron construction of *NlNF-Y*, open reading frames (ORFs) of *NlNF-YA*, *NlNF-YB*, and *NlNF-YC* were used to search a BPH genomic database (Xue et al., 2014). For phylogenetic analysis, 39 NF-Y sequences from 13 species including *D. melanogaster*, *N. lugens*, *Acyrthosiphon pisum*, *Apis cerana*, *Bemisia tabaci, Bombyx mori*, *Cryptotermes secundus*, *Halyomorpha halys*, *Monomorium pharaonis*, *Nasonia vitripennis*, *Nicrophorus vespilloides*, *Tribolium castaneum*, and *Zootermopsis nevadensis* were used for sequence alignment. A phylogenetic tree was constructed with maximum-likelihood method and 1000 bootstraps using the MEGA 7 program (Kumar et al., 2016).

Spatio-Temporal Expression Pattern of *NlNF-Y*

Total RNA was isolated from eggs ($n = 100$), first-instar ($n = 100$), second-instar ($n = 50$), third-instar ($n = 50$), fourth-instar ($n = 30$), fifth-instar nymphs ($n = 15$), and adult females ($n = 15$), which were laid or ecdysed within 24 h. To examine tissue distribution, we dissected the head ($n = 50$), antenna ($n = 200$), tergum ($n = 50$), leg ($n = 100$), fat body ($n = 30$), cuticle ($n = 50$), and gut ($n = 100$) from four-instar nymphs for RNA extraction. First-strand cDNA was synthesized from total RNA (450 ng) using HiScript QRT SuperMix (Vazyme #R223-01). The synthesized cDNAs were 10-fold diluted and used as templates for quantitative real-time PCR (qPCR). The qPCR primers for *NlNF-Y* (**Supplementary Table 1**) were designed using Primer-Blast.[1] The qPCR was conducted on a CFX96TM real-time PCR detection system (Bio-Rad) using the following conditions: denaturation for 3 min at 95°C, followed by 40 cycles at 95°C for 10 s, and 60°C for 30 s. The ribosomal protein S11 gene (*rps11*) was used as the internal reference gene (Yuan et al., 2014). The $2^{-\Delta\Delta Ct}$ method (Ct represents the cycle threshold) was used to measure the relative expression level (Livak and Schmittgen, 2001). Three independent biological replicates with three technical replicates were conducted for each experiment.

RNAi and Microinjection

The dsRNAs were synthesized using a T7 High Yield Transcription Kit (Vazyme #TR101-02) according to the manufacturer's instructions with primers containing the T7 RNA polymerase promoter at both ends (**Supplementary Table 1**). A dsRNA injection was carried out as in our previous study (Xu et al., 2015). Briefly, fourth-instar nymphs were anesthetized with carbon dioxide for 10–15 s. Approximately

[1] https://www.ncbi.nlm.nih.gov/tools/primer-blast/

150 ng dsRNA was microinjected into the mesothorax using a FemtoJet microinjection system (Eppendorf). To investigate whether disruption of *NlNF-YA* affected ecdysone signaling activity, fifth-instar nymphs (n = 10 for each of three replicates) were collected to examine the expression levels of *NlE74A* and *NlE75B* by qPCR using corresponding primers (**Supplementary Table 1**). To investigate RNAi efficiency, BPHs (n = 5 for each of three replicates) at 24 h after adult eclosion were collected for qPCR assay.

Forewing Size and Hind Tibiae Length

Fourth-instar nymphs (36–48 h after ecdysis, hAE) were microinjected with dsRNAs targeting *NlNF-YA* (ds*NlNF-YA*), *NlNF-YB* (ds*NlNF-YB*), *NlNF-YC* (ds*NlNF-YC*), or *GFP* (ds*GFP*). After adult eclosion (24 h), images of the forewings and hind tibiae were captured with a DFC320 digital camera attached to a Leica S8AP0 stereomicroscope using a LAS digital imaging system (v. 3.8). Digital images of forewings (n = 20) and hind tibias (n = 20) were collected for the measurement of forewing size and hind tibia length using ImageJ (v. 1.47).

Microinjection With 20-hydroxyecdysone (20E)

Fourth-instar nymphs (36–48 hAE) were microinjected with corresponding dsRNAs targeting each gene, and then nymphs were maintained on fresh rice seedings until the fifth-instar stage (within 48 h). Fifth-instar nymphs were microinjected with 20E (1 mg/ml) or distilled water, and the adult eclosion rate was calculated.

Transmission Electron Microscopy

Fourth-instar nymphs (36–48 hAE) were microinjected with dsRNAs targeting *NlNF-YA*, *NlNF-YB*, *NlNF-YC*, or *GFP*. The thoraxes were dissected from adult females (24 h after emergence) for Transmission Electron Microscopy (TEM) as in our previous study (Xue et al., 2013). Briefly, samples were fixed in 2.5% glutaraldehyde overnight at 4°C. After fixation, samples were post-fixed in 1% osmium tetroxide for 1.5 h. Then, samples were dehydrated in a standard ethanol/acetone series, infiltrated and embedded in Spurr medium, and then superthin sections were cut. The sections were stained with 5% uranyl acetate followed by Reynolds' lead citrate solution and observed under a JEM-1230 transmission electron microscope (JEOL).

Fecundity Assay

Newly emerged females and males (within 12 h after eclosion) were microinjected with ds*NF-YA*, ds-*NF-YB*, ds*NF-YC*, or ds*Gfp*. Then each female was allowed to match with two males in a glass tube. Insects were removed at 5 days after matching, and eggs were counted under a Leica S8AP0 stereomicroscope.

Data Analysis

Statistical analyses were performed using GraphPad Prism 7.0 (GraphPad Software). Means were compared using a two-tailed Student's t-test and log-rank (Mantel-Cox) test at a significance level set at $^{*}P < 0.05$, $^{**}P \leq 0.01$, and $^{***}P \leq 0.001$.

RESULTS

NlNF-YA, *NlNF-YB*, and *NlNF-YC* Sequence Analysis

We identified three genes encoding BPH NF-Y homologs, *NlNF-YA*, *NlNF-YB*, and *NlNF-YC*, in a BLAST search against BPH genomic (Xue et al., 2014) and transcriptome databases using the *D. melanogaster* NF-Y proteins as query sequences. The ORFs of *NlNF-YA*, *NlNF-YB*, and *NlNF-YC* were 1002-, 609-, and 1011-bp in length, encoding 333, 202, and 336 amino acid residues, respectively (**Supplementary Figures 1–3**). Exon-intron construction analysis showed that the *NlNF-YA*, *NlNF-YB*, and *NlNF-YC* ORFs consist of eight, five, and eight exons, located in scaffolds 6450/1657, 3414, and 1809, respectively. A phylogenetic analysis based on NF-Y homologs from 13 species showed that *Nl*NF-YA, *Nl*NF-YB, and *Nl*NF-YC together with their counterparts formed three distinct clusters (**Figure 1**), indicating that the BPH *NF-Y* genes we identified were authentic *NF-Y* homologs.

Spatio-Temporal Analysis of *NlNF-YA*, *NlNF-YB*, and *NlNF-YC*

Spatio-temporal expression of *NlNF-YA*, *NlNF-YB*, and *NlNF-YC* was examined by qPCR. *NlNF-YA*, *NlNF-YB*, and *NlNF-YC* transcripts were readily detected from egg to adult stages,

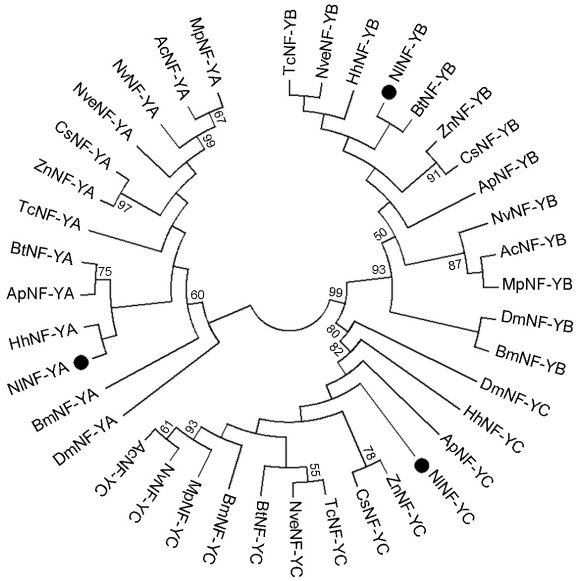

FIGURE 1 | Phylogenetic analysis of *Nl*NF-Y members. The phylogenetic tree was constructed with 39 full-length *Nl*NF-Y members from 13 species using the maximum-likelihood method and bootstrapping was set to 1,000 replications. *Nl*NF-YA, *Nl*NF-YB, and *Nl*NF-YC are indicated by dots. Nl, *Nilaparvata lugens*; Dm, *Drosophila melanogaster*; Ap, *Acyrthosiphon pisum*; Ac, *Apis cerana*; Bt, *Bemisia tabaci*; Bm, *Bombyx mori*; Cs, *Cryptotermes secundus*; Hh, *Halyomorpha halys*; Mp, *Monomorium pharaonis*; Nv, *Nasonia vitripennis*; Nve, *Nicrophorus vespilloides*; Tc, *Tribolium castaneum*, and Zn, *Zootermopsis nevadensis*.

and relatively high levels were detected in eggs laid within 24 h (Egg-24 h) (**Figure 2A**), indicating that they might play important functions in egg development. Tissue distribution analysis showed that *NlNF-YA*, *NlNF-YB*, and *NlNF-YC* were evenly expressed in head, antenna, tergum, leg, fat body, cuticle, and gut of fourth-instar nymphs (**Figure 2B**), indicating *NlNF-Y* genes might be important for BPH growth and development.

Knockdown of *NlNF-Y* Genes Leads to Small and Malformed Wings

To investigate whether *NlNF-YA*, *NlNF-YB*, and *NlNF-YC* played any roles in BPH development, fourth-instar short-wing-destined nymphs were microinjected with corresponding dsRNAs targeting each gene. At 48 h after microinjection, RNAi efficiency was examined by qPCR, which showed that dsRNA treatments significantly down-regulated the expression levels of *NlNF-YA*, *NlNF-YB*, and *NlNF-YC* by 63.7, 99.9, and 82.7%, respectively, relative to the GFP^{RNAi} treatment (**Figure 3A**). Notably, $NlNF\text{-}YA^{RNAi}$, $NlNF\text{-}YB^{RNAi}$, and $NlNF\text{-}YC^{RNAi}$ caused high mortality, leading to approximately 60, 60, and 40% of nymphs died before adult eclosion (**Figure 3B**), respectively. The remaining nymphs could successfully molt into adults. However, these adults had moderately smaller and slightly malformed forewings relative to GFP^{RNAi} BPHs

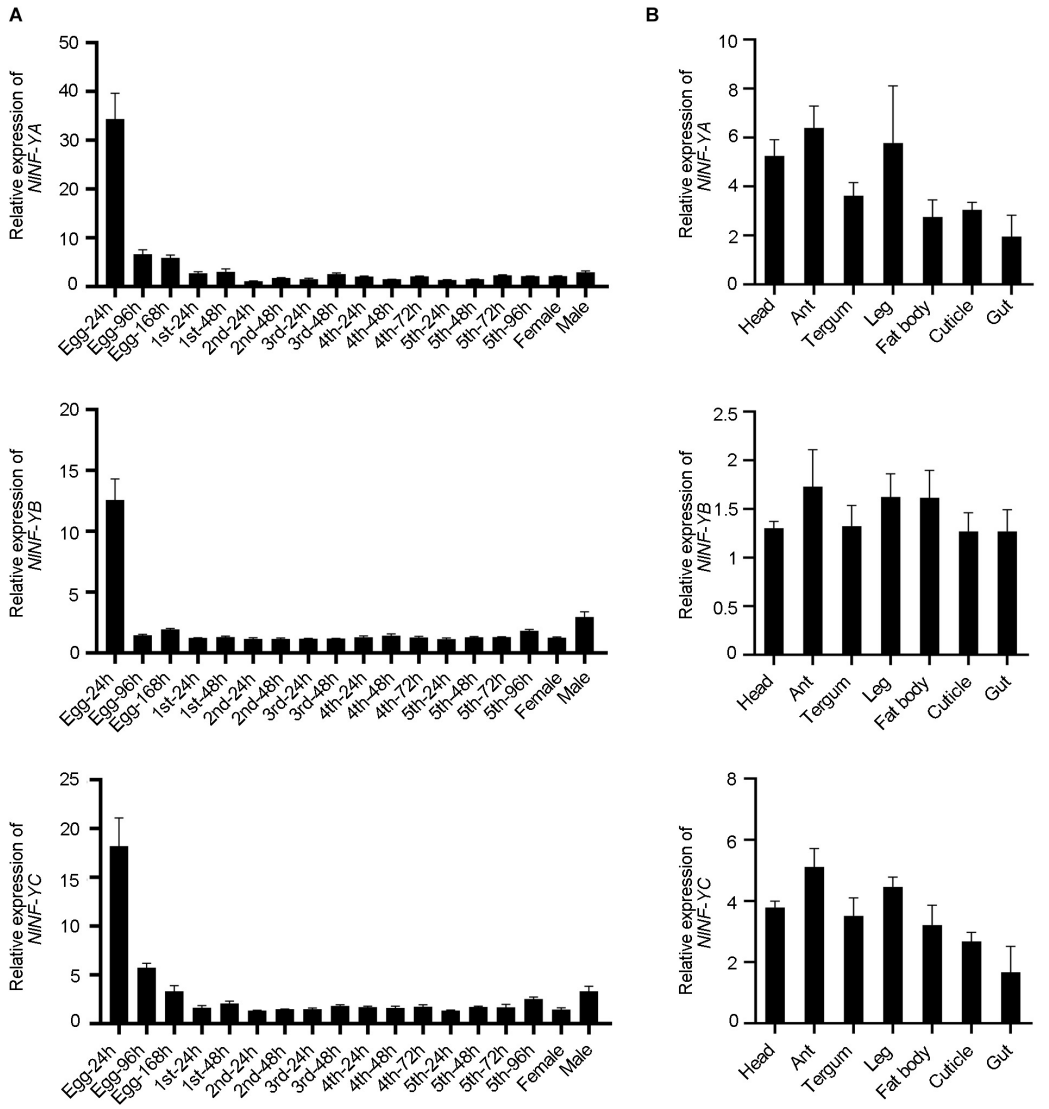

FIGURE 2 | Spatio-temporal expression of *NlNF-Y* genes. **(A)** Developmental profile of *NlNF-YA*, *NlNF-YB*, and *NlNF-YC*. Total RNAs were isolated from eggs (n = 100), first-instar (n = 100), second-instar (n = 50), third-instar (n = 50), fourth-instar (n = 30), fifth-instar nymphs (n = 15), and adult females (n = 15). **(B)** Tissue distribution of *Nl*NF-Y. Total RNAs were extracted from the head (n = 30), antenna (ant, n = 200), tergum (n = 50), leg (n = 100), fat body (n = 30), cuticle (n = 50), and gut (n = 100) from fourth-instar nymphs. First-strand cDNA was synthesized using random primers, and qPCR was conducted using specific primers corresponding to each gene. The relative expression level was normalized by the ribosomal S11 gene (*rps11*). Bars represent s.d. derived from three independent biological replicates.

(**Figures 4A,B**). *NlNF-YA*^{RNAi}, *NlNF-YB*^{RNAi}, and *NlNF-YC*^{RNAi} specifically reduced forewing size but had marginal roles on hind tibiae length (**Figure 4C**). These data indicated that *NlNF-YA*, *NlNF-YB*, and *NlNF-YC* were essential for normal wing growth in BPHs.

Knockdown of *NlNF-Y* Genes Leads to Defective IFM

Because short-wing BPHs lack hindwings and IFM, we used long-wing BPHs to investigate whether *NlNF-YA*, *NlNF-YB*, and *NlNF-YC* had any effect on IFM development. For this,

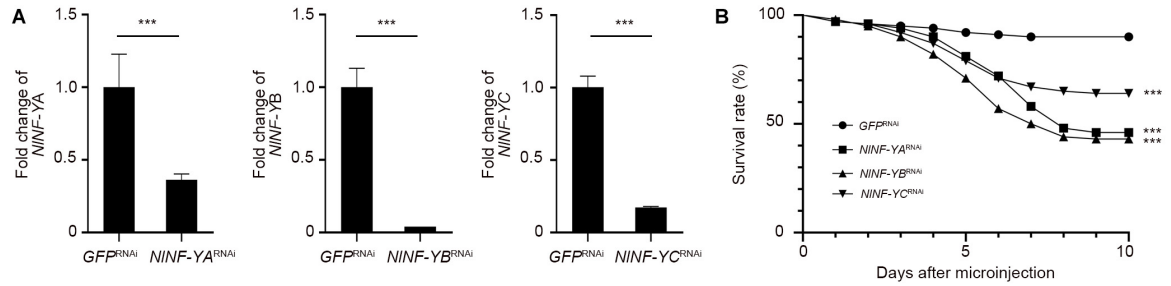

FIGURE 3 | The survival rate of BPHs after dsRNA treatment. **(A)** Examination of RNAi efficiency. Fifth-instar nymphs (0–24 hAE) were microinjected with dsRNAs, and BPHs (n = 5 for each of three replicates) at 24 h after adult eclosion were collected for qPCR assay. The relative expression of *NlNF-YA*, *NlNF-YB*, and *NlNF-YC* was normalized to the expression of *rps11*. **(B)** The survival rate of BPHs after dsRNA treatment. Fourth-instar nymphs (n = 100) were microinjected with dsRNAs targeting *NlNF-YA*, *NlNF-YB*, *NlNF-YC*, or *Gfp*. Statistical analysis was performed by log-rank (Mantel-Cox) test. *NlNF-YA*^{RNAi}, ds*NlNF-YB*^{RNAi}, or ds*NlNF-YC*^{RNAi} significantly decreased the survivability of nymphs compared to *GFP*^{RNAi} (***$P < 0.001$).

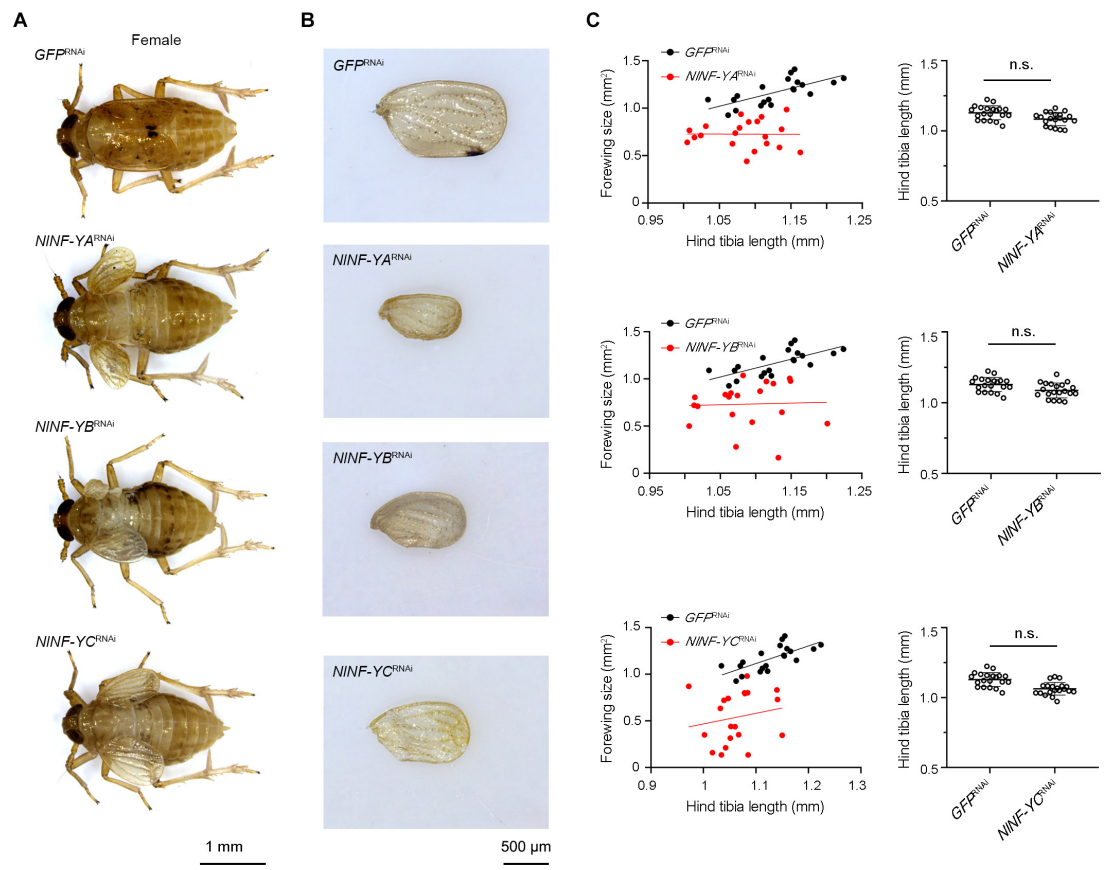

FIGURE 4 | Knockdown of *NlNF-Y* reduces forewing size in short-winged BPHs. **(A)** Morphology of dsRNA-treated short-winged BPHs. **(B)** The size of forewings after dsRNA treatment. **(C)** Relative wing size and tibia length in BPHs with *NlNF-Y* or *Gfp* knockdown. Each dot represents the wing size and tibia length derived from an individual female (n = 20). Bars represent the mean ± s.d. derived from independent biological replicates (n = 20). Statistical comparisons between two groups were performed using a two-tailed Student's t-test (n.s., non-significant).

fourth-instar long-wing-destined nymphs were microinjected with corresponding dsRNAs targeting each gene. *NlNF-YA*^{RNAi}, *NlNF-YB*^{RNAi}, and *NlNF-YC*^{RNAi} gave rise to adults with curved forewings and hindwings (**Figure 5A**). In line with the phenotype in short-winged BPHs, smaller forewings and hindwings were observed in adults previously treated with either *NlNF-YA*^{RNAi}, *NlNF-YB*^{RNAi}, or *NlNF-YC*^{RNAi} (**Figure 4B**), although there was no discernable effect on hind tibia length (**Figure 4C**). Next, these adults were collected for IFM ultrastructure examination using TEM. In *GFP*^{RNAi} adults, sarcomeres were clearly divided by Z discs and well-organized (**Figure 6**). In contrast, *NlNF-YA*^{RNAi}, *NlNF-YB*^{RNAi}, or *NlNF-YC*^{RNAi} led to defective sarcomeres, with deformed Z discs and weakly organized myofibrillar. These events indicated that the *Nl*NF-Y complex might be essential for IFM assembly in BPH.

Knockdown of *NlNF-Y* Genes Impairs Nymphal Growth and Adult Molting

Given that *NlNF-Y* genes were evenly expressed across nymphal stages (**Figure 2A**), we investigated whether knockdown of *NlNF-Y* genes would affect nymph growth. For this purpose, third-instar nymphs were microinjected with corresponding dsRNAs targeting each gene. Nymphs treated with *NlNF-YA*^{RNAi}, *NlNF-YB*^{RNAi}, or *NlNF-YC*^{RNAi} had an extended fifth-instar duration compared with those treated with *GFP*^{RNAi} (**Figure 7A**), with *NlNF-YA*^{RNAi} showing the most profound effect (**Figure 7A**). In addition, the majority of *NlNF-YA*^{RNAi}-treated nymphs died before adult emergence (**Figure 7B**), indicating that the disruption of the NF-Y complex impaired nymph-to-adult ecdysis.

Given that ecdysone is a hormone that initiates all major developmental transitions from the egg, to larva, to pupa, to adult in insects (Gilbert et al., 2002; Dubrovsky, 2005), we asked whether it mediated the effects of *Nl*NF-YA on adult molting. For this purpose, we first assessed the expression levels of two early ecdysone response genes, *NlE74A* and *NlE75E* (Dubrovsky, 2005), in the context of *NlNF-YA* knockdown. *NlNF-YA*^{RNAi} significantly reduced both *NlE74A* and *NlE75E* transcripts compared with *GFP*^{RNAi} (**Figure 7C**), indicating that knockdown of *NlNF-YA* might impair ecdyson signaling activity. Following this observation, we asked whether the addition

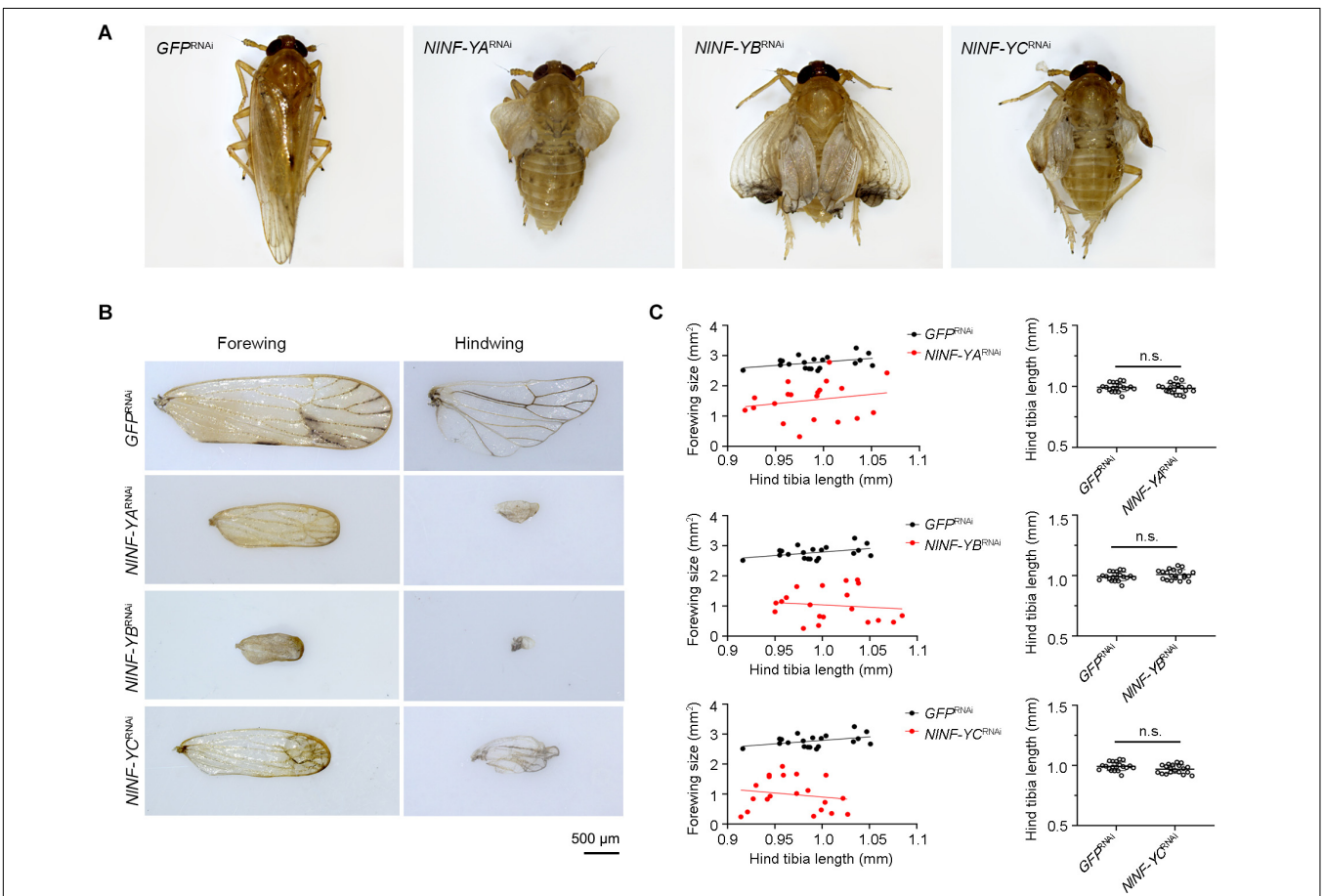

FIGURE 5 | Knockdown of *NlNF-Y* reduces forewing size in long-winged BPHs. **(A)** Morphology of dsRNA-treated long-winged BPHs. **(B)** The size of forewings and hindwings after dsRNA treatment. **(C)** Relative wing size and tibia length in BPHs with *NlNF-Y* or *Gfp* knockdown. Each dot represents the wing size and tibia length derived from an individual female (n = 20). Bar represents mean ± s.d. derived from independent biological replicates (n = 20). Statistical comparisons between two groups were performed using a two-tailed Student's t-test (n.s., non-significant).

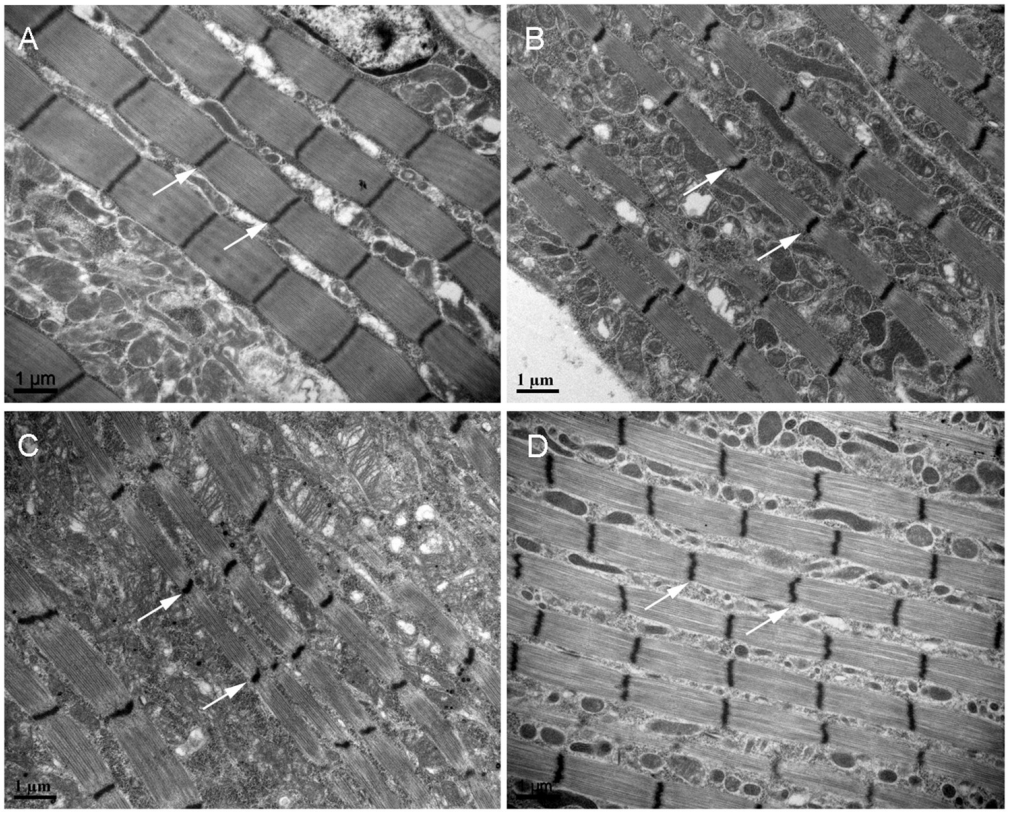

FIGURE 6 | TEM of the IFM of dsRNA-treated long-winged BPHs. Fourth-instar nymphs were treated with dsRNAs targeting Gfp **(A)**, NlNF-YA **(B)**, NlNF-YB **(C)**, or NlNF-YC **(D)**. Thorax was dissected from female adults (24 h after eclosion) for TEM. The Z discs are indicated by arrows.

of ecdysone could rescue the *NlNF-YA*^{RNAi} defect. To this end, fourth-instar nymphs were microinjected with ds*NlNF-YA*, followed by microinjection with 20E when nymphs proceeded to the fifth-instar at 48 h after eclosion. The addition of 20E could partially restore the molting defect caused by *NlNF-YA*^{RNAi} (**Figure 7B**) compared with the addition of water, indicating that *NlNF-YA*^{RNAi} decreased adult eclosion at least partially through the ecdysone signaling pathway.

Knockdown of *NlNF-Y* Genes Impairs Reproduction

Given that relatively high amounts of *NlNF-YA*, *NlNF-YB*, and *NlNF-YC* transcripts were detected at the early egg stage (**Figure 2A**), we asked whether *NlNF-YA, NlNF-YB*, and *NlNF-YC* contributed to BPH reproduction. Female and male adults at 12 h after eclosion were microinjected with corresponding dsRNAs targeting each gene, and then allowed to mate and to lay eggs for 5 days. BPHs treated with *NlNF-YA*^{RNAi}, *NlNF-YB*^{RNAi}, and *NlNF-YC*^{RNAi} laid substantially fewer eggs than those treated with *GFP*^{RNAi} (**Figure 8A**). In addition, the eggs laid by BPHs previously treated with *NlNF-YA*^{RNAi}, *NlNF-YB*^{RNAi}, or *NlNF-YC*^{RNAi} failed to develop eye pigmentation, a characteristic hallmark of egg development, indicating *NlNF-Y* genes might be essential for embryogenesis (**Figure 8B**).

DISCUSSION

In this study, we investigated the functions of individual *NlNF-Y* members in the BPH during nymphal development, adult molting, wing growth, IFM development, and reproduction. The results demonstrated that *Nl*NF-Y played pivotal roles in these processes. Depletion of *NlNF-YA*, *NlNF-YB*, and *NlNF-YC* resulted in extended nymphal duration, affected nymph-adult molting progress, reduced wing size, disrupted IFM assembly, reduced egg production, and impaired egg development. These findings provide an impetus to understand the function of NF-Y in life-history traits of insects.

The CCAAT box is one of the most common cis-acting elements found in the promoter and enhancer regions of various genes in eukaryotes (Li et al., 1992). An analysis of a large database of 1,031 human promoters indicated that the CCAAT box is present in 63% of them (Suzuki et al., 2001). NF-Y is the major CCAAT box recognizing protein that binds to DNA with high specificity and affinity (Bi et al., 1997; Mantovani, 1998). Knockdown or overexpression of the *Drosophila NF-YA* homolog with different GAL4 also drives lethality in the *Drosophila* pharate adult stage, possibly by influencing disc specification (Yoshioka et al., 2007; Ly et al., 2013). A similar phenomenon was observed in BPH,

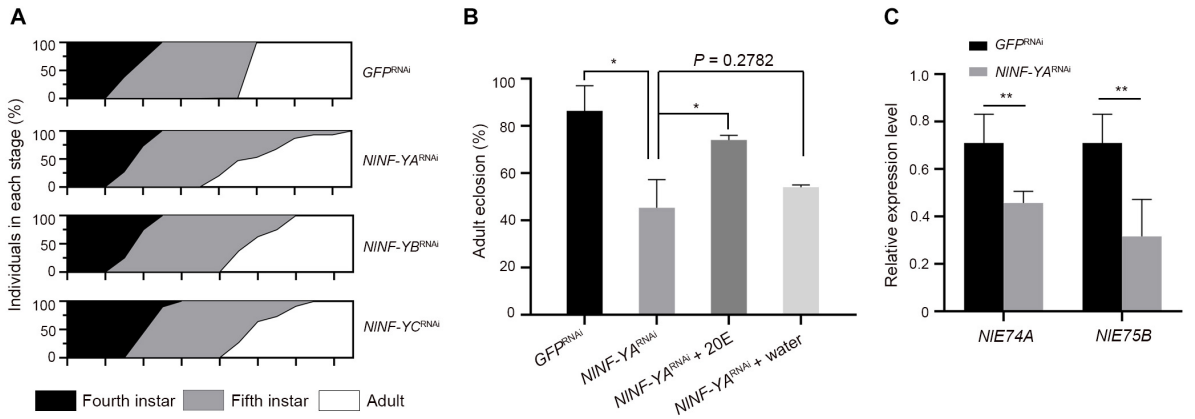

FIGURE 7 | Nymphal duration and adult eclosion of dsRNA-treated BPHs. **(A)** Third-instar nymphs (0–24 hAE) were microinjected with dsRNAs targeting *NlNF-YA* (n = 660), *NlNF-YB* (n = 435), *NlNF-YC* (n = 480), or *Gfp* (n = 442). The curve in different developmental stages indicates the molting ratio. (**B**) The nymph-adult eclosion rate of BPHs. Fourth-instar nymphs (36–48 hAE) were microinjected with dsRNAs targeting *NlNF-YA* or *Gfp*, and then 20E or distilled water was microinjected when nymphs proceeded the fifth-instar stage. **(C)** The expression of *NlE74A* and *NlE75B* in context of *NlNF-YA* knockdown. The relative expressions of *NlE74A* and *NlE75B* were normalized to the expression of *rps11*. Statistical comparisons between two groups were performed using two-tailed Student's t-test (*$P < 0.05$, and **$P < 0.01$).

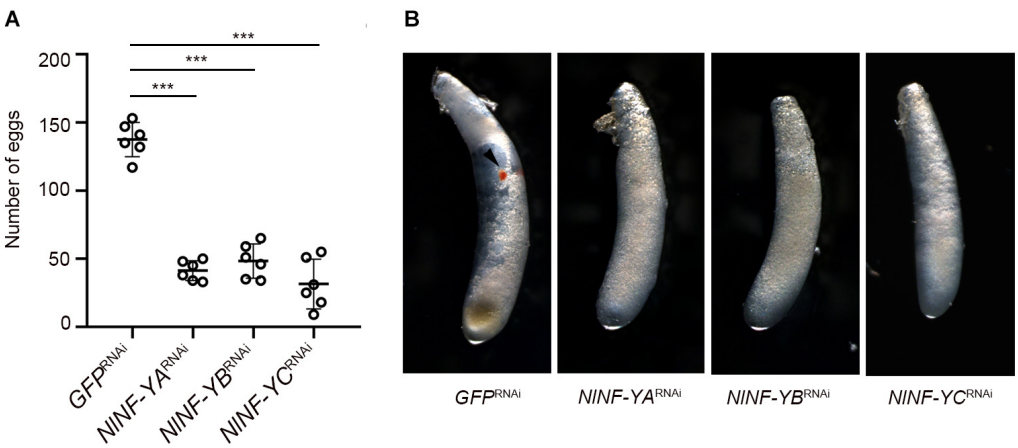

FIGURE 8 | Fecundity of adults with gene knockdown and phenotype of eggs produced. **(A)** Newly emerged adults (0–12 hAE) were treated with dsRNAs targeting each gene. The dsRNA-treated females and males were allowed to mate and laid eggs for 5 days. Each circle represents eggs produced by an individual female (n = 6). Bars represent the mean ± s.d. Statistical comparisons between two groups were performed using a two-tailed Student's t-test (***$P < 0.001$). **(B)** Morphology of eggs deposited after 5 days by dsRNA-treated BPHs. The eye pigmentation is indicated by an arrow head.

depleting *NlNF-YA*, *NlNF-YB*, and *NlNF-YC* delayed fifth-instar development and led to high lethality, indicating that the CCAAT box might also be a common cis-acting element in the BPH. In addition, we noticed that depletion either *NlNF-YA*, *NlNF-YB*, or *NlNF-YC* led to small and malformed forewings and hindwings. As a wing-dimorphic insect, fifth-instar BPH nymphs have the ability to develop into either short-winged or long-winged adults. A recent finding showed that cells of short wing pads are largely in the G2/M phase of the cell cycle, whereas those of long wings are largely in G1, indicating that cell cycle progression is necessary for wing morph determination (Lin et al., 2020). These observations are in line with previous reports that cell cycle-related genes are the main target genes of NF-Y (Zwicker et al., 1995; Bolognese et al., 1999; Farina et al., 1999; Kao et al., 1999; Korner et al., 2001; Manni et al., 2001). In addition, the depletion of *NlNF-Y* not only affected wing size, but also led to an IFM defect, the latter tissue is only present in long-winged adults. Based on these events, we speculate that NF-Y might be tightly involved in regulating alternative wing morphs in the BPH although this needs to be further confirmed experimentally.

It is of interest that the depletion of *NlNF-YA* significantly decreased the adult molting rate, and this defect could be partially rescued by the addition of 20E. In addition, the depletion of *Nl*NF-YA significantly reduced the expression levels of *NlE74A* and *NlE75B*, the downstream genes of the ecdysone pathway. These findings indicated that *Nl*NF-Y might affect the ecdysone pathway although the underlying mechanism remains unknown.

Although there remains much to be done, our findings provided a first glimpse of the function of NF-Y in hemipteran insects.

DATA AVAILABILITY STATEMENT

The original contributions presented in the study are included in the article/**Supplementary Material**, further inquiries can be directed to the corresponding author.

AUTHOR CONTRIBUTIONS

H-HC and H-JX designed the experiment and wrote the manuscript. H-HC, Y-LL, X-YL, and J-LZ conducted the experiments. H-JX managed and directed the project. All authors contributed to the article and approved the submitted version.

ACKNOWLEDGMENTS

This work was supported by the National Natural Science Foundation of China (31772158 and 31972261), and the National Natural Science Foundation of China for Excellent Young Scholars (31522047). The authors declare that they have no competing interest. We thank the International Science Editing company for polishing this manuscript.

SUPPLEMENTARY MATERIAL

The Supplementary Material for this article can be found online at: https://www.frontiersin.org/articles/10.3389/fgene.2020.585320/full#supplementary-material

Supplementary Table 1 | Primers used in this study.

REFERENCES

Backus, E. A., Serrano, M. S., and Ranger, C. M. (2005). Mechanisms of hopperburn: an overview of insect taxonomy, behavior, and physiology. *Annu. Rev. Entomol.* 50, 125–151. doi: 10.1146/annurev.ento.49.061802.123310

Bhattacharya, A., Deng, J. M., Zhang, Z., Behringer, R., de Crombrugghe, B., and Maity, S. N. (2003). The B subunit of the CCAAT box binding transcription factor complex (CBF/NF-Y) is essential for early mouse development and cell proliferation. *Cancer Res.* 63, 8167–8172.

Bi, W., Wu, L., Coustry, F., de Crombrugghe, B., and Maity, S. N. (1997). DNA binding specificity of the CCAAT-binding factor CBF/NF-Y. *J. Biol. Chem.* 272, 26562–26572. doi: 10.1074/jbc.272.42.26562

Bolognese, F., Wasner, M., Dohna, C. L., Gurtner, A., Muller, H., Manni, I., et al. (1999). The cyclin B2 promoter depends on NF-Y, a trimer whose CCAAT-binding activity is cell-cycle regulated. *Oncogene* 18, 1845–1853. doi: 10.1038/sj.onc.1202494

Dorn, A., Bollekens, J., Staub, A., Benoist, C., and Mathis, D. (1987). A multiplicity of CCAAT box-binding proteins. *Cell* 50, 863–872. doi: 10.1016/0092-8674(87)90513-7

Dubrovsky, E. B. (2005). Hormonal cross talk in insect development. *Trands Endocrino. Metab.* 16, 6–11. doi: 10.1016/j.tem.2004.11.003

Farina, A., Manni, I., Fontemaggi, G., Tlainen, M., Cenciarelli, C., Bellorini, M., et al. (1999). Down-regulation of cyclin B1 gene transcription in terminally differentiated skeletal muscle cells is associated with loss of functional CCAAT-binding NF-Y complex. *Oncogene* 18, 2818–2827. doi: 10.1038/sj.onc.1202472

Gilbert, L. I., Rybczynski, R., and Warren, J. T. (2002). Control and biochemical nature of the ecdysteroidogenic pathway. *Annu. Rev. Entomol.* 47, 883–916. doi: 10.1146/annurev.ento.47.091201.145302

Gurtner, A., Manni, I., Fuschi, P., Mantovani, R., Guadagni, F., Sacchi, A., et al. (2003). Requirement for down-regulation of the CCAAT-binding activity of the NF-Y transcription factor during skeletal muscle differentiation. *Mol. Biol. Cell.* 14, 2706–2715. doi: 10.1091/mbc.e02-09-0600

Kao, C. Y., Tanimoto, A., Arima, N., Sasaguri, Y., and Padmanabhan, R. (1999). Transactivation of the human cdc2 promoter by adenovirus E1A. *E*1A induces the expression and assembly of a heteromeric complex consisting of the CCAAT box binding factor, CBF/NF-Y, and a 110-kDa DNA-binding protein. *J. Biol. Chem.* 274, 23043–23051. doi: 10.1074/jbc.274.33.23043

Korner, K., Jerome, V., Schmidt, T., and Muller, R. (2001). Cell cycle regulation of the murine cdc25B promoter: essential role for nuclear factor-Y and a proximal repressor element. *J. Biol. Chem.* 276, 9662–9669. doi: 10.1074/jbc.M008696200

Kumar, S., Stecher, G., and Tamura, K. (2016). MEGA7: molecular evolutionary genetics analysis version 7.0 for bigger datasets. *Mol. Biol. Evol.* 33, 1870–1874. doi: 10.1093/molbev/msw054

Laloum, T., De Mita, S., Gamas, P., Baudin, M., and Niebel, A. (2013). CCAAT-box binding transcription factors in plants: Y so many? *Trends Plant Sci.* 18, 157–166. doi: 10.1016/j.tplants.2012.07.004

Li, G., Zhao, H., Wang, L., Wang, Y., Guo, X., and Xu, B. (2018). The animal nuclear factor Y: an enigmatic and important heterotrimeric transcription factor. *Am. J. Cancer Res.* 8, 1106–1125.

Li, X. Y., Mantovani, R., Hooft van Huijsduijnen, R., Andre, I., Benoist, C., and Mathis, D. (1992). Evolutionary variation of the CCAAT-binding transcription factor NF-Y. *Nucleic Acids Res.* 20, 1087–1091. doi: 10.1093/nar/20.5.1087

Lin, X., Gao, H., Xu, Y., Zhang, Y., Li, Y., Lavine, M. D., et al. (2020). Cell cycle progression determine wing morph in the polyphenic insect *Nilaparvata lugens*. *iScience* 23:101040. doi: 10.1016/j.isci.2020.101040

Livak, K. J., and Schmittgen, T. D. (2001). Analysis of relative gene expression data using real-time quantitative PCR and the $2-\Delta\Delta CT$ method. *Methods* 25, 402–408. doi: 10.1006/meth.2001.1262

Ly, L. L., Suyari, O., Yoshioka, Y., Tue, N. T., Yoshida, H., and Yamaguchi, M. (2013). dNF-YB plays dual roles in cell death and cell differentiation during Drosophila eye development. *Gene* 520, 106–118. doi: 10.1016/j.gene.2013.02.036

Manni, I., Mazzaro, G., Gurtner, A., Mantovani, R., Haugwitz, U., Krause, K., et al. (2001). NF-Y mediates the transcriptional inhibition of the cyclin B1, cyclin B2, and cdc25C promoters upon induced G2 arrest. *J. Biol. Chem.* 276, 5570–5576. doi: 10.1074/jbc.M006052200

Mantovani, R. (1998). A survey of 178 NF-Y binding CCAAT boxes. *Nucleic. Acids Res.* 26, 1135–1143. doi: 10.1093/nar/26.5.1135

Mantovani, R. (1999). The molecular biology of the CCAAT-binding factor NF-Y. *Gene* 239, 15–27. doi: 10.1016/s0378-1119(99)00368-6

McNabb, D. S., Xing, Y., and Guarente, L. (1995). Cloning of yeast HAP5: a novel subunit of a heterotrimeric complex required for CCAAT binding. *Genes Dev.* 9, 47–58. doi: 10.1101/gad.9.1.47

Otuka, A. (2013). Migration of rice planthoppers and their vectored re-emerging and novel rice viruses in East Asia. *Front. Microbiol.* 4:309. doi: 10.3389/fmicb.2013.00309

Sinha, S., Lu, J., Maity, S. N., and de Crombrugghe, B. (1995). Recombinant rat CBF-C, the third subunit of CBF-NFY, allows formation of a protein-DNA complex with CBF-A and CBF-B and with yeast HAP2 and HAP3. *Proc. Natl. Acad. Sci. U.S.A.* 92, 1624–1628. doi: 10.1073/pnas.92.5.1624

Suzuki, Y., Tsunoda, T., Sese, J., Taira, H., Mizushima-Sugano, J., Hata, H., et al. (2001). Identification and characterization of the potential promoter regions of 1031 kinds of human genes. *Genome Res.* 11, 677–684. doi: 10.1101/gr.gr-1640r

Wu, J., Ge, L., Liu, F., Song, Q., and Stanley, D. (2020). Pesticide-induced planthopper population resurgence in rice cropping system. *Annu. Rev. Entomol.* 65, 409–429. doi: 10.1146/annurev-ento-011019-025215

Xu, H. J., Chen, T., Ma, X. F., Xue, J., Pan, P. L., Zhang, X. C., et al. (2013). Genome-wide screening for components of small interfering RNA (siRNA) and micro-RNA (miRNA) pathways in the brown planthopper, *Nilaparvata lugens* (Hemiptera: Delphacidae). *Insect Mol. Biol.* 22, 635–647. doi: 10.1111/imb.12051

Xu, H. J., Xue, J., Lu, B., Zhang, X. C., Zhuo, J. C., He, S. F., et al. (2015). Two insulin receptors determine alternative wing morphs in planthoppers. *Nature* 519, 464–467. doi: 10.1038/nature14286

Xu, H. J., and Zhang, C. X. (2017). Insulin receptors and wing dimorphism in rice planthoppers. *Philos. Trans. R. Soc. Lond B Biol. Sci.* 372:20150489. doi: 10.1098/rstb.2015.0489

Xue, J., Zhang, X. Q., Xu, H. J., Fan, H. W., Huang, H. J., Ma, X. F., et al. (2013). Molecular characterization of the flightin gene in the wing-dimorphic planthopper, *Nilaparvata lugens*, and its evolution in Pancrustacea. *Insect Biochem. Mol. Biol.* 43, 433–443. doi: 10.1016/j.ibmb.2013.02.006

Xue, J., Zhou, X., Zhang, C. X., Yu, L. L., Fan, H. W., Wang, Z., et al. (2014). Genomes of the rice pest brown planthopper and its endosymbionts reveal complex complementary contributions for host adaptation. *Genome Biol.* 15:521. doi: 10.1186/s13059-014-0521-0

Xue, W. H., Liu, Y. L., Jiang, Y. Q., He, S. F., Wang, Q. Q., Yang, Z. N., et al. (2018). CRISPR/Cas9-mediated knockout of two eye pigmentation genes in the brown planthopper, *Nilaparvata lugens* (Hemiptera: Delphacidae). *Insect Biochem. Mol. Biol.* 93, 19–26. doi: 10.1016/j.ibmb.2017.12.003

Yoshioka, Y., Suyari, O., Yamada, M., Ohno, K., Hayashi, Y., and Yamaguchi, M. (2007). Complex interference in the eye developmental pathway by *Drosophila* NF-YA. *Genesis* 45, 21–31. doi: 10.1002/dvg.20260

Yuan, M., Lu, Y., Zhu, X., Wan, H., Shakeel, M., Zhan, S., et al. (2014). Selection and evaluation of potential reference genes for gene expression analysis in the brown planthopper, *Nilaparvata lugens* (Hemiptera: Delphacidae) using reverse-transcription quantitative PCR. *PLoS One* 9:e86503. doi: 10.1371/journal.pone.0086503

Zhang, C. X., Brisson, J. A., and Xu, H. J. (2019). Molecular mechanisms of wing polymorphism in insects. *Annu. Rev. Entomol.* 64, 297–314. doi: 10.1146/annurev-ento-011118-112448

Zwicker, J., Lucibello, F. C., Wolfraim, L. A., Gross, C., Truss, M., Engeland, K., et al. (1995). Cell cycle regulation of the cyclin A, cdc25C and cdc2 genes is based on a common mechanism of transcriptional repression. *EMBO J.* 14, 4514–4522. doi: 10.1002/j.1460-2075.1995.tb00130.x

Conflict of Interest: The authors declare that the research was conducted in the absence of any commercial or financial relationships that could be construed as a potential conflict of interest.

frontiers in Genetics

ORIGINAL RESEARCH
published: 17 December 2020
doi: 10.3389/fgene.2020.566961

Genetic Mapping of Climbing and Mimicry: Two Behavioral Traits Degraded During Silkworm Domestication

Man Wang[1†], Yongjian Lin[1†], Shiyi Zhou[1], Yong Cui[1], Qili Feng[1], Wei Yan[2] and Hui Xiang[1*]*

[1] Guangdong Provincial Key Laboratory of Insect Developmental Biology and Applied Technology, Institute of Insect Science and Technology, School of Life Sciences, South China Normal University, Guangzhou, China, [2] Guangdong Provincial Key Laboratory of Biotechnology for Plant Development, School of Life Sciences, South China Normal University, Guangzhou, China

OPEN ACCESS

Edited by:
Subba Reddy Palli,
University of Kentucky, United States

Reviewed by:
Min-Jin Han,
Center for Studies of Education and Psychology of Minorities in Southwest China, Southwest University, China
Quanyou Yu,
Chongqing University, China
Fangyin Dai,
Southwest University, China

***Correspondence:**
Hui Xiang
xiang_shine@foxmail.com
Wei Yan
yanwei_bio@126.com

[†] These authors have contributed equally to this work

Specialty section:
This article was submitted to Epigenomics and Epigenetics, a section of the journal Frontiers in Genetics

Received: 29 May 2020
Accepted: 17 November 2020
Published: 17 December 2020

Citation:
Wang M, Lin Y, Zhou S, Cui Y, Feng Q, Yan W and Xiang H (2020) Genetic Mapping of Climbing and Mimicry: Two Behavioral Traits Degraded During Silkworm Domestication. Front. Genet. 11:566961. doi: 10.3389/fgene.2020.566961

Behavioral changes caused by domestication in animals are an important issue in evolutionary biology. The silkworm, *Bombyx mori*, is an ideal fully domesticated insect model for studying both convergent domestication and behavior evolution. We explored the genetic basis of climbing for foraging and mimicry, two degraded behaviors during silkworm domestication, in combination of bulked segregant analysis (BSA) and selection sweep screening. One candidate gene, *ASNA1*, located in the 3–5 Mb on chromosome 19, harboring a specific non-synonymous mutation in domestic silkworm, might be involved in climbing ability. This mutation was under positive selection in Lepidoptera, strongly suggesting its potential function in silkworm domestication. Nine candidate domesticated genes related to mimicry were identified on chromosomes 13, 21, and 27. Most of the candidate domesticated genes were generally expressed at higher levels in the brain of the wild silkworm. This study provides valuable information for deciphering the molecular basis of behavioral changes associated with silkworm domestication.

Keywords: *Bombyx mori*, behavioral domestication, climbing, mimicry, bulked segregant analysis, selection sweep screening

INTRODUCTION

Compared with wild animals, domestic animals showed typical behavioral adaptation to artificial selection. Reduced fear of humans and increased tolerance to artificial stresses are two earliest and most important adaptations in animals. Artificial selection can reduce the effects of natural selection of animals, for example, foraging ability and predator avoidance (Solberg et al., 2020). Domesticated behaviors shared in disparate animals are considered as "domestication syndrome" (Wilkins et al., 2014). Deciphering the genetic basis of domesticated behaviors will improve the understanding of animal domestication. The developments of high-throughput sequencing and evolutionary genomics have greatly accelerated the reverse genetic studies on morphological traits in mammals and poultries (Frantz et al., 2015; Qiu et al., 2015; Pendleton et al., 2018; Zhang et al., 2018). However, behavioral traits are more difficult to assay than morphological traits in animals.

Mapping behavior-related loci in animals is largely hampered by the difficulties in constructing mapping populations and phenotype investigation.

During the breeding of silkworm, many behavioral and morphological traits have been domesticated. Domesticated genes and pathways involved in the nervous system in silkworm were also found in other animals, suggesting the "domestication syndrome" in silkworm (Xiang et al., 2018). The larval locomotion, especially the climbing for foraging ability, has been largely decreased in the domestic silkworm. Notably, the domestic silkworm has the greatest potential to climb at the wandering stage or been infected by baculovirus, indicating possible correlations with the nervous system (Kamita et al., 2005; Feiguin et al., 2009). Another novel adapted behavior in the domestic silkworm is the loss of larval mimicry response to exogenous stimulus. Usually, the wild silkworm larva at the end of instar stretches its body and holds tightly to imitate a mulberry branch immediately in response to exogenous stimulus. The climbing and mimicry abilities are essential for foraging and predator avoidance in the wild silkworm and other wild insects (Garrouste et al., 2016). However, the genetic basis for these two interesting behavioral traits is still unclear. Benefit from the high-throughput sequencing-based bulked segregant analysis (BSA), the trait-related loci can be identified rapidly using individuals with extreme phenotypes in a mapping population (Takagi et al., 2013; Zegeye et al., 2018; Liu et al., 2019). The feasible construction of mapping population between the wild silkworm and the domestic silkworm also enables the identification of domestic behavior-related loci in silkworm.

In this study, the two domestic behaviors, climbing for foraging and mimicry, were carefully observed in the mapping population between the wild silkworm and the domestic silkworm. Individuals showing fully loss of climbing ability for foraging or mimicry response were selected for bulked re-sequencing and compared with both parents and individuals with extreme climbing ability and mimicry response. Candidate genes related to these two behaviors were identified through BSA analysis, combined with selection sweep screening and estimation of expression patterns of domesticated genes in candidate region(s). This study provides an efficient method to illustrate the potential genetic basis related to behavioral evolution during silkworm domestication. Further study on behavior-related genes will provide important clues for understanding the genomic evolution of behavioral adaptation under artificial selection in animals.

MATERIALS AND METHODS

Construction of Mapping Population

The wild silkworm with climbing ability and mimicry response and the domestic silkworm P50 strain loss of these two characters were collected from a wild field in Zhejiang Province and maintained as indoor populations. The wild female moth with larger body and weaker flying ability was crossed with the domestic moth P50 (male) to generate the F1 generation. Then, the F1 (male) was backcrossed with the domestic moth P50 strain (female) to generate the BC1 mapping population. Climbing and mimicry behaviors were carefully observed in both F1 and BC1 generations. All the silkworms were fed at 27°C and 70% humidity.

Phenotypic Assay and Establishment of Segregation Groups

To examine the climbing ability, the BC1 individuals (∼200) were fed in boxes (with insufficient mulberry leaves) under mulberry seedlings at the beginning of the 5th instar for ∼7 days. Individuals with strong climbing ability could climb up ∼50 cm to the mulberry seedlings for foraging. Those climbed up to the branches were put back to the box for repeated observation (at least 3 times/day). Individuals that consistently climb or stay in boxes were considered as individuals with extreme distinct phenotypes in the segregation population and selected for bulked sequencing. We also observed individuals with white or dark body in both segregation groups. Therefore, four independent sets of different larval body colors were generated for re-sequencing, i.e., white body with climbing ability, white body loss of climbing ability, dark body with climbing ability, and dark body loss of climbing ability, 20 individuals for each set.

To estimate the mimicry traits, the BC1 individuals (∼200) were fed on mulberry branches. Then, the branches were shaken artificially to observe the mimicry response. Those extended their head and chest to simulate the dendrite shape and maintained for at least 10 s were considered as extreme mimic individuals (**Supplementary Video 1**). Those showed mimicry response were also verified by hand touch (**Supplementary Video 2**). On the contrary, individuals that kept eating even when touched by hand were considered as extreme non-mimic individuals (**Supplementary Video 3**). Eventually, 18 individuals with strong mimicry response and 20 non-mimicry individuals were selected for re-sequencing, respectively.

DNA Extraction and Sequencing

The total DNA was extracted for each individual using a traditional phenol–chloroform DNA extraction protocol and quantified by NanoDrop 2000 (Thermo). Equal quantity (1.5 μg) DNA of each individual in each set was pooled to obtain bulked DNA for sequencing on the Illumina Hiseq 4000 platform (PE150, with insert size around 350 bp). The sequencing libraries were constructed according to the manufacturer's instructions. In addition, both the wild silkworm (P_Wild) and the domestic silkworm (P_P50) were sequenced for comparison.

Sequence Alignment and SNP/InDel Calling

The reference genome of domestic silkworm was downloaded from the Silkbase[1]. The re-sequencing short reads of each bulk were aligned to the reference genome with BWA (Burrows–Wheeler Aligner) (-t 4 -k 32 -M -R) (Li and Durbin, 2009). Alignment files were converted to BAM files using the SAMtools software (-bS -t) (Li et al., 2009). Potential PCR

[1]http://sgp.dna.affrc.go.jp/ComprehensiveGeneSet/

duplications were excluded using the rmdup in SAMtools. If multiple read pairs were mapped to identical coordinates, only the pair with the highest mapping quality was retained. Reliable genome-wide single-nucleotide polymorphisms (SNPs) and insertions/deletions (InDels) were identified with the Unified Genotyper function in GATK (–filterExpression "QD < 4.0 || FS > 60.0 || MQ < 40.0," -G_filter "GQ < 20," –cluster WindowSize 4) (McKenna et al., 2010). InDels were further filtered with the Variant Filtration parameter (–filter Expression "QD < 4.0 || FS > 200.0 || Read PosRankSum < −20.0 || Inbreeding Coeff < −0.8 "). ANNOVAR was used to annotate SNP or InDel based on the GFF3 files of the reference genome (Wang et al., 2010). The gene models were derived from Xiang et al. (2018) that integrative assembled with GLEAN based on a combination of coding sequences from SilkDB, homology, and *ab initio* sets (AUGUSTUS, SNAP, and GENSCAN).

SNP/InDel Index Calculation

The homozygous SNPs/InDels between the two parents were extracted as markers for index calculation. Only SNPs/InDels covered by at least seven reads in both parents (∼1/3 of the sequencing depth of parents) were considered. The genotype of the P50 strain was used as the reference, and reads supporting the reference genotype or non-reference genotype were counted in each bulk. The SNP index and InDel index were calculated with reads supporting the non-reference genotype divided by the total reads in each sequenced bulk (Takagi et al., 2013). SNPs/InDels with depth < 7 in both segregation groups or missing in one group were excluded. The genome-wide SNP/InDel indexes were visualized in sliding window of 1 Mb with a step size of 10 kb. The average index of all the SNPs/InDels presented in each window was designated as the index of this window in each group. The ΔSNP/InDel index was calculated to represent the difference of index between the segregation groups, and 1,000 permutation tests were performed with 95% confidence level as threshold. The SNP/InDel index in each segregation group and the ΔSNP/InDel index were shown with ggplot package in RStudio.

Screening of Domestication Signature

Genes related to domesticated behaviors are usually under selection. Based on the published genome-wide SNPs of 137 domestic silkworm and 7 wild silkworm strains (Xiang et al., 2018), we calculated the selection signatures (*Fst* and π) of the chromosomes harboring the candidate regions related to climbing and mimicry to screen candidate domesticated genes as described previously (Zhu et al., 2019a). The allele frequency for each site was calculated with the reads supporting the reference genotype divided by the total covered reads. The effects of candidate SNPs were then estimated according to the annotation of the reference genome.

Evolution Analysis of the Candidate Genes Related to Climbing in Lepidoptera

The homologous sequences of candidate genes related to climbing were obtained using blastp against the NCBI database non-redundant nucleotide library[2] and the sequences of *Antheraea yamamai* in the GigaDB database[3] (Kim et al., 2018). Protein sequences with at least 80% identity in other insect genomes were downloaded for comparisons, including the five Lepidoptera species *A. yamamai*, *Danaus plexippus*, *Chilo suppressalis*, *Helicoverpa armigera*, and *Papilio machaon*. The downloaded protein sequences were aligned with ClustalW using default settings in MEGA 7 (Kumar et al., 2016). The minimum-evolution tree was constructed to show the evolution of candidate genes in all the collected insect genomes. Branch model (model = 0 and NSsites = 0 for one-ratio model, model = 2 and NSsites = 2 for two-ratio model) and branch-site model (model = 2, NSsites = 2) in PAML software (version 4.8) were used for phylogenetic analysis (Yang, 2007). The likelihood ratio test was used to estimate the fitness of different models.

Transcriptomic Analysis

RNA-seq data from different tissues of *B. mori* (5th instar day 3 larvae) were downloaded from the NCBI SRA database[4]. The accession numbers are SRR4425245 (ovary), SRR4425244 (testis), SRR4425250 (brain), SRR4425254 (anterior silk gland), SRR4425258 (middle silk gland), SRR4425260 (posterior silk gland), DRR095110 (midgut), SRR4425248 (fat body), SRR7812745 (integument), and DRR095113 (malpighian tubule). Reads were mapped to the silkworm reference genome with TopHat2 (Kim et al., 2013), and the expression levels (FPKM) were further determined with Resm (Li and Dewey, 2011). The expression heatmaps were constructed with normalized Z-scores on the OmicShare online platform[5].

We also sequenced the RNA of the brains of both parents at three key larval stages (middle larval stage, late larval stage, and wandering stage) to estimate the expression levels of candidate genes related to climbing and mimicry, three replicates for each sample. Reads were mapped to the reference genome of *B. mori* with TopHat2 (Kim et al., 2013). The expression levels (FPKM) of genes were further calculated with Cuffdiff (Trapnell et al., 2012). The expression heatmaps were constructed as described above. We also normalized the FPKM of each candidate gene according to the total numbers of sequencing depth of the corresponding samples, and Student's *t*-test was imported for estimation of the expression differences between wild silkworm and domestic silkworm.

RESULTS

Inheritance of Climbing and Mimicry Behaviors

The wild female moth with larger body and weaker flying ability was crossed with the domestic silkworm P50 strain (male) to generate the F1 generation (**Figures 1A–C**). Interestingly, all of the individuals in the F1 generation showed a strong

[2]https://blast.ncbi.nlm.nih.gov/Blast.cgi

[3]http://gigadb.org/dataset/100382

[4]https://www.ncbi.nlm.nih.gov/sra/

[5]https://www.omicshare.com/

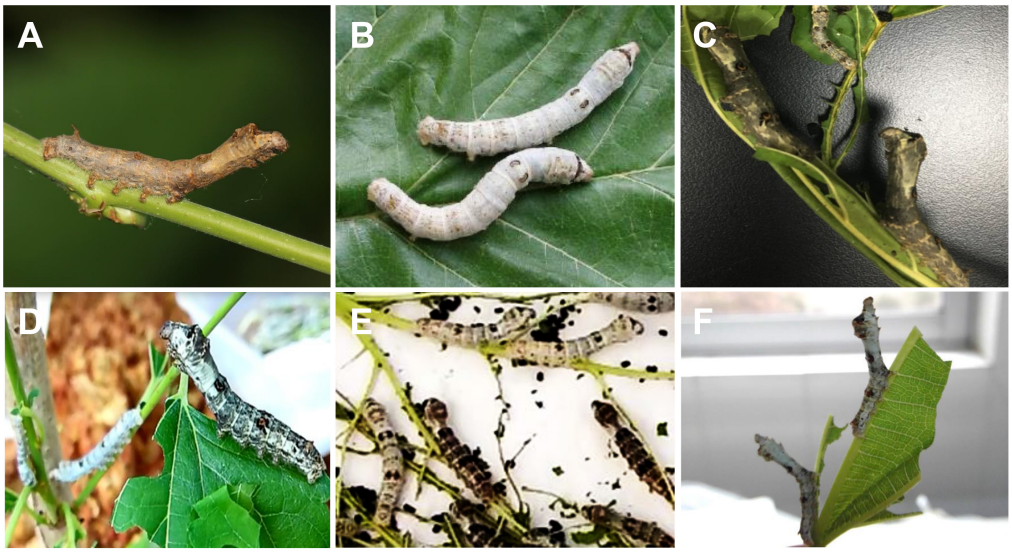

FIGURE 1 | Larvae of the wild silkworm, the domestic silkworms, and the hybrid populations. **(A)** The wild silkworm with the ability of climbing and mimicry. **(B)** The domestic silkworm unable to climb for foraging and mimicry. **(C)** F1 hybrids of the wild silkworm and the domestic silkworm. **(D)** Individuals with climbing ability. **(E)** Individuals unable to climb. Individuals with white or dark body color are observed in both the two segregation groups. **(F)** Backcrossed individuals with typical mimicry response.

ability of climbing and mimicry response, indicating that these two behaviors were dominant. The F1 was then backcrossed with the recessive parent (the domestic silkworm P50 strain) to generate the BC1 populations. Both climbing for foraging and mimicry response were segregated in the BC1 populations (**Supplementary Videos 1–3**). Individuals in BC1 with stronger climbing ability could climb up to over 50 cm from the foot of the mulberry seedling. We also found that the climbing ability for foraging was not linked to the body color (**Figures 1D,E**), i.e., individuals with strong climbing ability were detected in both individuals of white and dark bodies. Individuals in BC1 with strong ability to mimic could response to artificial shake and hand touch promptly and maintain for at least 10 s (**Figure 1F** and **Supplementary Videos 1, 2**). Those unable to mimic showed no response to artificial shaking and hand touching (**Supplementary Video 3**).

BSA to Identify the Candidate Region Related to Climbing Behavior

Because the body color was not linked to the climbing for foraging behavior, we therefore generated four bulks to identify the candidate region related to climbing, i.e., white body with climbing ability, dark body with climbing ability, white body unable to climb, and dark body unable to climb (**Figures 1D,E** and **Supplementary Table S1**). In total, 14.7–18.2 Gb data were obtained for the four bulks (**Supplementary Table S1**). The clean reads were mapped to the reference genome for SNP and InDel calling as described in "Materials and Methods" section. More than 93.34% clean reads could be aligned properly, covering 28–34 × of the reference genome in depth (**Supplementary Table S1**). The two parents, the wild silkworm (P_Wild) and the domestic silkworm P50 (P_P50), were also sequenced to 10.9 Gb (20.39 × in depth) and 10.0 Gb (21.08 × in depth) for comparison, respectively (**Supplementary Table S1**). Only SNPs/InDels with homozygous genotypes in both parents were extracted as markers for further analyses, resulting in 7,142,097 SNPs and 346,910 InDels in the white set and 7,063,453 SNPs and 340,067 InDels in the dark set, respectively.

To identify the candidate loci related to climbing, the genotypes of the parent P_P50 were used as reference for calculating the SNP/InDel index in sequenced bulks. If all short reads covering one position are identical to the genotype of P_P50, the SNP/InDel index will be 0. In contrast, if all of the short reads support a different genotype from the reference, the SNP/InDel index will be 1. The ΔSNP/InDel index was also calculated to represent the index differences between the climbing ability bulks and the non-climbing ability bulks. Ideally, the candidate loci related to climbing behavior are expected to be heterozygous, and the ΔSNP/InDel index should be 0.5. The candidate region will be outstanding in the ΔSNP/InDel index due to the strong linkages between closely linked SNPs/InDels with the causal mutation.

In comparison of the climbing and non-climbing bulks of white body, two candidate peaks located on chromosomes 14 and 19 were identified (**Figure 2A**, **Supplementary Figure S1**, and **Supplementary Data**). The peak on chromosome 19 nearly reached the 95% confidence interval. Interestingly, this peak was also detected in the comparison of climbing and non-climbing bulks of dark body (**Figure 2B**, **Supplementary Figure S2**, and **Supplementary Data**), indicating a strong linkage to the climbing behavior. By overlapping the SNPs/InDels with high index in both sets, the candidate region could be

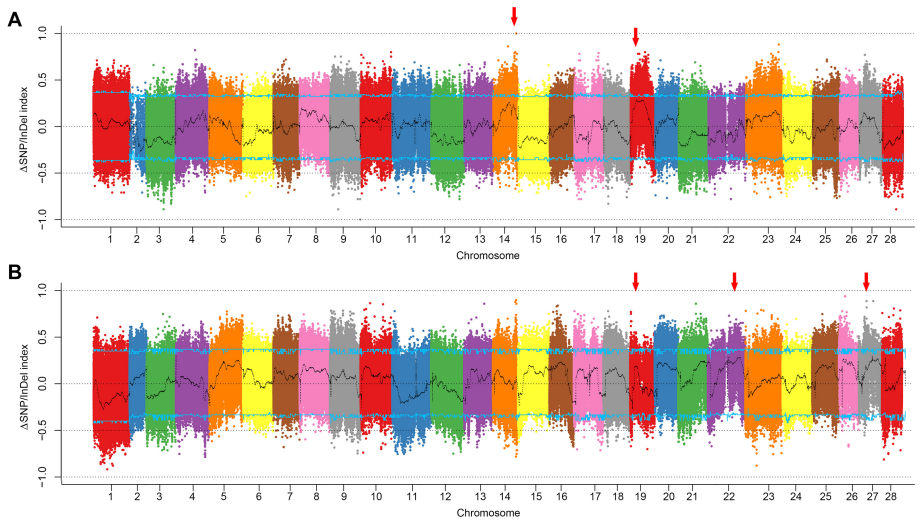

FIGURE 2 | Plotting of ΔSNP/InDel index of the climbing and non-climbing bulks. **(A)** White body color set. **(B)** Dark body color set. Curves in black are indexes calculated with 1 Mb sliding window with 10 kb step size. Blue lines indicate the cutoff of 95% confidence interval. Red arrows indicate the candidate regions for climbing.

roughly narrowed down to 3–5 Mb interval on chromosome 19 (**Figures 3A,B**).

Identification of Candidate Domesticated Genes Related to Climbing by Selective Sweep Screening

Considering the possible sequencing bias and errors that occurred in the candidate region, we extended the candidate region on 1–5 Mb on chromosome 19 for the identification of candidate domesticated genes related to climbing. We screened the selective sweep of domestication signatures in this region to discover candidate domesticated genes as described in "Materials and Methods" section (**Figure 3C**). As expected, strong selective sweep signatures were found in this region, especially in 3.7–4 Mb, in which four candidate domesticated genes were identified (**Figures 3A–C**). These four candidate domesticated genes were annotated as fanconi-associated nuclease 1-like (*FAN1*), GPI ethanolamine phosphate transferase 3 (*Pigo*), ATPase ASNA1 homolog (*ASNA1*), and uncharacterized protein, respectively (**Supplementary Table S2**). These four genes showed remarkable higher *Fst* and extremely lower π in the domestic silkworm than in the wild silkworm (**Figures 3C,D**). In the Silkworm Genome Informatics Database (SGID) (Zhu et al., 2019b), *FAN1*, *Pigo*, and *ASNA1* were possibly under positive selection (**Supplementary Table S2**). Consistently, the allele frequencies in this region were also quite different between the domestic silkworm and the wild silkworm, with nearly fixed alleles in the domestic silkworm population (**Figure 4A** and **Supplementary Figure S3**). Interestingly, non-synonymous variations divergent in allele frequency between the domestic and the wild silkworm were identified in the coding regions of *FAN1*, *Pigo*, and *ASNA1* (**Figure 4A** and **Supplementary Figure S3**). To further explore the potential significance of these non-synonymous variations, the homologous protein sequences in 5 Lepidoptera species and 62 other insect species were collected for comparative analysis. We found that only the non-synonymous variation on the ATPase ASNA1 was specific in the domestic silkworm, causing glycine (G) to aspartic acid (D) conversion at residue 115 (**Figures 4B,C** and **Supplementary Figures S4, S5**). This variation also appeared to be positively selected in the domestic silkworm clade, as detected in PAML analyses ($p < 0.0001$ using the branch-site model and $p = 0.06$ using the branch model) (**Figure 4D**). Of the 68 collected species, *ASNA1* was a single copy gene in *B. mori* and *B. mandarina* and possibly two copies in only four species (**Supplementary Figure S4**). The amino acids affected by the non-synonymous variations identified on FAN1 ($G_{105}D$ and $D_{155}E$) and Pigo ($K_{108}E$ and $I_{463}V$) were common between *B. mori*, *B. mandarina*, and some of the other Lepidoptera species, suggesting that these variations were not correlated with the loss of climbing ability in domestic silkworm (**Supplementary Figure S6**).

Mapping of Mimicry-Related Loci by BSA Analysis and Selective Sweep Screening

To identify candidate regions related to the mimicry phenotype, individuals with/without responses to artificial shaking or hand touching were collected and pooled separately for re-sequencing. The clean data covered about 32- and 37-fold of the reference genome in depth for mimicry and non-mimicry bulks, respectively (**Supplementary Table S1**). Compared with the genotypes of the recessive parent P_P50, there were 1,877,029 SNPs and 333,064 InDels retained for BSA. Candidate peaks related to the mimicry trait were detected in 13-17 Mb on chromosome 13, 10–14 Mb on chromosome 21, and 9–10 Mb on chromosome 27, respectively (**Figure 5** and

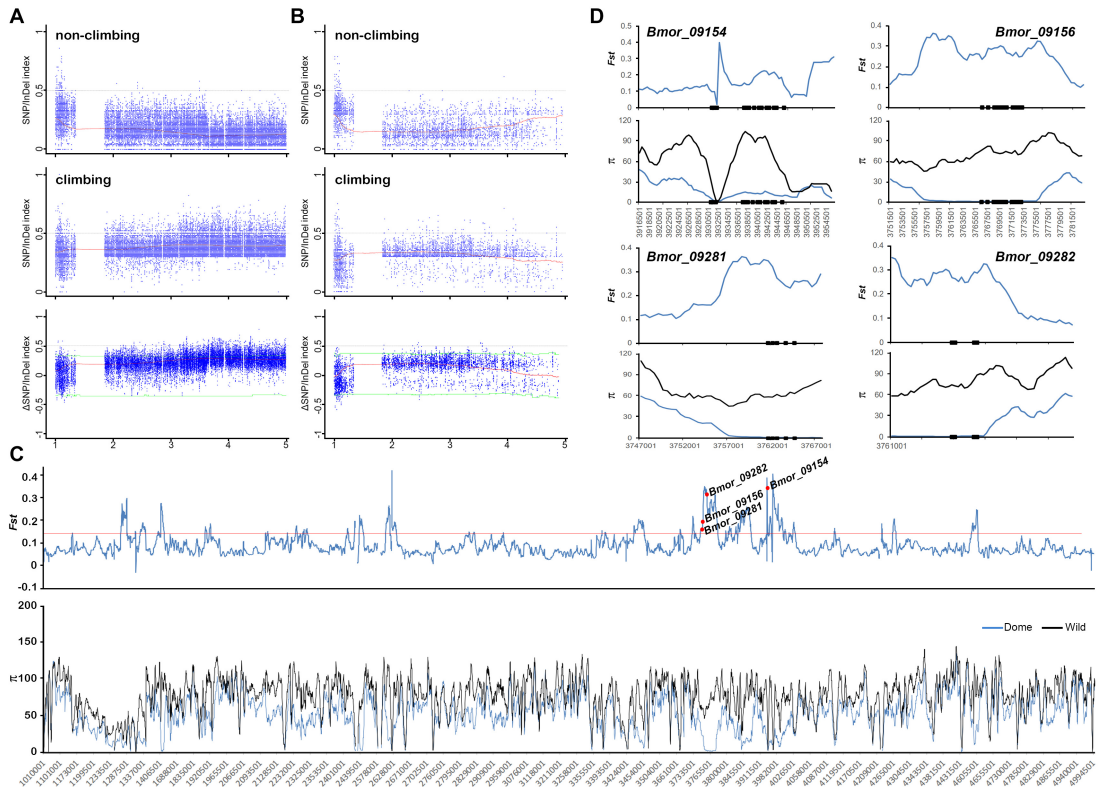

FIGURE 3 | Mapping of climbing-related loci through BSA analysis combined with selective sweep approaches. SNP/InDel index information of the candidate region (1–5 Mb on chromosome 19) detected by BSA in both the white color set **(A)** and the dark color set **(B)**. The first panel is the index in the group with climbing ability, and the second panel is the index in the group loss of climbing ability. The ΔSNP/InDel index shown in the third panel represents the difference of index between these two groups. Red curves indicate the index calculated with 1 Mb sliding window with 10 kb step size. Green lines indicate the cutoff of 95% confidence interval. **(C)** Selective sweep screening in the candidate region. Signature index, including population divergence coefficient (*Fst*) between the early domestic silkworm group and the wild silkworm group, and nucleic acid diversity (π) in the silkworm population are shown along the chromosome. Red line represents the top 5% *Fst* cutoff. The four domesticated genes are marked with red circles. Dome, domestic silkworm; Wild, wild silkworm. **(D)** Selection signatures of the four candidate domestication genes. The black blocks represent the genomic structure of corresponding genes.

Supplementary Figure S7). However, all the peaks were not beyond the 95% confidence interval, suggesting the difficulty of accurate mapping of behavior traits by BSA. Screening of the selective signatures resulted in 12 genes in total in these regions (**Figures 5B–D** and **Supplementary Table S2**). These genes were predicted to encode proteins with diverse functions, such as neuropeptide receptors, glycine receptor subunit alpha-4, transporters, kinase related genes, and TBC family member (**Supplementary Table S2**). Of these candidate genes, only six genes were predicted to be under positive selection in silkworm in SGID (**Supplementary Table S2**). The allele frequencies in these candidate genes were much higher in domestic silkworm than in wild silkworm (**Supplementary Figure S8**).

Tissue Expression Pattern of the Candidate Domestication Genes Potentially Related to Climbing and Mimicry

By investigating the published RNA-seq data of the domestic silkworm, we noticed that most of the candidate genes related to climbing for foraging and mimicry were expressed at higher levels in the brain than in the other tissues (**Figures 6A,B**), especially the mimicry-related candidate genes (**Figure 6B**). These patterns implied that the loci related to domesticated behaviors might primarily function in the brain. Therefore, we further compared the expression of these genes in the brain of the wild and domestic silkworms at three key larval developmental stages (middle larval stage, late larval stage, and wandering stage) as described in "Materials and Methods" section (**Figures 6C,D**). The expressions of *FAN1* and *Pigo* were higher in the wild silkworm than in the domestic silkworm but no significant differences in *ASNA1* (p = 0.2820 for middle larval stage brain, p = 0.2730 for late larval stage brain, and p = 0.1917 for wandering stage brain, respectively) (**Figure 6C** and **Supplementary Figure S9**). We also verified the expression levels of candidate genes related to mimicry in the brains of wild and domestic silkworms. It is interesting that most candidate genes related to mimicry except the three non-detected genes were generally expressed at higher levels in the brain of the wild silkworm (**Figure 6D** and **Supplementary Figure S9**).

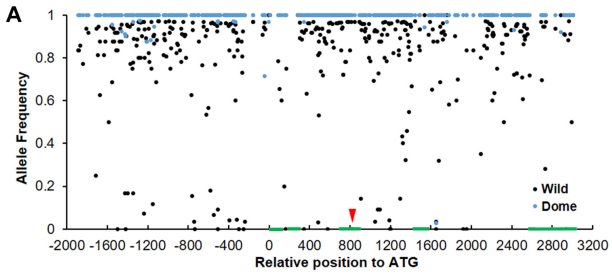

D

Model	ω0	ω1:ωback ground	2Δl	p-value
One ratio	0.0096	-	-	-
Two ratio	-	999. 0 : 0.009	3.490	0.06
2branchsite			55.256	0*

FIGURE 4 | SNP analysis of the candidate domesticated gene *Bmor_09281* (*ASNA1*) related to climbing ability. **(A)** Allele frequencies in the genetic region of *Bmor_09281* (*ASNA1*). Green blocks indicate the genomic structure of the genes. Red arrow shows the non-synonymous replacement in the domestic silkworm group compared with the wild silkworm group. Black dots and blue dots represent the allele frequencies in wild silkworm and domestic silkworm, respectively. **(B)** Predicted conserved domains in *ASNA1*. **(C)** Protein alignment of *ASNA1* with homologous collected from six other Lepidoptera species. The functional domain of *ASNA1* is shown in the top panel. Red arrow shows the non-synonymous replacement specific in the domestic silkworm. **(D)** Evolution analysis of *ASNA1* with PAML analysis. * significant fitness of the alternative model compared with the one ratio model using the likelihood ratio test.

DISCUSSION

In this study, we provided a novel example of behavioral domestication in silkworm. Degraded climbing for foraging and loss of mimicry in silkworm are attributed to tolerance to artificial condition and relaxation of natural selection. These behavior traits are usually designated as "domestication syndrome" (Wilkins et al., 2014). Particularly, mimicry is a special adaptive behavior formed over long-term evolution of insects in nature. We had observed that the larval wild silkworms occasionally mimicked the branch, by stretching their thorax and head and remaining still (**Figure 1A**).

Body color is another well documented morphological trait in "domestication syndrome" (Jensen, 2014). Associations between genes controlling pigmentation with behavior features have been reported in several domestic animals (Jensen, 2014). In the dog breed German shepherd, variation in attention and activity was reported to be associated with a polymorphism of tyrosine hydroxylase (*TH*), a key enzyme in the melanin synthesis pathway (Kubinyi et al., 2012). However, we found that the body color was not correlated to the climbing for foraging in the BC1 population. Therefore, two bulks with extreme phenotypes were generated for mapping the climbing behavior for both individuals with white and dark bodies. Comparisons between the candidate regions identified in bulks with different body colors efficiently narrowed the candidate region to chromosome 19.

Behavior is controlled by the interactions among neurons in their nervous systems (Haynes, 1988; Comer and Robertson, 2001). Genome-wide investigations consistently identified candidate domestication genes in the nervous systems that might be related to domestic behaviors (Schubert et al., 2014; Dong et al., 2015; Frantz et al., 2015; Qiu et al., 2015; Lawal et al., 2018; Pendleton et al., 2018; Xiang et al., 2018). Disability of climbing for foraging in the domestic silkworm might be attributed to the changes of the nervous system. Of the four candidate domesticated genes related to climbing loci that were identified (**Supplementary Table S2**), *FAN1* was reported to be associated with neurological disorders, such as schizophrenia (Li et al., 2012; Zhao et al., 2014; Segui et al., 2015). *FAN1* encodes a DNA repair nuclease that inhibits the progression of DNA replication forks and prevents chromosomal abnormalities, with endonuclease and exonuclease functions (Pizzolato et al., 2015; Lachaud et al., 2016). Variation of *FAN1* can lead to a series of psychiatric and neurodevelopmental phenotypes (Ionita-Laza et al., 2014). Glycosylphosphatidylinositol (GPI) ethanolamine phosphate transferase (*Pigo*) participates in glycosylphosphatidylinositol biosynthesis. Mutation of genes involved in GPI biosynthesis can induce hyperphosphatasia with mental retardation syndrome (Krawitz et al., 2012; Chiyonobu et al., 2014; Nakamura et al., 2014; Xue et al., 2016). *Pigo* encodes GPI ethanolamine phosphate transferase 3, catalyzing the final step of GPI-anchor synthesis. Mutations in *Pigo* caused epileptic encephalopathy and led to severe neurological impairment, dysmorphia, chorea, seizures, and early death (Freeze et al., 2012; Zehavi et al., 2017). *ASNA1* encodes an ATPase targeting tail-anchored protein that is versatile and important in various biological processes. In humans, mutations in *ASNA1* caused rapidly progressive pediatric cardiomyopathy (Verhagen et al., 2019) and might be related to early onset Parkinson's disease (Kun-Rodrigues et al., 2015). In comparisons with other Lepidoptera species, we found a non-synonymous variation specific to the domestic silkworm. This variation might be involved in the degraded climbing ability in the domestic silkworm. Although the function or biological significance of the four genes is still unknown in insects, evidence from mammals and particularly humans shed light on their roles in neural pathways. These genes were primarily expressed in the brain of the domestic silkworm. Functional verification in an insect model will be of great value.

The BSA-seq approaches in this study detected many relative weak peaks related to mimicry. Combination with selective sweep screening efficiently narrowed down the candidates. As expected,

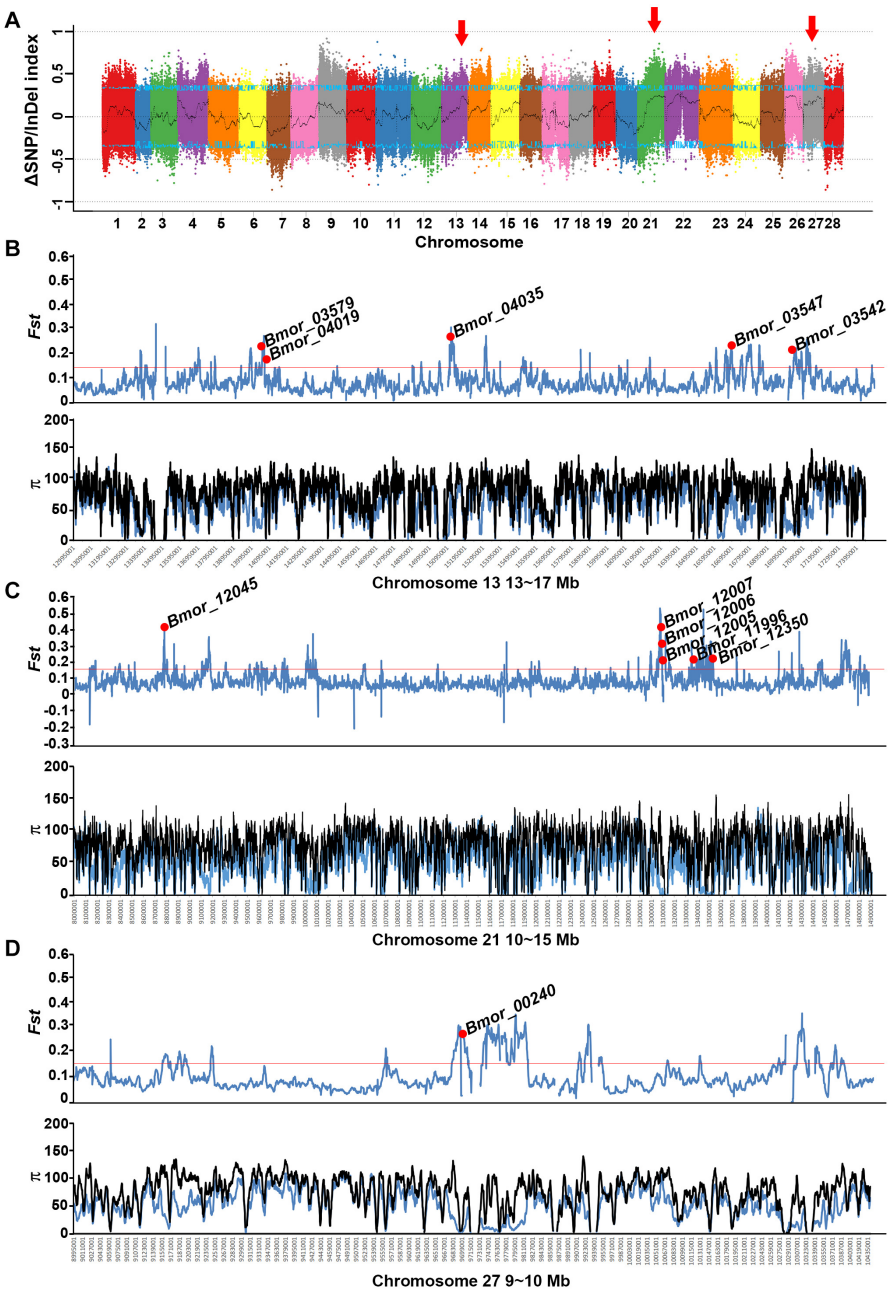

FIGURE 5 | Preliminary mapping of mimicry-related loci through BSA analysis combined with selective sweep approaches. **(A)** ΔSNP/InDel index of the mimicry and non-mimicry bulks. The candidate regions related to mimicry are marked with red arrows. **(B–D)** The selective sweep signatures in the three potential candidate regions located on chromosomes 13, 21, and 27. Black curves indicate the index calculated at 1 Mb sliding windows scale with 10 kb step size. Blue lines indicate the cutoff of 95% confidence interval. Red lines indicates 5% *Fst cutoff*.

many candidate genes related to mimicry were also involved in neural pathways. For example, neuropeptide receptors were reported to be facilitators of animal domestication (Herbeck and Gulevich, 2019). Glycine receptor subunit alpha-4 highly expressed in neural tissues might function in the regulation of neuronal activity in vertebrates (Wang and Slaughter, 2005). TBC family proteins are associated with the formation of multiple functional cilia and the growth of synapses in humans (Shi et al., 2018). In flies, pathogenic mutations of TBCs caused severe neurological defects (Fischer et al., 2016). These candidate genes were mostly highly expressed in the silkworm brain and higher expressed in the brain of the wild silkworm, suggesting the importance of neural pathways in larval mimicry of the wild silkworm. The findings of this study will be helpful for further exploration of insect climbing for foraging and larval mimicry behaviors.

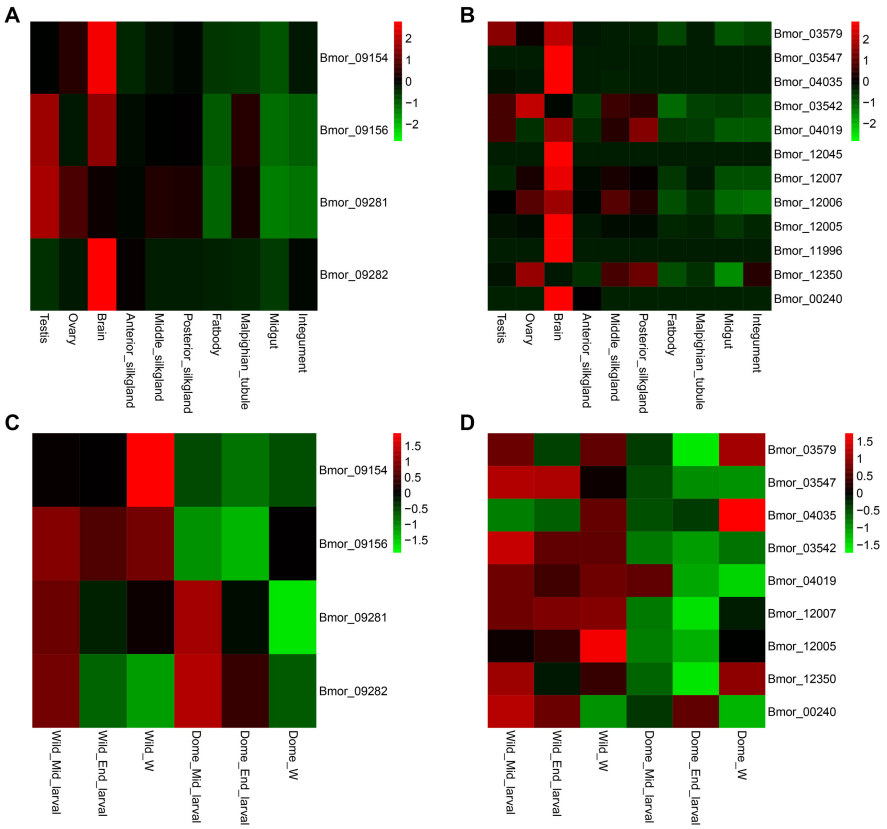

FIGURE 6 | Expression patterns of the candidate genes related to climbing and mimicry. Tissue expression pattern of the candidate domesticated genes related to climbing **(A)** and mimicry **(B)**. Expression levels of the candidate domesticated genes related to climbing **(C)** and mimicry **(D)** at different larval stages of the wild silkworm and domestic silkworm. Dome, domestic silkworm; Wild, wild silkworm; End_larval, the end of the last larval stage; Mid_larval, the middle of the last larval stage; W, wandering stage.

DATA AVAILABILITY STATEMENT

The datasets presented in this study can be found in online repositories. The names of the repository/repositories and accession number(s) can be found below: https://www.ncbi.nlm.nih.gov/, PRJNA607658.

AUTHOR CONTRIBUTIONS

HX conceived and supervised the study. MW drafted the manuscript. YL and MW performed the experiments and generated the mapping population construction, sample collection, BSA analyses, and selection sweep analyses. YC, YL, and SZ collected and analyzed the transcriptome data of the different tissues of the silkworm. HX, WY, and QF revised the manuscript. All authors have read and approved the manuscript.

FUNDING

This work was supported by the grant from the National Natural Science Foundation of China (32070411) and a grant from the Natural Science Foundation of Guangdong Province (2019A1515011012).

ACKNOWLEDGMENTS

We thank Prof. Muwang Li, Prof. Shuai Zhan, and Mr. Jian Zhang for their kind help and suggestions in characterizing the behavioral traits in silkworm.

SUPPLEMENTARY MATERIAL

The Supplementary Material for this article can be found online at: https://www.frontiersin.org/articles/10.3389/fgene.2020.566961/full#supplementary-material

Supplementary Figure 1 | Comparisons of index in climbing and non-climbing bulks of white body. **(A)** SNP/InDel index in non-climbing bulk. **(B)** SNP/InDel index in climbing bulk. **(C)** ΔSNP/InDel index between climbing and non-climbing bulks. The candidate region related to climbing are marked with red arrows.

Supplementary Figure 2 | Comparisons of index in climbing and non-climbing bulks of dark body. **(A)** SNP/InDel index in non-climbing bulk. **(B)** SNP/InDel index in climbing bulk. **(C)** ΔSNP/InDel index between climbing and non-climbing bulks. The candidate region related to climbing are marked with red arrows.

Supplementary Figure 3 | SNP analysis of the candidate domestication genes related to climbing. Allele frequencies in the genetic region of the other three genes. Green blocks indicate the geno mic structure of corresponding genes. The non-synonymous replacement between the domestic silkworm group and the wild silkworm are marked with red arrows.

Supplementary Figure 4 | Phylogenetic analysis of ASNA1 in insects. The protein sequence of ASNA1 from silkworm was used as query to blast against all the insect genomes in NCBI database with default settings. Protein sequences with at least 80% identity of ASNA1 in silkworm were downloaded and aligned with ClustalW in MEGA7. The minimum-evolution tree was constructed to show the evolution of ASNA1 in all the collected insect genomes. The ASNA1 in silkworm was marked with black filled circle, and species with two copies of ASNA1 were marked with black filled triangles.

Supplementary Figure 5 | Protein alignments of the candidate mutation of ASNA1 in insects. The candidate mutation was divided into two groups (highlighted with cyan and yellow colors, respectively).

Supplementary Figure 6 | Protein alignments of the candidate mutations of FAN1 and Pigo in silkworm and five Lepidoptera species. **(A)** Two candidate non-synonymous mutations on FAN1. **(B)** Two candidate non-synonymous mutations on Pigo.

Supplementary Figure 7 | Comparisons of index in mimicry and non-mimicry bulks. **(A)** SNP/InDel index in non-mimicry bulk. **(B)** SNP/InDel index in mimicry bulk. **(C)** ΔSNP/InDel index between mimicry and non-mimicry bulks. The candidate region related to climbing are marked with red arrows.

Supplementary Figure 8 | Allele frequencies of candidate genes related to mimicry response. **(A)** *Bmor_03579*. **(B)** *Bmor_03547*. **(C)** *Bmor_04035*. **(D)** *Bmor_04019*. **(E)** *Bmor_12045*. **(F)** *Bmor_12007*. **(G)** *Bmor_12006*. **(H)** *Bmor_12005*. **(I)** *Bmor_11996*. **(J)** *Bmor_12350*. **(K)** *Bmor_00240*. Blue, domestic silkworm; black, wild silkworm. The allele frequency in genomic region and flanking 2 kb were shown for each gene.

Supplementary Figure 9 | Expression levels of candidate genes related to climbing and mimicry in brains of wild silkworm and domestic silkworm. **(A–D)** Four candidate genes related to climbing ability. **(E–M)** Nine detected candidate genes related to mimicry response. Genes predicted to be positively selected in SGID were marked in red. The FPKM values were normalized to the total reads of corresponding samples and multiplied by 10^7. Student's *t*-test was used to estimate the differences between wild silkworm and domestic silkworm. $^*p < 0.05$; $^{**}p < 0.01$.

Supplementary Table 1 | Summary of sequence data of parental lines and segregation bulks.

Supplementary Table 2 | Annotation of the candidate genes for climbing and mimicry.

Supplementary Data | ΔSNP/InDel index calculated in the white and dark body sets used for mapping candidate regions related to climbing ability in silkworm. The average ΔSNP/InDel index was calculated with 1 Mb sliding window with 10 kb step size.

Supplementary Video 1 | Climbing and mimicry of BC1. Individuals with strong ability of climbing in BC1. The branches were shaken for observation of the responses of each individual. Individuals response to artificial shaking by stretching their head and thorax to mimic the branch.

Supplementary Video 2 | Individuals response to hand touching. Individuals showing strong response to artificial shaking were verified by hand touching.

Supplementary Video 3 | Non-mimicry traits of BC1. BC1 individual's loss of mimicry showed no response and kept eating when touched by hand.

REFERENCES

Chiyonobu, T., Inoue, N., Morimoto, M., Kinoshita, T., and Murakami, Y. (2014). Glycosylphosphatidylinositol (GPI) anchor deficiency caused by mutations in PIGW is associated with West syndrome and hyperphosphatasia with mental retardation syndrome. *J. Med. Genet.* 51, 203–207. doi: 10.1136/jmedgenet-2013-102156

Comer, C. M., and Robertson, R. M. (2001). Identified nerve cells and insect behavior. *Prog. Neurobiol.* 63, 409–439. doi: 10.1016/s0301-0082(00)00051-4

Dong, Y., Zhang, X., Xie, M., Arefnezhad, B., Wang, Z., Wang, W., et al. (2015). Reference genome of wild goat (*capra aegagrus*) and sequencing of goat breeds provide insight into genic basis of goat domestication. *BMC Genom.* 16:431. doi: 10.1186/s12864-015-1606-1

Feiguin, F., Godena, V. K., Romano, G., D'ambrogio, A., Klima, R., and Baralle, F. E. (2009). Depletion of TDP-43 affects *Drosophila motoneurons* terminal synapsis and locomotive behavior. *FEBS Lett.* 583, 1586–1592. doi: 10.1016/j.febslet.2009.04.019

Fischer, B., Luthy, K., Paesmans, J., De Koninck, C., Maes, I., Swerts, J., et al. (2016). Skywalker-TBC1D24 has a lipid-binding pocket mutated in epilepsy and required for synaptic function. *Nat. Struct. Mol. Biol.* 23, 965–973. doi: 10.1038/nsmb.3297

Frantz, L. A., Schraiber, J. G., Madsen, O., Megens, H. J., Cagan, A., Bosse, M., et al. (2015). Evidence of long-term gene flow and selection during domestication from analyses of Eurasian wild and domestic pig genomes. *Nat. Genet.* 47, 1141–1148. doi: 10.1038/ng.3394

Freeze, H. H., Eklund, E. A., Ng, B. G., and Patterson, M. C. (2012). Neurology of inherited glycosylation disorders. *Lancet. Neurol.* 11, 453–466. doi: 10.1016/s1474-4422(12)70040-6

Garrouste, R., Hugel, S., Jacquelin, L., Rostan, P., Steyer, J. S., Desutter-Grandcolas, L., et al. (2016). Insect mimicry of plants dates back to the Permian. *Nat. Commun.* 7:13735.

Haynes, K. F. (1988). Sublethal effects of neurotoxic insecticides on insect behavior. *Annu. Rev. Entomol.* 33, 149–168. doi: 10.1146/annurev.en.33.010188.001053

Herbeck, Y. E., and Gulevich, R. G. (2019). Neuropeptides as facilitators of domestication. *Cell Tissue Res.* 375, 295–307. doi: 10.1007/s00441-018-2939-2

Ionita-Laza, I., Xu, B., Makarov, V., Buxbaum, J. D., Roos, J. L., Gogos, J. A., et al. (2014). Scan statistic-based analysis of exome sequencing data identifies FAN1 at 15q13.3 as a susceptibility gene for schizophrenia and autism. *Proc. Natl. Acad. Sci. U.S.A.* 111, 343–348. doi: 10.1073/pnas.1309475110

Jensen, P. (2014). Behavior genetics and the domestication of animals. *Annu. Rev. Anim. Biosci.* 2, 85–104. doi: 10.1146/annurev-animal-022513-114135

Kamita, S. G., Nagasaka, K., Chua, J. W., Shimada, T., Mita, K., Kobayashi, M., et al. (2005). A baculovirus-encoded protein tyrosine phosphatase gene induces enhanced locomotory activity in a lepidopteran host. *Proc. Natl. Acad. Sci. U.S.A.* 102, 2584–2589. doi: 10.1073/pnas.0409457102

Kim, D., Pertea, G., Trapnell, C., Pimentel, H., Kelley, R., and Salzberg, S. L. (2013). TopHat2: accurate alignment of transcriptomes in the presence of insertions, deletions and gene fusions. *Genome Biol.* 14:R36.

Kim, S. R., Kwak, W., Kim, H., Caetano-Anolles, K., Kim, K. Y., Kim, S. B., et al. (2018). Genome sequence of the Japanese oak silk moth, *Antheraea yamamai*: the first draft genome in the family Saturniidae. *Gigascience* 7, 1–11.

Krawitz, P. M., Murakami, Y., Hecht, J., Kruger, U., Holder, S. E., Mortier, G. R., et al. (2012). Mutations in PIGO, a member of the GPI-anchor-synthesis pathway, cause hyperphosphatasia with mental retardation. *Am. J. Hum. Genet.* 91, 146–151. doi: 10.1016/j.ajhg.2012.05.004

Kubinyi, E., Vas, J., Hejjas, K., Ronai, Z., Bruder, I., Turcsan, B., et al. (2012). Polymorphism in the tyrosine hydroxylase (TH) gene is associated with activity-impulsivity in German Shepherd Dogs. *PLoS One* 7:e30271. doi: 10.1371/journal.pone.0030271

Kumar, S., Stecher, G., and Tamura, K. (2016). MEGA7: molecular evolutionary genetics analysis version 7.0 for bigger datasets. *Mol. Biol. Evol.* 33, 1870–1874. doi: 10.1093/molbev/msw054

Kun-Rodrigues, C., Ganos, C., Guerreiro, R., Schneider, S. A., Schulte, C., Lesage, S., et al. (2015). A systematic screening to identify de novo mutations causing sporadic early-onset Parkinson's disease. *Hum. Mol. Genet.* 24, 6711–6720. doi: 10.1093/hmg/ddv376

Lachaud, C., Slean, M., Marchesi, F., Lock, C., Odell, E., Castor, D., et al. (2016). Karyomegalic interstitial nephritis and DNA damage-induced polyploidy in Fan1 nuclease-defective knock-in mice. *Genes Dev.* 30, 639–644. doi: 10.1101/gad.276287.115

Lawal, R. A., Al-Atiyat, R. M., Aljumaah, R. S., Silva, P., Mwacharo, J. M., and Hanotte, O. (2018). Whole-genome resequencing of red junglefowl and indigenous village chicken reveal new insights on the genome dynamics of the species. *Front. Genet.* 9:264. doi: 10.3389/fgene.2018.00264

Li, B., and Dewey, C. N. (2011). RSEM: accurate transcript quantification from RNA-Seq data with or without a reference genome. *BMC Bioinformatics* 12:323. doi: 10.1186/1471-2105-12-323

Li, H., and Durbin, R. (2009). Fast and accurate short read alignment with Burrows-Wheeler transform. *Bioinformatics* 25, 1754–1760. doi: 10.1093/bioinformatics/btp324

Li, H., Handsaker, B., Wysoker, A., Fennell, T., Ruan, J., Homer, N., et al. (2009). The Sequence Alignment/Map format and SAMtools. *Bioinformatics* 25, 2078–2079. doi: 10.1093/bioinformatics/btp352

Li, Y., Zhao, L., Sun, H., Yu, J., Li, N., Liang, J., et al. (2012). Gene silencing of FANCF potentiates the sensitivity to mitoxantrone through activation of JNK and p38 signal pathways in breast cancer cells. *PLoS One* 7:e44254. doi: 10.1371/journal.pone.0044254

Liu, T., Wang, J., Wu, C., Zhang, Y., Zhang, X., Li, X., et al. (2019). Combined QTL-seq and traditional linkage analysis to identify candidate genes for purple skin of radish fleshy taproots. *Front. Genet.* 10:808. doi: 10.3389/fgene.2019.00808

McKenna, A., Hanna, M., Banks, E., Sivachenko, A., Cibulskis, K., Kernytsky, A., et al. (2010). The Genome analysis toolkit: a MapReduce framework for analyzing next-generation DNA sequencing data. *Genome Res.* 20, 1297–1303. doi: 10.1101/gr.107524.110

Nakamura, K., Osaka, H., Murakami, Y., Anzai, R., Nishiyama, K., Kodera, H., et al. (2014). PIGO mutations in intractable epilepsy and severe developmental delay with mild elevation of alkaline phosphatase levels. *Epilepsia* 55, e13–e17.

Pendleton, A. L., Shen, F., Taravella, A. M., Emery, S., Veeramah, K. R., Boyko, A. R., et al. (2018). Comparison of village dog and wolf genomes highlights the role of the neural crest in dog domestication. *BMC Biol.* 16:64. doi: 10.1186/s12915-018-0535-2

Pizzolato, J., Mukherjee, S., Scharer, O. D., and Jiricny, J. (2015). FANCD2-associated nuclease 1, but not exonuclease 1 or flap endonuclease 1, is able to unhook DNA interstrand cross-links in vitro. *J. Biol. Chem.* 290, 22602–22611. doi: 10.1074/jbc.m115.663666

Qiu, Q., Wang, L., Wang, K., Yang, Y., Ma, T., Wang, Z., et al. (2015). Yak whole-genome resequencing reveals domestication signatures and prehistoric population expansions. *Nat. Commun.* 6:10283.

Schubert, M., Jonsson, H., Chang, D., Der Sarkissian, C., Ermini, L., Ginolhac, A., et al. (2014). Prehistoric genomes reveal the genetic foundation and cost of horse domestication. *Proc. Natl. Acad. Sci. U.S.A.* 111, E5661–E5669.

Segui, N., Mina, L. B., Lazaro, C., Sanz-Pamplona, R., Pons, T., Navarro, M., et al. (2015). Germline mutations in FAN1 cause hereditary colorectal cancer by impairing DNA repair. *Gastroenterology* 149, 563–566. doi: 10.1053/j.gastro.2015.05.056

Shi, M. T., Zhang, Y., and Zhou, G. Q. (2018). The critical roles of TBC proteins in human diseases. *Yi Chuan* 40, 12–21.

Solberg, M. F., Robertsen, G., Sundt-Hansen, L. E., Hindar, K., and Glover, K. A. (2020). Domestication leads to increased predation susceptibility. *Sci. Rep.* 10:1929.

Takagi, H., Abe, A., Yoshida, K., Kosugi, S., Natsume, S., Mitsuoka, C., et al. (2013). QTL-seq: rapid mapping of quantitative trait loci in rice by whole genome resequencing of DNA from two bulked populations. *Plant J.* 74, 174–183. doi: 10.1111/tpj.12105

Trapnell, C., Roberts, A., Goff, L., Pertea, G., Kim, D., Kelley, D. R., et al. (2012). Differential gene and transcript expression analysis of RNA-seq experiments with TopHat and Cufflinks. *Nat. Protoc.* 7, 562–578. doi: 10.1038/nprot.2012.016

Verhagen, J. M. A., Van Den Born, M., Van Der Linde, H. C., Nikkels, P. G. J., Verdijk, R. M., Kivlen, M. H., et al. (2019). Biallelic variants in ASNA1, encoding a cytosolic targeting factor of tail-anchored proteins, cause rapidly progressive pediatric cardiomyopathy. *Circ. Genom. Precis. Med.* 12, 397–406.

Wang, K., Li, M., and Hakonarson, H. (2010). ANNOVAR: functional annotation of genetic variants from high-throughput sequencing data. *Nucleic Acids Res.* 38:e164. doi: 10.1093/nar/gkq603

Wang, P., and Slaughter, M. M. (2005). Effects of GABA receptor antagonists on retinal glycine receptors and on homomeric glycine receptor alpha subunits. *J. Neurophysiol.* 93, 3120–3126. doi: 10.1152/jn.01228.2004

Wilkins, A. S., Wrangham, R. W., and Fitch, W. T. (2014). The "domestication syndrome" in mammals: a unified explanation based on neural crest cell behavior and genetics. *Genetics* 197, 795–808. doi: 10.1534/genetics.114.165423

Xiang, H., Liu, X., Li, M., Zhu, Y., Wang, L., Cui, Y., et al. (2018). The evolutionary road from wild moth to domestic silkworm. *Nat. Ecol. Evol.* 2, 1268–1279. doi: 10.1038/s41559-018-0593-4

Xue, J., Li, H., Zhang, Y., and Yang, Z. (2016). Clinical and genetic analysis of two Chinese infants with Mabry syndrome. *Brain Dev.* 38, 807–818. doi: 10.1016/j.braindev.2016.04.008

Yang, Z. (2007). PAML 4: phylogenetic analysis by maximum likelihood. *Mol. Biol. Evol.* 24, 1586–1591. doi: 10.1093/molbev/msm088

Zegeye, W. A., Zhang, Y., Cao, L., and Cheng, S. (2018). Whole genome resequencing from bulked populations as a rapid QTL and gene identification method in rice. *Int. J. Mol. Sci* 19:4000. doi: 10.3390/ijms19124000

Zehavi, Y., Von Renesse, A., Daniel-Spiegel, E., Sapir, Y., Zalman, L., Chervinsky, I., et al. (2017). A homozygous PIGO mutation associated with severe infantile epileptic encephalopathy and corpus callosum hypoplasia, but normal alkaline phosphatase levels. *Metab. Brain Dis.* 32, 2131–2137. doi: 10.1007/s11011-017-0109-y

Zhang, Z., Jia, Y., Almeida, P., Mank, J. E., Van Tuinen, M., Wang, Q., et al. (2018). Whole-genome resequencing reveals signatures of selection and timing of duck domestication. *Gigascience* 7:giy027.

Zhao, Q., Saro, D., Sachpatzidis, A., Singh, T. R., Schlingman, D., Zheng, X. F., et al. (2014). The MHF complex senses branched DNA by binding a pair of crossover DNA duplexes. *Nat. Commun.* 5:2987.

Zhu, Y. N., Wang, L. Z., Li, C. C., Cui, Y., Wang, M., Lin, Y. J., et al. (2019a). Artificial selection on storage protein 1 possibly contributes to increase of hatchability during silkworm domestication. *PLoS Genet.* 15:e1007616. doi: 10.1371/journal.pgen.1007616

Zhu, Z., Guan, Z., Liu, G., Wang, Y., and Zhang, Z. (2019b). SGID: a comprehensive and interactive database of silkworm. *Database* 2019:baz134.

Conflict of Interest: The authors declare that the research was conducted in the absence of any commercial or financial relationships that could be construed as a potential conflict of interest.

frontiers in Genetics

ORIGINAL RESEARCH
published: 24 February 2021
doi: 10.3389/fgene.2021.611476

Dim Red Light During Scotophase Enhances Mating of a Moth Through Increased Male Antennal Sensitivity Against the Female Sex Pheromone

Qiuying Chen[1,2,3], Xi Yang[1,2,3], Dongrui You[1,2,3], Jiaojiao Luo[1,2,3], Xiaojing Hu[1,2,3], Zhifeng Xu[1,2,3] and Wei Xiao[1,2,3]**

[1]Key Laboratory of Entomology and Pest Control Engineering, College of Plant Protection, Southwest University, Chongqing, China, [2]Academy of Agricultural Sciences, Southwest University, Chongqing, China, [3]State Cultivation Base of Crop Stress Biology for Southern Mountainous Land of Southwest University, Southwest University, Chongqing, China

Insects are behaviorally and physiologically affected by different light conditions, including photoperiod, light intensity, and spectrum. Light at night has important influences on nocturnal insects, including most moth species. Moth copulation and mating usually occur at night. Although a few studies examine changes in insect mating under artificial light at night, detailed influences of light, such as that of monochromatic light, on moth mating remain largely unknown. In this study, on the basis of long-term insects rearing experience, dim red light (spectrum range: 610–710 nm, with a peak at 660 nm; 2.0 Lux) during scotophase was hypothesized to enhance mating in the yellow peach moth, *Conogethes punctiferalis*. To test the hypothesis, the mating of moths under dim red, blue, and white lights during scotophase was observed. Under the dim red light, the enhancement of mating in *C. punctiferalis* was observed. In addition, the electroantennografic response of males against the female sex pheromone increased with red light treatment during scotophase. In an analysis of the differentially expressed genes in the antennae of males under red light and dark conditions, the expression levels of two odorant-binding protein (OBP) genes, *CpunOBP2* and *CpunPBP5*, were up-regulated. Two genes were then expressed in *Escherichia coli*, and the recombinant proteins showed strong binding to female pheromone components in fluorescence-binding assays. Thus, the results of this study indicated that dim red light at night enhanced the mating of *C. punctiferalis*. One of the mechanisms for the enhancement was probably an increase in the antennal sensitivity of males to the female sex pheromone under red light that was caused by increases in the expression levels of pheromone-binding protein genes in male antennae.

Keywords: dim red light, scotophase, mating enhancement, *Conogethes punctiferalis*, electroantennography, odorant binding proteins

OPEN ACCESS

Edited by:
Fei Li,
Zhejiang University, China

Reviewed by:
Peng He,
Guizhou University, China
Yang Liu,
Chinese Academy of Agricultural Sciences, China
Shao-Hua Gu,
China Agricultural University, China

***Correspondence:**
Zhifeng Xu
xzf2018@swu.edu.cn
Wei Xiao
xiaowei@swu.edu.cn

Specialty section:
This article was submitted to Epigenomics and Epigenetics, a section of the journal Frontiers in Genetics

Received: *29 September 2020*
Accepted: *07 January 2021*
Published: *24 February 2021*

Citation:
Chen Q, Yang X, You D, Luo J, Hu X, Xu Z and Xiao W (2021) Dim Red Light During Scotophase Enhances Mating of a Moth Through Increased Male Antennal Sensitivity Against the Female Sex Pheromone. Front. Genet. 12:611476. doi: 10.3389/fgene.2021.611476

INTRODUCTION

Light influences many behaviors of insects, including host-finding, aggregation, mating, and oviposition (Matthews and Matthews, 2010). Different light conditions have different influences on insect mating behaviors. First, a prolonged photophase usually inhibits mating. For example, in *Heteroplcha jinyinhuaphaga*, when the photoperiod is changed from 6Light:18Dark to 22Light:2Dark, calling

and mating behaviors, including total calling percentage, onset time of calling, total mating percentage, and mating duration, decreased significantly (Xiang et al., 2018). In *Cnophalocrocis medinalis*, calling frequency decreased substantially under constant light, compared with a normal photoperiod of 15Light : 9Dark (Kawazu et al., 2011). Second, the wavelength of light also influences insect mating behaviors. For example, males of the cabbage butterfly *Pieris rapae crucivora* were more active in UV-rich environments, and they searched longer for females and approached them preferentially in the shade and then copulate there more frequently (Obara et al., 2008). In the tephritid fruit fly *Anastrepha ludens*, males exposed to red, blue, or shaded light treatments in the photoperiod were more frequently chosen as mating partners than dark-reared males, whereas females reared in blue light and darkness mated less compared with those reared in red and shaded light (Diaz-Fleischer and Arredondo, 2011). In a comprehensive study on the influences of light on the reproductive performance of the potential natural enemy *Propylea japonica*, the light intensity, wavelength and photoperiod had important effects on the mating behaviors of pursuit time, number of copulations, and duration of copula (Wang et al., 2014).

In addition to those studies that focus on the effects of photoperiod, intensity, and wavelength on insect mating behaviors, the effect of light in scotophase on insect mating behavior has also recently been investigated. Lifetime exposure to a high level of white light (100 lux) at night increased the probability of a successful mating in the cricket *Teleogryllus commodus* (Botha et al., 2017). In the oriental tobacco budworm *Helicoverpa assulta*, a dim white light (0.5 lux) during scotophase promoted mating, whereas a high-intensity light (50.0 lux) suppressed calling behavior, pheromone production, and mating (Li et al., 2015). Compared with many laboratory experiments, few field tests have been conducted on the influence of light on insect mating at night. van Geffen et al. (2015) investigated the effects of artificial lights (white, green, and red, with intensities <10 lux) at night on the mating of a geometrid moth, *Operophtera brumata*, in an oak-dominated forest in Wageningen, the Netherlands. In their study, fewer mated females were caught on artificially illuminated trees than on the dark control. In addition, fewer males were attracted to a synthetic sex pheromone trap on illuminated trees than to one on the control (van Geffen et al., 2015). These authors concluded that artificial light at night inhibits mating in the moth, although the details of mating under artificial light conditions were not directly observed.

Light in scotophase can also change gene expression levels in insects. For example, with 3 h of low light treatment at the beginning of scotophase, the expression of 16 genes decreased and that of 14 genes increased in male adults of the mosquito *Culex pipiens* (Honnen et al., 2016). In the heads of *Helicoverpa armigera* males, the genes *IMFamide*, *leucokinin*, and *sNPF* were differentially expressed between UV-A light (365 nm) treatments and the control (Wang et al., 2018).

The yellow peach moth *Conogethes punctiferalis* (Guenée; Lepidoptera: Crambidae) is widely distributed in Asia and Australia. The larvae damage many economically important orchard crops, spices, and vegetables (Xu et al., 2014). Female sex pheromone of the specie includes (*E*)-10-hexadecenal, (*Z*)-10-hexadecenal, (*Z*3, *Z*6, *Z*9)-tricosatriene and (*Z*9)-heptacosene (Konno et al., 1982; Xiao et al., 2011, 2012). In male antennae, chemosensory genes, including *CpunPBP2*, *CpunPBP5*, *CpunGOBP1*, and *CpunGOBP2*, have been demonstrated of pheromone binding function in recent years (Ge et al., 2018; Jing et al., 2019). Since 2012, a colony of the moth has been reared in our laboratory. On the basis of our long-term rearing experience and personal communications (Dr. Ballal, Indian Council of Agricultural Research), the continuous provision of a dim red light during scotophase was hypothesized to enhance mating in the yellow peach moth. Therefore, in this study, the mating behavior of *C. punctiferalis* was firstly observed under red light during scotophase. When the enhancement of mating under red light was confirmed, electroantennography (EAG) tests were conducted to test the antennal responses of male moths reared under red light or in the dark to female sex pheromone components. Finally, the expression levels of chemosensory genes in the antennae of male moths under those two light conditions were compared and the functions of the differentially expressed genes were investigated.

MATERIALS AND METHODS

Insects

A colony of yellow peach moths was started from larvae collected in chestnut orchards in Chongqing, China (N 28°40'38", E 115°50'20"). In the lab, larvae were reared on chestnuts or corn (Xiao et al., 2012). Pupae were sexed, and the sexes were kept in separate cages at 25 ± 1°C and 40–60% relative humidity under a 15Light : 9Dark photoperiod. A fluorescent lamp provided light in photophase. During scotophase, no light was provided unless operations were necessary, which were illuminated with a 15 W red, incandescent lamp. Adults were provided with 10% sugar solution on cotton pads. A fresh apple wrapped in cheesecloth was hung from the top of the cage to collect eggs.

Chemicals

The synthetic pheromone components including (*E*)-10-hexadecenal (E10-16 : Ald), (*Z*)-10-hexadecenal (Z10-16 : Ald), (*Z*3, *Z*6, *Z*9)-tricosatriene (Z3, Z6, Z9-23 : HC) and (*Z*9)-heptacosene (Z9-27 : HC) were purchased from Shanghai Udchem Technology Co., Ltd., China. N-phenyl-1-naphthylamine (1-NPN) was purchased from Sigma-Aldrich (purity ≥95%; Shanghai, China). All chemicals were stored as specified by the manufacturers.

Mating and Oviposition Observations

Pairs of newly eclosed adults (1-day-old, male : female, 1 : 1, 30 pairs) were put in a metal cage (50 cm × 50 cm × 50 cm). In each treatment, three cages of insects were treated as replicates. Temperature, photoperiod, and adult food were the same as those for rearing. For use in the light experiments during the 9 h of scotophase, red (spectrum range: 610–710 nm, with a peak at 660 nm), blue (spectrum range: 410–510 nm, with a peak at 460 nm), and white (spectrum range: mixed) light LED lamps (Shenzhen Ladeng Lighting Technology Co., Ltd., Shenzhen, China) were set approximately 3 m above the cages. The intensity

of light was approximately 2.0 lux at the middle point of the inner cage space. As a control, no light was provided during scotophase (dark treatment). The number of mating pairs (including both continuously mating and newly mating pairs) was recorded every hour from the 2nd day after eclosion. A video camera (HDR-CX560V in nightshot mode; Sony, Tokyo, Japan) was used to assist with observations in the dark treatment. In an additional red-light experiment, two other light intensities, 0.2 and 20.0 lux, were examined, in addition to 2.0 lux. A spectrometer (HR-350, Highpoint Corporation, Taiwan, China) and an illuminometer (Z-10, Everfine Corporation, Hangzhou, China) were used to measure the light spectra and intensities, respectively.

The cheesecloth with deposited eggs was changed daily, and the number of eggs on the cheesecloth was counted immediately.

Electroantennography

The EAG technique was applied as described by Beck et al. (2014) under a normal laboratory conditions illuminated with a fluorescent lamp (light intensity >1000 lux). The antennae of 3-day-old virgin males reared under the same conditions as those in the red-light experiment were cut at the base and the distal part of the flagellum tip amputated. Then, an excised antenna was quickly mounted on an electrode fork holder (Syntech, kirchzarten, Germany) with the flagellum tip on the recording electrode and the base end on the reference electrode. The fork holder with excised antenna was immediately connected to a pre-amplifier and placed 1.0 cm inside the open end of a glass tube provided with continuous airflow. An air stimulus controller (CS-55, Syntech, kirchzarten, Germany) generated continuous, humidified airflow (400 ml/min) or pulsed airflow (280 ml/min, 0.5-s pulse duration) for odor delivery. Twenty microliters of each stimulus dissolved in hexane were loaded on a rectangular filter paper (5 mm wide and 50 mm long), which was subsequently inserted into the wide section (8-mm diameter) of a Pasteur pipette. The pipette containing the stimulus was then inserted with its narrow end into a side port in the wall of the glass tube. Stimuli were tested with the solvent hexane tested as the blank at the start of a stimuli series. Each concentration of a stimulus was tested once with an antenna. The EAG amplitudes from four antennae of different moths were recorded as replicates for a stimulus. The analog signal of the antennal response was detected through a probe (INR-II, Syntech, kirchzarten, Germany), captured and processed with an Intelligent Data Acquisition Controller (IDAC-4, Syntech, kirchzarten, Germany), and analyzed using EAG 2000 software (Syntech, kirchzarten, Germany) on a PC. The dose of each synthetic pheromone component was tested as a ratio of a female equivalent (FE). For each of *E*10-16 : Ald, *Z*10-16 : Ald, *Z*3, *Z*6, *Z*9-23 : HC and *Z*9-27 : HC, one FE was 9.55, 0.45, 2.4 and 270 ng (Xiao et al., 2011, 2012).

Expression Levels and Functions of Antennal Chemosensory Genes

Reverse-Transcription Quantitative PCR of Chemosensory Genes

Based on the transcriptome sequencing (unpublished) of the antennae of 3-day-old male adults with red light and dark treatments during scotophase, six odorant-binding protein (OBP) genes were identified with expression levels that were significantly up-regulated by the red-light treatment. Then, the expression levels of those genes were verified by reverse-transcription quantitative PCR (RT-qPCR), primers showed in **Table 1**. Primer efficiency was tested using 3-fold diluted cDNA samples, and a standard curve was generated. The Ct values were plotted against the log of the cDNA dilutions, and the efficiency percentage and R^2 values were within the acceptable range. A two-step program was adopted. The reaction volume was set to 20 µl, which included 10 µl of SYBR Premix ExTaq mixture (Takara Biotechnology Co., Ltd., Dalian, China), 1 µl of each of the forward and reverse primers (concentration: 10 µM), 1 µl of cDNA, and 7 µl of RNase free water. The program was designed as follows: denaturation at 95°C for 2 min, followed by 39 cycles at 95°C for 15 s and 60°C for 30 s, with melting curve analysis performed from 60°C to 95°C to determine the specificity of PCR products. Three independent biological replicates were processed for all samples. The $2^{-\Delta\Delta CT}$ method was used to calculate the relative expression of genes according to that of the reference gene RP49 (GenBank number: KX668533; Yang et al., 2017).

Preparation of Recombinant Proteins

The signal peptides of *CpunOBP2* and *CpunPBP5* (GenBank number: KF026055.1 and KP985227, respectively) were predicted by the SignalP server (Petersen et al., 2011). Then, primers were designed with signal peptides removed from the complete open reading frame sequences. With antennal cDNA used as the templates, *CpunOBP2* and *CpunPBP5* were amplified and cloned using the Pclone-007 s vector (TsingKe Biotech, Beijing, China). The following forward and reverse primers were designed for *CpunOBP2* and *CpunPBP5* according to homologous recombination as **Table 2** shown.

The expected gene sequences were purified and cloned into the bacterial expression vector pET-32a (+), (TsingKe

TABLE 1 | The forward and reverse primers of quantitative PCR (qPCR).

Gene	Forward primer	Reverse primer
GOBP1	TACTTCAACCTGATCACCGA	CCTCCTCGAACTGCTTCT
PBP5	GTCAACGTACGAGTGGAAGC	CTCCCCTAGCTCAGAGTCCT
OBP2	ATGTTGGCGTGTTGGATGAC	CCGAGTTGACTGGAGAGCAA
OBP3	AGGAGTTAGAGTCGATTGCA	ATTTCAGAGCCAATATCGCC
OBP11	TCTTTTAGTGGTGTGGTGTGT	CTGGATTCACGTTCGTCTCC
OBP13	GTGCATGGATGACGAGATG	GCACTTGATGTAGCACTTGA

TABLE 2 | The forward and reverse primers were designed according to homologous recombination of *CpunOBP2* and *CpunPBP5*.

CpunOBP2	forward primer	GGCCATGGCTGATATCGGATCCA TGACAGAGGAACAAAGA
	reverse primer	CTCGAGTGCGGCCGCAAGC TTTTAGA CGTCGATGCCAA
CpunPBP5	forward primer	GGCCATGGCTGATATCGGATCC TCTCAGGA GGTGATGAAGAA
	reverse primer	CTCGAGTGCGGCCGCAAGCT TCTAGGCTTCACCTATCATCT

Biotech, Beijing, China) digested with the same enzymes. Then, the plasmid was transformed into BL21 (DE3) competent cells (TsingKe Biotech, Beijing, China), and colonies were grown on LB ampicillin agar plates. A single positive clone was first identified and then grown in liquid LB with ampicillin overnight at 37°C. The culture was diluted to 1 : 100 and cultured for 5–6 h at 37°C until its absorbance at OD (600 nm) reached 0.6–0.8. To induce the protein, isopropyl-β-D-thiogalactoside (Solarbio, Beijing, China) was added to the culture at a final concentration of 0.1 mM, and the culture was incubated at 15°C and 150 r.min^{-1} for 18 h. The induced bacterial cells were harvested from a volume of 200 ml of liquid LB medium and centrifuged at 4°C for 20 min (4,000 *g*). The pellets were subjected to ultrasonication and were centrifuged at 4°C for 20 min (9,000 *g*) to obtain the soluble proteins, and the recombinant protein were purified by the Ni^{2+}-IDA column (His tagged) with a gradient concentration imidazole washing. The western blot method was performed to analyze the correct expression. Ten microliters of purified protein sample were electrophoresed in 10% gel (BIO-RAD, Shanghai, China). The gel was sandwiched with a fluoride polyvinylidene fluoride (PVDF) membrane, and the sample in the gel was transferred to the PVDF (electrophoresis; 240 mA, 1 h). The film was washed three times using Tris-HCl buffer solution-Tween (TBST; Cebio, Beijing, China). Then, 5% skim milk powder in TBST was used as the blocking buffer for 1 h and then washed three times by TBST. The PVDF membrane was incubated with the primary antibody His (1 : 1,000) overnight at 4°C. The membrane was washed three times again using TBST and treated with the secondary antibody sheep anti-rabbit antibody (1 : 10,000) at room temperature for 1 h. After a final wash, the membrane was developed in Gel imager (Analytik Jena, Jena, Germany) using Super ECL reagent (ELC kit, Coolaber, Beijing, China). The purified protein was obtained with tags removed by enterokinase from recombinant proteins.

Fluorescence-Binding Assay

A fluorescence-binding assay was used to measure the affinity of the recombined CpunOBP2 and CpunPBP5 to female sex pheromone components (Liu et al., 2012; Ge et al., 2018). An F970CRT fluorescence spectrophotometer (Lengguang Technology Co., Ltd., Shanghai, China) with a 1-cm light path fluorimeter quartz cuvette was used for the assay. The fluorescent probe 1-NPN and all tested chemicals were dissolved in methanol of HPLC-grade purity, and the final concentration of chemicals used in the assay was 1 mM. To measure the affinity of the fluorescent ligand 1-NPN to each protein, a 2 μM solution of the protein in 30 mM Tris-HCl, pH 7.4, was titrated with aliquots of 1 mM ligand in methanol to final concentrations of 2–20 μM. The fluorescence of 1-NPN was excited at 337 nm, and emission spectra were recorded between 350 and 500 nm. The affinity of chemicals was measured in competitive binding assays, using 1-NPN as the fluorescent reporter at a concentration of 2 μM and each chemical at different concentrations from 0.5 to 8 μM (Liu et al., 2013; Sun et al., 2013; Hua et al., 2020).

GraphPad Prism 8 (GraphPad Software, Inc., San Diego, CA, United States) was used to estimate the $K_{1\text{-NPN}}$ (K_d of complex protein / 1-NPN) values by nonlinear regression for a unique site of binding. The proteins were assumed to be 100% active, with a stoichiometry of 1 : 1 (protein : ligand) at saturation. For other competitor ligands, the dissociation constants were calculated from the corresponding IC_{50} values (concentration of a ligand halving the initial fluorescence value of 1-NPN) using the following equation: $K_i = [IC_{50}]/(1 + [1\text{-NPN}]/K_{1\text{-NPN}})$. In the equation, [1-NPN] is the free concentration of 1-NPN, and $K_{1\text{-NPN}}$ is the dissociation constant of the complex protein/1-NPN (Ge et al., 2018; Jing et al., 2019).

Statistical Analyses

Data from different light (red, blue, and white) experiments were analyzed by independent sample *t*-tests. Data from different intensities of red light were subjected to the least significant difference test after ANOVA. Absolute EAG amplitudes of the blank were subtracted from the EAG amplitude of the stimuli (Ngumbi et al., 2010). Then, the data were analyzed by ANOVA, and the least significant difference test was used for multiple comparisons of means. Oviposition and gene expression data were analyzed by independent sample *t*-tests.

RESULTS

Mating Pairs Under Different Conditions During Scotophase

The numbers of mating pairs of *C. punctiferalis* under red light and dark conditions in scotophase during 6 days after adult eclosion are shown in **Figure 1**. Most of the mating

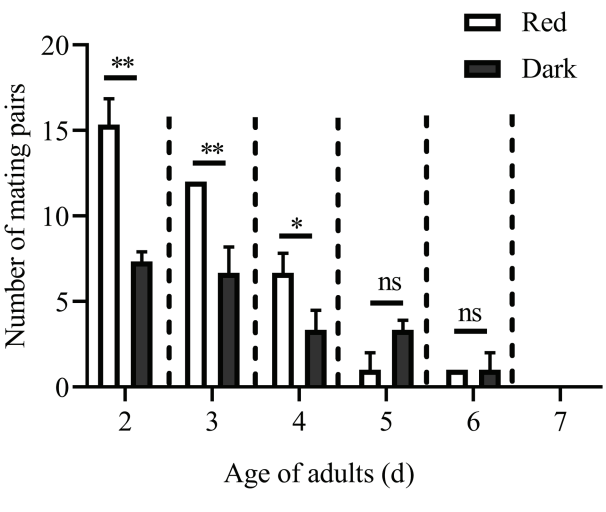

FIGURE 1 | Mating pairs of *Conogethes punctiferalis* under red light and dark conditions during scotophase. Data are shown as mean ± SD, from three replicates. Asterisks above columns mean significant differences ($^{*}p < 0.05$, $^{**}p < 0.01$, ns: no significant difference), by independent sample *t*-tests.

occurred in the 2 to 4-day-old adults under both light conditions. The number of mating pairs under red light was significantly higher than that in the dark on each of first 3 days. In the five and 6-day-old adults, the number of mating pairs was not significantly different under the two light conditions. In the 7-day-old adults, no mating was observed under either light condition. The oviposition of females is shown in **Table 3**. The numbers of eggs laid by 3 to 5-day-old females under red light were significantly higher than those in the dark. Meanwhile, the egg numbers under red light on those 3 days accounted for approximately 76% of the total recorded numbers during 5 days. In addition, the average number of eggs laid per female per day under red light was significantly higher than that in the dark.

Except for the 1st day, the numbers of mating pairs of *C. punctiferalis* were not significantly different between blue light and dark conditions in scotophase during 6 days of observation (**Figure 2**). On the 1st day, the number of mating pairs in blue light was significantly lower than that in the dark (**Figure 2**). A similar result was found in the white light experiment. There were no significant differences in numbers of mating pairs between white light and dark conditions during 6 days of observation (**Figure 3**).

Effects of Different Intensities of the Red Light on Mating

The effects of different intensities of red light on the number of mating pairs of *C. punctiferalis* in scotophase are shown in **Figure 4**. Similar to the results in **Figure 1**, most of the mating was observed in the first 3 days under all light intensities. In the 2-d-old adults, the number of mating pairs under 2.0 and 20.0-lux red light was significantly higher than that under 0.2 lux. No differences in the number of mating pairs were observed among the three light intensities for 3-d-old adults. In the 4-day-old adults, the number of mating pairs under the 2.0-lux red light was significantly higher than that under 0.2 and 20.0 lux. In addition, no differences were observed in the number of mating pairs among the three intensities in the 5-day-old adults. No mating was observed in the 6 to 7-day-old adults except a few mating was found under 2.0-lux red light in the 6-day-old adults.

EAG Responses

Figure 5 shows the EAG responses of male adults reared under red light and dark conditions during scotophase to the single female pheromones component (**Figures 5A–D**) and the pheromone mixture (**Figure 6**). For E10-16 : Ald (**Figure 5A**),

TABLE 3 | Oviposition of *C. punctiferalis* under red light and dark conditions during scotophase.

Lights	Age of adults (d)					Eggs /♀/d
	2	3	4	5	6	
Red light	311.0 ± 174.5a	1055.0 ± 121.8a	1046.0 ± 13.8a	951.0 ± 85.9a	626.0 ± 169.8a	26.6 ± 2.13a
Dark	277.0 ± 231.8a	520.0 ± 57.0b	635.0 ± 103.5b	681.0 ± 83.1b	677.0 ± 276.5a	18.3 ± 3.5b

Data are shown as mean ± SD, from three replicates. Data with different letters in the same column are significant different, $p < 0.05$, by independent sample t-tests.

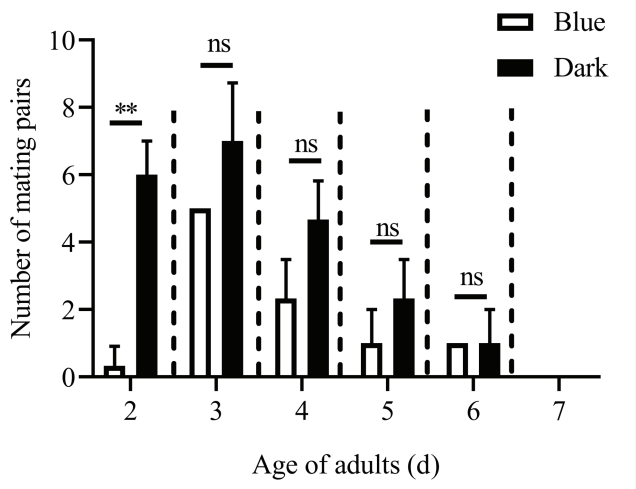

FIGURE 2 | Mating pairs of *C. punctiferalis* under blue light and dark conditions during scotophase. Data are shown as mean ± SD, from three replicates. Asterisks above columns mean significant differences ($^{**}p < 0.01$, ns: no significant difference), by independent sample *t*-tests.

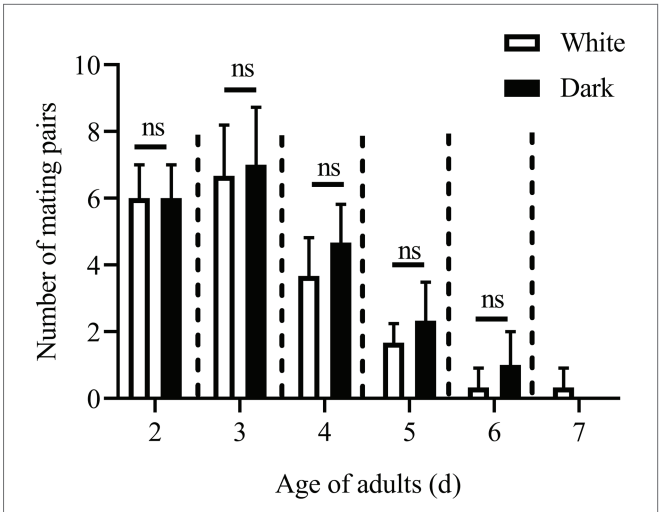

FIGURE 3 | Mating pairs of *C. punctiferalis* under white light and dark conditions during scotophase. Data are shown as mean ± SD, from three replicates. Asterisks above columns means significant differences ($p < 0.05$, ns: no significant difference), by independent sample *t*-tests.

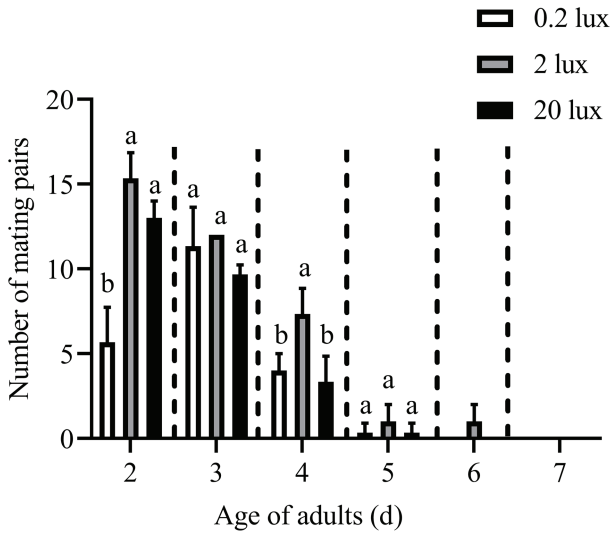

FIGURE 4 | Mating pairs of *C. punctiferalis* under different intensities of red light during scotophase. Data are shown as mean ± standard deviation, from three replicates. Different letters above columns mean significant differences ($p < 0.05$, ns: no significant difference), by Tukey's multiple comparisons after ANOVA.

among the five tested doses of E10-16 : Ald (**Figure 5A**), the EAG responses of male moths under red light were significantly higher than those of males in the dark at doses of 0.01, 0.1, and 100 FEs, respectively. However, at the dose of 10 FE, the EAG response of males in the dark was higher than that of males under red light. By contrast, for all doses of Z10-16: Ald except of 100FE (**Figure 5B**), there were no differences in EAG responses at other tested doses between male antennae under red light and in the dark. Additoanlly, for Z9-27 : HC, the EAG responses of male moths under red light were much higher than that in the dark at the only one dose, 100FE, among five tested doses (**Figure 5C**). While, for Z3, Z6, Z9-23 : HC, no difference of the EAG responses between male moths under red light and in the dark was found at the tested dose, except of 100FE, at which the EAG response of male moths in the dark was significantly higher than that under red light (**Figure 5D**). Finally, when all pheromone components were mixed and tested, the EAG response of male moths under red light was significantly higher than that in the dark at each of all tested doses (**Figure 6**).

Expression Levels of Genes

Reverse-transcription quantitative PCR was performed to determine the expression levels of six differentially expressed genes (under red light and dark conditions during scotophase) screened from the transcriptome analysis as shown in **Figure 7**, the relative expression of *CpunOBP2* and *CpunPBP5* in antennae of males under red light was significantly higher than that in the dark.

Fluorescent Ligand-Binding Assays

CpunOBP2 and *CpunPBP5* were expressed in *Escherichia coli*, and the recombined protein (about 1 mg/ml) was purified by affinity chromatography. The presence of recombinant CpunOBP2 and CpunPBP5 was checked by SDS-PAGE (**Figure 8**). With tags removed by enterokinase, proteins were then subjected to a fluorescence displacement-binding assay. Based on the binding curves and the Scatchard plots (**Figure 9**), the dissociation constant of the proteins/1-NPN complex was calculated as 7.88 ± 1.10 μM for *CpunOBP2* and 12.95 ± 4.48 μM for *CpunPBP5*. Then, the binding affinity of the proteins to the female sex pheromones E10-16 : Ald, Z10-16 : Ald, Z9-27 : HC and Z3, Z6, Z9-23 : HC was measured. As shown in **Figure 10**, the intensities of recombinant CpunOBP2 decreased with the increase in ligand concentration (E10-16 : Ald, Z10-16 : Ald and Z3, Z6, Z9-23 : HC). And for recombinant CpunPBP5, the lowest decrease of intensity was found in the ligand of E10-16 : Ald, among four pheromone components. Then, the IC_{50} and K_i values of the two proteins were calculated (**Table 4**). The binding affinity of the recombined CpunOBP2 was 8.48 ± 4.06 μM to E10-16 : Ald, 6.86 ± 2.50 μM to Z10-16 : Ald and 3.68 ± 2.33 μM to Z3, Z6, Z9-23 : HC (**Table 4**), which indicated the protein bound to the three pheromone components with a similar and relatively high affinity. Meanwhile, CpunOBP2 showed no binding to Z9-27 : HC. By contrast, the binding affinity of CpunPBP5 was 1.47 ± 0.62 μM to E10-16 : Ald, which indicated much stronger binding affinity of the protein to the ligand, compared with that of CpunOBP2. However, to Z10-16 : Ald Z3, Z6, Z9-23 : HC, and Z9-27 : HC, the recombined CpunOBP5 showed no binding affinity (**Table 4**).

DISCUSSION

When artificially rearing moths, dim red light is usually used to aid observations during scotophase. In this study, dim red light at night was hypothesized to increase mating in *C. punctiferalis*. To test this hypothesis, mating of *C. punctiferalis* was observed during scotophase with and without dim red light (610–710 nm, 2.0 lux). Many more adults were observed mating in red light compared with those in the dark. However, most mating was not enhanced under dim blue or white light. In addition, under different intensities of red light (0.2, 2.0, and 20.0 lux), similar enhancement in mating was observed. Moreover, the increased antennal sensitivity to female sex pheromones was found in male adults reared under red light during sctotophase. In a subsequent analysis, upregulation of expression levels of two OBP genes was determined in antennae of males under red light. The pheromone-binding affinities of the proteins of those two genes were confirmed in fluorescent-binding assays.

Insects are generally assumed to be essentially blind to red wavelengths (Shimoda and Honda, 2013). Therefore, red lights are frequently used to aid observations or operations while working with artificially reared insect populations during scotophase, because the influence on insects is negligible. However, different behaviors of insects were reported with or without red light. For example, red wavelengths influenced aggregation in the ant *Lasius niger*, and among colony individuals,

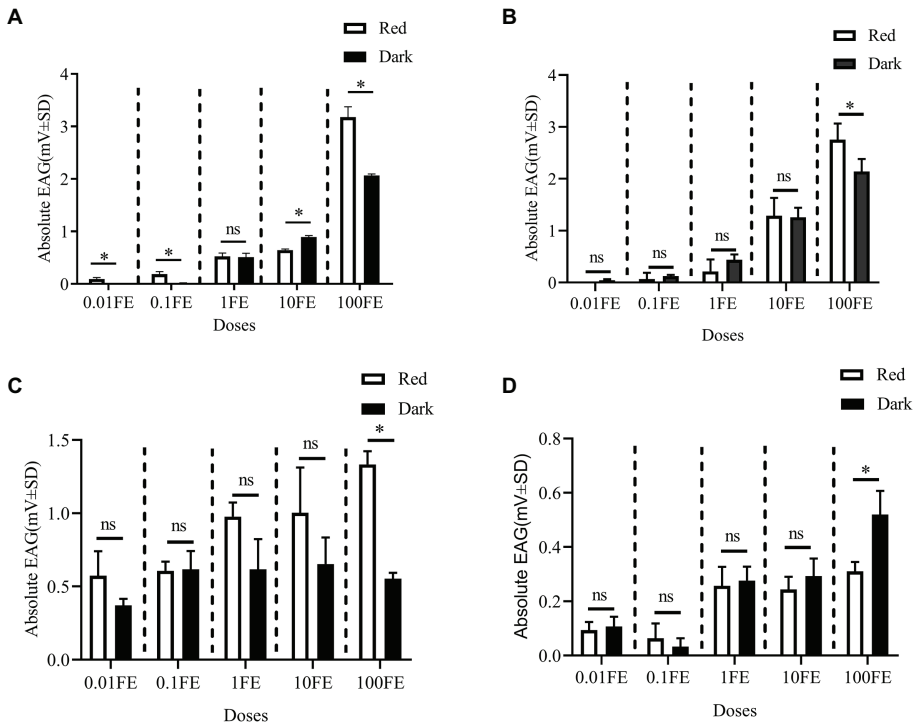

FIGURE 5 | Electroantennographic (EAG) responses of male *C. punctiferalis* reared under red light and dark conditions during scotophase. **(A)** E10-16:Ald; **(B)** Z10-16:Ald; **(C)** Z9-27:HC Z6; and **(D)** Z3, Z6, Z9-23:HC. Data are shown as mean ± SD, from four replicates. Asterisks above columns mean significant differences ($^{*}p < 0.05$, ns: no significant difference), by independent sample *t*-tests. FE, female equivalent.

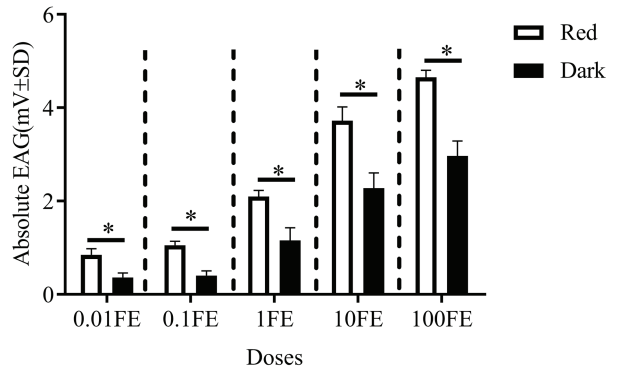

FIGURE 6 | Electroantennographic (EAG) responses to the mixture of sex pheromones of male *C. punctiferalis* reared under red light and dark conditions during scotophase. Data are shown as mean ± SD, from four replicates. Asterisks above columns mean significant differences ($^{*}p < 0.05$, ns: no significant difference), by independent sample *t*-tests. FE: female equivalent.

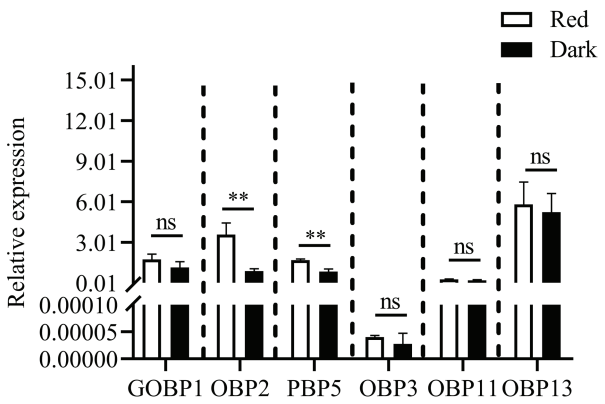

FIGURE 7 | Expression levels of odorant binding protein genes, in antennae of *C. punctiferalis* males (3-day-old) under red light and dark conditions during scotophase. Data are shown as mean ± SD, from three replicates. Asterisks above columns mean significant differences ($^{**}p < 0.01$, ns: no significant difference), by independent sample *t*-tests.

foragers aggregated well in total darkness but showed low assembly under red light, whereas brood-tenders aggregated well in both conditions (Depickere et al., 2004). The sexual performance of a lekking tephritid fruit fly (*A. luddens*) is also affected by red light (Diaz-Fleischer and Arredondo, 2011). Male flies exposed to red light were more frequently chosen as mating partners than dark-reared males. Similarly, females reared in red light mated more than those reared in blue light and in darkness.

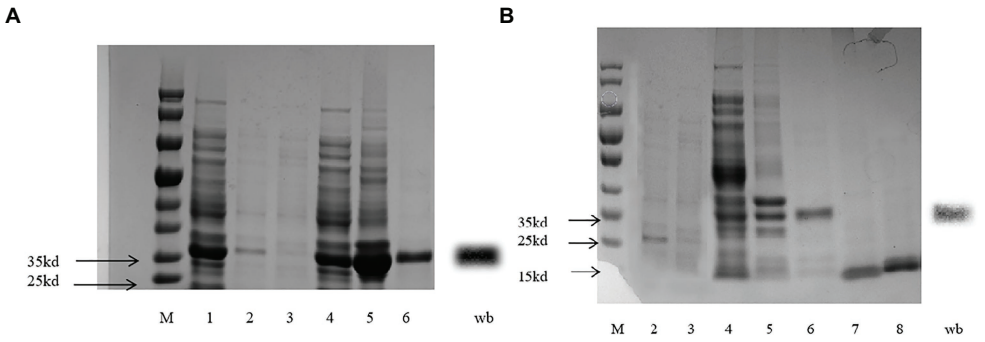

FIGURE 8 | SDS-PAGE for recombined CpunPBP5 **(A)** and CpunOBP2 **(B)**.

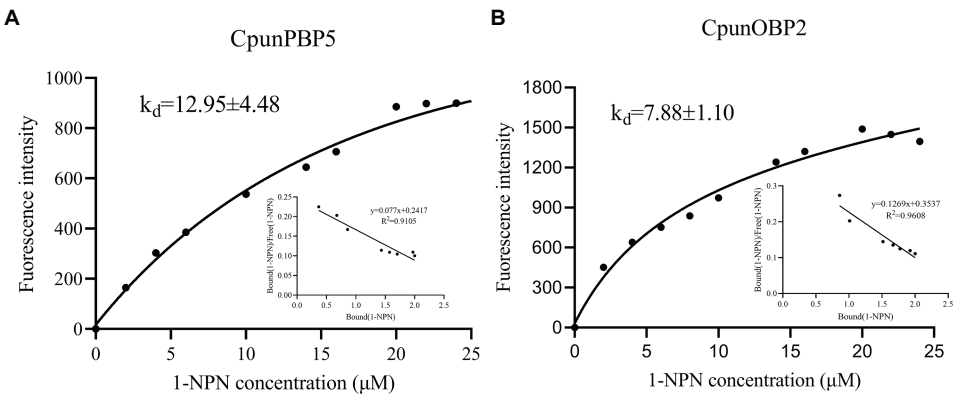

FIGURE 9 | Binding curve and relative Scatchard plot for 1-NPN/CpunOBP2 **(A)** and 1-NPN/CpunPBP5 **(B)**.

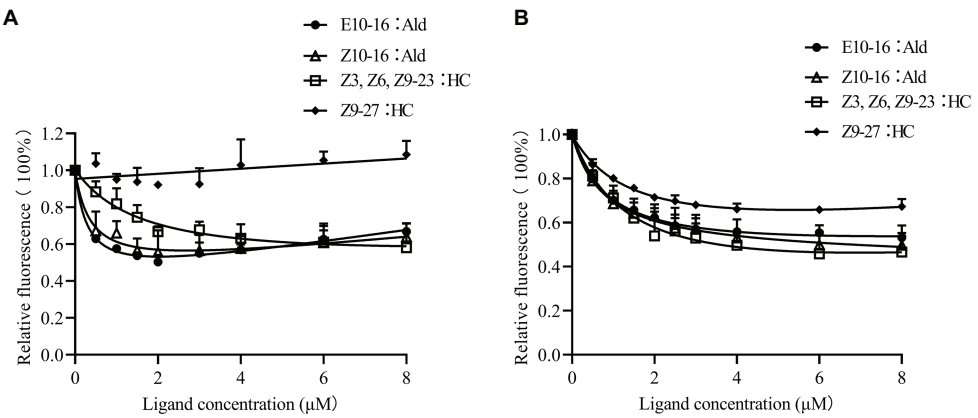

FIGURE 10 | Competitive binding curves of CpunPBP5 **(A)** and CpunOBP2 **(B)** to sex pheromones. Data are shown as mean ± SD, from three replicates.

Note that in the above publications, red lights were provided as a light source only in photophase, and no light was provided during scotophase. The effects of weak light on insect behavior in scotophase are rarely studied. Especially for many moth species, mating of which usually occurs at night. In the oriental tobacco budworm *H. assulta*, mating was increased by a dim white light (0.5 lux) during scotophase (Li et al., 2015). However, in that study, a 15 W incandescent bulb provided the light, which was probably broad-spectrum light rather than monochromatic one. In addition, the moths were held in cages with one pair (male

TABLE 4 | IC_{50} values (μM) and dissociation constants (K_i; μM) of CpunOBP2 and CpunPBP5 to different sex pheromones at pH = 7.4. Data are shown as mean ± SD, from three replicates.

Proteins	Ligand	IC_{50} (μM)	K_i (μM)
CpunOBP2	E10-16:Ald	9.55 ± 4.58	8.48 ± 4.06
	Z10-16:Ald	7.73 ± 2.82	6.86 ± 2.50
	Z3, Z6, Z9-23:HC	4.14 ± 2.63	3.68 ± 2.33
	Z9-27:HC	-	-
CpunPBP5	E10-16:Ald	1.58 ± 0.67	1.47 ± 0.62
	Z10-16:Ald	-	-
	Z3, Z6, Z9-23:HC	-	-
	Z9-27:HC	-	-

and female) per cage. As a result, the increase in mating was observed at only one time point, i.e., 1 h into scotophase. In this study, a monochromatic red light with the spectrum of 610–710 nm was used as the light source. Meanwhile, there were 30 pairs of males and females per cage (with three replicates), which gave individuals relatively free mate choice during mating. Thus, the increase in mating under red light during several consecutive scotophases was clearly observed in this study (**Figure 1**).

The EAG responses of male *C. punctiferalis* antennae under red light to single pheromone component, except of Z3, Z6, Z9-23:HC, was much higher than that of males in darkness, at the highest tested dose of 100FE (**Figures 5A–D**). When four pheromone components were further mixed and tested, the EAG response of male moths under red light was found increased significantly, compared with that in the dark at each of all tested doses (**Figure 6**). Generally, the sex pheromone of a Lepidopterous specie is composed of multi-components (Ando, 2018). Antennal responses of males usually could be elicited by a single component and the mixture of components. In natural environment, a male individual perceives female sex pheromone components as a mixture in spite of single ones. Therefore, the pheromone mixture elicits more comprehensive antennal response of males, compared with the single component does. In our results, obvious difference in EAG response between males under red light and in darkness against female sex pheromone was found when all pheromone components were tested as a mixture rather than singe ones. These results clearly indicate that red light enhances the antennal sensitivity of males to the female sex pheromone. The olfactory perception of female sex pheromones plays an essential role in the pheromone communication system of moths (Stengl, 2010). A variety of molecular components, including OBPs, chemosensory proteins, and odorant receptors, are involved in peripheral sensory reception and signal transduction in insects (Suh et al., 2014). Therefore, when the expression levels of chemosensory genes are up-regulated, increases in EAG responses are reasonably detected (Wan et al., 2015). In this study, the increase in the pheromone sensitivity of male adults with red light treatment was most likely due to the up-regulation of two OBP genes, i.e., *CpunOBP2* and *CpunPBP5*. The recombined proteins of these two genes, especially for CpunOBP2, showed strong binding to female sex pheromone components (**Figures 10A**,**B**). Of the two OBPs, CpunPBP5 has been previously identified as one of the pheromone-binding proteins in *C. punctiferalis* (Ge et al., 2018), whereas pheromone-binding affinity of CpunOBP2 was reported for the first time in our study.

Pre-exposure to various pheromones and plant volatiles frequently changes the expression levels of chemosensory genes in insect antennae (Wan et al., 2015). At the transcriptional level, artificial light at night was recently found to influence gene expression in *H. armigera* and *C. pipiens* (Honnen et al., 2016; Wang et al., 2018). In this study, the expression of OBP genes in male antennae of *C. punctiferalis* was up-regulated by red light during scotophase, with verification by RT-qPCR. With this finding, this study is the first to report that the expression of chemosensory genes in insects can be changed by monochromatic light. However, mechanisms of gene expression changed by red light remain largely unknown. Red light can penetrate animal tissues because of long wavelength (Fitzgerald et al., 2013; Zer-Krispil et al., 2018). And the cytochrome c oxidase of the mitochondrial respiratory chain is considered as the photoacceptor for the red light (Karu, 2008; Lunova et al., 2019). Irradiation of mammalian cells with red light causes an upregulation of various genes, most of which directly or indirectly play roles in the enhancement of cell proliferation and the suppression of apoptosis (Zhang et al., 2003). In our study, whether up-regulated expression of the two OBP genes in *C. punctiferalis* male antennae is relative to cytochrome *c* oxidase activated by red light is yet to be investigated.

In summary, we found that a dim red light enhanced mating of the yellow peach moth, *C. punctiferalis*, while a dim blue light and white light did not. Meanwhile, the red light increased expression of pheromone binding protein genes, *CpunOBP2* and *CpunPBP5*, in antennae of male adults, which showed increased antennal responses to female pheromone components. In brief, the increase in the antennal sensitivity of males to the female sex pheromone is probably one of the mechanisms for the increase in mating in *C. punctiferalis* under the dim red light during scotophase.

DATA AVAILABILITY STATEMENT

The raw data supporting the conclusions of this article will be made available by the authors, without undue reservation.

AUTHOR CONTRIBUTIONS

ZX and WX designed the research and wrote the article. QC, XY, DY, JL, and XH performed the experiments. All authors contributed to the article and approved the submitted version.

FUNDING

This work was supported by the National Key Research and Development Project (2017YFD0202002-7) and Fundamental Research Funds for the Central Universities, China (XDJK2018B040).

ACKNOWLEDGMENTS

We express sincere thanks to Dr. Lin He and Dr. Guangmao Shen for valuable suggestions in the experiments.

REFERENCES

Ando, T. (2018). Internet database. Available at: https://lepipheromone.sakura.ne.jp/lepi_phero_list_eng.html

Beck, J. J., Light, D. M., and Gee, W. S. (2014). Electrophysiological responses of male and female *Amyelois transitella* antennae to pistachio and almond host plant volatiles. *Entomol. Exp. Appl.* 153, 217–230. doi: 10.1111/eea.12243

Botha, L. M., Jones, T. M., and Hopkins, G. R. (2017). Effects of lifetime exposure to artificial light at night on cricket (*Teleogryllus commodus*) courtship and mating behaviour. *Anim. Behav.* 129, 181–188. doi: 10.1016/j.anbehav.2017.05.020

Depickere, S., Fresneau, D., and Deneubourg, J. L. (2004). The influence of red light on the aggregation of two castes of the ant, *Lasius niger*. *J. Insect Physiol.* 50, 629–635. doi: 10.1016/j.jinsphys.2004.04.009

Diaz-Fleischer, F., and Arredondo, J. (2011). Light conditions affect sexual performance in a lekking tephritid fruit fly. *J. Exp. Biol.* 214, 2595–2602. doi: 10.1242/jeb.055004

Fitzgerald, M., Hodgetts, S., Heuvel, C. V. D., Natoli, R., Hart, N. S., Valter, K., et al. (2013). Red/near-infrared irradiation therapy for treatment of central nervous system injuries and disorders. *Rev. Neurosci.* 24, 205–226. doi: 10.1515/revneuro-2012-0086

Ge, X., Ahmed, T., Zhang, T., Wang, Z., He, K., and Bai, S. (2018). Binding specificity of two PBPs in the yellow peach moth *Conogethes punctiferalis* (Guenee). *Front. Physiol.* 9:308. doi: 10.3389/fphys.2018.00308

Honnen, A. C., Johnston, P. R., and Monaghan, M. T. (2016). Sex-specific gene expression in the mosquito *Culex pipiens* f. molestus in response to artificial light at night. *BMC Genomics* 17:22. doi: 10.1181/s12864-015-2336-0

Hua, J., Pan, C., Huang, Y., Li, Y., Li, H., Wu, C., et al. (2020). Functional characteristic analysis of three odorant-binding proteins from the sweet potato weevil (*Cylas formicarius*) in the perception of sex pheromones and host plant volatiles. *Pest Manag. Sci.* 77, 300–312. doi: 10.1002/ps.6019

Jing, D. P., Zhang, T. T., Bai, S. X., Prabu, S., He, K. L., Dewer, Y., et al. (2019). GOBP1 plays a key role in sex pheromones and plant volatiles recognition in yellow peach moth, *Conogethes punctiferalis* (Lepidoptera: Crambidae). *Insects* 10:302. doi: 10.3390/insects10090302

Karu, T. I. (2008). Mitochondrial signaling in mammalian cells activated by red and near-IR radiation. *Photochem. Photobiol.* 84, 1091–1099. doi: 10.1111/j.1751-1097.2008.00394.x

Kawazu, K., Adati, T., and Tatsuki, S. (2011). The effect of Photoregime on the calling behavior of the rice leaf folder moth, *Cnaphalocrocis medinalis* (Lepidoptera: Crambidae). *Japan Agr. Res. Q.* 45, 197–202. doi: 10.6090/jarq.45.197

Konno, Y., Arai, K., Sekiguchi, K., and Matsumoto, Y. (1982). (*E*)-10-Hexadecenal, a sex pheromone component of the yellow peach moth, Dichocrocis punctiferalis Guenée (Lepidoptera: Pyralidae). *Appl. Entomol. Zool.* 17, 207–217. doi: 10.1303/aez.17.207

Li, H. T., Yan, S., Li, Z., Zhang, Q. W., and Liu, X. X. (2015). Dim Light during scotophase enhances sexual behavior of the oriental tobacco *Budworm Helicoverpa assulta* (Lepidoptera: Noctuidae). *Fla. Entomol.* 98, 690–696. doi: 10.1653/024.098.0244

Liu, N.-Y., He, P., and Dong, S.-L. (2012). Binding properties of pheromone-binding protein 1 from the common cutworm *Spodoptera litura*. *Comp. Biochem. Physiol. B* 161, 295–302. doi: 10.1016/j.cbpb.2011.11.007

Liu, N. Y., Liu, C. C., and Dong, S. L. (2013). Functional differentiation of pheromone-binding proteins in the common cutworm *Spodoptera litura*. *Comp. Biochem. Physiol. A Mol. Integr. Physiol.* 165, 254–262. doi: 10.1016/j.cbpa.2013.03.016

Lunova, M., Smolková, B., Uzhytchak, M., Janoušková, K. Ž., Jirsa, M., Egorova, D., et al. (2019). Light-induced modulation of the mitochondrial respiratory chain activity: possibilities and limitations. *Cell. Mol. Life Sci.* 77, 2815–2838. doi: 10.1007/s00018-019-03321-z

Matthews, R. W., and Matthews, J. R. (eds.) (2010). "Visual communication" in *Insect behavior*. *2nd Edn.* (New York, NY, United States: Springer), 261–290.

Ngumbi, E., Chen, L., and Fadamiro, H. (2010). Electroantennogram (EAG) responses of *Microplitis croceipes* and *Cotesia marginiventris* and their lepidopteran hosts to a wide array of odor stimuli: correlation between EAG response and degree of host specificity? *J. Insect Physiol.* 56, 1260–1268. doi: 10.1016/j.jinsphys.2010.03.032

Obara, Y., Koshitaka, H., and Arikawa, K. (2008). Better mate in the shade: enhancement of male mating behaviour in the cabbage butterfly, *Pieris rapae crucivora*, in a UV-rich environment. *J. Exp. Biol.* 211, 3698–3702. doi: 10.1242/jeb.021980

Petersen, T. N., Brunak, S., Heijne, G. V., and Nielsen, H. (2011). SignalP 4.0: discriminating signal peptides from transmembrane regions. *Nat. Methods* 8, 785–786. doi: 10.1038/nmeth.1701

Shimoda, M., and Honda, K. I. (2013). Insect reactions to light and its applications to pest management. *Appl. Entomol. Zool.* 48, 413–421. doi: 10.1007/s13355-013-0219-x

Stengl, M. (2010). Pheromone transduction in moths. *Front. Cell. Neurosci.* 4:133. doi: 10.3389/fncel.2010.00133

Suh, E., Bohbot, J. D., and Zwiebel, L. J. (2014). Peripheral olfactory signaling in insects. *Curr. Opin. Insect Sci.* 6, 86–92. doi: 10.1016/j.cois.2014.10.006

Sun, M. J., Liu, Y., and Wang, G. R. (2013). Expression patterns and binding properties of three pheromone binding proteins in the diamondback moth, *Plutella xyllotella*. *J. Insect Physiol.* 59, 46–55. doi: 10.1016/j.jinsphys.2012.10.020

van Geffen, K. G., Groot, A. T., van Grunsven, R. H. A., Donners, M., Berendse, F., and Veenendaal, E. M. (2015). Artificial night lighting disrupts sex pheromone in a noctuid moth. *Ecol. Entomol.* 40, 401–408. doi: 10.1111/een.12202

Wan, X. L., Qian, K., and Du, Y. J. (2015). Synthetic pheromones and plant volatiles alter the expression of chemosensory genes in *Spodoptera exigua*. *Sci. Rep.* 5:17320. doi: 10.1038/srep17320

Wang, L. J., Liu, X. H., Liu, Z. X., Wang, X. P., Lei, C. L., and Zhu, F. (2018). Members of the neuropeptide transcriptional network in *Helicoverpa armigera* and their expression in response to light stress. *Gene* 671, 67–77. doi: 10.1016/j.gene.2018.05.070

Wang, S., Wang, K., Michaud, J. P., Zhang, F., and Tan, X. L. (2014). Reproductive performance of *Propylea japonica* (Coleoptera: Coccinellidae) under various light intensities, wavelengths and photoperiods. *Eur. J. Entomol.* 111, 341–347. doi: 10.14411/eje.2014.053

Xiang, Y. Y., Zhang, X. W., and Xu, G. M. (2018). The timing of calling and mating in *Heterolocha jinyinhuaphaga* and the influence of environmental determinants. *J. Insect Behav.* 31, 334–346. doi: 10.1007/s10905-018-9682-0

Xiao, W., Honda, H., and Matsuyama, S. (2011). Monoenyl hydrocarbons in female body wax of the yellow peach moth as synergists of aldehydepheromone components. *Appl. Entomol. Zool.* 46, 239–246. doi: 10.1007/s13355-011-0035-0

Xiao, W., Matsuyama, S., Ando, T., Millar, J. G., and Honda, H. (2012). Unsaturated cuticular hydrocarbons synergize responses to sex attractant pheromone in the yellow peach moth, *Conogethes punctiferalis*. *J. Chem. Ecol.* 38, 1143–1150. doi: 10.1007/s10886-012-0176-9

Xu, L. R., Ni, X. Z., Wang, Z. Y., and He, K. L. (2014). Effects of photoperiod and temperature on diapause induction in *Conogethes punctiferalis* (Lepidoptera: Pyralidae). *Insect Sci.* 21, 556–563. doi: 10.1111/j.1744-7917.2012.01543.x

Yang, L., Hu, X. J., Xu, Z. F., and Xiao, W. (2017). Screening of reference genes for qRT-PCR in *Conogethes punctiferalis* (Lepidoptera:Crambidae). *Acta Entomol. Sin.* 60, 1266–1277. doi: 10.16380/j.kcxb.2017.11.004-015-2336-0

Zer-Krispil, S., Zak, H., Shao, L., Ben-Shaanan, S., Tordjman, L., Bentzur, A., et al. (2018). Ejaculation induced by the activation of Crz neurons is rewarding to drosophila males. *Curr. Biol.* 28, 1445.e3–1452.e3. doi: 10.1016/j.cub.2018.03.039

Zhang, Y. O., Song, S. P., Fong, N. C. C., Tsang, C. H., Yang, Z., and Yang, M. S. (2003). cDNA microarray analysis of gene expression profiles in human fibroblast cells irradiated with red Light. *J. Invest. Dermatol.* 120, 849–857. doi: 10.1046/j.1523-1747.2003.12133.x

Conflict of Interest: The authors declare that the research was conducted in the absence of any commercial or financial relationships that could be construed as a potential conflict of interest.

frontiers in Genetics

ORIGINAL RESEARCH
published: 05 July 2021
doi: 10.3389/fgene.2021.691382

OPEN ACCESS

Edited by:
Wei Guo,
Institute of Zoology, Chinese Academy of Sciences (CAS), China

Reviewed by:
Sufang Zhang,
Research Institute of Forest Ecology, Environment and Protection Chinese Academy of Forestry, Chinese Academy of Sciences, China
Jiasheng Song,
Henan University, China

***Correspondence:**
Yanping Luo
yanpluo2012@hainanu.edu.cn
Baoqian Lyu
lvbaoqian@hotmail.com

†ORCID:
Shakil Ahmad
orcid.org/0000-0003-2383-0798
Momana Jamil
orcid.org/0000-0003-3639-5705
Muhammad Fahim
orcid.org/0000-0002-5470-1641
Farman Ullah
orcid.org/0000-0001-6174-1425
Yanping Luo
orcid.org/0000-0002-1948-715X

Specialty section:
This article was submitted to Epigenomics and Epigenetics, a section of the journal Frontiers in Genetics

Received: *06 April 2021*
Accepted: *10 June 2021*
Published: *05 July 2021*

Citation:
Ahmad S, Jamil M, Fahim M, Zhang S, Ullah F, Lyu B and Luo Y (2021) RNAi-Mediated Knockdown of Imaginal Disc Growth Factors (IDGFs) Genes Causes Developmental Malformation and Mortality in Melon Fly, Zeugodacus cucurbitae. Front. Genet. 12:691382. doi: 10.3389/fgene.2021.691382

RNAi-Mediated Knockdown of Imaginal Disc Growth Factors (IDGFs) Genes Causes Developmental Malformation and Mortality in Melon Fly, *Zeugodacus cucurbitae*

Shakil Ahmad[1†], Momana Jamil[1†], Muhammad Fahim[2†], Shujing Zhang[1], Farman Ullah[3†], Baoqian Lyu[4*] and Yanping Luo[1*†]

[1] School of Plant Protection, Hainan University, Haikou, China, [2] Centre for Omic Sciences, Islamia College University, Peshawar, Pakistan, [3] Department of Entomology, College of Plant Protection, China Agricultural University, Beijing, China, [4] Environment and Plant Protection Institute, Chinese Academy of Tropical Agricultural Sciences/Key Laboratory of Integrated Pest Management on Tropical Crops, Ministry of Agriculture and Rural Affairs, Haikou, China

This study reports the first successful use of oral feeding dsRNA technique for functional characterization of imaginal disc growth factors (IDGFs) genes (*IDGF1*, *IDGF3_1*, *IDGF4_0*, *IDGF4_1*, and *IDGF6*) in melon fly *Zeugodacus cucurbitae.* Phylogenetic and domain analysis indicates that these genes had high similarity with other Tephritidae fruit flies homolog and contain only one conserved domain among these five genes, which is glyco-18 domain (glyco-hydro-18 domain). Gene expression analysis at different developmental stages revealed that these genes were expressed at larval, pupal, and adult stages. To understand their role in different developmental stages, larvae were fed dsRNA-corresponding to each of the five IDGFs, in an artificial diet. RNAi-mediated knockdown of *IDGF1* shows no phenotypic effects but caused mortality (10.4%), while *IDGF4_0* caused malformed pharate at the adult stage where insects failed to shed their old cuticle and remained attached with their body, highest mortality (49.2%) was recorded compared to dsRNA-green fluorescent protein (GFP) or DEPC. Silencing of *IDGF3_1* and *IDGF4_1* cause lethal phenotype in larvae, (17.2%) and (40%) mortality was indexed in *Z. cucurbitae*. *IDGF6* was mainly expressed in pupae and adult stages, and its silencing caused a malformation in adult wings. The developmental defects such as malformation in wings, larval–larval lethality, pupal–adult malformation, and small body size show that IDGFs are key developmental genes in the melon fly. Our results provide a baseline for the melon fly management and understanding of IDGFs specific functions in *Z. cucurbitae.*

Keywords: chitinase, mortality, RNA interference, wings malformation, Tephritidae

INTRODUCTION

RNA interference (RNAi) was simultaneously discovered as a tool for functional genomics (Fire et al., 1998) and antiviral resistance strategy (Waterhouse et al., 1998). Since then, it has been explored and applied as an effective tool for the control of aphids (Zhao et al., 2018; Tariq et al., 2019; Ullah et al., 2020b), whiteflies (Grover et al., 2019), beetles (Mehlhorn et al., 2020), and lepidopterans pests (Rana et al., 2020), etc. Because of RNAi's robustness and target precision, it has lowered pesticide pressure on humans and the atmosphere while minimizing negative effects on non-target and beneficial insects. Furthermore, RNAi knockdown and knock-out variants have opened new avenues in reverse genetics for functional characterization of previously uncharacterized genes. Numerous studies on RNAi use for transgenic insect resistance have been reported, either in cellular cytoplasm (Chung et al., 2021) or Chloroplast (Bally et al., 2018). Moreover, exogenous application of dsRNA is effective against herbivorous insect pests, both in the laboratory (San Miguel and Scott, 2016) and in field trials (Mehlhorn et al., 2020). Additionally, RNAi also has revolutionized sterile insect technique (SIT) through the use of dsRNAs targeted at genes involved in fertility or fecundity of insect pests (Darrington et al., 2017; Ullah et al., 2020b). However, the selection of efficient target genes for RNAi-mediated control strategy remains the pivotal player in the overall success and efficacy (Scott et al., 2013; Xu et al., 2016). In insects, the epithelial apical extracellular matrix (ECM) contains many fibrous proteins and polysaccharides synthesized or transmembrane, whose composition differs significantly, from insect chitinase to plants cellulose (Cosgrove, 2005; Öztürk-Çolak et al., 2016; Vuong-Brender et al., 2017). Exoskeleton is essential for epithelial barrier formation, maintaining body shape, homeostasis, and protect the insect from coming in contact with agrochemical, predators, and parasitoids (Galko and Krasnow, 2004; Yoshiyama et al., 2006; Turner, 2009; Shibata et al., 2010; Uv and Moussian, 2010; Jaspers et al., 2014). Many studies recently reported that ECM helps in the shaping of different organs, like *Drosophila* wings (Fernandes et al., 2010) and provide structural support to delicate internal organs but also protects them against damage caused by various environmental factors and microorganisms (Dittmer et al., 2015; Mun et al., 2015).

Various genes involved in cuticular synthesis and maintenance have been characterized (Pan et al., 2011). Among these, imaginal disc growth factors (IDGFs), which belong to Chitinase glycoside hydrolase 18 (GH18) family, are associated with insect's molting and cuticle maintenance (Zhao et al., 2020). IDGFs were first identified from *Drosophila* imaginal disc cell cultures by fractionating conditioned medium (Kawamura et al., 1999; Zhu et al., 2008). IDGFs were confirmed to be the proteins cooperating with insulin that promote cell lineages derived from imaginal discs in *Drosophila melanogaster* (Kawamura et al., 1999; Varela et al., 2002; Zurovcová and Ayala, 2002). RNAi has been widely used to find out the functions of vital genes in different insects of economic importance (Tomoyasu and Denell, 2004; Chen et al., 2008; Gong et al., 2012; Asokan et al., 2013; Zhang et al., 2013; Qi et al., 2015; Wang et al., 2017; Ullah et al., 2020a). Recently, a study reported that silencing of *IDGF6* in *Bactrocera correcta* through RNAi significantly decreases the expression of *IDGF6*, causes larval mortality and wing malformation in adult flies (Zhao et al., 2020). Similar reports using RNAi techniques for silencing essential genes were recorded in severe phenotypes abnormalities in different insect species (Zhu et al., 2008; Bellés, 2010; Scott et al., 2013; Xi et al., 2015). Although in model insects *D. melanogaster*, IDGFs have been reported systematically, and specific functional information in *Zeugodacus cucurbitae* are still unknown. In *Drosophila*, these five non-enzymatic IDGFs (*IDGF1*, *IDGF3_1*, *IDGF4_0*, *IDGF4_1*, and *IDGF6*) are involved in the maintenance of ECM scaffold against chitinolytic degradation, and plays a vital role in physiological processes such as adult eclosion, development regulation, and blood sugar reduction of insects (Galko and Krasnow, 2004). Among these genes, the function of the *IDGF4* gene has been recently described in the defense barrier and development of *Bactrocera dorsalis* (Diptera: Tephritidae) (Gu et al., 2019). However, very little information is available on the rest of the member genes. Targeting genes involved in cuticular formation may provide an effective way for pest control.

Melon fly, *Z. cucurbitae* Coquillett (Diptera: Tephritidae) is one of the most destructive pests that cause severe economic loss to cucurbit crops (Gogi et al., 2009). Different researchers reported its losses in various crops to range up to 30–100% (Dhillon et al., 2005; Subedi et al., 2021). Researchers reported many strategies to control fruit flies which includes pheromones (Shelly et al., 2004; Panhwar, 2005), cultural practices (Gogi et al., 2007, 2009), biological controls (Drew et al., 2003), lure mixtures (Vargas et al., 2008, 2010), and hot water treatment (Panhwar, 2005). Insecticide applications are less effective due to larvae developing and feeding inside the fruit, covered by fruit pulp, and not exposed to direct insecticides (Yee et al., 2007; Gogi et al., 2009; Sapkota et al., 2010). Also, insecticides contaminate the environment, have a deleterious impact on predators and parasitoids of insect pests, develop resistance, induces insect pest populations and have maximum residue levels (MRLs) issues (Desneux et al., 2007; Baig et al., 2009; Decourtye et al., 2013; Gebregergis, 2018; Jactel et al., 2019; Ullah et al., 2019a,b). Therefore, novel approaches such as RNAi will provide novel ways to control *Z. cucurbitae* and provide insight into functional genomics of the target genes in ECM formation.

In this paper, we cloned and identified full-length cDNA of five IDGF family genes from *Z. cucurbitae*, which are least characterized in Tehpritidae. We then analyzed gene expression patterns in eight different developmental stages of *Z. cucurbitae* using real-time quantitative PCR (RT-qPCR). dsRNA-mediated RNAi technology was applied to explore the function of five-member genes of IDGF family in *Z. cucurbitae* at larval and adult stages. Knockdown of *IDGF3_1*, *IDGF4_0*, *IDGF4_1*, and *IDGF6* genes led to various types of developmental defects and mortality except *IDGF1*, where the dsRNA treated larvae showed minimal mortality and no visible phenotypes. Our data provide a baseline for the role of IDGFs genes in developmental stages of *Z. cucurbitae*

and identify the potential target for RNAi mediated pest control strategy.

MATERIALS AND METHODS

Insects Rearing

Colony of *Z. cucurbitae* was reared for many generations in the insect rearing room at 25 ± 1°C and 75% relative humidity, with a 14:10 h (light: dark) photoperiod at Hainan University, Haikou, China. Larvae were fed with artificial food as described previously (Liu et al., 2020). Fruit flies were reared on a ratio of 3:1 of sugar and yeast for around 10–12 generations in 45 cm × 45 cm × 50 cm cages before the experiment to eradicate local environmental impact.

Cloning of IDGFs Genes

To detect the expression pattern of five different genes (*IDGF1*, *IDGF3_1*, *IDGF4_0*, *IDGF4_1*, and *IDGF6*), total RNA was isolated from eight different developmental stages of *Z. cucurbitae*. Briefly, A total of ten individuals according to the body size (Per replication: L2 20 larvae, L3-1 10 larvae, L3-2 10 larvae, P-E, P-M, P-L 5 pupae for each, A-E and A-M 2 adults for each) were randomly collected and mixed for RNA extraction. cDNA was synthesized using commercially available HiScript® III 1st Strand cDNA Synthesis Kit following the manufacturer's instructions. RT-qPCR was performed to verify IDGFs gene fragment (**Supplementary Table 3**) from *Z. cucurbitae* using Prime STAR® HS DNA Polymerase (Takara, Japan) under the following conditions: initial denaturation at 94°C for 5 min; followed by 30 cycles of Denaturation at 94°C for 30 s, annealing at 58°C for 30 s, extension at 72°C (according to the size of each gene) and final extension at 72°C for 5 min. Amplified products were examined by 1.2% agarose gel electrophoresis and purified using a Universal DNA Purification kit (Tiangen, China). Amplified PCR products were cloned into a pMD^{TM}18-T vector (Takara, Japan), and verified by sequencing at Sangon Biotech Company Shanghai, China.

Phylogenetic Analysis

We used MEGA 6.0 software to construct a phylogenetic tree through the maximum likelihood method JTT matrix-based model with 1,000 replications of bootstrap analysis (Tamura et al., 2013). The full name of species used in this tree construction and the short names used are all listed along with GenBank accession numbers in **Supplementary Table 1**.

dsRNA Preparation and Feeding

dsRNA was synthesized using T7 RiboMAX^{TM} Express RNAi System (Promega, United States). Each primer used for PCR contained a 5′ T7RNA polymerase binding site (GAATTAATACGACTCACTATAGGGAGA) followed by the sequence-specific for the target gene i.e., *IDGF1*, *IDGF3_1*, *IDGF4_0*, *IDGF4_1*, and *IDGF6* (**Supplementary Table 3**). These primers were used to amplify the template for the synthesis of forward and reverse RNA. dsRNA was purified according to manufacturer's instructions and the integrity and quantities of all synthesized dsRNA products were determined by 1.2% agarose gel electrophoresis. Their concentration was measured using the NanoDrop2000 spectrophotometer. dsRNA of green fluorescent protein (GFP) and DEPC was used as a negative control. To investigate the biological functions of each chitinase gene of *Z. cucurbitae*, dsRNA was fed to 2 days old third instar larvae for 48 h and then shifted to the new food contain dsRNA for another 48 h. Five biological replications were performed with sixty individuals in each replicate. Each replicates fed with 6 g artificial food contained 60 μl dsRNA (1,000 ng/μl), dsGFP, and DEPC. Larval body size, mortality, and phenotype were examined 24 h post-feeding at each developmental stage till the adult's sexual maturity.

Detection of Gene Expression by RT-qPCR

To understand the temporal gene expression profile of *IDGF1*, *IDGF3_1*, *IDGF4_0*, *IDGF4_1*, and *IDGF6* of *Z. cucurbitae*, RT-qPCR was performed at different developmental stages. RT-qPCR was performed using SYBR® Premix Ex Taq^{TM} II (TliRNaseH Plus) (Takara, Japan) on an ABI 7500 instrument (United States). The PCR reaction includes 10 μl SYBER Green mix, 1 μl cDNA, 1 μl each of forward and reverse primers and 7 μl of ddH_2O with three technical and three biological replicates for each gene expression. The elongation factor 1 alpha (*EF1α*) was used as endogenous reference genes for data normalization, and a relative transcript level of IDGFs was calculated with the $2^{-\Delta\Delta Ct}$ method (Livak and Schmittgen, 2001). All the primers used in this study are shown in **Supplementary Table 3**.

Silencing of Chitinase Genes of *Zeugodacus cucurbitae*

To observe phenotype, third early-instar larvae (2 days old) was fed with 6 g food mixed with 60 μl dsRNA or dsGFP (1,000 ng/μl) or DEPC for 48 h and transferred to a new artificial diet with the same treatment for another 48 h. After 96 h, larvae were shifted to soil for pupation. Two individuals from each replication of each group were killed every 24 h until the pupal stage to determine RNAi efficiency, while the others continued to feed. Similarly, two individuals were killed at the adult stage (24 h old), to test the RNAi efficiency. The stability of dsRNAs in the artificial diet, 1 g of each diet was collected 24 h post-feeding. The artificial diet was diluted in 50 μl distilled water, and the dsRNAs were observed in 1% agarose gel electrophoresis. Mortality was recorded by counting the flies number in each group after 24 h. The phenotype effects were observed in each developmental stage until 10 days of the adult's emergence.

Statistical Analysis

Statistical analysis was performed to measure the significant differences between each different group. Chitinase-like protein expression was quantified in the larvae, Pupae, and adults treated with dsRNA-GFP, DEPC, and gene-specific dsRNA. Statistical significance of differences in gene expression levels among samples was assessed using one-way ANOVA with a 0.05 level of

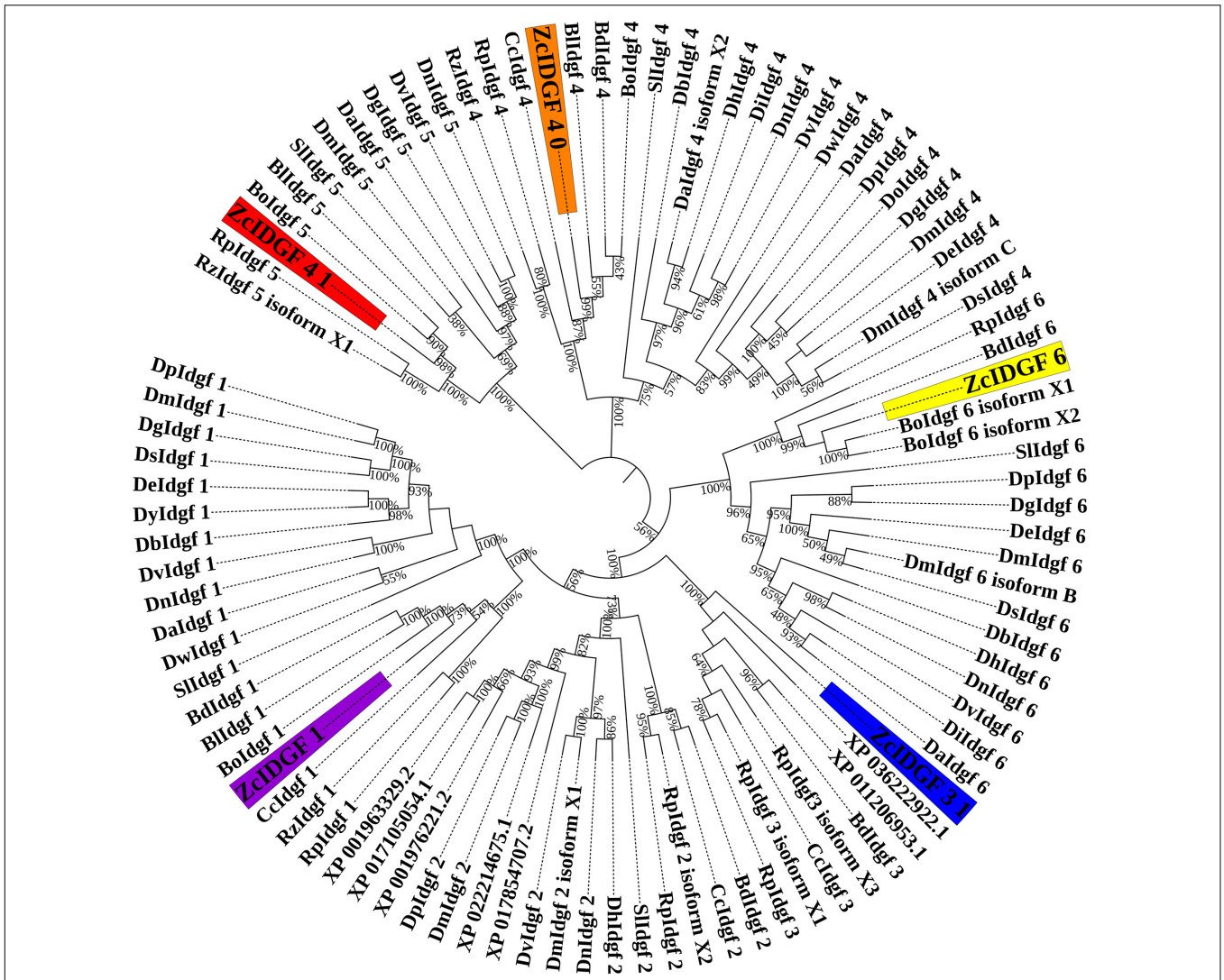

FIGURE 1 | Phylogenetic analysis of IDGFs genes with model family Tephritidae (taxid: 7211) and Drosophilidae (taxid: 7214) are shown in the tree. The highlighted part indicates our target genes. Tree indicates relationship between IDGFs gene and species tree. Maximum likelihood method was used to construct insects IDGFs coding sequences phylogenetic tree. Complete details of all IDGFs are listed in **Supplementary Table 1**.

significance (95% confidence interval) GraphPad Prism 8.01 for Windows (GraphPad Software, San Diego, CA, United States)[1].

RESULTS

Characterization and Phylogenetic Analysis of IDGFs of *Zeugodacus cucurbitae*

Imaginal disc growth factors genes (*IDGF1*, *IDGF3_1*, *IDGF4_0*, *IDGF4_1*, and *IDGF6*) were cloned from *Z. cucurbitae* (**Supplementary Table 2**). They were compared with IDGF genes with Tephritidae (taxid: 7211) and Drosophilidae (taxid: 7214) as a model family (**Supplementary Table 1**). The five IDGF genes were highly conserved and had high homology with members of Tephritidae than Drosophilidae (**Figure 1**).

Nucleotide sequence analysis shows that *IDGF1* of *Z. cucurbitae* had the maximum similarity with a homolog *Bison latifrons* and *B. dorsalis* (92%) followed by *Bactrocera oleae* (91%) and *Ceratitis capitata* (89%). Compared with similar in *Drosophila*, the highest identity was recorded with *Drosophila virilis* (69%). *IDGF3_1* shows highest similarity with *B. dorsalis* and *B. latifrons* (94%) followed by *B. oleae* (93%) and *Rhagoletis pomonella* (91%). Compared with the similar Drosophilidae, the highest identity was revealed with *Drosophila hydei* and *D. virilis* (71%). For *IDGF4_0*, the maximum similarity was recorded with *B. latifrons* and *B. dorsalis* (98%), followed by *B. oleae* (96%) and *C. capitata* (92%). Compared to the similar in Drosophilidae, the highest identity of *IDGF4_0* revealed with *D. hydei* and *D. virilis* (83%). Nucleotide sequence analysis revealed that the *IDGF4_1* of *Z. cucurbitae* had highest identity with a homolog from

[1]www.graphpad.com

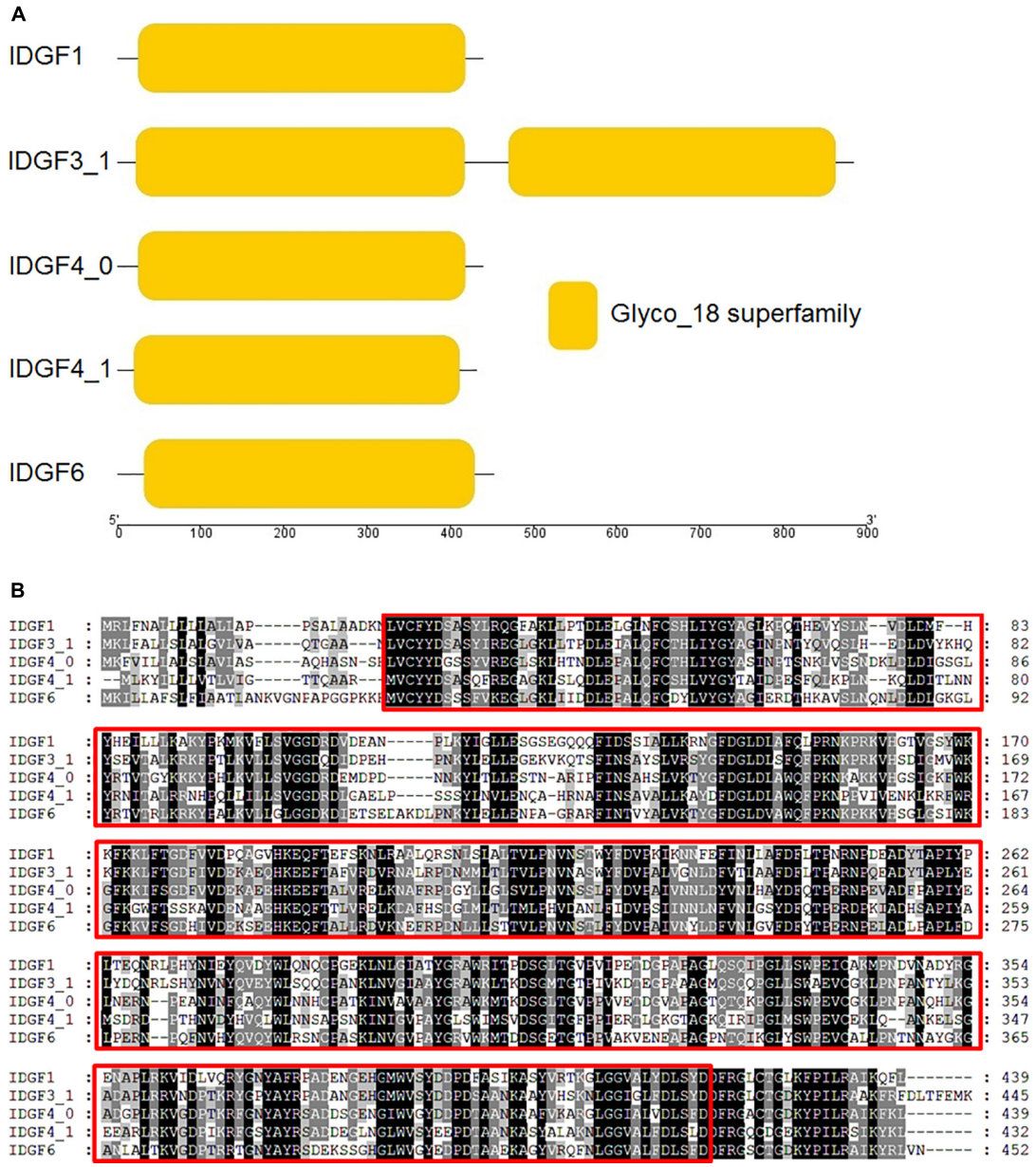

FIGURE 2 | (A) Imaginal disc growth factors gene, also their domain architecture and motif in *Z. cucurbitae.* The deduced amino acid sequences were used to predict the domain architectures of the five IDGFs genes using online conserved domain database (CDD) and presented through TBTool software. **(B)** Amino acid sequence alignment of IDGFs was performed using ClustalW alignment method in MEGA7. In GeneDoc program, ClustalW alignment was used to shade the identical and similar amino acids in the alignment. The conserved regions among five IDGFs sequences are tinted with red box. Dark shade indicates identical amino acids and gray shade represents similar amino acids.

B. oleae (79%), *B. latifrons* (76%), *C. capitata* (72%), followed by *Rhagoletis zephyria* and *R. pomonella* (71%). Compared to the same Drosophilidae, the highest identity of *IDGF4_1* revealed with *Drosophila mojavensis* (58%). Comparison of nucleotide sequence within Tephritidae family revealed that *IDGF6* of *Z. cucurbitae* has high homology with *B. dorsalis* (96%), *B. latifrons* (96%), followed by *B. oleae*, and *C. capitata* (94%). In the family Drosophilidae, the highest identity of *IDGF6* was observed with *D. melanogaster* (77%).

Architectures of Domain and Catalytic Motif of IDGFs in *Zeugodacus cucurbitae*

We used amino acid sequences of the five IDGFs genes, i.e., *IDGF1*, *IDGF3_1*, *IDGF4_0*, *IDGF4_1*, and *IDGF6*, for domain architectures using pfam online tool (**Figure 2A**). Our results show that all predicted amino acid sequences contained ≥ 1 Glyco_hydro_18 superfamily domain (PFAM accession: PF00704).

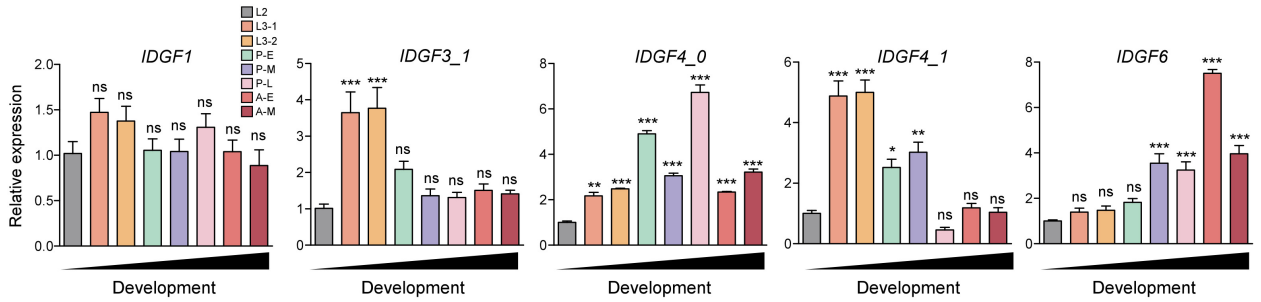

FIGURE 3 | Temporal expression of eight developmental stages of *Z. cucurbitae* was determined, RNA was extracted from the whole body of flies in different developmental stages including 2nd instar larvae (L2), 3rd early-instar larvae (L3-1), Third late instar larvae (L3-3), 1–2 days mixed pupae as early pupae (P-E), 5–6 days as mid pupae (P-M), and 7–9 days as of late pupae (P-L), 1–2 days adults as (A-E), and 10-day adults as (A-M). We had presented our results after normalization against reference gene *EFα1* as the relative expression. All IDGFs gene expression is relative to the gene expression of each gene in 2nd instar larvae. One-way ANOVA with *post hoc* Tukey test was used to test the statistical significance $*p < 0.05$; $**p < 0.01$; $***p \leq 0.001$, ns: not significant.

In particular, *IDGF3_1* had two copies of Glyco_hydro_18 superfamily domains, whereas the remaining amino acid sequences, *IDGF1*, *IDGF4_0*, *IDGF4_1*, and *IDGF6*, had only one copy. Sequence alignment showed that five IDGFs genes have well-conserved regions, including the specific sites for gene activity (**Figure 2B**). However, no chitin-binding domain (CBD) was found at the *C*-terminus. Further, *IDGF1* has two *N*-glycosylation sites at positions 208 and 220 in the N-terminal extracellular domain, while *IDGF3_1* has three potential *N*-glycosylation sites at positions 219, 665, and 791. The *IDGF4_0* has two *N*-glycosylation sites at positions 65 and 222, and *IDGF4_1* also has two potential *N*-glycosylation sites at positions 83 and 278 in the *N*-terminal extracellular domain. *IDGF6* has only one *N*-glycosylation site at position 233 (**Supplementary Figure 1**).

Temporal Expression Patterns of IDGFs in *Zeugodacus cucurbitae* Wild-Type

Temporal expression of five IDGFs genes in eight different developmental stages of *Z. cucurbitae* was determined using qPCR. IDGFs genes varied expression in certain developmental stages (*t*-tests: $P < 0.05$). We observed that the expression of *IDGF1* slightly increased in early larval instars and almost tended to stabilize until the pupal stage. The *IDGF3* significantly increased in expression at the first two larval stages. *IDGF4_0* significantly expressed in all stages. *IDGF4_1* was significantly expressed in larval and mid-pupal stage. While *IDGF6* was strongly expressed in pupal and adult stages only (**Figure 3**). The expression pattern of IDGFs indicates their pivotal roles in different developmental stages.

dsRNA-Mediated Knockdown of IDGFs Genes in *Zeugodacus cucurbitae*

RNAi technique has been used to inhibit target gene expression as a temporal knockdown strategy. Recently, RNAi techniques are being used in many studies for the management of different insects. *Z. cucurbitae* is an economically efficient fruit fly that causes a risk to many crop production and requires economically quarantine restrictions and eradication techniques. We developed a dsRNA feeding method for functional characterization of IDGF genes in *Z. cucurbitae* and identifying potential genes for effective management strategy. Compared to other strategies, dsRNA mixed with artificial food (Asimakis et al., 2019), is a non-invasive process and is less laborious in various systems, i.e., synthesized dsRNA (Turner et al., 2006), siRNA (Wuriyanghan et al., 2011), virus-derived RNA (Kumar et al., 2012), and transgenic hairpin RNA (Baum et al., 2007).

In all functional studies, two control groups, i.e., dsRNA-GFP and DEPC were used with no difference among these two control groups as compared to wild-type, e.g., no malformed wings, no pupal–adult malformation, and no larval–larval lethality in both the control groups, indicating that these phenotype abnormalities were related to the dsRNA homology depended on IDGFs genes knockdown. After knockdown for each gene, the expression level for other genes was determined by qPCR, and no non-target effects were observed, which prove the effectiveness of RNAi in *Z. cucurbitae* (**Figure 4**).

dsRNA-*IDGF1* Shows No Phenotypic Defects in *Zeugodacus cucurbitae*

Significant difference with a control group in the expression level of *IDGF1* was observed 24 h post-feeding of dsRNA-*IDGF1*, also a significant decrease in mRNA expression level was observed at 48, 72, 96, and 240 h. However, *IDGF1* knockdown causes (10.4%) mortality in *Z. cucurbitae.*

IDGF3_1 and *IDGF4_1* Contribute to the Larval–Larval Molt of *Zeugodacus cucurbitae*

Severe developmental defects and phenotypic abnormalities were observed when dsRNA-*IDGF3_1* or dsRNA-*IDGF4_1* were fed to the 2-day-old third instar larvae. Since these genes are highly expressed in the larval stage (**Figure 3**), therefore, the decrease in expression led to cuticular degradation in old larvae, resulting in the hindrance of larval molting

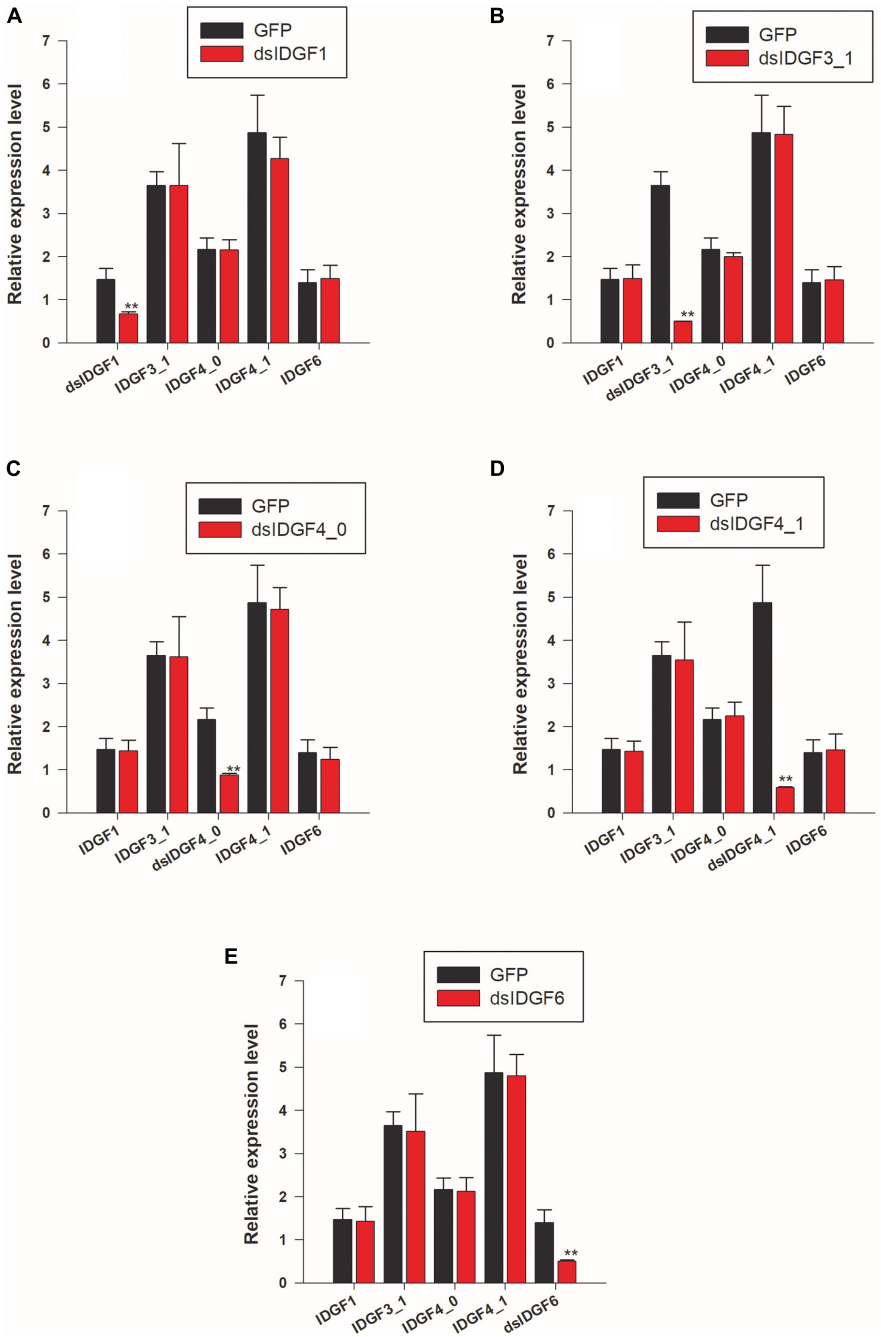

FIGURE 4 | RNAi suppresses only the target transcripts. **(A)** Larvae fed with ds*IDGF1* and the other four genes are non-target transcript. **(B)** Larvae fed with ds*IDGF3_1*. **(C)** Larvae fed with ds*IDGF4_0*. **(D)** Larvae fed with ds*IDGF4_1*. **(E)** Larvae fed with ds*IDGF6*. No effects observed on non-target transcript.

(**Figures 5**, **6**). After feeding dsRNA-*IDGF3_1*, the highest mortality recorded was (17.2%) at 24 h (**Figure 7**). The pupae size of dsRNA-*IDGF3_1* fed larvae reduced by 50% as compared to the control group. The remaining individuals completed metamorphosis into adults. Further, after feeding dsRNA-*IDGF4_1*, the highest mortality (40%) was recorded at 24 h compared to dsRNA-GFP and DEPC, and about (20%) individuals died and turned black with abnormal pigmentation. These results suggest that both *IDGF3_1* and *IDGF4_1* play an essential role in larval molting.

IDGF4_0 Is Required for Pupal–Adult Molt of *Zeugodacus cucurbitae*

Individuals fed with dsRNA-*IDGF4_0* exhibited phenotype at pharate adult stage as compared to the control group. After

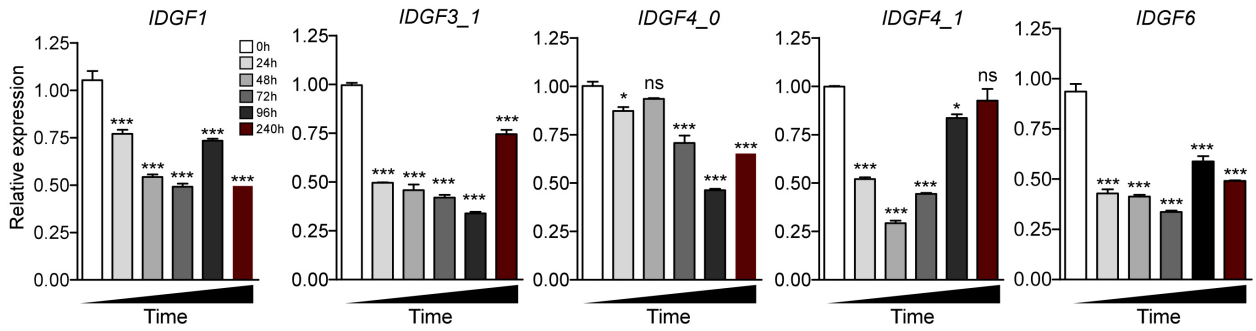

FIGURE 5 | Relative expression pattern of IDGFs in different time intervals post feeding to dsRNA or dsGFP or DEPC were determined as mean (±SE) of the three biological replicates, and two flies were used per pooled RNA sample with control as the calibrator, i.e., cDNA from non-RNAi flies (only fed on artificial diet with DEPC-water and dsGFP). *EF1α* is used as the internal control. One-way ANOVA with post hoc Tukey test was used to test the statistical significance $^{*}p < 0.05$; $^{**}p < 0.01$; $^{***}p \leq 0.001$, ns: not significant.

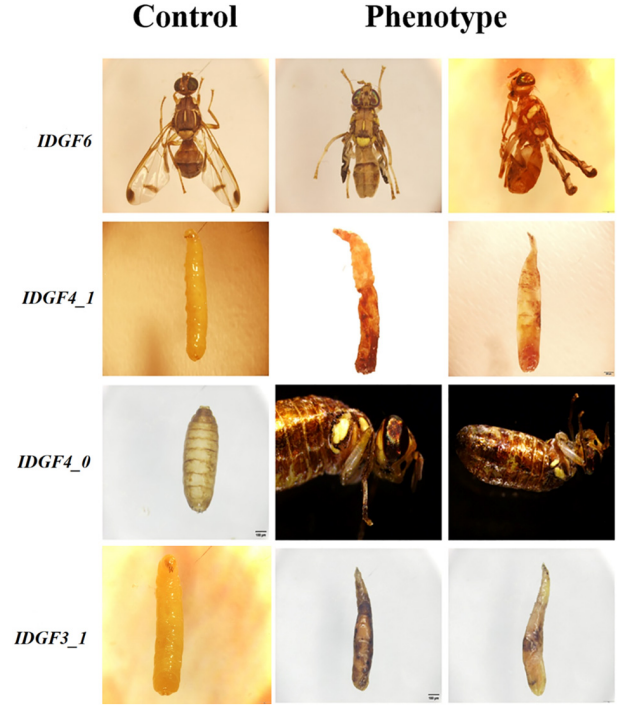

FIGURE 6 | Phenotypes, abnormalities after feeding dsRNA of IDGFs compared to control group dsGFP or DEPC in different developmental stages of *Z. cucurbitae*. All Pictures were taken with a scale bar 200 μm. The Control group represents either dsGFP or DEPC, and the Phenotype group represents abnormalities post feeding dsRNA for each gene. In phenotypes groups *IDGF6* represents wings malformation in *Z. cucurbitae, IDGF3_1* and *IDGF4_1* represents larval lethal phenotypes and *IDGF4_0* represents phenotype at pupal–adult stage where flies fail to shed their old cuticle.

5–6 days of pupation, a mortality of 49.2% was recorded (**Figure 7**). Furthermore, *Z. cucurbitae* failed to shed their old cuticle, and the mature cuticle was visible under the old cuticle resulting in the splitting of the old pronotal cuticle (**Figure 6**). In comparison, no abnormalities were recorded in control groups, either dsRNA-GFP or DEPC.

IDGF6 Is Required for Wings Formation of *Zeugodacus cucurbitae*

When dsRNA for *IDGF6* was fed to the third larval instar of *Z. cucurbitae* no phenotype was observed in larval or pupal stage. The larvae had completed the larval–larval and larval–pupal molts; however, there were some notable differences during the molts. The pupae usually contract their abdomens compared to control (dsRNA-GFP or DEPC) to the same extent. The adult's eclosion was also the same as the control group. A remarkable phenotype was observed at the adult stage, where the wings were malformed and curled, which did not spread normally (**Figure 6**). Approximately 90% of individuals with malformed wings died within 10 days of emergence. The highest mortality rate (20.8%) was recorded at 240 h post-feeding dsRNA-*IDGF6* compared to the control group (**Figure 7**). Moreover, no malformed wings were observed in the control group in dsRNA-GFP and DEPC, and all the flies lived normally.

DISCUSSION

Based on these results, we had applied the oral feeding dsRNA technique for the first time in melon fly *Z. cucurbitae* to know the specific function of IDGFs genes. IDGFs belong from a poorly described GH 18 Chitinase family with proteins without catalytic activity (Funkhouser and Aronson, 2007). Using five IDGFs genes (mentioned above) nucleotide sequences of Tephritidae, the Maximum likelihood method was applied to get a phylogenetic tree, which shows a high similarity with the homolog in other Tephritidae fruit flies (**Figure 1** and **Supplementary Table 1**). Chitinase is known to degrade chitin to the low molecular weight Chit oligosaccharides and play an important role in the growth and development of insects (Zhu et al., 2016). The number of chitinase family genes in different insects ranges from 9 *Acyrthosiphon pisum* to 24 in *Tribolium castaneum* (Zhu et al., 2008; Arakane and Muthukrishnan, 2010; Nakabachi et al., 2010; Tetreau et al., 2015; Omar et al., 2019). Zhao et al. (2018) reported that plant-mediated RNAi of chitin synthase 1 (*CHS1*) gene in

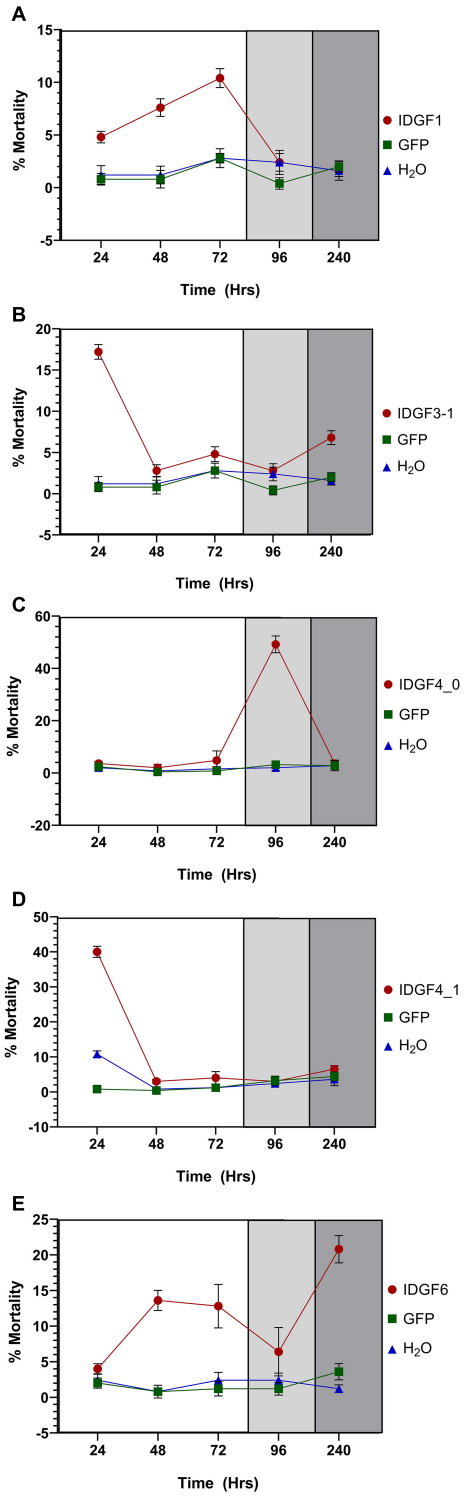

FIGURE 7 | Mortality rate (%) of *Z. cucurbitae* at different developmental stages after being artificially fed with dsGFP or DEPC or dsRNA of IDGFs. The letters **(A–E)** represents *IDGF1*, *IDGF3_1*, *IDGF4_0*, *IDGF4_1*, and *IDGF6*. The white portion represent larval stages, light gray indicates pupal stage, and dark gray indicates adult stage of *Z. cucurbitae*. The values are presented as the mean (±SE) of five biological replications (50 insects were used per replicate). Treatments were compared using one-way ANOVA (Turkey's test, $p < 0.05$).

Sitobion avenae causes ∼50% decreased expression, whereas ∼20% reduction was observed in number of aphids and ecdysis. RNAi-mediated knockdown of *MpNav* gene expression caused up to 65% mortality in 3rd instar nymphs and lowered the longevity and fecundity in adult peach-potato aphid, *Myzus persicae* (Tariq et al., 2019). Oral-delivery-mediated RNAi of *CHS1* causes mortality and also disrupted the adult longevity and fecundity of the cotton-melon aphid, *Aphis gossypii* (Ullah et al., 2020b).

Temporal expression analysis in eight different developmental stages showed that these genes are highly expressed in different stages: larval–larval, larval–pupal, and pupal–adults, which indicate a vital role in the growth and development of these stages. *IDGF1* was expressed in all stages, mostly in larval stages, and it's silencing caused mortality, but no phenotypic effects were observed. It would be an interesting study to compare the impact of IDGF family knockdown effect on the anatomy and histology of the melon fly. Furthermore, *IDGF3_1* and *IDGF4_1* were highly expressed in a larval stage, and silencing of both of these genes caused lethal phenotype in larvae (**Figure 6**) and caused mortality. Taken together, our results are consistent with few previous studies focused on IDGFs role in insect molting. A prior study on further vitro cell growth tests reported that combined with the insulin, *IDGF1* or *IDGF2* proteins stimulated the cultured imaginal disk cells growth (Hipfner and Cohen, 1999; Kawamura et al., 1999). Previously, it has been shown that *IDGF1* is expressed in the large salivary gland cells. Along with *IDGF3* its expression is lower as compared to *IDGF2* and *IDGF4* (Kawamura et al., 1999) *in vitro* cell growth tests combined with the insulin revealed that *IDGF1* or *IDGF2* proteins stimulated the cultured imaginal disk cells growth (Hipfner and Cohen, 1999; Kawamura et al., 1999). In a previous functional study of IDGFs, genes reported that individually *IDGF1* knocked down through RNAi in a model specie *Drosophila*, shows narrowed ECM thickness and displayed severe epidermal lesions in the larvae (Pesch et al., 2016). Similarly, expression levels of *IDGF3_1* after dsRNA feeding significantly decrease at 24, 48, 72, 96, and 240 h post-feeding. Pesch et al. (2016) found that in *Drosophila,* the IDGFs are essential for larval and adult molting. dsRNA-mediated silencing of IDGF family genes resulted in deformed cuticles, larval, and adult molting defects in *Drosophila*. Individual *IDGF3* knockdown via RNAi resulted in cuticle molting defects (Zurovcova et al., 2019). In similar studies, Espinoza and Berg (2020) found that overexpressing *IDGF3* leads to defects in the dorsal appendage with ∼50% frequency.

Individual knockdown of *IDGF4* in 3rd instar larvae through RNAi led to reduced larvae's survival rate under high temperature and caused malformation as adults. This finding indicates the role of *IDGF4* in the defense barrier and development of fruit flies (Gu et al., 2019). Several studies have mainly focused on the function of *IDGF4* in larval stages, while only two related research articles were founded about another key developmental stage: pupae. In *T. castaneum*, when ds*IDGF4* injected either into penultimate or to the last instar larvae shows normal pupation but caused mortality during adult eclosion (Zhu et al., 2008). In *B. mori*, proteins with a decisively different expression profile among wild-type and scale-less wing mutants were verified and

revealed that one *IDGF* gene was correlated to the differentiation of scale cells and development (Shi et al., 2013). Likewise, in homologs, specie *B. dorsalis*, dsRNA-*IDGF4* feeding in artificial food caused wings malformation and mortality (Gu et al., 2019). Furthermore, in *B. correcta*, dsRNA-*IDGF6* mediated strategy led to reduced gene expression of *IDGF6*, resulting in larval death and adult wing malformation. The knockdown of *IDGF6* led to decreased chitinase activity, resulting in stabilizing old cuticles and reduced body size (Zhao et al., 2020). Pesch et al., reported that *IDGF6* RNAi-induced mutants showed high mortality, and severe cuticle defects were observed in other mutants (Pesch et al., 2016). *IDGF6* is critical for larval cuticle barrier formation and protection against invasive microorganisms and mechanical stresses (Pesch et al., 2016). Therefore, *IDGF6* may prove to be an effective target for RNAi-based management.

In the current study, we observed differential responses to dsRNA uptake. For example, in *IDGF4_1*, the gene expression goes down in response to dsRNA feeding. However, the *IDGF4_1* expression recovers 48 h after dsRNA feeding. This phenomenon has been widely observed and attributed to various potential mechanisms, including the mutations of target genes or core RNAi machinery genes, enhanced dsRNA degradation, and lower dsRNA uptake (Zhu and Palli, 2020). For example, The Western Corn Cutworm (WCR) exhibited resistance to transgenic maize expressing *DvSnf7* dsRNA due to impaired luminal uptake. This resistance was not *DvSnf7* dsRNA specific, as indicated by cross-resistance to all other tested dsRNAs (Khajuria et al., 2018). The differential response of IDGF genes to the corresponding dsRNA may provide an excellent tool to further demystify the dsRNA resistance in insect pests. Overall, IDGFs can be used as potential target genes for pest control because of their function in different developmental stages. The malformation in wings, larval–larval lethality and pupal–adult malformation and small body size, and the highly conserved traits show that IDGFs are key genes for the pest. Furthermore, our results will pave the way for in-depth functional analysis of IDGFs family members and identify suitable insect control strategies through RNAi.

DATA AVAILABILITY STATEMENT

The original contributions presented in the study are included in the article/**Supplementary Material**, further inquiries can be directed to the corresponding authors.

AUTHOR CONTRIBUTIONS

SA and YL: designing research and funding acquisition. SA and MJ: methodology. SA, MF, and MJ: data curation and formal analysis. SA: performing research. SA, MF, FU, MJ, YL, BL, and SZ: writing – review and editing. YL and BL: supervision. All authors have read and agreed to the published version of the manuscript.

FUNDING

This study was supported by the National Natural Science Foundation of China (NSFC; Grant Nos. 31860513 and 31760526), the Chinese Government Scholarship, and Project of Innovation Research Team of the Hainan Natural Science Foundation (No. 2019cxtd409).

SUPPLEMENTARY MATERIAL

The Supplementary Material for this article can be found online at: https://www.frontiersin.org/articles/10.3389/fgene.2021.691382/full#supplementary-material

REFERENCES

Arakane, Y., and Muthukrishnan, S. (2010). Insect chitinase and chitinase-like proteins. *Cell. Mol. Life Sci. CMLS* 67, 201–216. doi: 10.1007/s00018-009-0161-9

Asimakis, Khan, M., Stathopoulou, P., Caceres, C., Bourtzis, K., and Tsiamis, G. (2019). The effect of diet and radiation on the bacterial symbiome of the melon fly, *Zeugodacus cucurbitae* (Coquillett). *BMC Biotechnol.* 19:88. doi: 10.1186/s12896-019-0578-7

Asokan, R., Chandra, G. S., Manamohan, M., and Kumar, N. K. (2013). Effect of diet delivered various concentrations of double-stranded RNA in silencing a midgut and a non-midgut gene of *Helicoverpa armigera*. *Bull. Entomol. Res.* 103, 555–563. doi: 10.1017/s0007485313000138

Baig, S. A., Akhtera, N. A., Muhammad, A., and Asi, M. R. (2009). Determination of the organophosphorus pesticide in vegetables by high-performance liquid chromatography. *Am.Eurasian J. Agricult. Environ. Sci.* 6, 513–519.

Bally, J., Fishilevich, E., Bowling, A. J., Pence, H. E., Narva, K. E., and Waterhouse, P. M. (2018). Improved insect-proofing: expressing double-stranded RNA in chloroplasts. *Pest Manag. Sci.* 74, 1751–1758. doi: 10.1002/ps.4870

Baum, J. A., Bogaert, T., Clinton, W., Heck, G. R., Feldmann, P., Ilagan, O., et al. (2007). Control of coleopteran insect pests through RNA interference. *Nat. Biotechnol.* 25, 1322–1326. doi: 10.1038/nbt1359

Bellés, X. (2010). Beyond *Drosophila*: RNAi in vivo and functional genomics in insects. *Annu. Rev. Entomol.* 55, 111–128. doi: 10.1093/bfgp/elp052

Chen, X., Tian, H., Zou, L., Tang, B., Hu, J., and Zhang, W. (2008). Disruption of Spodoptera exigua larval development by silencing chitin synthase gene a with RNA interference. *Bull. Entomol. Res.* 98, 613–619. doi: 10.1017/s0007485308005932

Chung, S. H., Feng, H., and Jander, G. (2021). Engineering pest tolerance through plant-mediated RNA interference. *Curr. Opin. Plant Biol.* 60:102029. doi: 10.1016/j.pbi.2021.102029

Cosgrove, D. J. (2005). Growth of the plant cell wall. *Nat. Rev. Mol. Cell Biol.* 6, 850–861.

Darrington, M., Dalmay, T., Morrison, N. I., and Chapman, T. (2017). Implementing the sterile insect technique with RNA interference - a review. *Entomol. Exp. et Appl.* 164, 155–175. doi: 10.1111/eea.12575

Decourtye, A., Henry, M., and Desneux, N. (2013). Overhaul pesticide testing on bees. *Nature* 497:188. doi: 10.1038/497188a

Desneux, N., Decourtye, A., and Delpuech, J. M. (2007). The sublethal effects of pesticides on beneficial arthropods. *Annu. Rev. Entomol.* 52, 81–106. doi: 10.1146/annurev.ento.52.110405.091440

Dhillon, M. K., Singh, R., Naresh, J. S., and Sharma, H. C. (2005). The melon fruit fly, Bactrocera cucurbitae: a review of its biology and management. *J. Insect. Sci.* 5:40.

Dittmer, N. T., Tetreau, G., Cao, X., Jiang, H., Wang, P., and Kanost, M. R. (2015). Annotation and expression analysis of cuticular proteins from the tobacco hornworm, *Manduca sexta*. *Insect Biochem. Mol. Biol.* 62, 100–113. doi: 10.1016/j.ibmb.2014.12.010

Drew, R. A. I., Prokopy, R. J., and Romig, M. C. (2003). Attraction of fruit flies of the genus Bactrocera to colored mimics of host fruit. *Entomol. Exp. et Appl* 107, 39–45. doi: 10.1046/j.1570-7458.2003.00039.x

Espinoza, C. Y., and Berg, C. A. (2020). Detecting new allies: modifier screen identifies a genetic interaction between imaginal disc growth factor 3 and combover, a rho-kinase substrate, during dorsal appendage tube formation in *Drosophila*. *G3* 10, 3585–3599. doi: 10.1534/g3.120.401476

Fernandes, I., Chanut-Delalande, H., Ferrer, P., Latapie, Y., Waltzer, L., Affolter, M., et al. (2010). Zona pellucida domain proteins remodel the apical compartment for localized cell shape changes. *Dev. Cell* 18, 64–76. doi: 10.1016/j.devcel.2009.11.009

Fire, A., Xu, S., Montgomery, M. K., Kostas, S. A., Driver, S. E., and Mello, C. C. (1998). Potent and specific genetic interference by double-stranded RNA in *Caenorhabditis elegans*. *Nature* 391, 806–811. doi: 10.1038/35888

Funkhouser, J. D., and Aronson, N. N. (2007). Chitinase family GH18: evolutionary insights from the genomic history of a diverse protein family. *BMC Evol. Biol.* 7:96. doi: 10.1186/1471-2148-7-96

Galko, M. J., and Krasnow, M. A. (2004). Cellular and genetic analysis of wound healing in *Drosophila larvae*. *PLoS Biol.* 2:E239. doi: 10.1371/journal.pbio.0020239

Gebregergis, Z. (2018). Incidence of a new pest, the cotton mealybug phenacoccus solenopsis tinsley, on sesame in north ethiopia. *Int. J. Zool.* 2018:3531495.

Gogi, M. D., Ashfaq, M., Arif, M., Khan, MJIJoA, and Biology. (2009). Screening of bitter gourd (*Momordica charantia*) germplasm for sources of resistance against melon fruit fly *Bactrocera cucurbitae* in Pakistan. *Int. J. Agricult. Biol.* 11, 746–750.

Gogi, M. D., Ashfaq, M., Arif, M. J., Khan, M. A., and Ahmad, F. (2007). Coadministration of insecticides and butanone acetate for its efficacy against melon fruit flies, *Bactrocera cucurbitae* (Insects: Diptera: Tephritidae). *Pak. Entomol.* 29, 111–116.

Gong, L., Luo, Q., Rizwan-ul-Haq, M., and Hu, M. Y. (2012). Cloning and characterization of three chemosensory proteins from *Spodoptera exigua* and effects of gene silencing on female survival and reproduction. *Bull. Entomol. Res.* 102, 600–609. doi: 10.1017/s0007485312000168

Grover, S., Jindal, V., Banta, G., Taning, C. N. T., Smagghe, G., and Christiaens, O. (2019). Potential of RNA interference in the study and management of the whitefly, *Bemisia tabaci*. *Arch. Insect Biochem. Physiol.* 100:e21522. doi: 10.1002/arch.21522

Gu, X., Li, Z., Su, Y., Zhao, Y., and Liu, L. (2019). Imaginal disc growth factor 4 regulates development and temperature adaptation in *Bactrocera dorsalis*. *Sci. Rep.* 9:931.

Hipfner, D. R., and Cohen, S. M. (1999). New growth factors for imaginal discs. *BioEssays* 21, 718–720. doi: 10.1002/(sici)1521-1878(199909)21:9<718::aid-bies2>3.0.co;2-z

Jactel, H., Verheggen, F., Thiéry, D., Escobar-Gutiérrez, A. J., Gachet, E., and Desneux, N. (2019). Alternatives to neonicotinoids. *Environ. Int.* 129, 423–429. doi: 10.1016/j.envint.2019.04.045

Jaspers, M. H. J., Pflanz, R., Riedel, D., Kawelke, S., Feussner, I., and Schuh, R. (2014). The fatty acyl-CoA reductase waterproof mediates airway clearance in *Drosophila*. *Dev. Biol.* 385, 23–31. doi: 10.1016/j.ydbio.2013.10.022

Kawamura, K., Shibata, T., Saget, O., Peel, D., and Bryant, P. J. (1999). A new family of growth factors produced by the fat body and active on *Drosophila* imaginal disc cells. *Development (Cambridge, England)* 126, 211–219. doi: 10.1242/dev.126.2.211

Khajuria, C., Ivashuta, S., Wiggins, E., Flagel, L., Moar, W., Pleau, M., et al. (2018). Development and characterization of the first dsRNA-resistant insect population from western corn rootworm, *Diabrotica virgifera* virgifera LeConte. *PLoS One* 13:e0197059. doi: 10.1371/journal.pone.0197059

Kumar, P., Pandit, S. S., and Baldwin, I. T. (2012). Tobacco rattle virus vector: a rapid and transient means of silencing manduca sexta genes by plant mediated RNA *Interference*. *PLoS One* 7:e31347. doi: 10.1371/journal.pone.0031347

Liu, X., Lin, X., Li, J., Li, F., Cao, F., and Yan, R. (2020). A novel solid artificial diet for *Zeugodacus cucurbitae* (Diptera: Tephritidae) larvae with fitness parameters assessed by two-sex life table. *J. Insect Sci.* 20:21.

Livak, K. J., and Schmittgen, T. D. (2001). Analysis of relative gene expression data using real-time quantitative PCR and the 2(-Delta Delta C(T)) Method. *Methods (San Diego, Calif)* 25, 402–408. doi: 10.1006/meth.2001.1262

Mehlhorn, S. G., Geibel, S., Bucher, G., and Nauen, R. (2020). Profiling of RNAi sensitivity after foliar dsRNA exposure in different European populations of Colorado potato beetle reveals a robust response with minor variability. *Pesticide Biochem. Physiol.* 166:104569. doi: 10.1016/j.pestbp.2020.104569

Mun, S., Noh, M. Y., Dittmer, N. T., Muthukrishnan, S., Kramer, K. J., Kanost, M. R., et al. (2015). Cuticular protein with a low complexity sequence becomes cross-linked during insect cuticle sclerotization and is required for the adult molt. *Sci. Rep.* 5:10484.

Nakabachi, A., Shigenobu, S., and Miyagishima, S. (2010). Chitinase-like proteins encoded in the genome of the pea aphid, *Acyrthosiphon pisum*. *Insect Mol. Biol.* 19(Suppl. 2), 175–185. doi: 10.1111/j.1365-2583.2009.00985.x

Omar, M. A. A., Ao, Y., Li, M., He, K., Xu, L., Tong, H., et al. (2019). The functional difference of eight chitinase genes between male and female of the cotton mealybug, *Phenacoccus solenopsis*. *Insect Mol. Biol.* 28, 550–567. doi: 10.1111/imb.12572

Öztürk-Çolak, A., Moussian, B., and Araújo, S. J. (2016). *Drosophila chitinous* a ECM and its cellular interactions during tracheal development. *Dev. Dyn.* 245, 259–267. doi: 10.1002/dvdy.24356

Pan, Z. Z., Li, H. L., Yu, X. J., Zuo, Q. X., Zheng, G. X., Shi, Y., et al. (2011). Synthesis and antityrosinase activities of alkyl 3,4-dihydroxybenzoates. *J. Agricult. Food Chem.* 59, 6645–6649. doi: 10.1021/jf200990g

Panhwar, F. (2005). *Mediterranean Fruit Fly (Ceratitis capitata) Attack on Fruits and its Control in Sindh Pakistan*. Germany: Digital Verlag GmbH.

Pesch, Y.-Y., Riedel, D., Patil, K. R., Loch, G., and Behr, M. (2016). Chitinases and Imaginal disc growth factors organize the extracellular matrix formation at barrier tissues in insects. *Sci. Rep.* 6:18340.

Qi, X. L., Su, X. F., Lu, G. Q., Liu, C. X., Liang, G. M., and Cheng, H. M. (2015). The effect of silencing arginine kinase by RNAi on the larval development of *Helicoverpa armigera*. *Bull. Entomol. Res.* 105, 555–565. doi: 10.1017/s0007485315000450

Rana, S., Rajurkar, A. B., Kumar, K. K., and Mohankumar, S. (2020). Comparative analysis of chitin SynthaseA dsRNA mediated RNA interference for management of crop pests of different families of lepidoptera. *Front. Plant Sci.* 11:427. doi: 10.3389/fpls.2020.00427

San Miguel, K., and Scott, J. G. (2016). The next generation of insecticides: dsRNA is stable as a foliar-applied insecticide. *Pest Manag. Sci.* 72, 801–809. doi: 10.1002/ps.4056

Sapkota, R., Dahal, K., and Thapa, R. (2010). Damage assessment and management of cucurbit fruit flies in spring-summer squash. *J. Entomol. Nematol.* 2, 007–012.

Scott, J. G., Michel, K., Bartholomay, L. C., Siegfried, B. D., Hunter, W. B., Smagghe, G., et al. (2013). Towards the elements of successful insect RNAi. *J. Insect Physiol.* 59, 1212–1221. doi: 10.1016/j.jinsphys.2013.08.014

Shelly, T. E., Pahio, E., and Edu, J. (2004). Synergistic and inhibitory interactions between methyl eugenol and cue lure influence trap catch of male fruit flies, *Bactrocera dorsalis* (Hendel) and B. cucurbitae (Diptera: Tephritidae). *Florida Entomol.* 87, 481–486. doi: 10.1653/0015-4040(2004)087[0481:saiibm]2.0.co;2

Shi, X.-F., Bin, H., Li, Y.-N., Yi, Y.-Z., Li, X.-M., Shen, X.-J., et al. (2013). Proteomic analysis of the phenotype of the scaleless wings mutant in the silkworm, *Bombyx mori*. *J. Proteom.* 78, 15–25. doi: 10.1016/j.jprot.2012.11.003

Shibata, T., Ariki, S., Shinzawa, N., Miyaji, R., Suyama, H., Sako, M., et al. (2010). Protein crosslinking by transglutaminase controls cuticle morphogenesis in *Drosophila*. *PLoS One* 5:e13477. doi: 10.1371/journal.pone.0013477

Subedi, K., Regmi, R., Thapa, R. B., and Tiwari, S. (2021). Evaluation of net house and mulching effect on Cucurbit fruit fly (Bactrocera cucurbitae Coquillett) on cucumber (*Cucumis sativus* L.). *J. Agricult. Food Res.* 3:100103. doi: 10.1016/j.jafr.2021.100103

Tamura, K., Stecher, G., Peterson, D., Filipski, A., and Kumar, S. (2013). MEGA6: molecular evolutionary genetics analysis version 6.0. *Mol. Biol. Evol.* 30, 2725–2729. doi: 10.1093/molbev/mst197

Tariq, K., Ali, A., Davies, T. G. E., Naz, E., Naz, L., Sohail, S., et al. (2019). RNA interference-mediated knockdown of voltage-gated sodium channel (MpNav) gene causes mortality in peach-potato aphid, *Myzus persicae*. *Sci. Rep.* 9:5291.

Tetreau, G., Cao, X., Chen, Y. R., Muthukrishnan, S., Jiang, H., Blissard, G. W., et al. (2015). Overview of chitin metabolism enzymes in *Manduca sexta*:

identification, domain organization, phylogenetic analysis and gene expression. *Insect Biochem. Mol. Biol.* 62, 114–126. doi: 10.1016/j.ibmb.2015.01.006

Tomoyasu, Y., and Denell, R. E. (2004). Larval RNAi in *Tribolium* (Coleoptera) for analyzing adult development. *Dev. Genes Evol.* 214, 575–578. doi: 10.1007/s00427-004-0434-0

Turner, C. T., Davy, M. W., MacDiarmid, R. M., Plummer, K. M., Birch, N. P., and Newcomb, R. D. (2006). RNA interference in the light brown apple moth, *Epiphyas postvittana* (Walker) induced by double-stranded RNA feeding. *Insect Mol. Biol.* 15, 383–391. doi: 10.1111/j.1365-2583.2006.00656.x

Turner, J. R. (2009). Intestinal mucosal barrier function in health and disease. *Nat. Rev. Immunol.* 9, 799–809. doi: 10.1038/nri2653

Ullah, F., Gul, H., Desneux, N., Gao, X., and Song, D. (2019a). Imidacloprid-induced hormesis effects on demographic traits of the melon aphid, *Aphis gossypii*. *Entomol. General.* 39, 325–337. doi: 10.1127/entomologia/2019/0892

Ullah, F., Gul, H., Desneux, N., Qu, Y., Xiao, X., Khattak, A. M., et al. (2019b). Acetamiprid-induced hormetic effects and vitellogenin gene (Vg) expression in the melon aphid, *Aphis gossypii*. *Entomol. General.* 39, 259–270. doi: 10.1127/entomologia/2019/0887

Ullah, F., Gul, H., Tariq, K., Desneux, N., Gao, X., and Song, D. (2020a). Functional analysis of cytochrome P450 genes linked with acetamiprid resistance in melon aphid, *Aphis gossypii*. *Pesticide Biochem. Physiol.* 175:104687. doi: 10.1016/j.pestbp.2020.104687

Ullah, F., Gul, H., Wang, X., Ding, Q., Said, F., Gao, X., et al. (2020b). RNAi-mediated knockdown of chitin synthase 1 (CHS1) gene causes mortality and decreased longevity and fecundity in *Aphis gossypii*. *Insects* 11:22. doi: 10.3390/insects11010022

Uv, A., and Moussian, B. (2010). The apical plasma membrane of *Drosophila* embryonic epithelia. *Eur. J. Cell Biol.* 89, 208–211. doi: 10.1016/j.ejcb.2009.11.009

Varela, P. F., Llera, A. S., Mariuzza, R. A., and Tormo, J. (2002). Crystal structure of imaginal disc growth factor-2. A member of a new family of growth-promoting glycoproteins from *Drosophila melanogaster*. *J. Biol. Chem.* 277, 13229–13236.

Vargas, R. I., Piñero, J. C., Jang, E. B., Mau, R. F., Stark, J. D., Gomez, L., et al. (2010). Response of melon fly (Diptera: Tephritidae) to weathered SPLAT-Spinosad-Cue-Lure. *J. Econ. Entomol.* 103, 1594–1602. doi: 10.1603/ec09406

Vargas, R. I., Stark, J. D., Hertlein, M., Neto, A. M., Coler, R., and Piñero, J. C. (2008). Evaluation of SPLAT with spinosad and methyl eugenol or cue-lure for "attract-and-kill" of oriental and melon fruit flies (Diptera: Tephritidae) in Hawaii. *J. Econ. Entomol.* 101, 759–768. doi: 10.1603/0022-0493(2008)101[759:eoswsa]2.0.co;2

Vuong-Brender, T. T. K., Suman, S. K., and Labouesse, M. (2017). The apical ECM preserves embryonic integrity and distributes mechanical stress during morphogenesis. *Development* 144, 4336–4349.

Wang, W. X., Zhu, T. H., Li, K. L., Chen, L. F., Lai, F. X., and Fu, Q. (2017). Molecular characterization, expression analysis and RNAi knockdown of elongation factor 1α and 1γ from *Nilaparvata lugens* and its yeast-like symbiont. *Bull. Entomol. Res.* 107, 303–312. doi: 10.1017/s0007485316000882

Waterhouse, P. M., Graham, M. W., and Wang, M. B. (1998). Virus resistance and gene silencing in plants can be induced by simultaneous expression of sense and antisense RNA. *Proc. Natl. Acad. Sci. U S A.* 95, 13959–13964. doi: 10.1073/pnas.95.23.13959

Wuriyanghan, H., Rosa, C., and Falk, B. W. (2011). Oral delivery of double-stranded RNAs and siRNAs induces RNAi effects in the Potato/Tomato psyllid. *Bactericerca cockerelli*. *PLoS One* 6:e27736. doi: 10.1371/journal.pone.0027736

Xi, Y., Pan, P. L., Ye, Y. X., Yu, B., Xu, H. J., and Zhang, C. X. (2015). Chitinase-like gene family in the brown planthopper, *Nilaparvata lugens*. *Insect Mol. Biol.* 24, 29–40. doi: 10.1111/imb.12133

Xu, J., Wang, X. F., Chen, P., Liu, F. T., Zheng, S. C., Ye, H., et al. (2016). RNA interference in moths: mechanisms, applications, and progress. *Genes* 7:88. doi: 10.3390/genes7100088

Yee, W. L., Oriki, J., and Meralee, J. N. (2007). Mortality of *Rhagoletis pomonella* (Diptera: Tephritidae) exposed to field-aged spinetoram, GF-120, and Azinphos-Methyl in Washington State. *Florida Entomol.* 90, 335–342. doi: 10.1653/0015-4040(2007)90[335:morpdt]2.0.co;2

Yoshiyama, T., Namiki, T., Mita, K., Kataoka, H., and Niwa, R. (2006). Neverland is an evolutionally conserved Rieske-domain protein that is essential for ecdysone synthesis and insect growth. *Development* 133, 2565–2574. doi: 10.1242/dev.02428

Zhang, X., Liu, X., Ma, J., and Zhao, J. (2013). Silencing of cytochrome P450 CYP6B6 gene of cotton bollworm (*Helicoverpa armigera*) by RNAi. *Bull. Entomol. Res.* 103, 584–591. doi: 10.1017/s0007485313000151

Zhao, Y., Li, Z., Gu, X., Su, Y., and Liu, L. (2020). Imaginal disc growth factor 6 (Idgf6) is involved in larval and adult wing development in *Bactrocera correcta* (Bezzi) (Diptera: Tephritidae). *Front. Genet.* 11:451. doi: 10.3389/fgene.2020.00451

Zhao, Y., Sui, X., Xu, L., Liu, G., Lu, L., You, M., et al. (2018). Plant-mediated RNAi of grain aphid CHS1 gene confers common wheat resistance against aphids. *Pest. Manag. Sci.* 747, 2754–2760. doi: 10.1002/ps.5062

Zhu, K. Y., Merzendorfer, H., Zhang, W., Zhang, J., and Muthukrishnan, S. (2016). Biosynthesis, turnover, and functions of chitin in insects. *Annu. Rev. Entomol.* 61, 177–196. doi: 10.1146/annurev-ento-010715-023933

Zhu, K. Y., and Palli, S. R. (2020). Mechanisms, applications, and challenges of insect RNA interference. *Ann. Rev. Entomol.* 65, 293–311. doi: 10.1146/annurev-ento-011019-025224

Zhu, Q., Arakane, Y., Beeman, R. W., Kramer, K. J., and Muthukrishnan, S. (2008). Functional specialization among insect chitinase family genes revealed by RNA interference. *Proc. Natl. Acad. Sci. U S A.* 105:6650. doi: 10.1073/pnas.0800739105

Zurovcová, M., and Ayala, F. J. (2002). Polymorphism patterns in two tightly linked developmental genes, Idgf1 and Idgf3, of *Drosophila melanogaster*. *Genetics* 162, 177–188. doi: 10.1093/genetics/162.1.177

Zurovcova, M., Benes, V., Zurovec, M., and Kucerova, L. (2019). Expansion of imaginal disc growth factor gene family in diptera reflects the evolution of novel functions. *Insects* 10:365. doi: 10.3390/insects10100365

Conflict of Interest: The authors declare that the research was conducted in the absence of any commercial or financial relationships that could be construed as a potential conflict of interest.

frontiers in Cell and Developmental Biology

ORIGINAL RESEARCH
published: 21 September 2021
doi: 10.3389/fcell.2021.647604

Comparative Transcriptomic Analyses of Antibiotic-Treated and Normally Reared *Bactrocera dorsalis* Reveals a Possible Gut Self-Immunity Mechanism

*Jiajin Fu†, Lingyu Zeng†, Linyu Zheng†, Zhenzhen Bai, Zhihong Li and Lijun Liu**

College of Plant Protection, China Agricultural University, Beijing, China

Bactrocera dorsalis (Hendel) is a notorious agricultural pest worldwide, and its prevention and control have been widely studied. Bacteria in the midgut of *B. dorsalis* help improve host insecticide resistance and environmental adaption, regulate growth and development, and affect male mating selection, among other functions. Insects have an effective gut defense system that maintains self-immunity and the balance among microorganisms in the gut, in addition to stabilizing the diversity among the gut symbiotic bacteria. However, the detailed regulatory mechanisms governing the gut bacteria and self-immunity are still unclear in oriental fruit flies. In this study, the diversity of the gut symbiotic bacteria in *B. dorsalis* was altered by feeding host fruit flies antibiotics, and the function of the gut bacteria was predicted. Then, a database of the intestinal transcriptome of the host fruit fly was established and analyzed using the Illumina HiSeq Platform. The gut bacteria shifted from Gram negative to Gram positive after antibiotic feeding. Antibiotics lead to a reduction in gut bacteria, particularly Gram-positive bacteria, which ultimately reduced the reproduction of the host flies. Ten immunity-related genes that were differentially expressed in the response to intestinal bacterial community changes were selected for qRT-PCR validation. Peptidoglycan-recognition protein SC2 gene (*PGRP-SC2)* was one of the 10 immunity-related genes analyzed. The differential expression of *PGRP-SC2* was the most significant, which confirms that *PGRP-SC2* may affect immunity of *B. dorsalis* toward gut bacteria.

Keywords: *Bactrocera dorsalis*, intestinal bacteria, immunity, transcriptome, antibiotic treatment, *PGRP-SC2*

OPEN ACCESS

Edited by:
Wei Guo,
Institute of Zoology, Chinese Academy of Sciences (CAS), China

Reviewed by:
Sufang Zhang,
Chinese Academy of Forestry, China
Qi-Long Qin,
Shandong University, China

***Correspondence:**
Lijun Liu
ljliu@cau.edu.cn

† These authors have contributed equally to this work

Specialty section:
This article was submitted to Epigenomics and Epigenetics, a section of the journal Frontiers in Cell and Developmental Biology

Received: *30 December 2020*
Accepted: *25 August 2021*
Published: *21 September 2021*

Citation:
Fu J, Zeng L, Zheng L, Bai Z, Li Z and Liu L (2021) Comparative Transcriptomic Analyses of Antibiotic-Treated and Normally Reared Bactrocera dorsalis Reveals a Possible Gut Self-Immunity Mechanism. Front. Cell Dev. Biol. 9:647604. doi: 10.3389/fcell.2021.647604

INTRODUCTION

Bactrocera dorsalis, also known as the oriental fruit fly, belongs to the Diptera (Tephritidae) family. As a member of the *Bactrocera* genus, it is listed as a quarantine pest in China. It has a wide host range and can damage more than 250 host plants (Verghese et al., 2012). It has been reported that the damage caused by oriental fruit flies can reach 100% of unprotected orchards, which causes huge losses to local agriculture and forestry (Zhang et al., 2010). Therefore, exploring effective control techniques for this notorious pest is of great significance.

Many studies have shown that different symbionts play an important role in the development of insects due to the different metabolic capacities of the host at different developmental stages

(e.g., Lindow and Brandl, 2003; Knief et al., 2011; Li et al., 2016). Among the bacteria in the insect gut, "resident bacteria" are mainly involved in immune function and decomposing toxins. Previous results have shown that intestinal bacteria can help host insects resist pathogens (Ning et al., 2009; Bonnay et al., 2013). Similarly, the intestinal tract of *B. dorsalis* also contains a large number of symbiotic bacteria, which are mainly Acetobacaceae, Lactobacillaceae, Enterobacteriaceae, Cystosporaceae, and Brevibacterium (e.g., Naaz et al., 2016; Bai et al., 2018; Noman et al., 2020). The number of commensal bacterial communities could be significantly reduced under antibiotic treatment (Yao et al., 2016). Intestinal bacteria could also enhance the ability of host oriental fruit flies to degrade pesticides (Damodaram et al., 2016; Yao et al., 2016; Cheng et al., 2017). In summary, intestinal symbiotic bacteria may play an important role in the development, health and reproduction of *B. dorsalis*, and studying the function of intestinal symbiotic bacteria will be helpful in the development of new control strategies for insects belonging to the *Bactrocera* genus (Lauzon and Prokopy, 2013).

Insect immunity is made up of innate immunity and acquired immunity. Intestinal immunity is a kind of innate immunity. The insect immune system has no immune cells, proteins, or specific antigen-antibody responses like those in higher animals (Zasloff, 2002), but it can activate immune effectors via resident intestinal bacteria or toxins and then participate in the corresponding cellular and humoral immunity to resist the infection of foreign pathogens (Bonnay et al., 2013). For insects, an effective gut immune defense system takes a long time to build up to maintain the immune balance within the body, among gut microbes, and between the body and gut microbes (Sansonetti, 2004; Artis, 2008). Physical defenses, the immune deficiency (Imd) pathway, dual oxidase–reactive oxygen species (Duox-ROS), the Janus kinase-signal transducer and activator of transcription (JAK/STAT) pathways, and the intestinal symbiotic flora have been reported to be the main regulatory mechanisms of microbial homeostasis in the insect gut (Bai et al., 2018). However, there has been little research on the intestinal immune mechanism of *B. dorsalis* thus far. Studies on the cascade of immune-related pathways and the relationship among immune-related genes are also still lacking in this notorious pest. Many researchers are most interested in what the most important regulatory pathways and the most important key genes in oriental fruit flies are.

Our previous study showed that the gut bacterial diversity in *B. dorsalis* and *Zeugodacus tau* can be changed by antibiotic feeding, which resulted in the suppression of ovary development; in particular, the ovary of *Z. tau* was totally suppressed and could not produce eggs when fed a diet with antibiotics (Bai et al., 2018; Noman et al., 2020). How the gut bacteria maintain balance and how they regulate the growth, development, and reproduction of host flies are the scientific questions we are working on now. In this study, female and male *B. dorsalis* adults before and after antibiotic treatment were sequenced, and the differentially expressed genes (DEGs) were analyzed by RNA-Seq. Immune-related genes and KEGG pathways were assessed, and their functions in the intestinal immune process of *B. dorsalis* were discussed. This study will lay a theoretical foundation for the study of the invasion mechanism and biological control strategy of *B. dorsalis*.

MATERIALS AND METHODS

Insects

Bactrocera dorsalis specimens were collected from Yunnan Province and reared in an artificial climate incubator for more than 20 generations. The rearing conditions were 25°C, 70% humidity, and 10 D:14 L (10 h dark and 14 h light). The fruit flies were reared using artificial food following the method described by Bai et al. (2018).

Antibiotic Feeding Treatment

Antibiotics [tetracycline 120 μg/ml, streptomycin 400 μg/ml, and ampicillin 400 μg/ml at a ratio of 3:10:10 (Bai et al., 2018)] were added to the artificial food. Both larvae and adults were treated with equal proportions of antibiotics. Thousands of eggs were transferred onto solid food containing antibiotics and normal solid feed and then reared in an incubator. The third-instar larvae were picked out and then put onto sterilized moist sand while waiting for pupation and eclosion.

Gut Bacterial Analysis

The methods used for fruit fly treatment and gut bacterial diversity analysis were from Bai et al. (2018). Bacterial diversity was analyzed via high-throughput sequencing of the V3–V4 variable region of the 16S rRNA gene, and then bacterial function prediction was performed via PICRUSt software.

Growth and Reproduction Parameters Measurement

Adult weight and survival rate of 10-day-old adults (10 days post eclosion) were chosen as two growth parameters. The number of pupae and 10-day-old adults were recorded and used for survival rate calculation. Four adults were directly weighed by an electronic balance. The data were recorded, and the average weight was calculated. The preoviposition period, continuous spawning period and egg number were measured to represent reproductive ability. The *B. dorsalis* adults were observed at a specific time every day, and when they began and finished producing eggs was recorded. Egg amounts from five pairs of fruit flies (five female adults and five male adults) were recorded every day. There were three biological replicates.

Sample and RNA Preparation

Female and male insects that were reared normally and treated with antibiotics for 15 days were washed with sterile water and then washed with 1% sodium hypochlorite, 75% alcohol, and sterile water for 1 min. In a disposable petri dish containing sterile water, the intestinal tract was dissected with sterile tweezers and Venus scissors. Each sample containing 10 intestinal tracts was immediately frozen in liquid nitrogen for 20 min and then transferred to −80°C for future use for intestinal tract transcriptome sequencing and analysis. Each

sample containing one male and one female adult whole body was also immediately frozen in liquid nitrogen for 20 min and then transferred to −80°C for future use for whole-body transcriptome sequencing and analysis. Three biological repeats were prepared for transcriptome sequencing. RNA was extracted by an RNA simple Total RNA Kit (Tiangen, China) and sent to a company (BMK Biotechnology Co., Ltd., Beijing, China) for transcriptome sequencing.

Isolation and Transcriptome Sequencing of Intestinal RNA

The whole genome of *B. dorsalis*, which was published in the National Center for Biotechnology Information (NCBI[1]) (PRJNA273958, ID: 10754), was used as a reference genome for the transcriptome assembly method. The raw RNA-Seq data has been deposited in the National Center for Biotechnology Information (NCBI) with accession code PRJNA694509 (ID: 694509). The sequencing data was obtained by constructing a transcriptome library (based on the Illumina HiSeq Platform). To verify the reliability of the data, three biological replicates were established for each treatment. For standardization, all paired reads from the clean data representing relative single gene expression levels were converted to fragments per kilobase per million mapped reads (FPKM) per thousand bases (Florea et al., 2013). Relative gene expression levels for each treatment were calculated using three repeated mean FPKMs. *p*-Values in multiple tests were corrected by a false discovery rate, according to Benjamini and Hochberg's approach (Reiner et al., 2003). DEGs were identified based on a fold-change (FC) ≥ 2 and $p < 0.01$. Clean reads were aligned with the reference genome sequence using TopHat2 (Kim et al., 2013) to obtain genetic information, sequence features, and sample information. Gene Ontology (GO) enrichment analysis of the DEGs was implemented by the GOseq R package (V 1.16.2) based on Wallenius non-central hypergeometric distribution (Young et al., 2010). KEGG (Kanehisa et al., 2008) is a database resource for understanding the high-level functions and utilities of biological systems, such as cells, organisms, and ecosystems, from molecular-level information, especially large-scale molecular datasets generated by genome sequencing and other high-throughput experimental technologies[2]. KOBAS (Mao et al., 2005) software (3.0) was used to analyze the enrichment of DEGs in KEGG pathways. The sequences of the DEGs were blasted (blastx) to the genome of a related species [the protein–protein interaction (PPI) of which exists in the STRING database[3]] to obtain the predicted PPIs of these DEGs. Then, the PPIs of these DEGs were visualized in Cytoscape (Shannon, 2003).

Quantitative Real-Time PCR

To verify the transcriptome data demonstrating *B. dorsalis* responding to changes in intestinal bacteria, 10 immunity-related genes were selected for quantitative real-time PCR (qRT-PCR) testing (Bai et al., 2018). Groups consisted of female and male insects with two types of controls and two types of treatments, and each group had three replicates ($2 \times 2 \times 3 = 12$). There were 12 groups and 10 intestines in each group. RNA was extracted using an RNA simple Total RNA Kit (Tiangen, China). The RNA was then reverse transcribed into cDNA by RT-PCR using the PrimeScript RT Reagent Kit (Takara, Beijing). The resulting cDNA was stored at −20°C and diluted 10 times before being used. The cDNA template was amplified by PCR with GoTaq Green Master Mix (Tiangen, China) using primers for the α-tubulin gene for template detection.

For quantitative real-time PCR, the 18S rRNA gene was selected as the internal reference gene. Primers were designed by Premier 5.0, and specificity was verified by NCBI. The reaction system and reaction conditions for qRT-PCR were established following the instructions of GoTaq® Green Master Mix (Tiangen, China). Reaction conditions were as follows: 95°C for 30 s; 95°C for 5 s, 60°C for 34 s (40 cycles); 95°C for 15 s, 60°C for 1 min, 95°C for 15 s, 60°C for 15 s. All primers were synthesized by Shanghai Bioengineering Company and their sequences are listed in **Supplementary Table 1**.

Statistical Analysis

For each biological replicate, three technical replicates were performed. The relative expression level of genes was analyzed by the $2^{-\Delta\ Ct}$ method (Chen and Wagner, 2012). The qRT-PCR results were statistically analyzed by Student's *t*-tests using SPSS 22.0, and $p < 0.05$ was considered significant. Independent *t*-tests using SPSS 22.0 were used to test the growth, mortality, and reproduction of treated and untreated flies, and $p < 0.05$ was considered significant.

RESULTS

Gut Bacterial Flora and Function Prediction

The gut bacterial flora was significantly changed with antibiotic feeding (Bai et al., 2018). **Table 1** shows that the major bacterial genera changed from *Enterobacter* to *Bacillus* and *Lactococcus* in males, while in females, the major genus was *Lactococcus* instead of *Pseudomonas*. The main bacteria in males and females shifted from Gram-negative bacteria to Gram-positive bacteria.

Bacterial function prediction showed that E (amino acid transport and metabolism), R (general function prediction only), and S (function unknown) were the top three important gene functions in adults (**Supplementary Figure 1**). In females, genes related to L (replication, recombination, and repair), A (RNA processing and modification), B (chromatin structure and dynamics), E (amino acid transport and metabolism), I (lipid transport and metabolism), K (translation), N (cell motility), Q (secondary metabolite biosynthesis transport and catabolism), and U (intracellular trafficking, secretion, and vesicular transport) decreased. By contrast, in males, genes related to A (RNA processing and modification), B (chromatin structure and dynamics), and K (translation) increased, while genes related to N (cell motility), U (intracellular trafficking, secretion, and vesicular transport), and W (extracellular structures) decreased.

[1] http://www.ncbi.nlm.nih.gov/

[2] http://www.genome.jp/kegg/

[3] http://string-db.org/

TABLE 1 | Top 10 bacterial genera in the *Bactrocera dorsalis* control and antibiotic treatment groups.

Bacteria (Genus)	Gram[1]	CKM	TRM	CKF	TRF
Enterobacter	G–	72.49	0.09	6.23	2.82
Pseudomonas	G–	6.45	5.42	83.07	29.04
Bacillus	G+	0.01	43.34	0.01	5.71
Lactococcus	G+	1.03	32.98	4.78	33.86
Stenotrophomonas	G–	0.06	0.46	0	15.8
Acinetobacter	G–	16.27	11.19	0	7.77
Leclercia	G–	0.2	0	5.27	0
Achromobacter	G–	3.44	0	0	0
Streptococcus	G+	0	3.79	0	2.61
Lactobacillus	G+	0	0	0	0.13

[1]*Gram stain; G+, Gram positive; G–, Gram negative.*
CKM, male in the control group; TRM, male intestinal tract in the antibiotic treatment group; CKF, female in the control group; TRF, female in the antibiotic treatment group.

Growth and Reproduction

The effect of gut bacteria on host oriental fruit flies was also investigated by testing two growth and four reproductive factors after the gut bacterial diversity was changed using antibiotics; the results are shown in **Figure 1**. Growth factors, including adult weight ($p = 0.38$) and survival rate ($p = 0.89$), were not significantly changed by gut bacterial changes (**Figures 1A,B**). However, the preoviposition period was significantly prolonged, increasing from 12.5 to 23.7 days ($p < 0.05$) (**Figure 1C**). Additionally, females in the control group could produce offspring for more than 37 days, while the females in the treatment group had only 12 days of spawning. The spawning period was shortened significantly ($p < 0.05$) (**Figure 1C**). In addition, the total egg number ($p < 0.01$) and the egg number per day of females in the treatment group decreased significantly compared with the control group (**Figures 1D,E**) (1, 5 days, $p < 0.05$; 7, 9, 11 days, $p < 0.01$).

Sequencing Data Analysis

After sequencing quality control was conducted by removing reads with an adapter, with null base and with low quality, a total of 95.60 GB of clean reads were obtained from 12 intestinal tract samples, and a total of 41.06 GB of clean reads were obtained from six adult whole-body samples. For each sample, no less than 7.05 GB of clean reads were obtained, and the percentage of Q30 bases for all the samples was more than 93.59%. Statistics of intestinal sequencing information are provided in **Supplementary Table 2**. The FPKM distribution of each sample is shown in **Supplementary Figures 2A,C**; this measured the expression level of each sample from the overall discrete angle of expression. The box plot shows that the overall gene expression levels of the different samples are similar. The correlation statistics between samples were plotted (**Supplementary Figures 2B,D**); the Pearson's correlation coefficients between the same samples were 1 and within the same groups were close to 1. No abnormal samples were found. These results suggested that sampling was reliable and suitable for further analysis. The RNA quality of CKM1, CKM2, CKM3, CKF2, CKF3, TRM1, TRM2, TRM3, TRF1, TRF2, and TRF3 was high enough for further analysis, while the RNA quality of CKF1 only reached level B; this resulted in only 11 samples being used for the intestinal tract studies.

Differentially Expressed Genes

A Venn diagram shows the differentially expressed genes (DEGs) shared between the groups (**Supplementary Figure 2**). In the adult whole body, there were 1,419 upregulated and 967 downregulated genes (**Supplementary Figure 3A**). In the male intestinal tract, there were 212 upregulated genes and 94 downregulated genes (**Supplementary Figure 3B**). In the female intestinal tract, 114 genes were upregulated and 168 genes were downregulated (**Supplementary Figure 3C**). There were also some non-differentially expressed genes in both males and females.

Functional Annotation and Enrichment Analysis of Differentially Expressed Genes

Gene ontology analyses can define and describe genes and proteins to clarify the function of each gene. The GO annotation system consists of three major components, namely, biological process, molecular function, and cellular component, and 8,186 sequences were classified into 58 functional groups (**Supplementary Figure 4**). In the biological process category, 5,329, 5,316, and 4,470 genes were enriched for the terms single-organism process, cell process, and metabolic process, respectively. In the molecular functions category, 3,912 and 3,497 genes were annotated with the terms binding and catalytic activity, respectively. The cell and cell parts were dominant terms in the cellular component category, and 4,350 and 4,353 genes were enriched, respectively. The top 10 GO terms were single-organism process, cellular process, metabolic process, cell part, cell, binding, catalytic activity, organelle, biological regulation, and developmental processing. In total, 5,404 genes were successfully annotated by COG and were classified into 25 COG groups. Most genes were enriched in general functional prediction (24.37%), followed by replication, recombination and repair (7.59%), transcription (7.44%), amino acid transport and metabolism (6.72%) and posttranslational modification, protein turnover, and chaperones (6.35%). We speculated that there may be some new unknown genes under the unknown function term (2.35%).

Functional Annotation and Enrichment Analysis of Adult Whole-Body Differentially Expressed Genes

A total of 12,610 DEGs were identified in antibiotic females (**Figure 2A**). Among the 4,656 secondary nodes related to cellular components, 5,524 and 2,430 genes were enriched for biological processes and molecular functions, respectively. Among the cellular components, the cell parts term was the most abundant and had 1,306 genes. In the secondary nodes related to biological processes and molecular functions, cellular process and binding were the most abundant terms and had 1,127 and 1,049 genes,

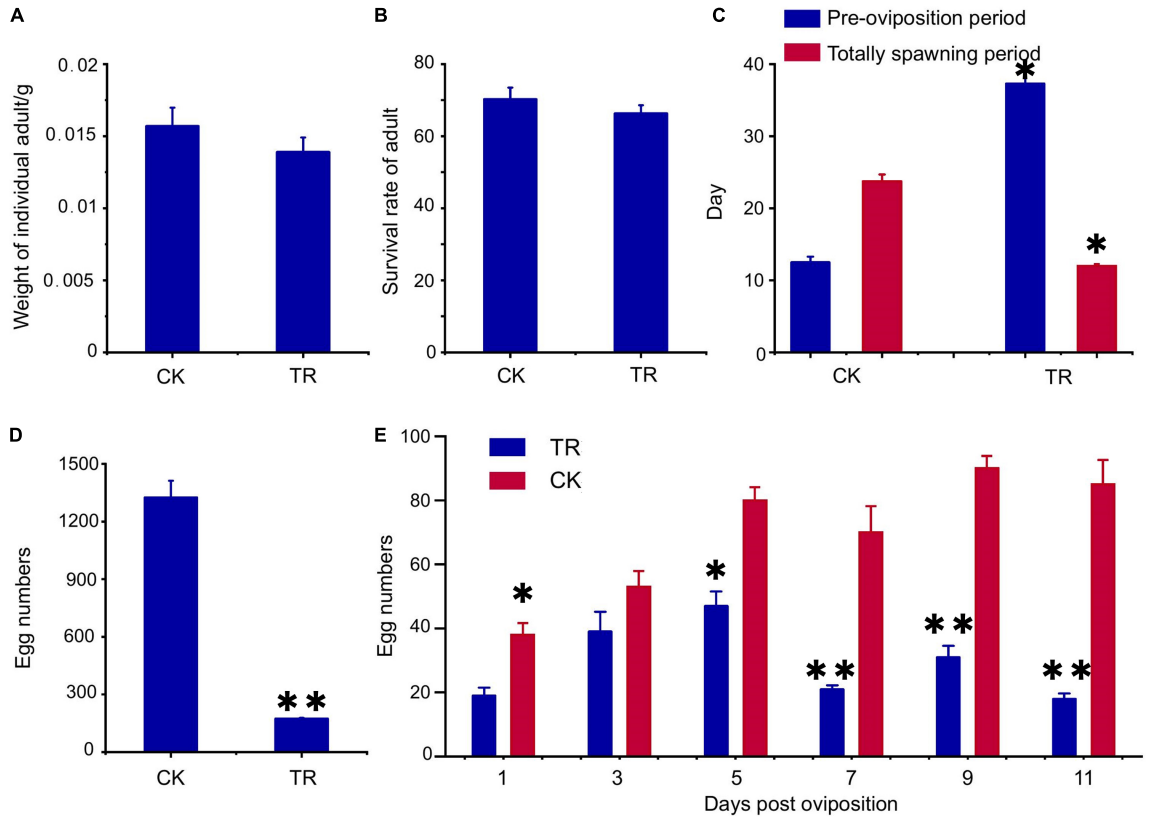

FIGURE 1 | Antibiotic feeding showed different effects on the growth and reproduction of *Bactrocera dorsalis*. **(A)** Antibiotic feeding did not decrease the weight of adults; **(B)** antibiotic feeding did not decrease the survival rate of adults; **(C)** antibiotic feeding prolonged the preoviposition period and shortened the total spawning period; **(D)** antibiotic feeding decreased the total number of eggs; **(E)** antibiotic feeding decreased the number of eggs per day after oviposition. CK, fruit flies reared under the normal conditions; TR, treatment group fed antibiotics. $^{*}p < 0.05$; $^{**}p < 0.01$.

respectively. All unigenes from antibiotic females were enriched in a total of 304 KEGG metabolic pathways. The top nine KEGG pathways are shown in **Figure 2B**. Among them, the most highly enriched factor was in the pathway named cardiac muscle contraction (KO04260), and the most DEGs were enriched for the term pathways in cancer (KO05200).

Functional Annotation and Enrichment Analysis of Male Intestinal Tract Differentially Expressed Genes

A total of 168 DEGs were identified in males (**Figure 3A**). Among the secondary nodes related to biological processes, 96, 91, and 68 genes were enriched for metabolic processes, single-organism processes, and cellular processes, respectively. Among the cellular components, cells and cell parts were the most abundant and had 48 genes. In the secondary nodes related to molecular function, catalytic activity and binding activity were the most abundant terms, with 87 and 55 genes, respectively. There were 142 differentially expressed genes in the 25 COG groups (**Figure 3C**). Among them, the most genes, with a percentage of 19.72% (28), were enriched for general functional prediction terms, followed by amino acid transport and metabolism and carbohydrate transport and metabolism, with percentages of 18.31% (26) and 16.2% (23), respectively. Three genes were enriched for unknown function items (2.21%). We speculated that these unknown sequences may contain some new unknown genes. All unigenes from males were enriched in a total of 58 KEGG metabolic pathways. The top 20 KEGG pathways are shown in **Figure 3B**. Among them, the most highly enriched factor was in the pathway named circadian rhythm-fly (KO04711), and most DEGs were enriched for the arginine and proline metabolism pathway (KO00330).

Functional Annotation and Enrichment Analysis of Female Intestinal Tract Differentially Expressed Genes

A total of 155 DEGs were identified in females (**Figure 4A**). Among the secondary nodes related to biological function, 91, 82, and 81 genes were enriched for metabolic processes, single-organism processes, and cellular processes, and 81 genes were enriched for the secondary nodes related to cellular components. Among the secondary nodes related to molecular function, catalytic activity and binding activity were found to be the most abundant terms, with 84 and 57 genes, respectively. There were 121 differentially expressed genes in the 25 COG groups (**Figure 4C**). Amino acid transport and metabolism had the most

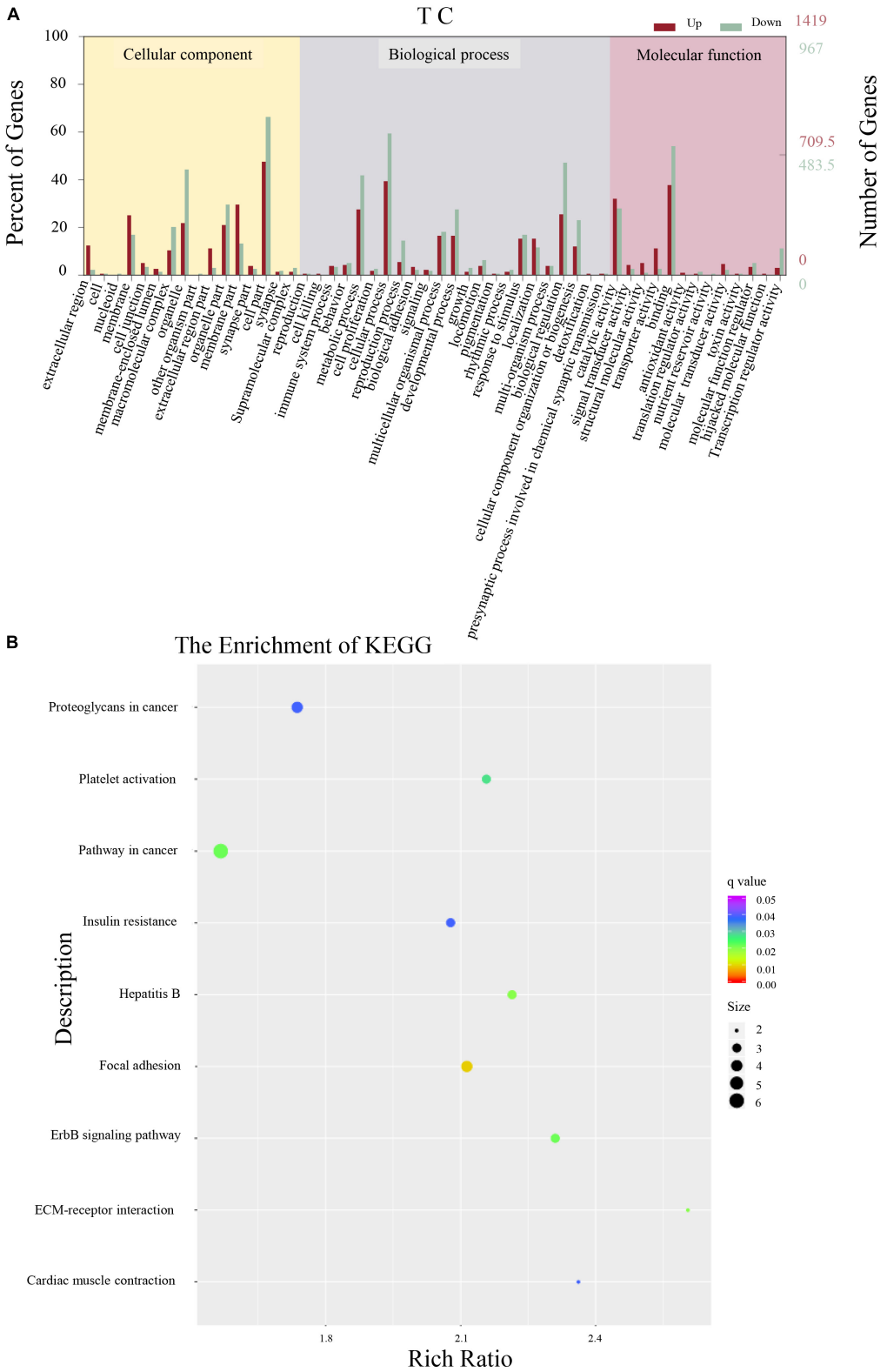

FIGURE 2 | Differentially expressed gene analysis of adult whole-body samples. **(A)** Annotated statistical graph of the Gene Ontology (GO) secondary nodes. Light colors represent all genes and dark colors represent all differentially expressed genes (DEGs) of *Bactrocera dorsalis* adults. **(B)** Scatter plot of enriched KEGG pathways. Each circle in the graph represents the number of genes enriched for a specific KEGG pathway. Enrichment factors represent the ratio of the number of differentially expressed genes to all the genes in the pathway.

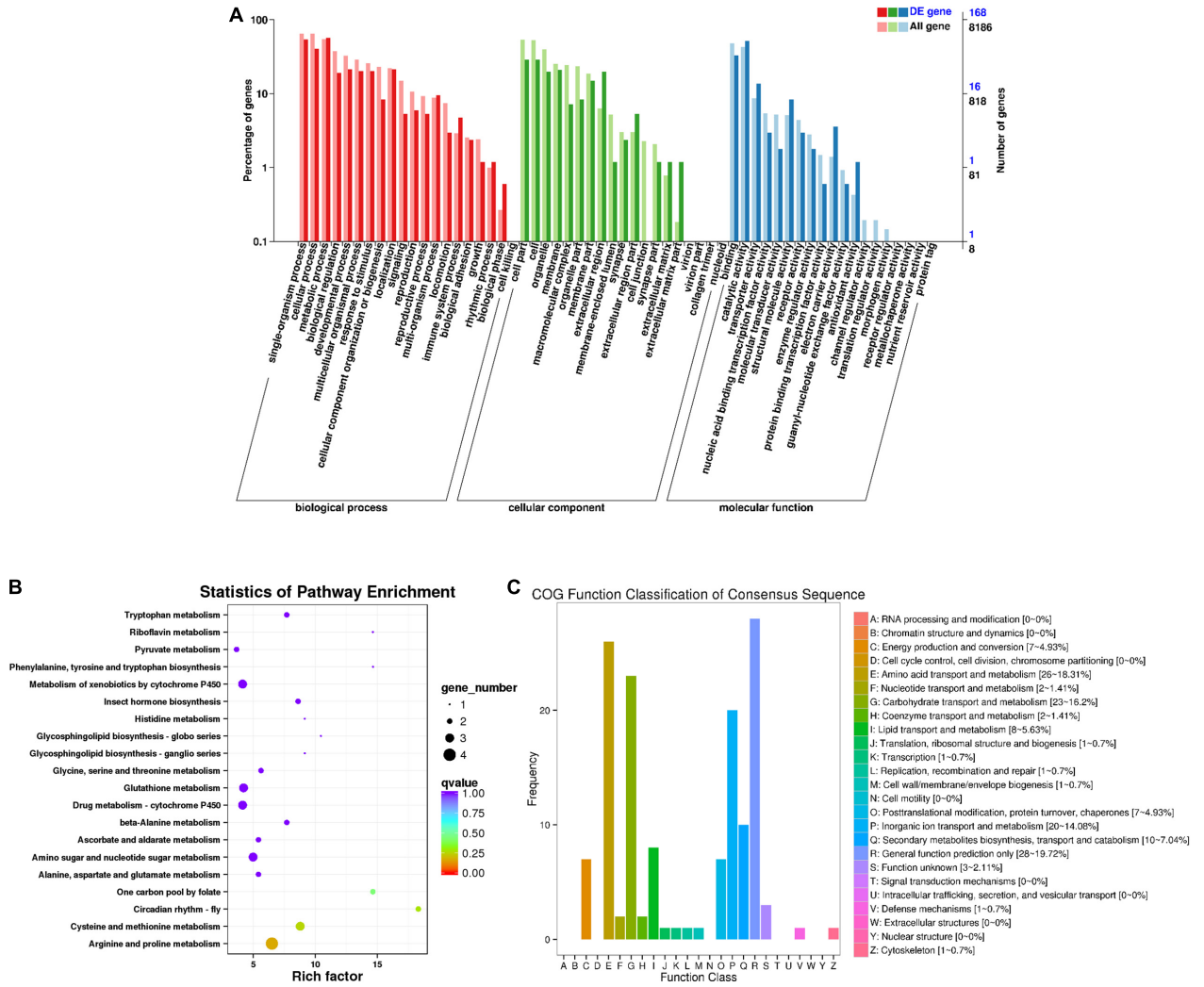

FIGURE 3 | Male differentially expressed gene analysis. **(A)** Annotated statistical graph of the GO secondary nodes. Light colors represent all genes and dark colors represent all differentially expressed genes (DEGs) of adult males. **(B)** Scatter plot of enriched KEGG pathways. Each circle in the graph represents the number of genes enriched for a specific KEGG pathway. Enrichment factors represent the ratio of the number of differentially expressed genes to all the genes in the pathway. **(C)** COG annotation classification statistics of differentially expressed genes in males. Frequency is the number of genes.

genes, with a percentage of 18.18% (22), followed by inorganic ion transport and metabolism and carbohydrate transport and metabolism, with percentages of 17.36% (21) and 14.05% (17), respectively. No genes with unknown function were found. All unigenes from females were enriched in a total of 55 KEGG metabolic pathways. The top 20 KEGG pathways are shown in **Figure 4B**. The most highly enriched factor and the most differentially expressed genes were in the folate biosynthesis pathway (KO00790).

Cluster Analysis of Differentially Expressed Genes Related to Immunity

Based on the KEGG pathway analysis of female adults 15 days post emergence of *B. dorsalis*, a total of 17 intestinal immune-related pathways were identified, including glycolysis, amino acid metabolism, pyruvate metabolism, and programmed cell death (**Table 2**). The results from male adults and adult whole-bodies (including females and males) were the same as those from females (**Table 2**). Ten immune-related genes were identified among the DEGs according to their RPFM values and gene function annotations; they are listed in **Table 3**. Among them, only three genes were speculated to play a role in males, including gram-negative bacteria-binding protein 3-like (*GNBP-3-like*), myb-like protein M (*MP-M*), and lysosome membrane protein 2 (*LMP-2*). Six genes were speculated to play a role in females, including *Laccase-1*, octopamine receptor beta-1R (*ORβ-1R*), probable multidrug resistance-associated protein lethal (2) 03659 (*PMRAPL(2)03659*), ubiquitin-60S ribosomal protein L40 (*URP-L40*), lysozyme B-like (*LB-like*), and cytosolic aminopeptidase-like (*CA-like*). One gene that was speculated to play a role in

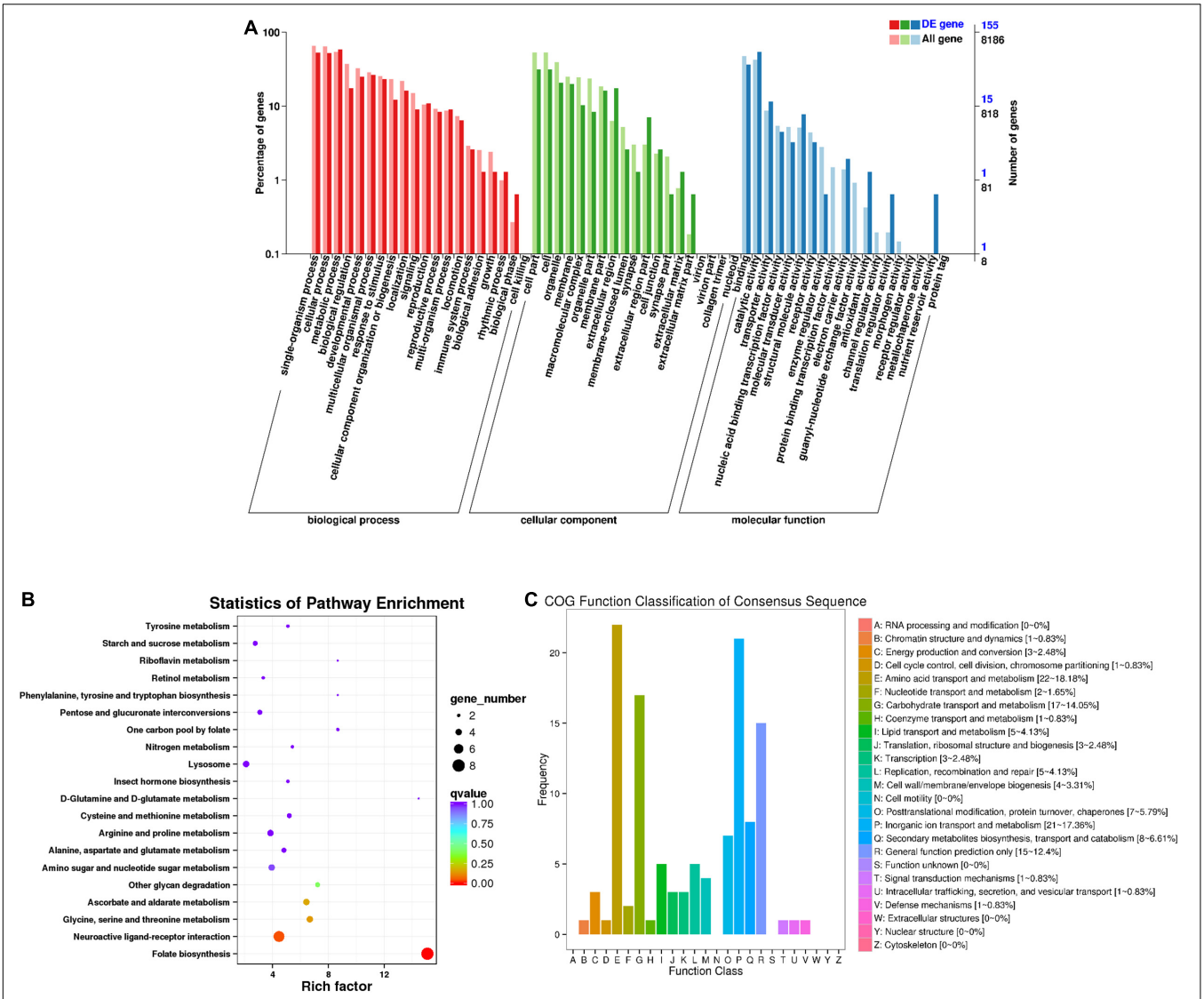

FIGURE 4 | Female differentially expressed gene analysis. **(A)** Annotated statistical graph of GO secondary nodes. Light colors represent all genes and dark colors represent all differentially expressed genes in females. **(B)** Scatter plot of enriched KEGG pathways. Each circle in the graph represents the number of genes enriched for a specific KEGG pathway. Enrichment factors represent the ratio of the number of differentially expressed genes to all the genes in the pathway. **(C)** COG annotation classification statistics of differentially expressed genes in females. **(B)** Frequency is the number of genes.

both males and females was peptidoglycan-recognition protein SC2 (*PGRP-SC2*). Based on the DEGs and KEGG pathway analysis, arginine and proline metabolism may be important pathways in the intestinal immune mechanisms of *B. dorsalis*.

Quantitative Real-Time-PCR Validation

To validate the sequencing quality, 10 immune-related genes were chosen for RT-qPCR. In the RT-qPCR assay, the expression of seven genes, *PGRP-SC2-M*, *PGRP-SC2-F*, *GNBP-3-like*, *MP-M*, *LMP-2*, *ORβ-1R*, *PMRAPL(2)03659*, and *CA-like*, were increased, while *LB-like*, *URP-L40*, and *Laccase-1* were decreased. Compared with the RNA-Seq results, the expression of *PGRP-SC2* and *URP-L40* was different from that of the transcriptome.

DISCUSSION

Bacteria in the midgut of *B. dorsalis* help improve host insecticide resistance and environmental adaptation, regulate growth and development, and affect male mating selection (Damodaram et al., 2016; Cheng et al., 2017; Raza et al., 2020). Many reports have attempted to uncover the function and regulatory mechanism of symbiotic bacteria in host insects. Amino acids have been confirmed to be the main factor that regulates the growth, development, and reproduction of host insects (Hoedjes et al., 2017; Ricardo et al., 2017). *Riptortus pedestris* gut bacteria can mediate growth, ovary development, and egg numbers by regulating three proteins stored in the hemolymph (Lee et al., 2016). During that process, food also plays an important part.

TABLE 2 | Immune-related KEGG pathways enriched in *Bactrocera dorsalis* adults.

Number	Pathway name
1	Pentose and glucuronate interconversions
2	Glycine, serine, and threonine metabolism
3	Pyruvate metabolism
4	Tryptophan metabolism
5	Metabolism of xenobiotics by cytochrome P450
6	Ascorbate and aldarate metabolism
7	Retinol metabolism
8	Cysteine and methionine metabolism
9	Phenylalanine, tyrosine, and tryptophan biosynthesis
10	Glycolysis/gluconeogenesis
11	Arginine and proline metabolism
12	Sphingolipid metabolism
13	Drug metabolism–cytochrome P450
14	Phagosome
15	Glycosphingolipid biosynthesis–globo series
16	ECM-receptor interaction
17	Drug metabolism–other enzymes

Together with essential amino acids, two important gut bacteria, *Acetobacter* and *Lactobacillus*, can increase the egg production of *Drosophila* by making host flies prefer to feed on yeast (Ricardo et al., 2017). In our study, the most important predicted function of the gut bacteria in oriental fruit flies was related to amino acid transport and metabolism, which was consistent with a previous report that amino acids may be important in regulating the growth and reproduction of host flies (Ricardo et al., 2017).

With the rapid development of high-throughput sequencing technology, RNA-Seq has become an important tool for transcriptome research (Wang et al., 2009). The genus *Bactrocera*, in which *B. dorsalis* belongs, is by far the most frequently identified genus. DEGs were identified according to the gene expression levels in the different samples, and functional annotations and enrichment analyses were also performed. Many reports have shown that the transcriptome can be used to uncover biological phenomes and mechanisms of molecular regulation in *B. dorsalis* (Gu et al., 2019, Guo et al., 2020). Gut bacteria can improve host fly fitness via gene overexpression. A good example is the gut symbiont *Citrobacter* sp., which can help its *B. dorsalis* host degrade trichlorphon via the expression of phosphatase hydrolase genes. High-throughput sequencing technology has become a useful tool to explore new genes in bacteria or genes in host insects that are associated with the function of bacteria. A comparative genomic analysis between the gut and wild *Citrobacter* strains showed that phosphatase hydrolase genes were highly expressed in gut *Citrobacter* when trichlorphon was present (Cheng et al., 2017). The pyroquinolinin-dependent alcohol dehydrogenase gene (*PQQ-ADH*) of symbiotic acetic acid bacteria in *Drosophila* can regulate the development rate, individual size, energy metabolism, and intestinal stem cell activity of the host insects via the insulin pathway (Shin et al., 2011).

In this study, DEGs were assigned to 58 functional subcategories within three main categories (biological processes, cellular components, and molecular function), and most of the enriched terms shared between males and females were related to metabolic processes, catalytic activity, and single-organism processes. For the COG database annotations, the largest proportion of genes in males (19.72%) were enriched for general functional prediction terms. In females, genes related to amino acid transport and metabolism were the most enriched, accounting for 18.18%. For the top 20 KEGG enrichment pathways, the most differentially expressed genes among males were related to arginine and proline metabolism (KO00330), and the most differentially expressed genes in females were related to folate biosynthesis (KO00790). Our result is consistent with one previous report that the immunity of the host *B. dorsalis* in response to low temperature stimulates the arginine and proline metabolism pathway, and that this is promoted by the gut microbiota (Raza et al., 2020). Folic acid is very important during the development of female ovaries (Song et al., 2014). Reports have also shown that folic acid can be synthesized by the intestinal microflora in animals (Hanson and Gregory, 2011). These reports provide a wealth of genetic information for our

TABLE 3 | Expression of immune-related genes and their RT-qPCR validation.

Sex	Annotation	RNA-Seq		RT-qPCR	
		log_2FC	*p*-Value	log_2FC	*p*-Value
Male	*GNBP-3-like*	2.2403	0.000	0.6906	0.034
	MP-M	2.2014	0.009	0.8030	0.010
	LMP-2	2.0973	0.007	0.6029	0.060
Female	*Laccase-1*	−2.8094	0.000	−0.7832	0.012
	LB-like	−3.2173	0.000	−0.0623	0.052
	ORβ-1R	3.3143	0.030	0.2238	0.031
	PMRAPL(2) 03659	2.1459	0.000	0.0804	0.142
	URP-L40	2.9374	0.000	−0.2237	0.306
	CA-like	3.3494	0.006	0.9409	0.004
Male and female	*PGRP-SC2*	Male: −2.64887 Female: −3.4597	0.000 0.000	2.4323 1.6164	0.000 0.000

follow-up experiments and will help us uncover the function of intestinal bacteria and the folate biosynthesis pathway in *B. dorsalis*.

Immunity is important for insects. Both diet and vertically transmitted bacteria can influence the fitness and immunity of *B. dorsalis* (Hassan et al., 2020). However, insects have an effective gut defense system that maintains self-immunity, thereby preserving the balance among microorganisms in the gut and stabilizing the diversity in gut symbiotic bacteria. It has been reported that the immune deficiency (Imd) pathway and dual oxidase–reactive oxygen species (Duox-ROS) are the main regulatory pathways in *B. dorsalis* (Wang, 2015; Liu et al., 2017; Iatsenko et al., 2018). Four genes, *PGRP-LB*, *PGRP-SB*, *cecropin*, and *defensin*, were confirmed to be key genes in the Imd pathway. In this study, to investigate the effect of intestinal bacteria on the intestinal immunity of *B. dorsalis*, differentially expressed genes and KEGG signaling pathways related to intestinal immunity were defined. As mentioned earlier, the *PGRP-SC2* and *URP-L40* validation results are controversial. For *URP-L40*, the different expression trends can be attributed to the high *p*-value obtained; the *p*-value for the qRT-PCR was larger; therefore, the data are less credible. It has been reported that *PGRP-SC2* can be downregulated with the activation of the Imd pathway in flies (Bischoff et al., 2006). *PGRP-SC2* has been confirmed to play an important role in innate immunity, and its expression level increased with increasing bacterial concentrations after challenge by Gram-positive bacteria in *Artemia sinica* (Zhu et al., 2017). Transcripts from different PGRP genes have been identified in immune regulatory organs such as the fat body, gut, and hemocytes in *Drosophila* (Werner et al., 2000). In our research, Gram-positive bacteria increased after the insects were fed antibiotics, and the expression of the *PGRP-SC2* gene in *B. dorsalis* rose accordingly, which was consistent with our experimental results. The *PGRP-SC2* gene and the arginine–proline metabolism pathway were identified and speculated to play a key role in the intestinal immunity of the *Drosophila* host, which provides a theoretical basis for revealing the function of intestinal bacteria. An advanced team showed that the *PGRP-SC2* gene could inhibit the intestinal overreaction of *B. dorsalis* caused by *E. coli* and that it plays a negative role in immune regulation (Yao, 2017). The key point of this study should be the effect of the *PGRP-SC2* gene on the intestinal commensal bacterial community of *B. dorsalis* and the role of *PGRP-SC2* in the immunity of *B. dorsalis*, which is also the target of our future research.

DATA AVAILABILITY STATEMENT

RNA-seq raw data have been deposited in National Center for Biotechnology Information (NCBI) with accession code PRJNA694509 (ID: 694509).

AUTHOR CONTRIBUTIONS

LL conceived and designed the study. LZe, LZh, and ZB performed the experiments. JF, LZh, and LL wrote the article. ZL and LL modified the manuscript. All authors have read and agreed to the published version of the manuscript.

FUNDING

This study received financial support from the National Natural Science Foundation of China (31801802), the Beijing Natural Foundation of China (6174043), and the Fundamental Research Funds for the Central Universities (2020SF004).

ACKNOWLEDGMENTS

We would like to thank all the members of the Plant Quarantine Laboratory of China Agricultural University (CAUPQL). Many thanks to all reviewers' comments on this manuscript.

SUPPLEMENTARY MATERIAL

The Supplementary Material for this article can be found online at: https://www.frontiersin.org/articles/10.3389/fcell.2021.647604/full#supplementary-material

Supplementary Figure 1 | COG-based functional distribution histogram of gut bacteria from *Bactrocera dorsalis* before and after antibiotic feeding. CKM, male in the control group; TRM, male in the antibiotic treatment group; CKF, female in the control group; TRF, female in the antibiotic treatment group.

Supplementary Figure 2 | Sample reliability verification diagram. **(A)** Box plot of the gene expression distribution of all intestinal tract samples. The abscissa represents different samples; the ordinate represents the logarithm of the sample expression FPKM. **(B)** Heatmap of the correlation in expression between two intestinal tract samples. **(C)** Box plot of the gene expression distribution of the adult whole-body samples. The abscissa represents different samples; **(D)** heatmap of the correlation in expression between two adult whole-body samples. The horizontal and vertical coordinates in the graph are sample numbers, and their order is determined by the results of correlation clustering. CKM, male intestinal tract in the control group; CKF, female intestinal tract in the control group; TRM, male intestinal tract in the antibiotic treatment group; TRF, female intestinal tract in the antibiotic treatment group. C, male and female whole-body in the control group; T, male and female whole-body in the antibiotic treatment group.

Supplementary Figure 3 | Overall analysis of differentially expressed genes. **(A)** Volcano plot of differentially expressed genes in the adult whole-body samples from the control and treatment groups. Yellow dots show upregulated genes, blue dots show downregulated genes, and black dots show non-differentially expressed genes. **(B)** Volcano plot of differentially expressed genes in the intestinal tract of males from the control and treatment groups. **(C)** Volcano plot of differentially expressed genes in the intestinal tract of females from the control and treatment groups. Red dots show upregulated genes, green dots show downregulated genes, and black dots show non-differentially expressed genes.

Supplementary Figure 4 | GO and COG DEG analysis results. **(A)** Statistical results of the GO classifications for all genes. Light colors represent all genes and dark colors represent all differentially expressed genes. **(B)** Statistical results of the COG classification for all genes. Frequency is the number of genes.

Supplementary Table 1 | Primers used for real time RT-qPCR amplification.

Supplementary Table 2 | Statistics of intestinal sequencing yield of *Bactrocera dorsalis*.

REFERENCES

Artis, D. (2008). Epithelial-cell recognition of commensal bacteria and maintenance of immune homeostasis in the gut. *Nat. Rev. Immunol*. 8, 411–420. doi: 10.1038/nri2316

Bai, Z. Z., Liu, L. J., Noman, S. M., Zeng, L. Y., Luo, M., and Li, Z. H. (2018). The influence of antibiotics on gut bacteria diversity associated with laboratory-reared *Bactrocera dorsalis*. *Bull. Entomol. Res*. 109, 500–509. doi: 10.1017/S0007485318000834

Bischoff, V., Vignal, C., Duvic, B., Boneca, I. G., Hoffmann, J. A., and Royet, J. (2006). Downregulation of the *Drosophila* immune response by peptidoglycan-recognition proteins SC1 and SC2. *PLoS Pathog.* 2:e14. doi: 10.1371/journal.ppat.0020014

Bonnay, F., Cohen-Berros, E., Hoffmann, M., Kim, S. Y., Boulianne, G. L., Hoffmanm, J. A., et al. (2013). Big bang gene modulates gut immune tolerance in *Drosophila*. *Proc. Natl. Acad. Sci. U.S.A.* 110, 2957–2962. doi: 10.1073/pnas.1221910110

Chen, B., and Wagner, A. (2012). Hsp90 is important for fecundity, longevity, and buffering of cryptic deleterious variation in wild fly populations. *BMC Evol. Biol.* 12:25. doi: 10.1186/1471-2148-12-25

Cheng, D. F., Guo, Z. J., Riegler, M., Xi, Z. Y., Liang, G. W., and Xu, Y. J. (2017). Gut symbiont enhances insecticide resistance in a significant pest, the oriental fruit fly *Bactrocera dorsalis* (Hendel). *Microbiome* 5:13. doi: 10.1186/s40168-017-0236-z

Damodaram, K. J. P., Ayyasamy, A., and Kempraj, V. (2016). Commensal bacteria aid mate-selection in the fruit fly, *Bactrocera dorsalis*. *Microb. Ecol.* 72, 725–729. doi: 10.1007/s00248-016-0819-4

Florea, L., Song, L., and Salzberg, S. L. (2013). Thousands of exon skipping events differentiate among splicing patterns in sixteen human tissues. *F1000 Res.* 2:188. doi: 10.12688/f1000research.2-188.v1

Gu, X. Y., Zhao, Y., Su, Y., Wu, J. J., Wang, Z. Y., Liu, L. J., et al. (2019). A transcriptional and functional analysis of heat hardening in two invasive fruit fly species, *Bactrocera dorsalis* and *Bactrocera correcta*. *Evol. Appl.* 12, 1147–1163. doi: 10.1111/eva.12793

Guo, S. K., Guo, X. Y., Zheng, L. Y., Zhao, Z. H., Liu, L. J., Shen, J., et al. (2020). A potential genetic control by suppression of the wing developmental gene wingless in a global invasive pest *Bactrocera dorsalis*. *J. Pest Sci*. 94, 517–529. doi: 10.1007/s10340-020-01263-1

Hanson, A. D., and Gregory, J. F. (2011). Folate biosynthesis, turnover, and transport in plants. *Annu. Rev. Plant Biol*. 62, 105–125. doi: 10.1146/annurev-arplant-042110-103819

Hassan, B., Siddiqui, J. A., and Xu, Y. (2020). Vertically transmitted gut bacteria and nutrition influence the immunity and fitness of *Bactrocera dorsalis* larvae. *Front. Microbiol* 11:596352. doi: 10.3389/fmicb.2020.596352

Hoedjes, K. M., Rodrigues, M. A., and Flatt, T. (2017). Amino acid modulation of lifespan and reproduction in *Drosophila*. *Curr. Opin. Insect Sci.* 23, 118–122. doi: 10.1016/j.cois.2017.07.005

Iatsenko, I., Boquete, J. P., and Lemaitre, B. (2018). Microbiota-derived lactate activates production of reactive oxygen species by the intestinal NADPH oxidase nox and shortens drosophila lifespan. *Immunity* 49, 929–942.e5. doi: 10.1016/j.immuni.2018.09.017

Kanehisa, M., Araki, M., Goto, S., Hattori, M., Hirakawa, M., Itoh, M., et al. (2008). KEGG for linking genomes to life and the environment. *Nucleic Acids Res*. 36, 480–484.

Kim, D., Pertea, G., Trapnell, C., Pimentel, H., and Kelley, R. (2013). TopHat2: accurate alignment of transcriptomes in the presence of insertions, deletions and gene fusions. *Genome Biol*. 14:R36. doi: 10.1186/gb-2013-14-4-r36

Knief, C., Delmotte, N., Chaffron, S., Stark, M., and Vorholt, J. A. (2011). Metaproteogenomic analysis of microbial communities in the phyllosphere and rhizosphere of rice. *ISME J.* 6, 1378–1390. doi: 10.1038/ismej.2011.192

Lauzon, C. R., and Prokopy, T. B. R. (2013). *Serratia marcescens* as a bacterial pathogen of *Rhagoletis pomonella* flies (Diptera: Tephritidae). *Eur. J. Entomol.* 100, 87–92. doi: 10.14411/eje.2003.017

Lee, J. B., Park, K. E., Lee, S. A., Jang, S. H., Eo, H. J., Jang, H. A., et al. (2016). Gut symbiotic bacteria stimulate insect growth and egg production by modulating hexamerin and vitellogenin gene expression. *Dev. Comp. Immunol*. 69, 12–22.

Li, Q., Fan, J., Sun, J., Wang, M., Francis, F., and Chen, J. (2016). Research progress in the interactions among the plants, insects and endosymbionts. *J. Plant Prot*. 43, 881–891.

Lindow, S. E., and Brandl, M. T. (2003). Microbiology of the phyllosphere. *Appl. Environ. Microbiol*. 69, 1875–1883. doi: 10.1128/aem.69.4.1875-1883.2003

Liu, S. H., Wei, D., Yuan, G. R., Jiang, H. B., Dou, W., and Wang, J. J. (2017). Antimicrobial peptide gene cecropin-2 and defensin respond to peptidoglycan infection in the female adult of oriental fruit fly, *Bactrocera dorsalis* (Hendel). *Comp. Biochem. Physiol. B Biochem. Mol. Biol*. 206, 1–7. doi: 10.1016/j.cbpb.2017.01.004

Mao, X., Tao, C., Olyarchuk, J. G., and Wei, L. (2005). Automated genome annotation and pathway identification using the KEGG Orthology (KO) as a controlled vocabulary. *Bioinformatics* 21, 3787–3793. doi: 10.1093/bioinformatics/bti430

Naaz, N., Choudhary, J. S., Prabhakar, C. S., Moanaro, and Maurya, S. (2016). Identification and evaluation of cultivable gut bacteria associated with peach fruit fly, *Bactrocera zonata* (Diptera: Tephritidae). *Phyto Parasitica* 44, 1–12.

Ning, Y. Y., You, M. M., and Wang, C. S. (2009). Advances in the study of insect immune identification and pathogen immune escape. *J. Entomol.* 52, 567–575. doi: 10.16380/j.kcxb.2009.05.007 (in Chinese).

Noman, M. S., Shi, G., Liu, L. J., and Li, Z. H. (2020). The diversity of bacteria in different life stages and their impact on the development and reproduction of *Zeugodacus tau* (Diptera: Tephritidae). *Insect Sci*. 28, 363–376. doi: 10.1111/1744-7917.12768

Raza, M. F., Wang, Y., Cai, Z., Bai, S., Yao, Z., and Awan, U. A. (2020). Gut microbiota promotes host resistance to low-temperature stress by stimulating its arginine and proline metabolism pathway in adult *Bactrocera dorsalis*. *PLoS Pathog*. 16:e1008441. doi: 10.1371/journal.ppat.1008441

Reiner, A., Yekutieli, D., and Benjamini, Y. (2003). Identifying differentially expressed genes using false discovery rate controlling procedures. *Bioinformatics* 19, 368–375. doi: 10.1093/bioinformatics/btf877

Ricardo, L. O. G. A., Zita, C. S., Patrícia, F. A., Tondolo, F. G., Margarida, A., Célia, B., et al. (2017). Commensal bacteria and essential amino acids control food choice behavior and reproduction. *PLoS Biol*. 15:e2000862. doi: 10.1371/journal.pbio.2000862

Sansonetti, P. J. (2004). War and peace at mucosal surfaces. *Nat. Rev. Immunol*. 4, 953–964. doi: 10.1038/nri1499

Shannon, P. (2003). Cytoscape: a software environment for integrated models of biomolecular interaction networks. *Genome Res*. 13, 2498–2504. doi: 10.1101/gr.1239303

Shin, S. C., Kim, S. H., You, H., Kim, B., Kim, A. C., Lee, K. A., et al. (2011). *Drosophila* microbiome modulates host developmental and metabolic homeostasis via insulin signaling. *Science* 334, 670–674. doi: 10.1126/science.1212782

Song, J., Xu, S. Y., Yang, S. Y., and Wu, D. (2014). The effect of folic acid on the quality of ovarian cells in animals and its mechanism of action. *J. Anim. Nutr.* 26, 63–68 (in Chinese).

Verghese, A., Soumya, C. B., Shivashankar, S., Manivannan, S., and Krishnamurthy, S. V. (2012). Phenolics as chemical barriers to female fruit fly, *Bactrocera dorsalis* (Hendel) in mango. *Curr. Sci*. 103, 563–566.

Wang, A. L. (2015). *Function Analysis of PGRP-LB and PGRP- SB in Immunity and Modulation of Intestinal Microbiota in Bactrocera Dorsalis*. Wuhan: Huazhong Agricultural University. doi: 10.7666/d.Y2803245 (in Chinese).

Wang, Z., Gerstein, M., and Snyder, M. (2009). RNA-seq: a revolutionary tool for transcriptomics. *Nat. Rev. Genet.* 10:57. doi: 10.1038/nrg2484

Werner, T., Liu, G., Kang, D., Ekengren, S., Steiner, H., and Hultmark, D. (2000). A family of peptidoglycan recognition proteins in the fruit fly *Drosophila melanogaster*. *Proc. Natl. Acad. Sci. U.S.A.* 97, 13772–13777. doi: 10.1073/pnas.97.25.13772

Yao, Z. C. (2017). *Study of the Duox-ROS System and IMD Signal Path Functionality in Bactrocera Dorsalis*. Wuhan: Huazhong Agricultural University (in Chinese).

Yao, Z., Wang, A., Li, Y., Cai, Z., Lemaitre, B., and Zhang, H. Y. (2016). The dual oxidase gene BdDuox regulates the intestinal bacterial community homeostasis of *Bactrocera dorsalis*. *ISME J.* 10, 1037–1050. doi: 10.1038/ismej.2015.202

Young, M. D., Wakefield, M. J., Smyth, G. K., and Oshlack, A. (2010). Gene ontology analysis for RNA-seq: accounting for selection bias. *Genome Biol.* 11:R14. doi: 10.1186/gb-2010-11-2-r14

Zasloff, M. (2002). Antimicrobial peptides of multicellular organisms. *Nature* 415, 389–395. doi: 10.1038/415389a

Zhang, X. Y., Meng, Y. Q., Huang, Z. D., Pu, Z. X., and Chen, G. Q. (2010). Research progress on the control technology of *Bactrocera dorsalis*. *Zhejiang Citrus* 27, 26–29 (in Chinese).

Zhu, X. L., Zhang, M. C., Yao, F., Yin, Y. L., Zou, X. Y., Hou, L., et al. (2017). Involvement of PGRP-SC2 from *Artemia* sinica in the innate immune response against bacteria and expression pattern at different developmental stages. *Dev. Comp. Immunol.* 67, 276–286. doi: 10.1016/j.dci.2016.09.009

Conflict of Interest: The authors declare that the research was conducted in the absence of any commercial or financial relationships that could be construed as a potential conflict of interest.

Publisher's Note: All claims expressed in this article are solely those of the authors and do not necessarily represent those of their affiliated organizations, or those of the publisher, the editors and the reviewers. Any product that may be evaluated in this article, or claim that may be made by its manufacturer, is not guaranteed or endorsed by the publisher.

Advantages of publishing in Frontiers

OPEN ACCESS
Articles are free to read for greatest visibility and readership

FAST PUBLICATION
Around 90 days from submission to decision

HIGH QUALITY PEER-REVIEW
Rigorous, collaborative, and constructive peer-review

TRANSPARENT PEER-REVIEW
Editors and reviewers acknowledged by name on published articles

Frontiers
Avenue du Tribunal-Fédéral 34
1005 Lausanne | Switzerland

Visit us: www.frontiersin.org
Contact us: frontiersin.org/about/contact

REPRODUCIBILITY OF RESEARCH
Support open data and methods to enhance research reproducibility

DIGITAL PUBLISHING
Articles designed for optimal readership across devices

FOLLOW US
@frontiersin

IMPACT METRICS
Advanced article metrics track visibility across digital media

EXTENSIVE PROMOTION
Marketing and promotion of impactful research

LOOP RESEARCH NETWORK
Our network increases your article's readership